NUREG/CR-3654
EPRI NP-3497
WCAP-10415

PWR FLECHT SEASET
Systems Effects Natural Circulation and Reflux Condensation

Data Evaluation and Analysis Report
NRC/EPRI/Westinghouse Report No. 14

Prepared by L. E. Hochreiter, S. D. Rupprecht, J. T. Dederer, S. Wong,
E. R. Rosal, B. R. Sinwell, F. J. Kovdalski, R. Quaglia

Jointly Sponsored by
USNRC, EPRI, and Westinghouse

Prepared for
U.S. Nuclear Regulatory
Commission

GPO Printed copy price: $15.00

FLECHT SEASET PROGRAM
NRC/EPRI/Westinghouse Report No. 14
NUREG/CR-3654
EPRI NP-3497
WCAP-10415

PWR FLECHT SEASET
SYSTEMS EFFECTS NATURAL CIRCULATION AND REFLUX CONDENSATION
DATA EVALUATION AND ANALYSIS REPORT

Manuscript Completed: August 1984
Date Published:

Prepared by: L.E. Hochreiter, S.D. Rupprecht, J.T. Dederer, S. Wong, E.R. Rosal, B.R. Sinwell, F.J. Kovdalski, R. Quaglia

Prepared for

Division of Accident Evaluation
Office of Nuclear Regulatory Research
U.S. Nuclear Regulatory Commission
Washington, DC 20555

Electric Power Research Institute
3412 Hillview Avenue
Palo Alto, California 94303

and

Westinghouse Electric Corporation
Nuclear Energy Systems
P. O. Box 355
Pittsburgh, Pennsylvania 15230

by

Westinghouse Electric Corporation
under
Contract No. NRC-04-77-127, EPRI Project No. RP959-1

Program Management Group

NRC - R. Lee
EPRI - A. Singh
Westinghouse - H. B. Rosenblatt

NRC FIN B6204

LEGAL NOTICE

This report was prepared as an account of work sponsored by the U.S. Nuclear Regulatory Commission, the Electric Power Research Institute, Inc., and the Westinghouse Electric Corporation. Neither the United States government nor any agency thereof, nor the Institute or members thereof, nor the Westinghouse Electric Corporation, nor any of their employes, makes any warranty, expressed or implied, or assumes any legal liability or responsibility for any third party's use or the result of such use of any information, apparatus, product, or process disclosed in this report or represents that its use by such third party would not infringe privately owned rights.

ACKNOWLEDGMENTS

The work of the following Westinghouse Nuclear Energy Systems contributors is hereby acknowledged:

TECHNOLOGY PROGRAMS
L. M. Williams

SAFEGUARDS ENGINEERING
M. Y. Young
K. F. McNamee
D. W. Sklarsky
D. P. Kitzmiller
D. P. Remlinger

TEST ENGINEERING AND OPERATIONS
D. P. Geisler
V. J. Grande
V. S. Petrillo
F. J. Mulligan
P. F. Orangio
R. W. Freudenberg
N. Washington
W. Russell
J. R. Latta

EQUIPMENT TECHNICAL PLANNING INTEGRATION
N. F. Falgione, Jr.

PUBLICATION PROGRAMS
J. G. Nagle

RESEARCH AND DEVELOPMENT CENTER
Dr. A. Pebler

The work of the following members of the Program Management Group, their colleagues, and their consultants is hereby acknowledged:

EPRI-K. H. Sun
NRC-RSR-L. H. Sullivan, R. Lee
NRC-NRR-W. Hodges, G. N. Lauben
EG&G-G. Wilson, D. M. Ogden
ITI-P. R. Davis

7124B:lb/073084

SPECIAL ACKNOWLEDGMENTS

The authors would like to acknowledge the efforts of several individuals who provided special assistance during this program. The authors would like to thank R. L. Kiang and P. Jeuck of SRI and J. P. Sursock and K. H. (Bill) Sun of EPRI for making the SRI material evaluation test facility available for testing operating procedures. The authors would also like to acknowledge the prompt and able assistance given by Mr. G. G. Loomis of the INEL Semiscale program in finalizing test procedures for successful operation in all three modes of natural circulation cooling. Finally the authors would like to thank Professor Peter Griffith of Massachusetts Institute of Technology for his review of the data analysis and for his insight into the complex two-phase phenomena and system effects observed in these experiments.

TABLE OF CONTENTS

TABLE OF CONTENTS (cont)

TABLE OF CONTENTS (cont)

LIST OF ILLUSTRATIONS

LIST OF ILLUSTRATIONS (cont)

LIST OF ILLUSTRATIONS (cont)

LIST OF ILLUSTRATIONS (cont)

LIST OF TABLES

SECTION 1
SUMMARY

As part of the NRC/EPRI/Westinghouse Full-Length Emergency Cooling Heat Transfer Separate Effects and Systems Effects Test (FLECHT SEASET) heat transfer and hydraulic program,[1] a series of natural circulation tests were conducted on a test facility whose dimensions were scaled to those of current PWRs with a scale factor of 1/307 on a volume basis, in which full lengths and full heights were prototypical. The purpose of these tests was to identify hydraulic and heat transfer phenomena during natural circulation cooling modes. The resulting test data, evaluation, and analysis are to be used for PWR code and model assessment as well as to provide a comparison to similar experiments in other scaled systems.

Steady-state single-phase, two-phase, and reflux condensation modes of natural circulation cooling were established in the FLECHT SEASET systems effects facility and the flow and heat transfer characteristics of the different cooling modes were identified.

Both single-phase and two-phase natural circulation are driven by an overall fluid density gradient between the hot and cold sides of the loop. During single-phase natural circulation, fluid in the core, hot leg, and upflow side of the steam generator is hotter, and therefore less dense, than fluid in the steam generator downflow side, pump suction, cold leg, and downcomer. This causes an unbalanced gravity head. During two-phase natural circulation, saturated steam bubbles in the core, hot leg, and upflow side of the steam generator cause the fluid in these regions to be less dense than that in the steam generator downflow side, pump suction, cold leg, and downcomer. Generally, two-phase natural circulation flow rates are higher than single-phase values because of the presence of the saturated steam bubbles, which creates a much higher overall loop density gradient. The reflux condensation mode occurs when the steam generator tubes and hot leg are nearly voided of

---

1. Conway, C. E., et al., "PWR FLECHT Separate Effects and Systems Effects Test (SEASET) Program Plan," NRC/EPRI/Westinghouse-1, December 1977.

liquid and steam created in the core is condensed in the steam generator tubes. Condensation occurs in both the upflow and downflow side of the steam generator tubes and the upflow/downflow of condensed fluid was evenly split.

Two different types of system behavior were observed in the FLECHT SEASET tests, as compared to the higher-pressure Semiscale natural circulation experiments. The single-loop simulation (broken loop) stopped circulating as the system moved from single-phase natural circulation to reflux condensation. Also, while in reflux condensation, the larger loop (representing three scaled PWR loops) vented through the loop seal. Detailed data analysis in this report indicates that this behavior is due to scaling compromises and facility design. The steam generator data were reduced such that local steam generator heat fluxes could be obtained for single-phase, two-phase, and reflux condensation natural circulation cooling modes.

This report presents the test data; data reduction, analysis, and evaluation; and resulting model development and analysis. The models which have been developed include a reflux tube condensation model as well as a single- and two-phase model for the overall system.

SECTION 2
INTRODUCTION

2-1. BACKGROUND

Since the Three Mile Island accident, an increased interest has developed in alternative cooling modes for pressurized water reactors following postulated accidents. The cooling modes of primary interest are single-phase natural circulation, two-phase natural circulation, and reflux condensation while the primary system is in a pressurized state. The information of interest is the heat transfer mechanisms which occur during each cooling mode and the coupled heat transfer-flow behavior of a closed loop natural circulation system. Cooling and flow stability are also of interest in a gravity-driven flow situation for natural circulation.

The FLECHT SEASET natural circulation test facility[1] offered an opportunity to investigate the alternative cooling modes, heat transfer processes, and flow behavior of a scaled closed system under natural circulation. The facility conceptual design, scaling rationale, and instrumentation have been covered in detail in the Task Plan.[1] Highlights of the facility design, test generation, and testing method are given in section 4 of this report. One drawback of the FLECHT SEASET natural circulation system is its low pressure [1.03 MPa (150 psia) maximum], which makes simulation of small breaks and operational transients difficult.

The information generated in this portion of the FLECHT SEASET program will be very useful for developing and assessing computer models for system behavior in single- and two-phase natural circulation. The analysis of the data and interpretation of the observed flow behavior can be used to benchmark complex systems analysis codes, which can then be used for both safety assessment and the writing of operational procedures for accident recovery. The models presented in this report will also serve as alternatives for existing models

---

1. Rosal, E. R., et al., "PWR FLECHT SEASET Systems Effects Natural Circulation and Reflux Condensation Task Plan Report," NRC/EPRI/Westinghouse-12, November 1982.

and can aid in interpretation of the test data. Computer code assessment against the FLECHT SEASET model would constitute an additional verification process to increase confidence in codes when applied to PWR performance.

2-2. TASK OBJECTIVES

The objcctives of the natural circulation tests were as follows:

- To provide a single-phase and two-phase natural circulation data base over a range of rod bundle powers such that natural circulation calculations can be verified
- To examine core cooling transitions between single-phase, two-phase, and reflux condensation and examine the steam generator heat transfer in these modes
- To examine system response and stability in a two-phase or reflux condensation mode and, in particular, characterize the steam generator behavior in these cooling modes

To accomplish these objectives, the FLECHT SEASET reflood systems effects test facility was modified and redesigned as described in the Task Plan to provide a low-pressure, closed loop simulation of a four-loop PWR. A substantial amount of instrumentation was added to the FLECHT SEASET facility to acheive the objectives. Details of the test facility are given in section 4.

2-3. PREVIOUS STUDIES

Because of the importance of the Three Mile Island accident, several reactor safety programs were reoriented to provide information and data for natural circulation system behavior. In addition, several new programs were initiated to provide quick answers as well as to study particular natural circulation phenomena. The programs of interest to the NRC/EPRI/Westinghouse cooperative program are the Semiscale small-break natural circulation test series, the EPRI/SRI natural circulation tests, the PKL small-break test, studies at MIT on multitube steam generator behavior, and the University of California (Santa Barbara) single-tube refluxing experiments.

These experimental programs are discussed in general terms in the following paragraphs, to give their design, range of conditions, and overall relationship to the FLECHT SEASET experiments. In the data analysis and evaluation, specific results of these programs are compared to the FLECHT SEASET data.

The Semiscale experiments[1] are the most prototypical two-phase natural circulation test in terms of simulating the pressure ranges expected in a postulated small-break LOCA or operational transient. Semiscale did have other scaling problems and compromises such as heat loss, small diameter pipes, and limited number of steam generator tubes; these were minimized for the natural circulation test. The heat loss problem was reduced to a second-order effect by strip-heating the piping. The small diameter of the piping and the limited number of steam generator tubes is a result of the volume scaling, which is the preferred scaling approach for these tests.

The Semiscale tests showed that all three cooling modes (single-phase, two-phase, and reflux condensation) could be achieved by draining incremental amounts of liquid from the facility such that it would undergo quasi-steady transitions from single-phase natural circulation to reflux condensation. The effects of noncondensible gas injection were also examined in the Semiscale program.

In Semiscale, the overall loop natural circulation mass flow rate was found to vary considerably, depending on system mass inventory. The variation in loop mass flow rate with inventory reflects a transition from single-phase natural circulation to two-phase natural circulation to reflux condensation. There was no significant change in loop mass flow rate between 0 and 4 percent system mass inventory, because the drain simply lowered the vessel coolant level to the top of the hot leg and no significant voiding occurred in the loop. The Semiscale test facility also had an upper head which could void first without changing the natural circulation cooling mode. Further draining caused the loop mass flow rate to increase sharply and eventually peak. The increase in flow was caused by increased voiding in the upflow portion, which

---

1. Loomis, G. G., and Soda, K., "Results of the Semiscale MOD-2A Natural Circulation Experiments," NUREG-CR-2335, September 1982.

increased the overall loop density gradient. The peak in flow occurred as steam bubbles in the hot side positions eventually spilled over into the downflow side of the steam generator, causing a reduction in overall loop density gradient between the upflow and downflow sides in the steam generator. The peak Semiscale loop flow occurred at system mass inventories between 86 and 90 percent. In this case, the maximum density driving head existed in the Semiscale facility; hence the loop flow was greatest. Eventually, as primary mass inventory was decreased below 70 percent, the steam generator tubes and plena were nearly voided of liquid and the reflux condenser mode was established. During the system drains, the system pressure followed the trend of the core differential temperature. As mass was expelled from the system and the loop flow rate increased, the core outlet temperature decreased. This decrease led to a reduced bulk system temperature and thus reduced system pressure. Further draining of system mass from the peak flow condition resulted in very little change in core differential temperature and system pressure. Therefore, the system pressure changed only negligibly with the system mass drains after the peak loop flow was achieved.

Regardless of natural circulation mode, the core heat (at scaled decay heat levels) was effectively removed in the steam generator(s) even though the mechanism changed from mode to mode.

The EPRI/SRI natural circulation tests[1] were the first series of experiments after the TMI accident. These experiments first modeled a Babcock & Wilcox once-through steam generator plant; then they also modeled a Combustion Engineering System 80 plant (two hot legs, four cold legs) and a Westinghouse four-loop PWR (four hot legs and four cold legs). The experiments were designed using linear scaling. As a result, elevations and transport times between the scaled system and the prototype were not preserved. The major contribution of the tests was the broad range of conditions and configurations tested and the flow visualization that could be achieved in some of the facility components. The other major benefit was that these tests could be

---

1. Fernandez, R. T., et al., "Reflux Boiling Heat Removal in a Scaled TMI-2 Systems Test Facility," ANS Topical Meeting on Reactor Safety, Knoxville, TN, April 1980.

quickly performed to scope out the phenomena, which could be investigated later at more prototypical conditions and scale in larger test facilities, such as Semiscale and FLECHT SEASET.

The U-tube steam generator experiments[1,2] were conducted in two modes. In the first, with single-phase natural circulation, the facility was allowed to void by having a heat source/heat sink mismatch such that the primary systems would push water into the pressurizer. In the second, the tests were started with less than 100 percent water and additional water was drained. Most of the tests were evaluated with only one of the two steam generators active. Tests were conducted in two-phase natural circulation and reflux condensation at pressures of 0.34 to 0.52 MPa (50 to 75 psia). The test results showed the following:

- Decay heat can be successfully removed by either single-phase or two-phase natural circulation, or reflux condensation.
- The unsteadiness in primary temperature indicated that single-phase natural circulation was not always steady, two-phase natural circulation was never steady, and reflux condensation was always steady.
- Two-phase natural circulation can assume many two-phase cooling modes, the existence of which is suggested by a great variety of primary temperature traces. The existence of a particular mode is a function of the input power, the secondary flow rate, and the water inventory in the active loop.
- In the reflux condensation mode, the system is highly tolerant of noncondensible gas since the system pressure will adjust itself such that sufficient condensing surface in the U-tubes is exposed to remove the heat. If secondary cooling is available, the amount of noncondensible gas that can be accommodated in the primary system undergoing reflux condensation is limited merely by the design pressure of the system.

All tests involving transition between forced and natural circulation went smoothly with no adverse effect on system pressure and temperature.

---

1. Kiang, R. L., and Marks, J. S., "Two-Phase Natural Circulation Experiment on Small-Break Accident Heat Removal," EPRI NP-2007, August 1981.
2. Kiang, R. L., et al., "Decay Heat Removal Experiment in a UTSG Two-Loop Test Facility," EPRI NP-2621, September 1982.

The SRI tests did show quasi-steady temperature traces in the hot and cold legs of the operating loop when in single- and two-phase circulation. This indicates that the flow was not steady but, rather, oscillatory. When the load was shifted from one generator to another, the quasi-steady temperatures would shift from one loop to the other. No loop stalling, when the generator was active, is mentioned in the SRI reports.

Another larger-scale test facility which also examined small-break and/or alternate reactor cooling modes was the Kraftwerk Union PKL Loop.[1,2] The PKL loop is an intermediate-pressure [2.76 MPa (400 psia)] facility with three full-height loops. One loop simulates two intact loops, complete with U-tube steam generators. The scale factor for the facility is 1/134. Both transient small-break tests and quasi-steady-state tests were conducted; in the latter, the system inventory was drained in a controlled manner.

The steady-state tests, similar to those performed in both Semiscale and FLECHT SEASET, involved draining discrete amounts of liquid from the system and then allowing the facility to obtain a steady state. The natural circulation flow would change from single-phase to two-phase and, when sufficient mass had been drained, into reflux condensation. The maximum two-phase flow point occurred at 95 percent of the original mass inventory, and reflux condensation occurred at mass inventories of less than 80 percent.

Two interesting tests were performed on PKL which have some bearing on some of the FLECHT SEASET results. The first test was to investigate flooding in the steam generators in the reflux condensation mode. Since the test power was limited, the investigators blocked off the equivalent of three steam generators such that the remaining generator carried the total load, which would be equal to 8.5 percent core decay heat. In this case, the remaining generator was above the flooding limit and all the condensate was pushed over the

---

1. Weirshaupt, H., and Brand, B., "PKL Small-Break Tests and Energy Transport Mechanisms", ANS Topical Meeting on Small-Break LOCA Analysis in LWRs, Monterey, CA, August 1981.

2. Maudl, R. M., and Weiss, P. A., "PKL Tests on Energy Transfer Mechanisms During Small Break LOCAs'," Nuclear Safety 23, No. 2, March-April 1982.

U-tubes to the cold legs. Flooding at this decay power and pressure agrees with the scaling calculations performed for FLECHT SEASET (given in section 3 of this report), which indicated that flooding would occur at about 6 percent decay power.

The addition of noncondensible gases during reflux condensation only increased the primary side temperatures to compensate for the lost heat transfer surface area. It was also observed that the noncondensible gases were swept to the downhill side of the generator by the condensing steam. The noncondensibles would then build up on the downhill side and in the exit plenum of the generator. This same effect was also observed in the single-tube tests performed by Ripple.[1] In these tests, the noncondensibles would change the fraction of steam condensed on the uphill and downhill sides of the generator. As the amount of noncondensible gas increased, or as the gas accumulated, the condensation on the downhill side of the generator was reduced, and most of the condensation occurred on the uphill side.

---

1. Ripple, R., "The Influence of Noncondensible Gases on the Heat Transfer in Steam Generators of Pressurized Water Reactors During a Loss-of-Coolant Accident," PhD Thesis, Technical University of Munich, March 1981.

SECTION 3
SCALING

3-1. INTRODUCTION

The FLECHT SEASET systems effects test facility was originally designed for low-pressure reflood systems effects testing. The nominal design of the facility was for 0.41 MPa (60 psia), which would be representative of a high-pressure PWR containment during the calculated reflood transient. However, when the Three Mile Island accident occurred, the priority of testing was rearranged and it was desired to modify the test facility to investigate natural circulation cooling modes typical of a small-break loss-of-coolant accident. The small-break transients of interest, however, are at much higher pressures [4.1 to 8.3 MPa (600 to 1200 psia)] than the FLECHT SEASET test facility was designed for. Therefore, lower-pressure effects of the FLECHT SEASET tests must be considered as well as scaling effects of the test apparatus.

3-2. DIFFERENT SCALING APPROACHES

Most of the FLECHT SEASET reflood systems effects test facility had been designed and some of it had been constructed before the decision was made to investigate small-break, loss-of-coolant, and natural circulation cooling modes. Therefore, the original facility scaling logic for reflood tests had to be examined to see if it was still valid for small-break accident simulation.

Originally, in the FLECHT Systems Effects Tests Programs,[1] different scaling rationales were examined to determine the appropriate basis for the reflood systems effects tests. Linear scaling and volume scaling were examined. Using linear scaling, a model of the prototype would have the thermal hydraulic pressures occurring on a reduced time scale relative to

---

1. Cadek, F. F., et al., "PWR FLECHT Systems Effects Tests Program Plan," WCAP-7906, April 1972.

the prototype. Linear scaling was investigated for the Semiscale facility.[1] It was decided that this would distort the geometry of the test facility since the lengths, areas, and volumes would scale as SF, $(SF)^2$, and $(SF)^3$ where SF is the scale factor. In the Semiscale core, the loop would have been so small that it would have been difficult (if not impossible) to build and instrument, and several scaling violations would have existed out of design necessity. A similar conclusion was also reached in the LOFT scaling study.[2]

The results of the Semiscale study, the original FLECHT SEASET program plan, and the LOFT scaling study all confirmed that the most prototypical system response would be obtained with a volume-scaled test facility in which the lengths of the piping and loop were the same as those of the prototype. Following the Semiscale approach, volume scaling results in

$$\frac{L_m}{L_p} = L^* = 1 = \text{length scale factor} \qquad (3\text{-}1)$$

$$\frac{q'''_m}{q'''_p} = q^* = 1 = \text{volumetric heat generation scale factor} \qquad (3\text{-}2)$$

where

L_m = model length

L_p = prototype length

q'''_m = model volumetric heat generation rate

q'''_p = prototype volumetric heat generation rate

---

1. Larsen, T. K., et al., "Scaling Criteria and an Assessment of Semiscale Mod-3 Scaling for Small-Break Loss-of-Coolant Transients," EGG-SEMI-5121, March 1980.

2. Ybarrondo, L. J., et al., "Examination of LOFT Scaling," ASME Winter Meeting, New York, NY, 1974.

Setting L* equal to 1 means that lengths, velocities, and accelerations should be the same in the model and prototype (assuming the same fluid physical properties). Since the pressure and temperature range of the FLECHT SEASET tests is different from the prototype small-break conditions, the velocities and accelerations will not be precisely preserved for all phases of natural circulation cooling. This aspect is carefully described in paragraph 3-3.

Using equation (3-1) for the volume ratio of the system, then

$$\frac{V_m}{V_p} = \frac{A_m \cancel{L_m}^{1}}{\cancel{A_p} \cancel{L_p}} = \frac{A_m}{A_p} = A^* \qquad (3\text{-}3)$$

which is the area ratio. Thus, when the flow path lengths in the model are kept the same as those of the prototype to preserve the real-time aspect of the experiment, the flow areas are reduced by the scale factor. Therefore, the pressure drop per unit length will be higher in the model compared to the prototype, and the pressure drop distribution around the simulated reactor coolant loop will be different in the model compared to a PWR reactor coolant system. In the FLECHT SEASET scaled model, the pressure drop distribution could not be preserved; however, the overall loop pressure drop and the pressure drop between major components was preserved using removable orifice plates. The cause of the largest pressure drop in the reactor loop is the pump; in the test, the cause of the largest pressure drop was the wall friction.

Equation (3-2) indicates that the volumetric heat generation rate would be the same in the model as in the prototype. Again following the Semiscale approach,

$$\frac{q_m}{q_p} = \frac{q'''_m V_m}{q'''_p V_p} = \frac{A_m L_m}{A_p L_p} = \frac{A_m}{A_p} = A^* \qquad (3\text{-}4)$$

since $L_m/L_p = 1$, where A* is the scale factor for the flow area and it is equal to the power ratio.

If one examines the heat flux ratio, where A_s is the heat transfer surface area,

$$\frac{q_m}{q_p} = \frac{q''_m}{q''_p} \quad \frac{As_m}{As} = A^* \tag{3-5}$$

if the heat flux scaling is to be maintained as unity ($q''_m/q''_p = 1$). Then, from equations (3-4) and (3-5),

$$\frac{q_m}{q_p} = \frac{q''_m}{q''_p} \quad \frac{As_m}{As_p} = A^* \tag{3-6}$$

or

$$\frac{As_m}{As_p} = \frac{N_m OD_m L_m}{N_p OD_p L_p} \tag{3-7}$$

for either the core or the steam generator. Again from equation (3-1), $L_m/L_p = L^* = 1$; thus

$$\frac{N_m D_m}{N_p D_p} = A^* \tag{3-8}$$

The designer is faced with a choice of having a scaled number of heat transfer surfaces (N_m) and preserving the characteristic dimension of the surface (D_p), or increasing the number of surfaces and reducing the characteristic dimension of the surface. From a scaled experiment point of view, the proper choice is to preserve the characteristic dimension of the heat transfer surface such that $D_m/D_p = 1$ and

$$\frac{N_m}{N_p} = A^* \tag{3-9}$$

Then the heater rods or steam generator tubes are prototypical, but there are fewer of them in the model.

By preserving the diameter, lengths, velocities, and accelerations, several single phase dimensionless numbers are preserved between the prototype and the

model, if the fluid conditions are the same. Since $D_m/D_p = 1$, in the bundle and steam generator, then for the same fluid conditions the Reynolds numbers of the model and prototype are the same, as are the Euler numbers and Prandtl numbers. The Euler number represents the loop pressure drop or the pressure drop of a major component such as the bundle, steam generator, or downcomer. As mentioned earlier, the Euler number for the interconnecting piping would not be preserved, since the volume scaling results in an increased pressure drop per foot for the model.

Considering single-phase heat transfer in the heater rod bundle (core) or steam generator,

$$\frac{q''_m}{q''_p} = \frac{h_m}{h_p} \quad \frac{\Delta T_m}{\Delta T_p} \tag{3-10}$$

Since by equation (3-5), $q''_m/q''_p = 1$, the heat transfer in the prototype is related to the model heat transfer as

$$h_p = h_m \frac{(T_w - T_f)_m}{(T_w - T_f)_p} \tag{3-11}$$

Therefore, for the heat transfer coefficient to be the same between the model and the prototype, the physical properties of the coolant in each case should be the same, as well as the temperature difference between the heat transfer surface and coolant. It should be noted that, if the physical properties are weakly dependent on the absolute value of the temperature, then the test results can be applied to other temperature or pressure levels with little error. Therefore, for the same physical properties, with volume scaling, the Nusselt numbers remain the same.

The Grashof number also remains the same between the prototype and model for volume scaling, since the lengths are preserved as well as the characteristic length (D_m/D_p).

Therefore, the scaling logic in the FLECHT SEASET facility employs the following criteria:

- The power input per fluid volume in the test bundle compared to that of an average power fuel assembly in a PWR is preserved so that the steam generation rates will be about the same.

- The steam generator is sized to preserve the same power (or heat source) per tube bundle flow area as that of a normal Westinghouse four-loop steam generator. This preserves the cooling capacity of the generator and the cooling length such that the proper elevation heads are available for natural circulation.

- The elevations are maintained at full height and the system components are at the same relative elevations as in a four-loop Westinghouse PWR. Since reflooding and natural circulation are gravity-driven processes, all elevations are maintained at full height so that important driving forces in the system will be simulated and the dominant term in the momentum equation for each component will be preserved.

- The real-time nature of the process was desired to be preserved so that thermal-hydraulic events would occur on a real-time scale basis. This requires that the piping and flow paths between components be full length so that the transport times between components are preserved.

- The total loop pressure drop is preserved.

The basic scaling factor for the test is 1:307. This ratio stems from the selection of the 161-heater rod bundle array to simulate the PWR core, with the result that the test bundle flow area and volume are 1/307 of the flow area and volume of the standard Westinghouse four-loop, 3425 MWt PWR core.

The sizing of the other system volumes has also been made on a 1/307 scale where possible. The energy release capability of the FLECHT-SET heater rod bundle has also been maintained compared to an average assembly of PWR fuel rods during the reflood and small-break phases of a LOCA transient. This is accomplished by providing identical heated lengths, heater rod diameters, and kw/ft ratings (for reflood power levels) and comparable peaking factors of each rod compared to PWR fuel rods.

The FLECHT SEASET facility and the required PWR scaled flow areas, pipe lengths, elevations, and resistance coefficients are compared in tables 3-1 and 3-2. Resistance coefficients were calculated based on the hot leg conditions for both the PWR and the FLECHT SEASET facility. Since natural circulation is a gravity-forced process, by preserving the component

TABLE 3-1

COMPARISON OF VENDOR DESIGNS

Dimension	Westinghouse[a]	Combustion Engineering[b]	Babcock & Wilcox[c]
Cold leg piping			
Diameter [m (in.)]	0.698 (27.5)	0.76 (30)	0.71 (28)
Area [m^2 (ft^2)]	0.3832 (4.125)	0.46 (4.9)	0.397 (4.27)
Scaled flow area [m^2 (ft^2)]	0.00124 (0.0134)	0.00148 (0.0159)	0.00129 (0.0139)
Percent difference[e]	--	(18.7)	3.7
Loop seal piping			
Diameter [m (in.)]	0.79 (31)	0.76 (30)	0.81 (32)
Area [m^2 (ft^2)]	0.487 (5.24)	0.456 (4.91)	0.518 (5.58)
Height [m (ft)]	2.7 (9.0)	1.8 (6.0)	3.26 (10.7)
Scaled flow area [m^2 (ft^2)]	0.00158 (0.0170)	0.00148 (0.0159)	0.00168 (0.0181)
Percent difference[e]	--	-6.5	6.5
Hot leg piping			
Diameter [m (in.)]	0.74 (29)	1.07 (42)	0.97 (38)
Area [m^2 (ft^2)]	0.426 (4.59)	0.894 (9.62)	0.331 (7.87)
Scaled flow area [m^2 (ft^2)]	0.00138 (0.0149)	0.00291 (0.0313)	0.00238 (0.0256)
Percent difference[e]	--	110.1	71.8

a. 4 x 4 3425 MWt PWR
b. 2 x 4 3817 MWt System 80 design
c. 2 x 4 3820 MWt 205 design
d. Based on scaling ratio of 307:1
e. Percent change from Westinghouse scaled area

elevations, flow path lengths, overall loop flow resistances, and scaling the volumes, flow areas, and major heat sources to represent a typical PWR plant, adequate overall simulation is maintained.

3-3. PRESSURE EFFECTS AND SCALING FOR FLECHT SEASET TESTS

For a small-break LOCA, the pressure range of interest is 4.1 to 8.3 MPa (600 to 1200 psia), which is significantly greater than the pressure capability of the FLECHT SEASET systems effects loop. In the natural circulation test plan, three types of tests were conducted:

- Single-phase circulation with single-phase steam generator secondary side
- Two-phase primary side natural circulation with boiling secondary steam generator side
- Reflux condensation primary side with boiling secondary side steam generators

For the single-phase tests, it is expected that the effect of pressure on the Nusselt number would be small, such that the resulting temperature rises for the model and prototype would be similar. It should be noted that for the volume scaling, $D_m/D_p = 1$, $V_m/V_p = 1$, and it was assumed that for the Grashof number $(T_w - T_f)_m/(T_w - T_f)_p = 1$.

The resulting impact of the property differences on the expected temperature rises in the model and prototype can be estimated as

$$\frac{q''_m}{q''_p} = \frac{h_m \Delta T_m}{h_p \Delta T_p} = \frac{Nu_m}{Nu_p} \frac{k_m}{k_p} \frac{D_p}{D_m} \frac{\Delta T_m}{\Delta T_p} = 1 \qquad (3\text{-}12)$$

where Nu could be forced turbulent convection or natural convection. Noting that $q''_m/q''_p = 1$, and assuming a Dittus-Boelter[1] expression for turbulent forced convection, the temperature rise ratio for the model and prototype becomes

1. Dittus, F. W., and Boelter, L. M. K., "Heat Transfer in Automobile Radiators of the Tubular Type," Univ. Calif. Berkeley Publ. Eng. 2, 13, 443-462 (1930).

COMPARISON OF PWR SCALED FLO

Component	Flow Area [m^2 (ft^2)]		
	PWR	PWR Scaled	
Core	4.76 (51.2)	0.01548 (0.1665)	
Lower plenum	11.098 (119.46)	0.0361 (0.3891)	
Upper plenum	11.098 (119.46)	0.0361 (0.3891)	
Downcomer	4.84 (52.1)	0.01577 (0.1697)	
Hot Leg			
o Broken	0.426 (4.59) [74 cm (29 in.) ID]	0.00139 (0.0149)	
o Unbroken	1.279 (13.77)	0.00416 (0.0448)	
Pump suction			
o Broken	0.487 (5.24) [78 cm (31 in.) ID]	0.00159 (0.01706)	
o Unbroken	1.460 (15.72)	0.00476 (0.0512)	
Cold leg			
o Broken	0.383 (4.12) [70 cm (27.5 in.) ID]	0.00125 (0.0134)	
o Unbroken	1.148 (12.36)	0.00374 (0.0402)	
Steam generator			
o Unbroken tubes	3.1674 (34.095)	0.01031 (0.1110)	
o Inlet/outlet plena	11.990 (129.06)	0.03906 (0.4204)	
o Broken tubes	1.0558 (11.365)	0.00344 (0.0370)	
o Inlet/outlet plena	3.997 (43.02)	0.01301 (0.1401)	

a. Based on PWR core flow area to FLECHT SEASET bundle flow area ratio
b. Empty
c. With 10 2.858 cm (1.125 in.) OD columns [64.1 cm^2 (9.94 $in.^2$)]
d. All 33 tubes unplugged
e. Volume was scaled.
f. All 11 tubes unplugged

TABLE 3-2

AREAS AND SYSTEMS EFFECTS TEST FLOW AREAS[a]

FLE_HT SEASET	FLECHT SEASET Pipe Size	Pipe ID [cm(in.)]	Flow Area Ratio (FS/PWR Scaled)
0.01548 (0.1665)	0.0508 cm (0.0200 in.) wall	19.36 (7.625)	1.0
0.3880 (0.4176)[b] 0.3238 (0.3485)[c]	25 cm (10 in.) sch 140	22.22 (8.750)	1.07 0.90
0.01603 (0.1726)	15 cm (6 in.) 1.3 cm (5 in.) wall	14.29 (5.625)	1.02
0.00145 (0.0155)	5 cm (2 in.) sch 160	4.290 (1.689)	1.04
0.00426 (0.0458)	7.6 cm (3 in.) sch 80	7.366 (2.900)	1.02
0.00159 (0.0170)	6.3 cm (2.5 in.) sch XXSTG	4.498 (1.771)	1.00
0.00477 (0.0513)	7.6 cm (3 in.) sch 40	7.793 (3.068)	1.003
0.00131 (0.0140)	3.8 cm (1.5 in.) sch 40	4.090 (1.610)	1.05
0.00426 (0.0458)	7.6 cm (3 in.) sch 80	7.366 (2.900)	1.14
0.01003 (0.1079)[d] 0.02162 (0.2327)[e]	2.2 cm (0.875 in.) 0.127 cm (0.05 in.) wall 25 cm (10 in.) sch 80	1.968 (0.775) 24.29 (9.564)	0.97 0.55
0.00335 (0.0360)[f] 0.007411 (0.0804)[e]	3.3 cm (0.875 in.) 0.172 cm (0.05 in.) wall 15 cm (6 in.) sch XSTG	1.968 (0.775) 14.63 (5.761)	0.97 0.57

51.2/0.1665 = 307; PWR is a 412 - SNUPPS.

$$\frac{\Delta T_m}{\Delta T_p} = \left(\frac{Re_p}{Re_m}\right)^{0.8} \left(\frac{Pr_p}{Pr_m}\right)^{0.4} \left(\frac{k_p}{k_m}\right) \qquad (3\text{-}13)$$

Similarly, for natural circulation where $Nu = 0.17\ (Gr \cdot Pr)^{1/4}$ (1) and noting that Gr has a ΔT dependence, a similar expression for the heat flux ratio can be derived to give

$$\frac{q''_m}{q''_p} = \frac{(Gr' \cdot Pr)^{1/4} k_m \Delta T_m^{5/4} D_p}{D_m (Gr' \cdot Pr)^{1/4} k_p \Delta T_p^{5/4}} = 1 \qquad (3\text{-}14)$$

where $Gr' = Gr/\Delta Tm$.

The temperature ratio then becomes

$$\frac{\Delta T_m}{\Delta T_p} = \left[\left(\frac{Gr'_p \cdot Pr_p}{Gr'_m \cdot Pr_m}\right)^{1/4} \left(\frac{k_p}{k_m}\right)\right]^{4/5} \qquad (3\text{-}15)$$

Comparisons of the Nusselt number ratios and the resulting temperature ratio between the model and prototype for both forced convection and natural convection are shown in table 3-3. There is a maximum of 25 percent variation between the expected model temperature rise and the prototype temperature rise at a scaling pressure of 8.3 MPa (1200 psia). For forced convection, the model temperature rise will be smaller than the prototype temperature rise, primarily due to the Prandtl number ratio. In natural circulation, the model temperature rise will be larger. In either case, the difference in the model and prototype temperature is approximately 20 percent; this is acceptable for the FLECHT SEASET tests.

For two-phase natural circulation and reflux condensation, the heat transfer mode of interest is condensation in the steam generator tubes. Assuming laminar film condensation on the vertical surfaces, the Nusselt analysis(1) gives

---

1. Eckert, E. R. G., and Drake, R. M., Analysis of Heat and Mass Transfer, McGraw-Hill, New York, 1972.

TABLE 3-3

INFLUENCE OF PRESSURE ON SINGLE-PHASE
HEAT TRANSFER AND TEMPERATURE RISE

Mode	Parameter	Value at Indicated Pressure	
		4.1 MPa (600 psia)	8.3 MPa (1200 psia)
Forced convection	$\frac{Nu_m}{Nu_p}$	1.12	1.062
	$\frac{\Delta T_m}{\Delta T_p}$	0.796	0.747
Natural convection	$\frac{Nu_m}{Nu_p}$	0.747	0.679
	$\frac{\Delta T_m}{\Delta T_p}$	1.15	1.19

$$\overline{h_c} = 0.943 \left[\frac{g(\rho_f - \rho_g)\rho_f k_f^3 h_{fg}}{\mu_f L (T_{sat} - T_w)} \right]^{1/4} \quad (3\text{-}16)$$

Therefore, the wall heat flux becomes

$$q'' = \overline{h_c} (T_{sat} - T_w) \quad (3\text{-}18)$$

Applying the scaling criteria where the heat flux ratio is unity gives

$$\frac{q''_m}{q''_p} = 1 = \frac{0.943 \left[\frac{g\rho_f(\rho_f - \rho_g)k_f^3 h_{fg}}{\mu_f L(T_{sat} - T_w)_m} \right]^{1/4}}{0.943 \left[\frac{g\rho_f(\rho_f - \rho_g)k_f^3 h_{fg}}{\mu_f L(T_{sat} - T_w)_p} \right]^{1/4}} \quad (3\text{-}19)$$

Simplifying the expression in equation (3-19) gives

$$1 = \left[\frac{(T_{sat} - T_w)_m}{(T_{sat} - T_w)_p}\right]^{3/4} \left[\frac{\rho_{f_m}(\rho_{f_m} - \rho_{g_m})k_{f_m}^3 h_{fg_m} \mu_{f_p}}{\rho_{f_p}(\rho_{f_p} - \rho_{g_p})k_{f_p}^3 h_{fg_p} \mu_{f_m}}\right]^{1/4} \quad (3\text{-}20)$$

Assuming that the prototype is at 4.1 MPa (600 psia), the condensation wall temperature wall ratio is 1.09, and at 8.3 MPa (1200 psia) the ratio becomes 1.25. This indicates that the condensation effects for the prototype and model are similar, and that the model will yield prototypical condensation heat transfer data.

There is a serious discrepancy between the density of the vapor at the model conditions and the corresponding vapor density at reactor conditions which can affect the two-phase flow behavior of the system. Assuming that the FLECHT SEASET test facility will simulate two-phase natural circulation and reflux condensation at a system pressure of 0.34 MPa (50 psia), the ratio of the steam densities ρ_m/ρ_p becomes 0.092 at 4.1 MPa (600 psia) and 0.0425 at 8.3 MPa (1200 psia). Therefore, for the scaled steam mass flow in the simulated hot leg, the resulting vapor velocity will be significantly higher in the FLECHT SEASET model compared to the prototype.

The concern is that larger steam velocities in the hot legs due to the lower system pressure for the FLECHT SEASET model could yield nonprototypical flow conditions or transitions compared to the reactor for two-phase natural circulation and reflux condensation cooling modes. These concerns are particularly important if a transient test is being conducted with a break simulation such that the system inventory is continuously decreasing. The scaled test could continue to promote two-phase natural circulation because of the higher steam velocity, whereas the PWR could be in a reflux condensation mode.

A similar concern exists in the steam generator inlet plenum at the tubesheet. The higher-than-scaled hot leg steam velocity could lead to a different flooding characteristic for the steam generator tubesheet compared to the PWR. Both the hot leg two-phase flow regime transitions and flooding behavior of the steam generator tubesheet are investigated next.

Examining the maximum possible steam flow in the hot legs, which the bundle would produce if completely covered with a two-phase mixture and no outlet subcooling comes from the downcomer,

$$\dot{M}_{s_m} = \frac{q_m}{h_{fg_m}} = \frac{q'''_m V_m}{h_{fg_m}} = \frac{q'''_m A_m L_m}{h_{fg_m}} \tag{3-21}$$

but in the hot leg

$$\dot{M}_s = \rho_m A_m^{HL} V_m^{HL} \tag{3-22}$$

where A_m^{HL} is the model hot leg flow area, and V_m^{HL} is the model hot leg velocity.

Thus,

$$V_m^{HL} = \frac{q'''_m A_m L_m}{h_{fg_m} \rho_m A_m^{HL}} \tag{3-23}$$

In the prototype,

$$V_p^{HL} = \frac{q'''_p A_p L_p}{h_{fg_p} \rho_p A_p^{HL}} \tag{3-24}$$

Taking the ratio yields

$$\frac{V_m^{HL}}{V_p^{HL}} = \frac{A_m}{A_p} \frac{h_{fg_p}}{h_{fg_m}} \frac{L_m}{L_p} \frac{q'''_m}{q'''_p} \frac{\rho_p}{\rho_m} \frac{A_p^{HL}}{A_m^{HL}} \tag{3-25}$$

where A_p^{HL} and V_p^{HL} are defined similarly to A_m^{HL} and V_p^{HL} in equation (3-22).

Using earlier identities,

$$\frac{q_m'''}{q_p'''} = 1 = \frac{L_m}{L_p}$$

$$\frac{A_m}{A_p} = \frac{1}{\text{scale factor}} = \frac{1}{307}$$

$$\frac{A_p^{HL}}{A_m^{HL}} = \text{scale factor} = 307$$

Thus,

$$\frac{V_m^{HL}}{V_p^{HL}} = \frac{h_{fg_p}}{h_{fg_m}} \quad \frac{\rho_p}{\rho_m} \qquad (3\text{-}26)$$

This ratio becomes 8.7866 at 4.1 MPa (600 psia) for the prototype and 15.59 at 8.3 MPa (1200 psia) for the prototype, assuming a 0.34 MPa (50 psia) pressure for the model.

To preserve the steam velocity in the hot leg, only two parameters can be changed, the volumetric heat generation rate (test power), and the hot leg flow area (A_m^{HL}), since the facility scale factor and pressure were already fixed.

The power generation in the experiment would have to be reduced by a factor of 8 to 15 below the scaled value to preserve the steam velocity in the hot leg. This would mean conducting tests at 0.2 percent of simulated reactor power rather than the preferred 2 percent of simulated reactor power. The lower test power would yield lower temperature rises, which would be difficult to measure. Also, unless the steam generator secondary side flow was correspondingly reduced by the same factor, the primary side heat would all be removed

at the immediate entrance of the steam generator. The measurement and control problems with such a low-power test made decreasing the test power an undesirable choice. Therefore, it was decided to enlarge the hot legs as much as possible consistent with the test vessel upper plenum and the existing steam generator plena. The hot leg inside diameters were increased from 42.9 to 76.2 mm (1.689 to 3.00 in.) for the broken loop and 73.6 to 152 mm (2.9 to 6 in.) for the unbroken loop simulation. Using these diameters to recalculate the hot leg area relative to the PWR flow areas, equation (3-25) can be recalculated for the steam flow in the hot leg for the model compared to the prototype. Therefore,

$$\frac{V_m^{HL}}{V_p^{HL}} = \left(\frac{h_{fg_p}}{h_{fg_m}}\right)\left(\frac{\rho_p}{\rho_m}\right)\left(\frac{18.36}{0.2454}\right)\left(\frac{1}{307}\right) \qquad (3\text{-}27)$$

resulting in a steam velocity ratio of 2.14 at 4.1 Mpa (600 psia) and 3.798 at 8.3 MPa (1200 psia). Therefore, when the hot leg diameter is increased, the steam velocity in the FLECHT SEASET hot legs is closer to the proper scaled value. However, the test steam velocity is still higher than the proper scaled value.

The flow regime transition which is of interest in the hot leg is the intermittent slug-plug to stratified flow regime. It is expected that co-current slug and plug flow would exist in the hot leg during two-phase natural circulation. However, as mass is drained from the system and reflux condensation occurs, eventually the hot leg will become stratified with liquid flowing back to the core at the same time that steam is flowing in the opposite direction toward the steam generators.

It was felt that the lower pressure of the FLECHT SEASET facility, which results in a higher hot leg vapor velocity, could delay the transition between the intermittent slug-plug flow (slug flow) and stratified flow in the FLECHT SEASET hot leg. This means that more mass would have to be drained from the FLECHT SEASET facility to obtain stratified flow, compared to a PWR.

Work by Taitel and Dukler[1] gives a criterion for the transition between the intermittent (plug and slug) flow regime and the stratified flow regime. The expression for the critical velocity for the transition vapor velocity U_g is

$$U_g = \left\{ \frac{(\rho_f - \rho_g)\, D \cdot g \cdot (1 - \tilde{h}_L)^2 \cdot Ag^2}{\rho_g \frac{1}{4} \left[1 - (2\tilde{h}_L - 1)^2 \right]^{1/2}} \right\}^{1/2} \qquad (3\text{-}28)$$

where

$$A_g = 0.25 \left\{ \cos^{-1} (2\tilde{h}_L - 1) - (2\tilde{h}_L - 1) \left[1 - (2\tilde{h}_L - 1)^2 \right]^{1/2} \right\}$$

and $\tilde{h}_L$ is h/D where h is the liquid height in the pipe of diameter D. Equation (3-28) was programmed and solved for the PWR dimensions and pressures of 4.1 and 8.3 MPa (600 and 1200 psia) for a range of h_L values as well as for the FLECHT SEASET facility at 0.34 MPa (50 psia) with the larger pipe diameter.

Figure 3-1 shows the calculated superficial velocity at the transition point between the intermittent and stratified flow regimes. Also shown is the superficial velocity, which is equal to 2 percent of core decay heat boiloff. The intersections of these two curves, for the PWR and for FLECHT SEASET, indicate the maximum value of h or liquid level in the pipe allowed at the transition point. As discussed above, the liquid level is lower in the FLECHT SEASET tests compared to the PWR because of the lower pressure (and corresponding higher hot leg steam velocity).

This means that the FLECHT SEASET test facility will remain in two-phase natural circulation with lower mass inventories as compared to the higher-pressure PWR. This difference in transition between one flow regime and

---

1. Taitel, Y., and Dukler, A. E., "A Model for Predicting Flow Regime Transitions in Horizontal and Near-Horizontal Gas-Liquid Flow," J. Amer. Inst. Ch. Eng. 22, 1, 47-55 (1976).

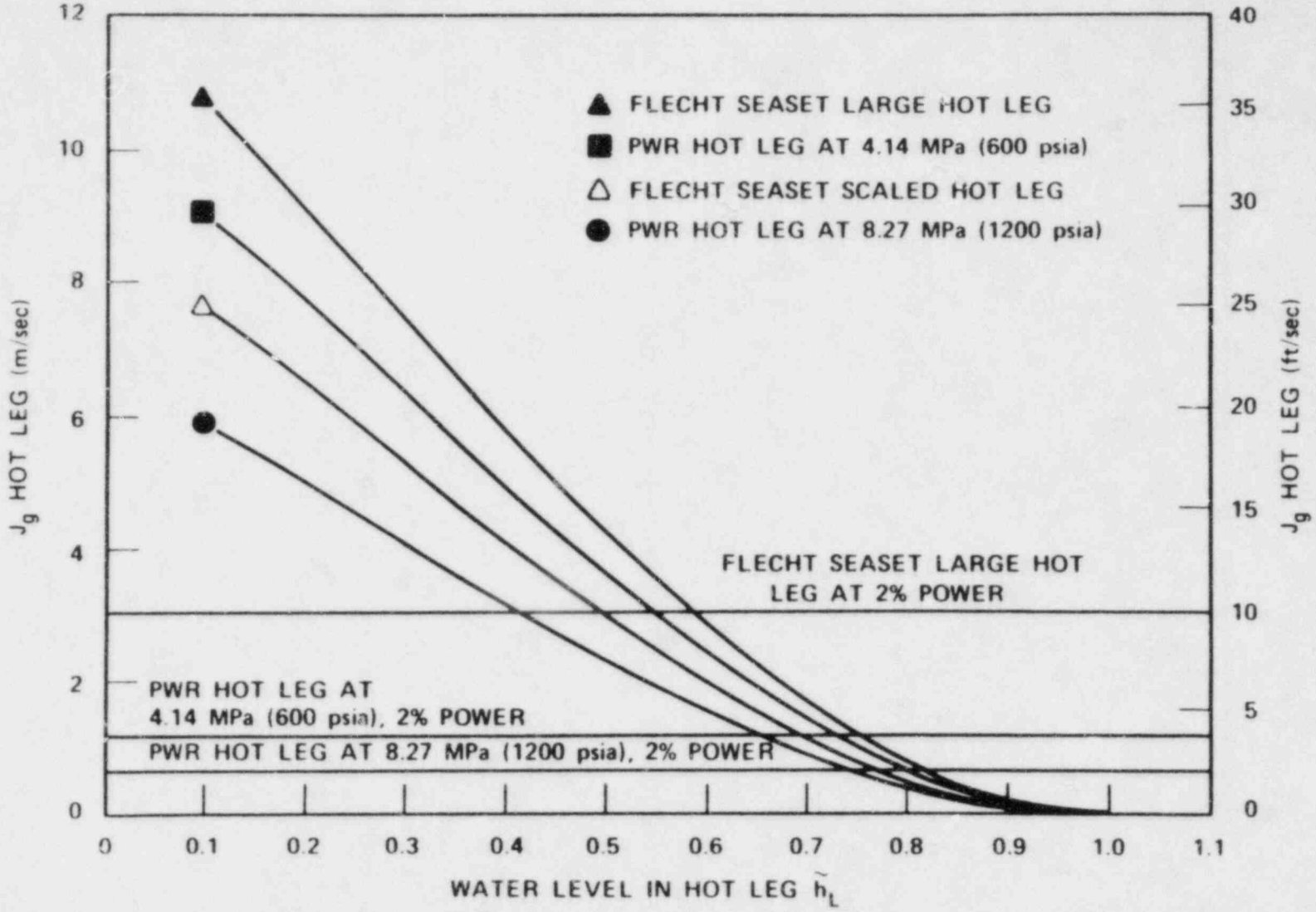

Figure 3-1. Calculation of Flow Regime Transition Points for PWR and FLECHT SEASET Facility

another is a result of the pressure scaling effect and has nothing to do with the volume scaling.

Zuber[1] performed a similar analysis for the Semiscale small-break tests and also showed that, even for the same pressure (and therefore coolant physical properties), the transition between intermittent and stratified flow does not scale with volume.

The other area of concern is the possible flooding effects at the steam generator tubesheet during the reflux condensation simulations in the FLECHT SEASET facility, resulting in liquid holdup in the steam generator. The higher vapor velocity in the hot legs and steam generator tubes could restrict the return of the condensate to the hot leg such that a pulsing flow similar to that observed by Banerjee[2] would exist in the FLECHT SEASET tests; pure reflux condensation would occur in the PWR. Since the flow area in the steam generator tubes was not increased, as was done with the hot legs, the steam velocity at the tubesheet is greater than the scaled value by a factor of 8 to 15.

The flooding characteristics of the steam generator tubesheet are assumed to obey the Wallis flooding correlation[3] given by

$$\sqrt{J_g^*} + m\sqrt{J_f^*} = C \qquad (3\text{-}29)$$

where

$$J_g^* = \frac{J_g\sqrt{\rho_g}}{\sqrt{gD(\rho_f-\rho_g)}} \qquad (3\text{-}30)$$

and

1. Zuber, N. "Scaling of Two-Phase Flow Transition in Horizontal Pipes of Semiscale, "NRC Memorandum, September 1979.

2. Banerjee, S., et al., "Reflux Condensation and Transition to Natural Circulation in a Vertical Tube," presented at 1981 Winter ASME meeting, Heat Transfer Aspects of Reactor Safety.

3. Wallis, G. B., One-Dimensional Two-Phase Flow, McGraw-Hill New York, 1969.

$$J_f^* = \frac{J_f \sqrt{\rho_f}}{\sqrt{gD(\rho_f - \rho_g)}} \qquad (3\text{-}31)$$

with values of m = 1.0 and C = 0.725 for sharp-edged tubes. For no liquid downflow, $J_f^* = 0$ and

$$J_{q\ crit}^* = C^2 \qquad (3\text{-}32)$$

Therefore,

$$J_{g_{crit}} = \frac{C^2 \sqrt{gD(\rho_f - \rho_g)}}{\sqrt{\rho_g}} \qquad (3\text{-}33)$$

The value of D is the inside diameter of the steam generator tube. The critical flooding velocities for the FLECHT SEASET test and the PWR are shown in figure 3-2, along with the steam velocity calculated for a given steam generator tube for different decay powers in the core. Figure 3-2 indicates that at decay powers above 3 percent, the FLECHT SEASET test facility could flood at the steam generator tubesheet.

If, for some reason, the steam flow would shift for both generators to a single generator, some tubes could operate above the flooding limit. Also, if a flow maldistribution would occur due to plugged or stalled tubes, the remaining tubes could operate above the flooding limit. A third possibility exists where the presence of noncondensible gas injection could result in a steam-helium mixture which would operate above the flooding limit.

At higher decay powers, it is speculated that the FLECHT SEASET test facility would not operate in a stable reflux mode. It is believed that some of the steam generator tubes of the facility would oscillate between a refluxing mode, in which the condensate accumulated in the steam generator tubes, and a two-phase natural circulation, in which the accumulated condensate would be pushed over the U-bend into the steam generator outlet plenum in much the same manner as in the single-tube experiments of Banerjee. The PWR, on the other hand, is nowhere near the flooding limit even at 5 percent decay power.

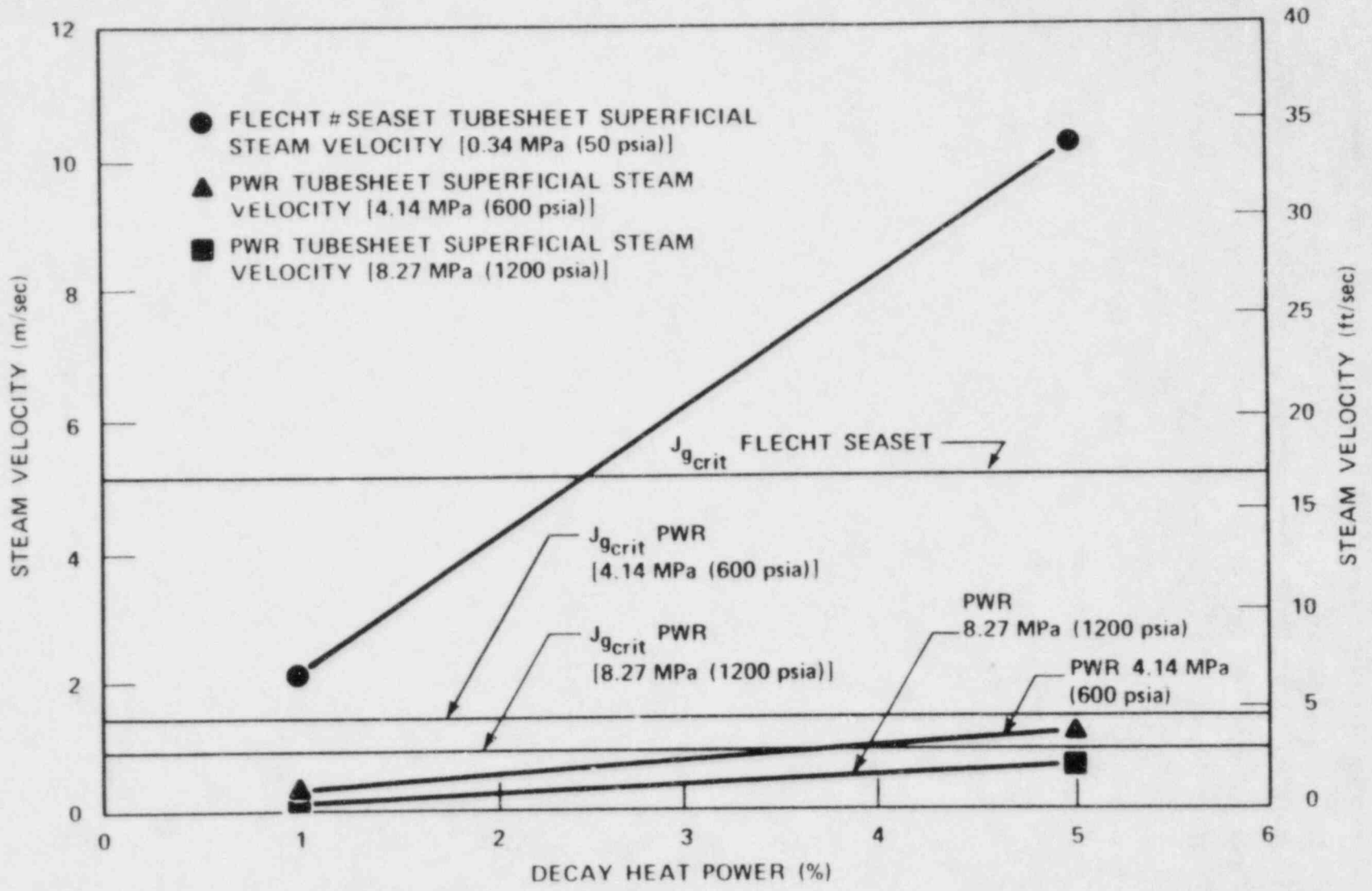

Figure 3-2. Critical Velocities for Tubesheet Flooding

3-4. SCALING CONCLUSIONS

The low-pressure facility has been examined for its applicability for simulating higher-pressure small-break natural circulation cooling modes. The lower pressure in the FLECHT SEASET facility requires lower system mass inventory to attain the same flow regimes in the hot leg compared to the PWR, even with the larger-than-scale leg diameters. Also, the FLECHT SEASET steam generators are closer to the flooding limit than those of the PWR; this can produce a delay from two-phase natural circulation to pure reflux condensation.

SECTION 4

TEST FACILITY DESCRIPTION AND TEST PROCEDURE

4-1. FACILITY COMPONENTS

The natural circulation test facility is a modification to the previous systems effects test facility used for the PWR FLECHT SEASET unblocked bundle test program.[1] The prior system consisted of the following:

- o A test vessel, one-dimensional downcomer, crossover leg and upper and lower plena, which collectively simulated the reactor
- o Two steam generator simulators, scaled 3:1, simulating three intact loops and one broken loop, termed "unbroken" and "broken," respectively
- o Containment and overflow tanks simulating containment backpressure
- o Two accumulators used as pressurizer and injection reservoirs
- o Overall system component design to operate at 0.41 MPa (60 psia)

For the system to accommodate the natural circulation series of tests, the following facility modifications were made:

- o New piping configuration eliminating the containment and overflow tanks and reconnecting the broken steam generator to the downcomer simulator
- o Additions of primary and secondary forced circulation capability
- o Addition of steam generator secondary side cooling
- o Upper head injection and cold leg injection capability
- o Addition of helium gas injection into the hot legs coupled with steam generator tube gas sampling
- o Extensive addition of temperature and pressure monitoring instrumentation to the loop piping and steam generator

1. Rosal, E. R., et al., "PWR FLECHT SEASET Systems Effects Natural Circulation and Reflux Condensation Task Plan Report," NRC/EPRI/Westinghouse-12, November 1982.

- o Reflux flowmeters on both hot and cold legs
- o Extensive insulation [up to 0.1 m (4 in.)] to minimize heat losses
- o Operating pressure increased to 1.03 MPa (150 psia), limited by existing components
- o New data acquisition and control facility with expanded capability

The components of the facility are described in the following paragraphs.

4-2. Test Vessel and Downcomer

The test vessel is very similar to the one used for the FLECHT SEASET unblocked bundle tests,[1] with the exception of the omission of sight glasses used for high speed photography. The bundle consisted of 161 electrically heated rods [3.66 m (12 ft) heated length with cosine heat flux distribution] with guide tubes and filler strips (to preserve flow area scaling) in a 17x17 Westinghouse fuel assembly configuration. It was instrumented by 300 1.0 mm (0.040 in.) diameter thermocouples on 50 rods, of which 33 thermocouples were used during these tests. Total bundle power was 1.2 megawatts, powered by a silicone-controlled rectifier in three zones with a common ground plate. A cross section of this bundle is shown in figure 4-1.

The downcomer was replaced, as well as the crossover leg which houses the bidirectional turbo-probe used for overall primary flow measurement. This section of piping was sent to Flow Technology, Inc. to generate a calibration curve for the probe.

Although the lower plenum from the previous tests was used, the upper plenum was new and featured sight glasses for observation of two-phase flow entering the hot legs.

The test vessel, downcomer, and crossover leg are shown in figure 4-2.

---

1. Loftus, M. J., et al., "PWR FLECHT SEASET Unblocked Bundle, Forced and Gravity Reflood Task Data Report," NRC/EPRI/Westinghouse-7, June 1980.

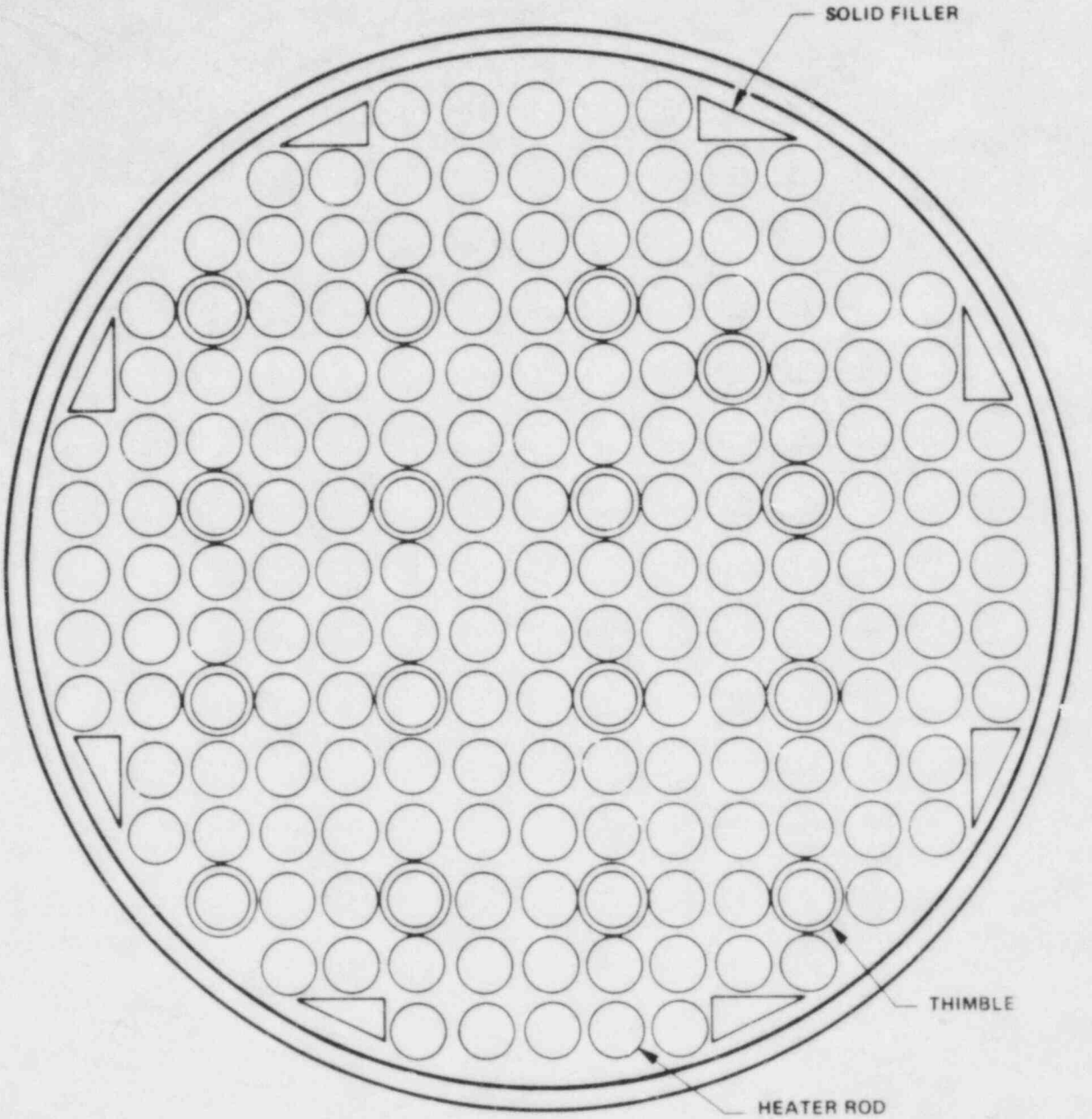

BUNDLE STATISTICS

HOUSING INSIDE DIAMETER	194.0 mm	7.625 in.
HOUSING WALL THICKNESS	5.08 mm	0.200 in.
ROD DIAMETER	9.50 mm	0.374 in.
THIMBLE DIAMETER	12.0 mm	0.474 in.
ROD PITCH	12.6 mm	0.496 in.
CROSS-SECTIONAL FLOW AREA	15476 mm^2	23.989 $in.^2$
FILLER DIMENSIONS	19.43 mm X 8.64 mm	0.765 in. X 0.340 in.
161 HEATER RODS		
16 THIMBLES		
8 FILLERS		

Figure 4-1. FLECHT SEASET Natural Circulation Bundle Cross Section

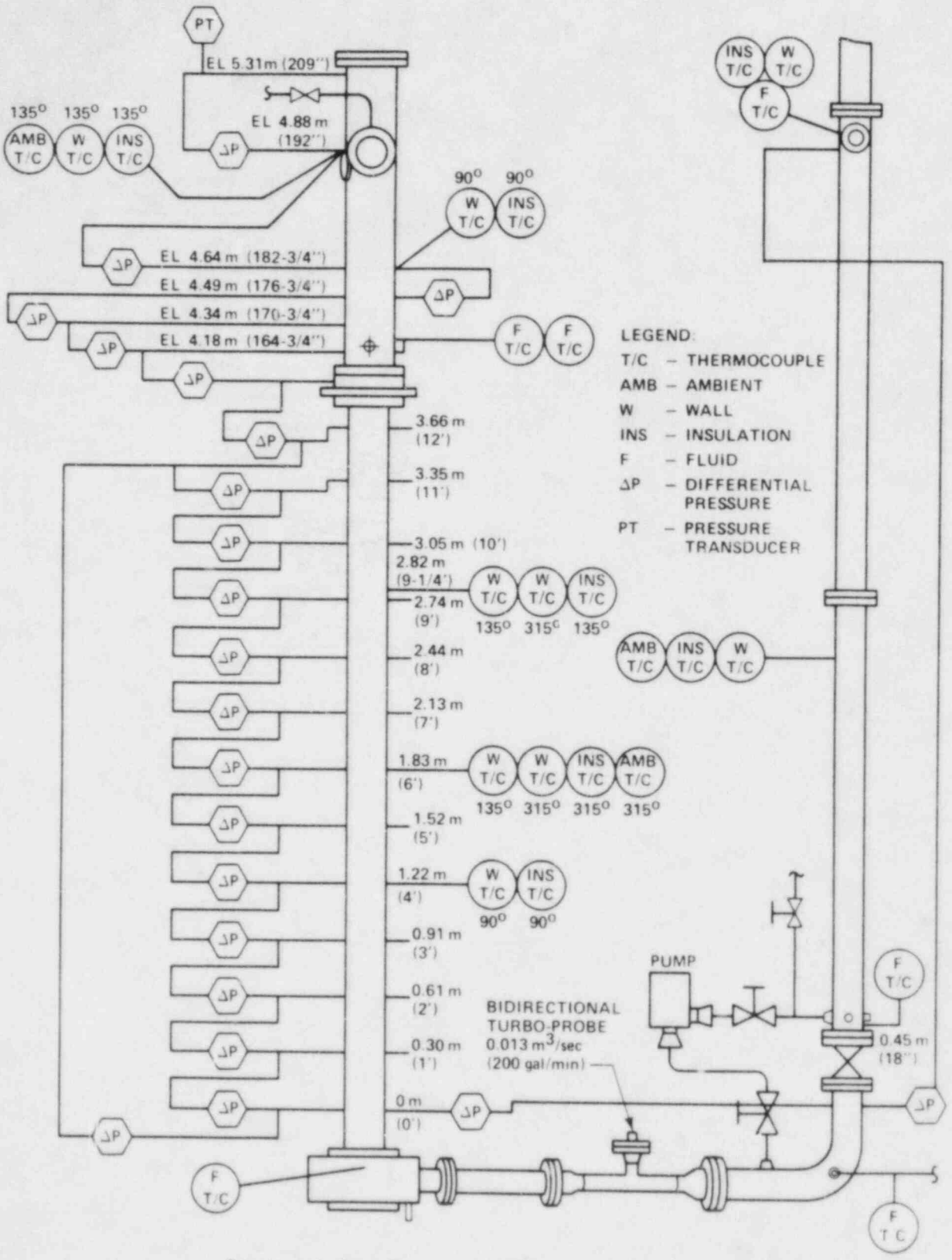

Figure 4-2. Test Vessel and Downcomer

4-3. Steam Generator Simulator

The two steam generator simulators are scaled 3:1 to each other; the unbroken has 33 0.222 m (0.875 in.) U-tubes and the broken has 11 0.222 m (0.875 in.) U-tubes. The unbroken generator is instrumented with 54 tube wall thermocouples, of which 38 were used; 57 primary fluid thermocouples, of which 44 were used; and 62 secondary fluid thermocouples, of which 34 were used. The broken generator is instrumented with 46 tube wall thermocouples, 42 primary fluid thermocouples, and 41 secondary thermocouples, all of which were used. Inlet and outlet plenum as well as secondary side levels were monitored with DP cells. In addition to temperature and level determination, aspirating steam probes were also utilized during the helium injection tests. Of the 55 present in the unbroken generator, 21 were used; 16 of the 42 present in the broken generator were used.

For observation of flow phenomena in the inlet and outlet plena of the generators, two sight glasses in each section of the plenum (a total of eight for both generators) located near the tubesheet were utilized. The generators are shown in figures 4-3 through 4-9 and the channel listing of instrumentation used is given in table 4-1.

4-4. Loop Piping

The completely new piping added to the system was scaled 3:1, in agreement with the steam generator scaling considerations, with the exception of the hot legs which were made as large as possible to compensate for low-pressure effects. (The 3:1 relationship was, however, maintained.) The flow split between broken and unbroken loop steam generators was determined by two bidirectional turbine meters located in the loop seal piping of each. These further served to confirm the readings taken by the turbo-probe located in the crossover leg used for overall loop flow.

The piping was heavily instrumented with thermocouples reading fluid, wall, and insulation temperatures (figure 4-10). For determining reflux fluid temperature, special thermocouples were devised and "hand fit" to each location such that the junction was located 0.13 mm (0.005 in.) from the wall

of the pipe into the flow stream, as shown in figure 4-11. The purpose of these thermocouples was to measure any subcooling the returning condensate might have. In addition, special mating of the flanges was done in order to assure minimum disturbance to the reflux flow.

At the end of each hot leg and cold leg, a small dam restricted returning flow from entering the upper plenum and downcomer, and caused the flow to be channeled through a 0 to 6.3 x 10^{-6} m^3/sec (0 to 1 gal/min) rotameter (two in parallel for the unbroken hot leg) and returned to the system slightly below the takeoff connections (figure 4-12).

A 4.7 x 10^{-4} m^3/sec (75 gal/min) pump was installed to supply primary side circulation during heating/cooldown operations. Identical pumps were also used in conjunction with a heat exchanger for cooling the secondary side; however, these were not used during operation. Cooling was supplied by venting steam from the secondary side and adding makeup water. Using a back-pressure regulator, constant pressure could be maintained in the generator secondary side.

DP cells were added for determination of the pressure drop from the piping as well as across the vessel. DP cells were also used to record all levels on all other vessels and piping (table 4-1).

4-5. Accumulators

Three large vessels were utilized for water supply and pressurization. Accumulator 2, of approximately 1.82 m^3 (400 gal) capacity, was used as a pressurizer during single-phase natural circulation and for injection during upper head injection and cold leg injection tests. Accumulator 2 was also used as a pressurizer during injection tests and as a standby water supply during other tests. The containment tank was used as a pressurizer for the secondary side before the boiling-makeup mode was used. All vessels had strip heaters to maintain the accumulator water at required temperatures.

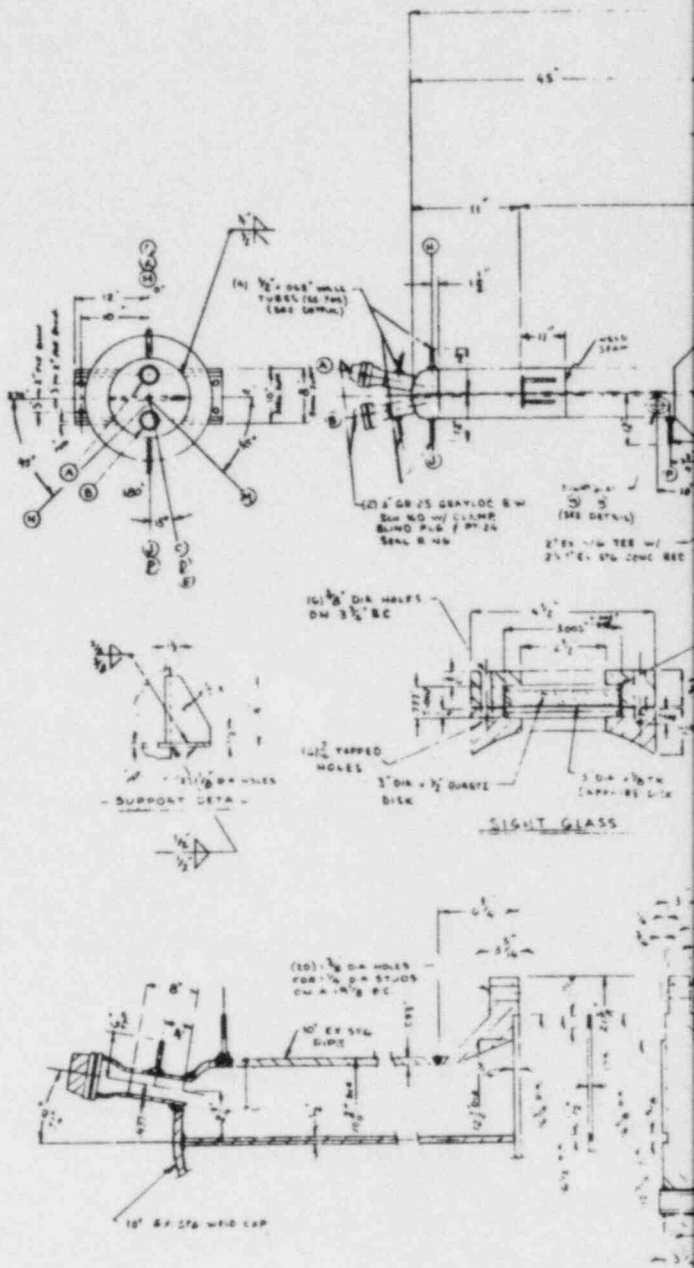

TI
APERTURE
CARD

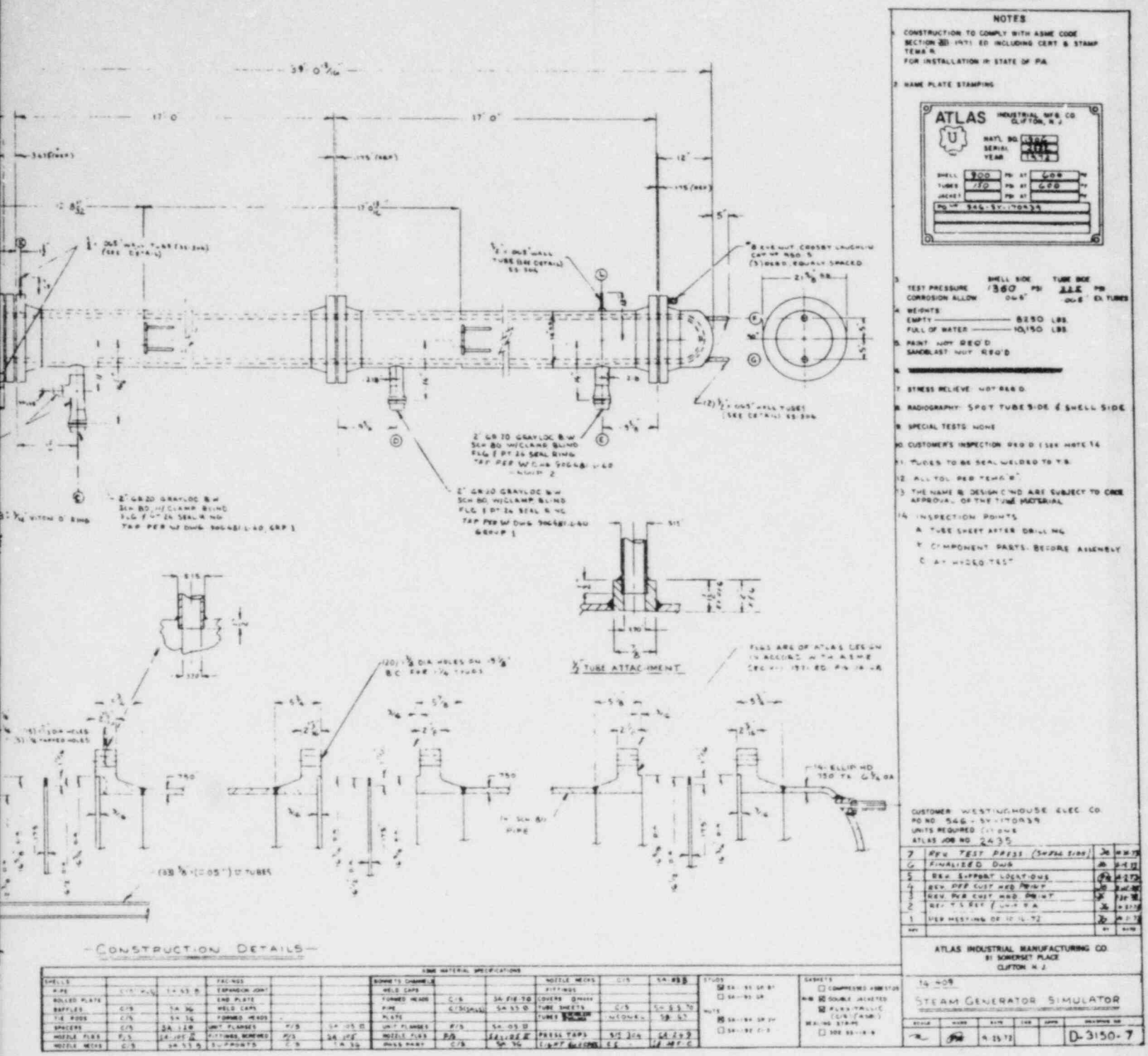

Figure 4-3. FLECHT SEASET Natural Circulation Broken Loop Steam Generator Construction Details (sheet 1 of 2)

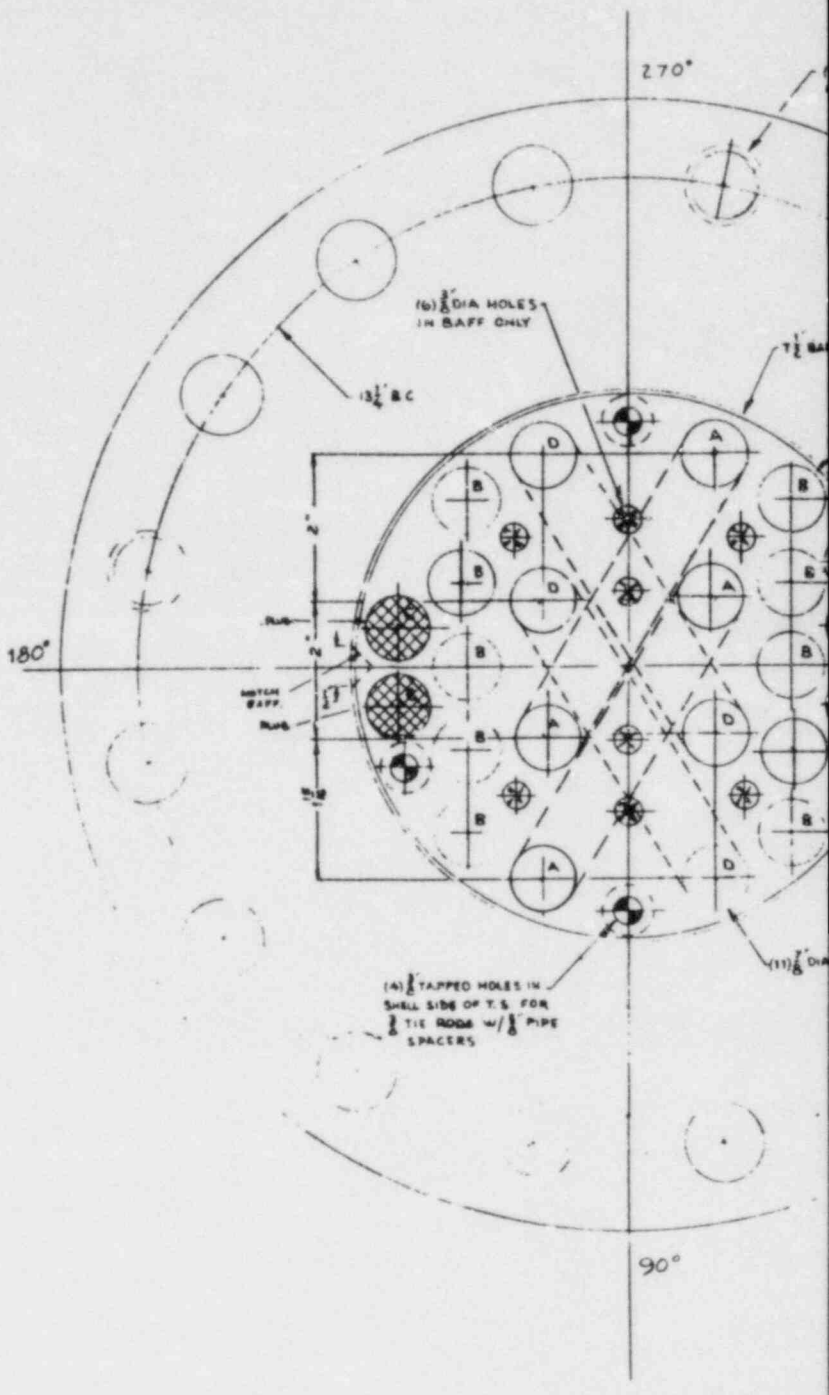

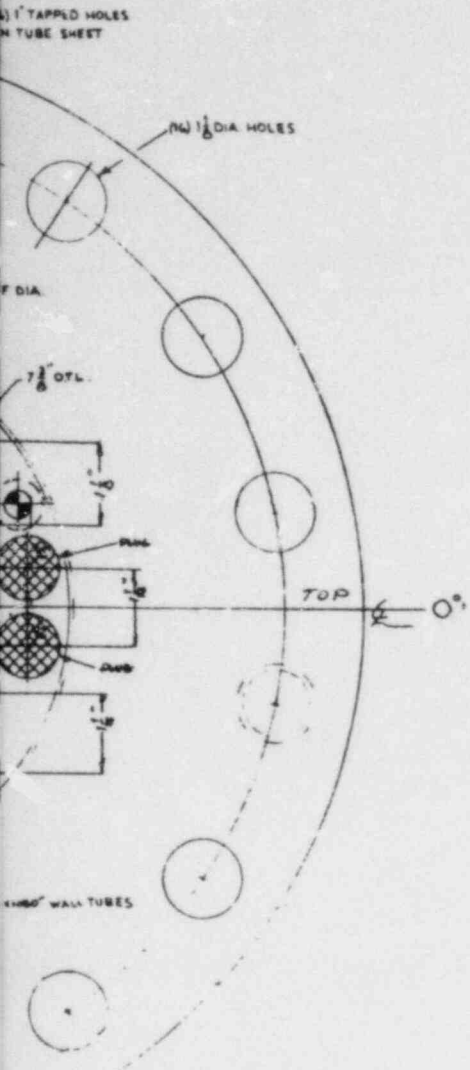

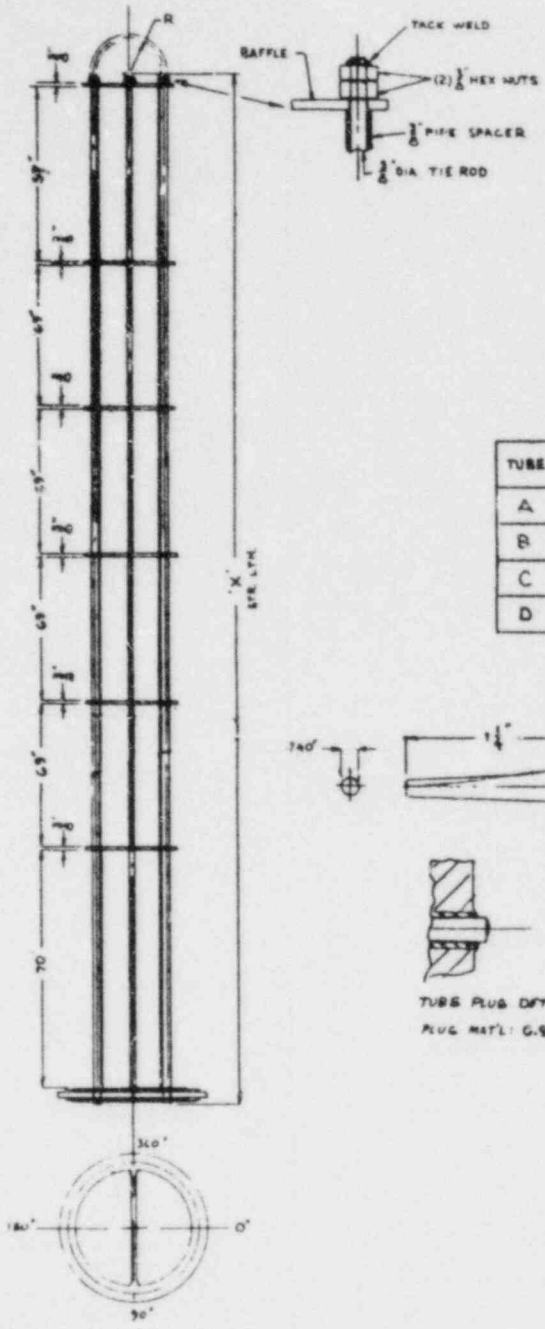

TUBE	R	X	DEV. LTH
A	$2\frac{3}{16}$"	34' $1\frac{1}{2}$"	68' $9\frac{1}{8}$"
B	$2\frac{3}{16}$"	34' $3\frac{1}{2}$"	69' $1\frac{1}{8}$"
C	$3\frac{3}{16}$"	34' $3\frac{1}{2}$"	69' 5"
D	$2\frac{3}{16}$"	34' $2\frac{1}{2}$"	68' $11\frac{3}{8}$"

TUBE PLUG DETAIL

PLUG MAT'L: C.S.

CUSTOMER: WESTINGHOUSE ELEC.
P.O. NO. 546-SY-170939
ATLAS JOB 2434
REF DWG. D-3138

*NOTE: ALL TOL PER TEMA 'R'

2	REV PER CUST MFR PRINT				
1	REV PER MEETING OF 10-16-72				

ATLAS INDUSTRIAL MANUFACTURING CO.
91 SOMERSET PLACE
CLIFTON, N. J.

TUBE BUNDLE DETAIL
#8-411

	JG	9-14-72			D-[illegible] 3189-2

Figure 4-3. FLECHT SEASET Natural Circulation Broken Loop Steam Generator Construction Details (sheet 2 of 2)

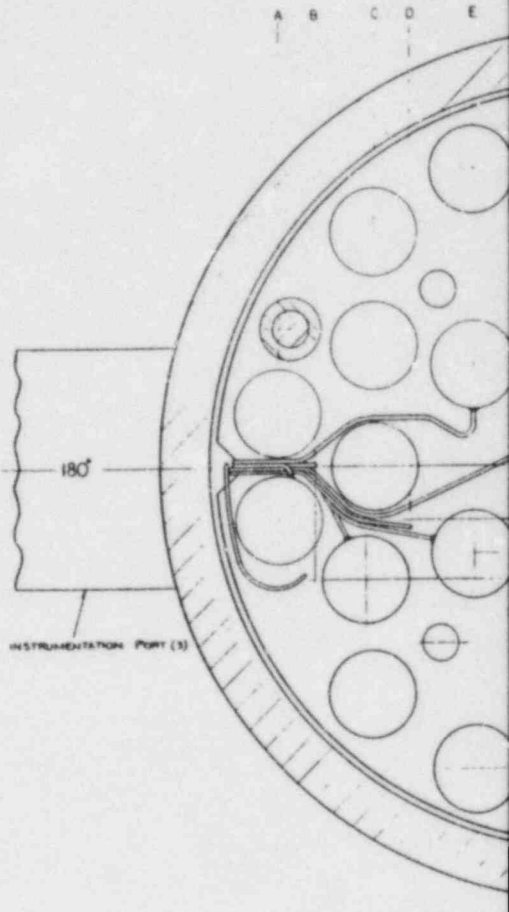

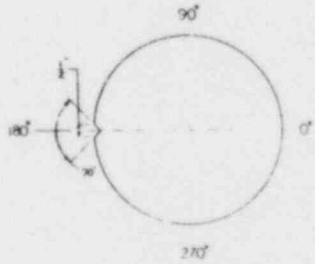

DETAIL B
SCALE 1:2

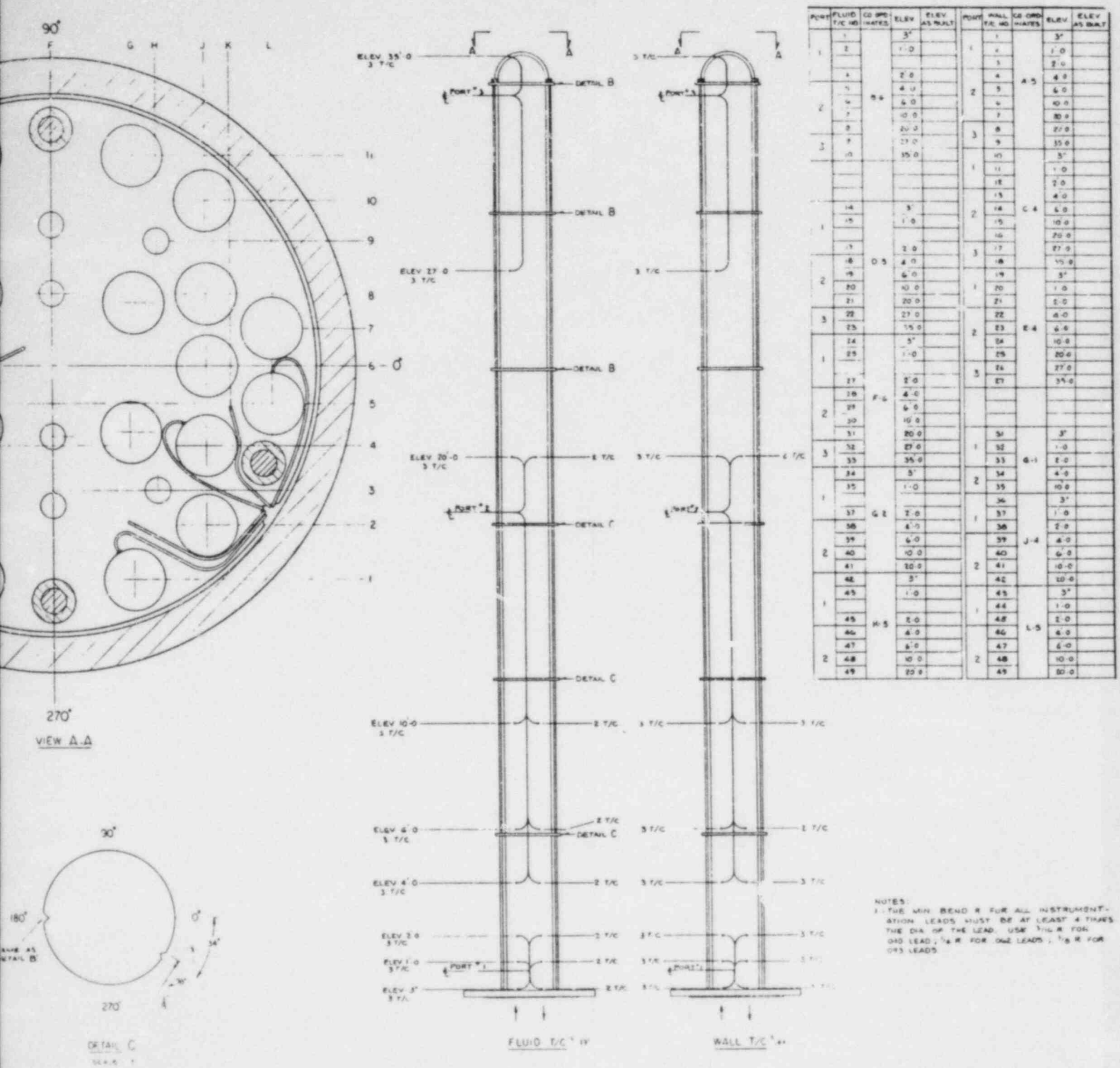

PORT	FLUID T/C NO	CO ORDINATES	ELEV	ELEV AS BUILT
1	1	B-6	3"	
	2		1'-0	
	3		2'-0	
	4		2'-0	
2	5		4'-0	
	6		6'-0	
	7		10'-0	
3	8		20'-0	
	9		27'-0	
	10		35'-0	
1	14	D-5	3"	
	15		1'-0	
2	16		2'-0	
	17		4'-0	
	18		6'-0	
	19		10'-0	
	20		20'-0	
3	21		27'-0	
	22		35'-0	
1	24	F-6	3"	
	25		1'-0	
2	27		2'-0	
	28		4'-0	
	29		6'-0	
	30		10'-0	
3	31		20'-0	
	32		27'-0	
	33		35'-0	
1	34	G-2	3"	
	35		1'-0	
2	37		2'-0	
	38		4'-0	
	39		6'-0	
	40		10'-0	
	41		20'-0	
1	42	K-5	3"	
	43		1'-0	
2	45		2'-0	
	46		4'-0	
	47		6'-0	
	48		10'-0	
	49		20'-0	

PORT	WALL T/C NO	CO ORDINATES	ELEV	ELEV AS BUILT
1	1	A-5	3"	
	4		1'-0	
	5		2'-0	
2	4		4'-0	
	5		6'-0	
	6		10'-0	
	7		20'-0	
3	8		27'-0	
	9		35'-0	
1	10	C-4	3"	
	11		1'-0	
	12		2'-0	
2	13		4'-0	
	14		6'-0	
	15		10'-0	
	16		20'-0	
3	17		27'-0	
	18		35'-0	
1	19	E-4	3"	
	20		1'-0	
	21		2'-0	
2	22		4'-0	
	23		6'-0	
	24		10'-0	
	25		20'-0	
3	26		27'-0	
	27		35'-0	
1	31	G-1	3"	
	32		1'-0	
	33		2'-0	
2	34		4'-0	
	35		10'-0	
1	36	J-4	3"	
	37		1'-0	
	38		2'-0	
2	39		4'-0	
	40		6'-0	
	41		10'-0	
	42		20'-0	
1	43	L-5	3"	
	44		1'-0	
	45		2'-0	
2	46		4'-0	
	47		6'-0	
	48		10'-0	
	49		20'-0	

NOTES:
1. THE MIN BEND R FOR ALL INSTRUMENTATION LEADS MUST BE AT LEAST 4 TIMES THE DIA OF THE LEAD. USE 1/16 R FOR .040 LEAD; 1/8 R FOR .062 LEADS; 1/4 R FOR .093 LEADS

Figure 4-4. FLECHT SEASET Natural Circulation Broken Loop Steam Generator Fluid and Tube Wall Thermocouples

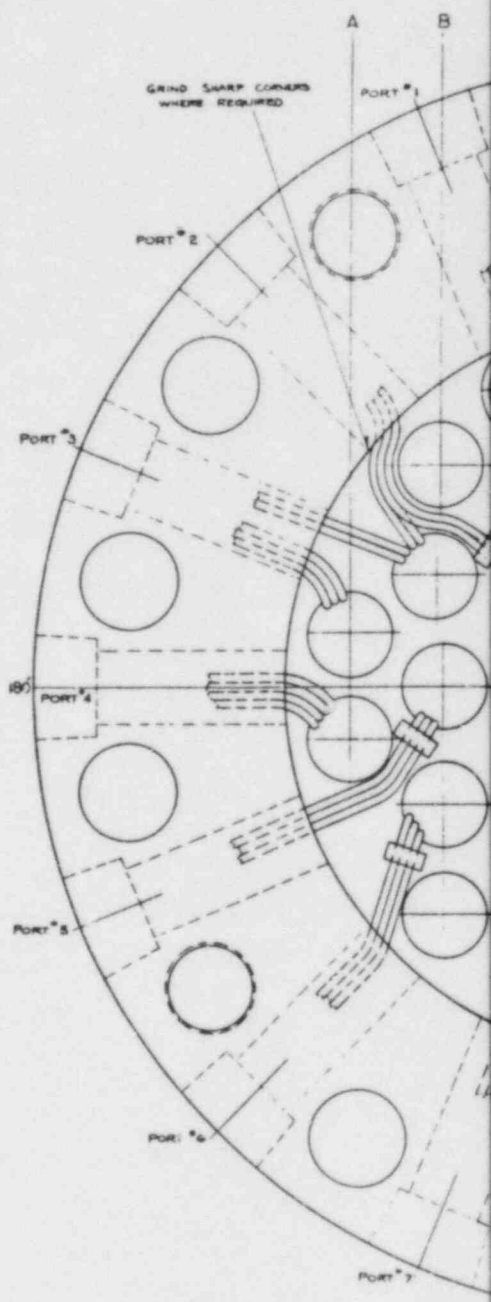

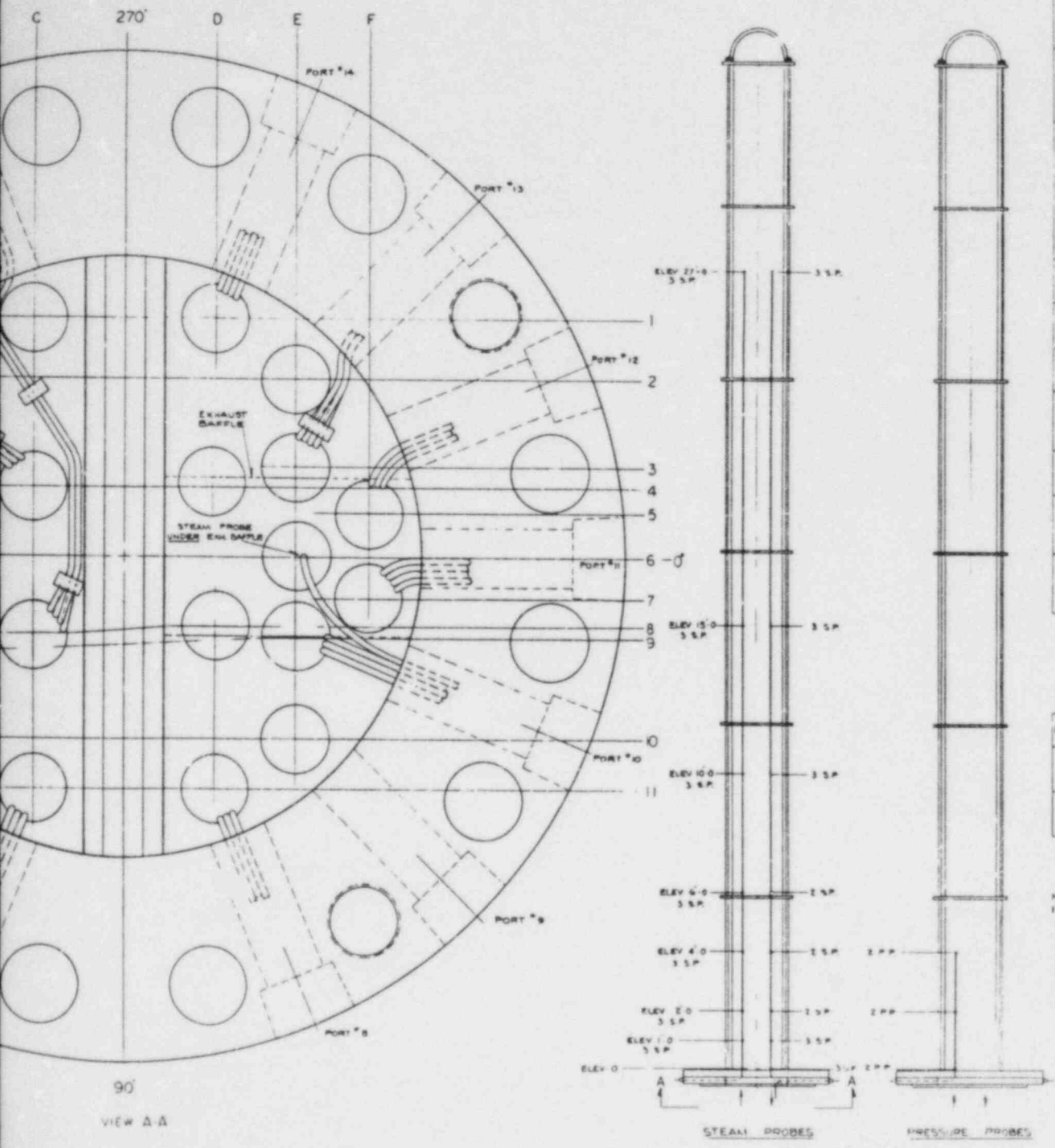

PORT	STEAM PROBE NO.	CO-ORD. NATES	ELEV	T/C TAG
1	S1	C-8	1'-0	
	S2		2'-0	
	S3		4'-0	
	S4		6'-0	
2	S5	C-4	10'-0	
	S6		15'-0	
	S7		27'-0	
	S8	B-3	1'-0	
	S9		2'-0	
3	S10	B-3	4'-0	
	S11		6'-0	
	S12	A-5	10'-0	
	S13		15'-0	
	S14		27'-0	
4	S15	A-7	1'-0	
	S16		2'-0	
	S17		4'-0	
	S18		6'-0	
6	S19	B-9	10'-0	
	S20		15'-0	
	S21		27'-0	
8	S22	D-11	2'-0	
	S23		15'-0	
	S24		27'-0	
10	S25	E-9	10'-0	
	S26		15'-0	
	S27		27'-0	
11	S28	F-7	0'-0	
	S29		1'-0	
	S30		4'-0	
	S31		6'-0	
12	S32	F-5	10'-0	
	S33		15'-0	
	S34		27'-0	
13	S35	E-3	0'-0	
	S36		1'-0	
	S37		4'-0	
	S38		6'-0	
14	S39	D-1	0'-0	
	S40		1'-0	
	S41		2'-0	
	S42		10'-0	

PORT	PRESSURE PROBE NO.	CO-ORD. NATES	ELEV	ELEV AS BUILT
5	P1	B-4	0'-0	
	P2		2'-0	
	P3		4'-0	
7	P4	C-11	0'-0	
	P5		2'-0	
	P6		4'-0	

NOTES:
1 - THE MIN. BEND R FOR ALL INSTRUMENTATION LEADS MUST BE AT LEAST 4 TIMES THE DIA. OF THE LEAD. USE 1/16 R FOR .040 LEAD, 1/8 R FOR .062 LEADS, 3/16 R FOR .093 LEADS.

Figure 4-5. FLECHT SEASET Natural Circulation Broken Loop Steam Generator Instrumentation Steam and Pressure Probes

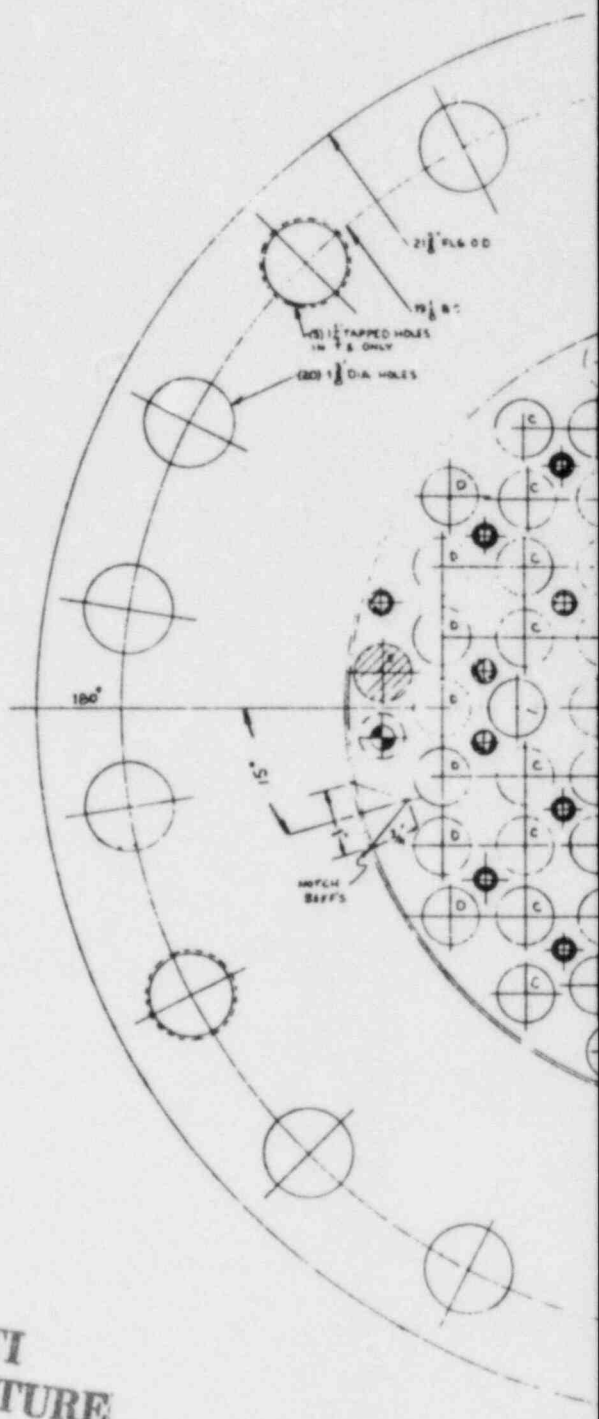

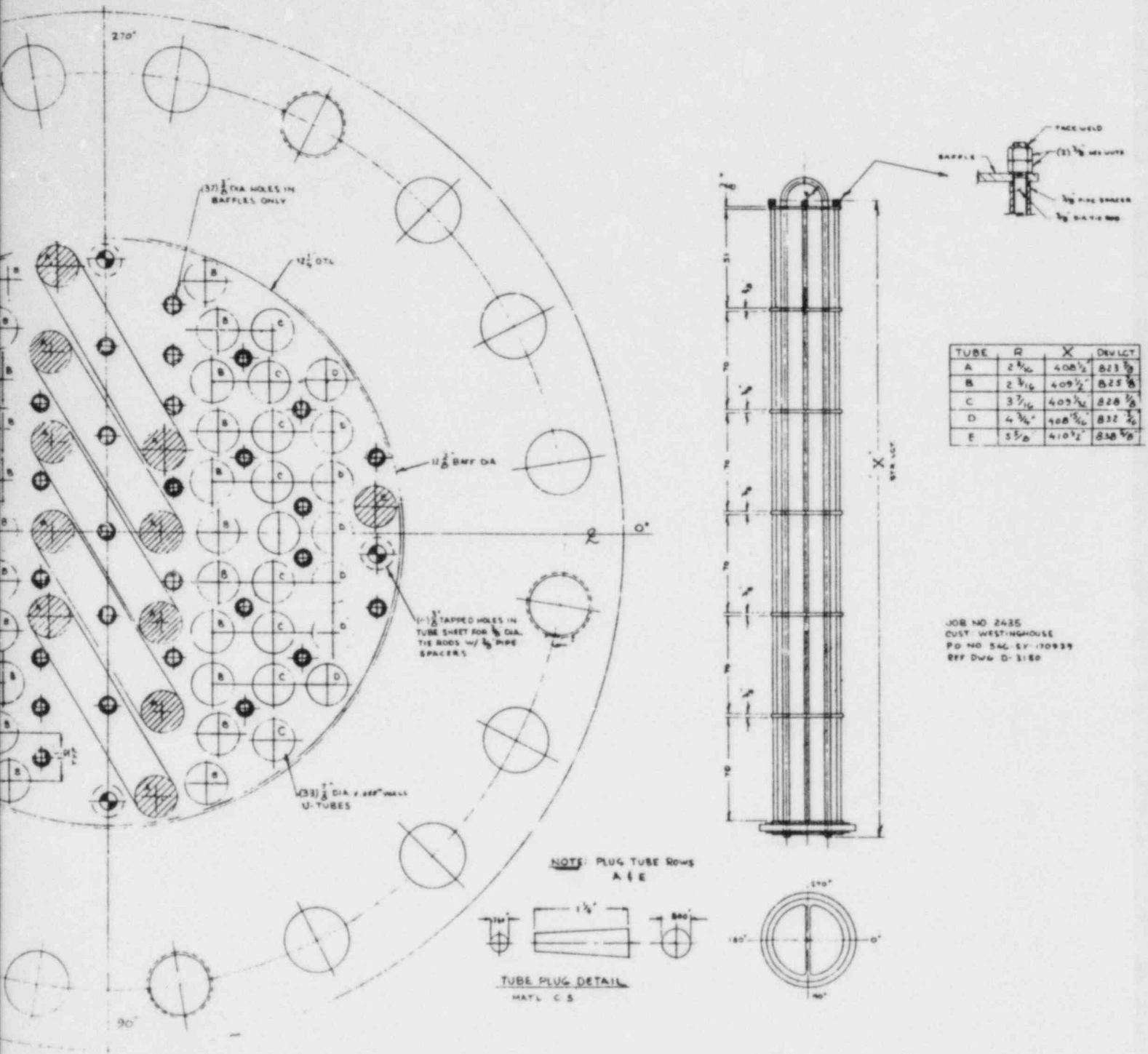

Figure 4-6. FLECHT SEASET Natural Circulation Unbroken Loop Steam Generator Construction Details (sheet 1 of 2)

Also Available On
Aperture Card

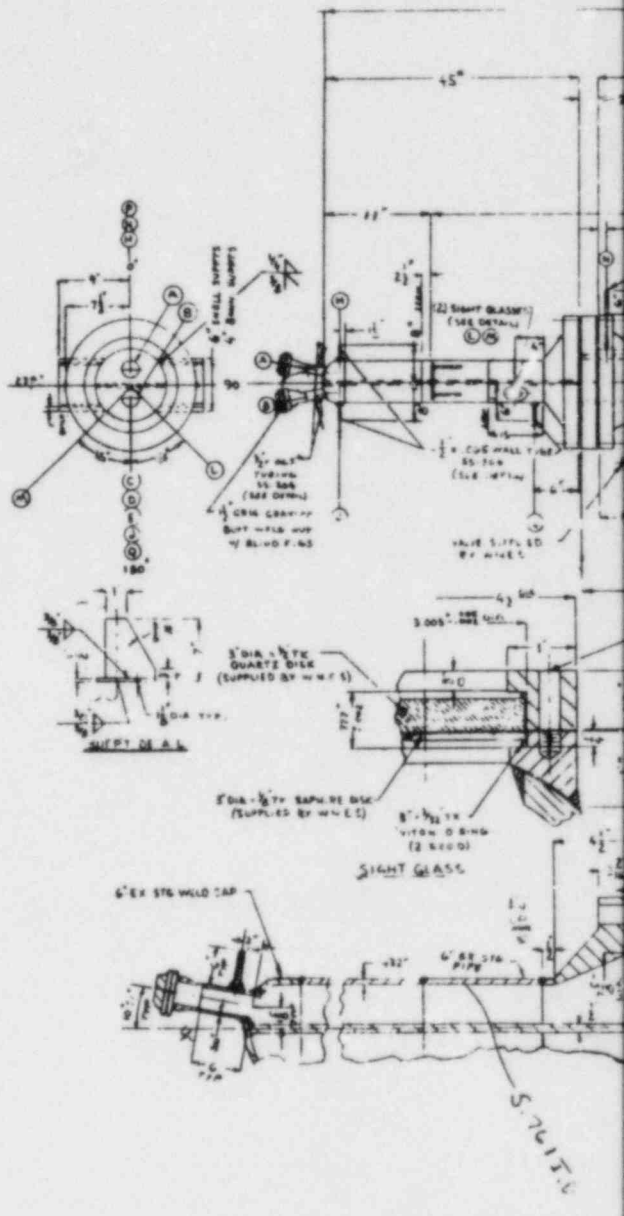

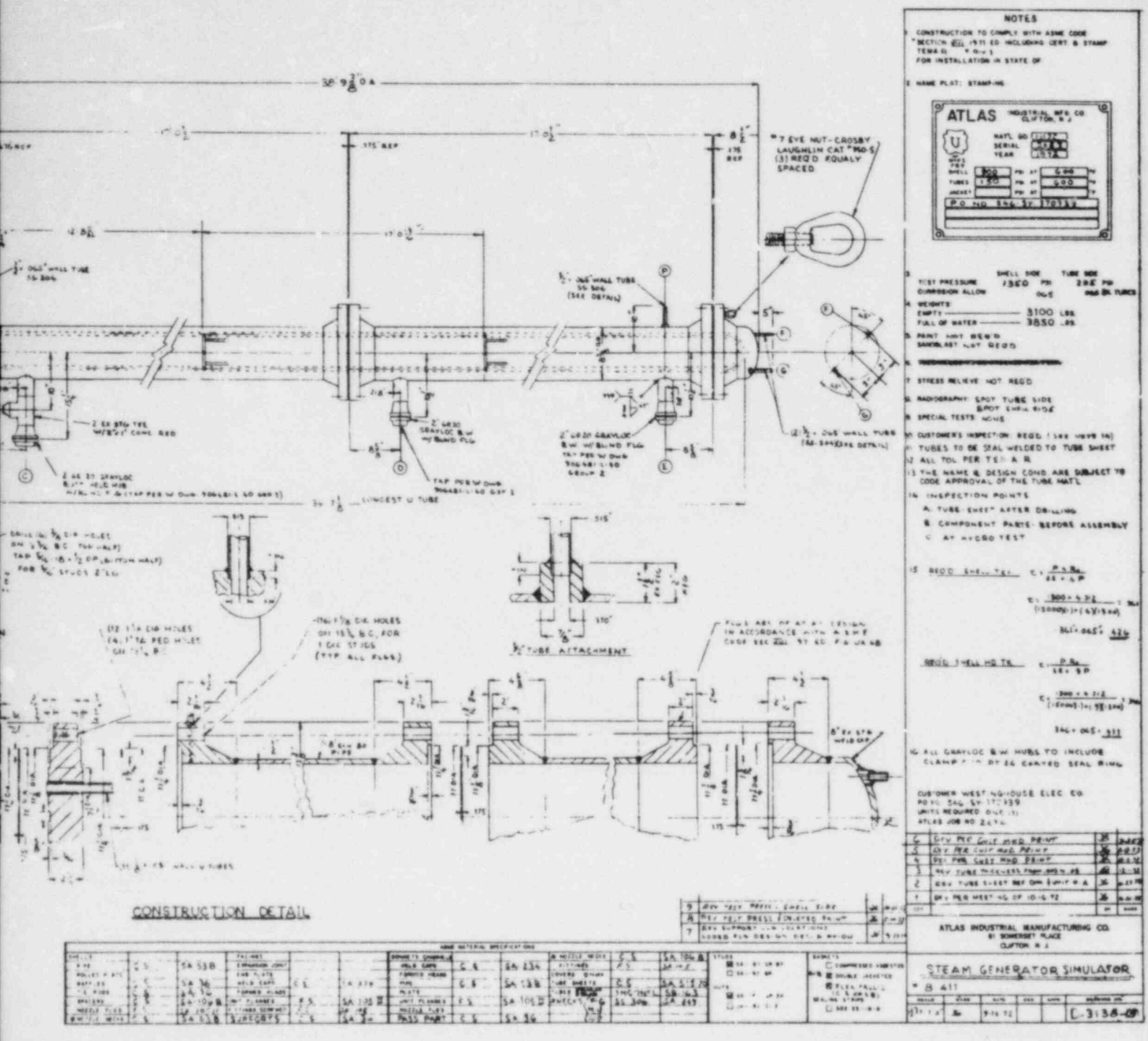

Figure 4-6. FLECHT SEASET Natural Circulation Unbroken Loop Steam Generator Construction Details (sheet 2 of 2)

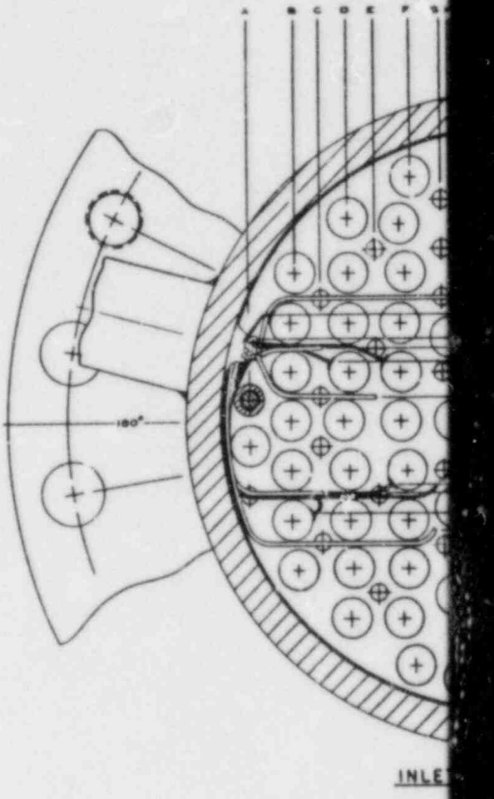

INLE

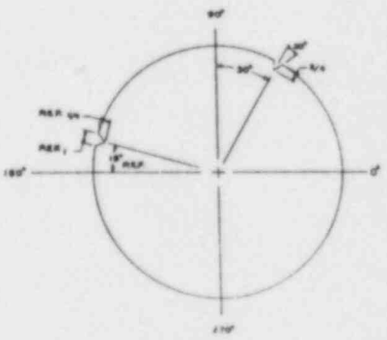

DETAIL A

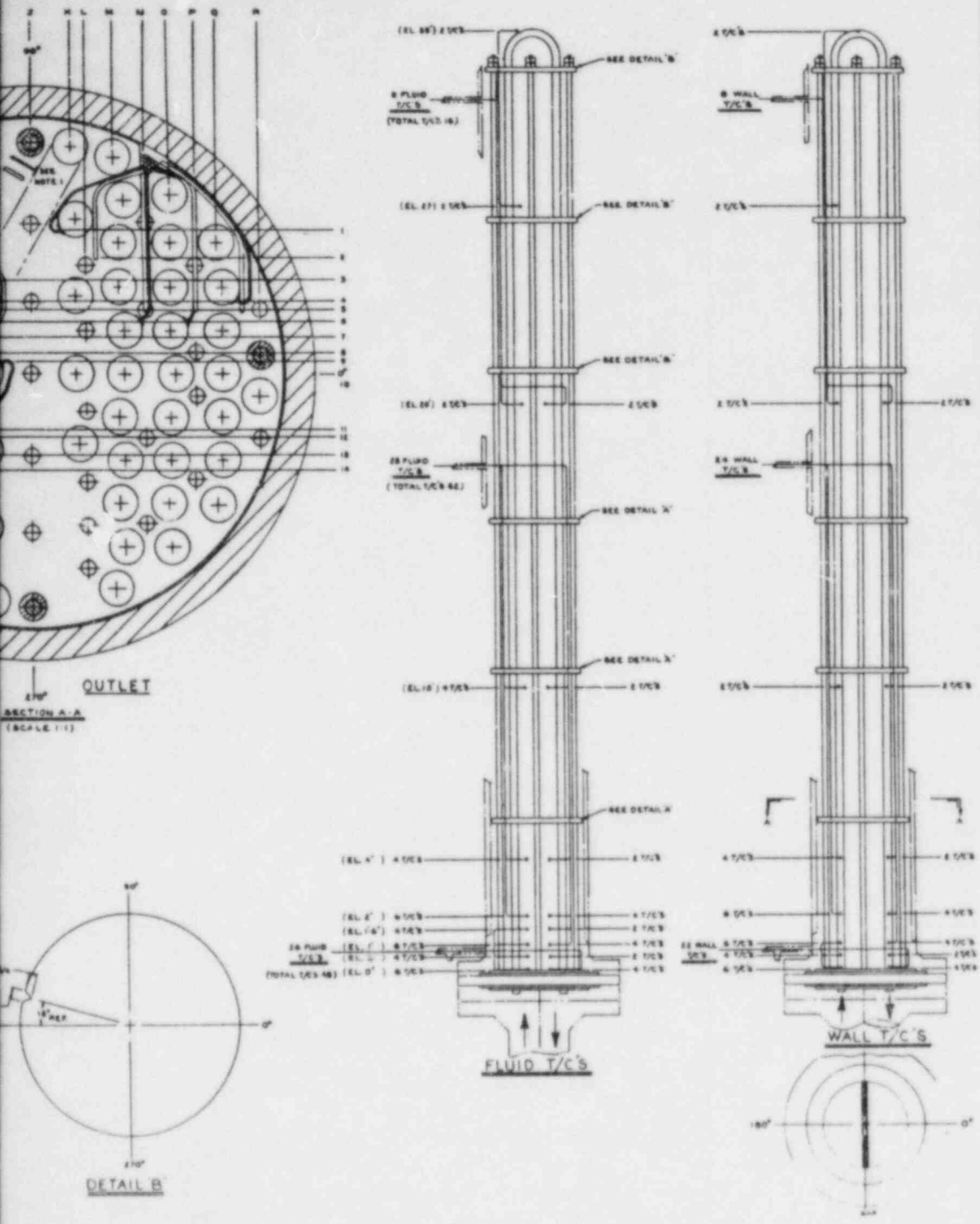

Figure 4-7. FLECHT SEASET Natural Circulation Unbroken Loop Steam Generator Fluid and Tube Wall Thermocouples

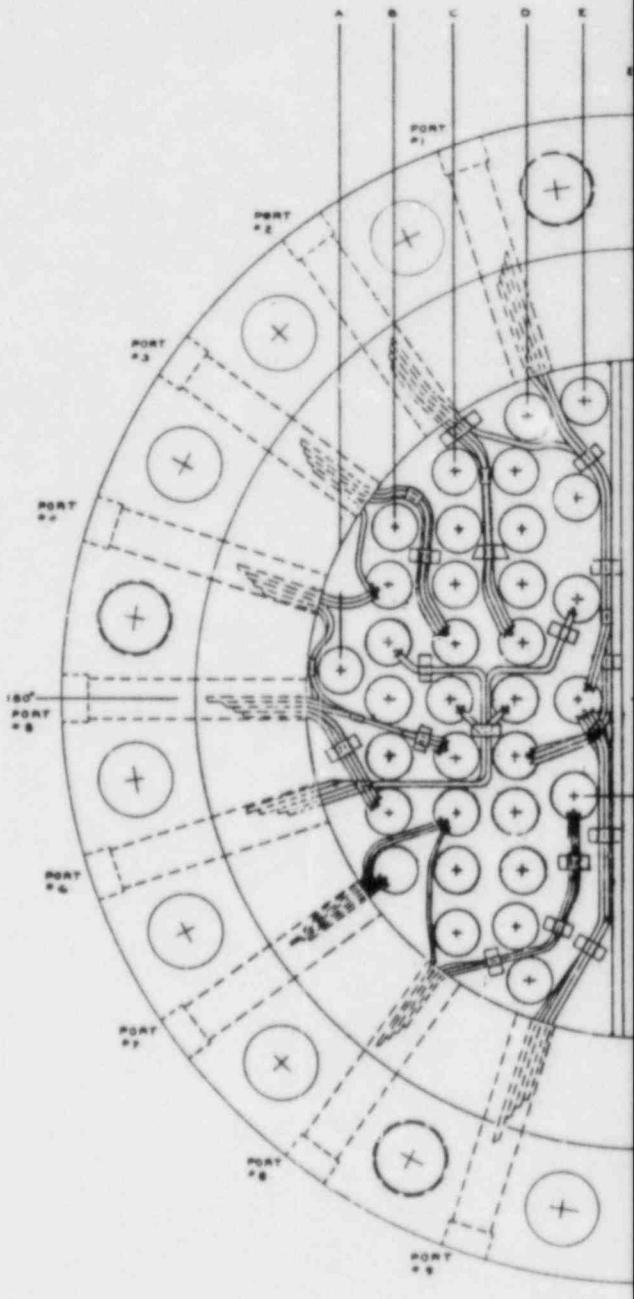

VIE

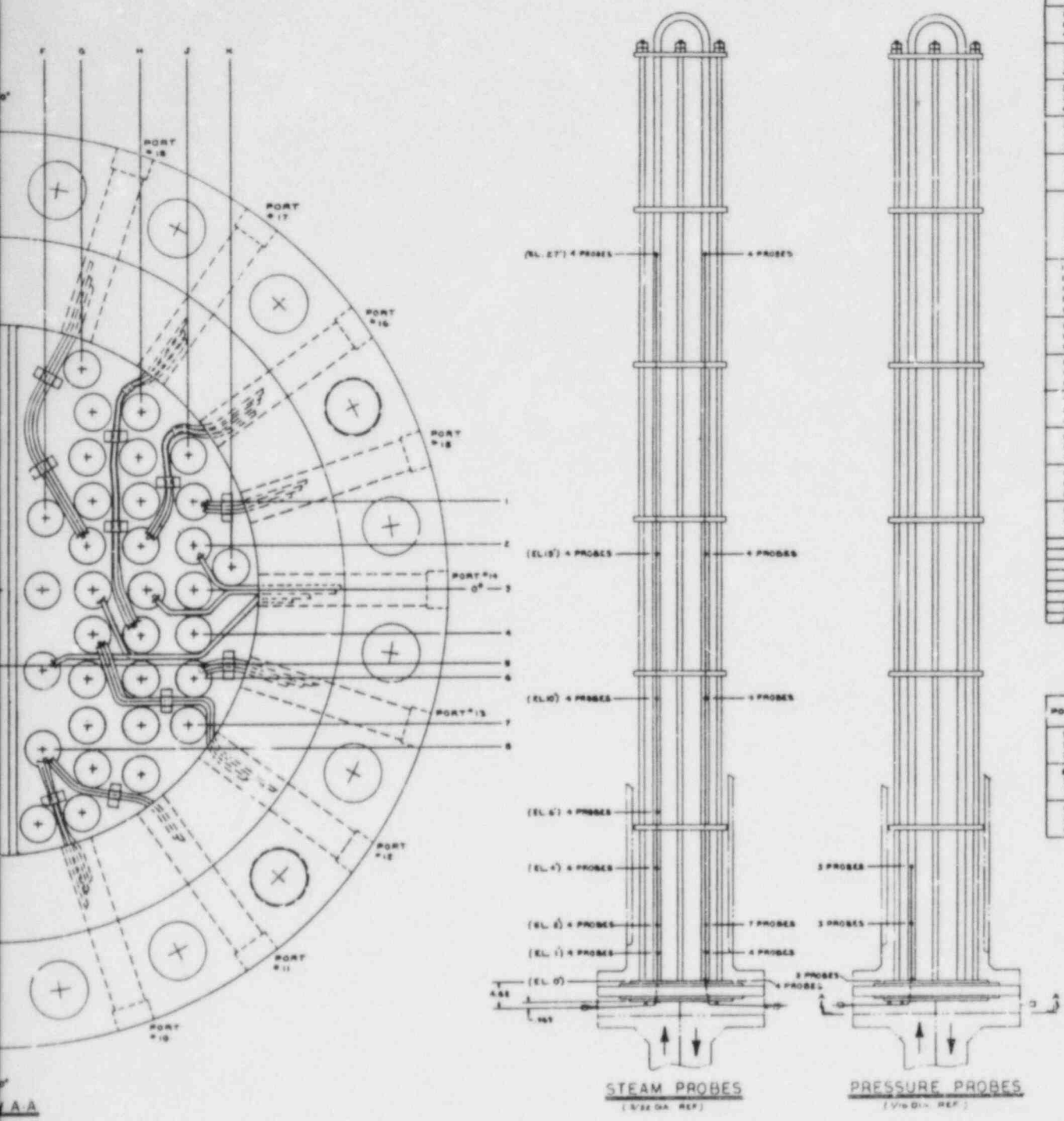

PORT	STEAM PROBE NO.	CO-ORDINATE	ELEV	T/C TAG
4	S 1	B - 1	6'	348
3	S 2		10'	343
4	S 3		15'	342
8	S 4	B - 8	1'	327
8	S 5		2'	326
8	S 6		4'	334
3	S 7	C - 2	6	333
3	S 8		10'	332
3	S 9		15'	345
5	S 10	C - 4	1'	319
5	S 11		2'	328
4	S 12		4'	336
2	S 13	D - 2	6'	347
2	S 14		10	346
2	S 15		15'	344
1	S 16	D - 4	1'	323
1	S 17		2'	322
2	S 18		4'	335
1	S 19	E - 3	1'	329
1	S 20		2'	328
9	S 21		4'	340
9	S 22		6'	331
9	S 23		10'	338
9	S 24		15'	337
10	S 25	F - 8	0'	330
11	S 26		1'	302
10	S 27		2'	301
11	S 28		10'	350
10	S 29		15'	341
15	S 30	G - 2	2'	316
15	S 31		10'	332
15	S 32		15'	351
12	S 33	G - 4	0'	318
12	S 34		1'	319
12	S 35		4'	307
16	S 36	H - 2	2'	320
16	S 37		10'	358
16	S 38		15'	349
17	S 39	H - 4	0'	305
17	S 40		1'	306
17	S 41		2'	308
18	S 42	J - 1	2'	317
18	S 43		10'	357
18	S 44		15'	360
13	S 45	J - 6	0'	303
13	S 46		1'	303
13	S 47		2'	304
6	S 48	B - 6	27'	
9	S 49	C - 1	27'	
5	S 50	C - 3	27'	
6	S 51	E - 1	27'	
7	S 52	F - 1	27'	
7	S 53	G - 1	27'	
7	S 54	J - 1	27'	
7	S 55	K - 1	27'	

PORT	PRESS. PROBE NO.	CO-ORDINATE	ELEV.	PROBE ELEV. AS BUILT
7	P 1	E - 7	0'	0'
7	P 2		2'	2'
7	P 3		4'	4'
8	P 4	C - 8	0'	0'
7	P 5		2'	2'
7	P 6		4'	4'
6	P 7	E - 9	0'	0'
8	P 8		2'	2'
8	P 9		4'	4'

Figure 4-8. FLECHT SEASET Natural Circulation Unbroken Loop Steam Generator Instrumentation Steam and Pressure Probes

TABLE 4-1

INSTRUMENTATION CHANNEL LIST FOR FLECHT SEASET
NATURAL CIRCULATION TESTS

********$$$$$$$$$******** COPYSEP,TABLNC,ZZZZZXY,999.									
1BUNDLE	HEATER ROD			T/C 1.00	8H	0-1000			
2BUNDLE	HEATER ROD			T/C 2.00	8G	0-1000			
3BUNDLE	HEATER ROD			T/C 2.00	5F	0-1000			
4BUNDLE	HEATER ROD			T/C 3.25	7J	0-1000			
5BUNDLE	HEATER ROD			T/C 3.25	7E	0-1000			
6BUNDLE	HEATER ROD			T/C 4.00	7K	0-1000			
7BUNDLE	HEATER ROD			T/C 4.00	7G	0-1000			
8BUNDLE	HEATER ROD			T/C 5.00	8H	0-1000			
9BUNDLE	HEATER ROD			T/C 5.00	6F	0-1000			
10BUNDLE	HEATER ROD			T/C 5.58	8G	0-1000			
11BUNDLE	HEATER ROD			T/C 5.58	5F	0-1000			
12BUNDLE	HEATER ROD			T/C 6.00	7K	0-1000			
13BUNDLE	HEATER ROD			T/C 6.50	7E	0-1000			
14BUNDLE	HEATER ROD			T/C 6.00	6C	0-1000			
15BUNDLE	HEATER ROD			T/C 6.00	8B	0-1000			
16BUNDLE	HEATER ROD			T/C 6.50	8G	0-1000			
17BUNDLE	HEATER ROD			T/C 6.50	5F	0-1000			
18BUNDLE	HEATER ROD			T/C 7.00	7K	0-1000			
19BUNDLE	HEATER ROD			T/C 7.00	7G	0-1000			
20BUNDLE	HEATER ROD			T/C 7.00	6L	0-1000			
21BUNDLE	HEATER ROD			T/C 7.00	8A	0-1000			
22BUNDLE	HEATER ROD			T/C 7.50	8H	0-1000			
23BUNDLE	HEATER ROD			T/C 7.50	6F	0-1000			
24BUNDLE	HEATER ROD			T/C 8.00	8G	0-1000			
25BUNDLE	HEATER ROD			T/C 8.00	5F	0-1000			
26BUNDLE	HEATER ROD			T/C 9.25	7J	0-1000			
27BUNDLE	HEATER ROD			T/C 9.25	7E	0-1000			
28BUNDLE	HEATER ROD			T/C10.00	7K	0-1000			
29BUNDLE	HEATER ROD			T/C10.00	10G	0-1000			
30BUNDLE	HEATER ROD			T/C11.00	8G	0-1000			
31BUNDLE	HEATER ROD			T/C11.00	5F	0-1000			
32BUNDLE	HEATER ROD			T/C11.50	7J	0-1000			
33BUNDLE	HEATER ROD			T/C11.50	7E	0-1000			
34BUNDLE	THIMBLE		BARE	F-T/C 5.00	7I	0-500			
35BUNDLE	THIMBLE		HEATED	F-T/C 5.00	7F	0-500			
36BUNDLE	THIMBLE		BARE	F-T/C 6.00	7I	0-500			
37BUNDLE	THIMBLE		HEATED	F-T/C 6.00	7F	0-500			
38BUNDLE	THIMBLE		BARE	F-T/C 7.00	7I	0-500			
39BUNDLE	THIMBLE		WALL	W-T/C 7.00	7L	0-500			
40BUNDLE	THIMBLE		BARE	F-T/C 7.50	10F	0-500			
41BUNDLE	THIMBLE		BARE	F-T/C 8.00	7I	0-500			
42BUNDLE	THIMBLE		HEATED	F-T/C 8.00	4F	0-500			
43BUNDLE	THIMBLE		BARE	F-T/C 9.25	7I	0-500			
44BUNDLE	THIMBLE		HEATED	F-T/C 9.25	7F	0-500			
45BUNDLE	THIMBLE		BARE	F-T/C10.00	10F	0-500			
46BUNDLE	THIMBLE		HEATED	F-T/C10.00	4F	0-500			
47BUNDLE	THIMBLE		HEATED	F-T/C11.00	10L	0-500			
48BUNDLE	THIMBLE		WALL	W-T/C 7.00	7L	0-500			
49BUNDLE	THIMBLE		HEATED	F-T/C11.50	7F	0-500			
50BUNDLE	THIMBLE		HEATED	F-T/C11.50	10I	0-500			
51UNBRK LOOP HOT LEG		TOP		F-T/C	ST-01	0-500			
52UNBRK LOOP HOT LEG		TOP		W-T/C	ST-01	0-500			
53UNBRK LOOP HOT LEG		TOP		I-T/C	ST-01	0-500			
54UNBRK LOOP HOT LEG		BOT		F-T/C	ST-01	0-500			
55UNBRK LOOP HOT LEG		BOT		W-T/C	ST-01	0-500			
56UNBRK LOOP HOT LEG		TOP		W-T/C	ST-03	0-500			
57UNBRK LOOP HOT LEG		BOT		W-T/C	ST-03	0-500			
58UNBRK LOOP HOT LEG		TOP		F-T/C	ST-03	0-500			
59UNBRK LOOP HOT LEG		BOT		F-T/C	ST-03	0-500			
60UNBRK LOOP HOT LEG		TOP		F-T/C	ST-04	0-500			
61UNBRK LOOP HOT LEG		BOT		F-T/C	ST-04	0-500			
62UNBRK LOOP HOT LEG		TOP		F-T/C	ST-05	0-500			
~~63UNBRK LOOP HOT LEG~~		~~TOP~~		~~W-T/C~~	~~ST-05~~	~~0-500~~			
64UNBRK LOOP HOT LEG		BOT		F-T/C	ST-05	0-500			
65UNBRK LOOP HOT LEG		BOT		W-T/C	ST-05	0-500			

TABLE 4-1 (cont)

INSTRUMENTATION CHANNEL LIST FOR FLECHT SEASET
NATURAL CIRCULATION TESTS

66	UNBRK	LOOP	HOT	LEG	BOT	I-T/C	ST-05	0-500	1	0
67	UNBRK	LOOP	HOT	LEG	TOP	F-T/C	ST-06	0-500	1	0
68	UNBRK	LOOP	HOT	LEG	TOP	W-T/C	ST-06	0-500	1	0
69	UNBRK	LOOP	HOT	LEG	TOP	I-T/C	ST-06	0-500	1	0
70	UNBRK	LOOP	HOT	LEG	BOT	F-T/C	ST-06	0-500	1	0
71	UNBRK	LOOP	HOT	LEG	BOT	W-T/C	ST-06	0-500	1	0
72	UNBRK	LOOP	HOT	LEG	TOP	F-T/C	ST-07	0-500	1	0
73	UNBRK	LOOP	HOT	LEG	BOT	F-T/C	ST-07	0-500	1	0
74	UNBRK	LOOP	HOT	LEG	TOP	F-T/C	ST-08	0-500	1	0
75	UNBRK	LOOP	HOT	LEG	BOT	F-T/C	ST-08	0-500	1	0
76	UNBRK	LOOP	HOT	LEG	TOP	F-T/C	ST-09	0-500	1	0
77	UNBRK	LOOP	HOT	LEG	BOT	F-T/C	ST-09	0-500	1	0
78	UNBRK	LOOP	HOT	LEG	TOP	F-T/C	ST-10	0-500	1	0
79	UNBRK	LOOP	HOT	LEG	TOP	W-T/C	ST-10	0-500	1	0
80	UNBRK	LOOP	HOT	LEG	TOP	I-T/C	ST-10	0-500	1	0
81	UNBRK	LOOP	HOT	LEG	BOT	F-T/C	ST-10	0-500	1	0
82	UNBRK	LOOP	HOT	LEG	BOT	W-T/C	ST-10	0-500	1	0
83	UNBRK	LOOP	LOOP	SEAL		F-T/C	ST-11	0-500	1	0
84	UNBRK	LOOP	LOOP	SEAL		W-T/C	ST-11	0-500	1	0
85	UNBRK	LOOP	LOOP	SEAL		F-T/C	ST-12	0-500	1	0
86	UNBRK	LOOP	LOOP	SEAL		W-T/C	ST-12	0-500	1	0
87	UNBRK	LOOP	LOOP	SEAL		I-T/C	ST-12	0-500	1	0
88	UNBRK	LOOP	LOOP	SEAL		F-T/C	ST-13	0-500	1	0
89	UNBRK	LOOP	LOOP	SEAL		W-T/C	ST-13	0-500	1	0
90	UNBRK	LOOP	LOOP	SEAL		I-T/C	ST-13	0-500	1	0
91	UNBRK	LOOP	LOOP	SEAL		F-T/C	ST-14	0-500	1	0
92	UNBRK	LOOP	LOOP	SEAL		W-T/C	ST-14	0-500	1	0
93	UNBRK	LOOP	LOOP	SEAL		F-T/C	ST-15	0-500	1	0
94	UNBRK	LOOP	LOOP	SEAL		W-T/C	ST-15	0-500	1	0
95	UNBRK	LOOP	LOOP	SEAL		I-T/C	ST-15	0-500	1	0
96	UNBRK	LOOP	COLD	LEG	TOP	F-T/C	ST-16	0-500	1	0
97	UNBRK	LOOP	COLD	LEG	BOT	F-T/C	ST-16	0-500	1	0
98	UNBRK	LOOP	COLD	LEG	TOP	F-T/C	ST-17	0-500	1	0
99	UNBRK	LOOP	COLD	LEG	TOP	W-T/C	ST-17	0-500	1	0
100	UNBRK	LOOP	COLD	LEG	TOP	I-T/C	ST-17	0-500	1	0
101	UNBRK	LOOP	COLD	LEG	BOT	F-T/C	ST-17	0-500	1	0
102	UNBRK	LOOP	COLD	LEG	BOT	W-T/C	ST-17	0-500	1	0
103	UNBRK	LOOP	COLD	LEG	TOP	F-T/C	ST-18	0-500	1	0
104	UNBRK	LOOP	COLD	LEG	BOT	F-T/C	ST-18	0-500	1	0
105	UNBRK	LOOP	COLD	LEG	TOP	F-T/C	ST-19	0-500	1	0
106	UNBRK	LOOP	COLD	LEG	BOT	F-T/C	ST-19	0-500	1	0
107	UNBRK	LOOP	COLD	LEG	SIDE	F-T/C	ST-20	0-500	1	0
108	UNBRK	LOOP	COLD	LEG	TOP	F-T/C	ST-21	0-500	1	0
109	UNBRK	LOOP	COLD	LEG	BOT	F-T/C	ST-21	0-500	1	0
110	UNBRK	LOOP	COLD	LEG	TOP	F-T/C	ST-22	0-500	1	0
111	UNBRK	LOOP	COLD	LEG	TOP	W-T/C	ST-22	0-500	1	0
112	UNBRK	LOOP	COLD	LEG	TOP	I-T/C	ST-22	0-500	1	0
113	UNBRK	LOOP	COLD	LEG	BOT	F-T/C	ST-22	0-500	1	0
114	UNBRK	LOOP	COLD	LEG	BOT	W-T/C	ST-22	0-500	1	0
115	UNBRK	LOOP	COLD	LEG	TOP	F-T/C	ST-23	0-500	1	0
116	UNBRK	LOOP	COLD	LEG	TOP	W-T/C	ST-23	0-500	1	0
117	UNBRK	LOOP	COLD	LEG	TOP	I-T/C	ST-23	0-500	1	0
118	UNBRK	LOOP	COLD	LEG	TOP	F-T/C	ST-24	0-500	1	0
119	UNBRK	LOOP	COLD	LEG	BOT	F-T/C	ST-24	0-500	1	0
120	UNBRK	LOOP	COLD	LEG	TOP	F-T/C	ST-26	0-500	1	0
121	UNBRK	LOOP	COLD	LEG	TOP	W-T/C	ST-27	0-500	1	0
122	UNBRK	LOOP	COLD	LEG	BOT	F-T/C	ST-27	0-500	1	0
123	UNBRK	LOOP	COLD	LEG	BOT	W-T/C	ST-27	0-500	1	0
124	UNBRK	LOOP	COLD	LEG	BOT	I-T/C	ST-27	0-500	1	0
125	BRK	LOOP	HOT	LEG	EXIT	F-T/C	ST-27	0-500	1	0
126	BRK	LOOP	HOT	LEG	TOP	F-T/C	ST-28	0-500	1	0
127	BRK	LOOP	HOT	LEG	TOP	W-T/C	ST-28	0-500	1	0
128	BRK	LOOP	HOT	LEG	TOP	I-T/C	ST-28	0-500	1	0
~~129~~	~~BRK~~	~~LOOP~~	~~HOT~~	~~LEG~~	~~BOT~~	~~F-T/C~~	~~ST-28~~	~~0-500~~	~~1~~	~~0~~
130	BRK	LOOP	HOT	LEG	BOT	W-T/C	ST-28	0-500	1	0
131	BRK	LOOP	HOT	LEG	TOP	F-T/C	ST-29	0-500	1	0

TABLE 4-1 (cont)

INSTRUMENTATION CHANNEL LIST FOR FLECHT SEASET
NATURAL CIRCULATION TESTS

132	BRK	LOOP	HOT LEG	BOT	F-T/C	ST-29	0-500	1	0
133	BRK	LOOP	HOT LEG	TOP	F-T/C	ST-30	0-500	1	0
134	BRK	LOOP	HOT LEG	BOT	F-T/C	ST-30	0-500	1	0
135	BRK	LOOP	HOT LEG	TOP	F-T/C	ST-31	0-500	1	0
136	BRK	LOOP	HOT LEG	TOP	W-T/C	ST-31	0-500	1	0
137	BRK	LOOP	HOT LEG	BOT	F-T/C	ST-31	0-500	1	0
138	BRK	LOOP	HOT LEG	BOT	W-T/C	ST-31	0-500	1	0
139	BRK	LOOP	HOT LEG	BOT	I-T/C	ST-31	0-500	1	0
140	BRK	LOOP	HOT LEG	TOP	F-T/C	ST-32	0-500	1	0
141	BRK	LOOP	HOT LEG	TOP	W-T/C	ST-32	0-500	1	0
142	BRK	LOOP	HOT LEG	TOP	I-T/C	ST-32	0-500	1	0
143	BRK	LOOP	HOT LEG	BOT	F-T/C	ST-32	0-500	1	0
144	BRK	LOOP	HOT LEG	BOT	W-T/C	ST-32	0-500	1	0
145	BRK	LOOP	HOT LEG	TOP	F-T/C	ST-33	0-500	1	0
146	BRK	LOOP	HOT LEG	BOT	F-T/C	ST-33	0-500	1	0
147	BRK	LOOP	HOT LEG	TOP	F-T/C	ST-34	0-500	1	0
148	BRK	LOOP	HOT LEG	BOT	F-T/C	ST-34	0-500	1	0
149	BRK	LOOP	HOT LEG	TOP	W-T/C	ST-34	0-500	1	0
150	BRK	LOOP	HOT LEG	BOT	W-T/C	ST-34	0-500	1	0
151	BRK	LOOP	HOT LEG	TOP	F-T/C	ST-35	0-500	1	0
152	BRK	LOOP	HOT LEG	TOP	W-T/C	ST-35	0-500	1	0
153	BRK	LOOP	HOT LEG	TOP	I-T/C	ST-35	0-500	1	0
154	BRK	LOOP	HOT LEG	BOT	F-T/C	ST-35	0-500	1	0
155	BRK	LOOP	HOT LEG	BOT	W-T/C	ST-35	0-500	1	0
156	BRK	LOOP	LOOP SEAL		F-T/C	ST-36	0-500	1	0
157	BRK	LOOP	LOOP SEAL		W-T/C	ST-36	0-500	1	0
158	BRK	LOOP	LOOP SEAL		F-T/C	ST-37	0-500	1	0
159	BRK	LOOP	LOOP SEAL		W-T/C	ST-37	0-500	1	0
160	BRK	LOOP	LOOP SEAL		I-T/C	ST-37	0-500	1	0
161	BRK	LOOP	LOOP SEAL		F-T/C	ST-38	0-500	1	0
162	BRK	LOOP	LOOP SEAL		W-T/C	ST-38	0-500	1	0
163	BRK	LOOP	LOOP SEAL		I-T/C	ST-38	0-500	1	0
164	BRK	LOOP	LOOP SEAL		F-T/C	ST-39	0-500	1	0
165	BRK	LOOP	LOOP SEAL		W-T/C	ST-39	0-500	1	0
166	BRK	LOOP	LOOP SEAL		F-T/C	ST-40	0-500	1	0
167	BRK	LOOP	LOOP SEAL		W-T/C	ST-40	0-500	1	0
168	BRK	LOOP	LOOP SEAL		I-T/C	ST-40	0-500	1	0
169	BRK	LOOP	COLD LEG	TOP	F-T/C	ST-41	0-500	1	0
170	BRK	LOOP	COLD LEG	BOT	F-T/C	ST-41	0-500	1	0
171	BRK	LOOP	COLD LEG	TOP	F-T/C	ST-42	0-500	1	0
172	BRK	LOOP	COLD LEG	TOP	W-T/C	ST-42	0-500	1	0
173	BRK	LOOP	COLD LEG	TOP	I-T/C	ST-42	0-500	1	0
174	BRK	LOOP	COLD LEG	BOT	F-T/C	ST-43	0-500	1	0
175	BRK	LOOP	COLD LEG	BOT	W-T/C	ST-43	0-500	1	0
176	BRK	LOOP	COLD LEG	TOP	F-T/C	ST-43	0-500	1	0
177	BRK	LOOP	COLD LEG	TOP	W-T/C	ST-43	0-500	1	0
178	BRK	LOOP	COLD LEG	TOP	I-T/C	ST-43	0-500	1	0
179	BRK	LOOP	COLD LEG	TOP	F-T/C	ST-44	0-500	1	0
180	BRK	LOOP	COLD LEG	BOT	F-T/C	ST-44	0-500	1	0
181	BRK	LOOP	COLD LEG	TOP	F-T/C	ST-45	0-500	1	0
182	BRK	LOOP	COLD LEG	BOT	F-T/C	ST-45	0-500	1	0
183	BRK	LOOP	COLD LEG	TOP	F-T/C	ST-46	0-500	1	0
184	BRK	LOOP	COLD LEG	TOP	W-T/C	ST-46	0-500	1	0
185	BRK	LOOP	COLD LEG	BOT	F-T/C	ST-46	0-500	1	0
186	BRK	LOOP	COLD LEG	BOT	W-T/C	ST-46	0-500	1	0
187	BRK	LOOP	COLD LEG	BOT	I-T/C	ST-46	0-500	1	0
188	BRK	LOOP	COLD LEG	TOP	F-T/C	ST-47	0-500	1	0
189	BRK	LOOP	COLD LEG	TOP	W-T/C	ST-47	0-500	1	0
190	BRK	LOOP	COLD LEG	TOP	I-T/C	ST-47	0-500	1	0
191	BRK	LOOP	COLD LEG	BOT	F-T/C	ST-47	0-500	1	0
192	BRK	LOOP	COLD LEG	BOT	W-T/C	ST-47	0-500	1	0
193	BRK	LOOP	COLD LEG	TOP	F-T/C	ST-48	0-500	1	0
194	BRK	LOOP	COLD LEG	TOP	W-T/C	ST-48	0-500	1	0
195	BRK	LOOP	COLD LEG	BOT	F-T/C	ST-48	0-500	1	0
196	BRK	LOOP	COLD LEG	BOT	W-T/C	ST-48	0-500	1	0
197	BRK	LOOP	COLD LEG	BOT	I-T/C	ST-48	0-500	1	0

TABLE 4-1 (cont)

INSTRUMENTATION CHANNEL LIST FOR FLECHT SEASET
NATURAL CIRCULATION TESTS

198UNBRK	LOOP	COLD LEG		INJ LN	F-T/C					0-500		1	C
199		ACCUM 1			F-T/C					0-500		1	C
200UNBRK	LOOP	HOT LEG	EXIT		F-T/C					0-500		1	C
201UNBRK	LOOP	STEAM GEN	INL	PLENUM	F-T/C					0-500		1	C
202UNBRK	LOOP	STEAM GEN	INL	PLENUM	W-T/C					0-500		1	C
203UNBRK	LOOP	STEAM GEN	OUTL	PLENUM	F-T/C					0-500		1	C
204UNBRK	LOOP	STEAM GEN	OUTL	PLENUM	W-T/C					0-500		1	C
205UNBRK	LOOP	STEAM GEN	INL	TUBE	W-T/C	0.00	101	B-	3	30-500		1	C
206UNBRK	LOOP	STEAM GEN	INL	TUBE	W-T/C	0.00	113	D-	6	20-500		1	C
207UNBRK	LOOP	STEAM GEN	INL	TUBE	W-T/C	0.00	126	H-	9	10-500		1	C
208UNBRK	LOOP	STEAM GEN	INL	SEC SIDE	F-T/C	0.00	1	A-	4	30-500		1	C
209UNBRK	LOOP	STEAM GEN	INL	SEC SIDE	F-T/C	0.00	8	C-	5	30-500		1	C
210UNBRK	LOOP	STEAM GEN	INL	SEC SIDE	F-T/C	0.00	21	E-	8	20-500		1	C
211UNBRK	LOOP	STEAM GEN	INL	SEC SIDE	F-T/C	0.00	31	H-	7	10-500		1	C
212UNBRK	LOOP	STEAM GEN	INL	TUBE	W-T/C	0.50	102	B-	3	30-500		1	C
213UNBRK	LOOP	STEAM GEN	INL	TUBE	W-T/C	0.50	114	D-	6	20-500		1	C
214UNBRK	LOOP	STEAM GEN	INL	TUBE	W-T/C	0.50	119	F-	6	20-500		1	C
215UNBRK	LOOP	STEAM GEN	INL	TUBE	W-T/C	0.50	127	H-	9	10-500		1	C
216UNBRK	LOOP	STEAM GEN	INL	SEC SIDE	F-T/C	0.50	2	A-	4	30-500		1	C
217UNBRK	LOOP	STEAM GEN	INL	SEC SIDE	F-T/C	0.50	9	C-	5	30-500		1	C
218UNBRK	LOOP	STEAM GEN	INL	SEC SIDE	F-T/C	0.50	32	H-	7	10-500		1	C
219UNBRK	LOOP	STEAM GEN	INL	TUBE	W-T/C	1.00	103	B-	3	30-500		1	C
220UNBRK	LOOP	STEAM GEN	INL	SHELL	I-T/C	1.00				0-500		1	C
221UNBRK	LOOP	STEAM GEN	INL	TUBE	W-T/C	1.00	128	H-	9	10-500		1	C
222UNBRK	LOOP	STEAM GEN	INL	SEC SIDE	F-T/C	1.00	3	A-	4	30-500		1	C
223UNBRK	LOOP	STEAM GEN	INL	SEC SIDE	F-T/C	1.00	19	C-12		30-500		1	C
224UNBRK	LOOP	STEAM GEN	INL	SEC SIDE	F-T/C	1.00	23	E-	8	20-500		1	C
225UNBRK	LOOP	STEAM GEN	INL	SHELL	I-T/C	15.00				0-500		1	C
226UNBRK	LOOP	STEAM GEN	INL	PRI SIDE	SP	1.00	327	B-	6	30-500		1	C
227UNBRK	LOOP	STEAM GEN	INL	SHELL	W-T/C	1.00				0-500		1	C
228UNBRK	LOOP	STEAM GEN	INL	PRI SIDE	SP	1.00	323	D-	4	10-500		1	C
229UNBRK	LOOP	STEAM GEN	INL	SHELL	I-T/C	27.00	329	E-	3	10-500		1	C
230UNBRK	LOOP	STEAM GEN	INL	SEC SIDE	F-T/C	1.50	4	A-	4	30-500		1	C
231UNBRK	LOOP	STEAM GEN	INL	SEC SIDE	F-T/C	1.50	11	C-	5	30-500		1	C
232UNBRK	LOOP	STEAM GEN	INL	SEC SIDE	F-T/C	1.50	24	E-	8	20-500		1	C
233UNBRK	LOOP	STEAM GEN	INL	SEC SIDE	F-T/C	1.50	34	H-	7	10-500		1	C
234UNBRK	LOOP	STEAM GEN	INL	TUBE	W-T/C	2.00	104	B-	3	30-500		1	C
235UNBRK	LOOP	STEAM GEN	INL	TUBE	W-T/C	2.00	116	D-	6	20-500		1	C
236UNBRK	LOOP	STEAM GEN	INL	TUBE	W-T/C	2.00	121	F-	6	20-500		1	C
237UNBRK	LOOP	STEAM GEN	INL	TUBE	W-T/C	2.00	129	H-	9	10-500		1	C
238UNBRK	LOOP	STEAM GEN	INL	SEC SIDE	F-T/C	2.00	5	A-	4	30-500		1	C
239UNBRK	LOOP	STEAM GEN	INL	SEC SIDE	F-T/C	2.00	12	C-	5	30-500		1	C
240UNBRK	LOOP	STEAM GEN	INL	SEC SIDE	F-T/C	2.00	25	E-	8	20-500		1	C
241UNBRK	LOOP	STEAM GEN	INL	PRI SIDE	SP	2.00	326	B-	6	30-500		1	C
242UNBRK	LOOP	STEAM GEN	INL	PRI SIDE	SP	2.00	325	C-	4	20-500		1	C
243UNBRK	LOOP	STEAM GEN	INL	SHELL	W-T/C	15.00				0-500		1	C
244UNBRK	LOOP	STEAM GEN	INL	TUBE	W-T/C	4.00	105	B-	3	30-500		1	C
245UNBRK	LOOP	STEAM GEN	INL	TUBE	W-T/C	4.00	117	D-	6	20-500		1	C
246UNBRK	LOOP	STEAM GEN	INL	TUBE	W-T/C	4.00	122	F-	6	20-500		1	C
247UNBRK	LOOP	STEAM GEN	INL	TUBE	W-T/C	4.00	130	H-	9	10-500		1	C
248UNBRK	LOOP	STEAM GEN	INL	SEC SIDE	F-T/C	4.00	13	C-	5	30-500		1	C
249UNBRK	LOOP	STEAM GEN	INL	PRI SIDE	SP	4.00	334	B-	6	30-500		1	C
250UNBRK	LOOP	STEAM GEN	INL	PRI SIDE	SP	4.00	336	C-	4	20-500		1	C
251UNBRK	LOOP	STEAM GEN	INL	PRI SIDE	SP	4.00	335	D-	4	10-500		1	C
252UNBRK	LOOP	STEAM GEN	INL	PRI SIDE	SP	6.00	333	C-	2	20-500		1	C
253UNBRK	LOOP	STEAM GEN	INL	PRI SIDE	SP	6.00	347	D-	2	10-500		1	C
254UNBRK	LOOP	STEAM GEN	INL	TUBE	W-T/C	10.00	106	B-	3	30-500		1	C
255UNBRK	LOOP	STEAM GEN	INL	TUBE	W-T/C	10.00	131	H-	9	10-500		1	C
256UNBRK	LOOP	STEAM GEN	INL	SEC SIDE	F-T/C	10.00	7	A-	4	30-500		1	C
257UNBRK	LOOP	STEAM GEN	INL	SEC SIDE	F-T/C	10.00	14	C-	5	30-500		1	C
258UNBRK	LOOP	STEAM GEN	INL	SHELL	W-T/C	27.00				0-500		1	C
259UNBRK	LOOP	STEAM GEN	INL	SHELL	W-T/C	35.00				0-500		1	C
260UNBRK	LOOP	STEAM GEN	INL	PRI SIDE	SP	10.00	343	B-	1	30-500		1	C
~~261UNBRK~~	~~LOOP~~	~~STEAM GEN~~	~~INL~~	~~PRI SIDE~~	~~SP~~	~~10.00~~	~~332~~	~~C-~~	~~2~~	~~20-500~~		~~1~~	~~C~~
262UNBRK	LOOP	STEAM GEN	INL	PRI SIDE	SP	10.00	346	D-	2	10-500		1	C
263UNBRK	LOOP	STEAM GEN	INL	PRI SIDE	SP	15.00	342	B-	1	30-500		1	C

TABLE 4-1 (cont)

INSTRUMENTATION CHANNEL LIST FOR FLECHT SEASET
NATURAL CIRCULATION TESTS

264	UNBRK	LOOP	STEAM	GEN	INL	PRI	SIDE	SP	15.00	348	C-	2	20-500			1	0
265	UNBRK	LOOP	STEAM	GEN	INL	PRI	SIDE	SP	15.00	344	D-	2	10-500			1	0
266	UNBRK	LOOP	STEAM	GEN	INL	SEC	SIDEF-T/C		20.00	15	C-	5	30-500			1	0
267	UNBRK	LOOP	STEAM	GEN	INL	TUBE	W-T/C		27.00	133	H-	9	10-500			1	0
268	UNBRK	LOOP	STEAM	GEN	INL	SEC	SIDEF-T/C		27.00	16	C-	5	*30-500			1	0
269	UNBRK	LOOP	STEAM	GEN	INL	PRI	SIDE	SP	27.00	F	B-	2	*30-500			1	0
270	UNBRK	LOOP	STEAM	GEN	INL	PRI	SIDE	SP	27.00	E	C-	3	20-500			1	0
271	UNBRK	LOOP	STEAM	GEN	INL	PRI	SIDE	SP	27.00	I	D-	3	10-500			1	0
272	UNBRK	LOOP	STEAM	GEN	INL	PRI	SIDE	SP	27.00	H	E-	1	10-500			1	0
273	UNBRK	LOOP	STEAM	GEN	INL	TUBE	W-T/C		35.00	109	B-	3	30-500			1	0
274	UNBRK	LOOP	STEAM	GEN	INL	TUBE	W-T/C		35.00	134	H-	9	10-500			1	0
275	UNBRK	LOOP	STEAM	GEN	INL	SEC	SIDEF-T/C		35.00	17	C-	5	30-500			1	0
276	UNBRK	LOOP	STEAM	GEN	INL	SEC	SIDEF-T/C		35.00	40	H-	7	10-500			1	0
277	UNBRK	LOOP	STEAM	GEN	OUTL	PRI	SIDE	SP	27.00	D	F-	5	10-500			1	0
278	UNBRK	LOOP	STEAM	GEN	OUTL	SHELL	I-T/C		27.00				0-500			1	0
279	UNBRK	LOOP	STEAM	GEN	OUTL	PRI	SIDE	SP	27.00	B	H-	3	20-500			1	0
280	UNBRK	LOOP	STEAM	GEN	OUTL	PRI	SIDE	SP	27.00	G	J-	2	30-500			1	0
281	UNBRK	LOOP	STEAM	GEN	OUTL	TUBE	W-T/C		20.00	144	M-	6	10-500			1	0
282	UNBRK	LOOP	STEAM	GEN	OUTL	PRI	SIDE	SP	15.00	341	F-	8	20-500			1	0
283	UNBRK	LOOP	STEAM	GEN	OUTL	PRI	SIDE	SP	15.00	349	H-	2	20-500			1	0
284	UNBRK	LOOP	STEAM	GEN	OUTL	TUBE	W-T/C		10.00	143	M-	6	10-500			1	0
285	UNBRK	LOOP	STEAM	GEN	OUTL	TUBE	W-T/C		10.00	153	Q-	4	30-500			1	0
286	UNBRK	LOOP	STEAM	GEN	OUTL	SEC	SIDEF-T/C		10.00	47	L-	2	20-500			1	0
287	UNBRK	LOOP	STEAM	GEN	OUTL	PRI	SIDE	SP	10.00	350	F-	8	20-500			1	0
288	UNBRK	LOOP	STEAM	GEN	OUTL	PRI	SIDE	SP	10.00	358	H-	2	20-500			1	0
289	UNBRK	LOOP	STEAM	GEN	OUTL	PRI	SIDE	SP	10.00	353	G-	2	10-500			1	0
290	UNBRK	LOOP	STEAM	GEN	OUTL	TUBE	W-T/C		4.00	142	M-	6	10-500			1	0
291	UNBRK	LOOP	STEAM	GEN	OUTL	TUBE	W-T/C		4.00	152	Q-	4	30-500			1	0
292	UNBRK	LOOP	STEAM	GEN	OUTL	SEC	SIDEF-T/C		4.00	60	R-	5	30-500			1	0
293	UNBRK	LOOP	STEAM	GEN	OUTL	TUBE	W-T/C		2.00	137	K-	1	20-500			1	0
294	UNBRK	LOOP	STEAM	GEN	OUTL	TUBE	W-T/C		2.00	141	M-	6	10-500			1	0
295	UNBRK	LOOP	STEAM	GEN	OUTL	SHELL	I-T/C		35.00				0-500			1	0
296	UNBRK	LOOP	STEAM	GEN	OUTL	TUBE	W-T/C		2.00	151	Q-	4	30-500			1	0
297	UNBRK	LOOP	STEAM	GEN	OUTL	SEC	SIDEF-T/C		2.00	51	N-	5	20-500			1	0
298	UNBRK	LOOP	STEAM	GEN	OUTL	SHELL	W-T/C		27.00				0-500			1	0
299	UNBRK	LOOP	STEAM	GEN	OUTL	PRI	SIDE	SP	2.00	307	G-	4	10-500			1	0
300	UNBRK	LOOP	STEAM	GEN	OUTL	PRI	SIDE	SP	2.00	317	J-	1	30-500			1	0
301	UNBRK	LOOP	STEAM	GEN	OUTL	PRI	SIDE	SP	2.00	304	J-	6	30-500			1	0
302	UNBRK	LOOP	STEAM	GEN	OUTL	TUBE	W-T/C		1.00	136	K-	1	20-500			1	0
303	UNBRK	LOOP	STEAM	GEN	OUTL	TUBE	W-T/C		1.00	140	M-	6	10-500			1	0
304	UNBRK	LOOP	STEAM	GEN	OUTL	TUBE	W-T/C		1.00	146	O-	6	20-500			1	0
305	UNBRK	LOOP	STEAM	GEN	OUTL	TUB.	W-T/C		1.00	150	Q-	4	30-500			1	0
306	UNBRK	LOOP	STEAM	GEN	OUTL	SEC	SIDEF-T/C		1.00	43	L-	2	20-500			1	0
307	UNBRK	LOOP	STEAM	GEN	OUTL	PRI	SIDE	SP	1.00	302	F-	8	20-500			1	0
308	UNBRK	LOOP	STEAM	GEN	OUTL	PRI	SIDE	SP	1.00	319	G-	4	10-500			1	0
309	UNBRK	LOOP	STEAM	GEN	OUTL	SHELL	W-T/C		15.00				0-500			1	0
310	UNBRK	LOOP	STEAM	GEN	OUTL	PRI	SIDE	SP	1.00	303	J-	6	30-500			1	0
311	UNBRK	LOOP	STEAM	GEN	OUTL	SEC	SIDE F-T/C HX INLET						0-500			1	0
312	UNBRK	LOOP	STEAM	GEN	OUTL	SEC	SIDEF-T/C		0.50	42	L-	2	20-500			1	0
313	UNBRK	LOOP	STEAM	GEN	OUTL	SEC	SIDEF-T/C		0.50	56	R-	5	30-500			1	0
314	UNBRK	LOOP	STEAM	GEN	OUTL	TUBE	W-T/C		0.00	148	Q-	4	30-500			1	0
315	UNBRK	LOOP	STEAM	GEN	OUTL	SEC	SIDEF-T/C		0.00	41	L-	2	20-500			1	0
316	UNBRK	LOOP	STEAM	GEN	OUTL	SEC	SIDEF-T/C		0.00	49	N-	5	20-500			1	0
317	UNBRK	LOOP	STEAM	GEN	OUTL	SEC	SIDEF-T/C	HX	INLT				30-500			1	0
318	UNBRK	LOOP	STEAM	GEN	OUTL	PRI	SIDE	SP	0.00	330	F-	8	20-500			1	0
319	UNBRK	LOOP	STEAM	GEN	OUTL	PRI	SIDE	SP	0.00	318	G-	4	10-500			1	0
320	UNBRK	LOOP	STEAM	GEN	OUTL	PRI	SIDE	SP	0.00	305	J-	6	30-500			1	0
321			ACCUM	2			F-T/C						0-500			1	0
322	BRK	LOOP	STEAM	GEN	INL	TUBE	W-T/C		0.25	73	A-	5	*30-500			1	0
323	BRK	LOOP	STEAM	GEN	INL	SHELL	W-T/C		1.00				0-500			1	0
324	BRK	LOOP	STEAM	GEN	INL	TUBE	W-T/C		0.25	48	E-	4	10-500			1	0
325	BRK	LOOP	STEAM	GEN	INL	SEC	SIDEF-T/C		0.25	19F	B-	6	*30-500			1	0
326	BRK	LOOP	STEAM	GEN	INL	SEC	SIDEF-T/C		0.25	7G	D-	5	20-500			1	0
~~327~~	~~BRK~~	~~LOOP~~	~~STEAM~~	~~GEN~~	~~INL~~	~~SEC~~	~~SIDEF-T/C~~		~~0.25~~	~~1A~~	~~F-~~	~~6~~	~~10-500~~			~~1~~	~~0~~
328	BRK	LOOP	STEAM	GEN	INL	TUBE	W-T/C		1.00	54	A-	5	*30-500			1	0
329	BRK	LOOP	STEAM	GEN	INL	TUBE	W-T/C		1.00	46	C-	4	20-500			1	0

TABLE 4-1 (cont)

INSTRUMENTATION CHANNEL LIST FOR FLECHT SEASET
NATURAL CIRCULATION TESTS

330	BRK	LOOP	STEAM	GEN	INL	TUBE	W-T/C	1.00	45	E-	4	10-500	1 0
331	BRK	LOOP	STEAM	GEN	INL	SEC SIDEF	T/C	1.00	20T	B-	6	*30-500	1 0
332	BRK	LOOP	STEAM	GEN	INL	SEC SIDEF	T/C	1.00	5E	D-	5	*20-500	1 0
333	BRK	LOOP	STEAM	GEN	INL	SEC SIDEF	T/C	1.00	11K	F-	6	10-500	1 0
334	BRK	LOOP	STEAM	GEN	INL	PRI SIDE	SP	1.00	105	C-	8	*10-500	1 0
335	BRK	LOOP	STEAM	GEN	INL	PRI SIDE	SP	1.00	113	B-	3	*20-500	1 0
336	BRK	LOOP	STEAM	GEN	INL	PRI SIDE	SP	1.00	112	A-	7	*30-500	1 0
337	BRK	LOOP	STEAM	GEN	INL	TUBE	W-T/C	2.00	53	A-	5	*30-500	1 0
338	BRK	LOOP	STEAM	GEN	INL	TUBE	W-T/C	2.00	70	C-	4	*20-500	1 0
339	BRK	LOOP	STEAM	GEN	INL	TUBE	W-T/C	2.00	49	E-	4	10-500	1 0
340	BRK	LOOP	STEAM	GEN	INL	SEC SIDEF	T/C	2.00	15	B-	6	*30-500	1 0
341	BRK	LOOP	STEAM	GEN	INL	SEC SIDEF	T/C	2.00	24A1	D-	5	*20-500	1 0
342	BRK	LOOP	STEAM	GEN	INL	SEC SIDEF	T/C	2.00	10J	F-	6	10-500	1 0
343	BRK	LOOP	STEAM	GEN	INL	SHELL	I-T/C	1.00				0-500	1 0
344	BRK	LOOP	STEAM	GEN	INL	PRI SIDE	SP	2.00	106	B-	3	20-500	1 0
345	BRK	LOOP	STEAM	GEN	INL	PRI SIDE	SP	2.00	108	A-	7	*30-500	1 0
346	BRK	LOOP	STEAM	GEN	INL	SHELL	W-T/C	15.00				0-500	1 0
347	BRK	LOOP	STEAM	GEN	INL	SHELL	I-T/C	15.00				0-500	1 0
348	BRK	LOOP	STEAM	GEN	INL	TUBE	W-T/C	4.00	24	E-	4	10-500	1 0
349	BRK	LOOP	STEAM	GEN	INL	SEC SIDEF	T/C	4.00	6F	B-	6	*30-500	1 0
350	BRK	LOOP	STEAM	GEN	INL	SEC SIDEF	T/C	4.00	25A2	D-	5	*20-500	1 0
351	BRK	LOOP	STEAM	GEN	INL	SEC SIDEF	T/C	4.00	2B	F-	6	10-500	1 0
352	BRK	LOOP	STEAM	GEN	INL	PRI SIDE	SP	4.00	102	C-	8	*10-500	1 0
353	BRK	LOOP	STEAM	GEN	INL	SHELL	W-T/C	27.00				0-500	1 0
354	BRK	LOOP	STEAM	GEN	INL	PRI SIDE	SP	4.00	119	A-	7	*30-500	1 0
355	BRK	LOOP	STEAM	GEN	INL	TUBE	W-T/C	6.00	10	A-	5	30-500	1 0
356	BRK	LOOP	STEAM	GEN	INL	TUBE	W-T/C	6.00	6	C-	4	*20-500	1 0
357	BRK	LOOP	STEAM	GEN	INL	TUBE	W-T/C	6.00	1	E-	4	10-500	1 0
358	BRK	LOOP	STEAM	GEN	INL	SEC SIDEF	T/C	6.00	43H	B-	6	*30-500	1 0
359	BRK	LOOP	STEAM	GEN	INL	SEC SIDEF	T/C	6.00	44I	D-	5	*20-500	1 0
360	BRK	LOOP	STEAM	GEN	INL	SEC SIDEF	T/C	6.00	47L	F-	6	10-500	1 0
361	BRK	LOOP	STEAM	GEN	INL	SHELL	I-T/C	27.00				0-500	1 0
362	BRK	LOOP	STEAM	GEN	INL	PRI SIDE	SP	6.00	160	B-	3	20-500	1 0
363	BRK	LOOP	STEAM	GEN	INL	SHELL	W-T/C	35.00				0-500	1 0
364	BRK	LOOP	STEAM	GEN	INL	TUBE	W-T/C	10.00	25	A-	5	*30-500	1 0
365	BRK	LOOP	STEAM	GEN	INL	TUBE	W-T/C	10.00	29	C-	4	*20-500	1 0
366	BRK	LOOP	STEAM	GEN	INL	TUBE	W-T/C	10.00	23	E-	4	10-500	1 0
367	BRK	LOOP	STEAM	GEN	INL	SEC SIDEF	T/C	10.00	32G	B-	6	*30-500	1 0
368	BRK	LOOP	STEAM	GEN	INL	SEC SIDEF	T/C	10.00	33H	D-	5	20-500	1 0
369	BRK	LOOP	STEAM	GEN	INL	SEC SIDEF	T/C	10.00	26A	F-	6	*10-500	1 0
370	BRK	LOOP	STEAM	GEN	INL	PRI SIDE	SP	10.00	156	C-	4	*10-500	1 0
371	BRK	LOOP	STEAM	GEN	INL	PRI SIDE	SP	10.00	166	A-	5	30-500	1 0
372	BRK	LOOP	STEAM	GEN	INL	SHELL	I-T/C	35.00				0-500	1 0
373	BRK	LOOP	STEAM	GEN	INL	TUBE	W-T/C	20.00	67	A-	5	*30-500	1 0
374	BRK	LOOP	STEAM	GEN	INL	TUBE	W-T/C	20.00	72	C-	4	20-500	1 0
375	BRK	LOOP	STEAM	GEN	INL	TUBE	W-T/C	20.00	36	E-	4	10-500	1 0
376	BRK	LOOP	STEAM	GEN	INL	SEC SIDEF	T/C	20.00	18R	B-	6	*30-500	1 0
377	BRK	LOOP	STEAM	GEN	INL	SEC SIDEF	T/C	20.00	29D	D-	5	20-500	1 0
378	BRK	LOOP	STEAM	GEN	INL	SEC SIDEF	T/C	20.00	14N	F-	6	10-500	1 0
379	BRK	LOOP	STEAM	GEN	INL	PRI SIDE	SP	15.00	152	C-	4	10-500	1 0
380	BRK	LOOP	STEAM	GEN	INL	PRI SIDE	SP	15.00	146	A-	5	30-500	1 0
381	BRK	LOOP	STEAM	GEN	INL	PRI SIDE	SP	15.00	149	B-	9	20-500	1 0
382	BRK	LOOP	STEAM	GEN	INL	TUBE	W-T/C	27.00	38	A-	5	*30-500	1 0
383	BRK	LOOP	STEAM	GEN	OUTL	SHELL	W-T/C	27.00				0-500	1 0
384	BRK	LOOP	STEAM	GEN	INL	TUBE	W-T/C	27.00	27	E-	4	10-500	1 0
385	BRK	LOOP	STEAM	GEN	INL	SEC SIDEF	T/C	27.00	28C	B-	6	*30-500	1 0
386	BRK	LOOP	STEAM	GEN	INL	SEC SIDEF	T/C	27.00	27B	D-	5	20-500	1 0
387	BRK	LOOP	STEAM	GEN	INL	SEC SIDEF	T/C	27.00	35J	F-	6	10-500	1 0
388	BRK	LOOP	STEAM	GEN	INL	PRI SIDE	SP	27.00	100	C-	4	10-500	1 0
389	BRK	LOOP	STEAM	GEN	INL	PRI SIDE	SP	27.00	K	A-	5	30-500	1 0
390	BRK	LOOP	STEAM	GEN	INL	PRI SIDE	SP	27.00	J	B-	9	*20-500	1 0
391	BRK	LOOP	STEAM	GEN	INL	TUBE	W-T/C	35.00	76	A-	5	30-500	1 0
392	BRK	LOOP	STEAM	GEN	INL	TUBE	W-T/C	35.00	75	C-	4	20-500	1 0
393	BRK	LOOP	STEAM	GEN	INL	TUBE	W-T/C	35.00	33	E-	4	10-500	1 0
394	BRK	LOOP	STEAM	GEN	INL	SEC SIDEF	T/C	35.00	3C	B-	6	30-500	1 0
395	BRK	LOOP	STEAM	GEN	INL	SEC SIDEF	T/C	35.00	3DF	D-	5	20-500	1 0

TABLE 4-1 (cont)

INSTRUMENTATION CHANNEL LIST FOR FLECHT SEASET
NATURAL CIRCULATION TESTS

396	BRK	LOOP	STEAM	GEN	INL	SEC SIDEF-T/C	35.00	4D	F- 6	10-500		1	0
397	BRK	LOOP	STEAM	GEN	OUTL	SHELL I-T/C	27.00			0-500		1	0
398	BRK	LOOP	STEAM	GEN	OUTL	PRI SIDE SP	27.00	L	E- 9	20-500		1	0
399	BRK	LOOP	STEAM	GEN	OUTL	PRI SIDE SP	27.00	N	D-11	30-500		1	0
400	BRK	LOOP	STEAM	GEN	OUTL	TUBE W-T/C	20.00	65	J- 4	20-500		1	0
401	BRK	LOOP	STEAM	GEN	OUTL	TUBE W-T/C	20.00	66	L- 5	*30-500		1	0
402	BRK	LOOP	STEAM	GEN	OUTL	SEC SIDEF-T/C	20.00	16P	G- 2	30-500		1	0
403	BRK	LOOP	STEAM	GEN	OUTL	SEC SIDEF-T/C	20.00	17Q	K- 5	*20-500		1	0
404	BRK	LOOP	STEAM	GEN	OUTL	PRI SIDE SP	15.00	UJ,	D-11	30-500		1	0
405	BRK	LOOP	STEAM	GEN	OUTL	PRI SIDE SP	15.00	150	E- 9	20-500		1	0
406	BRK	LOOP	STEAM	GEN	OUTL	SHELL W-T/C	15.00			0-500		1	0
407	BRK	LOOP	STEAM	GEN	OUTL	TUBE W-T/C	10.00	30	G- 1	30-500		1	0
408	BRK	LOOP	STEAM	GEN	OUTL	TUBE W-T/C	10.00	26	J- 4	*20-500		1	0
409	BRK	LOOP	STEAM	GEN	OUTL	TUBE W-T/C	10.00	31	L- 5	*30-500		1	0
410	BRK	LOOP	STEAM	GEN	OUTL	SEC SIDEF-T/C	10.00	34T	G- 2	30-500		1	0
411	BRK	LOOP	STEAM	GEN	OUTL	SEC SIDEF-T/C	10.00	31F	K- 5	*20-500		1	0
412	BRK	LOOP	STEAM	GEN	OUTL	PRI SIDE SP	10.00	165	E- 9	*20-500		1	0
413	BRK	LOOP	STEAM	GEN	OUTL	PRI SIDE SP	10.00	163	F- 5	30-500		1	0
414	BRK	LOOP	STEAM	GEN	OUTL	PRI SIDE SP	10.00	170	D- 1	30-500		1	0
415	BRK	LOOP	STEAM	GEN	OUTL	TUBE W-T/C	6.00	7	J- 4	*20-500		1	0
416	BRK	LOOP	STEAM	GEN	OUTL	TUBE W-T/C	6.00	8	L- 5	*30-500		1	0
417	BRK	LOOP	STEAM	GEN	OUTL	SEC SIDEF-T/C	6.00	39D	G- 2	30-500		1	0
418	BRK	LOOP	STEAM	GEN	OUTL	SEC SIDEF-T/C	6.00	40E	K- 5	*20-500		1	0
419	BRK	LOOP	STEAM	GEN	OUTL	PRI SIDE SP	6.00	159	F- 7	*30-500		1	0
420	BRK	LOOP	STEAM	GEN	OUTL	PRI SIDE SP	6.00	154	E- 3	20-500		1	0
421	BRK	LOOP	STEAM	GEN	OUTL	TUBE W-T/C	4.00	2	G- 1	30-500		1	0
422	BRK	LOOP	STEAM	GEN	OUTL	SHELL I-T/C	15.00			0-500		1	0
423	BRK	LOOP	STEAM	GEN	OUTL	TUBE W-T/C	4.00	5	L- 5	*30-500		1	0
424	BRK	LOOP	STEAM	GEN	OUTL	SEC SIDEF-T/C	4.00	37B	G- 2	30-500		1	0
425	BRK	LOOP	STEAM	GEN	OUTL	SEC SIDEF-T/C	4.00	38C	K- 5	*20-500		1	0
426	BRK	LOOP	STEAM	GEN	OUTL	PRI SIDE SP	4.00	115	F- 7	*30-500		1	0
427	BRK	LOOP	STEAM	GEN	OUTL	PRI SIDE SP	4.00	104	E- 3	20-500		1	0
428	BRK	LOOP	STEAM	GEN	OUTL	TUBE W-T/C	2.00	61	G- 1	30-500		1	0
429	BRK	LOOP	STEAM	GEN	OUTL	TUBE W-T/C	2.00	52	J- 4	*20-500		1	0
430	BRK	LOOP	STEAM	GEN	OUTL	TUBE W-T/C	2.00	74	L- 5	30-500		1	0
431	BRK	LOOP	STEAM	GEN	OUTL	SEC SIDEF-T/C	2.00	36A	G- 2	*30-500		1	0
432	BRK	LOOP	STEAM	GEN	OUTL	SEC SIDEF-T/C	2.00	13M	K- 5	*20-500		1	0
433	BRK	LOOP	STEAM	GEN	OUTL	PRI SIDE SP	2.00	107	D- 1	30-500		1	0
434	BRK	LOOP	STEAM	GEN	OUTL	TUBE W-T/C	1.00	56	G- 1	30-500		1	0
435	BRK	LOOP	STEAM	GEN	OUTL	TUBE W-T/C	1.00	44	J- 4	*20-500		1	0
436	BRK	LOOP	STEAM	GEN	OUTL	TUBE W-T/C	1.00	43	L- 5	*30-500		1	0
437	BRK	LOOP	STEAM	GEN	OUTL	SEC SIDEF-T/C	1.00	21U	G- 2	30-500		1	0
438	BRK	LOOP	STEAM	GEN	OUTL	SHELL W-T/C	1.00			0-500		1	0
439	BRK	LOOP	STEAM	GEN	OUTL	PRI SIDE SP	1.00	109	F- 7	*30-500		1	0
440	BRK	LOOP	STEAM	GEN	OUTL	PRI SIDE SP	1.00	103	E- 3	20-500		1	0
441	BRK	LOOP	STEAM	GEN	OUTL	PRI SIDE SP	1.00	110	D- 1	30-500		1	0
442	BRK	LOOP	STEAM	GEN	OUTL	TUBE W-T/C	0.25	63	G- 1	30-500		1	0
443	BRK	LOOP	STEAM	GEN	OUTL	TUBE W-T/C	0.25	47	J- 4	20-500		1	0
444	BRK	LOOP	STEAM	GEN	OUTL	TUBE W-T/C	0.25	57	L- 5	*30-500		1	0
445	BRK	LOOP	STEAM	GEN	OUTL	SEC SIDEF-T/C	0.25	22V	G- 2	30-500		1	0
446	BRK	LOOP	STEAM	GEN	OUTL	SEC SIDEF-T/C	0.25	23W	K- 5	*20-500		1	0
447	BRK	LOOP	STEAM	GEN	OUTL	PRI SIDE SP	2.00	111	D-11	*30-500		1	0
448	BRK	LOOP	STEAM	GEN	OUTL	PRI SIDE SP	0.00	114	E- 3	20-500		1	0
449	BRK	LOOP	STEAM	GEN	INL	PLENUM F-T/C				0-500		1	0
450	BRK	LOOP	STEAM	GEN	INL	PLENUM W-T/C				0-500		1	0
451	BRK	LOOP	STEAM	GEN	OUTL	PLENUM F-T/C				0-500		1	0
452	BRK	LOOP	STEAM	GEN	OUTL	PLENUM W-T/C				0-500		1	0
453	BRK	LOOP	STEAM	GEN	OUTL	PLENUM I-T/C				0-500		1	0
454	BRK	LOOP	STEAM	GEN	OUTL	FLANGE W-T/C				0-500		1	0
455	BRK	LOOP	STEAM	GEN	OUTL	FLANGE I-T/C				0-500		1	0
456	BRK	LOOP	STEAM	GEN	INL	FLANGE W-T/C				0-500		1	0
457	BRK	LOOP	STEAM	GEN	INL	FLANGE I-T/C				0-500		1	0
458			XOVER	LEG		F-T/C				0-500		1	0
~~459~~			~~XOVER~~	~~LEG~~		~~W-T/C~~				~~0-500~~		~~1~~	~~0~~
460			XOVER	LEG		I-T/C				0-500		1	0
461			LOWER	PLEN		F-T/C				0-500		1	0

TABLE 4-1 (cont)

INSTRUMENTATION CHANNEL LIST FOR FLECHT SEASET
NATURAL CIRCULATION TESTS

462			LOWER PLEN				W-T/C					0-500		1	0
463			LOWER PLEN				I-T/C					0-500		1	0
464			HOUSING				W-T/C	4.00		90	D	0-500		1	0
465			HOUSING				W-T/C	6.00		135	D	0-500		1	0
466			HOUSING				W-T/C	9.25		135	D	0-500		1	0
467			HOUSING				W-T/C	4.00		90	D	0-500		1	0
468			HOUSING				W-T/C	6.00		135	D	0-500		1	0
469			HOUSING				W-T/C	9.25		135	D	0-500		1	0
470			GRD PLATE				F-T/C					0-500		1	0
471			GRD PLATE				W-T/C					0-500		1	0
472			CORE PLATE				F-T/C					0-500		1	0
473			UPPER PLEN				W-T/C	13.58				0-500		1	0
474			UPPER PLEN				W-T/C	15.23		90	D	0-500		1	0
475			UPPER PLEN				I-T/C	15.23		90	D	0-500		1	0
476			UPPER PLEN				W-T/C	16.00		135	D	0-500		1	0
477			UPPER PLEN				I-T/C	16.00		135	D	0-500		1	0
478			DOWNCOMER				F-T/C	1.00				0-500		1	0
479			DOWNCOMER				W-T/C	8.00				0-500		1	0
480			DOWNCOMER				I-T/C	8.00				0-500		1	0
481			DOWNCOMER				F-T/C	15.83				0-500		1	0
482			DOWNCOMER				W-T/C	15.83				0-500		1	0
483			DOWNCOMER				I-T/C	15.83				0-500		1	0
484	UNBRK	LOOP	STEAM GEN	INL	FLANGE		W-T/C					0-500		1	0
485	UNBRK	LOOP	STEAM GEN	INL	FLANGE		I-T/C					0-500		1	0
486	UNBRK	LOOP	STEAM GEN	OUTL	FLANGE		W-T/C					0-500		1	0
487	UNBRK	LOOP	STEAM GEN	OUTL	FLANGE		I-T/C					0-500		1	0
488			INJECT LIN		INERT GS		F-T/C					0-500		1	0
489			ACCUM 1				F-T/C					0-500		1	0
490			HOUSING				D/P	0.0-1.0				+- 0.5		3	0
491			HOUSING				D/P	1.0-2.0				+- 0.5		3	0
492			HOUSING				D/P	2.00- 3.00				+- 0.5		3	0
493			HOUSING				D/P	3.00- 4.00				+- 0.5		3	0
494			HOUSING				D/P	4.00- 5.00				+- 0.5		3	0
495			HOUSING				D/P	5.00- 6.00				+- 0.5		3	0
496			HOUSING				D/P	6.00- 7.00				+- 0.5		3	0
497			HOUSING				D/P	7.00- 8.00				+- 0.5		3	0
498			HOUSING				D/P	8.00- 9.00				+- 0.5		3	0
499			HOUSING				D/P	9.00-10.00				+- 0.5		3	0
500			HOUSING				D/P	10.00-11.00				+- 0.5		3	0
501			HOUSING				D/P	11.00-12.00				+- 0.5		3	0
502			HOUSING				D/P	0.00-12.00				+- 5.0		3	0
503			HOUSING				D/P	12.00-13.23				+- 0.5		3	0
504			HOUSING				D/P	13.23-13.73				+- 0.5		3	0
505			UPPER PLEN				D/P	13.73-14.23				+- 0.5		3	0
506			UPPER PLEN				D/P	14.23-14.73				+- 0.5		3	0
507			UPPER PLEN				D/P	14.73-15.23				+- 0.5		3	0
508			UPPER PLEN				D/P	15.23-16.00				+- 0.5		3	0
509			UPPER PLEN				D/P	13.23-17.42				+- 0.5		3	0
510			DOWNCOMER				D/P	0.00-16.50				+- 8.0		3	0
511			DOWNCOMER				D/P	16.50-18.92				+- 1.0		3	0
512	UNBRK	LOOP	HOT LEG	INL	PLENUM		D/P					+- 2.0		3	0
513	UNBRK	LOOP	HOT LEG	RISE			D/P					+- 2.0		3	0
514	BRK	LOOP	HOT LEG	INL	PLENUM		D/P					+- 2.0		3	0
515	BRK	LOOP	HOT LEG	RISE			D/P					+- 2.0		3	0
516	UNBRK	LOOP	STEAM GEN	INL	PLENUM		D/P	0.17- 2.94				+- 2.0		3	0
517	UNBRK	LOOP	STEAM GEN	OUTL	PLENUM		D/P	0.17- 2.94				+- 2.0		3	0
518	UNBRK	LOOP	STEAM GEN		PLENUM		D/P	INL- OUTL				+- 1.0		3	0
519	UNBRK	LOOP	STEAM GEN	LEVEL	PRI TUBE		D/P	0.00- 2.00	B- 7			+- 0.5		3	0
520	UNBRK	LOOP	STEAM GEN	LEVEL	PRI TUBE		D/P	2.00- 4.00	B- 7			+- 0.5		3	0
521	UNBRK	LOOP	STEAM GEN	LEVEL	PRI TUBE		D/P	0.00- 2.00	C- 6			+- 0.5		3	0
522	UNBRK	LOOP	STEAM GEN	LEVEL	PRI TUBE		D/P	2.00- 4.00	C 6			+- 0.5		3	0
523	UNBRK	LOOP	STEAM GEN	LEVEL	PRI TUBE		D/P	0.00- 2.00	E- 5			+- 0.5		3	0
524	UNBRK	LOOP	STEAM GEN	LEVEL	PRI TUBE		D/P	2.00- 4.00	E- 5			+- 0.5		3	0
~~525~~	~~UNBRK~~	~~LOOP~~	~~STEAM GEN~~	~~LEVEL~~	~~SEC SIDE~~		~~D/P~~	~~0.00-35.00~~				~~+- 15.0~~		~~3~~	~~0~~
526	BRK	LOOP	STEAM GEN	INL	PLENUM		D/P	0.17- 3.08				+- 2.0		3	0
527	BRK	LOOP	STEAM GEN	OUTL	PLENUM		D/P	0.17- 3.08				+- 2.0		3	0

TABLE 4-1 (cont)

INSTRUMENTATION CHANNEL LIST FOR FLECHT SEASET
NATURAL CIRCULATION TESTS

528	BRK LOOP	STEAM GEN	PLENUM	D/P	INL- OUTL		+- 1.0	3	0
529	BRK LOOP	STEAM GEN LEVEL	PRI TUBE	D/P	0.00- 2.00	B- 6	+- 0.5	3	0
530	BRK LOOP	STEAM GEN LEVEL	PRI TUBE	D/P	2.00- 4.00	B- 6	+- 0.5	3	0
531	BRK LOOP	STEAM GEN LEVEL	SEC SIDE	D/P	0.00-35.00		+- 15.0	3	0
532	UNBRK LOOP	COLD LEG		D/P	OUTL-DOWNC		+- 1.0	3	0
533	UNBRK LOOP	CLD LEG INJ		D/P			+- 0.5	3	0
534	UNBRK LOOP	CLD LEG DOWNCOMER		D/P			+- 1.0	3	0
535		XOVER LEG		D/P			+- 0.5	3	0
536		ACCUM 1	PRESS	PT	21.00		0-200	7	0
537		ACCUM 2	PRESS	PT	13.70		0-200	7	0
538		ACCUM 2	LEVEL	D/P	0.55-13.80		+- 10.0	3	0
539		DOWNCOMER EXT	UPPER PL	D/P			+- 5.0	3	0
540		ACCUM 1	LEVEL	D/P	0.58-20.50		+- 10.0	3	0
541	UNBRK LOOP	STEAM GEN FLOW	SEC ORIF	D/P			+- 1.0	7	0
542	BRK LOOP	STEAM GEN FLOW	SEC ORIF	D/P			+- 1.0	7	0
543	UNBRK LOOP	LOOP SEAL LEVEL	DOWN LEG	D/P			+- 5.0	3	0
544	BRK LOOP	LOOP SEAL LEVEL	DOWN LEG	D/P			+- 5.0	3	0
545		UPPER PLEN	LEVEL	D/P	16.00-17.50		+- 1.0	7	0
546	SYSTEM	UPPER PLEN	PRESS	PT	17.50		0-150	7	0
547		DOWNCOMER EXT		PT	18.92		0-150	7	0
548	UNBRK LOOP	STM GEN OUTL	PLENUM	PT	0.17FT ELEV.		0-150	3	0
549	UNBRK LOOP	STEAM GEN PRESS	SEC SIDE	PT	35.00		0-150	7	0
550	BRK LOOP	STEAM GEN PRESS	SEC SIDE	PT	35.00		0-150	7	0
551		GAS INJ LI	PRESS				0-150	7	0
552	UNBRK LOOP	GAS INJ LI	FLOW HOT LEG	MTR			0-5000	7	0
553	BRK LOOP	GAS INJ LI	FLOW HOT LEG	MTR			0-1000	7	0
554	UNBRK LOOP	STEAM GEN FLW	INSEC SIDE	F-T/C			0-500	1	0
555	UNBRK LOOP	STEAM GEN FLW	OTSEC SIDE	F-T/C			0-500	1	0
556	BRK LOOP	STEAM GEN FLW	INSEC SIDE	F-T/C			0-500	1	0
557	BRK LOOP	STEAM GEN FLW	OTSEC SIDE	F-T/C			0-500	1	0
558	BUNDLE	POWER	PRI A.				0-100	4	0
559	BUNDLE	POWER	REDUNDNT				0-100	4	0
560	BUNDLE	POWER	PRI B.				0-100	4	0
561	BUNDLE	POWER	REDUNDNT				0-100	4	0
562	BUNDLE	POWER	PRI C.				0-100	4	0
563	BUNDLE	POWER	REDUNDNT				0-100	4	0
564		INJ LINE	FLOW BIDIRECT	MTR			.33-2.5	7	0
565	UNBRK LOOP	INJ LINE	FLOW TURBINE	MTR			2-20	7	0
566	UNBRK LOOP	STEAM GEN FLOW	SEC SIDE	PT			0-150	3	0
567	BRK LOOP	STEAM GEN FLOW	SEC SIDE	PT			0-150	3	0
568		GAS INJ	PRESS	PT			0-300	3	0
569	UNBRK LOOP	LIQ FILM	FLOW HOT LEGA	MTR			0-1.0	7	0
570	UNBRK LOOP	LIQ FILM	FLOW HOT LEGB	MTR			0-1.0	7	0
571	BRK LOOP	LIQ FILM	FLOW HOT LEG	MTR			0-1.0	7	0
572	UNBRK LOOP	LIQ FILM	FLOW COLD LEG	MTR			0-1.0	7	0
573	BRK LOOP	LIQ FILM	FLOW COLD LEG	MTR			0-1.0	7	0
574	UNBRK LOOP	LOOP SEAL	FLOW BIDIRECT	MTR			2.5-75.	7	0
575	BRK LOOP	LOOP SEAL	FLOW BIDIRECT	MTR			.9-27.	7	0
576		XOVER LEG	FLOW BIDIRECT	MTR			2.3-230	7	0

*EOS
*EOS
*EOP

4-6. Gas Sampling System

During the gas injection series of tests, a gas sampling/analysis system was used to determine the concentration of helium gas in particular tubes at various elevations. After the system had attained steady state, each of 37 tubes was individually sampled, condensed, and the helium stripped by argon in a stripping column. Each sample was then dried and measured against a pure argon standard for change in conductivity in a GOW-MAC gas analyzer. This process is shown in figure 4-13; the sensor locations are given in table 4-2.

4-7. TEST PROCEDURE

The following is the general procedure used to establish single-phase, two-phase, and reflux natural circulation modes:

(1) The primary system was evacuated, steam-purged, and filled with deaerated water to assure a gas-free system.

(2) The secondary side of the steam generator was filled with water to the 7.62 m (25 ft) level and the backpressure regulator was set to 0.28 MPa (40 psia).

(3) Accumulator 1 was filled about 50 percent, pressurized to 0.97 MPa (140 psia), and valved into the primary system.

(4) The downcomer isolation valve was closed and the pump bypass was opened.

(5) The primary circulation pump was started [about 4.7×10^{-4} m^3/sec (75 gal/min)].

(6) Power was turned on to the bundle (with equal power to each of three zones) and stepped up to 222 kw (total power). (System heatup took about 2 hours.)

(7) When steady state had been attained, the circulation pump was shut off and the downcomer isolation valve was opened. Single-phase natural circulation started within a few minutes.

(8) Secondary level was maintained by adding makeup water into the bottom of the secondary side to replace the water boiled off and vented through the backpressure regulator.

(9) When steady state had been attained, the data scan rates were increased once to every 2 seconds.

(10) With adequate data taken, the pressurizer (accummulator 1) was valved out and mass was removed from the system through a condenser and weighed.

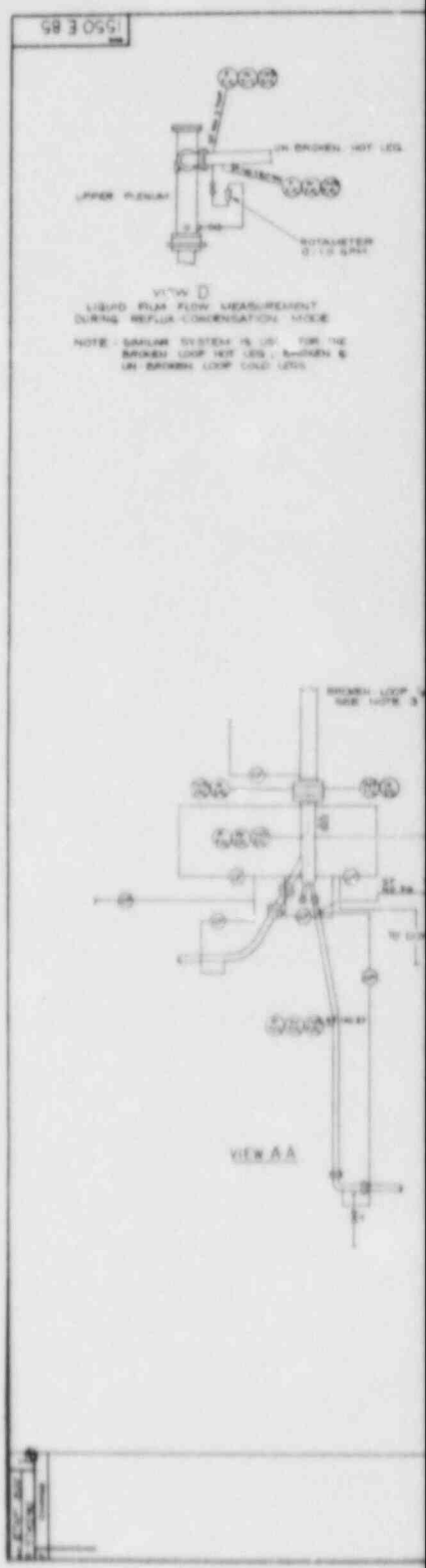
1350 E 85
UNBROKEN HOT LEG
LOWER PLENUM
ROTAMETER
VIEW D
LIQUID FILM FLOW MEASUREMENT
DURING REFLUX-CONDENSATION MODE
NOTE : SIMILAR SYSTEM IS USED FOR THE
BROKEN LOOP HOT LEG , BROKEN &
UN BROKEN LOOP COLD LEGS
VIEW A-A

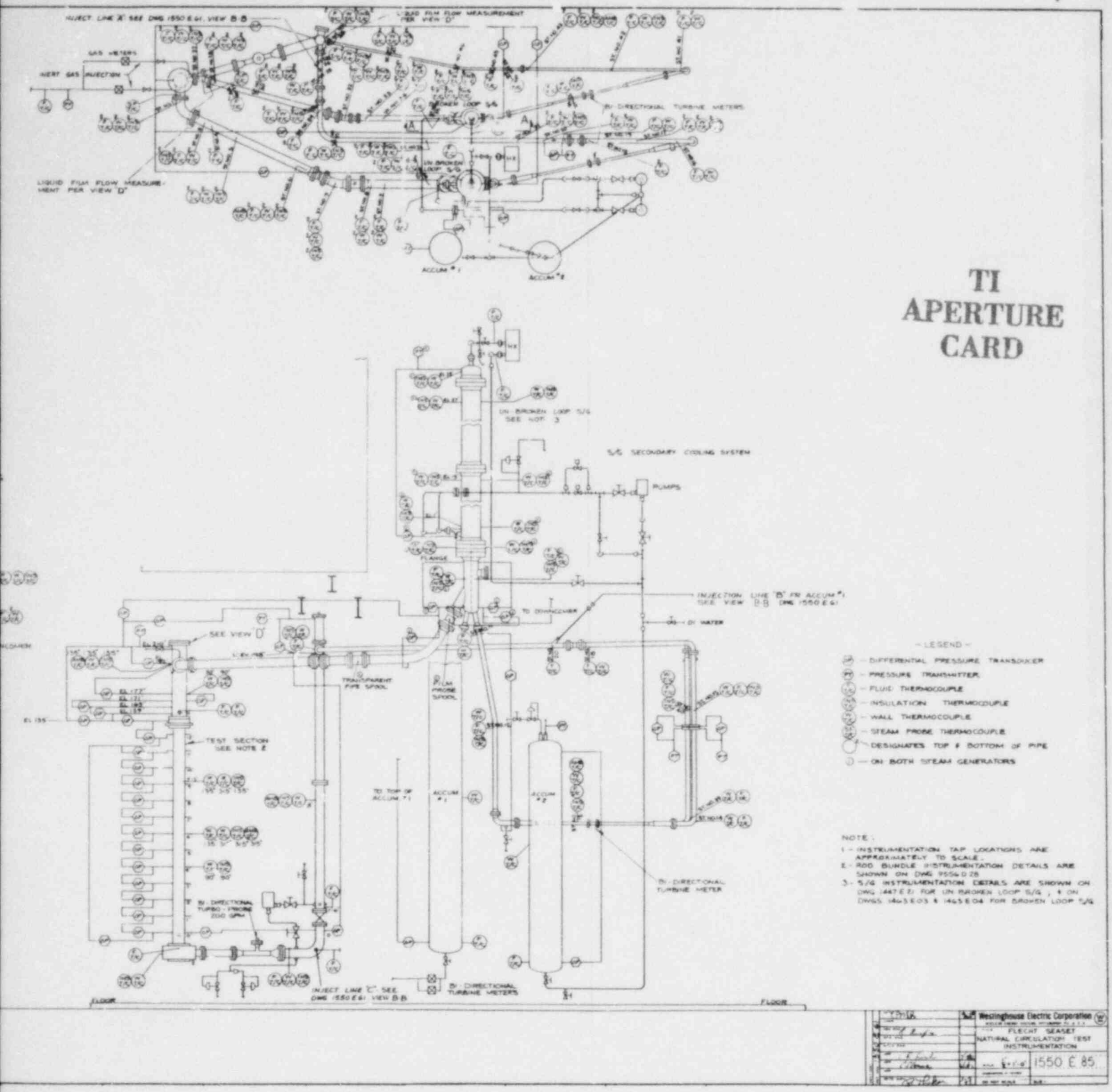

Figure 4-9. FLECHT SEASET Natural Circulation Test Instrumentation

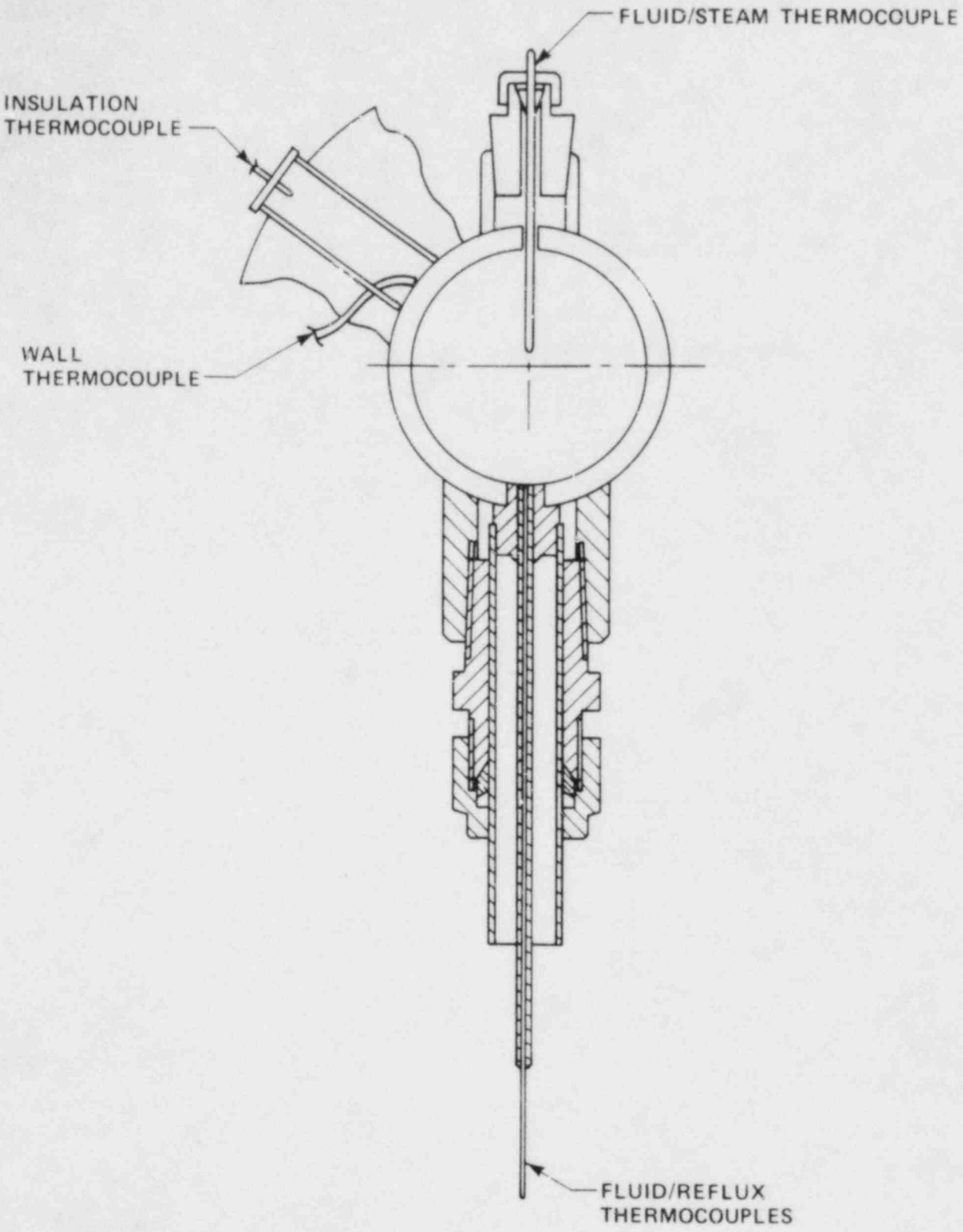

Figure 4-10. FLECHT SEASET Loop Piping Thermocouples

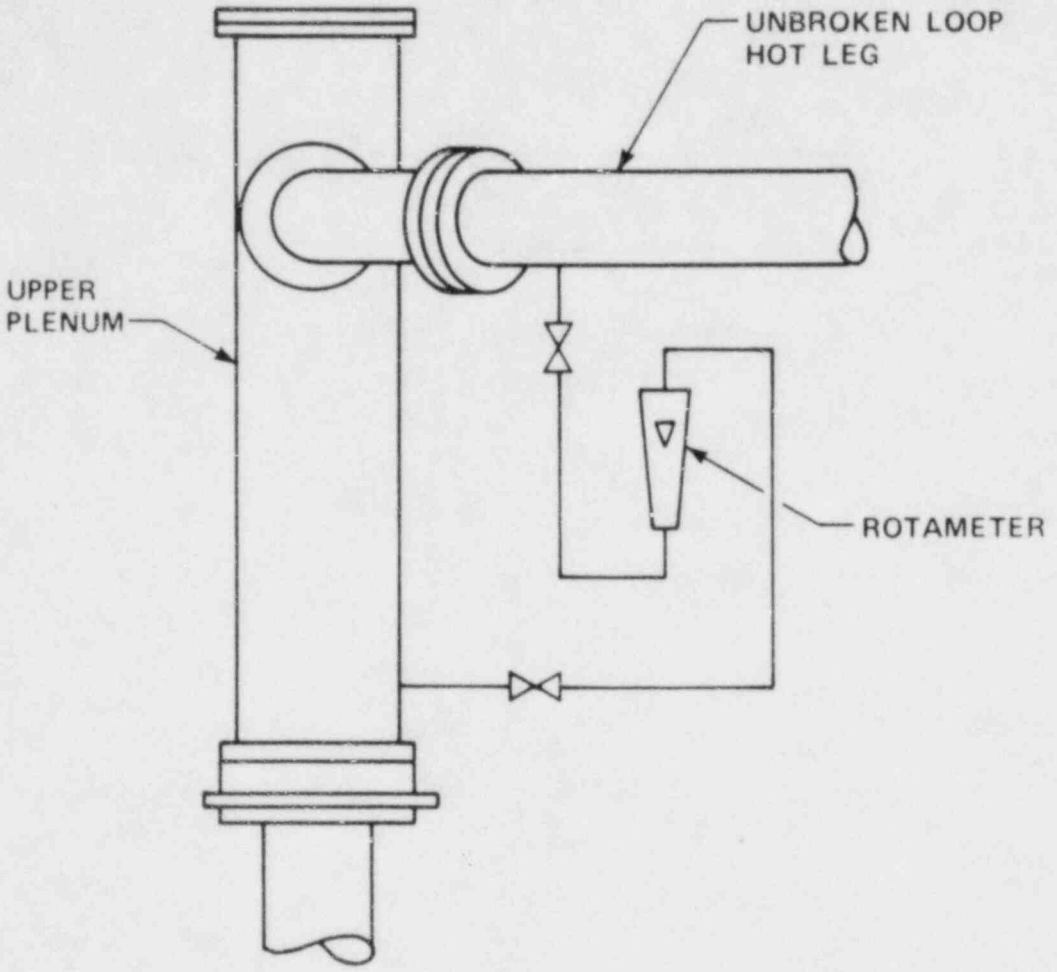

Figure 4-11. FLECHT SEASET Natural Circulation and Reflux Condensation Condensate Flow Measurement System

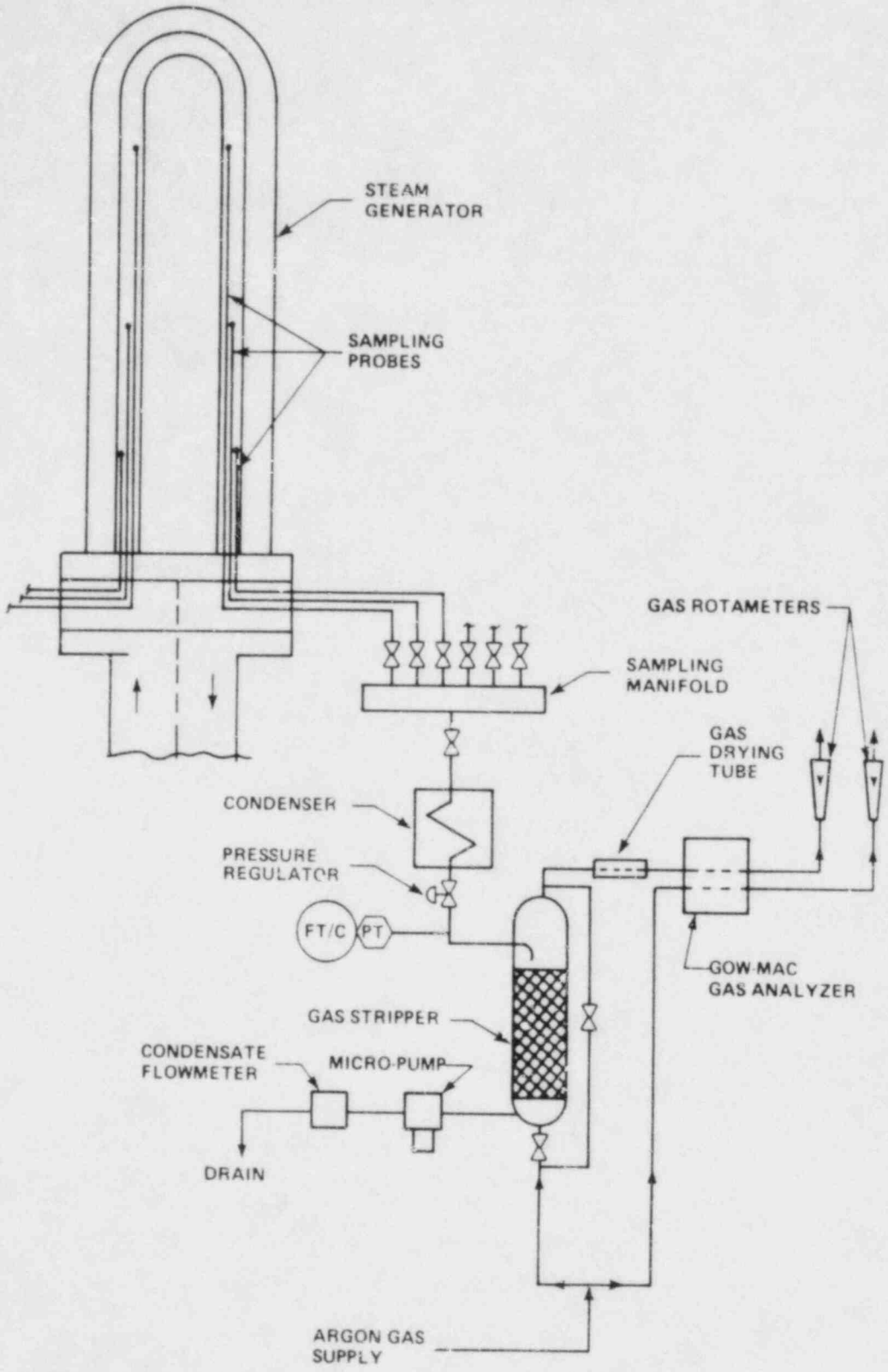

Figure 4-12. FLECHT SEASET Natural Circulation Noncondensible Gas Sampling System

TABLE 4-2

GAS SAMPLING SYSTEM SENSOR LOCATIONS

Sample Valve No.	Location Elevation [m (ft)] and Side[a]	
	Unbroken Loop Steam Generator	Broken Loop Steam Generator
1	8.23 (27)D	8.23 (27)U
2	8.23 (27)D	8.23 (27)U
3	8.23 (27)D	8.23 (27)D
4	8.23 (27)U	8.23 (27)D
5	8.23 (27)U	4.57 (15)U
6	8.23 (27)D	4.57 (15)D
7	8.23 (27)U	4.57 (15)D
8	8.23 (27)U	4.57 (15)U
9	4.57 (15)U[b]	3.05 (10)U
10	4.57 (15)D	3.05 (10)D
11	4.57 (15)U	3.05 (10)U
12	4.57 (15)U	3.05 (10)D
13	4.57 (15)U	1.83 (6)D[b]
14	3.05 (10)U	1.83 (6)D[b]
15	3.05 (10)U	1.83 (6)U
16	3.05 (10)U	1.83 (6)U[b]
17	3.05 (10)D[b]	
18	3.05 (10)U	
19	1.83 (6)U	
20	1.83 (6)U	
21	1.83 (6)U	

a. U - Uphill side
   D - Downhill side

b. Defective probe

(11) Drains were conducted in 18 kg (40 lb) increments, allowing approximately 15 minutes between each for the system to stabilize.

(12) When maximum two-phase flow was observed, drains were stopped and observation and data collection were conducted.

(13) Further draining was then conducted until all flow stopped in the turbine meters. This was determined to be the reflux mode of natural circulation.

(14) Further data were collected and observations made, after which the system was refilled from one of the accumulators with preheated water after shutting off the power.

Depending on the test matrix requirements, different operations were performed after steady-state conditions had been attained.

4-8. POWER CONTROL SYSTEM DESCRIPTION

The natural circulation test facility power control system consists of a main control cabinet and three water-cooled silicon-controlled rectifier (SCR) control cabinets. Each SCR unit is rated at 2000 amperes at 480/277 volts. Extensive monitoring and control capabilities have been incorporated into each unit. Both primary and redundant metering circuits are inherent to each of the three units.

The power demand signal may be fed to the SCRs by one of three means: a manual potentiometer located on the control cabinet, a momentary switch which increments the demand signal by a predetermined value, or directly from the computer. The units may also be operated in several feedback modes. In the open loop mode, instantaneous response is obtained; however, the output may not remain constant. In the closed loop mode, the feedback signal is proportional to either the power, the voltage, or the current. For natural circulation testing, closed loop voltage feedback was used.

Protection circuits built into the units provided an RMS overcurrent trip, instantaneous current trip, high-temperature SCR trip, and a water flow trip (for SCR protection). The RMS overcurrent trip and instantaneous trip will shut down the power controller within one-half cycle of line voltage.

Measurement of power is achieved by monitoring the voltage across the load and the current through the load. Each output is attenuated, converted to an RMS value, and scaled to its respective readout device. The actual power output is a result of a multiplier module (E x I). The output of this module is proportional to the instantaneous power consumed by the load. Additional stages also provide a scaled average power and scaled instantaneous power output.

4-9. DATA ACQUISITION SYSTEM

The data collection system for the FLECHT SEASET natural circulation test facility consisted of a Systems Engineering Laboratory (SEL) computer, a 600 lpm line printer, a nine-track magnetic tape unit, and signal processing equipment. The components which made up the complete computerized system are described below:

Manufacturer	Description
Systems Engineering Laboratory	SEL 32/77 high performance 32-bit computing system consisting of a 1 megabyte, 600 nsec MOS memory
Control Data Corporation	Single 80-megabyte disk processor subsystem with a maximum data transfer rate of 1.2 MB/sec
Pertec Corporation	Single 75 ips, 800/1600 bpi, 9-track magnetic tape transport system
Data Products	600 lpm, 136-column line printer with a 64-character set
Computer Products	RTP 7400 series low-level analog input system consisting of 576 input channels, a 10 vdc analog output system, and digital input and output capabilities
Tektronix	Model 4014 display terminal capable of providing alphanumeric communications and graphics
Tektronix	Model 4611 hard copy unit used in conjunction with the display terminal
Lear Seigler	Model ADM-3A display terminal

The natural circulation test software consisted of several primary programs or tasks and numerous subtasks. The following list provides a brief description of each task and a list of subtasks.

- NCDACP.P - The main data acquisition program; performs three important functions. First, it monitors all 576 analog input channels, which represent system temperatures, pressures, flows, and power levels, and stores these data on disk for retrieval at a later time. Second, it compares designated input channel data with predetermined limits and initiates alarms and shutdown procedures. Third, it simultaneously controls valves and bundle power during testing.

- NCPRNT.P - Lists run data on the line printer or display terminal or both at preselected intervals. Data may also be displayed in raw data format, millivolts, or engineering units.

- SCAN.A - Scans and displays up to eight channels of information every 3 seconds on the display terminal

- HIST - Samples designated channels and displays millivolt data in a histogram format

- HISTA - Same as HIST program except that millivolt data are displayed in engineering units

- ZEROES.A - Samples transducer channels during static loop conditions and places data placed into a calibration file

- CALIBR.A - A disk file which contains all calibration information for DP cells, PT cells, flowmeters, and power channels

- ORIFICE.B - A disk file containing orifice plate sizes and constant values

- PWTABL.D - A disk file containing a power-versus-time table providing an analog output signal to the power controllers

- CHANTABL - A disk file which provides a comprehensive listing of all data channels, a brief description, gain code information, and conversion codes

- DASTP.P - Generates a data tape for data reduction purposes

The following are subtasks used during testing:

- DASCLK.P
- DASSCN.P
- DASWTD.P

- o NCCALC.P
- o DASERR.P
- o 5XXXX.RT
- o 5XXXX.DA

Before a test was actually run, certain table changes were sometimes necessary. The appropriate file was initialized and completed per engineering direction, with a form must be filled out prior to testing (figure 4-14).

While the loop facility remained at static conditions, all transducer outputs were be sampled and read into a calibration file. This file was used during and after testing to provide necessary information for the conversion and printout to engineering units.

Once the data acquisition and control program had been initialized, the computer requested various responses by the computer operator. The computer dialog is as follows:

NATURAL CIRCULATION TEST
COMPUTER DIALOG
NCDACP.P

1. _____ Run length (in seconds)
2. _____ Scan delta (in seconds)
3. _____ Print interval (in seconds)
4. _____ Disk write interval (in seconds)
5. _____ Run number
6. _____ Delete previous run data
7. _____ Maximum rod temperature (150°F-2500°F)
8. _____ Critical rod temperature (150°F-2500°F)
9. _____ Initial power (0.0-10.0 volts)
10. _____ Power step (0.0-10.0 volts)
11. _____ Maximum system pressure (0.0-150 psia)
12. _____ System pressure alarm (0.0-150 psia)
13. _____ Injection flow
14. _____ Remote CRT
    _____ Channels

NATURAL CIRCULATION TEST

COMPUTER TABLE CHANGES

	Power Table		Flow Table	
	Time	Volts	Time	Volts
1.				
2.				
3.				
4.				
5.				
6.				
7.				
8.				
9.				
10.				
11.				
12.				

CHANNEL ASSIGNMENT TABLE CHANGES (Y/N) - List if (Y).

	Channel No.	Change
1.		
2.		
3.		
4.		
5.		
6.		
7.		
8.		
9.		
10.		

Figure 4-13. Natural Circulation Test Computer Table Change Form

When all systems were ready, the loop operator began the test by depressing the computer start button. The test began and the computer maintained complete control if desired. All input channels were recorded on disk, limits were maintained, data were displayed, and analog outputs were supplied.

The test could be terminated for any one of the following reasons:

- o Maximum run duration
- o Manual stop (loop operator)
- o Manual stop (computer operator)
- o Multiplexor failure
- o Software error
- o Computer power failure
- o Overtemperature condition
- o Overpressure condition

After test completion, a data reduction tape was generated which was compatible with the computer system at the Nuclear Center.

In addition to the computer system, analog strip-chart recorders were used periodically during heatup and testing by the loop operators and test director. For visual measurements, the recorders feature 11-step signal attenuation, 0.4-second full-scale response, variable chart speed, and $\pm$ 0.25 percent accuracy. The recorders measured temperatures, pressures, flows, levels, and power.

4-10. PROBLEMS AND CORRECTIVE ACTIONS

Most problems encountered during testing stemmed from reliability of equipment -- specifically turbine meters, computer, and DP cells.

The turbine meters in the loop seal piping experienced broken shafts on more than one occasion. Because it was believed that swaying of the pipes was a contributing factor, these pipes were supported by constraints and no further problems were experienced. There were also problems with the standard

pickoffs supplied with the meters. Even though rated for 149°C (300°F) they operated erroneously at 127°F to 138°C (260°F to 280°F). As a result, correcting high-temperature pickoffs were installed; this remedied the problem.

Since the computer system was entirely new, frequent debugging was necessary. However, once the debugging had been completed, it gave satisfactory performance.

A few of the DP cells used on the facility failed in the course of testing and were replaced. This was due mostly to the age of the units used.

The other main problem that occurred was related to the size of the steam generators relative to the test section heat input. Because of this disparity, the generators supplied too great a heat sink while the heat exchanger was in use. The solution was to run the secondary side boiling at a decreased elevation [7.62 versus 10.67 m (25 versus 35 ft when full] and reduced pressure [0.28 versus 0.69 MPa (40 psia versus 100 psia)], supplying makeup water to replace that which boiled off. This system worked well and was used for all of the matrix tests.

SECTION 5
NATURAL CIRCULATION CHARACTERISTICS

5-1. INTRODUCTION

Previous experimental programs[1,2,3] have established that there are three basic modes of natural circulation cooling: single-phase, two-phase, and reflux condensation modes. The mode in which a specific system will operate is primarily determined by core power, secondary side heat sink capability, and primary mass inventory. In this investigation, the three basic modes were established by maintaining the core power and secondary side heat sinks at constant values, while the primary system mass inventory was varied. This section provides a brief discussion of the test procedure, followed by detailed discussions of the observed phenomena associated with single-phase, two-phase, and reflux condensation natural circulation cooling modes. The discussions are limited, however, to the overall system behavior and stability. Detailed discussions of steam generator heat transfer behavior in each of these modes are presented in section 6.

Discussion of the parametric effects tests is also include in this section.

5-2. TEST PROCEDURE

The test was begun from a liquid-solid forced circulation cooling mode with the pressurizer valved in to the primary to maintain a primary pressure of 0.97 MPa (140 psi). Single-phase natural circulation was established after a

---

1. Loomis, G. G. and Soda, K., "Results of the Semiscale Mod-2A Natural Circulation Experiments," NUREG-CR-2335, September 1982.

2. Krang, k. L., et al., "Decay Heat Removal Experiments in a UTSG Two-Loop Test Facility," EPRI NP-2621, September 1982.

3. Mandl, R. M. and Weiss, P. A., "PKL Tests on Energy Transfer Mechanisms During Small Break LOCAs," Nuclear Safety 23, No. 2, March-April 1982.

short flow coastdown, when the circulation pump was shut down. Two-phase and reflux condensation modes of natural circulation were subsequently established by isolating the pressurizer and draining mass from the bottom of the downcomer.

Rod bundle power was maintained at a nominal value of 222.4 kw (2 percent scaled PWR power) during the course of the test. An effort was made to maintain the heat sink capability at a constant value throughout the test by operating the secondary in a feed-and-bleed pool boiling mode with a constant collapsed liquid level of 7.62 m (25 ft) and a regulated pressure of 0.28 MPa (40 psia). The collapsed liquid level criterion fixed the wetted surface area on the outside of the inverted U-tubes and, hence, fixed the effective heat transfer area. By regulating the secondary side pressure to 0.28 MPa (40 psia), the heat sink temperature was ideally fixed. (Feedwater subcooling at the tubesheet complicated this assumption, the implications of which are discussed in section 6.)

5-3. SINGLE-PHASE NATURAL CIRCULATION

During single-phase natural circulation, the decay heat was removed from the rod bundle and transferred to the secondary side by convection. The convective flow occurred naturally as a result of the temperature gradient experienced by the primary fluid as it circulated through the loop. Figure 5-1 is a schematic diagram of the FLECHT SEASET natural circulation facility and also shows the flow and temperature distribution typical of single-phase natural circulation. Fluid in the uphill side of the system (rod bundle, upper plenum, hot legs, and uphill sides of the steam generators) of the system was hotter and, hence, less dense than fluid in the relatively colder downhill side of the system (downhill sides of the steam generators, loop seals, cold legs, and downcomer). The resulting density gradient between the uphill and downhill sides of the system created a gravitational force imbalance that drove the flow through the system. A typical single-phase natural circulation mass flow rate through the core was 1.47 kg/sec (3.25 lbm/sec), with a flow split between the intact and broken loop of 3.1:1. This measured flow split differed by only 3 percent from the ideal ratio of 3:1.

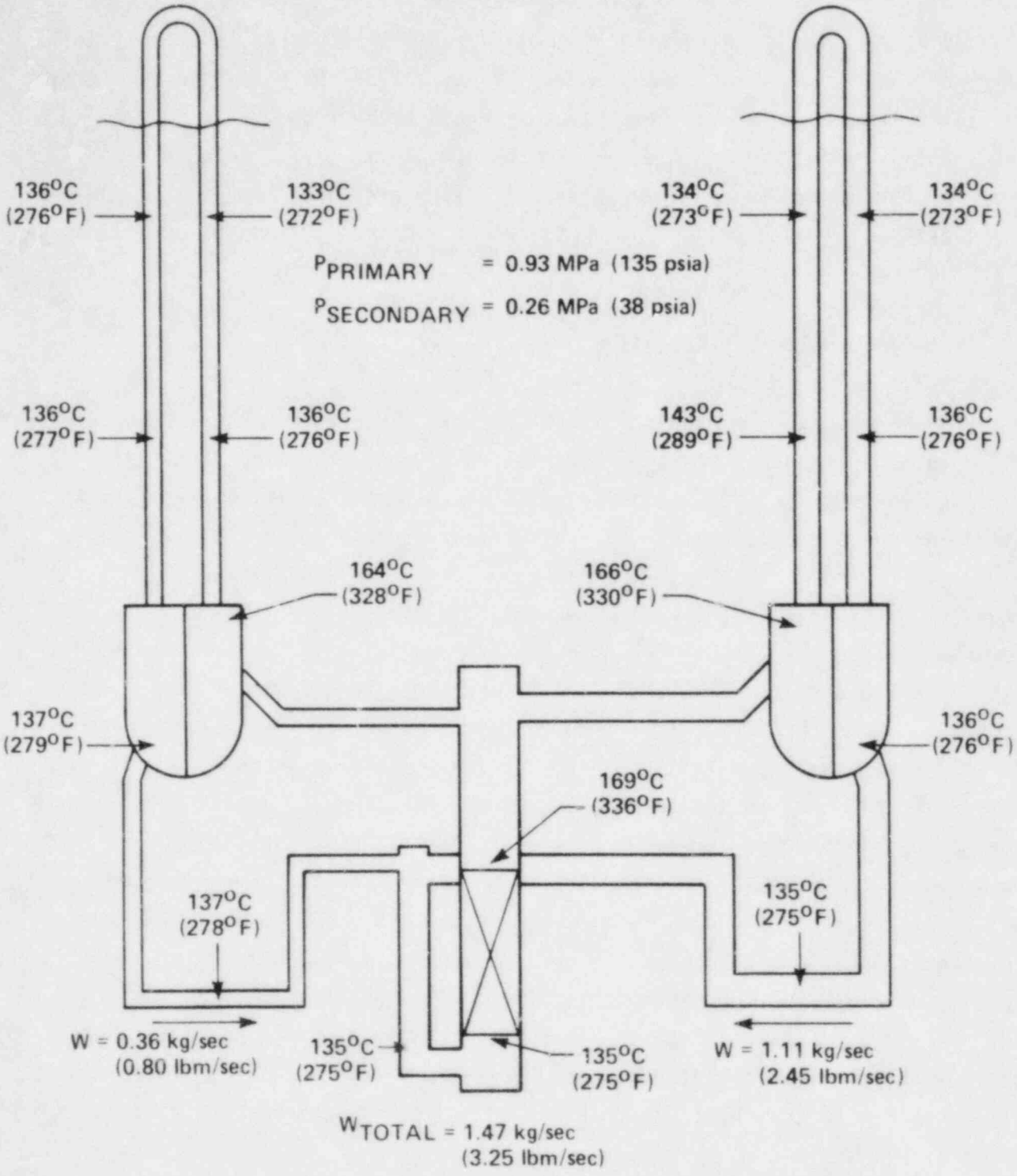

Figure 5-1. Temperature and Mass Flow Distribution During Single-Phase Natural Circulation

The temperature distribution shown in figure 5-1 indicates that most of the rod bundle's energy was transferred by convection to the secondary side in the lower elevations of the uphill side of both steam generators. Primary fluid on the downhill side of the U-tubes, however, increased in temperature slightly as a result of a relatively small amount of secondary-to-primary heat transfer. The reverse heat transfer was the result of the increased secondary side saturation temperature encountered by the primary fluid as it traversed the downhill portion of the U-tube. The saturation temperature increased as a result of the secondary side hydrostatic pressure gradient. The single-phase natural circulation steam generator heat transfer is discussed in more detail in section 6.

5-4. TWO-PHASE NATURAL CIRCULATION

In two-phase natural circulation, the decay heat was transported from the rod bundle to the secondary side by a combination of convection, boiling, and condensation heat transfer mechanisms. The makeup of the system may be described in general terms as follows. A subcooled single-phase fluid entered the bottom of the core through the downcomer. As the single-phase fluid flowed up into the rod bundle, its subcooling diminished as it removed heat from the heater rods by pure convection. At some point in the rod bundle, the subcooling vanished and the single-phase flow made the transition to a two-phase co-current flow, which removed the remainder of the heat from the rod bundle by convective boiling. The reverse process occurred as the decay heat was transferred to the secondary side. A saturated two-phase flow entered the steam generator U-tubes through the hot legs. As the two-phase fluid flowed co-currently in the U-tubes, the void fraction diminished as heat was transferred to the secondary by condensation. At some point in the steam generator U-tube, the void fraction became zero and the flow made the transition to a saturated single-phase flow. The interface between the single-phase and two-phase regions in the steam generator was dependent on the mass inventory. The saturated single-phase flow became subcooled as the remainder of the decay heat was transferred to the secondary by convection.

The basic system behavior associated with two-phase natural circulation may be summarized by figure 5-2. It should first be noted that two-phase natural

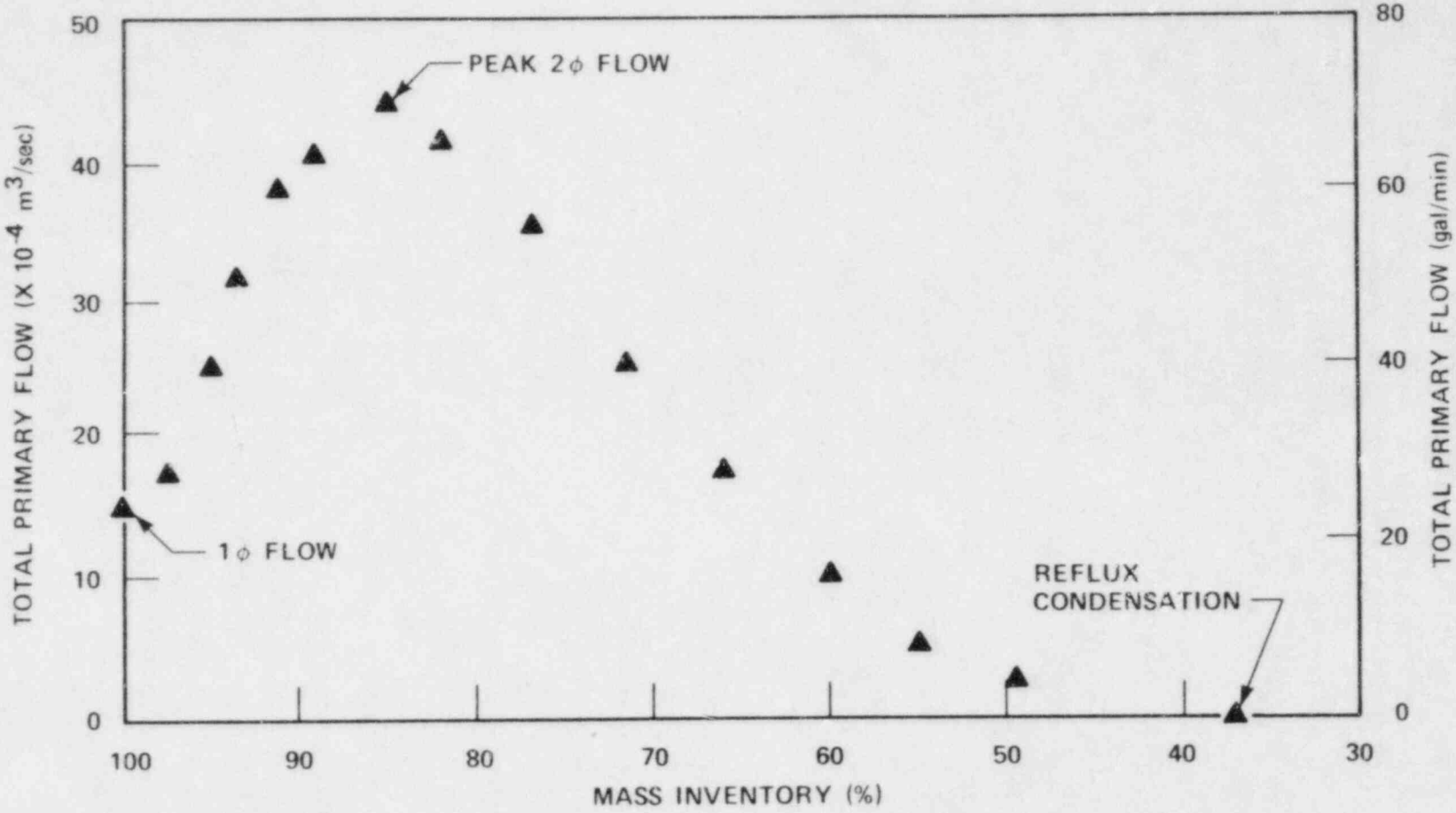

Figure 5-2. Natural Circulation Flow Rate as a Function of Primary System Mass Inventory

circulation cannot be characterized by a specific mass inventory or thermal-hydraulic state, but is a mode of cooling that encompasses a broad range of mass inventories, pressures, flows, and temperatures. The upper bound of the two-phase region was defined by the 100-percent mass inventory case, which corresponded to single-phase natural circulation. The lower bound of the two-phase natural circulation region occurred at the mass inventory associated with the transition to reflux condensation. In this investigation, that transition occurred at a mass inventory of approximately 38 percent.

Figure 5-2 shows that, as mass inventory was removed, the system pressure decayed in an exponential fashion. The flow through the core, however, increased significantly during the early phases of the mass removal and reached a peak value at approximately 84-percent mass inventory. This peak condition is known as the peak two-phase flow condition. Any further reduction in mass inventory resulted in a reduction in mass flow through the rod bundle. The net mass flow became zero as the system made the transition into the reflux condensation mode of cooling.

The detailed discussion of two-phase natural circulation that follows is divided into two parts. The first part deals with the transition from single-phase to two-phase peak flow; the second part deals with the transition from two-phase peak flow to reflux condensation.

5-5. Single-Phase to Two-Phase Peak Flow Transition

The system's behavior in this two-phase natural circulation region is documented in figures 5-3 through 5-51. Most of these figures are discussed below; all are included for completeness. The transition from single-phase to two-phase natural circulation was made by removing mass from the primary system. The mass inventory as a function of time is shown in figure 5-3. The primary pressure responded to this mass reduction by decaying in an exponential fashion (figure 5-7). It should be noted that the initial pressure decrease from 0.931 to 0.717 MPa (135 to 104 psia) was the result of the pressurizer being valved out of the primary system. Any pressure decrease beyond this point was the result of removal of mass from the bottom of the downcomer. Figure 5-3 accounts only for mass being removed from the bottom of the downcomer.

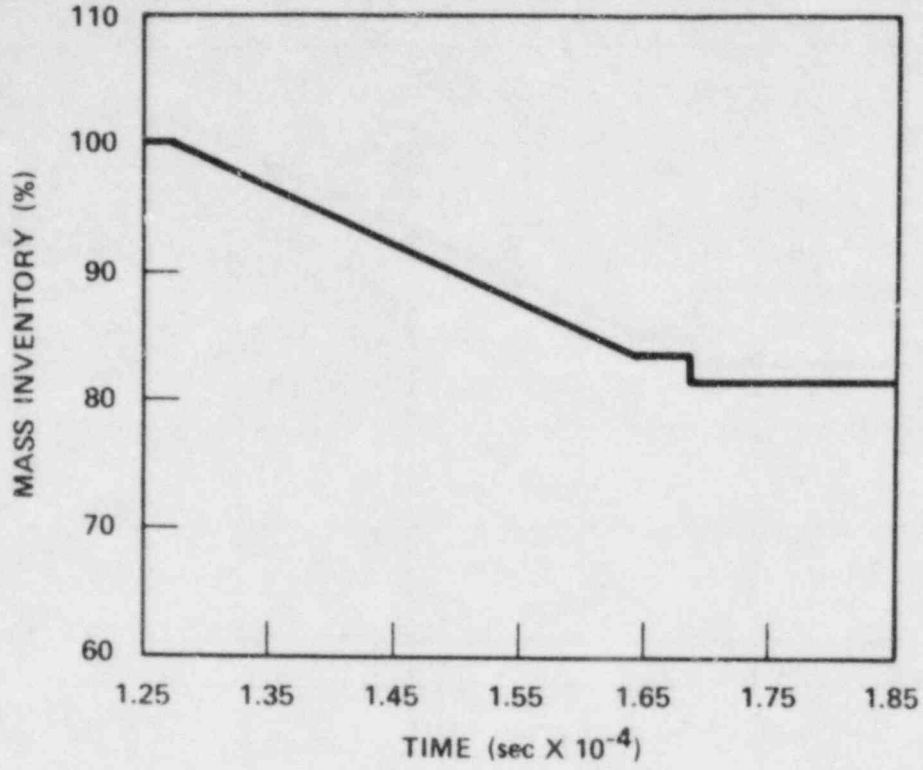

Figure 5-3. Mass Inventory as a Function of Time (12,500-17,800 sec)

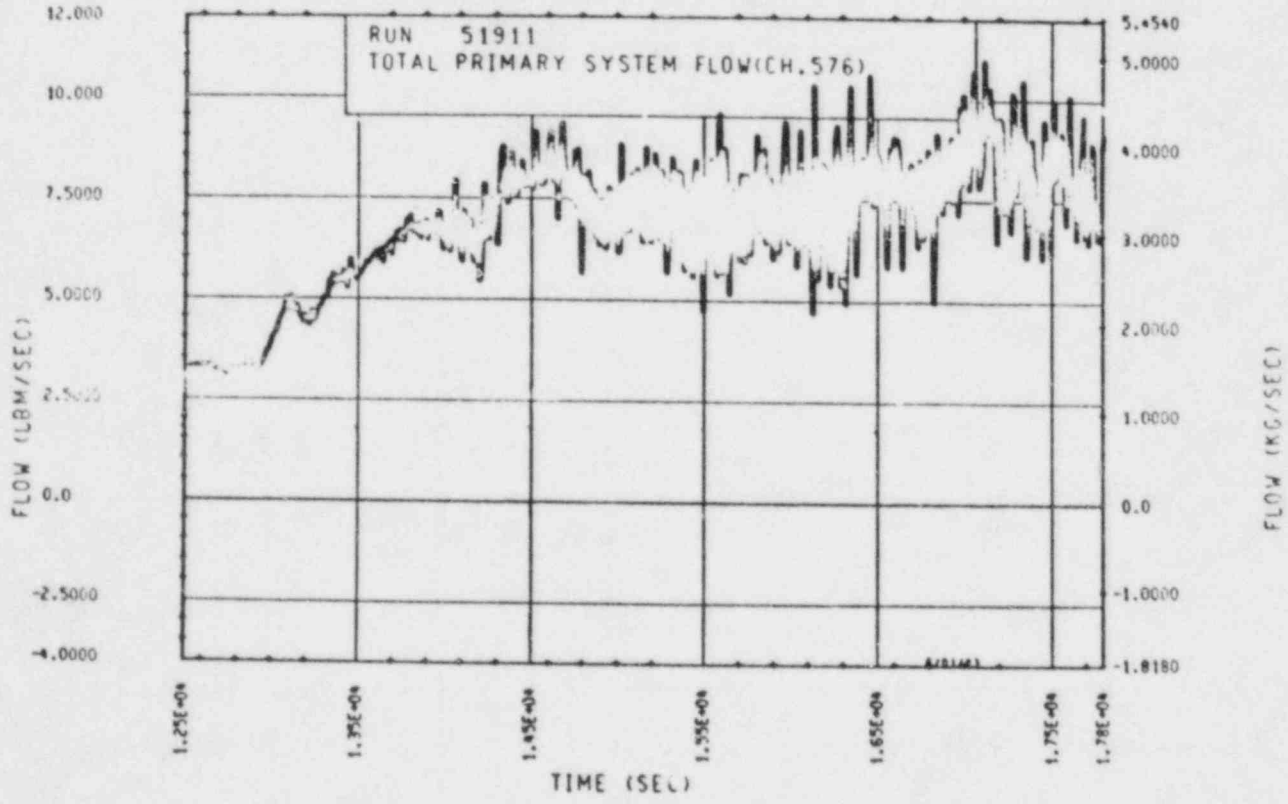

Figure 5-4. Mass Flow Rate Through Heater Rod Bundle (12,500-17,800 sec)

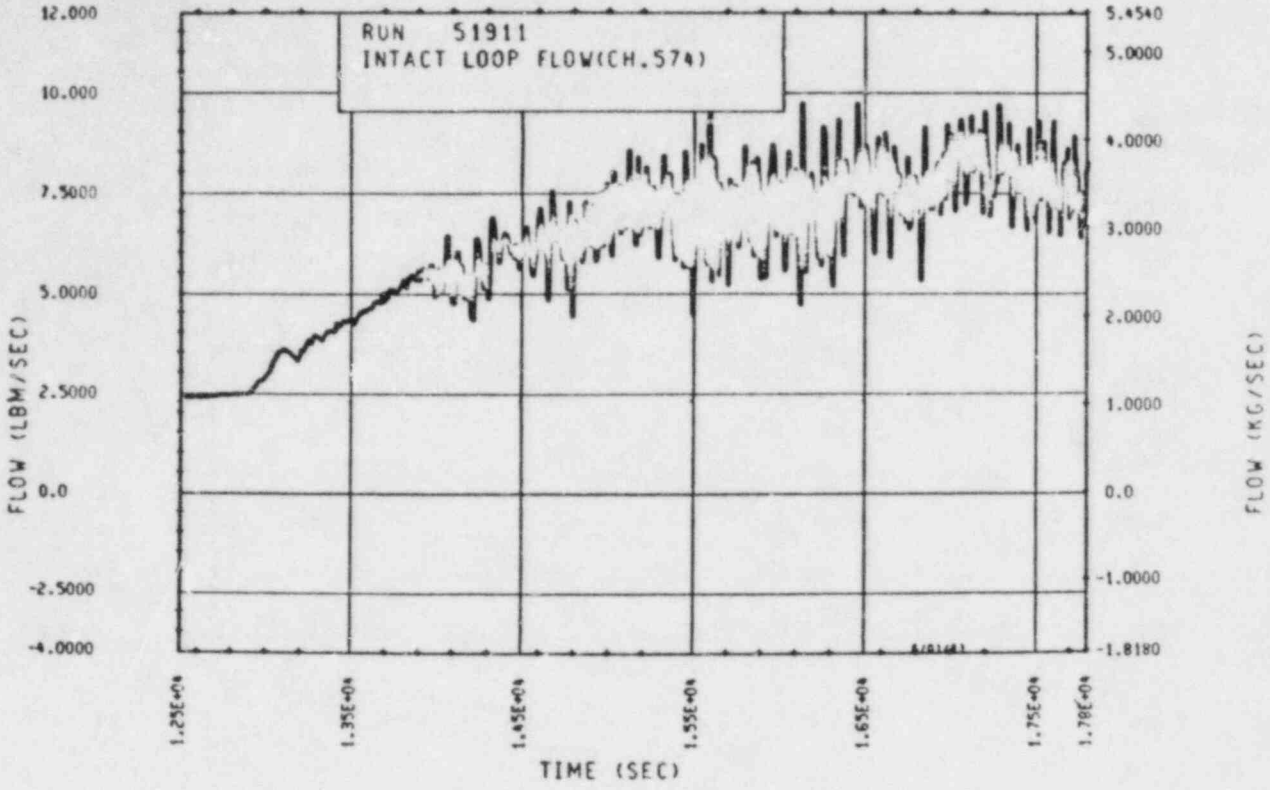

Figure 5-5. Mass Flow Rate Through Unbroken Loop (12 500-17,800 sec)

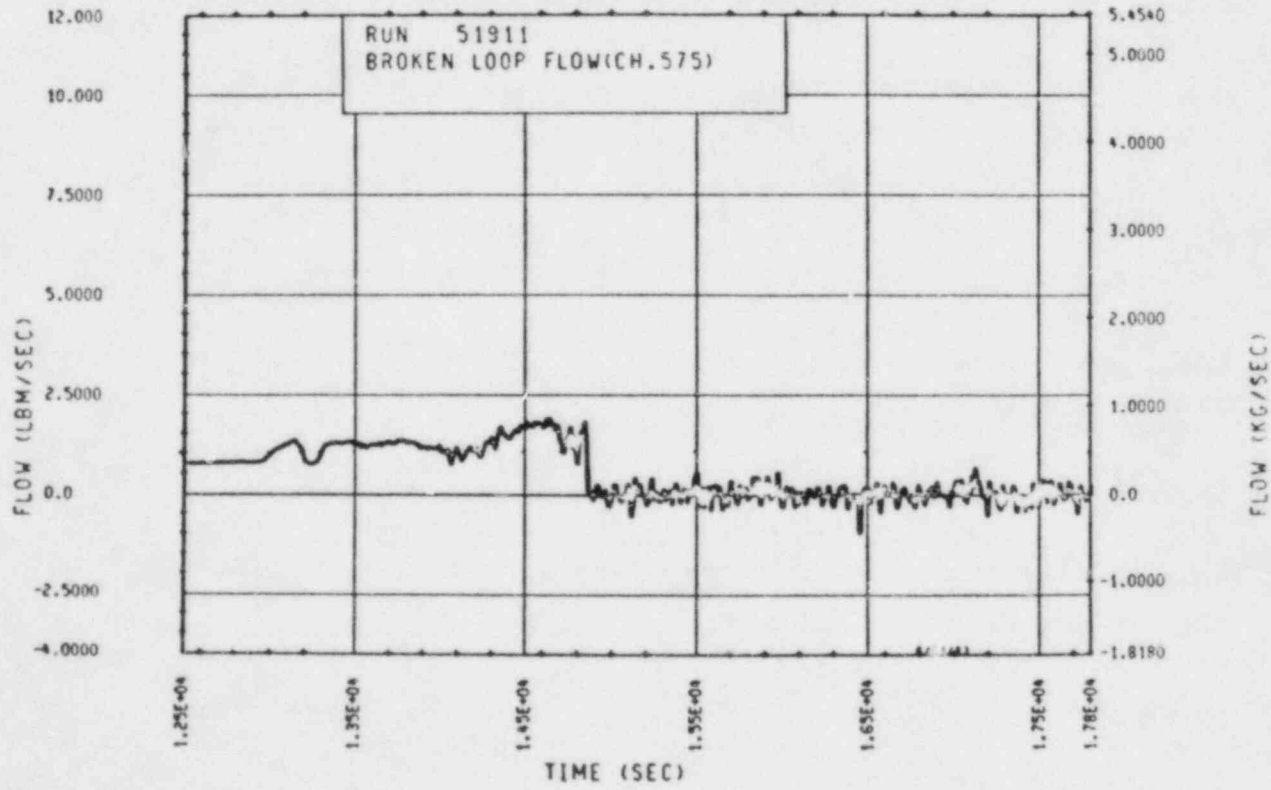

Figure 5-6. Mass Flow Rate Through Broken Loop (12,500-17,800 sec)

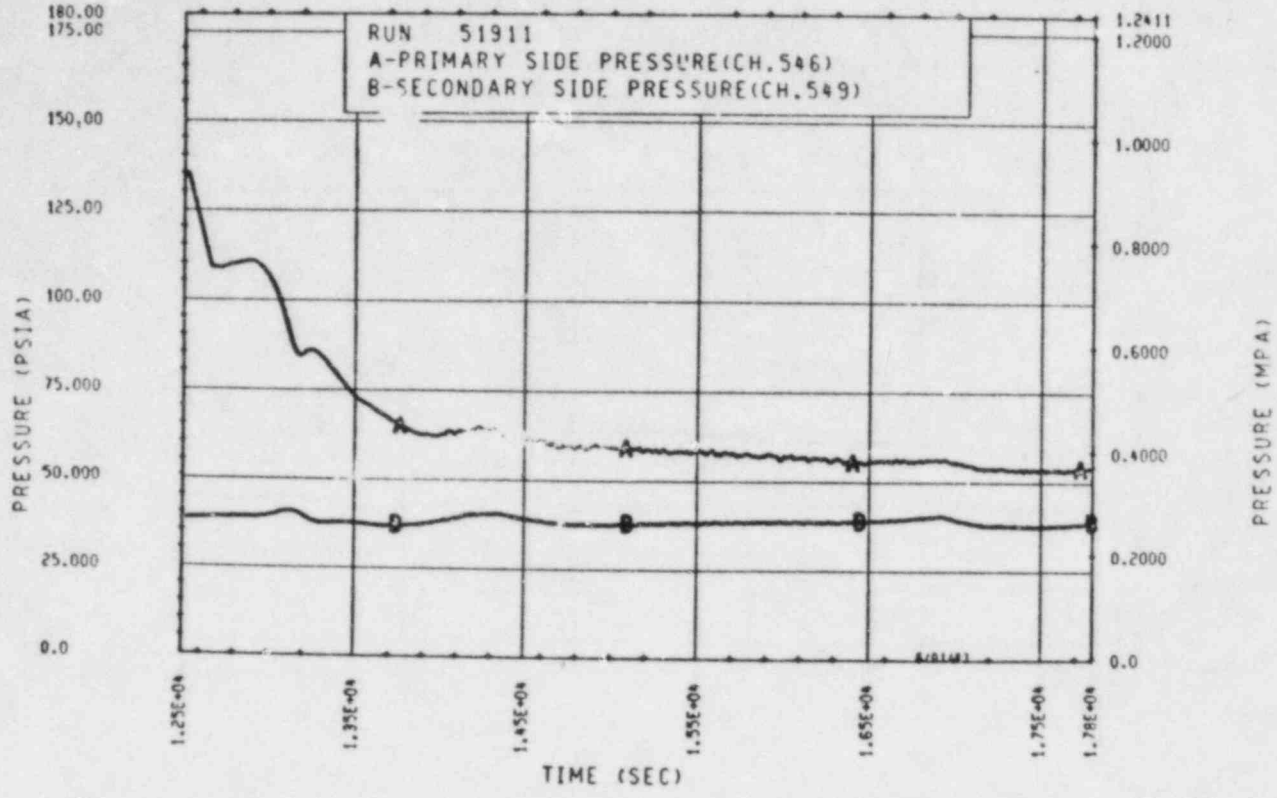

Figure 5-7. Primary and Secondary System Pressure (12,500-17,800 sec)

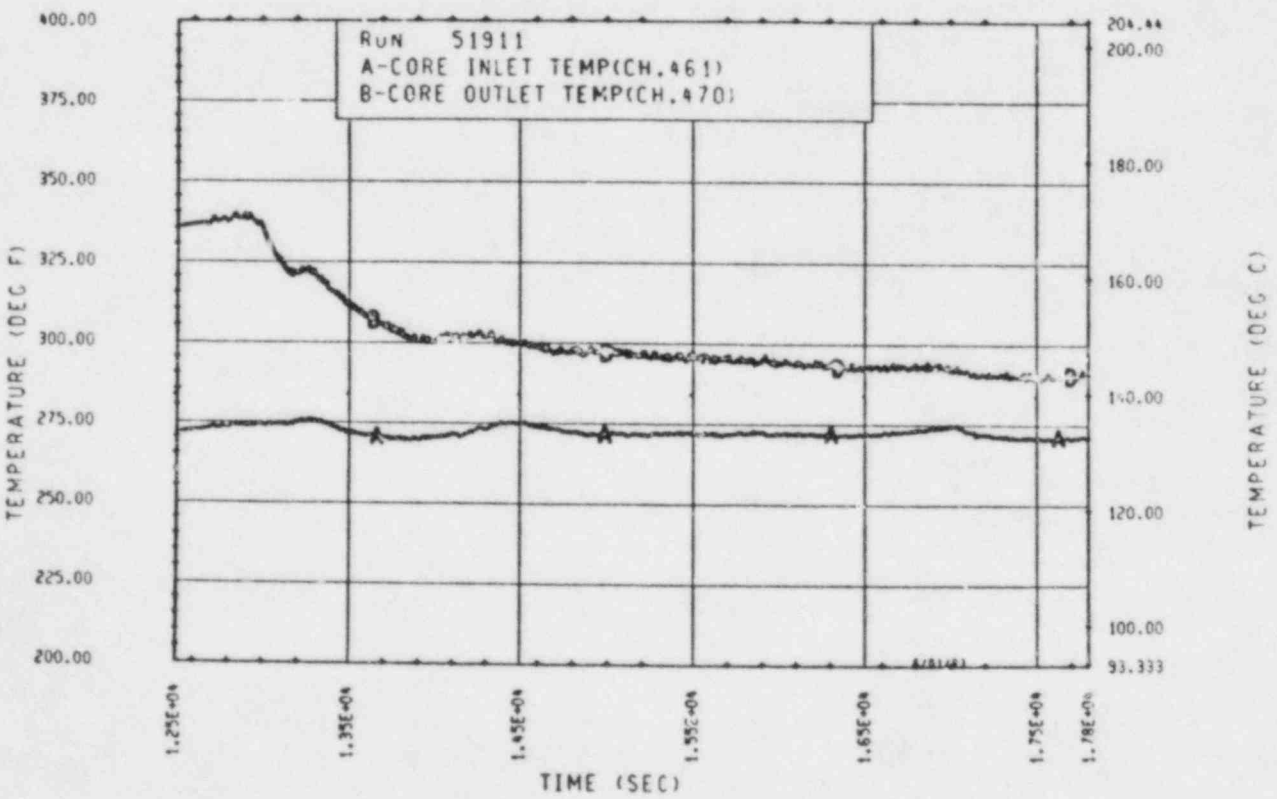

Figure 5-8. Heater Rod Bundle Inlet and Outlet Temperatures (12,500-17,800 sec)

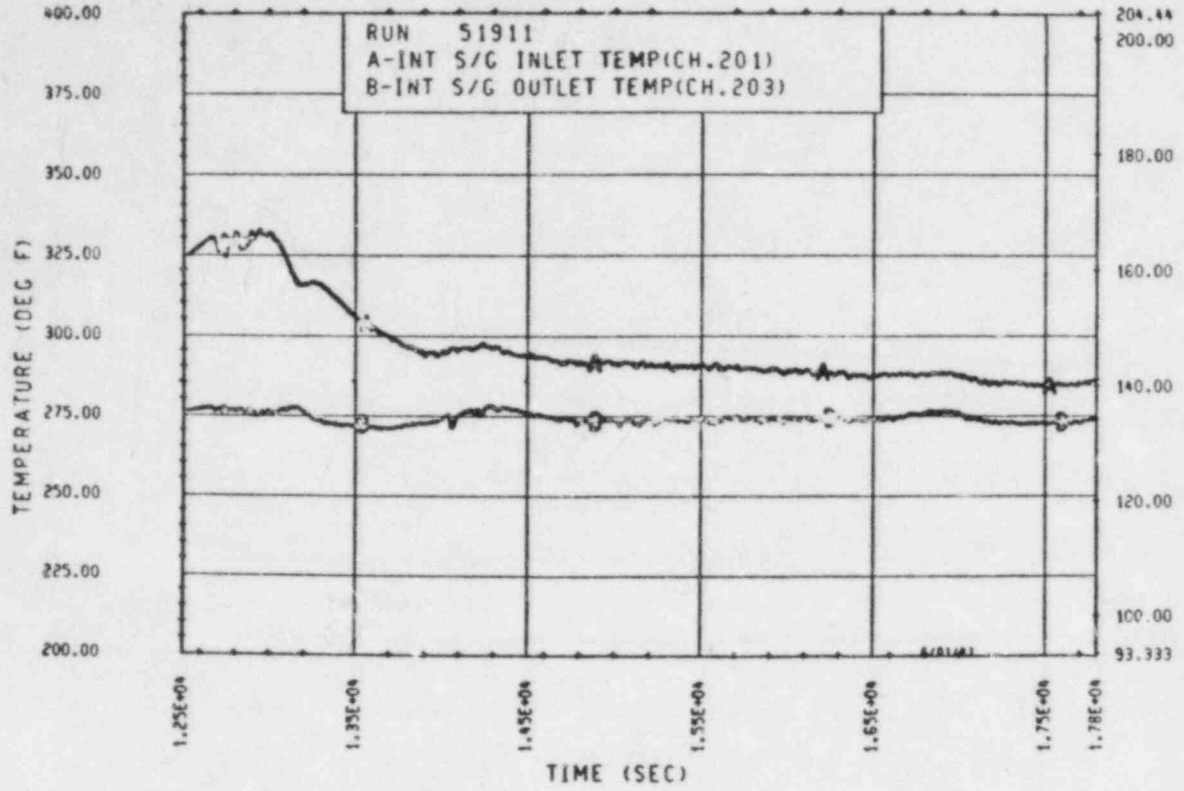

Figure 5-9. Unbroken Loop Steam Generator Inlet and Outlet Temperatures (12,500-17,800 sec)

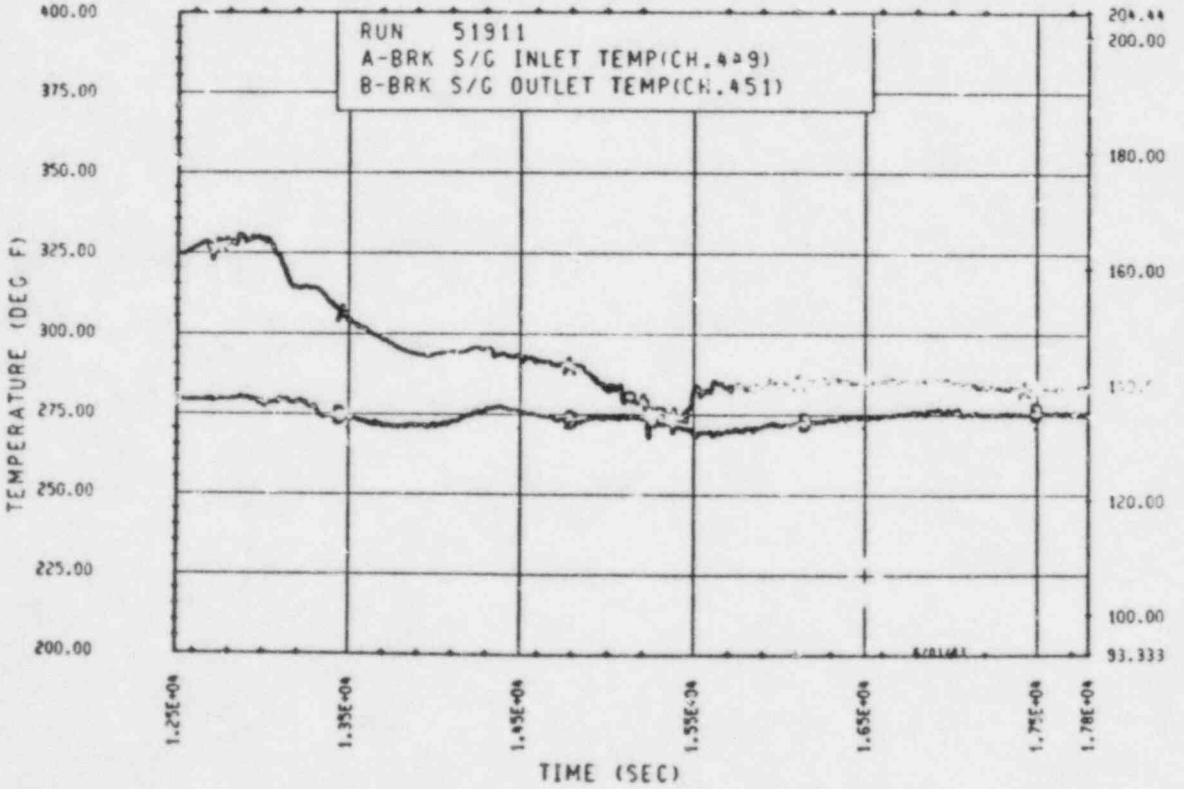

Figure 5-10. Broken Loop Steam Generator Inlet and Outlet Temperatures (12,500-17,800 sec)

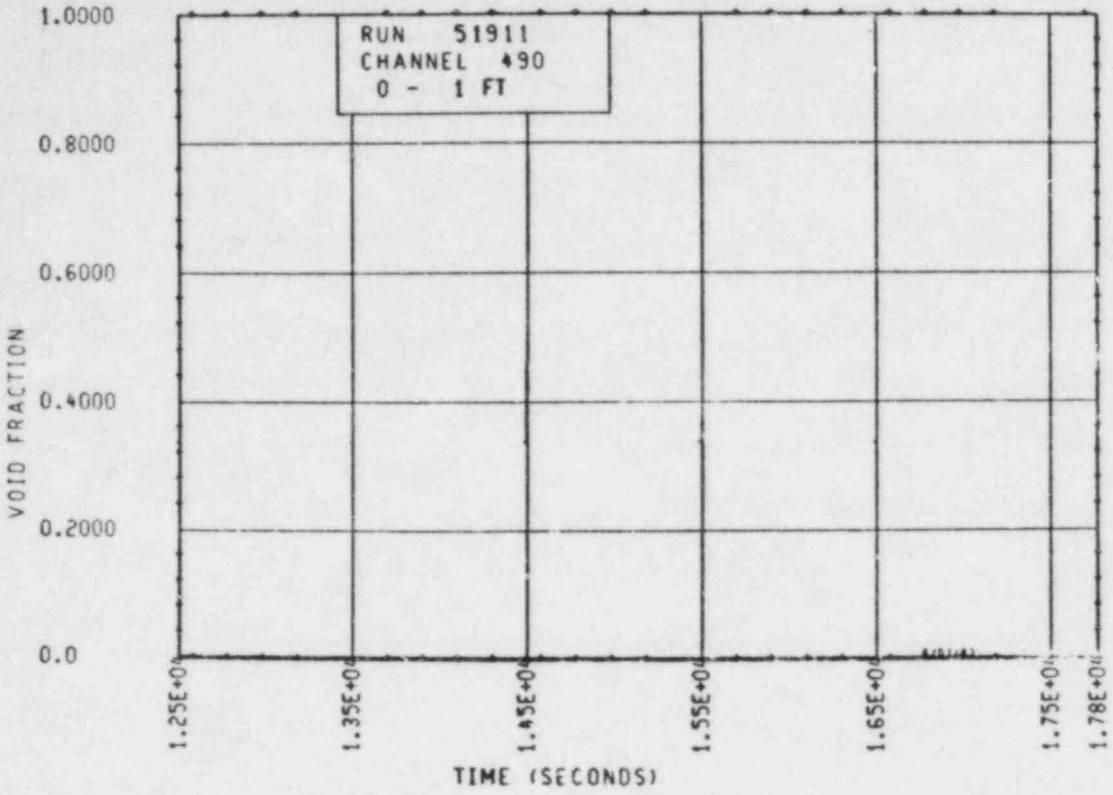

Figure 5-11. Heater Rod Bundle Void Fraction [0-0.30 m (0-1 ft)] (12,500-17,800 sec)

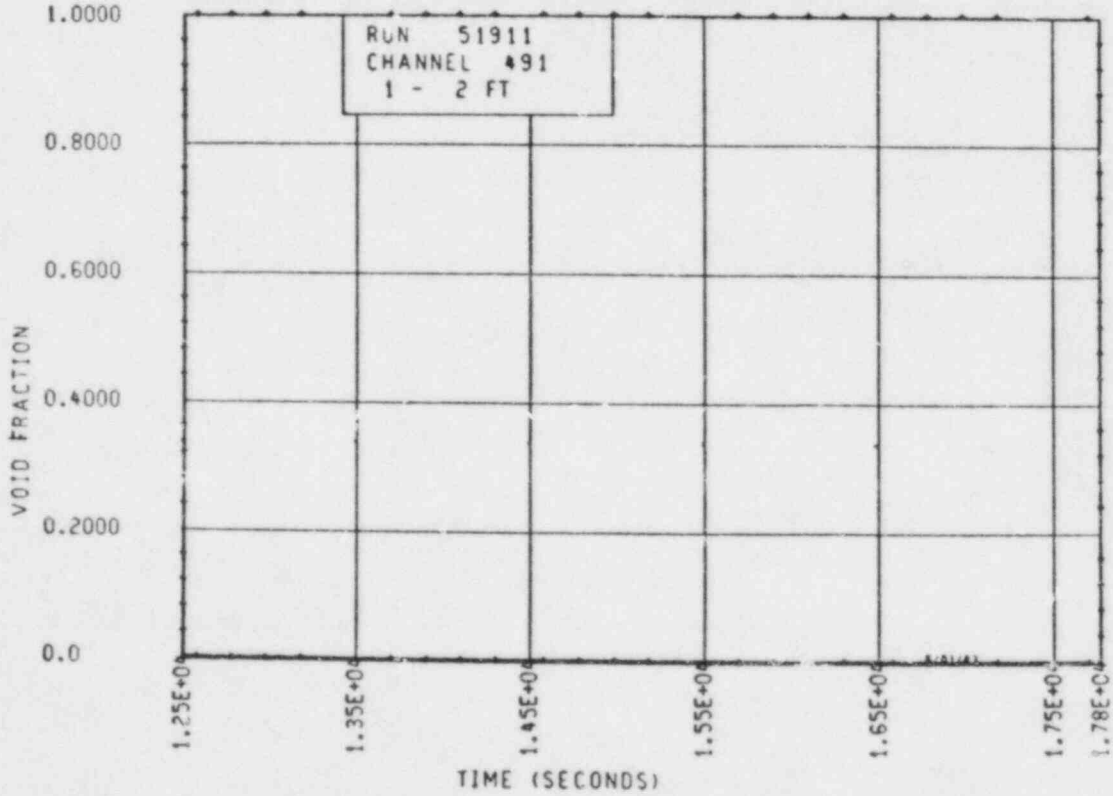

Figure 5-12 Heater Rod Bundle Void Fraction [0.30-0.61 m (1-2 ft)] (12,500-17,800 sec)

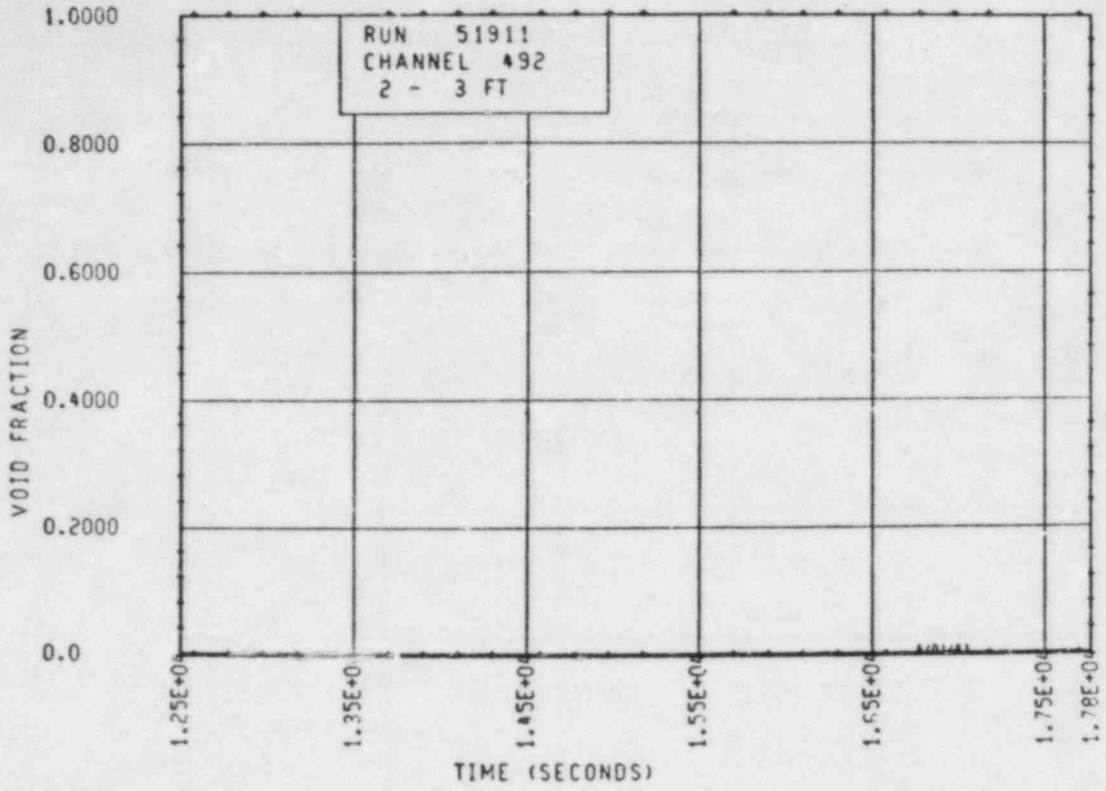

Figure 5-13. Heater Rod Bundle Void Fraction [0.61-0.91 m (2-3 ft)] (12,500-17,800 sec)

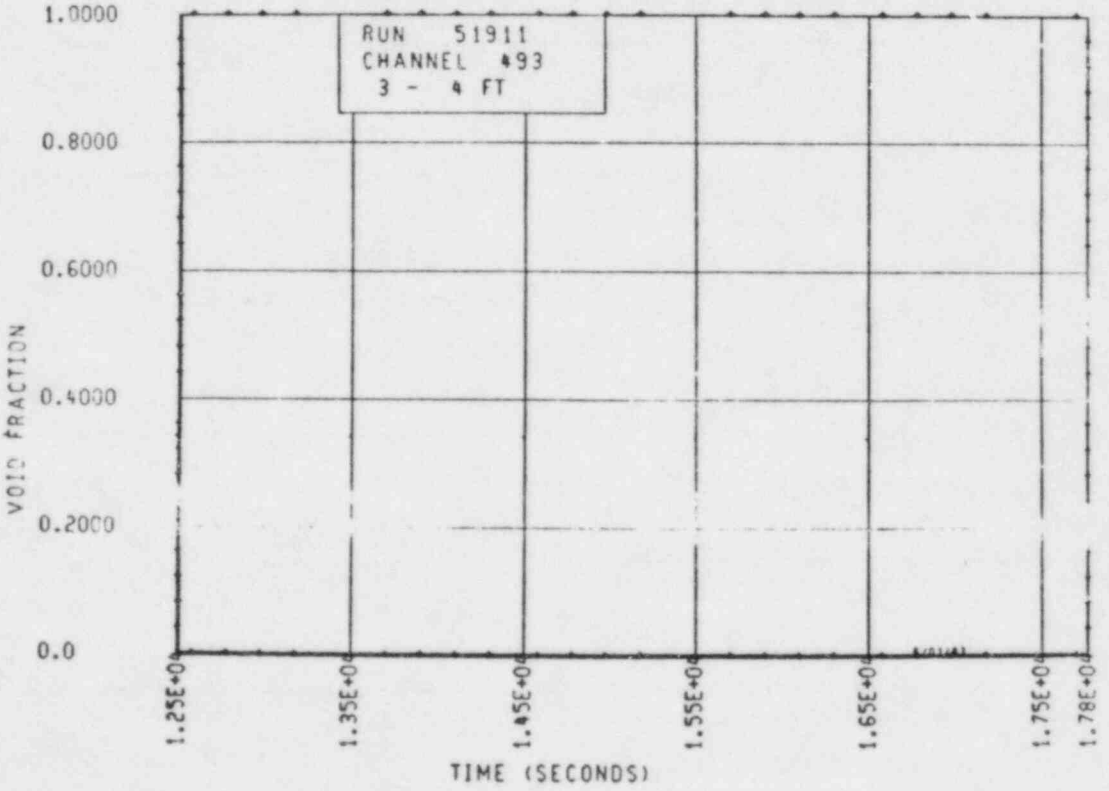

Figure 5-14. Heater Rod Bundle Void Fraction [0.91-1.22 m (3-4 ft)] (12,500-17,800 sec)

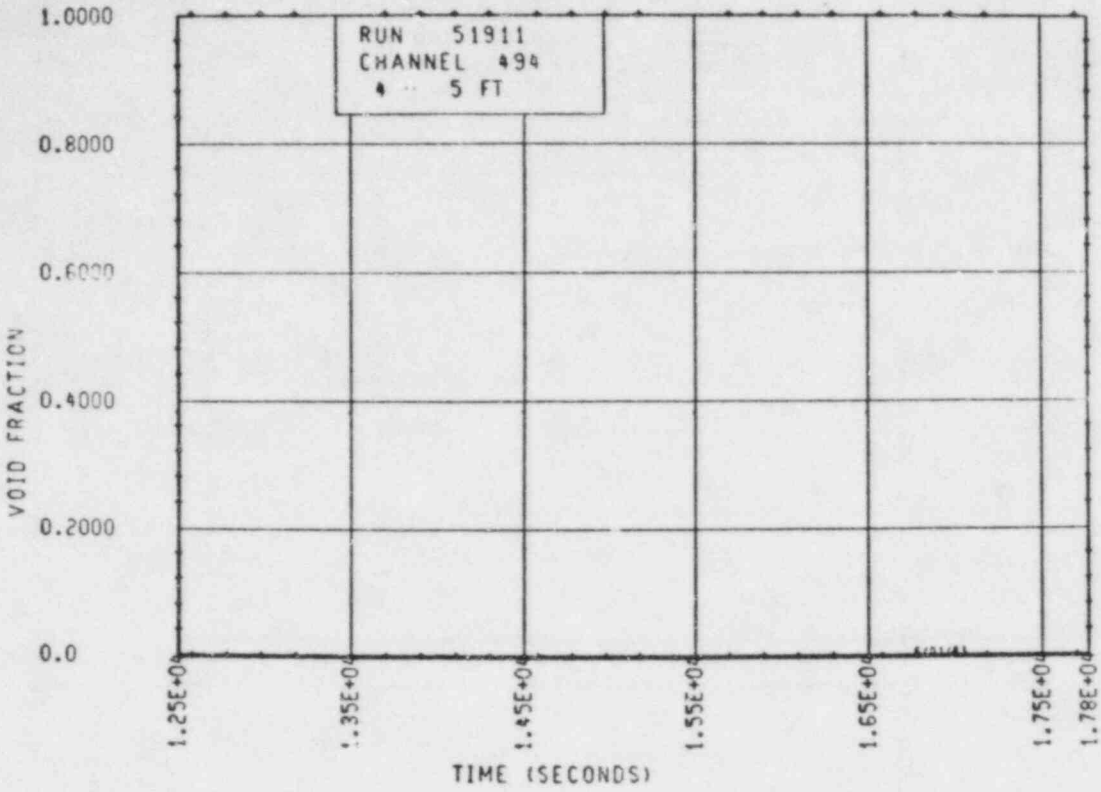

Figure 5-15. Heater Rod Bundle Void Fraction [1.22-1.52 m (4-5 ft)] (12,500-17,800 sec)

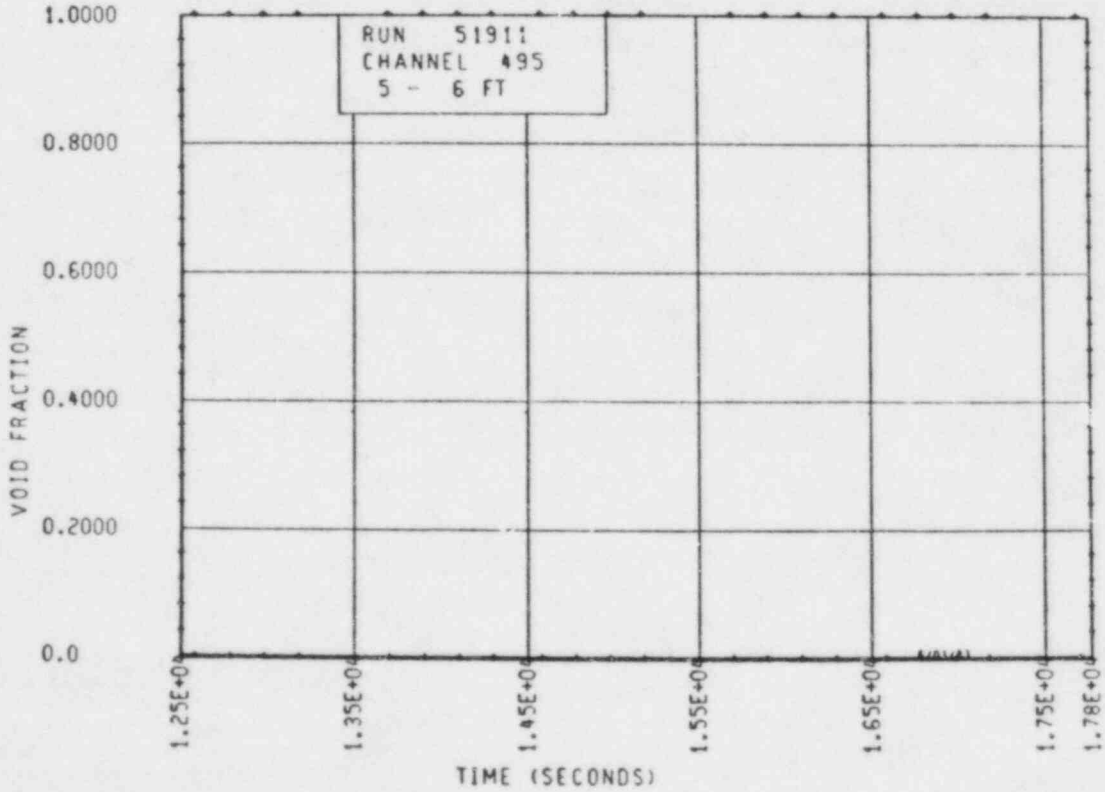

Figure 5-16. Heater Rod Bundle Void Fraction [1.52-1.83 m (5-6 ft)] (12,500-17,800 sec)

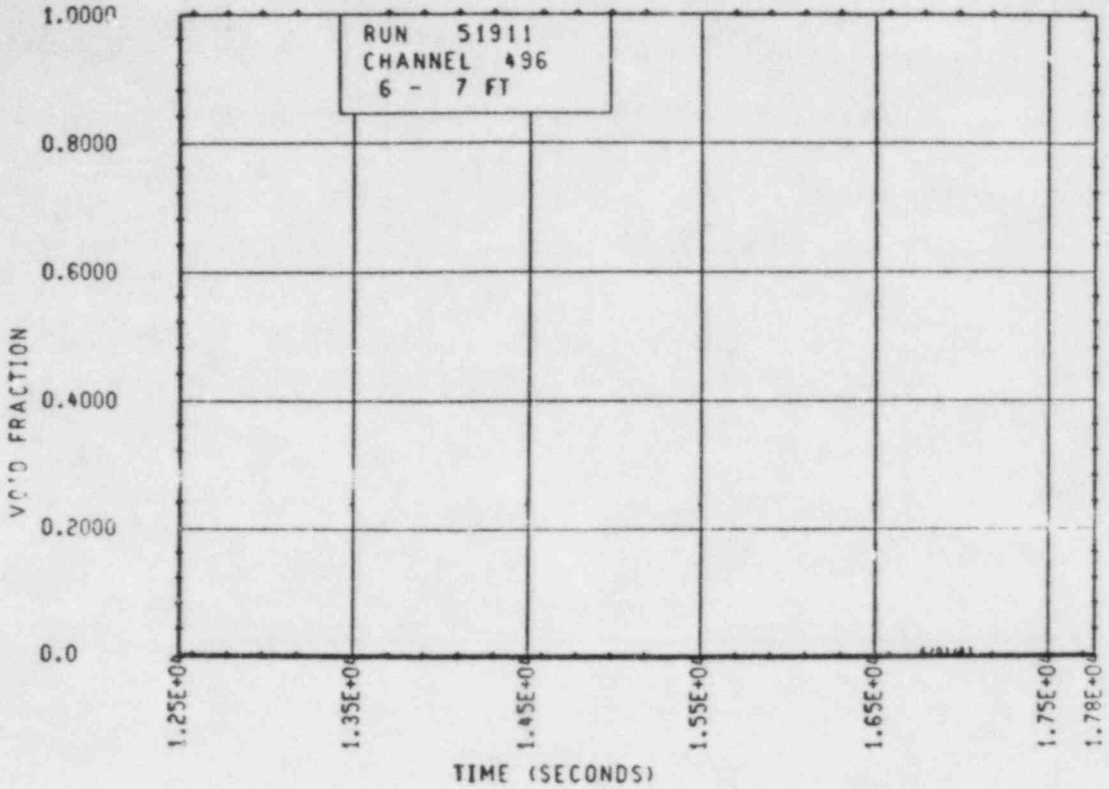

Figure 5-17. Heater Rod Bundle Void Fraction [1.83-2.13 m (6-7 ft)] (12,500-17,800 sec)

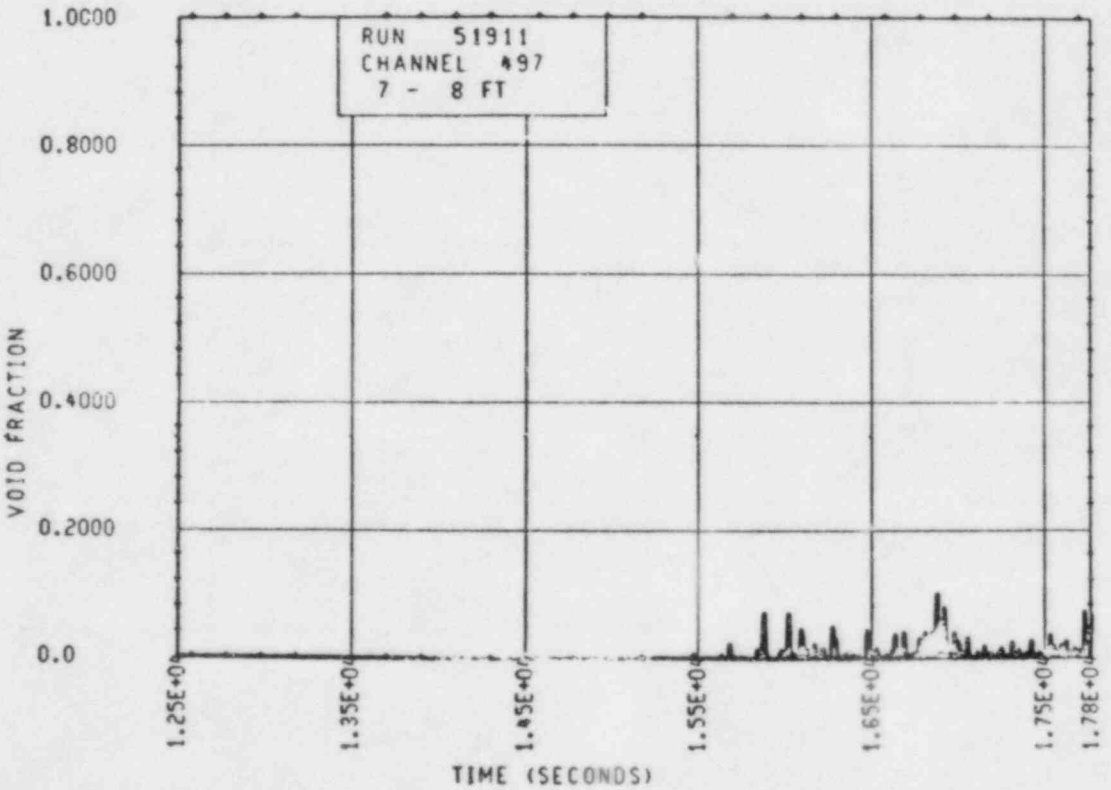

Figure 5-18. Heater Rod Bundle Void Fraction [2.13-2.44 m (7-8 ft)] (12,500-17,800 sec)

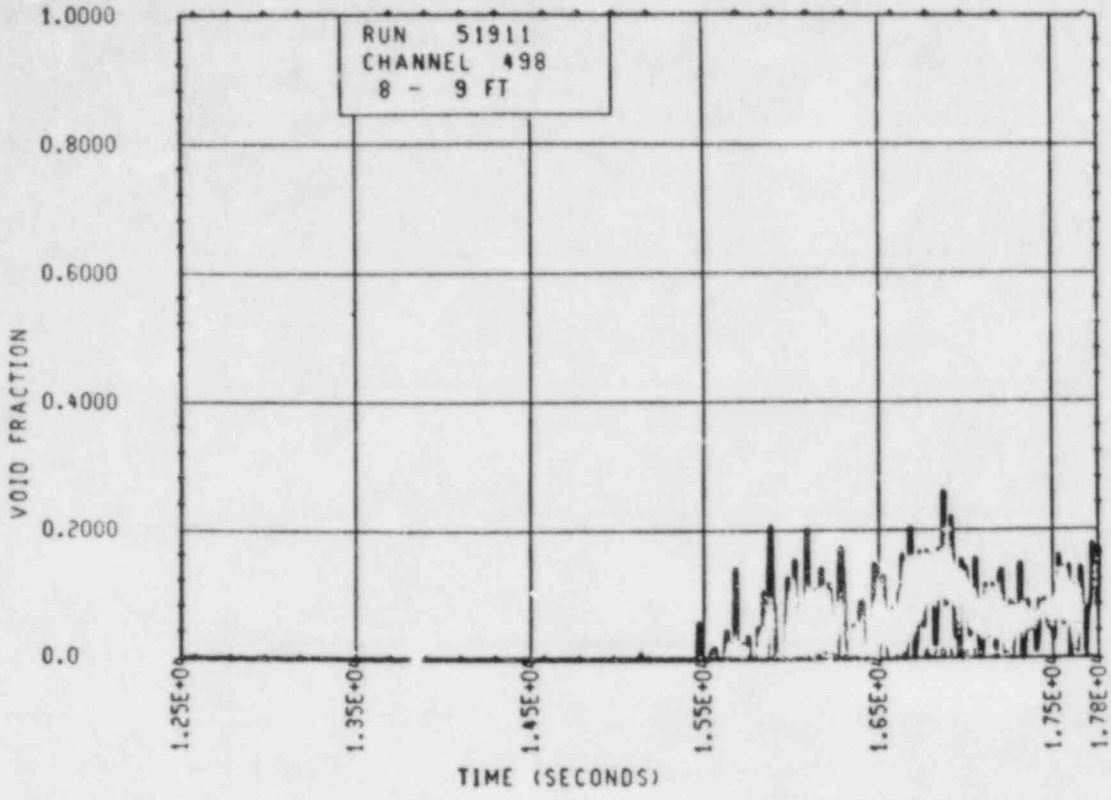

Figure 5-19. Heater Rod Bundle Void Fraction [2.44-2.74 m (8-9 ft)] (12,500-17,800 sec)

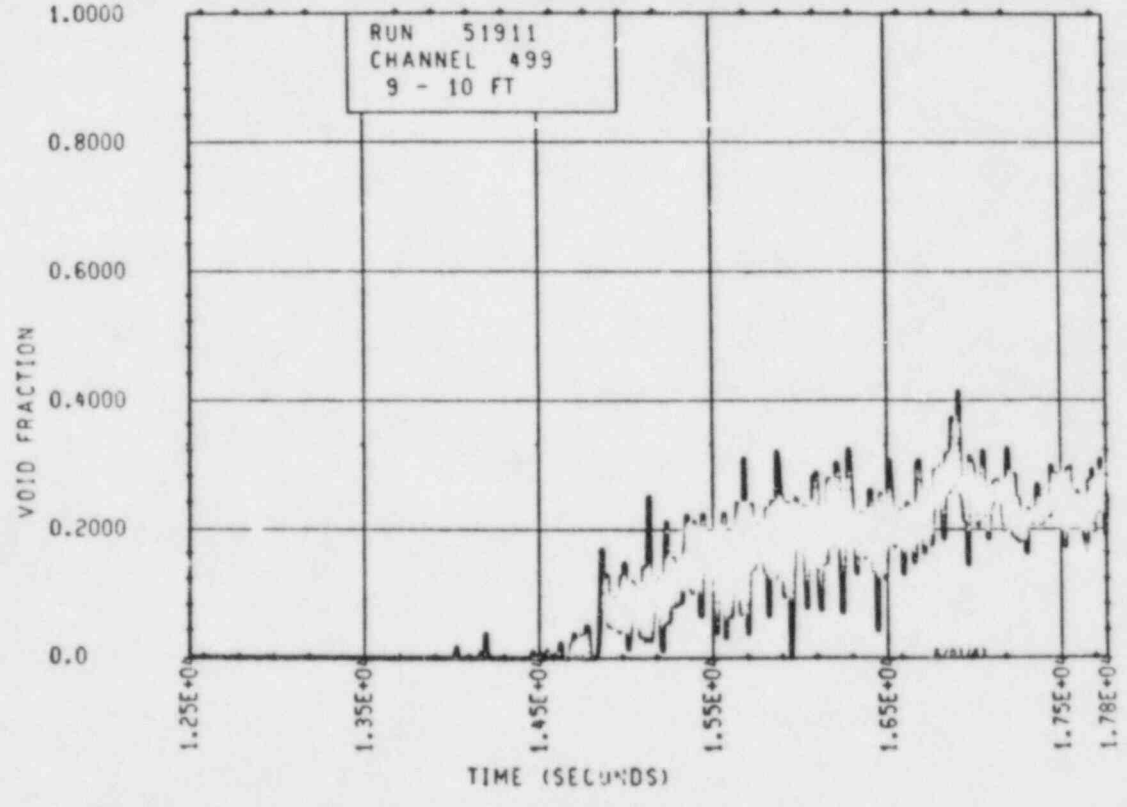

Figure 5-20. Heater Rod Bundle Void Fraction [2.74-3.05 m (9-10 ft)] (12,500-17,800 sec)

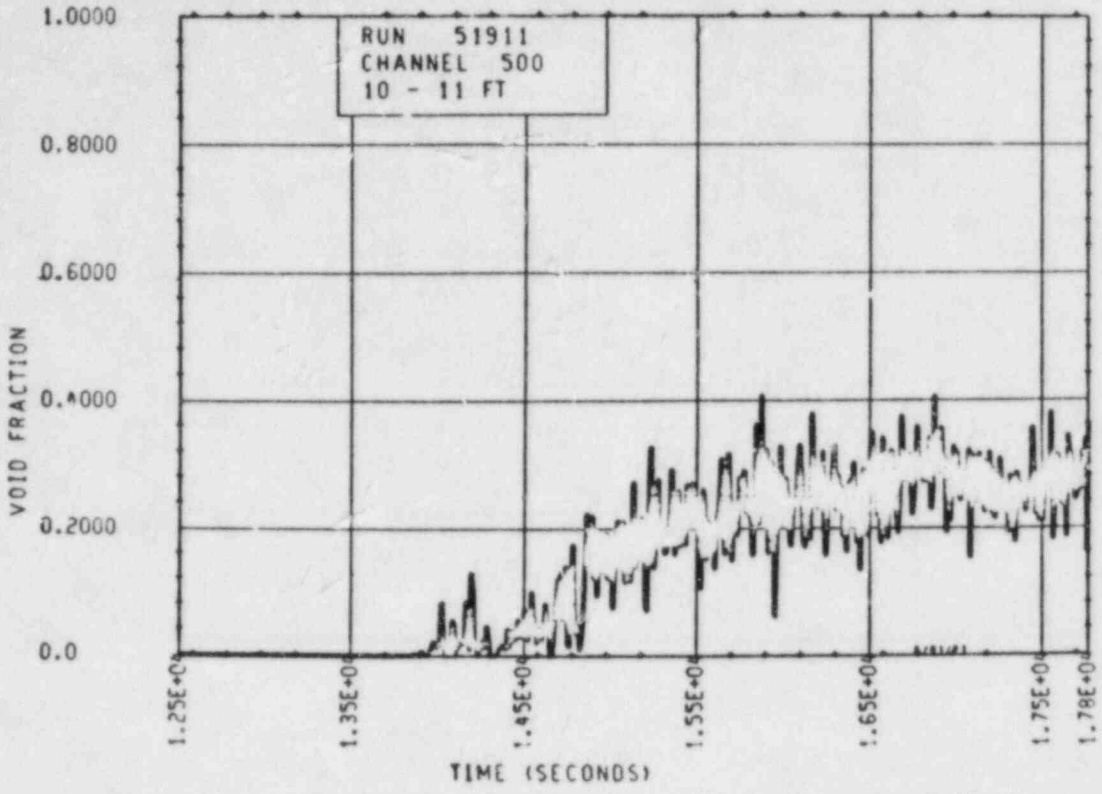

Figure 5-21. Heater Rod Bundle Void Fraction [3.05-3.35 m (10-11 ft)] (12,500-17,800 sec)

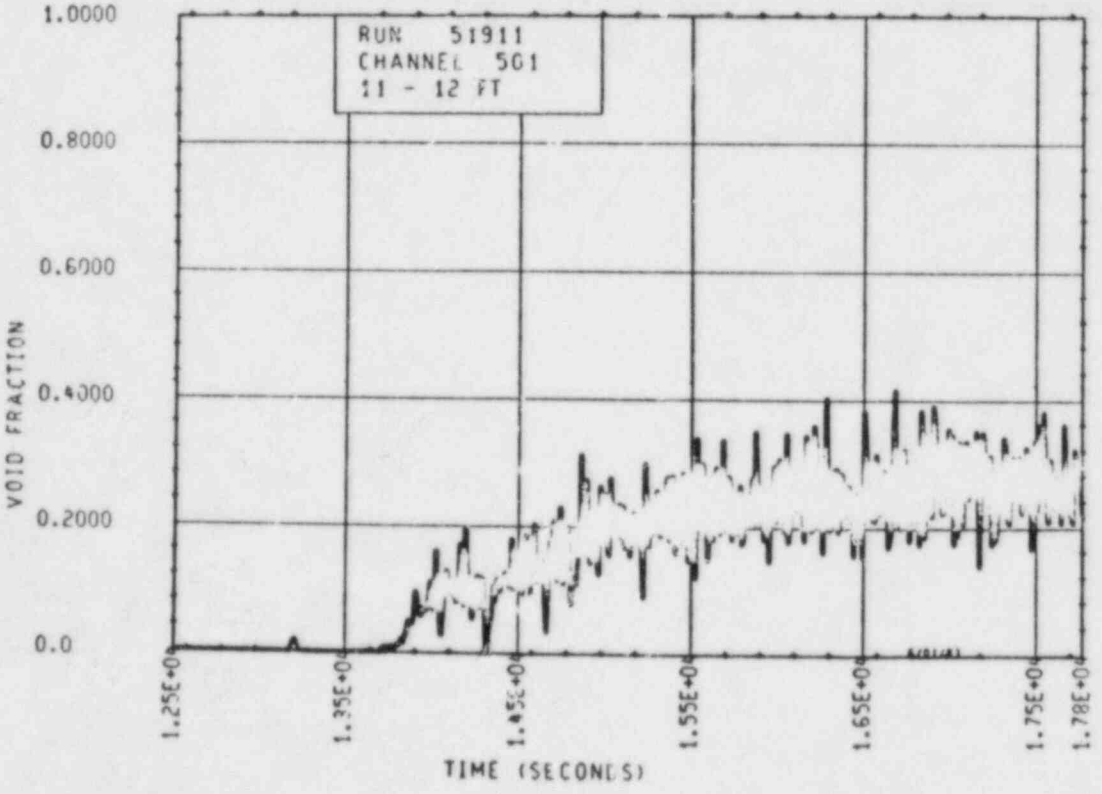

Figure 5-22. Heater Rod Bundle Void Fraction [3.35-3.66 m (11-12 ft)] (12,500-17,800 sec)

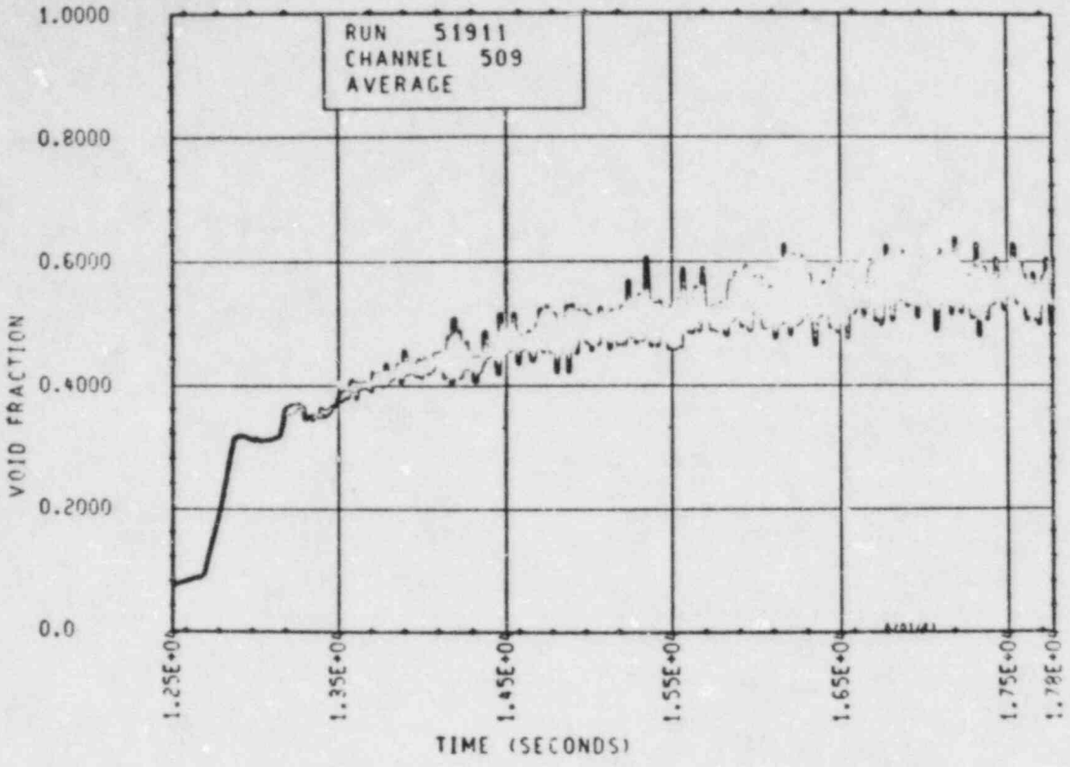

Figure 5-23. Upper Plenum Void Fraction (12,500-17,800 sec)

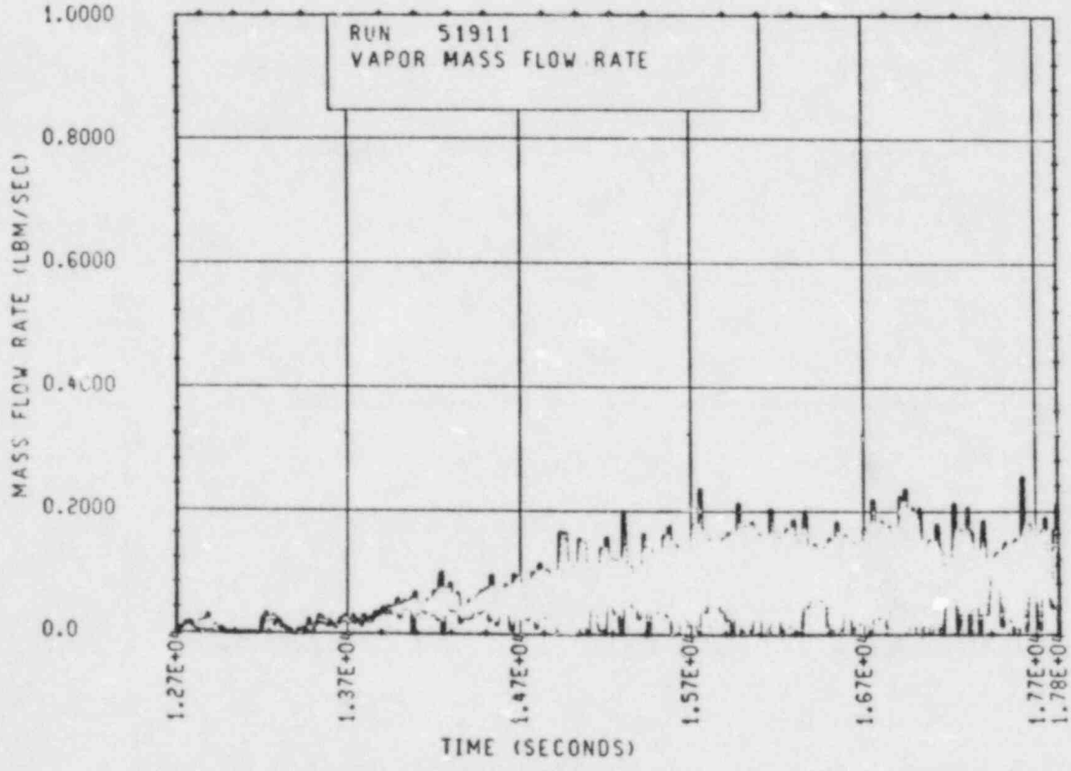

Figure 5-24. Calculated Heater Rod Bundle Vapor Generation Rate (12,500-17,800 sec)

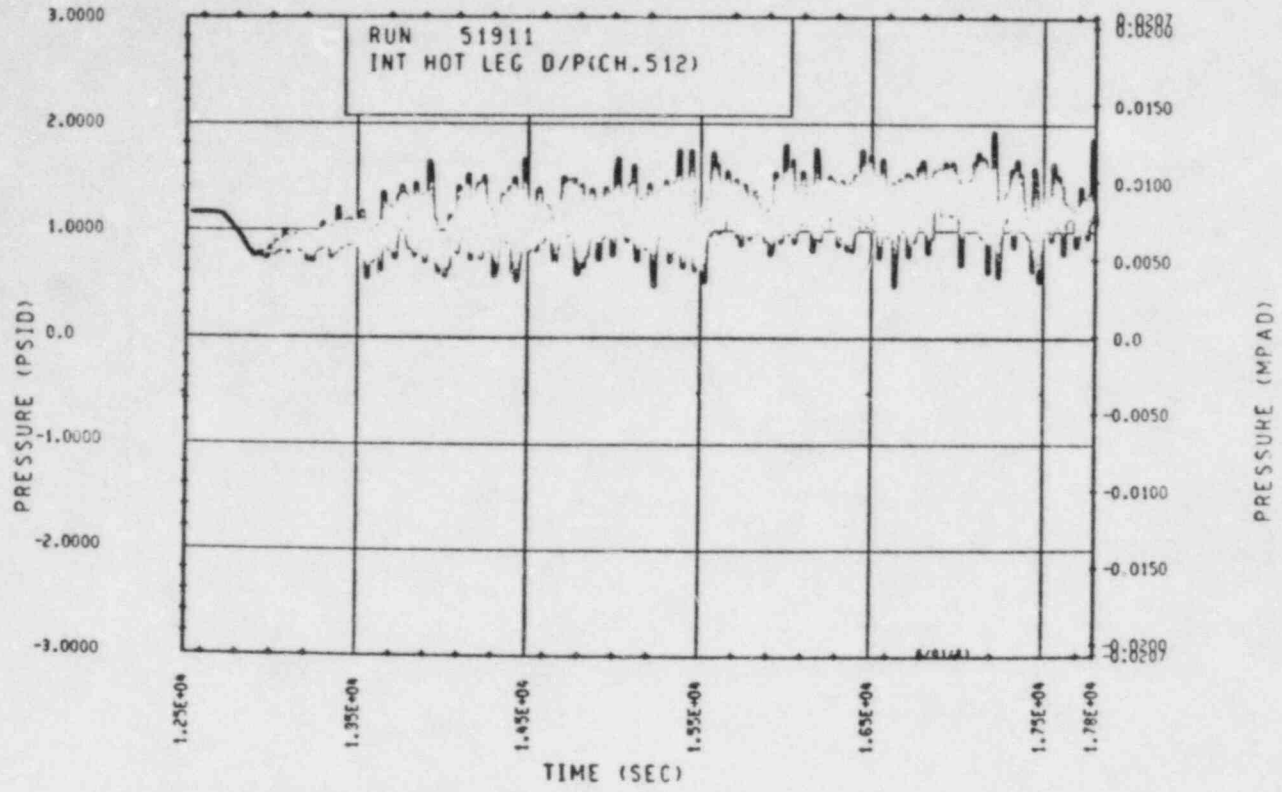

Figure 5-25. Unbroken Loop Hot Leg Differential Pressure (12,500-17,800 sec)

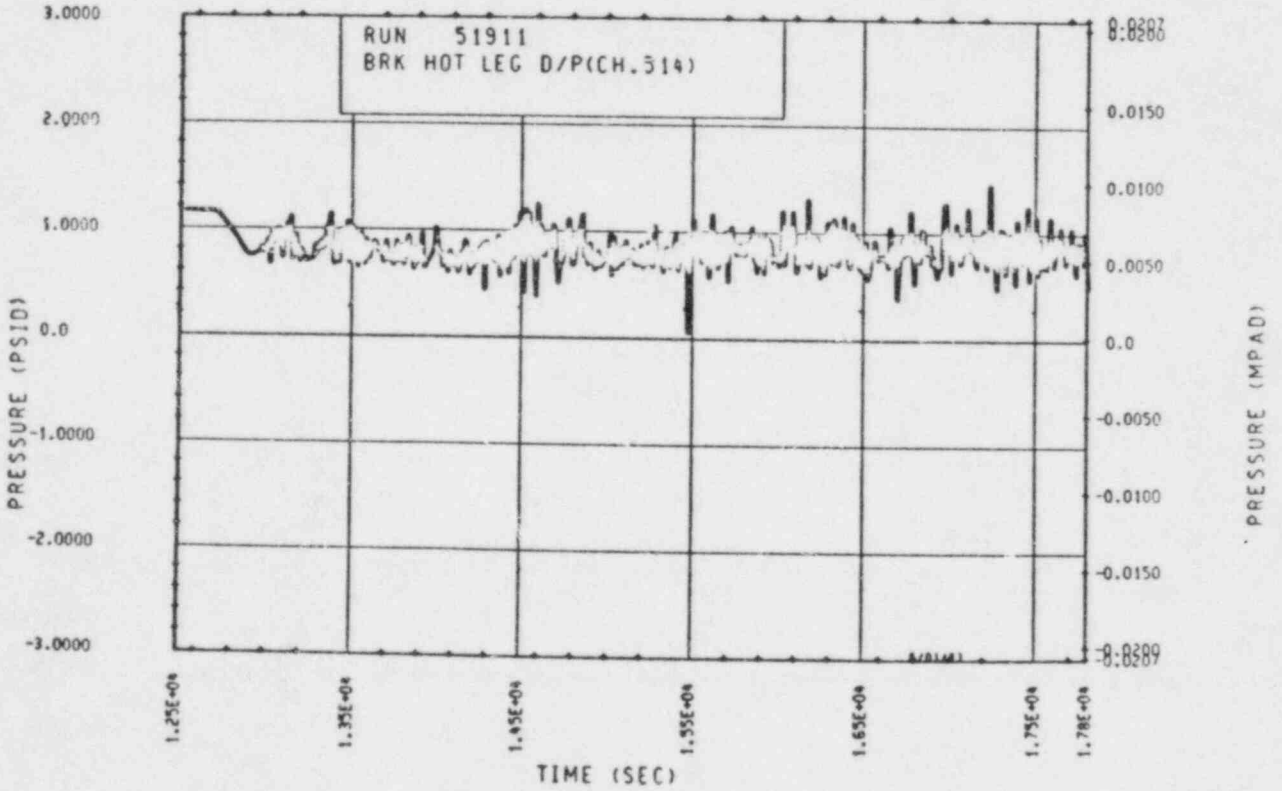

Figure 5-26. Broken Loop Hot Leg Differential Pressure (12,500-17,800 sec)

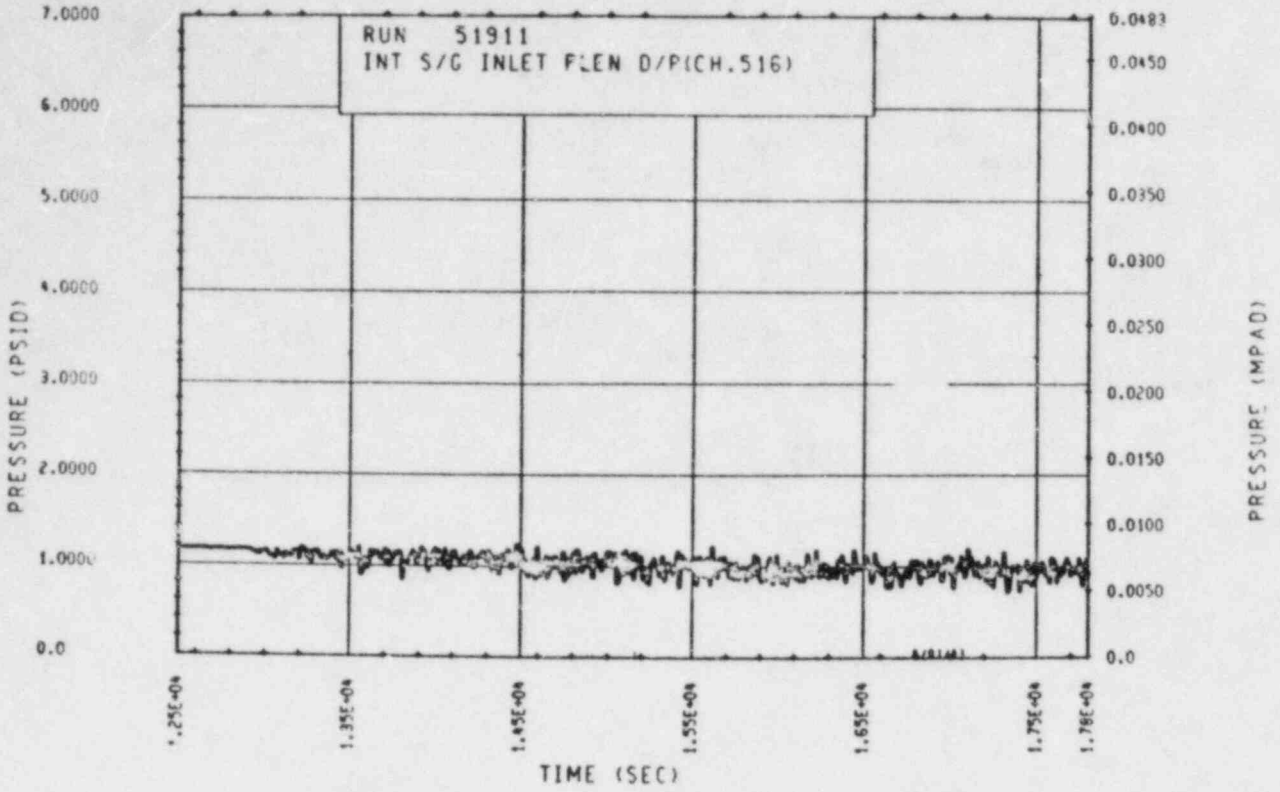

Figure 5-27. Unbroken Loop Steam Generator Inlet Plenum Differential Pressure (12,500-17,800 sec)

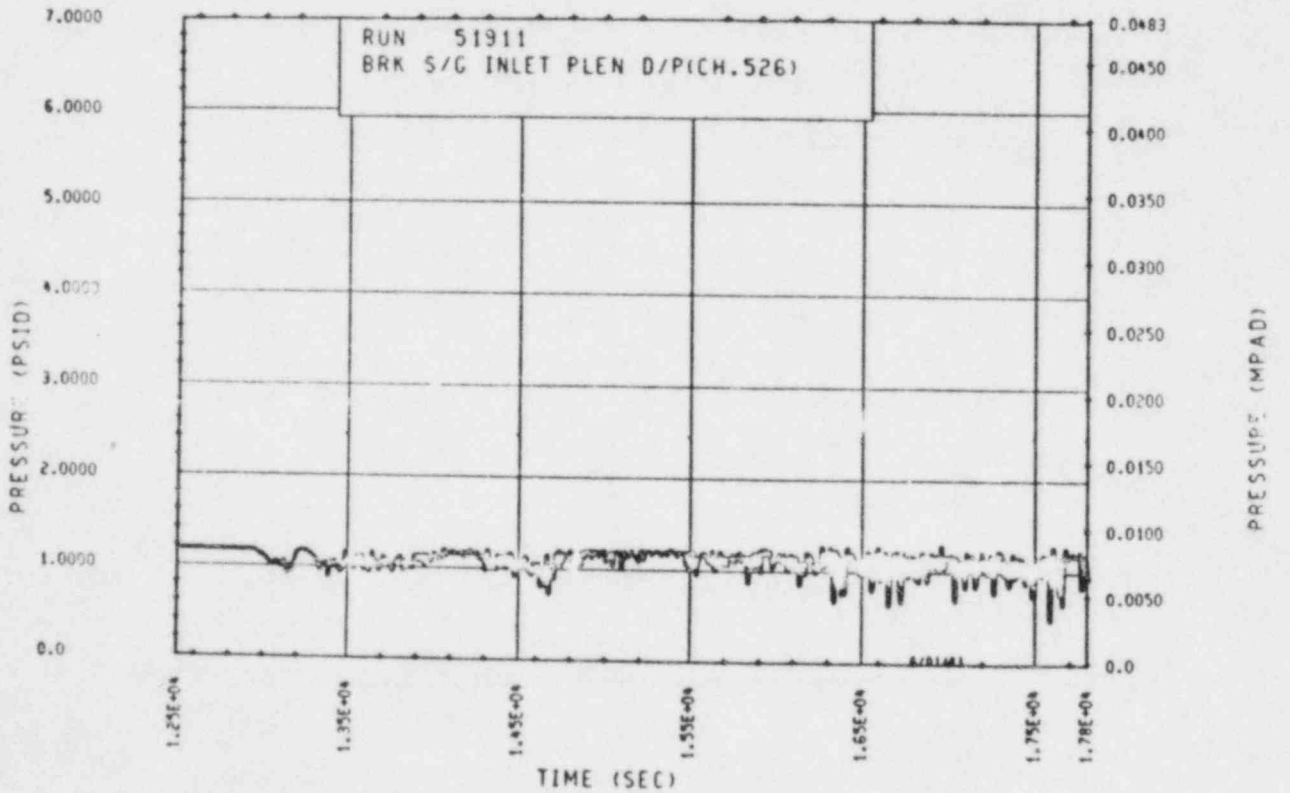

Figure 5-28. Broken Loop Steam Generator Inlet Plenum Differential Pressure (12,500-17,800 sec)

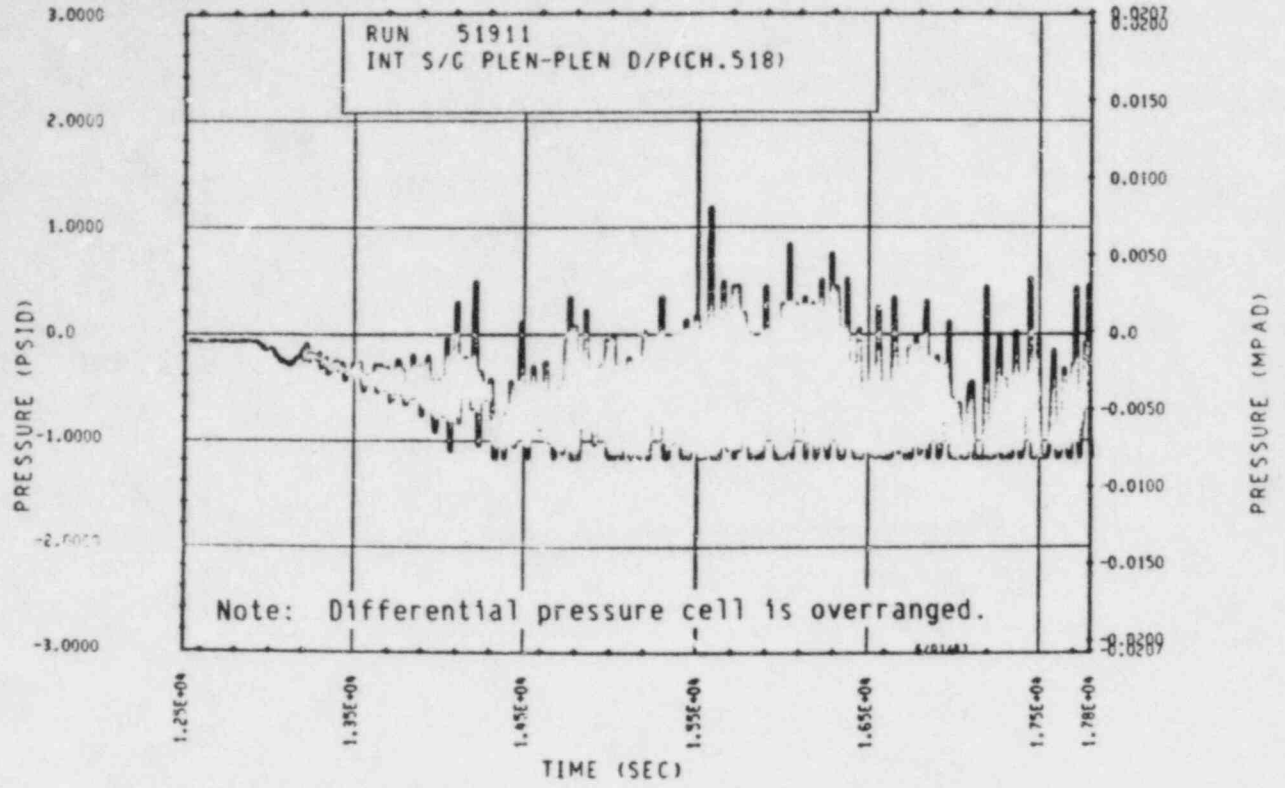

Figure 5-29 Unbroken Loop Steam Generator Plenum-to-Plenum Differential Pressure (12,500-17,800 sec)

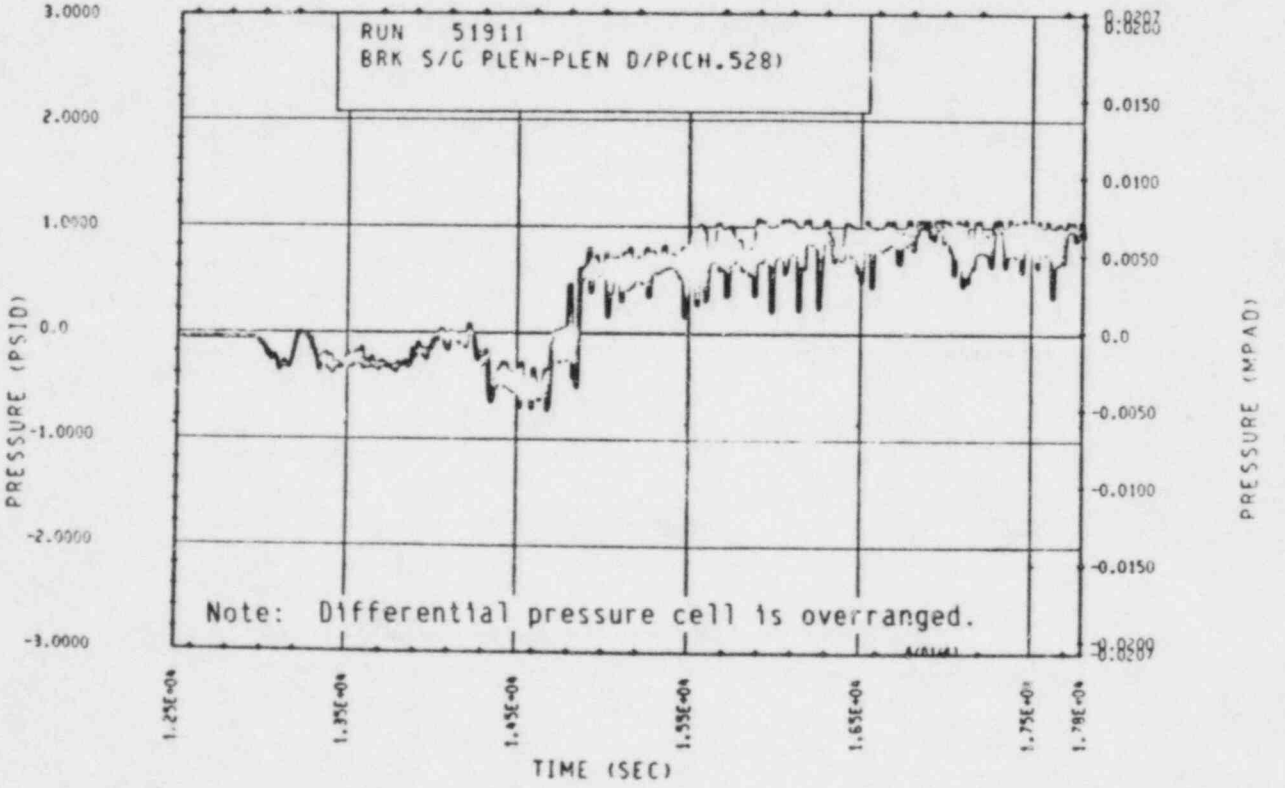

Figure 5-30. Broken Loop Steam Generator Plenum-to-Plenum Differential Pressure (12,500-17,800 sec)

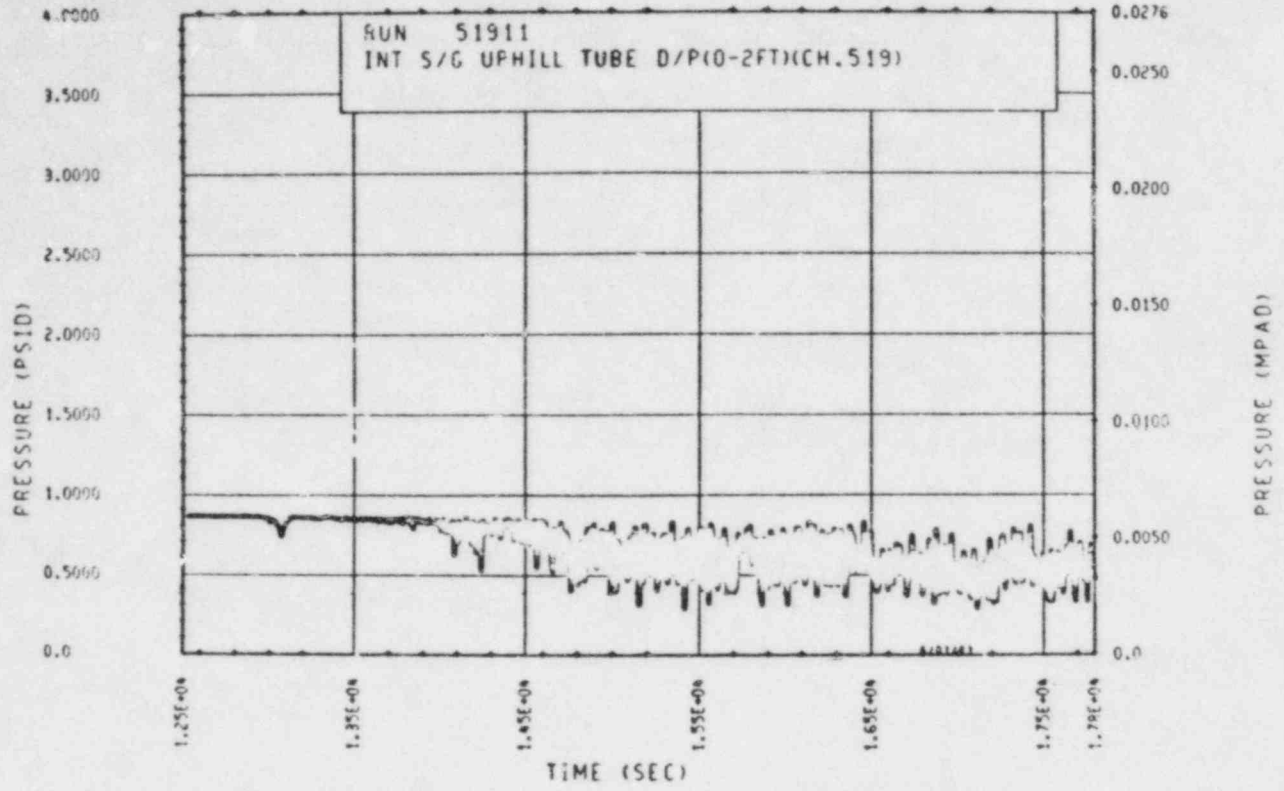

Figure 5-31. Unbroken Loop Steam Generator Uphill Tube B-7 Differential Pressure [0-0.61 m (0-2 ft)] (12,500-17,800 sec)

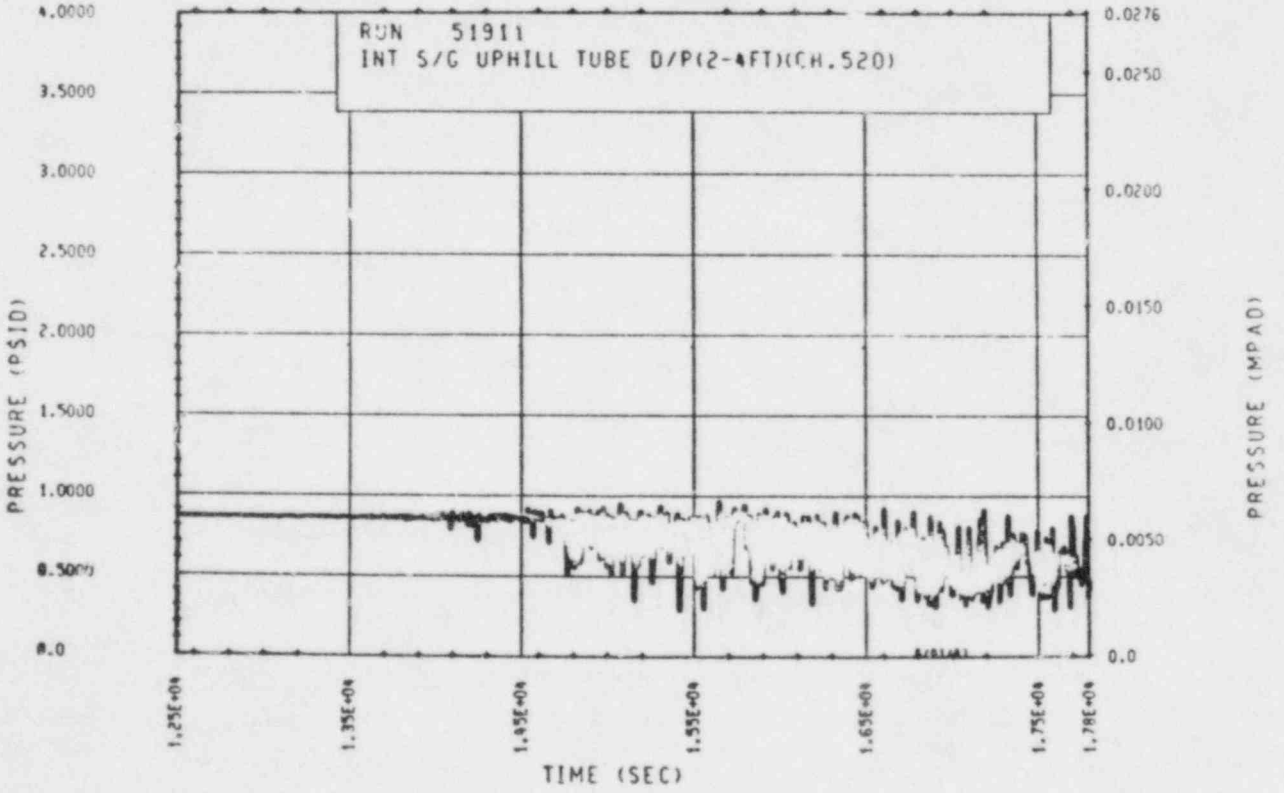

Figure 5-32. Unbroken Loop Steam Generator Uphill Tube B-7 Differential Pressure [0.61-1.22 m (2-4 ft)] (12,500-17,800 sec)

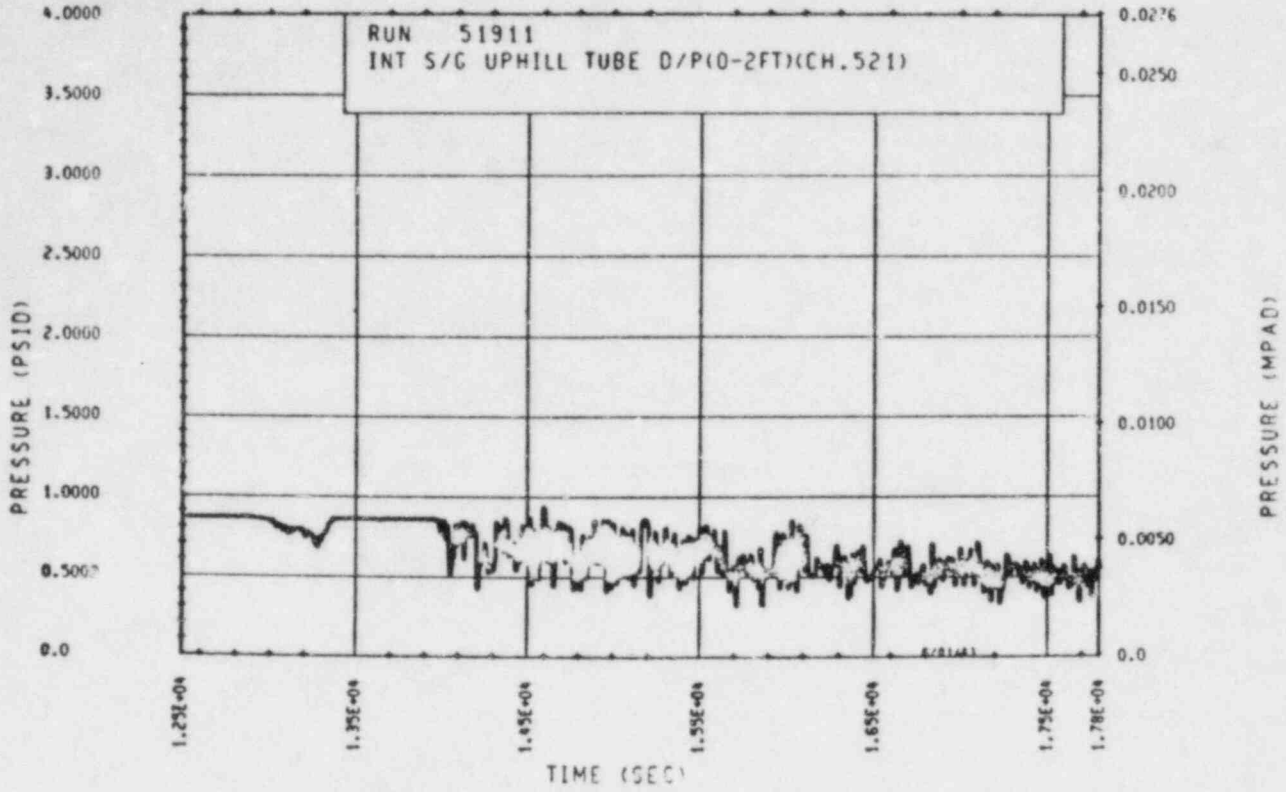

Figure 5-33. Unbroken Loop Steam Generator Uphill Tube C-6 Differential Pressure [0-0.61 m (0-2 ft)] (12,500-17,800 sec)

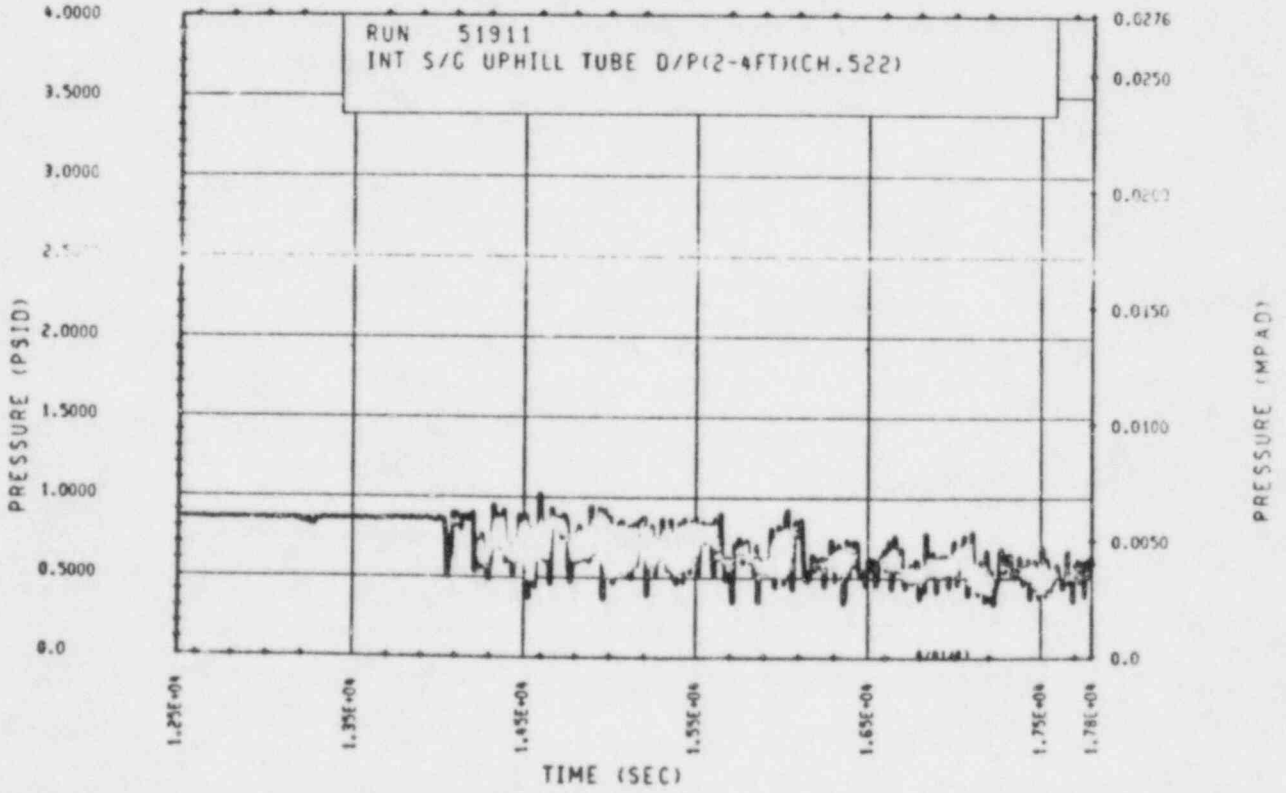

Figure 5-34. Unbroken Loop Steam Generator Uphill Tube C-6 Differential Pressure [0.61-1.22 m (2-4 ft)] (12,500-17,800 sec)

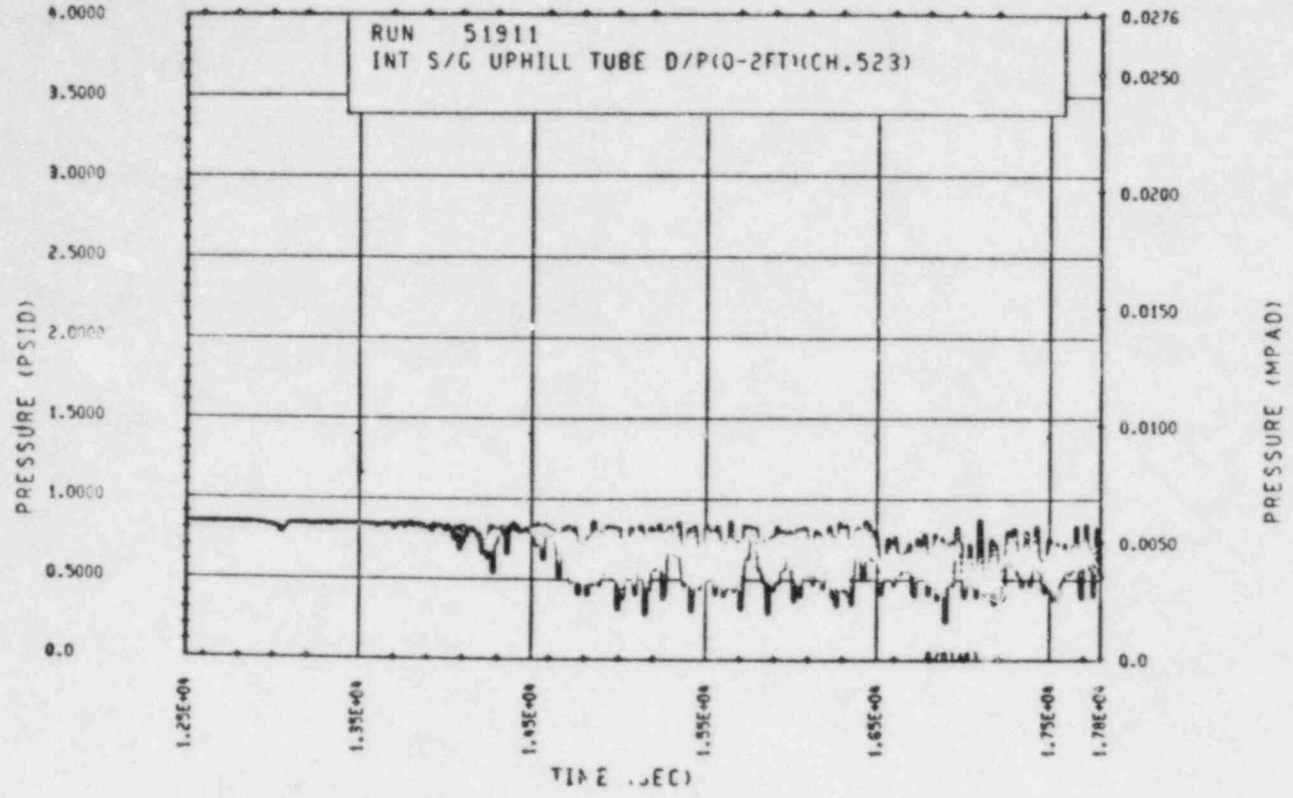

Figure 5-35. Unbroken Loop Steam Generator Uphill Tube E-5 Differential Pressure [0-0.61 m (0-2 ft)] (12,500-17,800 sec)

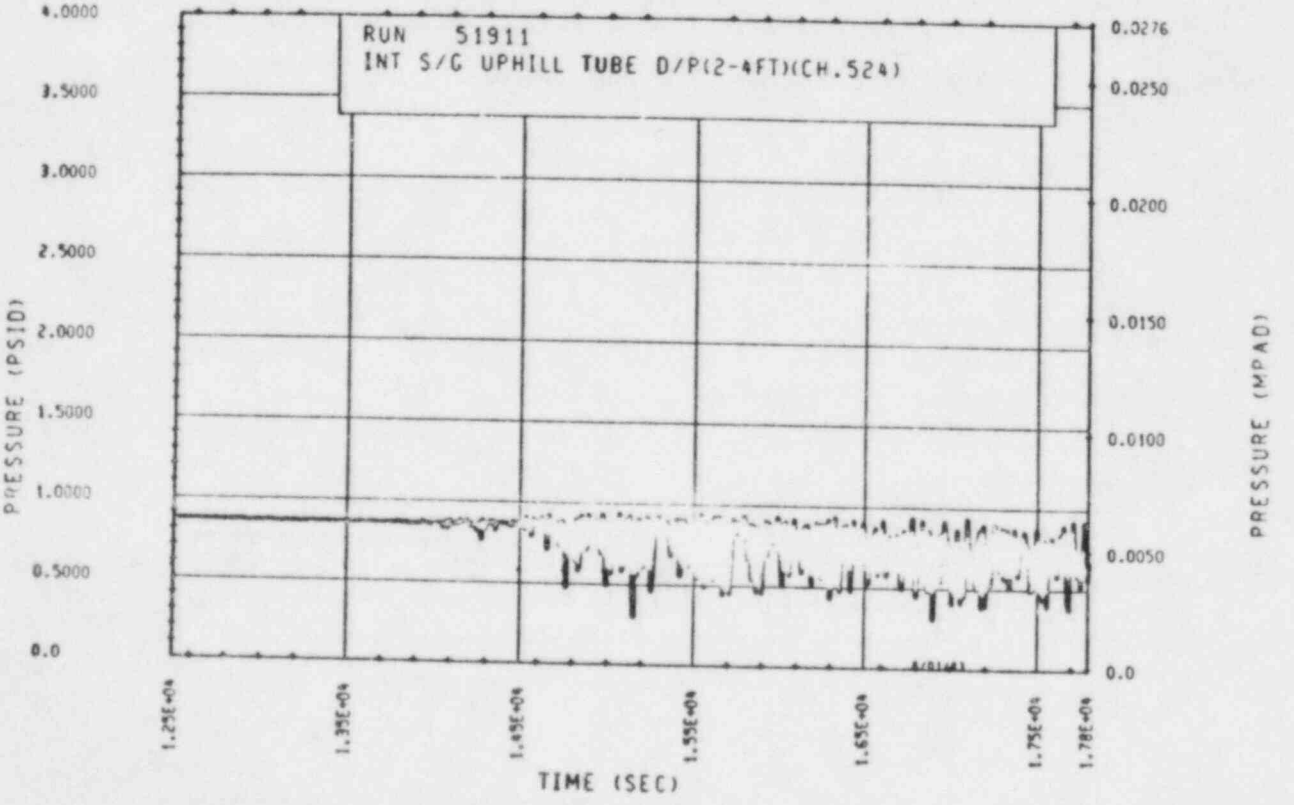

Figure 5-36. Unbroken Loop Steam Generator Uphill Tube E-5 Differential Pressure [0.61-1.22 m (2-4 ft)] (12,500-17,800 sec)

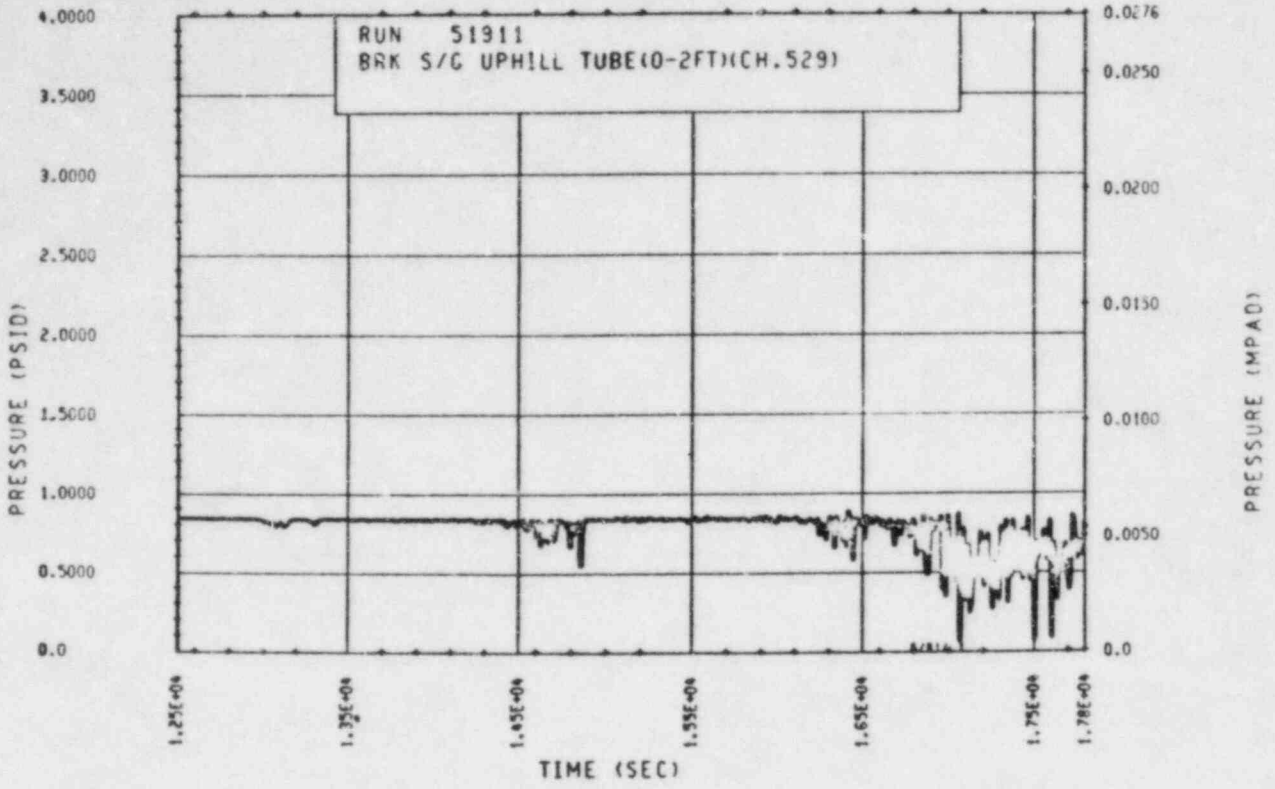

Figure 5-37. Broken Loop Steam Generator Uphill Tube B-6 Differential Pressure [0-0.61 m (0-2 ft)] (12,500-17,800 sec)

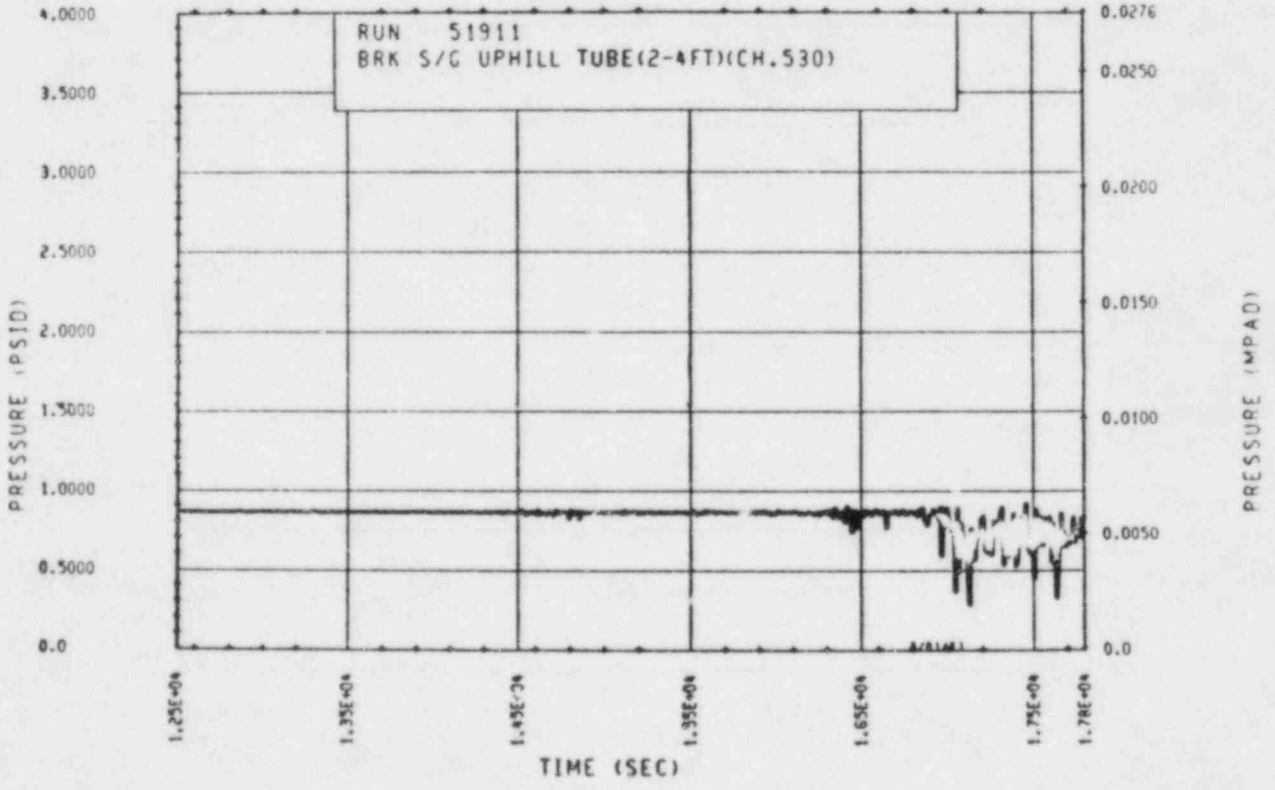

Figure 5-38. Broken Loop Steam Generator Uphill Tube B-6 Differential Pressure [0.61-1.22 m (2-4 ft)] (12,500-17,800 sec)

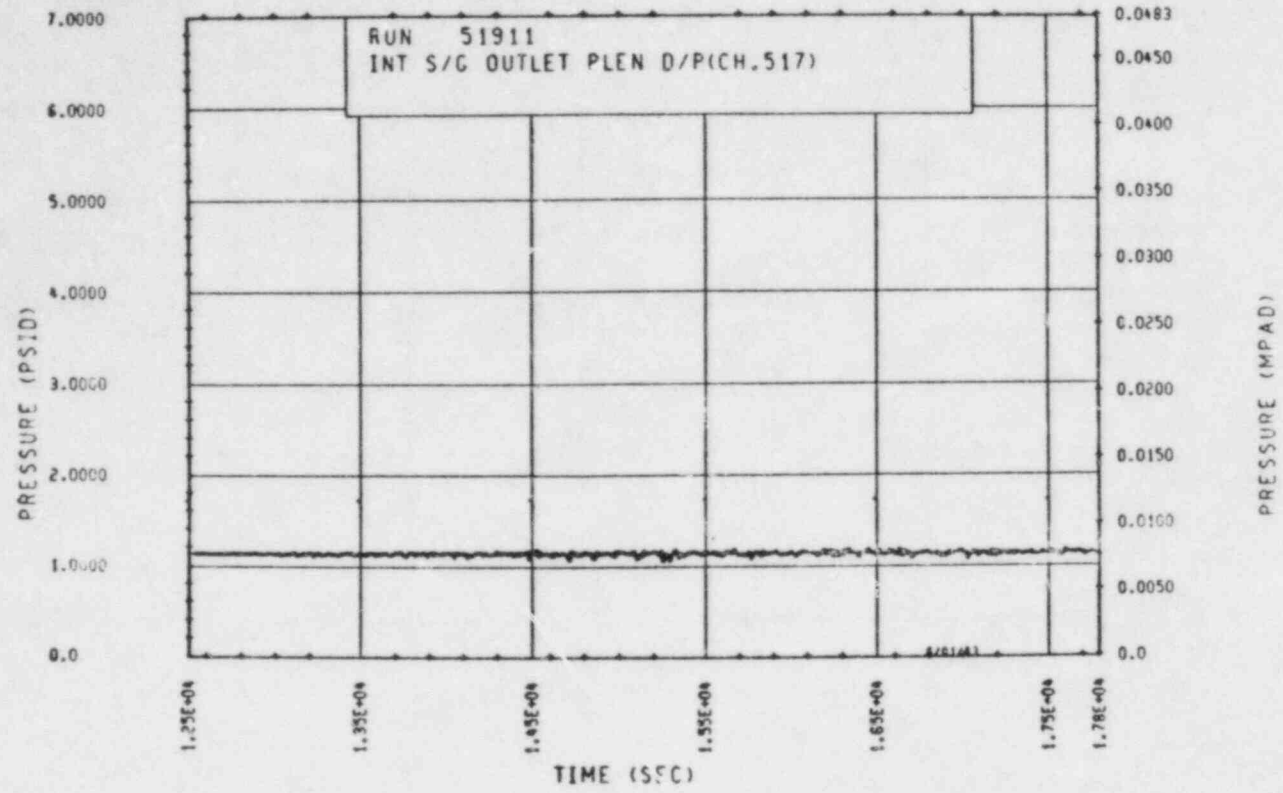

Figure 5-39. Unbroken Loop Steam Generator Outlet Plenum Differential Pressure (12,500-17,800 sec)

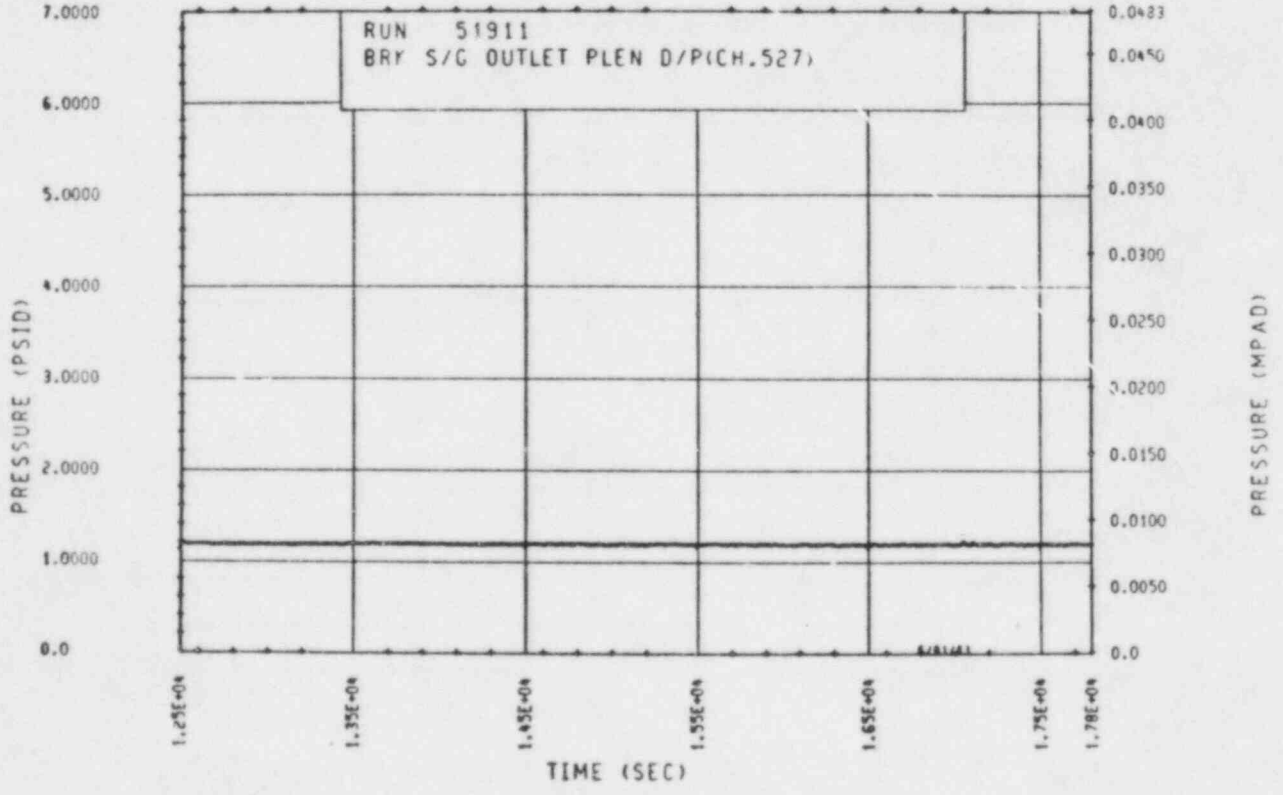

Figure 5-40. Broken Loop Steam Generator Outlet Plenum Differential Pressure (12,500-17,800 sec)

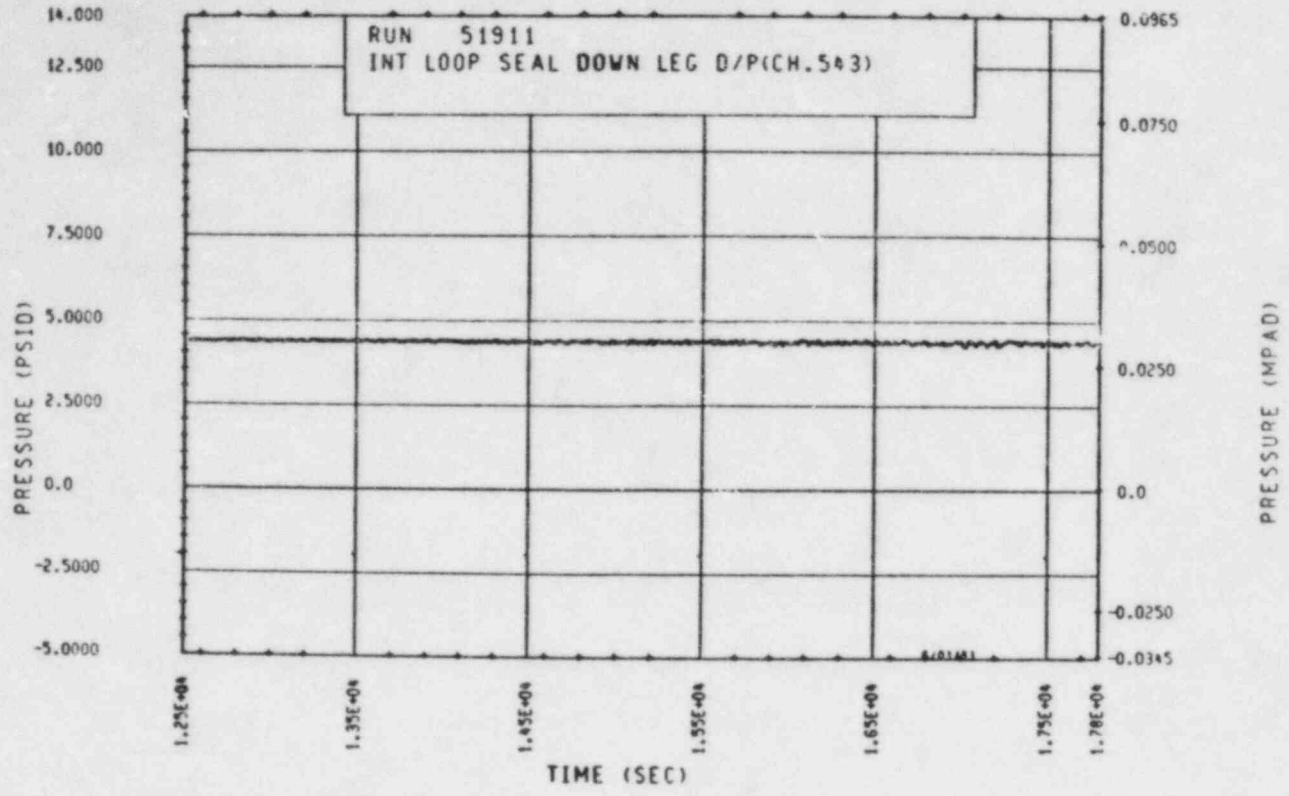

Figure 5-41. Unbroken Loop Seal Descending Leg Differential Pressure (12,500-17,800 sec)

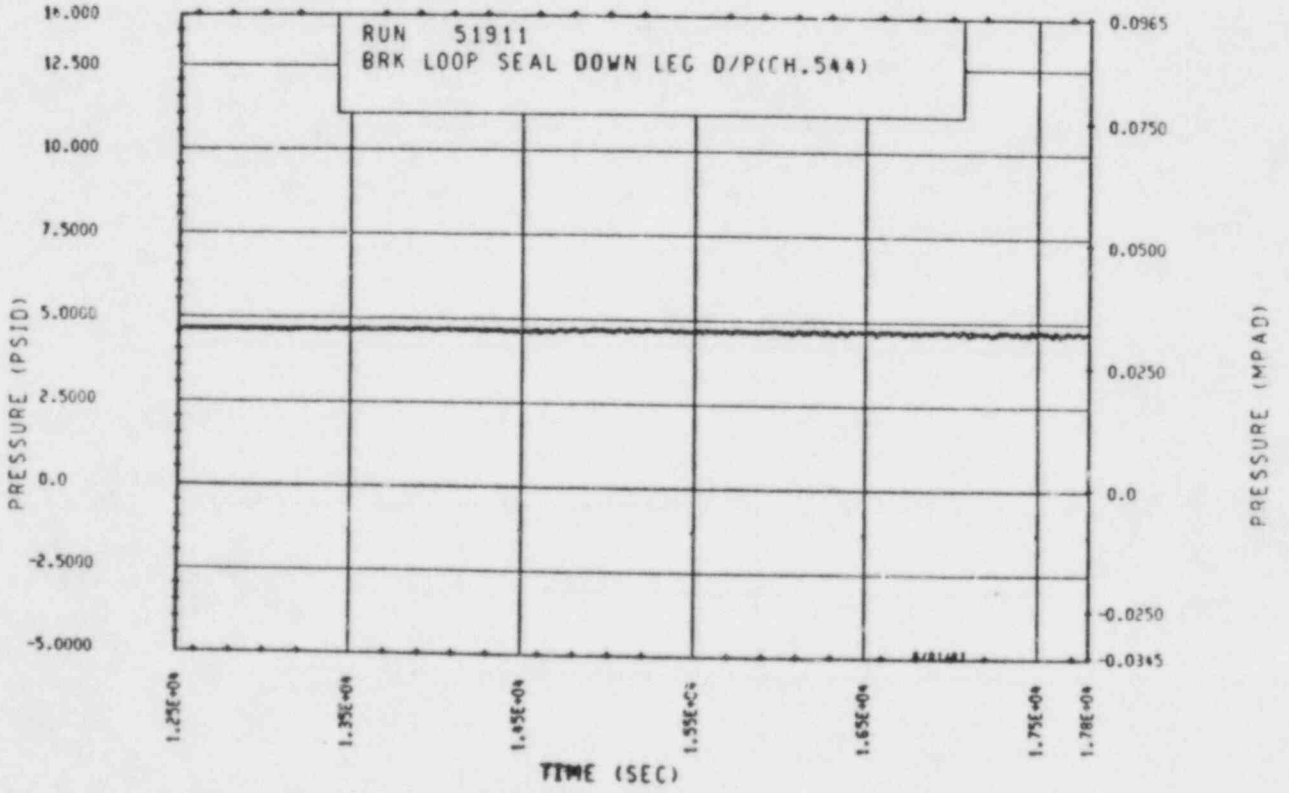

Figure 5-42 Broken Loop Seal Descending Leg Differential Pressure (12,500-17,800 sec)

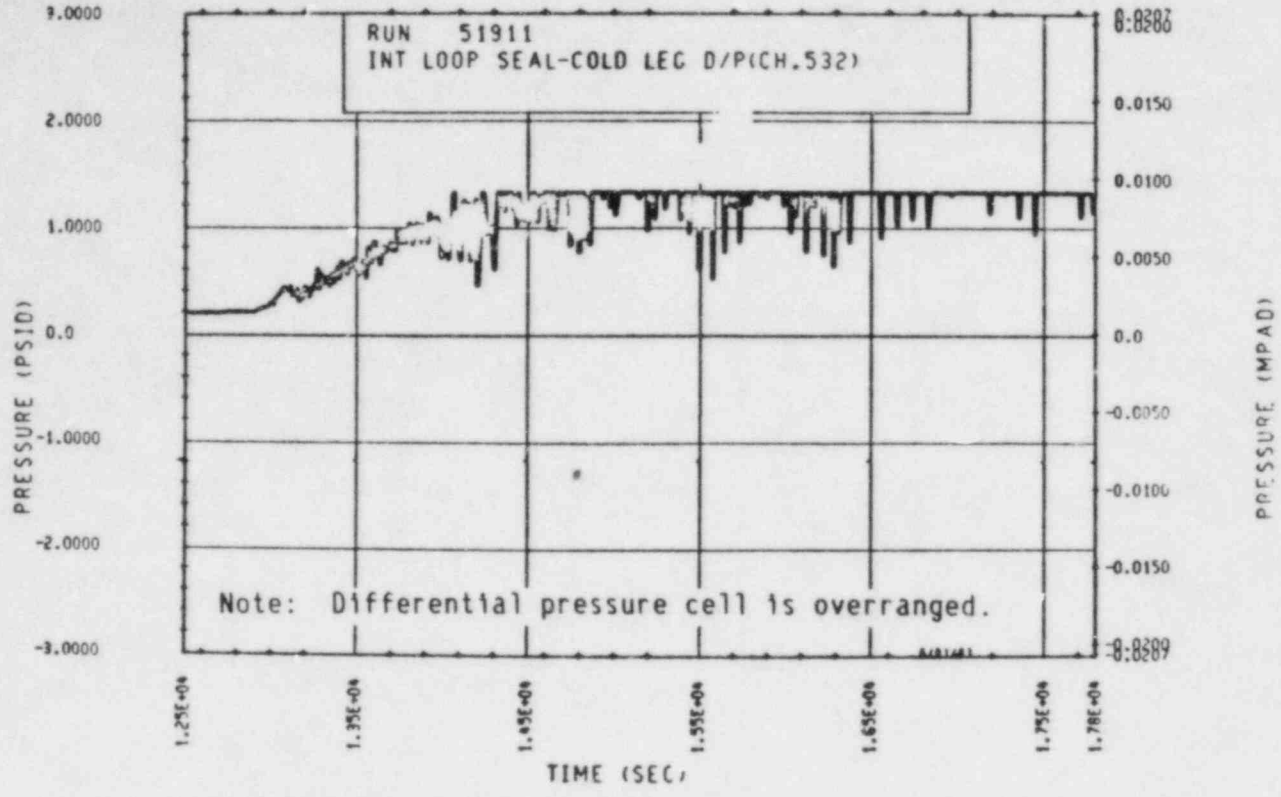

Figure 5-43. Unbroken Loop Seal Cold Leg Differential Pressure (12,500-17,800 sec)

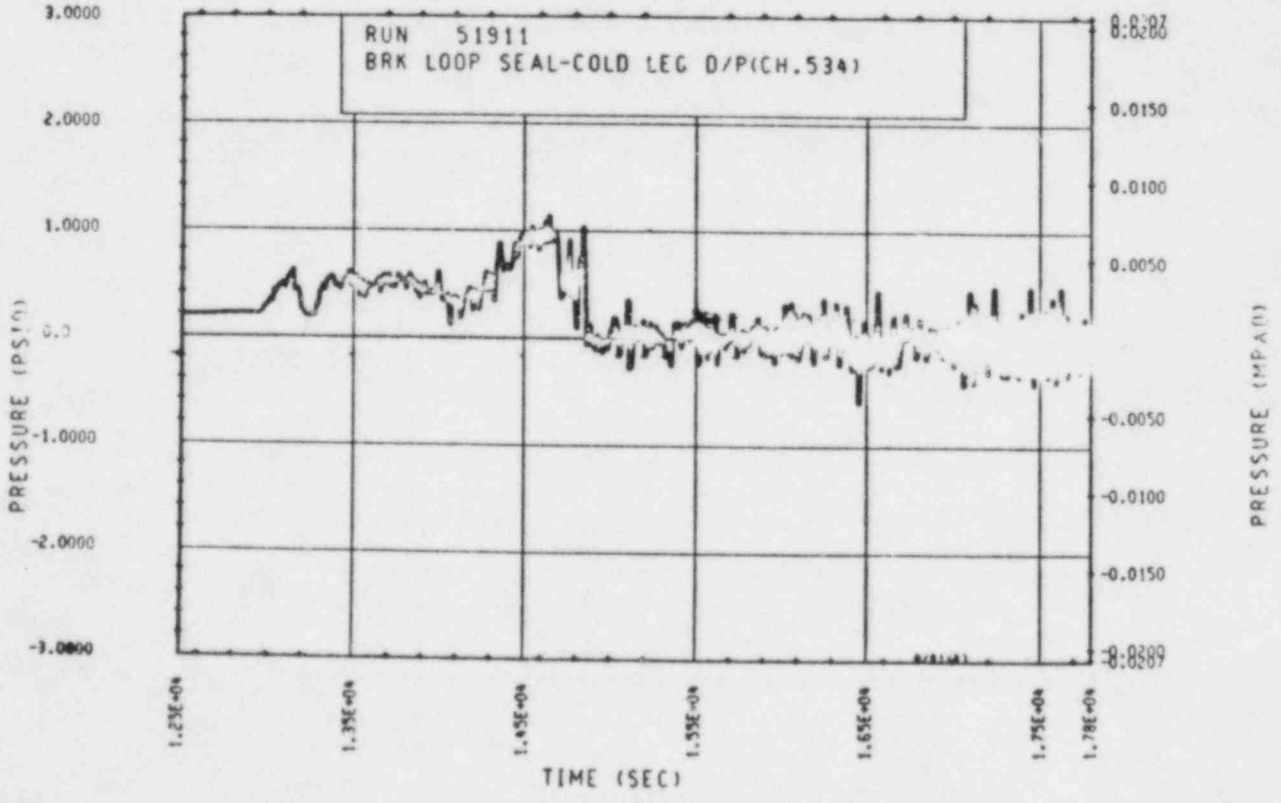

Figure 5-44. Broken Loop Seal Cold Leg Differential Pressure (12,500-17,800 sec)

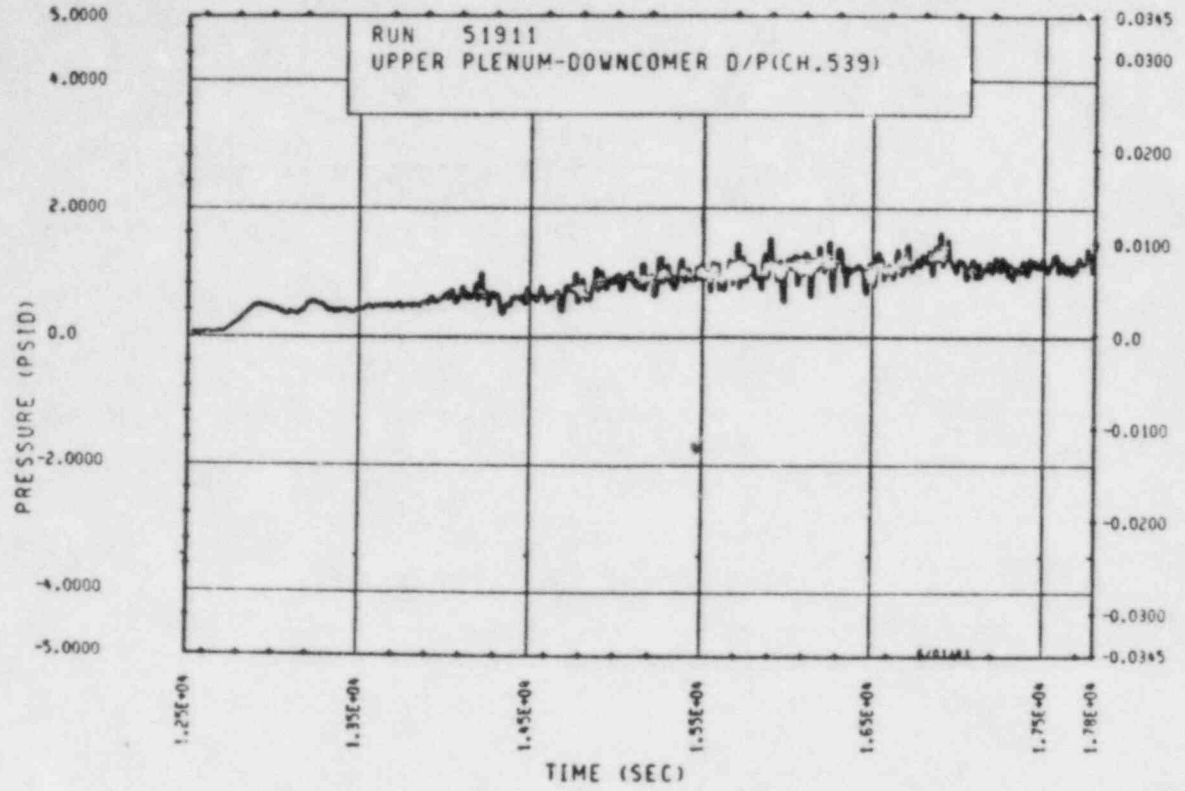

Figure 5-45. Upper Plenum-Downcomer Extension Differential Pressure (12,500-17,800 sec)

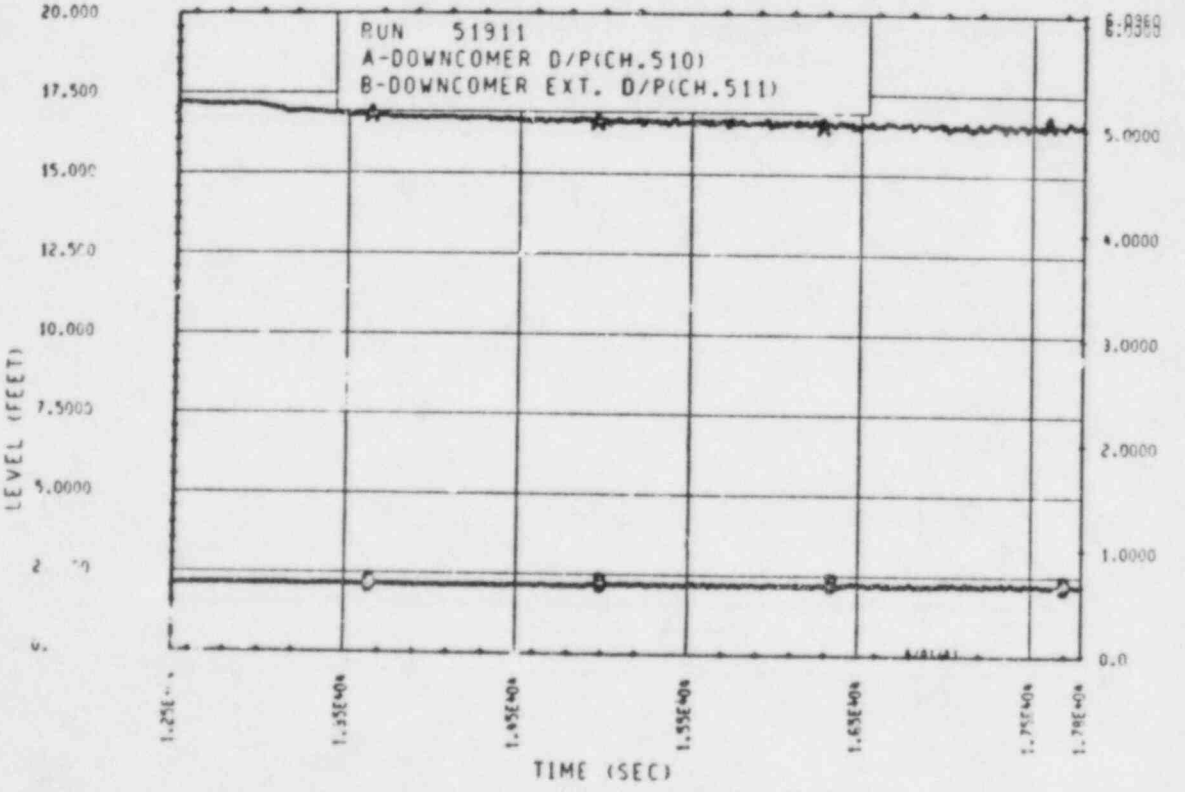

Figure 5-46. Downcomer and Downcomer Extension Liquid Levels (12,500-17,800 sec)

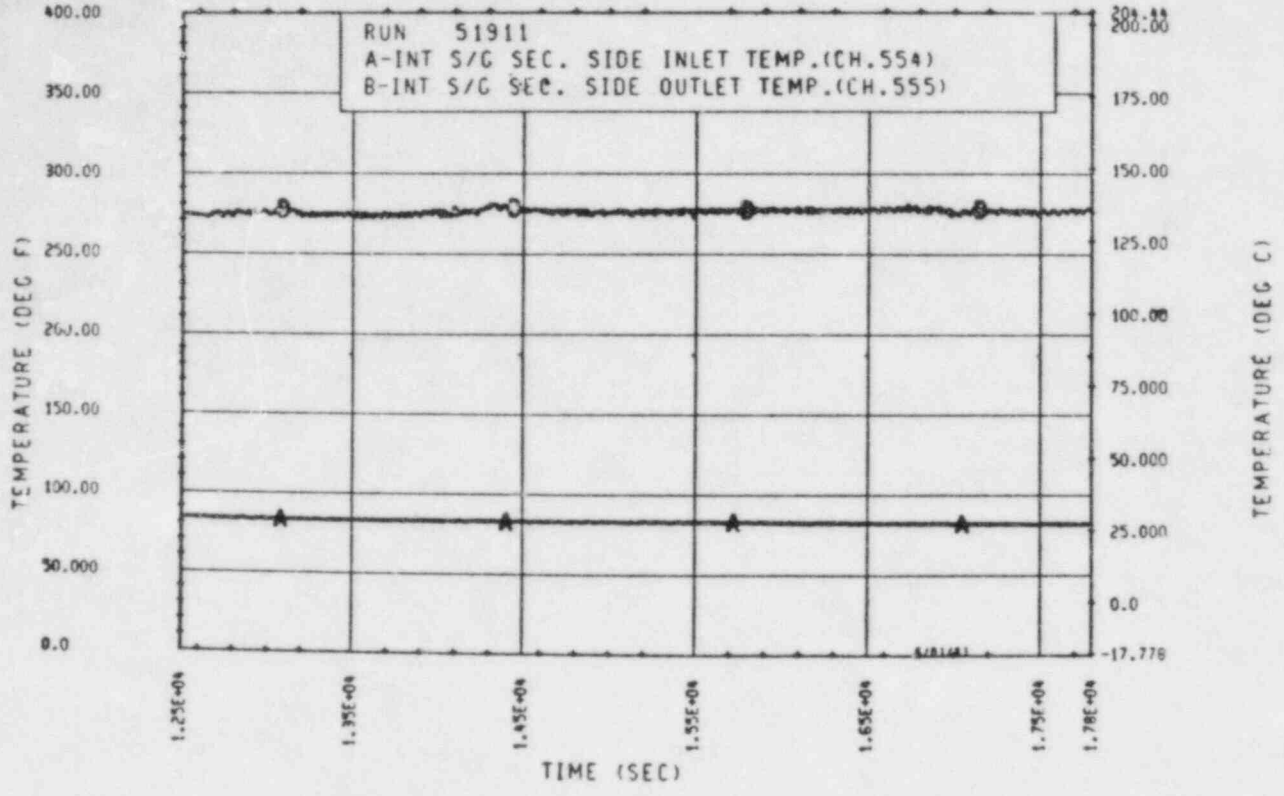

Figure 5-47. Unbroken Loop Steam Generator Secondary Side Inlet and Outlet Temperatures (12,500-17,800 sec)

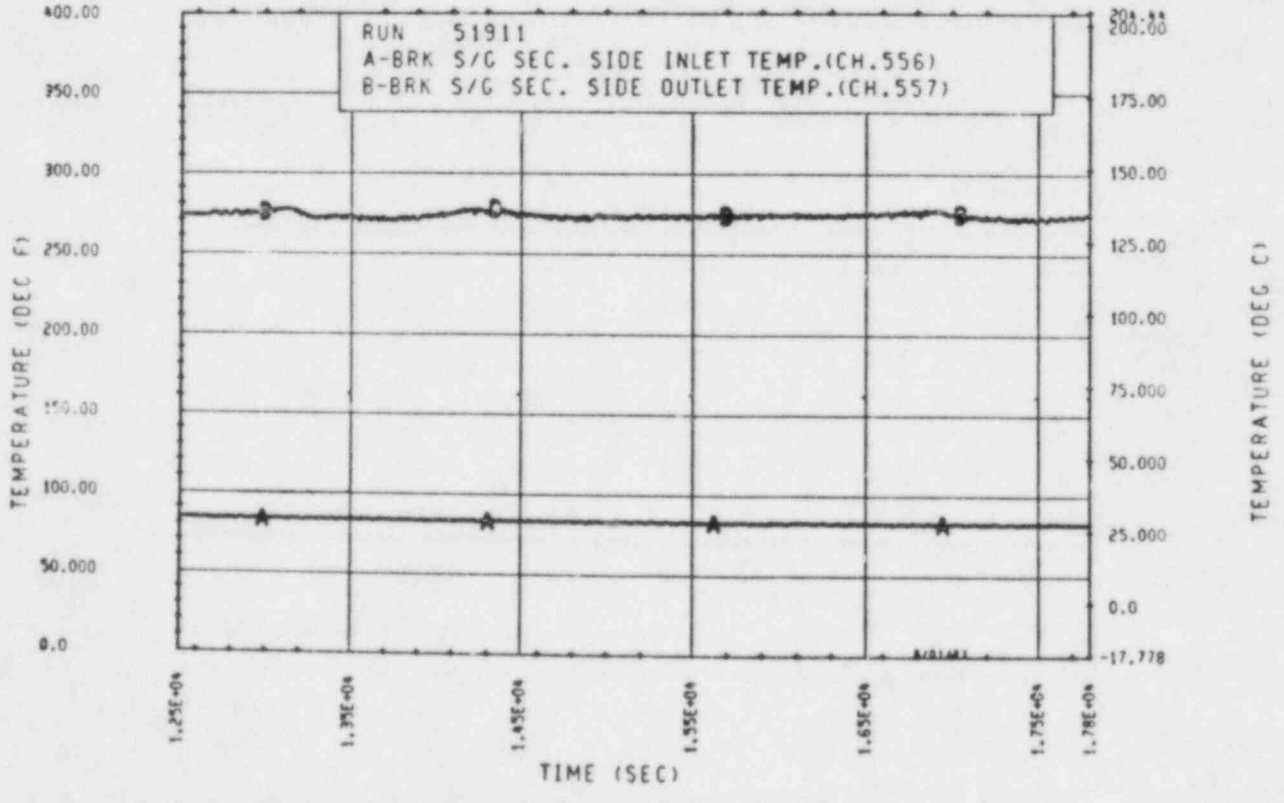

Figure 5-48. Broken Loop Steam Generator Secondary Side Inlet and Outlet Temperatures (12,500-17,800 sec)

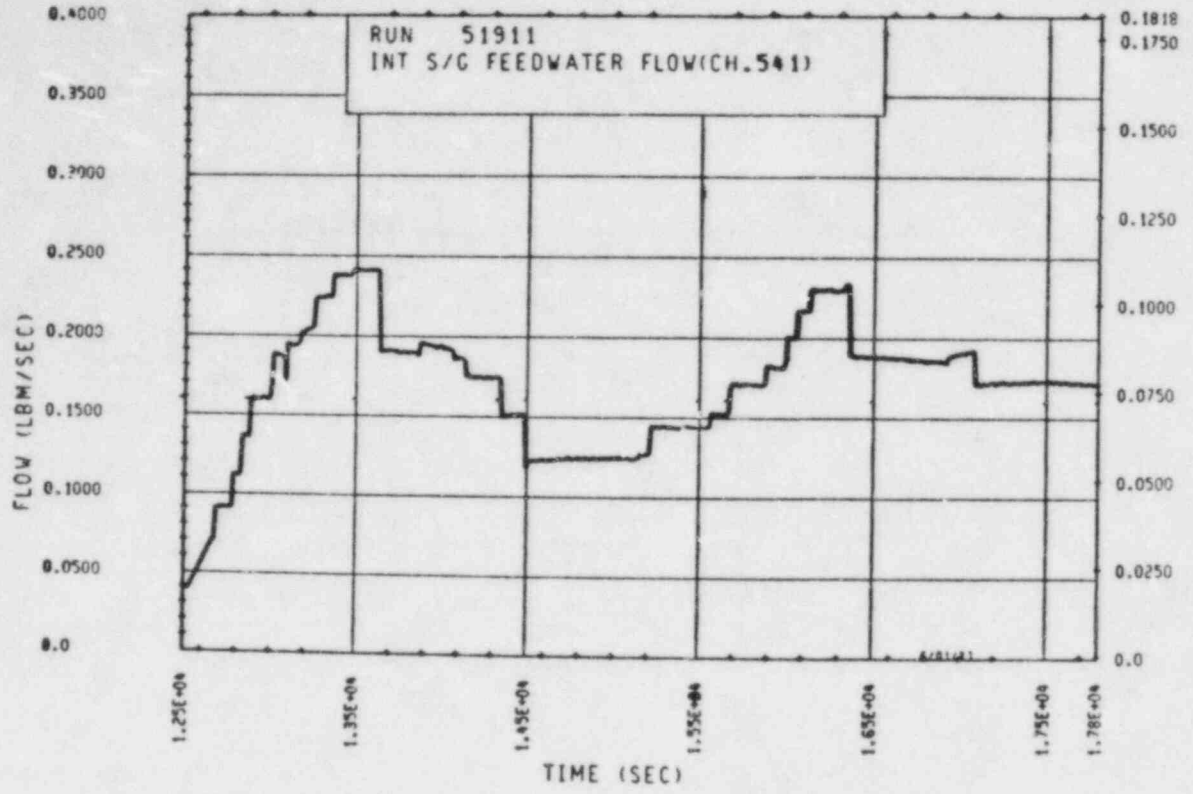

Figure 5-49. Unbroken Loop Steam Generator Feedwater Mass Flow Rate (12,500-17,800 sec)

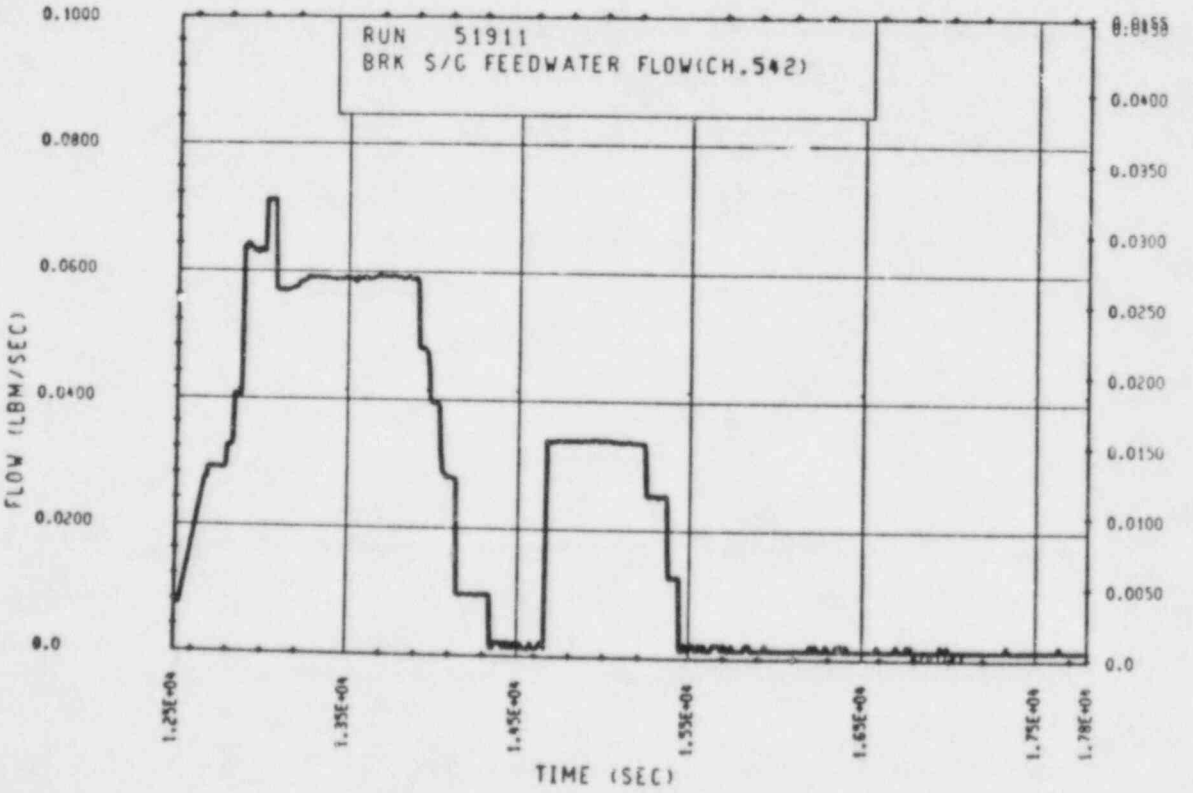

Figure 5-50. Broken Loop Steam Generator Feedwater Mass Flow Rate (12,500-17,800 sec)

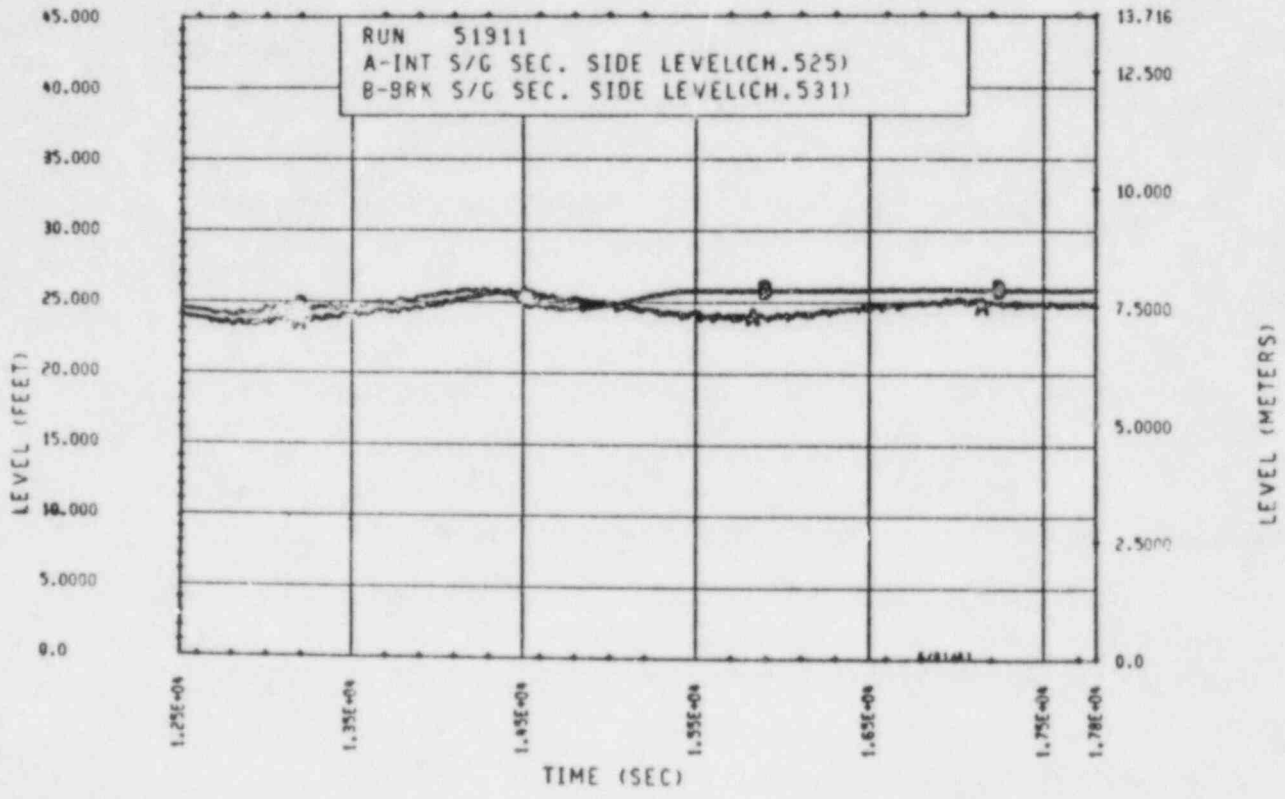

Figure 5-51. Unbroken and Broken Loop Steam Generator Secondary Side Collapsed Liquid Levels (12,500-17,800 sec)

The pressure decrease that resulted from the pressurizer being valved out was sufficient to remove the subcooling in the upper elevations of the upper plenum, so that flashing occurred. Further depressurization of the system by mass removal resulted in more flashing as well as vapor generation in the upper elevations of the rod bundle. Figures 5-11 through 5-23 show the resulting change in void fraction in the upper plenum and throughout the rod bundle. As the figures indicate, most of the boiling was occurring in the rod bundle above the 2.13 m (9 ft) elevation. Figure 5-24 shows the vapor generation rate increasing as the mass inventory was reduced. The vapor generation rate was calculated from a mass and energy balance performed on the rod bundle using quasi-steady-state data as boundary conditions. The two-phase condition at the rod bundle exit was verified by the fact that the rod bundle exit temperature was saturated. Figure 5-8 shows the rod bundle exit temperature decaying in an exponential fashion, reflecting the correspondence between saturation temperature and pressure. The rod bundle inlet temperature, also shown in figure 5-8, remained at a relatively constant value. Its degree of subcooling, however, decreased as mass was removed.

The single-phase to two-phase peak flow region was characterized by the single-phase/two-phase interface in the steam generator being located on the uphill side of the U-tubes. During the early stages of the mass inventory reduction, the vapor generation rate in the rod bundle was low and the single-phase/two-phase interface occurred in the lower elevations of the U-tubes. As the vapor generation rate increased with mass depletion and loss of inlet subcooling, the required U-tube condensation length increased and the interface consequently moved up the uphill side of the U-tubes. Evidence of this is shown in figure 5-29, which shows the unbroken loop steam generator plenum-to-plenum pressure drop. As the interface moved up the uphill side of the U-tubes, the total pressure drop shown in figure 5-29 became increasingly negative as a result of the increasingly negative gravitational pressure drop component. This reflects the increased gravitational force imbalance that occurred between the uphill and downhill portions of the entire loop as more and more vapor was generated. The unbroken loop counteracted this increasing imbalance by increasing the mass flow rate through the loop, as shown in figure 5-5. This flow increase was felt in the total mass flow rate through the core, as shown in figure 5-4.

The broken loop, however, did not experience a mass flow rate increase as the vapor generation rate increased. Figure 5-6 shows the broken loop mass flow rate increasing slightly, only to go to zero when the mass inventory was reduced to 91 percent. The broken loop would stall during every single-phase to two-phase peak flow transition. The stalling of the broken loop, however, had no impact on the system's ability to remove the decay heat from the rod bundle. The unbroken loop became the sole heat sink and the system operated in a N-1 loop configuration with no problems. This stalling phenomenon is discussed in more detail below.

Theoretically, the maximum gravitational force imbalance will occur when the single-phase/two-phase interface in the steam generator is coincident with the very top of the U-tubes. This condition, which would drive the maximum amount of flow through the loop, corresponds to the peak two-phase flow point. In this investigation, the secondary side was operated with a collapsed liquid level of only 7.62 m (25 ft) (71 percent full). As a result, the peak two-phase flow point occurred when the interface was coincident with the secondary side froth level, which is above the 7.62 m (25 ft) elevation. With any further increase in steam generation rate, the two-phase/single-phase interface would flow over the top of the U-tube to the downhill side in search of additional surface for condensation. The gravitational force imbalance would consequently decrease, and so would flow. This region of two-phase natural circulation is discussed in more detail in paragraph 5-6.

Unfortunately, the location of the single-phase/two-phase interface that occurred at peak two-phase flow cannot be verified. Figure 5-29 shows that the plenum-to-plenum differential pressure cell was not sized correctly to measure the phenomenon. The cell saturated at approximately $\pm$7 kPa ($\pm$1.0 psid), which explains why all the differential pressure oscillations are truncated below -7 kPa (-1.0 psid). A cell with a capability of 96 kPa ($\pm$14 psi) would be needed to cover the entire range of the U-tubes.

The peak two-phase mass flow rate was characteristically three times greater than that normally exhibited during single-phase natural circulation. The condition occurred at mass inventories of approximately 80 to 85 percent. For the case discussed in this section, the peak two-phase flow condition occurred

at a mass inventory of 81 percent. The variation in mass inventory could be the result of slight differences in the secondary side collapsed liquid levels and associated froth levels that may have occurred from test to test. As previously discussed, the peak two-phase flow condition was an unbroken loop phenomenon. The broken loop consistently stalled and became inactive prior to reaching the peak flow condition. Had the broken loop not stalled, the peak flow condition would have probably occurred at a mass inventory lower than 80 to 85 percent. The generated vapor would have distributed itself to both loops accordingly, and the corresponding single-phase/two-phase interfaces would have occurred at lower elevations on the uphill sides of the U-tubes. It would take a lower mass inventory and correspondingly higher vapor generation rate to move the interfaces to a peak two-phase flow condition.

5-6. Two-Phase Peak Flow to Reflux Condensation Transition

The system's behavior in this two-phase natural circulation region is documented in figures 5-52 through 5-104 during the time period 17,300 seconds to approximately 20,600 seconds.

As discussed in paragraph 5-5, the system operated in the peak two-phase flow condition in a N-1 loop configuration as a result of the broken loop stalling. The move from the peak two phase flow condition was accomplished by further depleting the primary side mass inventory (figure 5-52). As the mass inventory decreased, the vapor generation rate from the rod bundle correspondingly increased (figure 5-73), the rod bundle void fraction distribution changed considerably (figures 5-60 through 5-71), and more vapor was generated. The coolant entering the bottom of the bundle was nearly at the saturation temperature, so that nearly the entire bundle surface area was in the boiling mode. Vapor was consequently carried over the top of the unbroken loop U-tubes as more heat transfer area was required to accommodate the increased vapor generation rate. The single-phase/two-phase interface in the unbroken loop steam generator now existed on the downhill side of the U-tubes. The presence of vapor on the downhill side decreased the peak two-phase gravitational force imbalance that previously existed around the unbroken loop and flow consequently decreased (figures 5-53 and 5-54).

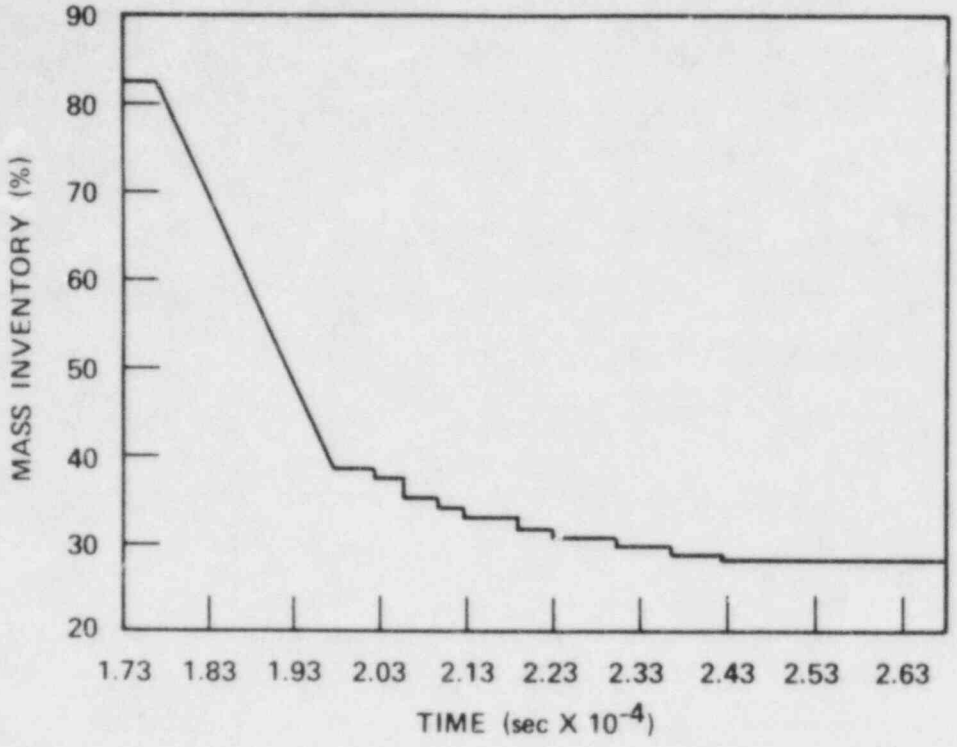

Figure 5-52. Mass Inventory as a Function of Time (17,300-26,500 sec)

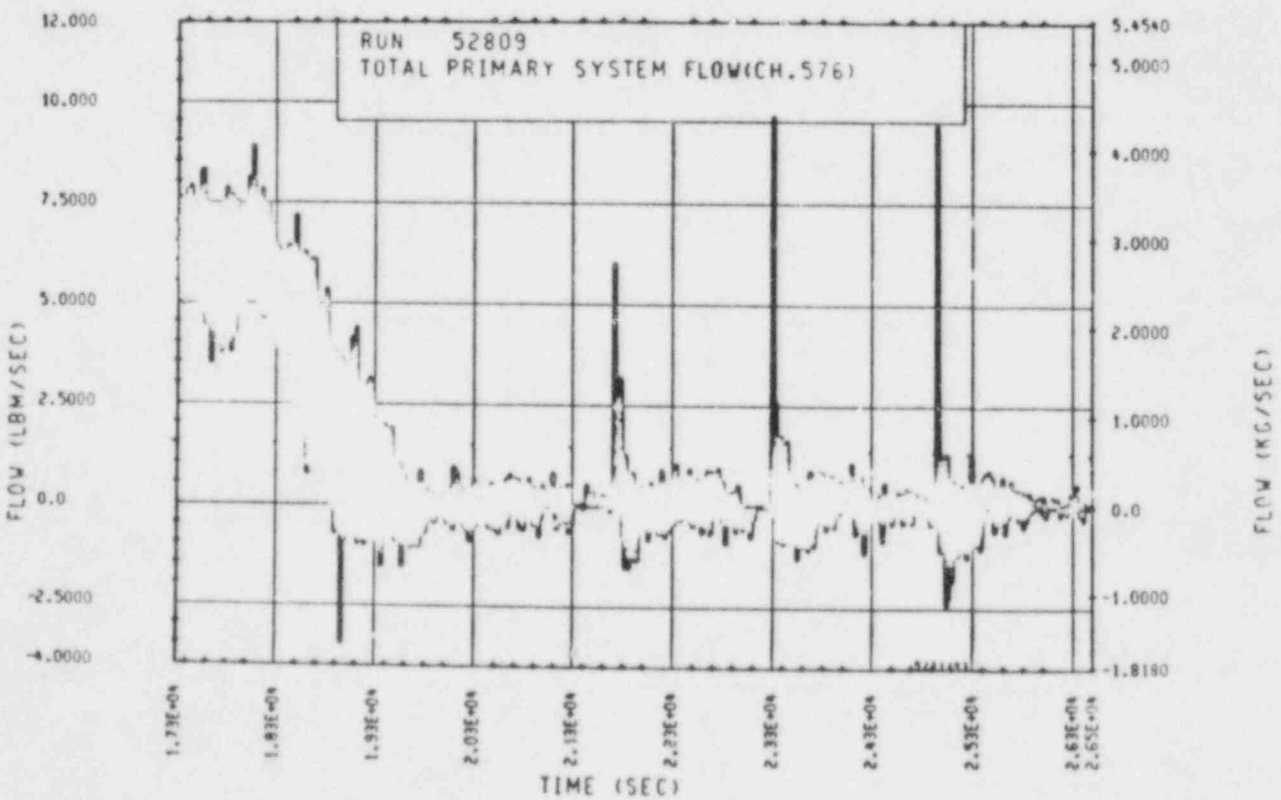

Figure 5-53. Mass Flow Rate Through Heater Rod Bundle (17,300-26,500 sec)

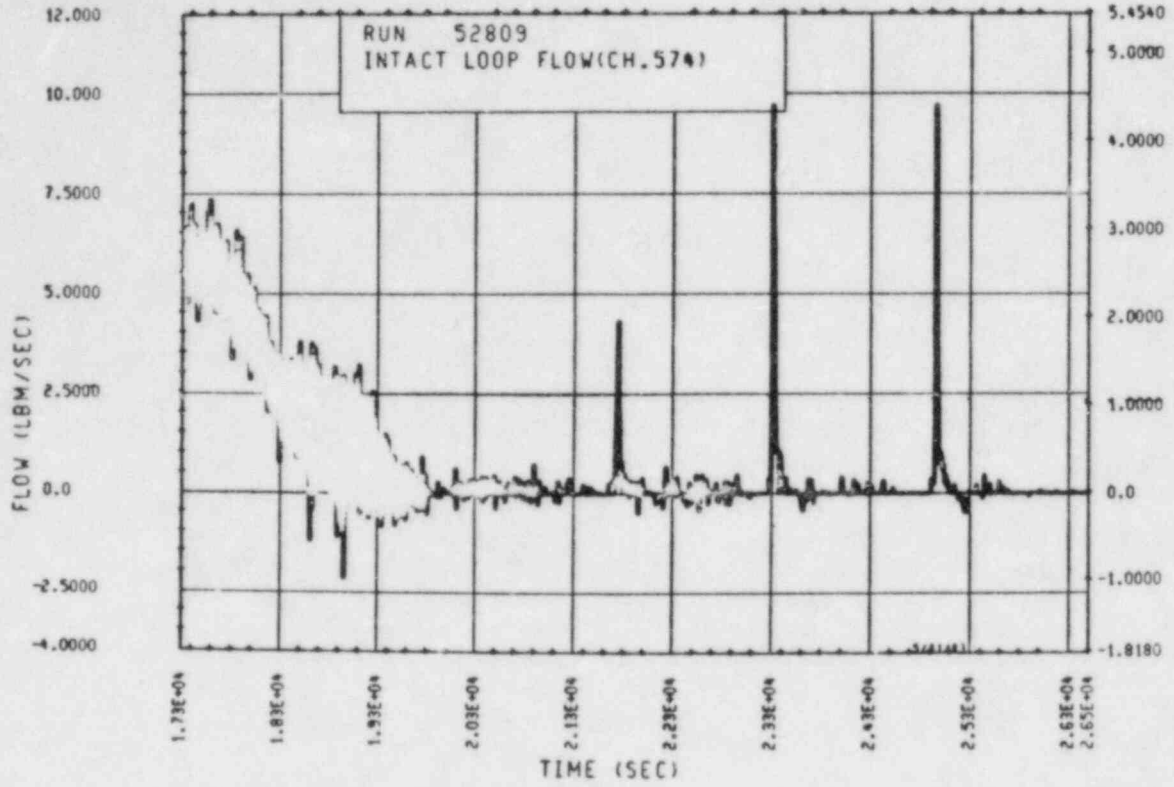

Figure 5-54. Mass Flow Rate Through Unbroken Loop (17,300-26,500 sec)

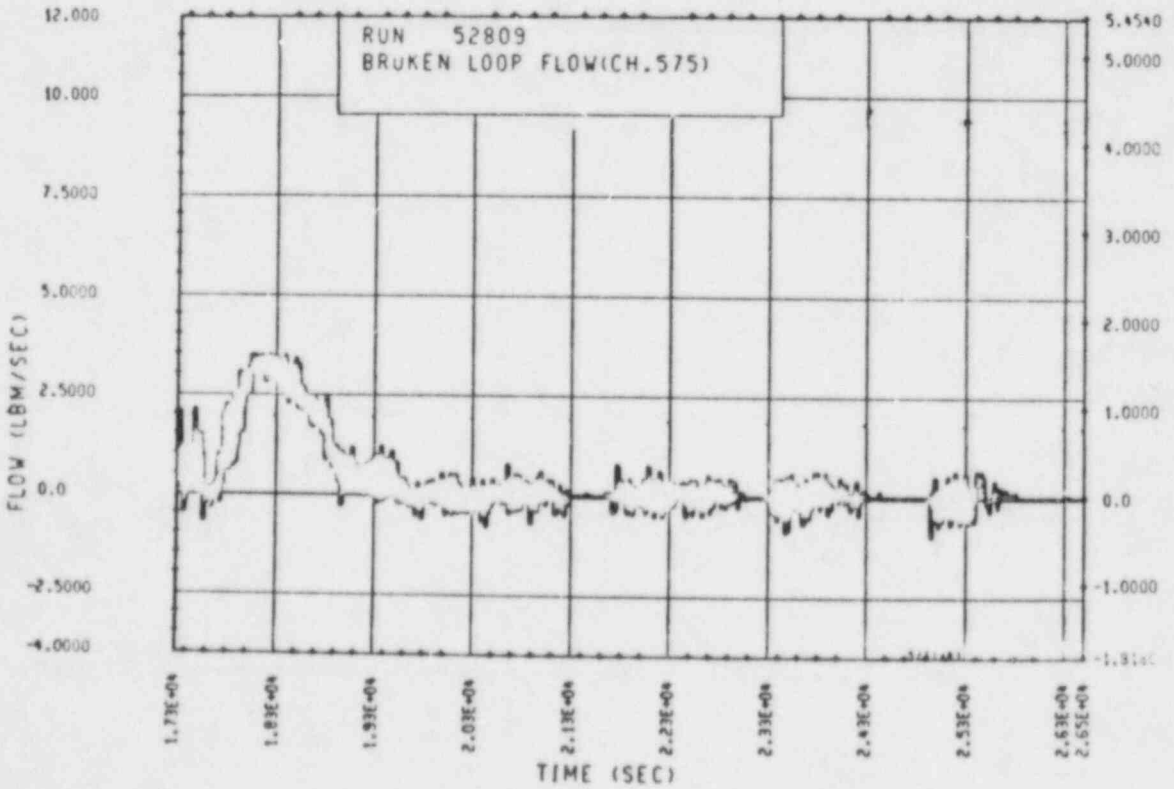

Figure 5-55. Mass Flow Rate Through Broken Loop (17,300-26,500 sec)

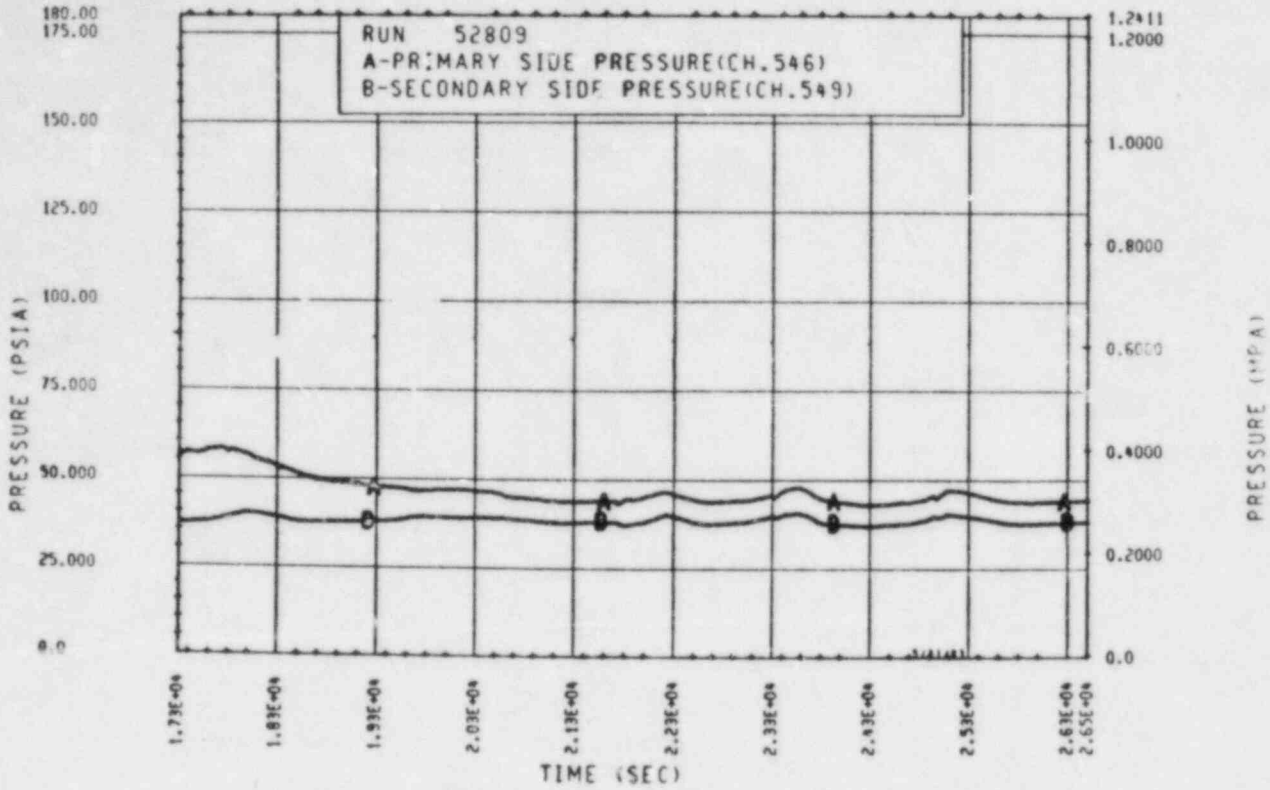

Figure 5-56. Primary and Secondary System Pressure (17,300-26,500 sec)

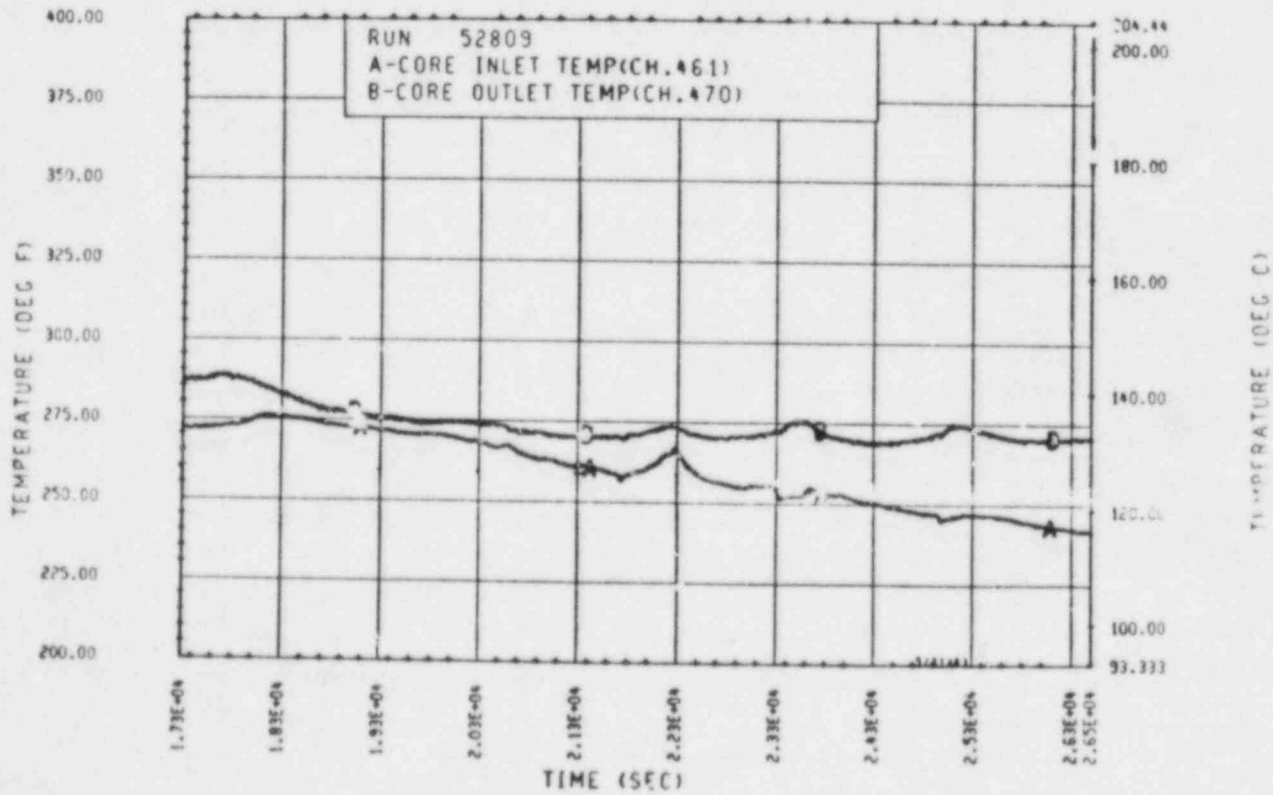

Figure 5-57. Heater Rod Bundle Inlet and Outlet Temperatures (17,300-26,500 sec)

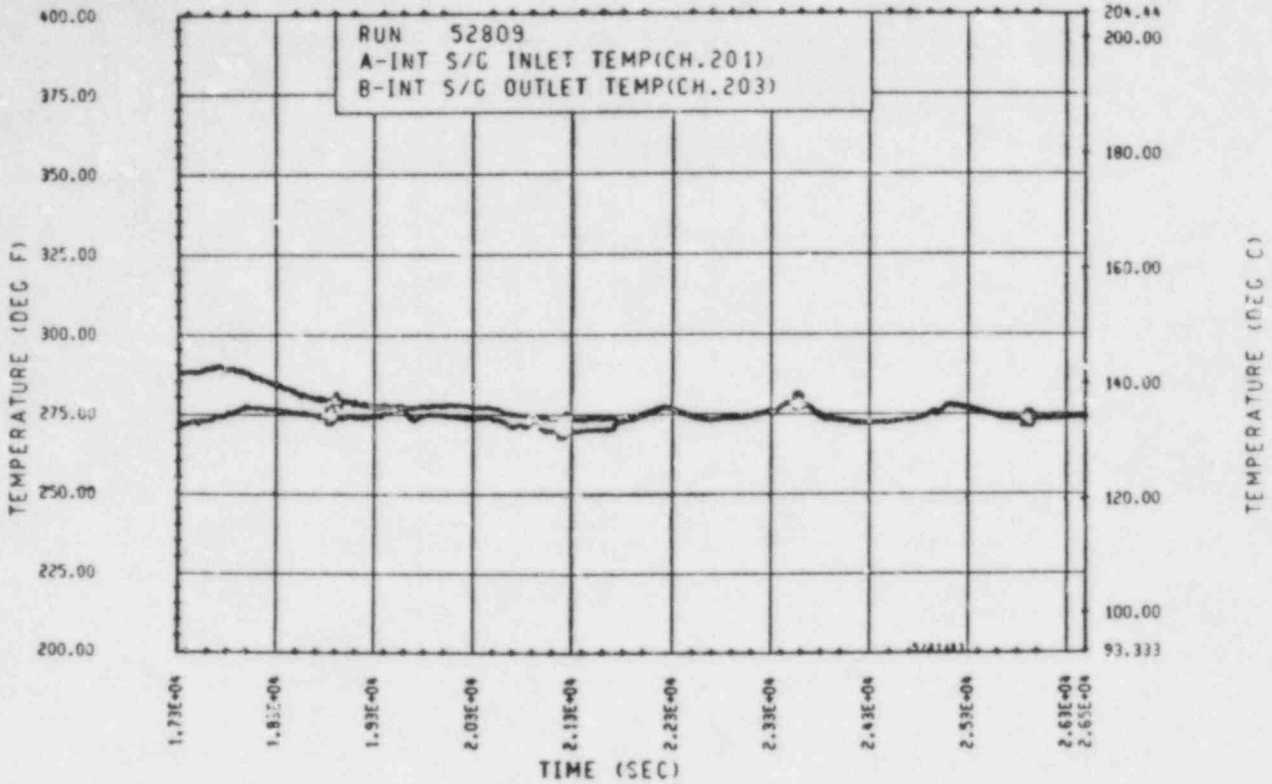

Figure 5-58. Unbroken Loop Steam Generator Inlet and Outlet Temperatures (17,300-26,500 sec)

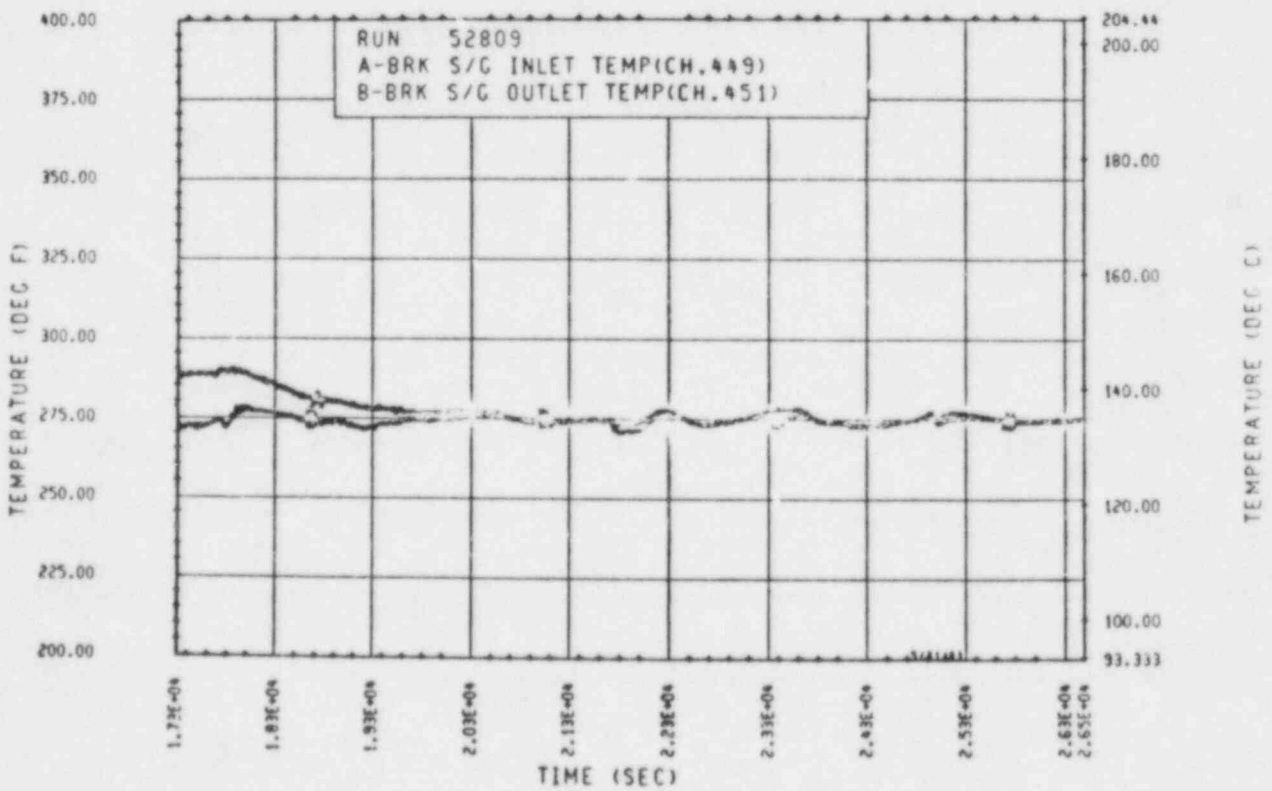

Figure 5-59. Broken Loop Steam Generator Inlet and Outlet Temperatures (17,300-26,500 sec)

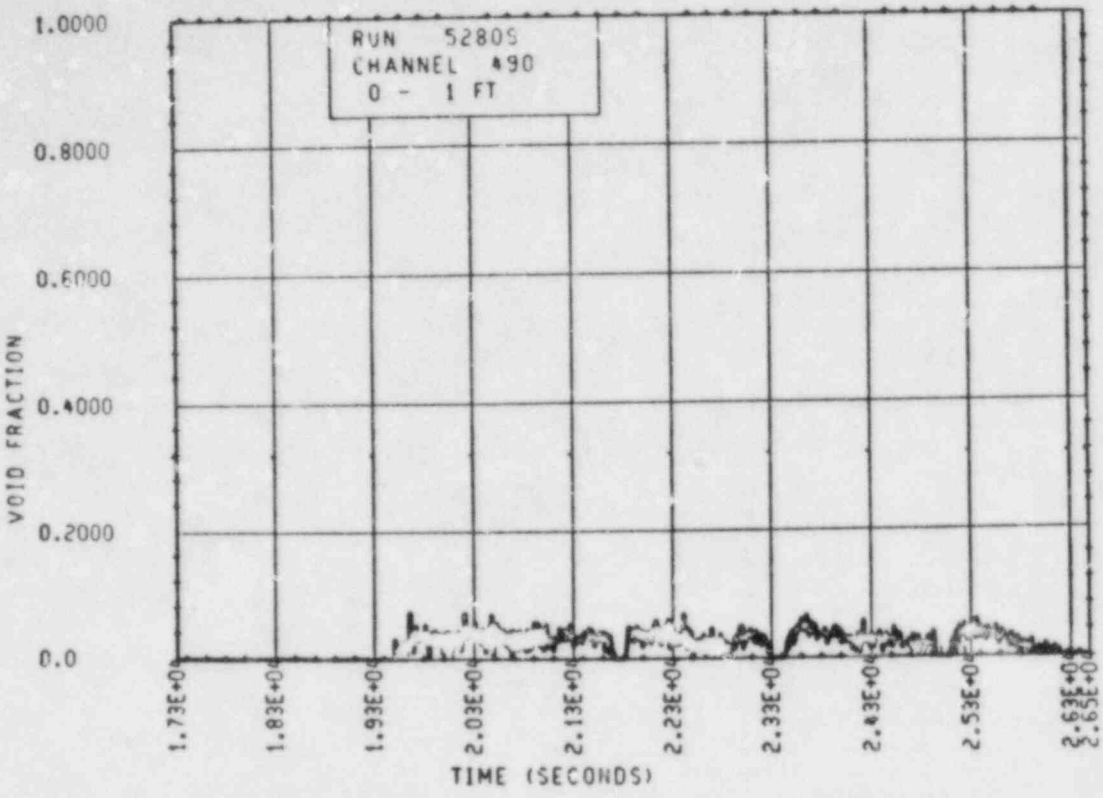

Figure 5-60. Heater Rod Bundle Void Fraction [0-0.30 m (0-1 ft)] (17,300-26,500 sec)

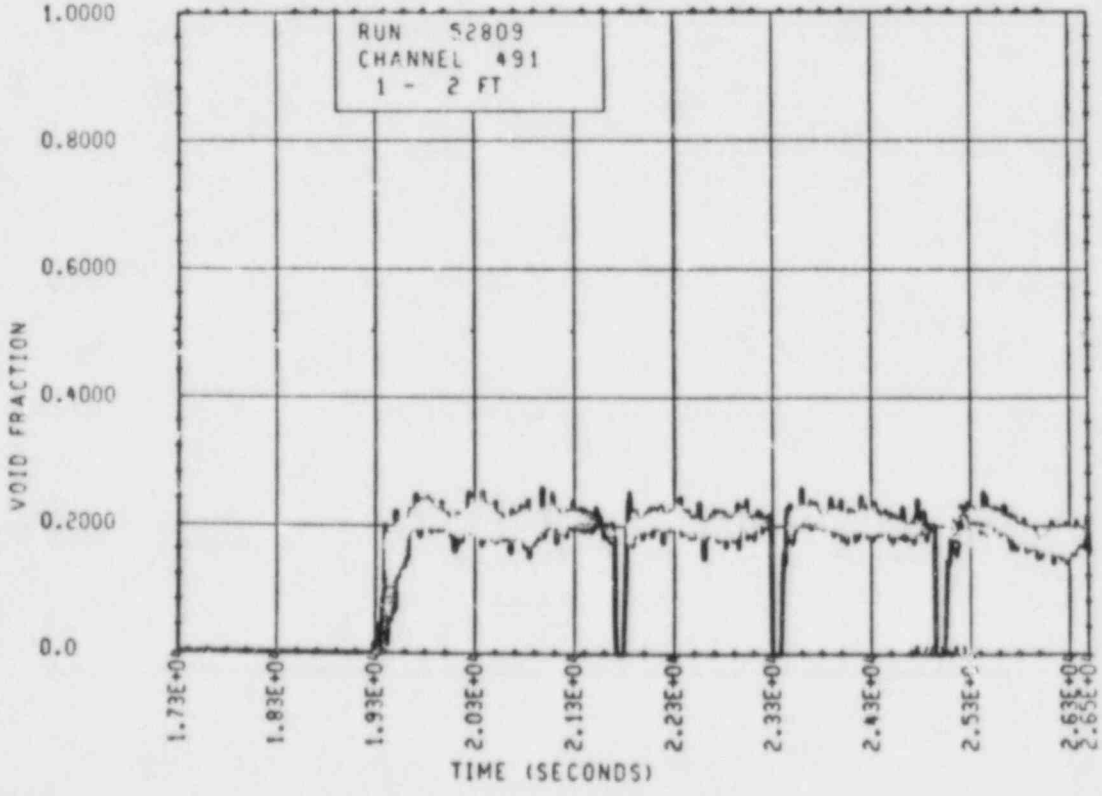

Figure 5-61. Heater Rod Bundle Void Fraction [0.30-0.61 m (1-2 ft)] (17,300-26,500 sec)

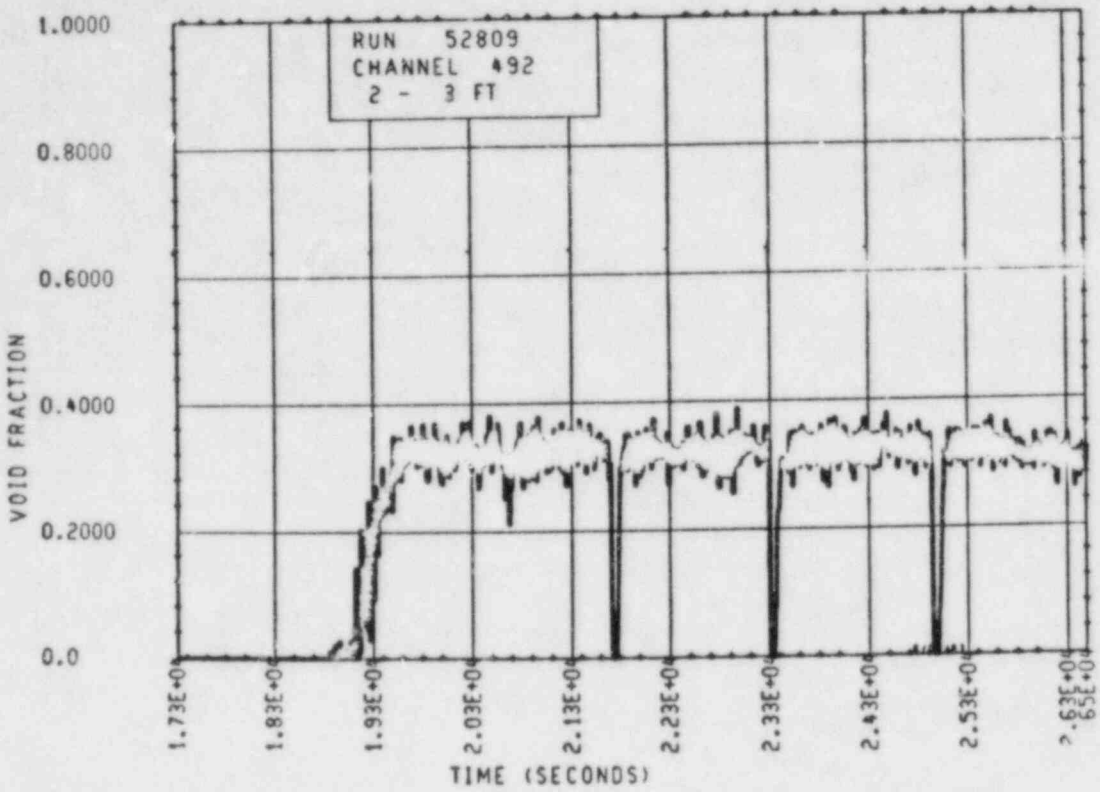

Figure 5-62. Heater Rod Bundle Void Fraction [0.61-0.91 m (2-3 ft)] (17,300-26,500 sec)

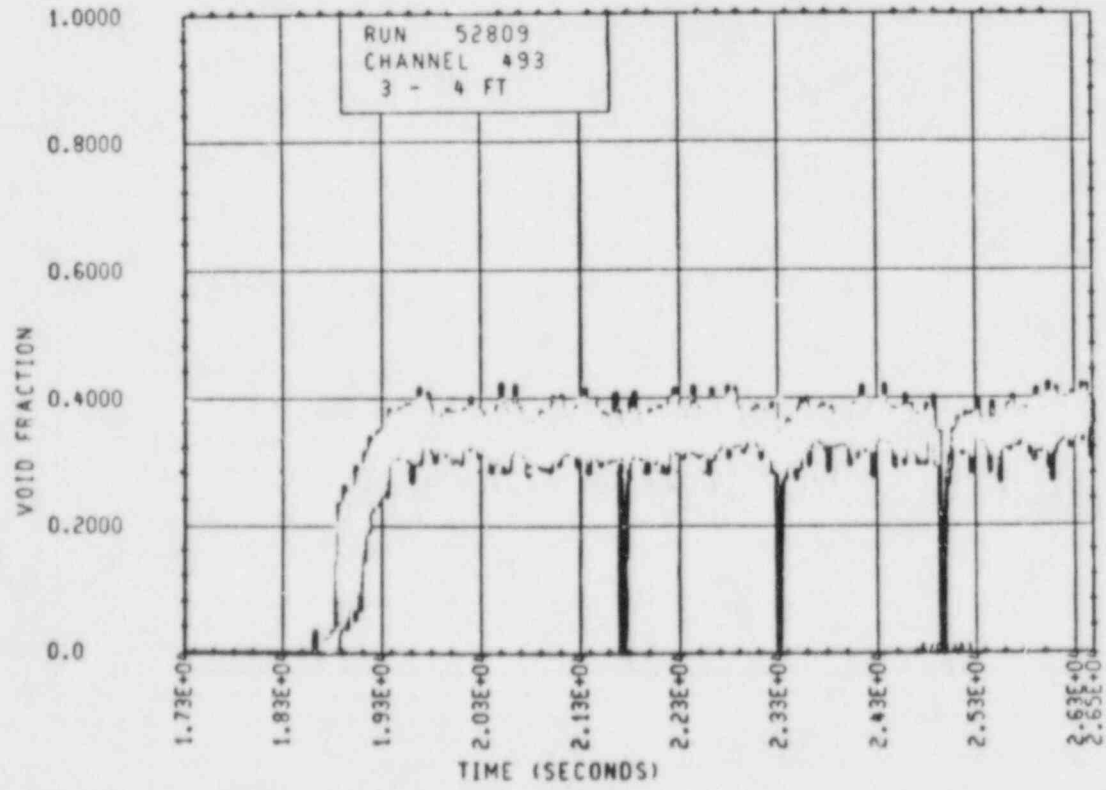

Figure 5-63. Heater Rod Bundle Void Fraction [0.91-1.22 m (3-4 ft)] (17,300-26,500 sec)

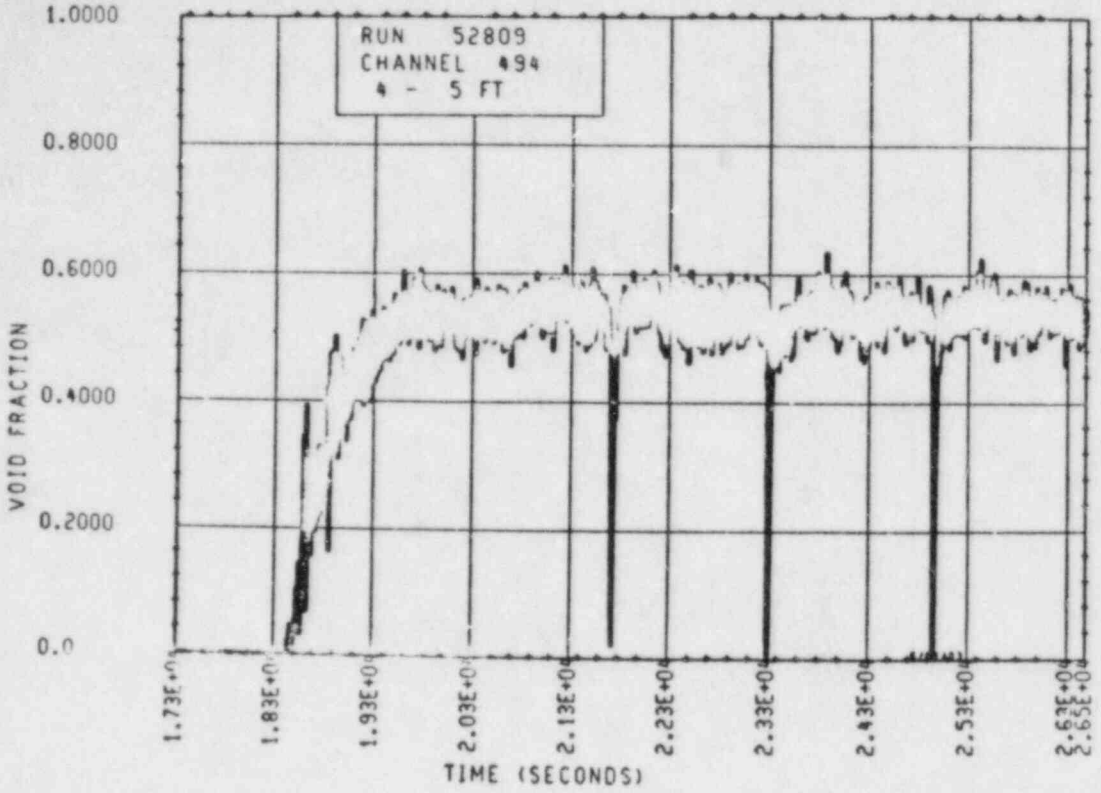

Figure 5-64. Heater Rod Bundle Void Fraction [1.22-1.52 m (4-5 ft)] (17,300-26,500 sec)

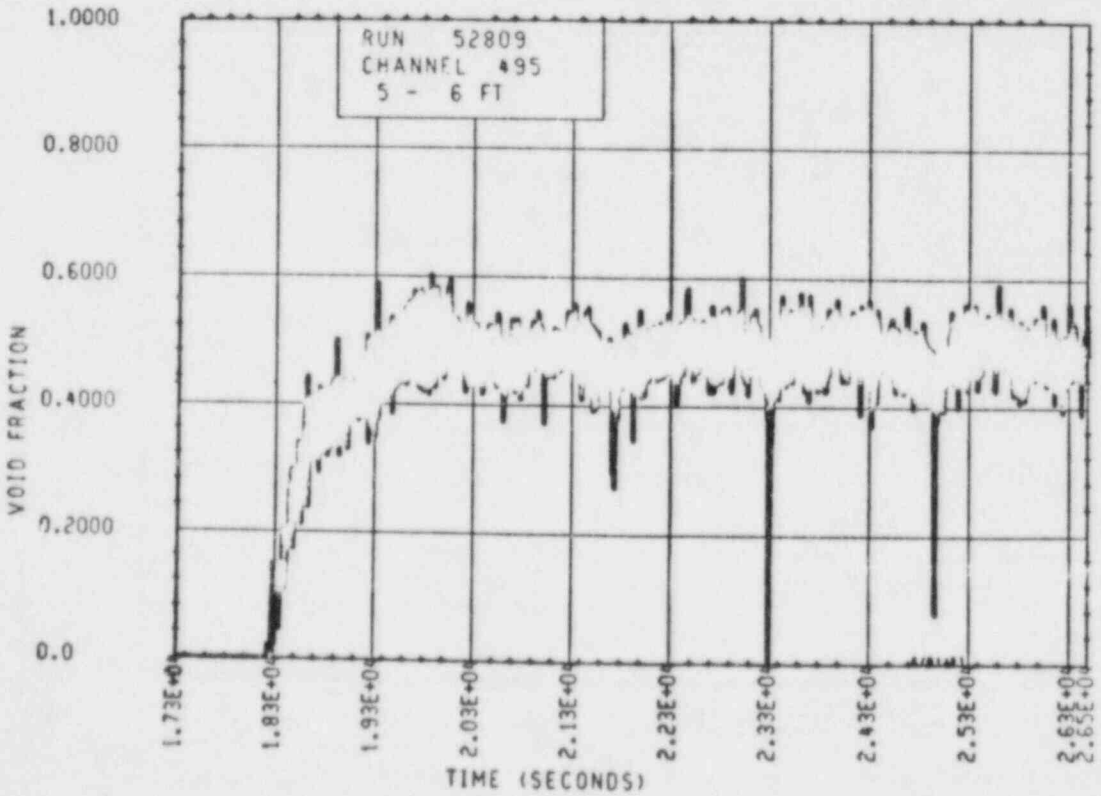

Figure 5-65. Heater Rod Bundle Void Fraction [1.52-1.83 m (5-6 ft)] (17,300-26,500 sec)

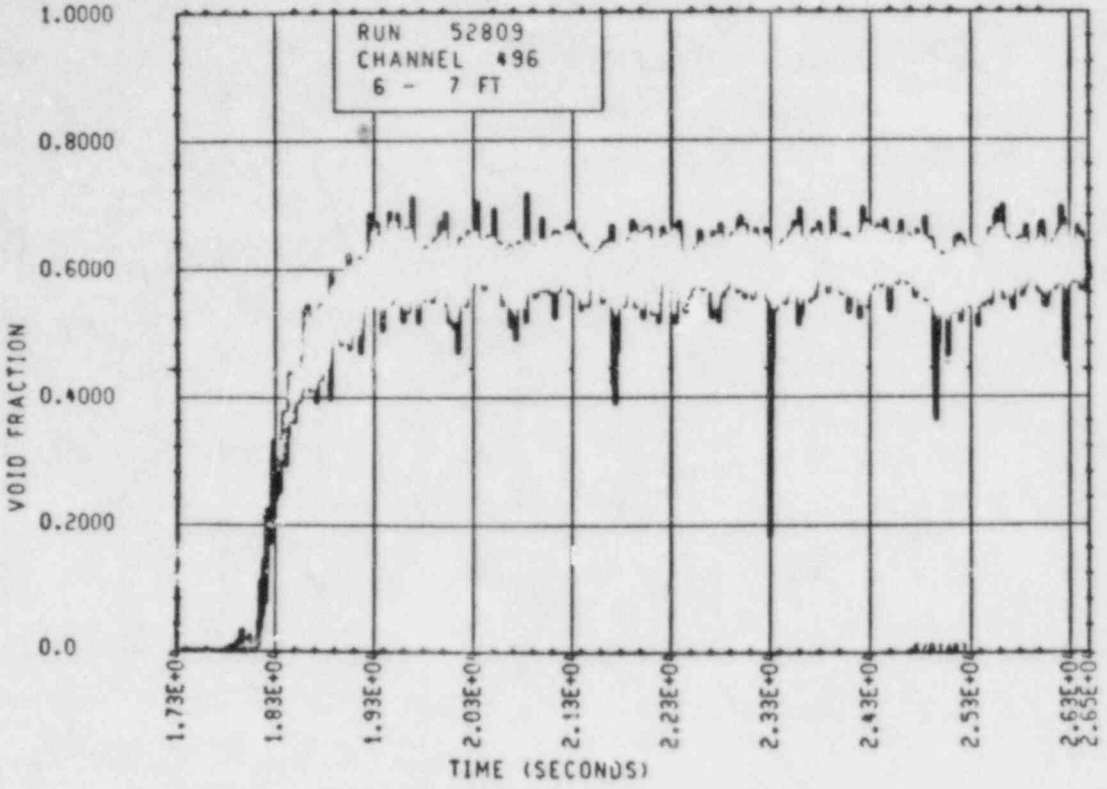

Figure 5-66. Heater Rod Bundle Void Fraction [1.83-2.13 m (6-7 ft)] (17,300-26,500 sec)

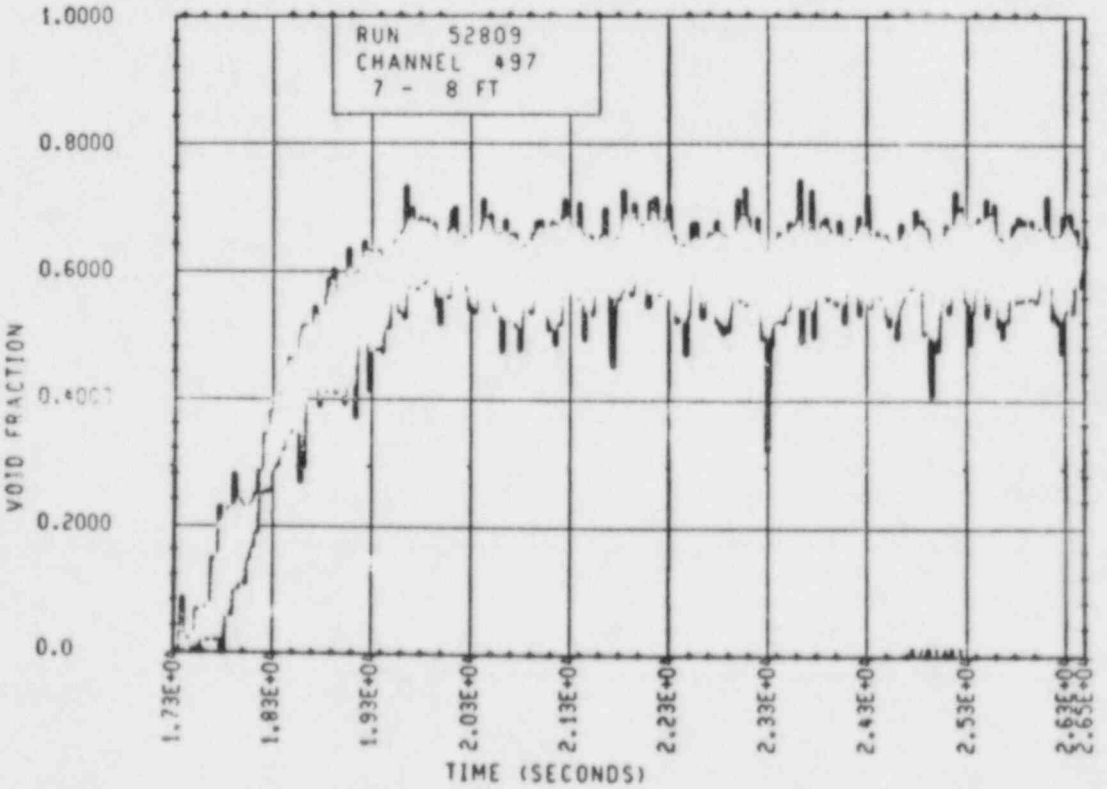

Figure 5-67. Heater Rod Bundle Void Fraction [2.13-2.44 m (7-8 ft)] (17,300-26,500 sec)

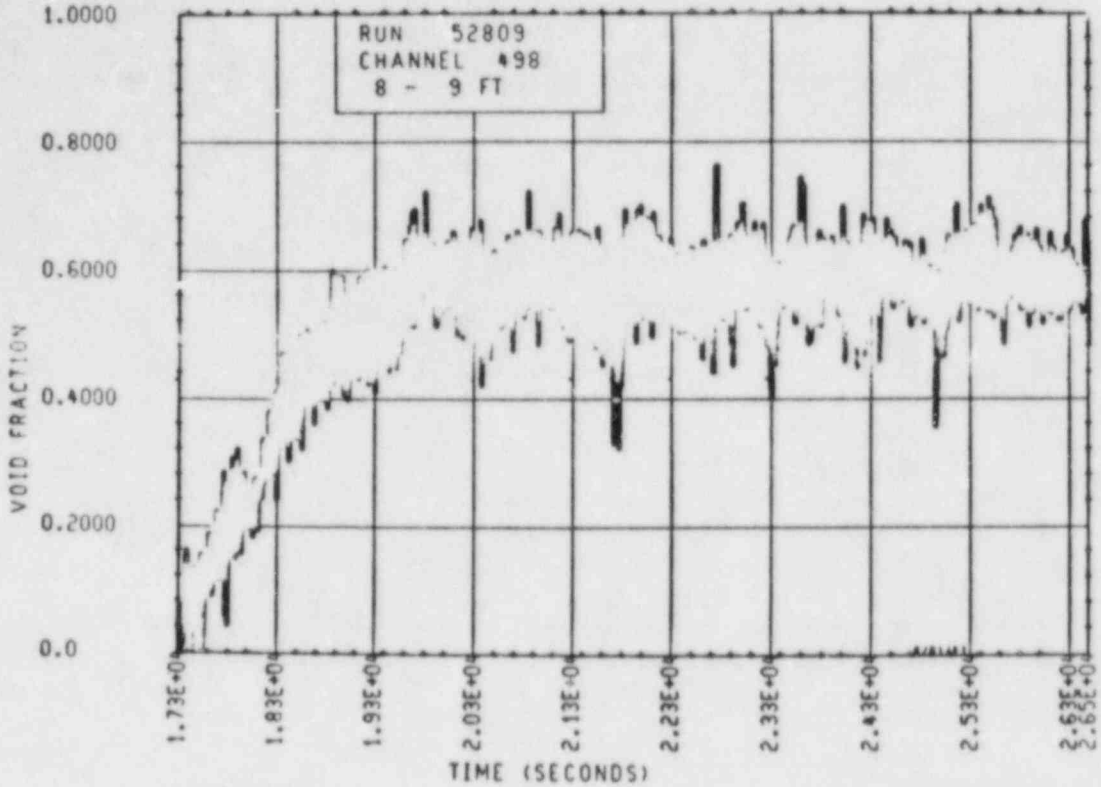

Figure 5-68. Heater Rod Bundle Void Fraction [2.44-2.74 m (8-9 ft)] (17,300-26,500 sec)

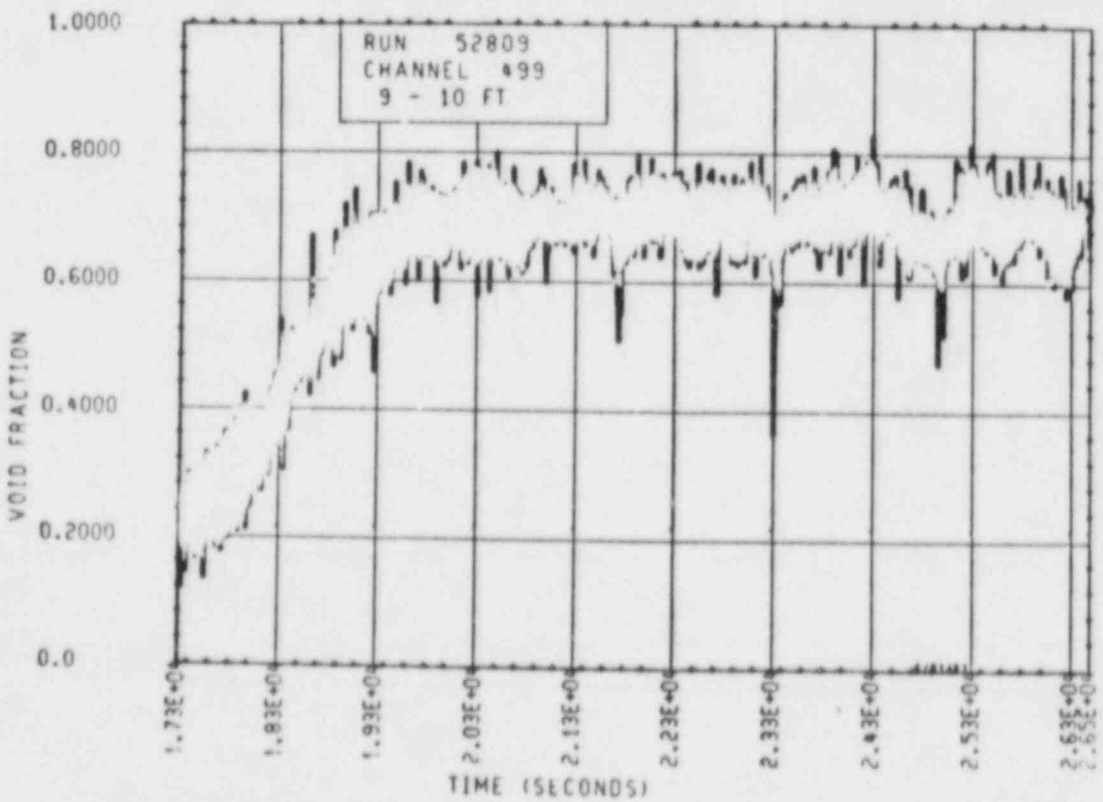

Figure 5-69. Heater Rod Bundle Void Fraction [2.74-3.05 m (9-10 ft)] (17,300-26,500 sec)

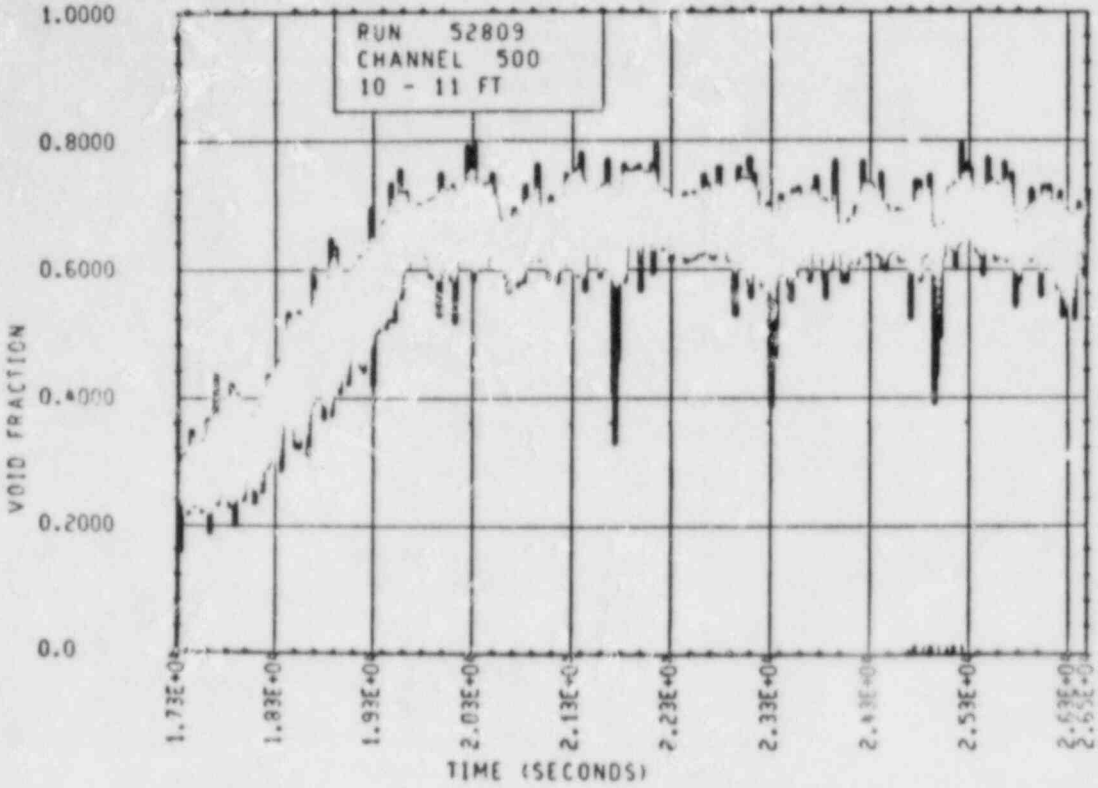

Figure 5-70. Heater Rod Bundle Void Fraction [3.05-3.35 m (10-11 ft)] (17,300-26,500 sec)

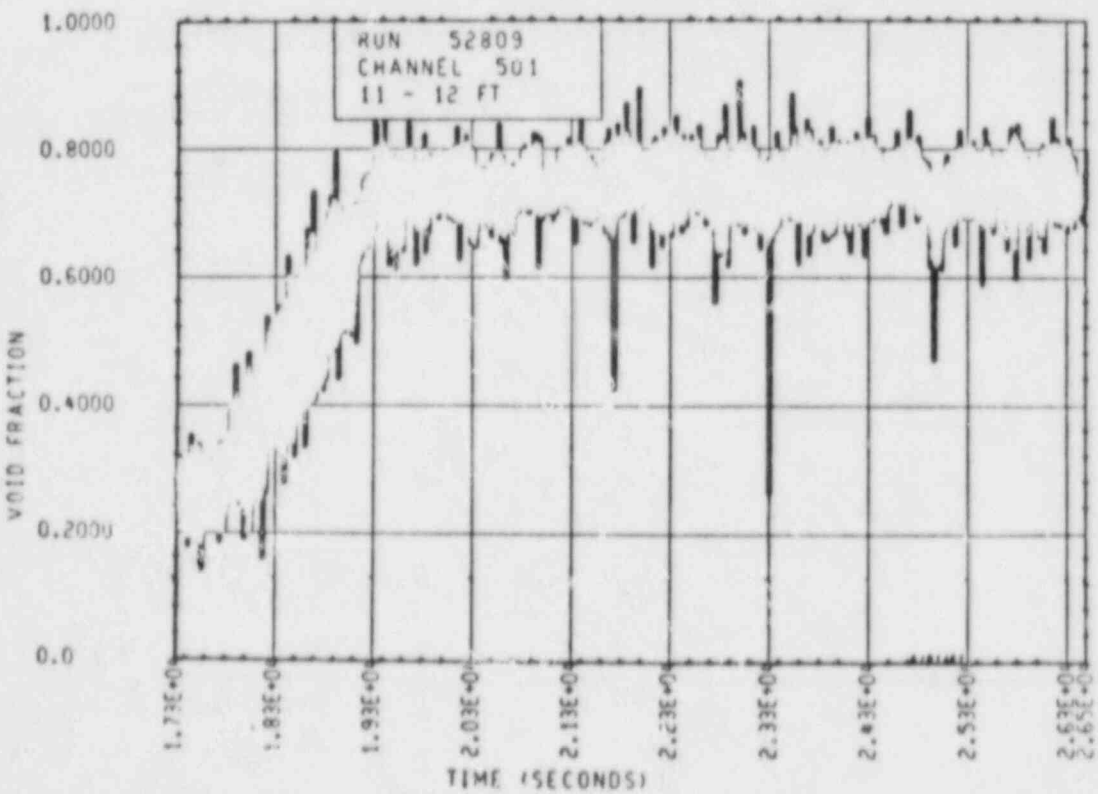

Figure 5-71. Heater Rod Bundle Void Fraction [3.35-3.66 m (11-12 ft)] (17,300-26,500 sec)

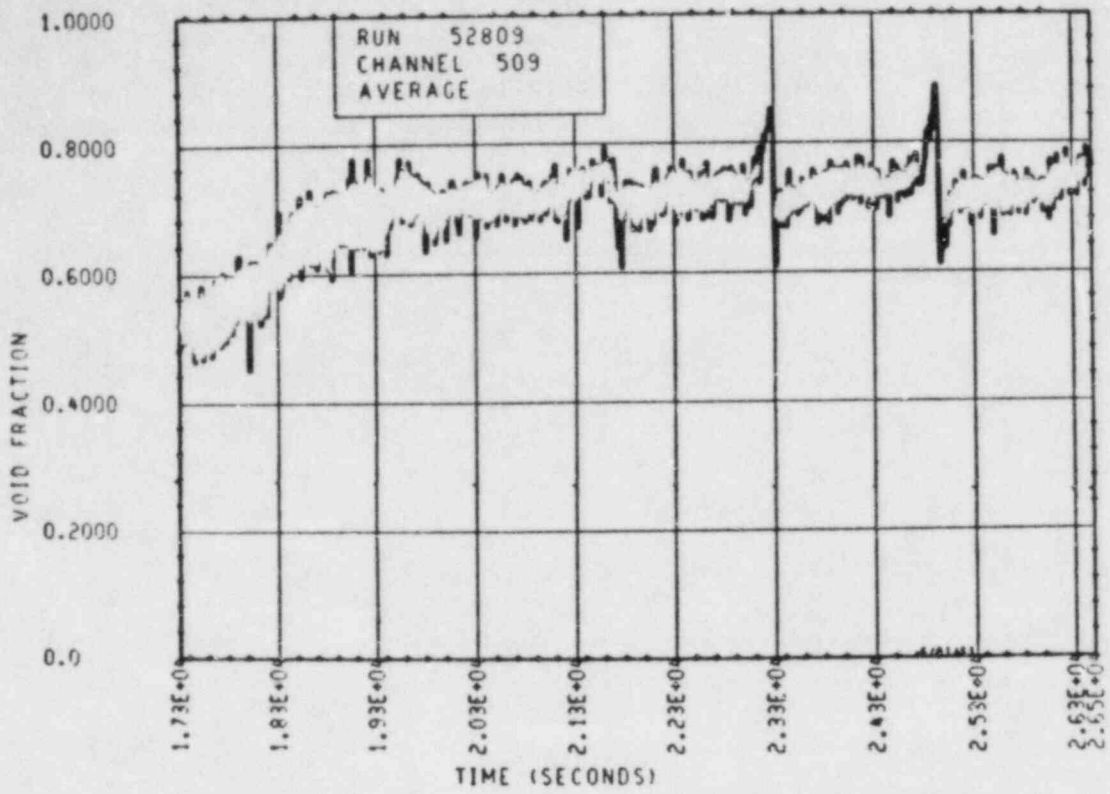

Figure 5-72. Upper Plenum Void Fraction (17,300-26,500 sec)

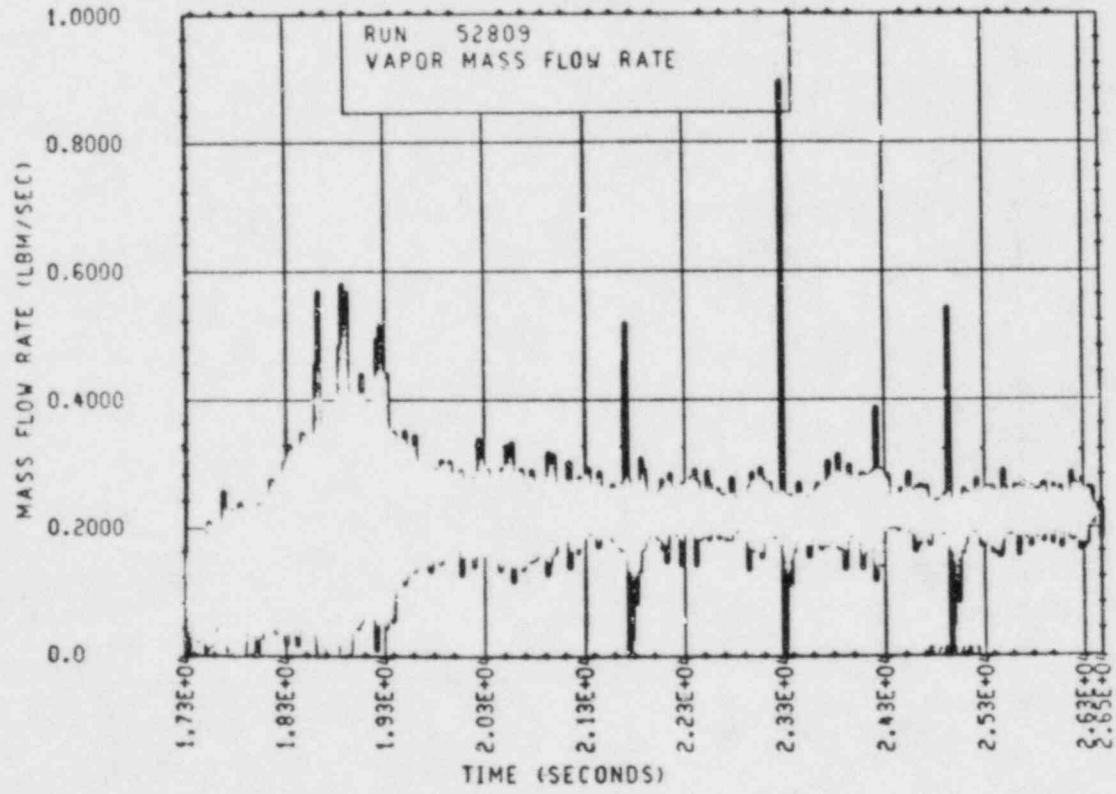

Figure 5-73. Calculated Heater Rod Bundle Vapor Generation Rate (17,300-26,500 sec)

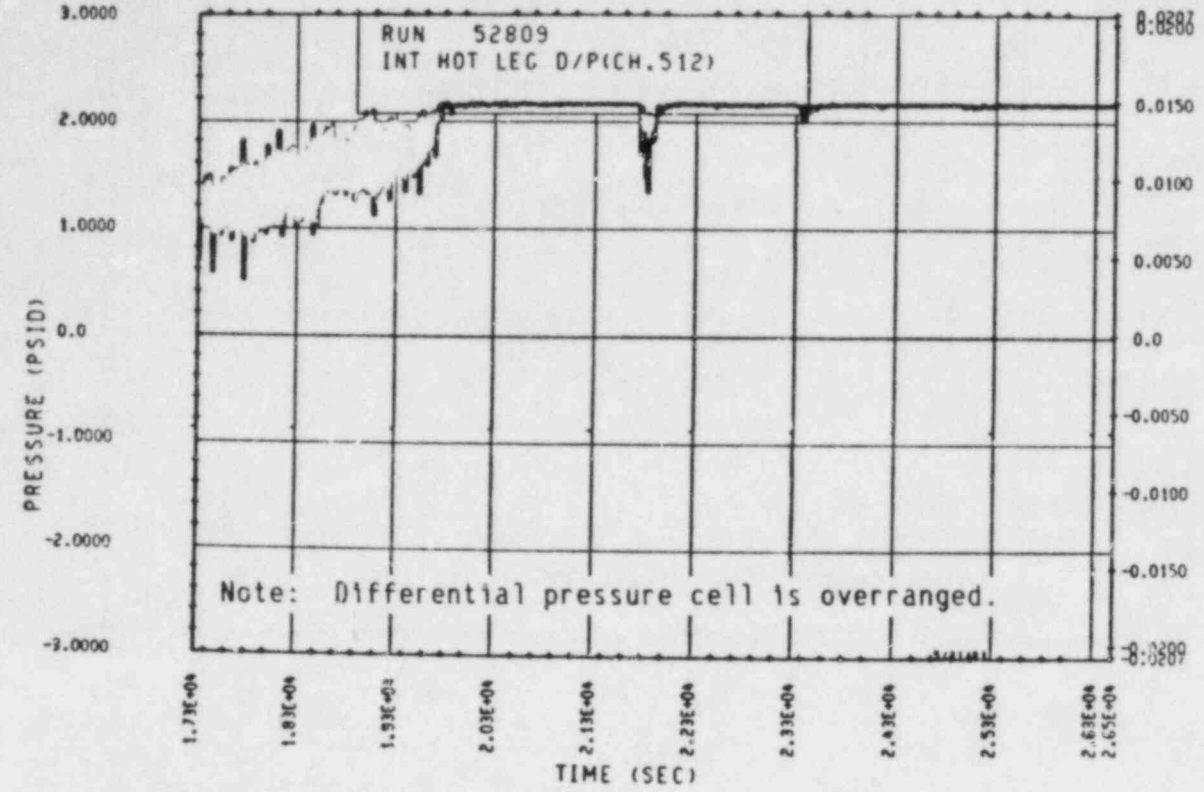

Figure 5-74. Unbroken Loop Hot Leg Differential Pressure (17,300-26,500 sec)

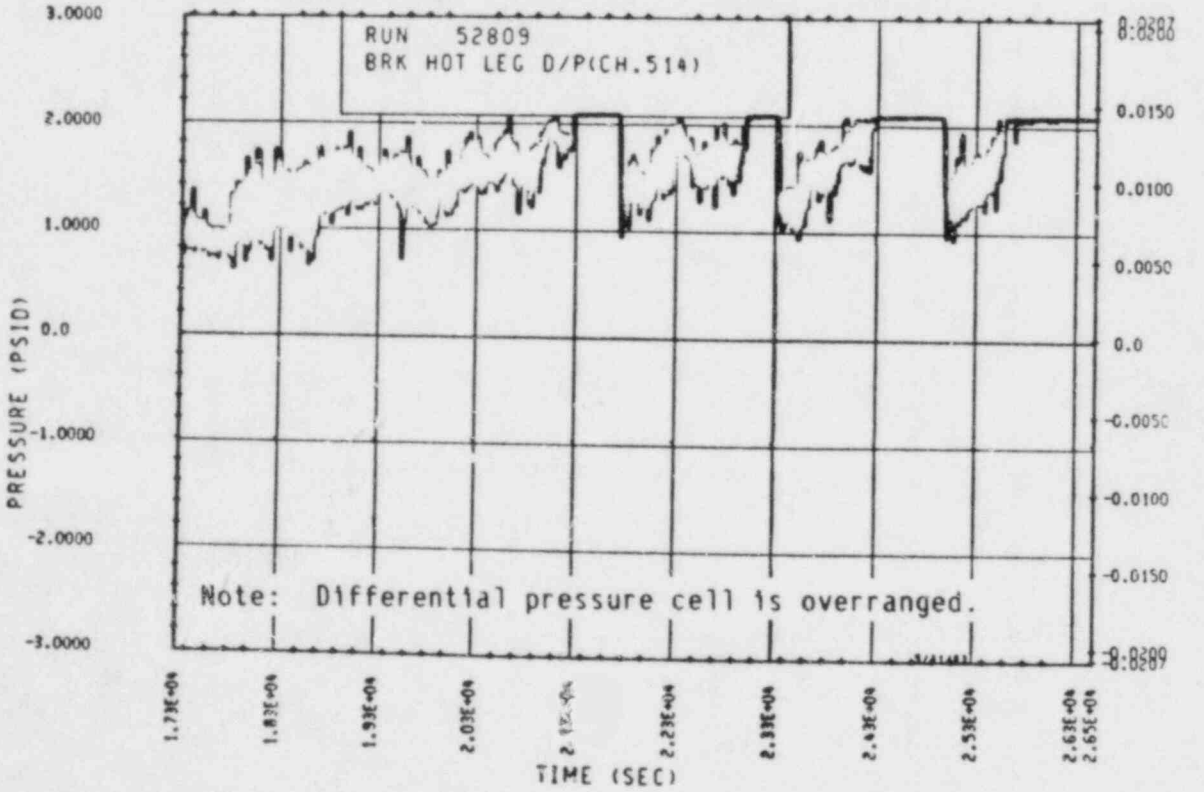

Figure 5-75. Broken Loop Hot Leg Differential Pressure (17,300-26,500 sec)

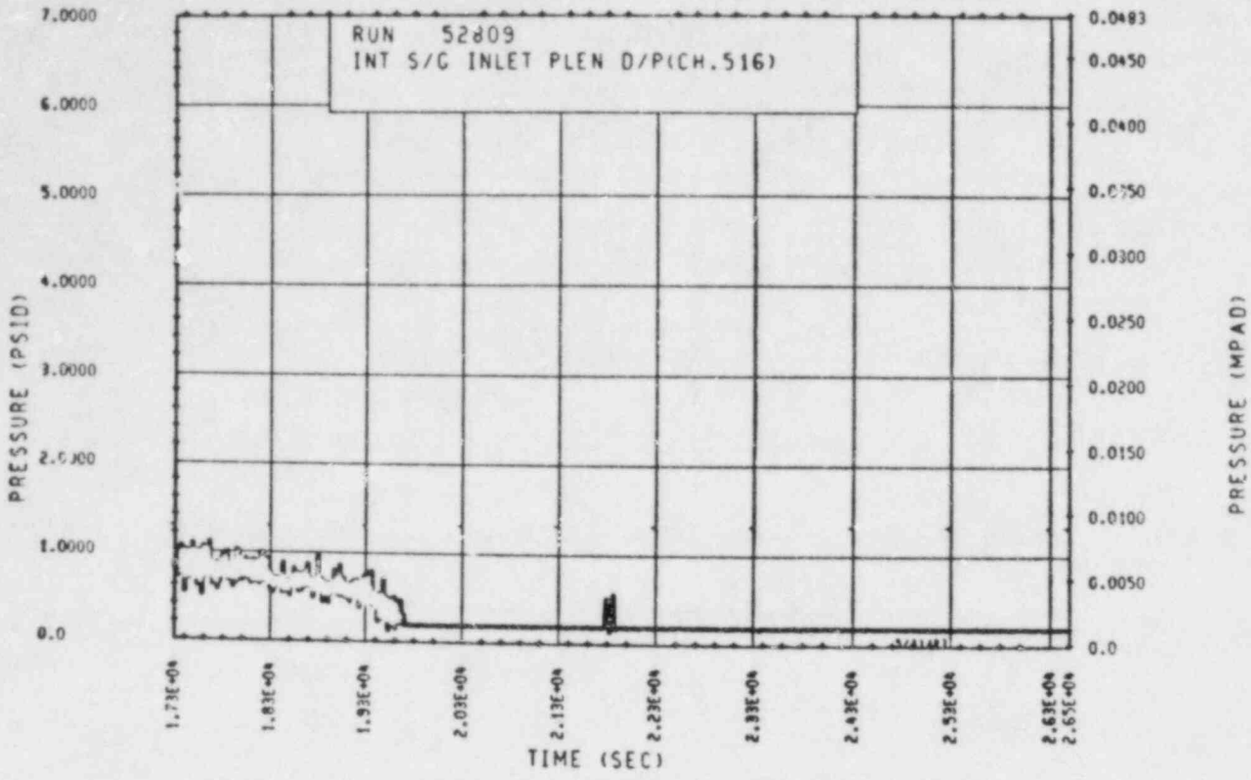

Figure 5-76. Unbroken Loop Steam Generator Inlet Plenum Differential Pressure (17,300-26,500 sec)

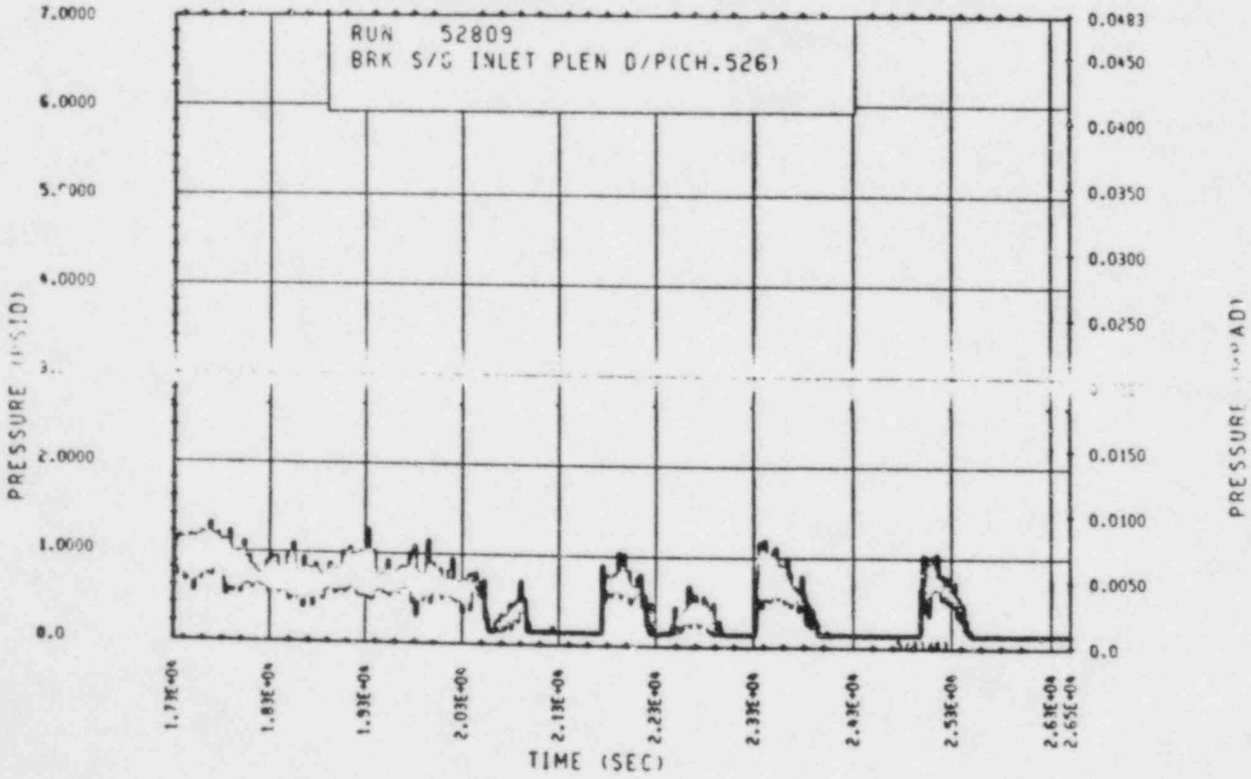

Figure 5-77. Broken Loop Steam Generator Inlet Plenum Differential Pressure (17,300-26,500 sec)

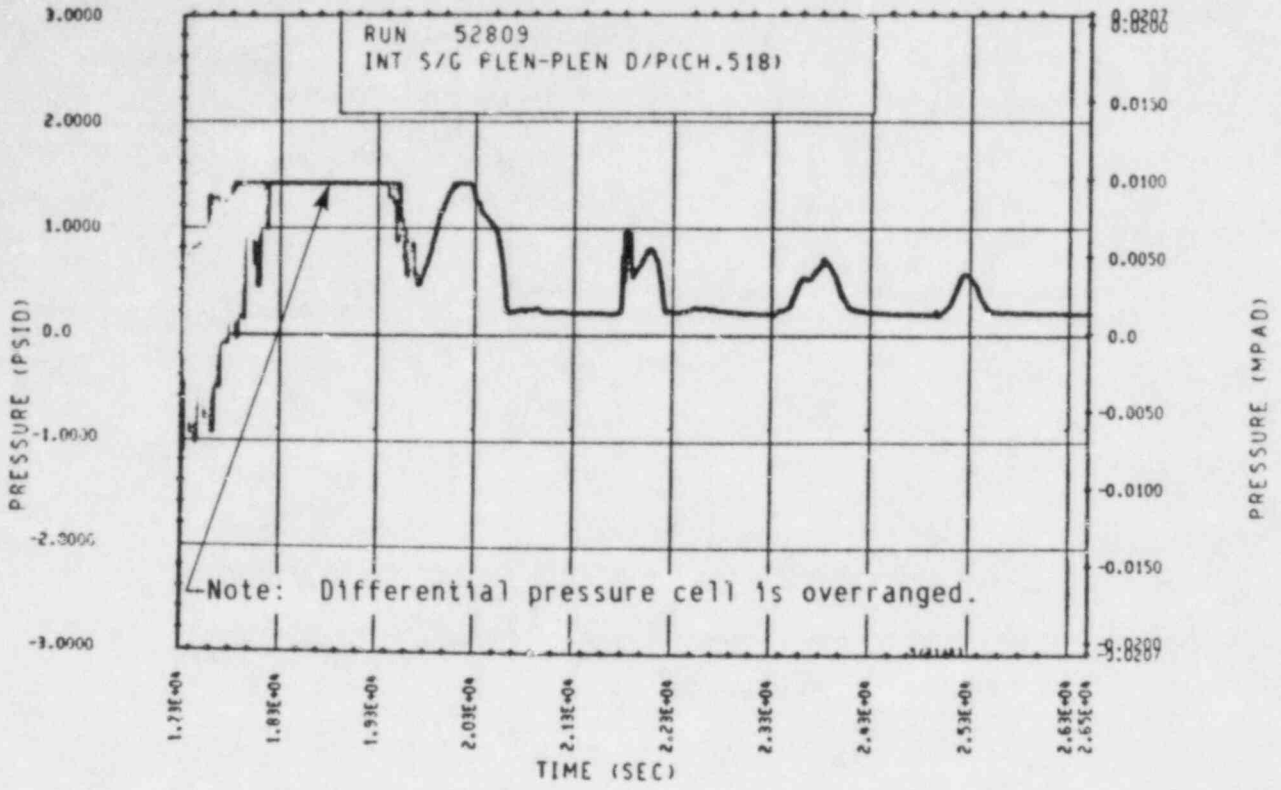

Figure 5-78. Unbroken Loop Steam Generator Plenum-to-Plenum Differential Pressure (17,300-26,500 sec)

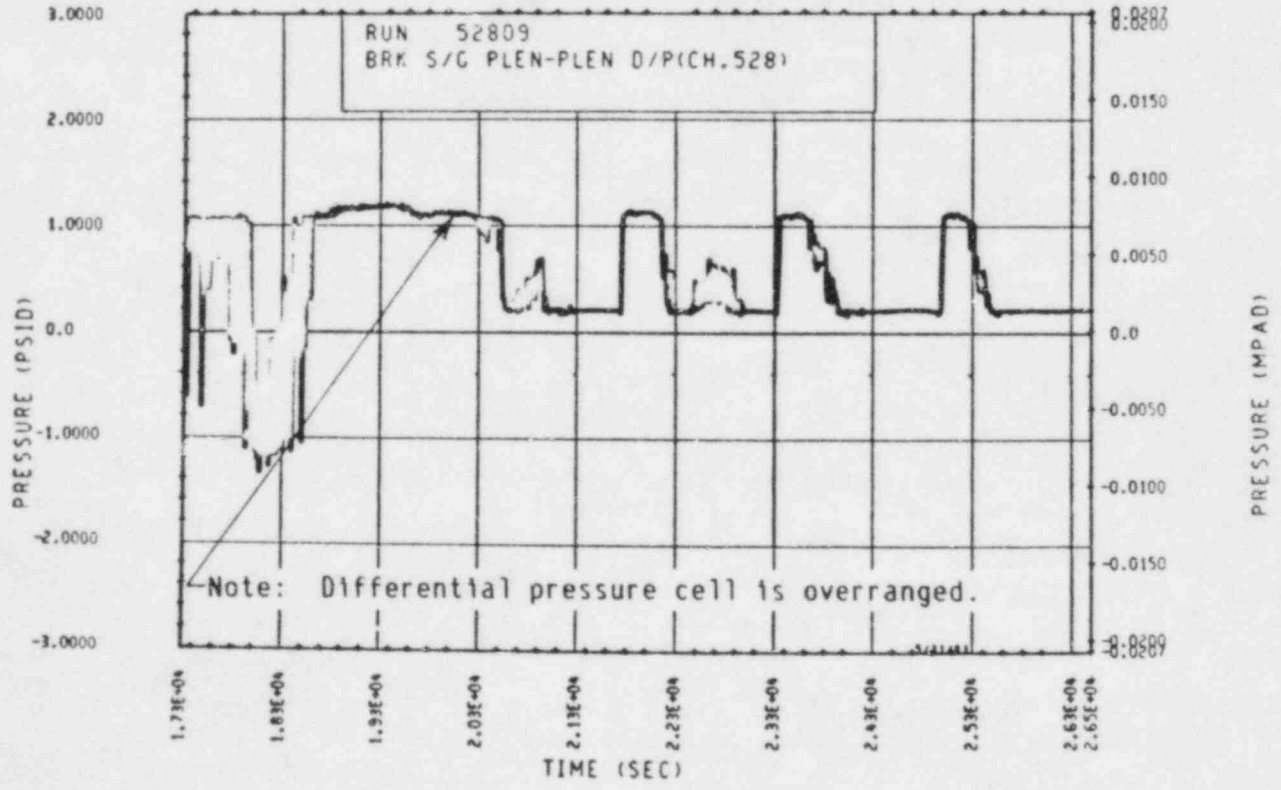

Figure 5-79. Broken Loop Steam Generator Plenum-to-Plenum Differential Pressure (17,300-26,500 sec)

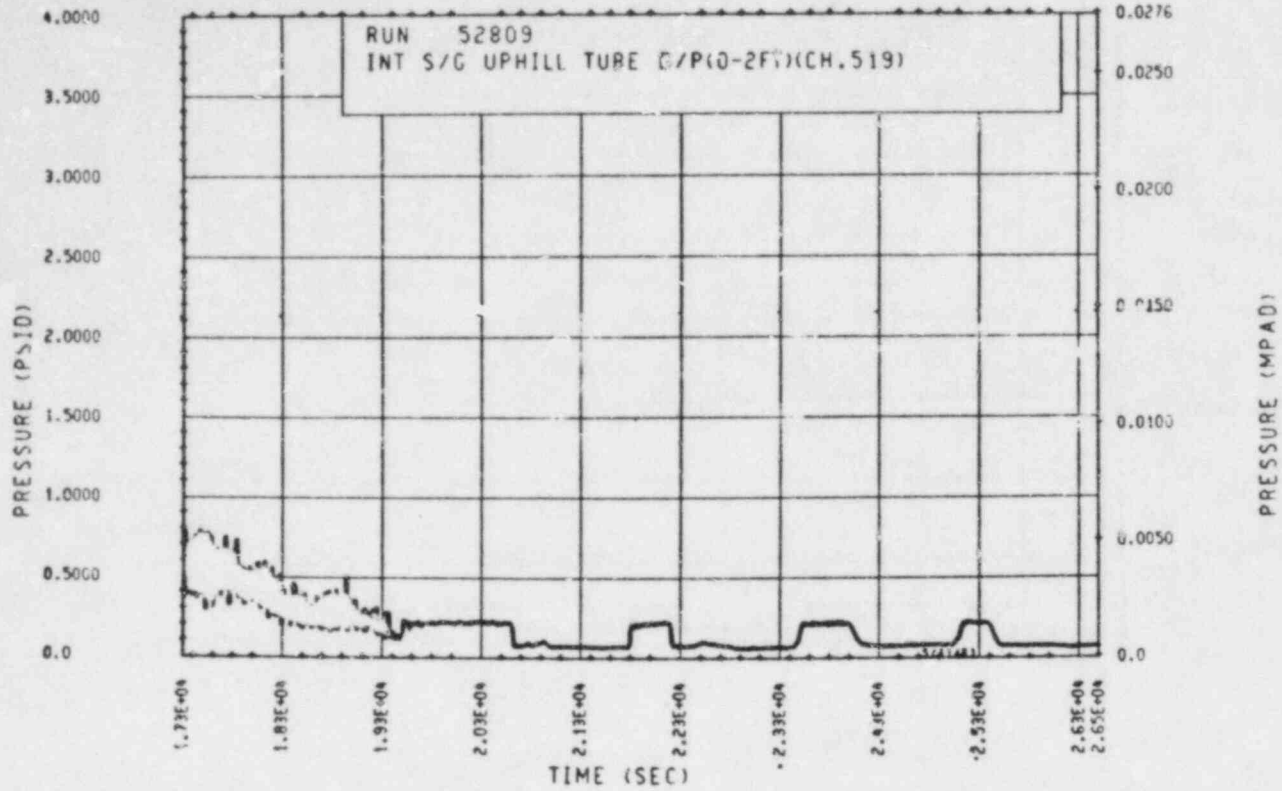

Figure 5-80. Unbroken Loop Steam Generator Uphill Tube B-7 Differential Pressure [0-0.61 m (0-2 ft)] (17,300-26,500 sec)

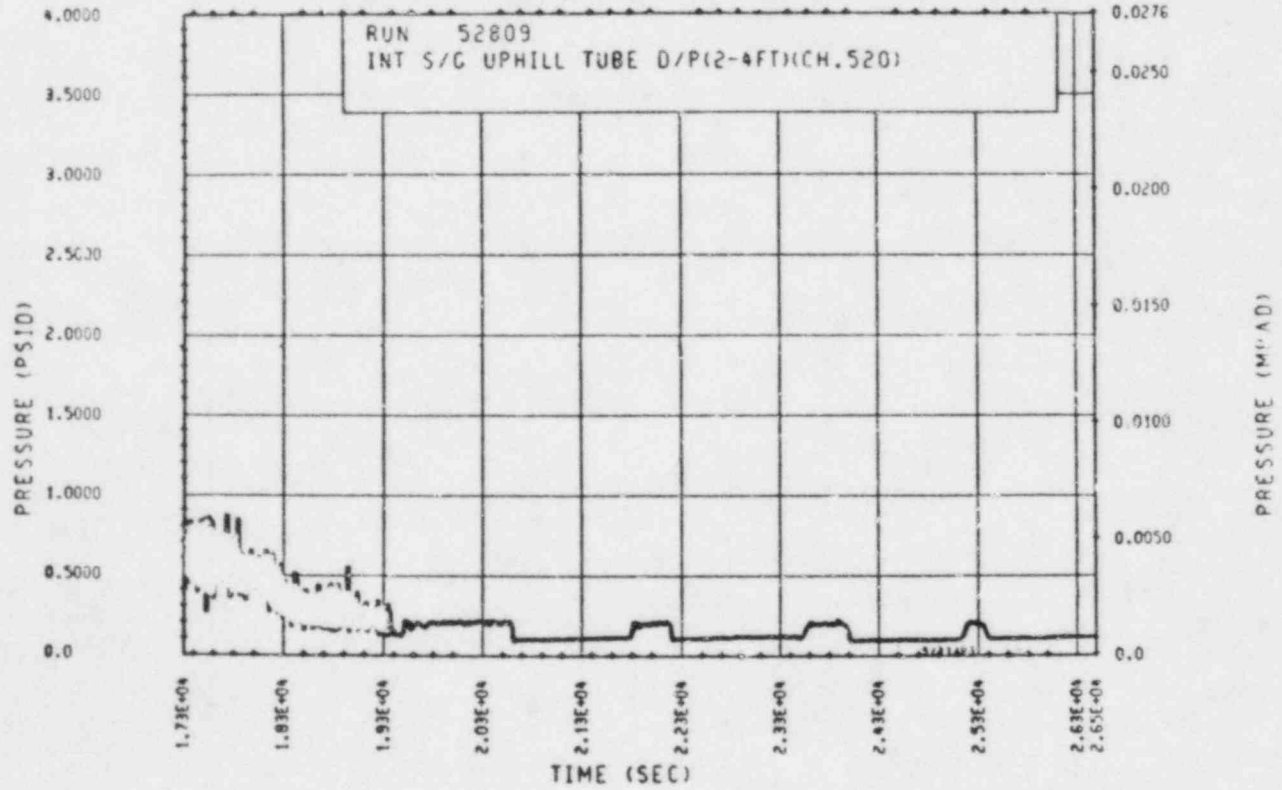

Figure 5-81. Unbroken Loop Steam Generator Uphill Tube B-7 Differential Pressure [0.61-1.22 m (2-4 ft)] (17,300-26,500 sec)

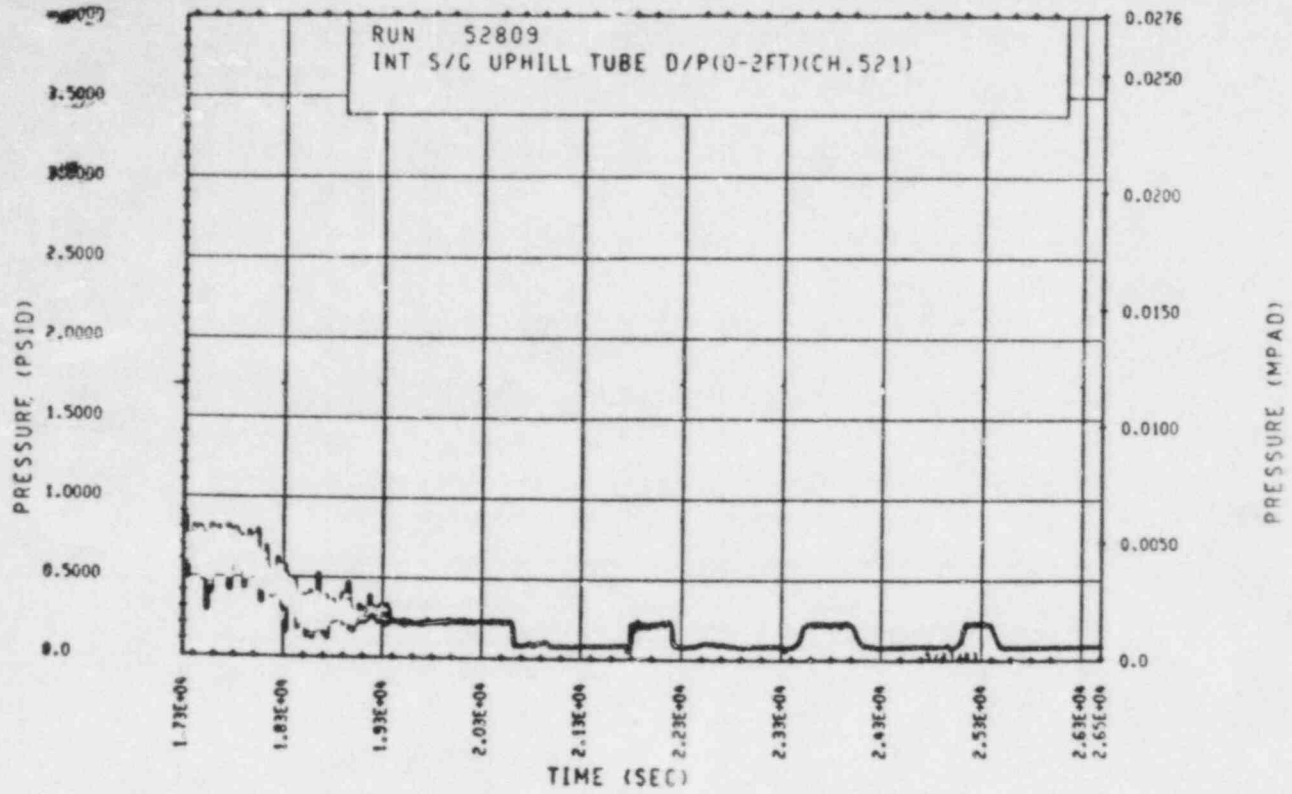

Figure 5-82. Unbroken Loop Steam Generator Uphill Tube C-6 Differential Pressure [0-0.61 m (0-2 ft)] (17,300-26,500 sec)

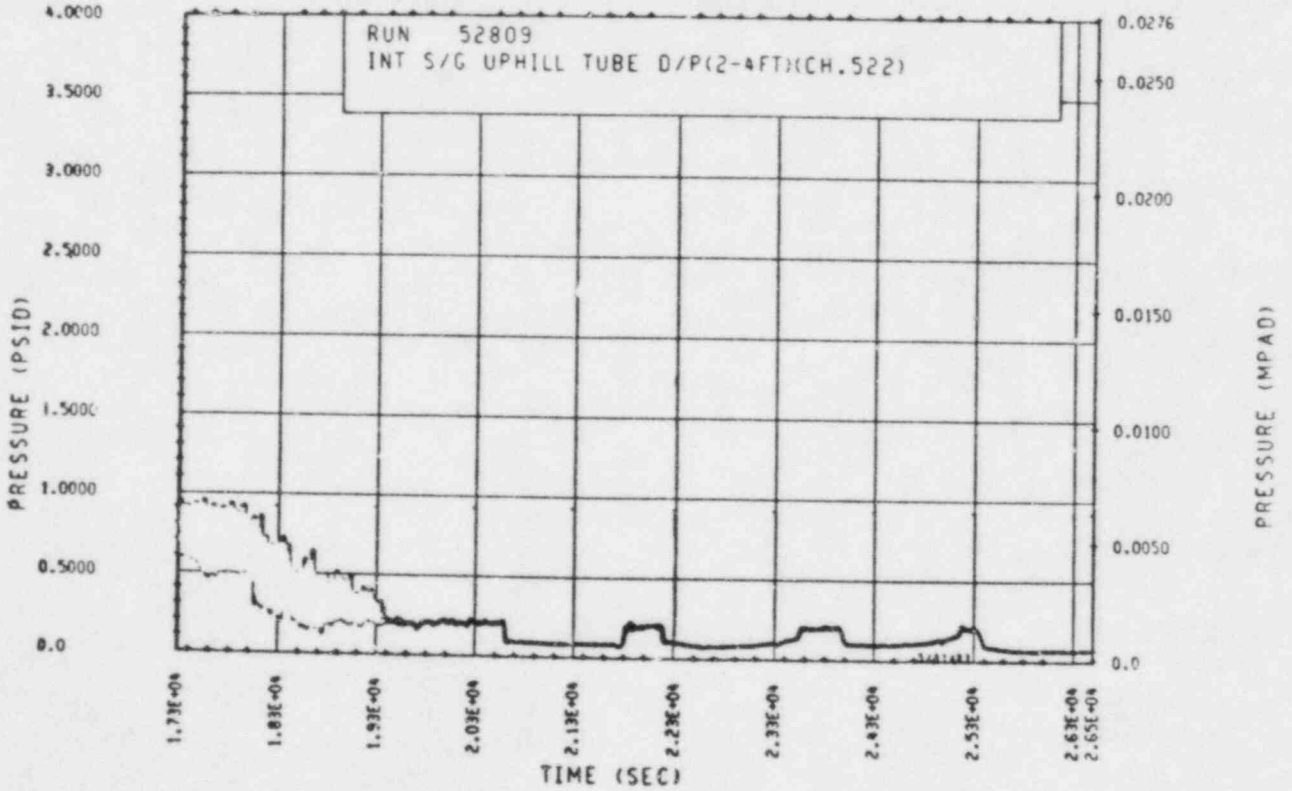

Figure 5-83. Unbroken Loop Steam Generator Uphill Tube C-6 Differential Pressure [0.61-1.22 m (2-4 ft)] (17,300-26,500 sec)

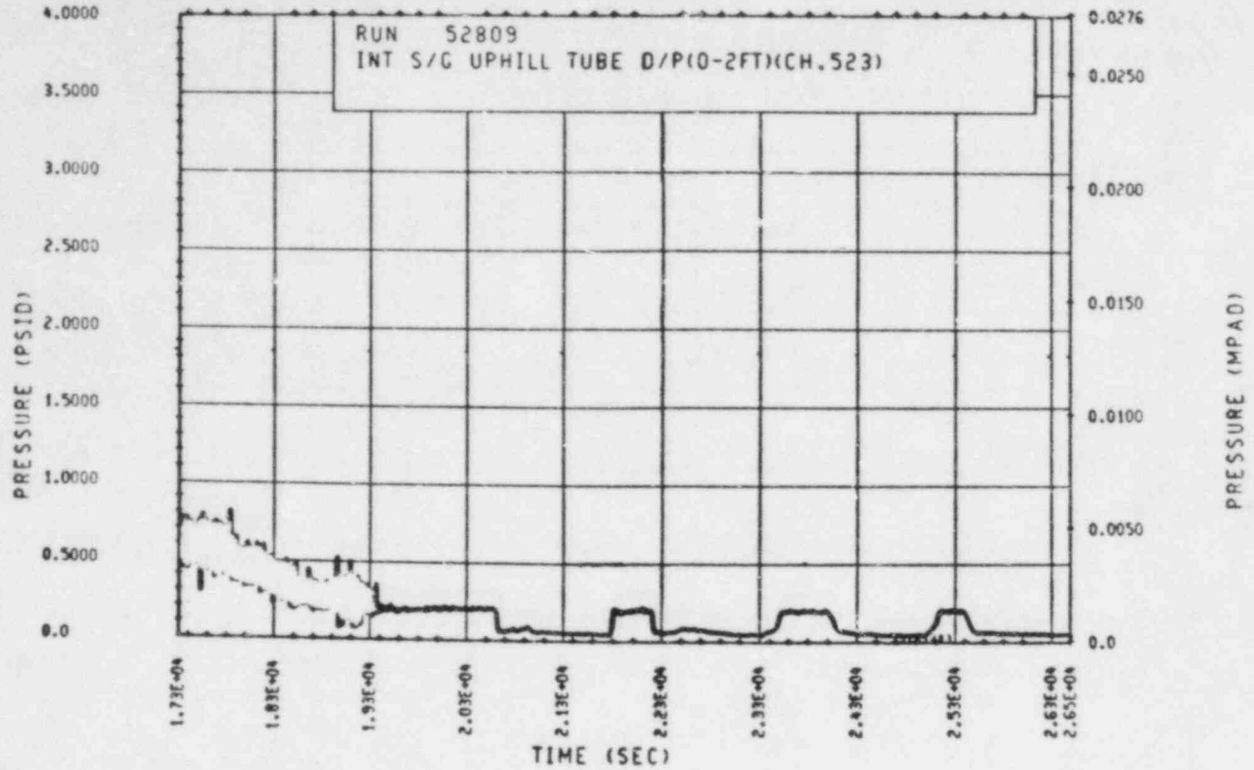

Figure 5-84. Unbroken Loop Steam Generator Uphill Tube E-5 Differential Pressure [0-0.61 m (0-2 ft)] (17,500-26,500 sec)

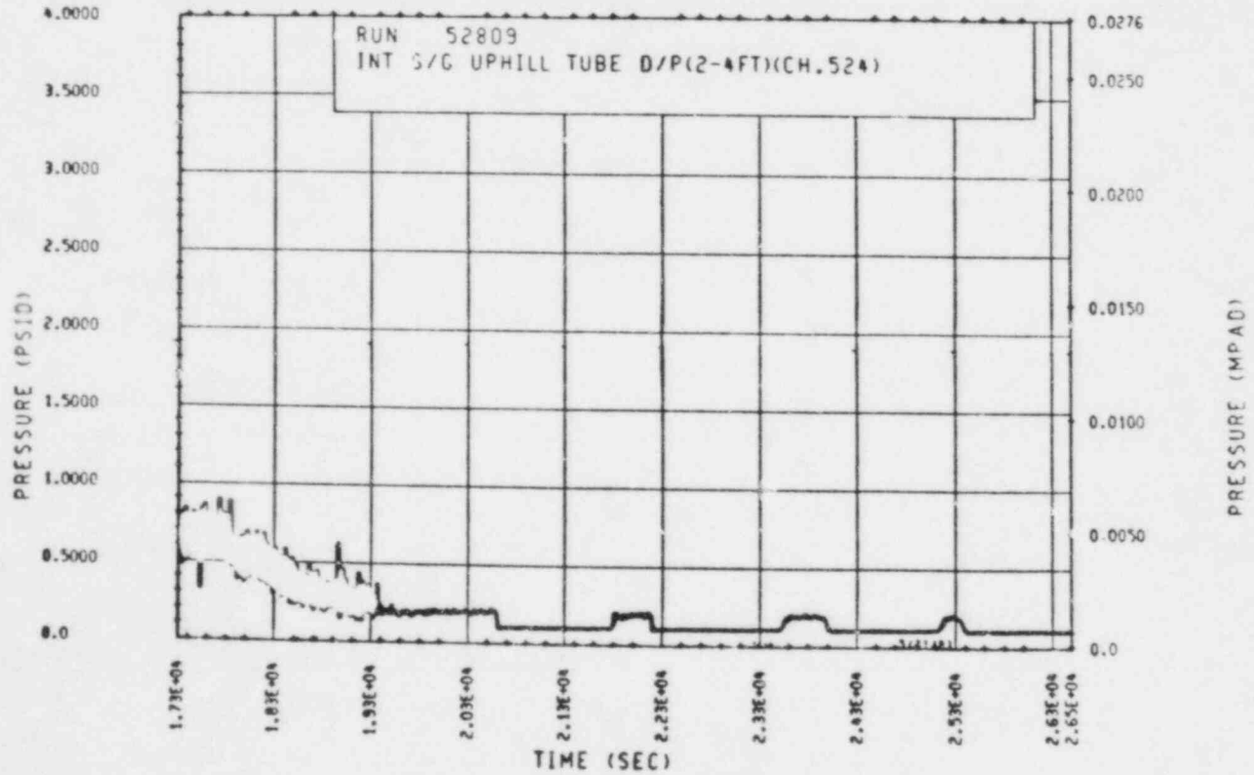

Figure 5-85. Unbroken Loop Steam Generator Uphill Tube E-5 Differential Pressure [0.61-1.22 m (2-4 ft)] (17,500-26,500 sec)

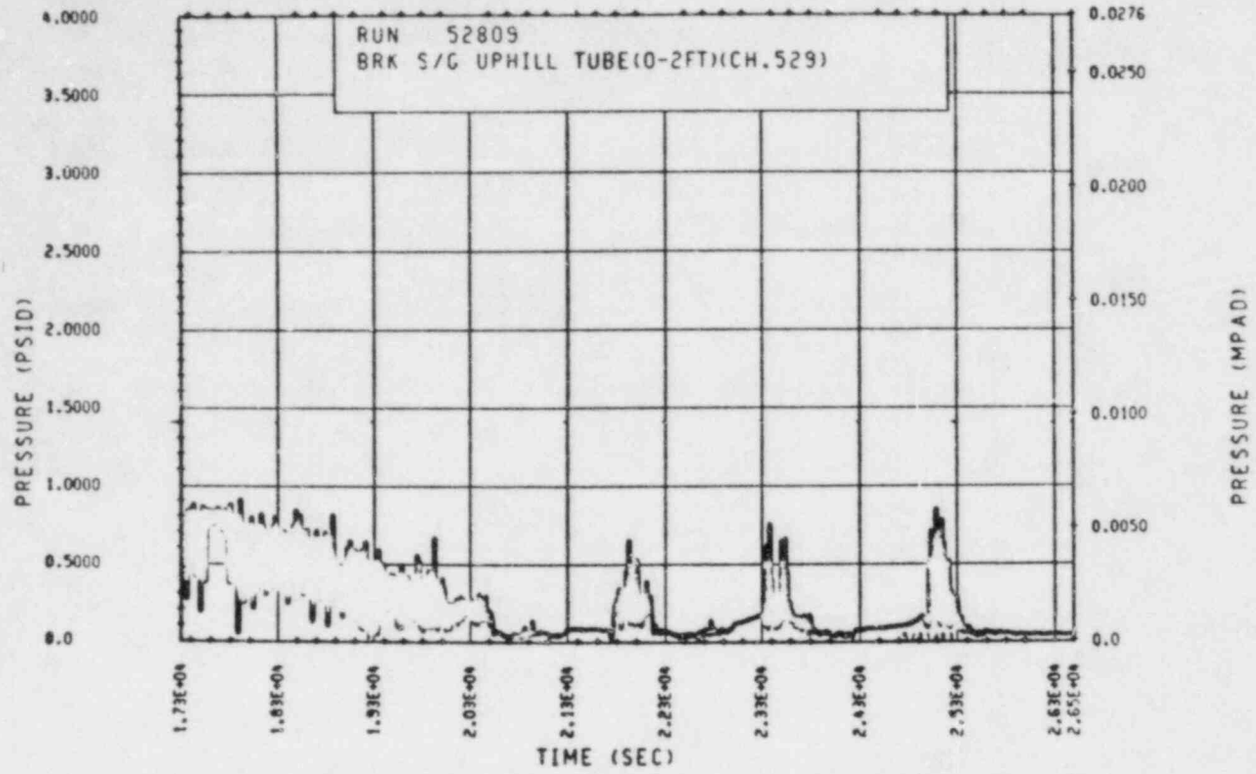

Figure 5-86. Broken Loop Steam Generator Uphill Tube B-6 Differential Pressure [0-0.61 m (0-2 ft)] (17,300-26,500 sec)

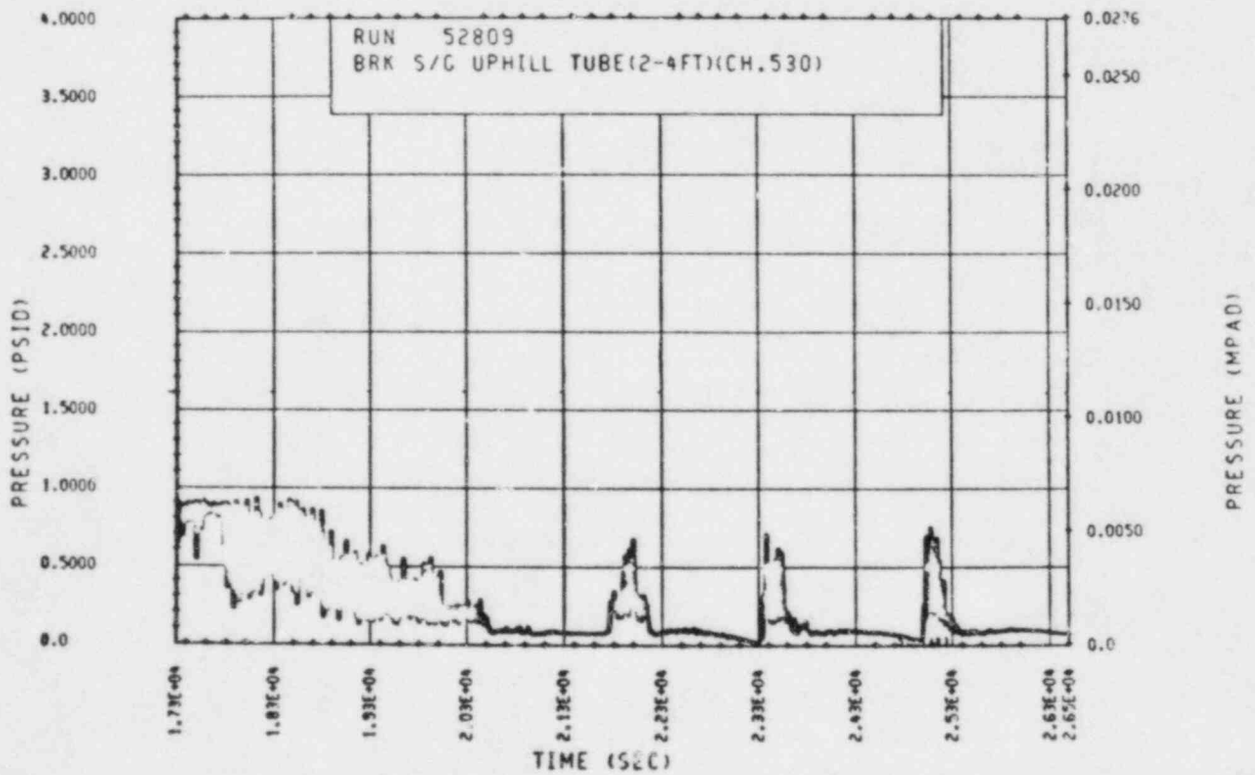

Figure 5-87. Broken Loop Steam Generator Uphill Tube B-6 Differential Pressure [0.61-1.22 m (2-4 ft)] (17,300-26,500 sec)

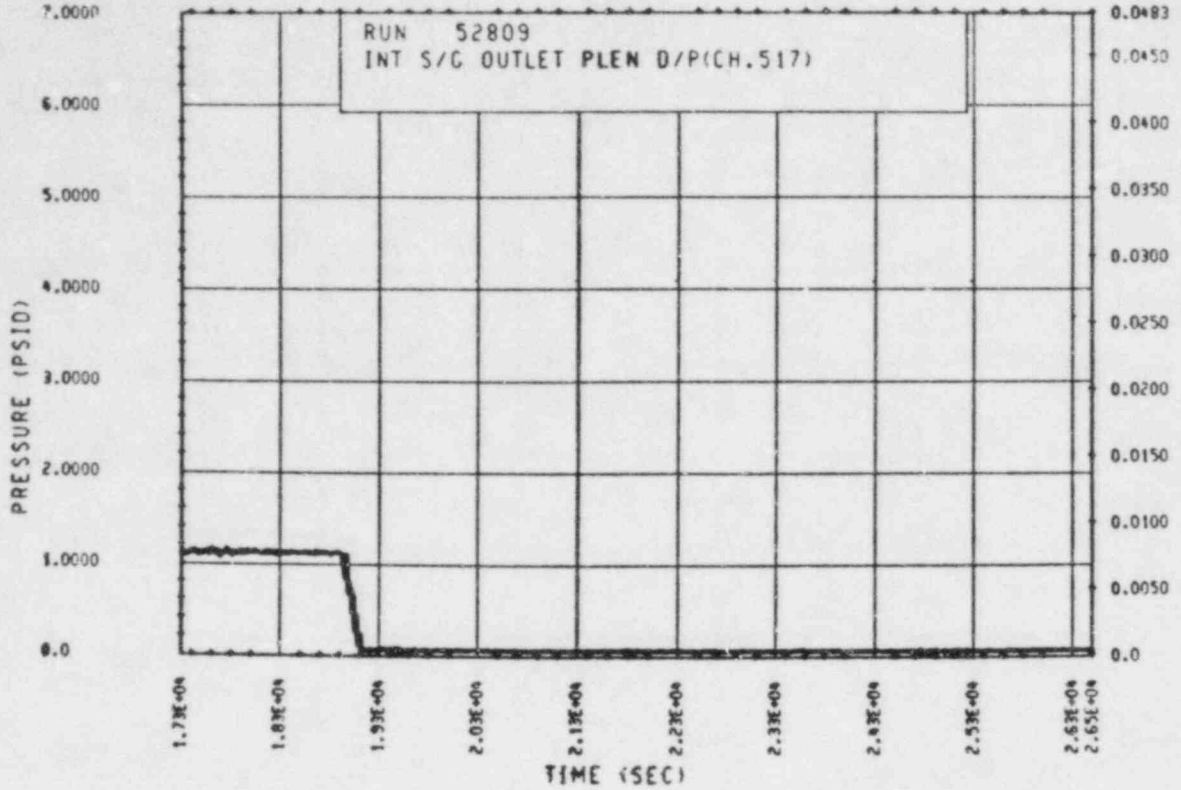

Figure 5-88. Unbroken Loop Steam Generator Outlet Plenum Differential Pressure (17,300-26,500 sec)

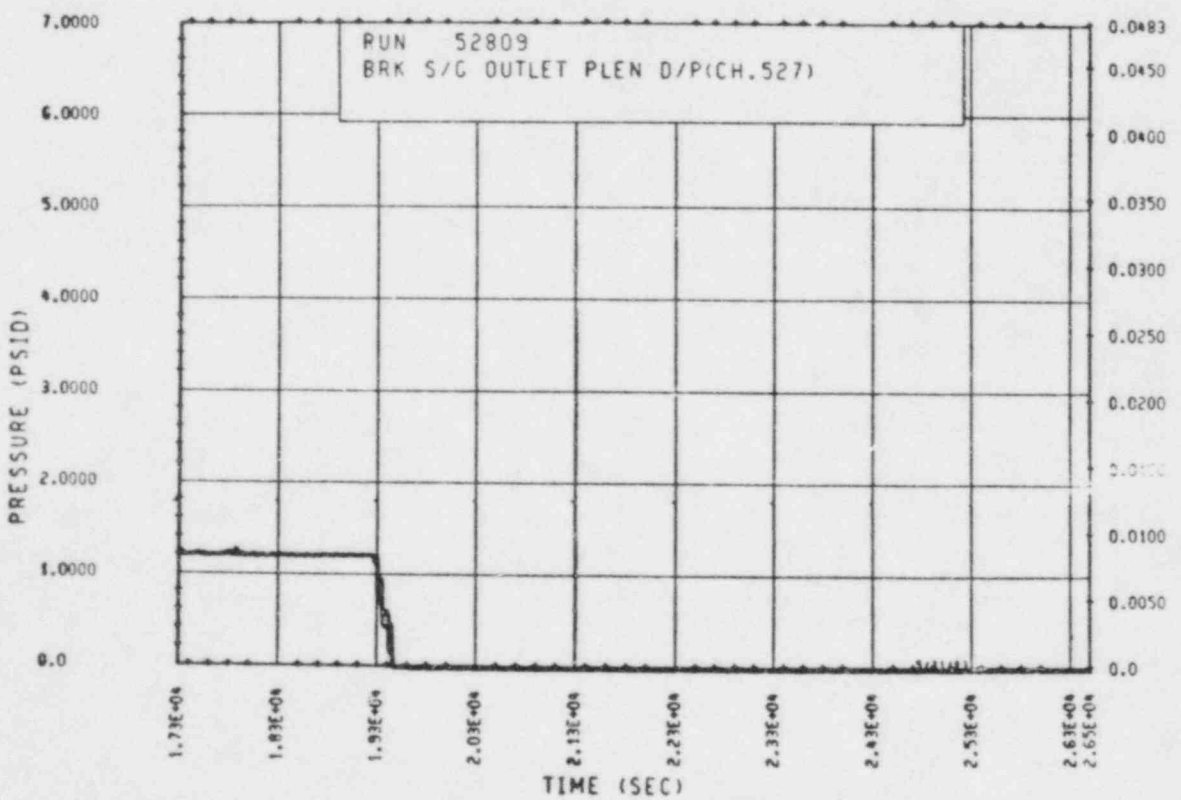

Figure 5-89. Broken Loop Steam Generator Outlet Plenum Differential Pressure (17,300-26,500 sec)

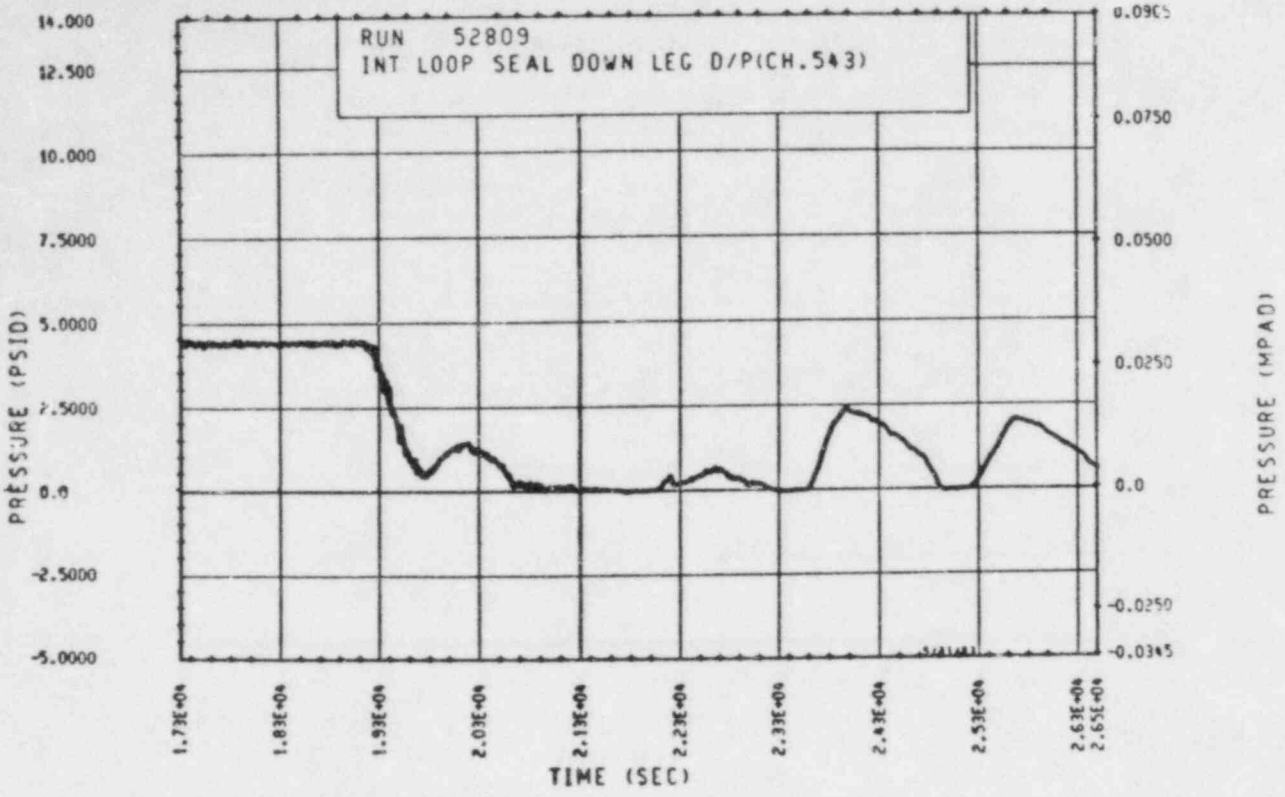

Figure 5-90. Unbroken Loop Seal Descending Leg Differential Pressure (17,300-26,500 sec)

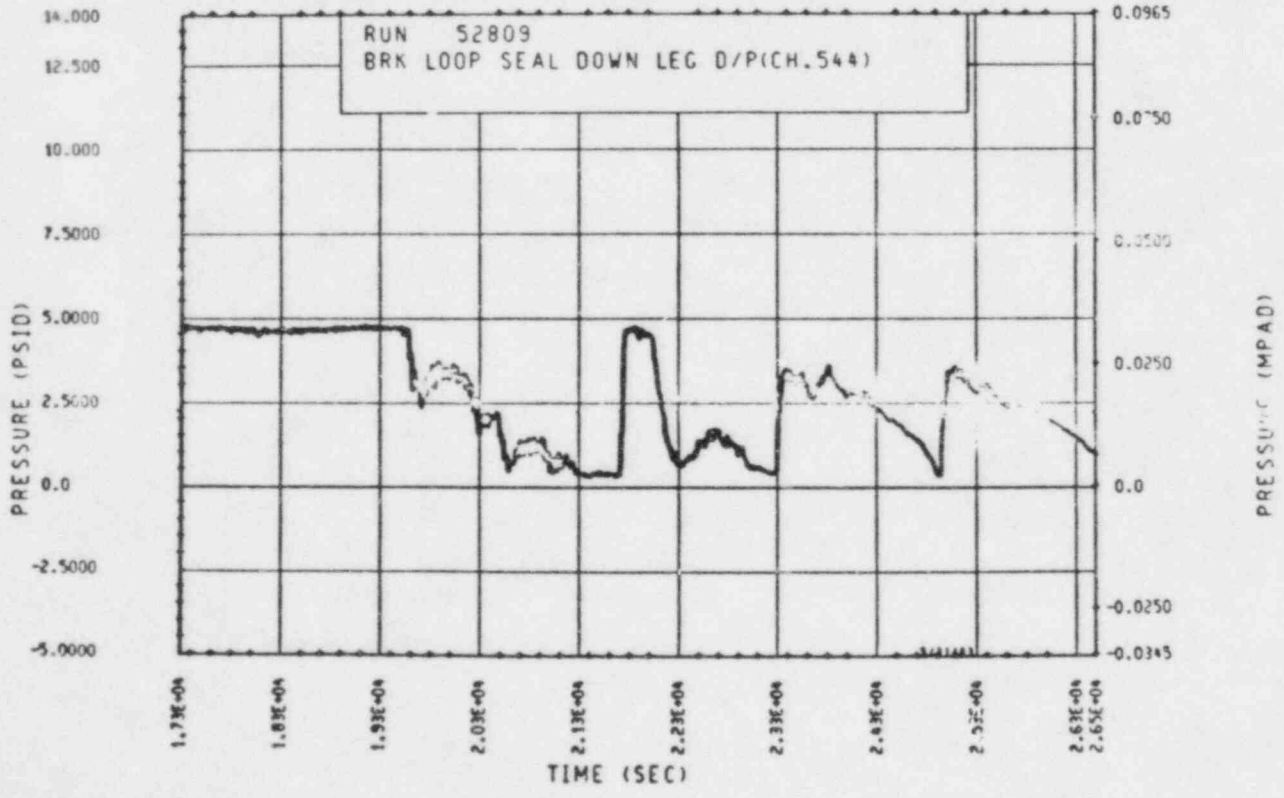

Figure 5-91. Broken Loop Seal Descending Leg Differential Pressure (17,300-26,500 sec)

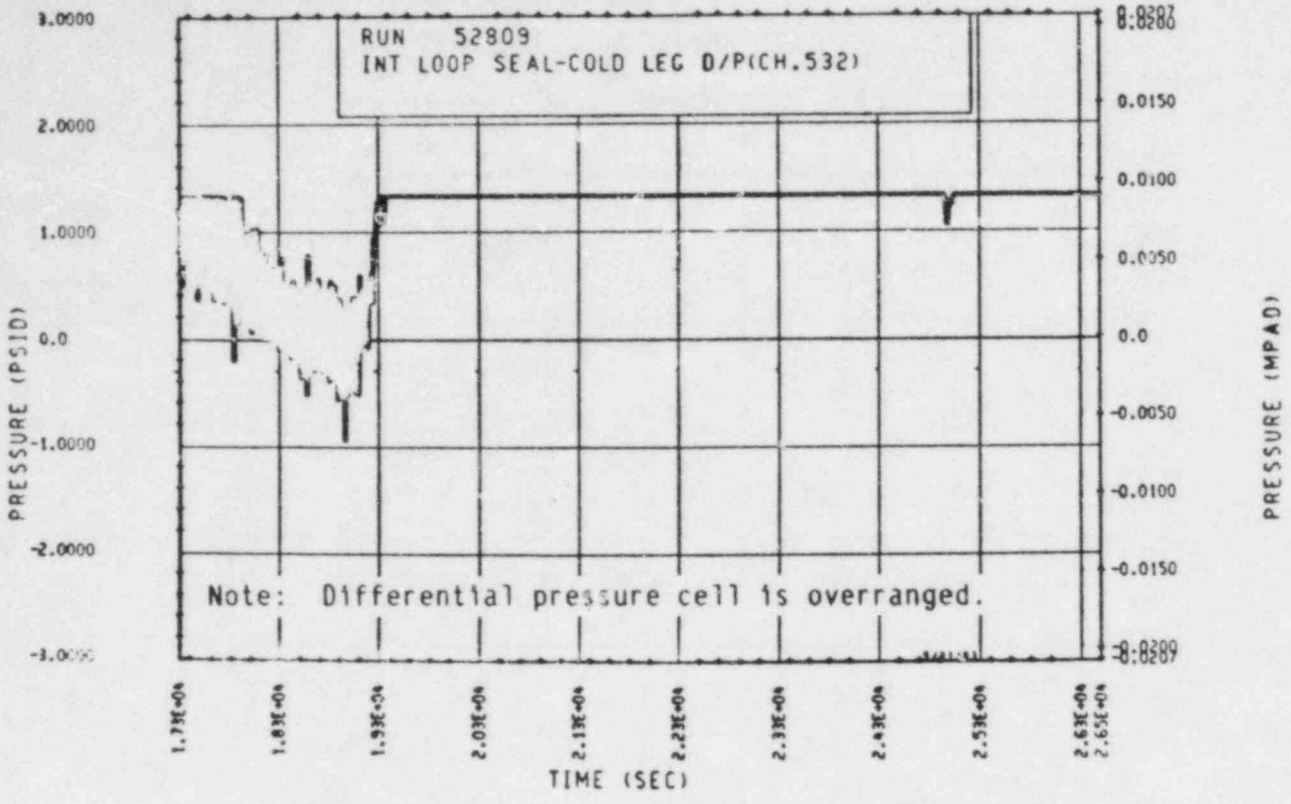

Figure 5-92. Unbroken Loop Seal Cold Leg Differential Pressure (17,300-26,500 sec)

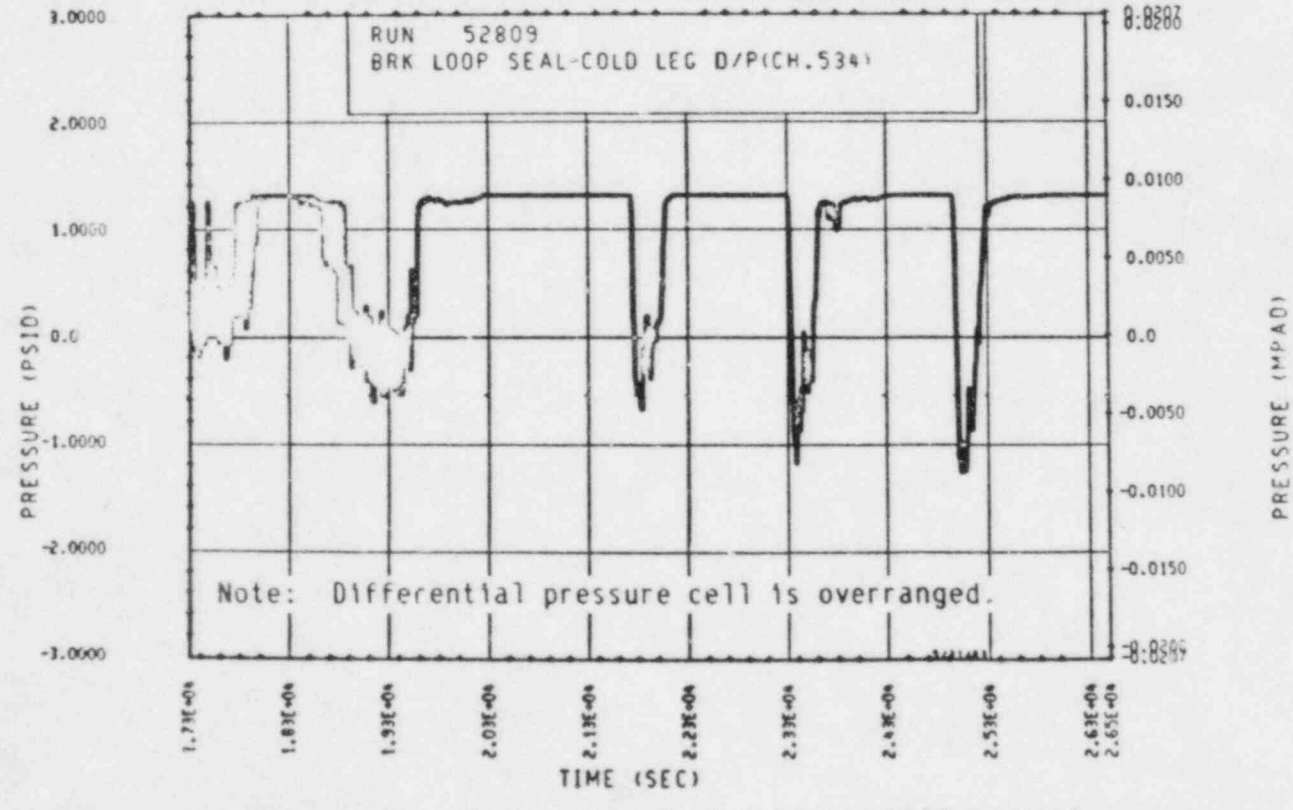

Figure 5-93. Broken Loop Seal Cold Leg Differential Pressure (17,300-26,500 sec)

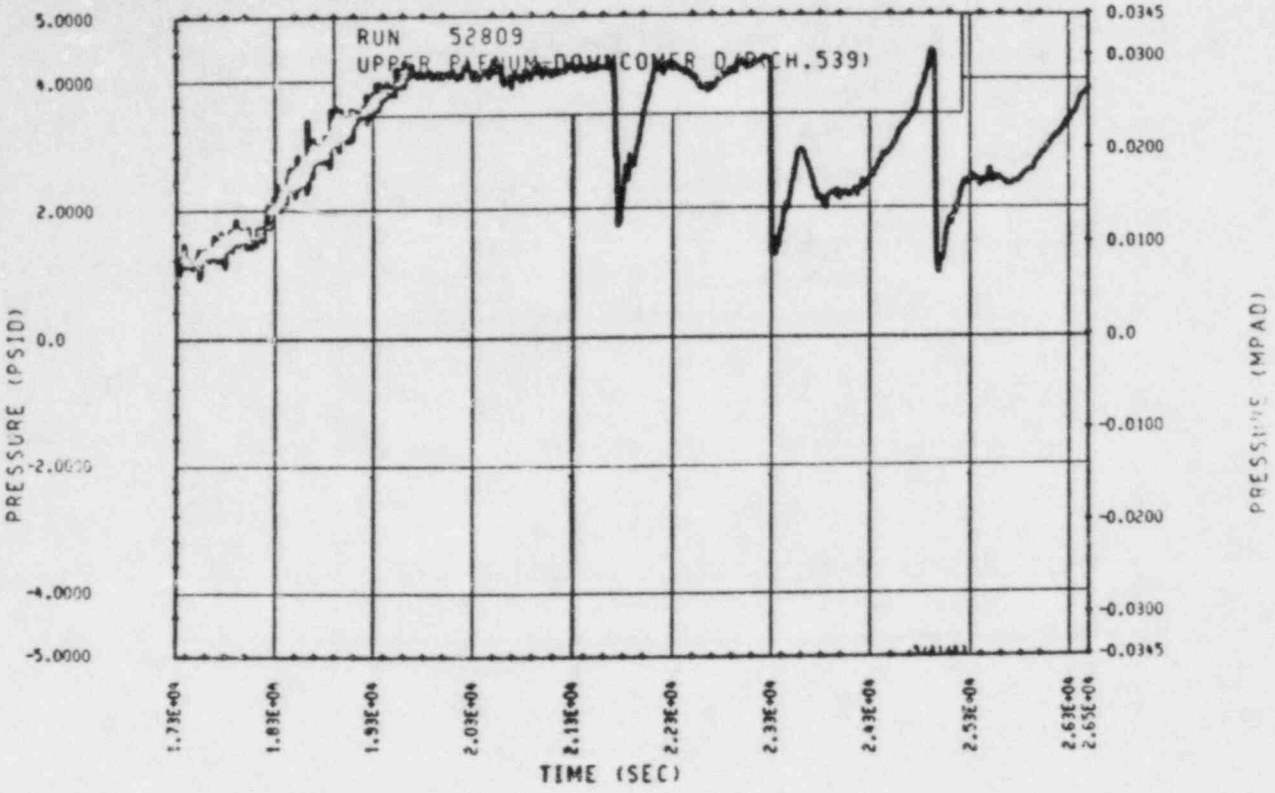

Figure 5-94. Upper Plenum-Downcomer Extension Differential Pressure (17,300-26,500 sec)

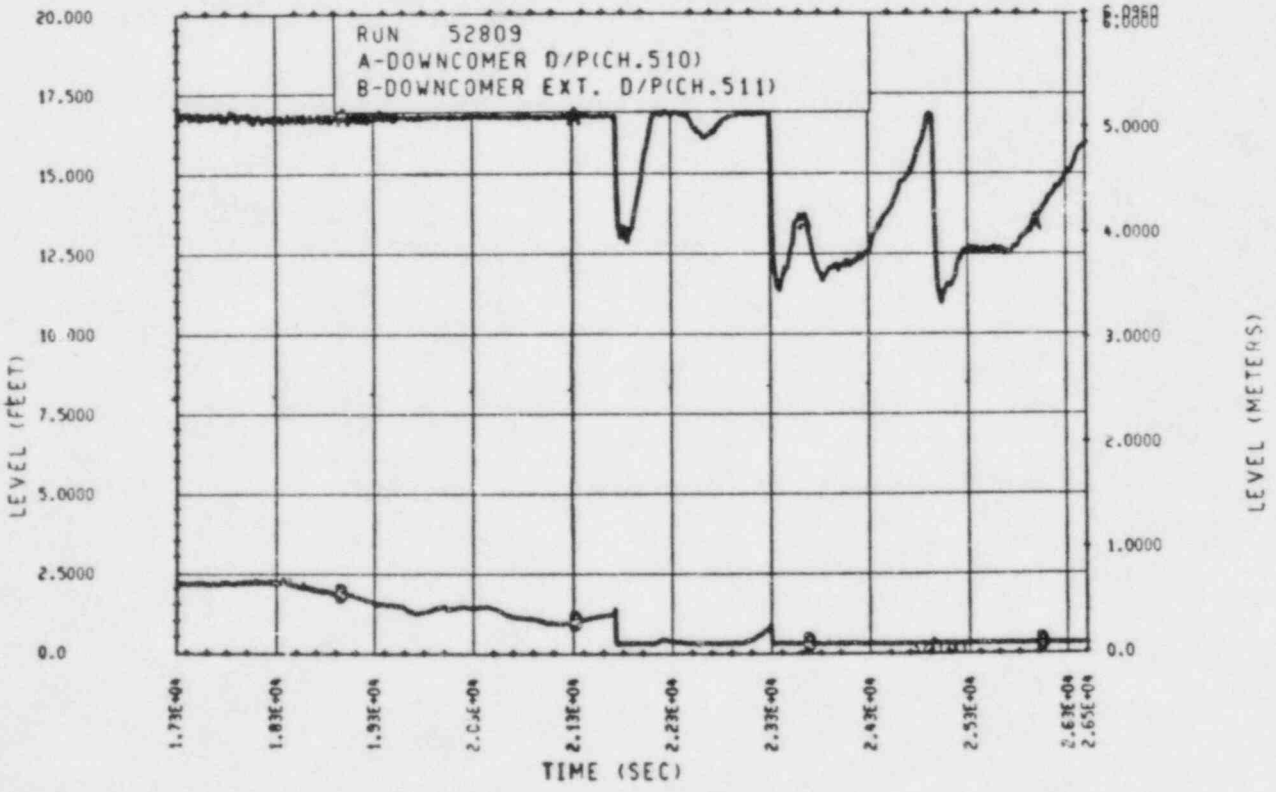

Figure 5-95. Downcomer and Downcomer Extension Liquid Levels (17,300-26,500 sec)

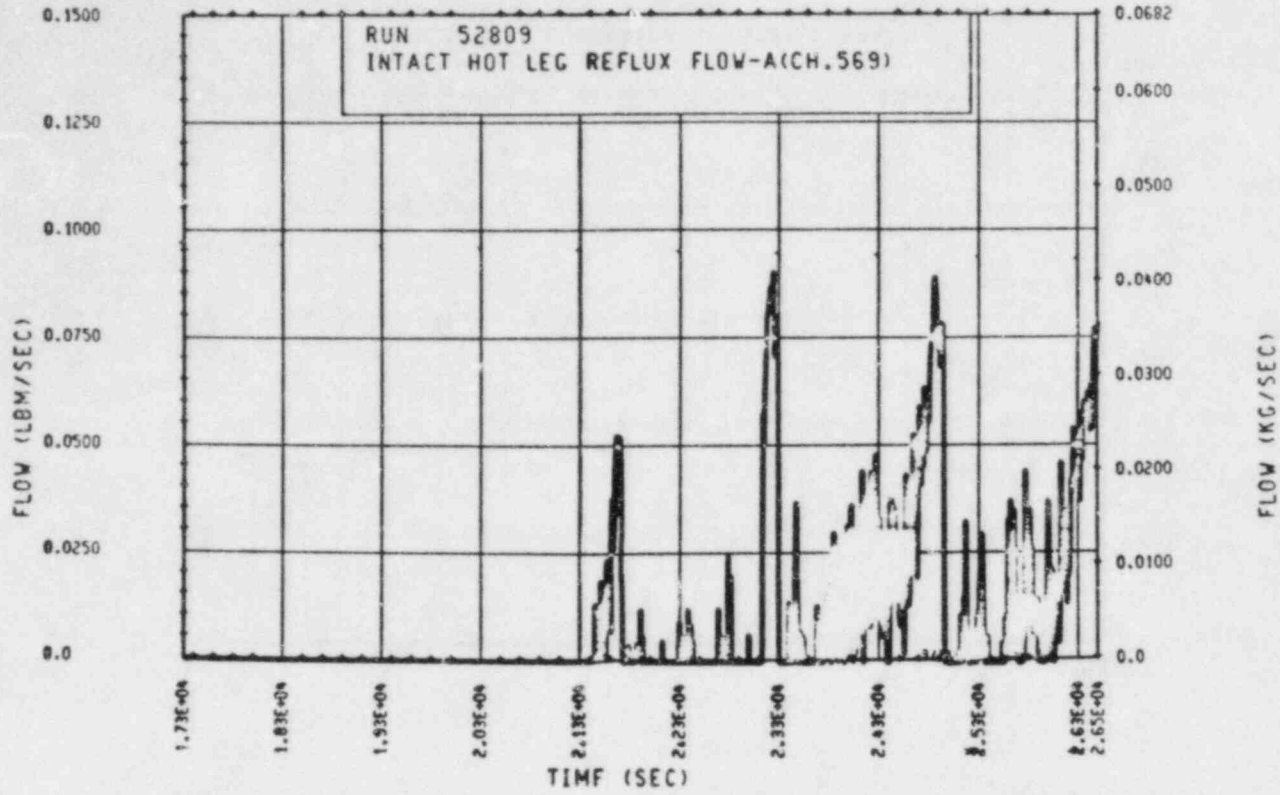

Figure 5-96. Unbroken Loop Hot Leg Reflux Condensation Mass Flow Rate (17,300-26,500 sec)

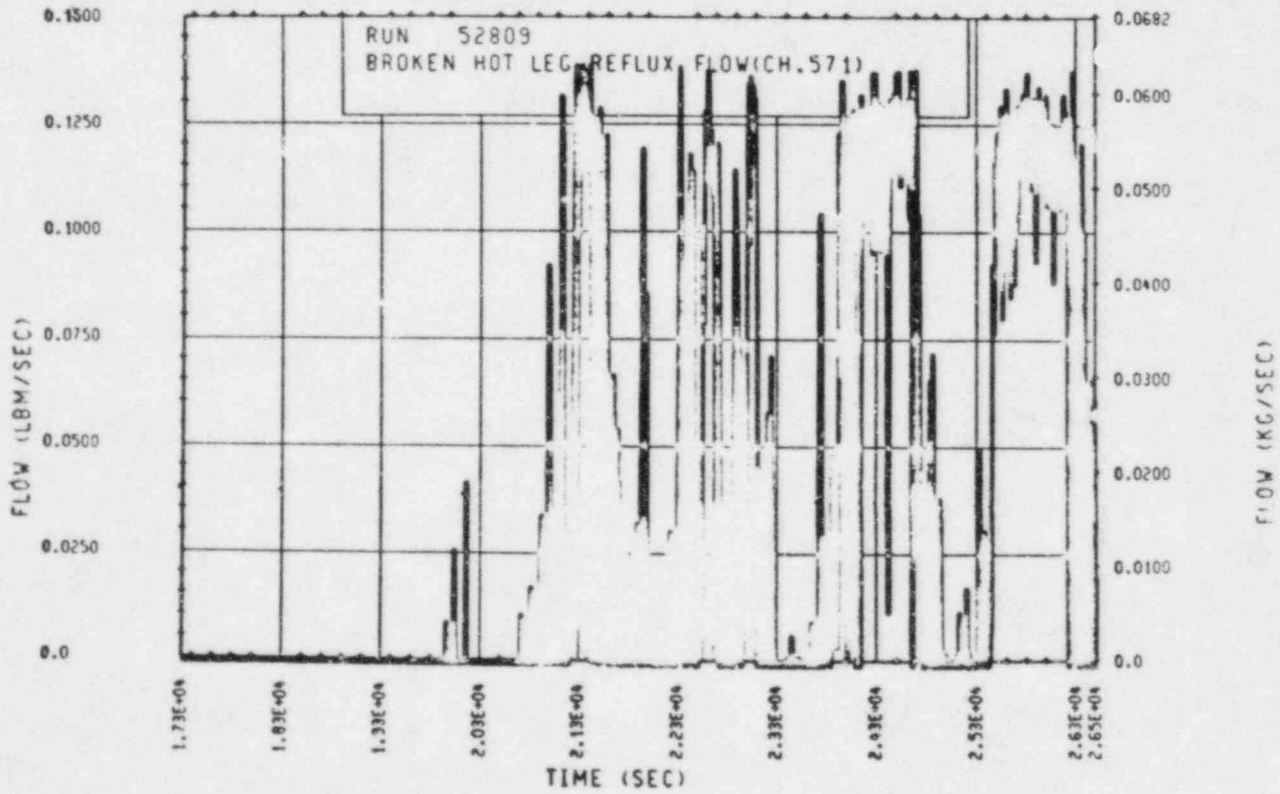

Figure 5-97. Broken Loop Hot Leg Reflux Condensation Mass Flow Rate (17,300-26,500 sec)

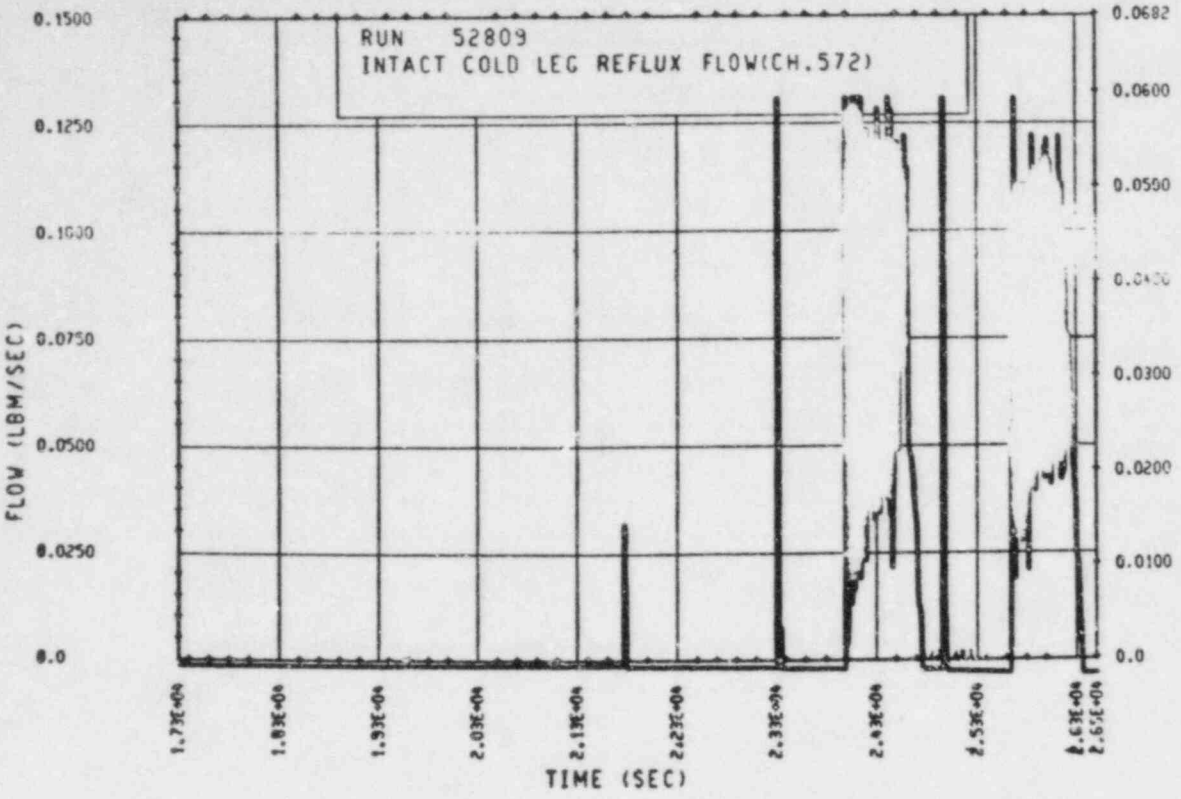

Figure 5-98. Unbroken Loop Cold Leg Reflux Condensation Mass Flow Rate (17,300-26,500 sec)

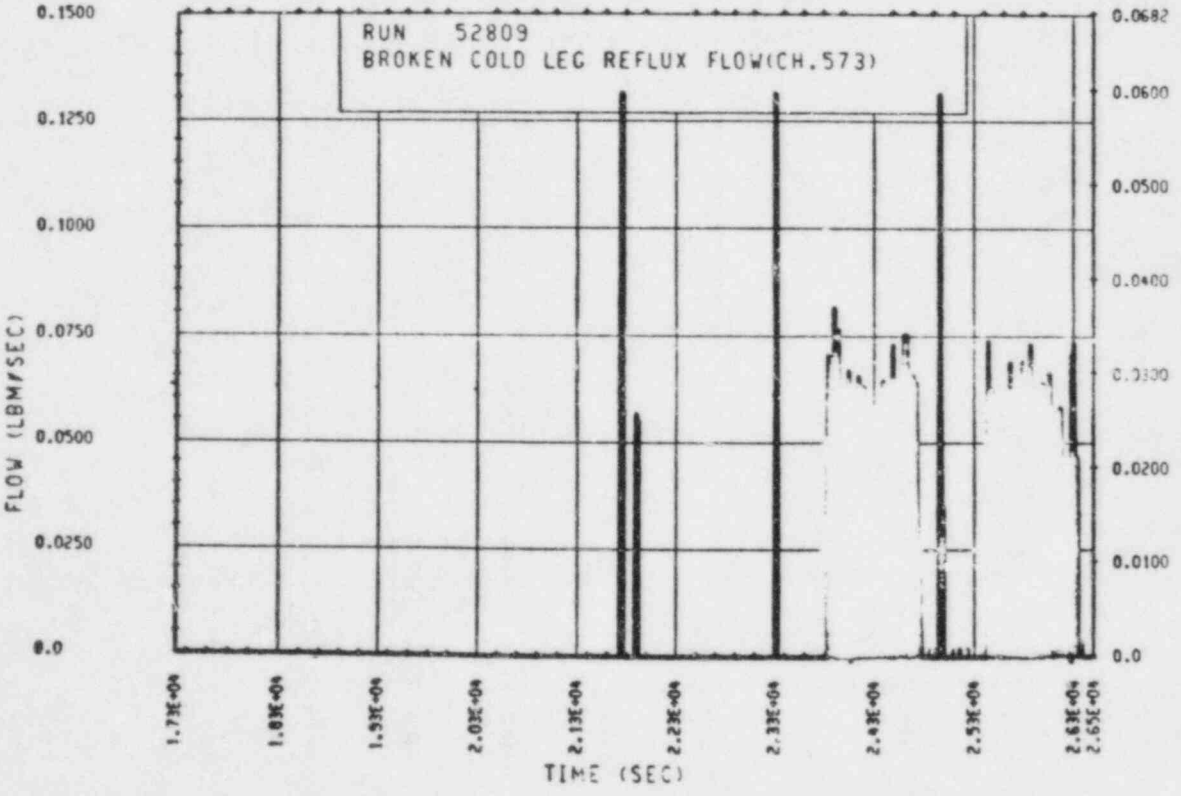

Figure 5-99. Broken Loop Cold Leg Reflux Condensation Mass Flow Rate (17,300-26,500 sec)

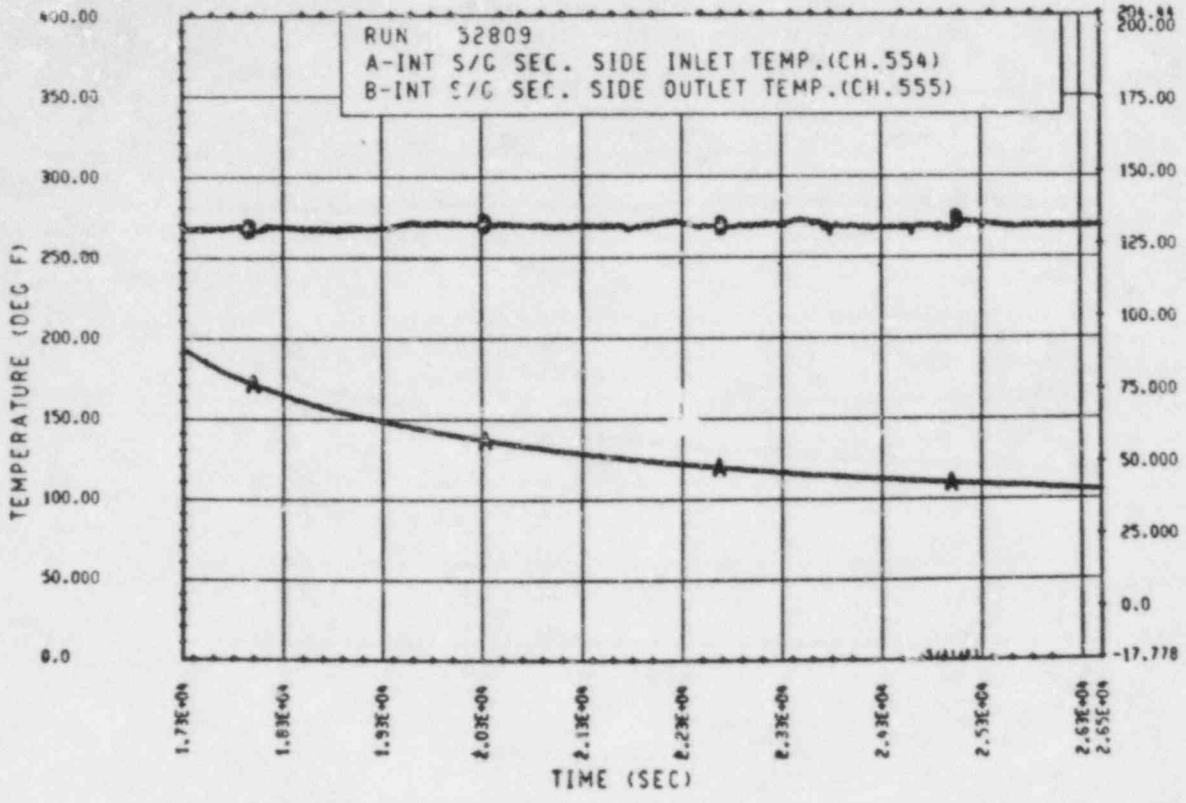

Figure 5-100. Unbroken Loop Steam Generator Secondary Side Inlet and Outlet Temperatures (17,300-26,500 sec)

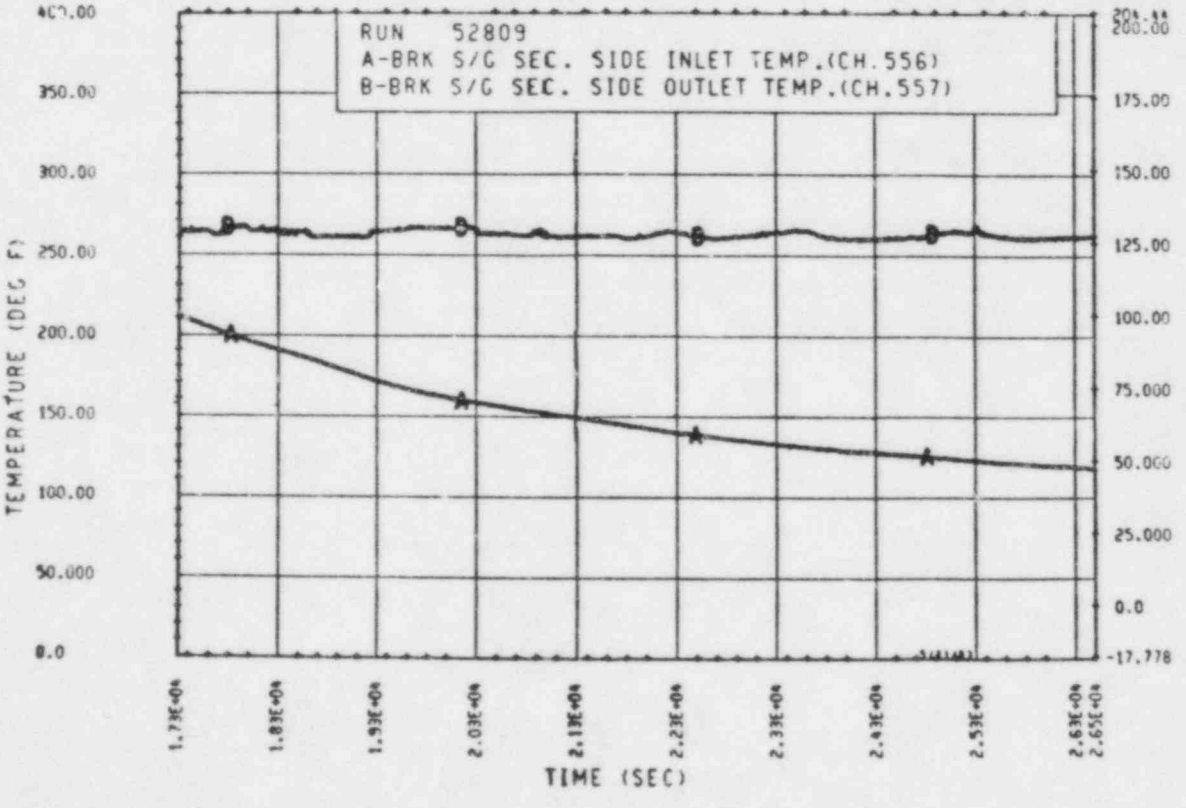

Figure 5-101. Broken Loop Steam Generator Secondary Side Inlet and Outlet Temperatures (17,300-26,500 sec)

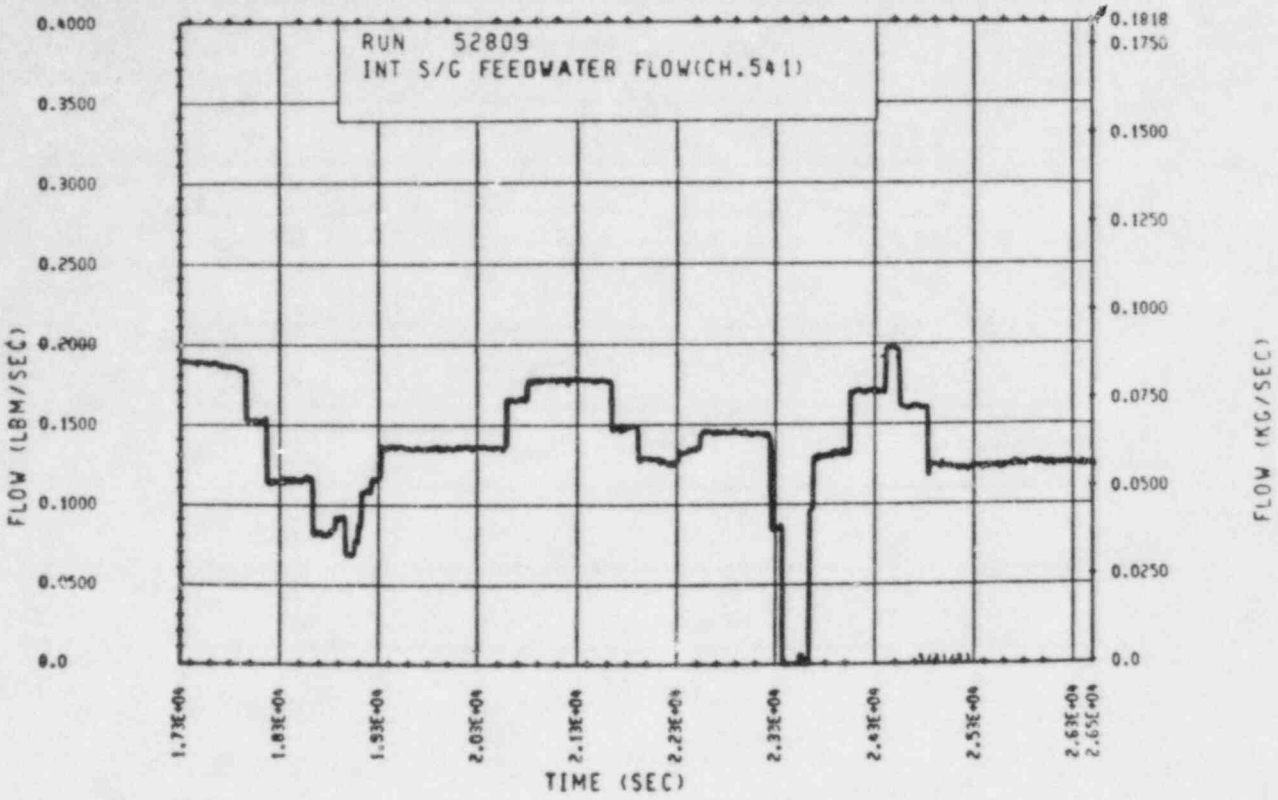

Figure 5-102. Unbroken Loop Steam Generator Feedwater Mass Flow Rate (17,300-26,500 sec)

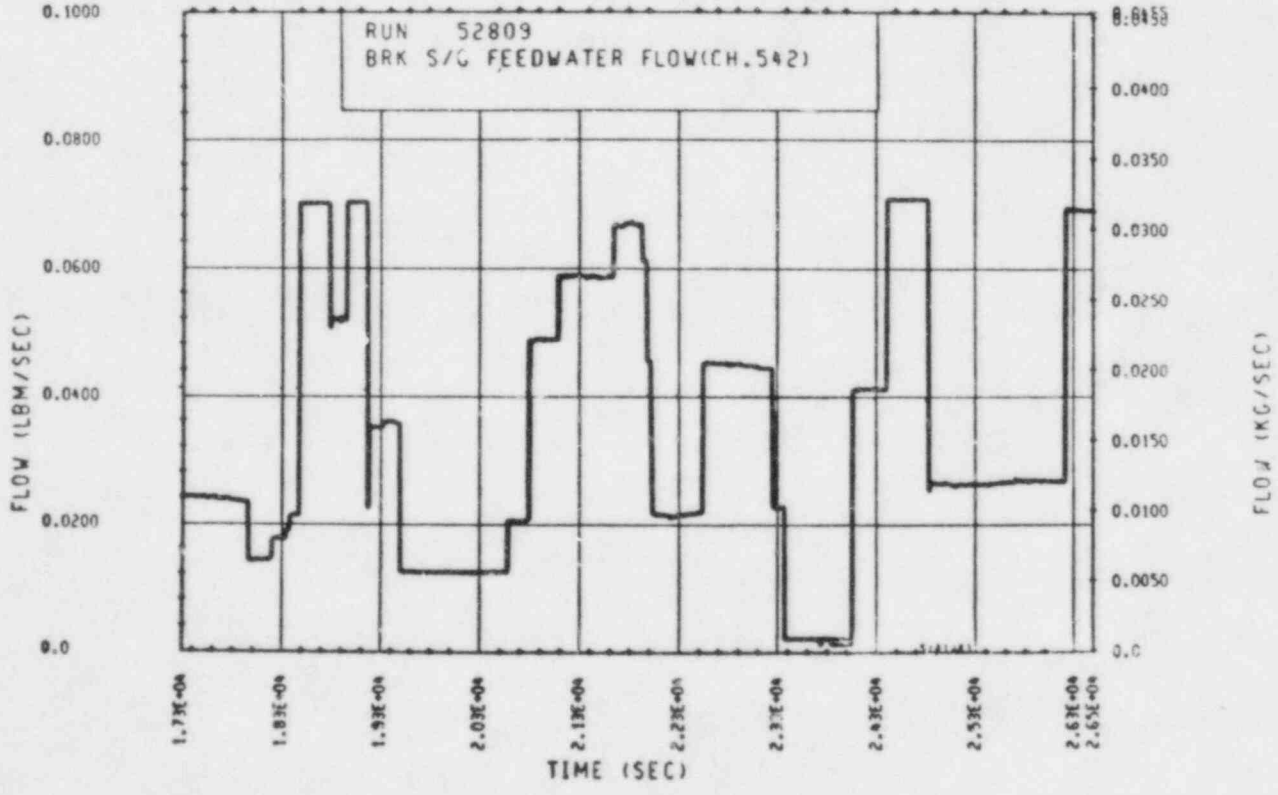

Figure 5-103. Broken Loop Steam Generator Feedwater Mass Flow Rate (17,300-26,500 sec)

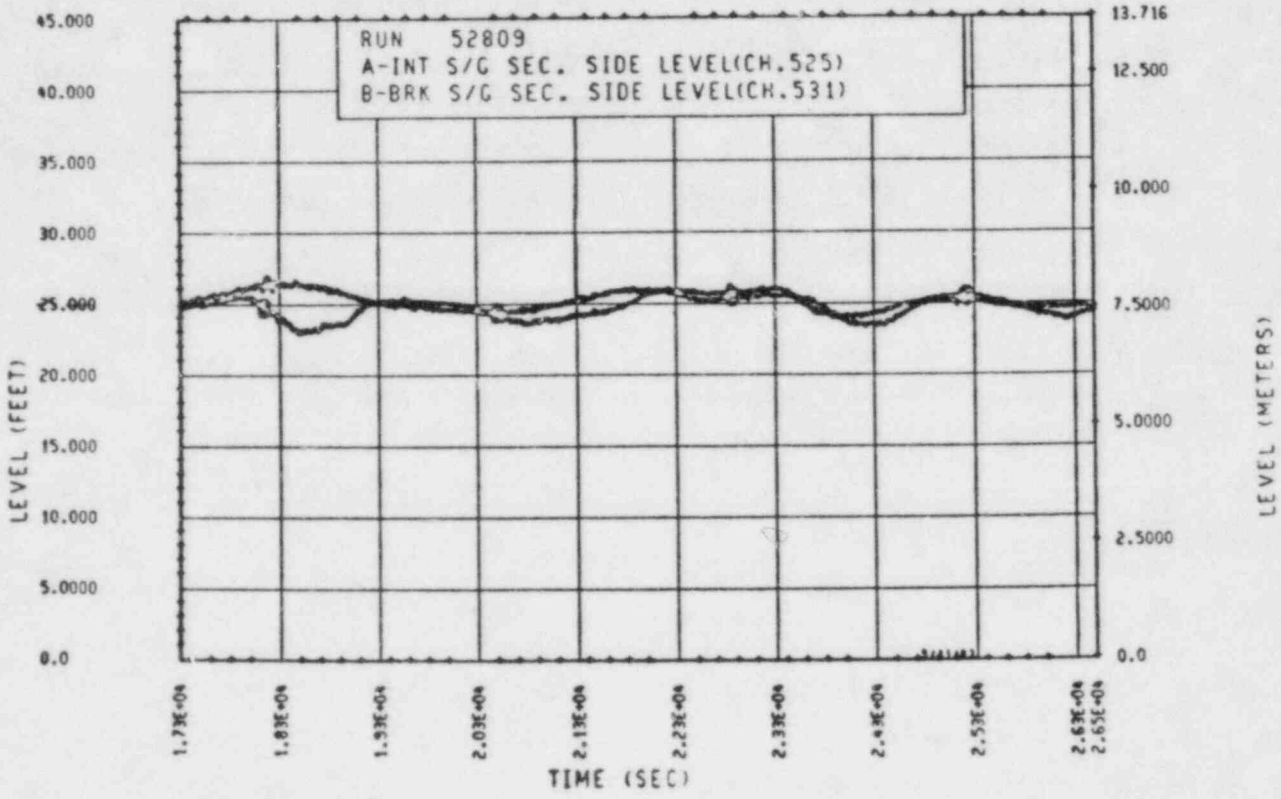

Figure 5-104. Unbroken and Broken Loop Steam Generator Secondary Side Collapsed Liquid Levels (17,300-26,500 sec)

The behavior of the broken loop during this period of two-phase natural circulation is shown in figure 5-55. The broken loop was stalled at the peak two-phase flow condition, but became unstalled shortly thereafter. The flow increased, peaked, and then decreased in a manner analogous to the two-phase natural circulation flow behavior shown in figure 5-2. The addition of the broken loop heat sink had little effect on the rest of the system. Figure 5-53 shows the total flow through the rod bundle increasing slightly at the moment the unbroken loop became active. This unstalling phenomenon is discussed in more detail below.

As the mass inventory decreased further, the gravitational force imbalance around the loop began to vanish as the downhill sides of the loop became increasingly voided. The voiding of the downhill portion of the loop is reflected by the unbroken loop plenum-to-plenum pressure drop (figure 5-78). As the single-phase/two-phase interface moved down the downhill side of the U-tubes, the negative gravitational pressure drop component became less influential. The inherently positive two-phase frictional component, however, became more influential as more of the U-tube was exposed to two-phase flow, as well as because of the increase in vapor velocity. The character of the total pressure drop consequently changed from one governed by gravity to one governed by friction. This resulted in a total pressure drop transition from a two-phase peak flow negative value to a positive value associated with reflux condensation.

At a mass inventory of approximately 53 percent, the unbroken loop steam generator was unable to condense all of the vapor that entering it. The unbroken loop steam generator outlet plenum (figure 5-88) began to void as a result of the excess vapor and system mass removal. Shortly thereafter, the broken loop steam generator outlet plenum began to void (figure 5-89). Both steam generator outlet plenums emptied of liquid quickly and the single-phase/two-phase interface subsequently penetrated into the descending legs of the loop seals (figures 5-90 and 5-91). The flow through both loops decreased because of the increasing downhill side voidage. The average flow became zero when the mass inventory decreased to 38 percent. As shown below, this zero flow condition provides only an approximate indication of the onset of reflux condensation.

A better indication of the transition to reflux condensation is provided by monitoring the condition of the steam generator inlet plena. Figure 5-76 shows the differential pressure cell measurement of the unbroken loop steam generator inlet plenum. As mass is removed from the primary system, the differential pressure reading decreases; this decrease indicates an increase in void. Most of this void increase with time is due to the increasing void fraction associated with the co-current two-phase flow entering the inlet plenum. At some point, however, the gravitational force acting on the liquid dominates, and the transition is made from a co-current to a counter-current stratified flow in the hot legs. The void fraction in the inlet plenum now increases as a result of liquid draining in a counter-current fashion out of the plenum and into the hot leg. The inlet plenum empties of liquid as a result. This was confirmed by visual observation. The stage is now set for condensate from the uphill side of the U-tubes to reflux back into the rod bundle through the hot leg. The unbroken loop inlet plenum emptied at approximately t = 19,700 seconds (38 percent mass inventory), signalling the transition to a counter-current flow regime in the intact loop hot leg. The steady differential pressure cell reading of 1.4 kPa (0.2 psi) after this time was primarily due to the liquid that collected in the inlet plenum dead space. This dead space is located below the hot leg entrance, so any liquid there can not drain out into the hot leg.

A comparison of the inlet plena from both steam generators (figure 5-76 and 5-77) shows that the broken loop inlet plenum emptied approximately 1,266 seconds after the unbroken loop inlet plenum. As a result, it is concluded that the transition to reflux condensaton did not occur in the broken loop until a mass inventory of approximately 37 percent was reached. It is believed that the modeling of the four prototypical loops into two loops, one unbroken (three loops) and one broken (one loop), is responsible for the difference in the transition to counter-current hot leg flow between the two modeled loops. Figure 5-105 is a detailed drawing of the facility's upper plenum. Of particular interest is the fact that the broken and unbroken loop hot leg nozzles were installed with the bottoms of the hot leg pipes at the identical elevation. In fact, the hot legs were installed so that the bottoms of both hot leg pipes were at the same elevation for the entire length of the hot leg. As a result of the modeling of the unbroken loop as three loops, the

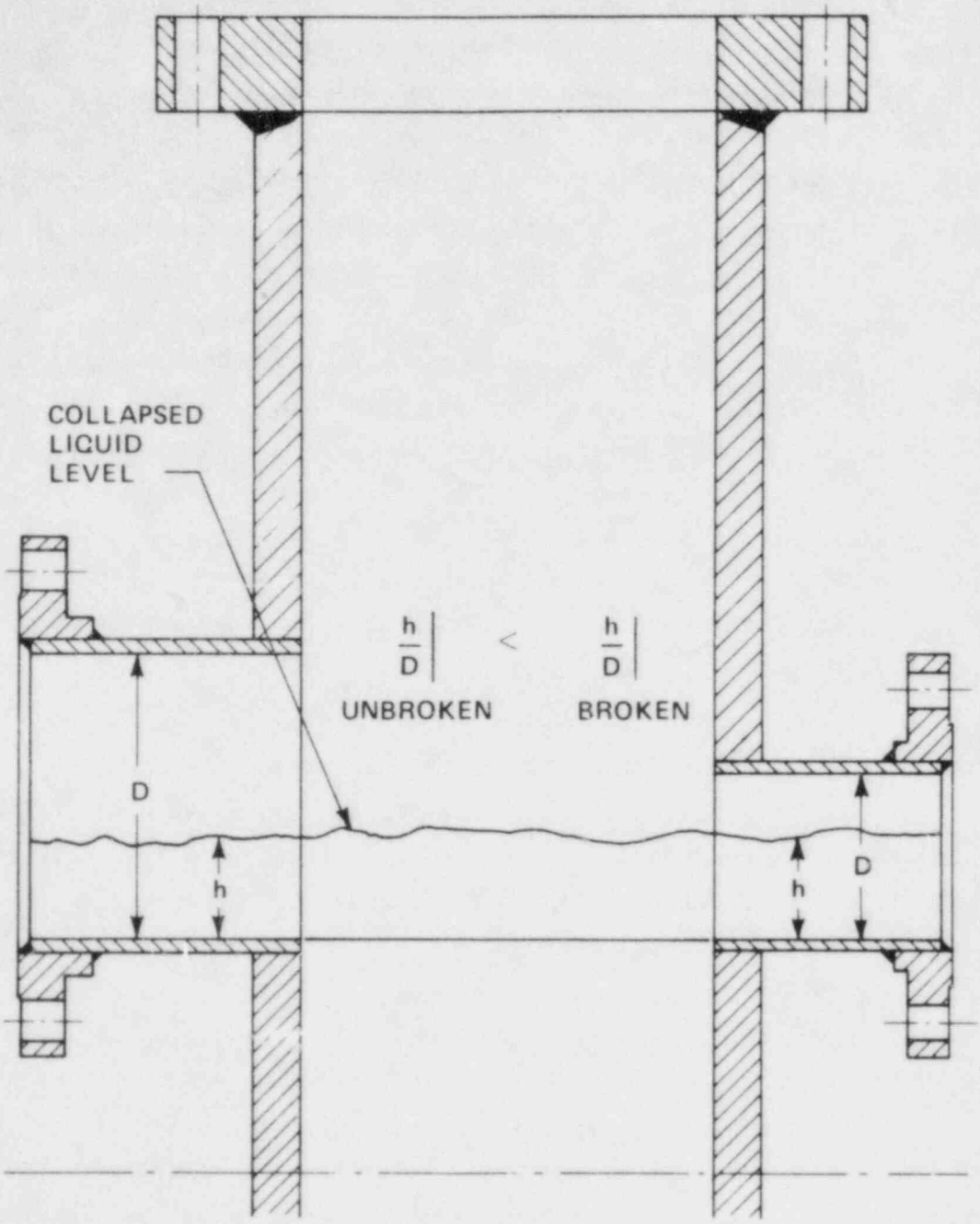

Figure 5-105. FLECHT SEASET Natural Circulation Facility Upper Plenum and Corresponding Unbroken and Broken Loop Hot Leg h/D Parameters

hot leg diameter is 0.064 m (2.5 in.) larger than that diameter associated with the broken loop. The implication of this hot leg geometrical configuration is as follows.

As discussed in detail in section 3, the transition from a co-current bubbly-slug flow to a stratified counter-current flow is influenced by the h/D that would exist if the flow were stratified. The smaller the h/D, the more likely that the flow will become stratified, and counter-current. Figure 5-105 is a schematic diagram of the broken and unbroken loop hot legs and the relationships between their individual h/D's. Because the bottoms of the two hot legs are at identical elevations, the h associated with both pipes will be identical. Because of the difference in diameters, however, the h/D of the unbroken loop will always be less than that associated with the broken loop. Hence, the unbroken loop hot leg will make the transition from co-current to counter-current stratified flow before the broken loop hot leg. This explains why the onset of counter-current hot leg flow occurs in the unbroken loop prior to the broken loop.

The behavior of the two-phase fluid in the steam generator U-tubes during the transition from two-phase natural circulation to reflux condensation is best described by the steam generator plenum-to-plenum differential pressure readings, as well as the readings from differential pressure cells located on the uphill side of a total of four U-tubes (figures 5-78 through 5-87). As previously discussed, the unbroken loop steam generator inlet plenum to outlet plenum pressure drop made the transition from a negative value to a positive value as the downhill portion of the loop voided. Figure 5-78 shows that the pressure drop became so positive that it saturated the differential pressure cell. It is believed that this large positive pressure drop measurement is the result of friction as well as liquid holdup on the uphill side of the steam generator. Figure 5-73 shows the rod bundle vapor mass flow rate increasing as the onset to reflux condensation was approached in the unbroken loop. There is no doubt that this will contribute to the positive nature of the total pressure drop as the result of an ever increasing frictional pressure drop component.

Hand calculations, however, indicate that the two-phase frictional pressure drop would only be on the order of 0.7 kPa (0.1 psi). The balance of the relatively large positive pressure drop shown in figure 5-78 must be due to liquid holdup on the uphill side of the steam generator. The holdup is believed to be the result of the flow in the U-tubes making the transition from a co-current to a counter-current flow regime. This transition is shown qualitatively in figure 5-106. As mass is drained from the primary, the superficial gas velocity increases. The void fraction associated with the co-current flow also increases. Evidence that the void fraction in the tubes increases is provided by the decreasing differential pressure measurement in the four instrumented U-tubes (figure 5-80 through 5-87.) As a result, figure 5-106 shows the superficial liquid velocity decreasing. Eventually the threshold for co-current/counter-current flow is reached ($j_f^*=0$), and there is a temporary liquid holdup in the uphill side of the steam generator U-tubes. It is this holdup that causes the large plenum-to-plenum positive pressure increase shown in figure 5-78. The plenum-to-plenum pressure drop decreases to a measurable value as the transition is made into the counter-current flow regime, and subsequent liquid fallback (reflux condensation) relieves the liquid buildup. Close examination of figure 5-78 shows that the unbroken loop plenum-to-plenum pressure drop did not reach a steady-state value until approximately 20,600 seconds (35 percent mass inventory). This is indicative of a steady-state reflux condensation condition in the unbroken loop. It should be noted that this steady-state condition occurred approximately 872 seconds after the flow through the loops went to an average value of zero.

Once the broken loop became unstalled, its plenum-to-plenum pressure drop behavior was similar to that of the unbroken loop (figure 5-79). It is interesting to note that the transition from co-current to counter-current flow occurred in the unbroken hot leg prior to the broken hot leg for reasons already discussed. Comparison of figures 5-78 and 5-79, however, shows that the transition to a steady-state reflux condensation condition occurred for both steam generators at roughly the same moment, t = 20,600 seconds.

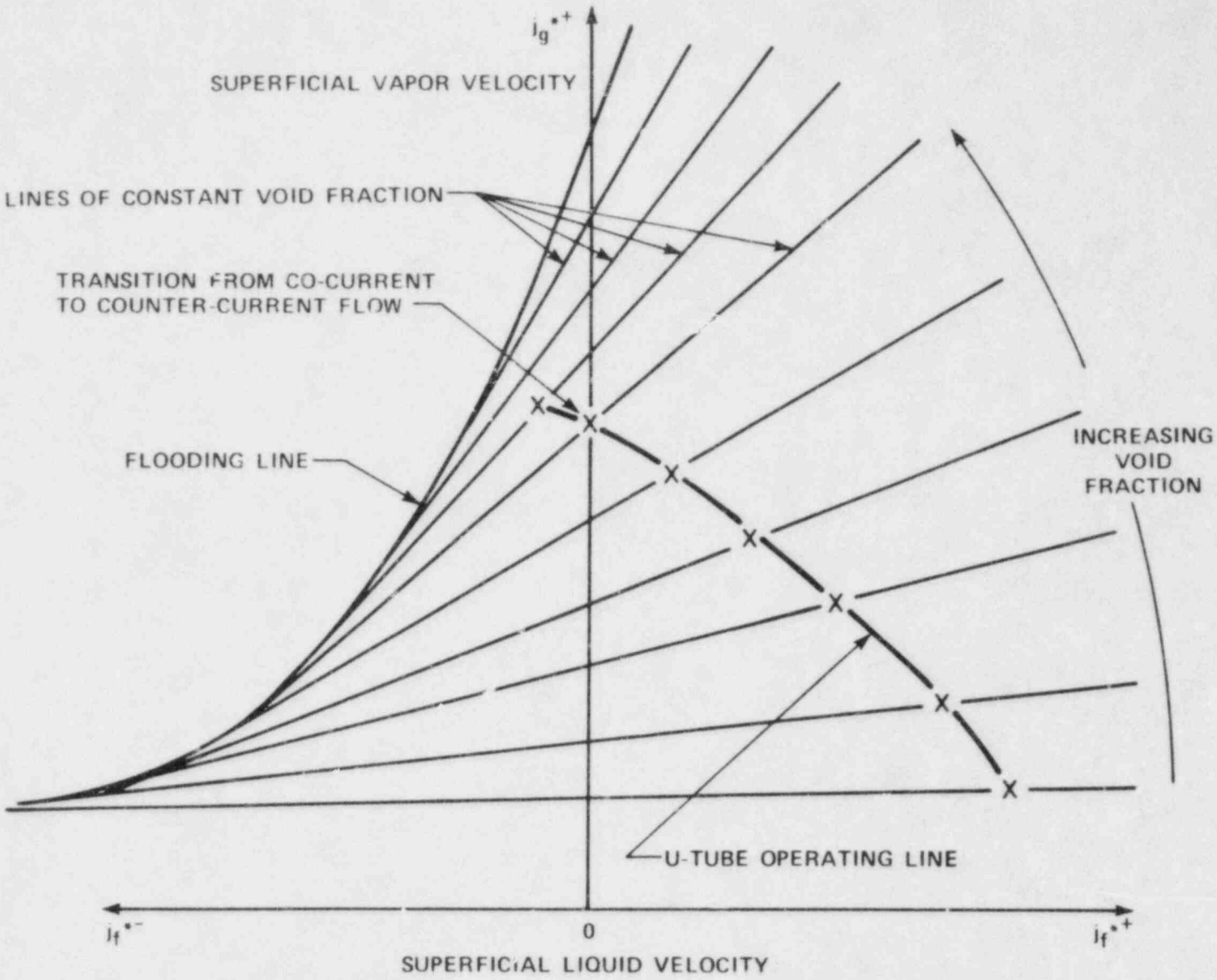

Figure 5-106. Qualitative Description of Transition From Co-Current to Counter-Current Flow in Uphill Side of Steam Generator U-Tubes

5-7. REFLUX CONDENSATION

The transition from a two-phase natural circulation cooling mode to a reflux condensation cooling mode has been discussed in detail above. In general terms, the reflux condensation mode of natural circulation can be described as follows. During reflux condensation, the rod bundle heat was transported to the secondary side by pool boiling in the core and filmwise condensation on both the uphill and downhill sides of the steam generator U-tubes. The rod bundle was kept supplied with liquid by condensate which returned to the rod bundle through two different paths. Condensate on the uphill portion of the U-tubes fell counter-current to steam rising out of the rod bundle and returned directly to the core through the hot legs. Condensate on the downhill side of the U-tubes returned to the rod bundle indirectly by falling into the loop seal and displacing water from the loop seal, cold leg, and downcomer into the bottom of the rod bundle. This mode of natural circulation cooling is documented in figures 5-52 through 5-104 for the time period 20,600 seconds to 26,500 seconds.

In paragraph 5-6, it is noted that a steady-state reflux condensation mode of cooling was momentarily established at approximately 26,500 seconds, which corresponds to a mass inventory of 35 percent. Visual observations in the upper plenum indicated that the mixture height was well above the tops of the hot legs. It was desirable for investigative purposes to bring this mixture height down below the hot legs, so that any liquid in the hot legs was due to reflux condensation. The flowmeters installed to measure reflux condensation operate best when this condition is achieved. To achieve this condition, more mass was removed from the primary in discrete drains (figure 5-52), until a mass inventory of 28 percent was reached. The response of the hot leg reflux meters is shown in figures 5-96 and 5-97.

During the course of these drains, however, it was difficult to achieve a steady-state reflux condensation condition for more than 28 minutes. The system would experience a periodic surge of flow through the rod bundle which would push the mixture height significantly above the hot leg nozzles. These periodic flow surges are shown as very large flow spikes in the crossover leg (figure 5-53) and unbroken loop (figure 5-54) flowmeters. The broken loop

flowmeter (figure 5-55) did not measure a flow spike. This flow surge phenomenon was very consistent, with a period of approximately 26 to 28 minutes. A comparison of figures 5-52 and 5-53 indicates that the phenomenon is independent of the discrete mass drains.

A detailed investigation of the system instrumentation revealed that the driving force behind the periodic flow surges was the periodic venting of steam through the unbroken loop seal. Figures 5-90 and 5-91 show differential pressure cell measurements on the descending leg of the loop seal. A decrease in pressure indicates a depression of the liquid level. Both figures show that the liquid levels began to be depressed by steam, which had passed through the steam generator uncondensed, well before the onset of reflux condensation. During this liquid depression (19,566 seconds to 21,700 seconds), the ascending leg of the loop seal was liquid solid, as indicated by the saturated loop seal/cold leg differential pressure cell readings in figures 5-92 and 5-93. This liquid distribution is shown in figure 5-107.

The liquid level in the descending leg of the unbroken loop seal reached the top of the loop seal horizontal pipe run at approximately 21,700 seconds. As it did so, a path was cleared for the steam to vent through the unbroken loop seal. This event is shown in figure 5-107. The fact that this occurred was confirmed by fluid thermocouples located in the horizontal, as well as the ascending, leg of the unbroken loop seal. These thermocouples registered a 3°C to 4°C (5°F to 7°F) temperature increase during the event, confirming that hot steam had indeed passed through the unbroken loop seal. Looking ahead to subsequent steam vents, a comparison of figures 5-90 and 5-91 shows that the levels in the descending legs of both loop seals depressed at the same rate. The unbroken loop seal, however, was the only loop seal to vent. This was the result of the unbroken loop seal modeling three-loops of a four loop system. The unbroken loop seal piping was subsequently bigger; hence, the depressing liquid level would reach the top of this piping sooner, allowing for steam to be vented through the loop seal.

As the steam vented through the intact loop seal, the event was measured by the flowmeter in the intact loop as the periodic flow spike alluded to earlier. Some of the vapor was condensed as it bubbled up through the

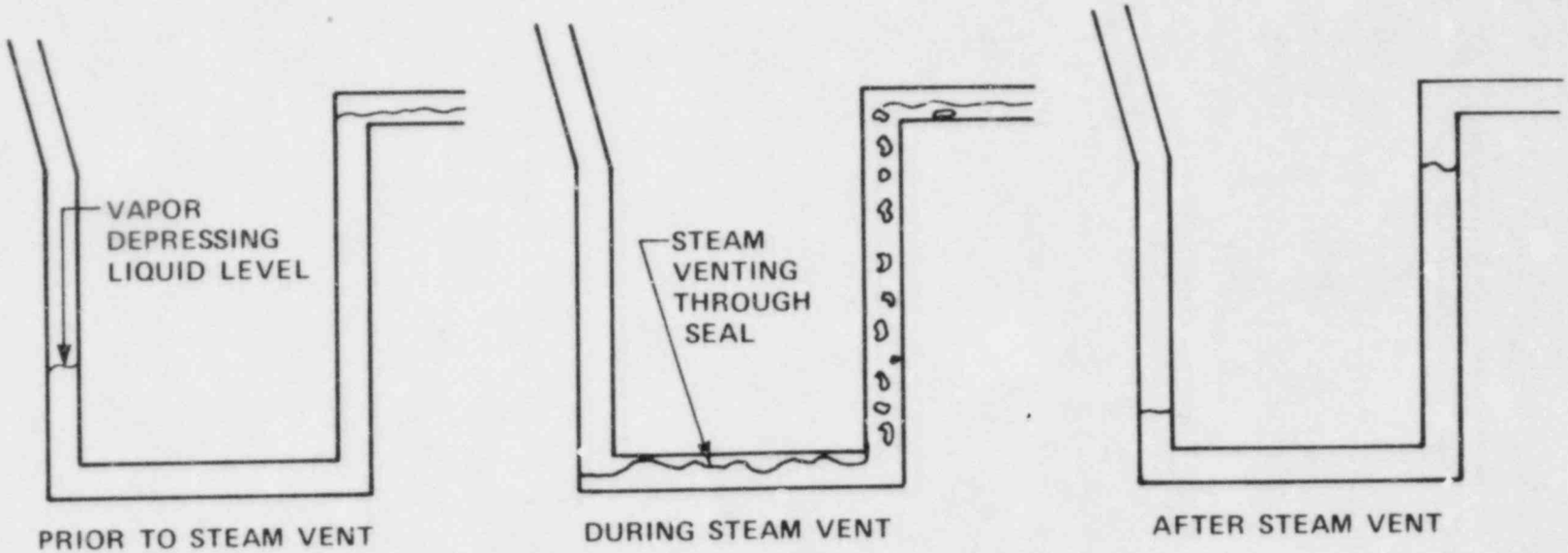

Figure 5-107. Unbroken Loop Seal Liquid Distribution

ascending leg of the loop seal. The 3°C to 4°C (5°F to 7°F) temperature increase noted earlier reflects a large condensation potential in the ascending leg of the loop seal. However, not all of the steam which vented through the loop seal was condensed right away. The liquid level in the downcomer shows a stepwise decrease coincident with the venting of steam (figure 5-95). This stepwise depression was the result of vapor rushing into the downcomer and displacing liquid out of the previously full downcomer. The vapor did not confine itself to the downcomer, but also rushed into the broken loop cold leg and consequently displaced water back into the broken loop seal. Evidence of this is shown in figure 5-92, as the step change recovery of liquid level in the descending leg of the broken loop seal. The slight cooling of fluid thermocouples on the broken loop seal confirmed that the source of this liquid level recovery was the water previously contained in the cold leg side of the loop seal.

The venting of steam through the unbroken loop seal was only momentary, as indicated by the momentary flow surge recorded by unbroken loop flowmeter (figure 5-59). As previously indicated, as the steam bubbled through the subcooled water in the unbroken loop seal, some of it condensed. This venting and subsequent condensation relieved the differential pressure that existed across the loop seal, and the unbroken loop seal resealed with water. The pressure decrease is reflected in the upper plenum/downcomer extension differential pressure measurement (figure 5-94), which shows a 1.8 to 2.2 kPa (2 to 2.5 psi) stepwise pressure decrease coincident with an unbroken loop seal vent. It should be noted, however, that the pressure decrease was only temporary. The pressure gradually increased following the vent and subsequent reseal of the loop seal.

The steam that rushed into the downcomer displaced subcooled water into the heater rod bundle through the crossover leg. This slug of cold water was measured by the crossover leg flowmeter as the flow spike alluded to earlier. The effect of the slug of cold water as it entered the rod bundle was two-fold. First, the slug of cold water displaced the two-phase mixture in the lower elevations of the rod bundle.

The mixture front was consequently forced up into the upper elevations of the upper plenum above the hot leg nozzles. This rising mixture level was visually observed through the windows in the upper plenum. The vapor flow rate out of the rod bundle increased momentarily as a result of vapor being displaced out of the rod bundle. This is seen in figure 5-73 as the momentary vapor mass flow spiked. Second, once the cold slug established itself in the rod bundle, vapor generation momentarily stopped in the lower elevations of the rod bundle. This can be seen in figures 5-60 through 5-69, where the void fraction went momentarily to zero in the first 1.5 m (5 ft) of the rod bundle. The cessation of boiling was only momentary. As figure 5-73 shows, the vapor mass flow rate out of the rod bundle momentarily dropped to zero, but quickly returned to its nominal pool boiling value.

As a result of the sudden and momentary surge of vapor out of the rod bundle immediately following an unbroken loop seal steam vent, a two-phase mixture was forced up into the broken loop steam generator inlet plenum (figure 5-77). In general, a two-phase mixture was not forced up into the unbroken loop steam generator plenum (figure 5-76). This behavorial difference between the two loops is believed to be the result of the tendency for the broken loop hot leg to make the transition from a counter-current to a co-current flow regime before the unbroken loop hot leg. This difference has already been discussed.

It is believed that the momentary surge of vapor out of the rod bundle also resulted in a transition from counter-current to co-current flow in both sets of steam generator U-tubes. Evidence of this is offered by the steam generator plenum-to-plenum pressure drop measurements (figures 5-78 and 5-79), which show significant pressure drop increases immediately following a loop seal vent. As discussed in paragraph 5-6, a small portion of this pressure drop increase is due to friction, but the balance is believed to be due to liquid holdup on the uphill side of the U-tubes. The sudden surge of vapor into the steam generators results in a momentary transition from a counter-current to a co-current flow regime. As the vapor surge subsides, the tubes make the transition back into a counter-current flow regime. As the transition is made back and forth between counter-current and co-current flow, there is liquid holdup. This phenomenon is complicated by the fact that the tubes

do not al act in unison; some tubes make the transition before others. The liquid holdup is relieved by the return to a counter-current flow regime. The counter-current flow is restricted, however, as the tubes operate along the flooding curve. As a result, it takes the tubes a finite amount of time to drain and return to a steady-state reflux condensation condition.

The liquid holdup explanation is supported by the fact that the vapor flow surge, which would contribute a large frictional pressure drop component, was only momentary (figure 5-73), whereas the total plenum-to-plenum pressure drop increase shown in figures 5-78 and 5-79 occurred over a period of 6 to 7 minutes. The long period associated with this plenum-to-plenum pressure drop increase could only be the result of liquid holdup, which was gradually relieved by liquid fallback as the tubes made the transition back into a steady-state reflux condensation condition. Evidence that fallback was restricted is provided by the unbroken loop hot leg reflux meter (figure 5-96), which shows the rate of reflux gradually increasing following a loop seal vent.

However, the return to a quasi-steady-state reflux condensation mode of cooling was only temporary. As soon as the unbroken loop seal vented and subsequently resealed, the cycle began again with the depression of the liquid levels of the descending legs of the loop seals. Approximately 26 to 28 minutes after the unbroken loop seal vented, it would vent again and initiate the chain of events described above.

5-8. PARAMETRIC EFFECTS TESTS

Several different parametric tests were evalu[illegible] to investigate the behavior of the natural circulation systems effect[illegible] when a parameter such as injection flow, loss of heat sink, or inj[illegible] a noncondensible gas was varied. Each parametric test was initiated from a steady-state condition such as single-phase natural circulation, peak two-phase flow point, or reflux condensation. The results of each test type are summarized below; the details of each test are given in appendix A.

5-9. Cold Leg Injection Tests

In the cold leg injection tests, the natural circulation systems effects test facility was operating in a stable natural circulation cooling mode (single-phase, two-phase, or reflux condensation); a set amount of water was injected into the cold leg during each of these cooling modes to see the system response. It was expected that cold water injection on the cold side of the system (the steam generator downhill side, cold leg, downcomer) would help to increase the natural circulation flow when the system was solid, since the cold injection enhances the density difference. It was expected that the same effects would occur in the two-phase natural circulation mode, unless the cold water decreased the boiling in the bundle. For reflux condensation, it was expected that the cold leg injection would act to fill the system.

For single-phase natural circulation (test 5), the primary pressure was reduced to 0.52 MPa (75 psia) to prevent possible overpressurization of the loop if the natural circulation flow would stall. The pressurizer was valved in to the primary system; however, the cold leg injection overwhelmed the pressurizer control and the system pressurized to 0.77 MPa (112 psia). The loop flow first increased, and then slowly decreased to the preinjection value. The pressure control, however, was restored to a lower steady-state value [0.41 MPa (60 psia)] such that some boiling occurred in the top of the bundle. The system did not return to its original state before the injection; however, the bundle always remained in a coolable state.

For two-phase natural circulation (test 11), the primary system was 81.2 percent full and, at 0.37 MPa (53 psia), at the peak two-phase flow point. The effect of cold leg injection was to initially increase the loop flow and then stall it as the cold water collapsed the vapor generated in the rod bundle. This caused the loss of the driving head on the uphill side of the steam generator. The loop quickly recovered from the stagnation condition as the colder injection water heated and boiling returned to the core. The rod bundle was always cooled even though the flow stalled.

In reflux condensation (test 12), the primary system was operating in a stable cooling mode with an inventory of 32.3 percent at a pressure of 0.32 MPa

(46 psia). The cold leg injection increased the total mass in the primary system such that two-phase natural circulation was restored for a short time period. Then it decayed to zero loop mass flow approximately 10 minutes after injection and the primary system returned to stable reflux condensation. Again, the rod bundle remained covered and coolable during the transient. For the small mass that was injected [37.0 kg (81.6 lbm)], the final mass inventory of the primary systems were approximately 36 percent; therefore it was within the stable reflux condensation range for the FLECHT SEASET tests.

5-10. Upper Head Injection Tests

In contrast to the cold leg injection tests, it was expected that cold water injected on the hot side of the system (bundle, hot leg, and uphill side of the generator) would act to retard the natural circulation flow, since the favorable density gradient would be momentarily upset by the cold water. The system would compensate for the cold water blockage by pressurizing. In both tne two-phase flow and reflux condensation, the injection of cold water would collapse the voids on the hot side of the system and further reduce the driving head for flow.

For single-phase natural circulation with upper head injection (test 10A), the system was operated at 0.52 MPa (75 psia) such that pressure margin existed up to the scram pressure of 0.97 MPa (140 psia). As expected, the upper head injection flow resulted in a stalling of the natural circulation loop flow. The primary system also went through a pressurization to a peak value of 0.61 MPa (88 psia); then the pressure decayed to 0.48 MPa (70 psia) approximately 6 minutes after the completion of the upper head injection. The loop flow, which was reduced below its initial steady-state value, slowly increased to its original steady flow value 3 minutes after the termination of the upper head injection. The rod bundle always remained covered with water and was coolable.

During the two-phase natural circulation tests with upper head injection (test 10B), the injection of the upper head water completely stalled the loop flow and collapsed all the void in the bundle and upper plenum. The primary

pressure also decreased from 0.46 to 0.41 MPa (67 to 60 psia), and then the primary system began to pressurize rapidly. The facility high-pressure alarm at 0.90 MPa (130 psia) was tripped and the upper head injection was terminated because of the higher primary side pressure. As the primary system pressurized, the loop flow was reestablished. However, the primary pressure exceeded the set system pressure of 0.97 MPa (140 psia) and the rod bundle power was tripped. The flow through the primary system increased and reached 25 percent of the peak two-phase flow before the power was terminated. If the allowable primary system pressure had been higher, it is felt that the two-phase flow would have been reestablished and the pressure excursion would have been terminated.

The upper head injection (UHI) during reflux condensation (test 10C) basically acted to refill the primary system, which had 33 percent of the original mass inventory, to approximately 49 percent of the original mass inventory. The primary system then went from a stable reflux condensation mode to a weak two-phase natural circulation cooling mode with a low loop flow of approximately 20 percent of the peak two-phase flow value. The upper head injection water initially condensed the voids in the bundle and upper plenum and the collapsed levels in each volume increased. After the termination of the UHI flow, the levels in the bundle and plenum returned to their pre-UHI values; however, the primary system never returned to stable reflux condensation because of the high mass inventory as compared to the smaller mass injection with the cold leg injection. The rod bundle remained covered and coolable during the entire transient.

5-11. Heat Sink Effects Tests

Several experiments were conducted to determine the effects of loss of heat sink on the primary system response. As the system lost its heat sink, it was expected that the natural circulation driving head would be reduced; this would then reduce the loop flow. With the heat source/heat sink mismatch, the primary system would then pressurize to compensate for the loss of heat sink.

For the FLECHT SEASET tests, the initial pressure conditions for the tests were 0.52 MPa (75 psia), single-phase natural circulation; 0.39 MPa (56 psia),

two-phase natural circulation; and 0.30 MPa (44 psia), reflux condensation. The overpressure alarm was set at 0.69 MPa (100 psia); at this pressure, emergency feedwater from a pressurized accumulator would be added to the generators to refill them to their normal operating level and thus restore the heat transfer area in the steam generator.

For the single-phase natural circulation test with loss of heat sink (test 9A), the primary system was operating at a steady pressure of 0.52 MPa (75 psia) with a collapsed secondary side steam generator level of 7.62 m (25 ft). The pressurizer and steam generator feed flow were isolated at the same time; this resulted in a superimposed pressure transient. The primary system recovered from this imposed transient and reached a quasi-steady state until the steam generator secondary level reached 2.74 m (9 ft) (26 percent full). At this level, the primary flow began to decrease slowly and the primary pressure increased. As the secondary level decreased to below 2.44 m (8 ft), the primary pressure rise increased more rapidly. When the level was approaching 1.83 m (6 ft), the primary pressure exceeded 0.69 MPa (100 psia). At this point, the steam generator feed flow was restored and the primary side pressure rise was terminated.

In the two-phase natural circulation test (test 9B), the primary system was operating at the peak two-phase flow point at 82.3 percent of the original mass inventory at a pressure of 0.39 MPa (56 psia). At these conditions, the broken loop was stalled and the unbroken loop was acting as the primary heat sink. When the steam generator feed flow was terminated, an almost immediate response was felt in the primary system. When the steam generator level reached 7.62 m (25 ft), the primary loop flow rate began to decrease. This indicates that nearly the entire surface area of the generator was needed to reject the generated heat at the given primary system pressure and flow. As the steam generator secondary sides boiled away, the primary system flow correspondingly decreased and the primary pressure increased, to increase the primary to secondary side temperature difference. The flow decrease was believed to be the result of vapor being carried over the top of the steam generator U-tubes, which reduced the total driving head for the primary system.

At a secondary steady generator level of 1.22 m (4 ft), the primary pressure reached 0.69 MPa (100 psia). The transient was terminated when the steam generator levels reached 0.76 m (2.5 ft) when the primary pressure reached 0.83 MPa (120 psia). At this time, the accumulator was used to restore the liquid inventory on the steam generator secondary side; the pressure rise transient was terminated and the peak loop flow was restored. The pressure rise in the two-phase flow tests was less abrupt than that in the single-phase test because of the compressibility of the two-phase mixture.

The transient in test 9C was similar to the previous two transients except that the primary system was in the reflux condensation cooling mode. The primary system was initially operating in a stable reflux mode, with the exception of the unbroken loop venting, with a mass inventory of approximately 35 percent at a pressure of 0.30 MPa (44 psia). As the steam generator level was decreased from 7.62 m (25 ft), there was only a slight pressure increase [14-21 kPa (2-3 psia)] as the level was boiled the 3.05 m (10 ft) collapsed level. The pressure behavior of the primary system does show the cyclic behavior of the unbroken loop vent-through, which can reduce the primary system pressure by condensation in the loop seal and downcomer. This condensation was caused by the cooler water in this region, which had lost energy because of heat loss through the insulation. However, since the collapsed liquid level dropped below 3.05 m (10 ft), a steady rapid rise in the primary pressure was measured. This indicates that as the secondary side is drained, the heat flux distribution moves down the steam generator tubes towards the inlet until there is insufficient surface area to transfer the heat. Then the primary system pressure increases so as to create a large primary to secondary side temperature rise. Once the steam generator level was restored, the primary system pressure quickly dropped to its original value. In fact, the pressure decreased to its original value when the steam generator level increased past 3.66 m (12 ft).

Test 14 examined the minimum secondary side heat sink in single-phase natural circulation to maintain a steady-state situation. The primary system was operating in steady state at 0.93 MPa (135 psia) with the steam generator secondary pressure at 0.21 MPa (30 psia) with a level of 7.62 m (25 ft). The pressurizer was valved in such that the primary system pressure would remain

constant. The effect of decreasing the secondary side steam generator level was detected by examining the primary loop flow. The loop flow remained constant until the secondary side steam generator collapsed level boiled down to 4.11 m (13.5 ft). Below this level, a mismatch occurred between power generated in the rod bundle and the surface area needed in the steam generator to remove the generated energy at the initial primary side pressure and natural circulation flow. Therefore, for the above primary conditions, the steam generator level had to be maintained at 4.11 m (13.5 ft) or greater; otherwise a transient would occur which would reduce the loop flow and result in higher primary side temperatures.

In test 16, the effects of increasing the secondary side heat sink were tested by depressurizing the steam generator secondary side while it was in a boiling mode and thereby lowering its sink temperature. The primary system was initially operating at its peak two-phase flow condition at 86.9 percent mass inventory at a pressure of 0.41 MPa (60 psia). As the secondary side depressurized, it cooled down; the result was a gradual cooldown of both the primary and secondary loops of the system. The primary flow behavior is not clear; it first increased, and then decreased. However, the changes were small, as expected, since both the hot side and cold side of the primary system were cooled.

In test 17, the broken loop steam generator was allowed to boil dry while the primary system operated at the peak two-phase flow condition. The primary system was operating at a pressure of 0.38 MPa (55 psia) with 81.4 percent of the original mass inventory. The secondary system was operating at 0.24 MPa (35 psia) with a collapsed level of 7.62 m (25 ft). Since the broken loop stalled while the primary system was in two-phase natural circulation, losing the heat sink to the stalled loop had no effect on the primary system behavior. This result again indicates that, because of the oversized heat sink (for the given bundle power), one generator can adequately carry the heat load from the bundle.

In test 18, the reflux condensation behavior of the primary system was investigated as the steam generator secondary side was depressurized. The pressure system was operating with a mass inventory of 36 percent and a pressure of 0.31 MPa (45 psia). The secondary system was in the boiling mode

of a pressure of 0.28 MPa (40 psia) with a collapsed level of 7.62 m (25 ft). The pressure on the secondary side was slowly decreased to 0.14 MPa (20 psia). The secondary and primary side temperature gradually cooled down to the new saturation temperature at a steam generator pressure of 0.14 MPa (20 psia). As both systems depressurized, the liquid level in the bundle decreased, indicating an additional voiding in the bundle. As the pressure decreased, the vapor generation rate increased because of the flashing caused by the superheat stored in the liquid at the initially higher pressure. This increase in the primary side vaporization resulted in an increase in the reflux flow, as measured by the cold and hot leg reflux condensation meters. Severe spikes in the broken and unbroken loop reflux meters were observed. While the hot leg reflux meters indicated oscillations, the measured flow values steadily increased as the secondary side pressure, and therefore the primary side pressure, decreased. The rod bundle remained coolable for all times in this test.

In test 19, the unbroken loop steam generator was allowed to boil dry while the primary system operated in a reflux condensation cooling mode. The primary inventory was approximately 39 percent and the system operated at 0.31 MPa (45 psia). The secondary system was in a boiling mode at a pressure of 0.28 MPa (40 psia) and an initial level of 7.62 m (25 ft) in both generators. Refluxing was occurring in both generators before the broken loop feed flow was isolated. As the broken loop generator boiled dry, the primary pressure slowly increased by a very small amount [estimated at 7-14 kPa (1-2 psia)]; since the secondary side pressure was fixed, this small increase was large from a percentage point of view. At t = 48,680 seconds, the primary to secondary pressure difference was 43 kPa (6.3 psia), at 57,000 seconds, the pressure difference was 56 kPa (8.1 psia). This corresponds to an average increase in the primary to secondary side temperature difference of 1°C (2°F). The increased temperature difference indicates that the primary system was compensating for the loss of surface area to remove heat. As the broken loop secondary level decreased, the reflux flow returning to the core from the broken loop hot leg and cold leg correspondingly decreased while the reflux flow in unbroken loops increased. Therefore, since there was an excess of surface area, the loss of the broken loop steam generator did not affect the overall primary system response, and the rod bundle remained in a coolable state.

5-12. Single-Phase Reference Tests

A series of four single-phase reference tests were performed to investigate the parametric effects of core power snd secondary side heat sink on single-phase natural circulation. These four tests differed from other single-phase tests in that the secondary side was not operated in a feed-and-bleed pool boiling mode. Rather, the secondary side was operated in a liquid-solid forced circulation mode with heat being removed from the secondary working fluid by a tertiary heat exchanger.

Tests 1 and 2 confirmed the analytical relationship developed by Lewis[1] that flow would vary with core power raised to the 1/3 power. The comparison between theory and experiment is shown in figure 5-108. The scatter of data is minimal at low power ratios, but becomes more significant as the power ratio approaches 12. The increase in scatter could possibly be the result of power and/or flow measurement uncertainties that become influential at large power ratios.

Tests 3 and 4 examined the effect of varying the secondary side heat sink while maintaining a constant power. The heat sink was varied by adjusting the secondary side forced circulation flow rate while maintaining a constant inlet temperature. The range of forced circulation flow in the broken loop secondary side was 0.003 to 0.024 kg/sec (0.007 to 0.054 lbm/sec). The corresponding range of forced circulation flow in the unbroken loop secondary side was 0.010 to 0.077 kg/sec (0.023 to 0.17 lbm/sec). It was originally expected that this flow rate variation would cause the local secondary side heat transfer coefficients to change and hence affect the overall primary-to-secondary heat transfer. This in turn would be reflected by a decrease or increase in the primary single-phase natural circulation flow rate. The primary, however, remained unaffected over the range of secondary flows investigated. An analysis of the fluid conditions in a secondary side flow channel indicated that the flow will be laminar for the entire range of secondary flow conditions. Hence, the secondary side local heat transfer coefficients did not vary with flow rate and consequently the primary remained unaffected.

---

1. Lewis, E. E., Nuclear Power Reactor Safety, John Wiley and Sons, New York, 1977.

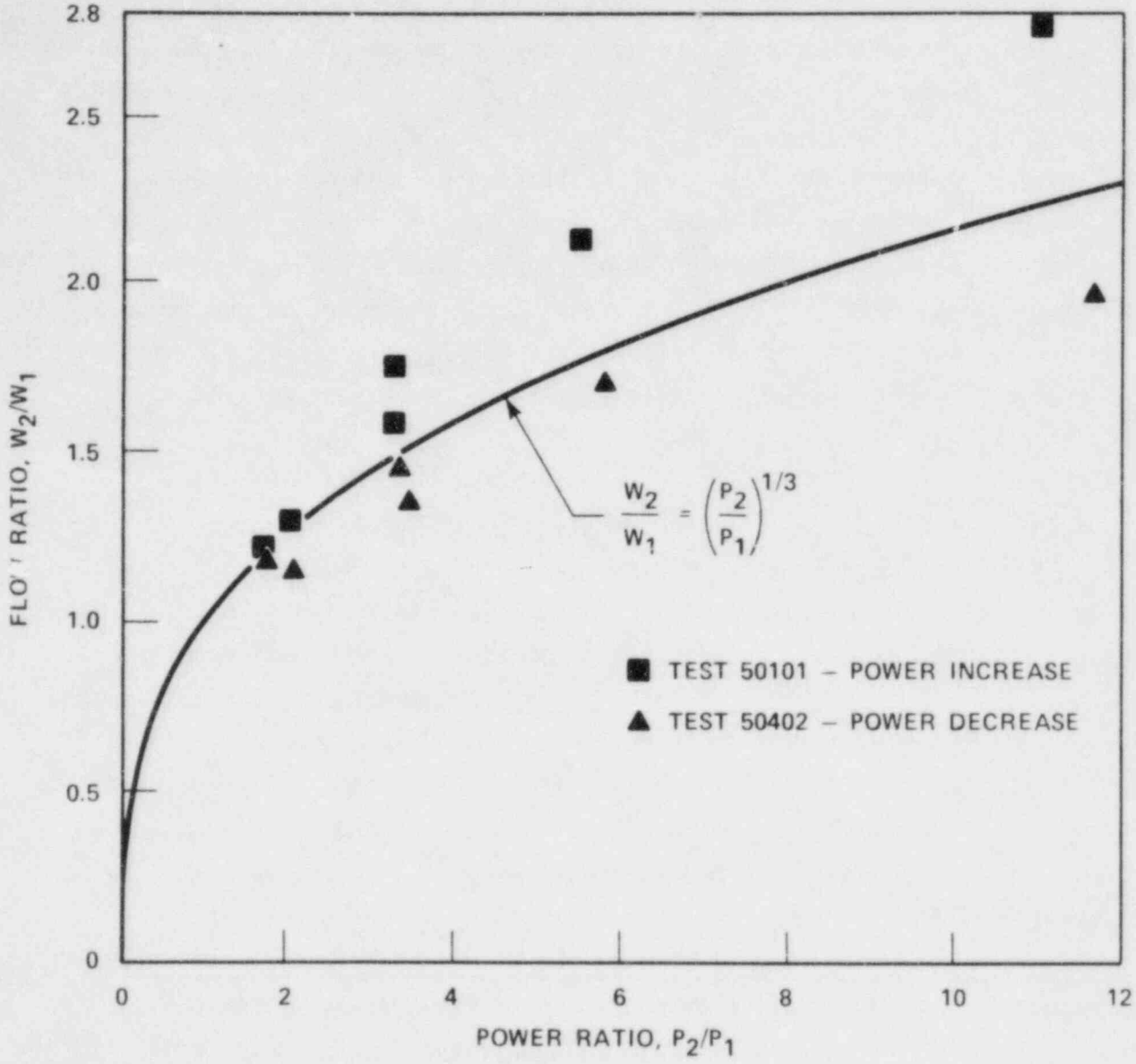

Figure 5-108. Single-Phase Flow Ratio as a Function of Power Ratio

5-13. Noncondensible Gas Tests

A series of three tests were performed to examine the effect of noncondensible gas on single-phase, two-phase, and reflux condensation modes of natural circulation. Helium was chosen as the noncondensible gas to be tested because it is the most common noncondensible gas expected to be found in a PWR during a small-break LOCA and because it is used as a fill gas in PWR fuel rods and would escape if the rods burst. In general, helium was placed into the primary system following the steady-state estab- lishment of the desired natural circulation mode of cooling. The helium entered the primary system by means of a series of simultaneous discrete injections through porous plugs into the hot legs of both the broken and unbroken loops.

Test 6 was designed to examine the effects of noncondensible gas on single-phase natural circulation. During the test, a total of 11.5 moles (2.53×10^{-2} lbm-moles) of helium were injected into the primary system in a series of nine injections. The primary system responded to the addition of noncondensible gas by reducing the single-phase flow from 0.0015 to 0.0011 m^3/sec (24 to 18 gal/min) during the first three injections. The six subsequent injections of helium had no impact on the system. It is believed that the flow decrease observed during the first three noncondensible gas injections was the result of helium accumulation at the top of selected steam generator U-tubes. The helium consequently formed a vapor plug at the top of the U-tubes, which blocked flow through these tubes. As a result of the tube blockage, the effective flow area through the steam generators' was reduced. This translated into an increase in frictional flow resistance through the steam generators and the system responded by reducing flow. It is postulated that flow was not reduced during the last six helium injections because this helium found its way to previously plugged tubes rather than plugging additional steam generator U-tubes. The manner in which the helium was injected (at the top of the hot leg) may have caused the helium to flow preferentially into selected tubes in the generator.

Test 13 was designed to examine the effect of noncondensible gas on two-phase natural circulation. The test was initiated from a two-phase peak flow condition at a mass inventory of 82 percent. Consistent with previous FLECHT

SEASET two-phase peak flow conditions, the system was operating in a N-1 loop configuration as a result of the broken loop being stalled. A total of 20.5 moles (4.51×10^{-2} lbm-moles) of helium were injected into the primary systems by means of a series of nine discrete injections. The primary system responded to the addition of noncondensible gas by making the transition from a two-phase flow condition to a single-phase flow condition. This phase transition was accompanied by an increase in primary system pressure and a decrease in flow. These pressure and flow trends are shown quantitatively in figure 5-109 as a function of the volume of helium injected.

Similar to the single-phase case discussed above, it is believed that these trends were the result of helium collecting in selected unbroken loop steam generator U-tubes and consequently blocking flow through those tubes. The flow blockage served to remove available heat transfer area as well as to increase the unbroken loop flow resistance. A portion of the observed flow decrease can be credited to the increased flow resistance. The remaining portion of the flow decrease can be attributed to the pressure increase and its effect on the rod bundle vapor generation rate. The pressure increased because of the increasing heat transfer area and volume displacement by the helium gas. The pressure effect, however, fed back onto the flow characteristics by virtue of the fact that a pressure increase will decrease the vapor generation rate in the rod bundle because of enhanced subcooling at the rod bundle inlet. The void fraction correspondingly decreased on the uphill side of the system. In response to this decrease in density gradient around the loop, flow decreased. During test 13, this flow decrease was accented by the fact that the pressure increase was significant enough to suppress vapor generation completely and force the system to operate in a single-phase natural circulation mode. It should be noted, however, that the addition of helium did not unstall the broken loop. The system operated in a N-1 loop configuration for the duration of the test.

Test 15 was designed to examine the effect of noncondensible gas on the reflux condensation mode of natural circulation. Before the initiation of noncondensible gas injections, the primary system was brought to a quasi-steady-state reflux condensation condition by reducing the primary system mass inventory to approximately 25.1 percent of its original single-phase liquid-solid condition. In this preinjection condition, the primary system exhibited periodic loop

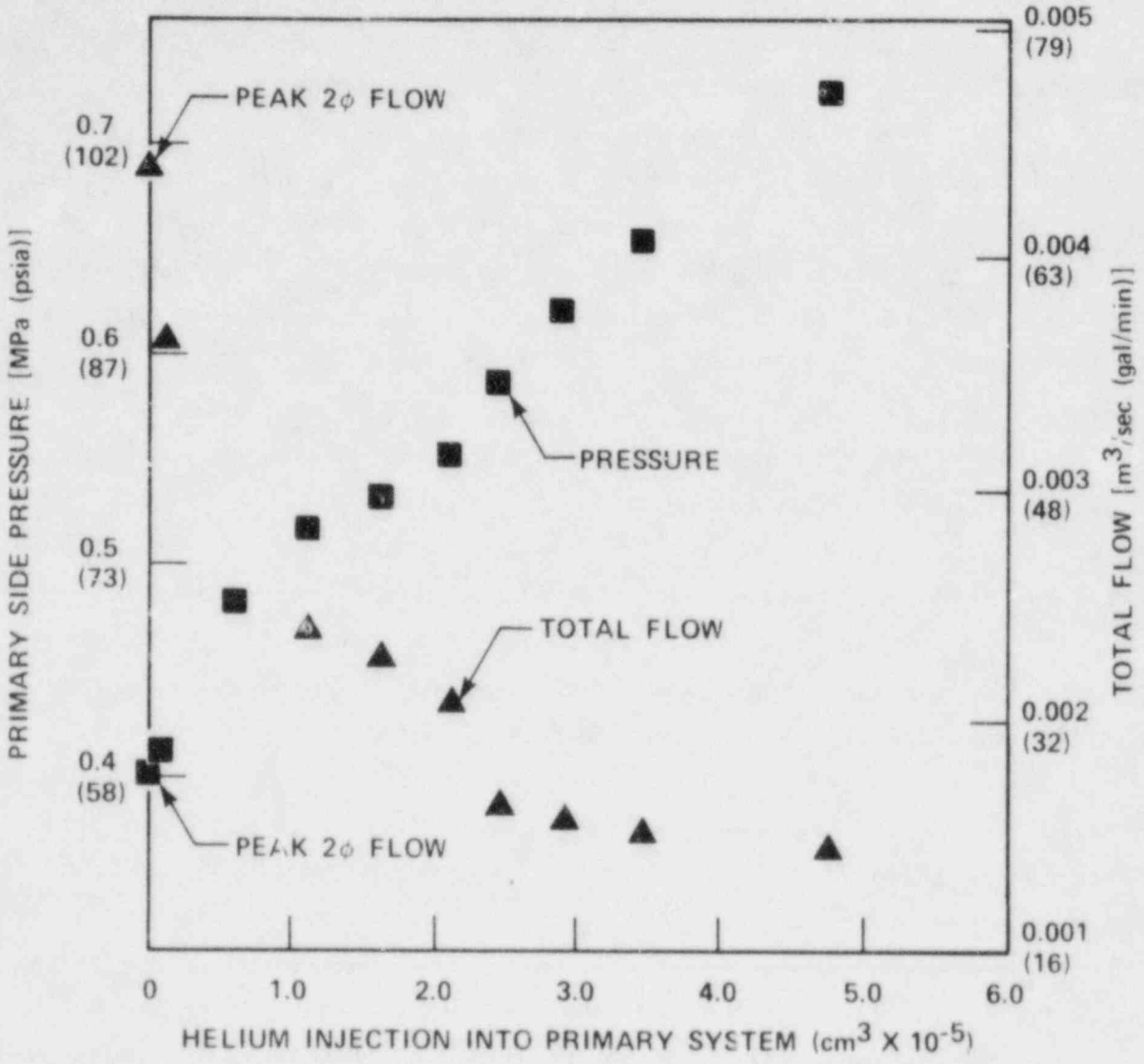

Figure 5-109. Natural Circulation Total Flow and Primary Pressure as a Function of Helium Injected Into Primary System

seal venting behavior consistent with that previously discussed in paragraph 5-6. During the course of the test, a total of 44.9 moles (9.89×10^{-2} lbm-moles) of helium were injected into t.e primary system by means of a series of three injections. As helium gas was introduced into the primary system, it was swept to the downhill side of the steam generators and loop seals, where it accumulated and reached thermal equilibrium with the secondary side. The pockets of helium gas on the downhill side of the steam generators blocked off previously available heat transfer area and forced more of the condensation process to occur on the uphill side of the steam generator U-tubes. This same phenomenon was observed by Hein, et al.[1] As more helium was introduced into the primary system, these helium pockets blanketed the downhill side of the U-tubes and spread to the uphill side, removing more heat transfer area. Fluid thermocouple readings indicate that, by the test's end, at least one pocket of helium in the unbroken steam generator had blanketed as much as 99 percent of a single U-tube.

The primary system was affected by this distribution of helium gas in four major wa s. First, the condensation process was forced to occur exclusively on the uphill side of the steam generators. Second, the system pressure increased to accommodate the degraded heat sink condition caused by the noncondensible gas effective removal of heat transfer area. Third, the period of the periodic loop seal venting behavior increased from minutes to hours as a result of noncondensible gas, rather than steam, being passed through the loop seal during loop seal vents. The noncondensible nature of the helium gas now trapped in the cold leg cavity usurped the cold leg steam condensation mechanism that previously drove the loop seal venting phenomenon. Any subsequent pressure decrease in the cold leg cavity was not due to the cooling of the trapped noncondensible gas as a result of ambient heat losses. The fourth and final effect involved the propensity of the uphill sides of the steam generator U-tubes to flood. As helium gas accumulation on the downhill side forced the total condensation burden to the uphill side, the thickness of the condensate film on the uphill side correspondingly increased twofold. This agrees with the flooding analyis described in section 3, which indicated that

1. Hein, D., et al., "The Distribution of Gas in a U-Tube Heat Exchanger and its Influence on the Condensation Process," The 7th International Heat Transfer Conference, Mun'ch, Germany, September 6-10, 1982.

the generators are operating near the flooding curve at 2-percent power. If all the condensate must now run back on the uphill side of the generator, some liquid holdup would be expected. As a result, the flow of condensate back to the heater rod bundle was periodically restricted by the counter-current flow of steam. The increased loop Δp associated with this periodic flooding behavior was sufficient to cause a core liquid level depression 0.61 m (2 ft) below the elevation coincident with the bottom of the loop seal. Core liquid level depressions triggered by U-tube flooding occurred four times during the course of the test. In the first three cases, core liquid level recoveries occurred as a result of loop seal vents which relieved the Δp across the core/downcomer. The fourth core liquid level depression resulted in a degraded core cooling condition because of the absence of a loop seal vent. the test was consequently terminated by a heater rod overtemperature signal of 399°C (750°F).

SECTION 6
STEAM GENERATOR HEAT TRANSFER ANALYSIS

6-1. INTRODUCTION

The purpose of the steam generator data reduction and analysis effort was to provide a data base from which local steam generator heat fluxes could be calculated during different natural circulation modes, namely, single-phase, two-phase, and reflux condensation. In addition, the secondary side heat transfer regimes were characterized and compared to published data. Recommendations for improvements in future tests were also made.

6-2. STEAM GENERATOR DATA ANALYSIS METHOD

The objective of the steam generator data reduction effort was to use thermal hydraulic data obtained during single-phase primary conditions to develop a heat transfer correlation for the steam generator secondary side fluid and correction factors for the wall thermocouples. This correlation and wall temperature correction factors, which are derived as a function of wall heat flux, can then be used to calculate steam generator heat fluxes, condensation rates, and primary side conditions when the primary operates with two-phase operating conditions.

For purposes of analysis, each steam generator was divided into three regions referred to as tube models (figures 6-1 and 6-2). In turn, each tube model contains many control volumes, each situated between instrumentation locations, as shown in figure 6-3. The instrumentation at a typical location is illustrated in figure 6-4. An axial energy balance is then performed on each control volume to determine the heat flux q'' during the single-phase portion of each test as shown in figure 6-5 and equation (6-1). That is:

$$\dot{m}\ Cp\ \frac{\Delta T_{pri}}{\Delta Z} = q'' \pi D \qquad (6\text{-}1)$$

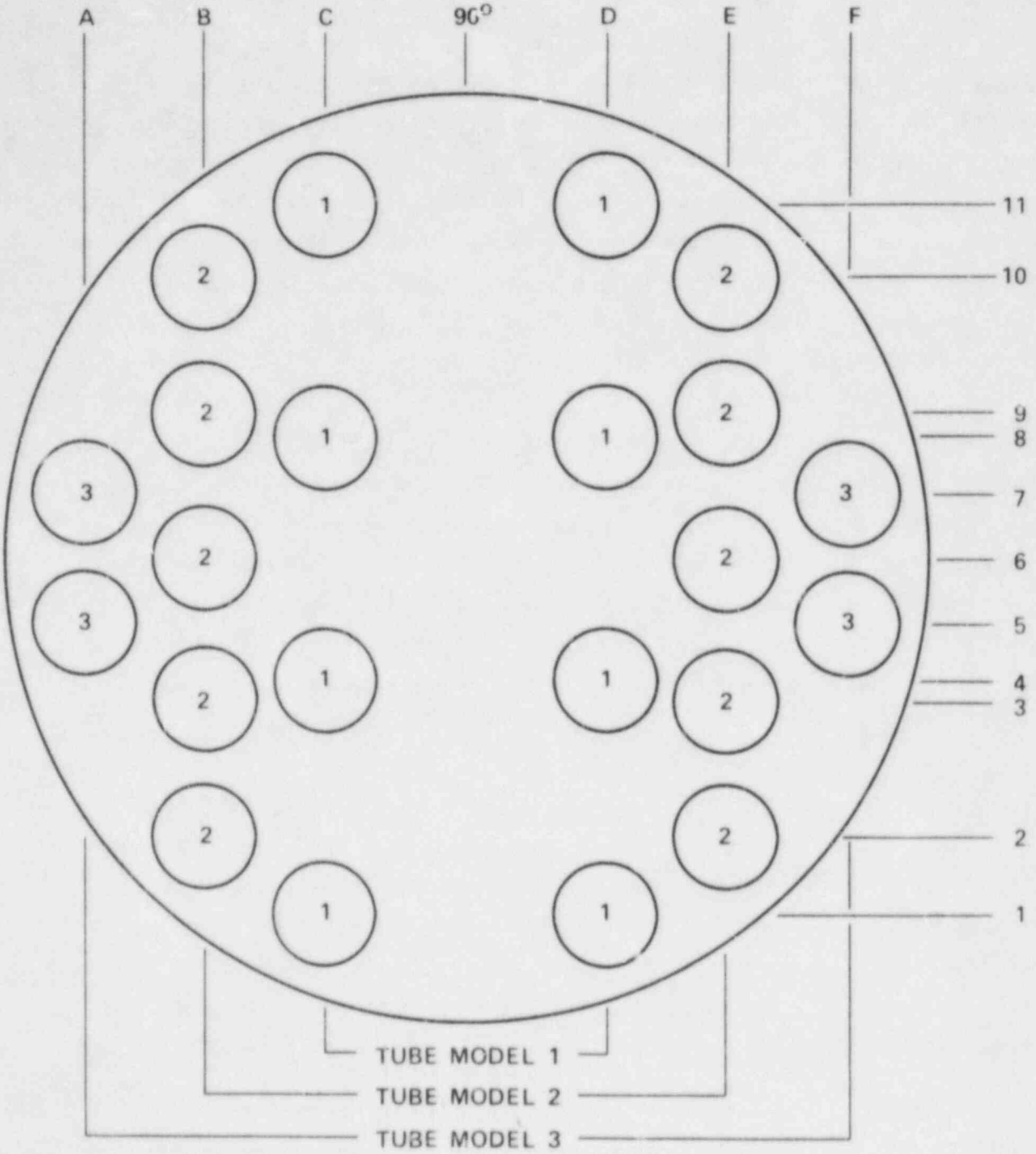

Figure 6-1. Broken Loop Steam Generator Cross Section Showing Tube Models

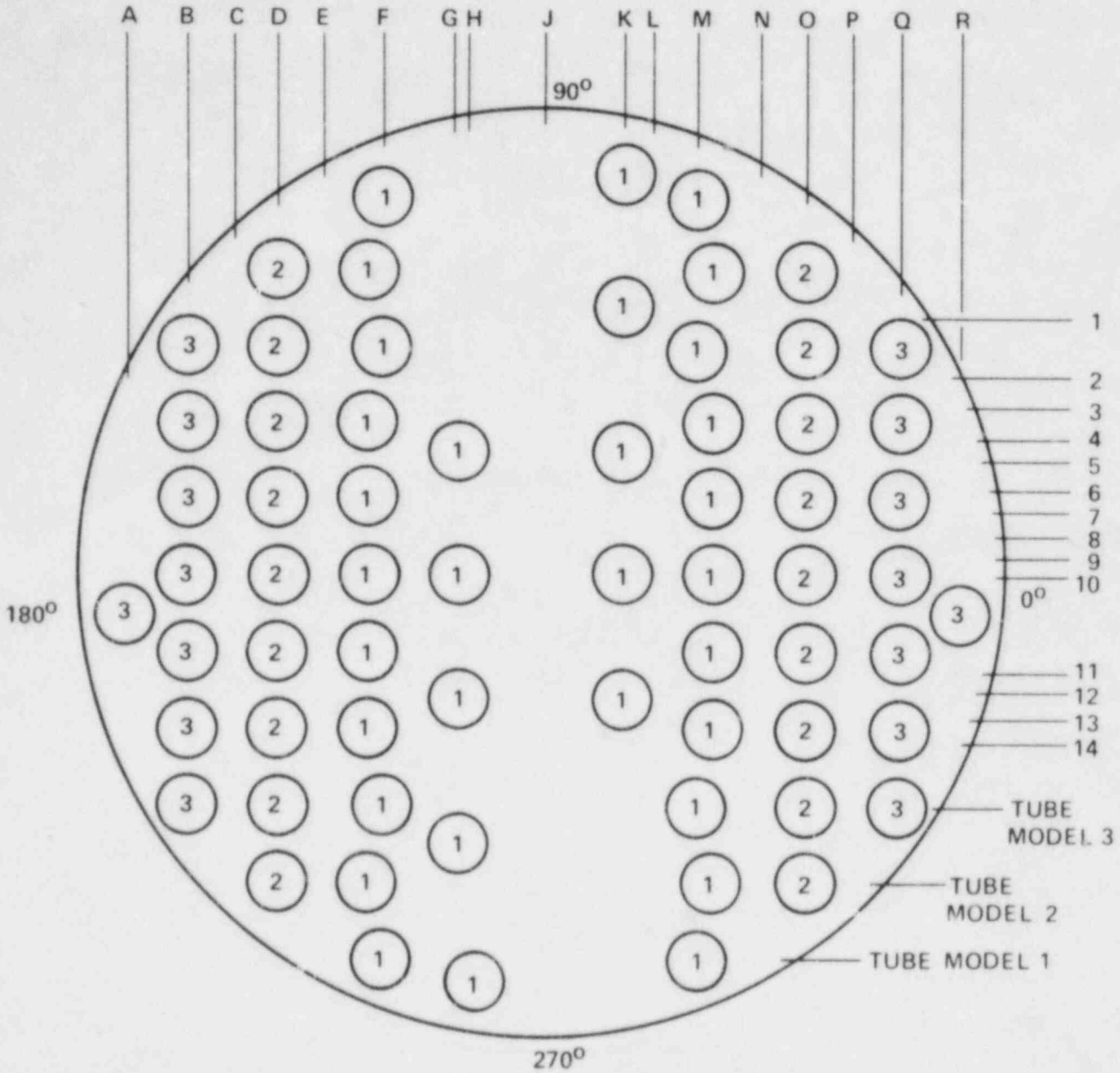

Figure 6-2. Unbroken Loop Steam Generator Cross Section Showing Tube Models

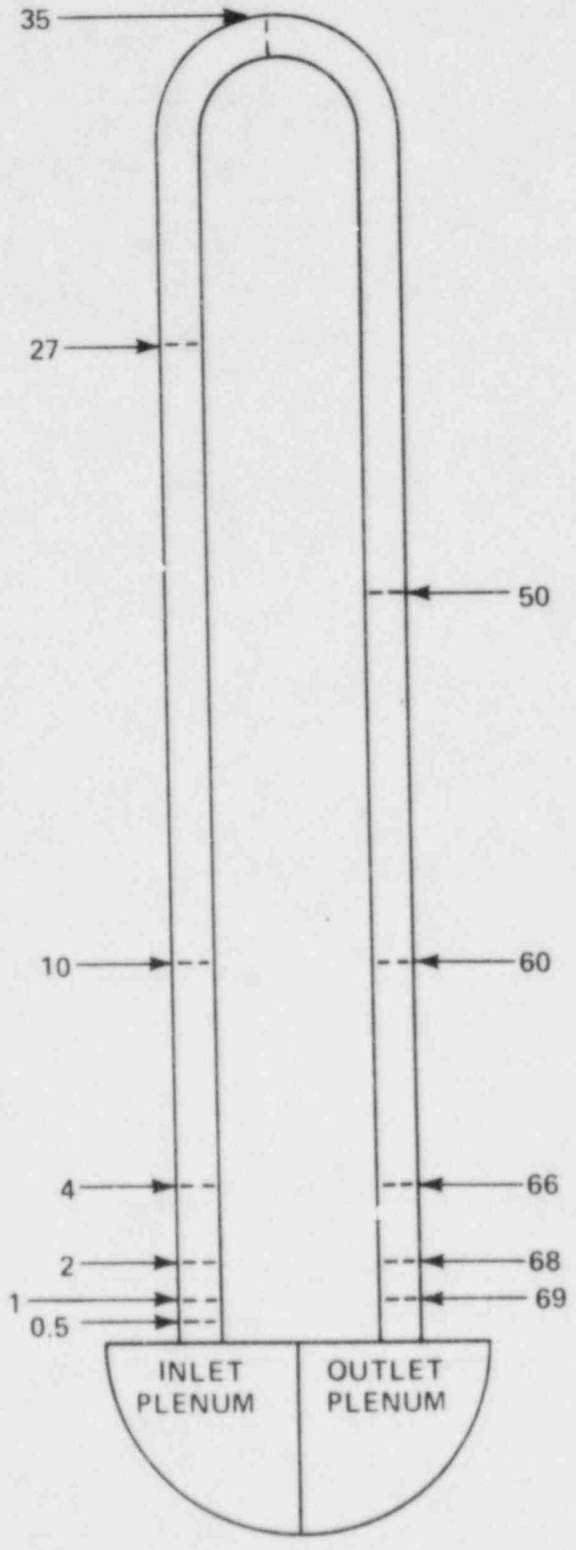

Figure 6-3. Instrumentation Locations and Primary Control Volumes -- Tube Model 1, Unbroken Loop

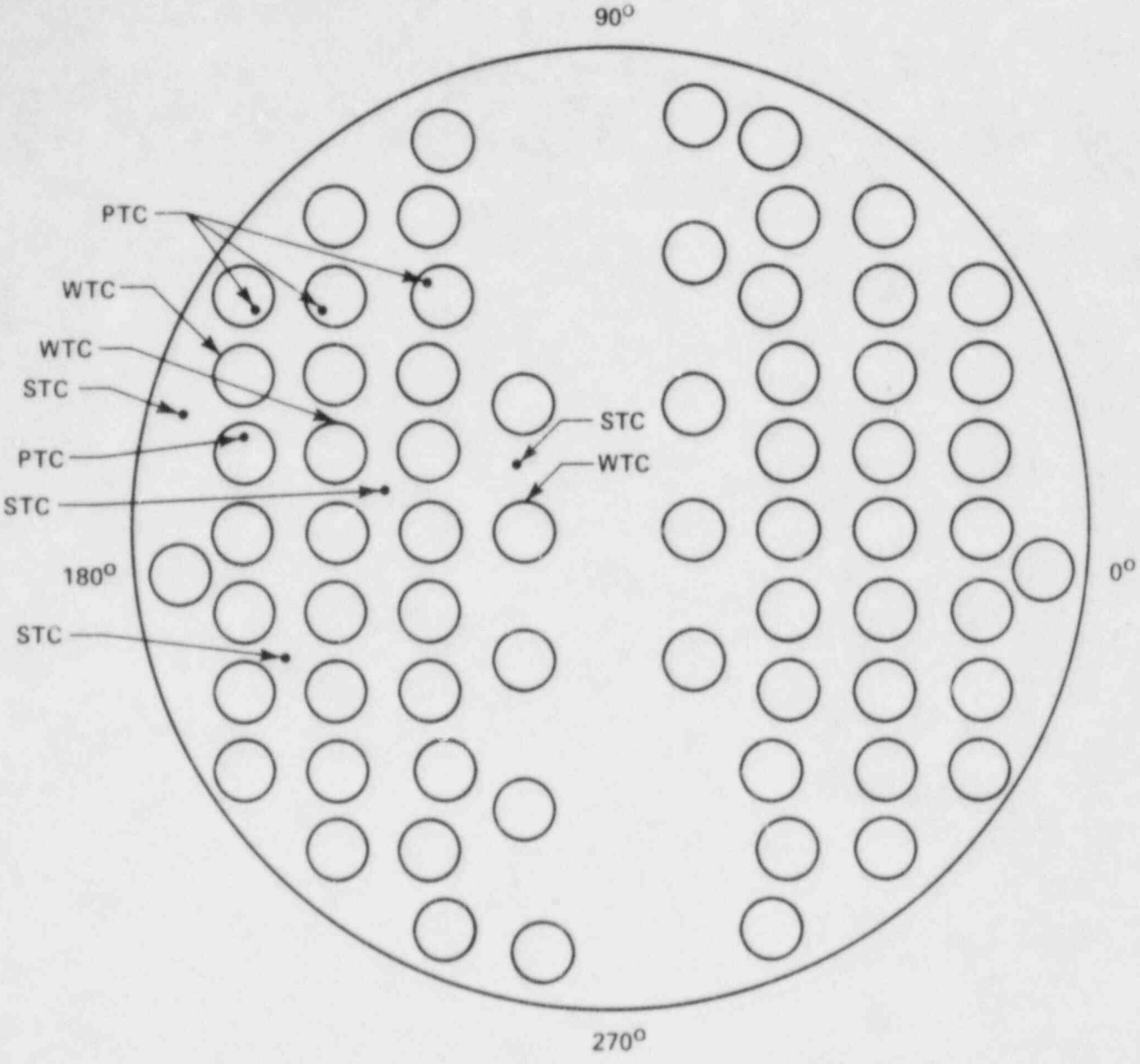

WTC – WALL THERMOCOUPLE
STC – SECONDARY FLUID THERMOCOUPLE
PTC – PRIMARY FLUID THERMOCOUPLE

Figure 6-4. Typical Instrumentation at a Given Elevation for Unbroken Loop Steam Generator

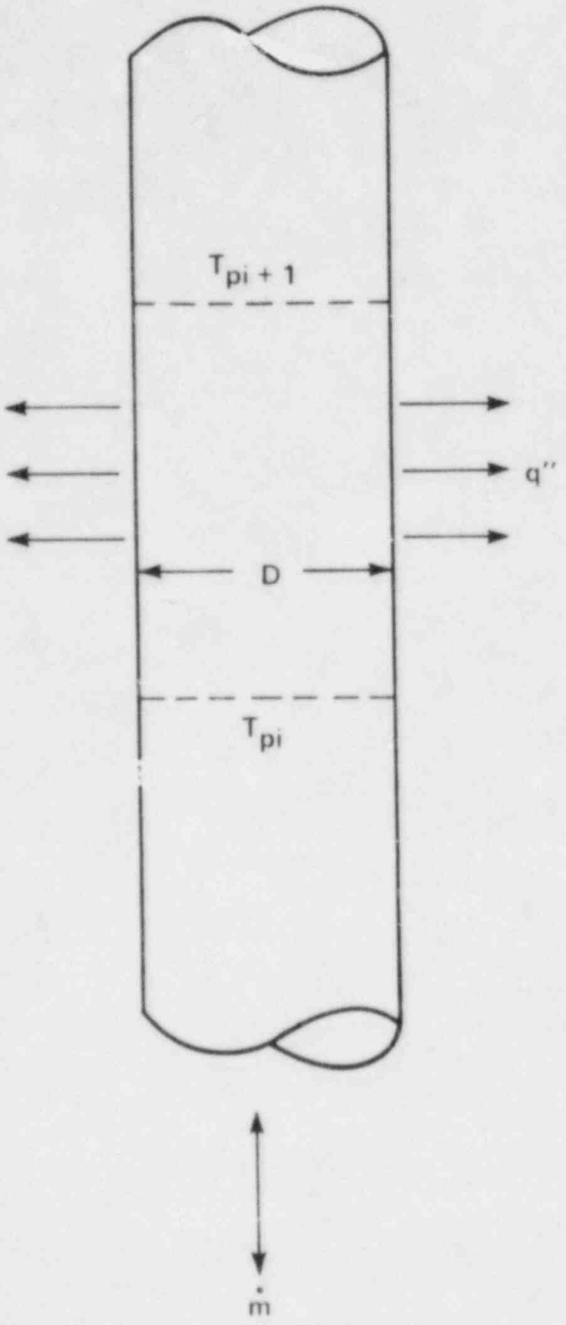

Figure 6-5. Energy Balance Scheme

where

m = mass flow per tube (lbm/hr)

Cp = specific heat (Btu/lbm-°F)

ΔT_{Pri} = difference in the steam generator primary fluid temperatures (°F)

q'' = calculated wall heat flux (Btu/ft^2-hr)

D = tube inside diameter (ft)

With the system in steady state, all energy lost by the fluid appears as a wall heat flux. The variation of heat flux values with tube location is illustrated in figures 6-6 through 6-11 for each of the six tube models. The Z coordinate is not actual elevation relative to the tubesheet, but rather linear distance along the tube starting at the tubesheet on the uphill side of each bundle.

The plots show that the largest heat fluxes are on the uphill side near the tubesheet, as would be expected for these generators. A region of higher heat flux, not shown on these curves, that occurs at the tubesheet level is due to the presence of a cold [27°C-38°C (80°F-100°F)] layer of secondary fluid immediately adjacent to the tubesheet. It is estimated that as much as 2 to 3 percent of the generator heat rejection could occur through tubesheet conduction between this cold liquid layer and the inlet/outlet plena of the generators. In most cases, regions of reverse heat transfer (secondary to primary) occur on the downhill side of the tubes at axial locations between 15.24 and 21.33 m (50 and 70 ft). This is attributed to the higher secondary saturation temperature near the bottom of the shell, due to increased hydrostatic pressure, and reduced primary temperatures due to cooling on the uphill side of the tubes.

The steam tube wall thermocouples were brazed to the tube wall as shown in figure 6-12. The effect of this attachment method is to produce a measured

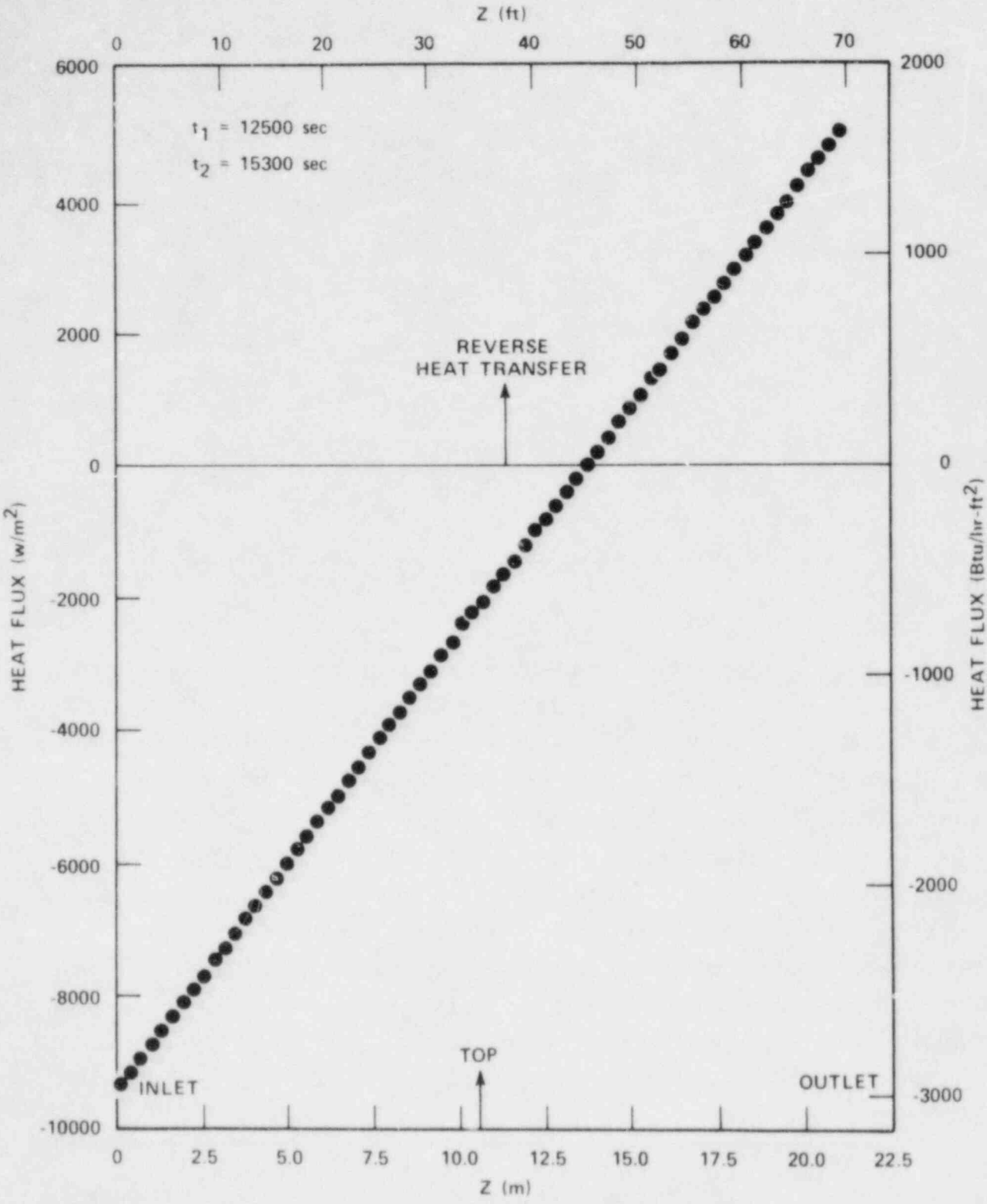

Figure 6-6. Unbroken Loop Single-Phase Tube Model 1

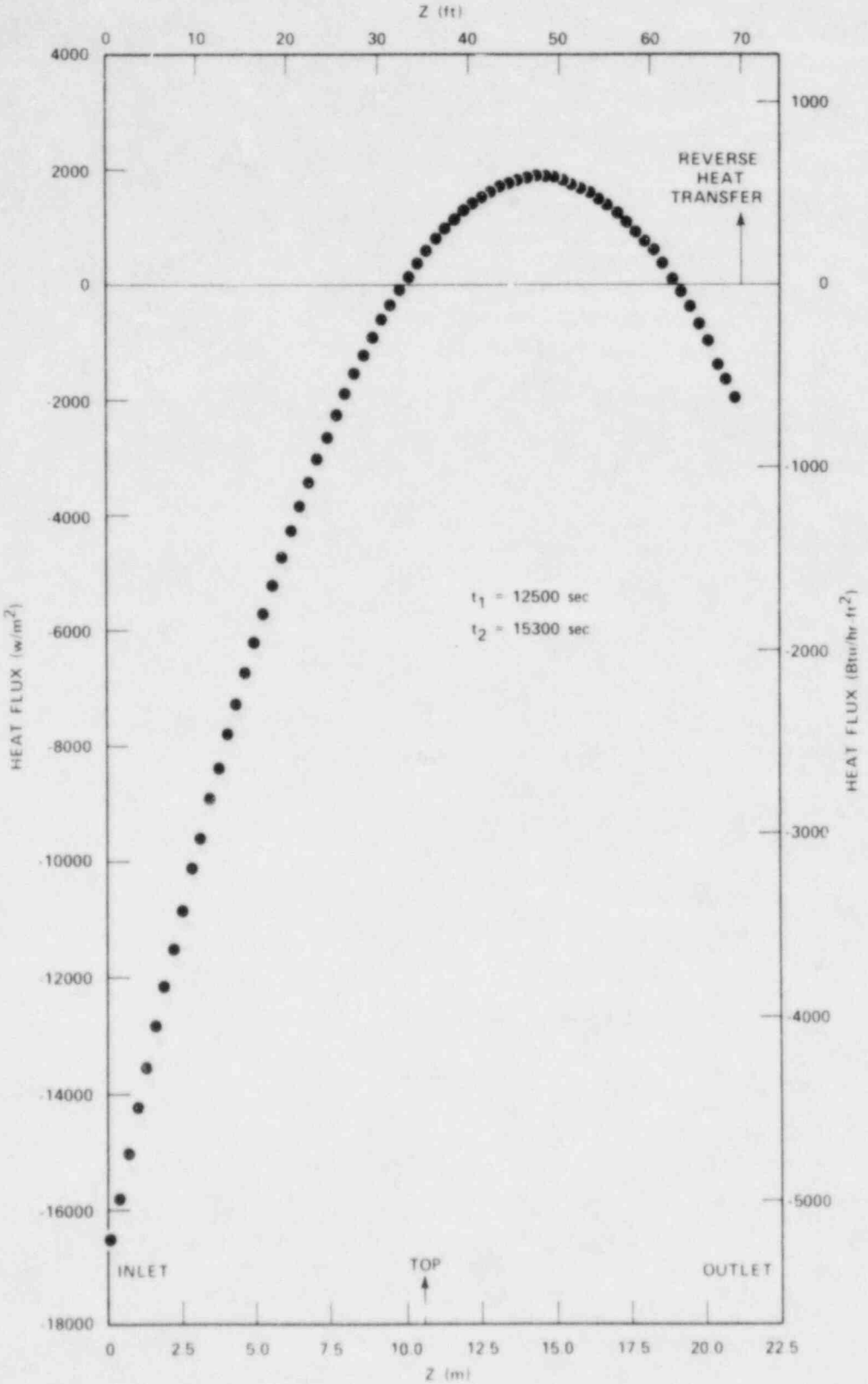

Figure 6-7. Unbroken Loop Single-Phase Tube Model 2

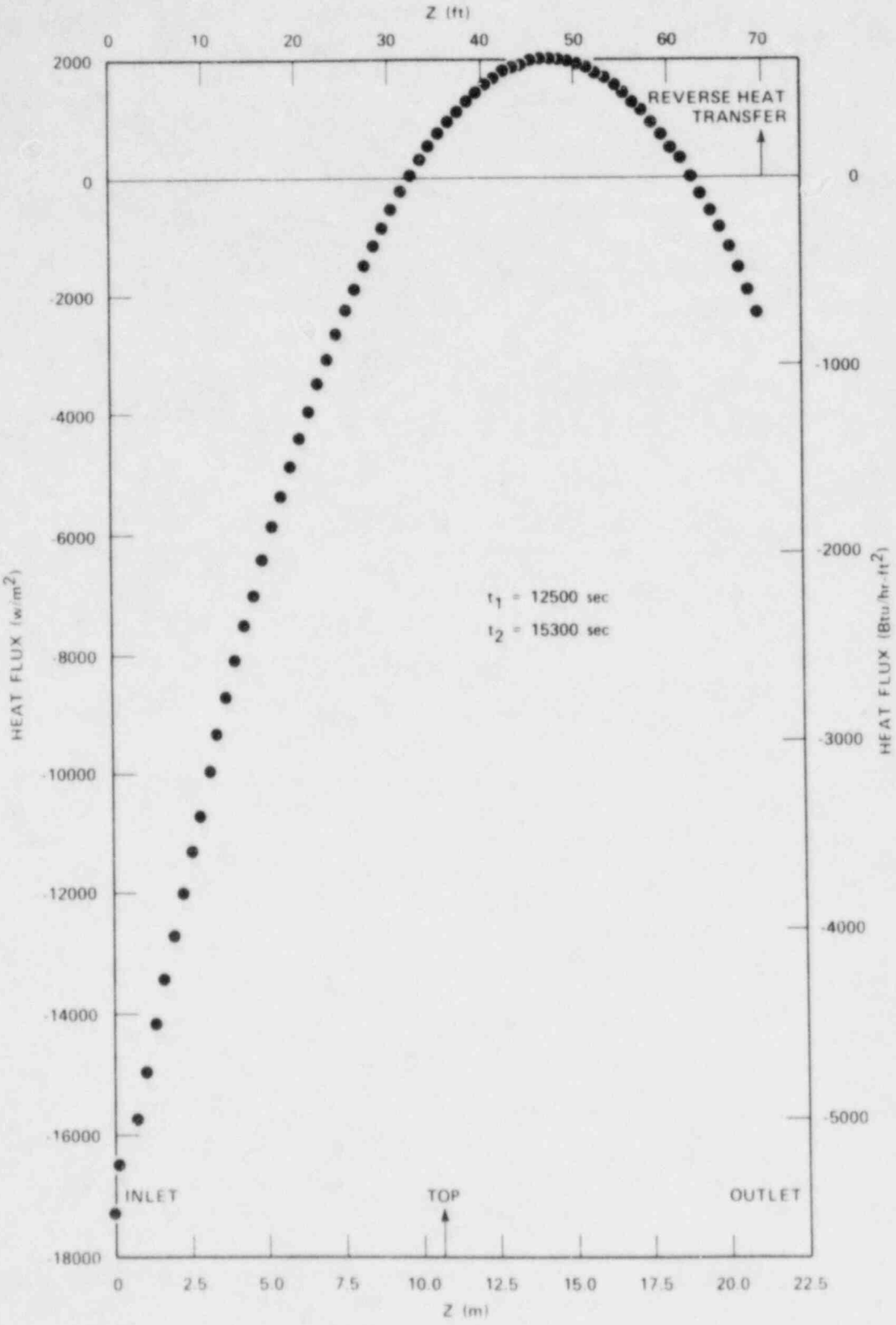

Figure 6-8. Unbroken Loop Single-Phase Tube Model 3

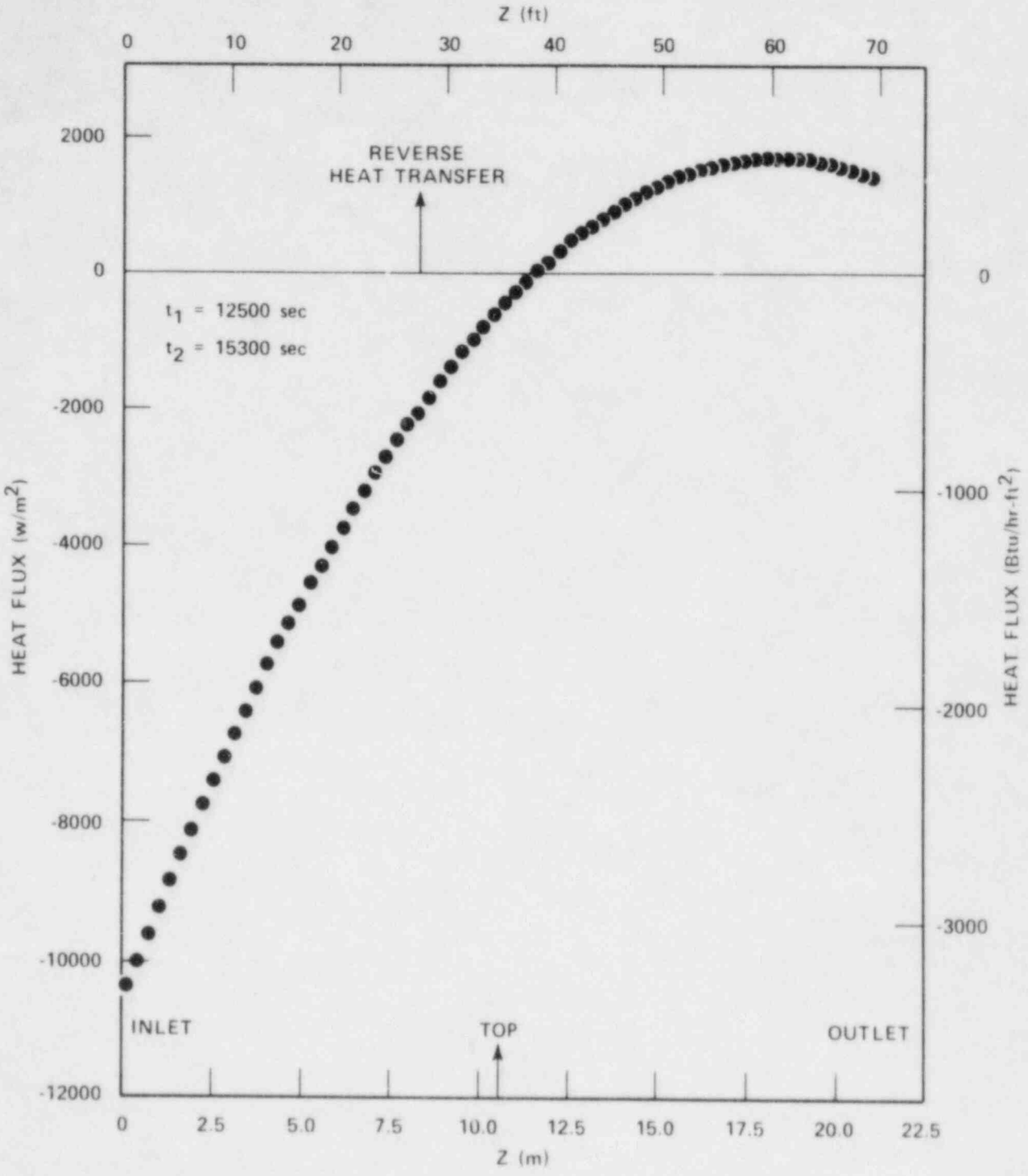

Figure 6-9. Broken Loop Single-Phase Tube Model 1

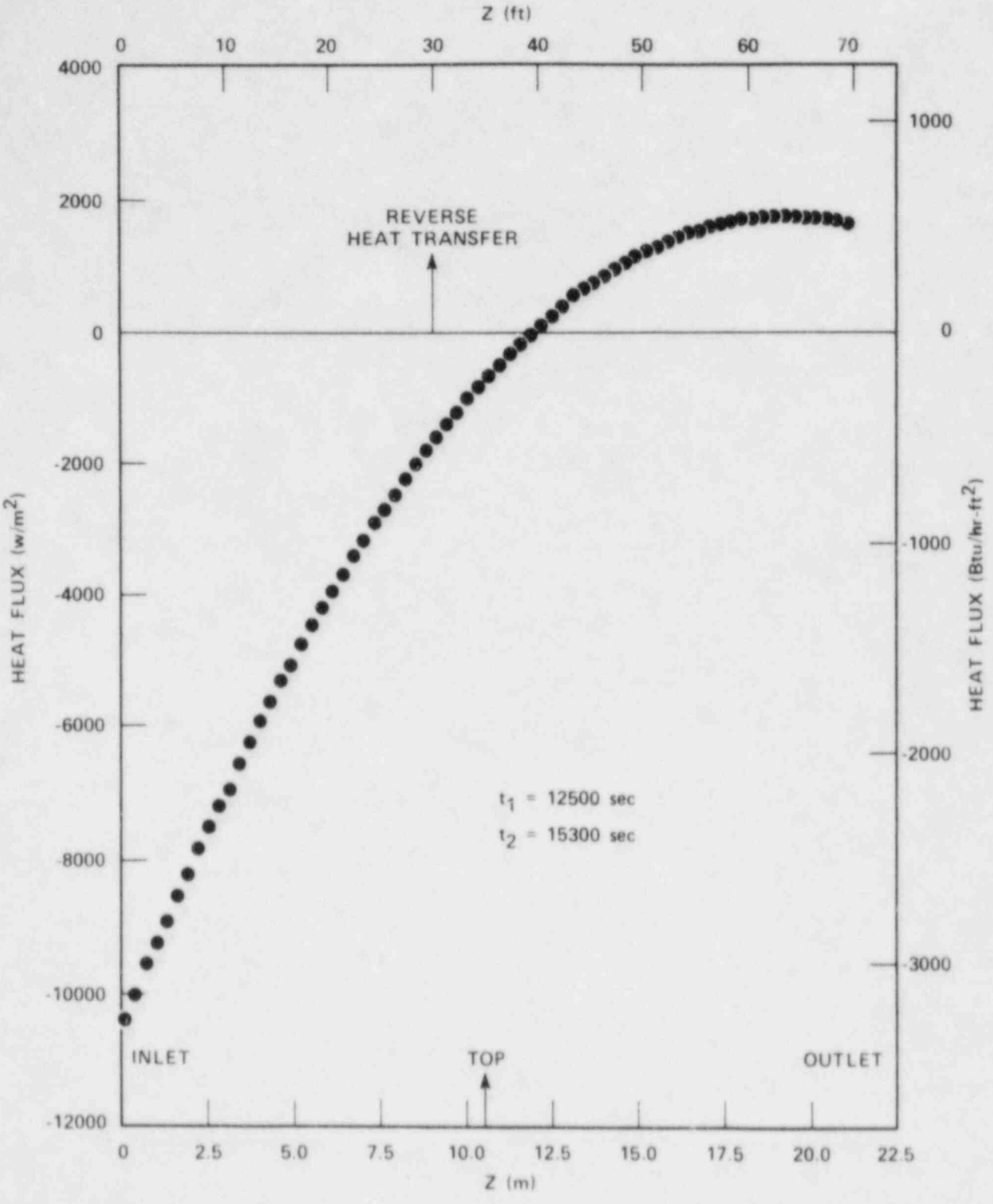

Figure 6-10. Broken Loop Single-Phase Tube Model 2

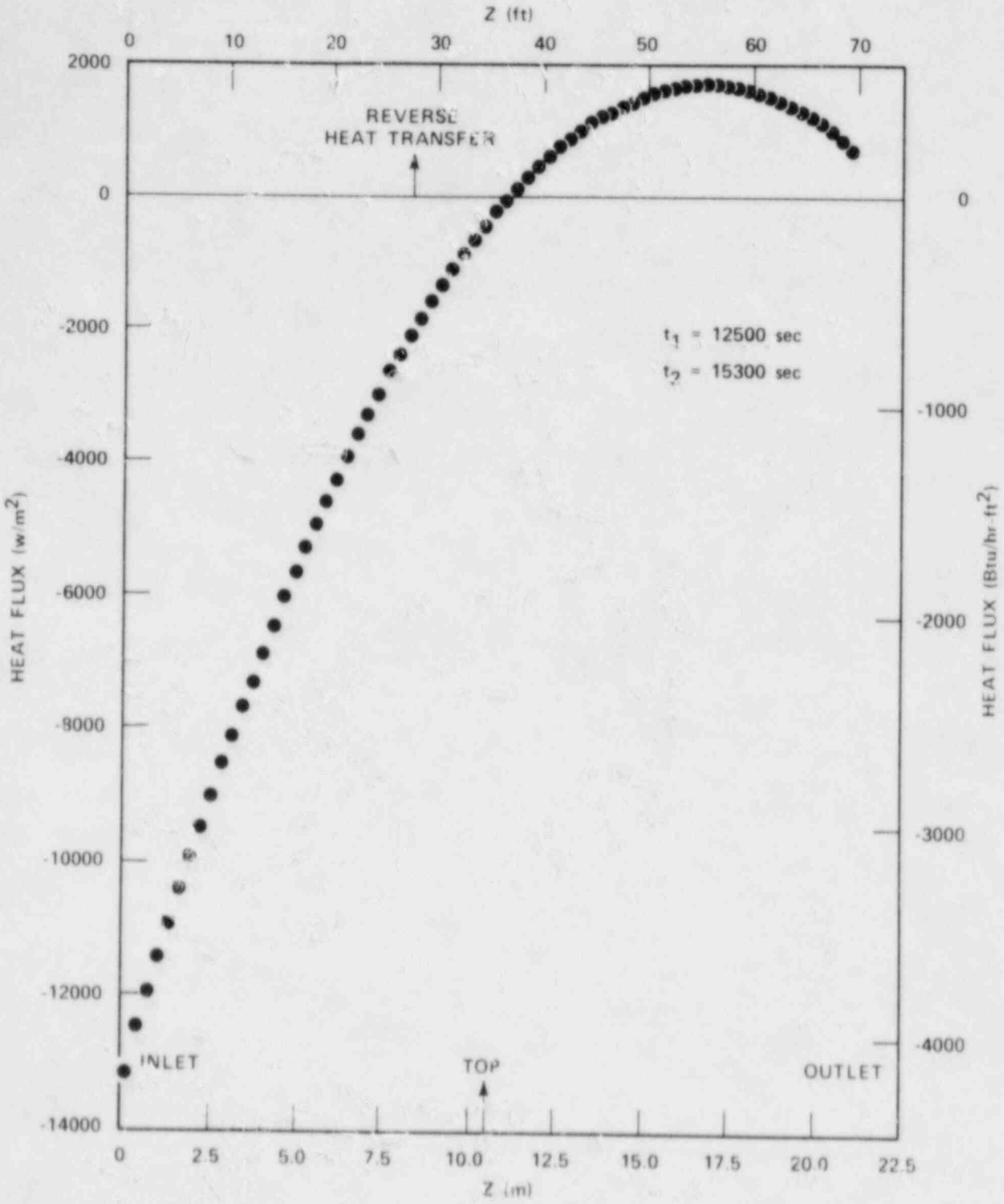

Figure 6-11. Broken Loop Single-Phase Tube Model 3

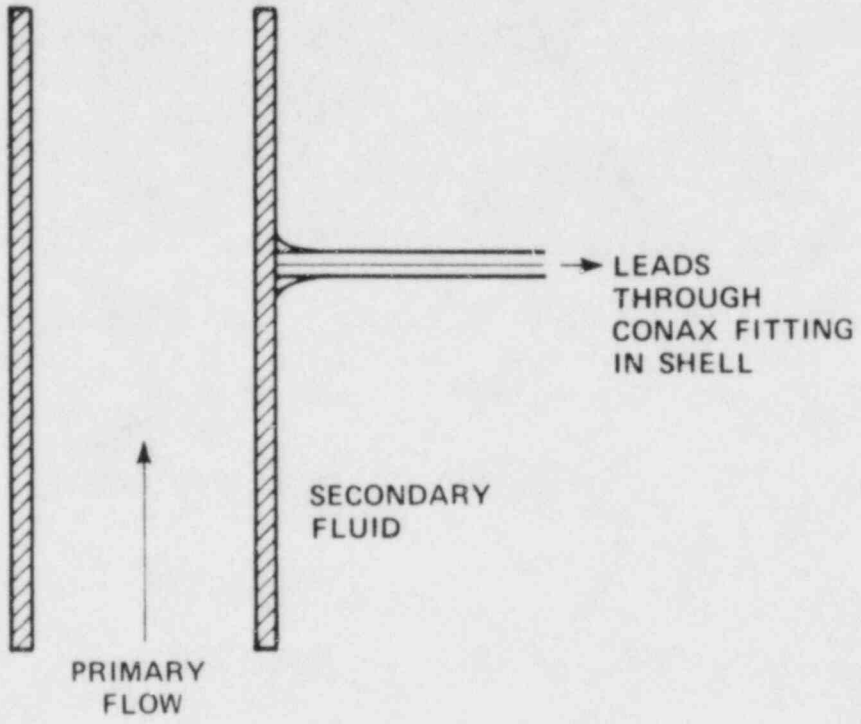

Figure 6-12. Wall Thermocouple Mounting

wall temperature that is lower than the actual wall temperature when heat is transferred from primary to secondary fluid. Conversely, the measured wall temperature is higher than the actual temperature during reverse heat transfer. Concerns about the wall thermocouple attachment method were addressed in the steam generator separate effects test program,[1] in which there was a natural circulation flow in the steam generator secondary side. Once the heat flux has been determined, an inside tube wall temperature can then be computed using the Dittus-Boelter heat transfer correlation.[2] The outside tube wall temperature is then computed using the steady-state conduction equation through the steam generator tube wall. From these calculations, a plot of the calculated wall temperature minus measured wall temperature versus wall heat flux can be obtained for each wall thermocouple.

The secondary side fluid temperature was measured at elevations corresponding to the primary side control volumes. The secondary fluid pressure can be determined at the tubesheet and, by subtracting the density head at each elevation, a close approximation to the secondary fluid pressure can then be obtained. The corresponding saturation temperature can then be found and plots of wall heat flux versus calculated wall temperature minus saturation temperature can be constructed for each wall thermocouple location. Similar plots can be drawn using the measured secondary fluid temperature, although these are of less value in understanding the heat transfer regimes that may be present. Representative secondary fluid and wall temperatures are shown for a single-phase primary case in figure 6-13. These data represent tube model 1 in the unbroken loop steam generator. The large drops in calculated and measured wall temperatures at low elevations are the result of cold secondary feedwater entering the shell at this location. It is also apparent that sufficent wall superheat exists to cause boiling at some locations. The secondary side differential pressure cells indicated a collapsed liquid level of approximately 7.92 m (26 ft) above the tubesheet. The calculated saturation temperature is taken to be essentially constant above this point, where it is assumed that only two two-phase flow is present.

1. Howard, R. C., et al., "PWR FLECHT SEASET Steam Generator Separate Effects Task Data Report," NRC/EPRI/Westinghouse-4, 1980.

2. Dittus, F. W., and Bolter, L. M. K., "Heat Transfer in Automobile Radiators of the Tubular Type," University of California, Berkeley Publ. Eng. 2, 13, 442-462 (1930).

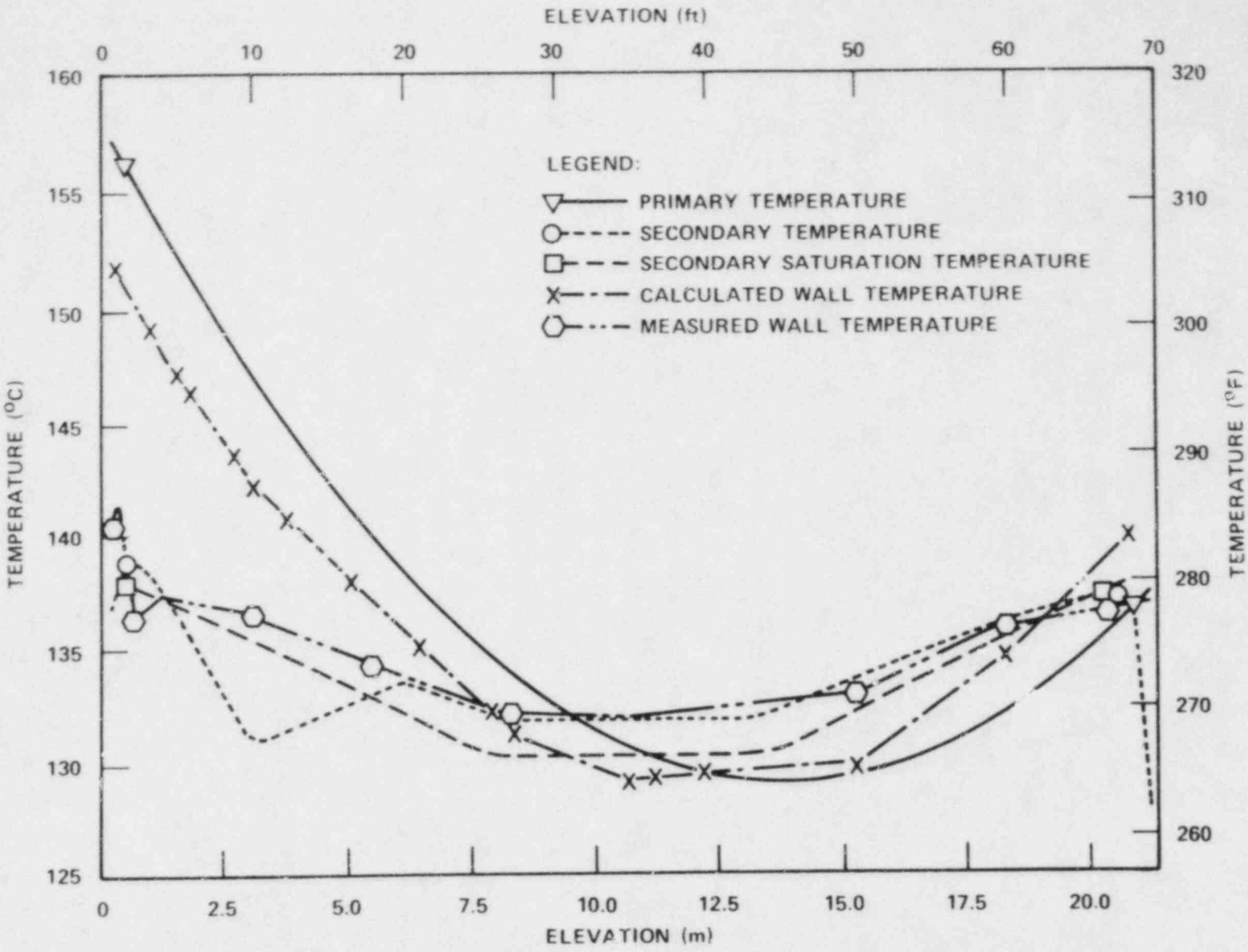

Figure 6-13. Temperature Distributions During Single-Phase Circulation

The data in this form can then be used to calculate wall heat fluxes during two-phase primary conditions. The general method is illustrated in figure 6-14. An initial estimate for the heat flux is made and subsequent wall thermocouple corrections are determined from the single-phase data. The corrected wall temperature is then found by adding this correction to the measured wall temperature. With either the secondary saturation or fluid temperature known, a new heat flux is determined from plots of heat flux versus wall temperature minus saturation temperature (or wall temperature minus secondary temperature) from the single-phase data base. The procedure is thus iterative in nature and will ultimately converge to a wall heat flux from which primary side conditions can be determined. It was decided that a correlation should be developed for each wall thermocouple rather than for each steam generator as a whole, because of the likelihood of variation in thermocouple brazing, geometry, and the like, which could cause each to respond differently to a given heat flux. Representative plots from the data base are presented in appendix B for each instrumented elevation in the steam generators.

A fair degree of scatter was noted in the primary side temperatures at lower elevations on the uphill side of the tubes. This was attributed to the presence of cold secondary inlet flow at this point. Examination of the secondary side temperatures and calculated wall heat fluxes indicated that more than one heat transfer regime is likely to be present in this area. In addition, several regions of primary fluid exhibited nonphysical behavior, such as lower temperatures than the surrounding secondary fluid. This was believed to be a result of the tube grouping and instrumentation location. The data were carefully reviewed and those data points which indicated physically unrealistic behavior from test to test were eliminated. Approximately 10 percent of the data was judged to be unreliable using these criteria.

One difficulty that arises in tests of this sort is the practicality of installing sufficient instrumentation to determine the local secondary fluid behavior. To reduce calculated heat flux scatter, a least-squares curve fit was applied to the primary side temperatures, enabling temperature values to be obtained at any point. In each generator, feedwater enters the shell very near to the tubesheet and creates a highly stratified region. Secondary fluid

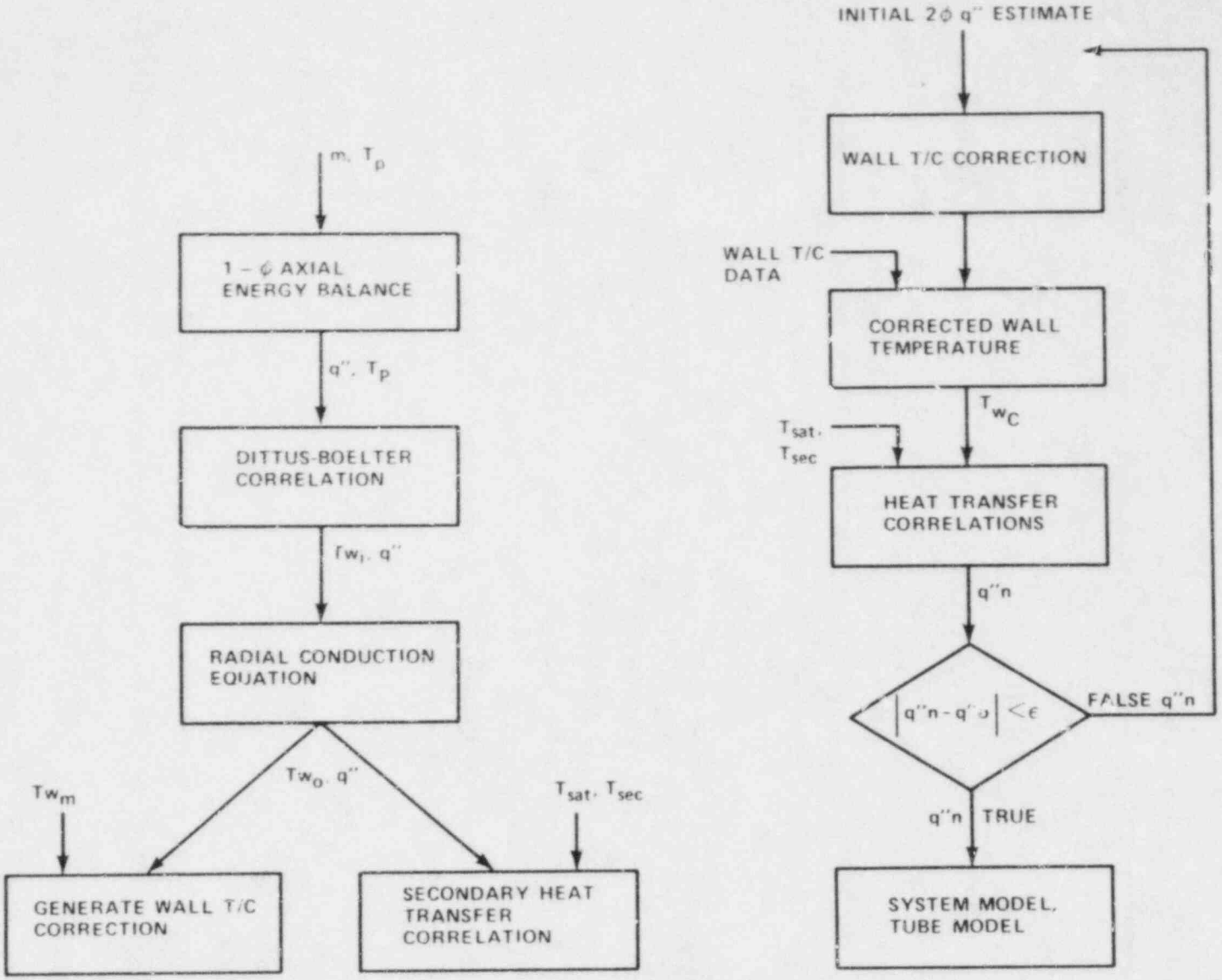

Figure 6-14. Method of Heat Flux Calculation

thermocouples indicated a stratification of as much as 364°C per meter (200°F per foot) at some locations. In addition, since the feedwater enters from one side only, the stratification is not likely to be uniform radially within the steam generator. Important checks on the validity of calculated heat fluxes are a comparison of the integrated heat flux with core power, and a plenum-to-plenum energy balance on each generator (appendix C). These calculations were performed for each test; the energy balanced within 4 to 21 percent. There are several possible causes for this discrepancy. All thermocouples have some inherent uncertainty due to manufacturing tolerances and the like. It has been estimated (appendix D) that the total accumulated uncertainty from all sources is approximately 0.3°C (0.6°F) at a temperature of 149°C (300°F) (0.2 percent error). This estimated uncertainty was obtained after calibrating each thermocouple to a National Bureau of Standards standard temperature measurement. However, typical temperature rises across the core or generators are 11°C (20°F) for forced flow cases and 28°C (50°F) for natural circulation cases. Thus, in forced flow, a discrepancy of 6 percent could result from thermocouple uncertainty alone.

Another source of possible error is the ambient losses that occur from the test vessel, hot legs, and steam generators. Since heat loss is a difficult quantity to measure accurately, the total loss was estimated at 1 to 2 percent.

In addition, significant stratification was observed in both hot legs during single-phase primary conditions. The temperature rise from bottom to top of the unbroken hot leg was as much as 11°C (20°F); for the broken leg a stratification of 8°C (14°F) was observed. Examination of all hot leg thermocouples (figure 6-15) did not clearly indicate the cause of this phenomenon. At the upper plenum exit, the top and bottom fluid temperatures were nearly the same [within 1°C (2°F)], and stratification developed as the flow progressed through the hot legs. It is possible that entrance effects due to the upper plenum geometry disturbed the flow field sufficiently to give the appearance of mixed flow at the entrance. There is not enough heat loss from the hot legs themselves to cause this degree of stratification. As the flow reaches the upward bend of the hot legs approaching the inlet plenum of the generators, the fluid momentum changes will cause some mixing to occur and this is reflected in a reduced fluid temperature variation across the pipe.

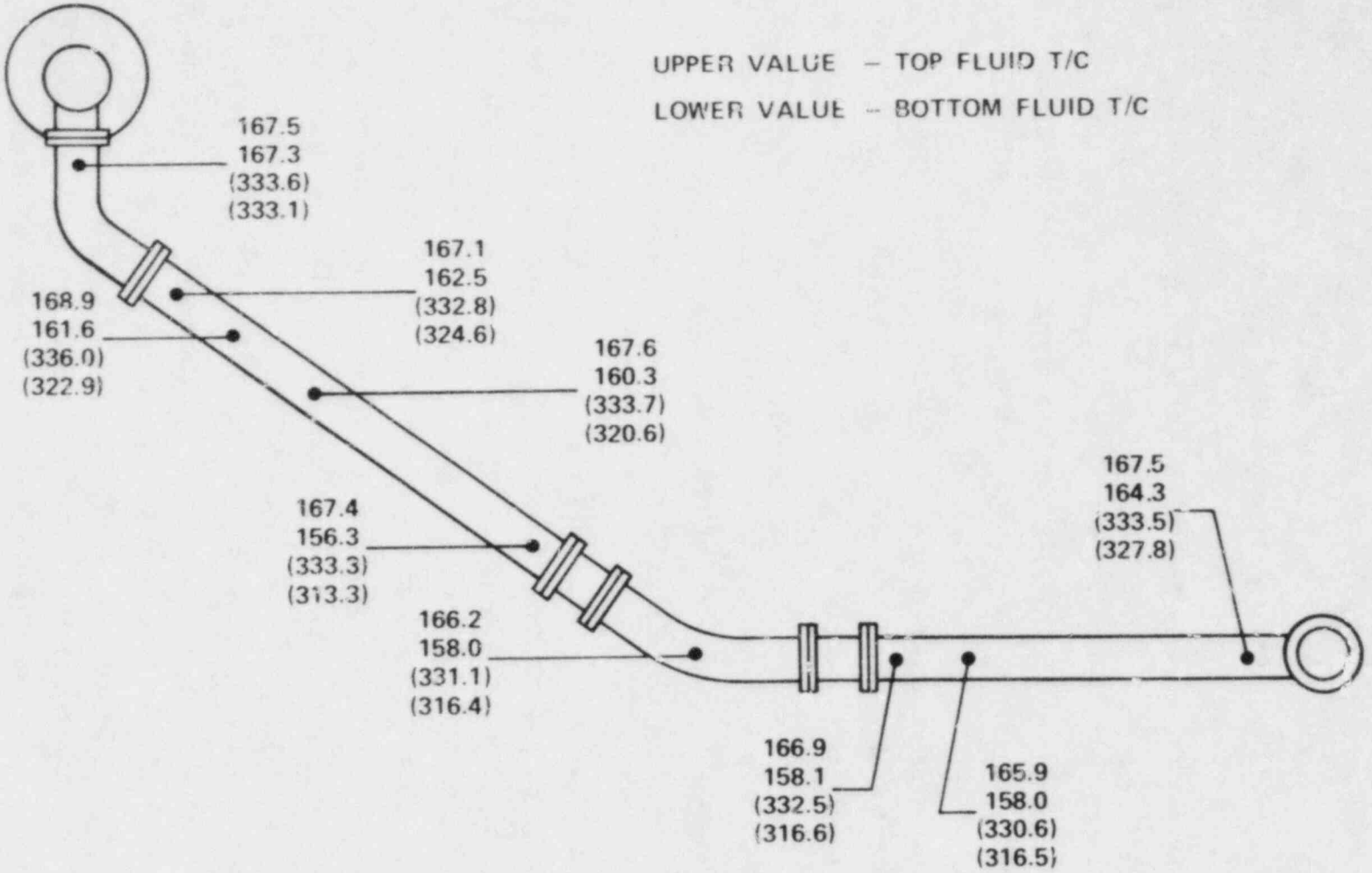

Figure 6-15. Unbroken Loop Hot Leg Thermocouple Measurements During Single-Phase Circulation

Thermocouples near the inlet plenum entrance showed a variation in fluid temperature of 2.7°C to 3.3°C (5°F to 6°F). With these inlet conditions, it is difficult to know whether or not the plenum fluid thermocouples are measuring an average fluid temperature. This uncertainty can lead to additional discrepancy in calculating a steam generator energy balance.

Finally, another small source of heat balance uncertainty is the conduction of heat through the tubesheet of each generator. The secondary feedwater enters and forms a cold layer of liquid on the shell side of each tubesheet. A temperature difference of as much as 139°C (250°F) can exist between this fluid layer and the primary fluid in the inlet plenum. Calculations show this heat loss can be 2.75 percent (appendix E). The accumulation of these sources of uncertainty could account for much of the observed discrepancy in the overall energy balances.

A calculation was performed (appendix F) to estimate the uneven distribution of flow among the tubes in the unbroken loop steam generator. A one-dimensional force balance was written for the longest and shortest U-tubes. The density was computed from primary temperature and pressure data as a function of elevation for each tube, and the plenum-to-plenum differential pressure was of course the same for both tubes. The result of this calculation shows a possible difference in flow between tubes of 8.7 percent for the case studied. This would also have some impact on the calculation of the local heat fluxes, because it was assumed that all tubes have equal flow. However, it appears that the flow in the tubes should be nearly the same.

In theory, the iterative scheme previously described for determining the steam generator secondary side heat flux when the primary side is two-phase will converge to a solution at each wall thermocouple location. However, the accuracy and convergence are strongly dependent on the accuracy of the secondary side heat flux versus ΔT_{sat} curve fit. The slope of this curve is on the order of 72 w/m-K (500 Btu/hr-ft^2-°F) ΔT, which is in general agreement with that of the Jens-Lottes correlation[1] for boiling. It should be noted,

---

1. Jens, W. H., and Lottes, P. A., "Analysis of Heat Transfer, Burnout, Pressure Digs, and Density Data for High-Pressure Water," ANL-4527, 1951.

however, that these are low-pressure tests and that the Jens-Lottes data were taken at high-pressure conditions.

Because of the fin effect of the steam generator tube wall thermocouples, it is believed that boiling initiates at these locations. The data for the steam generator wall thermocouple correction curves indicate that the ΔT_w (calculated minus measured temperature) remains essentially independent of heat flux over most of the heat flux range. For very low heat fluxes, the heat flux varies almost linearly with ΔT_w, and a curve would clearly pass through the point (0,0). It is believed that up to a given ΔT_w which is characteristic of each thermocouple, heat is transferred to or from the wall thermocouple by natural convection. When boiling initiates, this linear behavior vanishes and the curve flattens as more thermocouple sites and surrounding wall areas become active boiling sites. The resulting wall thermocouple corrections are similar to that shown in figure 6-17.

The steep slope of the heat flux versus ΔT_{sat} curve makes the iteration very sensitive to slight changes in ΔT_{sat}. Preliminary calculations made using this scheme showed that, for many channels, the solution did not converge to rational values of heat flux, and for others, the number of iterations to convergence was excessive. To bypass this problem, it was decided to eliminate the iteration by applying a constant steam generator wall thermocouple correction. This can be justified by the fact that most of the data constructing these curves lie in the region where a constant correction is adequate, and that for most cases, a best-curve fit through this data will suffice.

As mentioned, the heat flux used in these data bases is calculated from an axial energy balance on the primary fluid in each tube model. That calculation assumes a uniform distribution of flow into each tube in each generator. Calculations given in appendix F show that, for single-phase conditions, the different measured density gradients between tubes are not sufficient to cause a large bias in flow toward one group of tubes under natural circulation conditions. Nevertheless, a nonuniformity in flow of 7 to 8 percent between tubes is predicted in some cases. For this reason, the data composing the steam generator wall thermocouple correction curves were examined for natural

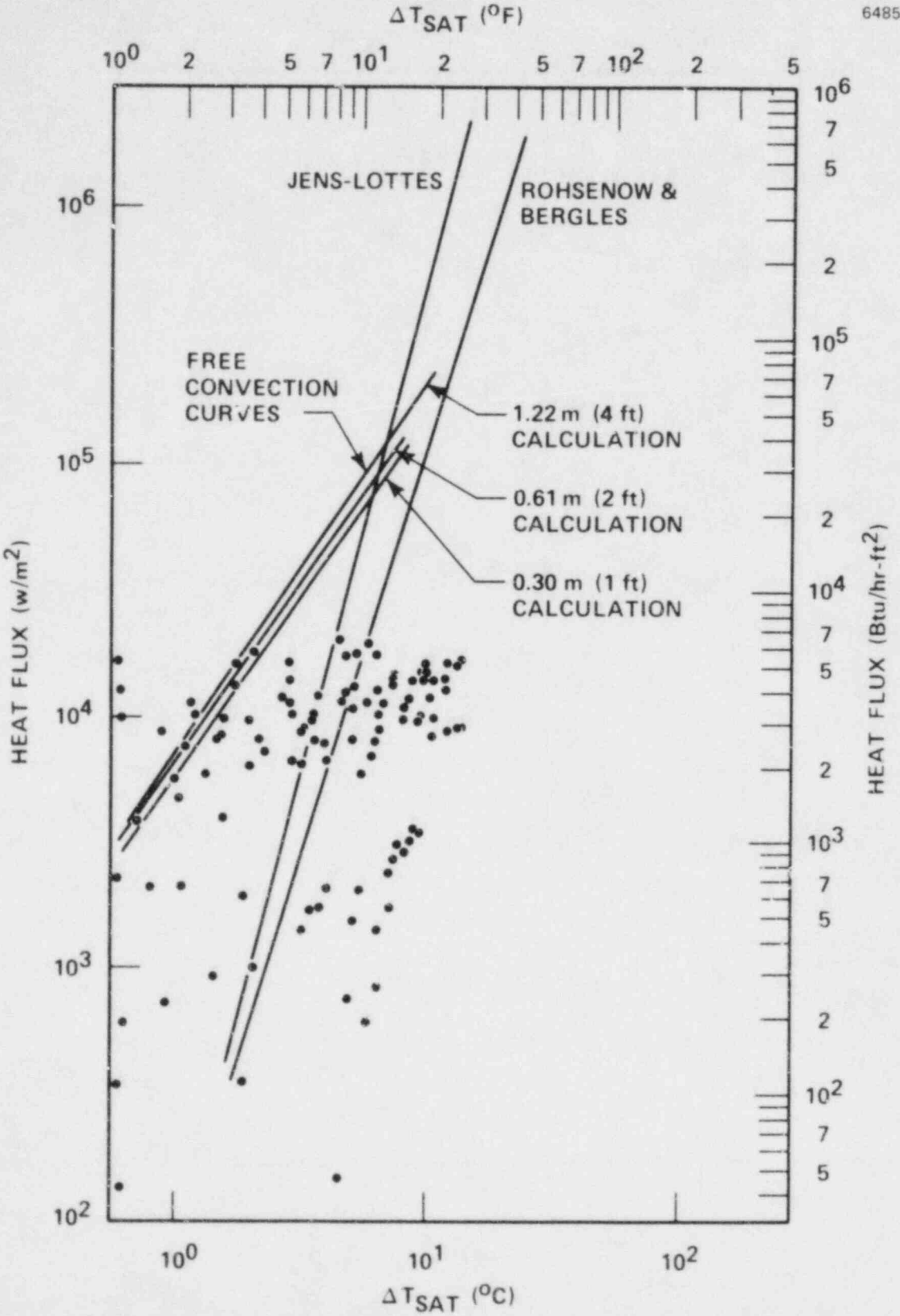

Figure 6-16. FLECHT SEASET Data Compared to Existing Correlations

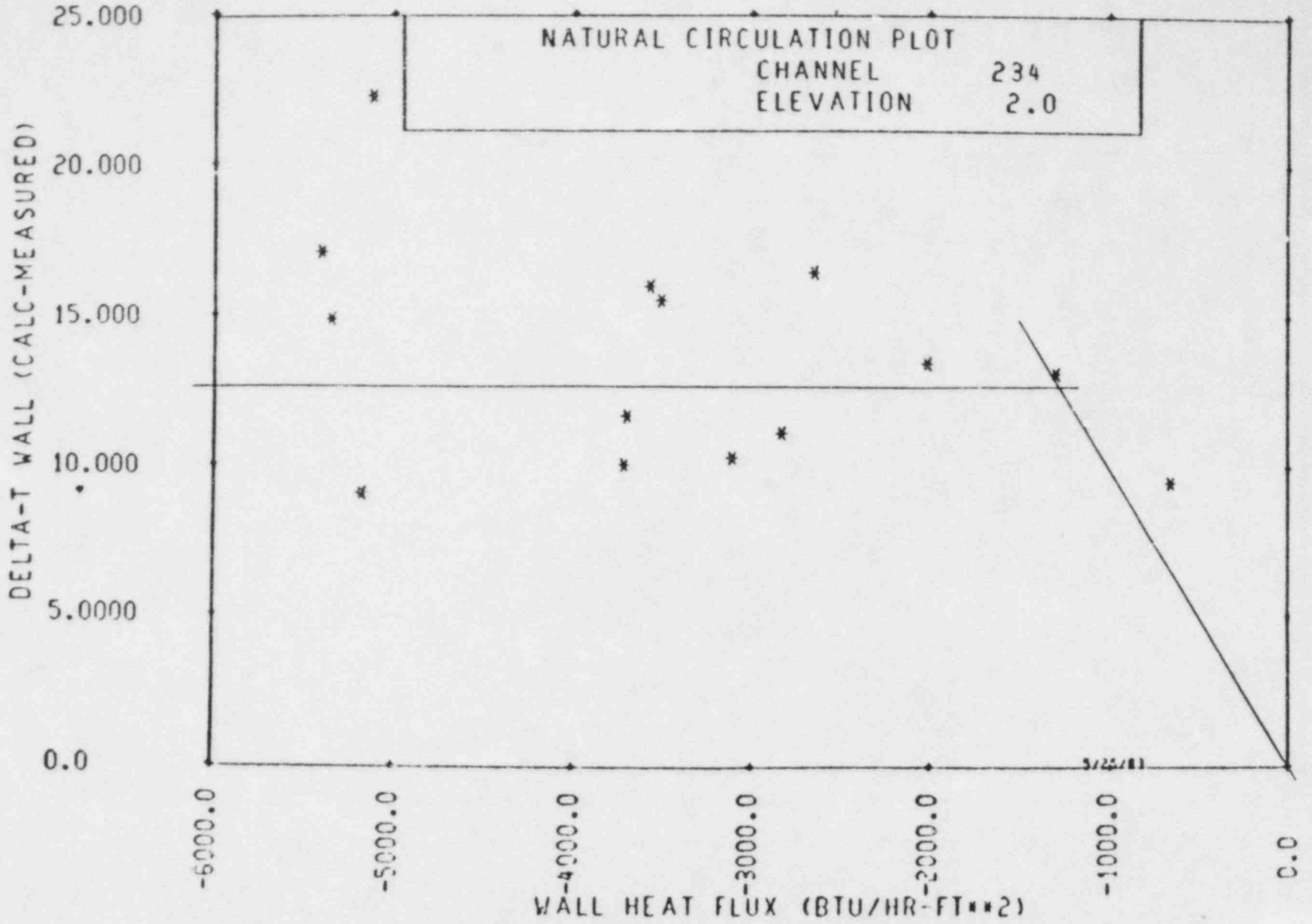

Figure 6-17. Typical Wall Thermocouple Correction Curve

circulation and forced circulation tests separately. Where a significant difference in ΔT_w correction was seen between these two groups of data, the final correction was weighted toward the forced flow tests, where the primary fluid is presumed to be uniformly split between tubes. The reason for this choice is that the uncertainties in the primary flow and primary thermocouple behavior are smaller than those in the single-phase natural circulation tests.

Successive calculations performed with this noniterative scheme yielded heat fluxes that converged and were physically more realistic. Representative plots of heat flux versus tube location for two-phase conditions are shown in figures 6-18 through 6-23. Similar plots for a reflux condensation test are given in figures 6-24 through 6-29.

It should be noted that the predicted heat fluxes for two-phase and reflux condensation cases are only as accurate as the data base curve fits, the test measurements, and the Dittus-Boelter correlation used in calculating wall temperatures. They do however, indicate the steam generator heat flux behavior.

6-3. DISCUSSION OF RESULTS

The data obtained in the FLECHT SEASET natural circulation tests can be used to calculate heat fluxes during single-phase, two-phase, and reflux condensation modes of operation. The overall heat transfer coefficients for each generator have been calculated using equation (6-2):

$$U = \frac{Q_T}{A\ \Delta T} \qquad (6\text{-}2)$$

where

U = overall heat transfer coefficient (Btu/hr-ft^2-°F)

Q_T = total heat rejected by steam generators (Btu/hr)

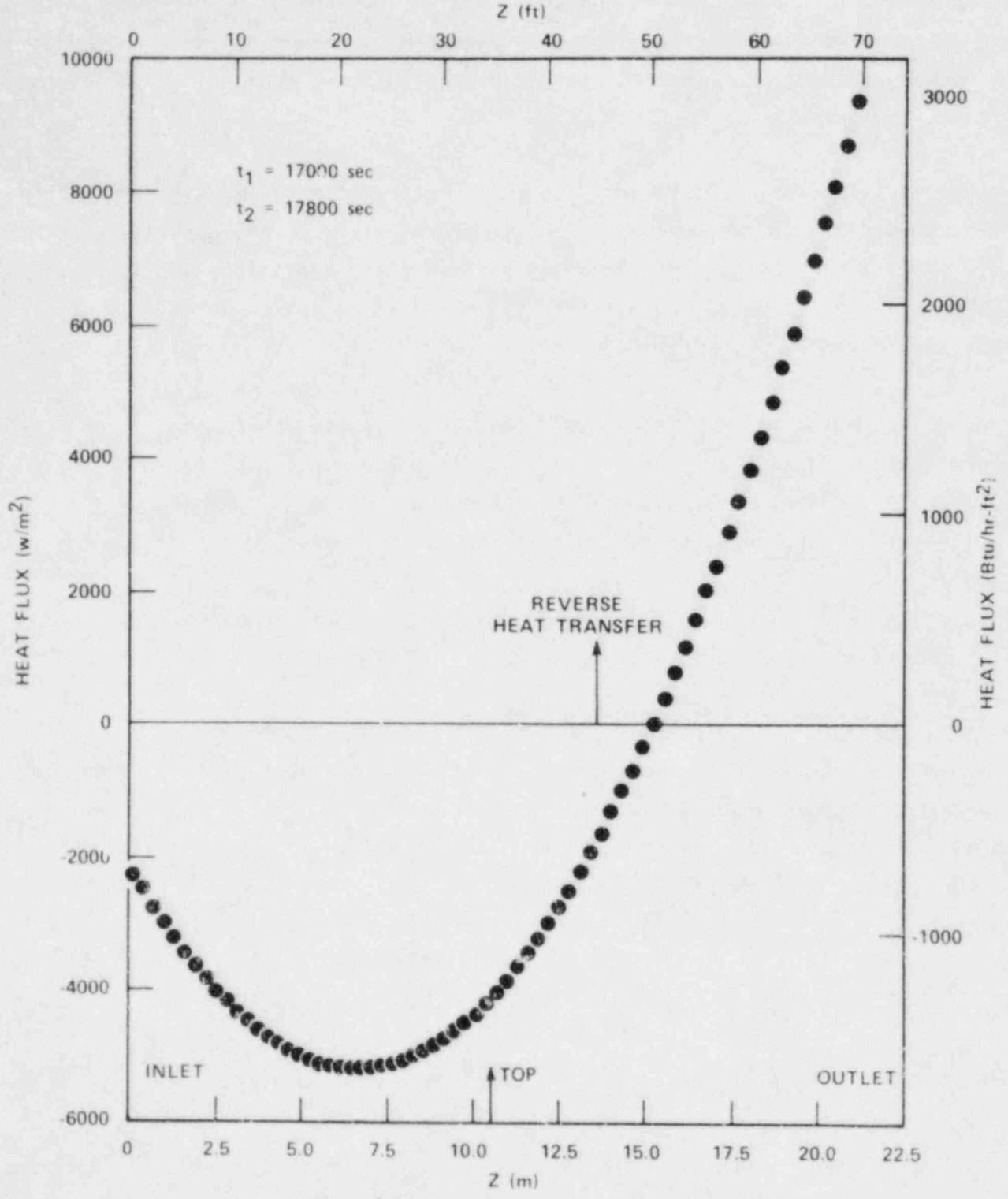

Figure 6-18. Unbroken Loop Two-Phase Heat Flux Plot, Tube Model 1

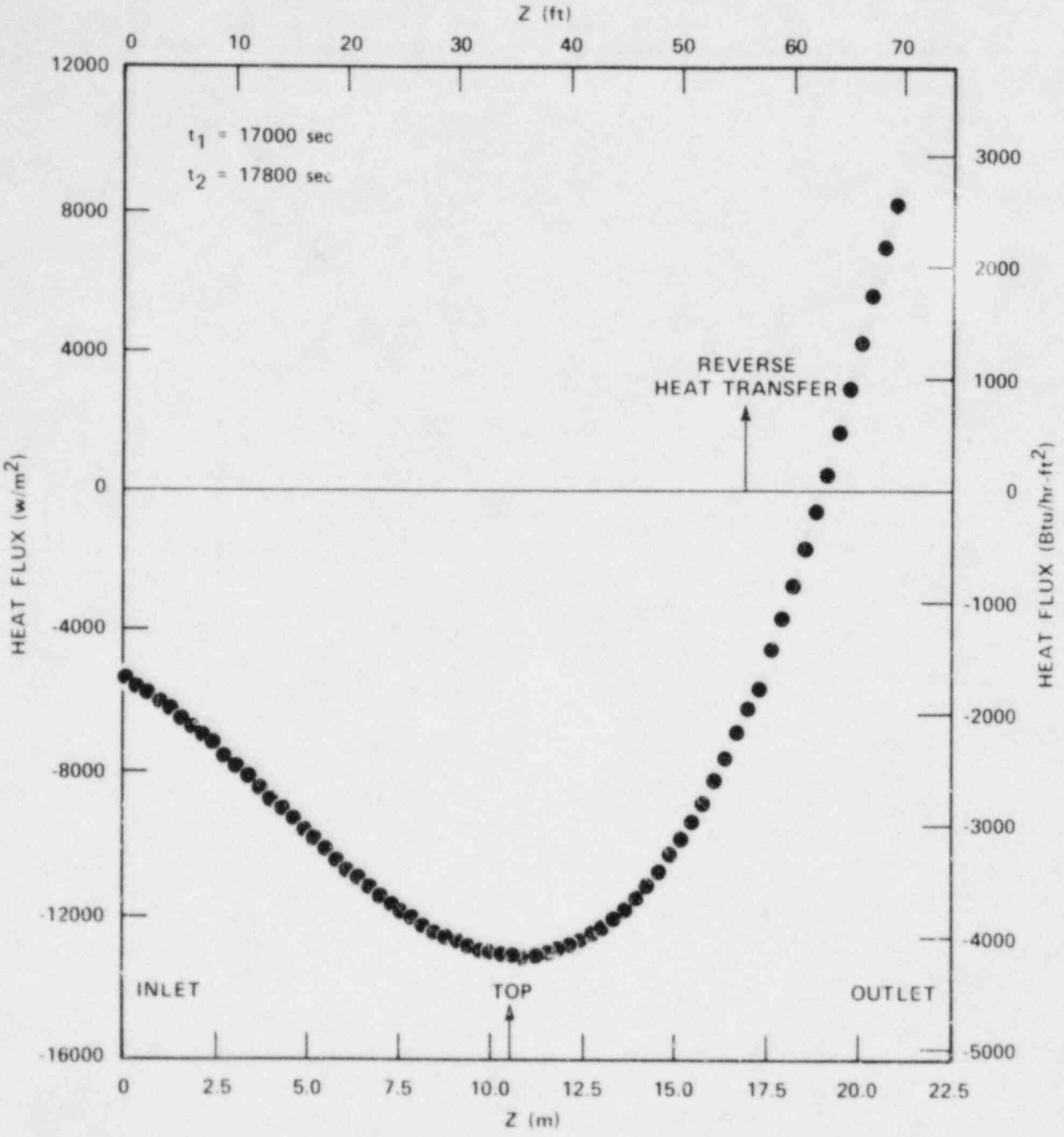

Figure 6-19. Unbroken Loop Two-Phase Heat Flux Plot, Tube Model 2

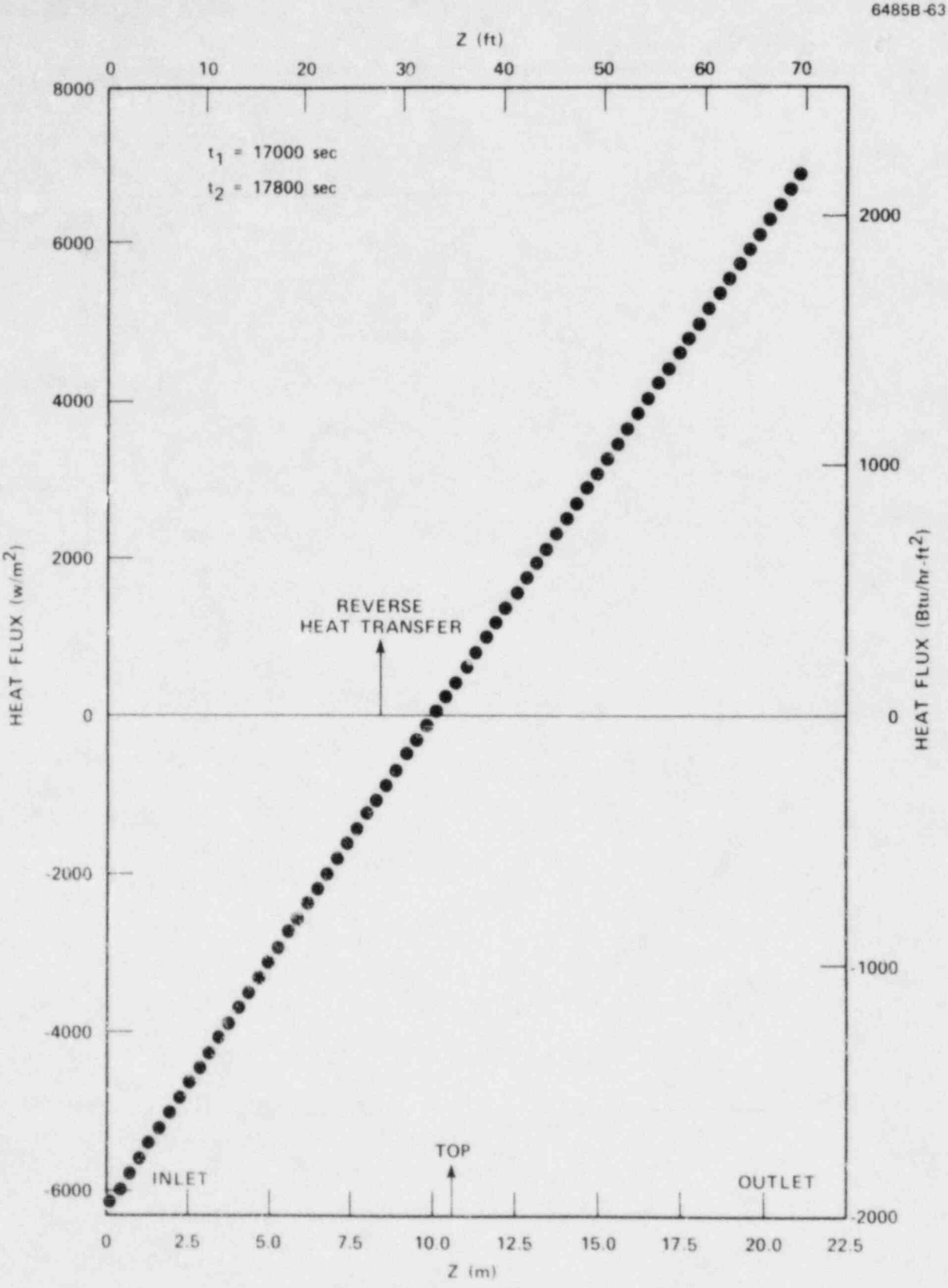

Figure 6-20. Unbroken Loop Two-Phase Heat Flux Plot, Tube Model 3

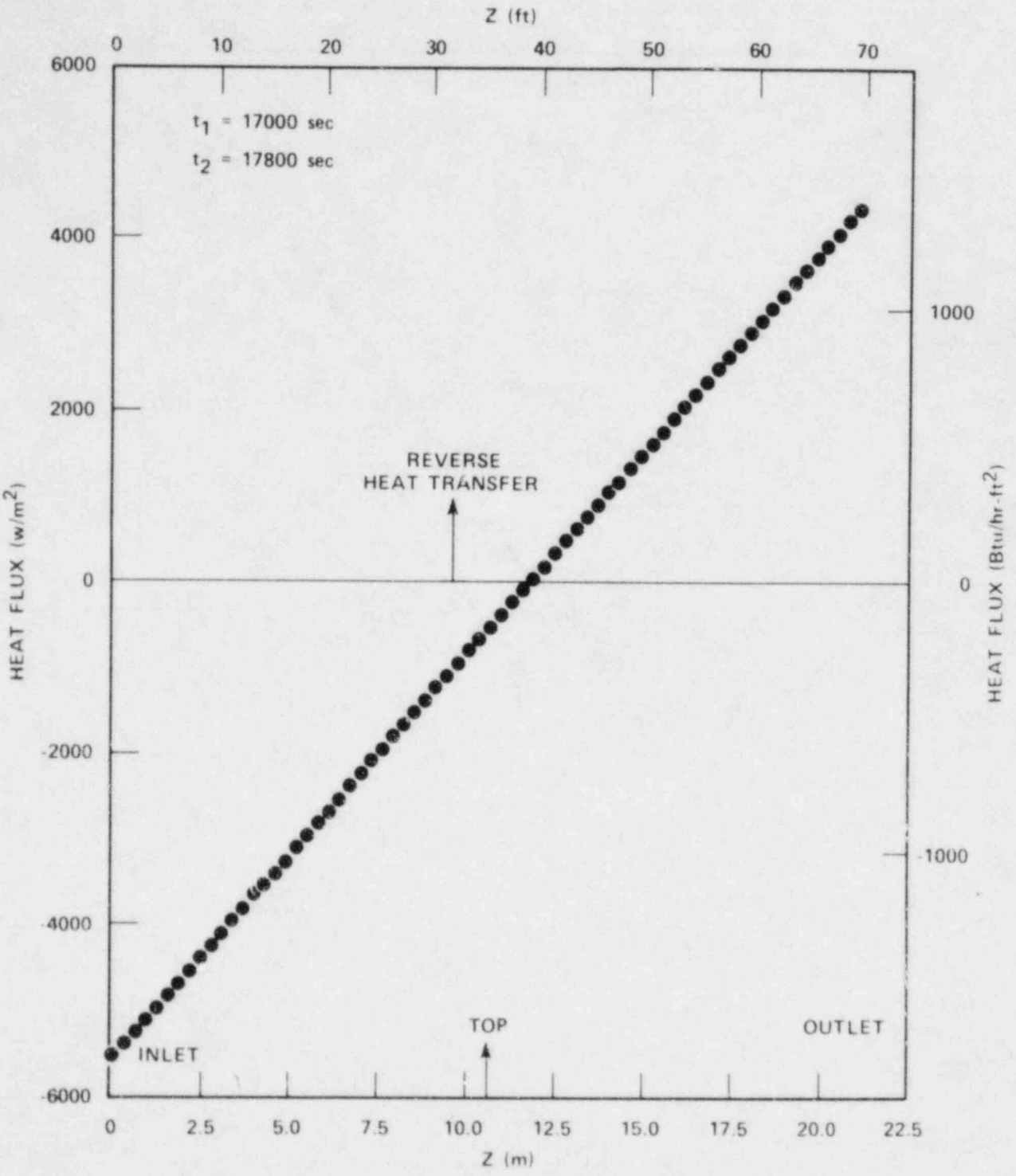

Figure 6-21. Broken Loop Two-Phase Heat Flux Plot, Tube Model 1

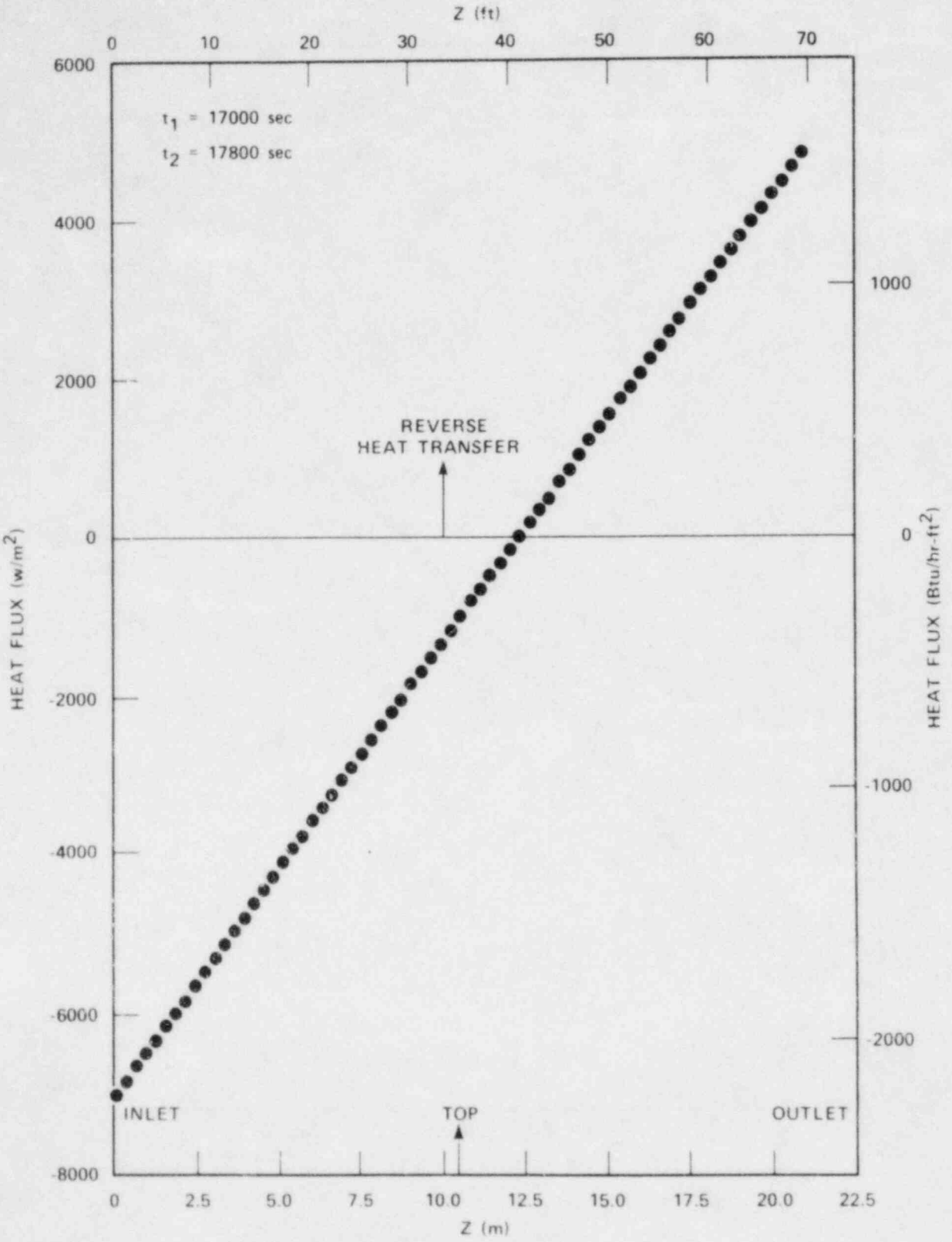

Figure 6-22. Broken Loop Two-Phase Heat Flux Plot, Tube Model 2

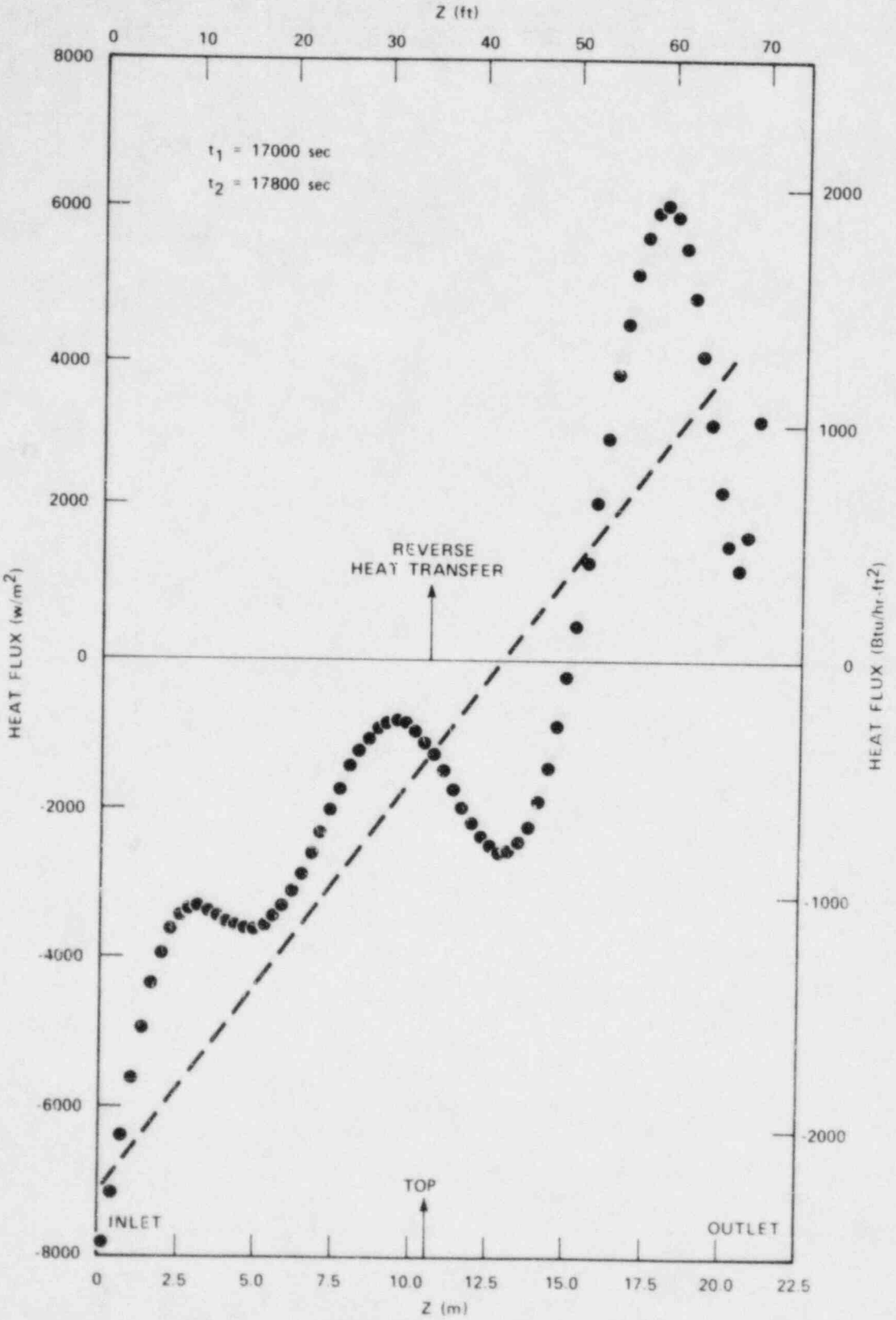

Figure 6-23. Broken Loop Two-Phase Heat Flux Plot, Tube Model 3

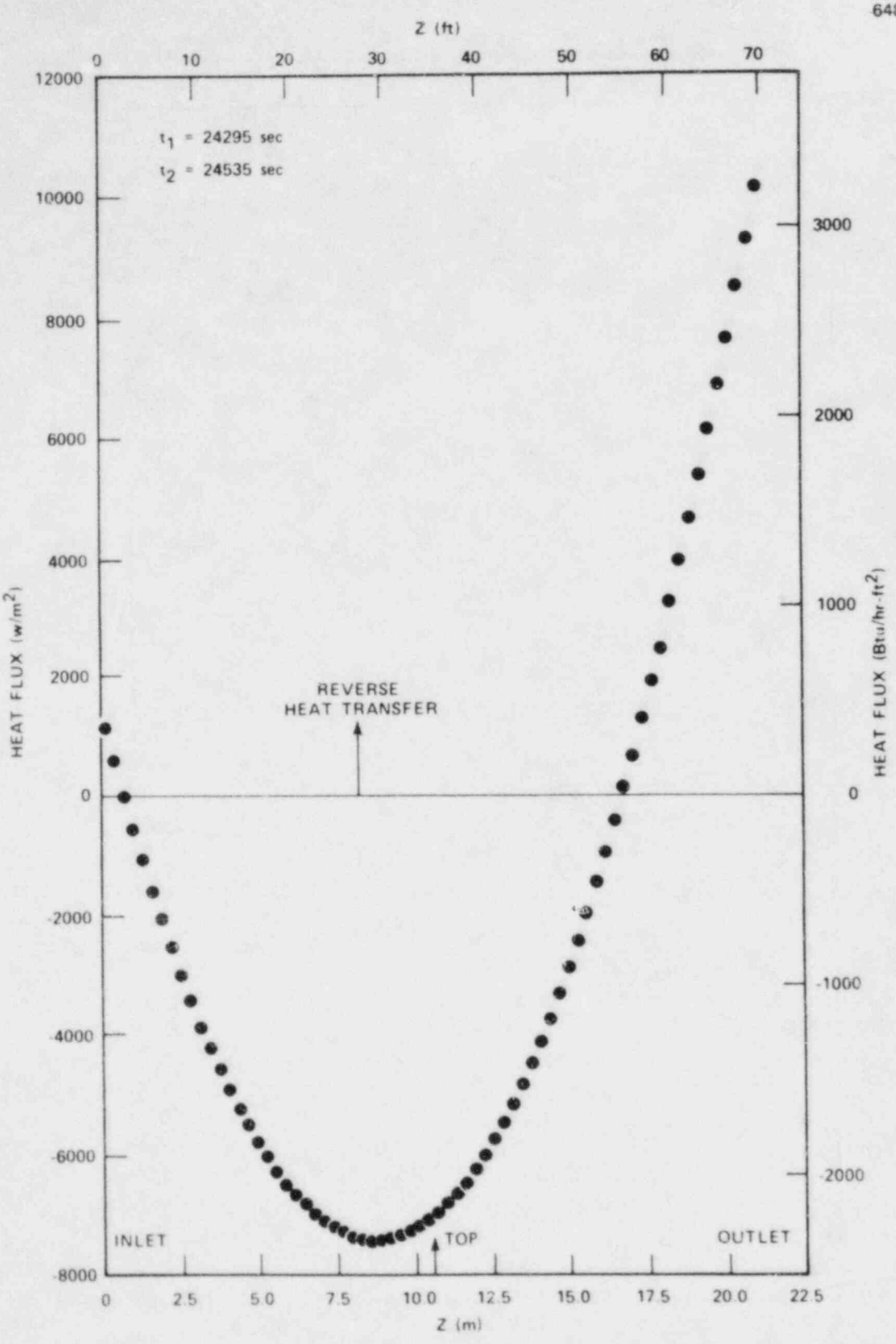

Figure 6-24. Unbroken Loop Reflux Condensation Heat Flux Plot, Tube Model 1

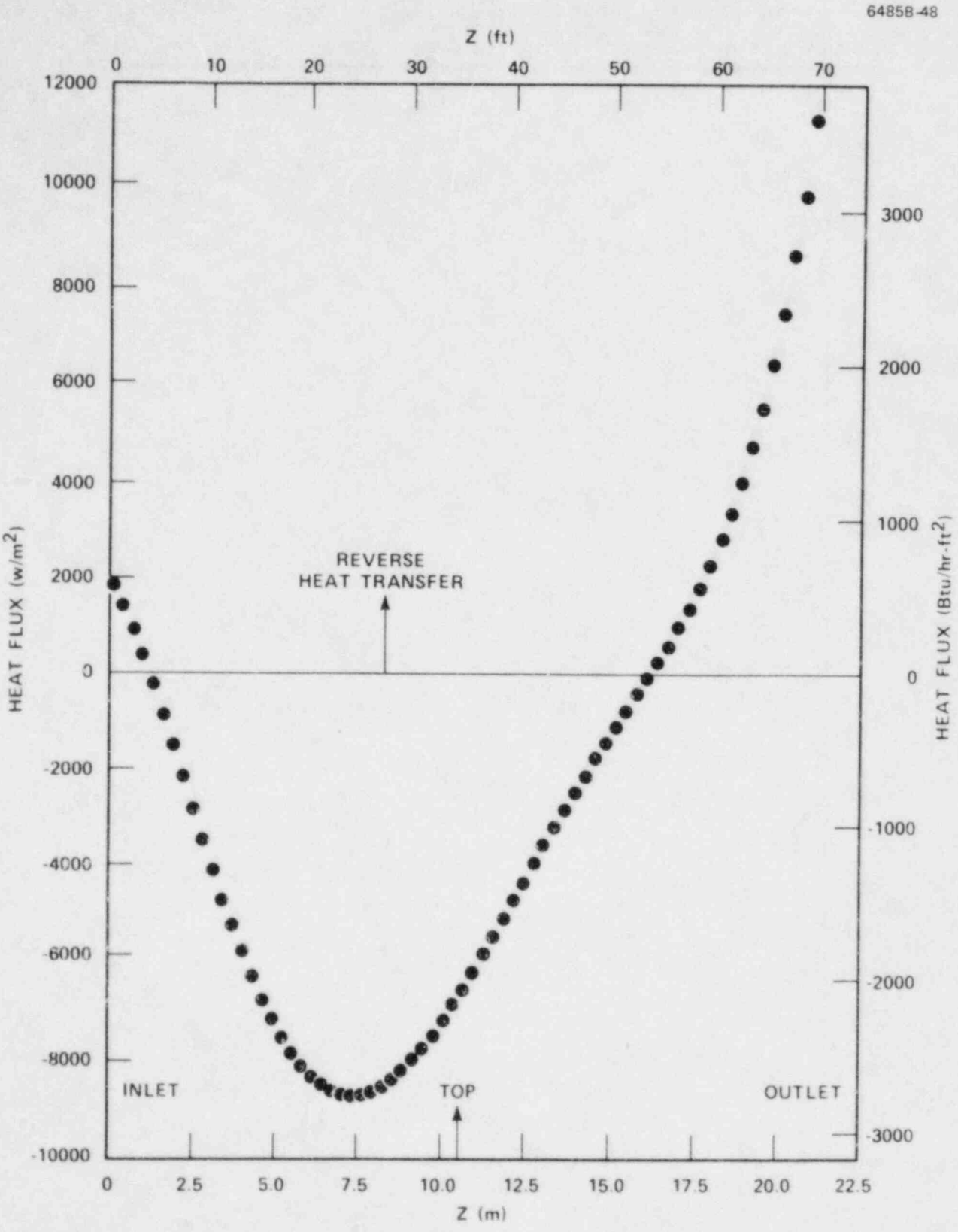

Figure 6-25. Unbroken Loop Reflux Condensation Heat Flux Plot, Tube Model 2

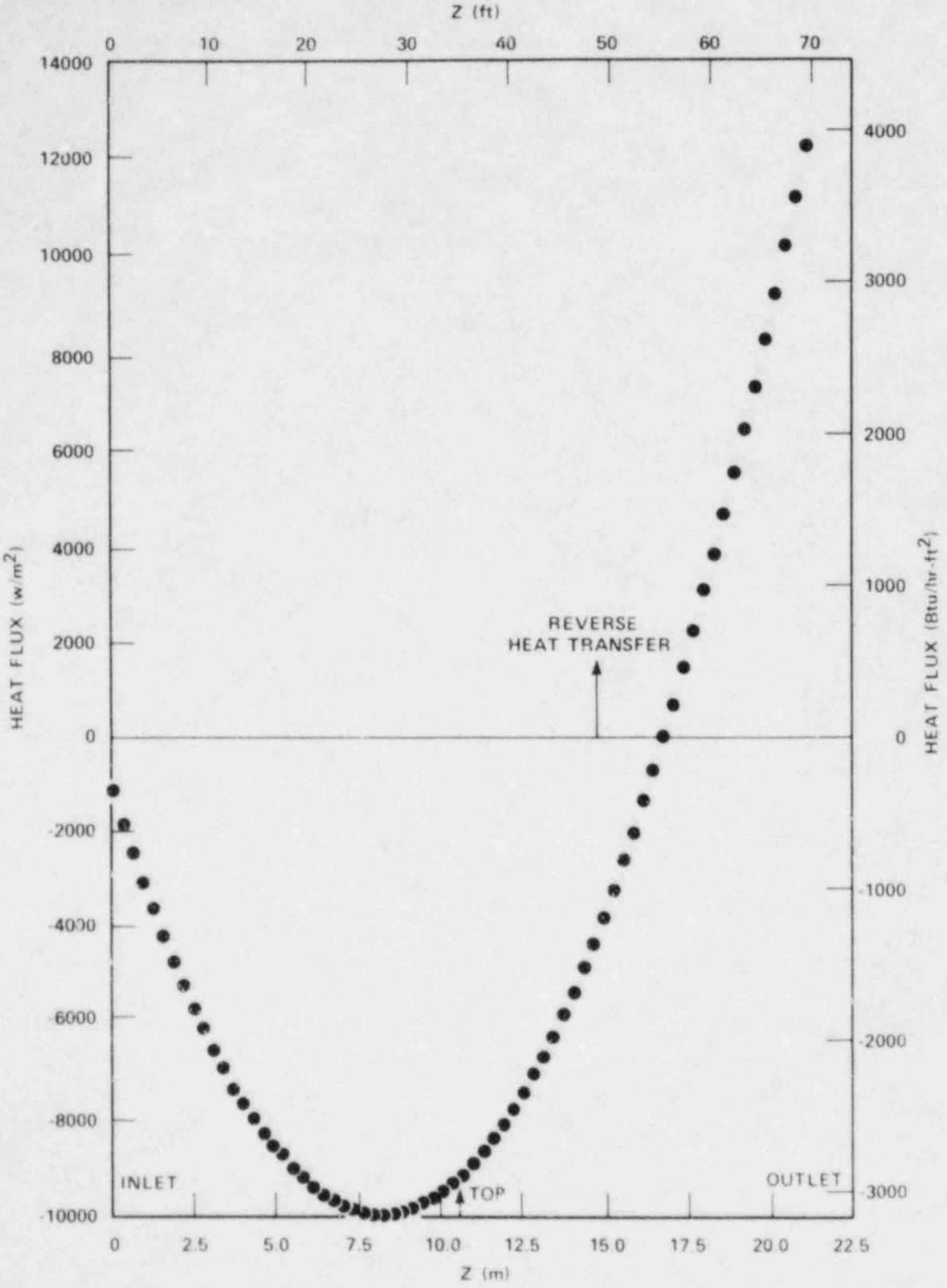

Figure 6-26. Unbroken Loop Reflux Condensation Heat Flux Plot, Tube Model 3

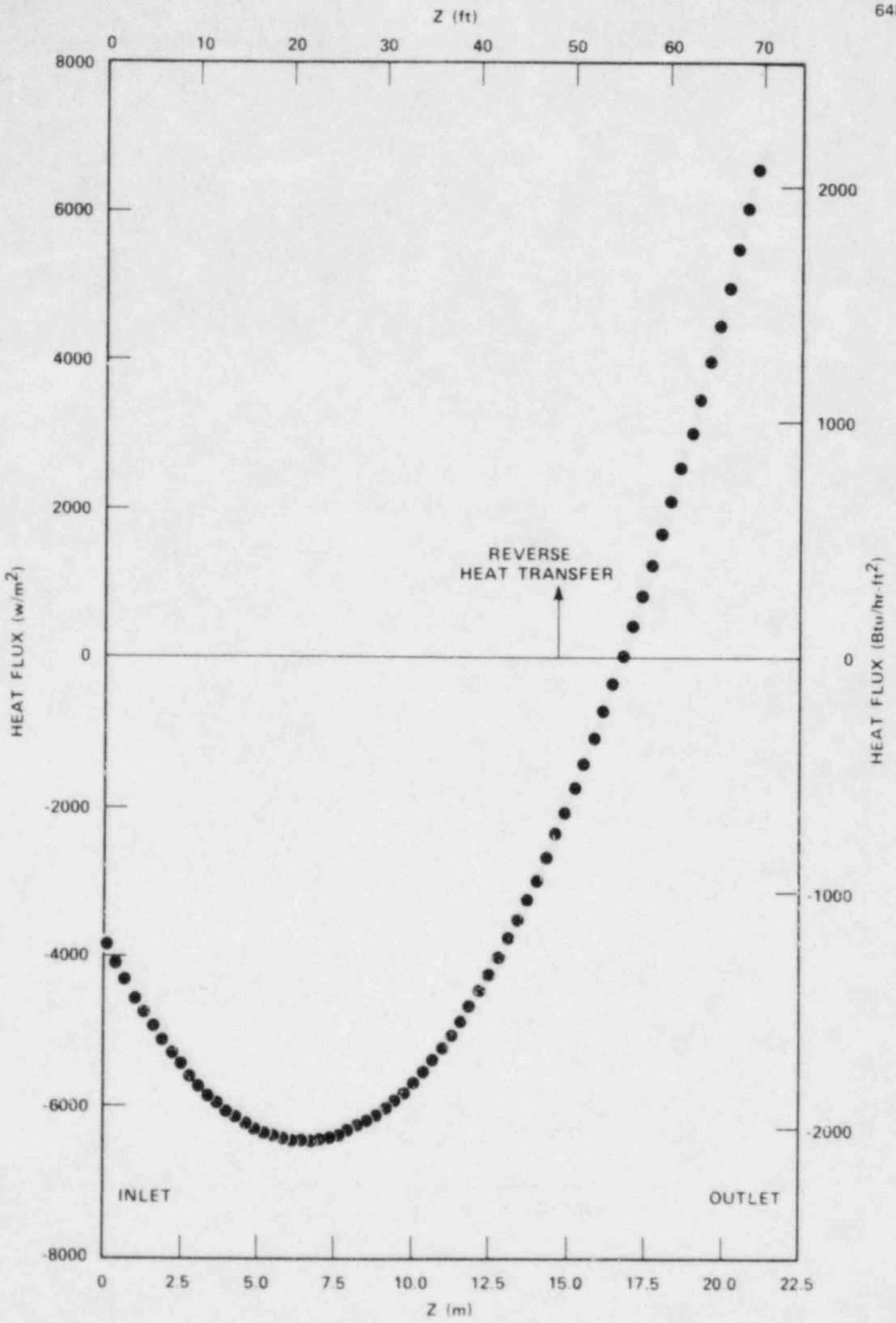

Figure 6-27. Broken Loop Reflux Condensation Heat Flux Plot, Tube Model 1

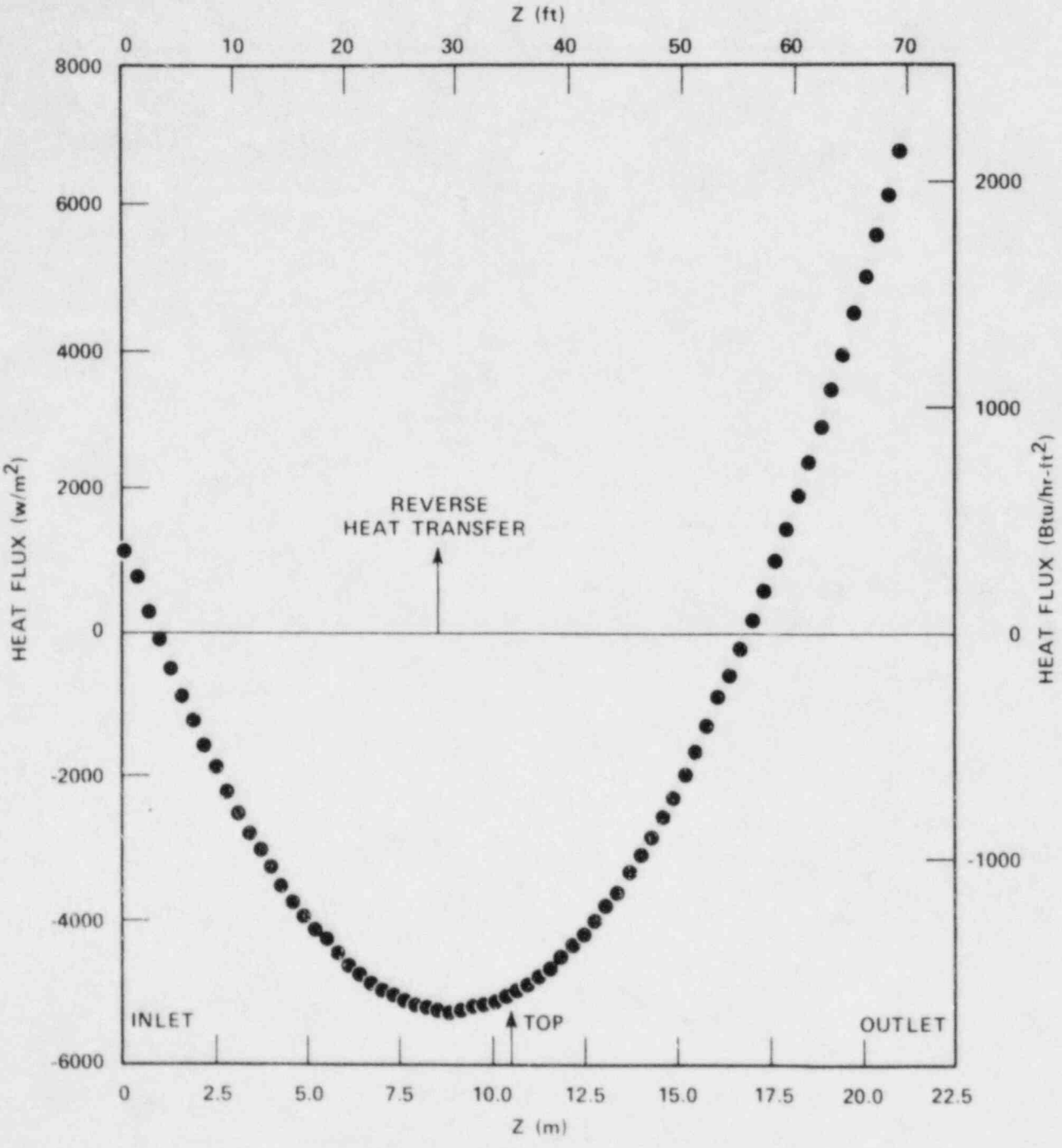

Figure 6-28. Broken Loop Reflux Condensation Heat Flux Plot, Tube Model 2

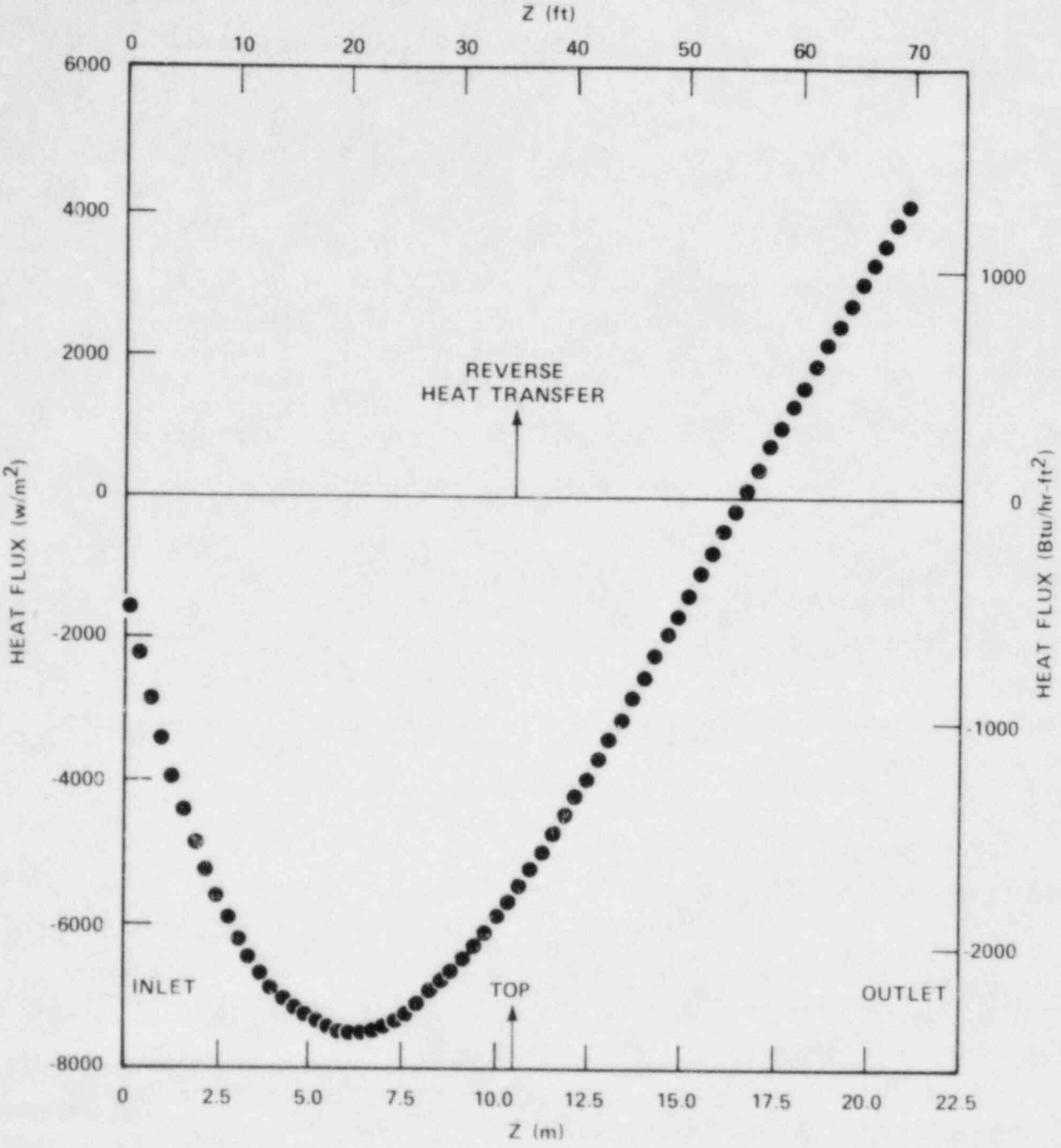

Figure 6-29. Broken Loop Reflux Condensation Heat Flux Plot, Tube Model 3

A = total generator tube area (ft^2)

ΔT = inlet to exit primary fluid temperature difference (°F)

The data (table 6-1) show that the reflux condensation heat transfer coefficient is larger than that for either single- or two-phase flow. However, this larger heat transfer coefficient is counterbalanced by a smaller driving primary-to-secondary side temperature difference.

TABLE 6-1

OVERALL STEAM GENERATOR HEAT TRANSFER DATA

Mode	Broken Loop Steam Generator Heat Transfer Coefficient [w/m-K (Btu/hr-ft^2-°F)]	Unbroken Loop Steam Generator Heat Transfer Coefficient [w/m-K (Btu/hr-ft^2-°F)]
Single-phase	2.58 (17.9)	2.71 (18.8)
Two-phase	8.44 (58.6)	13.5 (93.7)
Reflux condensation	168.65 (1170.4)	135.7 (941.7)

Before the steam generator heat flux results for the different modes of natural circulation are examined, the basis for the data analysis should be reviewed.

As previously mentioned, several assumptions have been made to reduce the data to a workable form. It is felt that the single-phase heat fluxes are fairly accurate, particularly in the sense that they describe the global behavior of the generator heat flux. The assumptions that are inherent in this calculation are that the primary flow is evenly split between tubes, and that all the tubes in a given tube model experience the same secondary environment. This latter assumption precludes the possibility of some tubes in a tube model being in a free convection mode while others are rejecting heat through nucleate boiling. Because of the finite amount of instrumentation available, such detailed information cannot be quantitatively determined; however the existing data suggest that nucleate boiling may occur near the tubesheet on the uphill side.

The curve fit applied to the primary side temperatures was necessary to eliminate some local effects created by the entering feed flow. A radial temperature gradient exists between the center of the primary liquid and the inside tube wall. It is important that the ΔT used in the energy balance is taken for the same radial position at different elevations. To achieve this, each primary thermocouple is held at the center of its tube by a clip. In at least one case, a clip was found to be dislodged; hence it is unclear whether the temperature reading at that location is accurate. It should be noted, however, that a steam generator energy balance comparing integrated heat flux with a plenum-to-plenum energy loss calculation was nearly the same for the curve-fit data and the raw data. This method eliminated unrealistic predictions such as both primary and secondary fluid losing energy at a given elevation with no apparent energy sink present.

Additional uncertainty may be introduced through the use of the Dittus-Boelter correlation for the primary side heat transfer coefficient, although this is a well-established correlation and valid for the Reynolds number range of these tests.

The single-phase steam generator heat flux plots are shown in figures 6-6 through 6-11, which clearly indicate the regions of reverse heat transfer that occur during single-phase tests. The convention in all heat flux calculations is that a negative heat flux represents heat flow from primary to secondary fluids. Significant reverse heat transfer is seen to occur only on the downhill side as previously noted.

Figures 6-18 through 6-23 show the steam generator heat fluxes for each tube model during peak two-phase flow. In general, the heat flux increases linearly with axial position, with each tube model experiencing reverse heat transfer. Tube model 3 of the broken loop basically follows this trend, although the numerical curve-fitting routine used with the data selected a higher-order polynomial and introduced apparent oscillations in the heat flux rate. This is not thought to be a physical phenomenon but rather particular to the curve-fitting procedure. The dashed line through these oscillations is a best-estimate curve through the data.

Tube models 1 and 2 of the unbroken loop exhibit an increasing heat flux over much of the uphill side. This behavior is seen in reflux condensation cases and is believed to be caused by a liquid film on the tube walls. The reflux condensation heat flux plots in figures 6-24 through 6-29 show a consistent behavior pattern for all tube models. The heat flux increases with axial position up to the top of the U-tube bundle. On the downhill side, the heat flux then decreases, forming a nearly symmetrical plot. This is strongly suggestive of a developed liquid film existing on the tube walls. Near the bottom, where the film is thickest, the heat transfer is the worst because of the added fluid resistance; near the top, heat transfer is improved where the film is thinner. In addition, the reflux flowmeters located in each hot leg and cold leg showed approximately equal amounts of condensate formed on uphill and downhill sides of the tube bundles. This independent measurement supports the symmetrical heat flux distribution shown in these figures.

The secondary side thermal behavior can be characterized for each tube model by constructing plots of fluid and wall temperature (figure 6-13). Near the tubesheet, there are some tubes that have sufficient wall superheat to sustain nucleate boiling. The inlet 0.61 m (2 ft) of the steam generator bundle can be characterized by nucleate boiling on the uphill side and partial boiling or natural convection on the downhill side. Above this point, the secondary fluid becomes more mixed and the primary fluid has been reduced in temperature. As a consequence, the secondary fluid experiences both partial boiling and natural convection heat transfer regimes on the uphill and downhill side of the bundle.

Figure 6-16 shows the calculated secondary side heat flux values, which are scattered near both calculated natural convection[1] and Jens-Lottes[2] boiling curves. This supports the notion of a mixed heat transfer regime as described above. The natural convection curves were computed from a correlation given by Eckert and Jackson and shown in equation (6-3):

---

1. Eckert, E. R. G., and Jackson, T. W., "Analysis of Turbulent Free Convection Boundary Layer on Flate Plates," NACAQ-1015, 1951.

2. Jens, W. H., and Lottes, P. A., "Analysis of Heat Transfer, Burnout, Pressure Digs, and Density Data for High-Pressure Water," ANL-4527, 1951.

$$Nu = 0.21 (Gr \quad Pr)^{0.4} \qquad (6\text{-}3)$$

The secondary side fluid was found to be in the turbulent range for the conditions studied. In the calculation of the Grashof number, the density was taken as that of saturated liquid. Actually, if some boiling is occurring, the density will be lower, and hence the Grashof number will be lower. From test data, it is not possible to accurately compute the degree of vapor generation at any secondary elevation; this introduces some uncertainty. The three different curves are obtained by choosing different elevations for the Grashof number, as shown. The free convection heat transfer curves are intended to be used as a trend and basis to examine the local calculated steam generator heat fluxes.

The boiling curves are from correlations taken by Jens and Lottes and Bergles-Rohsenow.[1] Examination of the data from which these curves were extracted shows considerable scatter, particularly in that of Jens and Lottes. In fact, the data scatter from the Jens-Lottes experiments overlaps with the the natural circulation test data presented in this report.

It is expected that the presence of noncondensibles in the primary side of the steam generator will reduce the area available for heat transfer and hence modify the primary side temperature and heat flux distribution in the steam generators. Previous tests, such as those performed by PKL[2] and the single-tube experiments by Ripple,[3] examined this phenomenon by injecting nitrogen into the system and plotting temperature variation with axial tube position. Ripple's results show a threshold of nitrogen injection below which

---

1. Bergles, A. E., and Rohsenow, W. N., "The Determination of Forced Convection Surface Boiling Heat Transfer," Paper 63-HT-22 presented at the 6th National Heat Transfer Conference, Boston, August 1963.

2. Mandl, R. M., and Weiss, P. A., "PKL Tests on Energy Transfer Mechanisms During Small-Break LOCAs," Nuclear Safety, 23, No. 2, 1982.

3. Ripple, R., "The Influence of Noncondensible Gases on the Heat Transfer in Steam Generators of Pressurized Water Reactors During a Loss-of-Coolant Accident," PhD thesis, Technical University of Munich, March 1981.

no effect on temperature distribution was noticed. Above this threshold, the primary to secondary ΔT was much reduced on the downhill side of the tube, indicating the accumulation of nitrogen at that location, such that the primary temperature equals the secondary and no transfer occurs. As more nitrogen was injected, this low ΔT "front" moved back within the tube, as shown in figure 6-30.

Analysis of the FLECHT SEASET natural circulation tests shows a region of reduced steam generator heat transfer due to the presence of noncondensible gas, in this case, helium. The calculated heat flux distribution is shown for the six tube models in figures 6-31 through 6-36. The data show that, before the injection of helium, the tubes are at least in a partial reflux condensation mode, as indicated by the reduced heat flux near the tubesheet. After injection, two main changes occurred. First, the regions near the top of the U-tubes [7.62-13.72 m (25-45 ft)] exhibited a reduced heat transfer, due to the presence of helium migrating, through buoyancy forces, to the top of the tubes and thus providing a mixture with a lower percentage of condensible fluid at this location. Second, since the total amount of heat rejected in the steam generator was constant, this reduced heat transfer area was compensated for by an increased heat transfer regime near the tubesheet on the uphill side of the tube bundle.

One reason for the difference in the heat flux distribution between Ripple's experiments and the FLECHT SEASET tests is the difference in molecular weights of the noncondensible gas. Nitrogen with a molar mass of 13 kg (28 lb) per mole is heavier than steam at 8.2 kg (18 lb) per mole; thus it accumulated at a lower point in the generators. It would also appear that, in both the PKL tests and Ripple's experiments, the nitrogen accumulated in a bubble on the downhill side and virtually no heat transfer occurred there. In the FLECHT SEASET tests, the lighter gas tended to migrate to the highest region of the generator. However, figures 6-31 through 6-36 show that heat transfer was still occurring in this region. One possible inference is that the helium was fairly well mixed with the steam and did not block off the primary flow entirely.

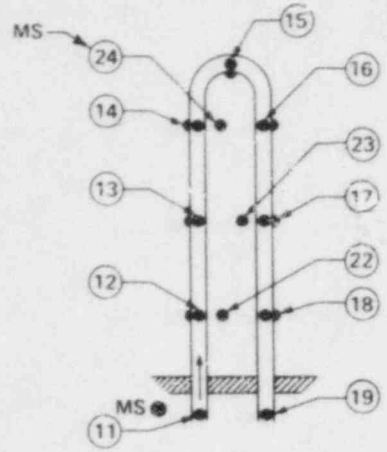

LEGEND:

x TEMPERATURE IN CENTERLINE OF U-TUBE (MS 12 - MS 18)

□ TEMPERATURE IN WALL OF U-TUBE (MS 2 - MS 8)

○ TEMPERATURE OF SECONDARY (MS 22 – MS 24)

64858-7
64858-8

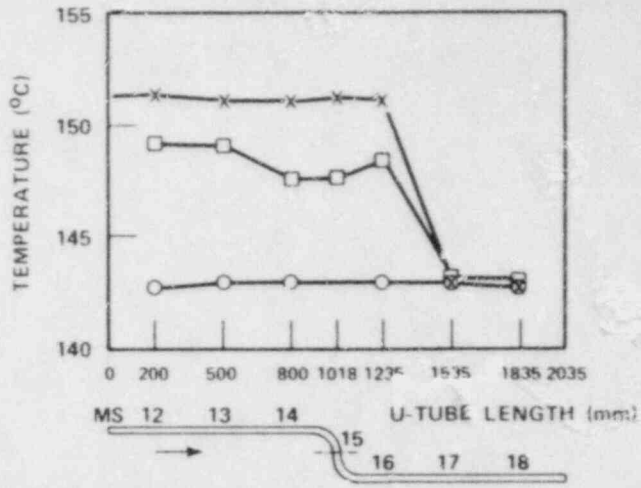

CONDENSATE DISTRIBUTION:
ASCENDING U-TUBE BRANCH 74%
DESCENDING U-TUBE BRANCH 26%

NITROGEN: 1.94 g, OF WHICH 0.67 g IS ACTIVE

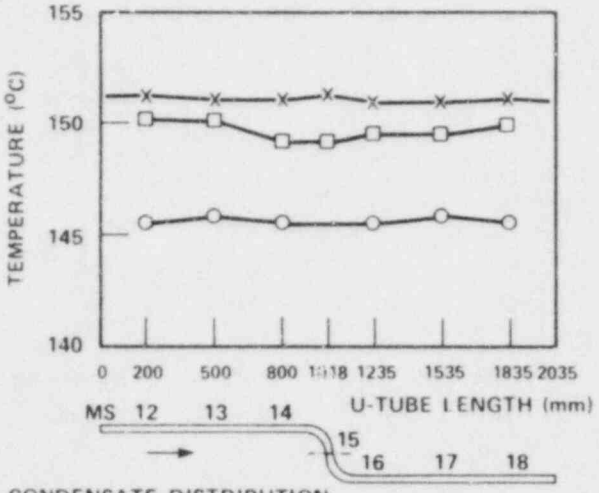

CONDENSATE DISTRIBUTION:
ASCENDING U-TUBE BRANCH 56%
DESCENDING U-TUBE BRANCH 44%

NITROGEN: 0.97 g, OF WHICH NONE IS ACTIVE

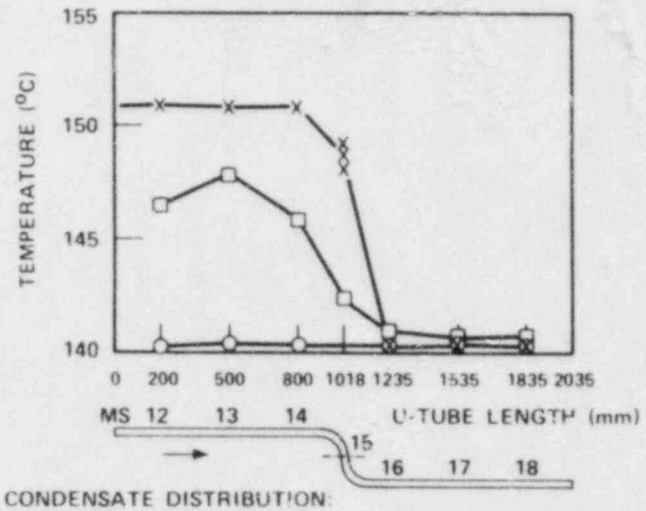

CONDENSATE DISTRIBUTION:
ASCENDING U-TUBE BRANCH 98%
DESCENDING U-TUBE BRANCH 2%

NITROGEN: 2.92 g, OF WHICH 0.83 g IS ACTIVE

Figure 6-30. Temperature Variation Versus Axial Tube Position, Single-Tube Experiments of Ripple

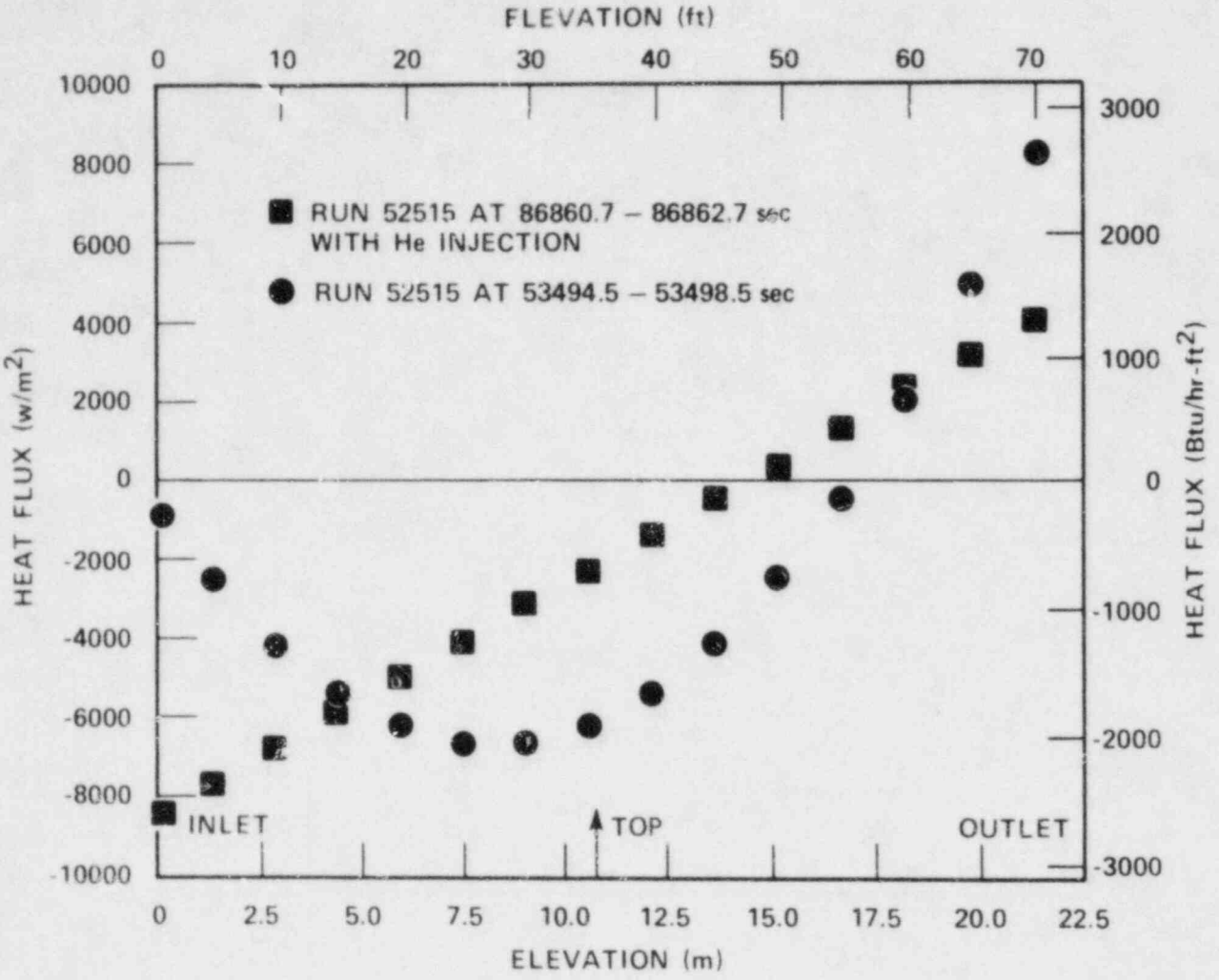

Figure 6-31. Effect of Noncondensible Injection on Steam Generator Heat Transfer, Unbroken Loop Tube Model 1

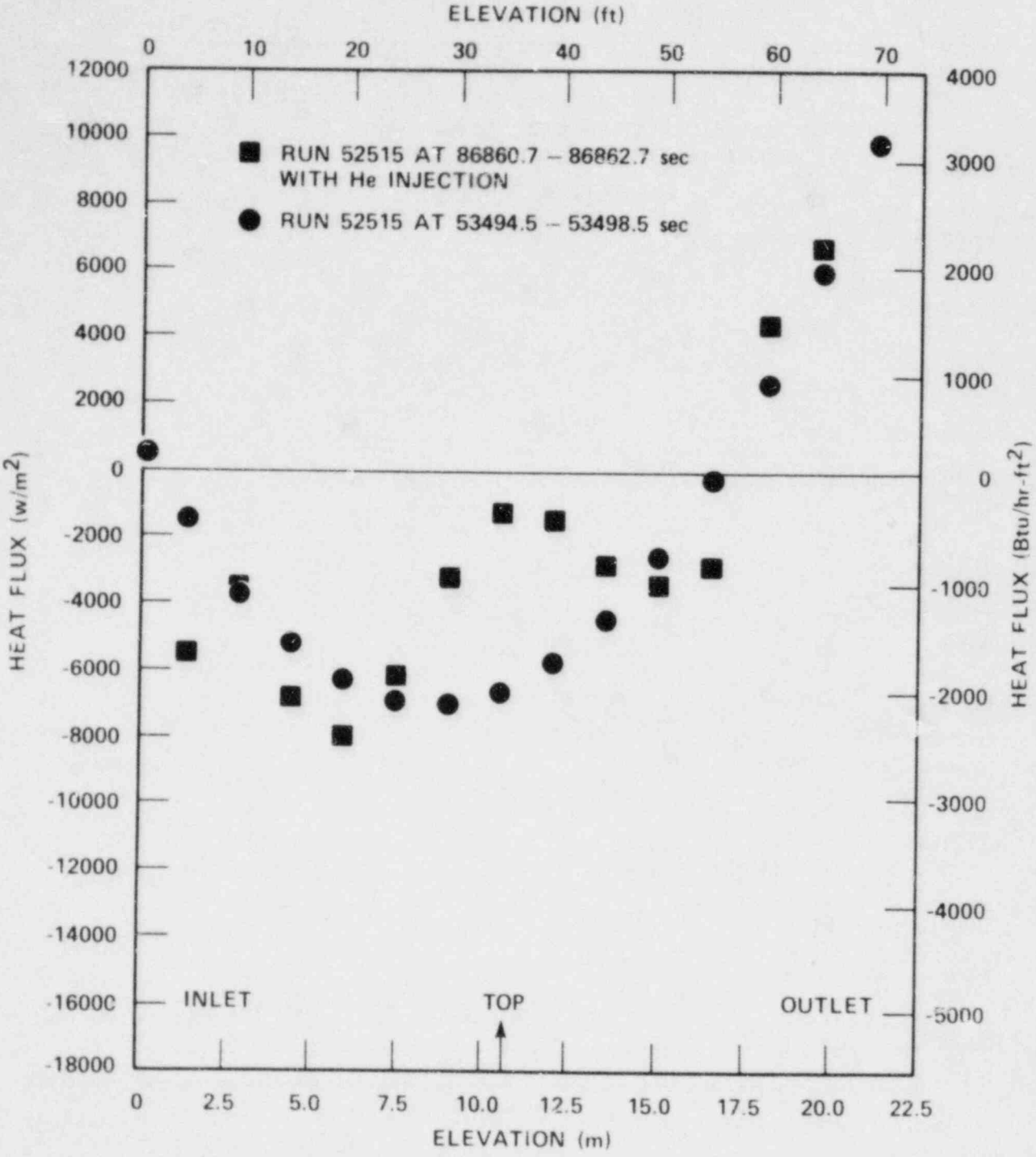

Figure 6-32. Effect of Noncondensible Injection on Steam Generator Heat Transfer, Unbroken Loop Tube Model 2

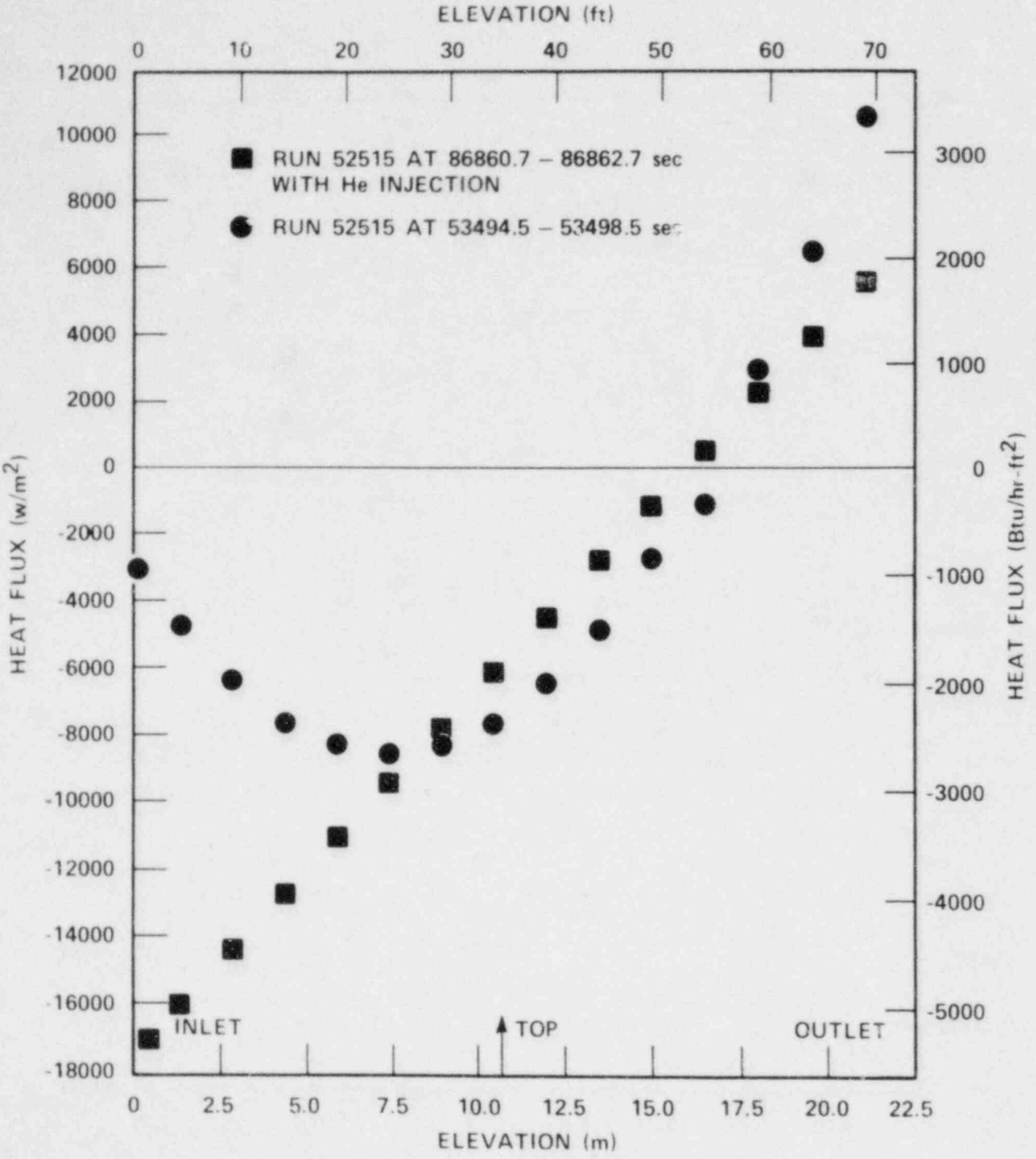

Figure 6-33. Effect of Noncondensible Injection on Steam Generator Heat Transfer, Unbroken Loop Tube Model 3

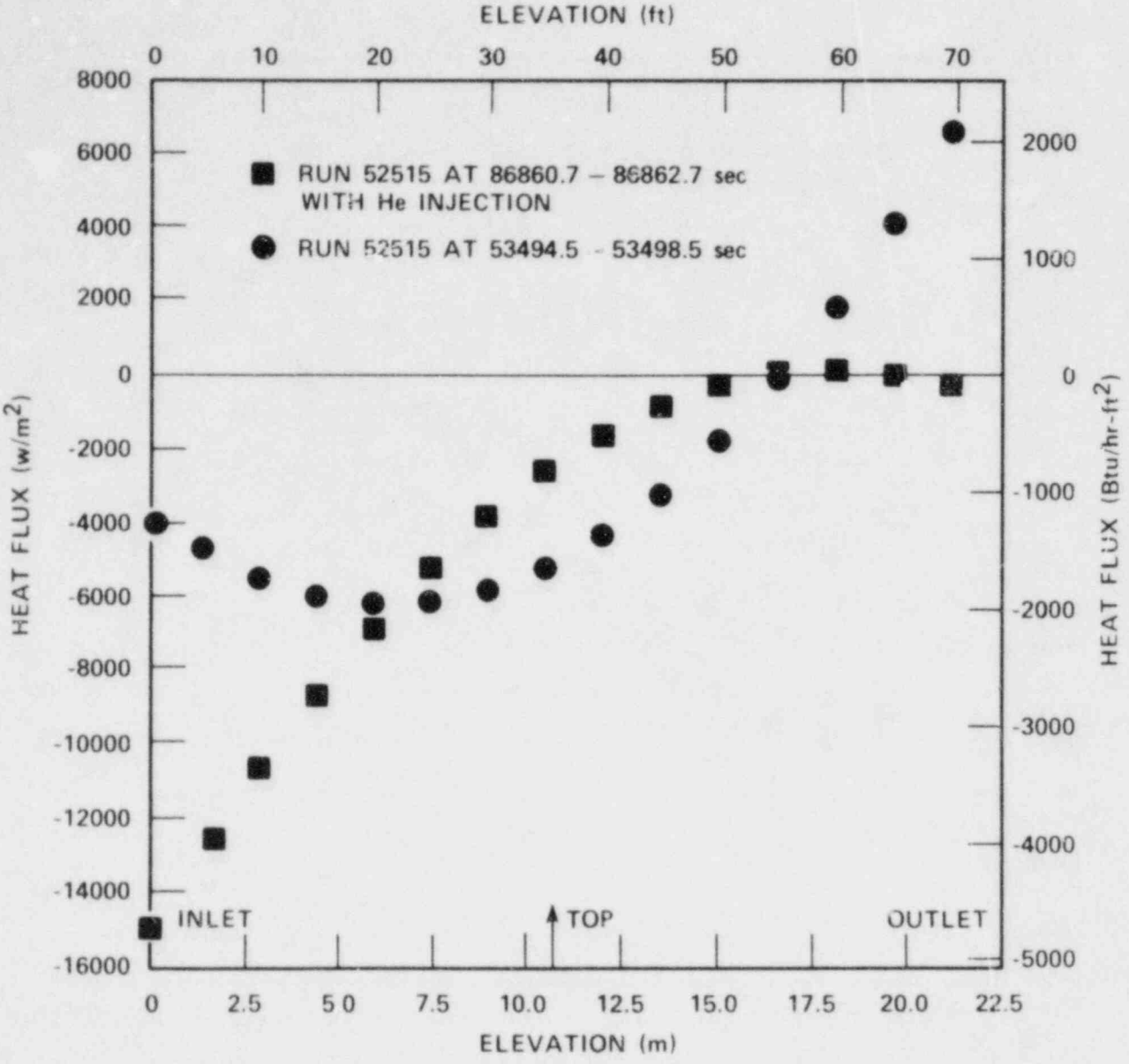

Figure 6-34. Effect of Noncondensible Injection on Steam Generator Heat Transfer, Broken Loop Tube Model 1

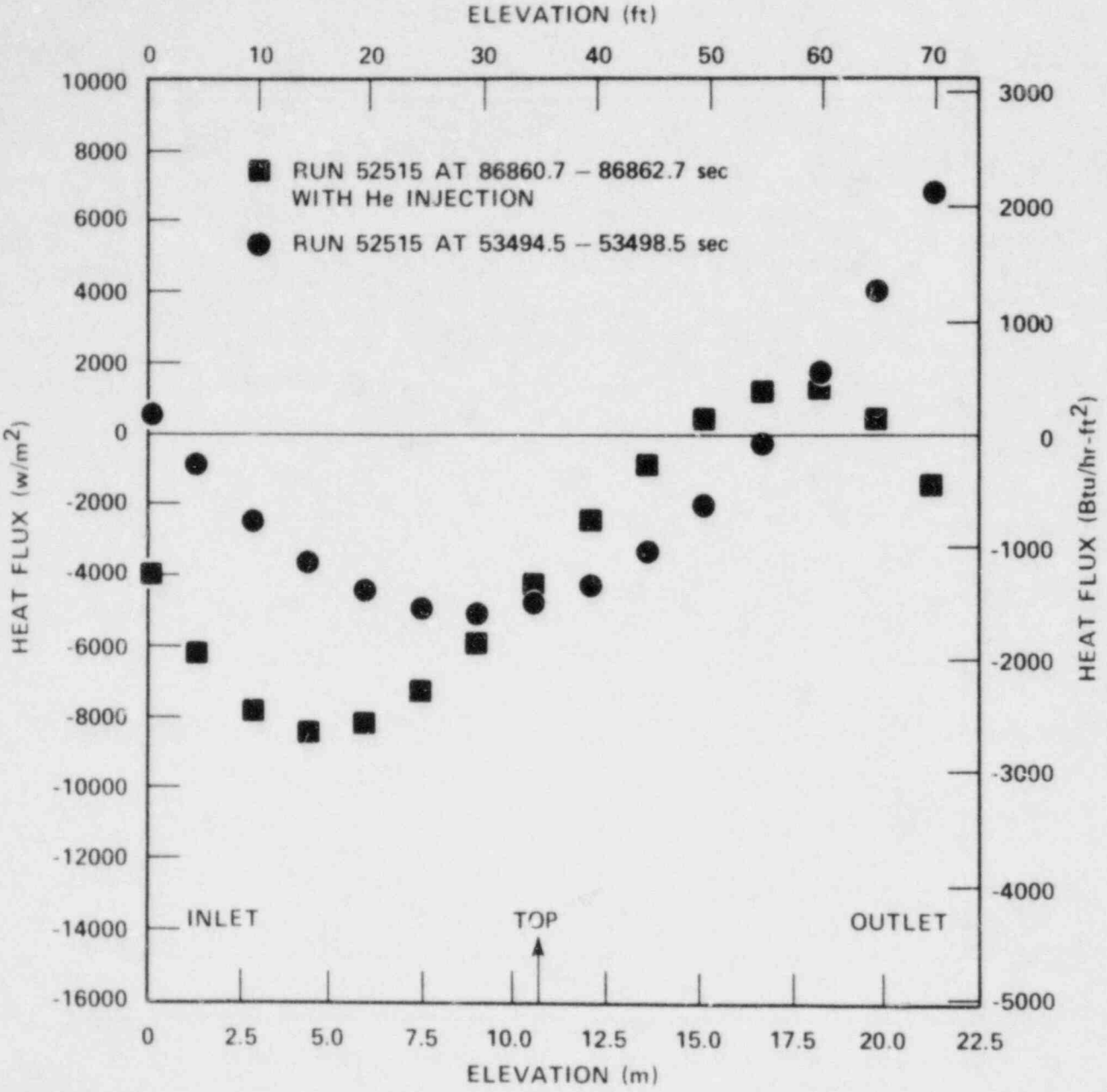

Figure 6-35. Effect of Noncondensible Injection on Steam Generator Heat Transfer, Broken Loop Tube Model 2

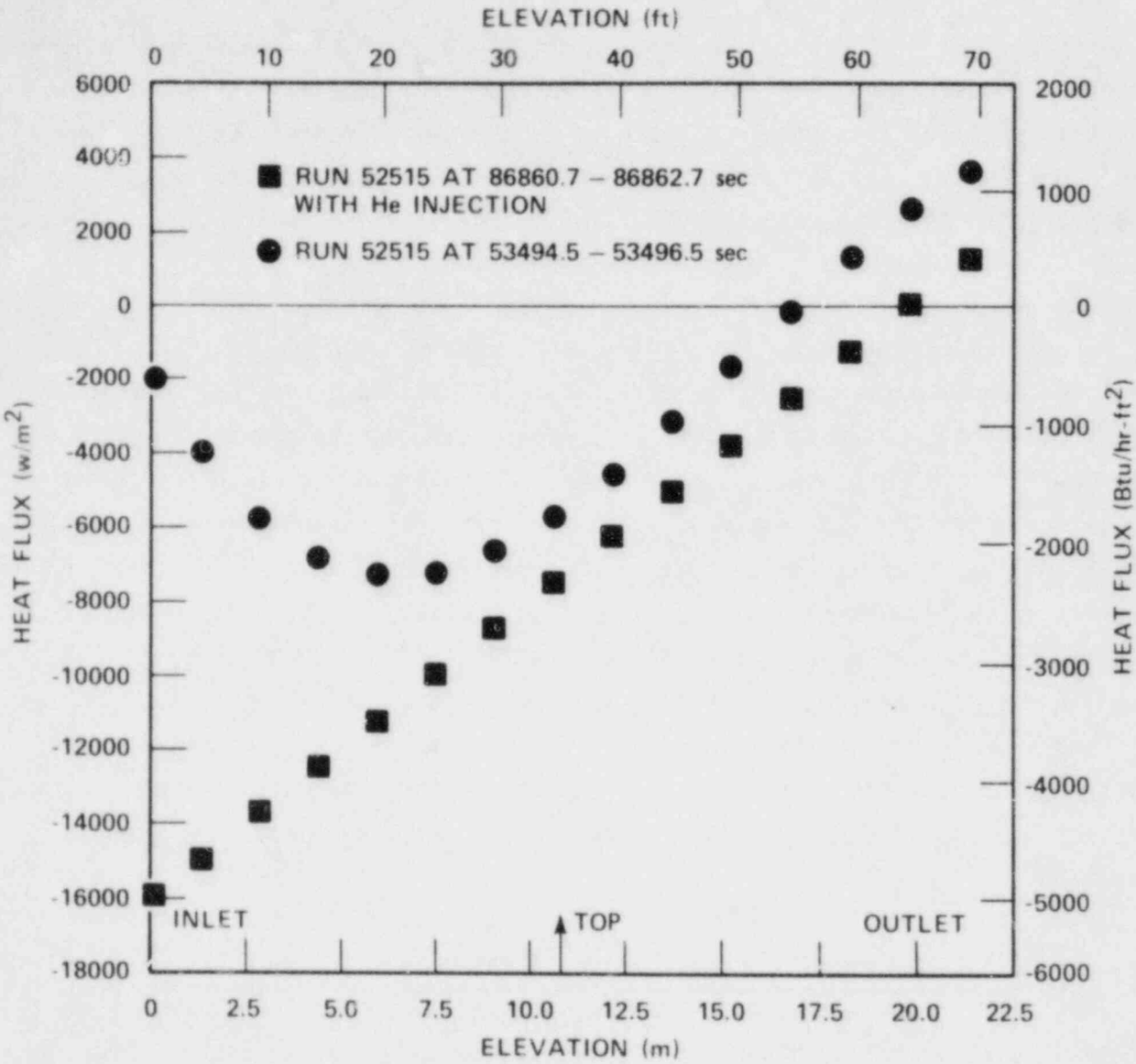

Figure 6-36. Effect of Noncondensible Injection on Steam Generator Heat Transfer, Broken Loop Tube Model 3

In comparison of the FLECHT SEASET results with those of Ripple's single-tube experiments, it should be noted that the FLECHT SEASET heat flux values represent the average effects of several tubes in each tube model. Some individual tubes could contain more helium; others could contain less.

6-4. ANALYTICAL HEAT TRANSFER MODEL FOR STEAM GENERATORS

Preliminary work was begun on an analytical tube model for predicting primary side heat transfer and flow conditions when the steam generator is in a reflux condensation mode. The basic approach is to begin with the steady-state two-phase continuity equations and a constant relative velocity between phases. Flow boundary conditions and heat flux values are obtained from test data. The equation formulation is outlined in appendix G.

For the simple case that was studied, a void fraction of 0.95 was assumed in the inlet plenum and an inlet volumetric flux (j) was computed from data to be approximately 1.12 m/sec (13,200 ft/hr). The steam generator heat flux distribution which was used for this example calculation was taken from a single-phase primary side natural circulation test. The outlet boundary condition on j was taken to be zero; this overspecifies the problem considering its first-order governing equation. Physically, these conditions represent a two-phase mixture entering the bundle and condensing. At the outlet, the (j=0) condition represents a constant loop seal liquid level. Actually, j does not exactly go to zero because the loop seal spills over into the cold leg to accommodate the condensate flow. However, the combination of high void fraction and relatively low liquid velocity will produce a near-zero j condition.

The tube is divided into 70 segments each approximately 0.3 m (1 ft) long to coincide with the heat flux data already calculated. The solution begins at the inlet plenum and marches along the tube using local values of heat flux until a value of j is calculated in the outlet plenum. This value is then compared to the zero j condition, the heat fluxes are adjusted, and the scheme is repeated until the outlet condition is satisfied. Void fraction values can then be calculated from equations (G-11) through (G-16), appendix G.

This model is clearly a first cut at the problem. There is no accounting for the possibility of liquid film subcooling or flooding at the tube inlet and exit. In addition, the constant relative velocity assumption [7.62 m/sec (25 ft/sec)] should be replaced with a suitable drift flux model.

The results of this preliminary model show the void fraction increasing as liquid condenses, as would be expected. However, the final heat flux values attained after iterating to satisfy the outlet condition are approximately 2 percent more than the heat flux available in the generator. This is attributed to the simplification of the model. Figure 6-37 shows the values of void fraction within the tube, and the final heat flux distribution is shown in figure 6-38.

Future work on this analysis should include the use of a suitable drift flux model and inclusion of subcooling in the liquid film.

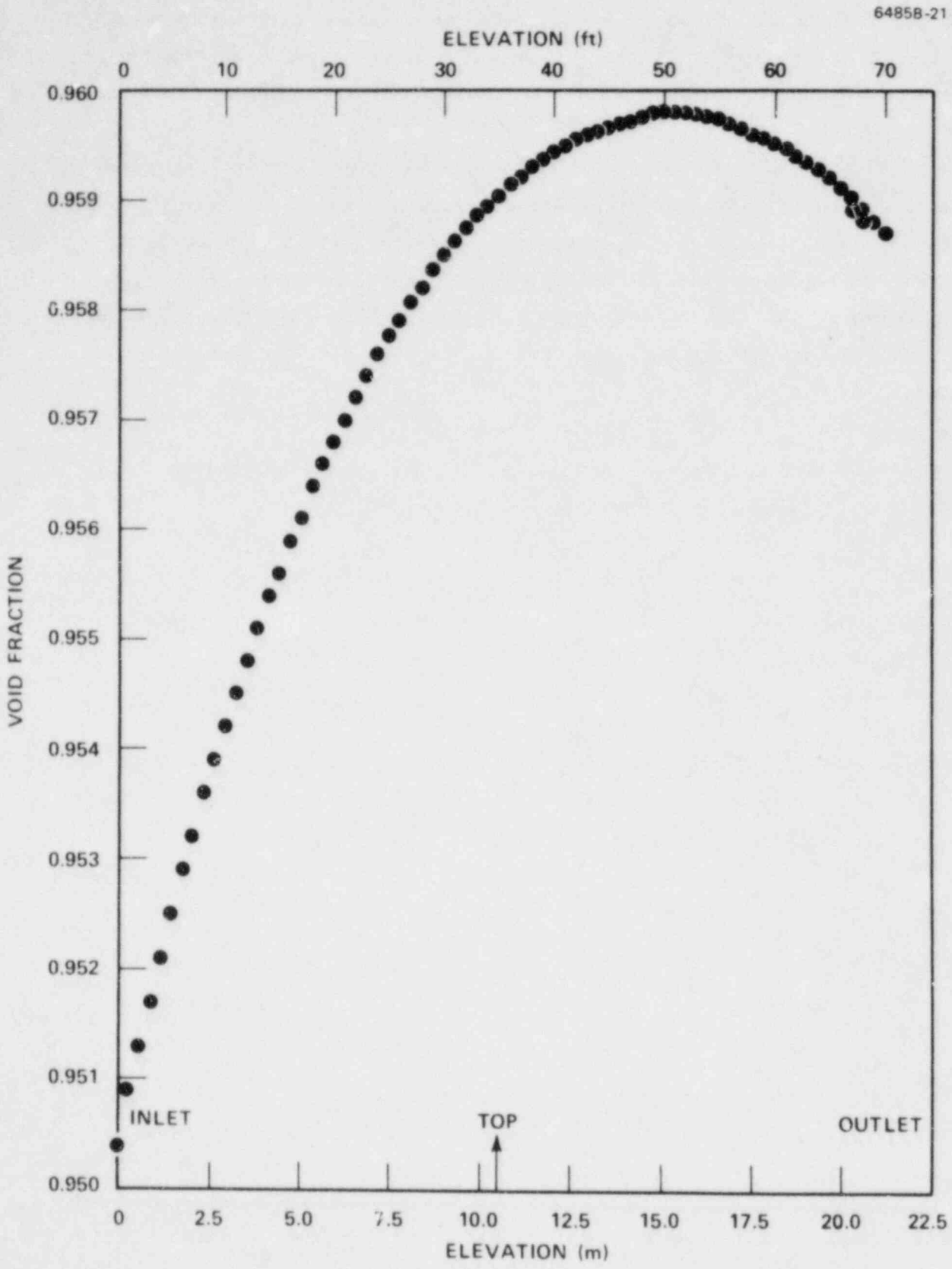

Figure 6-37. Analytical Prediction of Void Fraction

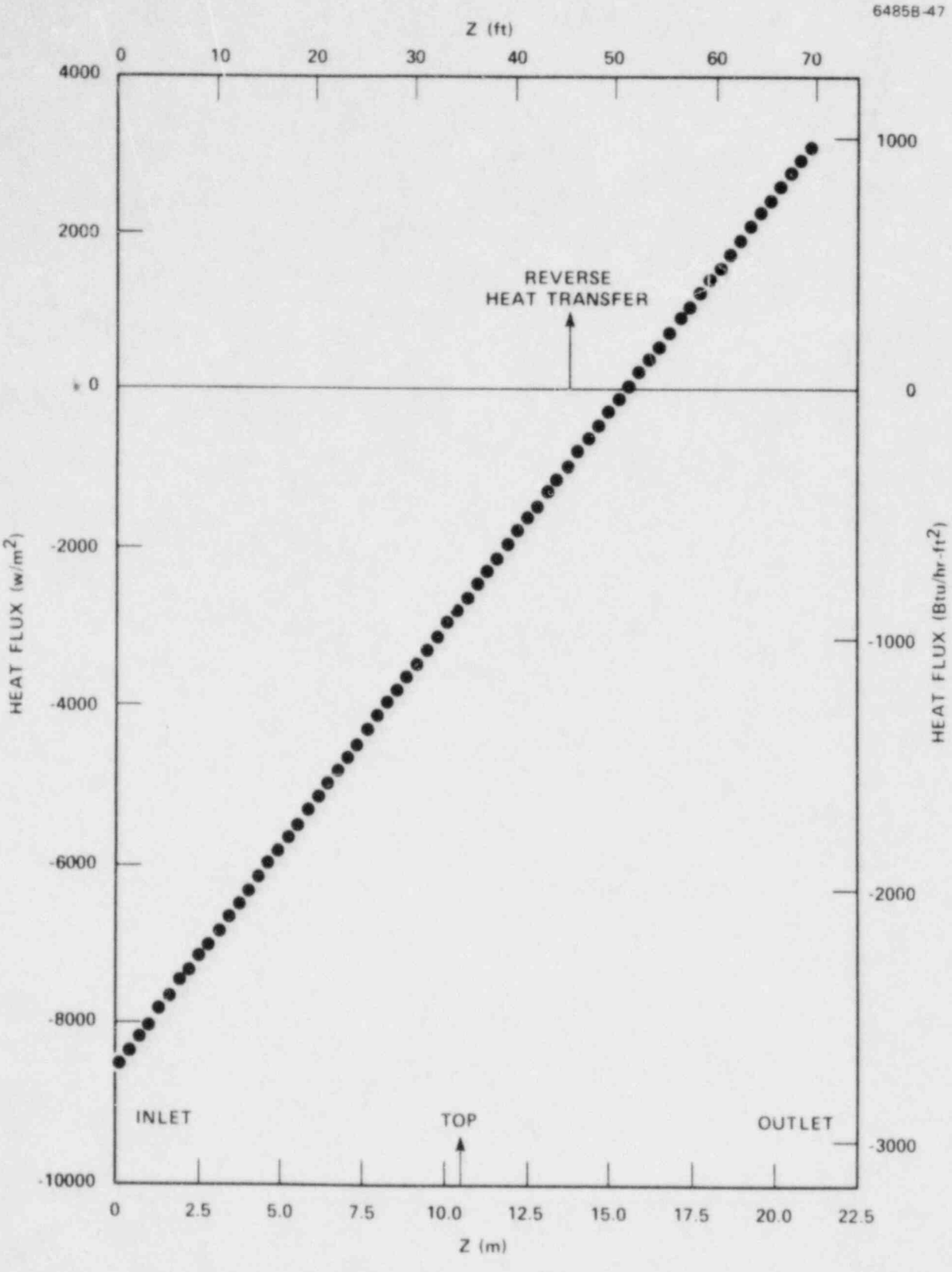

Figure 6-38. Heat Flux Used in Computing Void Fraction

SECTION 7
SYSTEM BEHAVIOR PREDICTIONS

7-1. INTRODUCTION

A system predictive model was to be developed for the FLECHT SEASET natural circulation program. The main objectives of the model development efforts were as follows:

- To predict the system transient natural circulation flow in the primary loop components of the FLECHT SEASET facilities
- To provide an independent system prediction capability for the natural circulation program
- To serve as an analytical check against other available system codes
- To predict average (cross-sectional) volumetric concentrations of liquid water, steam, and noncondensible gas in the primary loop components
- To study effects of noncondensible gas injection into the system on natural circulation transient behavior
- To develop or assess mechanistic heat transfer and hydrodynamic models (especially in the steam generators) by comparing predicted system transients with data

To meet the above objectives, and to allow for sufficient flexibilities for future improvements and modifications, the code developed contains the following features:

- The computer program allows detailed noding at each loop component (for instance, steam generator U-tubes) so that steam and noncondensible gas concentration distributions can be computed accurately.
- The program calculates system flow transients with relatively short computer time.
- The noncondensible gas field is added explicitly to a drift flux formulation which allows for different velocities among liquid water, steam vapor, and noncondensible gas.

- o Multitube steam generators are allowed.
- o Each loop component (for example, a rod bundle flow channel or a steam generator U-tube) can be isolated to study heat transfer and hydrodynamic models in detail.

Because of attempts to make the program more general and yet able to handle complex situations, considerable unforeseen difficulties were encountered in the convergence of the numerical solutions, especially when the noncondensible gas field has a different velocity than the steam, and in calculation of flow split between the unbroken and broken loops and in multitube steam generators. At this writing, not all the potential capabilities of the code mentioned above have been implemented, and some of the features in the program has not been checked and verified. Also, many of the observed phenomena in the natural circulation tests (for instance, broken loop flow stalling during two-phase mode) were not fully analyzed and no models were developed to describe them. Therefore, a complete prediction of the entire natural circulation test program behavior is not possible with the present status of the code. In this report, only limited predictions are presented, and some simplifying assumptions had to be made in performance of the analysis. Despite all these shortcomings, the code showed promising potential for development into a valuable analysis tool, given more time to solve all the numerical problems and to develop and implement more accurate heat transfer and hydrodynamic models.

The basic equations, the system geometry, and the numerical solution procedures are described in paragraphs 7-2 through 7-6 and appendix H. In paragraphs 7-7 through 7-10, the prediction procedures and data comparisons are given. Recommendations for future development efforts are suggested in paragraph 7-11.

7-2. BASIC EQUATIONS

The conservation equations developed are expected to be applicable to a wide range of reactor transients including steam generator transients. An attempt has been made to write the equations in their most general form, so they can easily accommodate future modifications and model improvements.

7-3. Continuity Equations

The one-dimensional continuity equations for the liquid water, steam vapor, and noncondensible gas field are as follows:

$$\frac{\partial}{\partial t}(\rho_{\ell}\alpha_{\ell}) + \frac{\partial G_{\ell}}{\partial z} = \Gamma_{\ell} + S_{\ell} \tag{7-1}$$

$$\frac{\partial}{\partial t}(\rho_{v}\alpha_{v}) + \frac{\partial G_{v}}{\partial z} = \Gamma_{v} \tag{7-2}$$

$$\frac{\partial}{\partial t}(\rho_{h}\alpha_{h}) + \frac{\partial G_{h}}{\partial z} = S_{h} \tag{7-3}$$

where

ρ = density (lbm/ft^3)

α = volumetric fraction or concentration

G = mass flux (lbm/ft^2-sec)

Γ = mass generation rate as a result of phase transition (lbm/ft^3-sec)

S = external mass source term (due, for instance, to mass injection into the system) (lbm/ft^3-sec)

t = time (sec)

z = space coordinate measured along loop components (ft)

ℓ = liquid water

v = steam vapor

h = noncondensible gas (for example, helium)

Also, equations (7-1), (7-2), and (7-3) imply that there is no steam injection ($S_v = 0$), and there is no phase transition for the noncondensible gas field ($\Gamma_h = 0$).

The volumetric concentrations, of course, must add up to unity:

$$\alpha_\ell + \alpha_v + \alpha_h = 1 \tag{7-4}$$

and the mass generation rates due to phase transition must be related by

$$\Gamma_\ell = -\Gamma_v \tag{7-5}$$

Also, it is apparent from the above equations that the cross-sectional variations of all flow parameters are neglected. For example, in terms of the drift flux formulation originally proposed by Zuber and Findley,[1] the distribution coefficient, C_o, which describes the cross-sectional variation of volumetric concentrations and mixture velocity, is assumed to be equal to unity.

The phase velocities, drift velocities, volumetric flux, and mass flux are related by the following equations:

$$j_v = \alpha_v u_v \tag{7-6}$$

$$j_\ell = \alpha_\ell u_\ell \tag{7-7}$$

$$j_h = \alpha_h u_h \tag{7-8}$$

---

1. Zuber, N., and Findley, J., "Average Volumetric Concentrations in Two-Phase Flow Systems," J. Heat Transfer 87, 453, 1965.

$$j = j_v + j_\ell + j_h \tag{7-9}$$

$$G_v = \rho_v j_v \tag{7-10}$$

$$G_\ell = \rho_\ell j_\ell \tag{7-11}$$

$$G_h = \rho_h j_h \tag{7-12}$$

$$G = G_v + G_\ell + G_h \tag{7-13}$$

$$u_v = j + \alpha_\ell u_{v\ell} + \alpha_h u_{vh} \tag{7-14}$$

$$u_\ell = j + \alpha_v u_{\ell v} + \alpha_h u_{\ell h} \tag{7-15}$$

$$u_h = j + \alpha_v u_{hv} + \alpha_\ell u_{h\ell} \tag{7-16}$$

$$u_{vj} = u_v - j = \alpha_\ell u_{v\ell} + \alpha_h u_{vh} \tag{7-17}$$

$$u_{\ell j} = u_\ell - j = \alpha_v u_{\ell v} + \alpha_h u_{\ell h} \tag{7-18}$$

$$u_{hj} = u_h - j = \alpha_v u_{hv} + \alpha_\ell u_{h\ell} \tag{7-19}$$

$$G_v = \rho_v \alpha_v (j + u_{vj}) \tag{7-20}$$

$$G_\ell = \rho_\ell \alpha_\ell (j + u_{\ell j}) \tag{7-21}$$

$$G_h = \rho_h \alpha_h (j + u_{hj}) \tag{7-22}$$

where

j = volumetric flux (ft^3/ft^2-sec or ft/sec)

u = velocity (ft/sec)

$u_{\gamma\beta}$ = relative velocity between γ and β phases, γ, β = v, h, or ℓ (ft/sec)

$u_{\gamma j}$ = drift velocity for γ phase, γ = v, ℓ, or h (ft/sec)

Elimination of the $\partial\alpha_\gamma/\partial t$ terms from equations (7-1), (7-2), and (7-3) gives an equation describing the variation of j (the mixture velocity or volumetric flux) along the loop components:

$$\sum_{\gamma=v,\ell,h}\left[\frac{1}{\rho_\gamma}\frac{\partial}{\partial_z}(\rho_\gamma\alpha_\gamma j)\right]=\sum_{\gamma=v,\ell,h}\left[-\frac{1}{\rho_\gamma}\frac{\partial}{\partial_z}(\rho_\gamma\alpha_\gamma u_{\gamma j})-\frac{\alpha_\gamma}{\rho_\gamma}\frac{\partial\rho_\gamma}{\partial_t}+\frac{\Gamma_\gamma}{\rho_\gamma}+\frac{S_\gamma}{\rho_\gamma}\right] \quad (7\text{-}23)$$

Equation (7-23) and equations (7-1) and (7-2) are to be solved simultaneously with known physical properties and with appropriate models for the drift velocity ($u_{\gamma j}$) or relative velocities ($u_{\gamma\beta}$) in order to predict the system transients and void distributions. When the predictions of the code are compared with data, the results of the comparisons can be used to study the sensitivity and to evaluate or verify various drift velocity and slip models.

The solution methods are described in more detail later in this section and in appendix H; the drift velocity or relative velocity (slip) models used are described in paragraphs 7-7 through 7-10.

7-4. Energy Equation

The computer code which was developed has the potential to handle general situations where all phases are not in thermal equilibrium, and heat transfer and phase-transition occur among all applicable phases. For the present application, however, simplifying assumptions have been made and only the following cases are considered:

- The enthalpy of the noncondensible gas field is neglected; that is, the energy equation for the noncondensible gas field is ignored.

- The energy equation for the liquid water field is

$$\frac{\partial}{\partial_t}(\alpha_\ell \rho_\ell h_\ell) + \frac{\partial}{\partial_z}(G_\ell h_\ell) = \dot{q}'''_\ell + S_\ell h_{in_\ell} \qquad (7\text{-}24)$$

where

h = enthalpy (Btu/lbm)

q'''_ℓ = total heat addition rate to the liquid per unit channel volume (Btu/ft^3-sec)

h_{in} = enthalpy of fluid injected into the system (Btu/lbm)

The above equation is applicable to single-phase liquid water flow, and to two-phase steam-water flow where no phase transition occurs and the wall-liquid and steam-liquid heat transfer is assumed to be described collectively by q'''_l.

- When steam and liquid water coexist and boiling takes place, it is assumed that

$$h_v = h_{sat_v} \qquad (7\text{-}25)$$

$$h_\ell = h_{sat_\ell} \qquad (7\text{-}26)$$

$$\Gamma_v = -\Gamma_\ell = \frac{\dot{q}'''_\ell}{h_{\ell v}} \qquad (7\text{-}27)$$

where

h_{sat} = enthalpy at saturation conditions (Btu/lbm)

$h_{\ell v}$ = latent heat of steam generation (Btu/lbm)

- Steam condensation is calculated by an input model and is described in paragraph 7-9.

For the single-phase liquid water natural circulation mode, only equation (7-24) is required. The value for q'''_ℓ in the rod bundle is from input

power; q_ℓ''' in the steam generator U-tubes is obtained by an input heat transfer model described in paragraph 7-9, and q_ℓ''' is zero elsewhere in the loop.

For the two-phase natural circulation mode, calculations are performed as follows:

- In the rod bundle flow channel and below the saturation line, equation (7-24) is used (with $S_\ell = 0$, and q_ℓ''' obtained from bundle power) to calculate the enthalpy rise of the liquid until it reaches saturation.
- In the rod bundle flow channel and above the saturation line, equations (7-25) through (7-27) are used to calculate the steaming rate.
- Adiabatic conditions are assumed for the rest of the loop except in the steam generator U-tubes.
- In the steam generator U-tubes, as mentioned above, the steam condensation rate is calculated by an input model as described in paragraph 7-9. The liquid enthalpy change is calculated by the same method as in the single-phase mode.

7-5. Momentum Equation

The standard assumption of neglecting the pressure variation across the flow cross-sectional area is employed. The mixture momentum equation is then written as

$$\Delta P = \frac{\partial G}{\partial t}\Delta z - \Delta\left(\frac{G^2}{\rho_m}\right) - \frac{4\tau_w}{D_h}\Delta z + (\rho_v\alpha_v + \rho_\ell\alpha_\ell + \rho_n\alpha_h)\, g\, \hat{z}\cdot\hat{g}\, \Delta z + (\Delta P)_s + (\Delta P)_f \qquad (7\text{-}28)$$

where

ΔP = total pressure drop across an increment loop component of length Δz (lbm/ft-sec^2)

Δz = length of reactor component increment (ft)

ρ_m = mixture momentum flux density [described in equation (7-29) (lbm/ft^3)]

τ_w = wall friction shear stress ($lbm/ft\text{-}sec^2$)

D_h = hydraulic diameter (ft)

g = gravitational acceleration (ft/sec^2)

$\hat{z} \cdot \hat{g}$ = cosine of the angle of inclination of Δz

$(\Delta P)_s$ = pressure drop due to fluid injection ($lbm/ft\text{-}sec^2$)

$(\Delta P)_f$ = pressure drop due to form loss, such as area changes ($lbm/ft\text{-}sec^2$)

The mixture momentum flux density is defined as

$$\frac{1}{\rho_m} = \sum_{\gamma=v,\ell,h} \frac{X_\gamma^2}{\rho_\gamma \alpha_\gamma} \tag{7-29}$$

where the flow quality X is defined as

$$x_\gamma = \frac{G_\gamma}{G} \quad , \gamma=v,\ell,h \tag{7-30}$$

The frictional pressure drop is evaluated by

$$\tau_w = \frac{1}{2} (C_f)_{\ell o} \frac{G^2}{\rho_\ell} \phi^2_{\ell o} \tag{7-31}$$

where

$$(C_f)_{\ell o} = 0.316 \, (Re)_{\ell 0}^{-0.25} \tag{7-32}$$

$$(Re)_{\ell o} = \frac{G D_h}{\mu_\ell} \tag{7-33}$$

The two-phase friction multiplier $\phi^2_{\ell o}$ is supplied by an input model[1] described in paragraph 7-9.

---

1. In fact, the entire expression for the two-phase wall shear stress τ_ω can be calculated by a user input model.

Pressure drop due to mass injection is neglected in the present calculations. The only loss coefficients considered in the present calculations are the following:

- At the loop seals of both broken and unbroken loops, where

$$K_{IL} = K_{BL} = 15 \tag{7-34}$$

$$(\Delta P_F)_{\substack{\text{loop}\\\text{seal}}} = -\frac{1}{2} K \rho j^2 \tag{7-35}$$

- At the crossover leg with

$$K_{CO} = 5 \tag{7.36}$$

and

$$(\Delta P_F)_{\substack{\text{cross-}\\\text{over}}} = -\frac{1}{2} K_{CO} \rho j^2 \tag{7-37}$$

7-6. Equation of State

The above conservation equations are supplemented by the equation of state:

$$\rho = \rho (P,h) \tag{7.38}$$

Other physical properties (such as viscosity and specific heat) are evaluated as a function of the system pressure and fluid enthalpy (or temperature).

It is apparent from the above descriptions that, to solve the conservation equations, one must supplement the equations with at least four hydrodynamic and heat transfer models:

- A drift velocity or slip model for the relative velocities between the gas phases and the liquid phase
- A heat transfer model between the liquid water and the steam-generator U-tube walls

- o A steam condensation model in the steam generator U-tubes
- o A model for the two-phase friction multiplier

In the following paragraphs, the models chosen in the present calculations are described. The numerical methods used to solve the system of conservation equations are described in appendix H.

7-7. ANALYSIS AND DATA COMPARISONS

As mentioned in previous paragraphs, considerable unforeseen difficulties were encountered in developing a stable convergent numerical solution for the model. Also, little time could be devoted to mechanistic hydrodynamic and heat transfer model developments. Therefore, only very limited predictions can be presented here; they represent an attempt to demonstrate the potential capabilities of the predictive code.

7-8. Single-Phase Natural Circulation Mode

Little problem was encountered in analyzing the single-phase natural circulation mode. A mode for the steam generator heat transfer was required. The analysis was performed for the following two cases:

- o Uniform constant heat sink in the steam generators
- o Heat sink in the steam generator calculated by

$$\dot{q}_{\ell}''' = h_{SG} (T_p - T_{REF}) \qquad (7\text{-}39)$$

where

h_{SG} = heat transfer coefficient in the steam generators (Btu/ft^3-sec-°F)

T_p = primary fluid temperature (°F)

T_{REF} = reference secondary heat sink temperature (°F)

The heat transfer coefficient, h_{SG}, was assumed to be a constant, and was a user input. In the present analysis, h_{SG} was obtained by examining test data and by fitting the predictions with data.

T_{REF} was simply taken to be the steam generator secondary fluid temperature at the outlet. Also, the flow was assumed to split uniformly among all steam generator U-tubes (since no data have shown otherwise); this assumption saves considerable computing time.

Test run 50708 was analyzed with the results shown in f'gures 7-1 and 7-2. In both these figures, a "pump" was first turned on to drive the flow. In the numerical analysis, the pump was simulated simply by adding an input ΔP of 7 kPa (1 psi) at the crossover leg. It was found that this particular value of pump power gave about the same forced flow around the loop as indicated by actual test data. After the forced flow became steady, the pump was turned off and the flow started to be driven only by the hydrostatic head difference around the loop.

Figure 7-1 shows that when the heat sink is constant in the steam generators, the system undergoes a smooth transient with a period of about 15 minutes. In figure 7-2, the heat sink and the primary fluid temperature are coupled by means of equation (7-39). The system undergoes more rapid oscillations with smaller amplitudes before becoming steady. Because figure 7-2 simulates the actual phenomena better, it represents a better prediction. Also, the analysis predicted a flow split ratio of about 3:1 between the unbroken and broken loops, which agrees well with the test data.

7-9. Two-Phase Natural Circulation Mode

Because of numerical instability problems, a full anlysis for two-phase situations is not possible at this writing. The code was used to study the following two cases:

- Calculating void fraction distributions around the loop, given the system flow
- Predicting the two-phase system flow

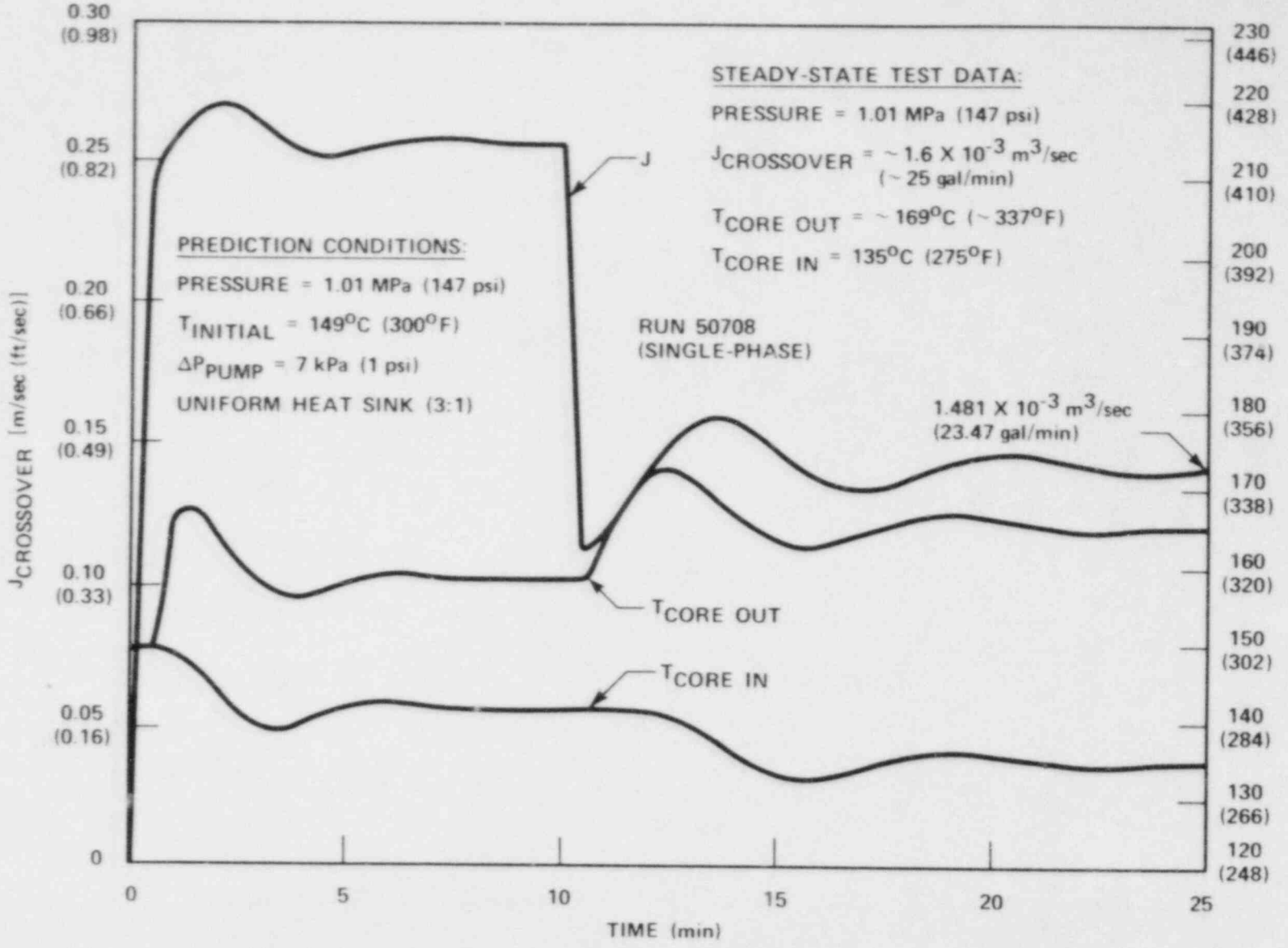

Figure 7-1. Single-Phase Predictions With Uniform Heat Sink in Steam Generator

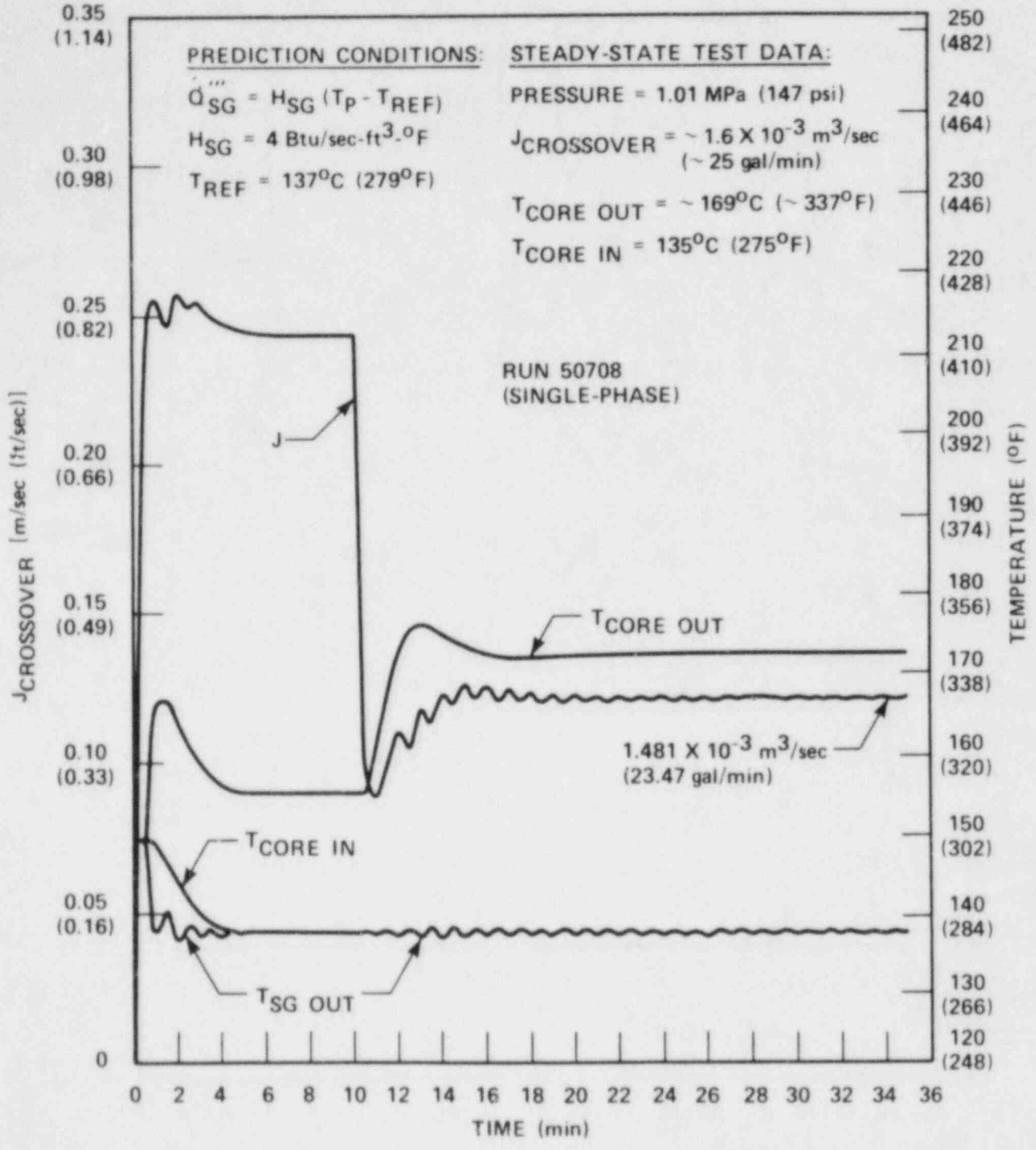

Figure 7-2. Single-Phase Predictions With Input Heat Transfer Coefficient in Steam Generator

In the analysis, however, a steam generator heat transfer model, a hydrodynamic slip or drive velocity model, and a two-phase friction model were required. Because of lack of time for an extensive model development effort, the following simple models and assumptions were used.

For simplicity, instead of a heat transfer model, steam was assumed to condense in the steam generator at a rate proportional to the local void fraction:

$$\Gamma_v = -K \frac{\rho_v \alpha_v}{\delta t} \tag{7-40}$$

When the two-phase natural circulation flow is at its peak value, all steam will be condensed at the uphill side of the U-tubes, and the downhill side of the U-tubes will be practically water solid. Therefore, the constant K in equation (7-40) is given a higher value at the uphill side than at the downhill side so that the desirable two-phase peak void distribution in the U-tubes can be achieved.

To calculate the slip between the gas and liquid phases for vertical components, the correlation recommended by Holmes[1] was used. This correlation was chosen because of its validity for the entire range of void fraction and for its simplicity of application:

$$V_{gj} = \frac{(1-\alpha C_o)\, C_o\, K(\alpha)\, u_c}{\alpha C_o \sqrt{\frac{\rho_g}{\rho_\ell}} + 1 - \alpha C_o} \tag{7-41}$$

The distribution coefficient, C_o, was assumed to be 1 in equation (7-41), and $K(\alpha)$ is void fraction dependent:

$$K(\alpha) = 1.53 \qquad , \; 0 \leq \alpha < \alpha_1$$

---

1. Holmes, J. A., "The Drift Flux Correlation in RELAP-UK," AEEW-R1143.

$$K(\alpha) = \frac{1.53\ (\alpha_2 - \alpha)^2 + Ku\ (\alpha - \alpha_1)^2}{(\alpha_2 - \alpha)^2 + (\alpha - \alpha_1)^2} \quad , \alpha_1 \leq \alpha < \alpha_2 \tag{7-42}$$

$$K(\alpha) = Ku \quad , \alpha_2 \leq \alpha < 1$$

The recommended value of α_1 is 0.05 and of α_2, 0.03 except at low pressure [no higher than 0.34 MPa (50 psia)], where the value of α_2 = -0.15 is recommended. The value of u_c is calculated by

$$u_c = \left[\frac{\sigma g\ (\rho_\ell - \rho_v)}{\rho_\ell^2}\right]^{0.25} \tag{7-43}$$

and σ = surface tension (lbm/sec^2).

Finally, Ku is the critical Kutateladze number and is related to the dimensionless pipe or hydraulic diameter, D*, as tabulated in table 7-1:

$$D^* = \sqrt{\frac{g(\rho_\ell - \rho_v)}{\sigma}}\ D_h \tag{7-44}$$

TABLE 7-1

VALUES OF CRITICAL KUTATELADZE NUMBER

D*	≤ 2	4	10	14	20	28	≥ 50
Ku	0	1.0	2.1	2.5	2.8	3.0	3.2

For horizontal two-phase flow, which occurs only at the hot legs since practically all steam is condensed in the steam generator, it was simply assumed that the gas and liquid move at the same velocity.

To calculate the friction for two-phase flow, a simple two-phase friction multiplier was used:

$$\phi_{\ell o}^2 = \left[1 + X\left(\frac{\rho_\ell}{\rho_v}\right)\right]\left[1 + X\left(\frac{\mu_v}{\mu_\ell} - 1\right)\right]^{0.25} \qquad (7\text{-}45)$$

For void distribution calculations, test runs 50708 and 52613 were analyzed. However, the broken loop of the FLECHT SEASET facility stalled during operation of the two-phase natural circulation mode. The present code does not have a mechanistic mode to predict such a phenomenon. Hence, in the two-phase analysis, the broken loop was simply discarded and, as in the single-phase case, the flow split among U-tubes in the steam generator was assumed to be uniform. That is, a single-tube steam generator model was used. The results are shown in figures 7-3 and 7-4.

As mentioned above, to condense most of the steam on the uphill side of the steam generator U-tubes, a K value (equation (7-40)) must be chosen carefully. It was found that a K value of 5 on the uphill side and a K value of 1 on the downhill side of the steam generator will condense more than 90 percent of the steam when the flow goes uphill. Although it cannot be verified by data, the void distributions shown in the figures are thought to resemble quite closely the actual void distributions in the natural circulation loop under two-phase peak flow conditions. [Except perhaps in the actual system, no steam (zero void) will be coming out of the steam generators; in the present calculations, steam comes out of the steam generator with a void fraction of 1 to 2 percent.] Figures 7-5 and 7-6 show the steam condensation rate in the steam generator U-tubes as calculated by equation (7-40), plotted together with the void distributions for comparison. The discontinuities of the void distributions that appear at the fluid volumes are due to differences in the relative velocities between steam and liquid water in different flow channels, which cause accumulation or depletion of void in the fluid volumes connecting these flow channels.

Test run 50708 was analyzed to predict the system flow rate using the momentum equation. The prediction methods are described in detail in appendix H; it is useful to mention here that the flow velocity at the crossover leg was iterated until the total pressure drop around the loop was zero. The results are shown in figure 7-7. The predicted flow at the crossover leg was 0.67 m/sec

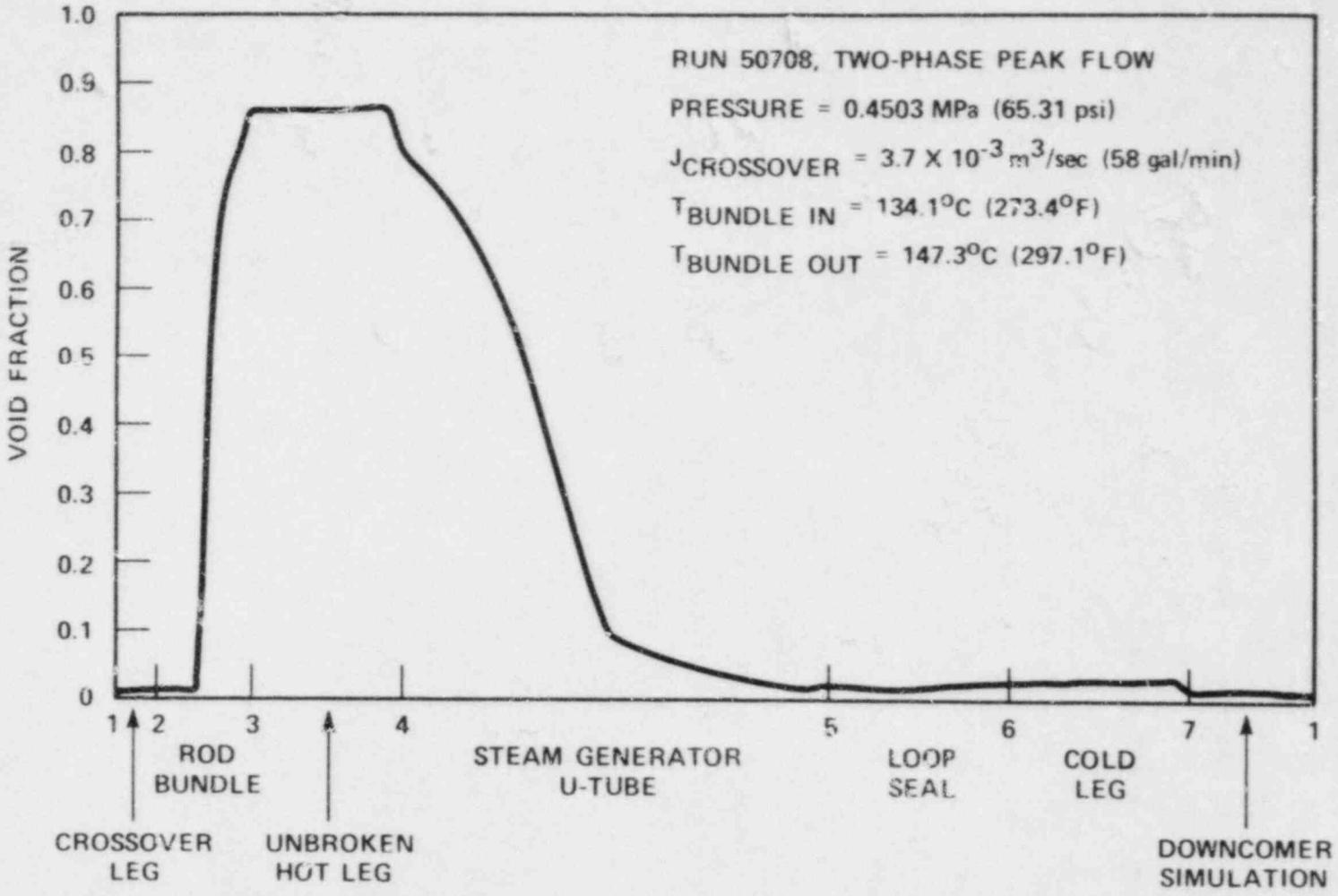

Figure 7-3. Void Fraction Distributions for Two-Phase Peak Flow Conditions (Run 50708)

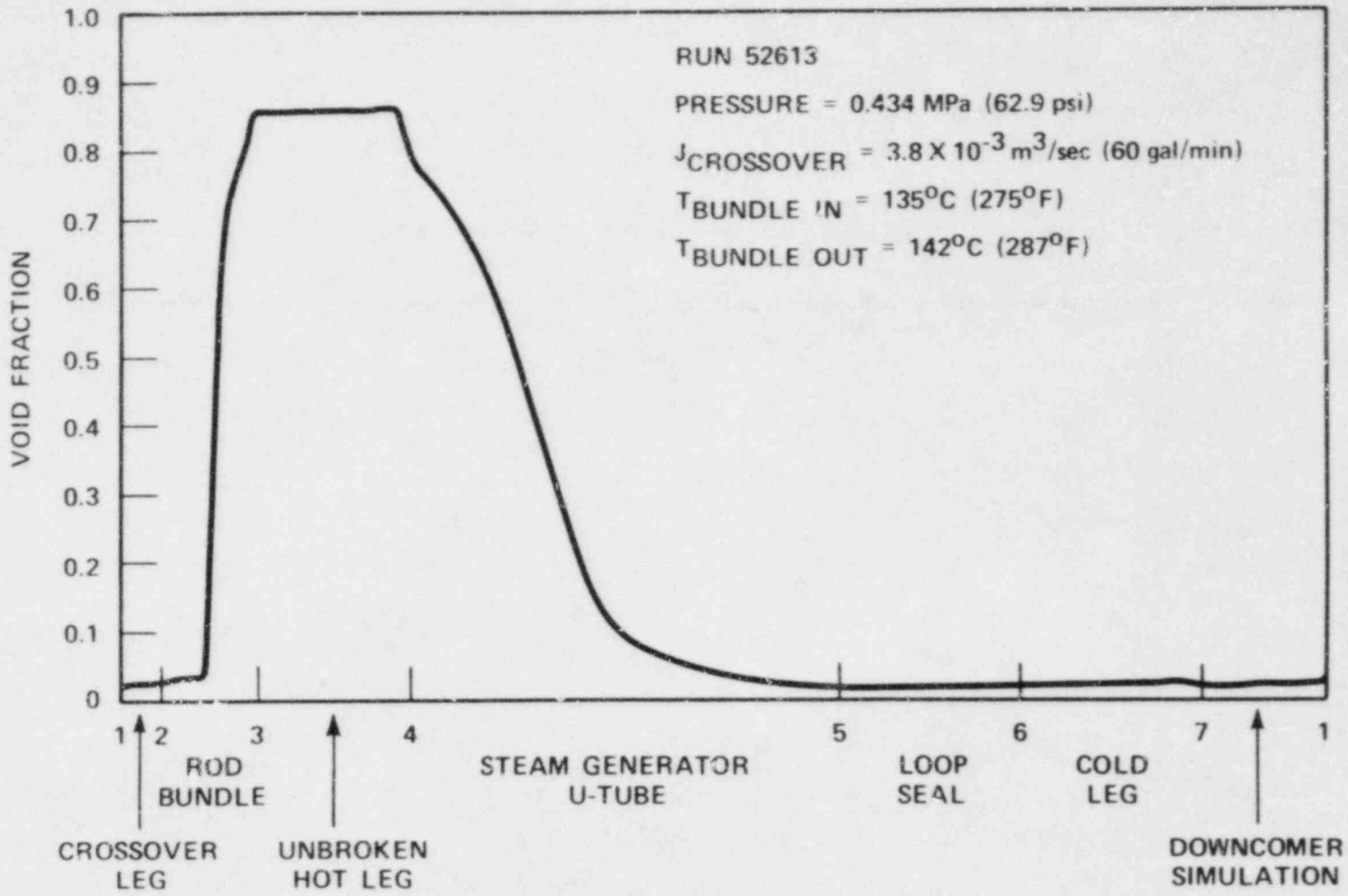

Figure 7-4. Void Fraction Distributions for Two-Phase Peak Flow Conditions (Run 52613)

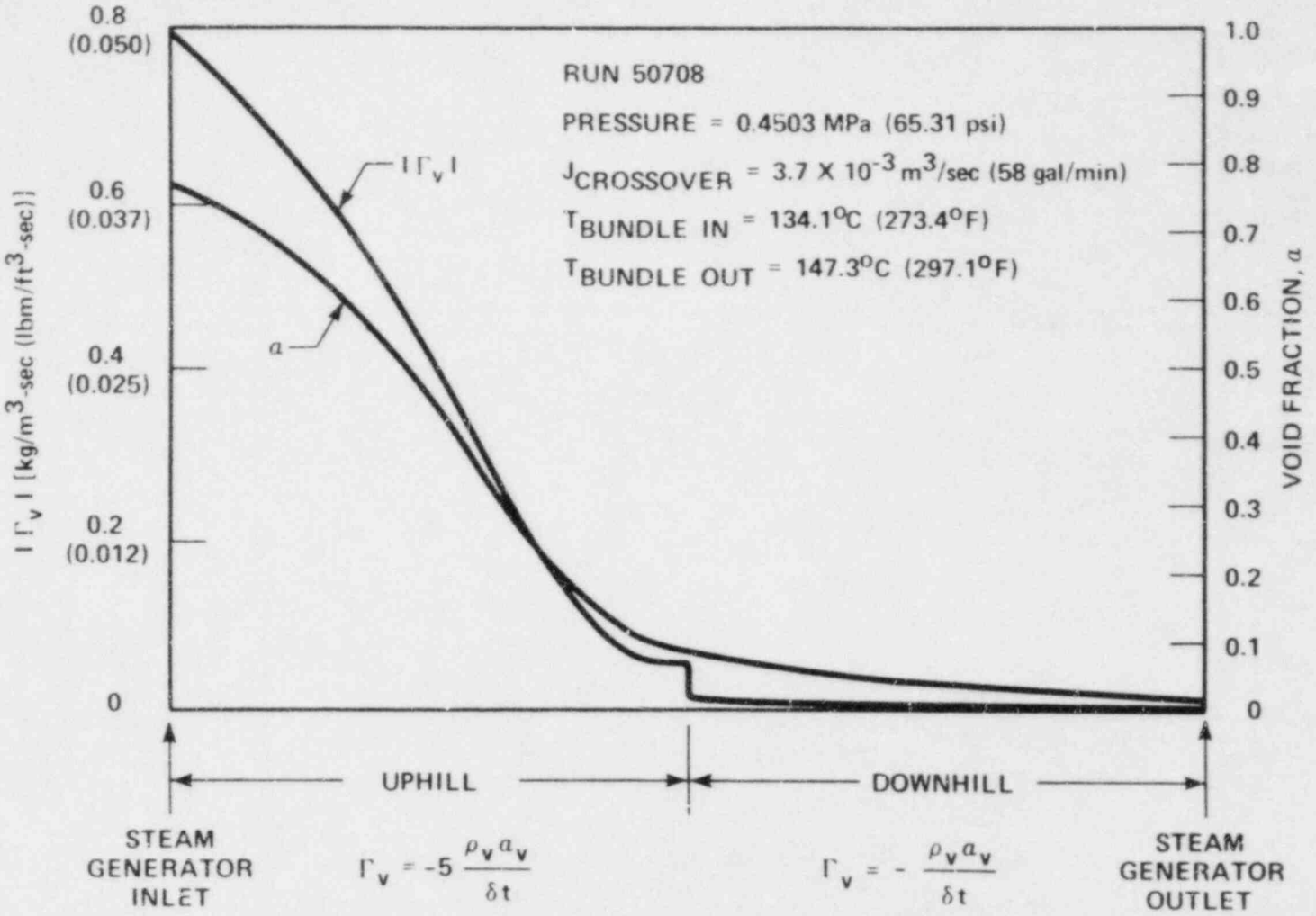

Figure 7-5. Steam Condensation Rate and Void Fraction Distributions in Steam Generators (Run 50708)

6485B-13

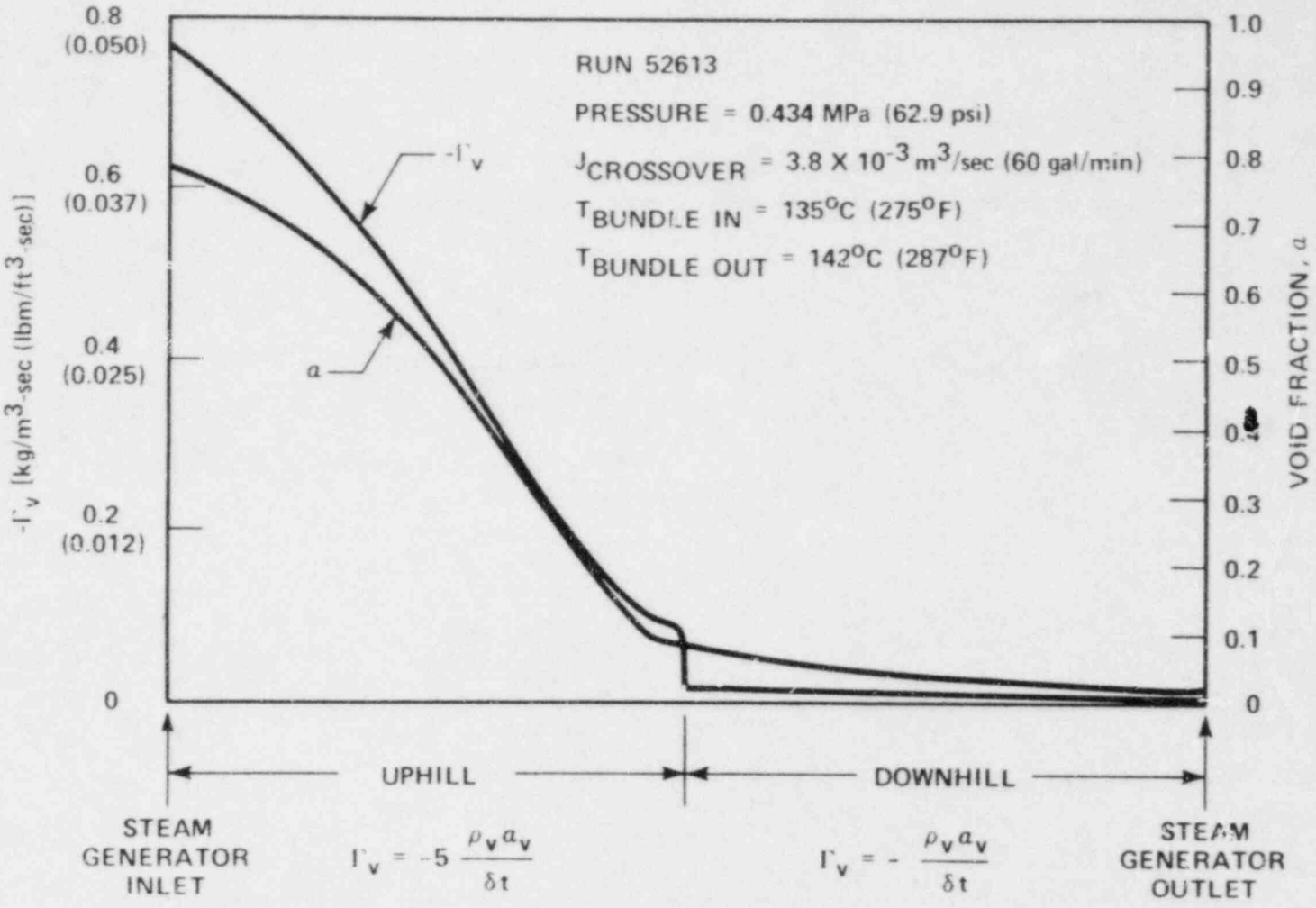

Figure 7-6. Steam Condensation Rate and Void Fraction Distributions in Steam Generators (Run 52613)

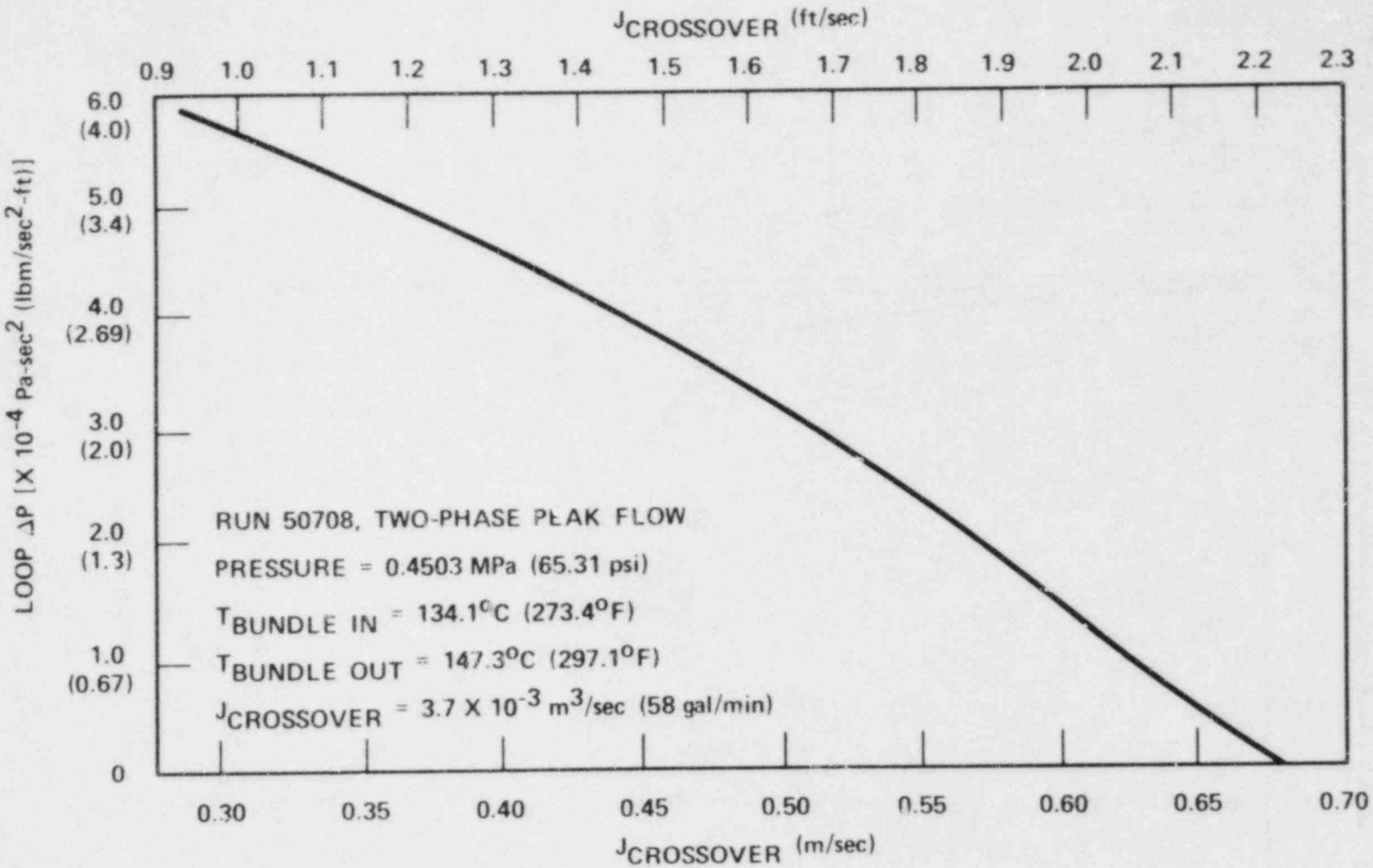

Figure 7-7. Variation of Total Pressure Drop Around Loop Versus Mixture Flow at Crossover Leg

or 8.7×10^{-3} m^3/sec (2.2 ft/sec or 138 gal/min), more than twice the measured two-phase peak flow rate of about 3.7×10^{-3} m^3/sec (58 gal/min). Although several factors could have contributed to the discrepancy between the prediction and data (for example, form losses in the fluid volumes were neglected), the most significant contribution of error seems to have come from the calculation of friction. (After all, the present calculation is essentially a balance between friction and hydrostatic pressure.) A sensitivity of the two-phase friction multiplier was performed as follows. The two-phase friction multiplier (equation (7-45)) was multiplied by a constant:

$$\Phi^{*}_{\ell o}{}^{2} = K^{*} \Phi^{2}_{\ell o} \tag{7-46}$$

K* was then varied between 1.0 and 10, and the total pressure drop around the loop was calculated using the measured flow rate of 3.7×10^{-3} m^3/sec (58 gal/min) at the crossover leg. The results are plotted in figure 7-8.

Figure 7-8 is interpreted as follows. Using the measured flow rate from data and a two-phase friction multiplier of

$$\Phi^{*}_{\ell o}{}^{2} = 3.8 \Phi^{2}_{\ell o} \tag{7-47}$$

where $\Phi^{2}_{\ell o}$ is give by equation (7-45), the friction and hydrostatic pressure head will just balance each other around the loop. Conversely, if equation (7-47) was used to predict the system flow using the same method as in figure 7-7, one would have predicted the system flow correctly.

7-10. Two-Phase Natural Circulation With Helium Injection

One of the objectives was to study the effects of noncondensible gas injection on system natural circulation behavior. However, because of unresolved numerical problems and lack of an adequate model to describe the possibility of trapping the noncondensible gas tat the U-tubes, any noncondensible gas injected into the system was simply calculated to be entrained by the liquid and kept circulating around the loop. More modeling effort is required to make full use of the code developed.

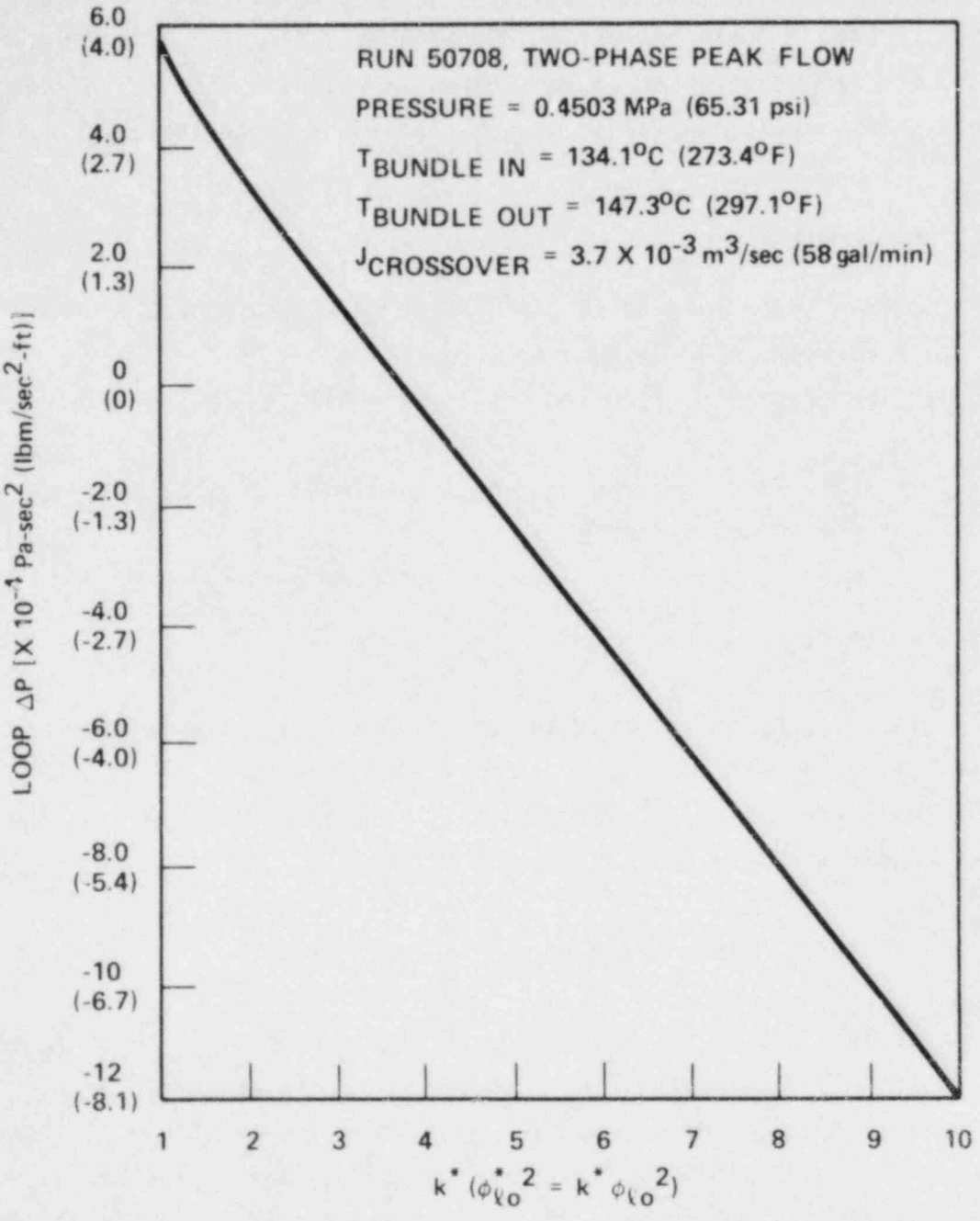

Figure 7-8. Variation of Total Pressure Drop Around Loop Versus Two-Phase Friction Multiplier

7-11. RECOMMENDATIONS FOR FUTURE WORK

Although only limited analysis is possible at this time, it is apparent from the work already done that the code developed can be turned into a valuable analysis tool if the numerical problems are corrected and mechanistic thermal-hydraulic models are developed. The following modifications are particularly recommended to improve the code:

- Numerical convergence problems must be solved so that the code can handle multitube steam generator models.
- The steam generator heat flux analysis presented in this report and other information available in the literature should be used to develop a mechanistic model or a data-based correlation for steam generator heat removal under similar natural circulation conditions.
- Drift velocities or relative velocities as affected by the presence of noncondensible gas field should be studied carefully. Especially, a model should be developed to predict the possibility of trapping the helium at the steam generator U-tube bends.
- Special attention should be directed to the frictional pressure drop calculations, especially in the steam generator U-tubes. The present analysis seems to indicate that homogeneous two-phase friction multipliers such as that in equation (7-45) are not adequate to predict the system natural circulation flow.

SECTION 8
CONCLUSIONS AND RECOMMENDATIONS

8-1. CONCLUSIONS OF PRESENT STUDY

The FLECHT SEASET natural circulation tests confirm that stable cooling can be achieved with less than a full primary system in different natural circulation cooling modes. Although the mass inventories were different in the FLECHT SEASET tests for a given mode of two-phase cooling as compared to those in other facilities, such as the Semiscale and PKL facilities, it is felt that this was a result of the lower system pressures used in the FLECHT SEASET tests.

The single-phase natural circulation tests performed as expected and the power-flow relationships verified single-phase natural circulation calculational methods given in such texts as Lewis.[1] Cooling remained stable for such parametric tests as cold leg injection, upper plenum injection, and noncondensible gas injection. When the heat sink was decreased, the primary system pressurized as expected, but quickly returned to its steady pressure when the steam generator feed flow was reintroduced. One piece of information which was interesting and had not been previously shown in other experiments was the large thermal stratification in single-phase natural circulation, which occurred in the hot legs. There was as much as 11°C (20°F) temperature difference between the top and bottom of the hot leg. The flow entered the steam generator with a reduced stratification. The heat flux calculation confirmed the original hypothesis that most of the heat was transferred to the secondary side at the steam generator inlet below 1.22 m (4 ft). Reverse heat transfer (secondary to primary) was also calculated to occur.

It was found that the FLECHT SEASET two-phase natural circulation tests had a peak flow with a lower system inventory as compared to other tests. The two-phase loop flow curve as a function of mass inventory showed the same

---

1. Lewis, E. E., Nuclear Reactor Safety, Academic Press, 1975

behavior as previous Semiscale, PKL, and SRI tests; namely, as the mass inventory initially decreased, the loop flow increased because of the hot side voiding.

The peak flow occurred with a mass inventory of approximately 85 percent. As the mass was further drained, the loop flow would decrease until reflux was obtained at inventories of 35 to 45 percent. The amount of mass that had to be drained to reach these states was larger than that in Semiscale and PKL but similar to that in the SRI tests. The differences between FLECHT SEASET, Semiscale, and PKL are most likely due to the pressure difference between the test facilities. The FLECHT SEASET and SRI mass inventories were similar because both facilities had lower pressure.

There were scaling effects which did affect the system behavior in the FLECHT SEASET tests. When the system progressed through the two-phase natural circulation cooling transient as mass was drained, the broken loop stalled, became inactive, and then became active at later times after the peak two-phase flow point had been reached. It is believed that the hot leg diameter difference between the broken and unbroken loops is responsible for the preferential stalling of the smaller broken loop. Since the bottoms of the pipes were maintained at the same elevation, the larger unbroken loop could uncover and take more than its scaled fraction of steam flow, and thus stall the broken loop. Alignment of the pipe bottoms is the proper approach for a reflood systems effects test. If the pipe top surfaces were aligned, this might not have occurred.

Another flow transient which occurred during reflux condensation and which is believed to have been caused by the low pressure in the facility is the loop seal blow-through. Again, since the loop seal piping was aligned such that the bottom elevations of the pipes were maintained, the larger unbroken loop piping would always blow through. The question of prototypicality of this transient is difficult to answer without a PWR analysis for similar conditions. At this time, it is believed that a PWR would not show such a behavior at nominal small-break LOCA conditions [approximately 8.3 MPa (1200 psia)]. The transient observed in FLECHT SEASET is a result of the larger-than-scaled heat

loss from the cold leg and upper downcomer, which resulted in condensation of the steam space in these regions. The experiments with noncondensible gas during reflux condensation showed that it was the condensation which drove the whole transient. A similar effect of condensation cuasing the loop seal to vent was observed in PKL.[1] Again it should be noted that heater rod bundle coolability was not impaired during this transient, since the loop is a closed system and no mass was lost. This type of transient has not been observed for similar tests in Semiscale which have been performed at higher, more prototypical, pressures and in which trace heating was used.

During two-phase natural circulation, it was found that noncondensible gas injection would act to pressurize the primary system; selected tubes in the steam generator would stall and be gas filled. The primary system pressure would become equal to the original single-phase pressure and the peak two-phase loop flow would decrease to the single-phase value. It was found that small amounts of noncondensible gas injection during reflux condensation would shift the heat flux distribution such that primary side vapor would be condensed on the uphill side of the generator. This is consistent with the observations in the PKL[2] tests and the single-tube experiments by Ripple.[3] As more noncondensibles were injected, the primary pressure increased and the two-phase froth level dropped below the top of the heated length. It is felt that this is a low-pressure effect of the FLECHT SEASET facility; a similar effect would not be expected in a PWR because of the higher system pressure.

The analysis of the steam generator heat transfer data yielded results which gave the overall steam generator heat transfer coefficient as well as the local heat flux distribution. This analysis and these data represent a unique contribution of the FLECHT SEASET program in this area and will help model

---

1. D. Hein, personal communication with S. D. Rupprecht and L. E. Hochreiter.

2. Mandl, R. M., and Weiss, P. A., "PKL Tests on Energy Transfer Mechanisms During Small Break LOCAs," Nuclear Safety 23, No. 2, March-April 1982.

3. Ripple, R., "The Influence of Noncondensible Gases on the Heat Transfer in Steam Generators of Pressurized Water Reactors During a Loss-of-Coolant Accident," PhD thesis, Technical University of Munich, March 1981.

development and assessment activities for these types of experiments. The heat flux calculations confirmed that it was the bottom 1.22 m (4 ft) of the steam generator which was most active as a heat sink. With regard to the steam generator analysis, it is felt that the available data were analyzed as thoroughly as possible and the most important results were obtained.

The steam generator data presented in this report indicate global generator behavior, enable calculation of overall heat transfer coefficients, predict heat flux distributions and their changes with each mode of operation.

8-2. RECOMMENDATIONS

It was apparent from the data analysis reported herein that additional analysis of the data could enhance understanding of observed phenomena. Specific recommendations include the following actions:

- Complete analysis of the noncondensible gas injection data, automate the GOW-MAC readings, and reduce and analyze these data to find which tubes filled with gas.
- Perform single-phase flow calculations using the measured loss coefficients from the shakedown tests.
- Perform PWR calculations for similar transients but at prototypical PWR pressures to ascertain the effects of low pressure on the experimental results relative to the PWR behavior. A more systematic comparison of the FLECHT SEASET, Semiscale, and PKL data would also indicate the effects of low pressure.

The two main areas of uncertainty in the steam generator heat flux calculation are the secondary side fluid temperature distribution and the flow field and temperature distribution in the inlet plenums. An inherent assumption in this data reduction effort is that all tubes in a tube model experience the same secondary side effects, and further, that the flow is evenly split between tube models. The following recommendations are made for future natural circulation tests aimed at investigating more of the physics of this phenomenon:

- A bench model constructed of glass, lexan, or similar material would enable an experimenter to actually see the boiling on the

secondary side, and determine how uniform this is between tubes. Dye injection could possibly be used to characterize the flow field in the inlet plenum. Of particular interest should be the geometry effects in the inlet plenum. That is, a large plenum will act as a "stagnation chamber" and effectively convert incoming velocity head to a pressure head. This would eliminate momentum effects that may carry more flow into some tubes. This study, of course, would not account for the heat transfer differences that occur between tubes and thereby affect the flow, but it would eliminate one uncertainty in computing an axial energy balance on the primary flow.

- Future tests might consider using fewer tubes and more instrumentation per tube. Imbedded wall thermocouples would also reduce the data uncertainty.

- Future tests should be supported by analyses of the inlet plenum and lower portion of the secondary fluid. Although even state-of-the-art codes have difficulty predicting local boiling regimes and the like, it is possible to examine the manner in which cold feedwater distributes itself around tubes at the bottom of the generators. This would remove much of the uncertainty in the primary fluid temperature data at these locations.

APPENDIX A
DATA FROM PARAMETRIC TESTS

The results of the parametric tests are detailed on the following pages. For each test, the objective and test procedure are included along with a test overview; the test schedule precedes the data plots.

Figures A-1 and A-2 show the test facility used and the basic system instrumentation, respectively.

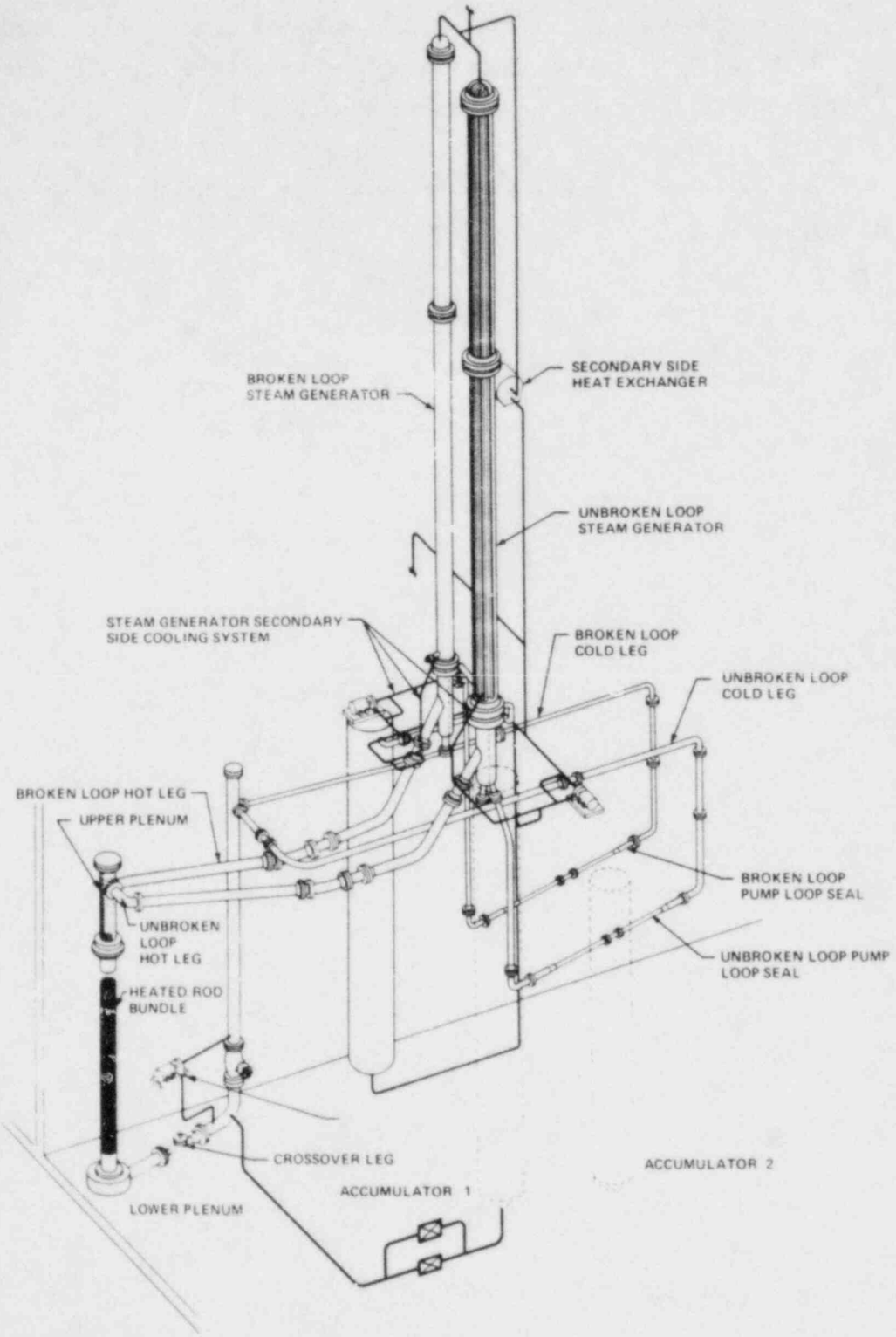

Figure A-1. FLECHT SEASET Systems Effects Natural Circulation and Reflux Condensation Test Facility

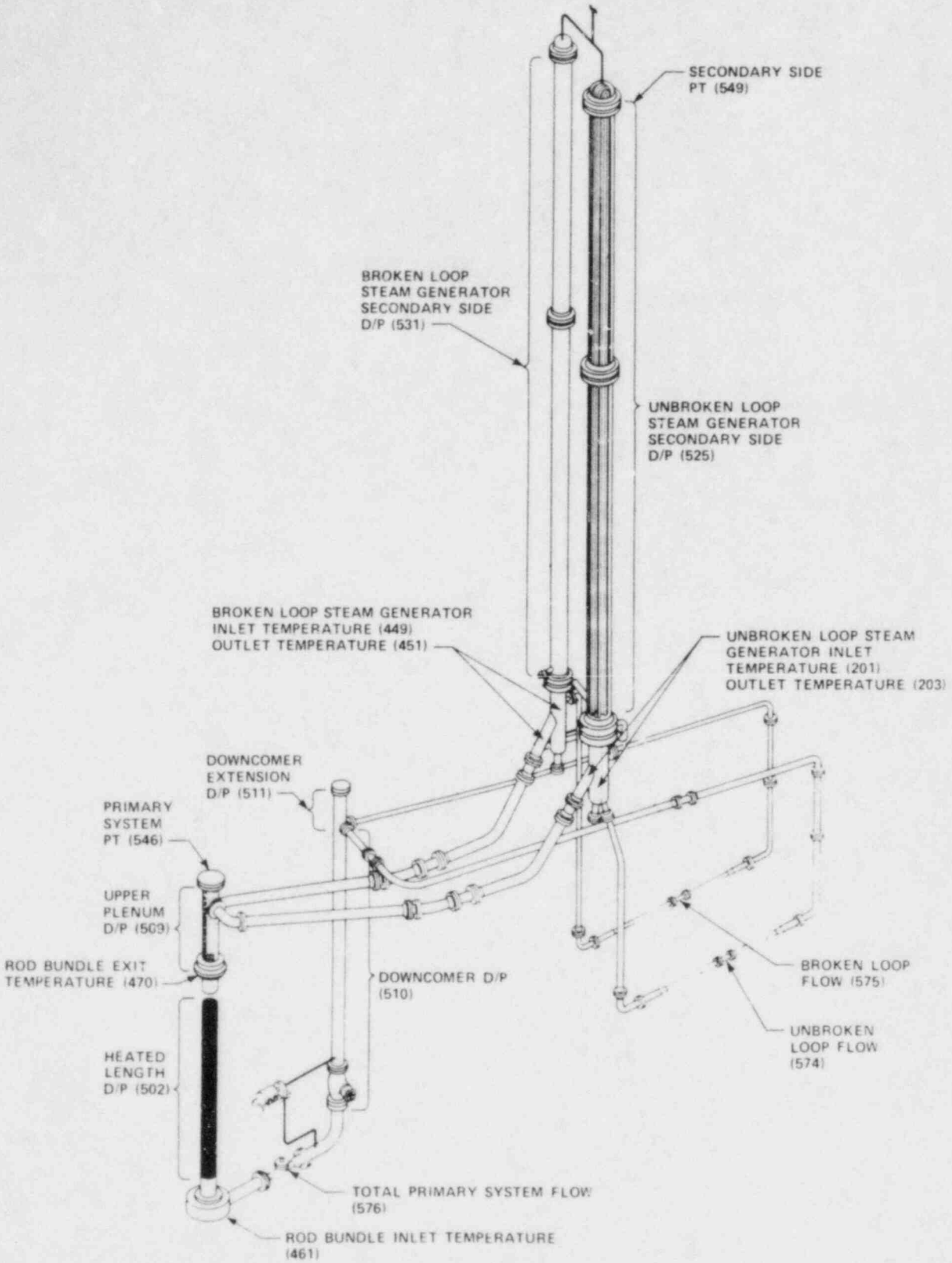

Figure A-2. Natural Circulation Facility Basic System Instrumentation

TEST 5: SINGLE-PHASE NATURAL CIRCULATION COLD LEG INJECTION TEST

Objective

To determine the effects of intact loop cold leg injection on single-phase natural circulation

Test Procedure

The test was begun from a single-phase natural circulation mode with a nominal primary system pressure of 0.52 Mpa (75 psia) and a nominal bundle power of 222 kw (simulated 2 percent of full power). The primary system was operated at 0.52 MPa (75 psia), as opposed to the 0.97 MPa (140 psia) reference condition, to allow primary system pressure margin in the event of a pressure spike during cold leg injection. As a result, the secondary side was operated at atmospheric pressure, as opposed to the 0.28 MPa (40 psia) reference condition, to maintain sufficient primary side subcooling. The secondary side was operated in a feed-and-bleed boiling mode with a constant level being maintained at approximately 7.62 m (25 ft) (71 percent full). Accumulator 1 was used to inject 34°C (93°F) water into the unbroken loop cold leg at a nominal rate of 0.77 kg/sec (1.7 lbm/sec). The duration of the injection was 48 seconds. The pressurizer was valved out of the primary system when cold leg injection was terminated. The test was terminated when the system returned to a steady-state condition.

Test Overview

Prior to the unbroken loop cold leg injection (CLI), the primary system operated in a steady-state single-phase natural circulation mode with a total mass flow rate of 1.5 kg/sec (3.2 lbm/sec) through the rod bundle. Both the unbroken and broken loops were active, with a flow split of 3 to 1, respectively. The single-phase fluid entered tne rod bundle at an average of 111°C (232°F) and exited at an average of 148°C (298°F) [ΔT = 37°C (66°F)]. Use of the measured mass flow rate and the measured rod bundle fluid temperature rise [37°C (66°F)] led to an axial energy balance estimate that 222.8 kw was

removed from the heater rods. This agrees favorably with the measured average of 224 kw of energy input to the rod bundle (0.54 percent difference). Because the primary system was operated at a pressure of 0.52 MPa (75 psia), the inlet and outlet rod bundle temperatures were approximately 22°C (40°F) cooler than those measured in the single-phase portion of reference test 8. The 0.52 MPa (75 psia) primary pressure in conjunction with the 0.11 MPa (16 psia) secondary side pressure resulted in a 5°C (9°F) fluid subcooling at the rod bundle exit. The primary side steam generator inlet plenum temperatures were observed to be, on the average, 6°C (10°F) lower than the rod bundle outlet temperature (3.3 percent difference).

Cold leg injection (CLI) was initiated in the unbroken loop cold leg at 8,984 seconds and was terminated 48 seconds later. The short injection of cold water caused the total flow through the rod bundle to increase momentarily from an average value of 1.5 kg/sec (3.2 lbm/sec) to a peak value of 1.75 kg/sec (3.86 lbm/sec) (20.6 percent increase). The flow then returned to its original 1.5 kg/sec (3.2 lbm/sec) value. The entire cycle lasted for only about 150 seconds. A similar effect was observed in the unbroken loop, and only a small effect was observed in the broken loop.

During the course of the 48-second injection, the CLI system overwhelmed the capability of the pressurizer to control pressure and subsequently pressurized the primary system from 0.52 to 0.77 Mpa (75 to 112 psia). The primary pressure returned to 0.52 MPa (75 psia) upon the termination of CLI. Seconds after CLI was terminated, the pressurizer was valved out of the primary system and the primary pressure began to decrease. At 124 seconds after the termination of CLI, the primary pressure reached a fairly steady value of 0.41 MPa (60 psi). The secondary side was unaffected.

The primary system was unable to recover to its original single-phase mode because of the depressurization of the primary side after the pressurizer was valved out. The saturation temperature at 0.41 MPa (60 psia) is 144.84°C (292.73°F). This represents a 8°C (15°F) reduction in saturation temperature at the rod bundle exit. As a result, the 5°C (9°F) subcooling that originally existed at the rod bundle exit prior to injection no longer existed shortly after the system depressurized to 0.41 MPa (60 psia). Subsequently, voids

began to form at the rod bundle exit. The voiding was initially delayed, however, as cold water from the CLI reached the rod bundle and momentarily decreased the inlet temperature from 111°C to 98°C (232°F to 208°F). This trend was echoed at the rod bundle exit, where the temperature momentarily decreased from 148°C to 142°C (298°F to 288°F). As the CLI cold water was convected through the rod bundle and its effect dissipated through the system, the rod bundle exit temperature gradually increased from its low value of 142°C (288°F) to a value of 144°C (292°F) 210 seconds after CLI was terminated. At this temperature and pressure, voids should be forming at the rod bundle exit. At 278 seconds after CLI termination, voiding was confirmed by the fact that the upper plenum collapsed liquid level began to decrease. The steam generator inlet and outlet plenum temperatures showed no discernible effects from the CLI.

TEST SCHEDULE
TEST 5

Time (sec)	Event
0	Computer on
464	Power to 222 kw; primary system operating in a forced circulation mode
7922	Steady-state single phase natural circulation established at a nominal primary pressure of 0.52 MPa (75 psi)
8984	Began cold leg injection; nominal injection rate = 7.64×10^{-4} m^3/sec (12.1 gal/min)
9032	Ended cold leg injection
9423	Steady-state single-phase natural circulation reestablished
9932	End of test 5

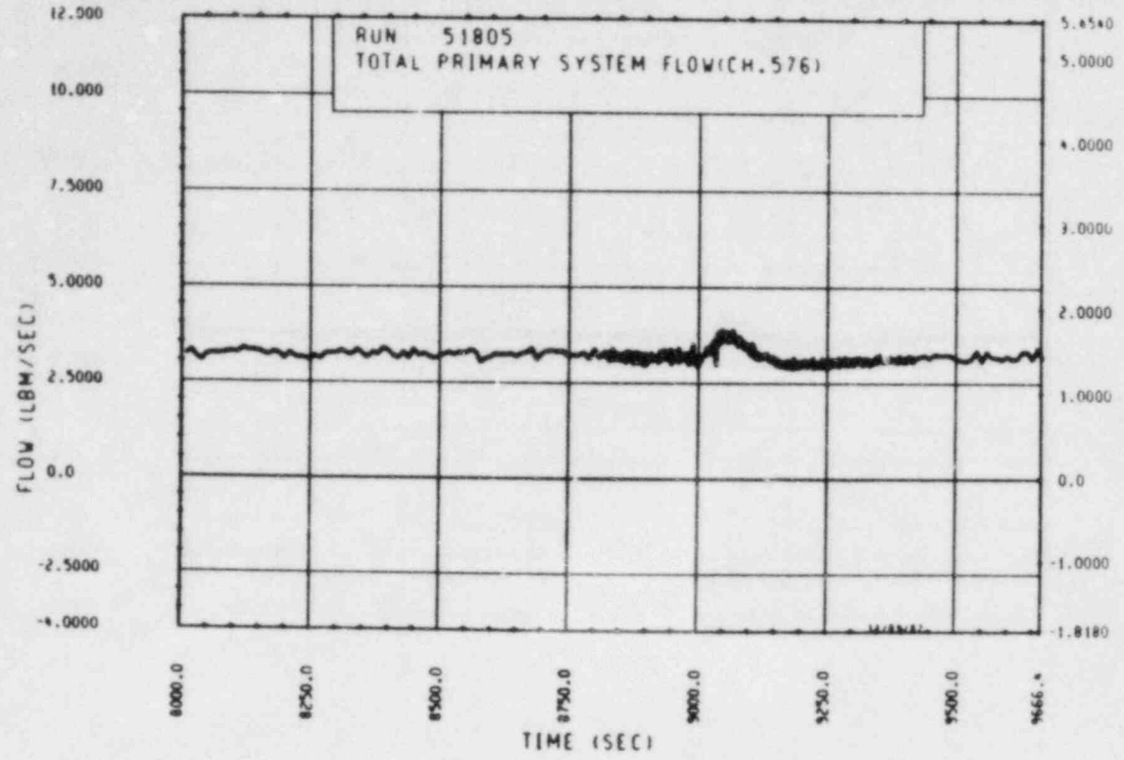

Figure A-3. Mass Flow Rate Through Rod Bundle, Test 5

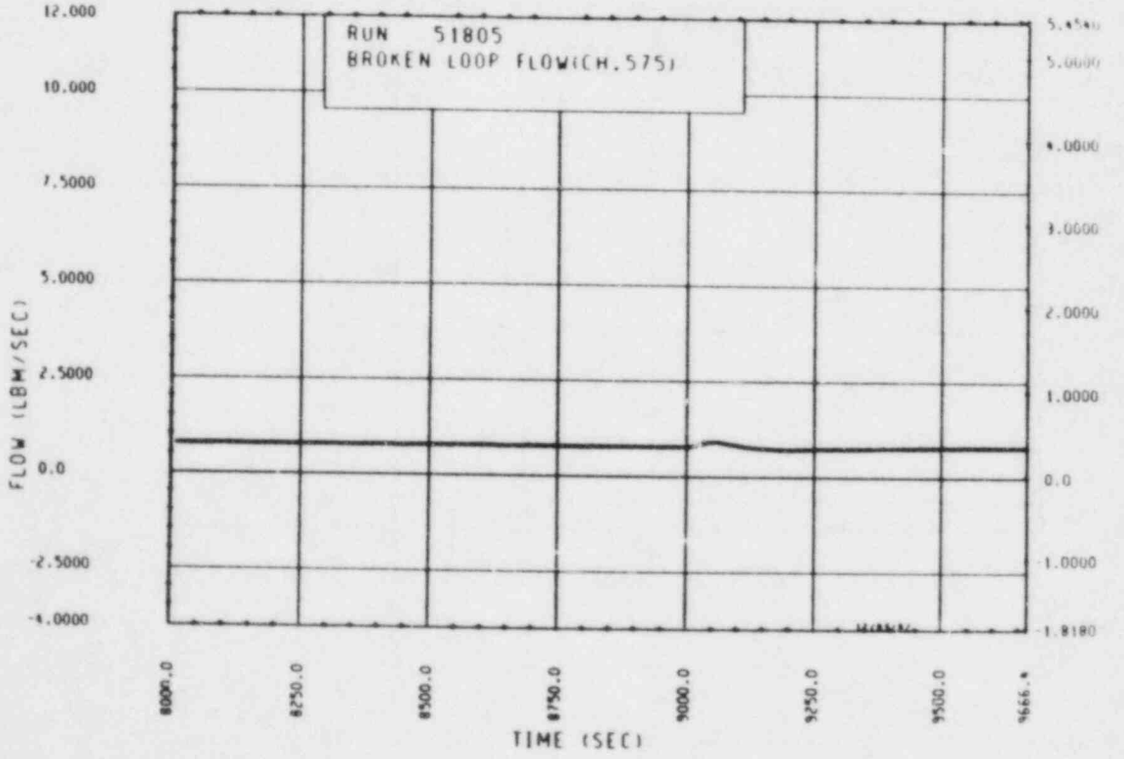

Figure A-4. Mass Flow Rate Through Broken Loop, Test 5

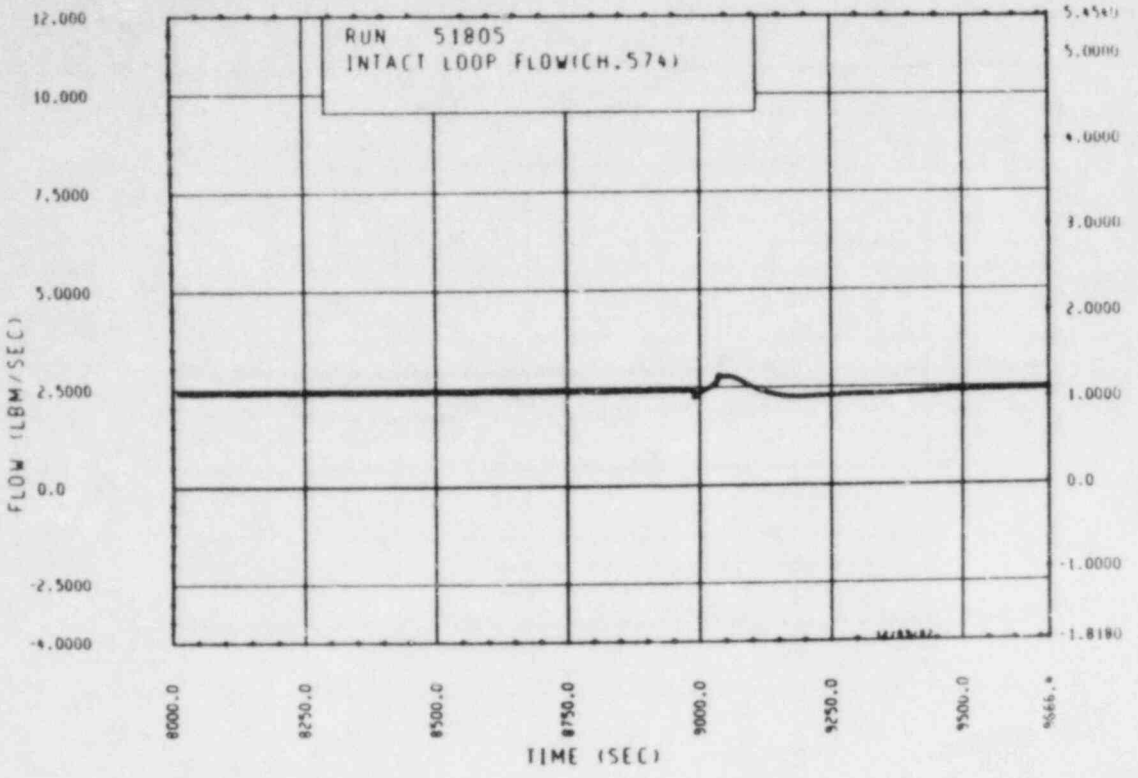

Figure A-5. Mass Flow Rate Through Unbroken Loop, Test 5

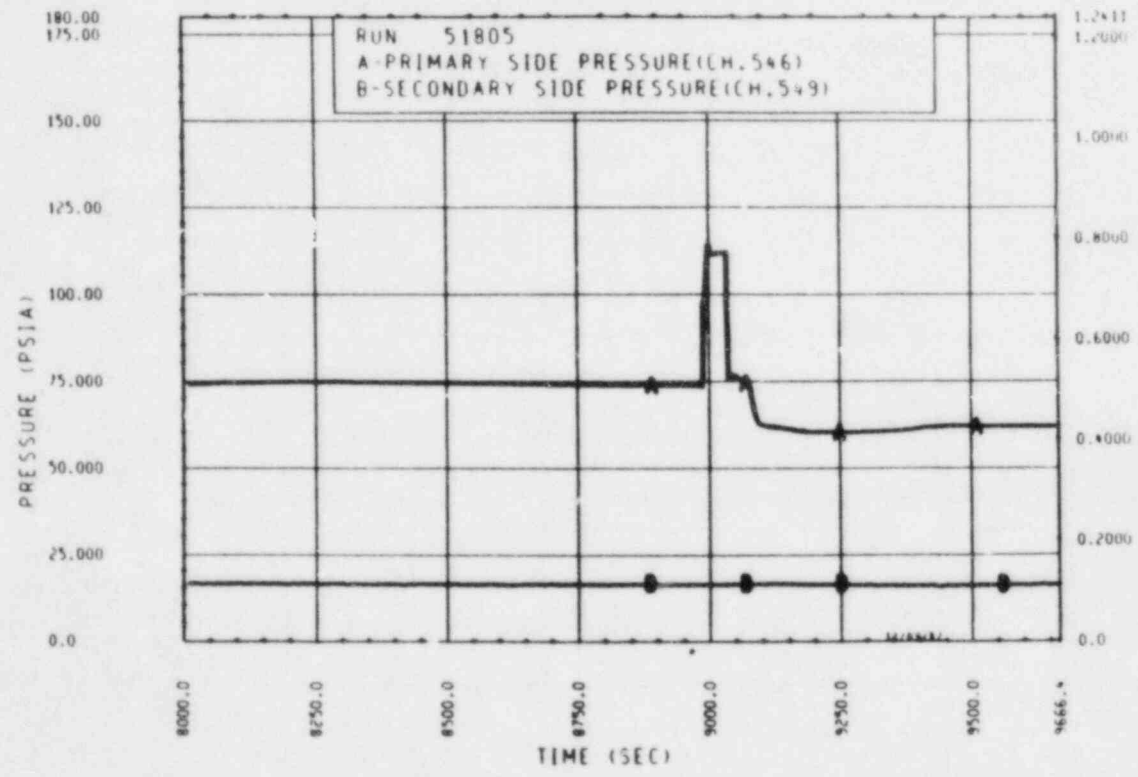

Figure A-6. Primary and Secondary System Pressure, Test 5

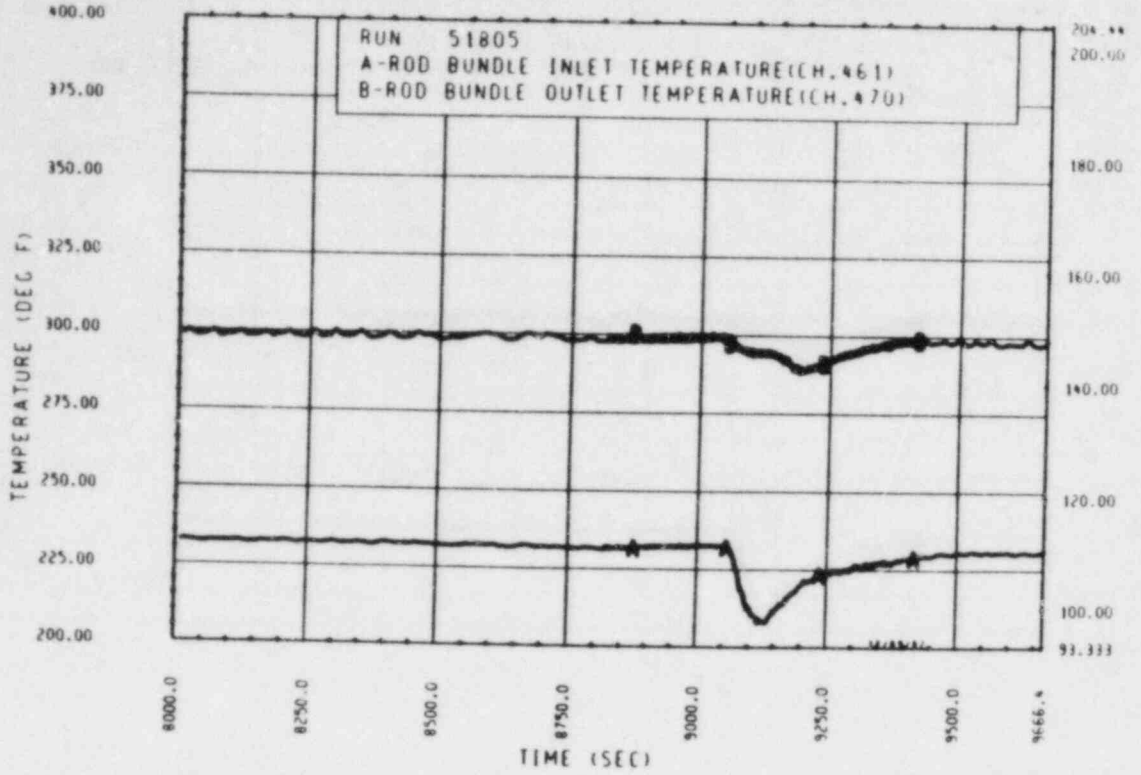

Figure A-7. Heater Rod Bundle Inlet and Outlet Temperature, Test 5

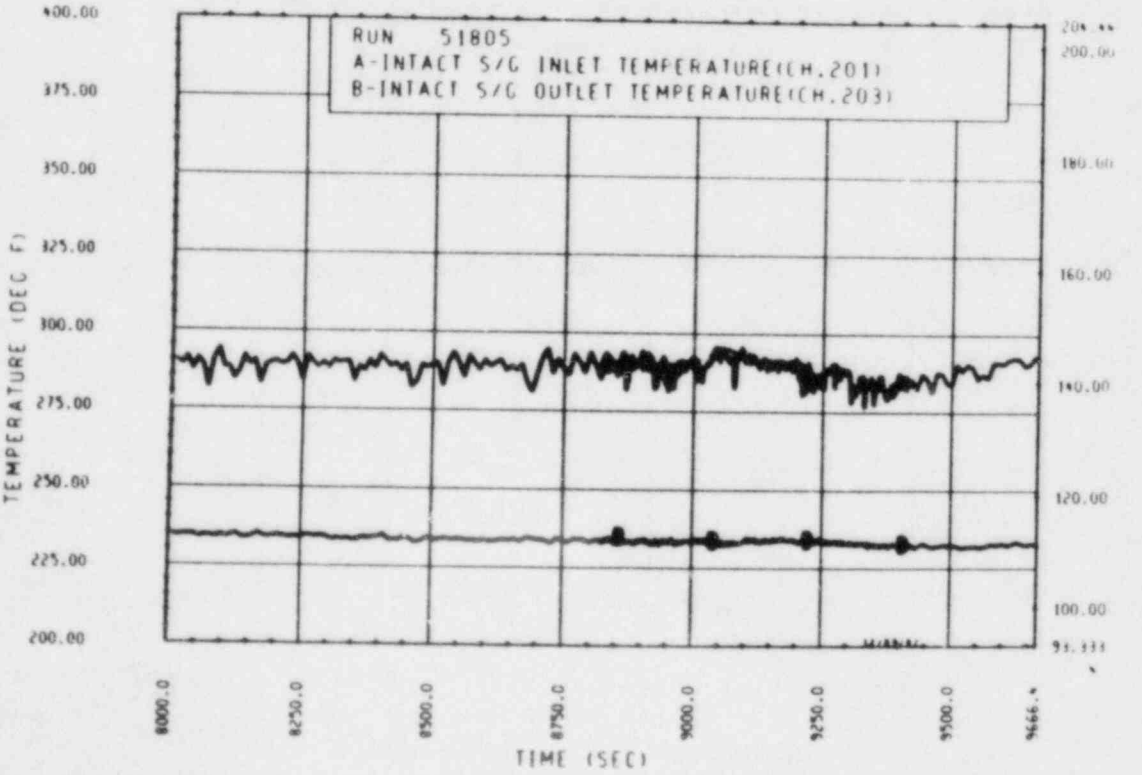

Figure A-8. Unbroken Loop Steam Generator Inlet and Outlet Temperature, Test 5

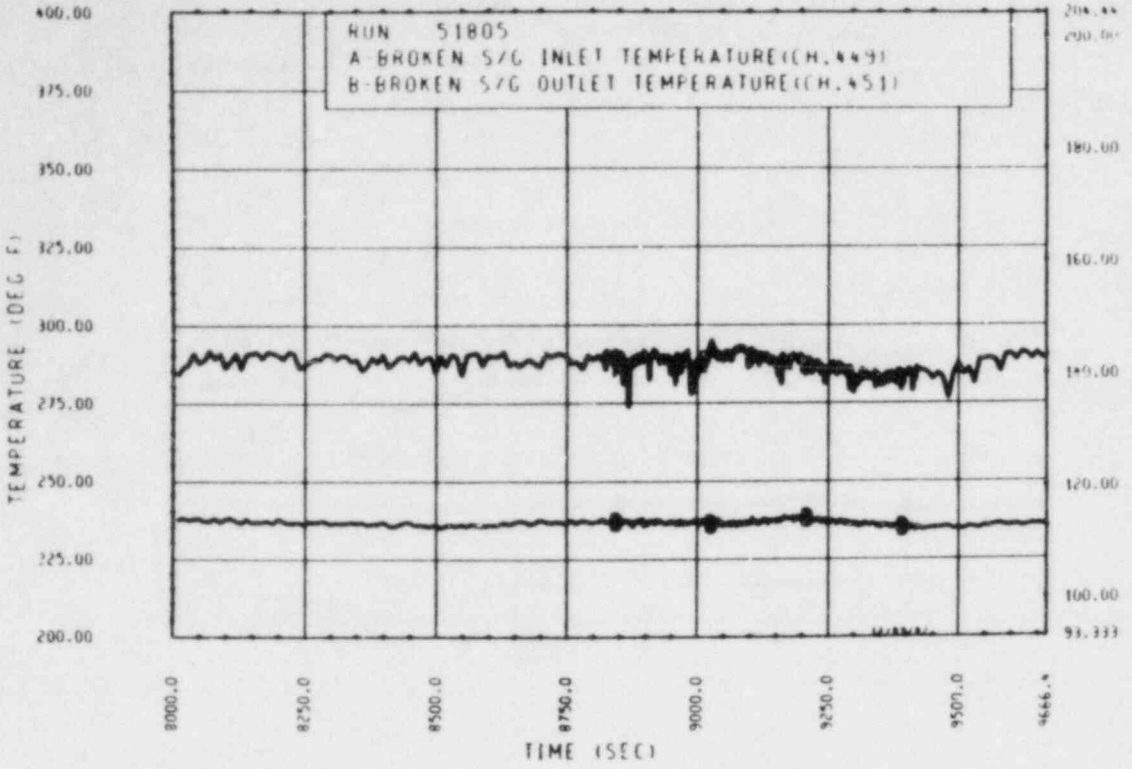

Figure A-9. Broken Loop Steam Generator Inlet and Outlet Temperature, Test 5

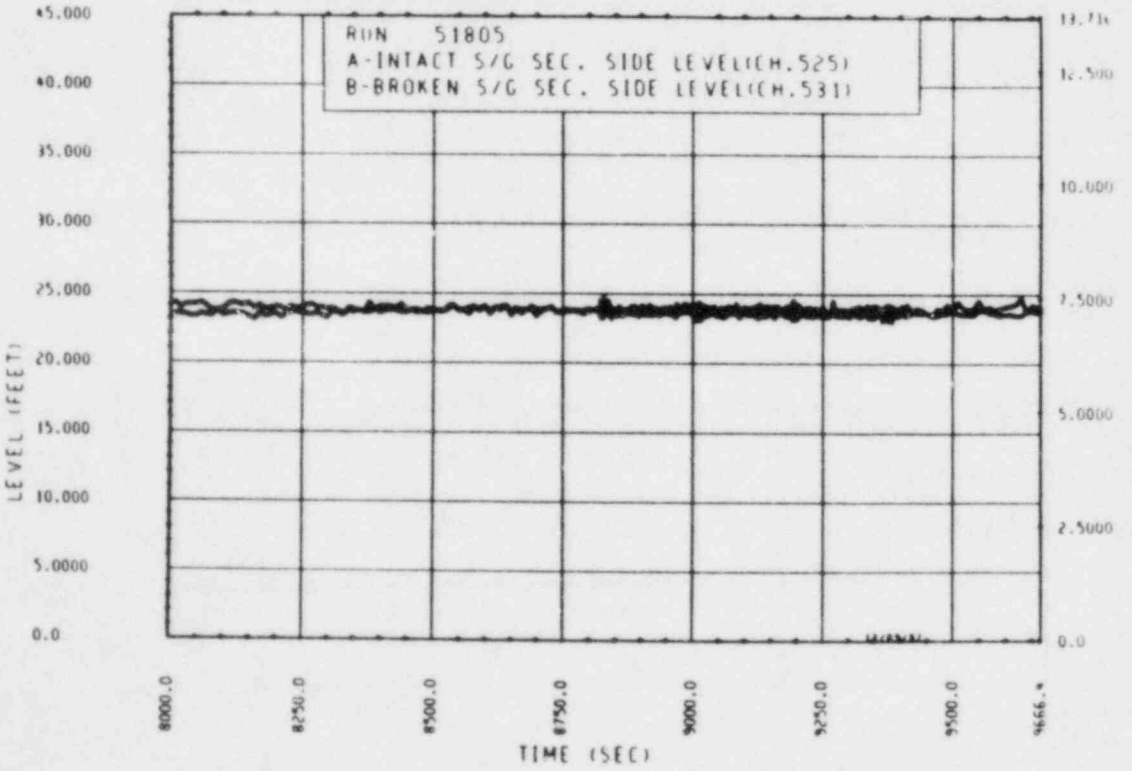

Figure A-10. Unbroken and Broken Loop Steam Generator Secondary Side Collapsed Liquid Levels, Test 5

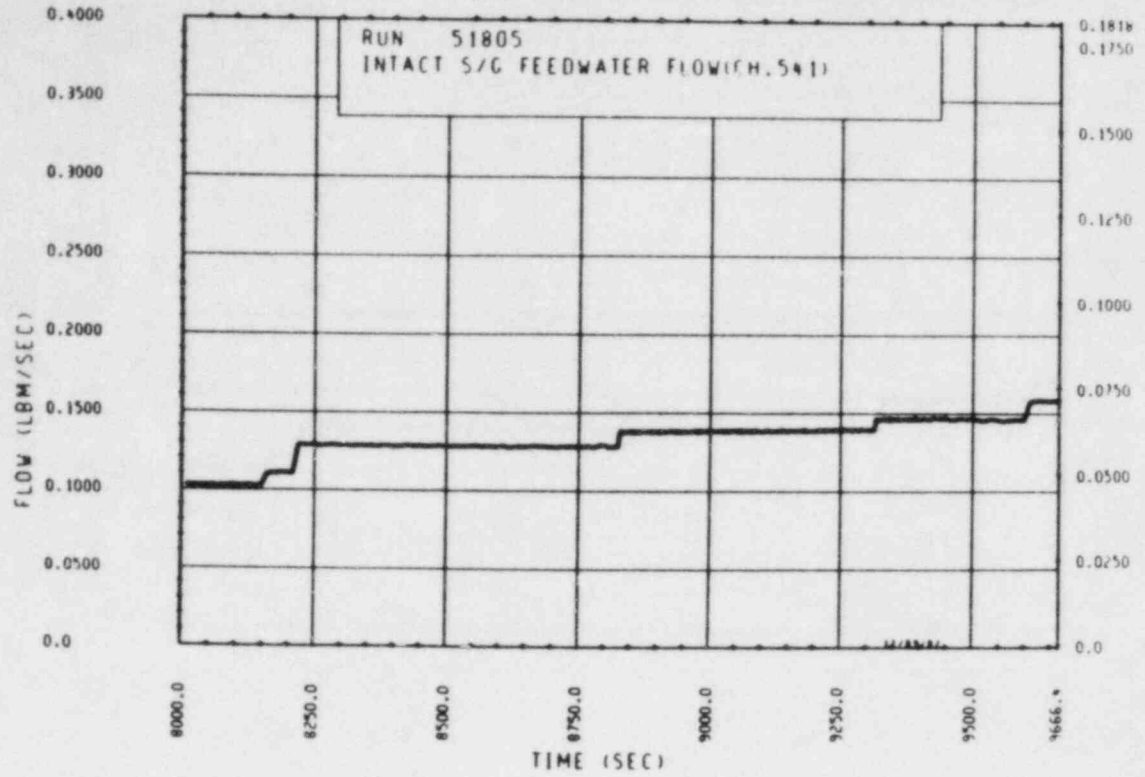

Figure A-11. Unbroken Loop Steam Generator Feedwater Mass Flow Rate, Test 5

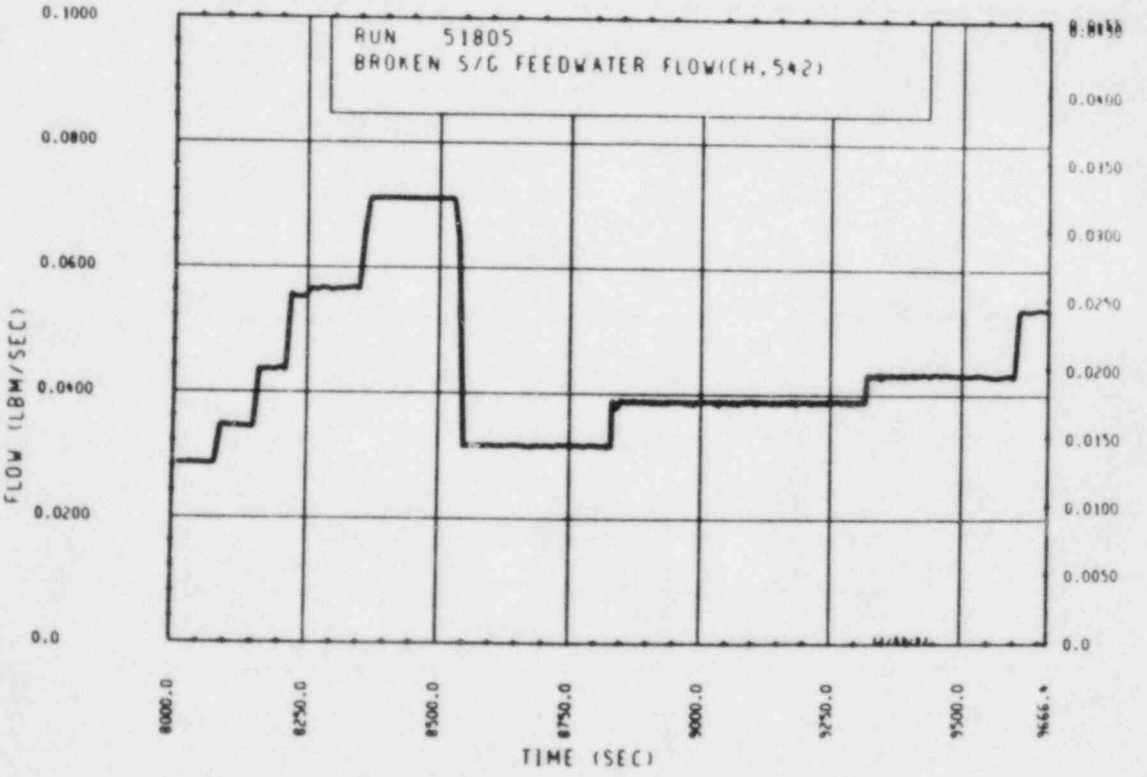

Figure A-12. Broken Loop Steam Generator Feedwater Mass Flow Rate, Test 5

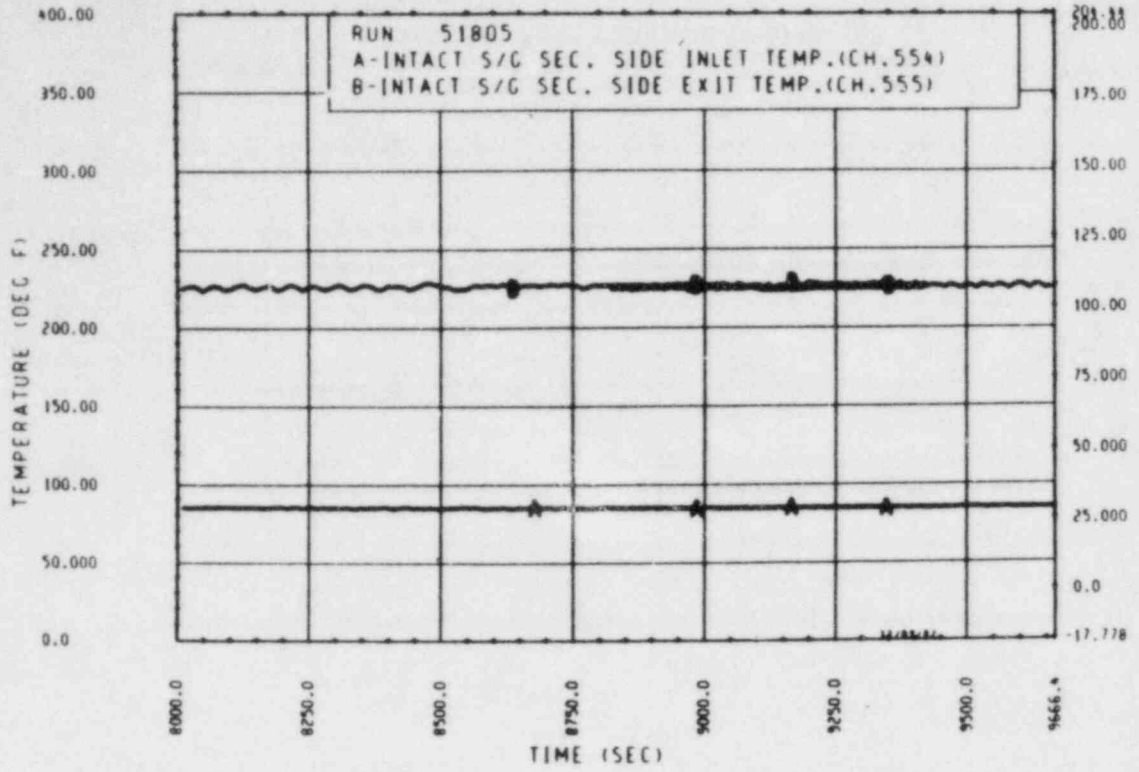

Figure A-13. Unbroken Loop Steam Generator Secondary Side Inlet and Outlet Temperature, Test 5

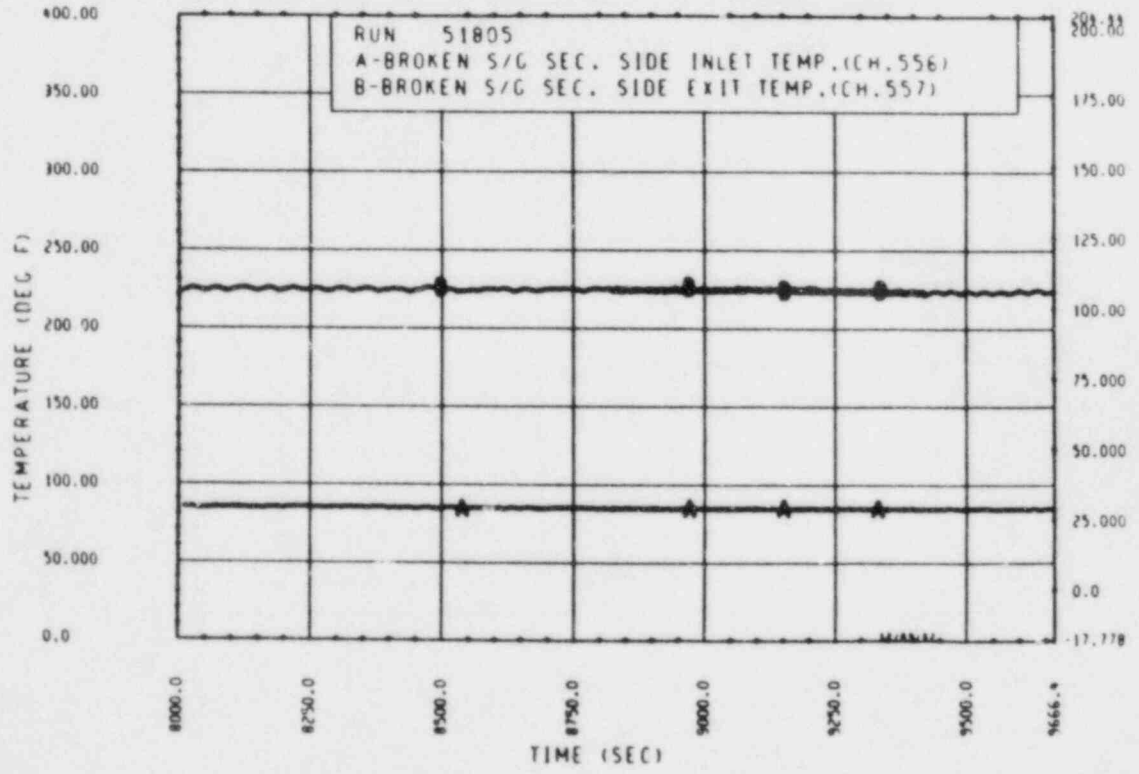

Figure A-14. Broken Loop Steam Generator Secondary Side Inlet and Outlet Temperature, Test 5

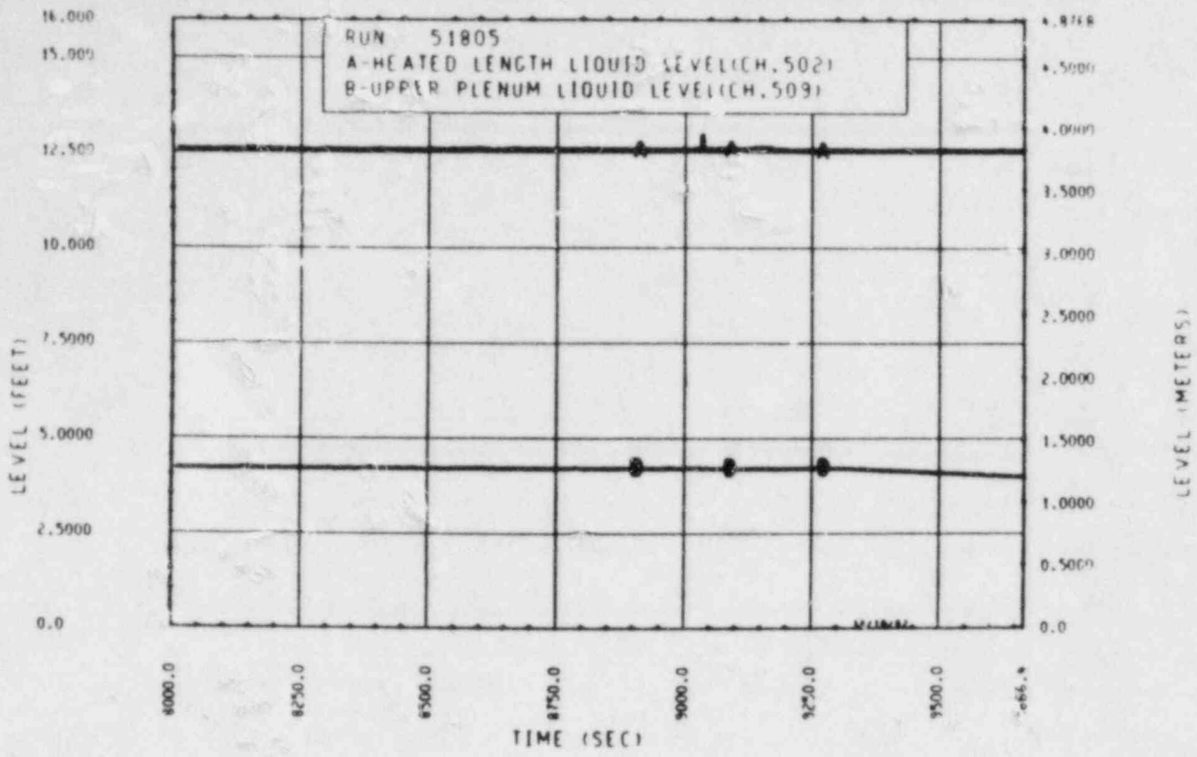

Figure A-15. Heated Length and Upper Plenum Liquid Levels, Test 5

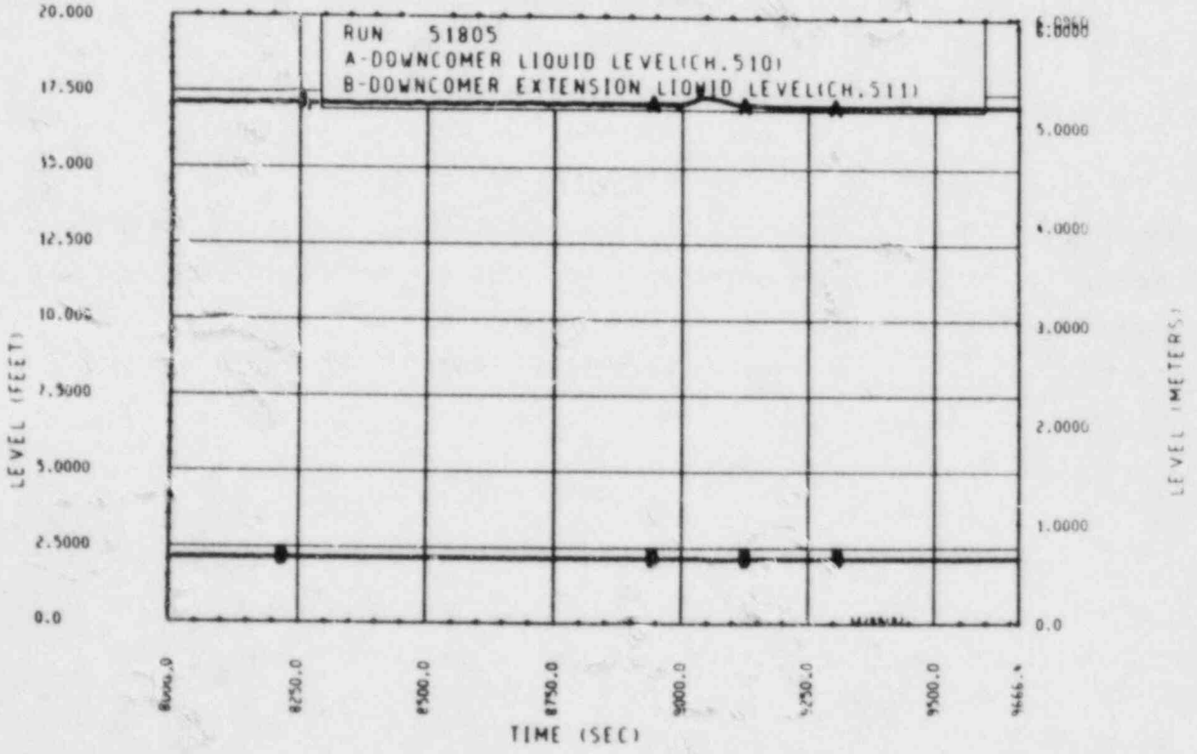

Figure A-16. Downcomer and Downcomer Extension Liquid Levels, Test 5

TEST 6: SINGLE-PHASE NONCONDENSIBLE GAS EFFECTS

Objective

To determine the effect of noncondensible gas on the single-phase natural circulation cooling mode

Test Procedure

The test was begun in a single-phase forced circulation mode with a nominal bundle power of 222 kw (simulated 2 percent of full power). Approximately 4650 cm^3 of helium were injected into the primary system during this forced circulation period, to saturate the liquid-solid system. Following the saturation injection, the circulation pump was turned off and the system made the transition into a steady-state single-phase natural circulation condition. The primary system was operated at 0.69 MPa (100 psia) as opposed to the 0.97 MPa (140 psia) reference condition, in order to allow primary system pressure margin in the event of a pressure spike during the test. As a result, the secondary side was operated at 0.17 MPa (25 psia) as opposed to the 0.28 MPa (40 psia) reference condition, to maintain sufficient primary side subcooling. The secondary side was operated in a feed-and-bleed boiling mode with a constant level being maintained at approximately 7.62 m (25 ft) (71 percent full). Helium was proportionally injected into both the unbroken and broken loop hot legs in a series of nine injections following the transition to single-phase natural circulation. Following each injection, the pressurizer was valved out to detect any primary system pressure effects due to degraded steam generator heat transfer in the presence of noncondensible gas. The pressurizer was valved in prior to each helium injection.

Test Overview

Including the saturation injection, a total of 2.47×10^5 standard cm^3 of helium were injected into the primary system during the duration of the test. The primary system responded to the addition of helium by reducing flow

through the heater rod bundle from 1.5×10^{-3} to 1.1×10^{-3} m^3/sec (24 to 18 gal/min). The flow reduction through the broken loop [3.8×10^{-4} to 1.3×10^{-4} m^3/sec] (6 to 2 gal/min) was more significant than that observed in the unbroken loop [1.1×10^{-3} to 1.0×10^{-3} m^3/sec] (18 to 16 gal/min). This flow reduction, however, only occurred during the first three helium injections. There was no discernible flow reduction during the six subsequent helium injections.

It is believed that the observed decrease in flow was due to accumulation of helium at the top of selected U-tubes and consequently blockage of flow through these tubes. The flow blockage translates into a reduction of flow area in the steam generators, which in turn results in an increased frictional pressure loss coefficient. The primary system responded to this frictional increase by reducing flow through the loops. System flow continued to decrease during the first three helium injections as more U-tubes became blocked during each injection. Subsequent helium injections, however, did not block off additional tubes, as a result of helium's propensity to accumulate in zero flow regions of the loop. The helium from these last injections deposited itself in tubes that were already blocked. Hence, flow through the loop was unaffected by the last six helium injections.

TEST SCHEDULE

TEST 6

Time (sec)	Event
0	Computer on
366	Power to 150 kw; primary system operating in forced circulation mode
1026	Power to 222 kw; primary system operating in forced circulation mode
23766	Began baseline sampling for the helium sampling system
24846	Ended baseline sampling
27796	Began He injection to saturate the primary system
27976	Ended He saturation injection; approximately 0.193 mole (4.26×10^{-4} lbm-mole) of He injected into primary system
29166	Began sampling steam generator U-tubes to determine helium concentration and distribution
30606	Ended helium sampling
31266	Single-phase natural circulation established
34386	Began first He injection
34566	Ended first He injection; approximately 0.640 mole (1.41×10^{-3} lbm-mole) of He injected into primary system

Time (sec)	Event
34596	Pressurizer valved out
35806	Pressurizer valved in
36606	Began second He injection
36876	Ended second He injection; approximately 0.676 mole (1.49×10^{-3} lbm-mole) of He injected into primary system
36901	Pressurizer valved out
37686	Began adjusting pressurizer to the current primary system pressure [0.738 MPa (107 psia)]
37951	Pressurizer adjusted to 0.738 MPa (107 psia); pressurizer valved in.
38286	Began third He injection
38466	Ended third He injection; approximately 0.447 mole (9.86×10^{-4} lbm-mole) of He injected into primary system
38496	Pressurizer valved out
39898	Pressurizer adjusted to 0.745 MPa (108 psi) and valved in
40026	Began fourth He injection
40926	Ended fourth He injection; approximately 2.35 moles (5.19×10^{-3} lbm-mole) of He injected into primary system; pressurizer valved out

Time (sec)	Event
42006	Pressurizer valved in
42126	Began fifth He injection
42426	Ended fifth He injection; approximately 0.735 mole (1.62×10^{-3} lbm-mole) of He injected into primary system
42471	Pressurizer valved out
43593	Pressurizer valved in for sampling
43626	Began sampling steam generator U-tubes to determine helium concentration and distribution
46626	Sampling halted after water forced its way into GOW-MAC analyzer; only broken loop steam generator sampled
49326	Began sixth helium injection
50226	Ended sixth helium injection; approximately 2.24 moles (4.94×10^{-3} lbm-mole) of helium injected into primary system.
50256	Pressurizer valved out
51126	Pressurizer valved in; began sampling steam generator U-tubes to determine helium concentration and distribution

Time (sec)	Event
52326	Sampling halted after water forced its way into the GOW-MAC analyzer; only three U-tubes sampled in broken loop steam generator
52566	Pressurizer valved out
59176	Pressurizer valved in
59526	Helium sampling resumed
64686	Helium sampling halted after water forced its way into GOW-MAC analyzer; approximately 75 percent of the designated U-tubes sampled
65526	Began seventh helium injection
65976	Ended seventh helium injection; approximately 1.06 moles (2.33×10^{-3} lbm-mole) of helium injected into primary system
65996	Pressurizer valved out
66881	Pressurizer valved in
67086	Began eighth helium injection
67526	Ended eighth helium injection; approximately 1.04 moles (2.30×10^{-3} lbm-mole) of helium injected into primary system
67556	Pressurizer valved out

Time (sec)	Event
68706	Pressurizer valved in; began ninth helium injection
69606	Ended ninth helium injection; approximately 2.09 moles (4.60×10^{-3} lbm-mole) of helium injected into primary system
69615	Pressurizer valved out
70386	Began "quick-look" sampling of steam generator U-tubes to determine helium concentration and distribution
71826	Ended "quick-look" sampling
72066	Power/computer off

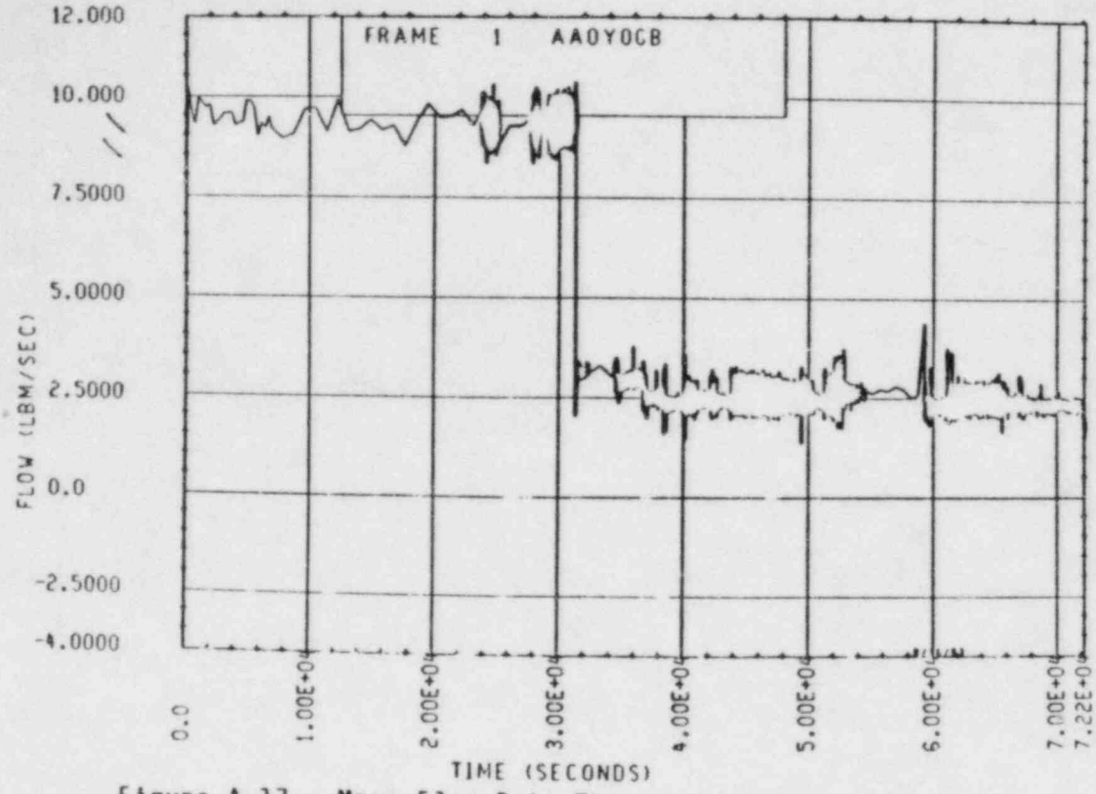

Figure A-17. Mass Flow Rate Through Rod Bundle, Test 6

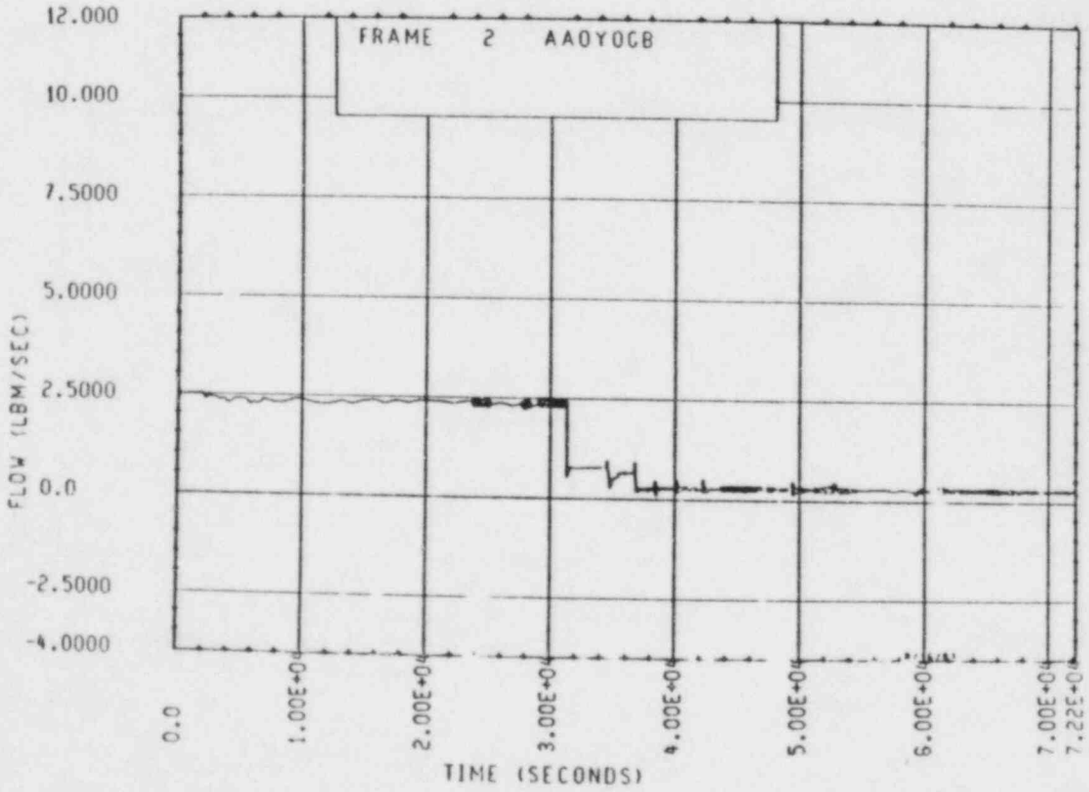

Figure A-18. Mass Flow Rate Through Broken Loop, Test 6

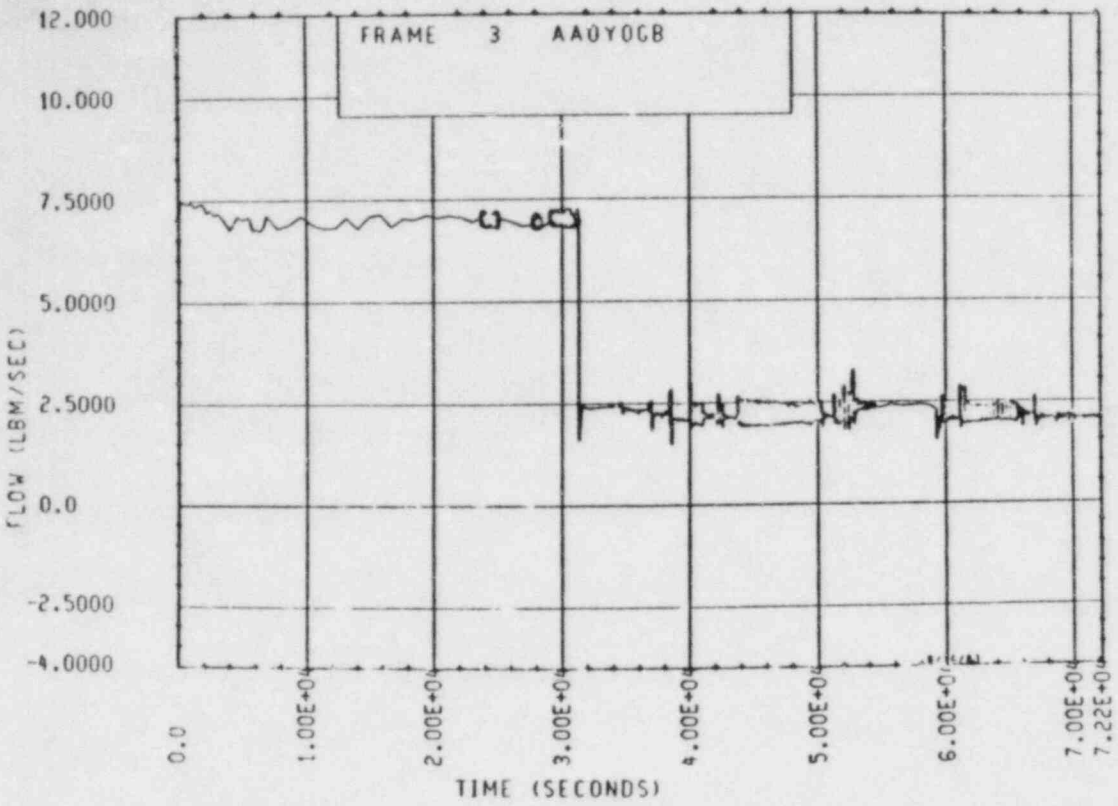

Figure A-19. Mass Flow Rate Through Unbroken Loop, Test 6

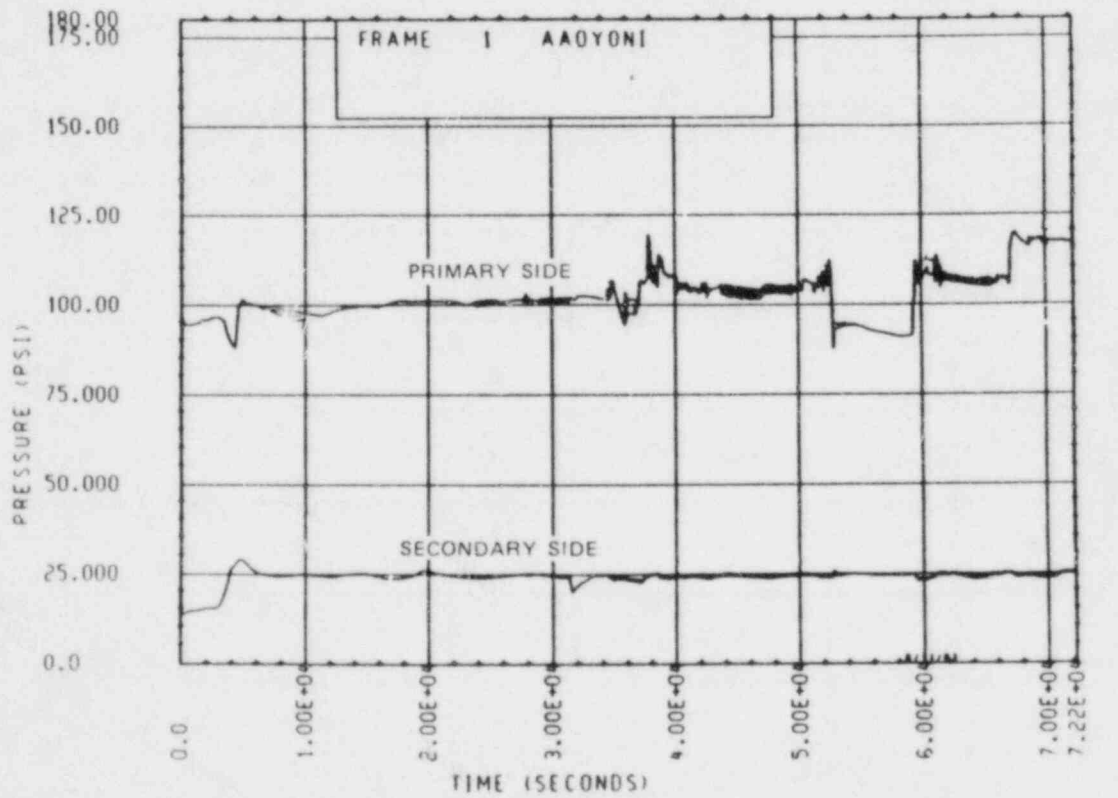

Figure A-20. Primary and Secondary System Pressure, Test 6

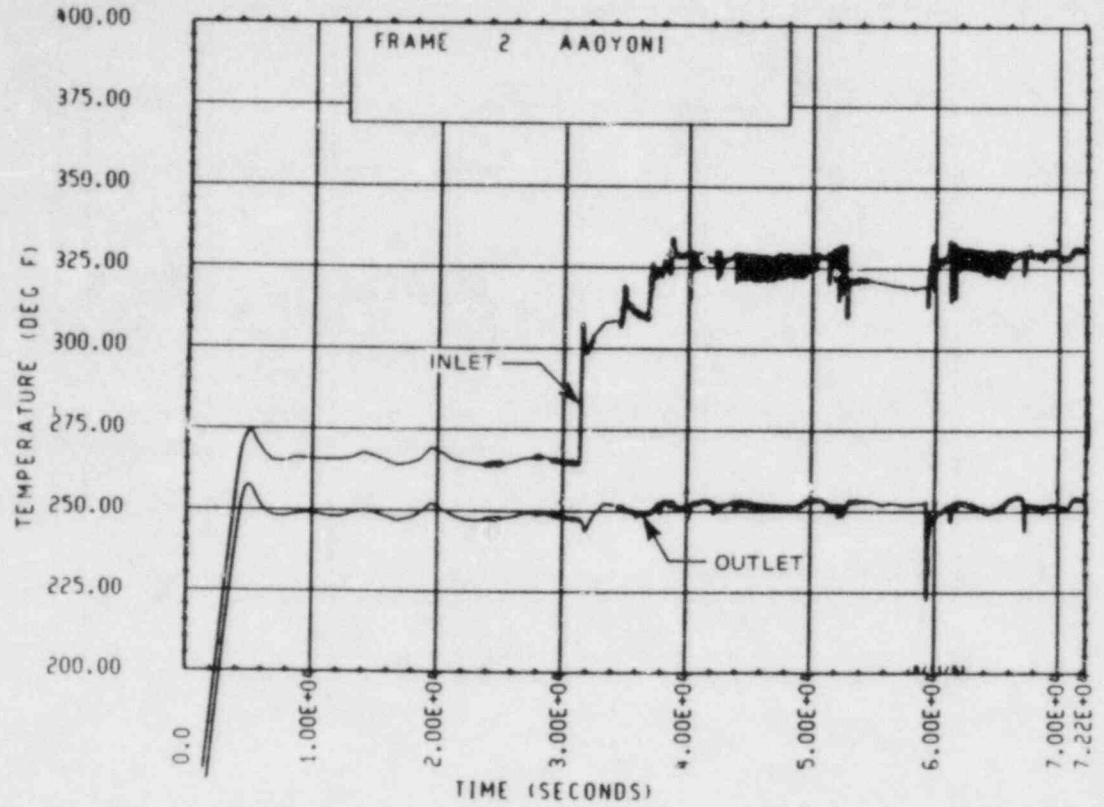

Figure A-21. Heater Rod Bundle Inlet and Outlet Temperature, Test 6

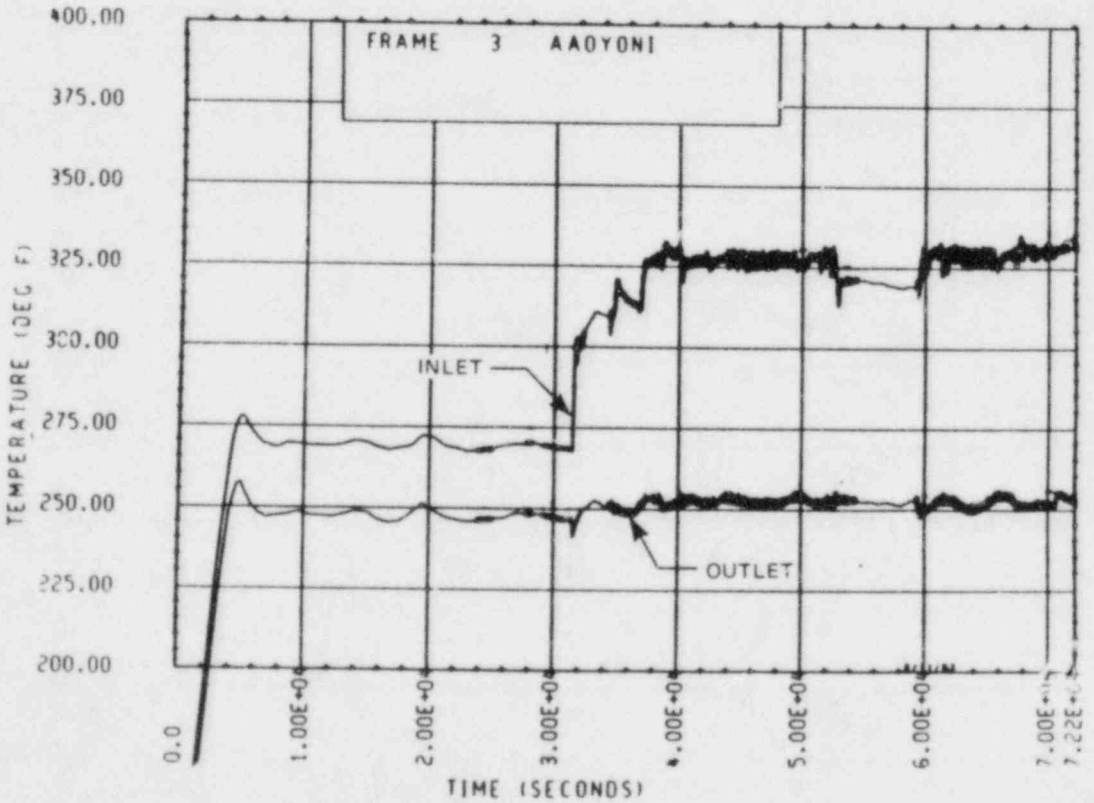

Figure A-22. Unbroken Loop Steam Generator Inlet and Outlet Temperature, Test 6

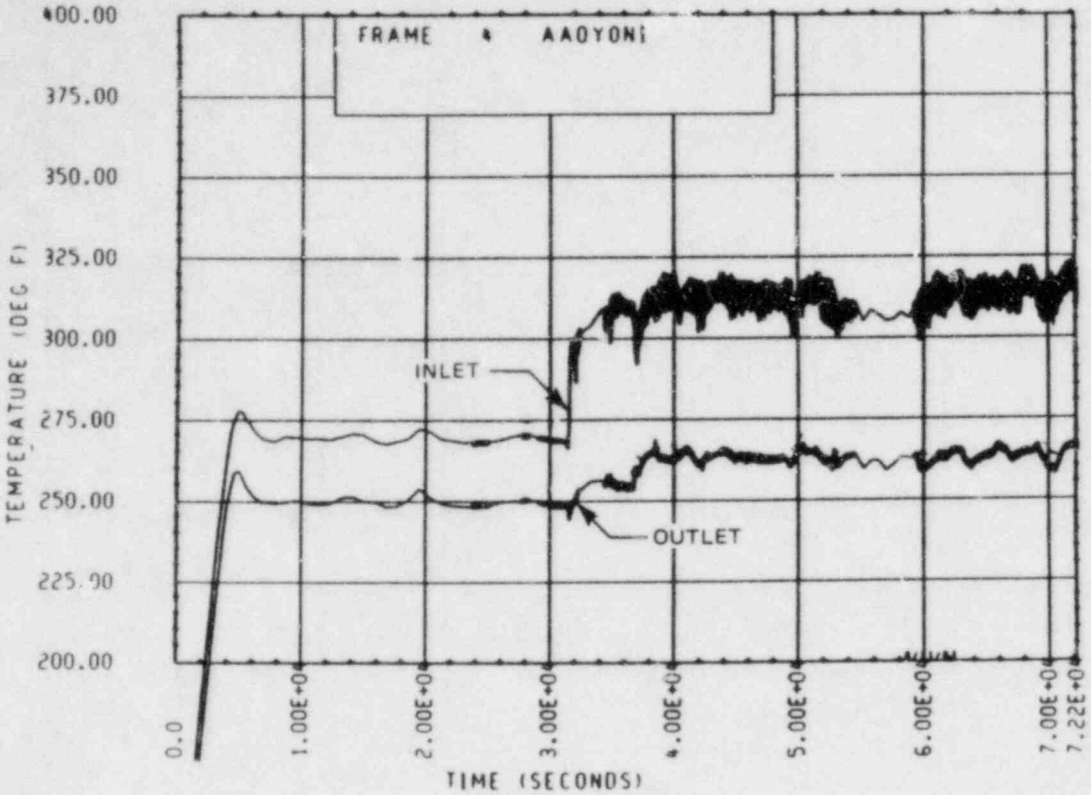

Figure A-23. Broken Loop Steam Generator Inlet and Outlet Temperature, Test 6

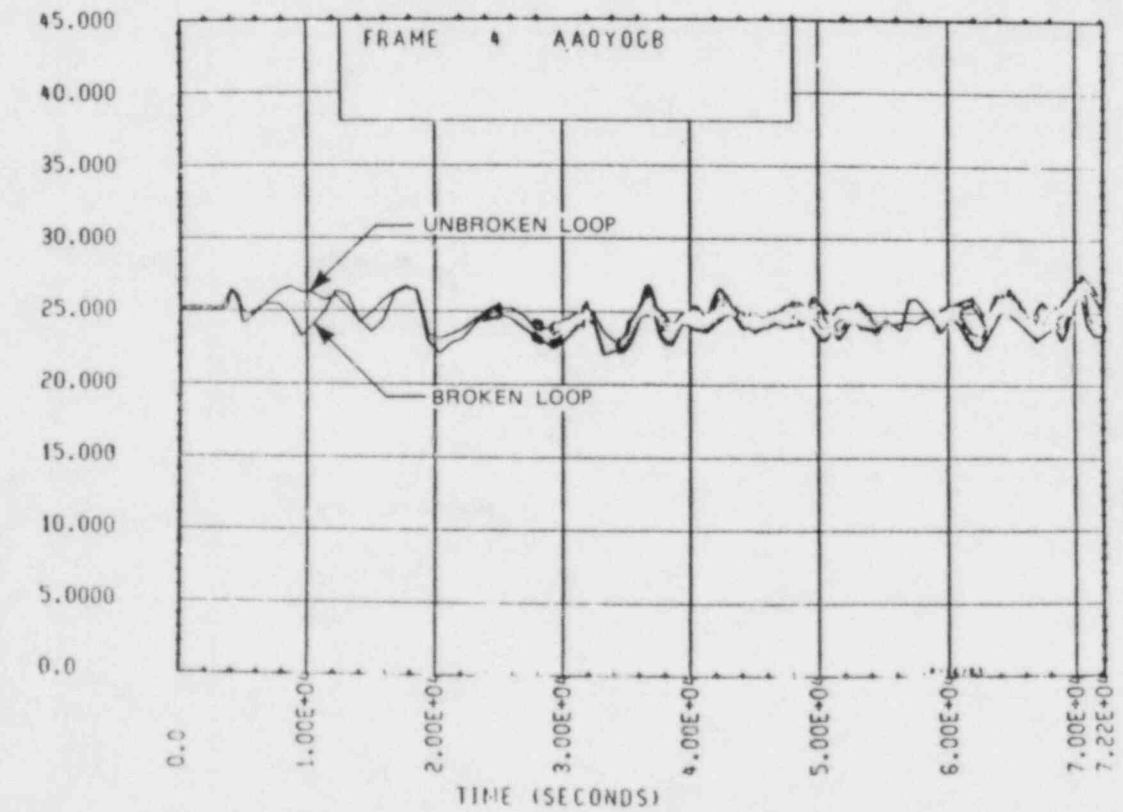

Figure A-24. Unbroken and Broken Loop Steam Generator Secondary Side Collapsed Liquid Levels, Test 6

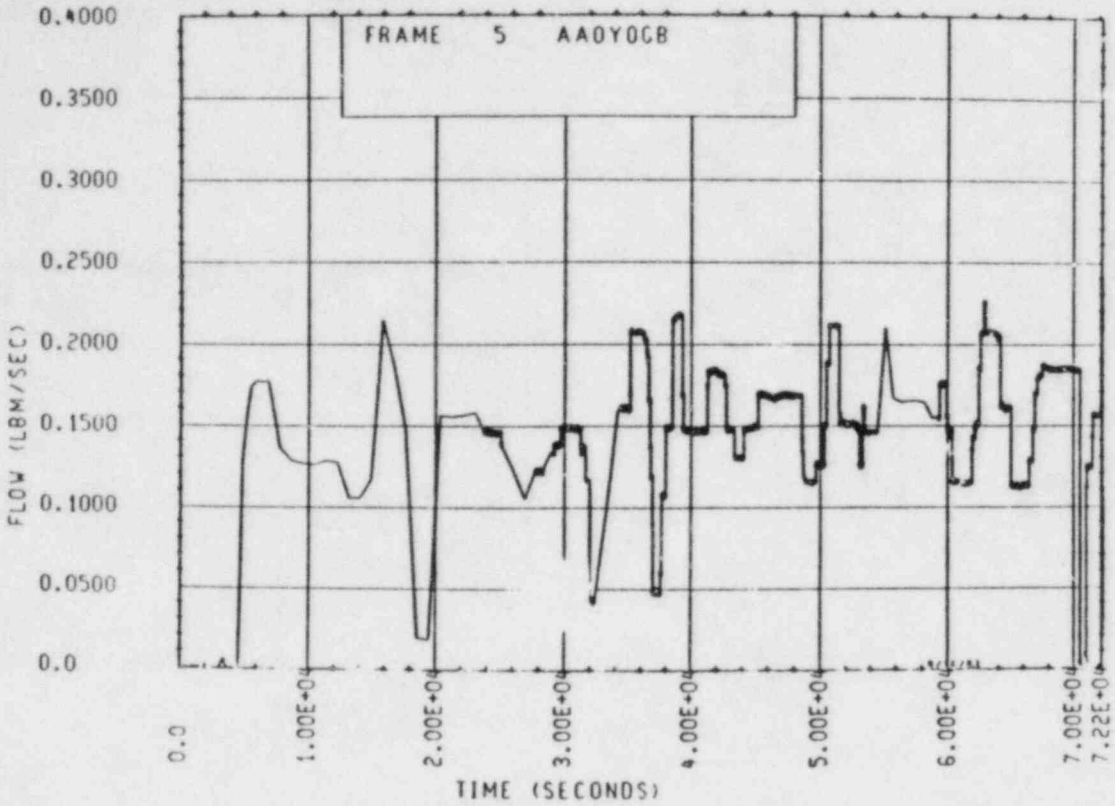

Figure A-25. Unbroken Loop Steam Generator Feedwater Mass Flow Rate, Test 6

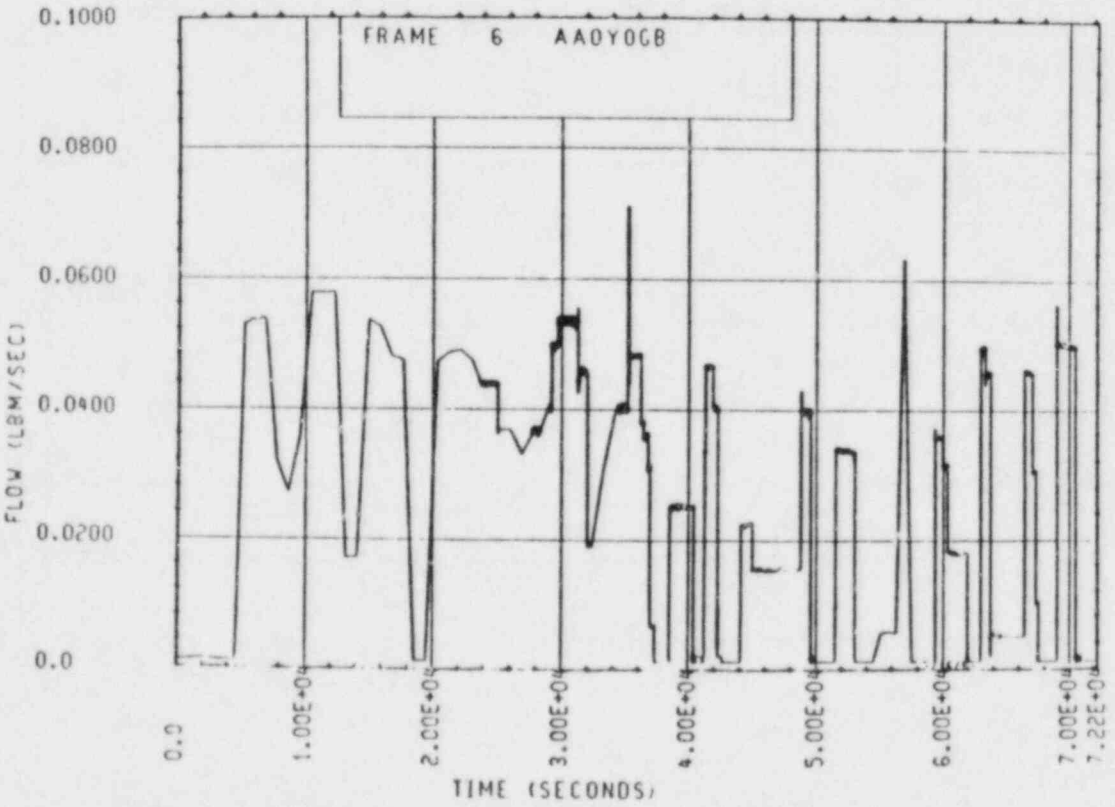

Figure A-26. Broken Loop Steam Generator Feedwater Mass Flow Rate, Test 6

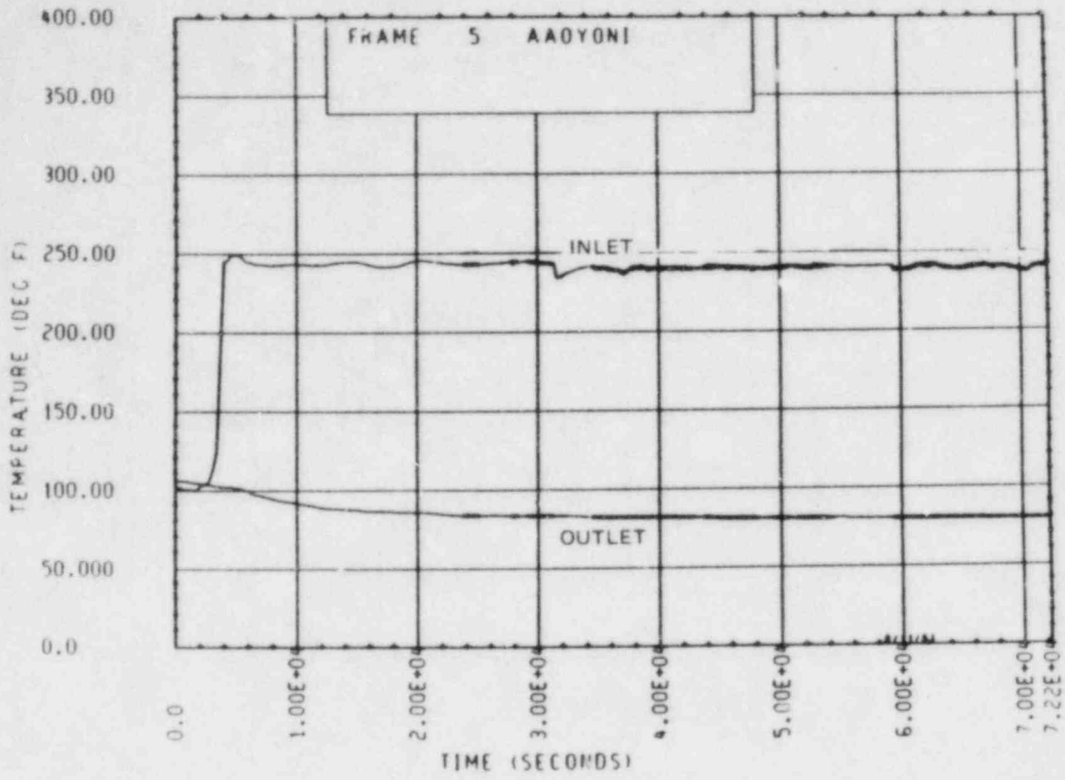

Figure A-27. Unbroken Loop Steam Generator Secondary Side Inlet and Outlet Temperature, Test 6

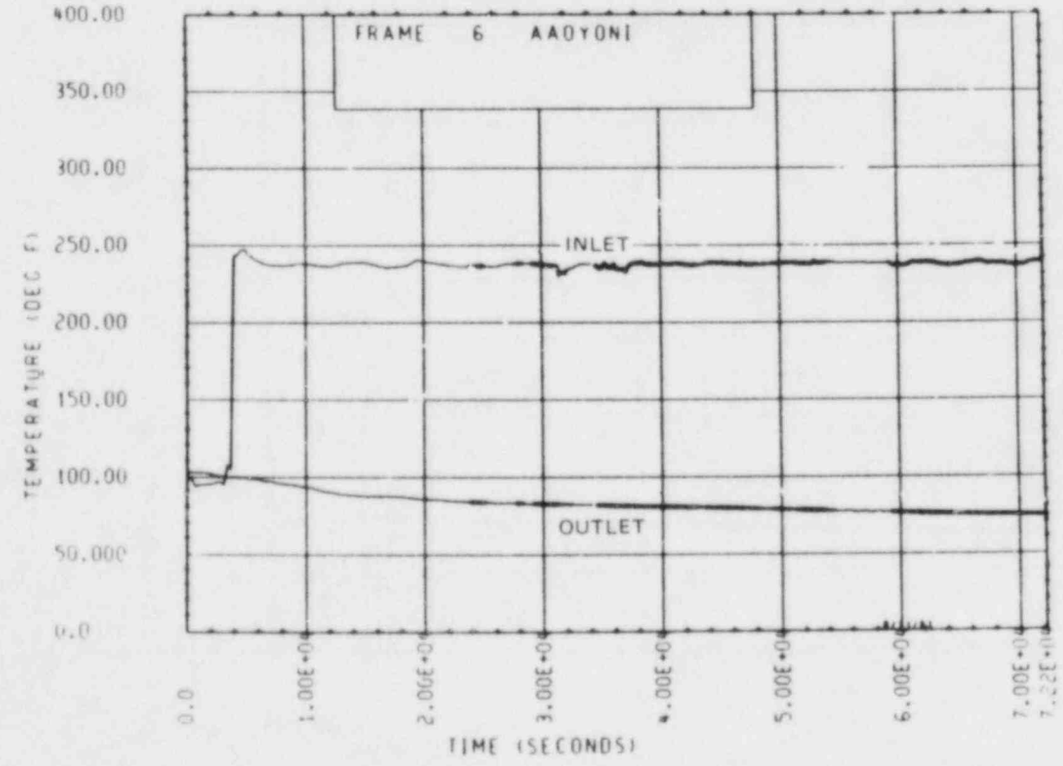

Figure A-28. Broken Loop Steam Generator Secondary Side Inlet and Outlet Temperature, Test 6

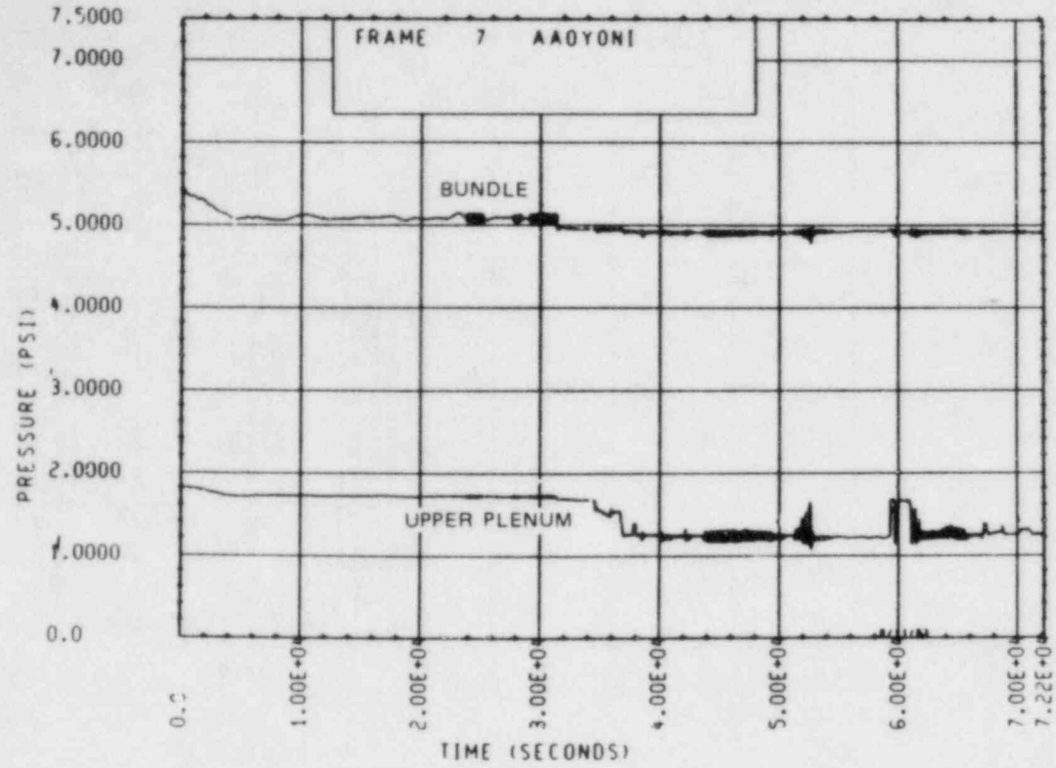

Figure A-29. Heater Rod Bundle and Upper Plenum Differential Pressure, Test 6

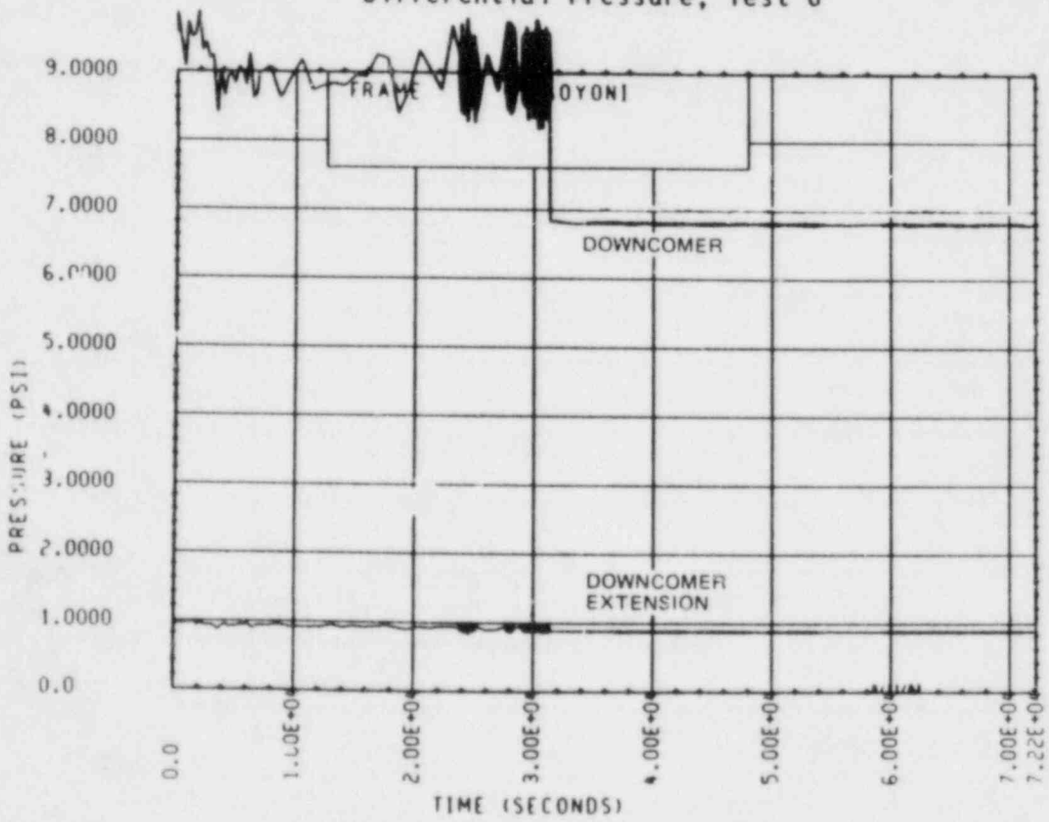

Figure A-30. Downcomer and Downcomer Extension Differential Pressure, Test 6

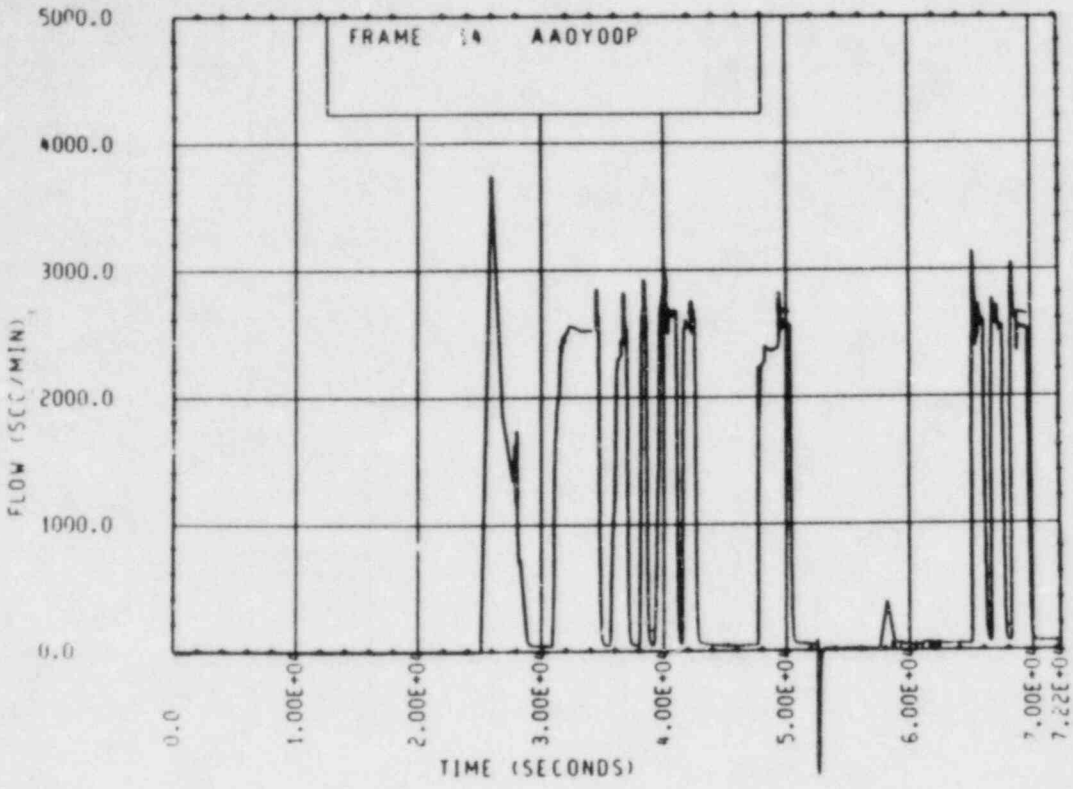

Figure A-31. Unbroken Loop Noncondensible Gas Injection Line Volumetric Flow Rate, Test 6

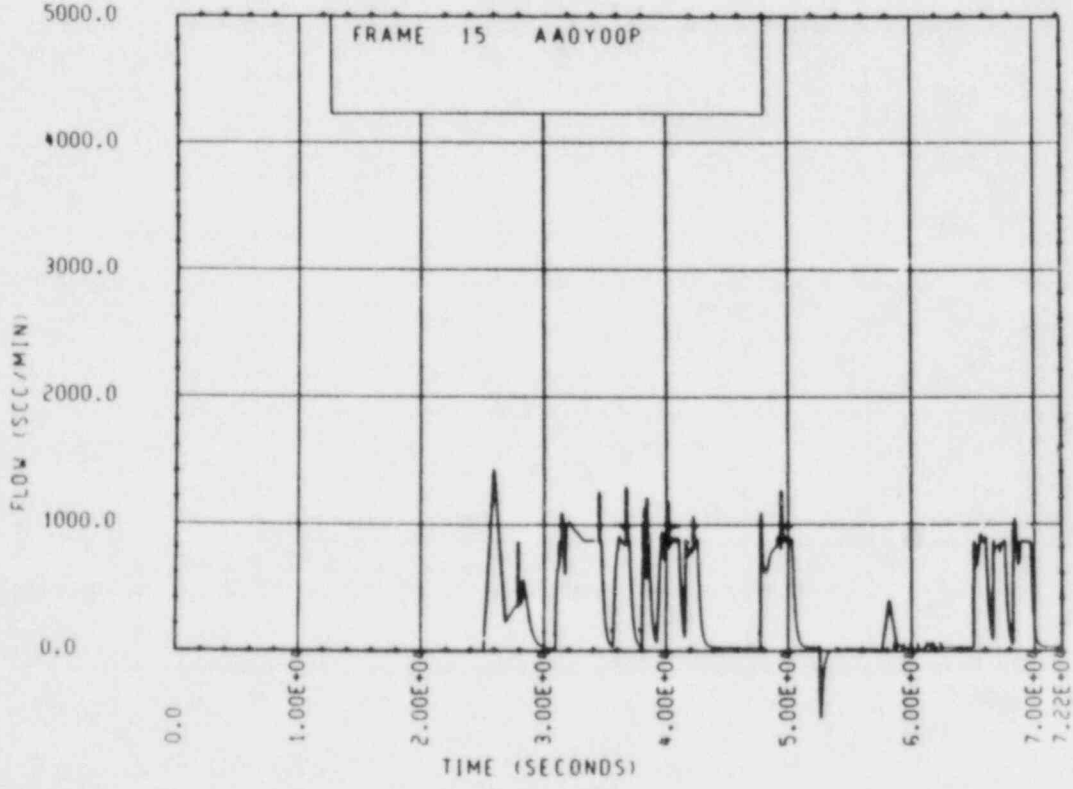

Figure A-32. Broken Loop Noncondensible Gas Injection Line Volumetric Flow Rate, Test 6

TEST 9A: SINGLE-PHASE NATURAL CIRCULATION WITH SECONDARY SIDE BOILOFF

Objective

To determine the effect of decreasing steam generator heat transfer area (by means of secondary side boiloff) on single-phase natural circulation

Test Procedure

The test was begun from a single-phase natural circulation mode with a primary system pressure of approximately 75 psia and a nominal bundle power of 222 kw. The primary system was operated at 0.52 MPa (75 psia), as opposed to the 0.97 MPa (140 psia) reference condition, to allow primary system pressure margin in the event that a pressure spike occurred during the secondary side boiloff. As a result, the secondary side was operated at atmospheric pressure as opposed to the 0.28 MPa (40 psia) reference condition, to maintain sufficient primary side subcooling. The secondary side was initially operated in a feed-and-bleed boiling mode with an initial collapsed liquid level of 7.62 m (25 ft) (71 percent full). The secondary side feedwater lines were then valved out and the secondary side levels were allowed to decrease by means of boiloff. During the course of the boiloff, the pressurizer was valved out, resulting in a constant-volume primary system. Boiloff was terminated when the primary system pressure increased to 0.69 MPa (100 psia). At that time, 110°C (230°F) water was injected into the secondary sides from accumulator 1. Injection continued until the secondary sides of both steam generators were recovered to their original 7.62 m (25 ft) levels. The test was terminated when the system returned to a steady-state condition.

Test Overview

The single-phase test may be characterized by two very distinct pressure transients that occurred during the course of the secondary side boiloff. The first pressure transient was initiated when the secondary side feedwater and the primary system pressurizer were valved off simultaneously. The primary system immediately began to experience a gradual pressure increase which

peaked at 0.65 MPa (94 psi) and then gradually decreased to a quasi-steady-state value of 0.42 MPa (61 psi). (At this low pressure, there probably was some void generation at the exit of the rod bundle.) It has been concluded that this first pressure transient was not the result of the secondary side boiloff, but rather the result of the feedwater and pressurizer being valved off simultaneously. This conclusion is based on experience from a previous single-phase boiloff test (test 14) as well as experience with the facility pressurizer.

In test 14 the secondary side was boiled off while the primary side operated in a single-phase mode at a constant pressure (pressurizer valved in to the primary). The primary system was oblivious to the secondary side boiloff until secondary side levels decreased to at least the 4.11 m (13.5 ft) level. During the first pressure transient described above, the secondary side levels remained in the 6.10 to 7.62 m (20 to 25 ft) range. It was therefore concluded that this pressure transient was not the result of a decrease in effective heat transfer area, as caused by a secondary side boiloff. Rather, it is believed that the pressure increase was the result of a loss of feedwater, and the subsequent heatup of secondary side fluid in the lower elevations of the tube bundle. This decrease in primary to secondary ΔT, accompanied by a loss of forced convection in the secondary side, could cause the primary to heat up. In a constant volume (pressurizer was valved out), liquid-solid system, only a very small temperature increase is required to cause a very dramatic pressure increase.

A plausible explanation for the subsequent pressure decrease from 0.65 to 0.42 MPa (94 to 61 psi) is not offered. It can only be said that a primary pressure decrease has been observed during other single-phase portions of tests when the pressurizer was valved out.

Whereas the first pressure transient was apparently the result of the feedwater and pressurizer being valved out together, the second pressure transient was the result of a decrease in steam generator effective heat transfer area (boiloff effect). The steam generator effective heat transfer area was sufficient to maintain primary side steady-state operation for secondary side

collapsed liquid levels as low as 2.74 m (9 ft) (26 percent full). The second primary system pressure transient began once levels started to decrease below the 2.74 m (9 ft) level. The pressure increase was gradual at first, but became rapid as levels boiled off to the 2.44 m (8 ft) (23 percent full) mark. The 0.69 MPa (100 psi) pressure alarm tripped with levels approaching the 1.83 m (6 ft) (17 percent full) mark. The pressure transient was accompanied by very subtle decreases in primary flow and very subtle increases in primary fluid temperature. As previously mentioned, this is to be expected in a single-phase constant volume system where only very small temperature increases are required to cause a dramatic pressure increase.

TEST SCHEDULE
TEST 9a

Time (sec)	Event
0	Computer on
2514	Power to 222 kw; primary system operating in a single-phase forced circulation mode
20273.6	Steady-state single-phase natural circulation established
21361	Feedwater valved out to both steam generators; pressurizer valved out
23274	Started draining broken loop steam generator secondary side, to maintain identical levels in both steam generators
23394	Stopped draining broken loop steam generator
24884	Injection valves set for accumulator 1 injection into steam generator secondary sides
24894	0.69 MPa (100 psi) primary system pressure alarm; injection into secondary initiated
25758	Injection terminated; normal feedwater flow initiated
26531	Unbroken loop steam generator secondary side level recovered to 7.62 m (25 ft)

Time (sec)	Event
26614	Broken loop steam generator secondary side level recovered to 7.62 m (25 ft)
27234	End of test 9a

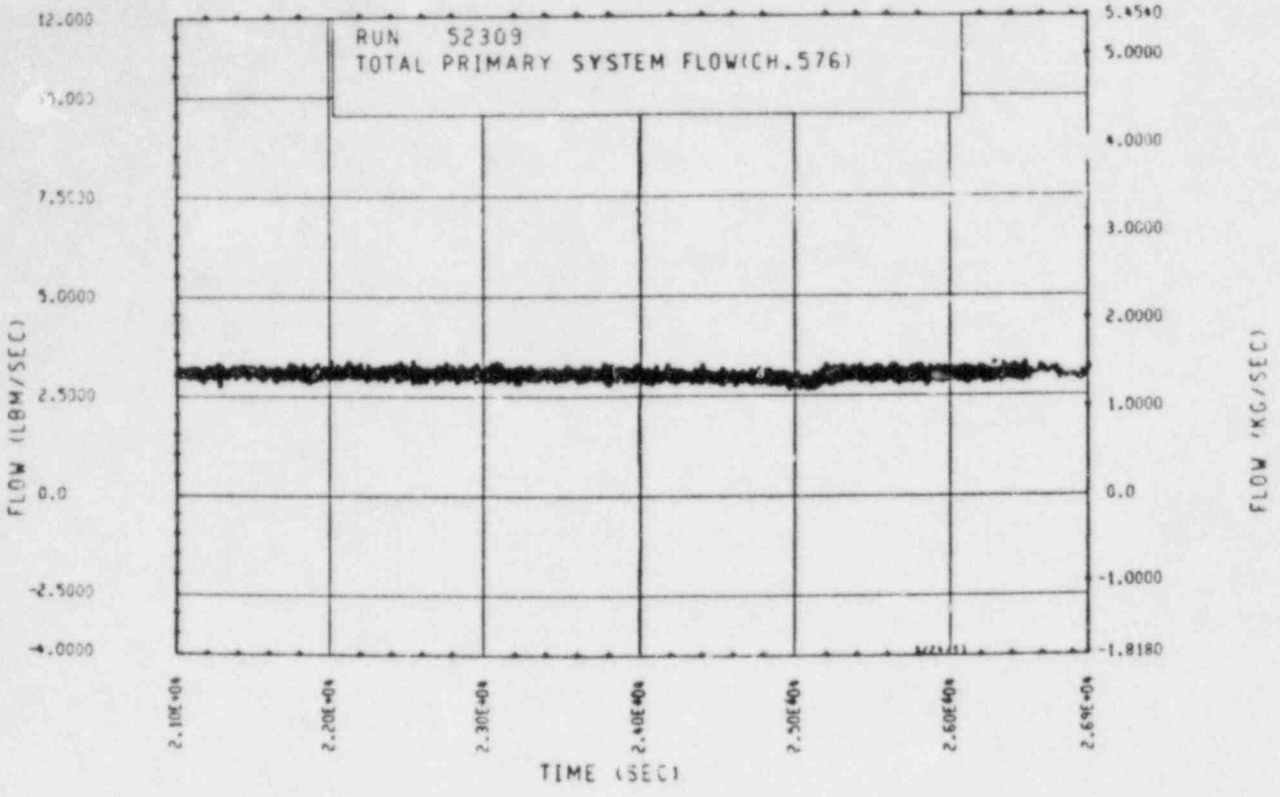

Figure A-33. Mass Flow Rate Through Rod Bundle, Test 9A

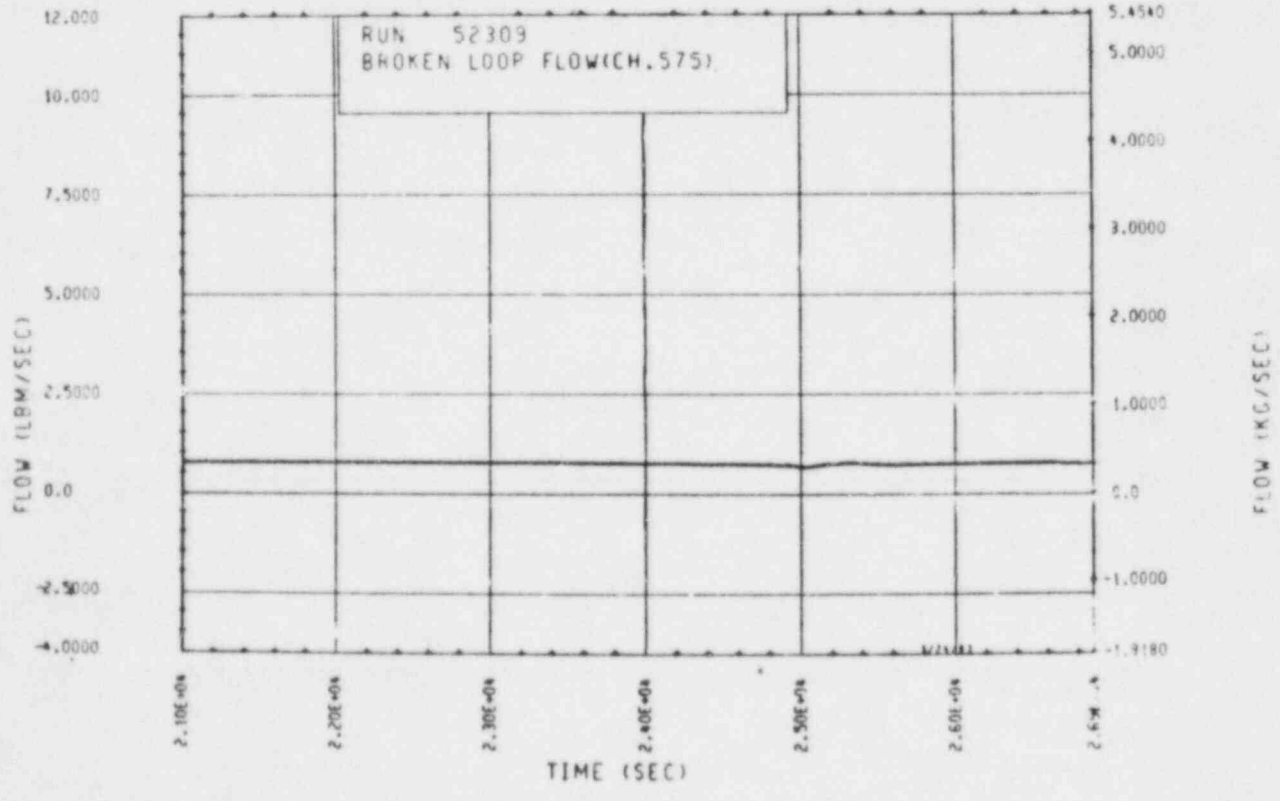

Figure A-34. Mass Flow Rate Through Broken Loop, Test 9A

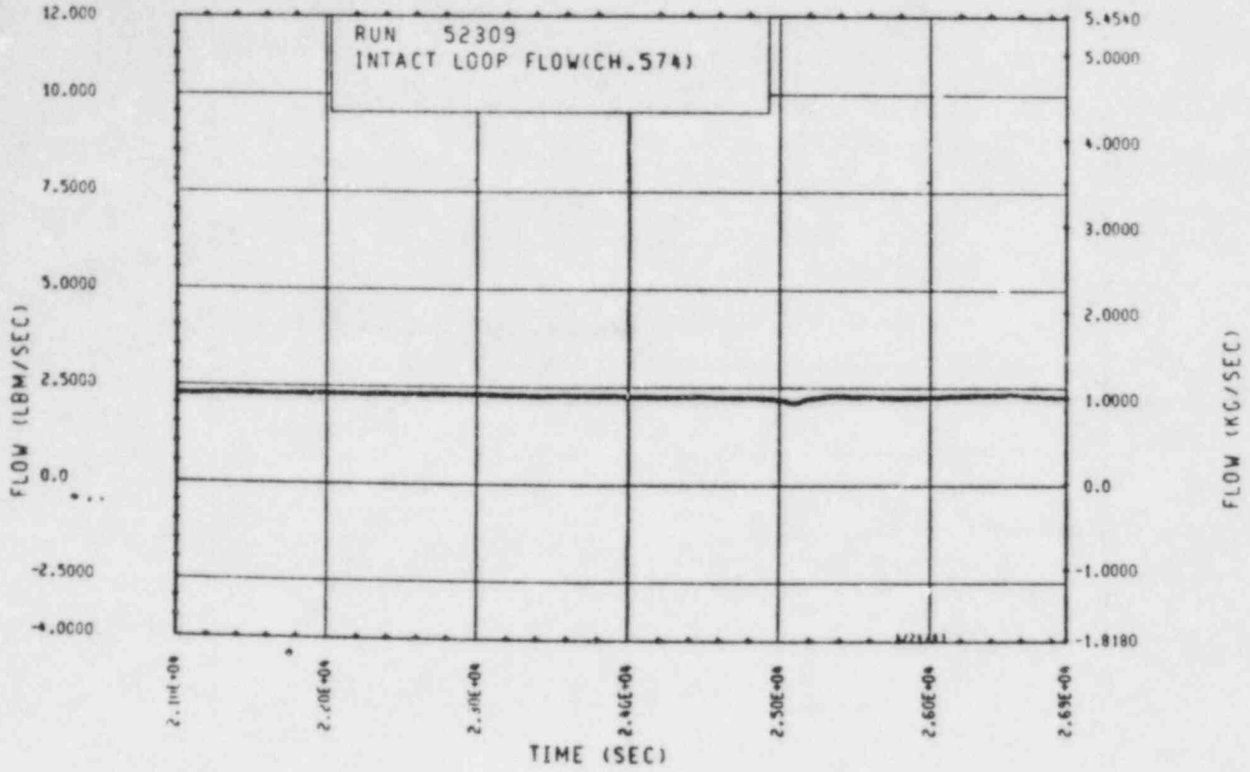

Figure A-35. Mass Flow Rate Through Unbroken Loop, Test 9A

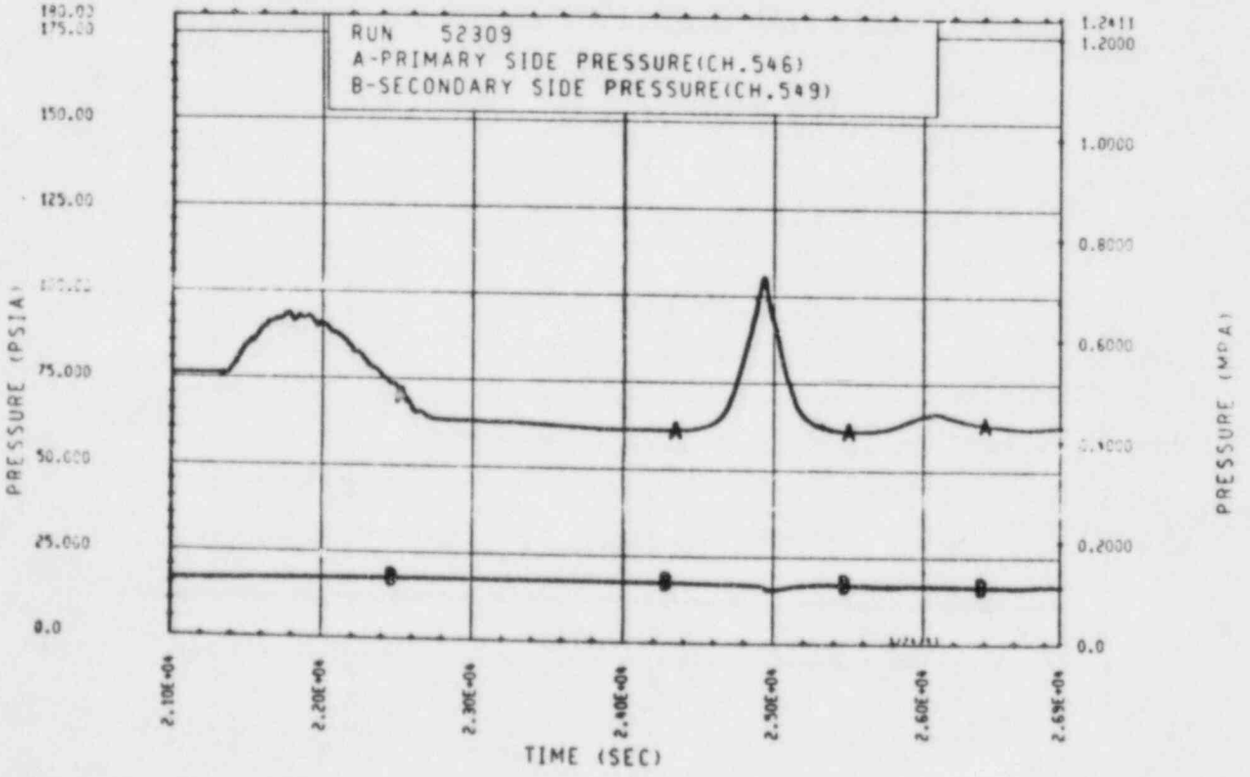

Figure A-36. Primary and Secondary System Pressure, Test 9A

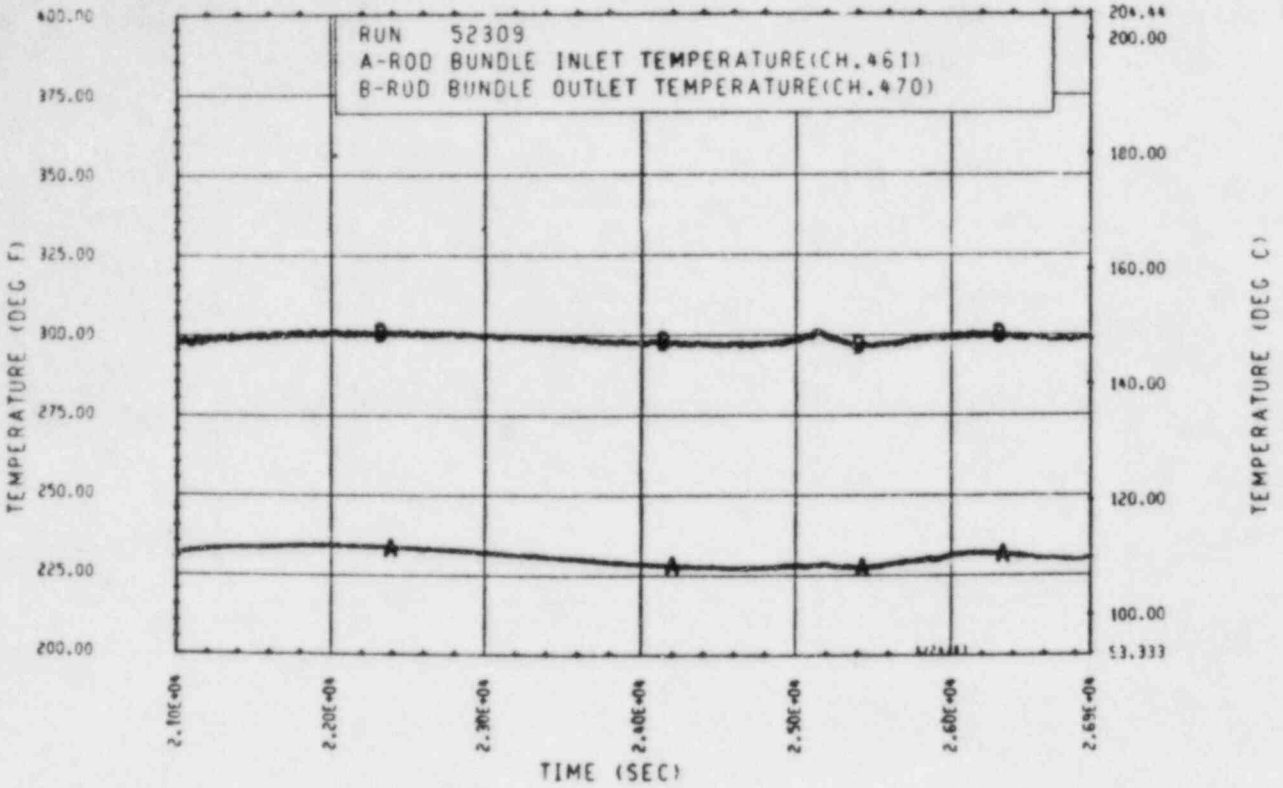

Figure A-37. Heater Rod Bundle Inlet and Outlet Temperature, Test 9A

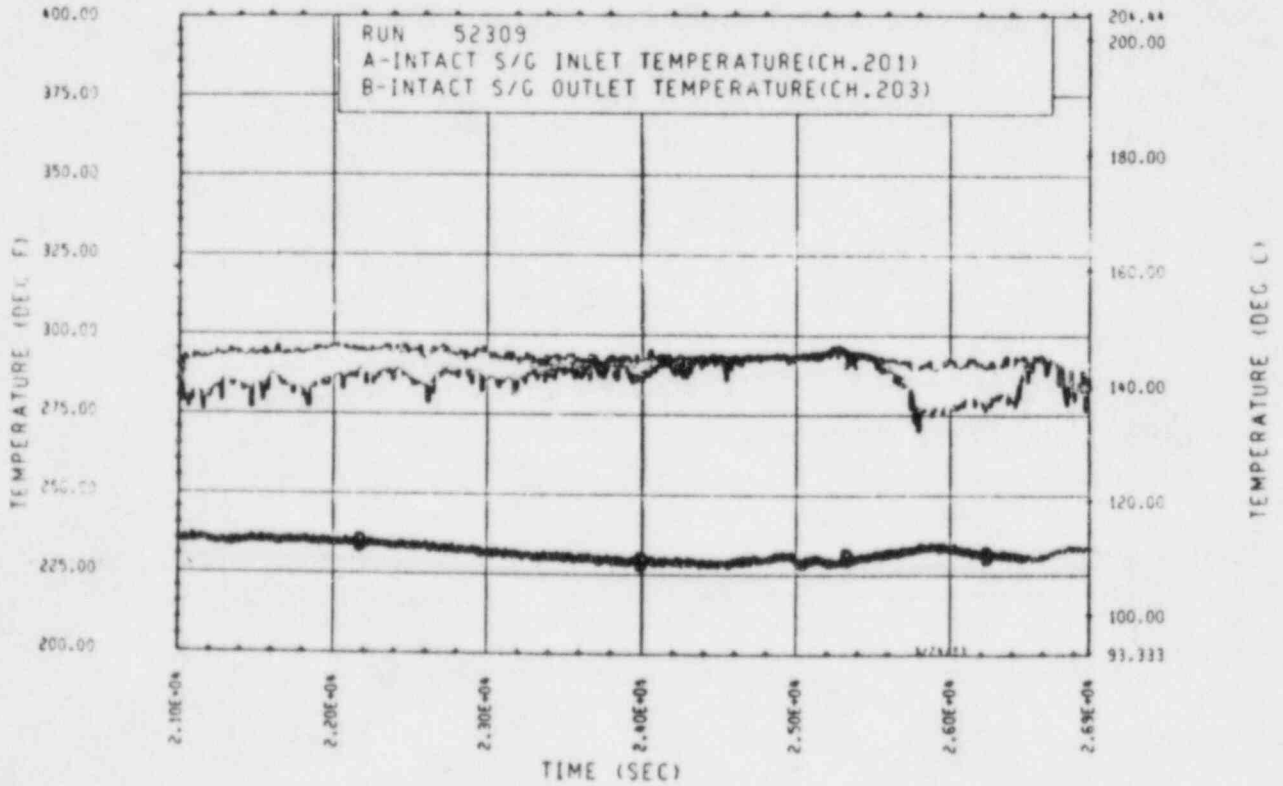

Figure A-38. Unbroken Loop Steam Generator Inlet and Outlet Temperature, Test 9A

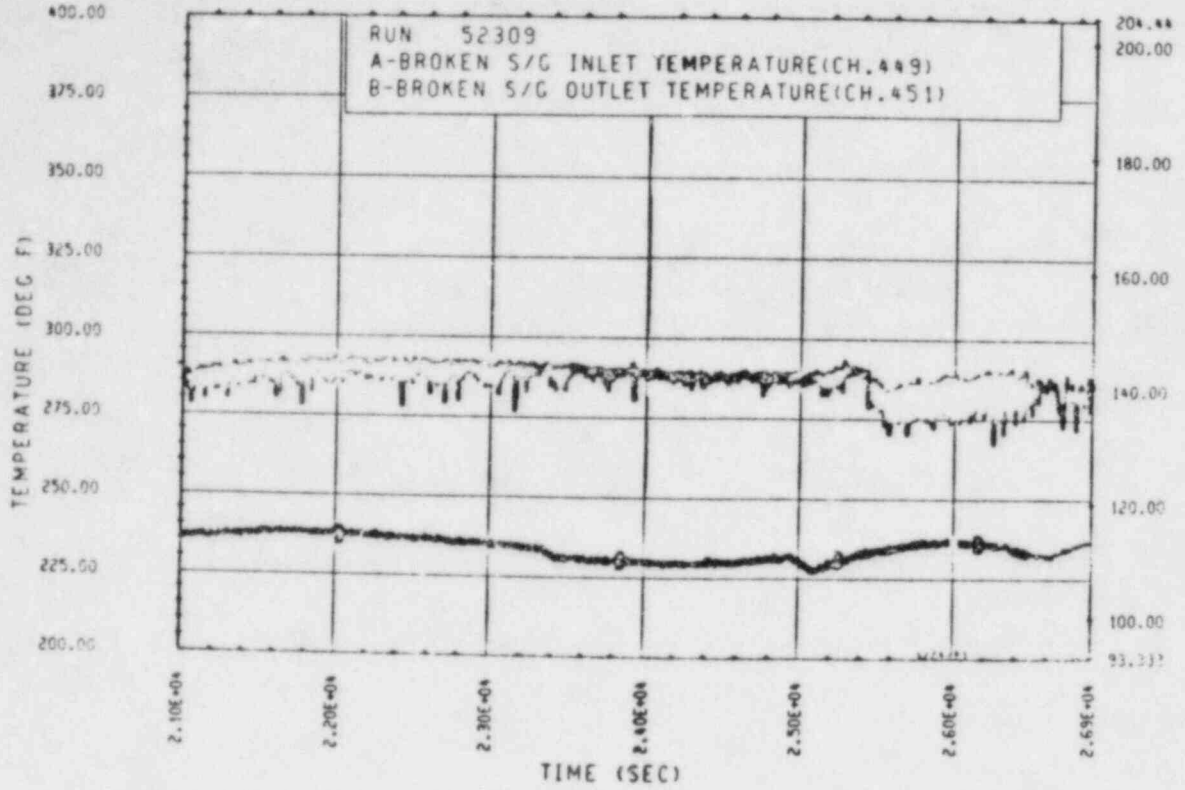

Figure A-39. Broken Loop Steam Generator Inlet and Outlet Temperature, Test 9A

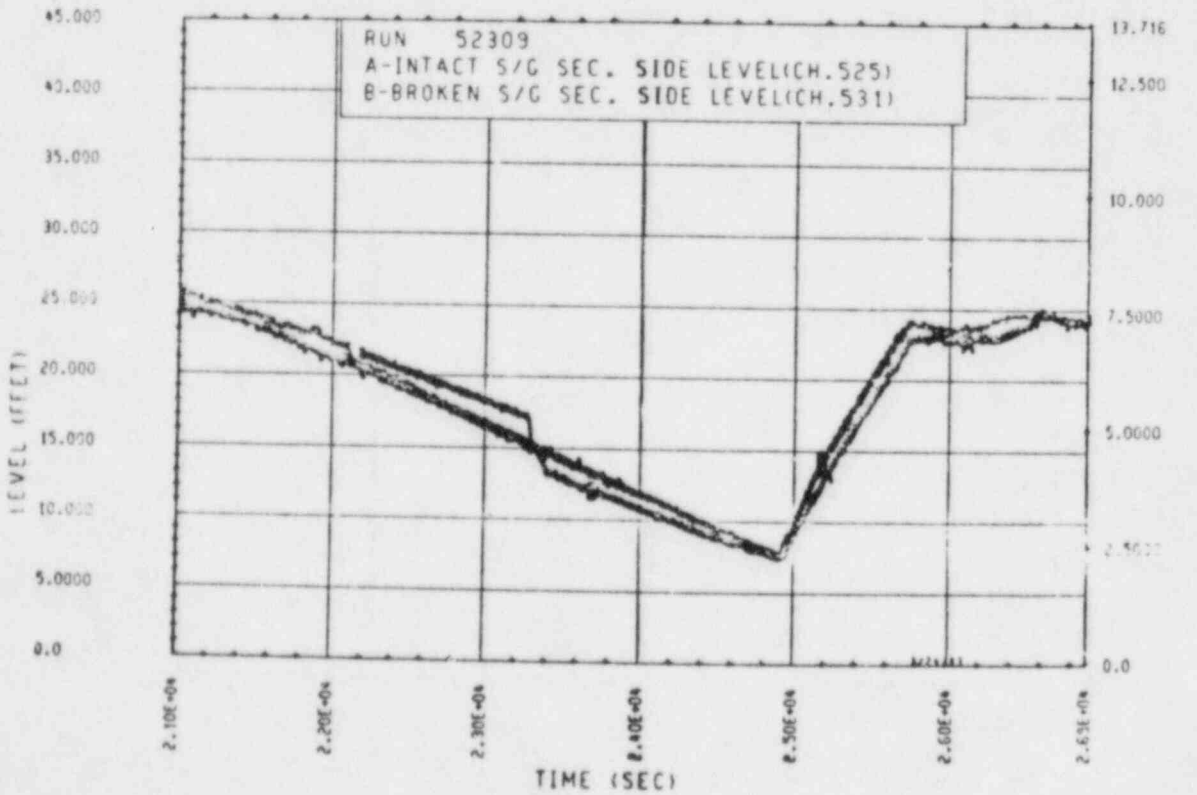

Figure A-40. Unbroken and Broken Loop Steam Generator Secondary Side Collapsed Liquid Levels, Test 9A

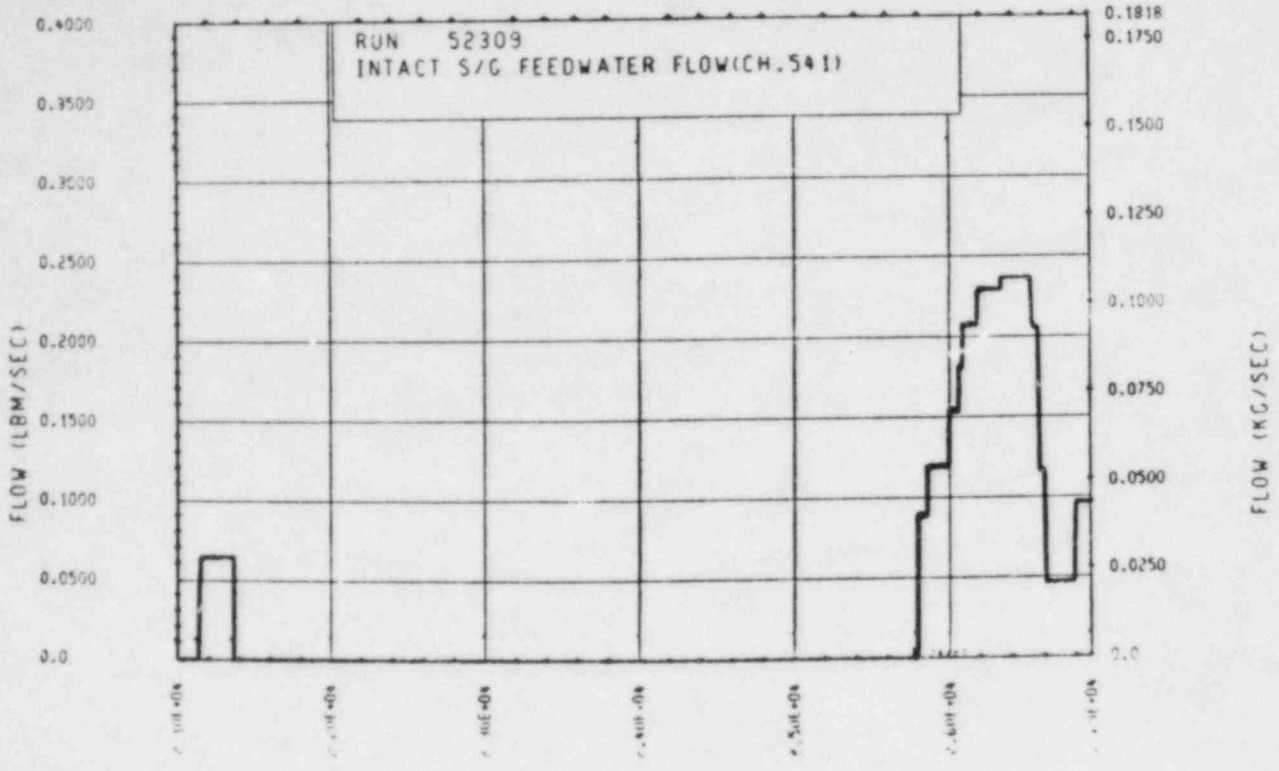

Figure A-41. Unbroken Loop Steam Generator Feedwater Mass Flow Rate, Test 9A

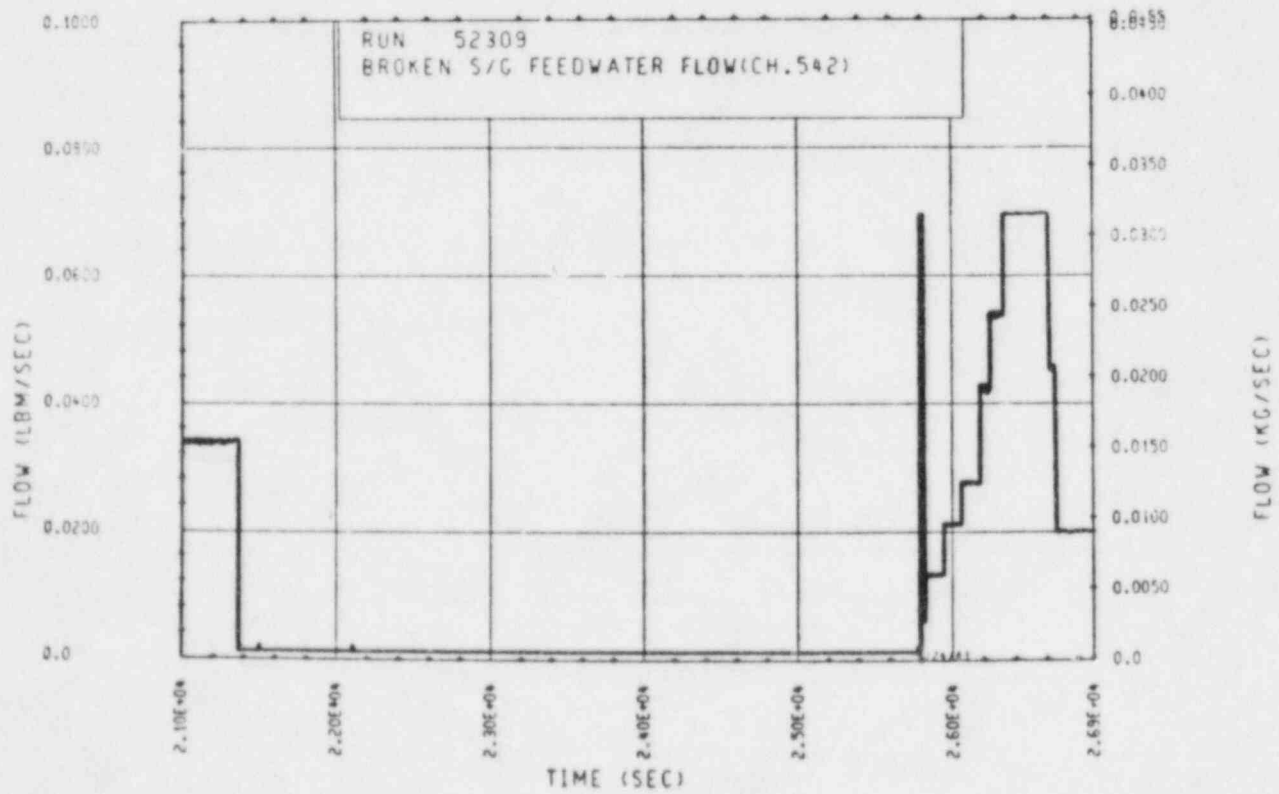

Figure A-42. Broken Loop Steam Generator Feedwater Mass Flow Rate, Test 9A

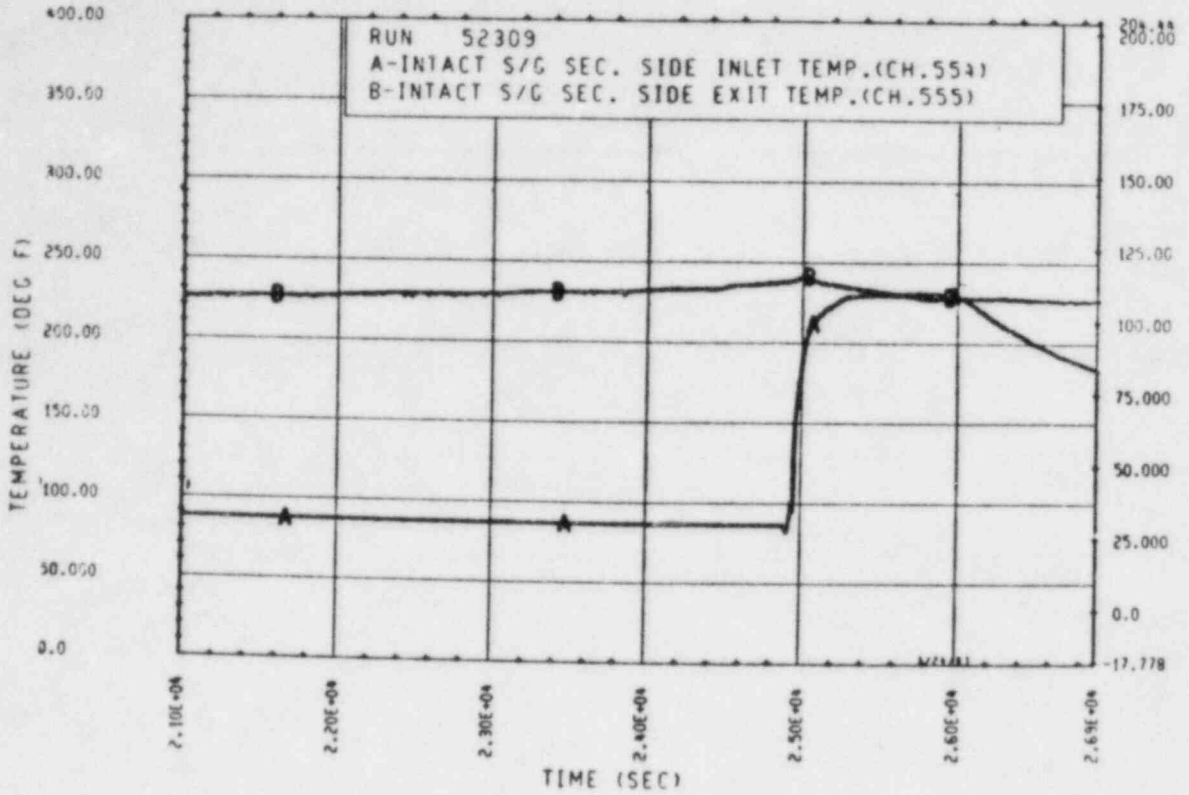

Figure A-43. Unbroken Loop Steam Generator Secondary Side Inlet and Outlet Temperature, Test 9A

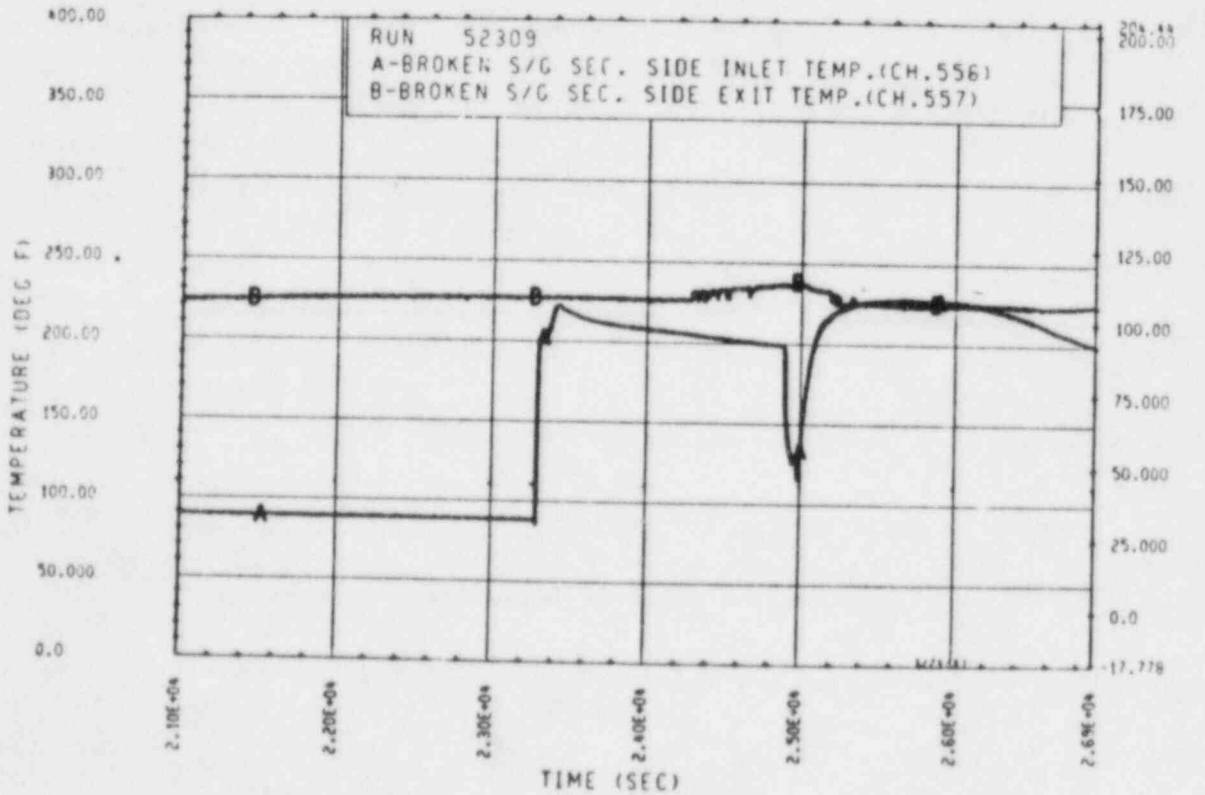

Figure A-44. Broken Loop Steam Generator Secondary Side Inlet and Outlet Temperature, Test 9A

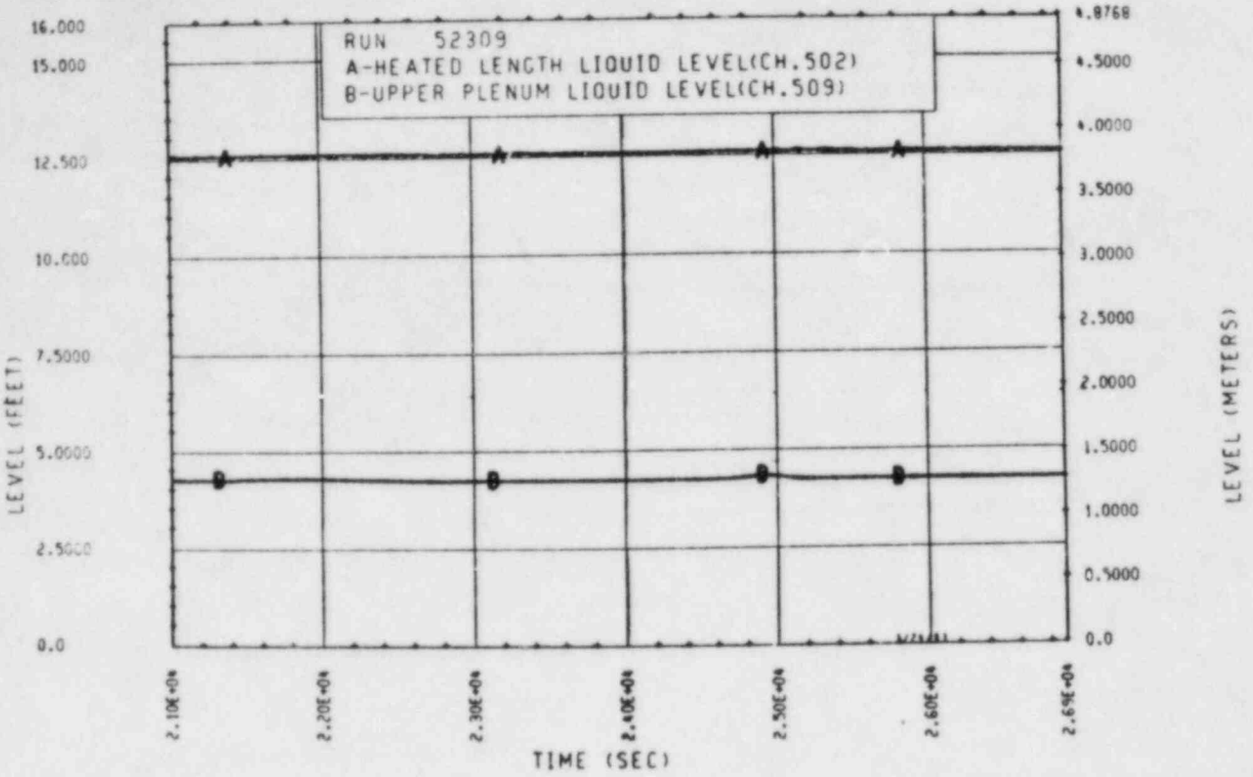

Figure A-45. Heated Length and Upper Plenum Liquid Levels, Test 9A

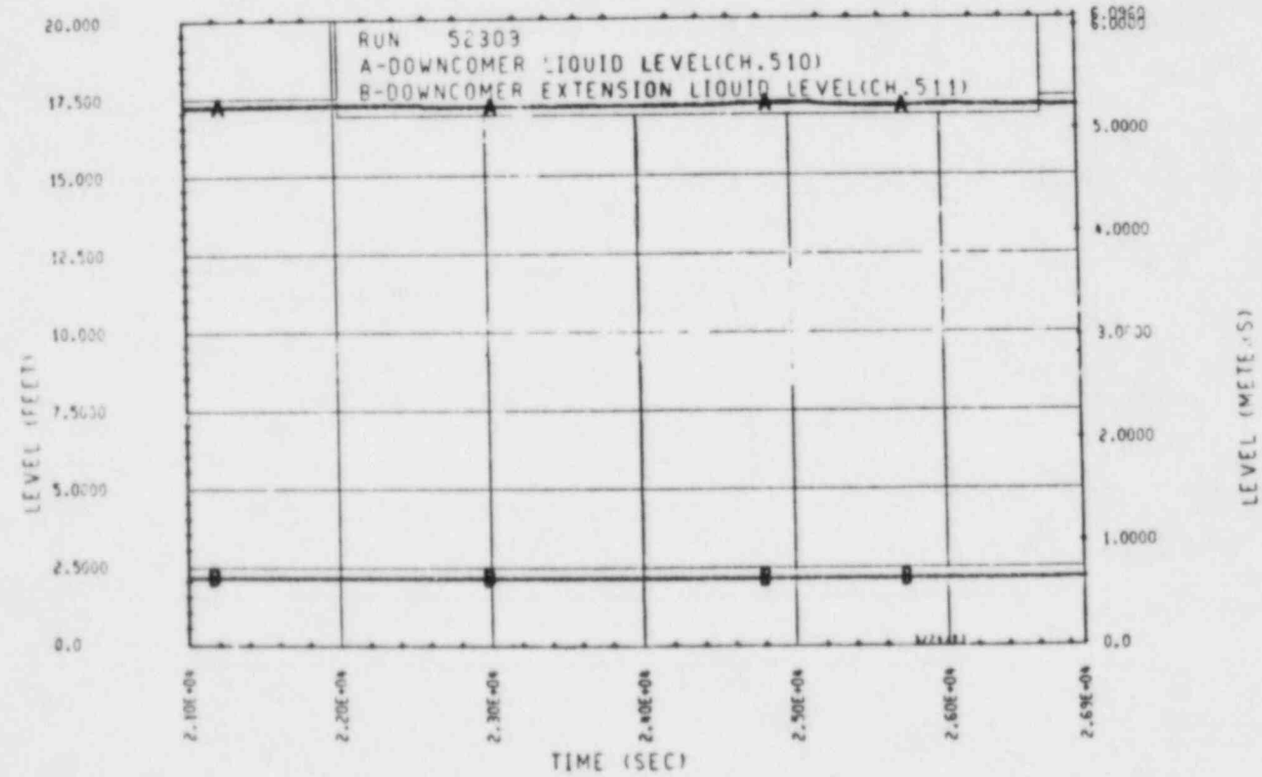

Figure A-46. Downcomer and Downcomer Extension Liquid Levels, Test 9A

TEST 9B: TWO-PHASE NATURAL CIRCULATION WITH SECONDARY SIDE BOILOFF

Objective

To determine the effect of decreasing steam generator heat transfer area (by means of secondary side boiloff) on two-phase natural circulation

Test Procedure

The test was begun from a steady-state peak two-phase flow natural circulation mode with a nominal bundle power of 222 kw. The primary system was brought to the two-phase condition by draining 17.73 percent of the original single-phase mass inventory. The primary system was operated with the pressurizer valved out. The secondary side was operated in a boiling mode with a nominal pressure of 0.28 MPa (40 psia) and an initial collapsed liquid level of 7.62 m (25 ft) (71 percent full). The secondary side feedwater lines were valved out, allowing the secondary side levels to decrease by means of boiloff. Boiloff was terminated when the rod bundle inlet temperature increased to 149°C (300°F). At that time, injection of 110°C (230°F) water from accumulator 1 was initiated into the steam generator secondary sides. Injection continued until the secondary sides of both steam generators were recovered to their original 7.62 m (25 ft) levels. The test was terminated when the system returned to a steady-state condition.

Test Overview

Prior to the initiation of the secondary side boiloff, the primary system was operated in a two-phase peak flow natural circulation mode. The broken loop was stalled, however, as it characteristically would do whenever the system was operated in a two-phase mode. Hence, the system was operating in a N-1 loop configuration, with the unbroken loop steam generator acting as the sole heat sink.

The primary system response to the secondary side boiloff was almost immediate. As soon as the unbroken loop secondary side collapsed liquid level reached the 7.62 (25 ft) mark, the mass flow rate through the unbroken loop began to decrease. This mass flow decrease was, of course, echoed by a total flow decrease through the rod bundle. Thus, the two-phase peak flow mode of natural circulation was significantly more sensitive to secondary side collapsed liquid levels than the single-phase natural circulation mode. Single-phase natural circulation was not affected by a decrease in secondary side collapsed liquid levels until those levels reached the 3.96 m (13 ft) level. The two-phase peak flow sensitivity is the result of the dynamics which inherently create a peak flow situation. Such a situation occurs when the entire length of the uphill side of the steam generator tubes is utilized to condense the two-phase mixture. This results in the lightest possible uphill situation which, when coupled with a relatively heavy liquid-solid downhill, creates a peak density imbalance between the uphill and downhill sides. The net result is a peak mass flow rate through the loop. Any degradation of the secondary side heat sink will result in vapor carryover from the uphill to downhill sides. The pressure of vapor in the downhill side will, of course, decrease the peak density imbalance that previously existed between the uphill and downhill sides. The net result is a decrease in mass flow rate through the loop.

As the secondary side collapsed liquid levels were allowed to decrease further, the mass flow rate decreased correspondingly. As expected, the mass flow decrease was accompanied by increases in temperature throughout the loop, as well as increases in primary system pressure.

It should be noted that, as the primary system pressure increased, the broken loop gradually became more active. It eventually became unstalled to the point where it participated in a steady manner as a heat sink (14,500-16,500 seconds). As pressure decreased during the recovery of the secondary side levels (16,500-17,300 seconds), the broken loop gradually became less active and eventually stalled. This suggests that the broken loop stalling may be a pressure-dependent phenomenon.

TEST SCHEDULE
TEST 9b

Time (sec)	Event
0	Computer on
552	Power to 222 kw; primary system operating in a forced circulation mode
5712	Steady-state single phase natural circulation established
6640	Pressurizer valved out (accumulator 2)
6707	System pressure fell from 0.97 MPa (140 psi) to a steady 0.75 MPa (109 psi).
7010	Began 136 kg (300 lbm) continuous drain from the primary system. Mass was drained from the primary until a two-phase peak-flow natural circulation mode was established.
7268	45 kg (100 lbm) drained
7576	91 kg (200 lbm) drained
7906	End of 136 kg (300 lbm) continuous drain
8263	Began 9 kg (20 lbm) drain
8325	Ended 9 kg (200 lbm) drain: 145 kg (320 lbm) drained from the primary system

Time (sec)	Event
8549	Two-phase peak-flow natural circulation condition established; primary system pressure = 0.385 MPa (55.9 psia)
9488	Feedwater shut off to unbroken loop steam generator (broken loop steam generator feedwater flow already shut off because of earlier stalling of the broken loop); beginning of secondary side boiloff
10084	Because of broken loop flow stalling, the small steam generator secondary had to be drained to maintain a collapsed liquid level equal to that of the unbroken loop steam generator secondary. Unbroken loop steam generator secondary was boiling off rapidly.
10332	Ended draining of broken loop steam generator secondary
10477	To maintain secondary side collapsed liquid levels, broken loop secondary required continuous draining. This draining was controlled by control panel ball valves.
11472	Broken loop steam generator became active and began to boil off secondary. Draining was halted.
12069	Primary pressure = 0.488 MPa (70.8 psia); gradual primary pressure increase observed during the entire boiloff

Time (sec)	Event
14101	Primary system pressure alarm sounded at 0.69 MPa (100 psia)
14577	Began injection of 110°C (232°F) accumulator 1 water into both steam generator secondaries
17038	Both steam generator secondary side levels recovered to approximately 7.62 m (25 ft)
17688	Began 363 kg (800 lbm) continuous drain from the primary system. Mass was drained from the primary until a reflux mode of natural circulation was established.
17922	45 kg (100 lbm) drained
19728	Ended 363 kg (800 lbm) continuous drain; total mass drained from the primary system = 508 kg (1120 lbm)
19932	Weir meters valved in
20184	Began 9 kg (20 lbm) drain
20251	Ended 9 kg (20 lbm) drain; 517 kg (1140 lbm) drained from the primary system
20457	Began 18 kg (40 lbm) drain
20575	Ended 18 kg (40 lbm) drain; 535 kg (1180 lbm) drained from the primary system
20582	Slight power adjustment

Time (sec)	Event
20907	Began 9 kg (20 lbm) drain
20978	Ended 9 kg (20 lbm) drain; 544 kg (1200 lbm) drained from the primary system
21220	Began 9 kg (20 lbm) drain
21289	Ended 9 kg (20 lbm) drain; 553 kg (1200 lbm) drained from the primary system
21804	Began 9 kg (20 lbm) drain
21869	Ended 9 kg (20 lbm) drain; 562 kg (1240 lbm) drained from the primary system
22218	Began 9 kg (20 lbm) drain
22284	Ended 9 kg (20 lbm) drain; 571 kg (1260 lbm) drained from the primary system
22947	Began 9 kg (20 lbm) drain
23011	Ended 9 kg (20 lbm) drain; 580 kg (1280 lbm) drained from the primary system. Weir meters indicated intermittent reflux.
23550	Began 9 kg (20 lbm) drain
23624	Ended 9 kg 20 lbm drain; 590 kg (1300 lbm) drained from the primary system

Time (sec)	Event
24192	Began 4.5 kg (10 lbm) drain
24222	Ended 4.5 kg (10 lbm) drain; 594 kg (1310 lbm) drained from the primary system
25632	Reflux natural circulation established; primary system pressure = 0.30 MPa (44 psia)
26520	Feedwater to both steam generator secondaries shut off. Began secondary side boiloff.
29663	Broken loop steam generator secondary side drained to equilibrate secondary side levels of both steam generators
31674	Primary system pressure alarm sounded at 0.69 MPa (100 psia.
31789	Began injection of 111°C (232°F) accumulator 1 water into both steam generator secondaries
32813	Both steam generator secondary side levels recovered to approximately 7.62 m (25 ft)
33983	Power off

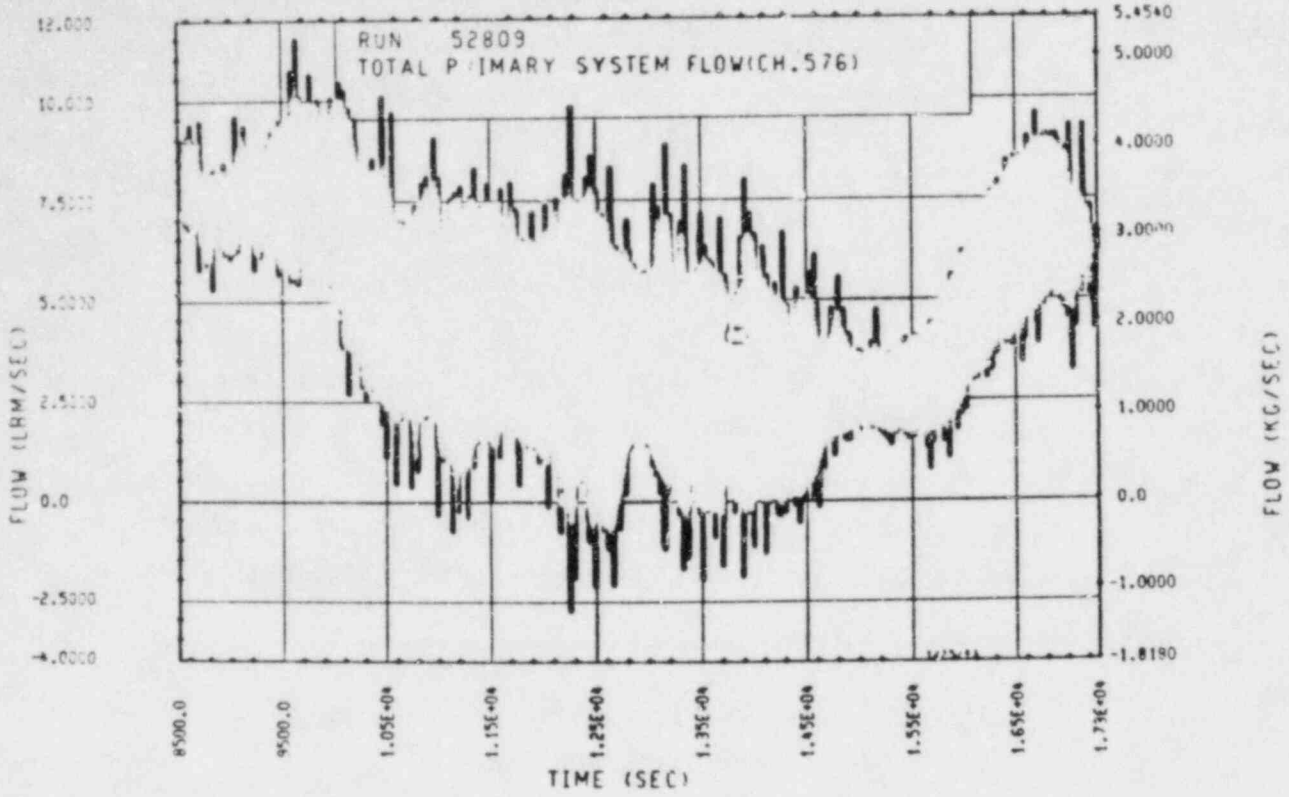

Figure A-47. Mass Flow Rate Through Rod Bundle, Test 9B

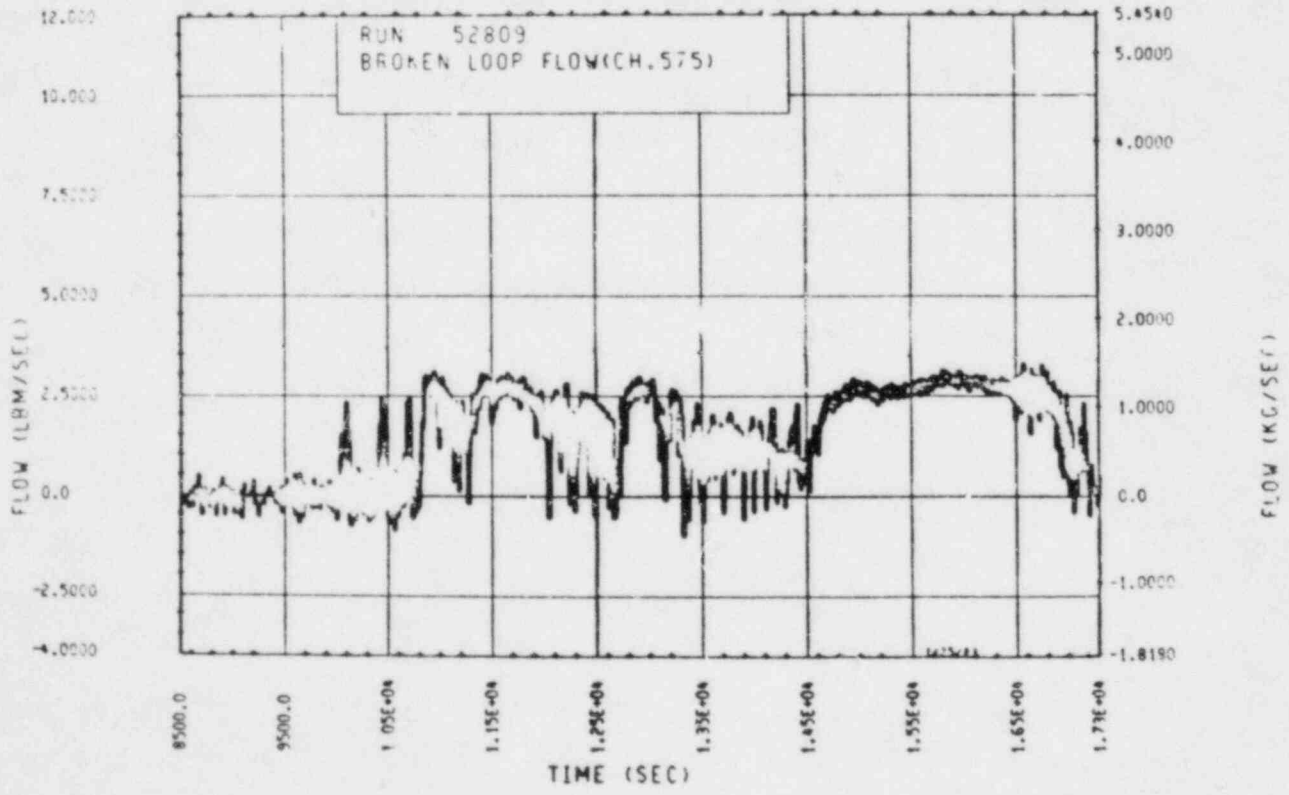

Figure A-48. Mass Flow Rate Through Broken Loop, Test 9B

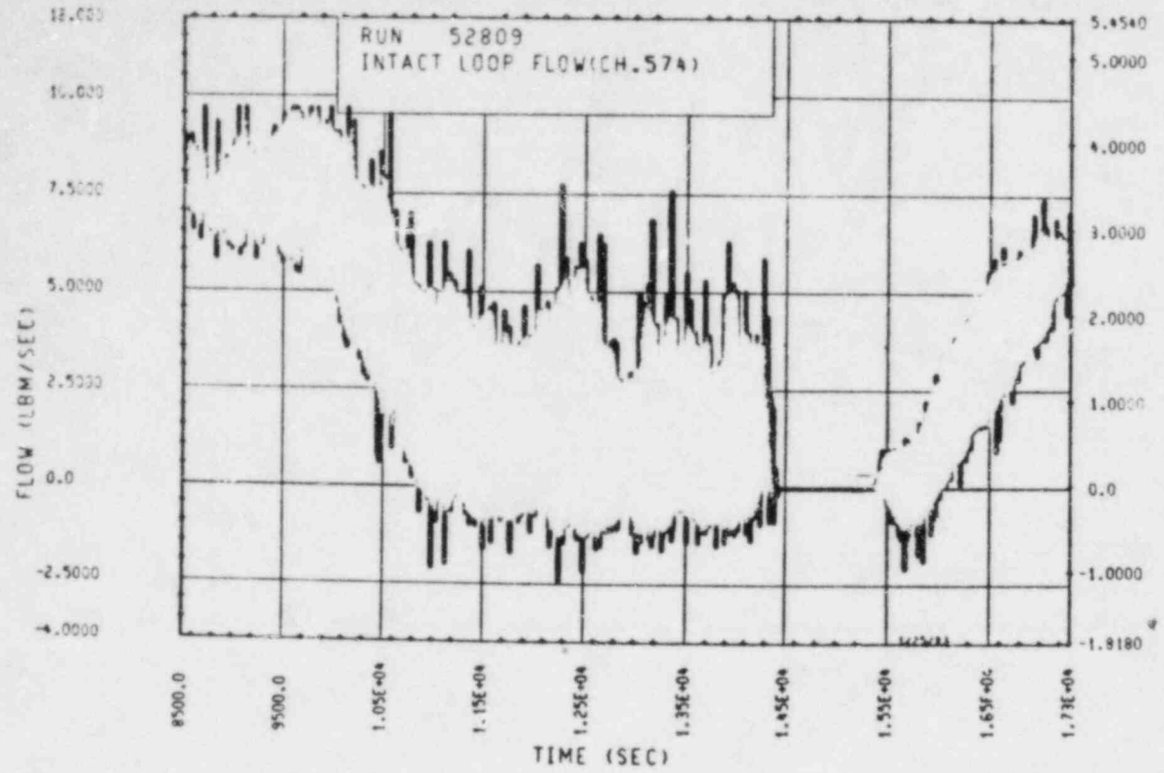

Figure A-49. Mass Flow Rate Through Unbroken Loop, Test 9B

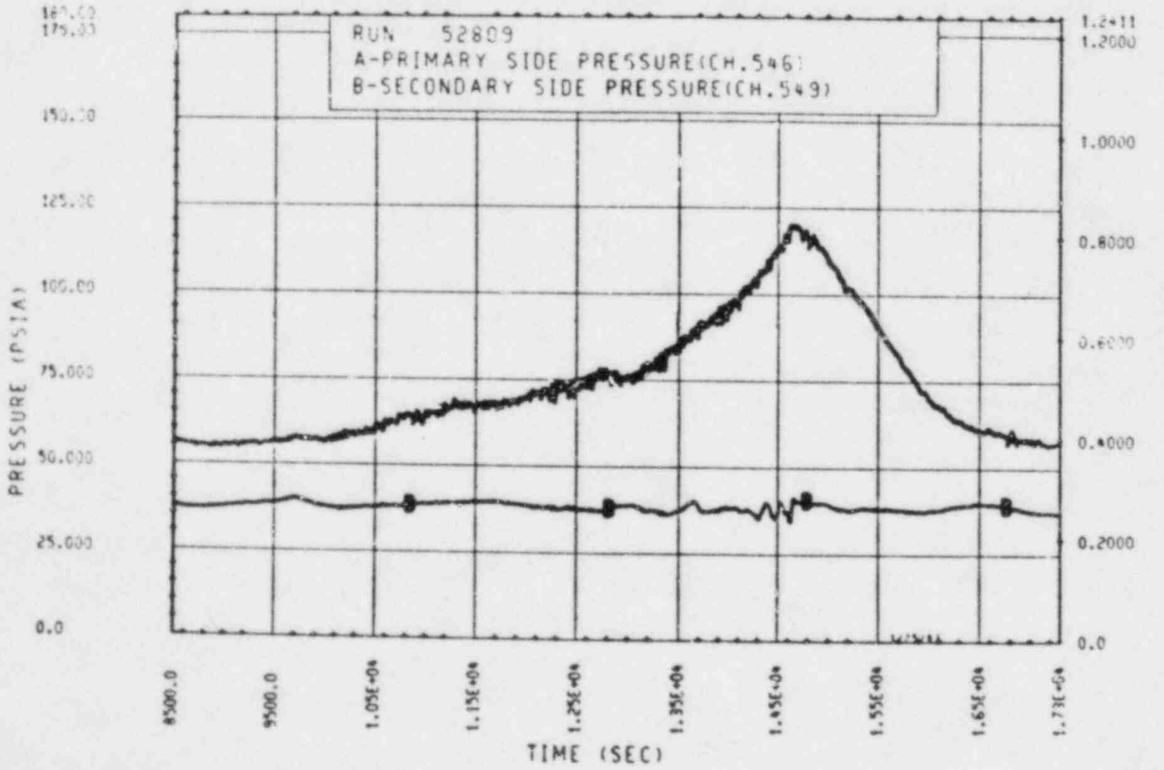

Figure A-50. Primary and Secondary System Pressure, Test 9B

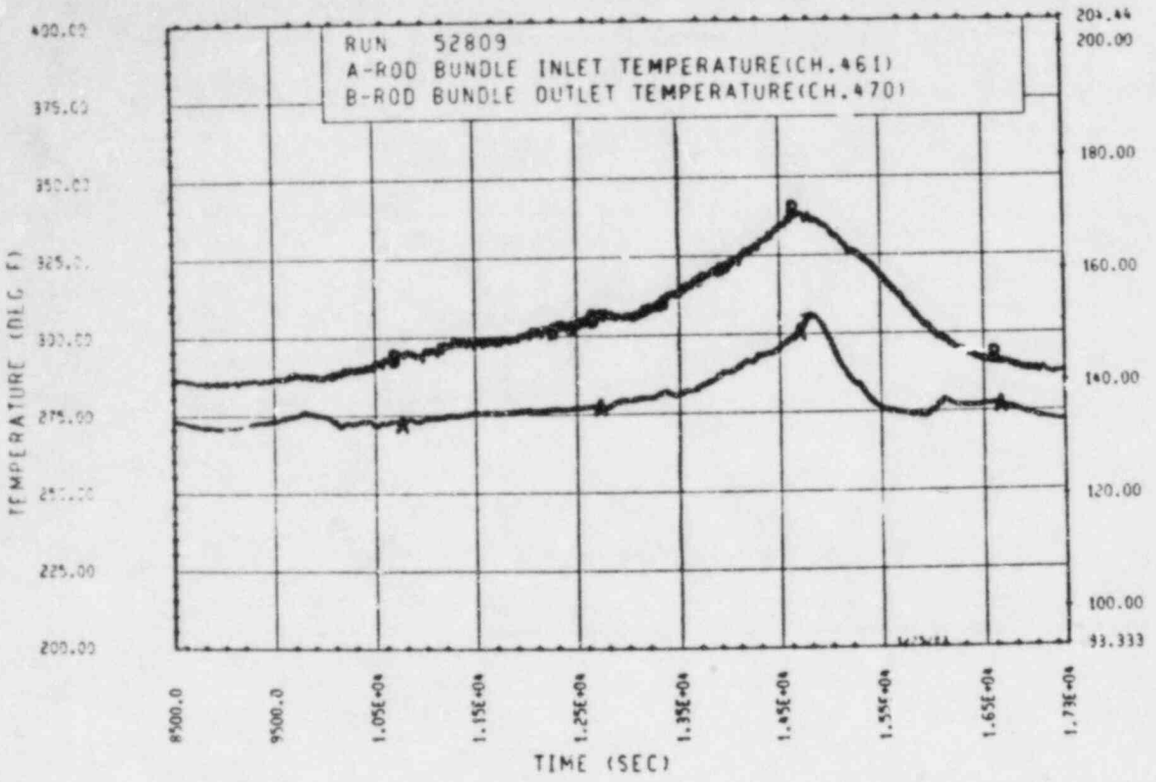

Figure A-51. Heater Rod Bundle Inlet and Outlet Temperature, Test 9B

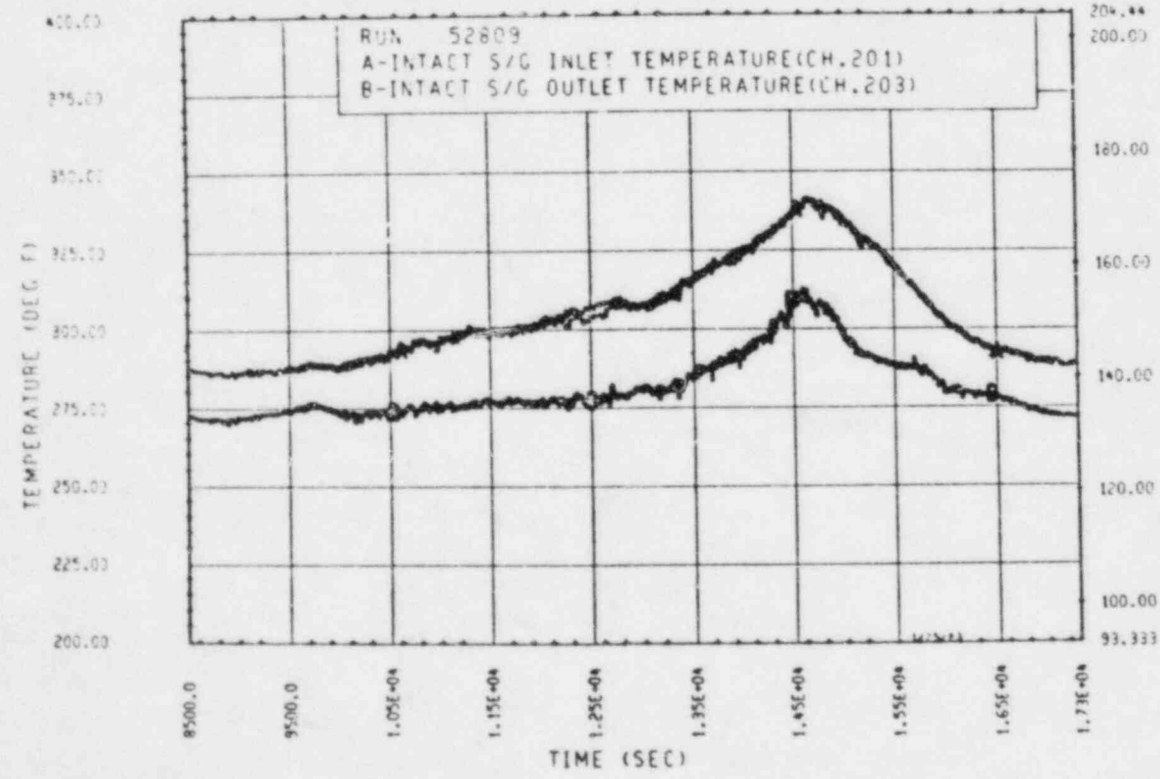

Figure A-52. Unbroken Loop Steam Generator Inlet and Outlet Temperature, Test 9B

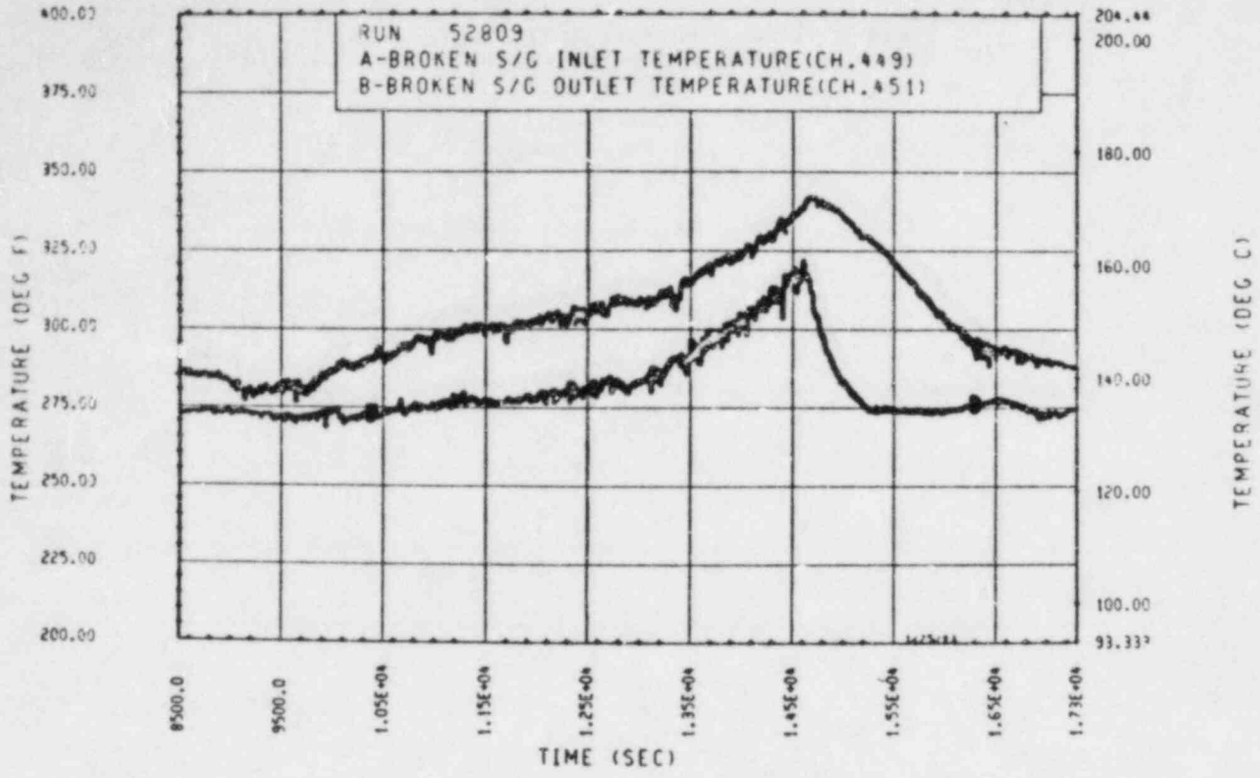

Figure A-53. Broken Loop Steam Generator Inlet and Outlet Temperature, Test 9B

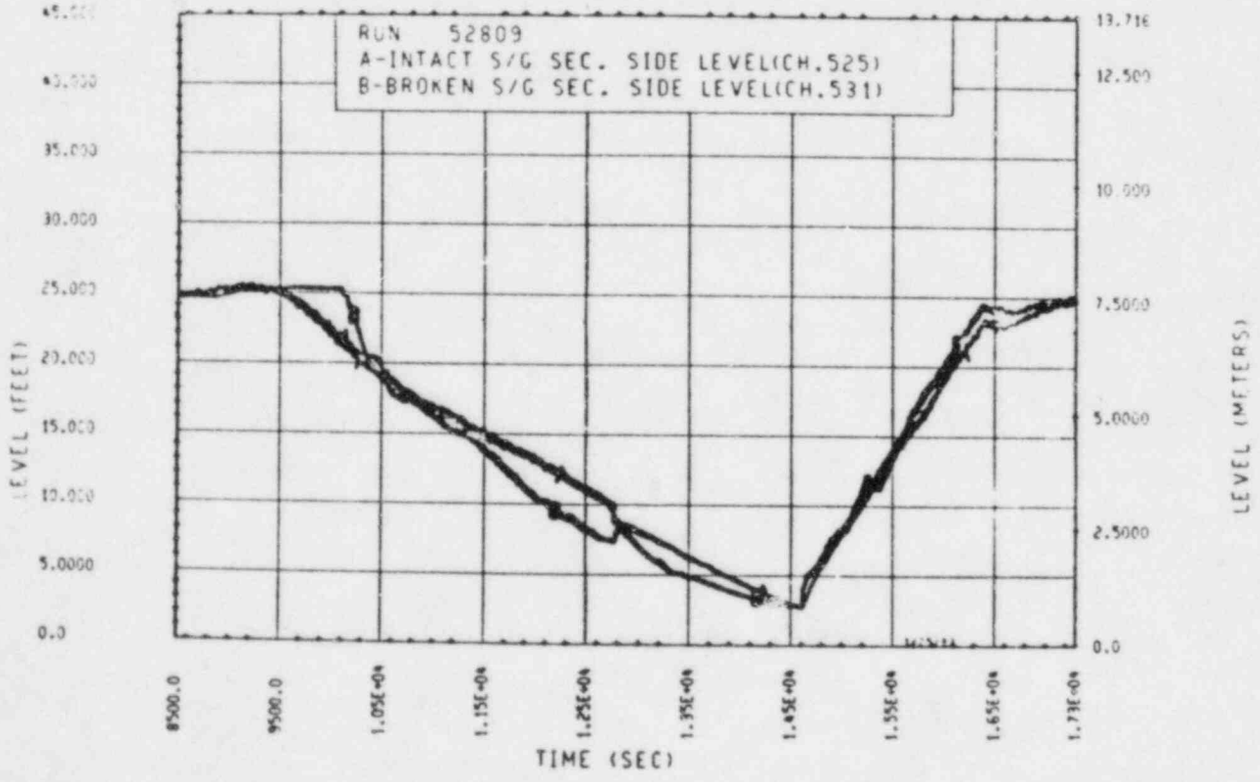

Figure A-54. Unbroken and Broken Loop Steam Generator Secondary Side Collapsed Liquid Levels, Test 9B

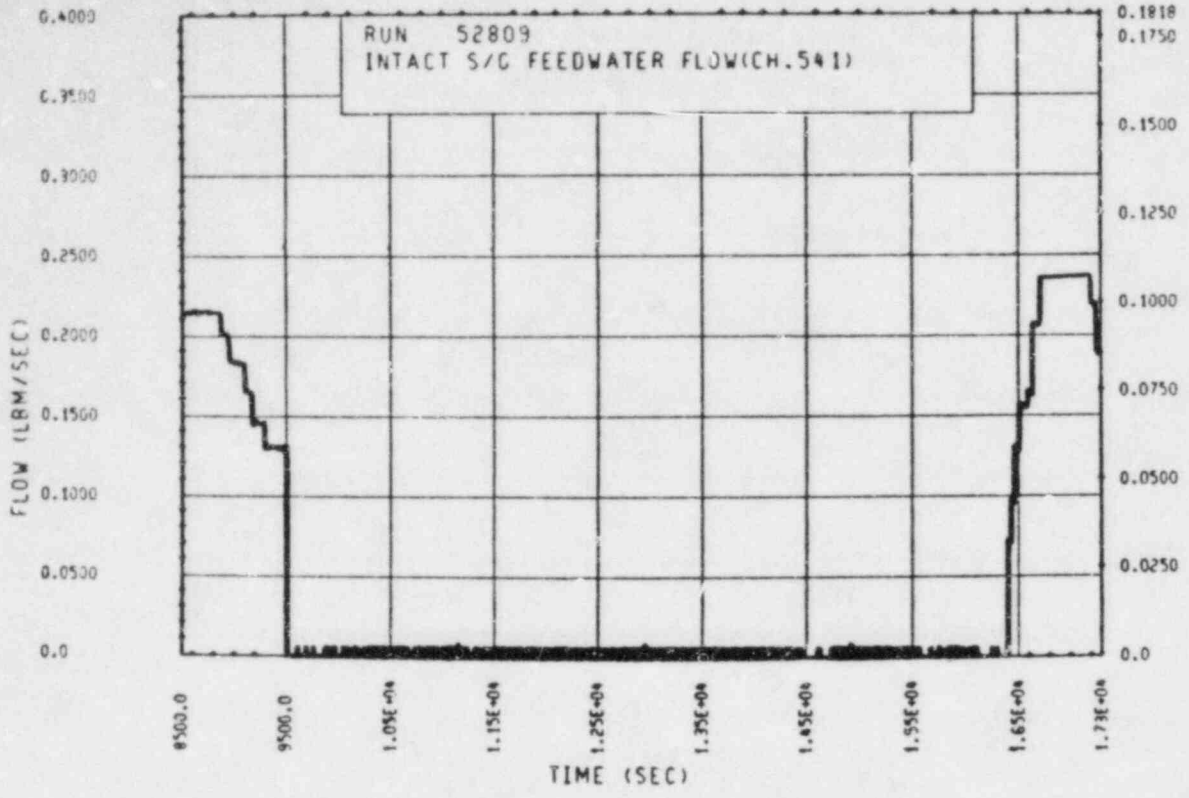

Figure A-55. Unbroken Loop Steam Generator Feedwater Mass Flow Rate, Test 9B

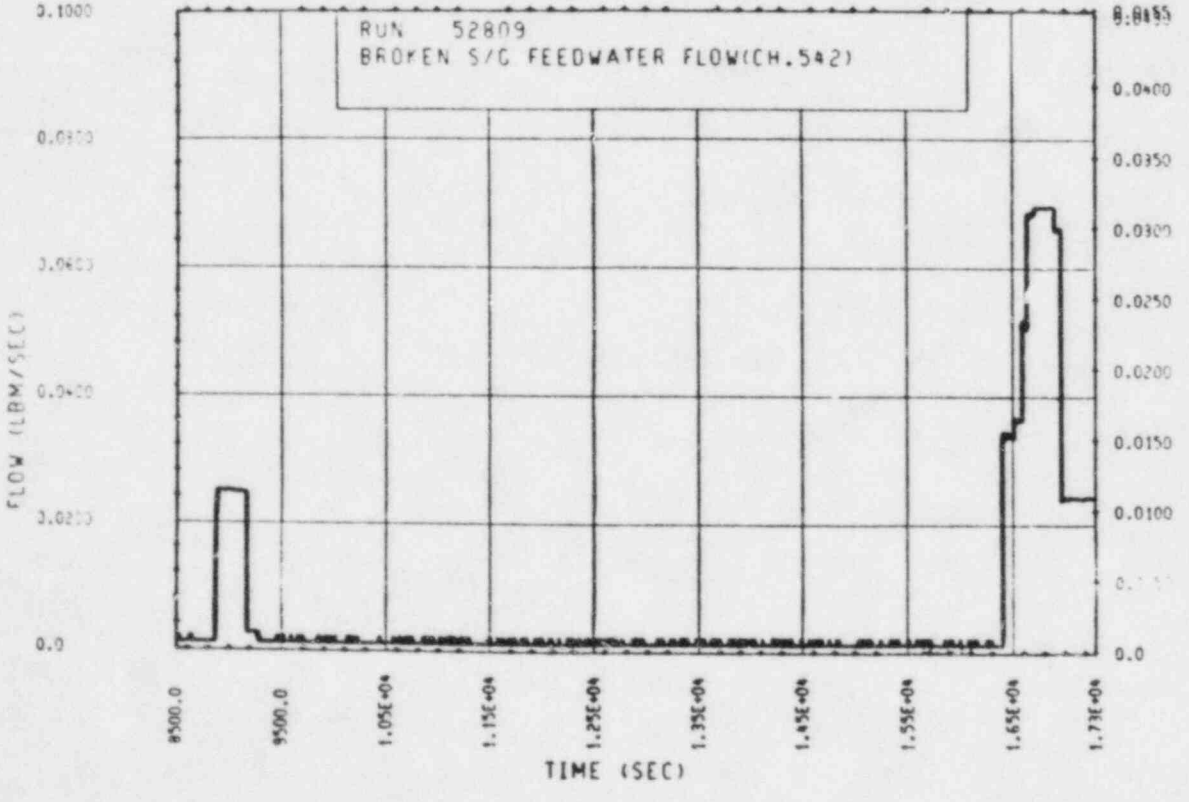

Figure A-56. Broken Loop Steam Generator Feedwater Mass Flow Rate, Test 9B

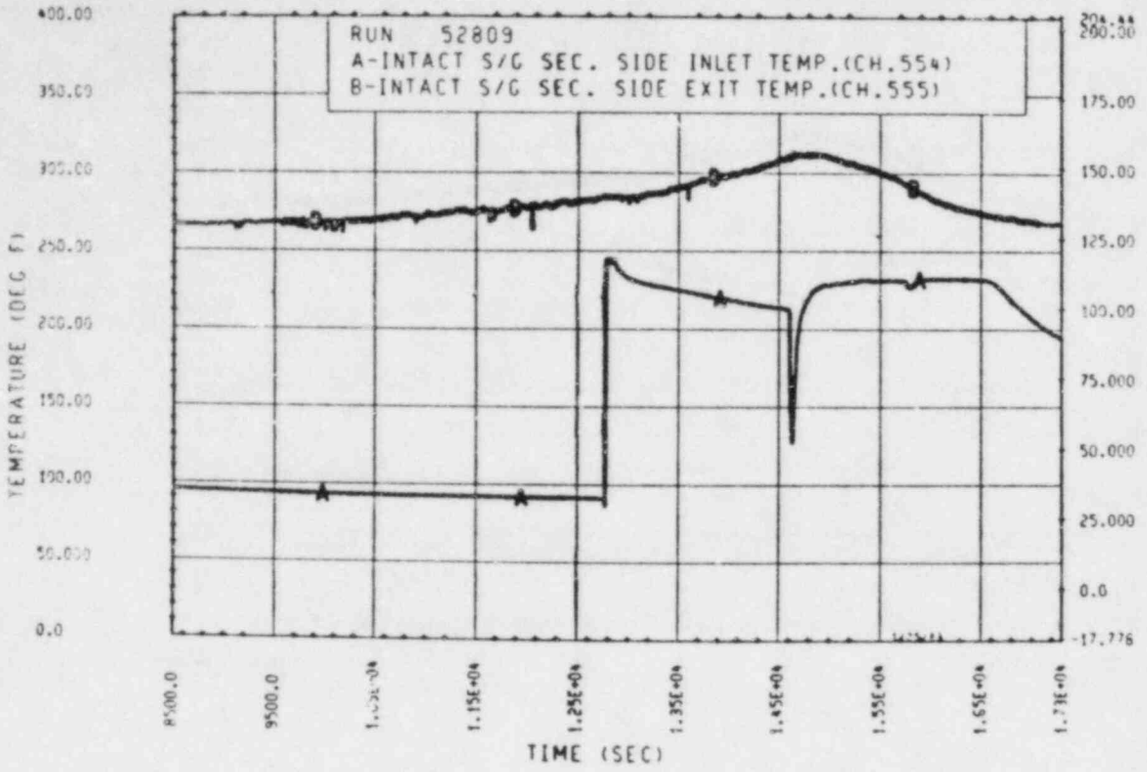

Figure A-57. Unbroken Loop Steam Generator Secondary Side Inlet and Outlet Temperature, Test 9B

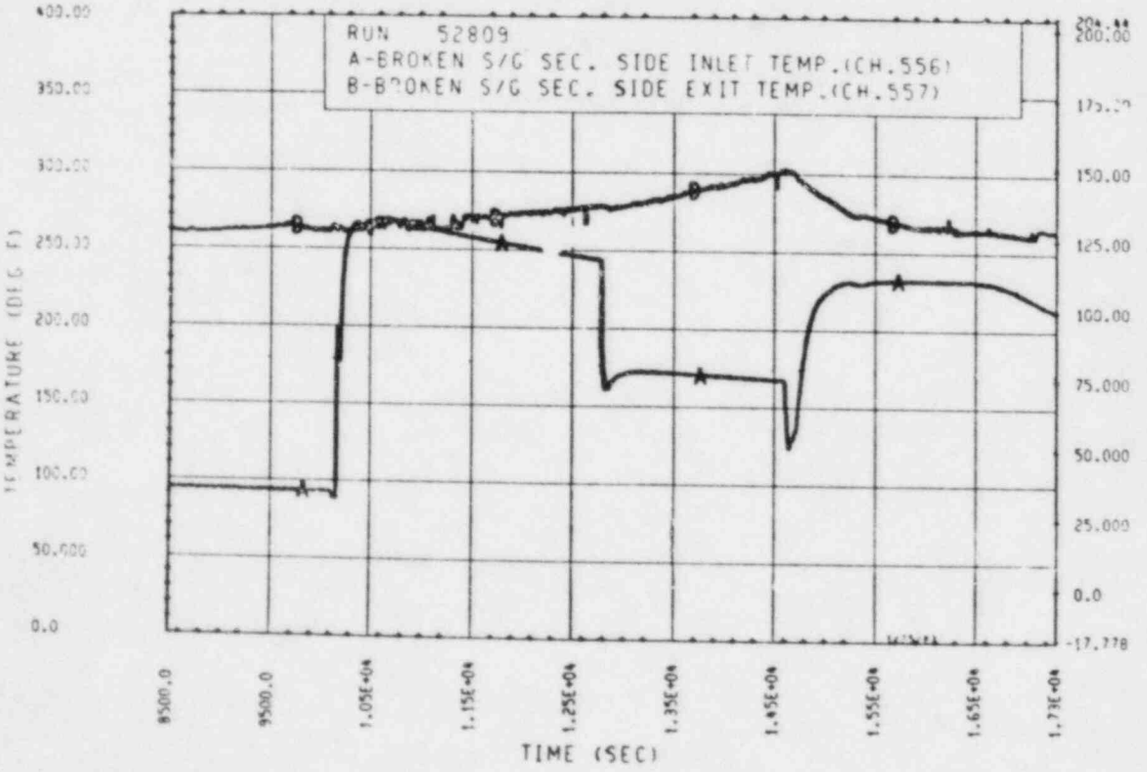

Figure A-58. Broken Loop Steam Generator Secondary Side Inlet and Outlet Temperature, Test 9B

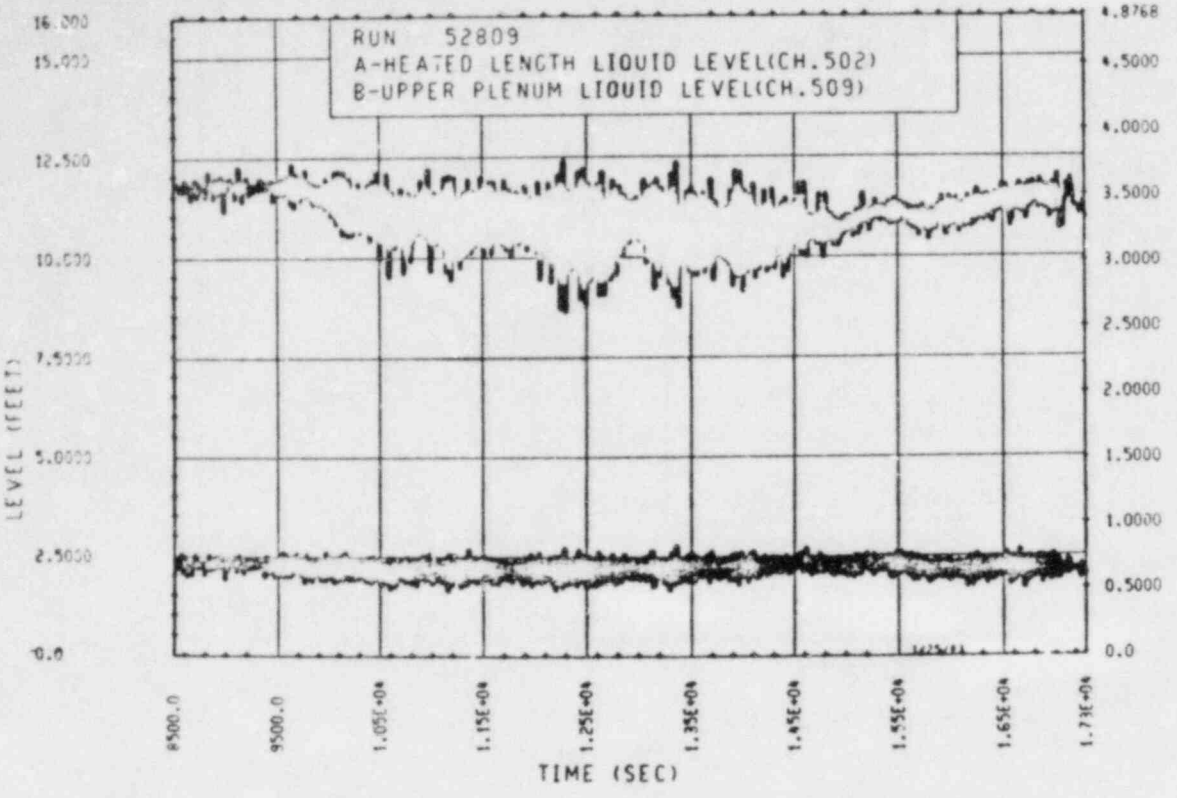

Figure A-59. Heated Length and Upper Plenum Liquid Levels, Test 9B

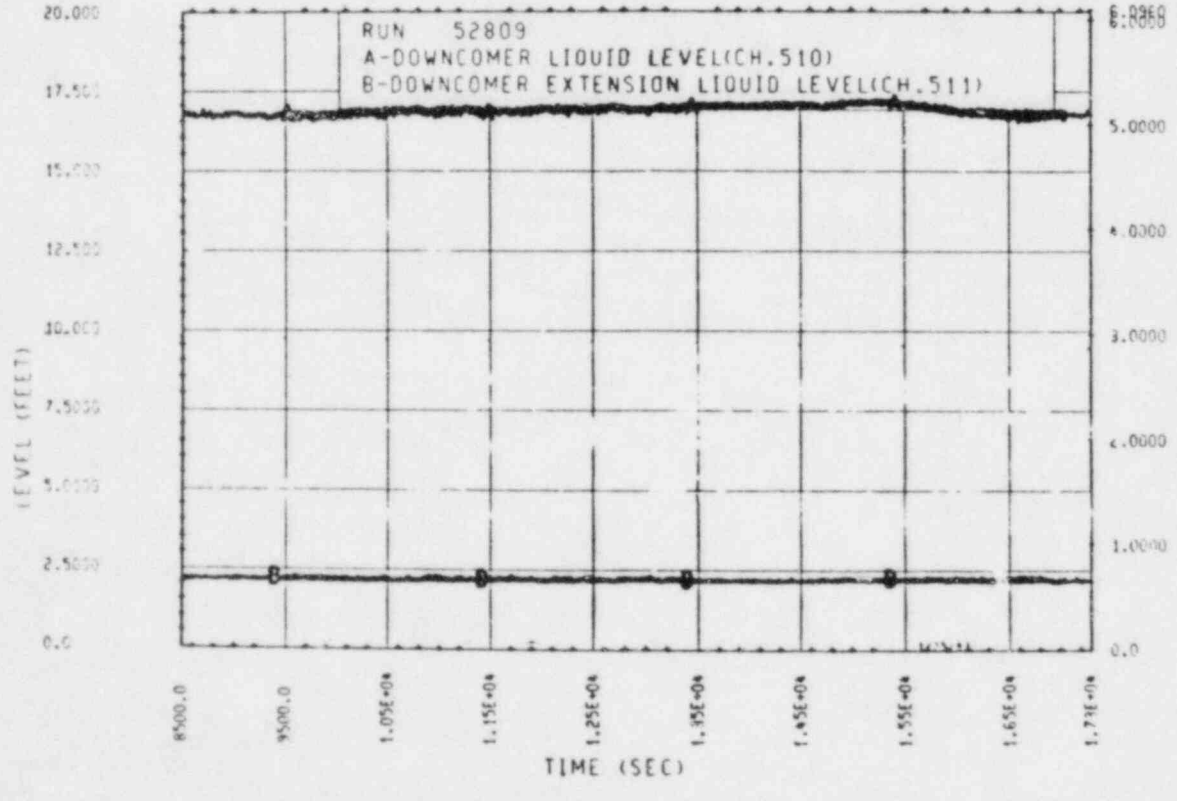

Figure A-60. Downcomer and Downcomer Extension Liquid Levels, Test 9B

TEST 9C: REFLUX CONDENSATION WITH SECONDARY SIDE BOILOFF

Objective

To determine the effect of decreasing steam generator heat transfer area (by means of secondary side boiloff) on the reflux condensation mode of natural circulation

Test Procedure

The test was begun from a steady-state reflux condensation mode with a nominal bundle power of 222 kw. The primary system was operated with the pressurizer valved out and a reduced mass inventory consistent with previously established reflux condensation conditions. The secondary side was operated in a boiling mode with a nominal pressure of 0.28 MPa (40 psia) and an initial collapsed liquid level of 7.62 m (25 ft) (71 percent full). The secondary side feedwater lines were valved out, allowing the secondary side levels to decrease by means of boiloff. Boiloff was terminated when the primary system pressure increased to 0.69 MPa (100 psia). At that time, 93°C (200°F) water was injected into the secondary sides from accumulator 1. Injection continued until the secondary sides of both steam generators were recovered to their original 7.62 m (25 ft) levels. The test was terminated when the system returned to a steady-state condition.

Test Overview

The secondary side feed flows were isolated and both the unbroken and broken loop steam generators levels decreased close together; however, it was observed that the broken loop level came down slower and in steps. This indicates that the heat load was not perfectly split between the two generators and did vary as the inventory was boiled away in the generators. The effect of losing the heat sink or steam generator surface area was felt only mildly by the primary system until the steam generator collapsed liquid level reached approximately 2.44 m (8 ft). It should be noted that there were several loop seal blow-through transients, which would help to depressurize the primary

systems by mixing the generated steam with the colder loop seal water. However, once the secondary side steam generator level had dropped below 2.44-3.05 m (8-10 ft), there was insufficient surface area to condense all the generated vapor and the primary system pressurizer to create a larger driving force ΔT from primary to secondary to compensate. The primary system pressure rapidly responded to this heat source (heat sink mismatch) and rapidly rose. The transient was terminated when the secondary side steam generator level was at the 0.76 m (2.5 ft) elevation. At this point, the primary pressure was at 0.87 MPa (126 psia) and the accumulator was activated to fill the secondary sides of the generators. It should be noted that the primary pressure quickly dropped to its steady value as the generators filled past the 3.05-3.66 m (10-12 ft) elevation. This indicates that stable refluxing could be maintained with a secondary level as low as approximately 3.05 m (10 ft) in the generators without a significant primary side pressure rise.

The reflux meters indicated a stoppage of reflux flow as the system began to pressurize. Reflux flow was restored when the steam generator levels were increased past the 3.05-3.66 m (10-12 ft) elevations.

TEST SCHEDULE
TEST 9c

Time (sec)	Event
0	Computer on
552	Power to 222 kw; primary system operating in a forced circulation mode
5712	Steady-state single phase natural circulation established
6640	Pressurizer valved out (accumulator 2)
6707	System pressure fell from 0.97 MPa (140 psi) to a steady 0.75 MPa (109 psi)
7010	Began 136 kg (300 lbm) continuous drain from the primary system. Mass was drained from the primary until a two-phase peak-flow natural circulation mode was established.
7268	45 kg (100 lbm) drained
7576	91 kg (200 lbm) drained
7906	End of 136 kg (300 lbm) continuous drain
8263	Began 9 kg (20 lbm) drain
8325	Ended 9 kg (200 lbm) drain; 145 kg (320 lbm) drained from the primary system

Time (sec)	Event
8549	Two-phase peak-flow natural circulation condition established; primary system pressure = 0.385 MPa (55.9 psia)
9488	Feedwater shut off to unbroken loop steam generator (broken loop steam generator feedwater flow already shut off because of earlier stalling of the broken loop); beginning of secondary side boiloff
10084	Because of broken loop flow stalling, the small steam generator secondary had to be drained to maintain a collapsed liquid level equal to that of the unbroken loop steam generator secondary. Unbroken loop steam generator secondary was boiling off rapidly.
10332	Ended draining of broken loop steam generator secondary
10477	To maintain secondary side collapsed liquid levels, broken loop secondary required continuous draining. This draining was controlled by control panel ball valves.
11472	Broken locp steam generator became active and began to boil off secondary. Draining was halted.
12069	Primary pressure = 0.488 MPa (70.8 psia); gradual primary pressure increase observed during the entire boiloff

Time (sec)	Event
14101	Primary system pressure alarm sounded at 0.69 MPa (100 psia)
14577	Began injection of 110°C (232°F) accumulator 1 water into both steam generator secondaries
17038	Both steam generator secondary side levels recovered to approximately 7.62 m (25 ft)
17688	Began 363 kg (800 lbm) continuous drain from the primary system. Mass was drained from the primary until a reflux mode of natural circulation was established.
17922	45 kg (100 lbm) drained
19728	Ended 363 kg (800 lbm) continuous drain; total mass drained from the primary system = 508 kg (1120 lbm)
19932	Weir meters valved in
20184	Began 9 kg (20 lbm) drain
20251	Ended 9 kg (20 lbm) drain; 517 kg (1140 lbm) drained from the primary system
20457	Began 18 kg (40 lbm) drain
20575	Ended 18 kg (40 lbm) drain; 535 kg (1180 lbm) drained from the primary system
20582	Slight power adjustment

Time (sec)	Event
20907	Began 9 kg (20 lbm) drain
20978	Ended 9 kg (20 lbm) drain; 544 kg (1200 lbm) drained from the primary system
21220	Began 9 kg (20 lbm) drain
21289	Ended 9 kg (20 lbm) drain; 553 kg (1200 lbm) drained from the primary system
21804	Began 9 kg (20 lbm) drain
21869	Ended 9 kg (20 lbm) drain; 562 kg (1240 lbm) drained from the primary system
22218	Began 9 kg (20 lbm) drain
22284	Ended 9 kg (20 lbm) drain; 571 kg (1260 lbm) drained from the primary system
22947	Began 9 kg (20 lbm) drain
23011	Ended 9 kg (20 lbm) drain; 580 kg (1280 lbm) drained from the primary system. Weir meters indicated intermittent reflux.
23550	Began 9 kg (20 lbm) drain
23624	Ended 9 kg 20 lbm drain; 590 kg (1300 lbm) drained from the primary system

Time (sec)	Event
24192	Began 4.5 kg (10 lbm) drain
24222	Ended 4.5 kg (10 lbm) drain; 594 kg (1310 lbm) drained from the primary system
25632	Reflux natural circulation established; primary system pressure = 0.30 MPa (44 psia)
26520	Feedwater to both steam generator secondaries shut off. Began secondary side boiloff.
29663	Broken loop steam generator secondary side drained to equilibrate secondary side levels of both steam generators
31674	Primary system pressure alarm sounded at 0.69 MPa 100 psia.
31789	Began injection of 111°C (232°F) accumulator 1 water into both steam generator secondaries
32813	Both steam generator secondary side levels recovered to approximately 7.62 m (25 ft)
33983	Power off

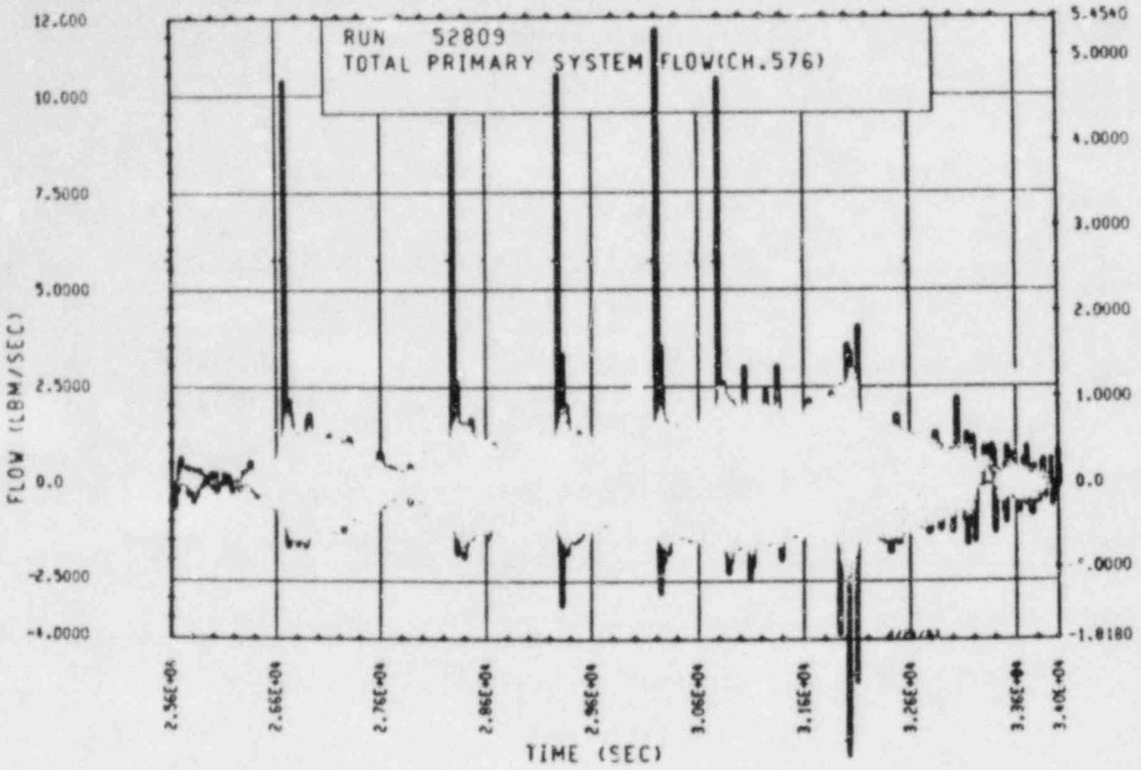

Figure A-61. Mass Flow Rate Through Rod Bundle, Test 9C

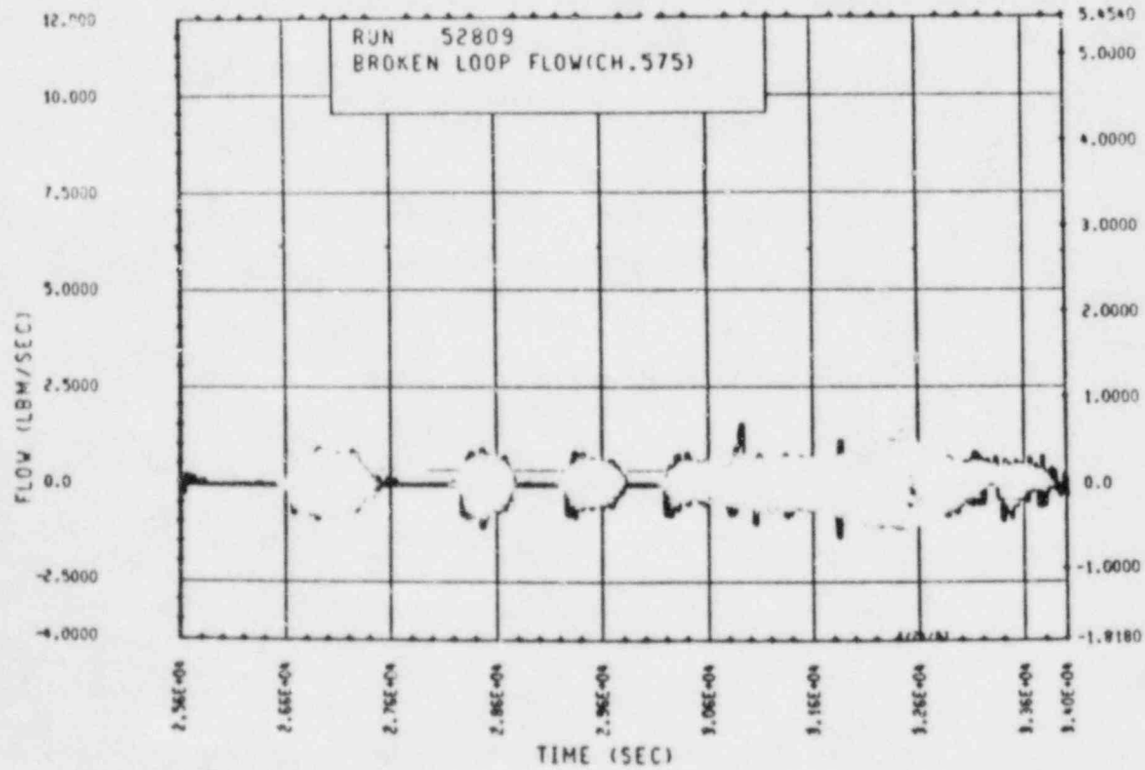

Figure A-62. Mass Flow Rate Through Broken Loop, Test 9C

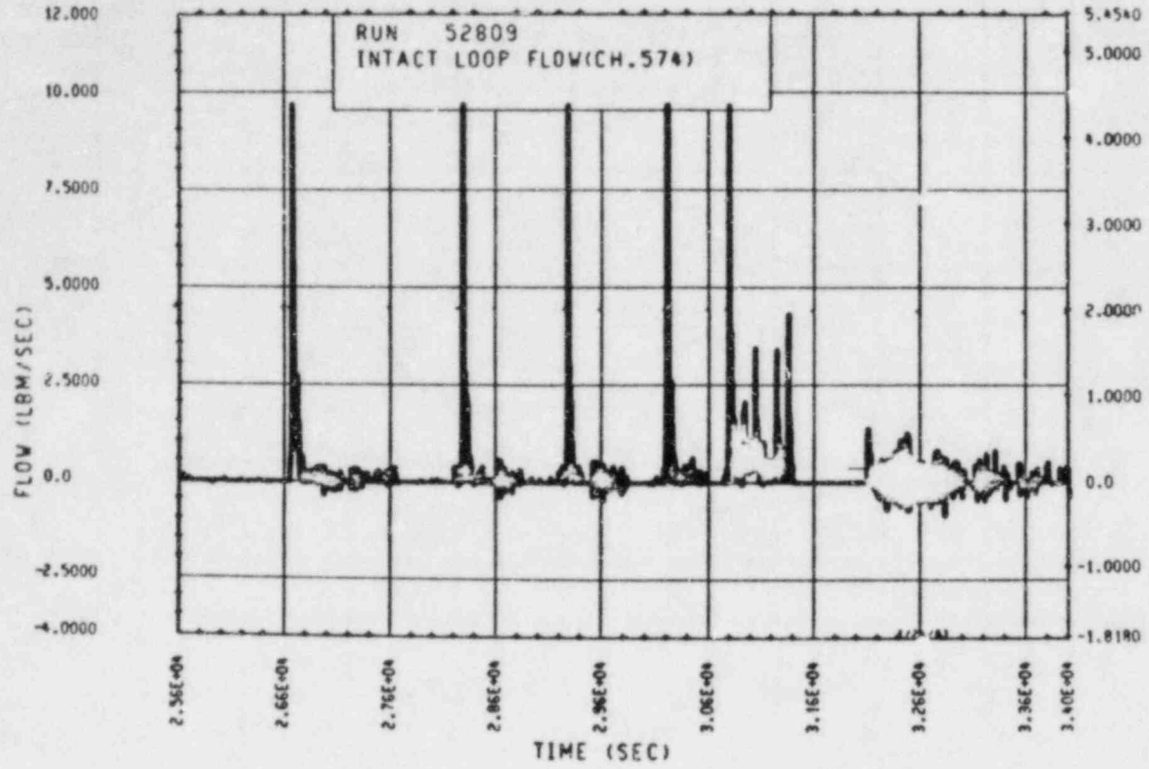

Figure A-63. Mass Flow Rate Through Unbroken Loop, Test 9C

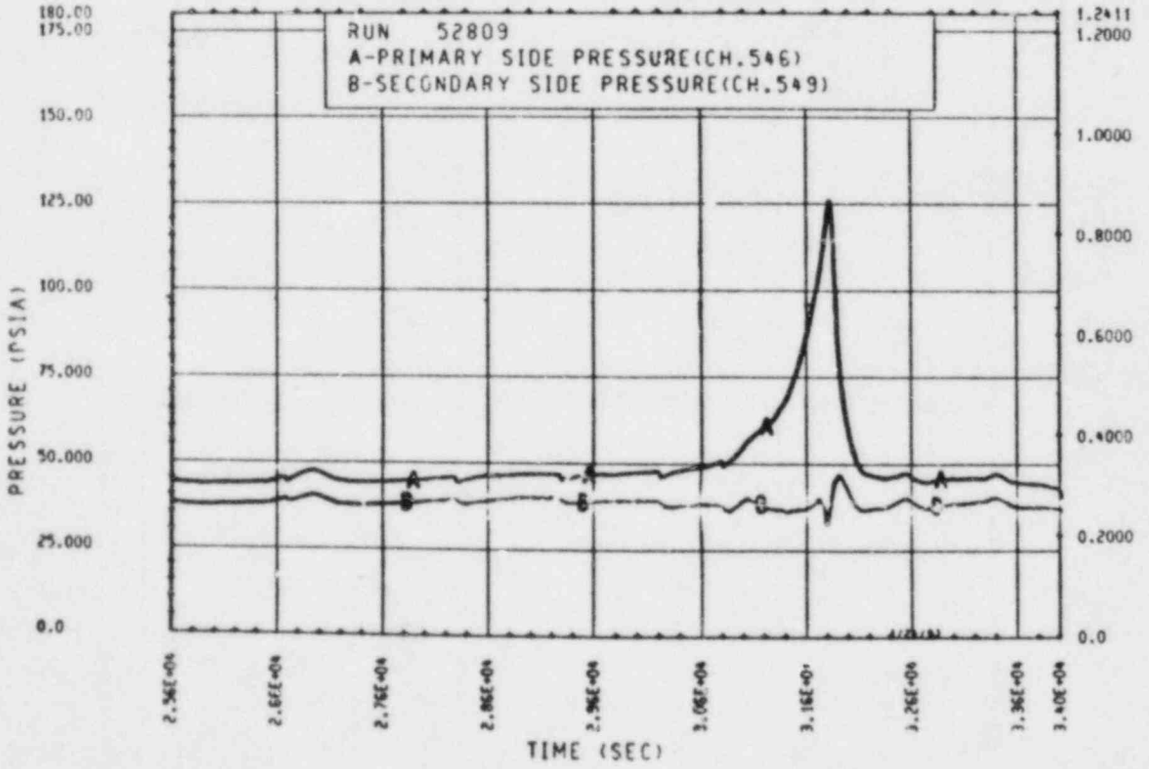

Figure A-64. Primary and Secondary System Pressure, Test 9C

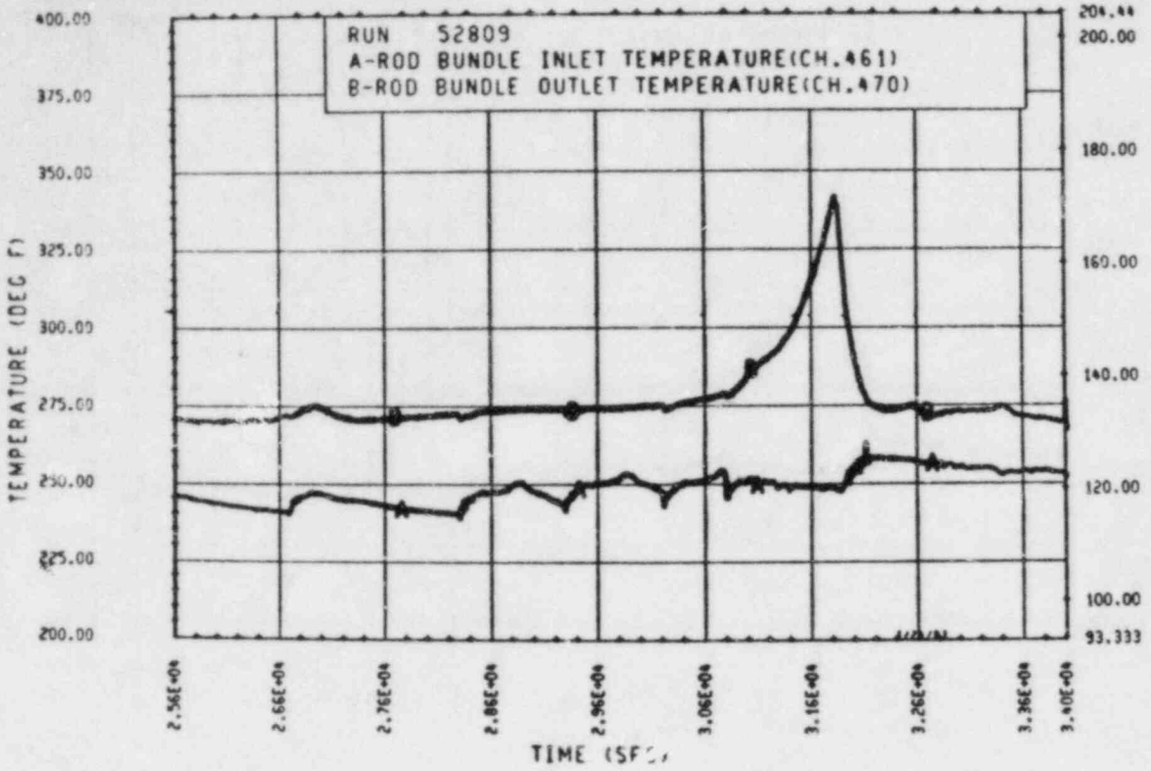

Figure A-65. Heater Rod Bundle Inlet and Outlet Temperature, Test 9C

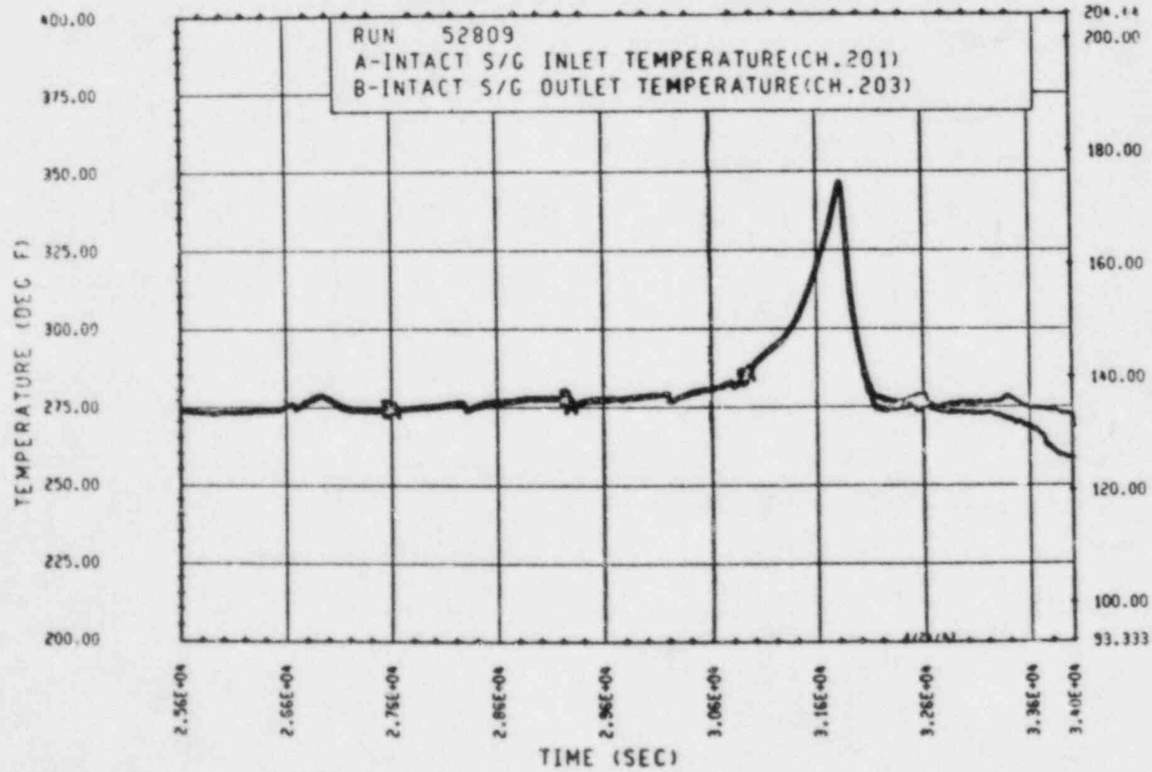

Figure A-66. Unbroken Loop Steam Generator Inlet and Outlet Temperature, Test 9C

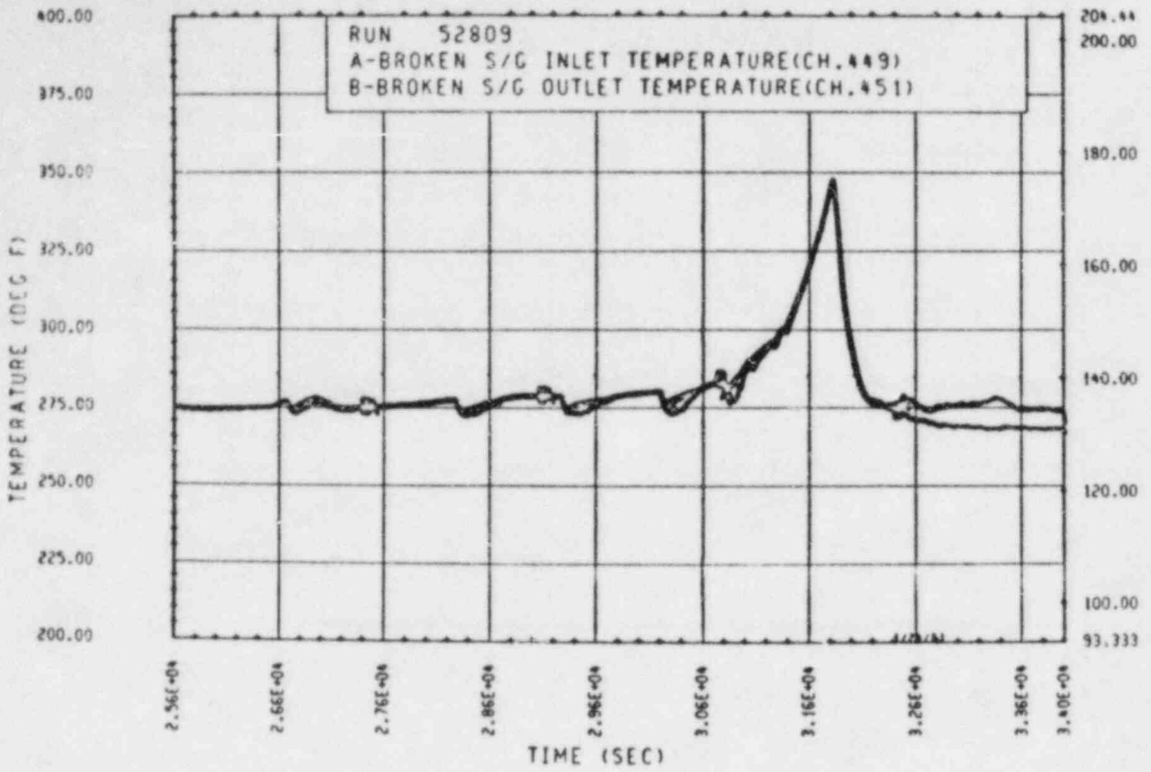

Figure A-67. Broken Loop Steam Generator Inlet and Outlet Temperature, Test 9C

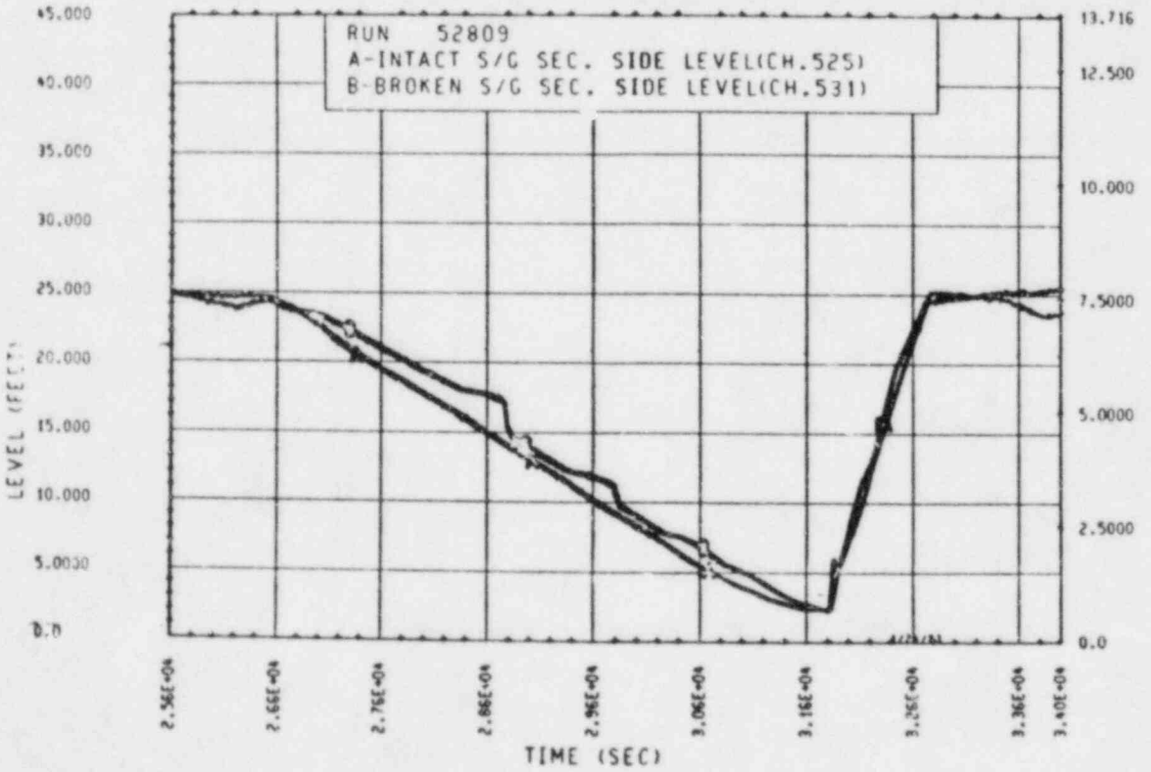

Figure A-68. Unbroken and Broken Loop Steam Generator Secondary Side Collapsed Liquid Levels, Test 9C

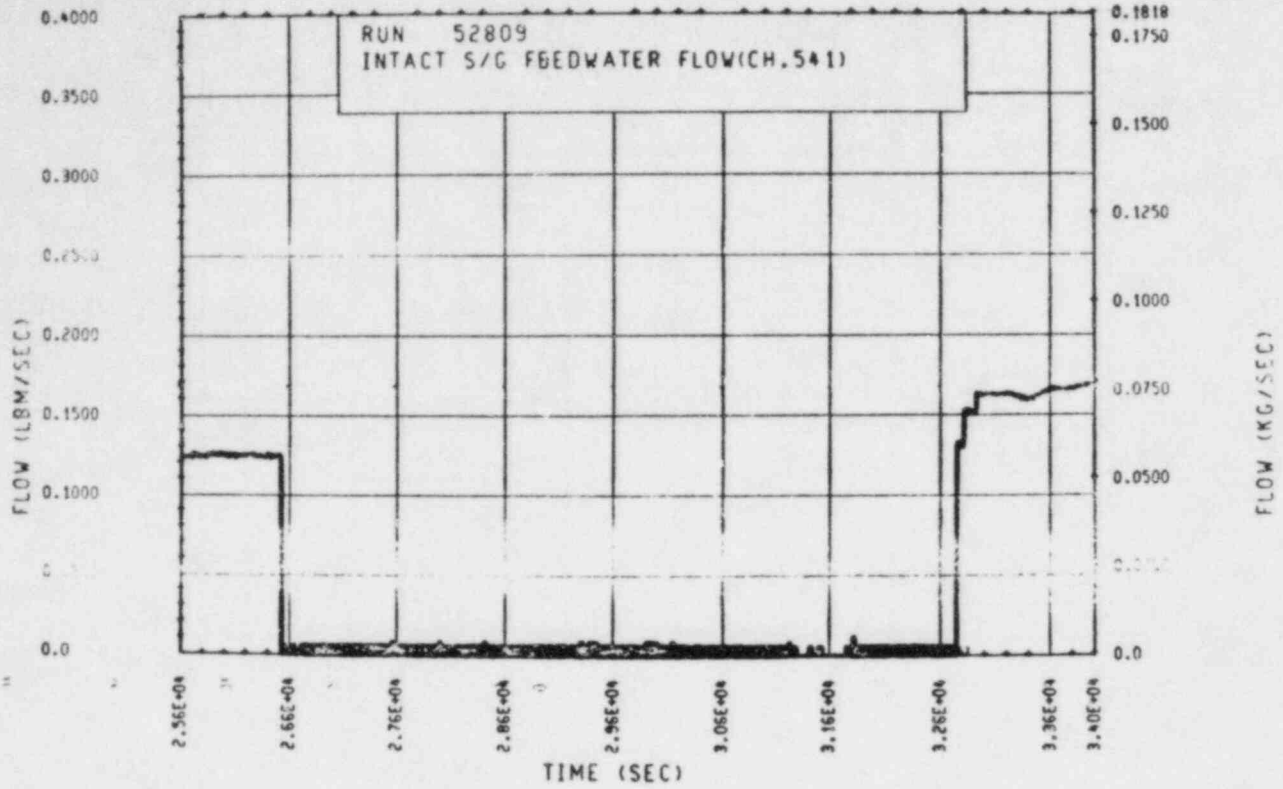

Figure A-69. Unbroken Loop Steam Generator Feedwater Mass Flow Rate, Test 9C

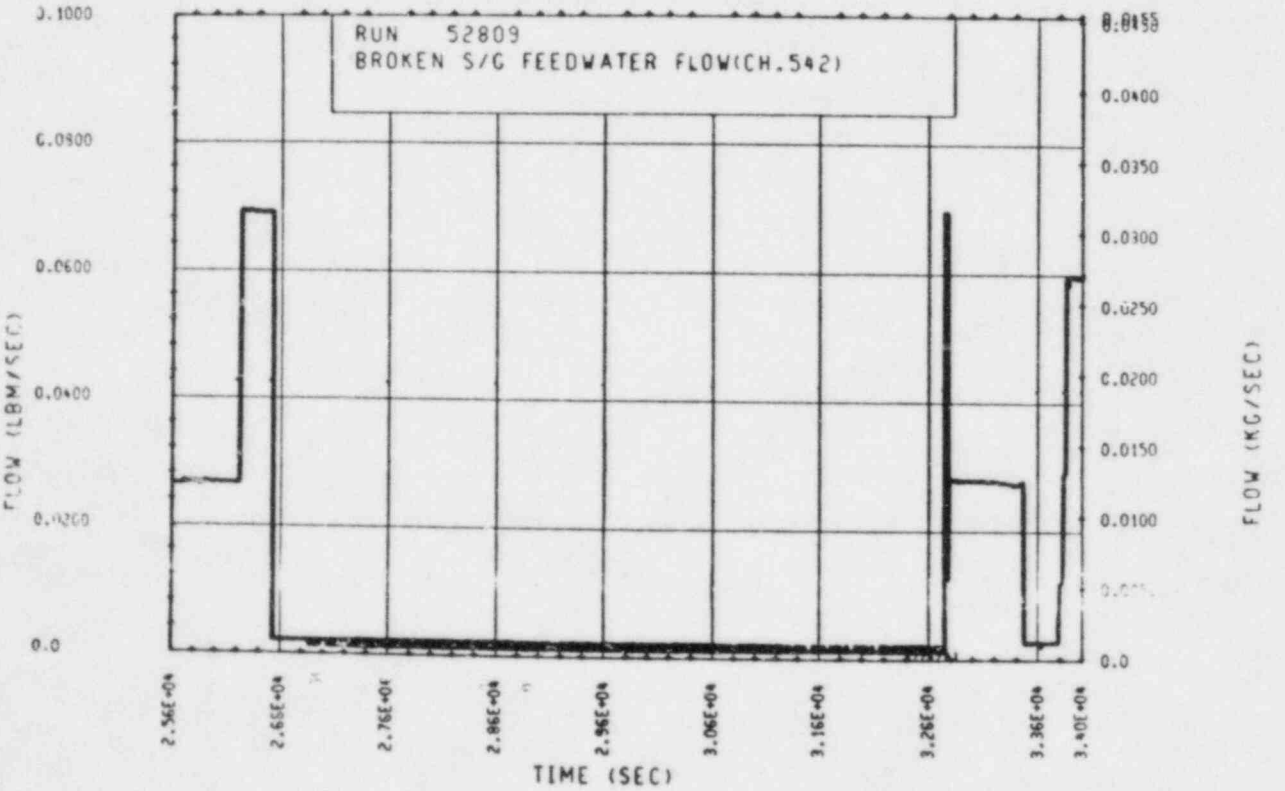

Figure A-70. Broken Loop Steam Generator Feedwater Mass Flow Rate, Test 9C

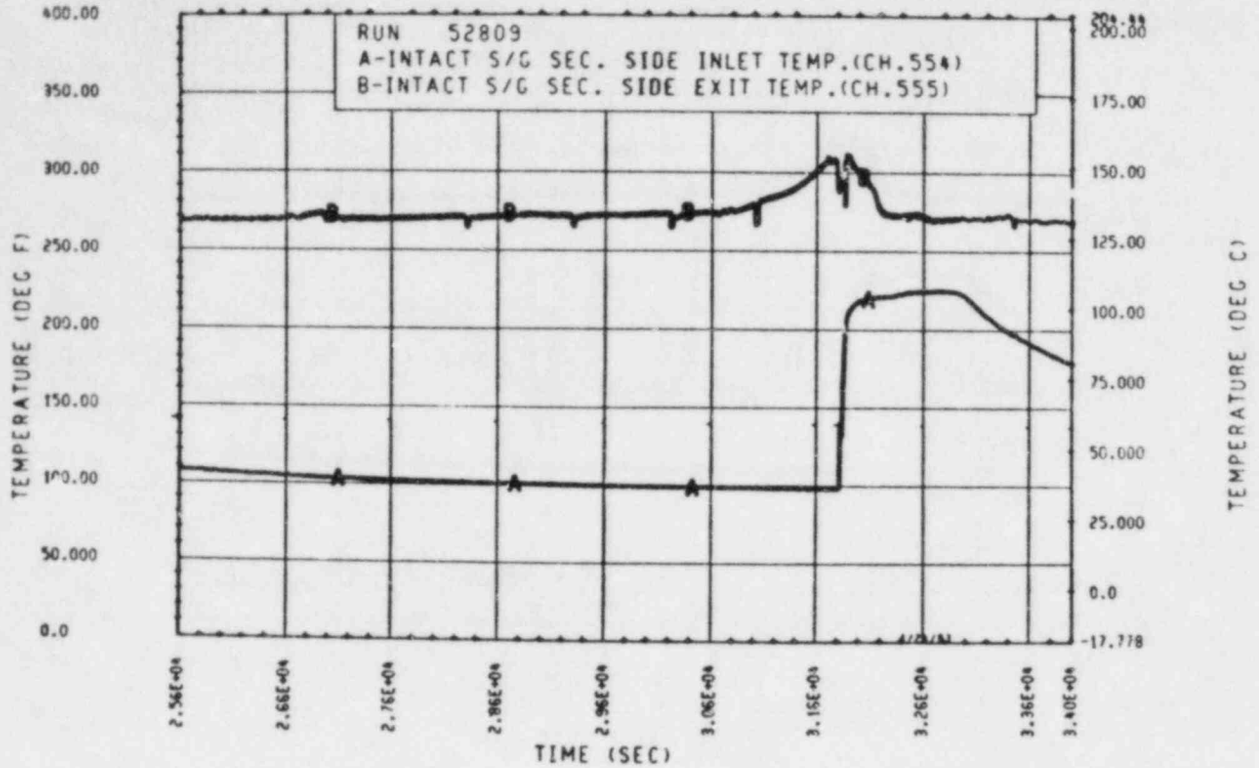

Figure A-71. Unbroken Loop Steam Generator Secondary Side Inlet and Outlet Temperature, Test 9C

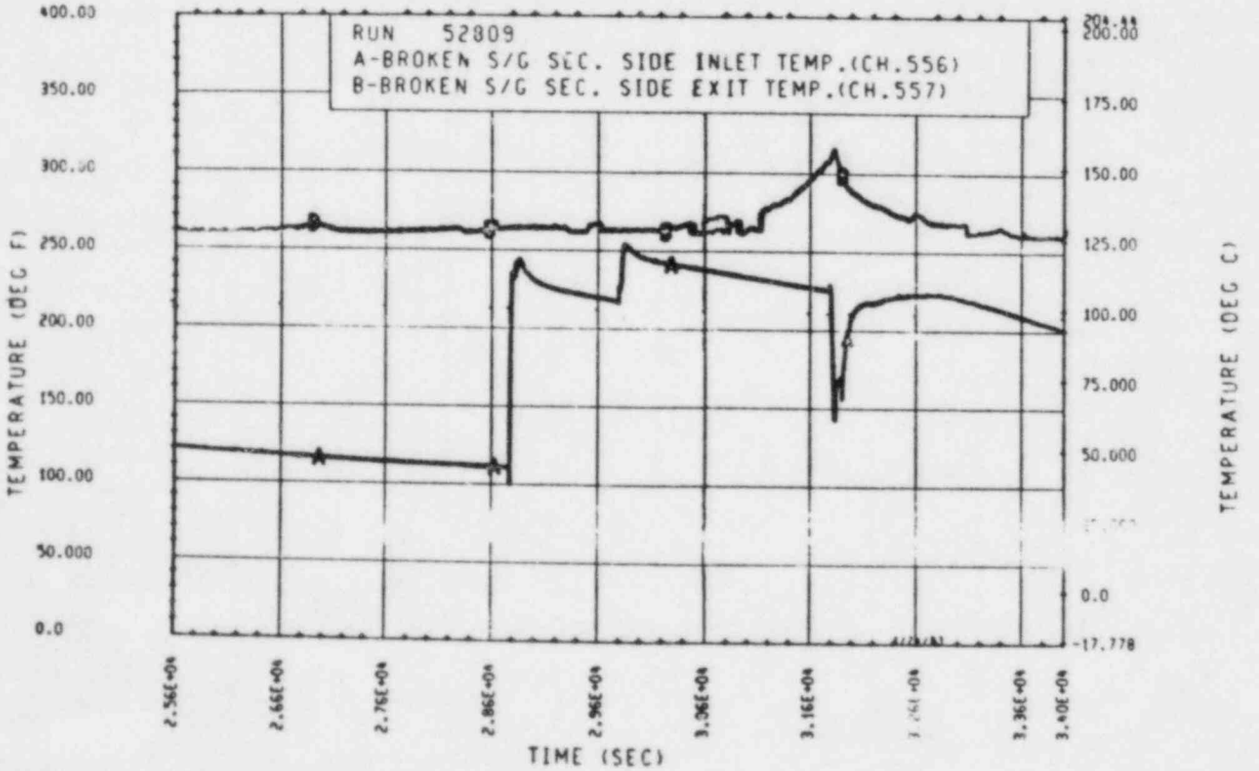

Figure A-72. Broken Loop Steam Generator Secondary Side Inlet and Outlet Temperature, Test 9C

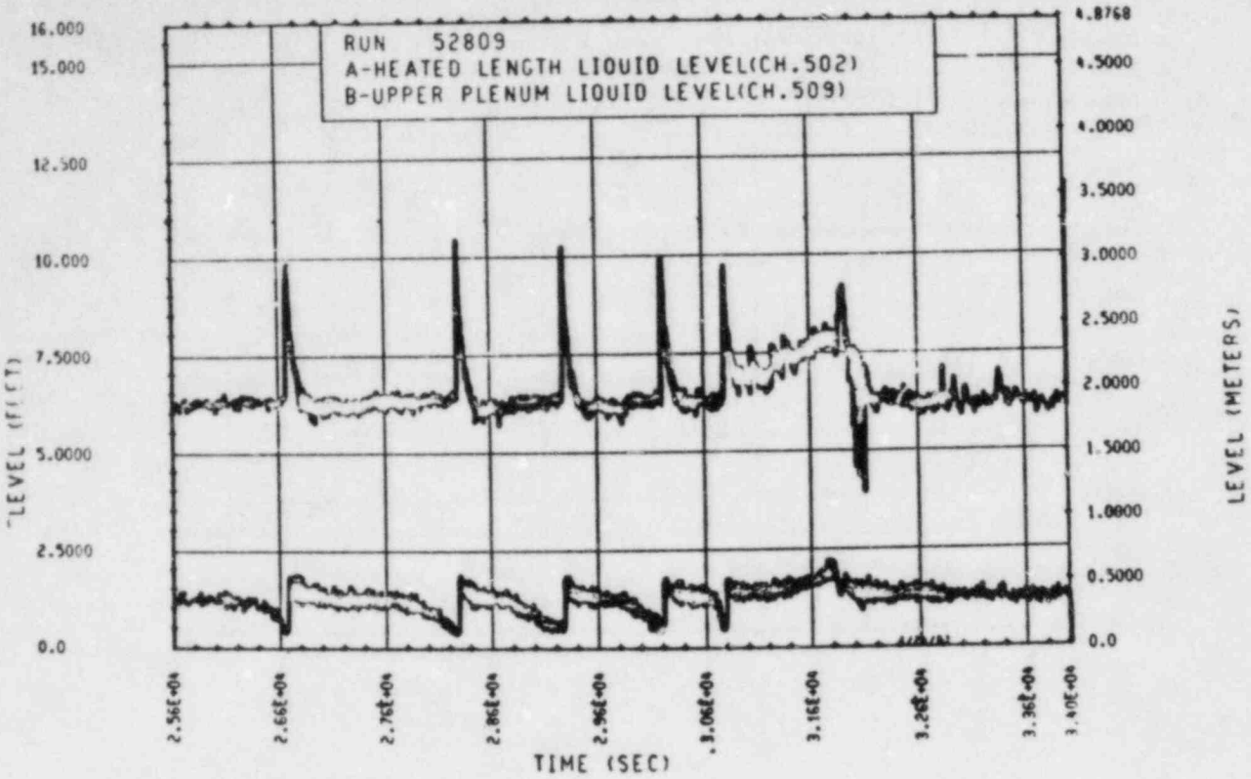

Figure A-73. Heated Length and Upper Plenum Liquid Levels, Test 9B

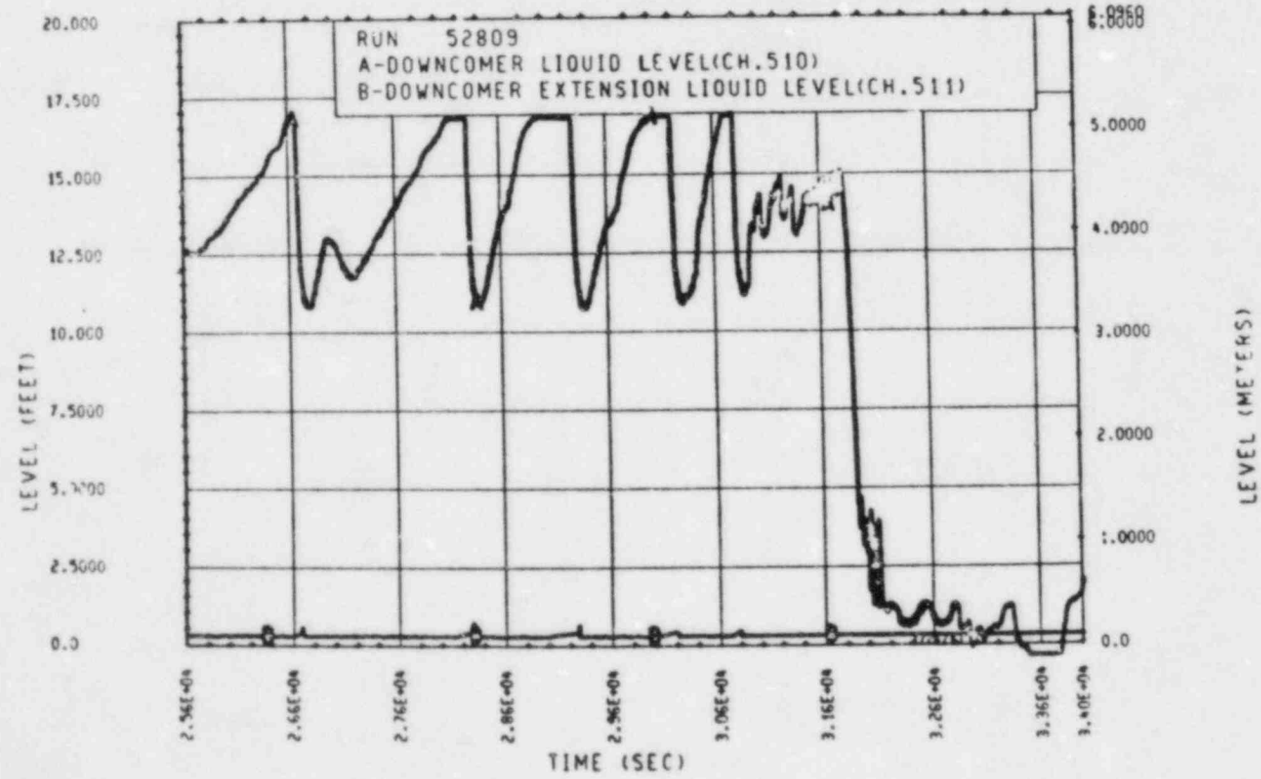

Figure A-74. Downcomer and Downcomer Extension Liquid Levels, Test 9C

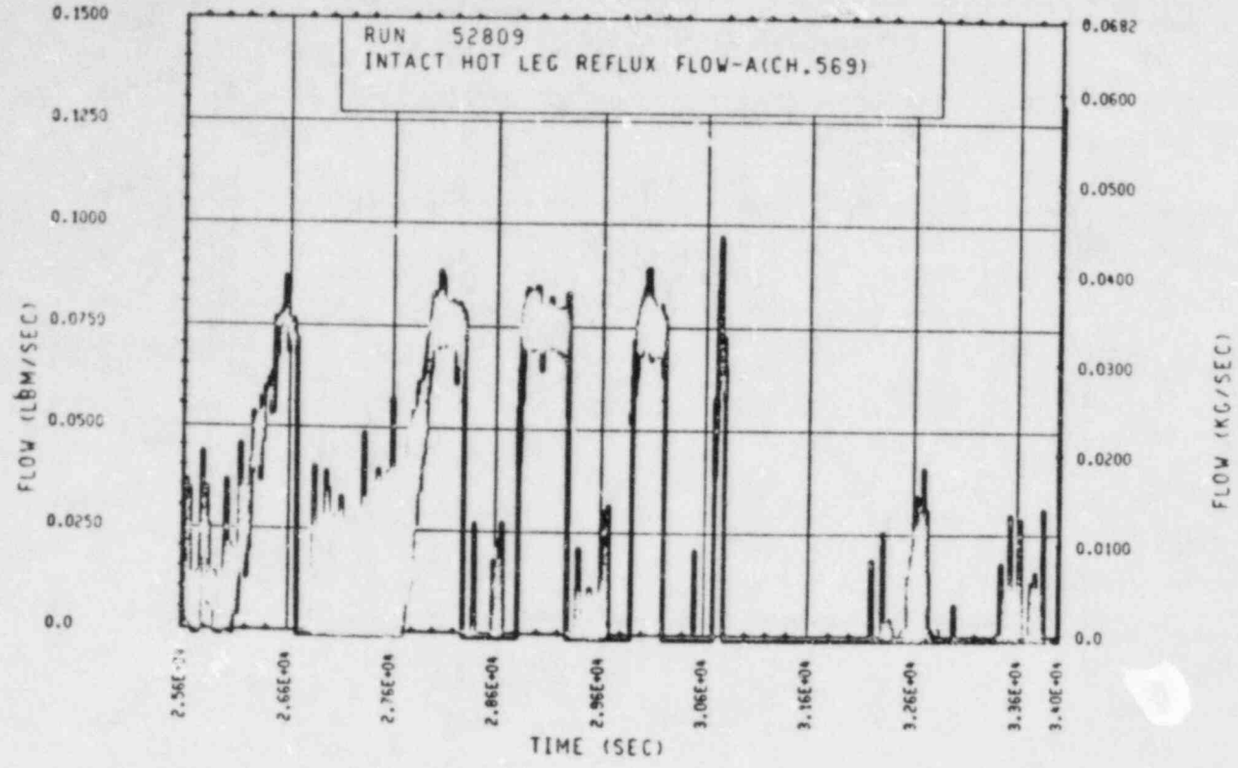

Figure A-75. Unbroken Loop Hot Leg Reflux Condensation Mass Flow Rate, Test 9C

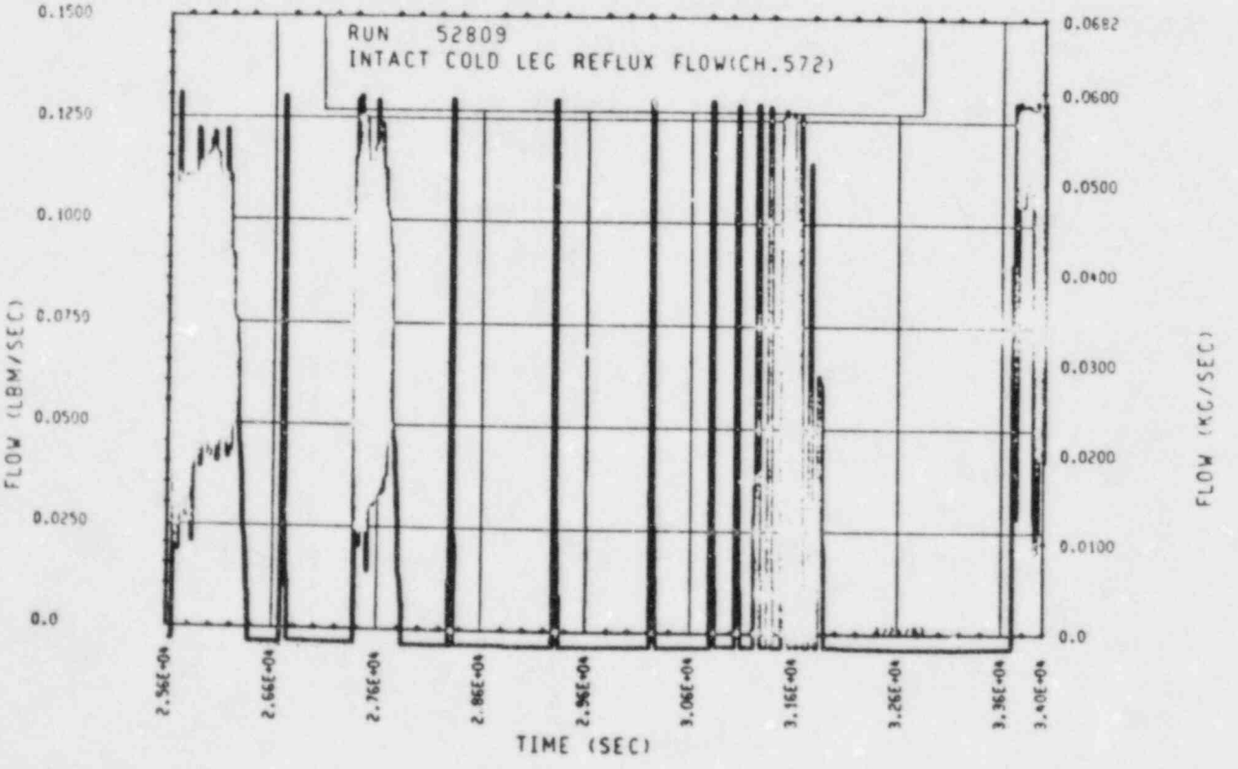

Figure A-76. Unbroken Loop Cold Leg Reflux Condensation Mass Flow Rate, Test 9C

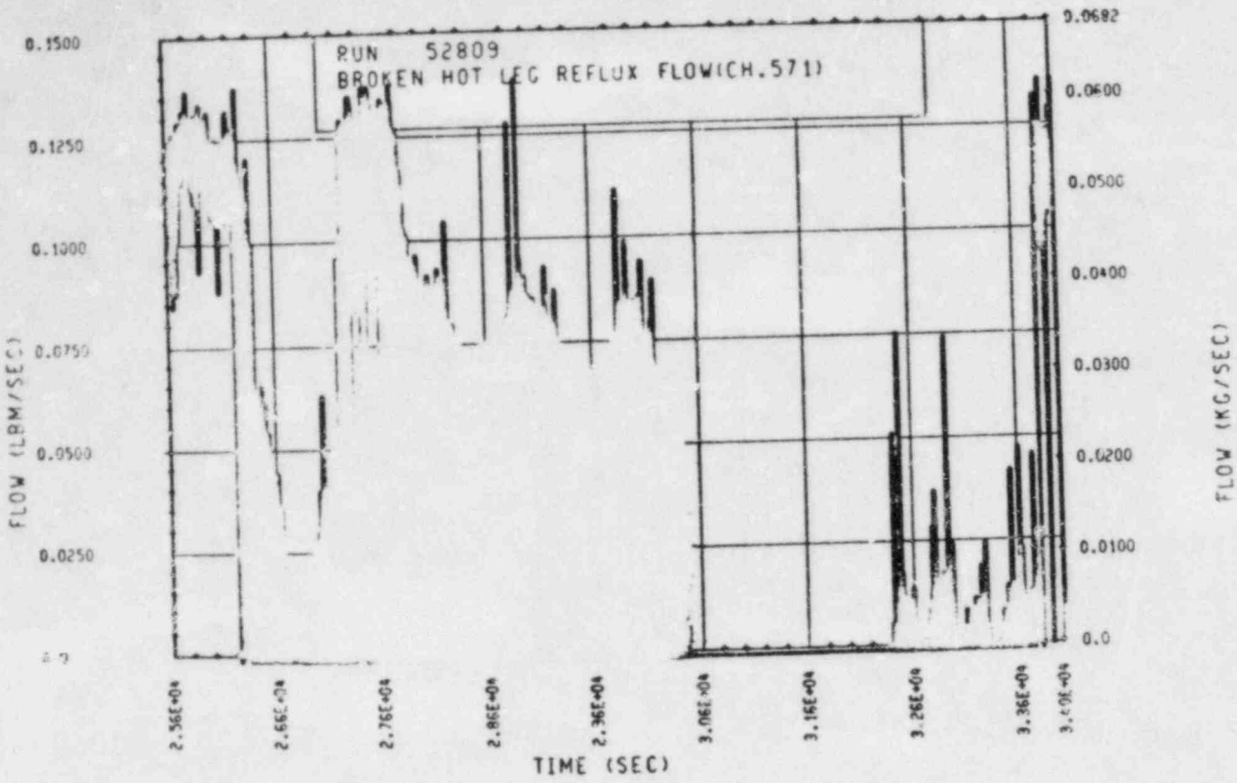

Figure A-77. Broken Loop Hot Leg Reflux Condensation Mass Flow Rate, Test 9C

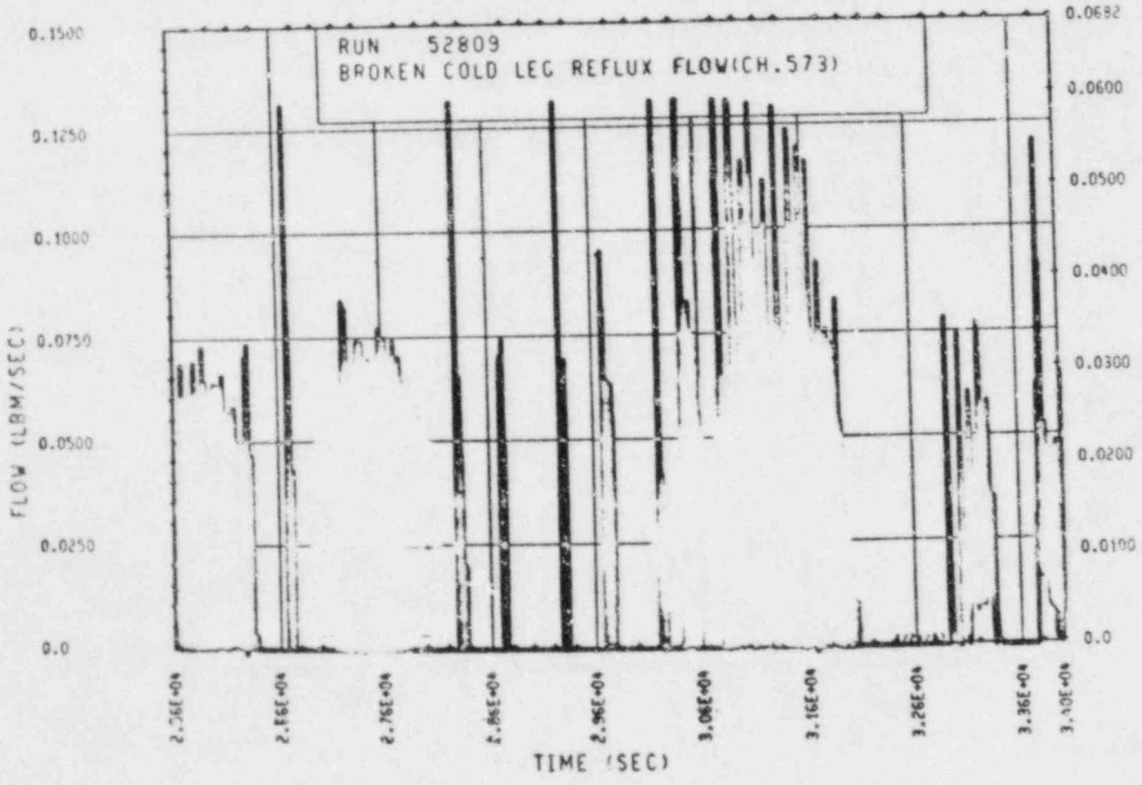

Figure A-78. Broken Loop Cold Leg Reflux Condensation Mass Flow Rate, Test 9C

TEST 10A: SINGLE-PHASE NATURAL CIRCULATION UPPER HEAD INJECTION TEST

Objective

To determine the effect of upper head injection (UHI) on single-phase natural circulation

Test Procedure

The test was begun from a steady-state single-phase natural circulation mode with a nominal primary system pressure of 0.52 MPa (75 psia) and a nominal bundle power of 222 kw (simulated 2 percent of full power). The primary system was operated at 0.52 MPa (75 psia), as opposed to the 0.97 MPa (140 psia) reference condition, to allow primary system pressure margin in the event of a pressure spike during UHI. As a result, the secondary side was operated at atmospheric pressure, as opposed to the 0.28 MPa (40 psia) reference condition, to maintain sufficient primary side subcooling. The secondary side was operated in a feed-and-bleed boiling mode with a constant level being maintained at approximately 7.62 m (25 ft) (71 percent full). Accumulator 1 was used to inject 36°C (97°F) water into the upper plenum at a nominal rate of 0.43 kg/sec (0.94 lbm/sec). The duration of the injection was 347 seconds. The pressurizer was valved out of the primary system when UHI was terminated. The test was terminated when the system returned to a steady-state condition.

Test Overview

Prior to UHI, the primary system operated in a steady-state single-phase natural circulation mode with a total mass flow rate of 1.5 kg/sec (3.2 lbm/sec) through the rod bundle. Both the unbroken and broken loops were active, with a flow split of 3.1 to 1, respectively. The single-phase fluid entered the rod bundle at an average value of approximately 111°C (231°F), and exited at an average value of approximately 147°C (297°F) [ΔT = 37°C (66°F)]. Use of the measured mass flow rate and the measured rod bundle fluid temperature rise led to an axial energy balance estimate that 222.8 kw was removed from the heater rods. This agrees favorably with the measured average of 224 kw of energy input to the rod bundle (0.54 percent difference).

Because the primary system was operated at a nominal pressure of 0.52 MPa (75 psia), the inlet and outlet rod bundle fluid temperatures were approximately 22°C (40°F) cooler than those measured in the single-phase portion of reference test 8. The 0.52 MPa (75 psi) primary pressure, in conjunction with the 0.11 MPa (16 psi) secondary side pressure resulted in a 5°C (9°F) fluid subcooling at the rod bundle exit. The primary side steam generator inlet plenum temperatures were observed to be on the average 6°C (10°F) lower than the rod bundle outlet temperature (3.3 percent difference). Examination of the hot leg temperature data indicated severe thermal stratification with large differences between the hot leg top and bottom. (See appendix C.)

During the course of the test, two single-phase UHI tests were attempted. The first attempt occurred at 11,671 seconds and was aborted because the pressurizer was inadvertently adjusted. The second attempt occurred at 14,311 seconds and was successfully terminated 347 seconds later. The following discussion focuses on this second successful attempt.

The initiation of UHI at 14,311 seconds caused the mass flow rate through the rod bundle to initially step change from its steady-state value of 1.5 kg/sec (3.2 lbm/sec) to a value of approximately 0.91 kg/sec (2.0 lbm/sec). The mass flow rate then gradually decreased until it bottomed out at 0.7 kg/sec (1.57 lbm/sec), 278 seconds after the initiation of UHI. When UHI was terminated at 14,658 seconds (347 seconds after initiation), the mass flow rate step-changed from 0.712 to 1.1 kg/sec (1.57 to 2.5 lbm/sec). It gradually returned to its original steady-state value of 1.4 kg/sec (3.2 lbm/sec) 175 seconds after the termination of UHI. A similar effect was observed in the intact loop, and only a small effect was observed in the broken loop.

During the course of the 347-second injection, the UHI system pressurized the primary system from 0.52 to 0.55 MPa (75 to 80 psia). The primary pressure returned to 0.52 MPa (75 psia) upon termination of UHI. Seconds after UHI was terminated, the pressurizer was valved out of the primary system and the primary pressure began to increase gradually. The primary pressure increased to a peak value of 0.61 MPa (88 psia) 107 seconds after the termination of UHI. The primary system pressure then gradually decreased to a steady value of 0.48 MPa (70 psia) 371 seconds after the termination of UHI. The secondary side was unaffected.

The rod bundle outlet temperature step-changed from 148°C (299°F) to an average temperature of 107°C (225°F) during the course of the injection. The rod bundle outlet temperature was lower than the rod bundle inlet temperature during the course of the injection. The rod bundle inlet maintained a steady temperature of about 112°C (233°F). The rod bundle exit temperature returned to a value of 147°C (297°F) 161 seconds after the termination of UHI. The steam generator inlet plenum temperatures showed trends similar to those of the rod bundle exit temperatures, although the temperature decrease was not as dramatic. The steam generator outlet plenum temperatures showed only a slight decrease.

TEST SCHEDULE
TEST 10A

Time (sec)	Event
0	Computer on
211	Power to 90 kw
991	Power to 150 kw
1771	Power to 222 kw; primary system operating in a forced circulation mode
5371	Pump off; began primary transition into a natural circulation mode
7831	Adjusted pressurizer to lower the primary pressure from 0.69 to 0.62 MPa (100 to 90 psi). Lowering pressure is a safety precaution. During a previous single-phase UHI attempt at 0.88 MPa (127 psi), the crossover leg ruptured during injection.
8462	Adjusted pressurizer to lower primary pressure from 0.61 to 0.55 MPa (87.9 to 80 psi)
9561	Adjusted pressurizer to lower primary pressure from 0.55 to 0.52 MPa (80 to 75 psi)
11191	Set up UHI injection flows to 4.3×10^{-4} m^3/sec (6.8 gal/min)

Time (sec)	Event
11671	Began UHI injection with a nominal flow rate of 4.3×10^{-4} m^3/sec (6.8 gal/min)
11987	UHI terminated; test aborted. The pressurizer was inadvertently adjusted. Primary pressure reset to 0.52 MPa (75 psi).
13912	Set up UHI flows to 4.3×10^{-4} m^3/sec (6.8 gal/min)
14311	Began UHI with a nominal flow rate of 4.3×10^{-4} m^3/sec (6.8 gal/min)
14658	Ended UHI
14636	Pressurizer valved out; pressure observed to peak at about 0.61 MPa (88 psi)
15098	Pressure settling down to approximately 0.49 MPa (71 psi)
15732	Single-phase UHI test terminated; pressurizer valved in; pressurizer adjusted to bring primary pressure to 0.93 MPa (135 psi)
16531	Primary pressure = 0.93 MPa (135 psi); secondary exhaust valves adjusted to increase secondary pressure to 0.28 MPa (40 psi); prepared to drain mass from the primary side to achieve a two-phase peak flow condition

Time (sec)	Event
18791	Pressurizer valved out
18823	Began 136 kg (300 lbm) continuous drain
19996	45 kg (100 lbm) drained
20971	91 kg (200 lbm) drained
22064	136 kg (300 lbm) drained; ended continuous drain
22313	Began 18 kg (40 lbm) drain
22403	Ended 18 kg (40 lbm) drain; total of 154 kg (340 lbm) drained
22531	Began two-phase peak flow steady-state reference run
23611	Ended two-phase peak flow steady-state reference run
23820	Adjusted UHI rate to 4.3×10^{-4} m^3/sec (6.8 gal/min)
24091	Began UHI; nominal flow rate of 4.3×10^{-4} m^3/sec (6.8 gal/min)
24281	Pressure alarm; primary pressure = 0.90 MPa (130 psi) UHI unable to inject due to high primary pressure.

Time (sec)	Event
24302	Bundle scram; primary pressure of 0.97 MPa (140 psi). Never finished injection. Injection was scheduled to finish at 24,438 sec. End of two-phase peak flow UHI test.
0	Computer back on. Note that the computer scrams with a bundle scram. The computer subsequently writes to a new tape when it is brought back on line. Thus the computer time is resequenced to zero.
1214	Power restarted to 60 kw. Pumps not on.
1314	Began a continuous mass drain to bring the system to a reflux mode of natural circulation. It was estimated that 81.00 kg (178.6 lbm) of mass was added to the primary inventory by the UHI. The net mass drained was 73.19 kg (161.4 lbm).
1466	Power increased to 107.7 kw
1634	Power increased to 222.3 kw
2727	166 kg (366 lbm) drained; total net amount of mass drained from the primary = 239.2 kg (527.4 lbm)
4369	380 kg (838 lbm) drained; total net amount of mass drained form the primary = 453.2 kg (999.4 lbm); continucus drain stopped
5316	Began 23 kg (50 lbm) drain

Time (sec)	Event
5457	Ended 23 kg (50 lbm) drain; net amount of mass drained from the primary = 475.90 kg (1049.4 lbm)
5671	Began 45 kg (100 lbm) drain
5928	Ended 45 kg (100 lbm) drain; net amount of mass drained from the primary = 521.25 kg (1149.4 lbm)
6032	Began 23 kg (50 lbm) drain
6177	Ended 23 kg (50 lbm) drain; net amount of mass drained from the primary = 543.93 kg (1199.4 lbm)
6679	Began 14 kg (30 lbm) drain
	Ended 14 kg (30 lbm) drain; net amount of mass drained from the primary = 557.53 kg (1229.4 lbm)
6914	Loss of feedwater to both steam generators. Both feedwater lines shut to keep the secondary from draining. Technicians realigned valves to draw feedwater from an alternate source.
8109	Computer operator reported a disk allocation error. Power ramped to zero. Power trip. Computer trip. Computer operator reallocated disk space.
0	Computer time resychronized for new disk
229	Power to bundle 75 kw

Time (sec)	Event
552	Power to bundle 222 kw
1282	Began 9 kg (20 lbm) drain
1349	Ended 9 kg (20 lbm) drain; net amount of mass drained from the primary = 566.60 kg (1249.4 lbm)
1681	Valved in weir meters
1749	Began 9 kg (20 lbm) drain
1807	Ended 9 kg (20 lbm) drain; net amount of mass drained from the primary = 575.67 kg (1269.4 lbm)
2559	Began 9 kg (20 lbm) drain
2631	Ended 9 kg (20 lbm) drain; net amount of mass drained from the primary = 584.74 kg (1289.4 lbm)
2851	Began 9 kg (20 lbm) drain
2922	Ended 9 kg (20 lbm) drain; net amount of mass drained from the primary = 593.81 kg (1309.4 lbm)
3053	Began 9 kg (20 lbm) drain
3113	Ended 9 kg (20 lbm) drain; net amount of mass drained from the primary = 602.88 kg (1329.4 lbm)
3354	Began 9 kg (20 lbm) drain

Time (sec)	Event
3417	Ended 9 kg (20 lbm) drain; net amount of mass drained from the primary = 611.95 kg (1349.4 lbm)
3680	Began 9 kg (20 lbm) drain
3743	Ended 9 kg (20 lbm) drain; net amount of mass drained from the primary = 621.02 kg (1369.4 lbm)
3958	Began 9 kg (20 lbm) drain
4024	Ended 9 kg (20 lbm) drain; net amount of mass drained from the primary = 630.09 kg (1389.4 lbm)
4317	Began 4.5 kg (10 lbm) drain
4349	Ended 4.5 kg (10 lbm) drain; net amount of mass drained from the primary = 634.63 kg (1399.4 lbm)
4648	Began 4.5 kg (10 lbm) drain
4686	Ended 4.5 kg (10 lbm) drain; net amount of mass drained from the primary = 639.16 kg (1409.4 lbm)
4955	Began steady-state reflux run
5559	UHI set up to deliver 4.3×10^{-4} m^3/sec (6.8 gal/min)
6039	Began UHI at a nominal flow rate of 4.3×10^{-4} m^3/sec (6.8 gal/min)

Time (sec)	Event
6386	Ended UHI
6939	Steady-state after UHI
7616	Ramped power down to zero
7732	Computer off

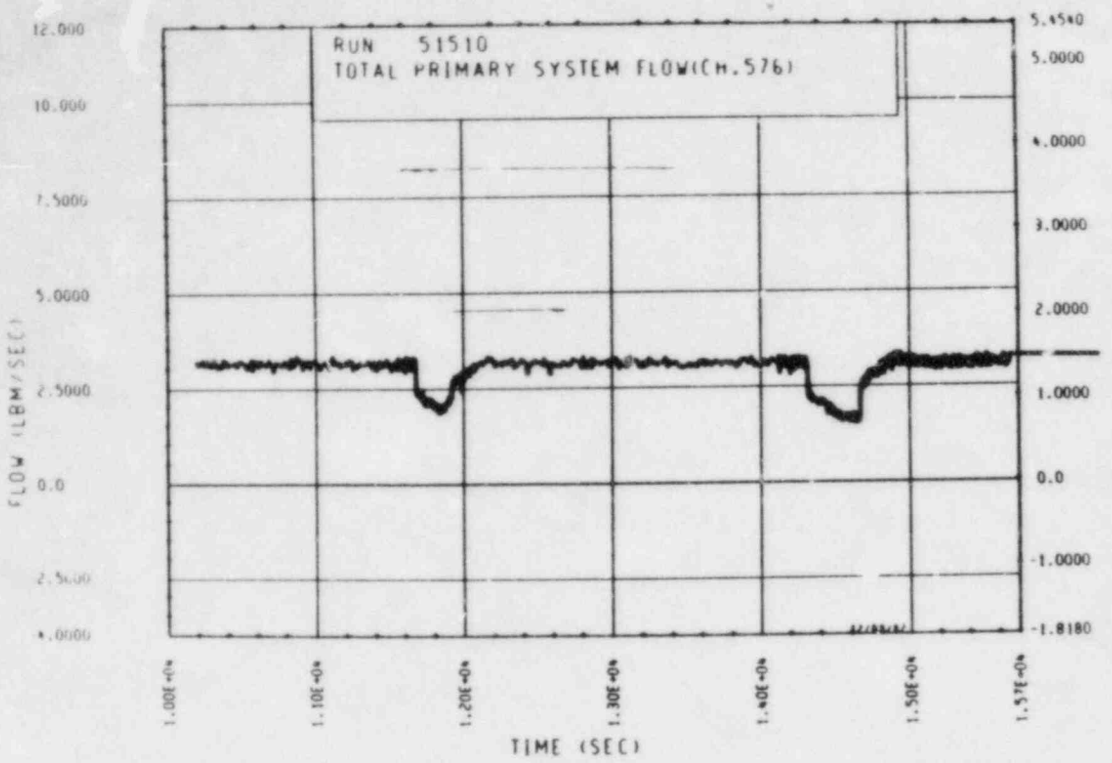

Figure A-79. Mass Flow Rate Through Rod Bundle, Test 10A

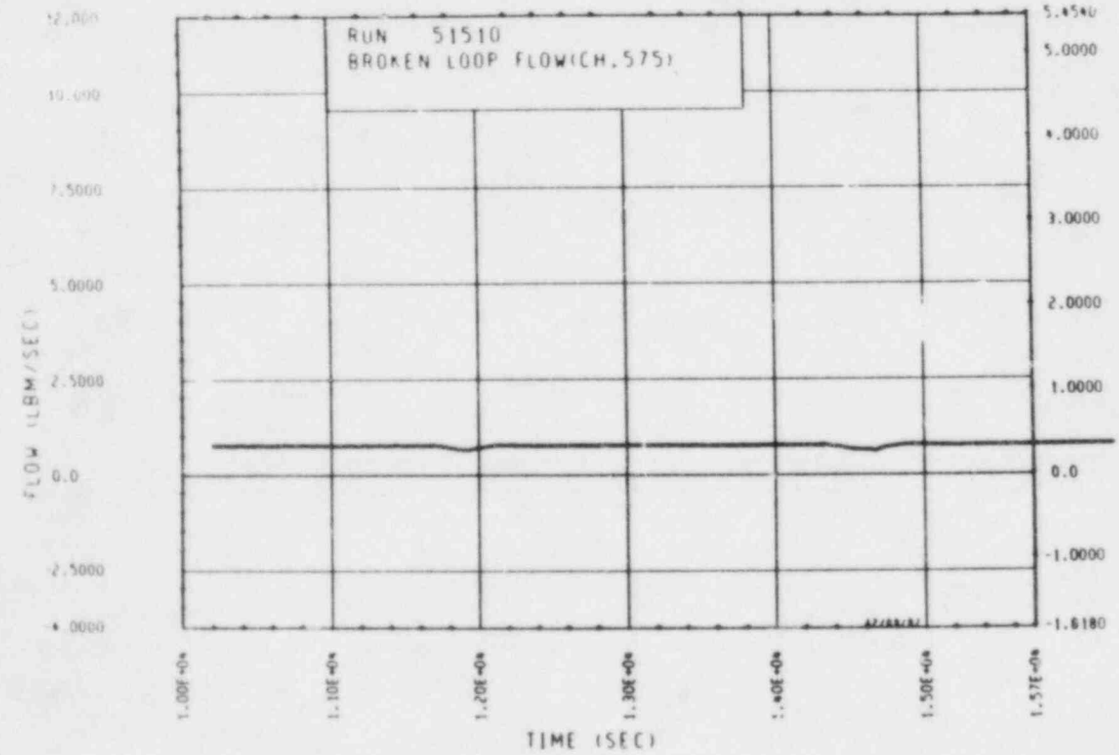

Figure A-80. Mass Flow Rate Through Broken Loop, Test 10A

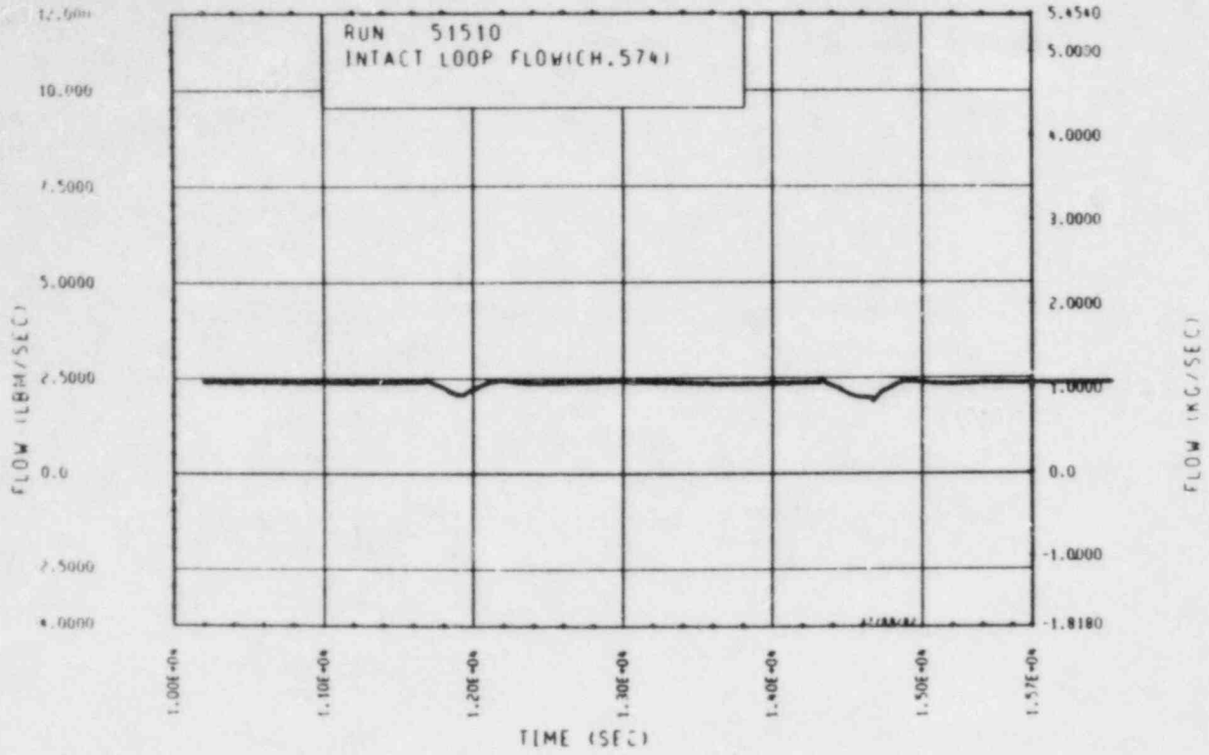

Figure A-81. Mass Flow Rate Through Unbroken Loop, Test 10A

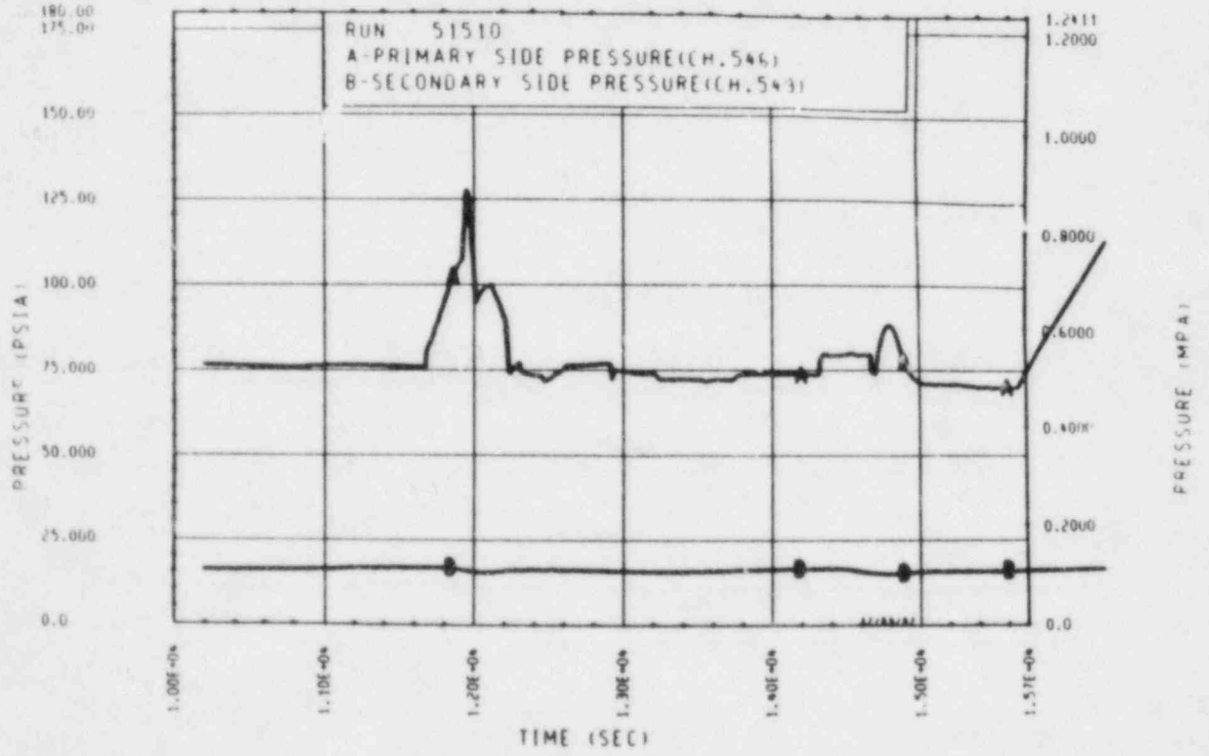

Figure A-82. Primary and Secondary System Pressure, Test 10A

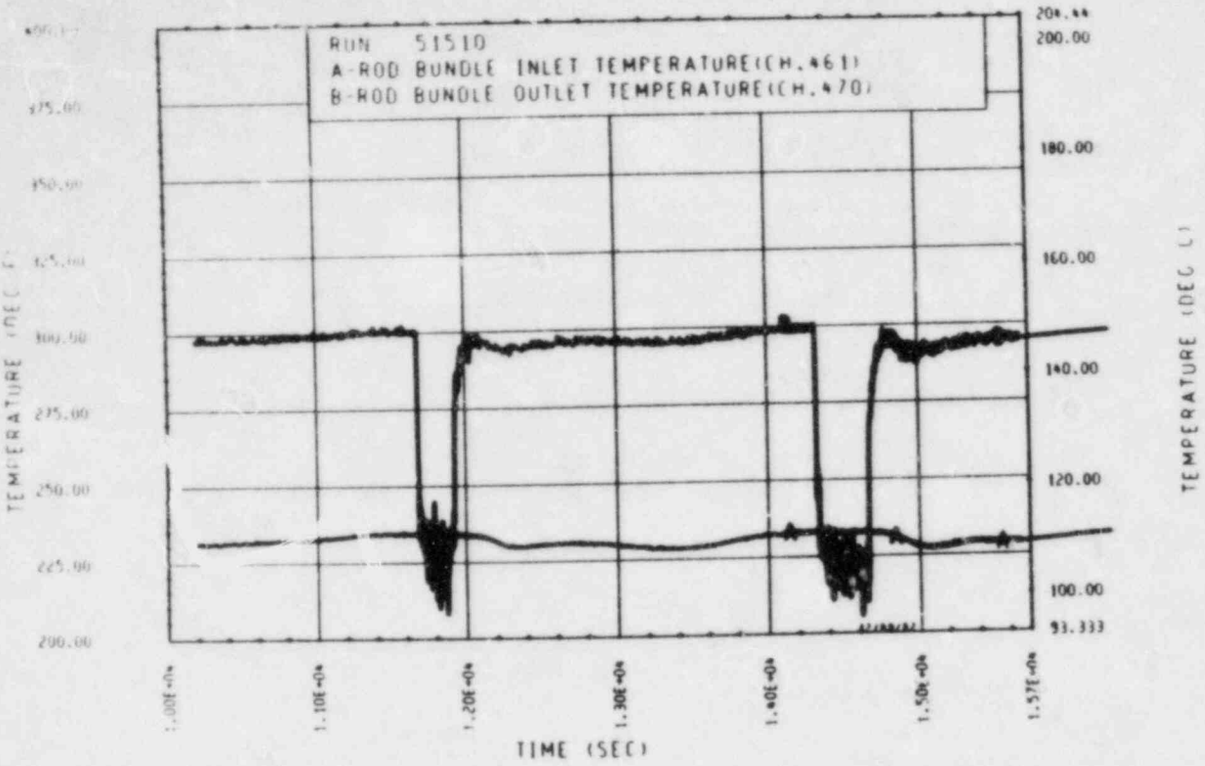

Figure A-83. Heater Rod Bundle Inlet and Outlet Temperature, Test 10A

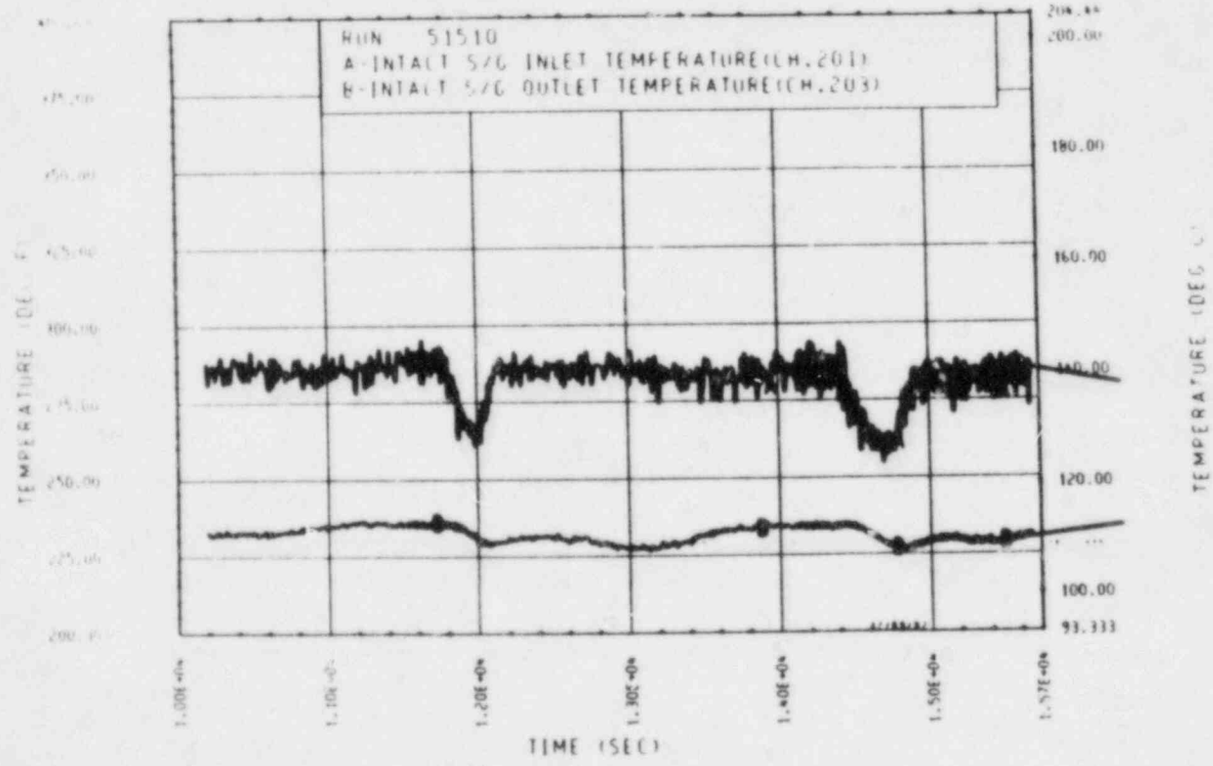

Figure A-84. Unbroken Loop Steam Generator Inlet and Outlet Temperature, Test 10A

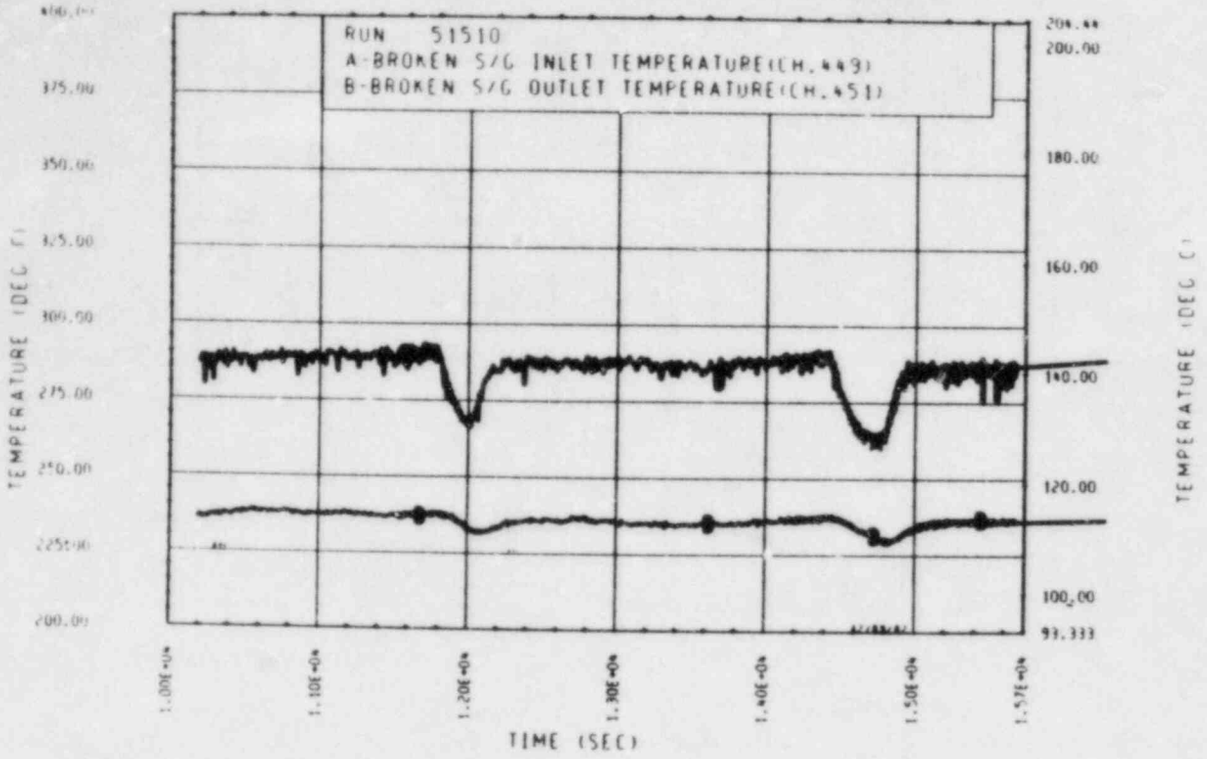

Figure A-85. Broken Loop Steam Generator Inlet and Outlet Temperature, Test 10A

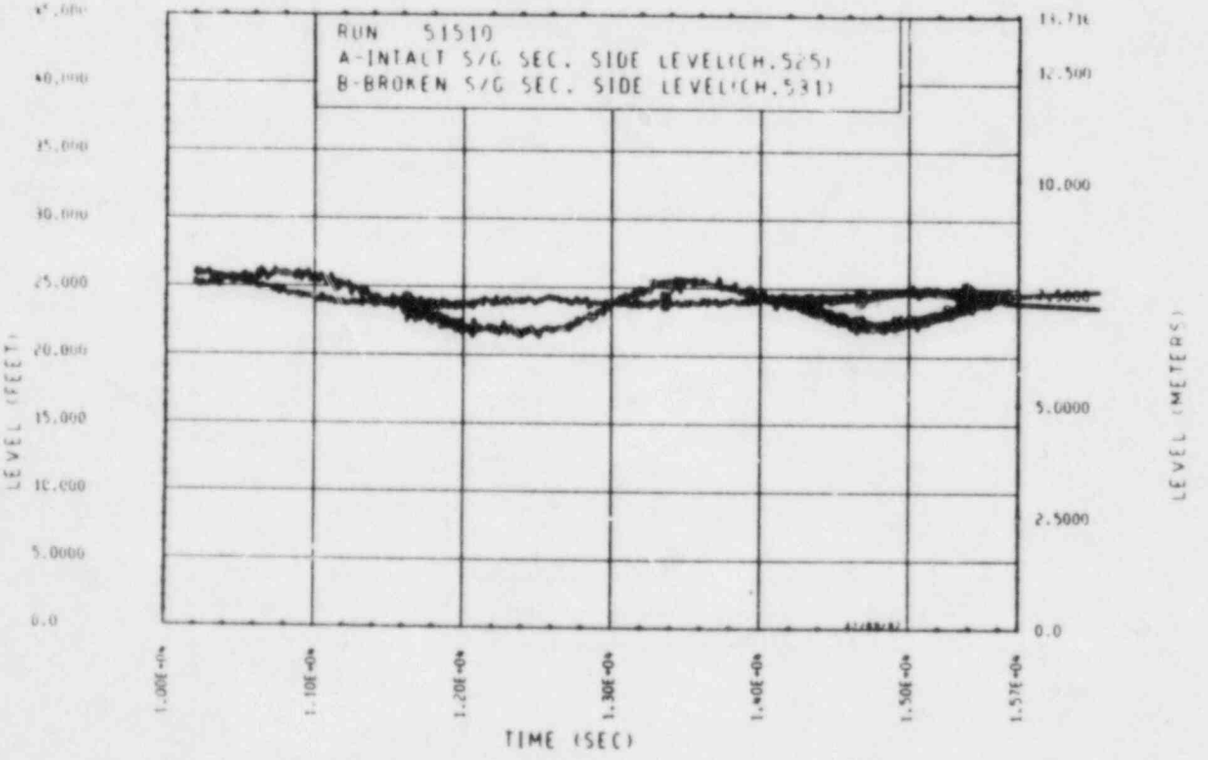

Figure A-86. Unbroken and Broken Loop Steam Generator Secondary Side Collapsed Liquid Levels, Test 10A

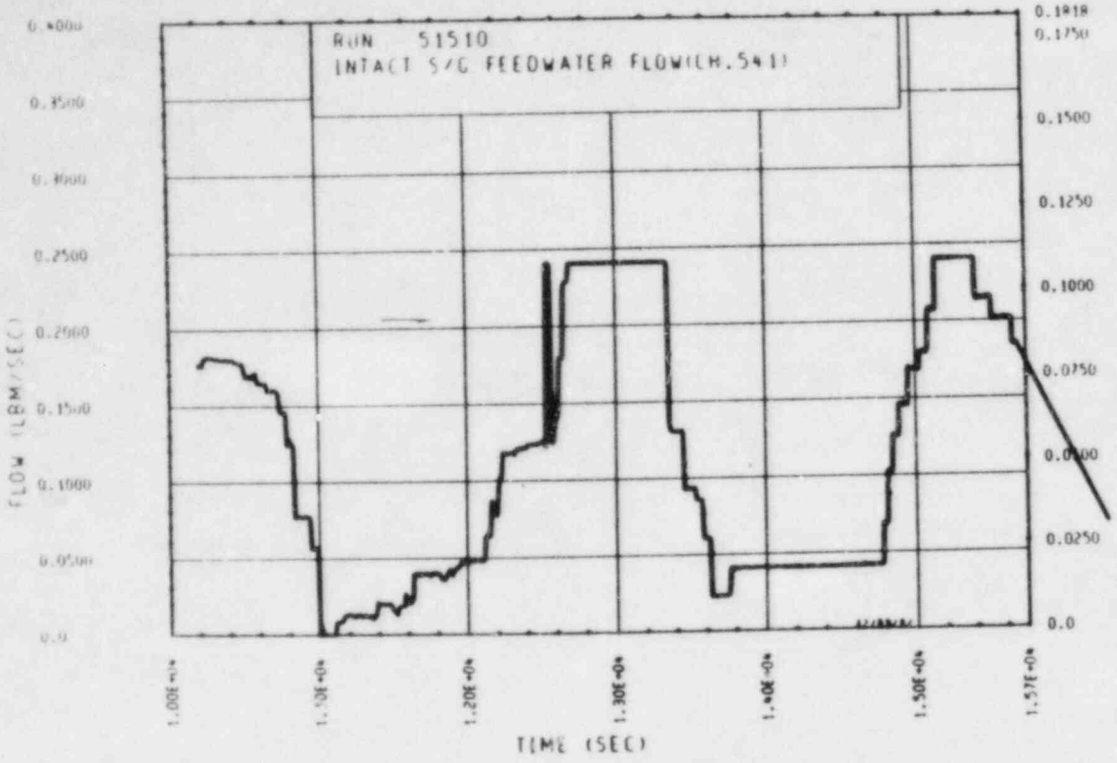

Figure A-87. Unbroken Loop Steam Generator Feedwater Mass Flow Rate, Test 10A

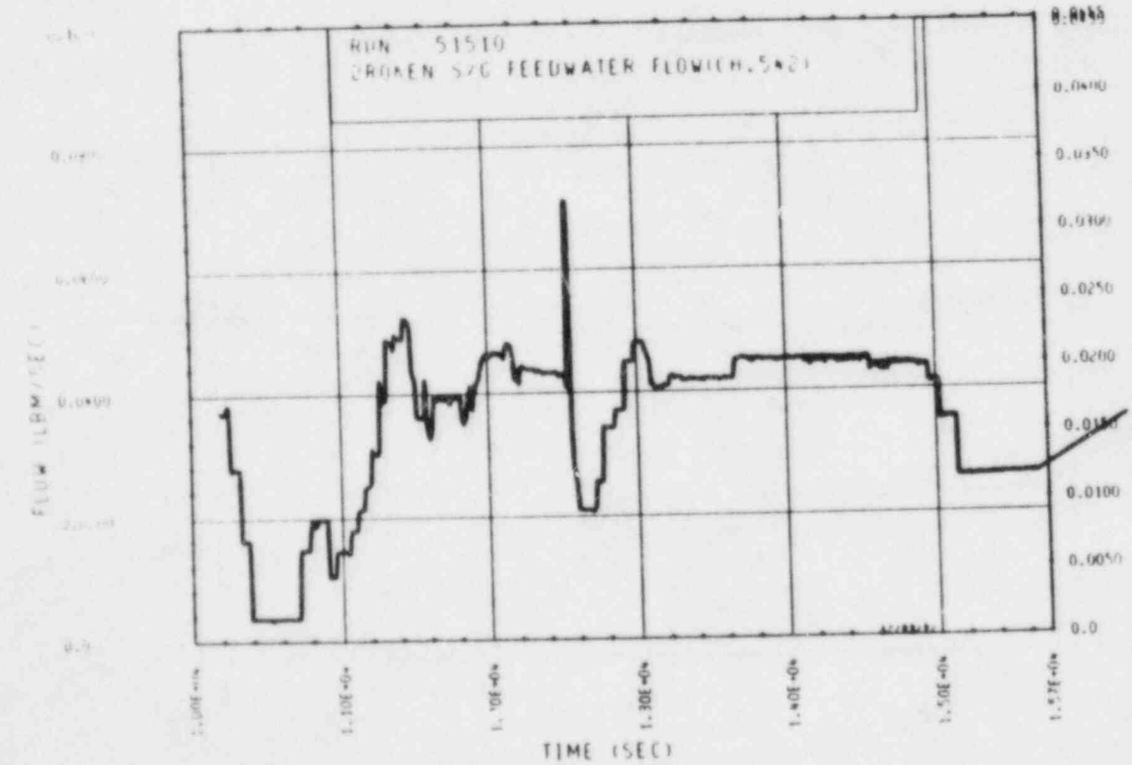

Figure A-88. Broken Loop Steam Generator Feedwater Mass Flow Rate, Test 10A

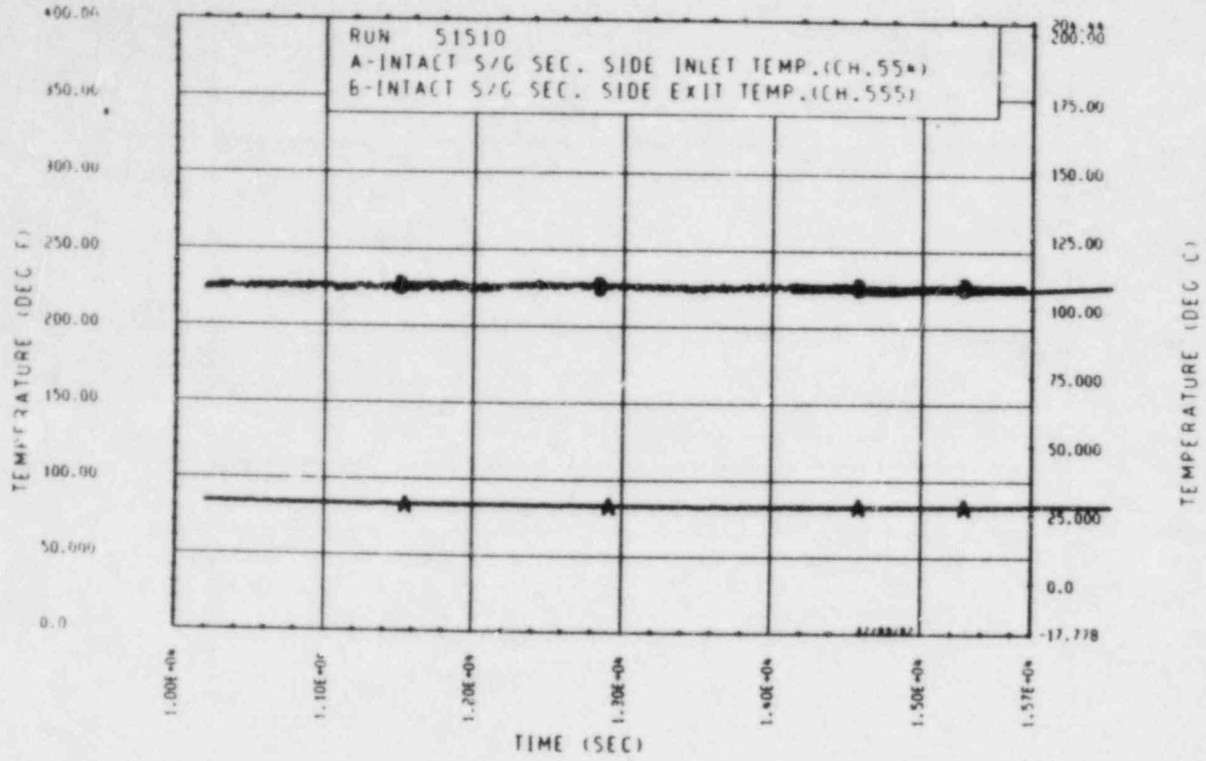

Figure A-89. Unbroken Loop Steam Generator Secondary Side Inlet and Outlet Temperature, Test 10A

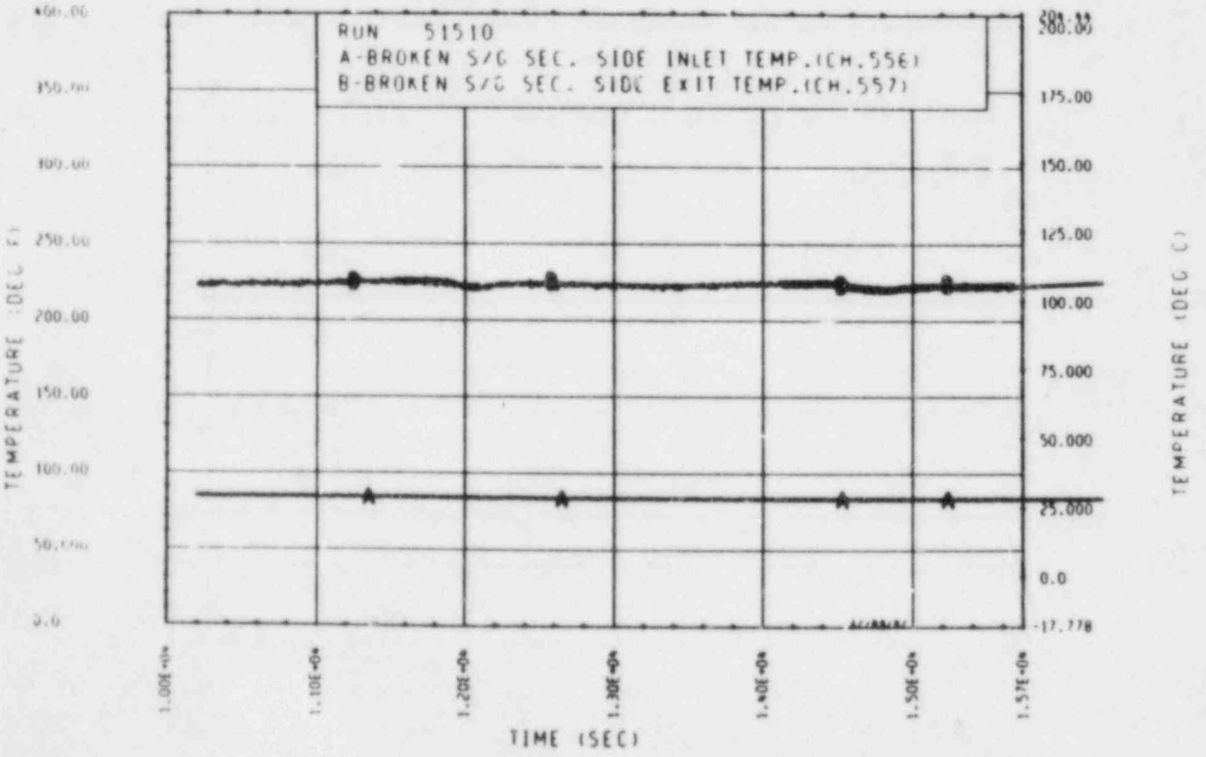

Figure A-90. Broken Loop Steam Generator Secondary Side Inlet and Outlet Temperature, Test 10A

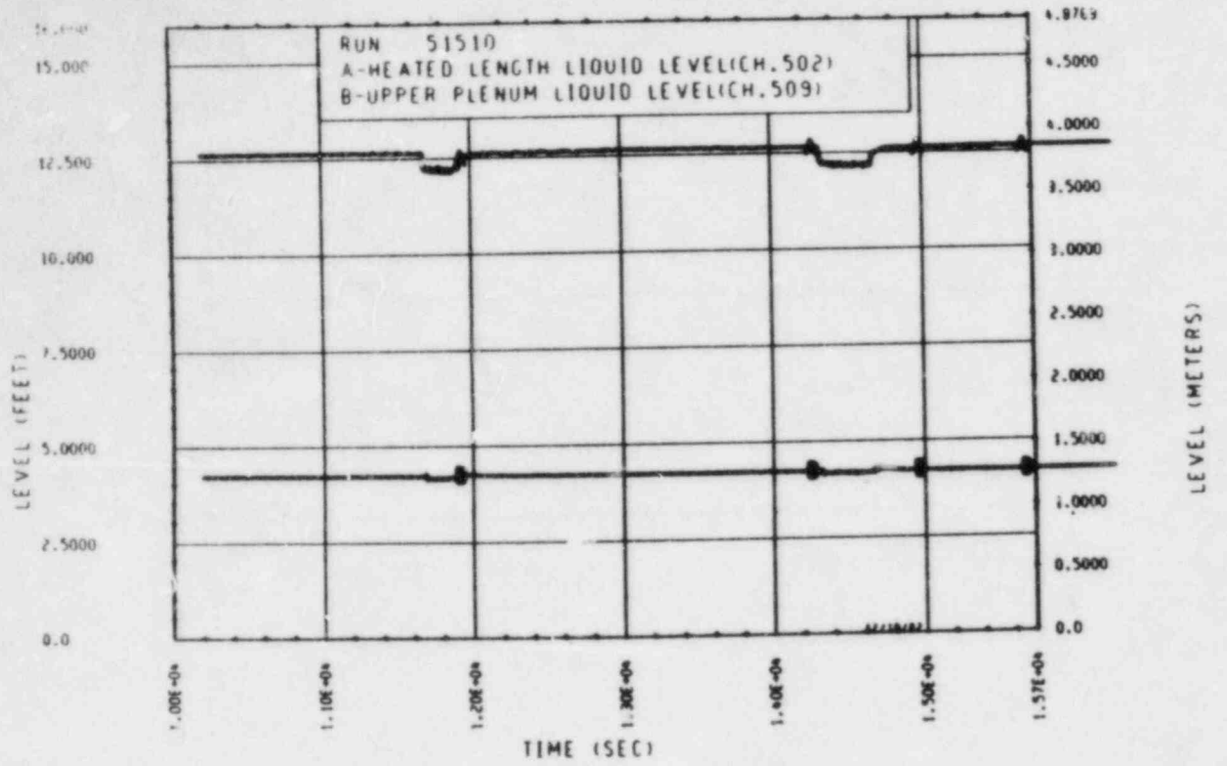

Figure A-91. Heated Length and Upper Plenum Liquid Levels, Test 10A

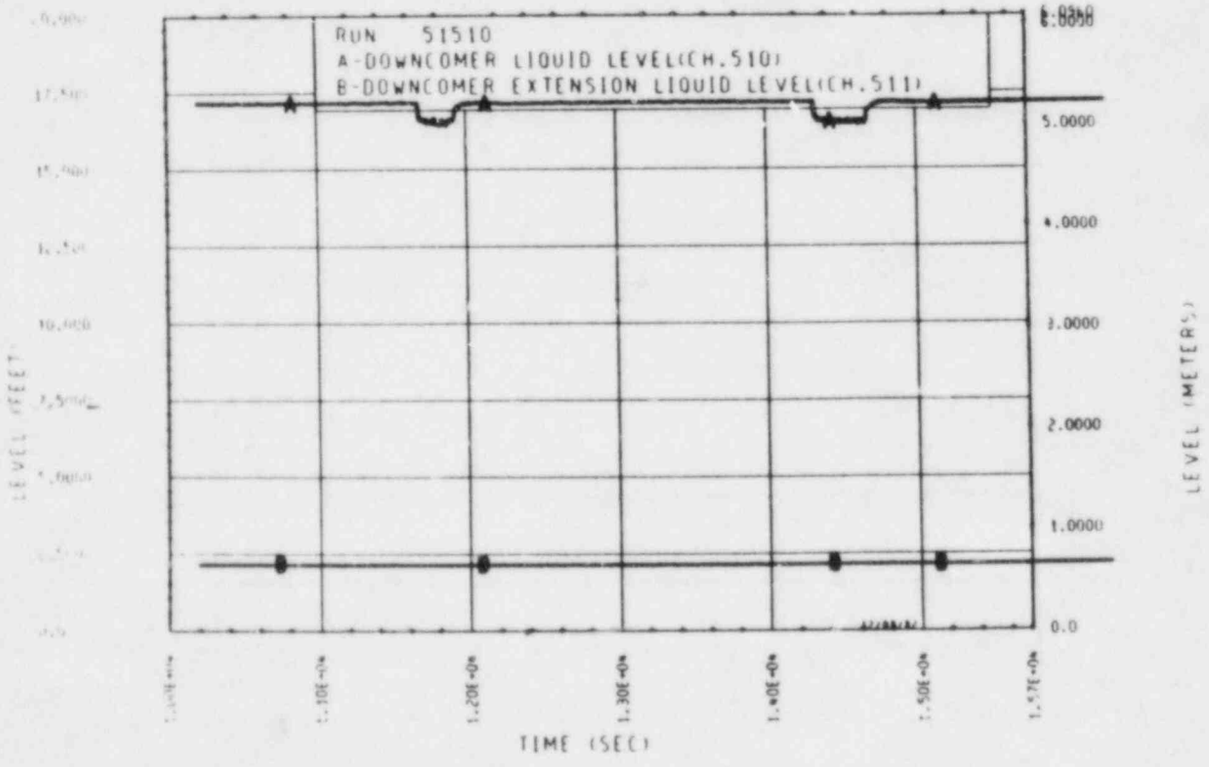

Figure A-92. Downcomer and Downcomer Extension Liquid Levels, Test 10A

TEST 10B: TWO-PHASE PEAK FLOW NATURAL CIRCULATION UPPER HEAD INJECTION TEST

Objective

To determine the effect of upper head injection (UHI) on two-phase peak flow natural circulation

Test Procedure

The test was begun from a steady-state two-phase peak flow natural circulation mode with a nominal bundle power of 222 kw (simulated 2 percent of full power). The primary system was operated with the pressurizer valved out and a reduced mass inventory consistent with previously established two-phase peak flow conditions. The secondary side was operated in a constant level feed-and-bleed boiling mode with a nominal pressure of 0.28 MPa (40 psia). The secondary side level was maintained at 7.62 m (25 ft) (71 percent full). Accumulator 1 was used to inject 36°C (97°F) water into the upper plenum at a nominal rate of 0.43 kg/sec (0.94 lbm/sec). The duration of the injection was scheduled to be 347 seconds. The test was terminated when the rod bundle automatically scrammed in response to a primary system overpressurization signal.

Test Overview

Prior to UHI, the primary system was brought to a steady-state two-phase peak flow natural circulation mode. This was accomplished by removing 18.6 percent of the original single-phase primary system mass inventory. At this peak two-phase flow condition, the average mass flow rate through the rod bundle was approximately 3.06 kg/sec (6.75 lbm/sec). The broken loop was initially stalled, but became active just prior to UHI. The flow ratio of the unbroken to broken loop was 5.5 to 1. Single-phase fluid entered the rod bundle inlet at an average temperature of 132°C (270°F) and a two-phase saturated mixture exited at an average temperature of 149°C (300°F). The average measured primary system pressure was approximately 0.43 MPa (63 psi), which has a

corresponding saturation temperature of 146.59°C (295.89°F). The rod bundle exit temperature of 149°C (300°F) indicates a 2°C (4°F) superheat based on the measured upper plenum pressure. Comparison of the rod bundle exit temperature with other adjacent fluid thermocouples shows excellent agreement. Based on visual observations of the upper plenum, it is believed that the exit was saturated and not superheated. This is confirmed by the collapsed liquid level reading of 0.76 m (2.5 ft) (54 percent full) on the upper plenum. Based on a 149°C (300°F) saturation temperature, the upper plenum pressure cell should have read 0.46 MPa (67 psia) (6.35 percent error).

UHI was initiated at 24,091 seconds and was scheduled to be terminated 347 seconds later. The mass flow rate through the rod bundle decreased from a local peak value of 3.4 to 0 kg/sec (7.5 to 0 lbm/sec) 65 seconds after the initiation of UHI. This flow stagnation is reflected in both the broken and unbroken loops. The rod bundle inlet temperature was generally unaffected by the UHI. The 36°C (97°F) UHI water significantly cooled the exit of the rod bundle, resulting in exit temperatures which averaged 129°C (265°F). Subsequently, void generation ceased in the rod bundle and the primary system pressure momentarily decreased from 0.44 MPa (64 psia) to a low value of 0.41 MPa (60 psia). The pressure reached 0.41 MPa (60 psi) 39 seconds after the initiation of UHI. At 71 seconds after UHI initiation, the primary system pressure began to climb dramatically, tripping the 0.90 MPa (130 psia) pressure alarm 166 seconds after UHI initiation. Continued injection was impossible because of the high primary pressure; it was terminated 181 seconds before its scheduled termina- tion. Termination of UHI decreased the rate of pressure increase but not enough to keep the rod bundle from scramming on a high-pressure signal [0.97 MPa (140 psia)] 200 seconds after UHI initiation. During the primary pressure rise, the secondary side pressure decreased from 0.26 to 0.24 MPa (38 to 35 psia).

The sharp primary pressure rise at the end of the test was accompanied by a general resumption of natural circulation flow through the primary system and a sharp rise in rod bundle exit temperature. Natural circulation flow began to be reestablished 135 seconds after UHI initiation, or 31 seconds before the

0.90 MPa (130 psia) pressure alarm was tripped (coincident with UHI termination). The total flow through the rod bundle was increasing and had established a value of approximately 0.9 kg/sec (2 lbm/sec) when the rod bundle was scrammed. Both the broken and unbroken loops showed similar trends. No explanation is offered regarding the general resumption of natural circulation flow 31 seconds before UHI termination. The rod bundle exit temperature began its sharp increase the moment UHI was terminated. The bundle exit temperature rose from 111°C to 151°C (232°F to 304°F).

TEST SCHEDULE
TEST 10B

Time (sec)	Event
0	Computer on
211	Power to 90 kw
991	Power to 150 kw
1771	Power to 222 kw; primary system operating in a forced circulation mode
5371	Pump off; began primary transition into a natural circulation mode
7831	Adjusted pressurizer to lower the primary pressure from 0.69 to 0.62 MPa (100 to 90 psi). Lowering pressure is a safety precaution. During a previous single-phase UHI attempt at 0.88 MPa (127 psi), the crossover leg ruptured during injection.
8462	Adjusted pressurizer to lower primary pressure from 0.61 to 0.55 MPa (87.9 to 80 psi)
9561	Adjusted pressurizer to lower primary pressure from 0.55 to 0.52 MPa (80 to 75 psi)
11191	Set up UHI injection flows to 4.3×10^{-4} m^3/sec (6.8 gal/min)

Time (sec)	Event
11671	Began UHI injection with a nominal flow rate of 4.3×10^{-4} m^3/sec (6.8 gal/min)
11987	UHI terminated; test aborted. The pressurizer was inadvertently adjusted. Primary pressure reset to 0.52 MPa (75 psi).
13912	Set up UHI flows to 4.3×10^{-4} m^3/sec (6.8 gal/min)
14311	Began UHI with a nominal flow rate of 4.3×10^{-4} m^3/sec (6.8 gal/min)
14658	Ended UHI
14636	Pressurizer valved out; pressure observed to peak at about 0.61 MPa (88 psi)
15098	Pressure settling down to approximately 0.49 MPa (71 psi)
15732	Single-phase UHI test terminated; pressurizer valved in; pressurizer adjusted to bring primary pressure to 0.93 MPa (135 psi)
16531	Primary pressure = 0.93 MPa (135 psi); secondary exhaust valves adjusted to increase secondary pressure to 0.28 MPa (40 psi); prepared to drain mass from the primary side to achieve a two-phase peak flow condition

Time (sec)	Event
18791	Pressurizer valved out
18823	Began 136 kg (300 lbm) continuous drain
19996	45 kg (100 lbm) drained
20971	91 kg (200 lbm) drained
22064	136 kg (300 lbm) drained; ended continuous drain
22313	Began 18 kg (40 lbm) drain
22403	Ended 18 kg (40 lbm) drain; total of 154 kg (340 lbm) drained
22531	Began two-phase peak flow steady-state reference run
23611	Ended two-phase peak flow steady-state reference run
23820	Adjusted UHI rate to 4.3×10^{-4} m^3/sec (6.8 gal/min)
24091	Began UHI; nominal flow rate of 4.3×10^{-4} m^3/sec (6.8 gal/min)
24281	Pressure alarm; primary pressure = 0.90 MPa (130 psi). UHI unable to inject due to high primary pressure.

Time (sec)	Event
24302	Bundle scram; primary pressure of 0.97 MPa (140 psi). Never finished injection. Injection was scheduled to finish at 24,438 sec. End of two-phase peak flow UHI test.
0	Computer back on. Note that the computer scrams with a bundle scram. The computer subsequently writes to a new tape when it is brought back on line. Thus the computer time is resequenced to zero.
1214	Power restarted to 60 kw. Pumps not on.
1314	Began a continuous mass drain to bring the system to a reflux mode of natural circulation. It was estimated that 81.00 kg (178.6 lbm) of mass was added to the primary inventory by the UHI. The net mass drained was 73.19 kg (161.4 lbm).
1466	Power increased to 107.7 kw
1634	Power increased to 222.3 kw
2727	166 kg (366 lbm) drained; total net amount of mass drained from the primary = 239.2 kg (527.4 lbm)
4369	380 kg (838 lbm) drained; total net amount of mass drained form the primary = 453.2 kg (999.4 lbm); continuous drain stopped
5316	Began 23 kg (50 lbm) drain

Time (sec)	Event
5457	Ended 23 kg (50 lbm) drain; net amount of mass drained from the primary = 475.90 kg (1049.4 lbm)
5671	Began 45 kg (100 lbm) drain
5928	Ended 45 kg (100 lbm) drain; net amount of mass drained from the primary = 521.25 kg (1149.4 lbm)
6032	Began 23 kg (50 lbm) drain
6177	Ended 23 kg (50 lbm) drain; net amount of mass drained from the primary = 543.93 kg (1199.4 lbm)
6679	Began 14 kg (30 lbm) drain
	Ended 14 kg (30 lbm) drain; net amount of mass drained from the primary = 557.53 kg (1229.4 lbm)
6914	Loss of feedwater to both steam generators. Both feedwater lines shut to keep the secondary from draining. Technicians realigned valves to draw feedwater from an alternate source.
8109	Computer operator reported a disk allocation error. Power ramped to zero. Power trip. Computer trip. Computer operator reallocated disk space.
0	Computer time resychronized for new disk
229	Power to bundle 75 kw

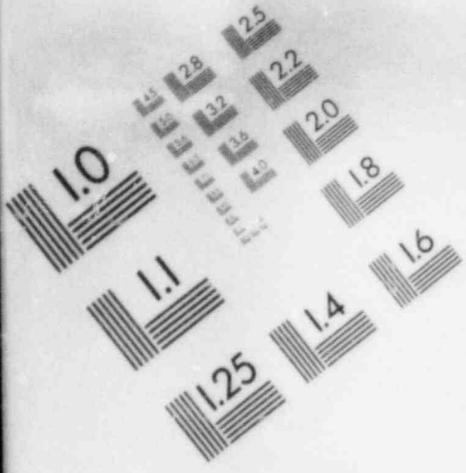

IMAGE EVALUATION TEST TARGET (MT-3)

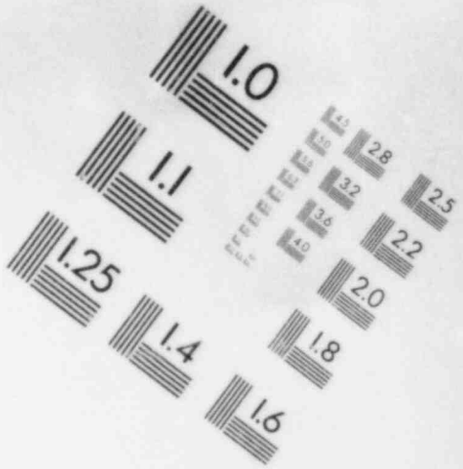

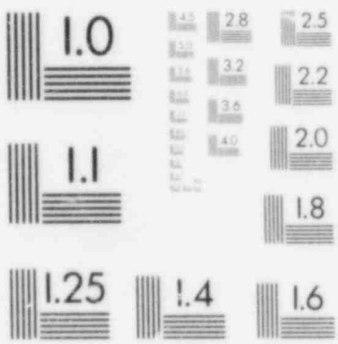

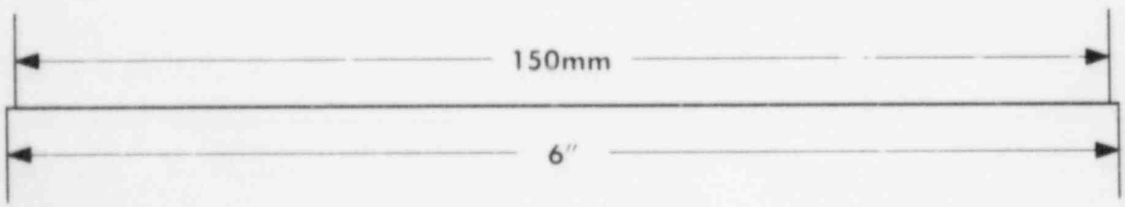

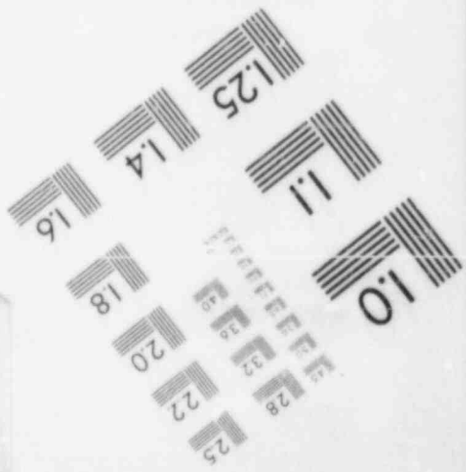

Time (sec)	Event
552	Power to bundle 222 kw
1282	Began 9 kg (20 lbm) drain
1349	Ended 9 kg (20 lbm) drain; net amount of mass drained from the primary = 566.60 kg (1249.4 lbm)
1681	Valved in weir meters
1749	Began 9 kg (20 lbm) drain
1807	Ended 9 kg (20 lbm) drain; net amount of mass drained from the primary = 575.67 kg (1269.4 lbm)
2559	Began 9 kg (20 lbm) drain
2631	Ended 9 kg (20 lbm) drain; net amount of mass drained from the primary = 584.74 kg (1289.4 lbm)
2851	Began 9 kg (20 lbm) drain
2922	Ended 9 kg (20 lbm) drain; net amount of mass drained from the primary = 593.81 kg (1309.4 lbm)
3053	Began 9 kg (20 lbm) drain
3113	Ended 9 kg (20 lbm) drain; net amount of mass drained from the primary = 602.88 kg (1329.4 lbm)
3354	Began 9 kg (20 lbm) drain

Time (sec)	Event
3417	Ended 9 kg (20 lbm) drain; net amount of mass drained from the primary = 611.95 kg (1349.4 lbm)
3680	Began 9 kg (20 lbm) drain
3743	Ended 9 kg (20 lbm) drain; net amount of mass drained from the primary = 621.02 kg (1369.4 lbm)
3958	Began 9 kg (20 lbm) drain
4024	Ended 9 kg (20 lbm) drain; net amount of mass drained from the primary = 630.09 kg (1389.4 lbm)
4317	Began 4.5 kg (10 lbm) drain
4349	Ended 4.5 kg (10 lbm) drain; net amount of mass drained from the primary = 634.63 kg (1399.4 lbm)
4648	Began 4.5 kg (10 lbm) drain
4686	Ended 4.5 kg (10 lbm) drain; net amount of mass drained from the primary = 639.16 kg (1409.4 lbm)
4955	Began steady-state reflux run
5559	UHI set up to deliver 4.3×10^{-4} m^3/sec (6.8 gal/min)
6039	Began UHI at a nominal flow rate of 4.3×10^{-4} m^3/sec (6.8 gal/min)

Time (sec)	Event
6386	Ended UHI
6939	Steady-state after UHI
7616	Ramped power down to zero
7732	Computer off

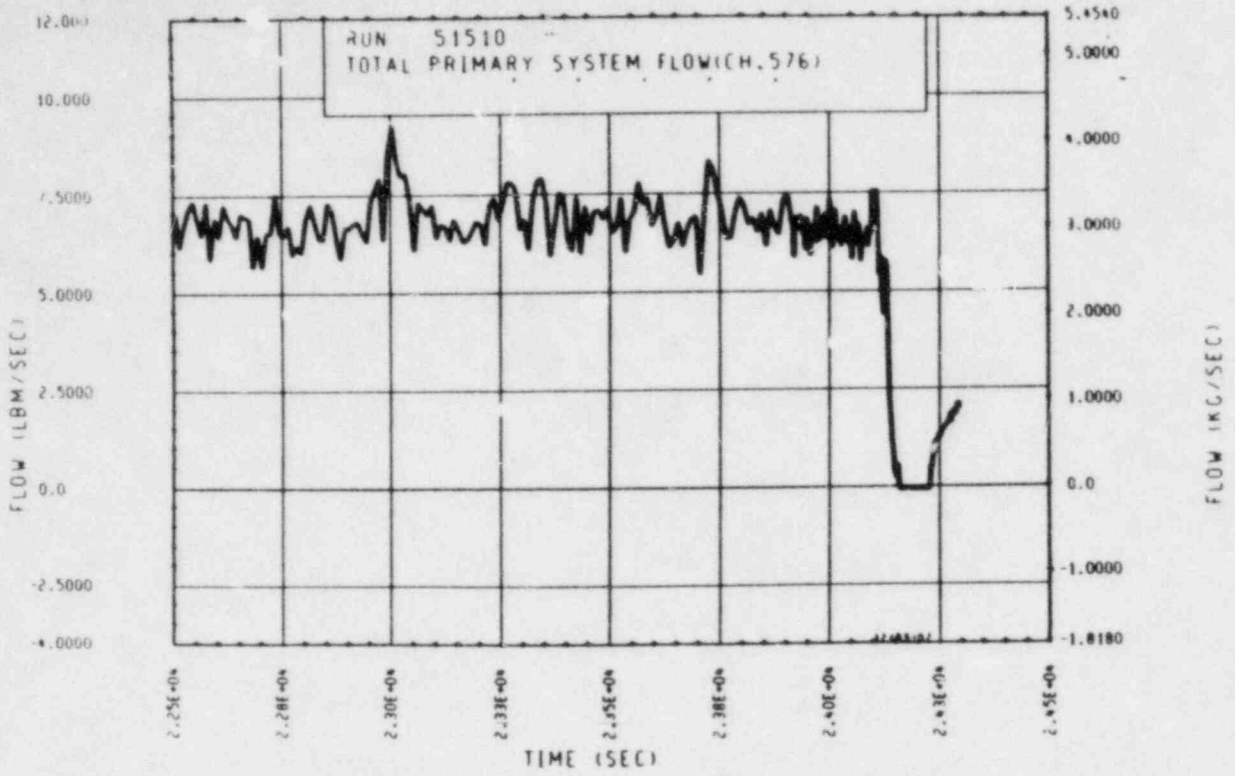

Figure A-93. Mass Flow Rate Through Rod Bundle, Test 10B

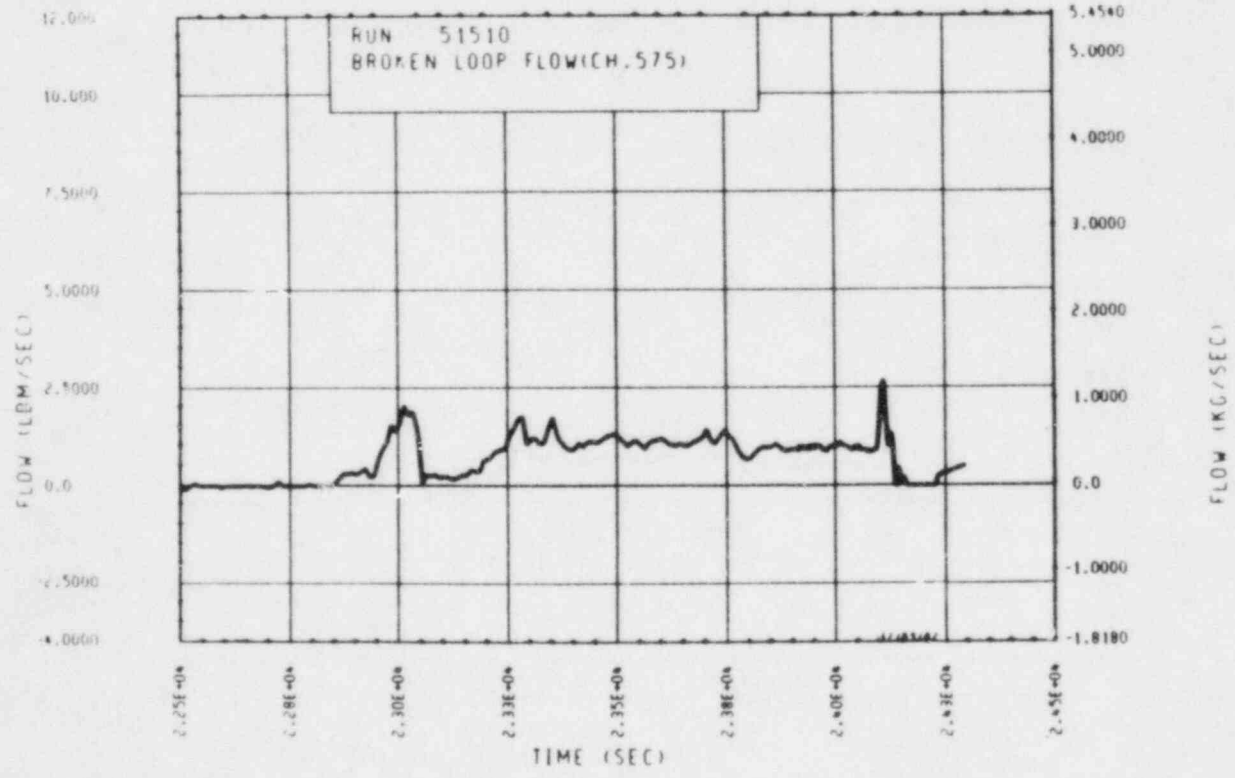

Figure A-94. Mass Flow Rate Through Broken Loop, Test 10B

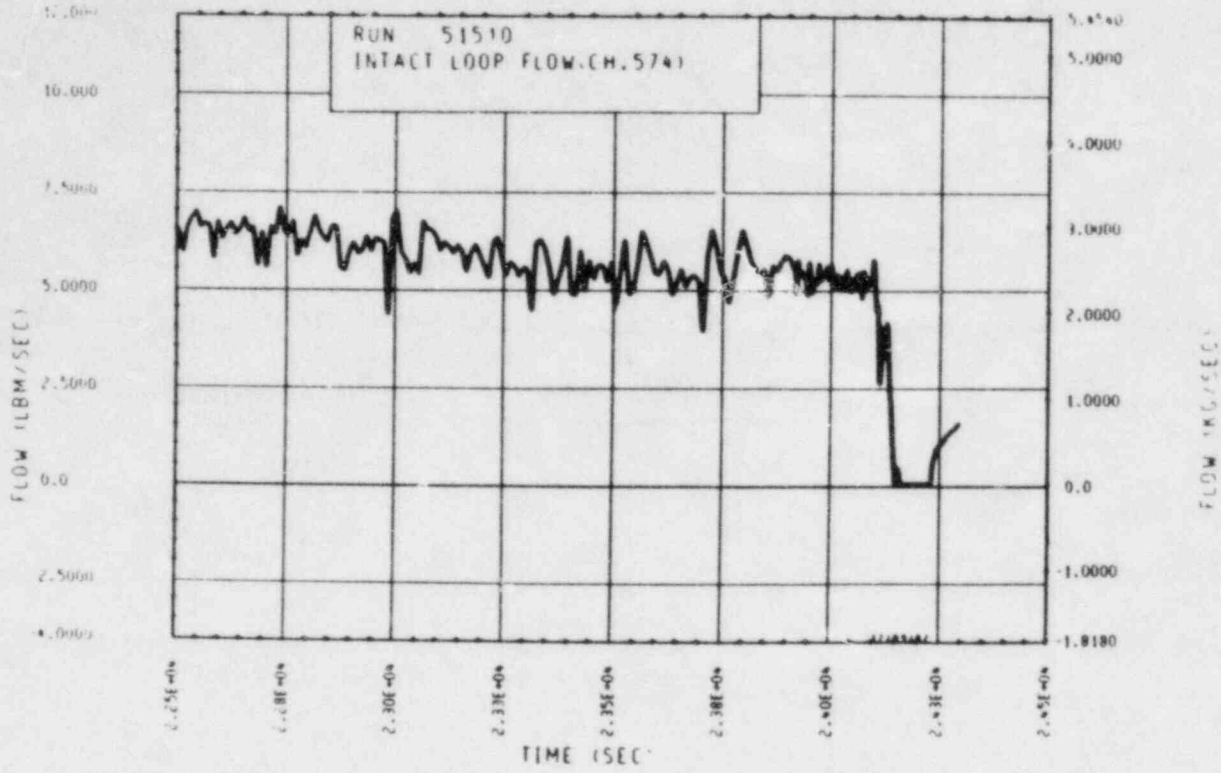

Figure A-95. Mass Flow Rate Through Unbroken Loop, Test 10B

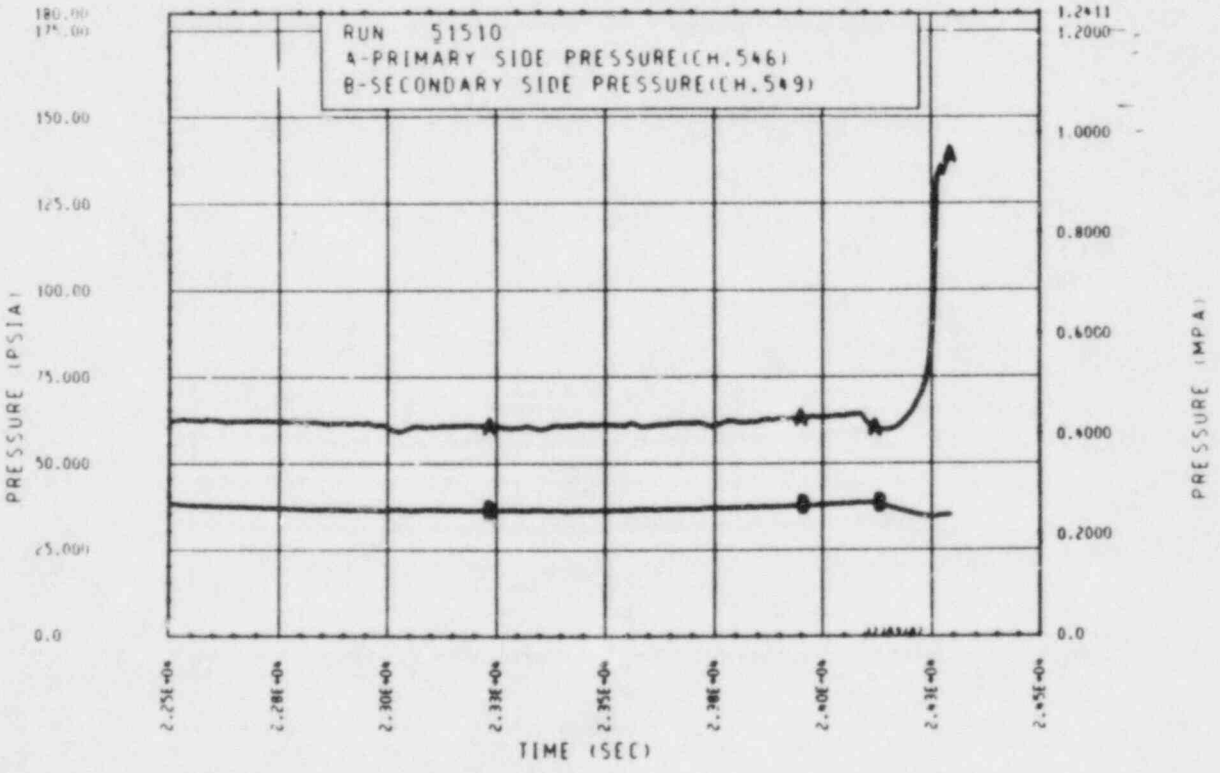

Figure A-96. Primary and Secondary System Pressure, Test 10B

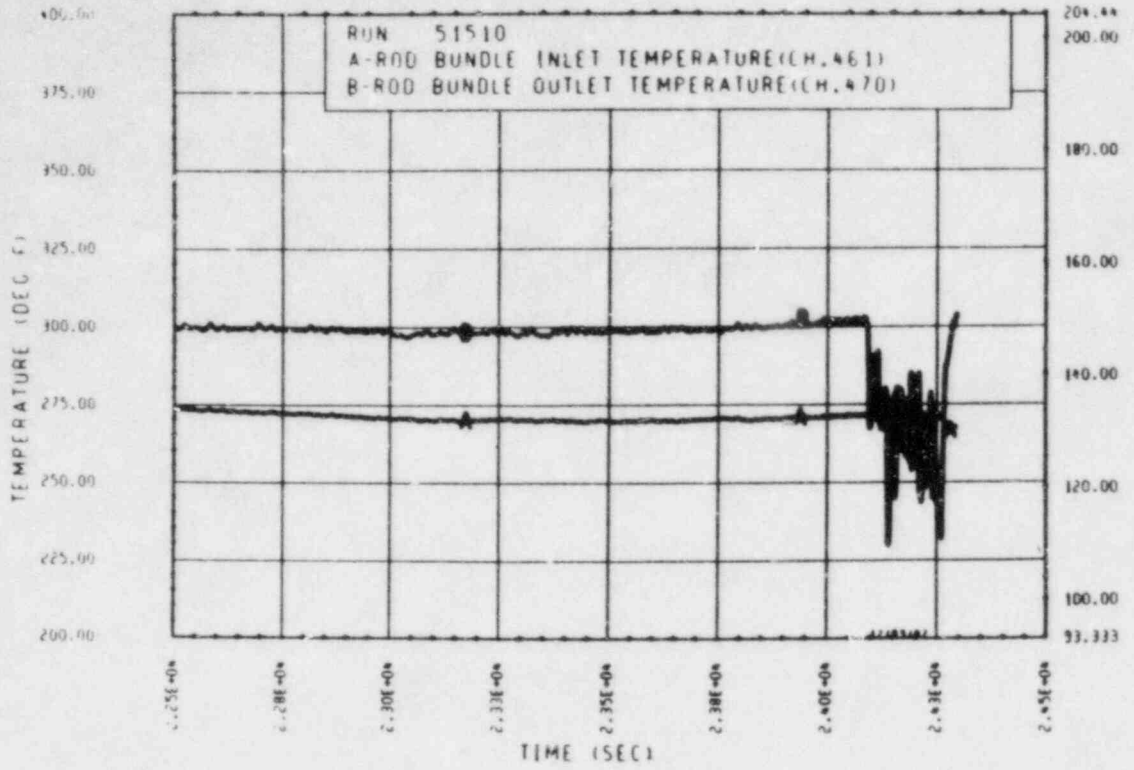

Figure A-97. Heater Rod Bundle Inlet and Outlet Temperature, Test 10B

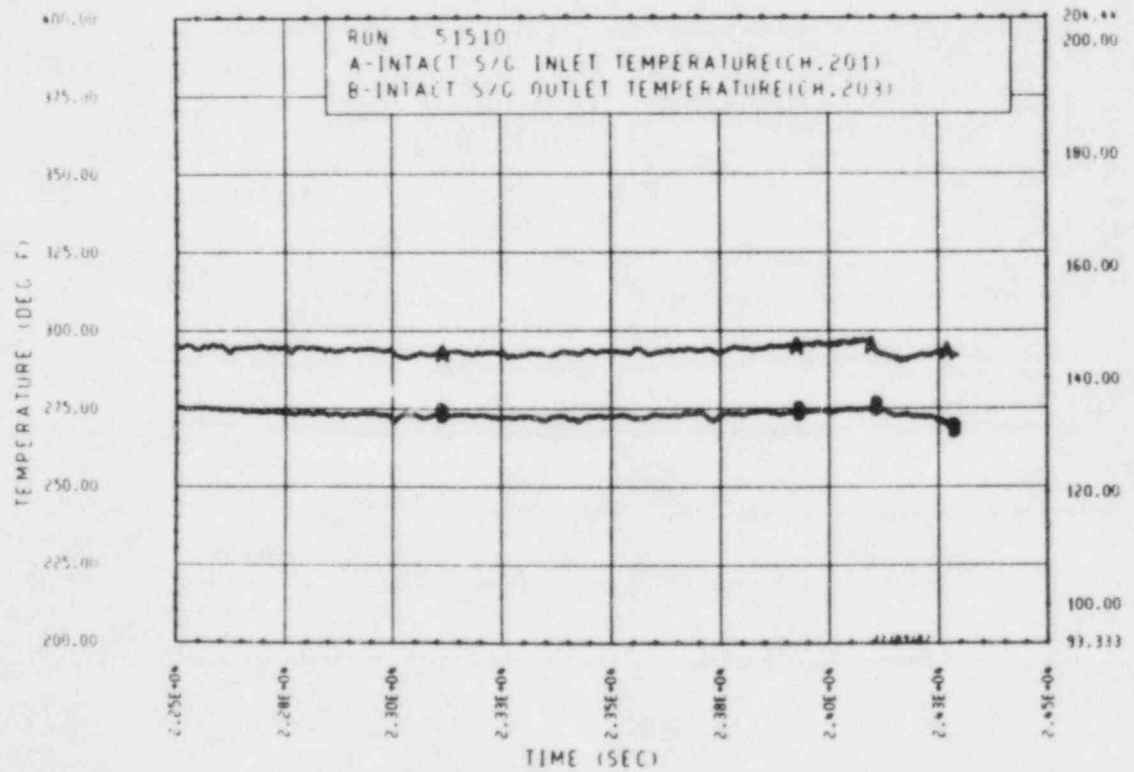

Figure A-98. Unbroken Loop Steam Generator Inlet and Outlet Temperature, Test 10B

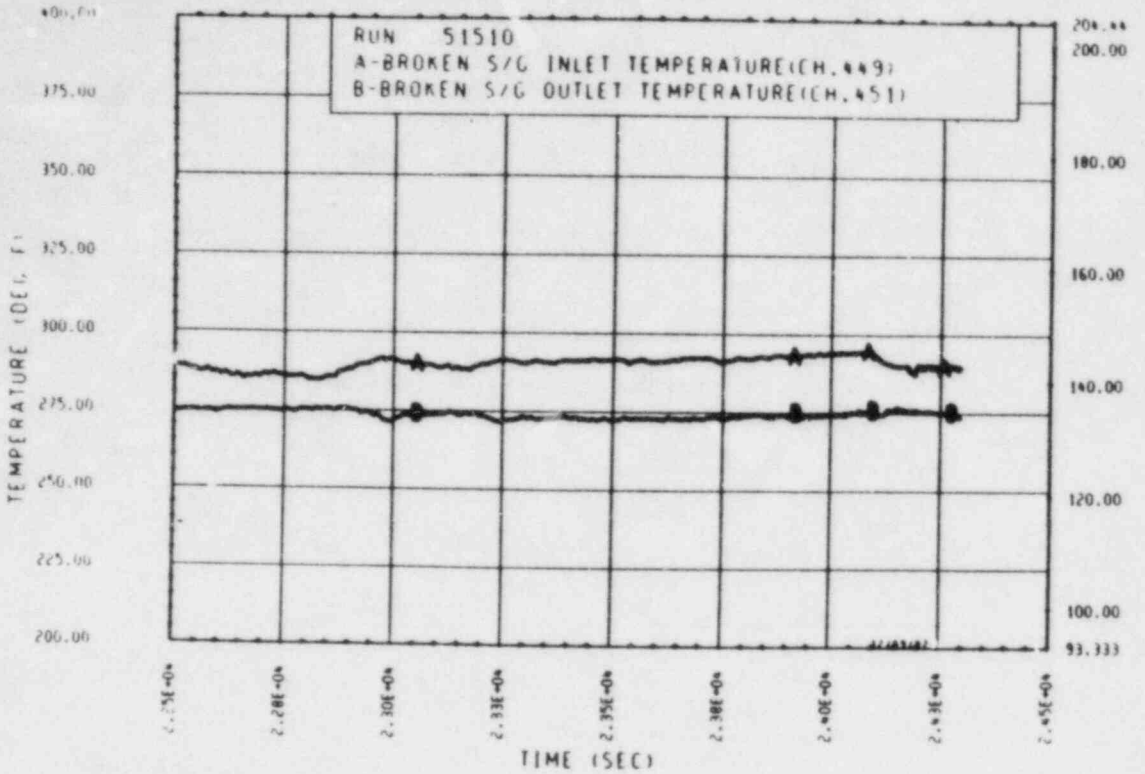

Figure A-99. Broken Loop Steam Generator Inlet and Outlet Temperature, Test 10B

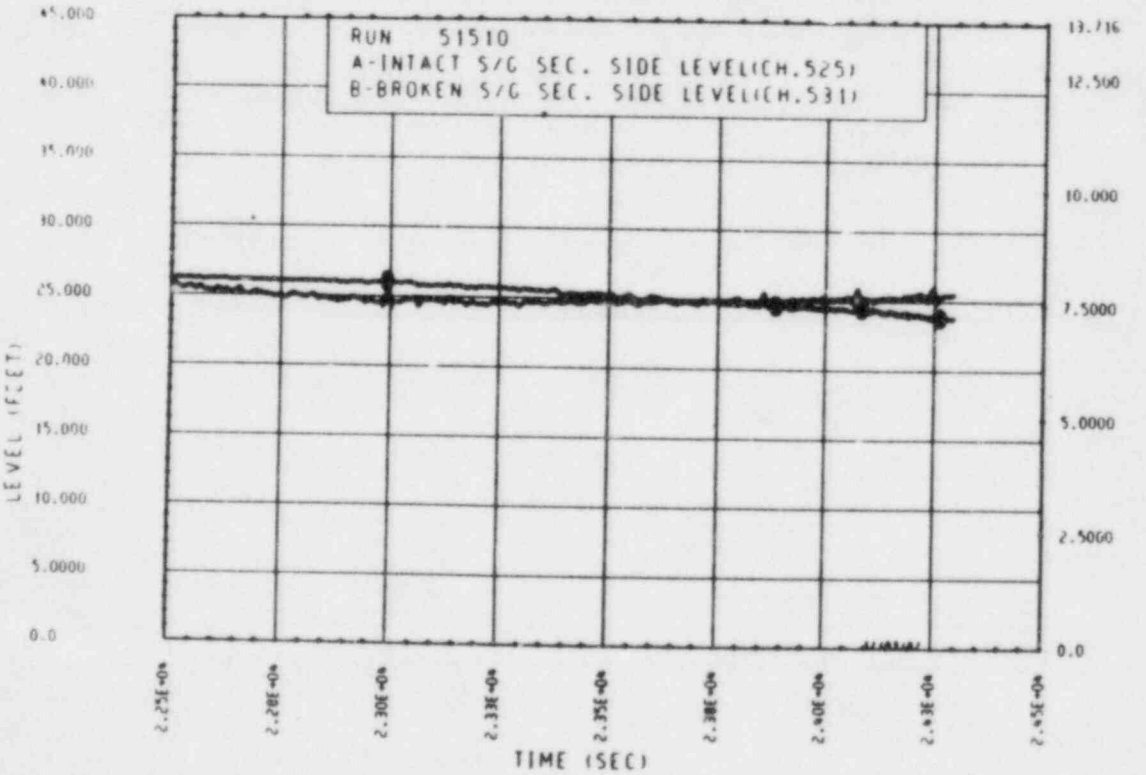

Figure A-100. Unbroken and Broken Loop Steam Generator Secondary Side Collapsed Liquid Levels, Test 10B

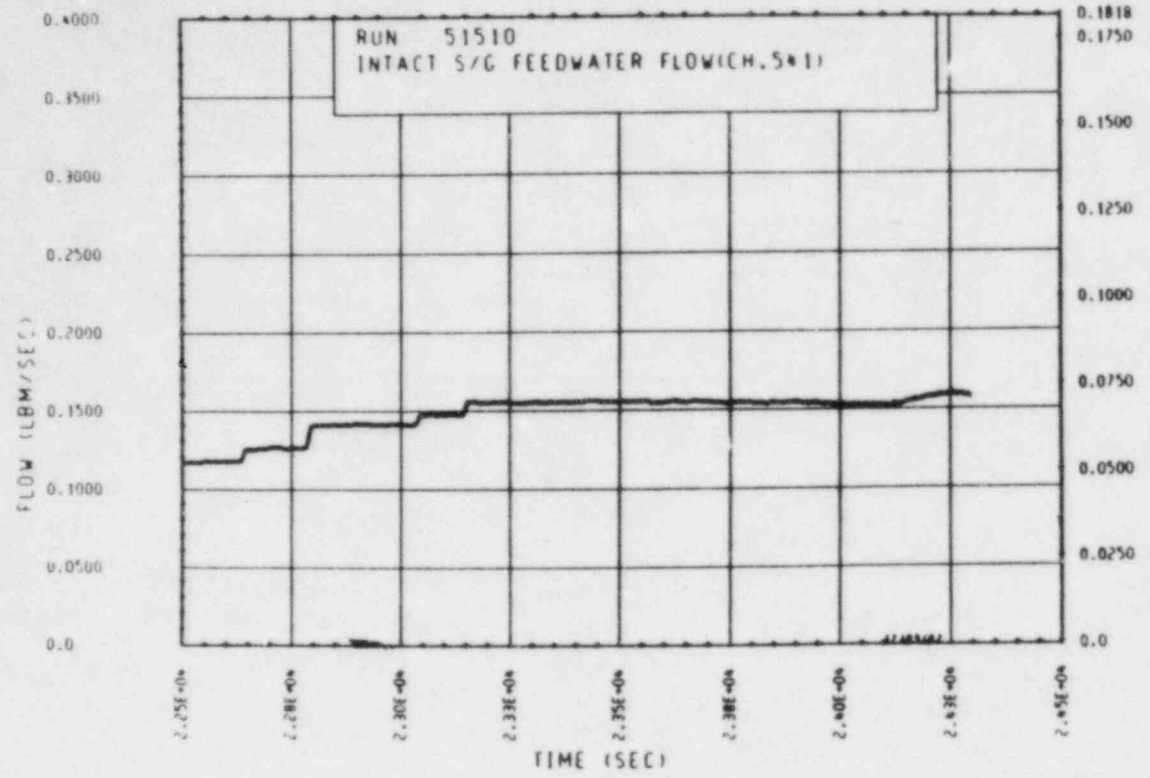

Figure A-101. Unbroken Loop Steam Generator Feedwater Mass Flow Rate, Test 10B

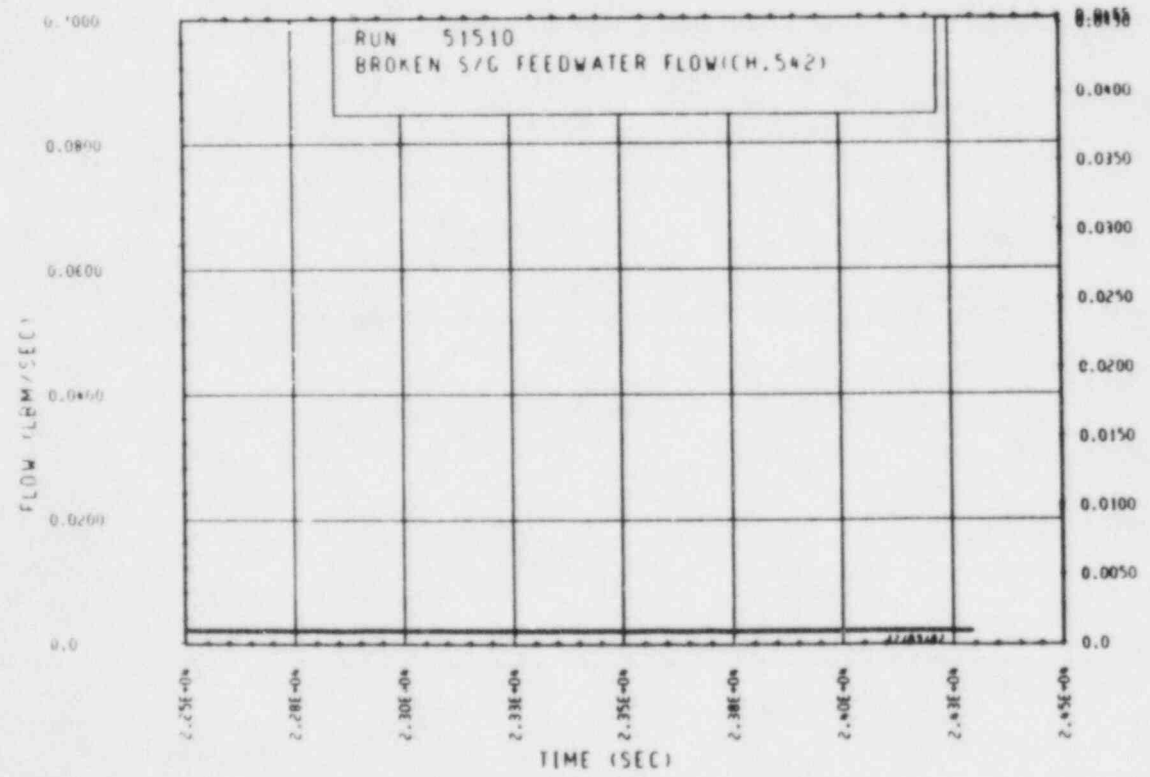

Figure A-102. Broken Loop Steam Generator Feedwater Mass Flow Rate, Test 10B

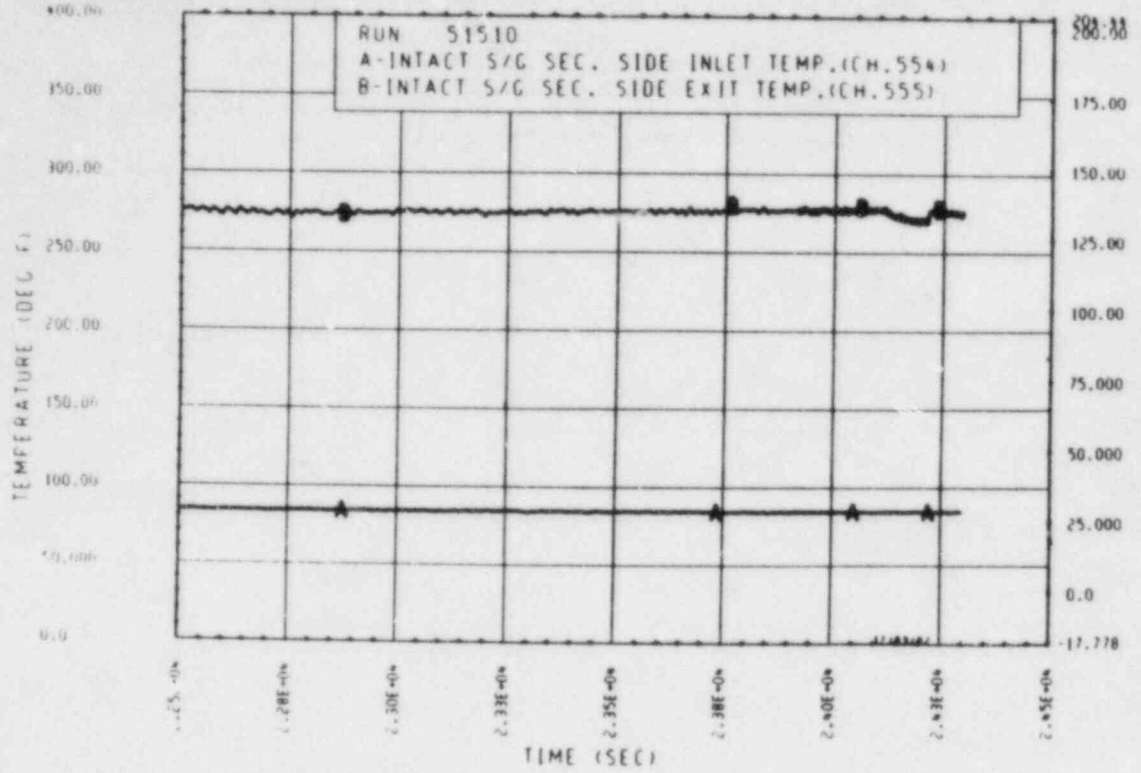

Figure A-103. Unbroken Loop Steam Generator Secondary Side Inlet and Outlet Temperature, Test 10B

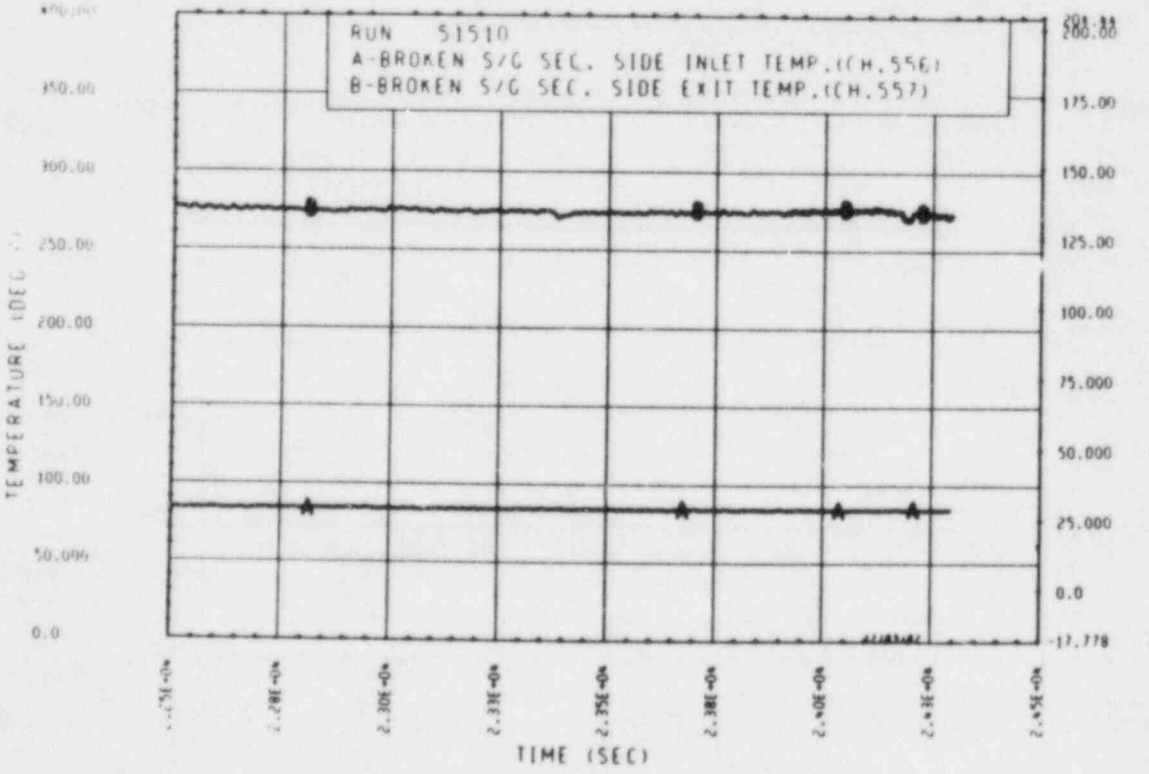

Figure A-104. Broken Loop Steam Generator Secondary Side Inlet and Outlet Temperature, Test 10B

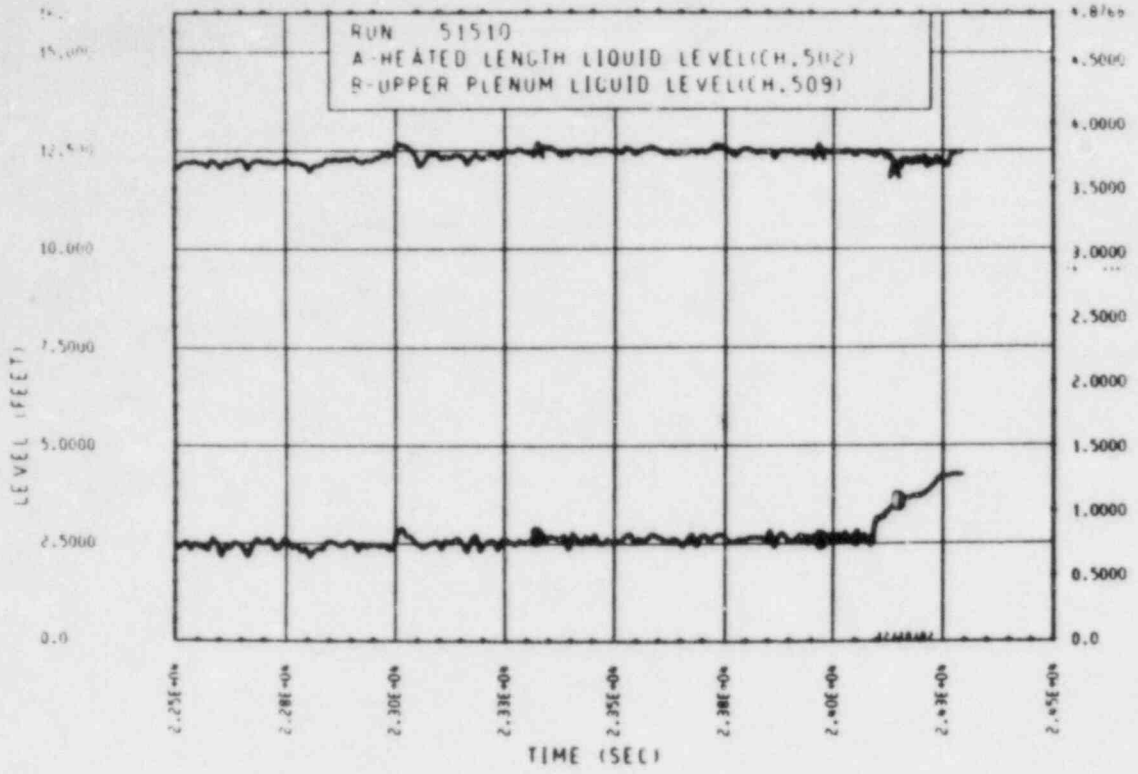

Figure A-105. Heated Length and Upper Plenum Liquid Levels, Test 10B

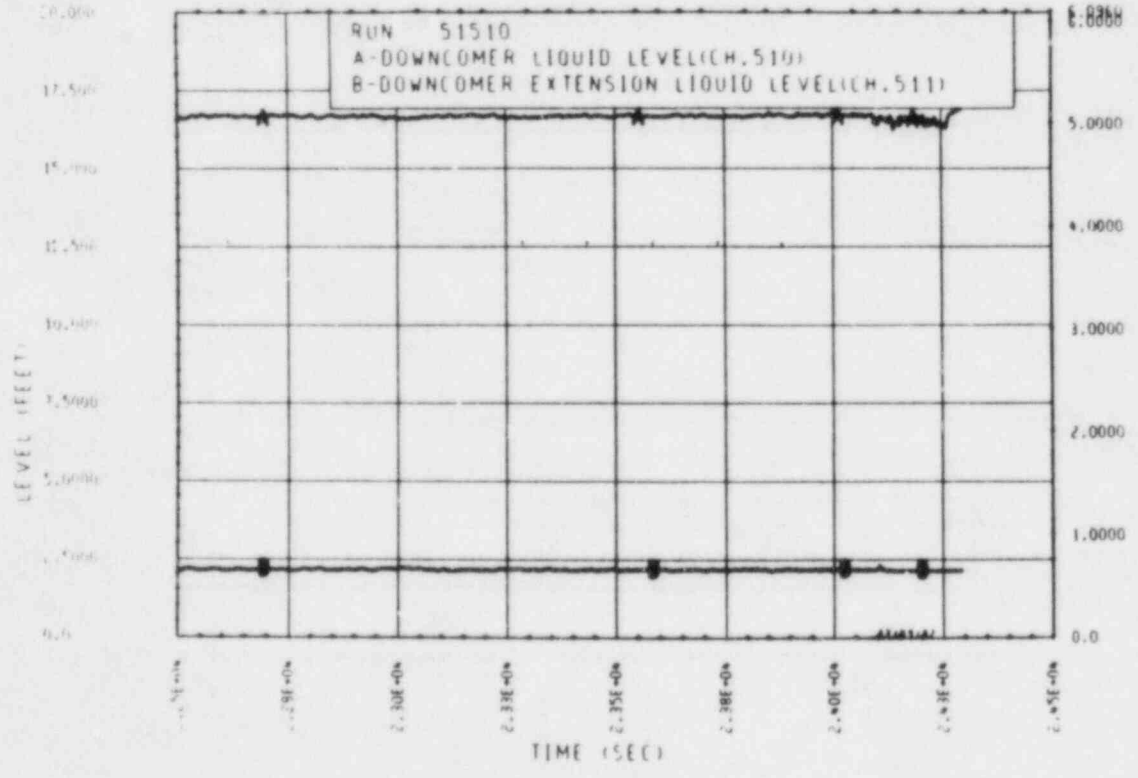

Figure A-106. Downcomer and Downcomer Extension Liquid Levels, Test 10B

TEST 10C: REFLUX CONDENSATION UPPER HEAD INJECTION TEST

Objective

To determine the effect of upper head injection (UHI) on reflux condensation

Test Procedure:

The test was begun from a steady-state reflux condensation mode with a nominal bundle power of 222 kw. The primary system was operated with the pressurizer valved out and a reduced mass inventory consistent with previously established reflux condensation conditions. The secondary side was operated in a constant level feed-and-bleed boiling mode with a nominal pressure of 0.28 MPa (40 psia). The secondary side level was maintained at 7.62 m (25 ft) (71 percent full). Accumulator 1 was used to inject 36°C (97°F) water into the upper plenum at a nominal rate of 0.43 kg/sec (0.94 lbm/sec). The duration of the injection was 347 seconds. The test was terminated when the system returned to a steady-state condition.

Test Overview

Prior to UHI, the primary system was brought to a steady-state reflux condensation mode of natural circulation. This was accomplished by removing 77 percent of the original single-phase primary system mass inventory. At the reflux condensation condition, the average measured primary system pressure was 0.31 MPa (45 psia). The secondary side pressure was 0.27 MPa (39 psia). Reflux condensation from the cold legs entered the rod bundle with a 22°C (39°F) subcooling at 113°C (236°F). A two-phase saturated mixture exited at the rod bundle exit at 132°C (270°F). At a primary pressure of 0.31 MPa (45 psia), the saturation temperature is 135°C (275°F). The rod bundle exit temperature of 132°C (270°F) indicates a 3°C (5°F) subcooling based on the measured upper plenum pressure. Comparison of the rod bundle exit thermocouple with other adjacent fluid thermocouples shows excellent agreement, and

indicates that the pressure cell in the upper plenum was probably in error by approximately 7 percent. Based on a saturation temperature of 132°C (270°F), the upper plenum pressure was 0.29 MPa (42 psia). The net mass flow through the rod bundle was zero. Hence, the rod bundle operated in a pool boiling mode. The collapsed liquid level in the heated length was approximately 1.83 m (6 ft) and quite steady. The upper plenum collapsed liquid level was less stable, but main- tained a level of 0.38 m (1.25 ft) (27 percent full) just prior to UHI.

The rod bundle collapsed liquid level was maintained by reflux condensation from both sets of hot legs and cold legs. The unbroken loop hot leg, unbroken loop cold leg, and the broken loop hot leg exhibited steady reflux condensation flows. The broken loop hot leg exhibited a more sporadic reflux condensation flow. Approximations of these reflux condensation flow rates are summarized below:

Unbroken loop hot leg ~ 0.034 kg/sec (0.075 lbm/sec)
Broken loop hot leg ~ 0.016 kg/sec (0.035 lbm/sec)
Unbroken loop cold leg ~ 0.041 kg/sec (0.090 lbm/sec)
Broken loop cold leg ~ 0.016 kg/sec (0.035 lbm/sec)
Total reflux condensation = 0.107 kg/sec (0.235 lbm/sec)

The reflux condensation (RC) flow splits between and within the broken and unbroken loops are summarized below:

Unbroken loop total RC/total RC = 0.70
Hot leg total RC/total RC = 0.47
Unbroken loop hot leg RC/unbroken loop total RC = 0.45
Broken loop hot leg RC/broken loop total RC = 0.50

Employing an average measured power of 224 kw and accounting for a 19°C (34°F) subcooling [accounting for a postulated 3°C (5°F) change in saturation temperature due to pressure cell error] at the rod bundle inlet, a steady-state energy balance predicts a steaming rate of 0.102 kg/sec (0.224 lbm/sec) in the rod bundle. This agrees favorably with the total measured RC rate of 0.107 kg/sec (0.235 lbm/sec) (4.7 percent discrepancy).

It should be noted that, prior to UHI, all three primary system bidirectional flowmeters showed very smooth and steady values of zero. After an unexplained flow surge at approximately 5800 seconds (UHI occurred at 6039 seconds), the flowmeters indicated oscillatory flow. At first it was believed that these flow oscillations were the result of the write-to-disk (WTD) rate change that occurred at 5,915.5 seconds. The rate changed from a WTD every 10 seconds to a WTD every 1 second. Comparisons, however, with independent strip-chart recordings show the same smooth-to-oscillatory flow transition phenomenon. Hence, it is concluded that the smooth and oscillatory flow phenomenon, respectively before and after the unexplained flow surge, is real and not the result of the inability of the WTD rate to capture the phenomenon.

UHI was initiated at 6039 seconds and was terminated 347 seconds later. The relatively long injection delivered a total of 147.92 kg (326.18 lbm) of cold water to the primary system. This represents an increase in pre-UHI reflux condensation mass inventory of approximately 79 percent. The injection resulted in an increase in the amplitude of the oscillatory flow in the rod bundle and in both loop seals. This oscillatory flow did not decrease to pre-UHI levels after termination of UHI. The oscillatory flow exhibited by both loop seal bidirectional turbine meters was about zero, whereas the oscillatory flow exhibited by the crossover leg bidirectional turbine meter showed an average flow up through the rod bundle of approximately 0.68 kg/sec (1.5 lbm/sec).

The rod bundle exit temperature decreased immediately upon initiation of UHI from 133°C (272°F) to an average of approximately 121°C (250°F). The exit temperature oscillated about 121°C (250°F) with 14°C (25°F) peak-to-peak oscillations. The exit temperature increased to 135°C (275°F) within seconds after the termination of UHI. The rod bundle inlet temperature began a steady but gradual increase during the initial portions of UHI. At UHI initiation, the inlet temperature was 114°C (237°F); 297 seconds later it measured 115°C (239°F). The rate of increase, however, increased at this point such that at UHI termination (347 seconds after UHI initiation), the inlet temperature measured 118°C (245°F). At 21 seconds later, the inlet temperature peaked at 128°C (262°F), and subsequently began to decrease.

During UHI, the collapsed liquid level in the heated length increased from 1.83 to 2.59 m (6 to 8.5 ft). The upper plenum collapsed liquid level increased from 0.38 to 0.69 m (1.25 to 2.25 ft) (48 percent full). These levels were stable during the course of the UHI, but decreased immediately after termination of UHI. The upper plenum recovered to its pre-UHI level of approximately 0.38 m (1.25 ft). The heated length recovered to the 2.13 m (7 ft) level, which is slightly higher than the pre-UHI level. This reflects the increase in primary system mass inventory as a result of UHI. The downcomer liquid level behaved quite differently. When UHI was initiated, the downcomer level began a steady decrease from 3.35 m (11 ft) to a level of 2.29 m (7.5 ft). The level reached the 2.29 m (7.5 ft) point 176 seconds after UHI initiation. The downcomer liquid level subsequently began a steady increase, reaching the 3.35 m (11 ft) level when UHI was terminated. During the 70 seconds following termination of UHI, the downcomer level increased rapidly to the cold leg nozzle level of 5.03 m (16.5 ft).

All reflux condensation flow was reduced to zero during the course of UHI. The unbroken and broken loop hot leg reflux condensation flowmeters became sporadically active after the termination of UHI, but never recovered to pre-UHI levels. The cold leg reflux condensation flowmeters never recovered, measuring no reflux condensation flow during or after UHI.

TEST SCHEDULE
TEST 10C

Time (sec)	Event
0	Computer on
211	Power to 90 kw
991	Power to 150 kw
1771	Power to 222 kw; primary system operating in a forced circulation mode
5371	Pump off; began primary transition into a natural circulation mode
7831	Adjusted pressurizer to lower the primary pressure from 0.69 to 0.62 MPa (100 to 90 psi). Lowering pressure is a safety precaution. During a previous single-phase UHI attempt at 0.88 MPa (127 psi), the crossover leg ruptured during injection.
8462	Adjusted pressurizer to lower primary pressure from 0.61 to 0.55 MPa (87.9 to 80 psi)
9561	Adjusted pressurizer to lower primary pressure from 0.55 to 0.52 MPa (80 to 75 psi)
11191	Set up UHI injection flows to 4.3×10^{-4} m^3/sec (6.8 gal/min)

Time (sec)	Event
11671	Began UHI injection with a nominal flow rate of 4.3×10^{-4} m^3/sec (6.8 gal/min)
11987	UHI terminated; test aborted. The pressurizer was inadvertently adjusted. Primary pressure reset to 0.52 MPa (75 psi).
13912	Set up UHI flows to 4.3×10^{-4} m^3/sec (6.8 gal/min)
14311	Began UHI with a nominal flow rate of 4.3×10^{-4} m^3/sec (6.8 gal/min)
14658	Ended UHI
14636	Pressurizer valved out; pressure observed to peak at about 0.61 MPa (88 psi)
15098	Pressure settling down to approximately 0.49 MPa (71 psi)
15732	Single-phase UHI test terminated; pressurizer valved in; pressurizer adjusted to bring primary pressure to 0.93 MPa (135 psi)
16531	Primary pressure = 0.93 MPa (135 psi); secondary exhaust valves adjusted to increase secondary pressure to 0.28 MPa (40 psi); prepared to drain mass from the primary side to achieve a two-phase peak flow condition

Time (sec)	Event
18791	Pressurizer valved out
18823	Began 136 kg (300 lbm) continuous drain
19996	45 kg (100 lbm) drained
20971	91 kg (200 lbm) drained
22064	136 kg (300 lbm) drained; ended continuous drain
22313	Began 18 kg (40 lbm) drain
22403	Ended 18 kg (40 lbm) drain; total of 154 kg (340 lbm) drained
22531	Began two-phase peak flow steady-state reference run
23611	Ended two-phase peak flow steady-state reference run
23820	Adjusted UHI rate to 4.3×10^{-4} m^3/sec (6.8 gal/min)
24091	Began UHI; nominal flow rate of 4.3×10^{-4} m^3/sec (6.8 gal/min)
24281	Pressure alarm; primary pressure = 0.90 MPa (130 psi). UHI unable to inject due to high primary pressure.

Time (sec)	Event
24302	Bundle scram; primary pressure of 0.97 MPa (140 psi). Never finished injection. Injection was scheduled to finish at 24,438 sec. End of two-phase peak flow UHI test.
0	Computer back on. Note that the computer scrams with a bundle scram. The computer subsequently writes to a new tape when it is brought back on line. Thus the computer time is resequenced to zero.
1214	Power restarted to 60 kw. Pumps not on.
1314	Began a continuous mass drain to bring the system to a reflux mode of natural circulation. It was estimated that 81.00 kg (178.6 lbm) of mass was added to the primary inventory by the UHI. The net mass drained was 73.19 kg (161.4 lbm).
1466	Power increased to 107.7 kw
1634	Power increased to 222.3 kw
2727	166 kg (366 lbm) drained; total net amount of mass drained from the primary = 239.2 kg (527.4 lbm)
4369	380 kg (838 lbm) drained; total net amount of mass drained form the primary = 453.2 kg (999.4 lbm); continuous drain stopped
5316	Began 23 kg (50 lbm) drain

Time (sec)	Event
5457	Ended 23 kg (50 lbm) drain; net amount of mass drained from the primary = 475.90 kg (1049.4 lbm)
5671	Began 45 kg (100 lbm) drain
5928	Ended 45 kg (100 lbm) drain; net amount of mass drained from the primary = 521.25 kg (1149.4 lbm)
6032	Began 23 kg (50 lbm) drain
6177	Ended 23 kg (50 lbm) drain; net amount of mass drained from the primary = 543.93 kg (1199.4 lbm)
6679	Began 14 kg (30 lbm) drain
	Ended 14 kg (30 lbm) drain; net amount of mass drained from the primary = 557.53 kg (1229.4 lbm)
6914	Loss of feedwater to both steam generators. Both feedwater lines shut to keep the secondary from draining. Technicians realigned valves to draw feedwater from an alternate source.
8109	Computer operator reported a disk allocation error. Power ramped to zero. Power trip. Computer trip. Computer operator reallocated disk space.
0	Computer time resychronized for new disk
229	Power to bundle 75 kw

Time (sec)	Event
552	Power to bundle 222 kw
1282	Began 9 kg (20 lbm) drain
1349	Ended 9 kg (20 lbm) drain; net amount of mass drained from the primary = 566.60 kg (1249.4 lbm)
1681	Valved in weir meters
1749	Began 9 kg (20 lbm) drain
1807	Ended 9 kg (20 lbm) drain; net amount of mass drained from the primary = 575.67 kg (1269.4 lbm)
2559	Began 9 kg (20 lbm) drain
2631	Ended 9 kg (20 lbm) drain; net amount of mass drained from the primary = 584.74 kg (1289.4 lbm)
2851	Began 9 kg (20 lbm) drain
2922	Ended 9 kg (20 lbm) drain; net amount of mass drained from the primary = 593.81 kg (1309.4 lbm)
3053	Began 9 kg (20 lbm) drain
3113	Ended 9 kg (20 lbm) drain; net amount of mass drained from the primary = 602.88 kg (1329.4 lbm)
3354	Began 9 kg (20 lbm) drain

Time (sec)	Event
3417	Ended 9 kg (20 lbm) drain; net amount of mass drained from the primary = 611.95 kg (1349.4 lbm)
3680	Began 9 kg (20 lbm) drain
3743	Ended 9 kg (20 lbm) drain; net amount of mass drained from the primary = 621.02 kg (1369.4 lbm)
3958	Began 9 kg (20 lbm) drain
4024	Ended 9 kg (20 lbm) drain; net amount of mass drained from the primary = 630.09 kg (1389.4 lbm)
4317	Began 4.5 kg (10 lbm) drain
4349	Ended 4.5 kg (10 lbm) drain; net amount of mass drained from the primary = 634.63 kg (1399.4 lbm)
4648	Began 4.5 kg (10 lbm) drain
4686	Ended 4.5 kg (10 lbm) drain; net amount of mass drained from the primary = 639.16 kg (1409.4 lbm)
4955	Began steady-state reflux run
5559	UHI set up to deliver 4.3×10^{-4} m^3/sec (6.8 gal/min)
6039	Began UHI at a nominal flow rate of 4.3×10^{-4} m^3/sec (6.8 gal/min)

Time (sec)	Event
6386	Ended UHI
6939	Steady-state after UHI
7616	Ramped power down to zero
7732	Computer off

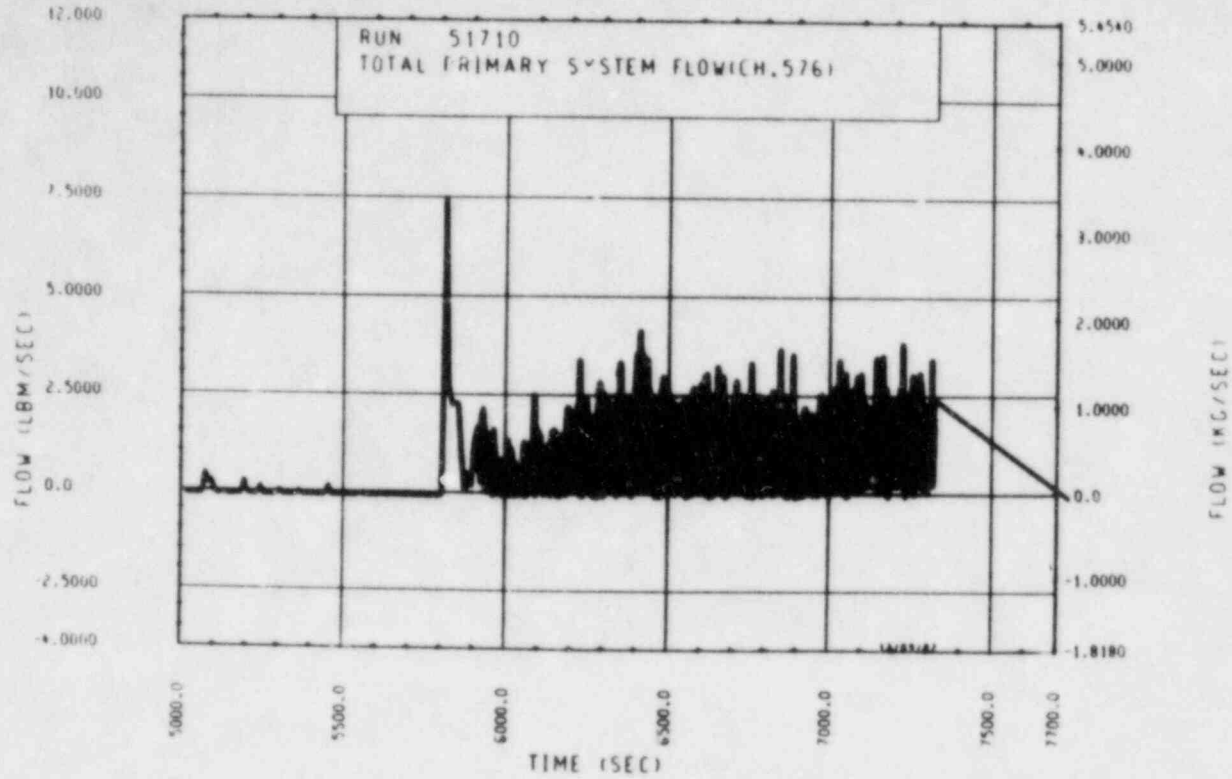

Figure A-107. Mass Flow Rate Through Rod Bundle, Test 10C

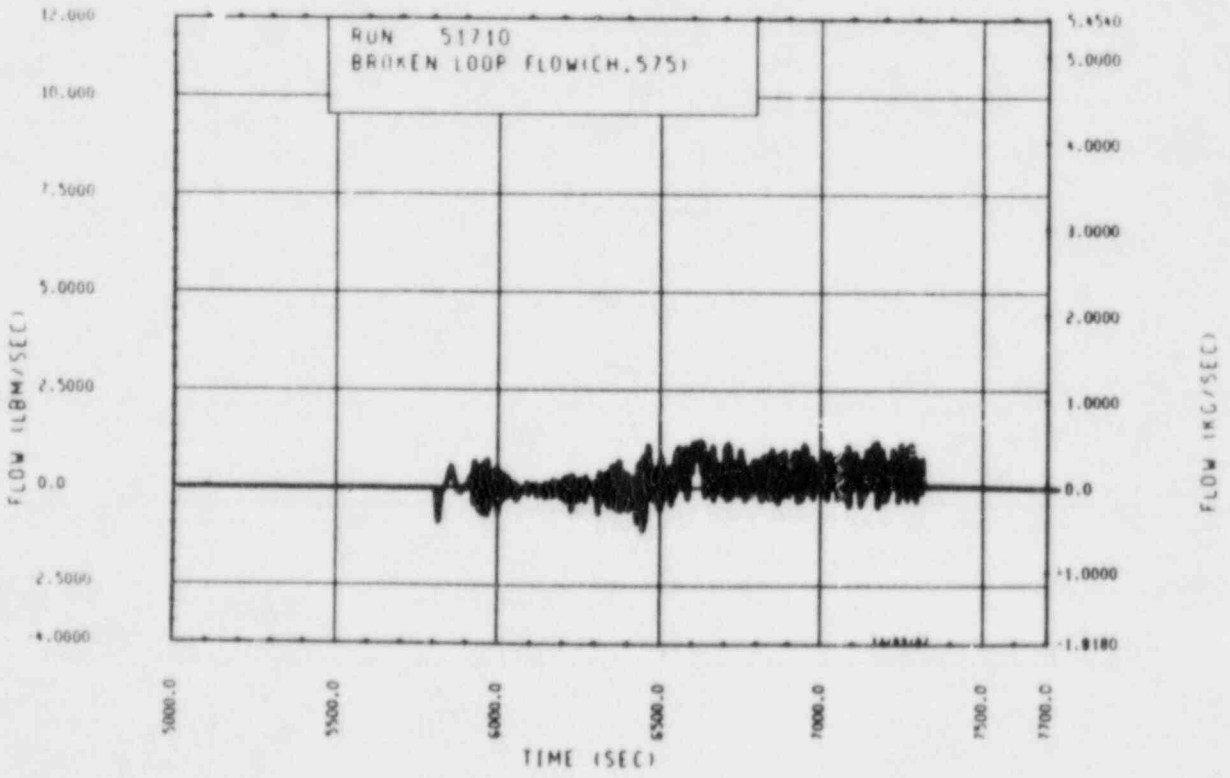

Figure A-108. Mass Flow Rate Through Broken Loop, Test 10C

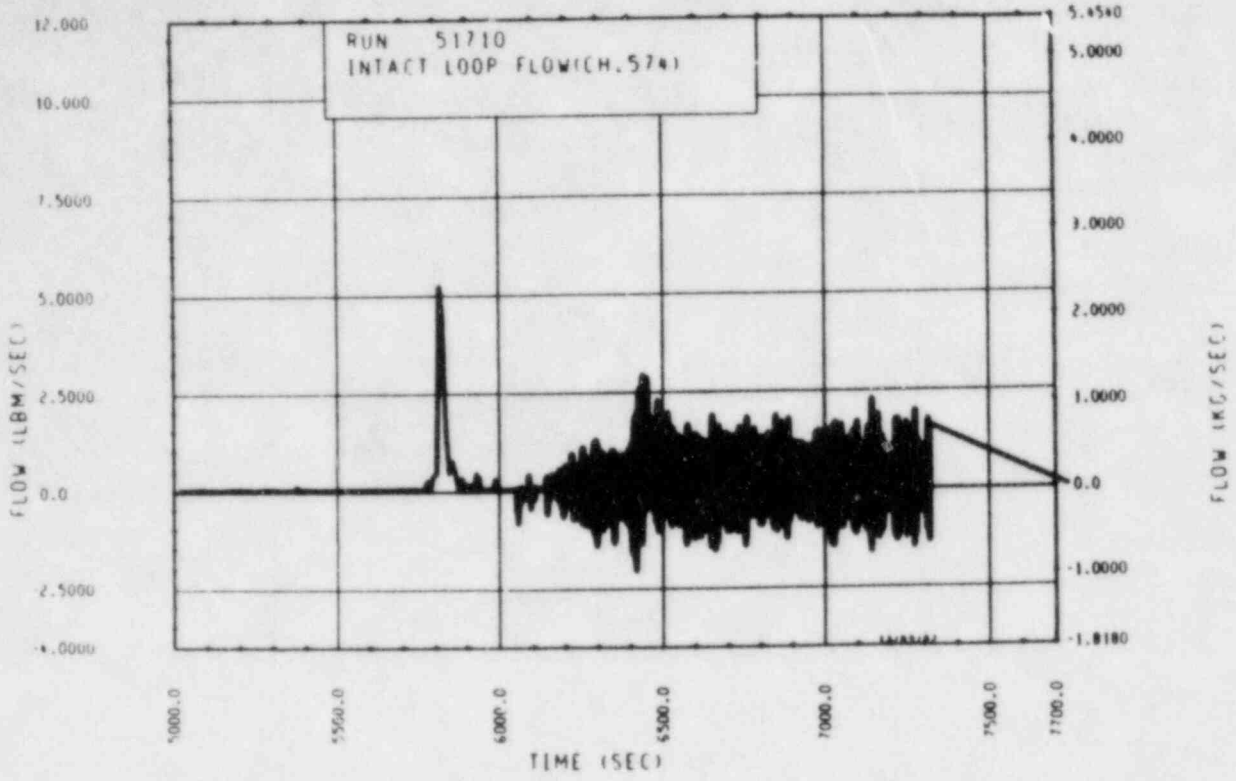

Figure A-109. Mass Flow Rate Through Unbroken Loop, Test 10C

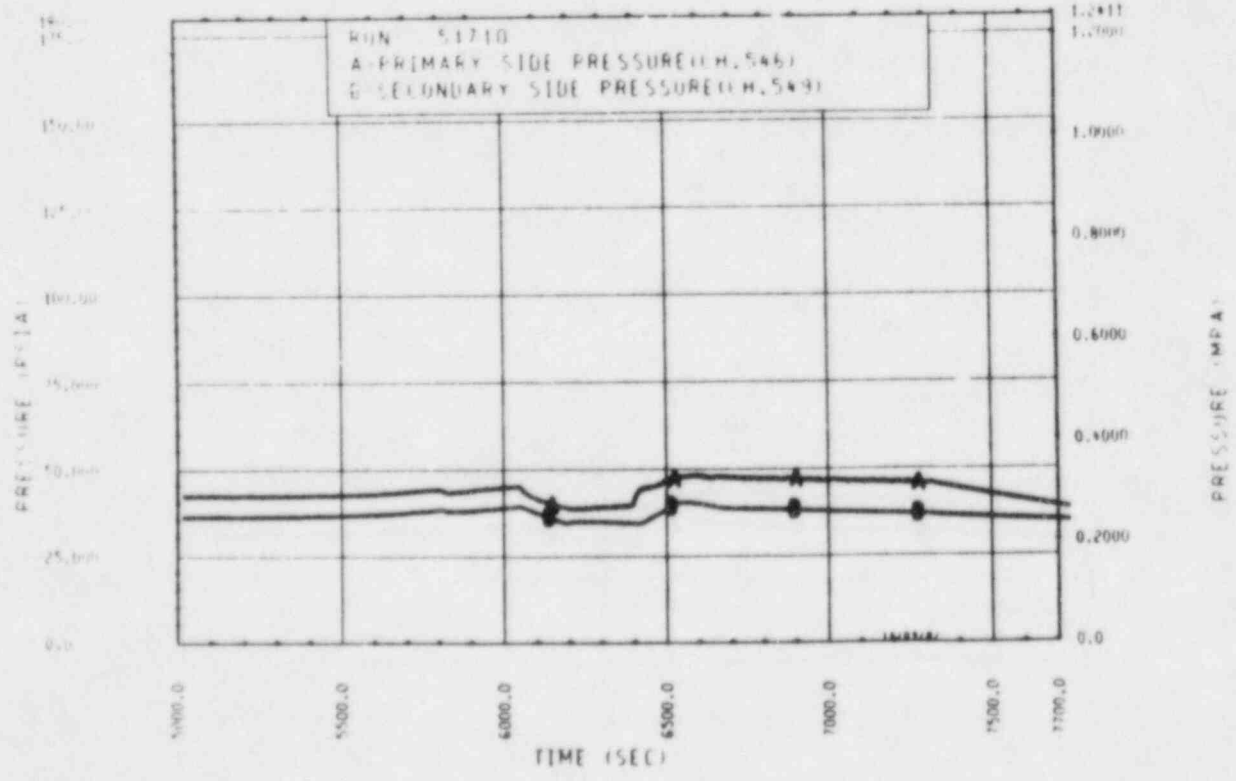

Figure A-110. Primary and Secondary System Pressure, Test 10C

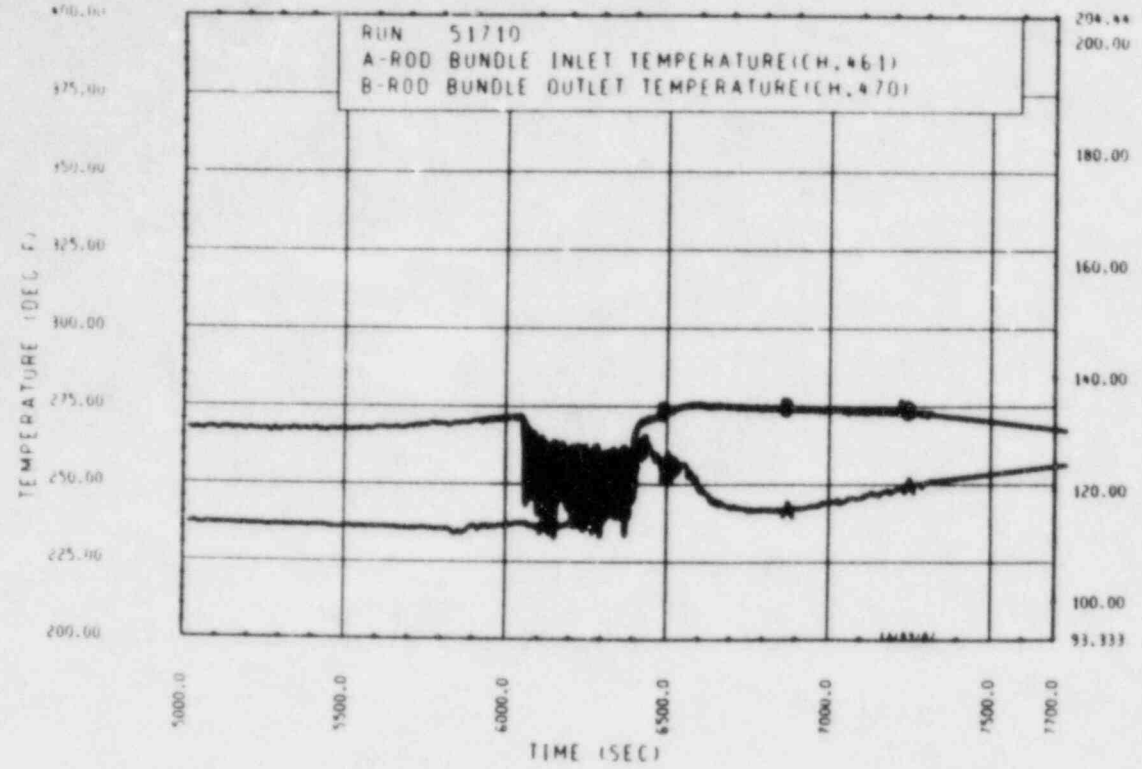

Figure A-111. Heater Rod Bundle Inlet and Outlet Temperature, Test 10C

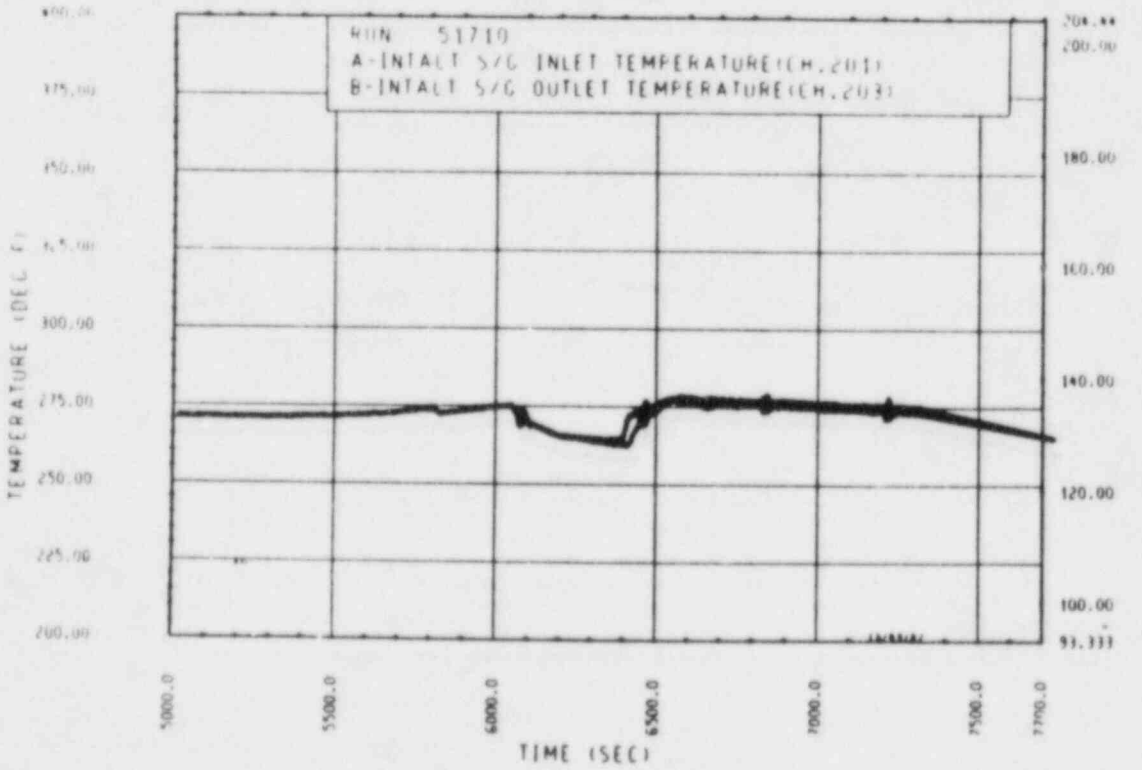

Figure A-112. Unbroken Loop Steam Generator Inlet and Outlet Temperature, Test 10C

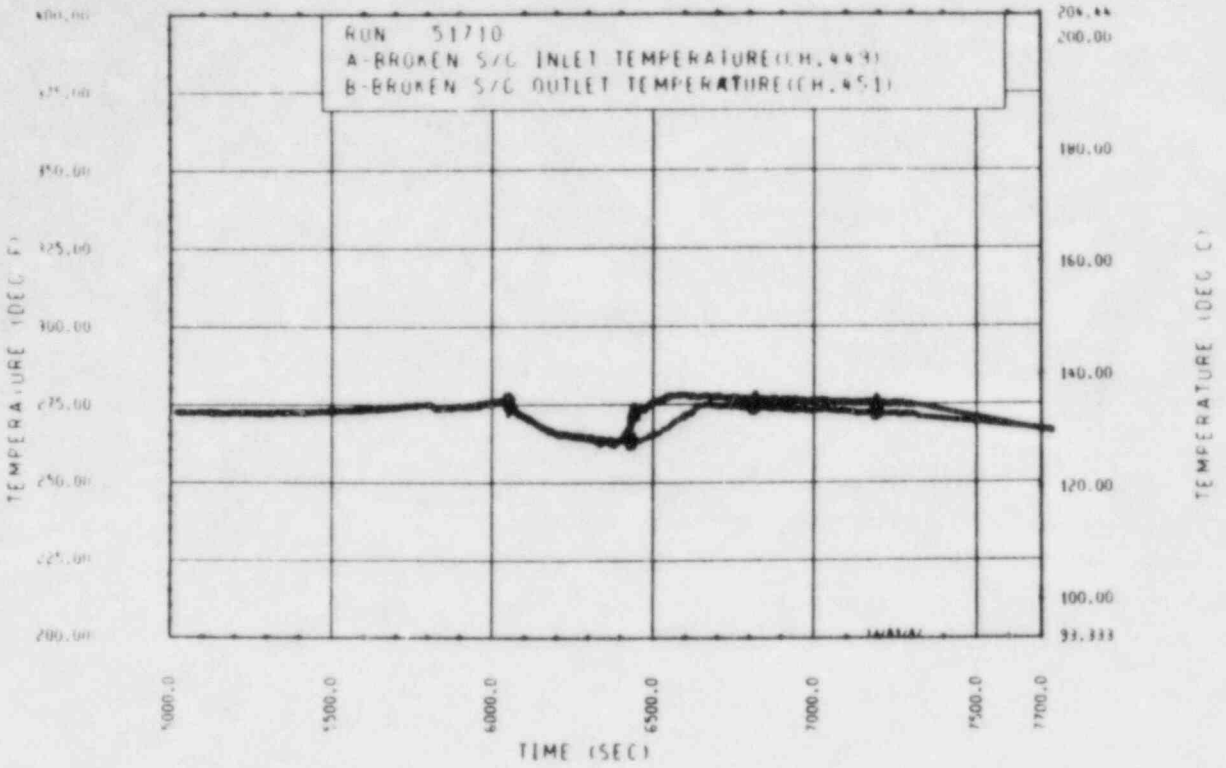

Figure A-113. Broken Loop Steam Generator Inlet and Outlet Temperature, Test 10C

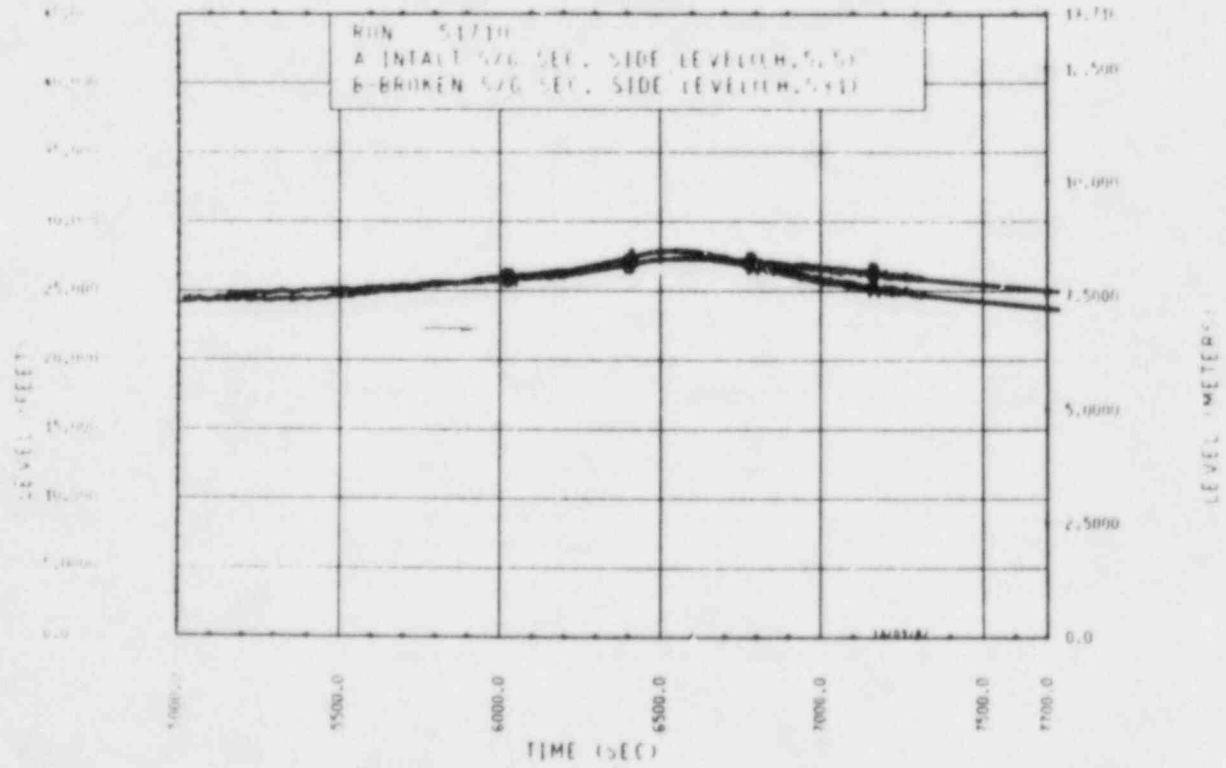

Figure A-114. Unbroken and Broken Loop Steam Generator Secondary Side Collapsed Liquid Levels, Test 10C

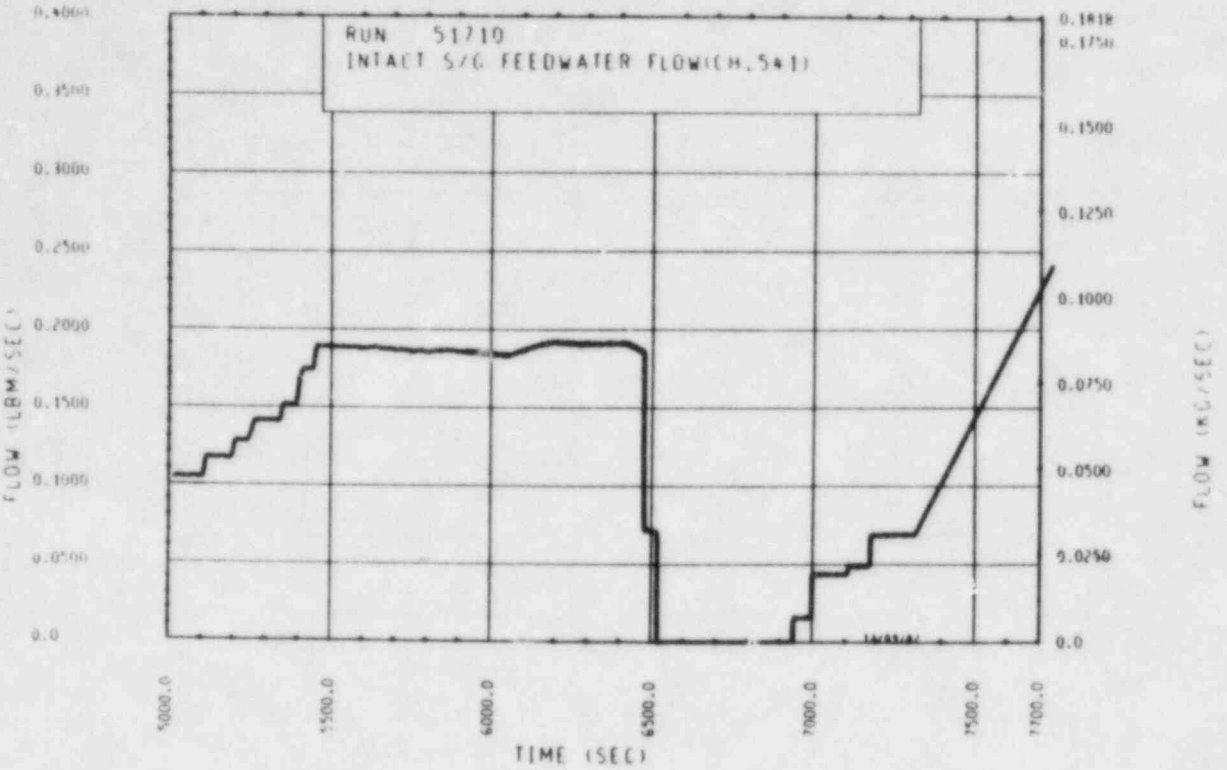

Figure A-115. Unbroken Loop Steam Generator Feedwater Mass Flow Rate, Test 10C

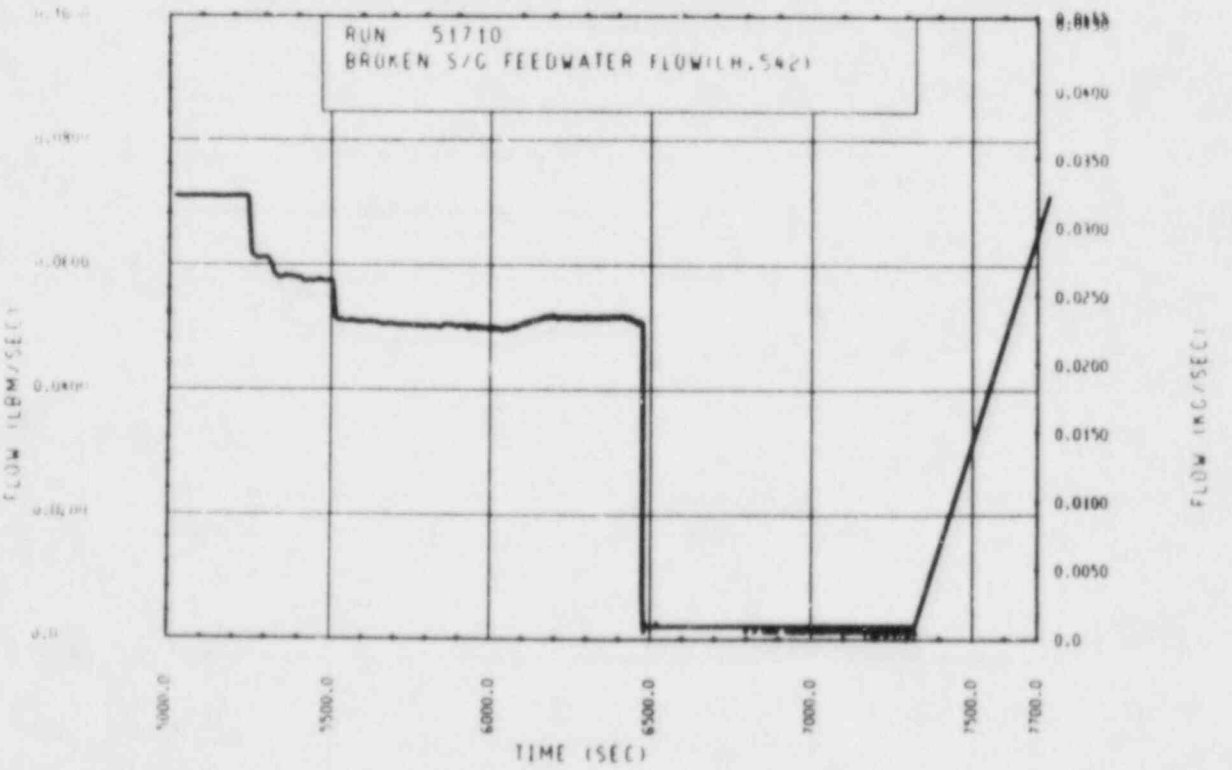

Figure A-116. Broken Loop Steam Generator Feedwater Mass Flow Rate, Test 10C

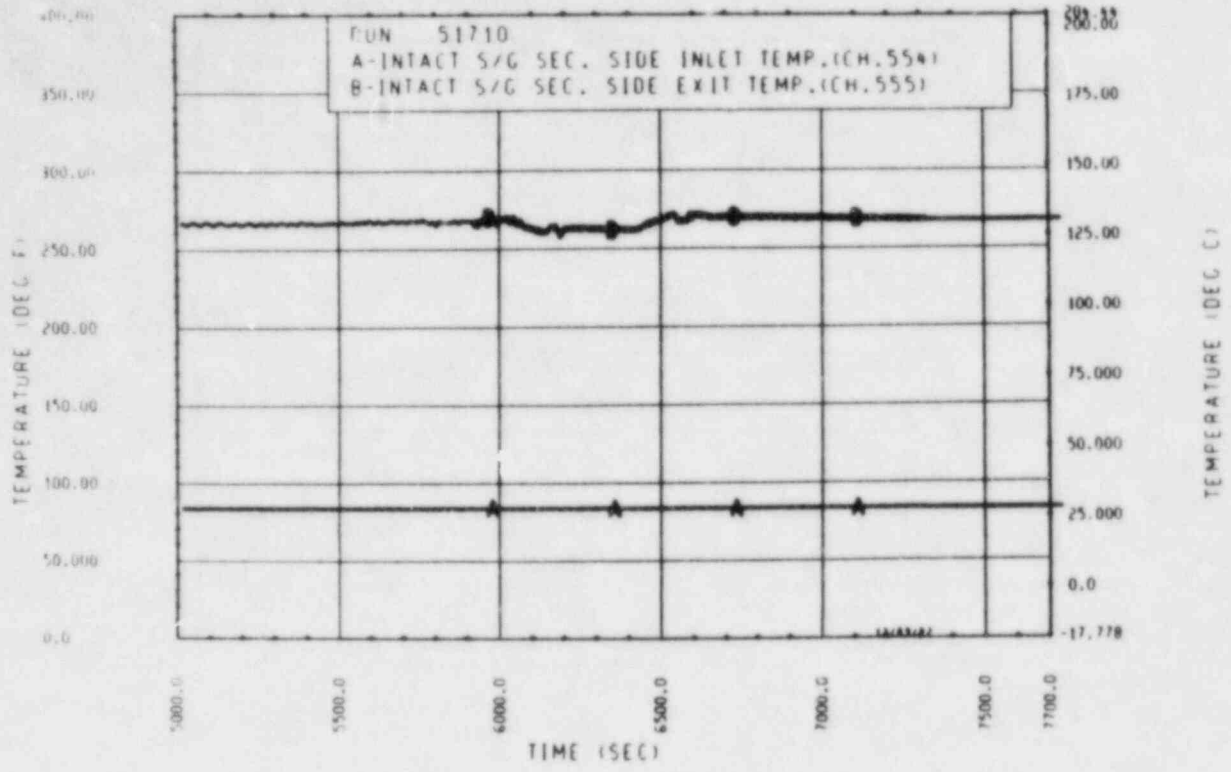

Figure A-117. Unbroken Loop Steam Generator Secondary Side Inlet and Outlet Temperature, Test 10C

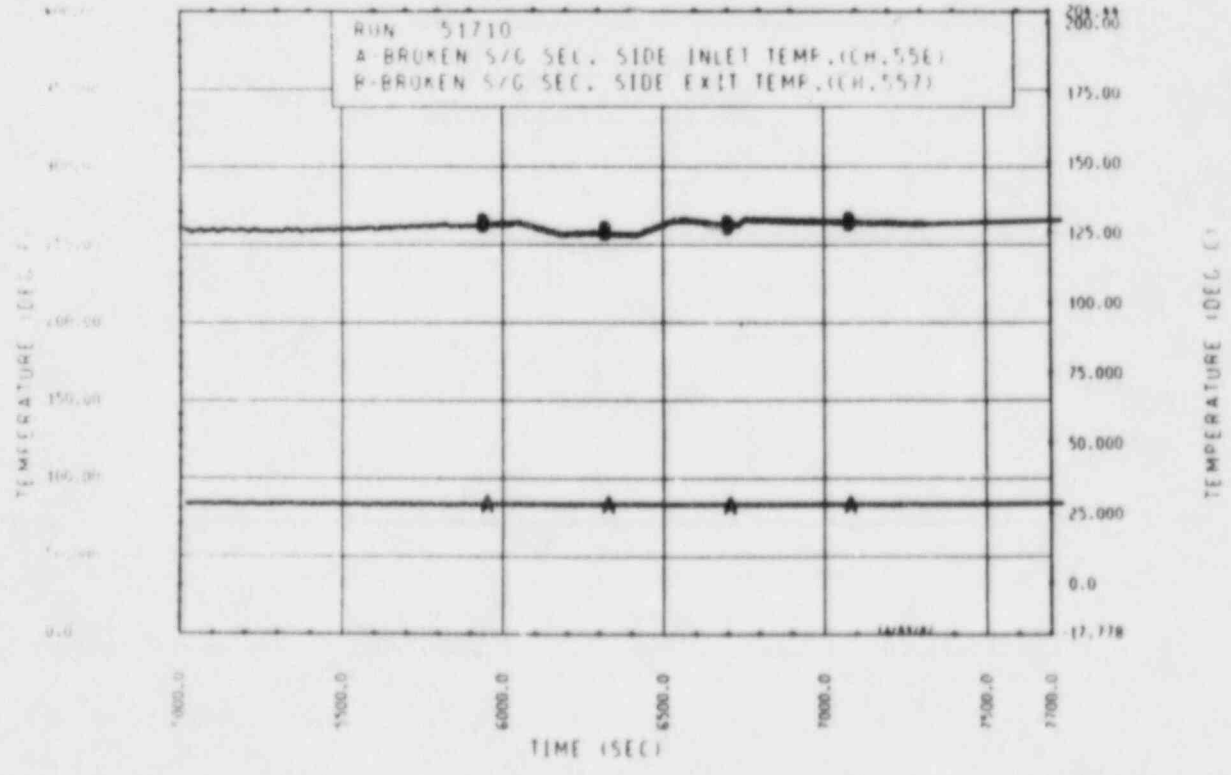

Figure A-118. Broken Loop Steam Generator Secondary Side Inlet and Outlet Temperature, Test 10C

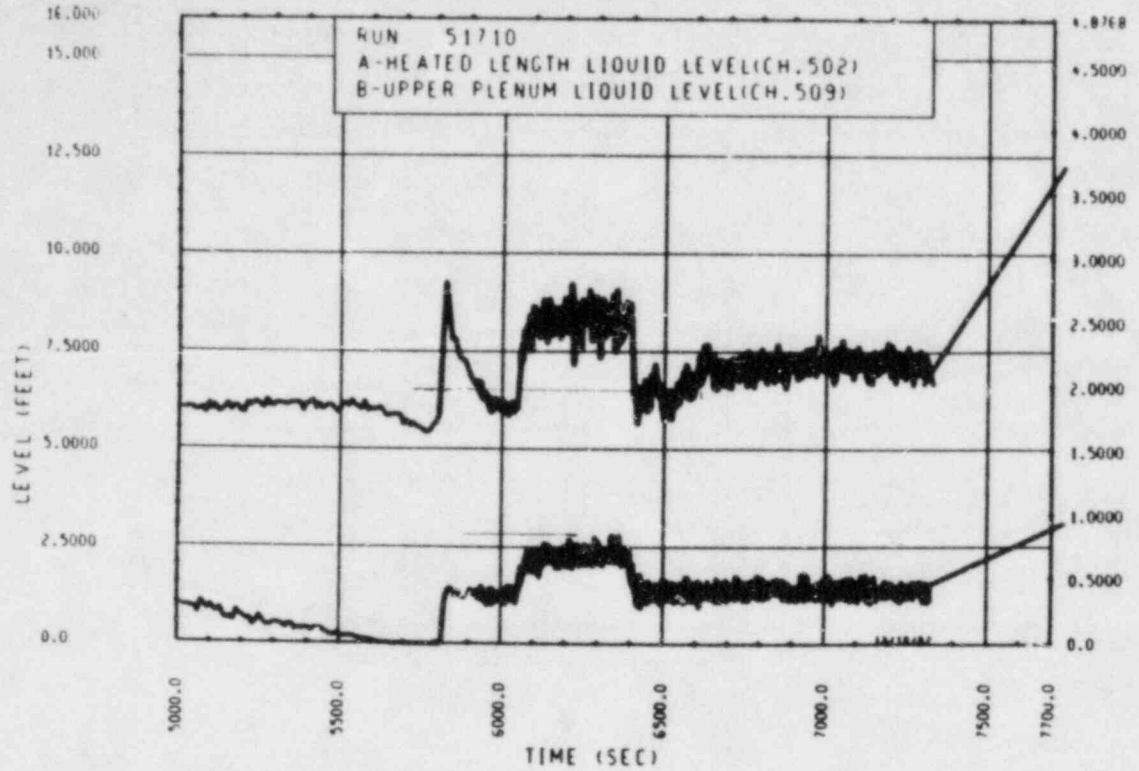

Figure A-119. Heated Length and Upper Plenum Liquid Levels, Test 10C

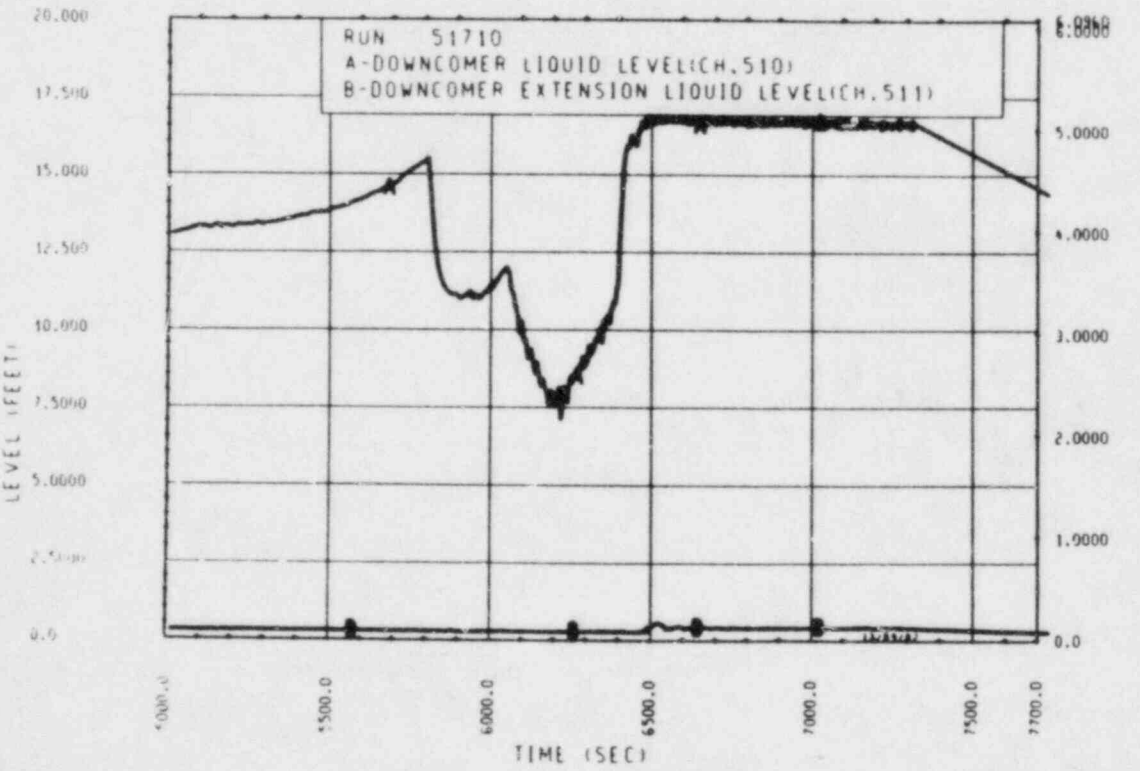

Figure A-120. Downcomer and Downcomer Extension Liquid Levels, Test 10C

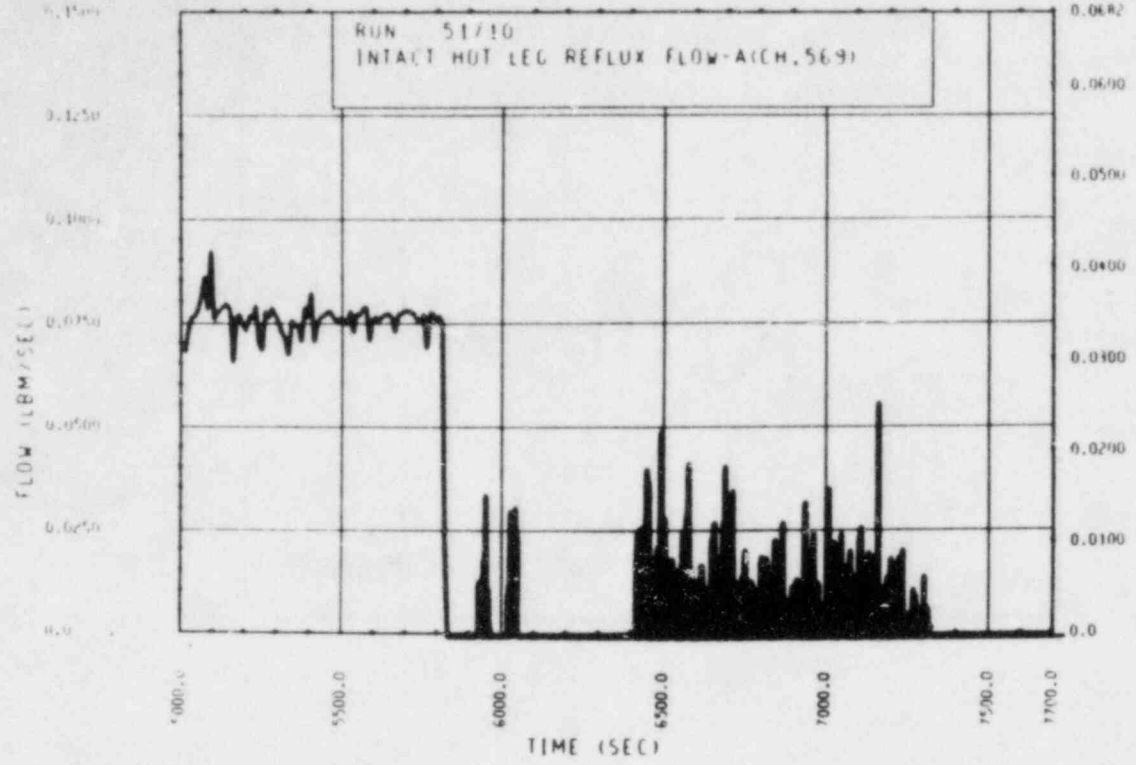

Figure A-121. Unbroken Loop Hot Leg Reflux Condensation Mass Flow Rate, Test 10C

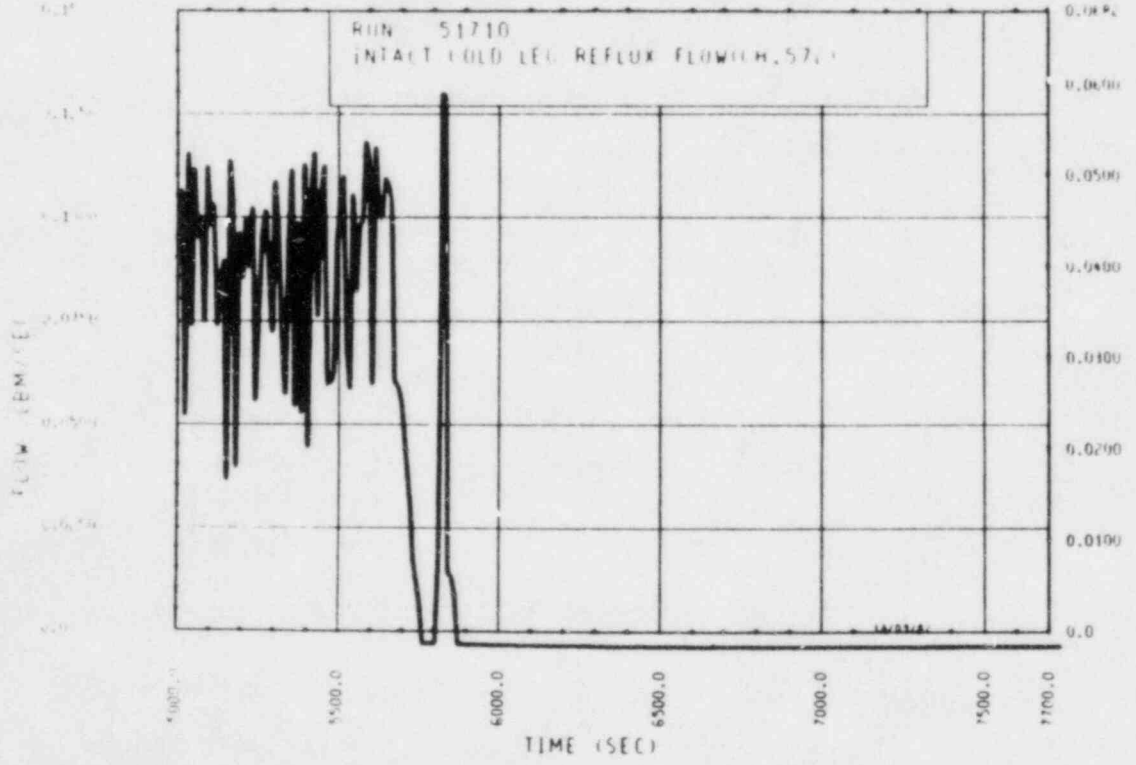

Figure A-122. Unbroken Loop Cold Leg Reflux Condensation Mass Flow Rate, Test 10C

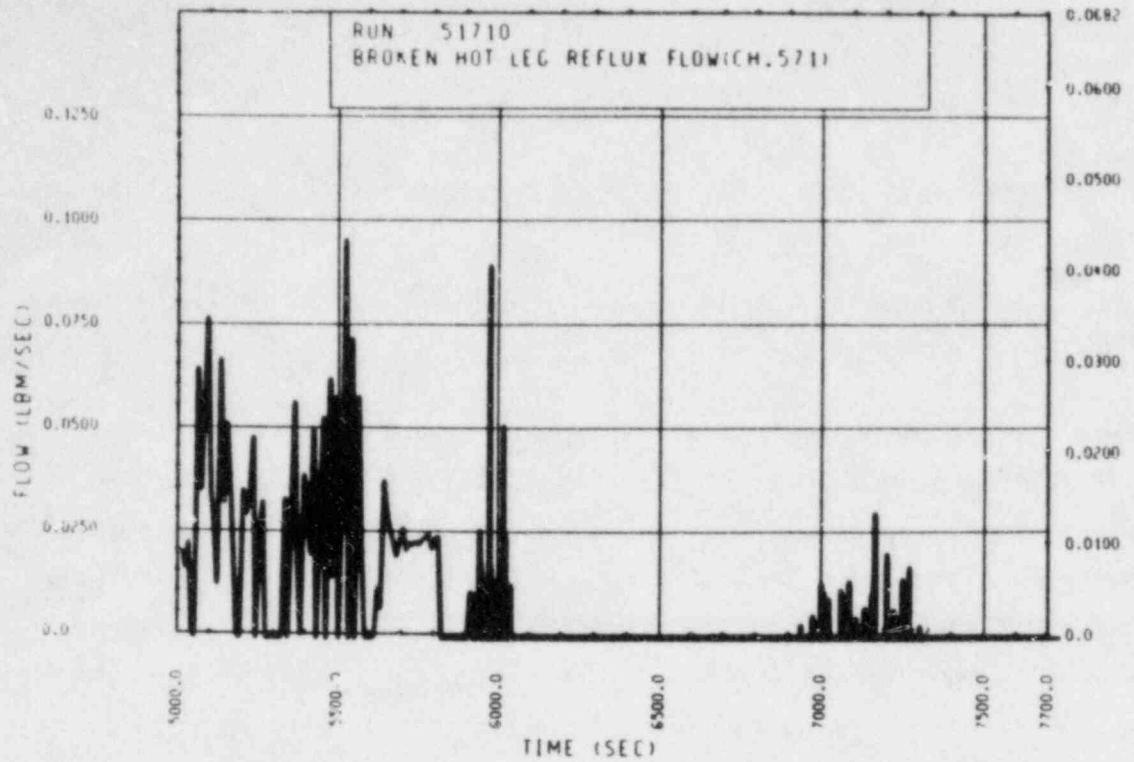

Figure A-123. Broken Loop Hot Leg Reflux Condensation Mass Flow Rate, Test 10C

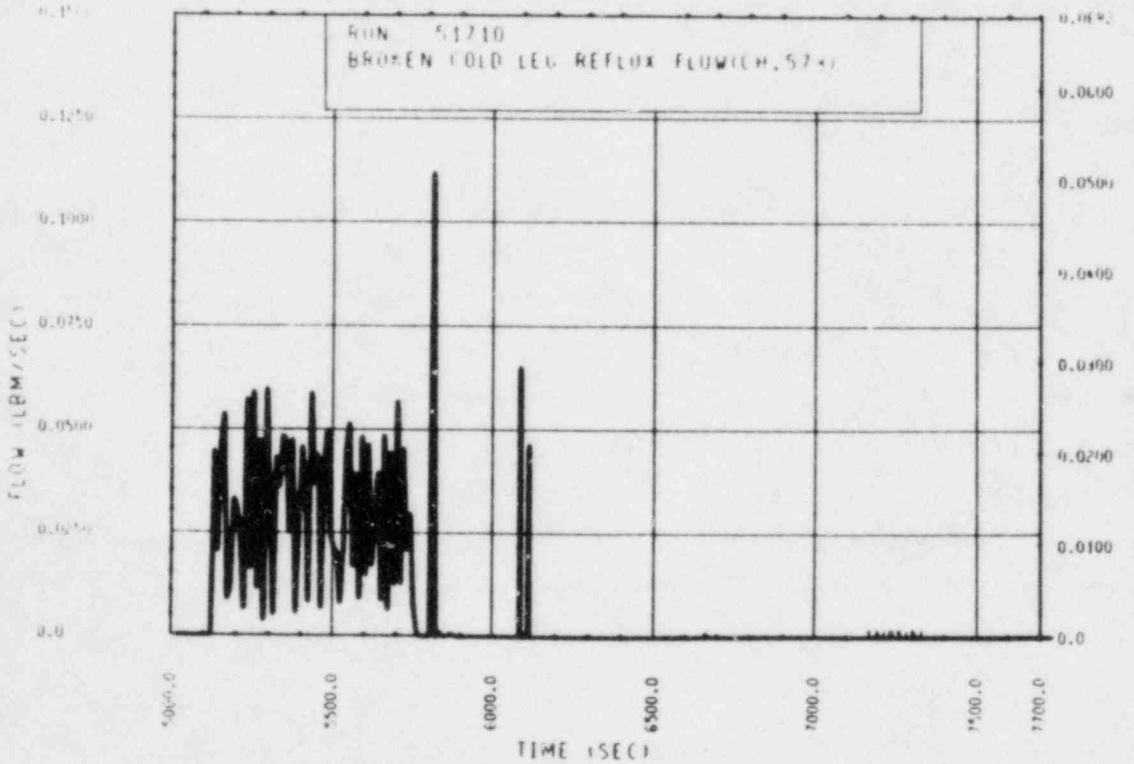

Figure A-124. Broken Loop Cold Leg Reflux Condensation Mass Flow Rate, Test 10C

TEST 11: TWO-PHASE PEAK FLOW NATURAL CIRCULATION COLD LEG INJECTION TEST

Objective

To determine the effects of unbroken loop cold leg injection on two-phase peak flow natural circulation

Test Procedure

The test was begun from a steady-state two-phase peak flow natural circulation mode with a nominal bundle power of 222 kw (simulated 2 percent of full power). The primary system was operated with the pressurizer valved out and a reduced mass inventory consistent with previously established two-phase peak flow conditions. The secondary side was operated in a constant level feed-and-bleed boiling mode with a nominal pressure of 0.28 MPa (40 psia). The secondary side level was maintained at 7.62 m (25 ft) (71 percent full). Accumulator 1 was used to inject 35°C (95°F) water into the unbroken loop cold leg at a nominal rate of 0.77 kg/sec (1.7 lbm/sec). The duration of the injection was 48 seconds. The test was terminated when the system returned to a steady-state condition.

Test Overview:

Prior to the unbroken loop cold leg injection (CLI), the primary system was brought to a steady-state two-phase peak flow natural circulation mode. This was accomplished by removing 18.8 percent of the original single-phase primary system mass inventory. At this peak two-phase flow condition, the average mass flow rate through the rod bundle was approximately 3.6 kg/sec (8.0 lbm/sec). The unbroken loop was stalled, causing the system to act as a single-loop system with the unbroken loop handling all of the natural circulation flow. Single-phase fluid entered the rod bundle at an average temperature of 133°C (271°F), and a two-phase mixture exited at an average temperature of 143°C (290°F). The average measured primary system pressure was

approximately 0.37 MPa (53 psia), which has a corresponding saturation temperature of 140.36°C (284.67°F). The rod bundle exit temperature of 143°C (290°F) indicates a 3°C (5°F) superheat based on the measured upper plenum pressure. Comparison of the rod bundle exit temperature with other adjacent fluid thermocouples shows excellent agreement. Based on visual observations of the upper plenum, it is believed that the exit was saturated and not superheated. This is confirmed by the collapsed liquid level reading of 0.61 m (2.0 ft) (43 percent full) in the upper plenum. Based on a 143°C (290°F) saturation temperature, the upper plenum pressure cell should have read 0.40 MPa (58 psia) (9.53 percent error).

Cold leg injection was initiated in the unbroken loop cold leg at 17,924 seconds and terminated 48 seconds later. The short injection of cold water caused the total flow through the rod bundle to initially increase from an average value of approximately 3.6 kg/sec (8.0 lbm/sec) to a peak value of 4.939 kg/sec (10.89 lbm/sec) 8 seconds after CLI initiation. Upon termination of CLI, the total flow returned momentarily to an average value of approximately 3.4 kg/sec (7.5 lbm/sec) before steadily decreasing to zero 96 seconds after the termination of CLI. This temporary flow stagnation was the result of the CLI water being convected into the rod bundle inlet and increasing the rod bundle inlet subcooling from approximately 8°C (14°F) to approximately 20°C (36°F). The increase in rod bundle inlet subcooling was accompanied by a slight decrease in primary system pressure, which was indicative of a decreasing steam generation rate. This was confirmed by the sudden decrease in the heated length collapsed liquid level at the moment of flow stagnation. As the void generation rate decreased, there was a subsequent loss of driving head between the downcomer and the rod bundle, thus producing a temporary flow stagnation. The stagnation condition was only temporary, with the primary system returning to a two-phase peak flow steady-state condition approximately 228 seconds after CLI termination. A similar flow effect was observed in the unbroken loop. The broken loop became momentarily active 58 seconds after CLI termination, yet stalled seconds later. The secondary side was not significantly affected.

TEST SCHEDULE
TEST 11

Time[a] (sec)	Event
10121.2	Pressurizer adjusted to bring primary side pressure to 0.93 MPa (135 psi); secondary side pressure regulator adjusted for 0.28 MPa (40 psi)
12404	Steady-state single-phase natural circulation conditions established
12544	Accumulator 2 (pressurizer) valved out
12714	Began 136 kg (300 lbm) continuous drain from the primary system. Mass was drained from the primary until a two-phase peak-flow natural circulation mode was established.
13710	Total of 45 kg (100 lbm) drained
16417	Ended 45 kg (300 lbm) continuous drain
16536	Began 18 kg (40 lbm) drain

a. Test 11 was run in series with test 5. Time zero therefore corresponds with time zero of test 5.

Test 5 was run at a nominal primary side pressure of 0.52 MPa (75 psi). To drain mass out of the primary side and achieve a peak two-phase flow reference condition, the primary side pressure had to be brought to 0.93 MPa (135 psi).

Time (sec)	Event
16885	Ended 18 kg (40 lbm) drain; total of 154 kg (340 lbm) drained
16904	Began 15-minute steady-state period for two-phase peak-flow
17804	Ended 15-minute steady-state period for two-phase peak-flow
17924	Began cold leg injection; nominal injection rate = 7.6×10^{-3} m^3/sec (121.1 gal/min)
17972	Ended cold leg injection; estimated 36.35 kg (80.16 lbm) of water injected. The net mass drained from the primary system was estimated to be approximately 118 kg (260 lbm).
18399	Steady-state two-phase natural circulation established
18884	End of test 11

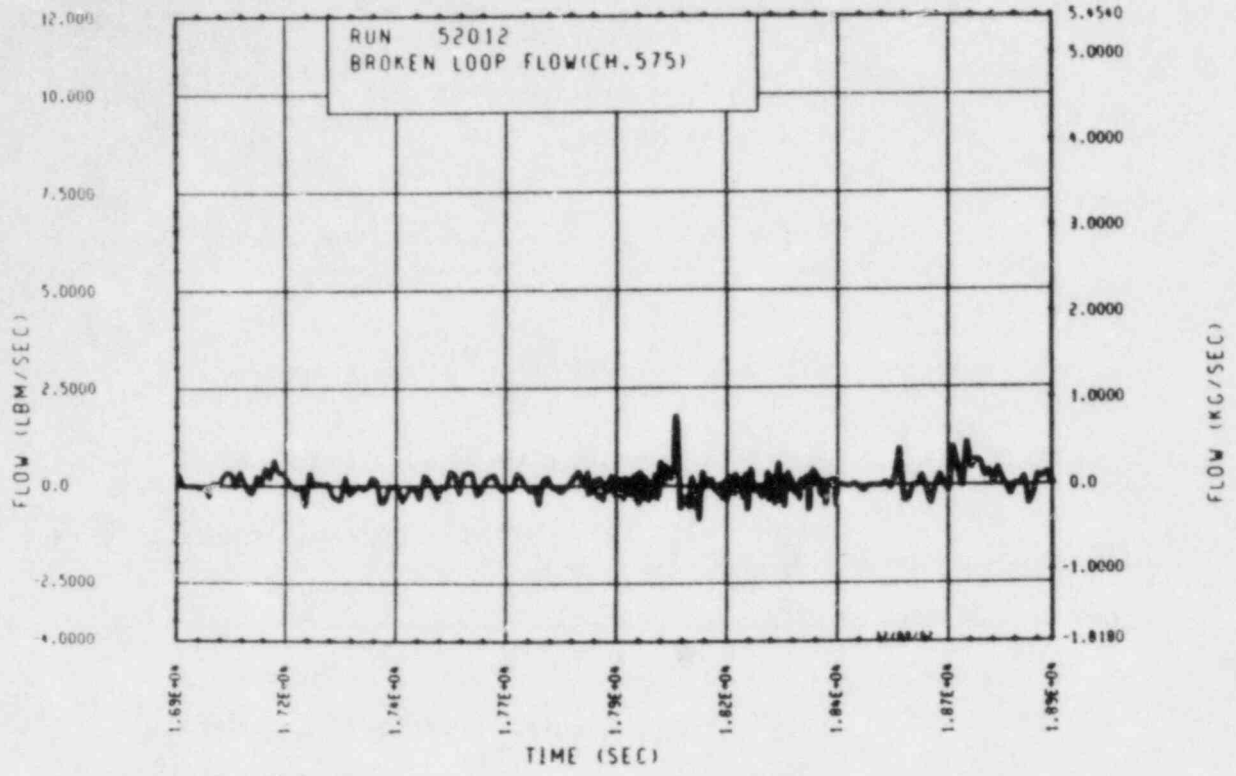

Figure A-125. Mass Flow Rate Through Rod Bundle, Test 11

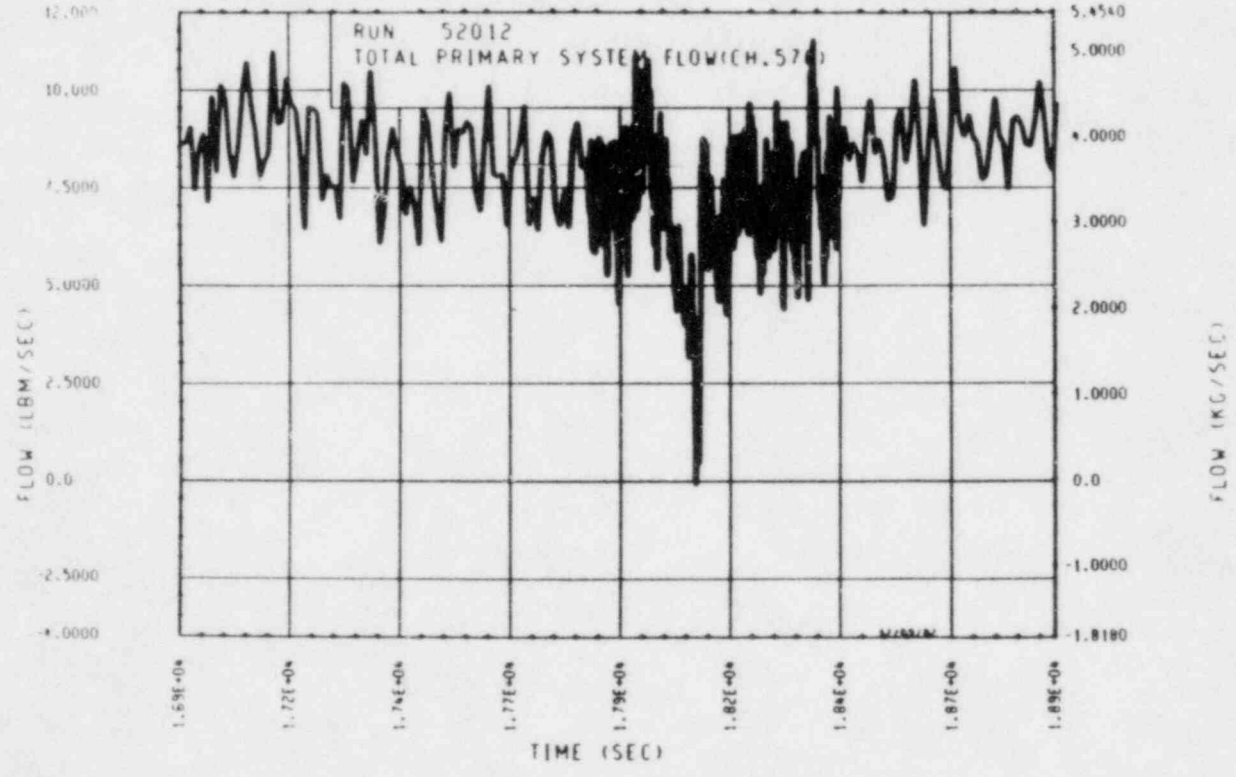

Figure A-126. Mass Flow Rate Through Broken Loop, Test 11

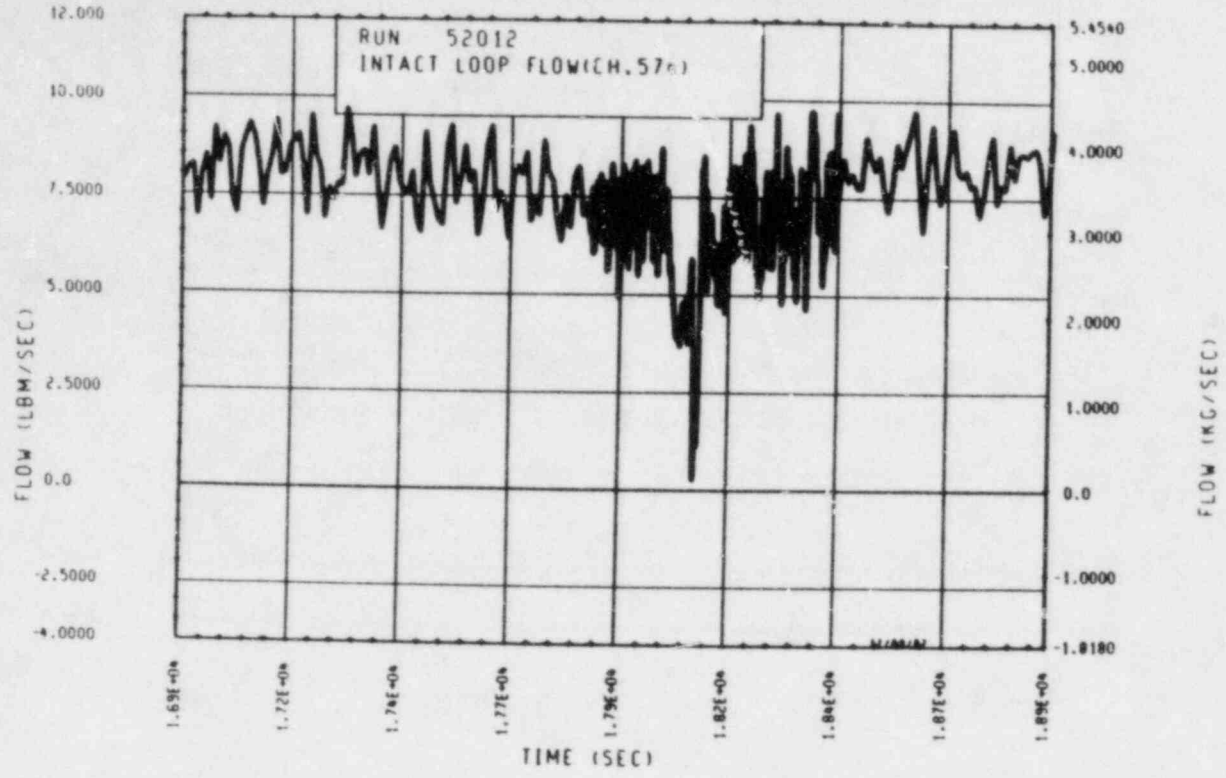

Figure A-127. Mass Flow Rate Through Unbroken Loop, Test 11

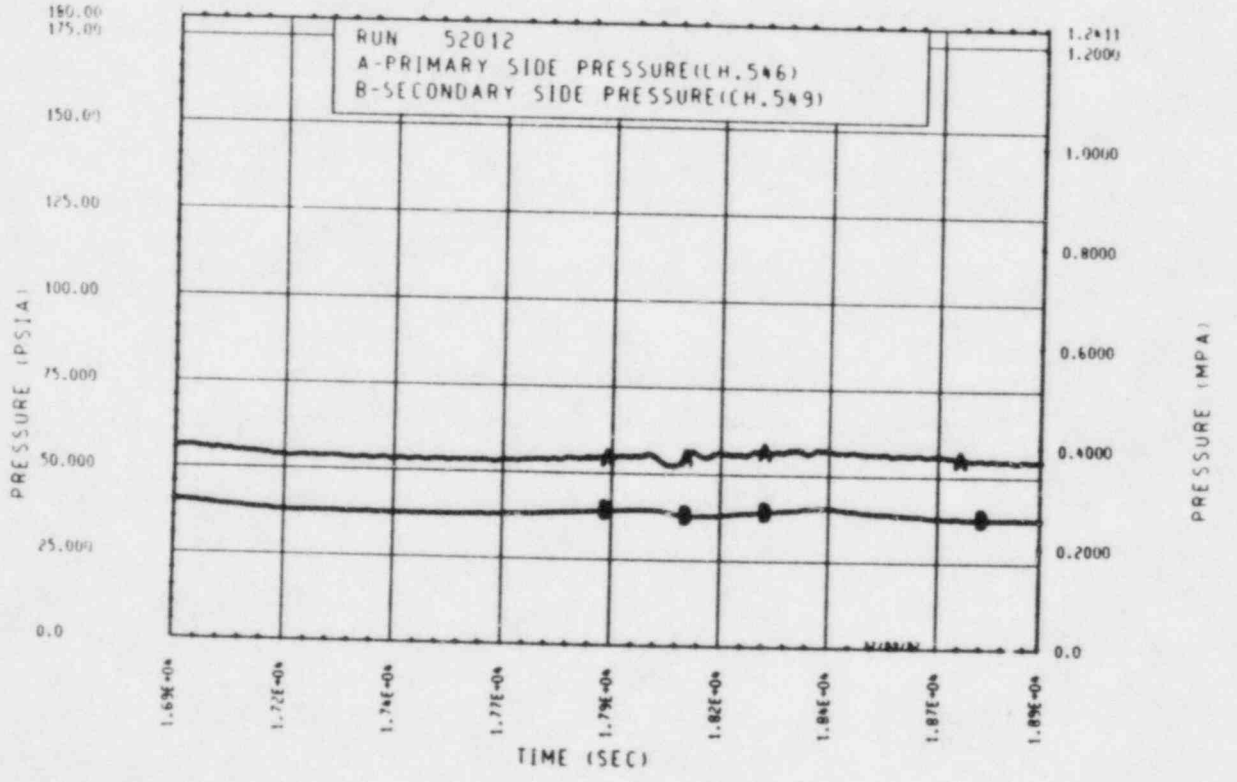

Figure A-128. Primary and Secondary System Pressure, Test 11

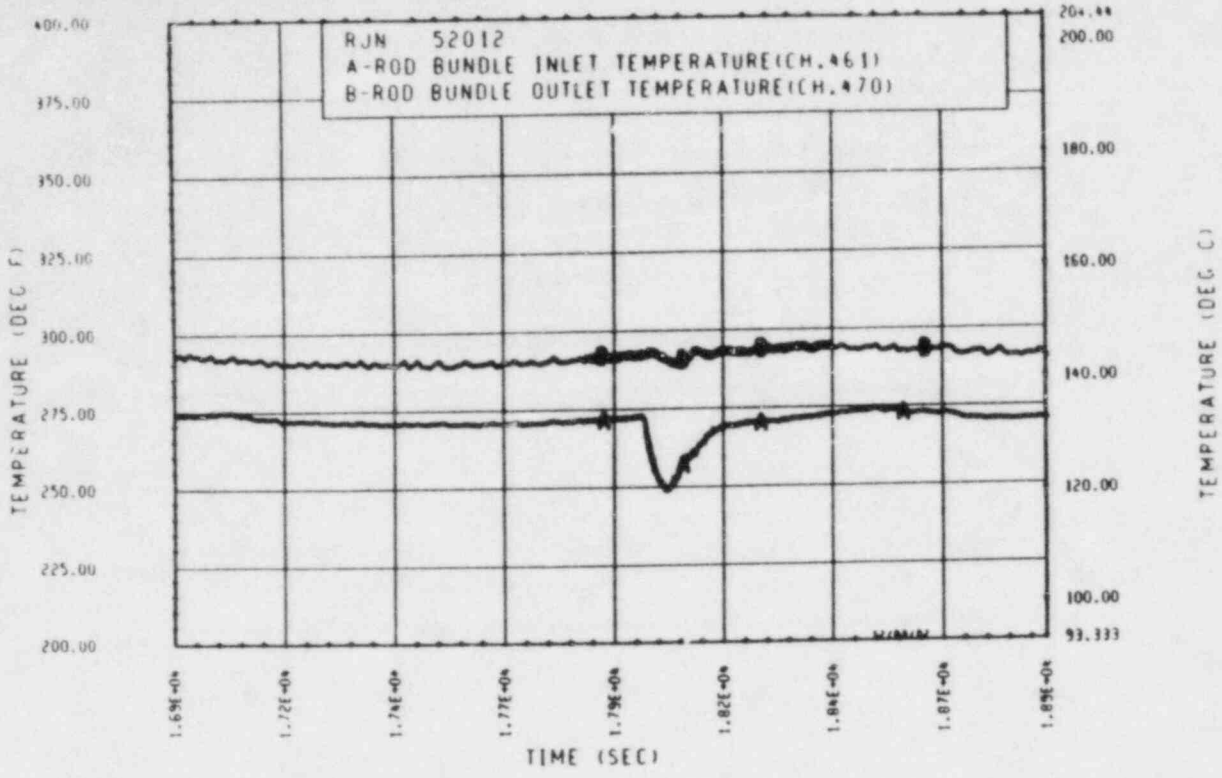

Figure A-129. Heater Rod Bundle Inlet and Outlet Temperature, Test 11

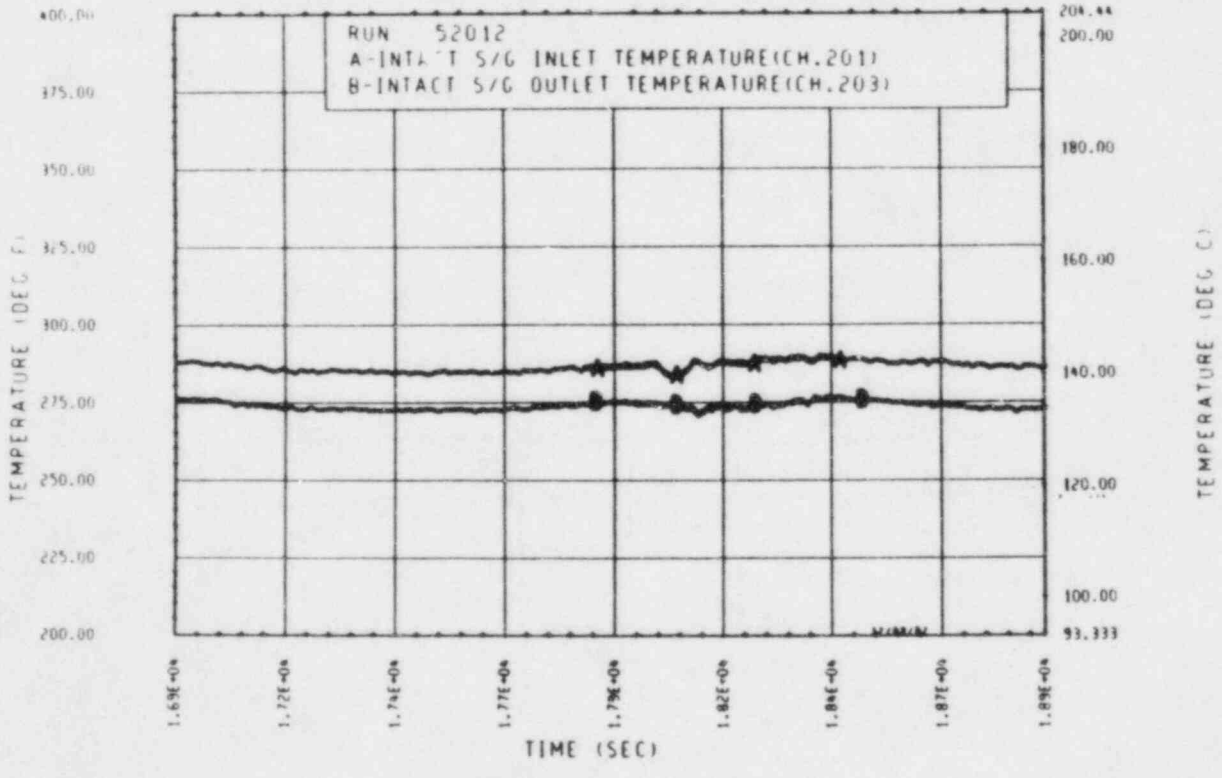

Figure A-130. Unbroken Loop Steam Generator Inlet and Outlet Temperature, Test 11

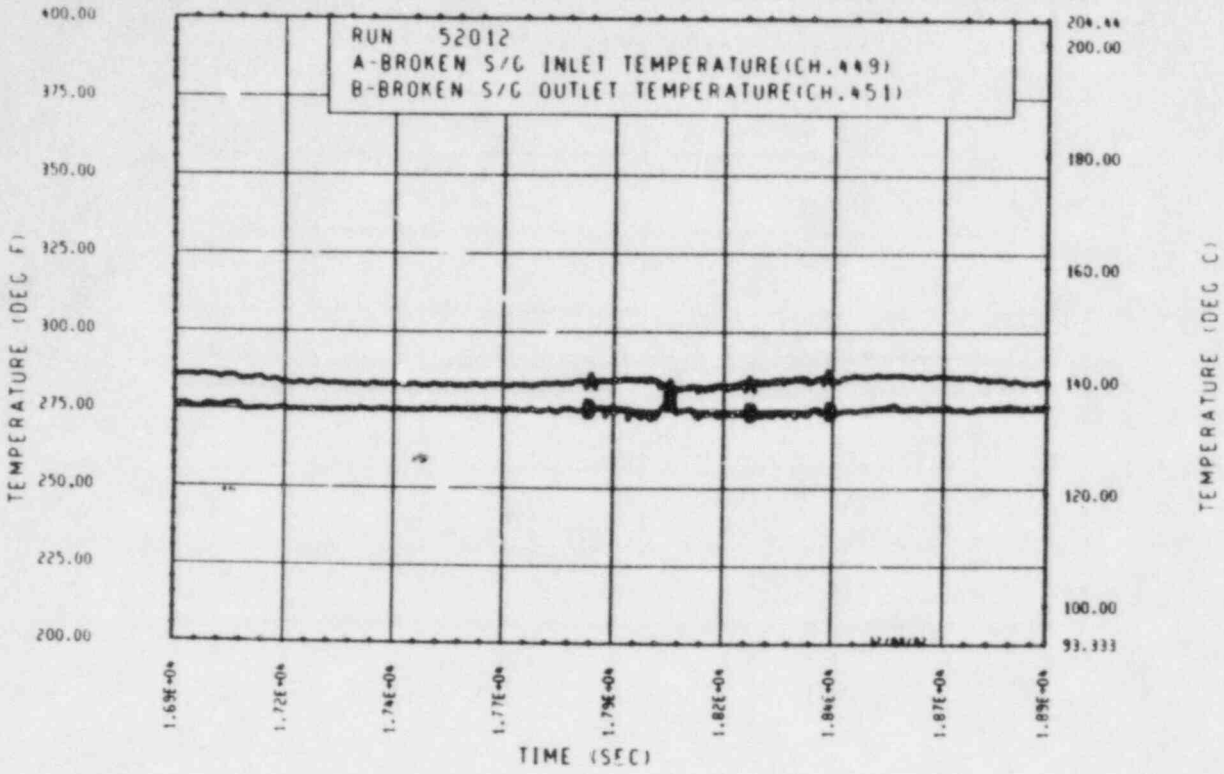

Figure A-131. Broken Loop Steam Generator Inlet and Outlet Temperature, Test 11

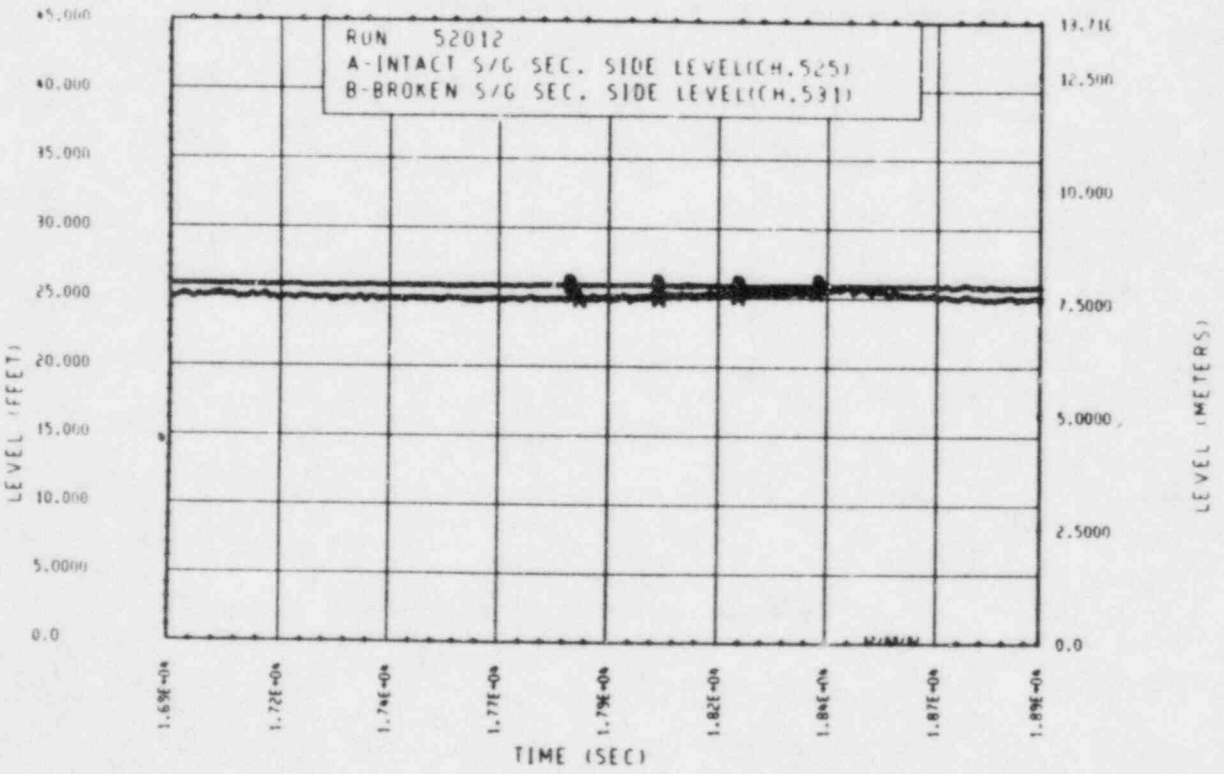

Figure A-132. Unbroken and Broken Loop Steam Generator Secondary Side Collapsed Liquid Levels, Test 11

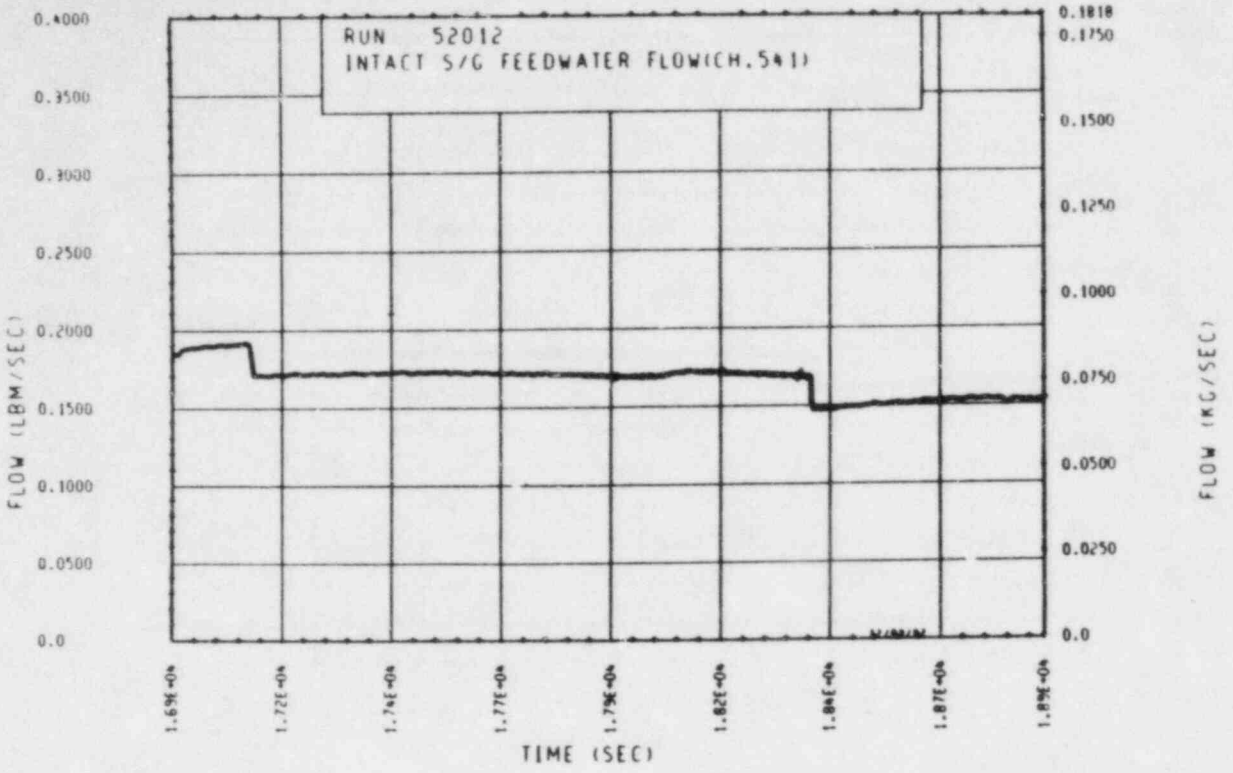

Figure A-133. Unbroken Loop Steam Generator Feedwater Mass Flow Rate, Test 11

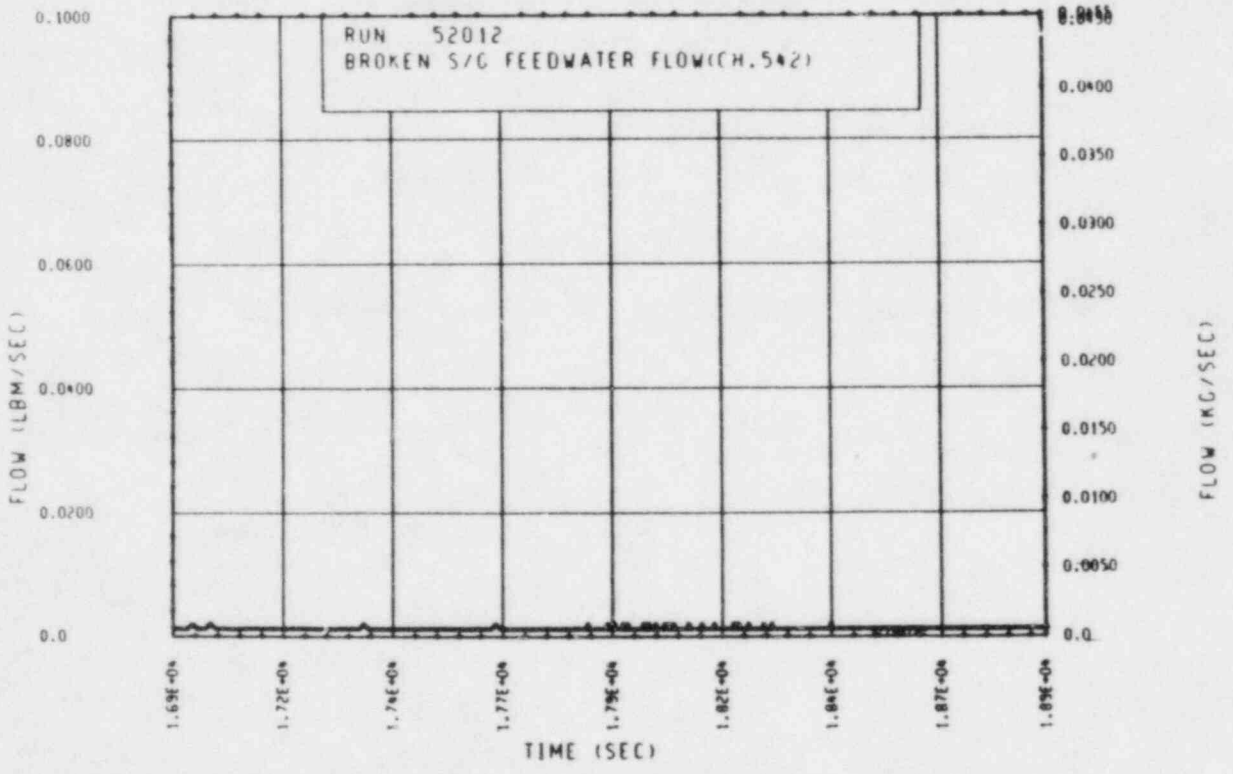

Figure A-134. Broken Loop Steam Generator Feedwater Mass Flow Rate, Test 11

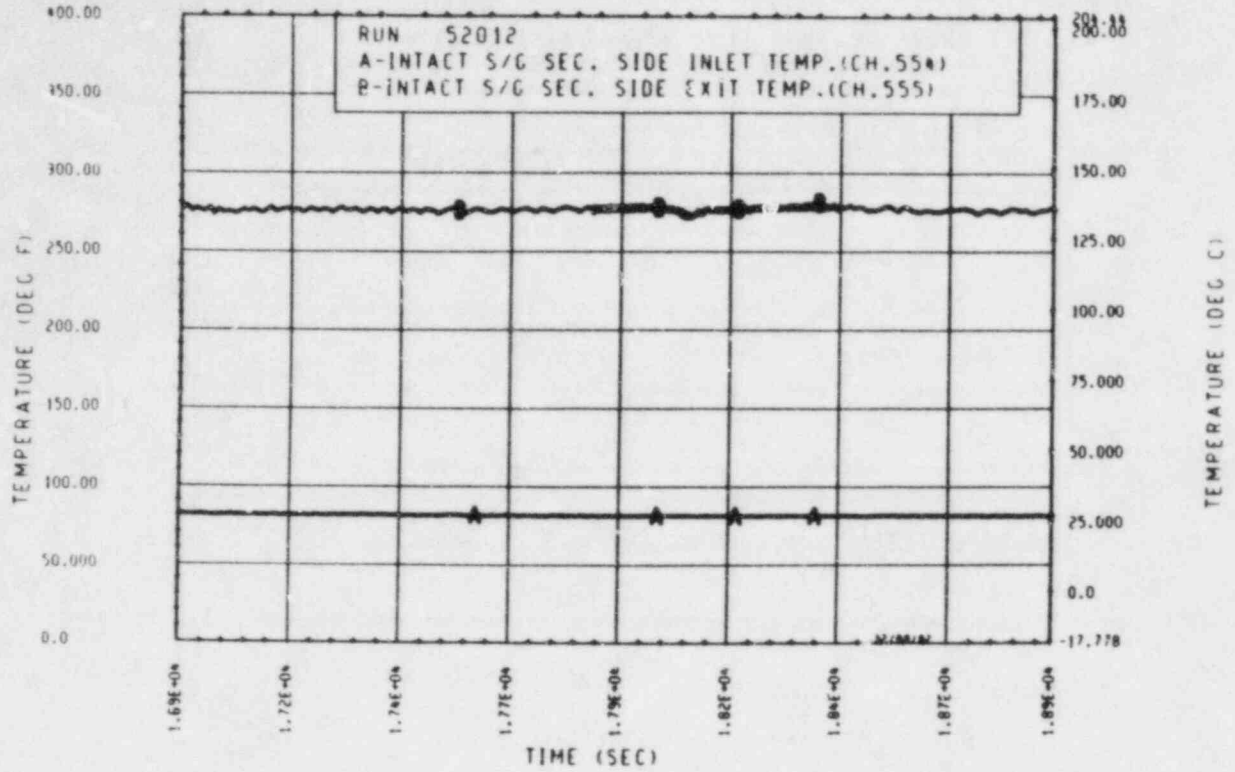

Figure A-135. Unbroken Loop Steam Generator Secondary Side Inlet and Outlet Temperature, Test 11

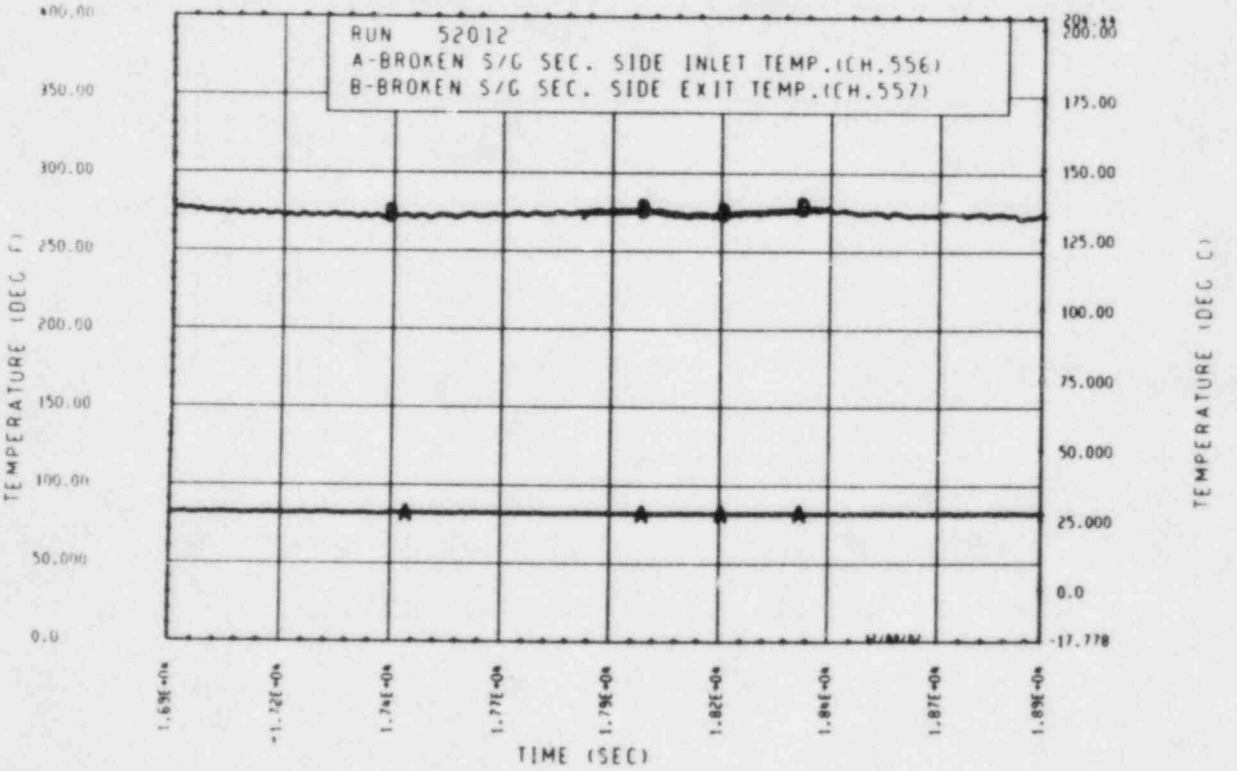

Figure A-136. Broken Loop Steam Generator Secondary Side Inlet and Outlet Temperature, Test 11

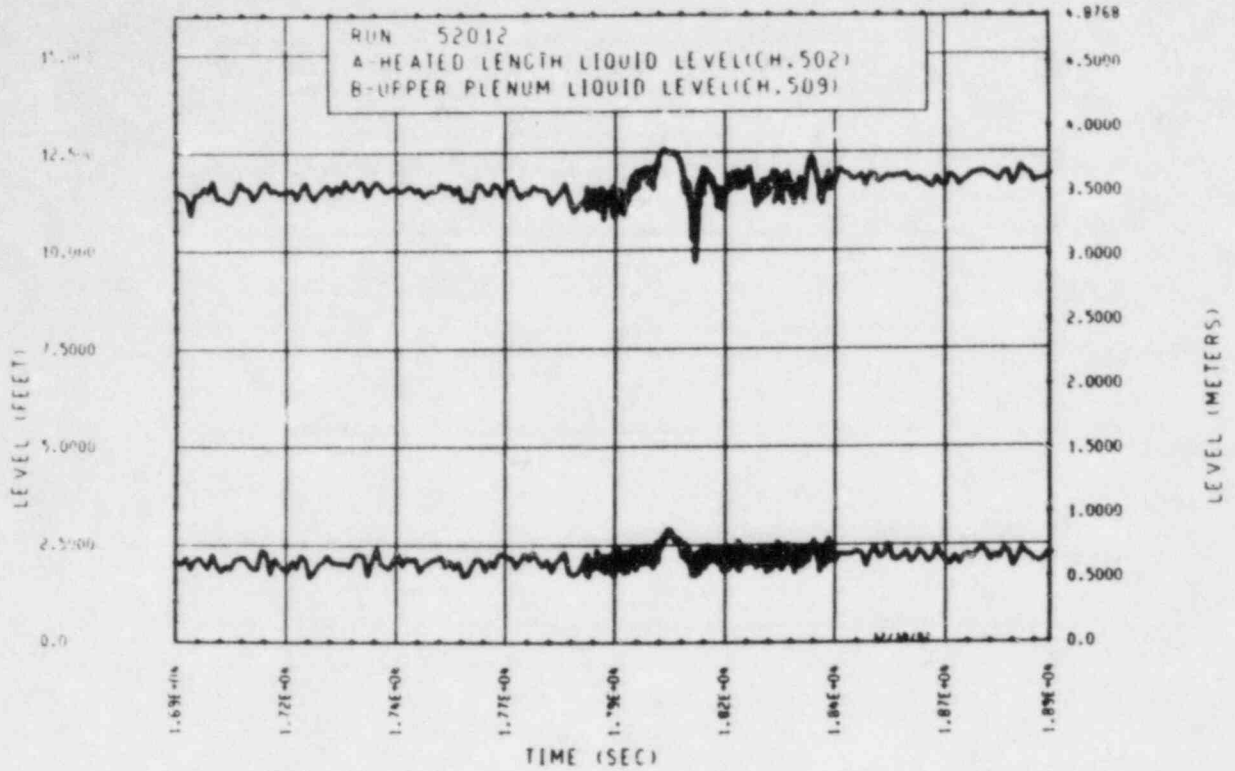

Figure A-137. Heated Length and Upper Plenum Liquid Levels, Test 11

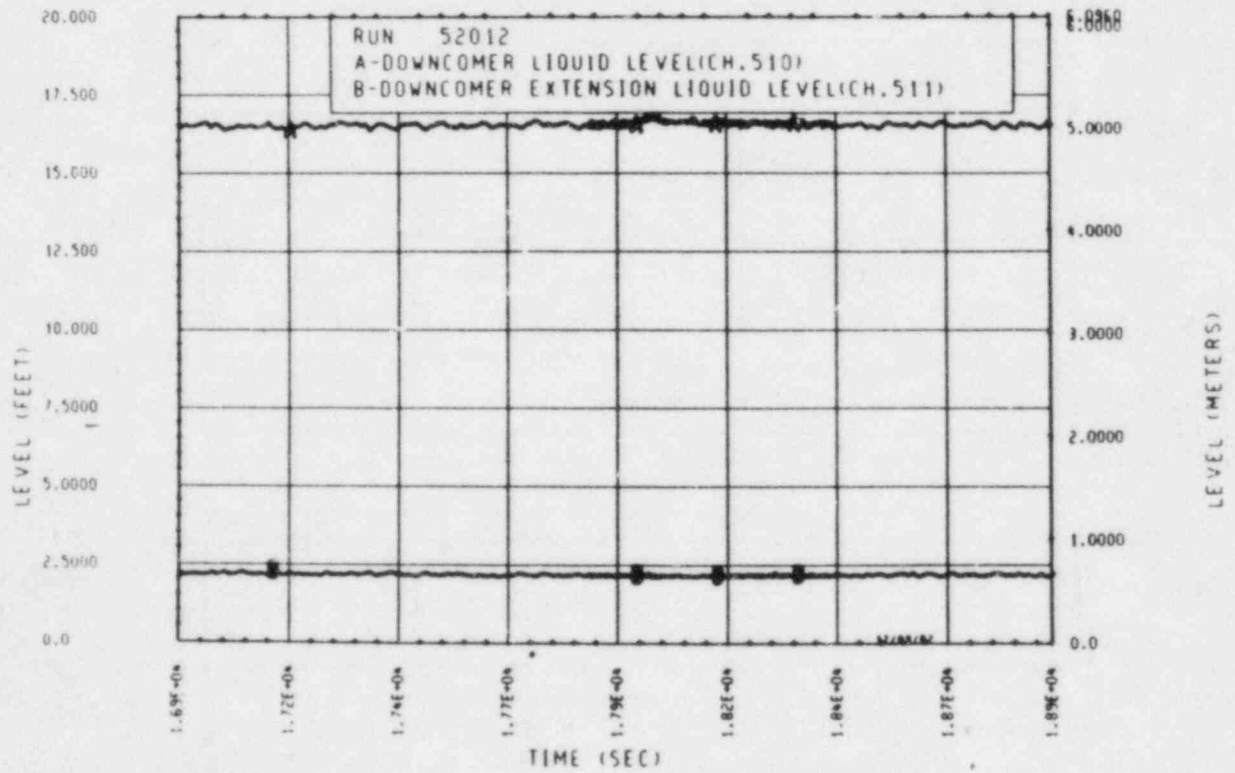

Figure A-138. Downcomer and Downcomer Extension Liquid Levels, Test 11

TEST 12: REFLUX CONDENSATION COLD LEG INJECTION TEST

Objective

To determine the effects of unbroken loop cold leg injection on reflux condensation

Test Procedure

The test was begun from a steady-state reflux condensation mode with a nominal bundle power of 222 kw. The primary system was operated with the pressurizer valved out and a reduced mass inventory consistent with previously established reflux condensation conditions. The secondary side was operated in a constant level feed-and-bleed boiling mode with a nominal pressure of 0.28 MPa (40 psia). The secondary side level was maintained at 7.62 m (25 ft) (71 percent full). Accumulator 1 was used to inject 35°C (95°F) water into the intact cold leg at a nominal rate of 0.77 kg/sec (1.7 lbm/sec). The duration of the injection was 48 seconds. The test was terminated when the system returned to a steady-state condition.

Test Overview:

Prior to unbroken loop cold leg injection (CLI), the primary system was brought to a steady-state reflux condensation mode of natural circulation. This was accomplished by removing 67.7 percent of the original single-phase primary system mass inventory. At this reflux condensation condition, the average primary system pressure was 0.32 MPa (46 psia). Reflux condensation from the cold legs entered the rod bundle with a 11°C (20°F) subcooling at 124°C (255°F). A two-phase saturated mixture exited at the rod bundle exit at 136°C (277°F). The net mass flow through the rod bundle was zero. Hence, the rod bundle operated in a pool boiling mode. The collapsed liquid level in the heated length was approximately 1.83 m (6 ft) and quite steady. The upper plenum collapsed liquid level was less stable and hovered about the 0.38 m (1.25 ft) (27 percent full) level.

The rod bundle collapsed liquid level was maintained by reflux condensation (RC) from both sets of hot legs and cold legs. The unbroken loop hot leg RC flowmeter indicated the most stable flow of condensate, whereas RC flowmeters associated with the unbroken loop cold legs, broken loop hot leg, and broken loop cold leg indicated unstable and sporadic condensate flow. Approximations of these reflux condensation flow rates are summarized below:

Unbroken loop hot leg ~ 0.034 kg/sec (0.075 lbm/sec)
Broken loop hot leg ~ 0.023 kg/sec (0.050 lbm/sec)
Unbroken loop cold leg ~ 0.045 kg/sec (0.10 lbm/sec)
Broken loop cold leg ~ 0.011 kg/sec (0.025 lbm/sec)
Total reflux condensation = 0.113 kg/sec (0.250 lbm/sec

The reflux condensation flow splits between and within the broken and intact loops are summarized below:

Unbroken loop total RC/total RC = 0.70
Hot leg total RC/total RC = 0.50
Unbroken loop hot leg RC/unbroken loop total RC = 0.43
Broken loop hot leg RC/broken loop total RC = 0.67

Employing an average measured power of 222 kw and accounting for 11°C (20°F) subcooling at the rod bundle inlet, a steady-state energy balance predicts a steaming rate of 0.102 kg/sec (0.224 lbm/sec) in the rod bundle. This agrees favorably with the total measured reflux condensation rate of 0.113 kg/sec (0.250 lbm/sec) (10 percent discrepancy).

Cold leg injection was initiated at 23,804 seconds and terminated 48 seconds later. The short injection of cold water into the unbroken loop cold leg resulted in the momentary resumption of natural circulation flow through the rod bundle and through the intact loop. The response of the broken loop was minimal. The rod bundle experienced a peak flow of 6.267 kg/sec (13.82 lbm/sec) 4 seconds after the termination of CLI. Simultaneously, the intact loop bidirectional flowmeter was saturated at 4.44 kg/sec (9.78 lbm/sec). These flow rates were significantly higher than mass flow rates observed

during peak two-phase conditions [typically 3.6 kg/sec (8 lbm/sec) through the rod bundle]. These high flow rates were only momentary; both the rod bundle and the intact loop subsequently experienced a gradual decay of mass flow. The mass flow returned to low values (about zero) approximately 548 seconds after the termination of CLI.

These flow surges were accompanied by a momentary 0.03 MPa (4 psia) decrease in upper plenum pressure, which was most likely the result of a momentary increase in frictional and form pressure losses in the rod bundle. The rod bundle inlet temperature was only slightly affected by CLI. The rod bundle exit temperatures decreased with the upper plenum pressure, reflecting the slight change in saturation temperature. This effect was echoed in the steam generator inlet and outlet plenum fluid temperatures. The broken loop steam generator outlet plenum fluid temperature did not recover, however, with the primary pressure. Its recovery lagged the system pressure by approximately 300 seconds. The secondary side pressure also echoed the primary pressure decrease and subsequent recovery. The secondary side exit temperatures reflected this trend.

The collapsed liquid level in the upper plenum showed only a slight increase in level during CLI. The heated length collapsed liquid level decreased from an average 1.83 m (6 ft) to 1.13 m (3.71 ft) 12 seconds after CLI initiation. This may be indicative of the cessation of boiling during the early moments of CLI. The collapsed liquid level quickly increased to a peak value of 2.78 m (9.12 ft) at a time coincident with the peak rod bundle flow surge. This collapsed liquid level indicated that void generation was continuing in the upper elevations of the rod bundle, even during the peak flow surges. The heated length collapsed liquid level recovered to 1.83 m (6 ft) as the rod bundle flow decayed to zero.

The sudden surge of mass flow coincident with CLI disrupted the reflux condensation occurring in the unbroken loop such that it never recovered to previously attained levels after CLI was terminated. The same held true for the broken loop hot leg. The broken loop cold leg, however, exhibited its most stable and prolonged period of reflux condensation beginning approximately 250

seconds after the termination of CLI. Coincident with this broken loop cold leg reflux condensation activity was the gradual refilling of the downcomer, which was previously depleted by the aforementioned mass flow surge.

TEST SCHEDULE
TEST 12

Time[a] (sec)	Event
18953	Began continuous drain of 426 kg (940 lbm)
19102	23 kg (50 lbm) drained
21704	Weir meters valved in
21874	Ended 426 kg (940 lbm) continuous drain; total mass drained from primary = 544 kg (1200 lbm)
22094	Redundant weir meter 570 valved out
22334	Began 9 kg (20 lbm) drain
22417	Ended 9 kg (20 lbm) drain; total mass drained from primary = 553 kg (1220 lbm)
22604	Weir meters indicated stable reflux; upper plenum froth level observed to be just below hot leg inlets
23804	Began cold leg injection; nominal injection rate = 7.6×10^{-4} m^3/sec (12 gal/min)

a. Test 12 was run in series with tests 5 and 11. Time zero therefore corresponds with time zero of test 5. It estimated that test 11 left the primary system drained of 112 kg (260 lbm).

Time (sec)	Event
23852	Ended cold leg injection
25004	End of test 12

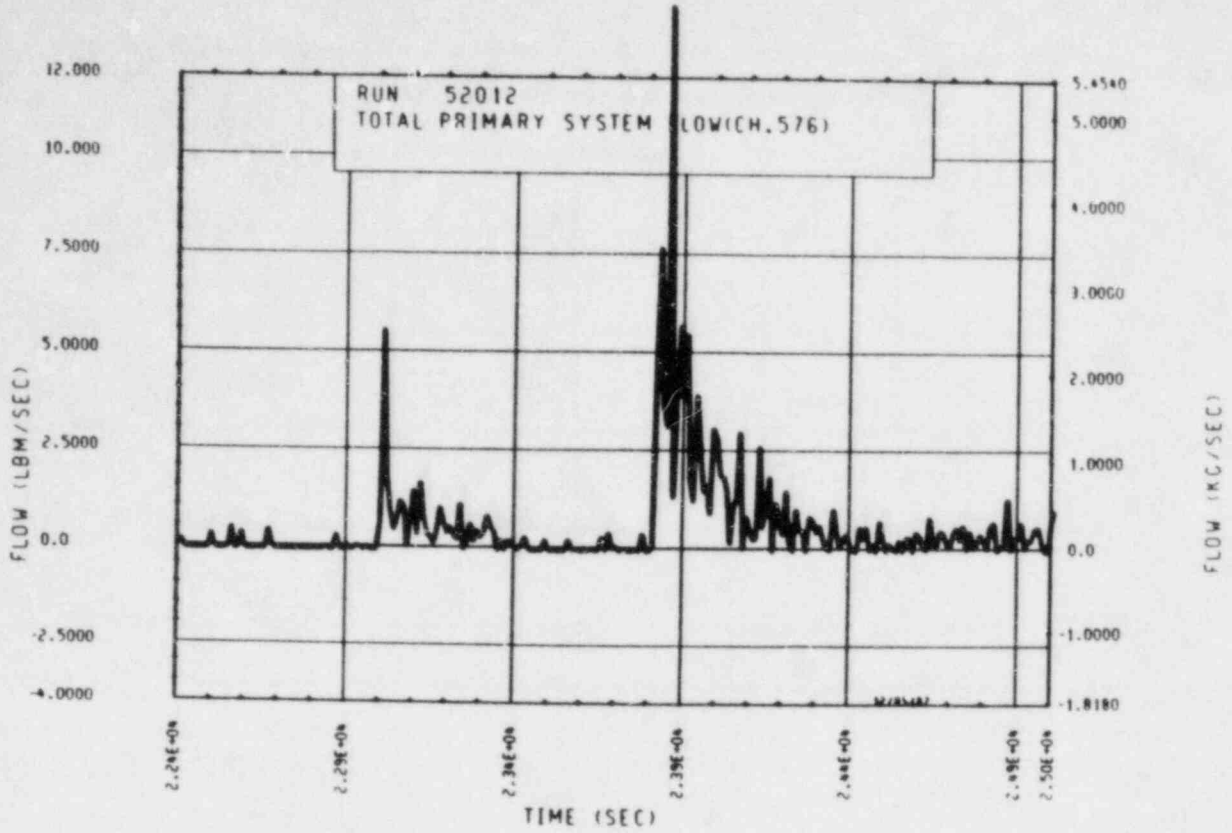

Figure A-139. Mass Flow Rate Through Rod Bundle, Test 12

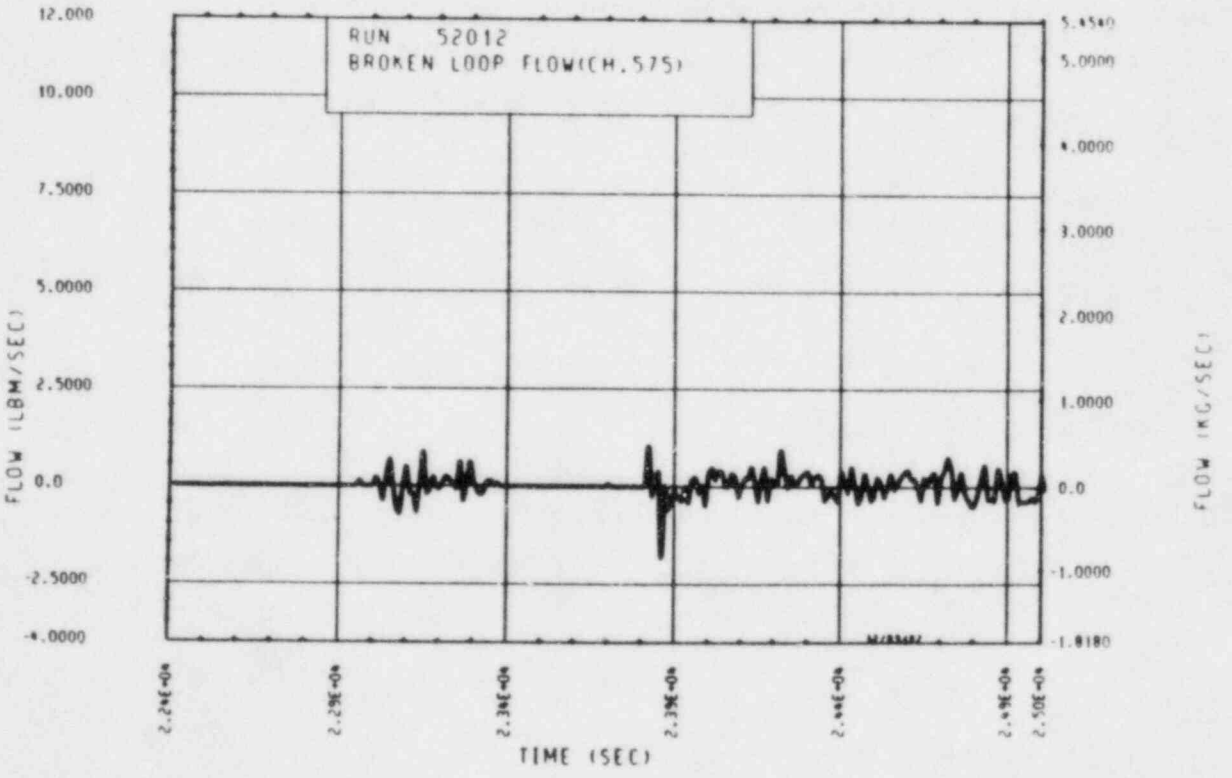

Figure A-140. Mass Flow Rate Through Broken Loop, Test 12

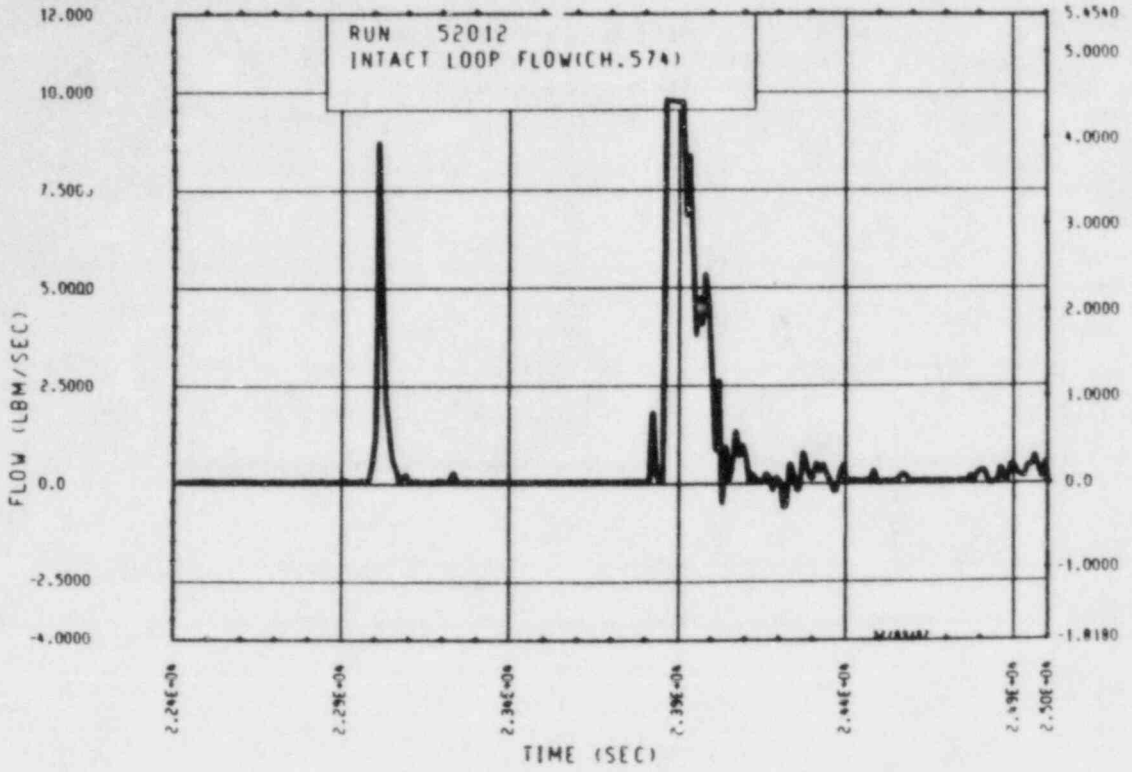

Figure A-141. Mass Flow Rate Through Unbroken Loop, Test 12

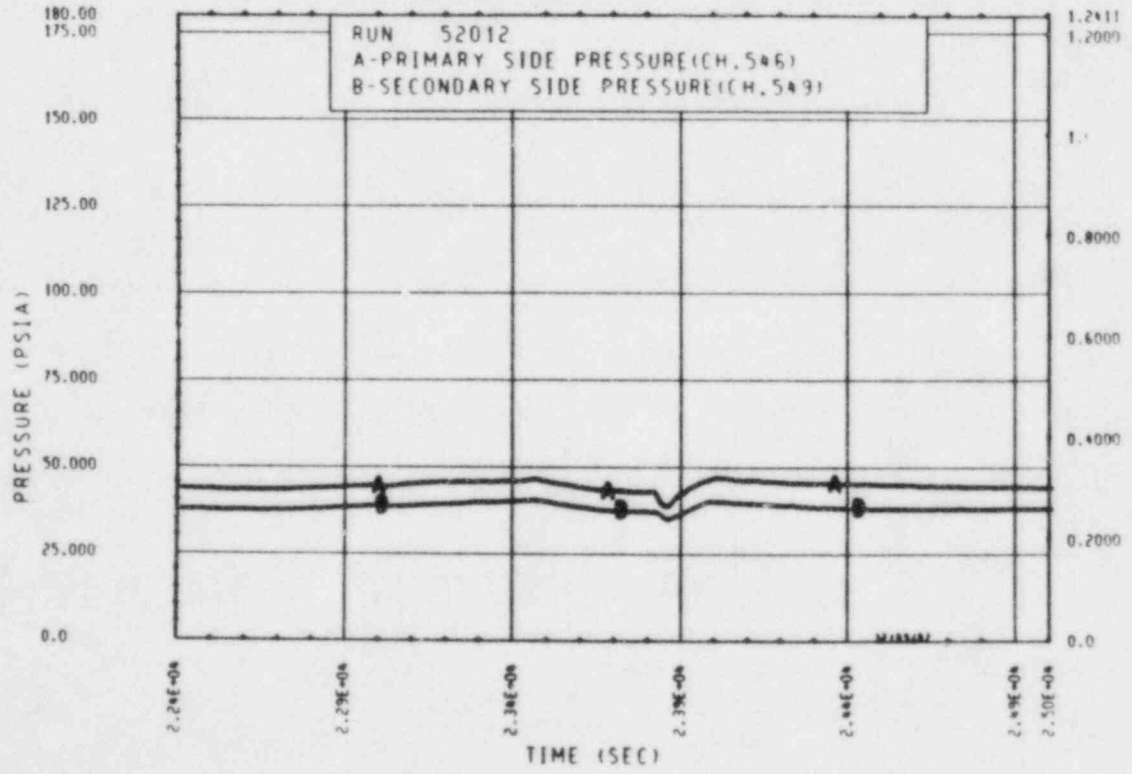

Figure A-142. Primary and Secondary System Pressure, Test 12

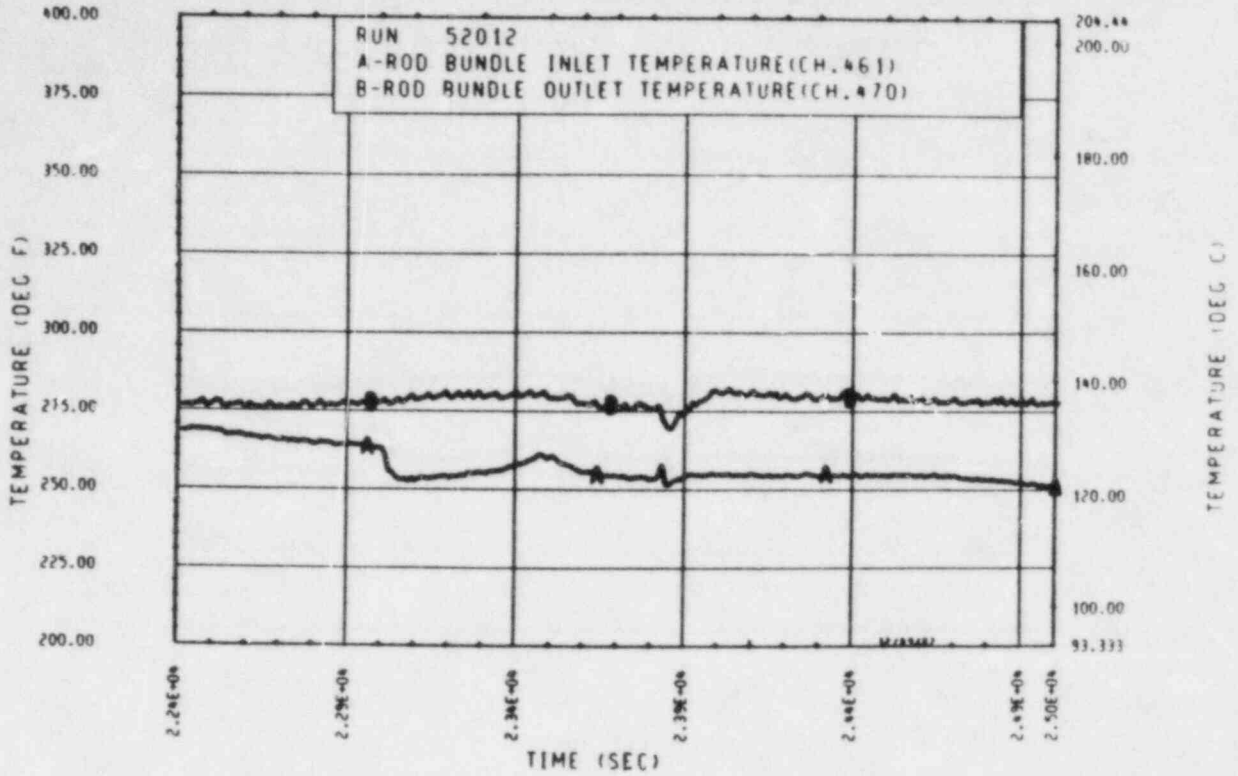

Figure A-143. Heater Rod Bundle Inlet and Outlet Temperature, Test 12

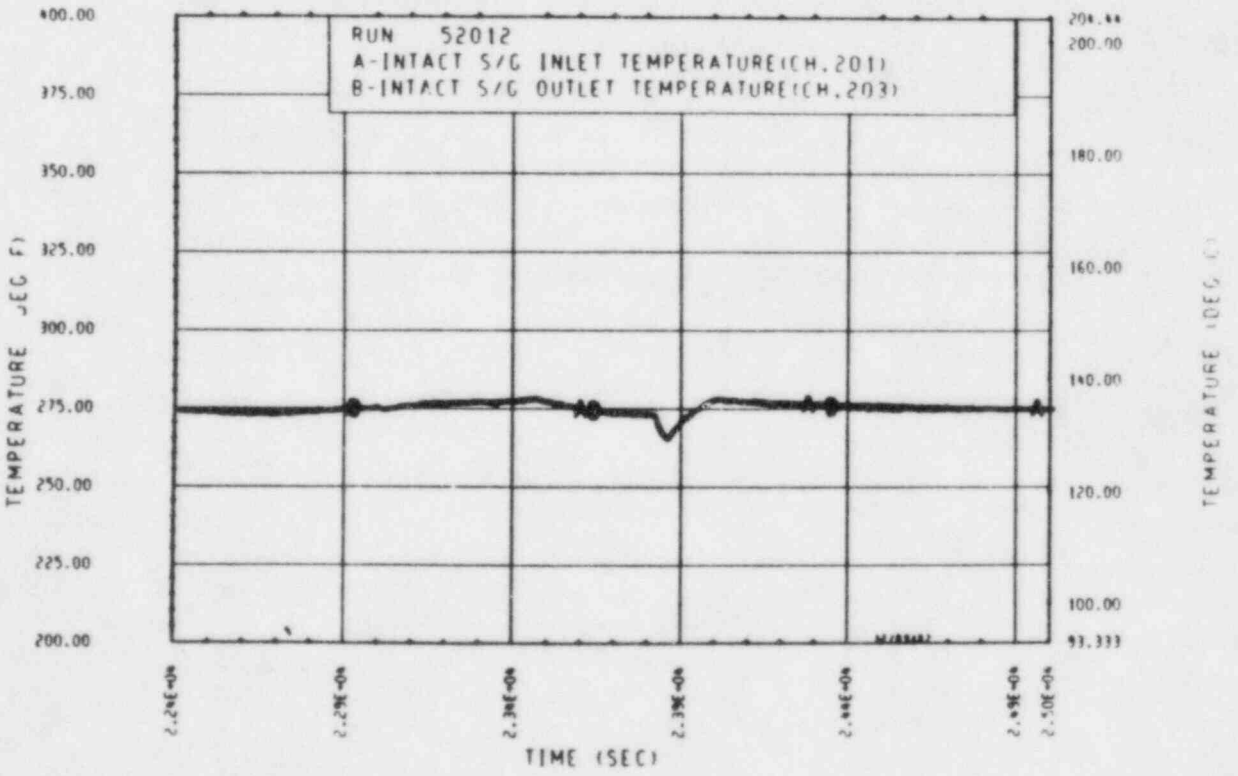

Figure A-144. Unbroken Loop Steam Generator Temperature, Test 12

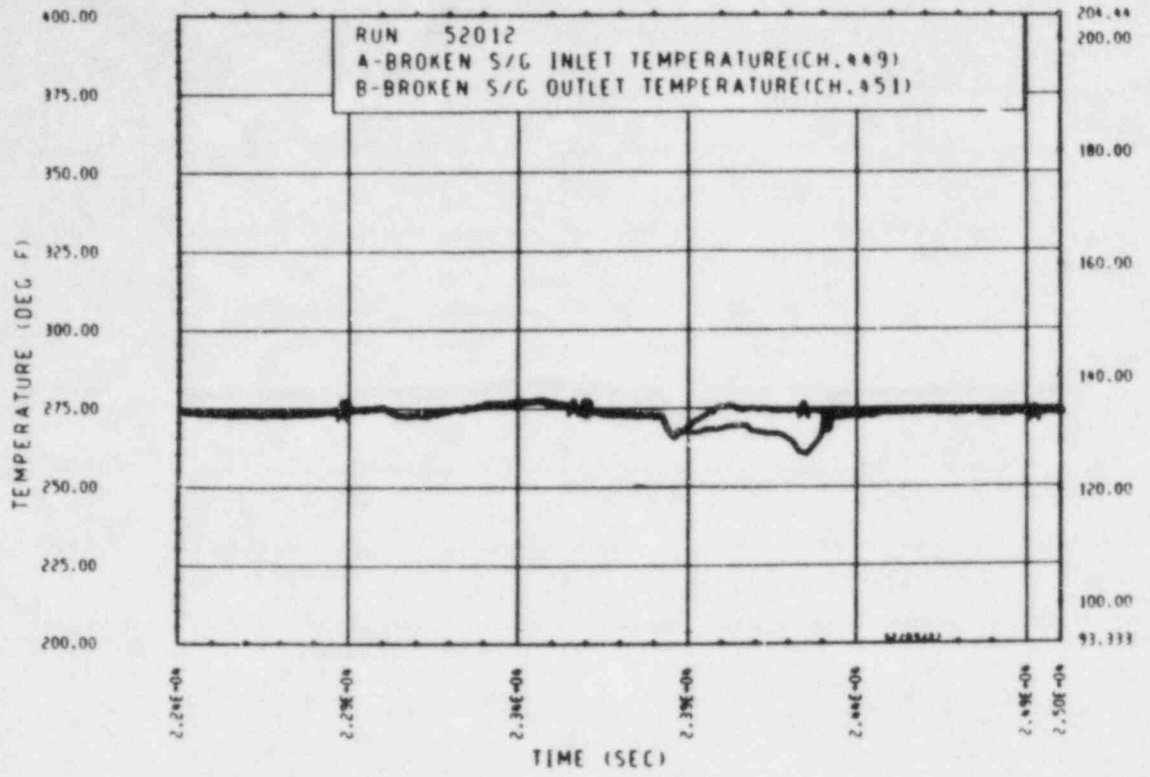

Figure A-145. Broken Loop Steam Generator Inlet and Outlet Temperature, Test 12

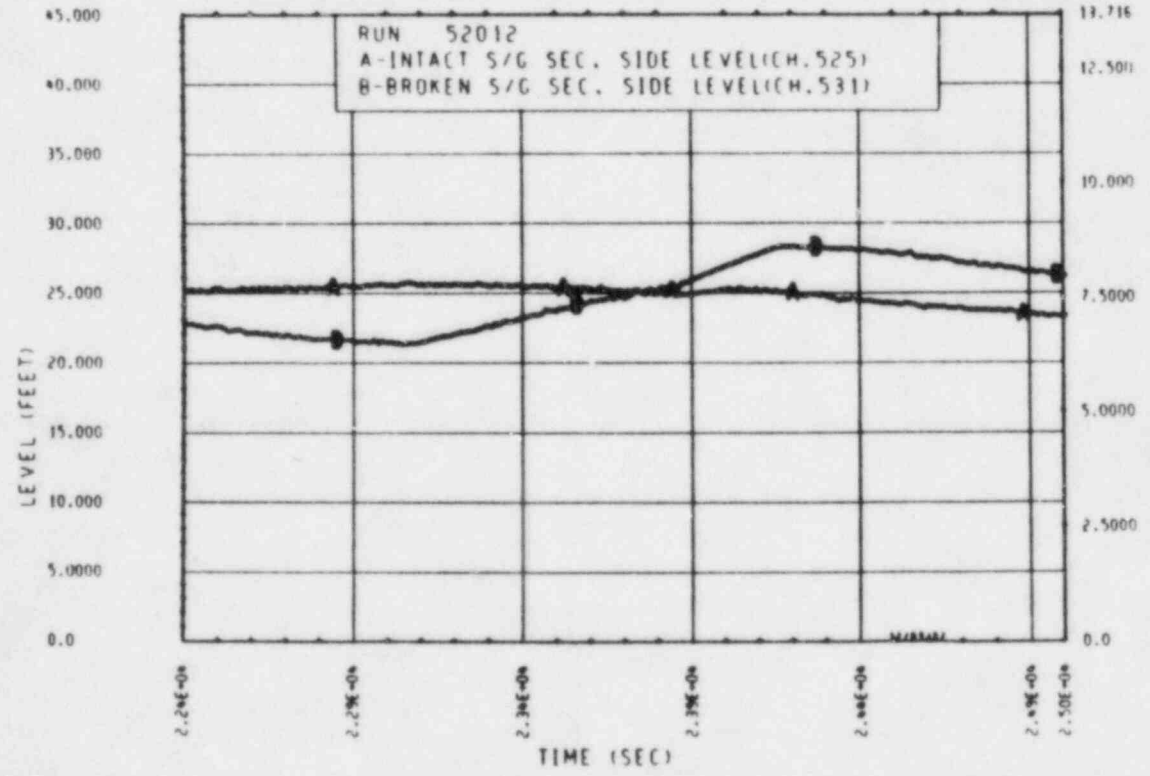

Figure A-146. Unbroken and Broken Loop Steam Generator Secondary Side Collapsed Liquid Levels, Test 12

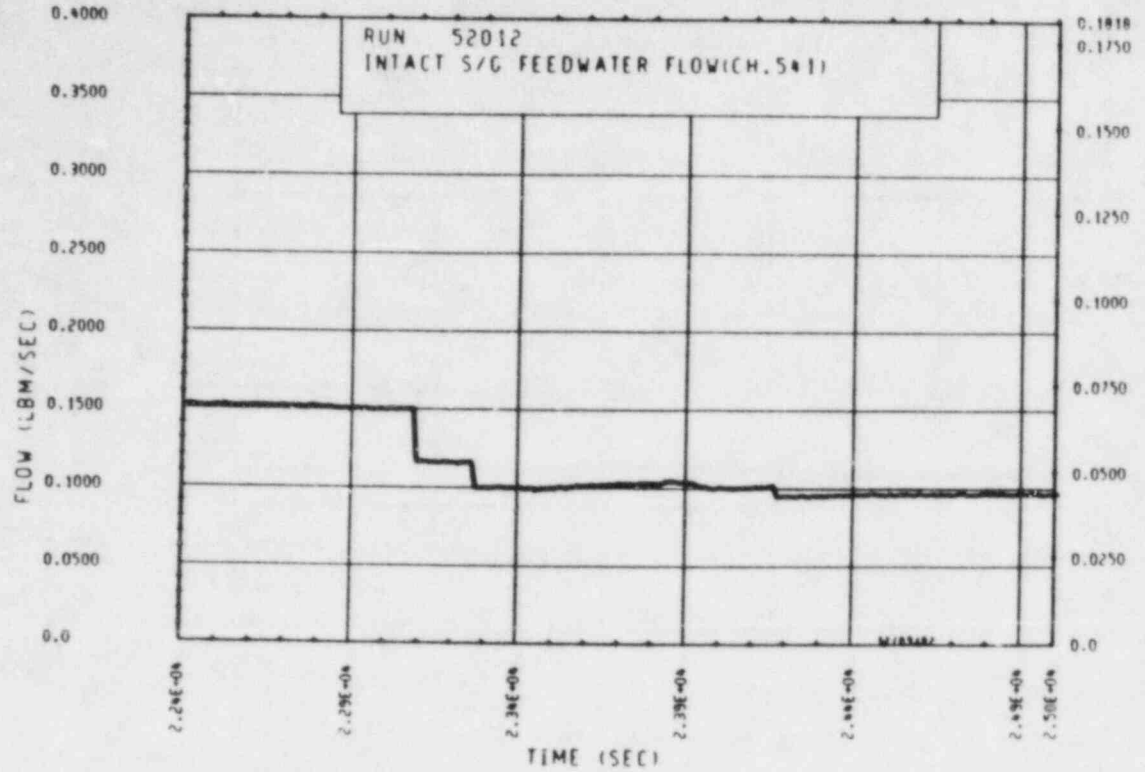

Figure A-147. Unbroken Loop Steam Generator Feedwater Mass Flow Rate, Test 12

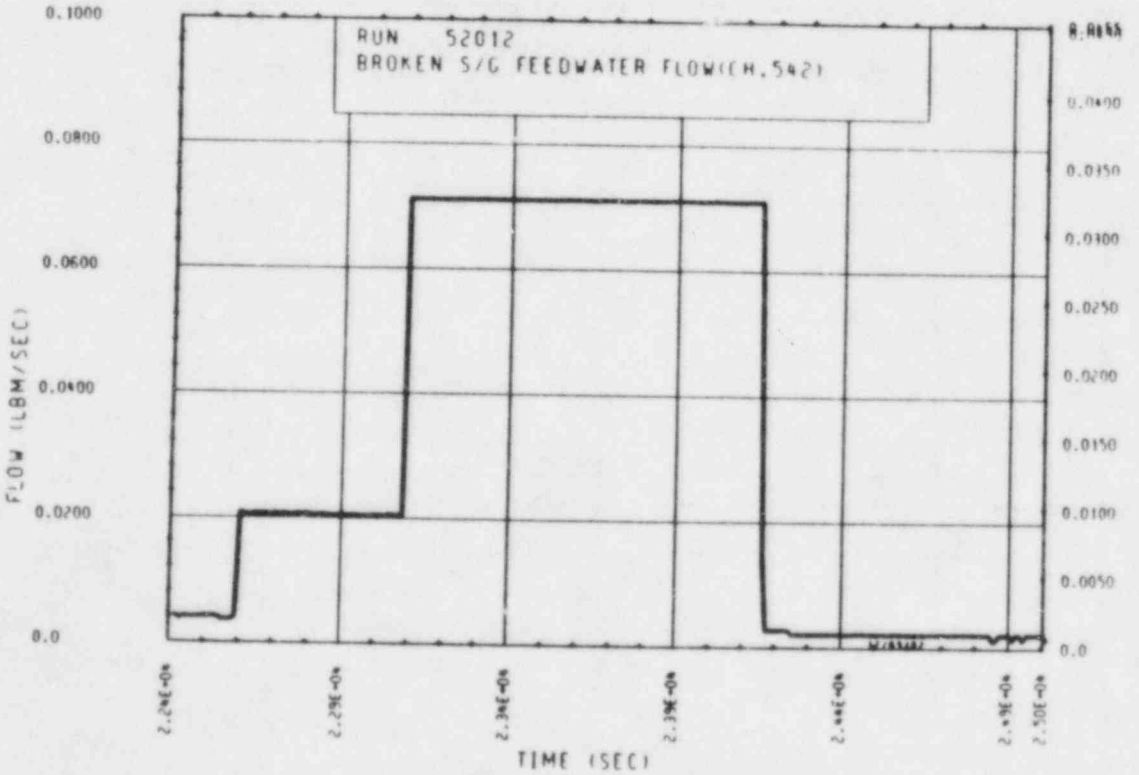

Figure A-148. Broken Loop Steam Generator Feedwater Mass Flow Rate, Test 12

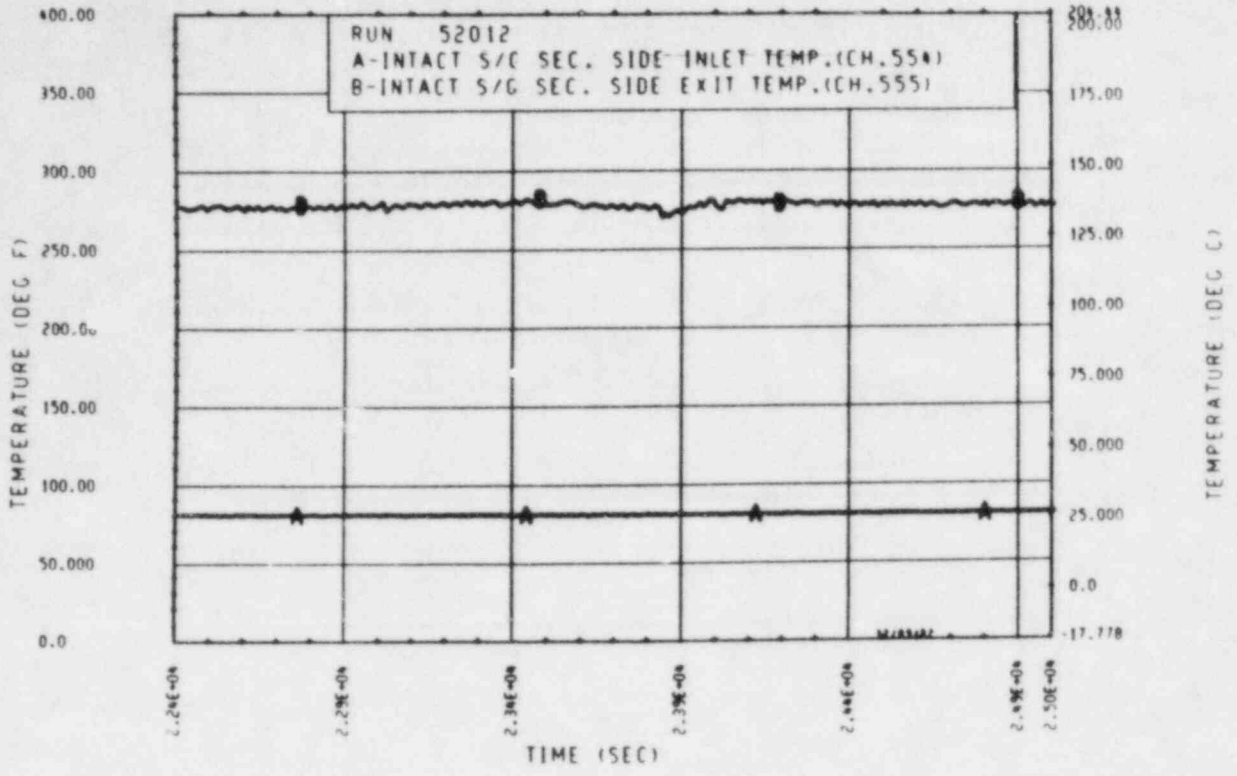

Figure A-149. Unbroken Loop Steam Generator Secondary Side Inlet and Outlet Temperature, Test 12

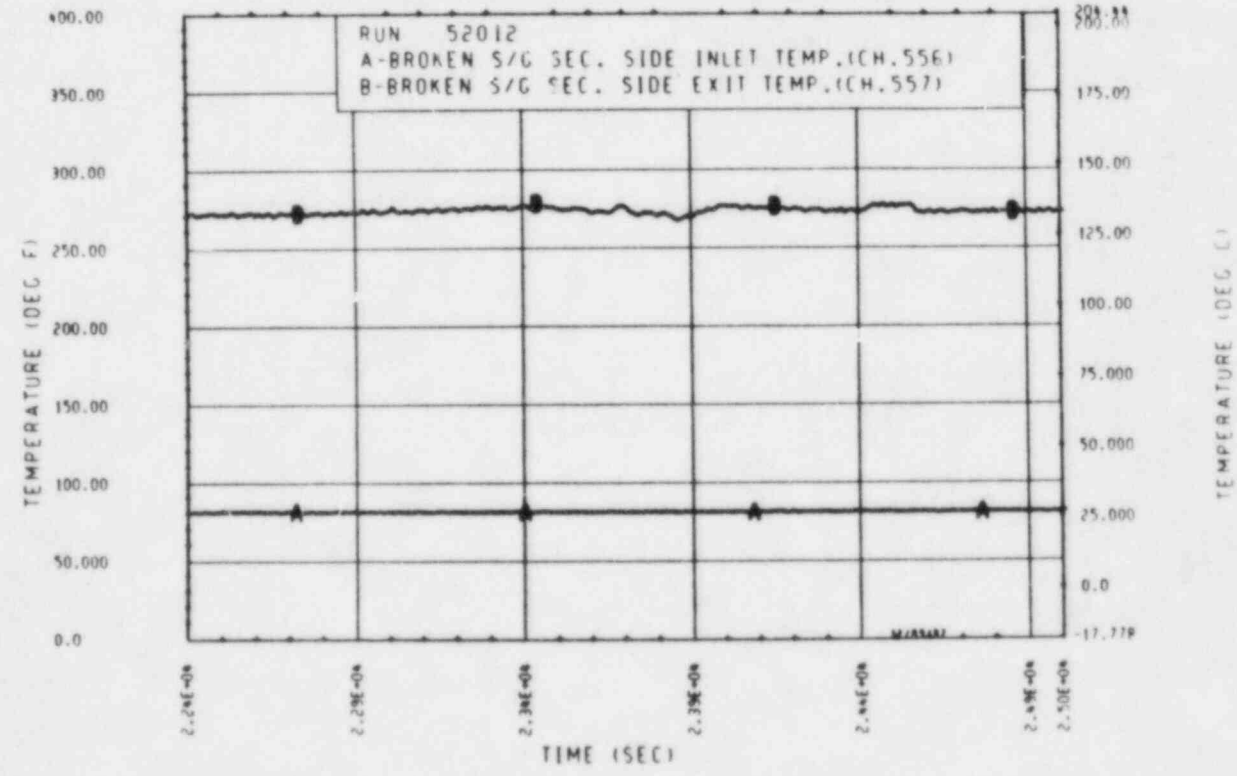

Figure A-150. Broken Loop Steam Generator Secondary Side Inlet and Outlet Temperature, Test 12

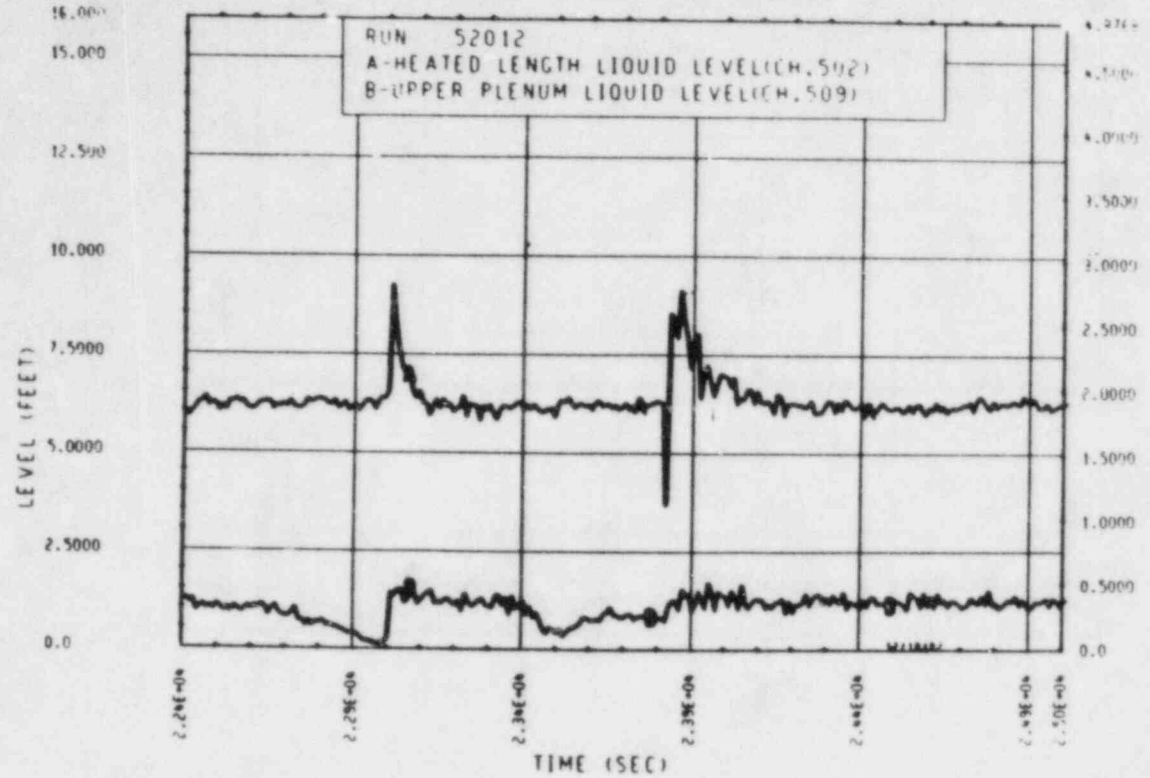

Figure A-151. Heated Length and Upper Plenum Liquid Levels, Test 12

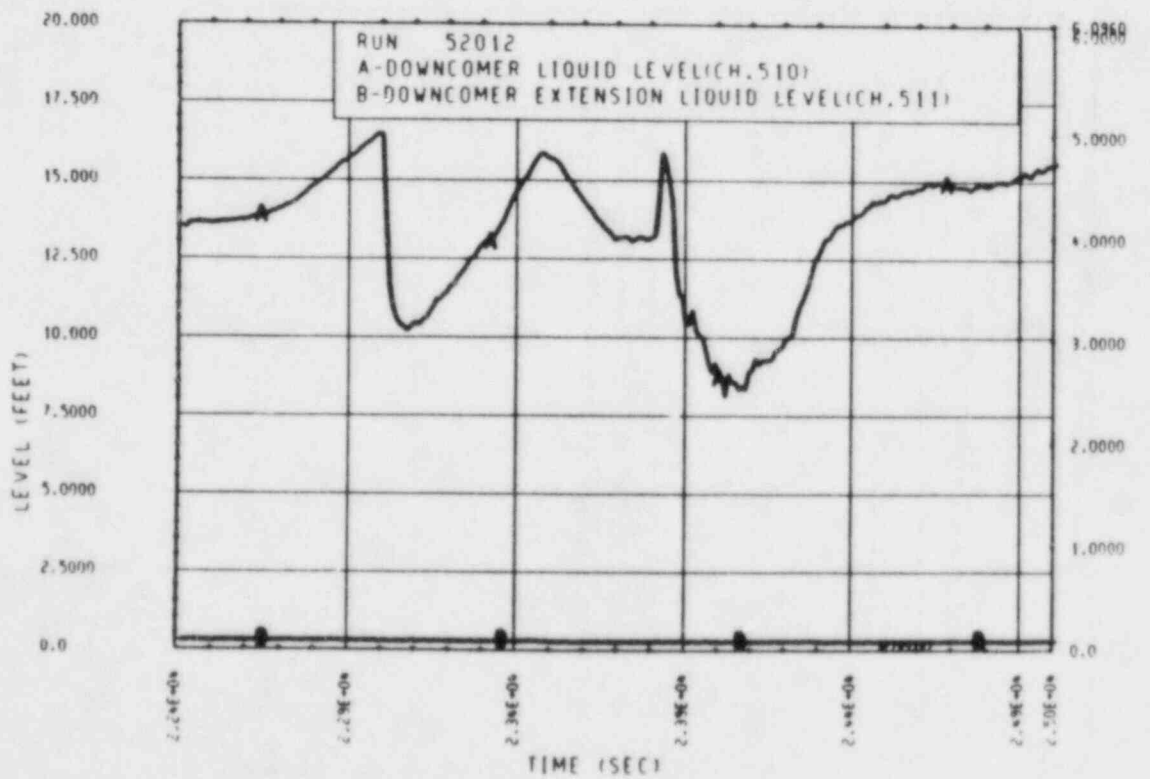

Figure A-152. Downcomer and Downcomer Extension Liquid Levels, Test 12

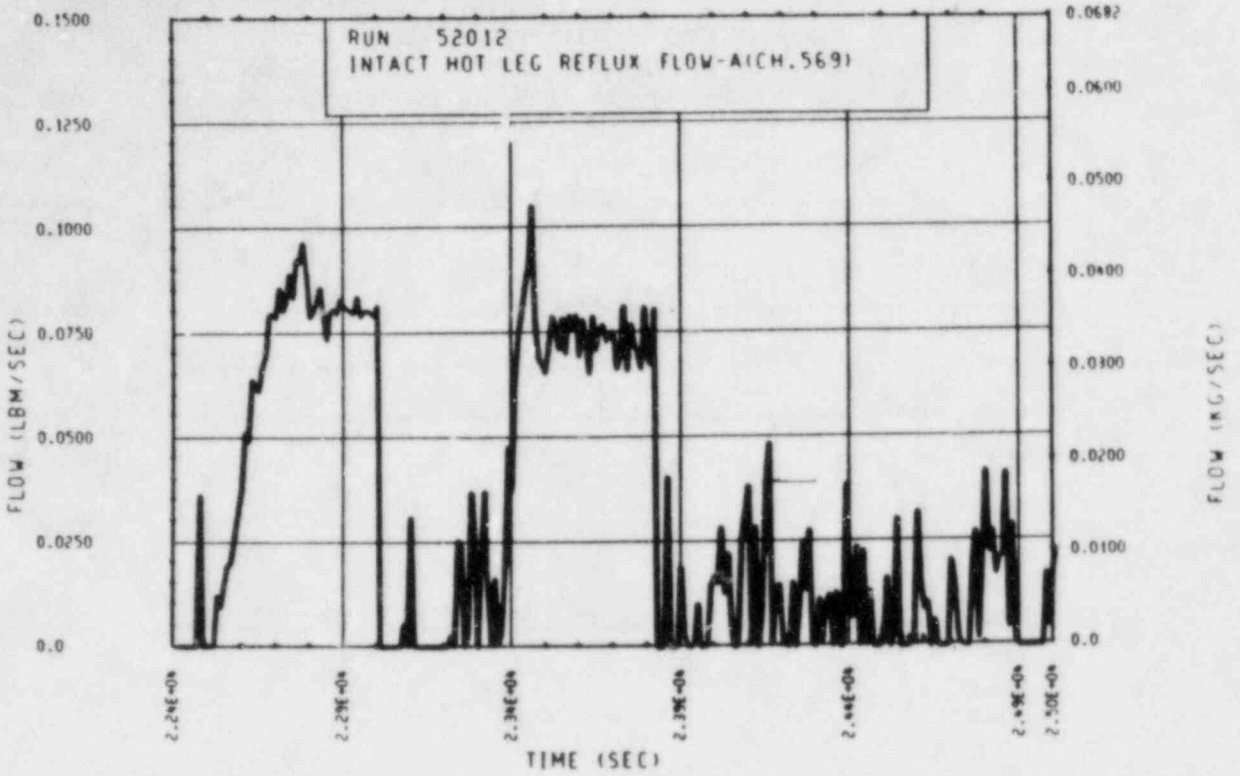

Figure A-153. Unbroken Loop Hot Leg Reflux Condensation Mass Flow Rate, Test 12

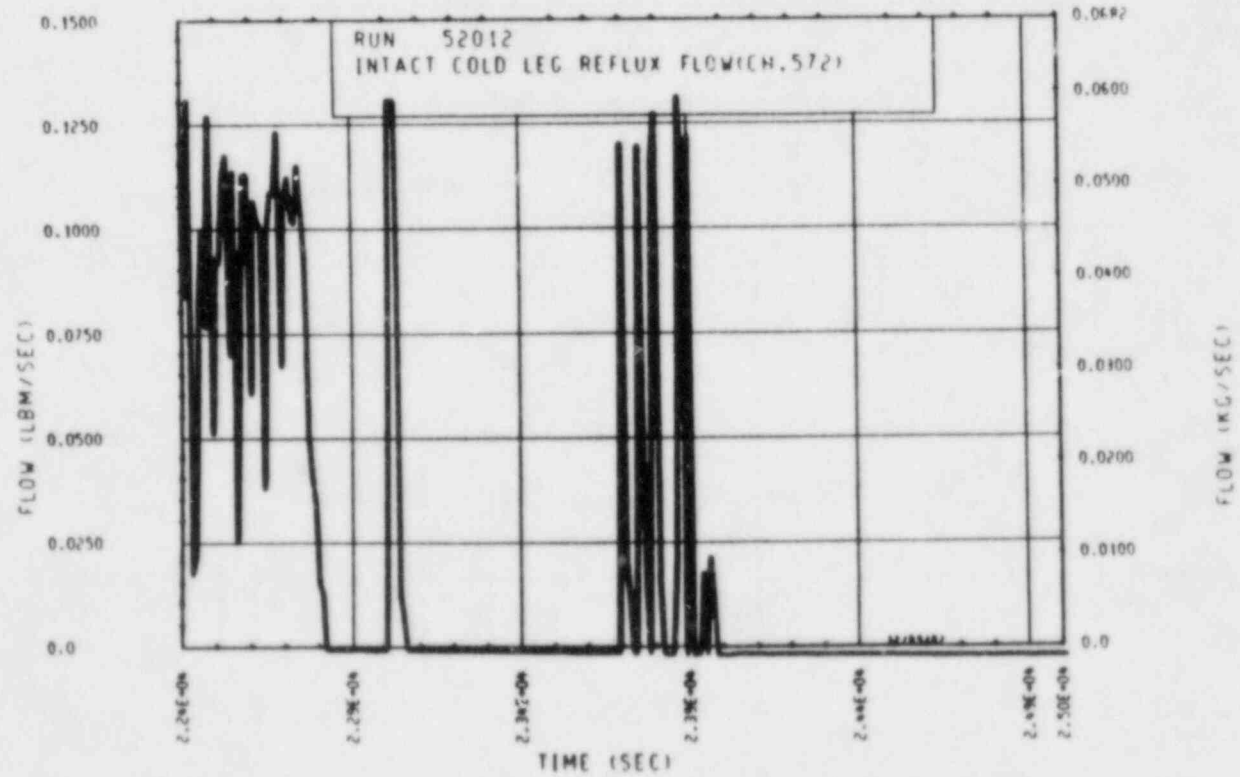

Figure A-154. Unbroken Loop Cold Leg Reflux Condensation Mass Flow Rate, Test 12

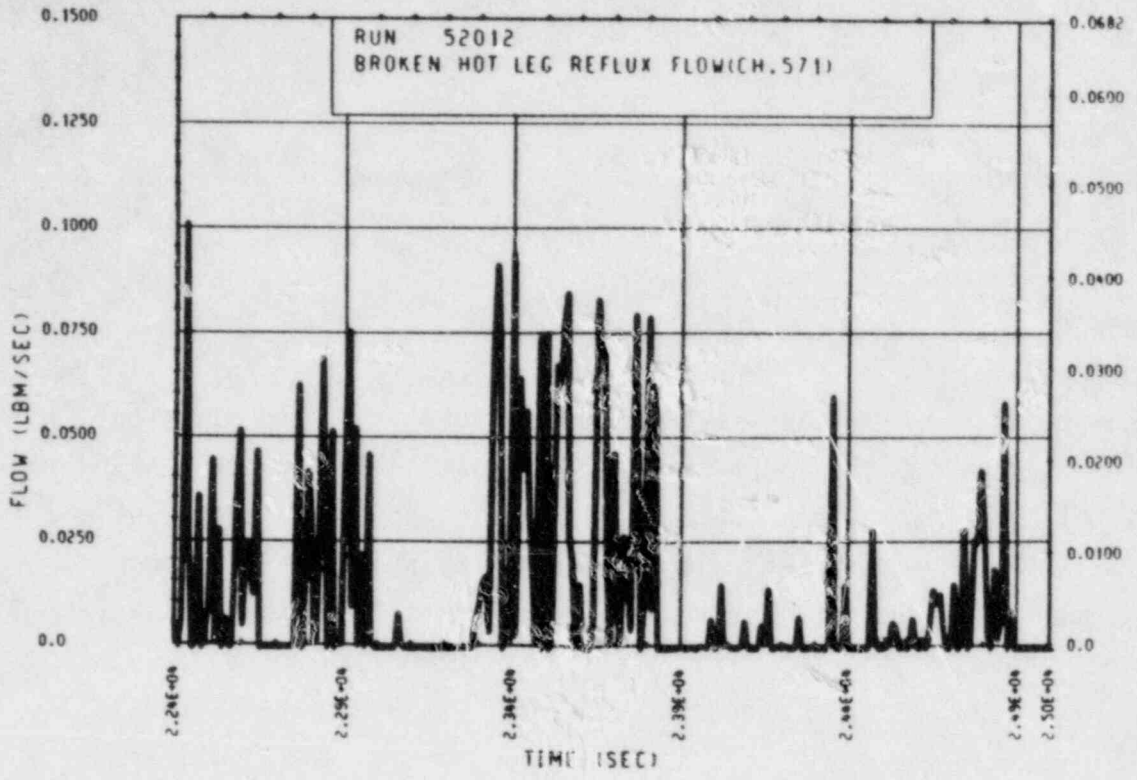

Figure A-155. Broken Loop Hot Leg Reflux Condensation Mass Flow Rate, Test 12

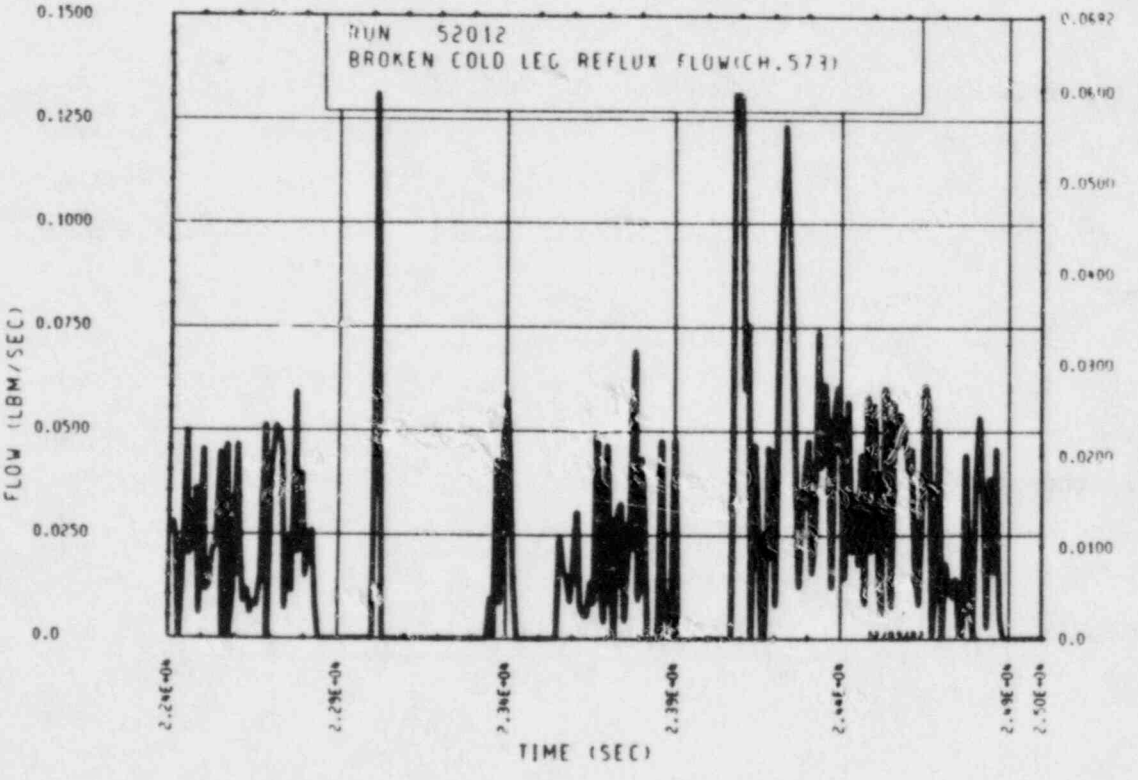

Figure A-156. Broken Loop Cold Leg Reflux Condensation Mass Flow Rate, Test 12

TEST 13: TWO-PHASE NONCONDENSIBLE GAS EFFECTS

Objective

To determine the effect of noncondensible gas on the two-phase peak flow natural circulation cooling mode

Test Procedure

The test was begun from a steady-state two-phase peak flow natural circulation condition with a nominal bundle power of 222 kw (simulated 2 percent of full power). The primary system was operated with the pressurizer valved out and a reduced mass inventory consistent with previously established two-phase peak flow conditions. The secondary system was operated at a constant level feed-and-bleed boiling mode with a nominal pressure of 0.28 MPa (40 psia). The secondary side level was maintained at 7.62 m (25 ft) (71 percent full). Helium was proportionally injected into both the unbroken and broken hot legs in a series of nine injections.

Test Overview

Prior to the initiation of noncondensible gas injections, the primary system was operated in a two-phase peak flow natural circulation mode. The broken loop was stalled, however, as it characteristically did whenever the system operates in a N-1 loop configuration with the intact loop acting as the sole heat sink.

A total of 4.92×10^{-5} standard cm^3 of helium were injected into the primary system by means of nine discrete injections. It should be noted that approximately 25 percent of this gas was injected into the stalled broken loop hot leg. The primary system responded to the addition of helium by making the transition from a two-phase flow system to a single-phase flow system while simultaneously increasing pressure and decreasing flow. It is believed that the system responded in this manner as a result of helium collecting in

selected U-tubes in the unbroken steam generator and consequently blocking flow through those tubes. Flow blockage in the intact loop steam generator resulted in a reduction in available heat transfer surface area as well as a reduction in flow area through the steam generator. The reduction in flow area increased the flow resistance across the unbroken loop steam generator; hence flow decreased. The flow decrease was further enhanced by the loss of available heat transfer area and volume displacement in the steam generator U-tubes, both of which caused system pressure to increase. The increase in system pressure was accompanied by a corresponding increase in system saturation temperature. Consequently, system subcooling increased and vapor generation decreased. The void fraction decrease in the heater rod bundle and uphill side of the steam generator U-tubes resulted in a loss of driving head around the loop, and substantially contributed to the decrease in flow. As helium displaced more and more active primary sytem volume, the pressure eventually increased to a point at which the subcooling was sufficient to suppress any vapor generation. The active portion of the system then returned to a single-phase mode of operation. This single-phase mode of operation, however, was different from those observed in other tests. The major difference was that the system continued to operate in a N-1 loop configuration as a result of the stalled broken loop.

TEST SCHEDULE
TEST 13

Time (sec)	Event
0	Computer on
4363	Power to 222 kw
12283	Primary system operating in single-phase natural circulation.
15133	Pressurizer valved out
15193	Began 136 kg (300 lbm) continuous drain to get the primary system into two-phase peak-flow natural circulation mode
16944	Ended continuous drain; 137 kg (301 lbm) actually drained from the primary system
17183	Began 9 kg (20 lbm) drain.
17227	Ended 9 kg (20 lbm) drain; 146 kg (321 lbm) drained from the primary thus far
24433	Began taking quick-look baseline samples from the steam generator U-tubes
25153	Ended baseline sampling
29773	Began a first helium injection
29953	Ended first helium injection; approximately 0.126 mole (2.77×10^{-4} lbm-mole) of helium injected into primary system

Time (sec)	Event
35653	Began sampling steam generator U-tubes to determine helium concentration and distribution
41473	Ended helium sampling
49873	Began second helium injection
50773	Ended second helium injection; approximately 2.04 moles (4.49×10^{-3} lbm-mole) of helium injected into primary system
53053	Began third helium injection
53953	Ended third helium injection; approximately 2.07 moles (4.56×10^{-3} lbm-mole) of helium injected into primary system
55453	Began sampling steam generator U-tubes to determine helium concentration and distribution
61033	Ended helium sampling
62893	Began fourth helium injection
63793	Ended fourth helium injection; approximately 2.10 moles (4.62×10^{-3} lbm-mole) of helium injected into primary system
65413	Began fifth helium injection

Time (sec)	Event
66313	Ended fifth helium injection; approximately 2.16 moles (4.76×10^{-3} lbm-mole) of helium injected into primary system
67273	Began sixth helium injection
67873	Ended sixth helium injection; approximately 2.16 moles (4.76×10^{-3} lbm-mole) of helium injected into primary system
68953	Began seventh helium injection
69853	Ended seventh helium injection; approximately 2.14 moles (4.71×10^{-3} lbm-mole) of helium injected into primary system
71113	Began eighth helium injection
72013	Ended eighth helium injection; approximately 2.14 moles (4.71×10^{-3} lbm-mole) of helium injected into primary system
73273	Began sampling steam generator U-tubes to determine helium concentration and distribution
78853	Ended helium sampling
79483	Began ninth helium injection
81831	Ended ninth helium injection; approximately 5.53 moles (1.22×10^{-2} lbm-mole) of helium injected into primary system; power shut off

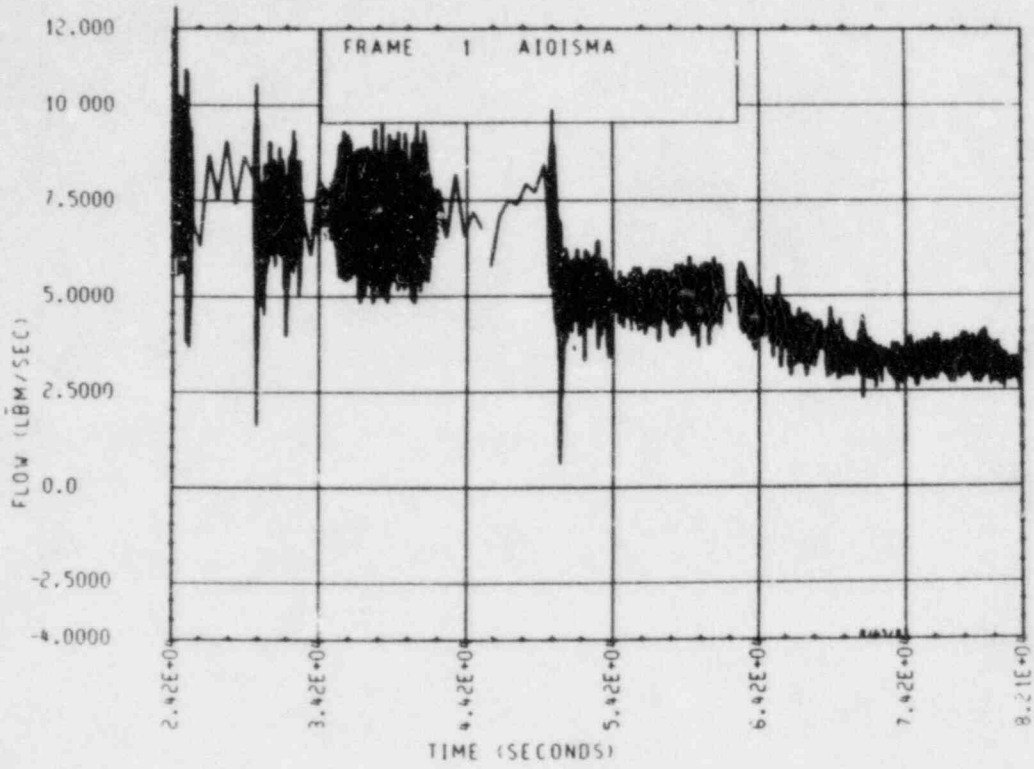

Figure A-157. Mass Flow Rate Through Rod Bundle, Test 13

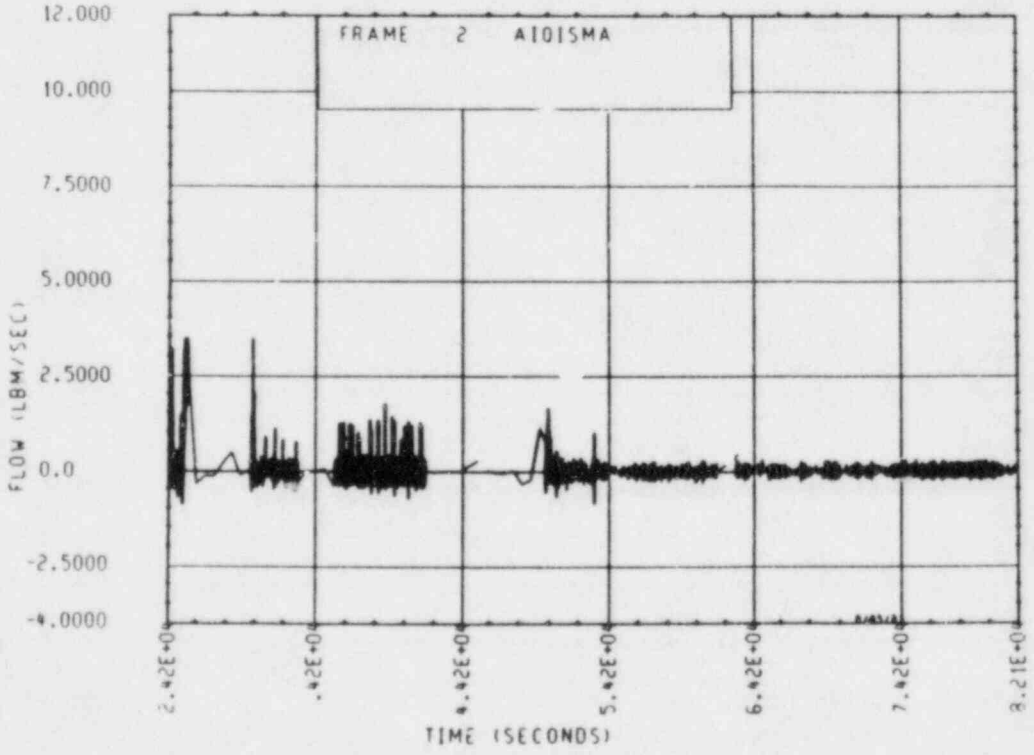

Figure A-158. Mass Flow Rate Through Broken Loop, Test 13

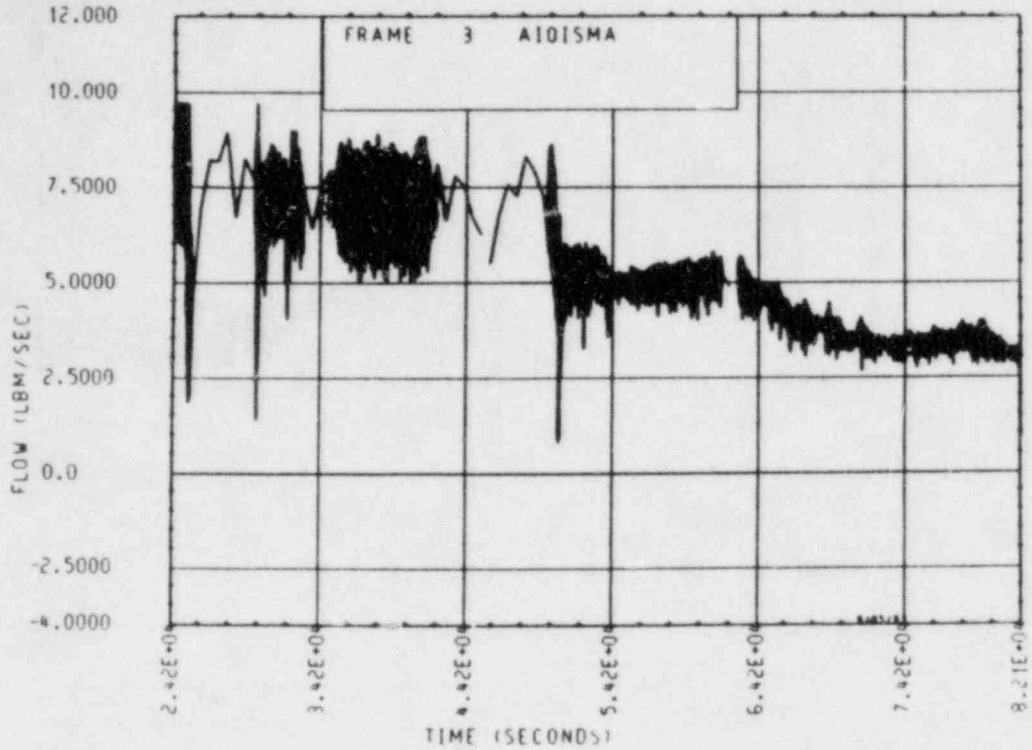

Figure A-159. Mass Flow Rate Through Unbroken Loop, Test 13

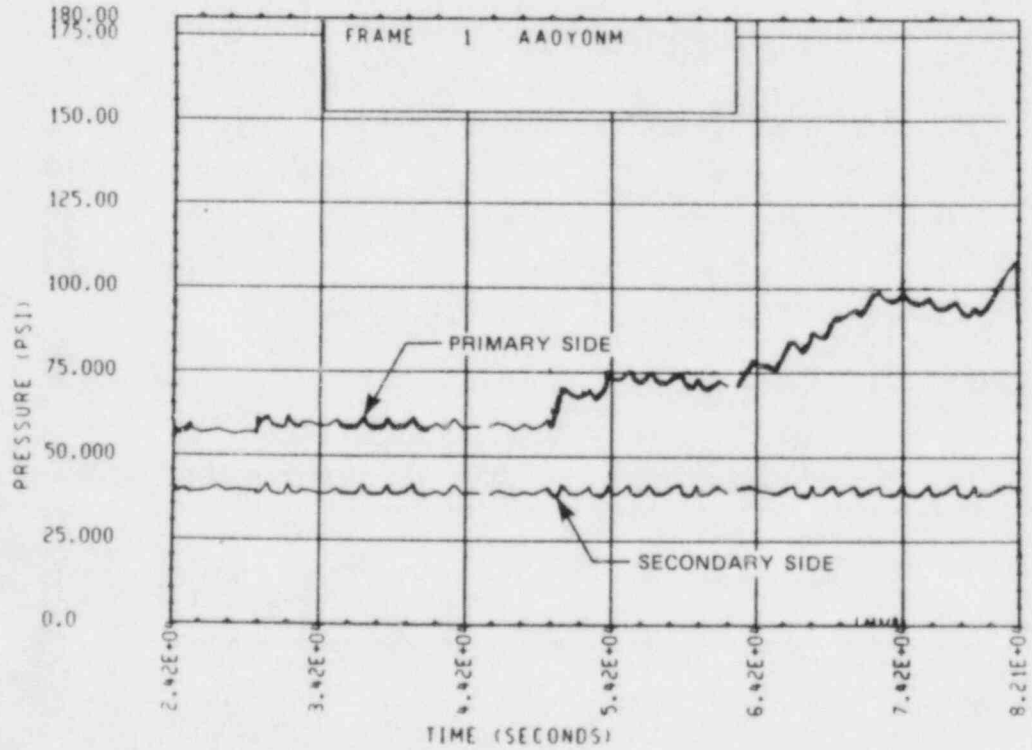

Figure A-160. Primary and Secondary System Pressure, Test 13

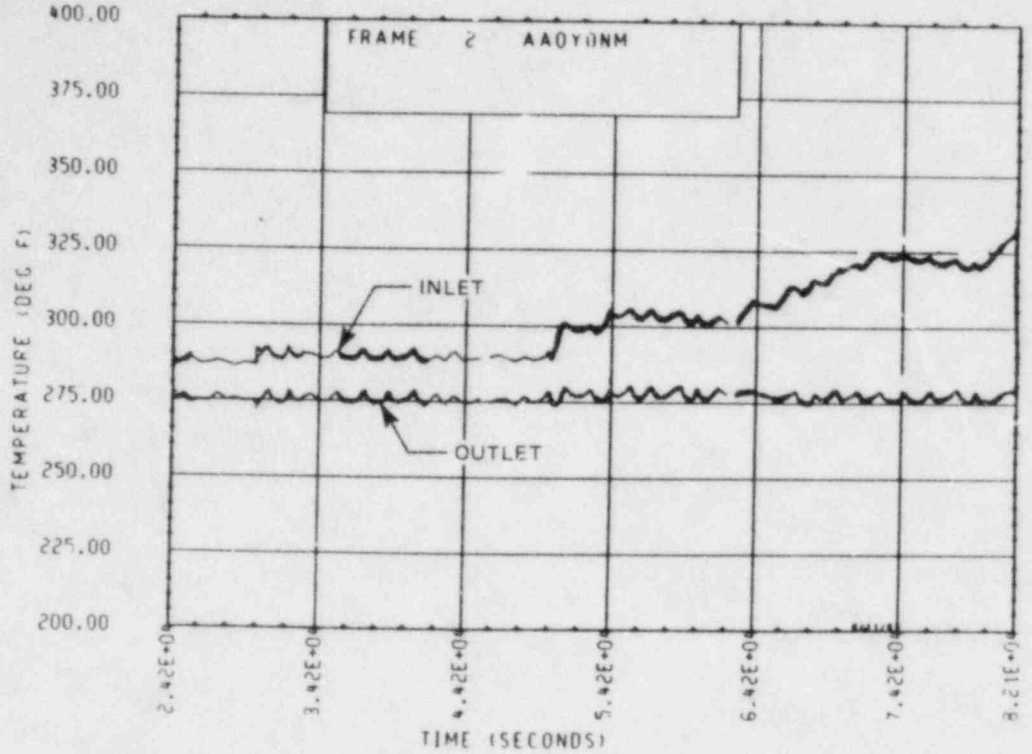

Figure A-161. Heater Rod Bundle Inlet and Outlet Temperature, Test 13

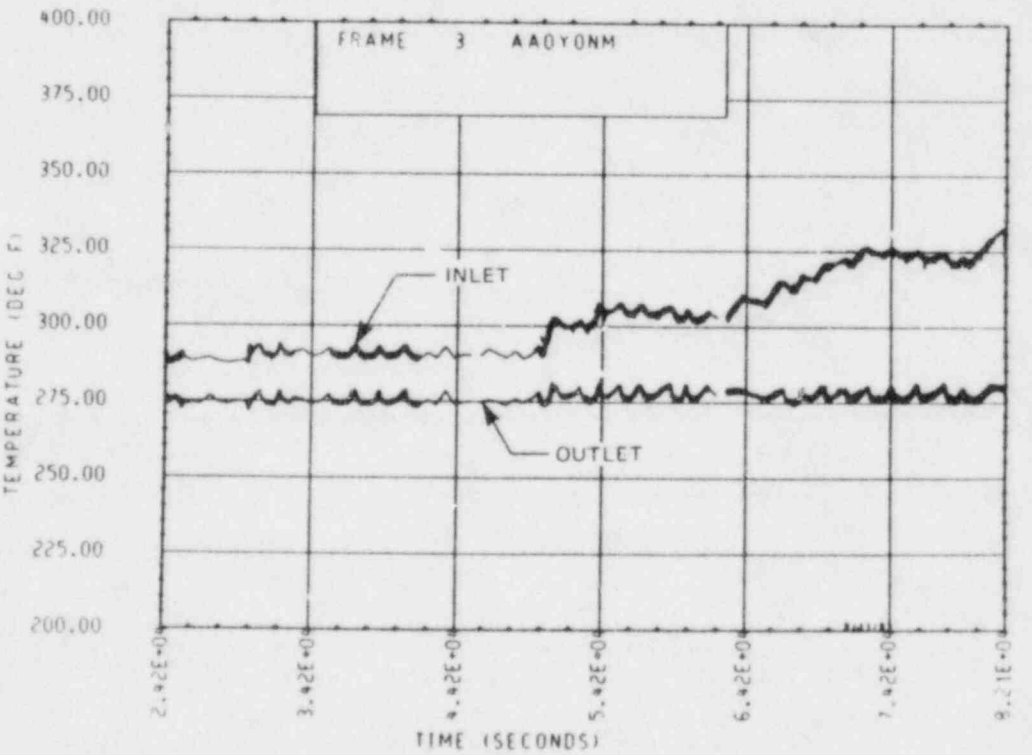

Figure A-162. Unbroken Loop Steam Generator Inlet and Outlet Temperature, Test 13

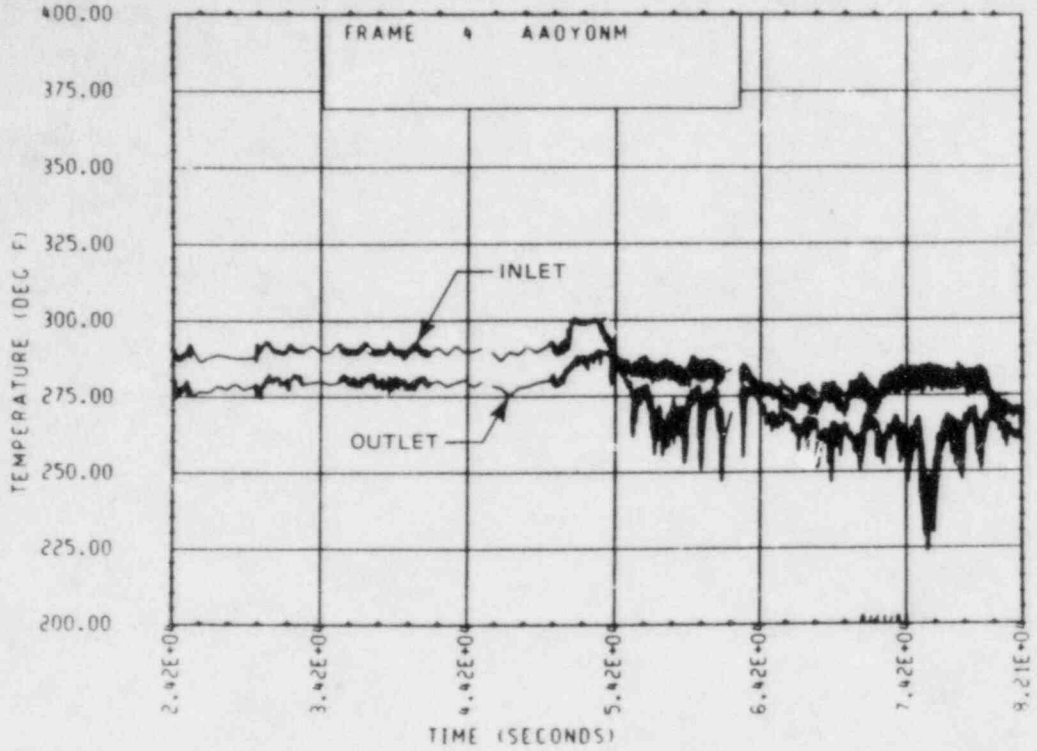

Figure A-163. Broken Loop Steam Generator Inlet and Outlet Temperature, Test 13

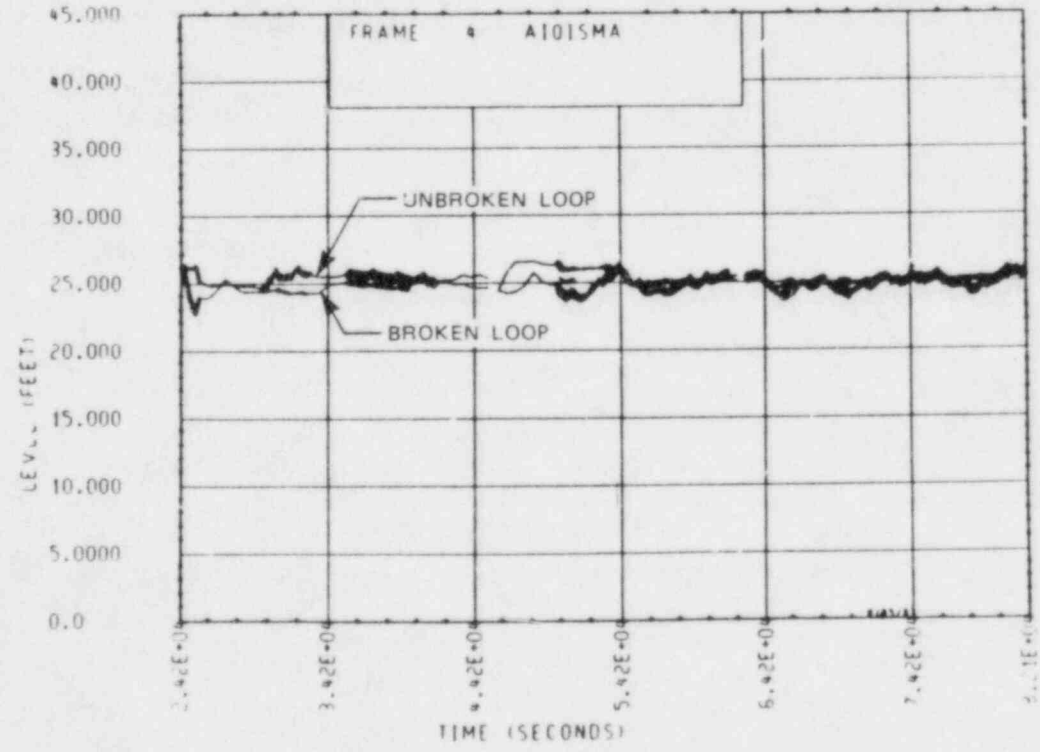

Figure A-164. Unbroken and Broken Loop Steam Generator Secondary Side Collapsed Liquid Levels, Test 13

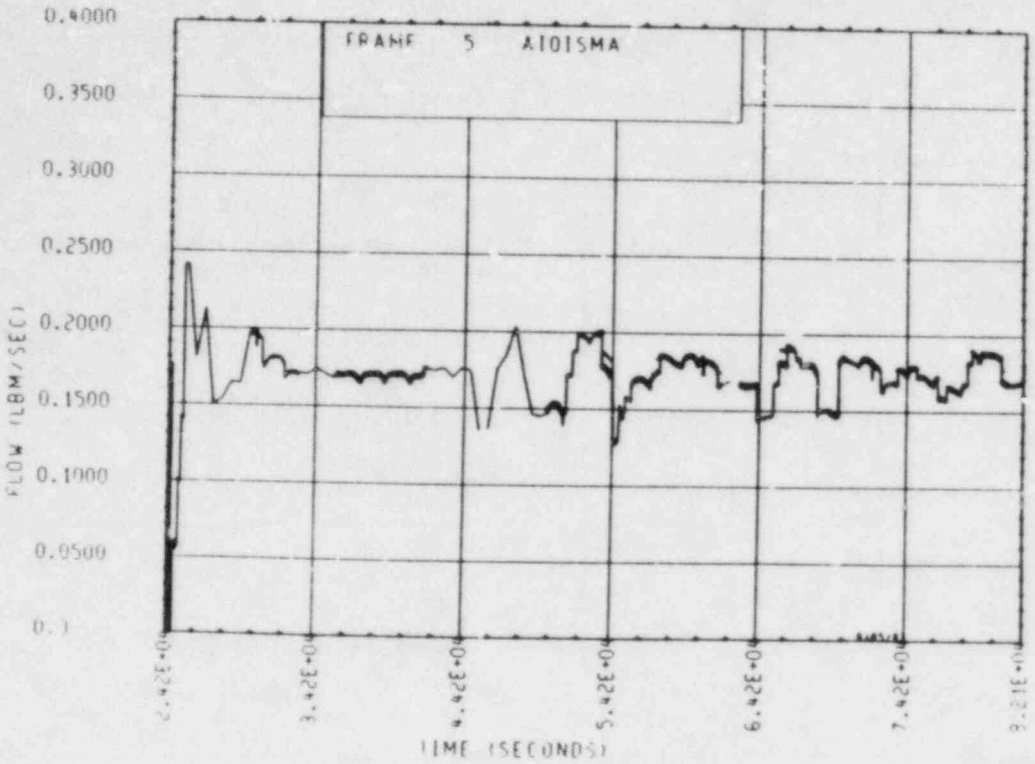

Figure A-165. Unbroken Loop Steam Generator Feedwater Mass Flow Rate, Test 13

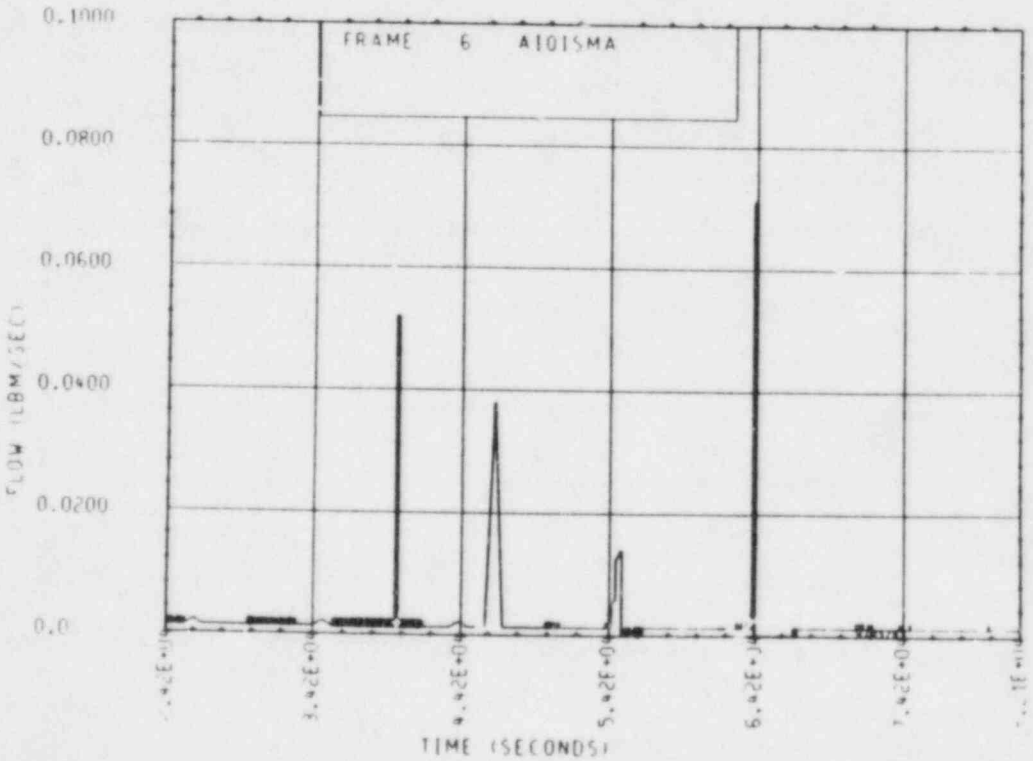

Figure A-166. Broken Loop Steam Generator Feedwater Mass Flow Rate, Test 13

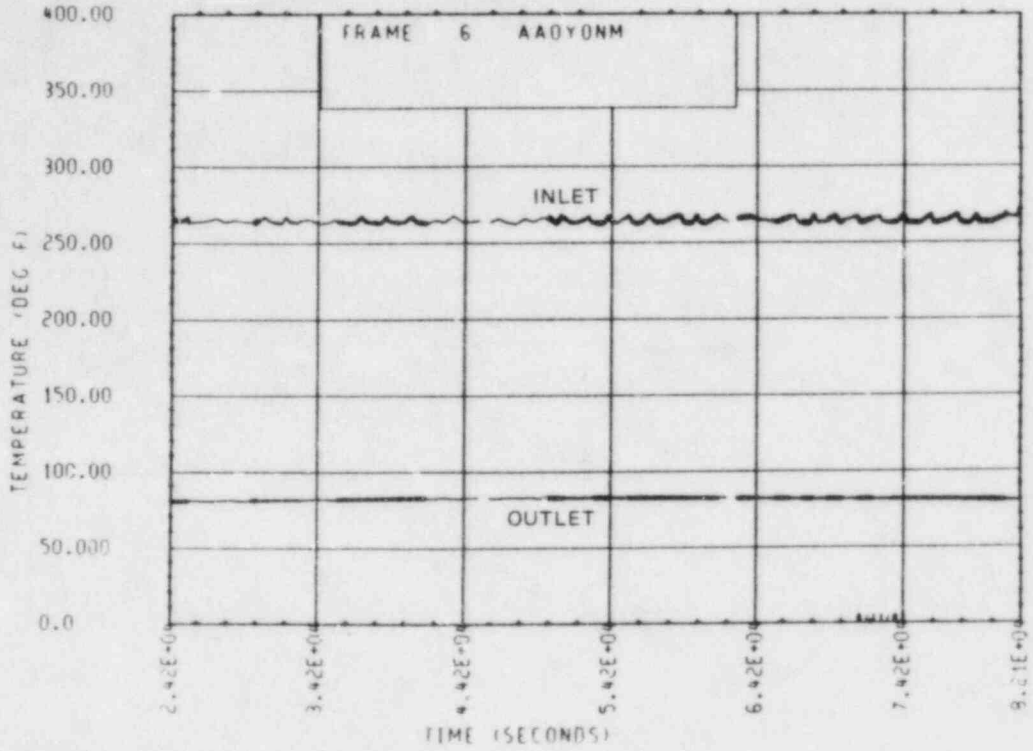

Figure A-167. Unbroken Loop Steam Generator Secondary Side Inlet and Outlet Temperature, Test 13

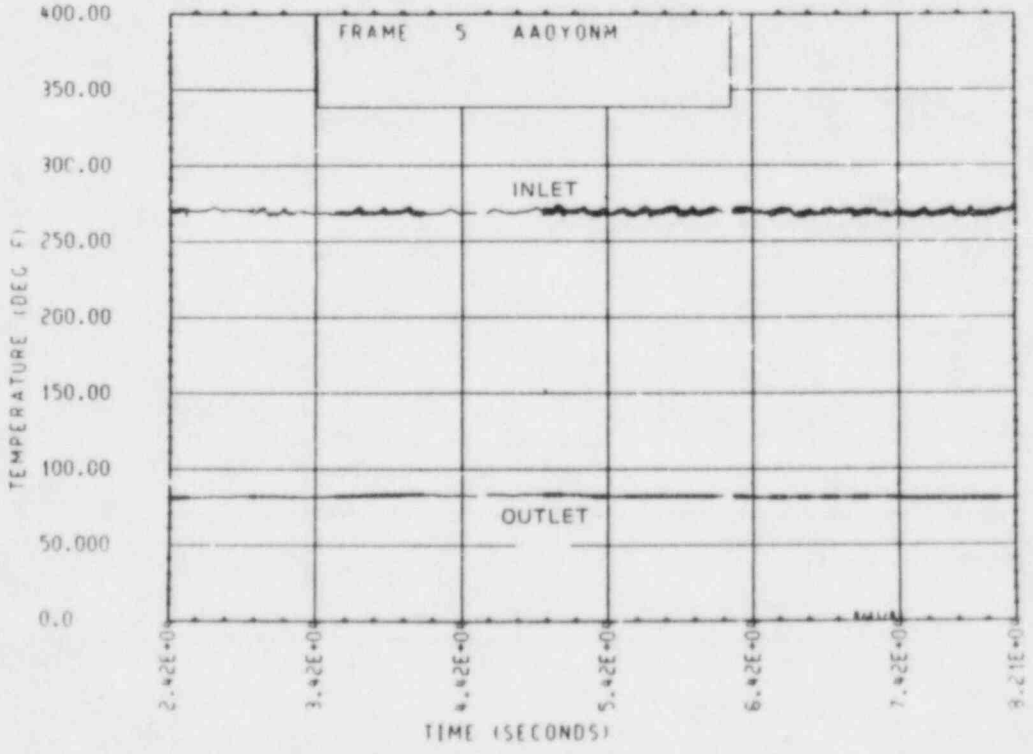

Figure A-168. Broken Loop Steam Generator Secondary Side Inlet and Outlet Temperature, Test 13

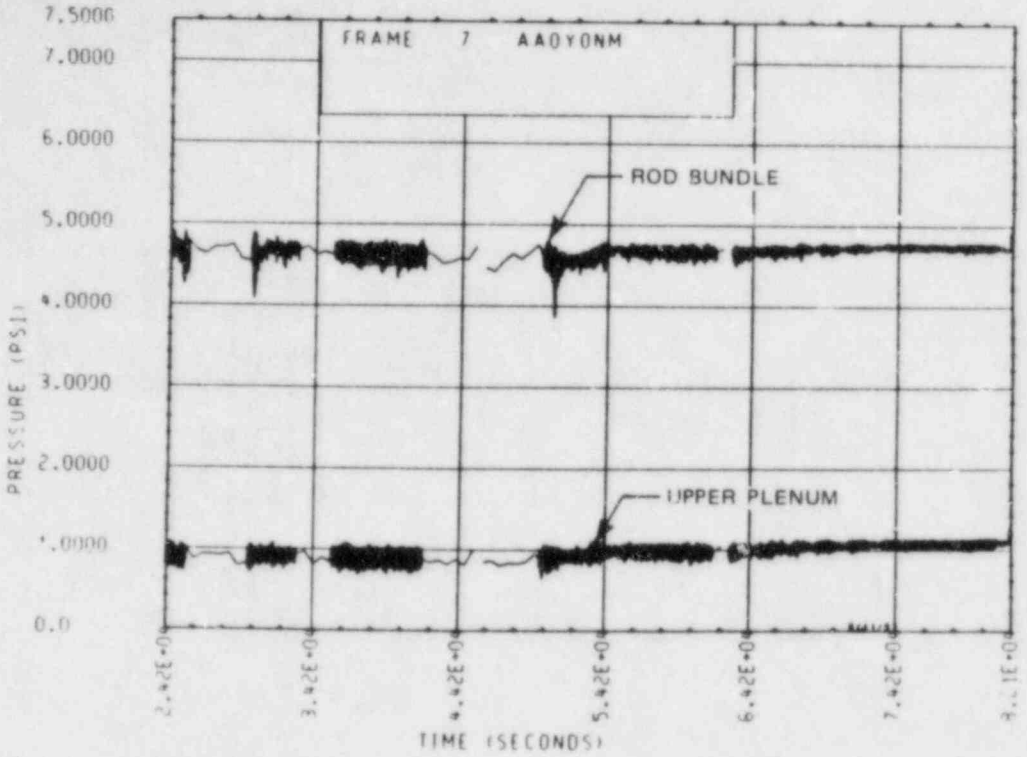

Figure A-169. Heater Rod Bundle and Upper Plenum Differential Pressure, Test 13

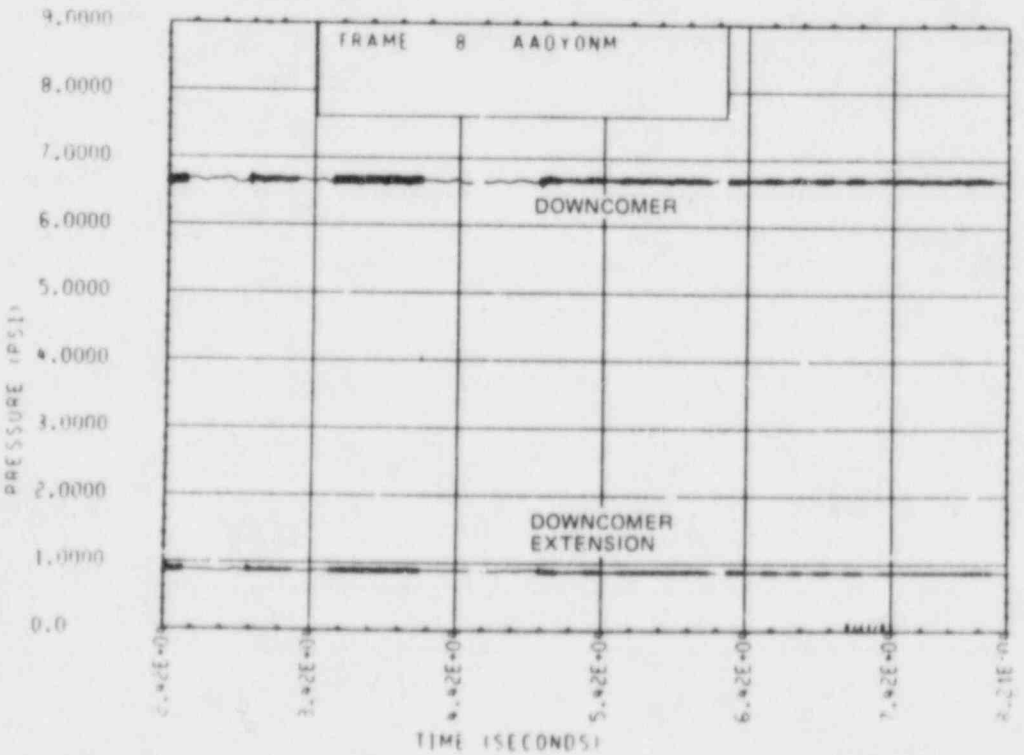

Figure A-170. Downcomer and Downcomer Extension Differential Pressure, Test 13

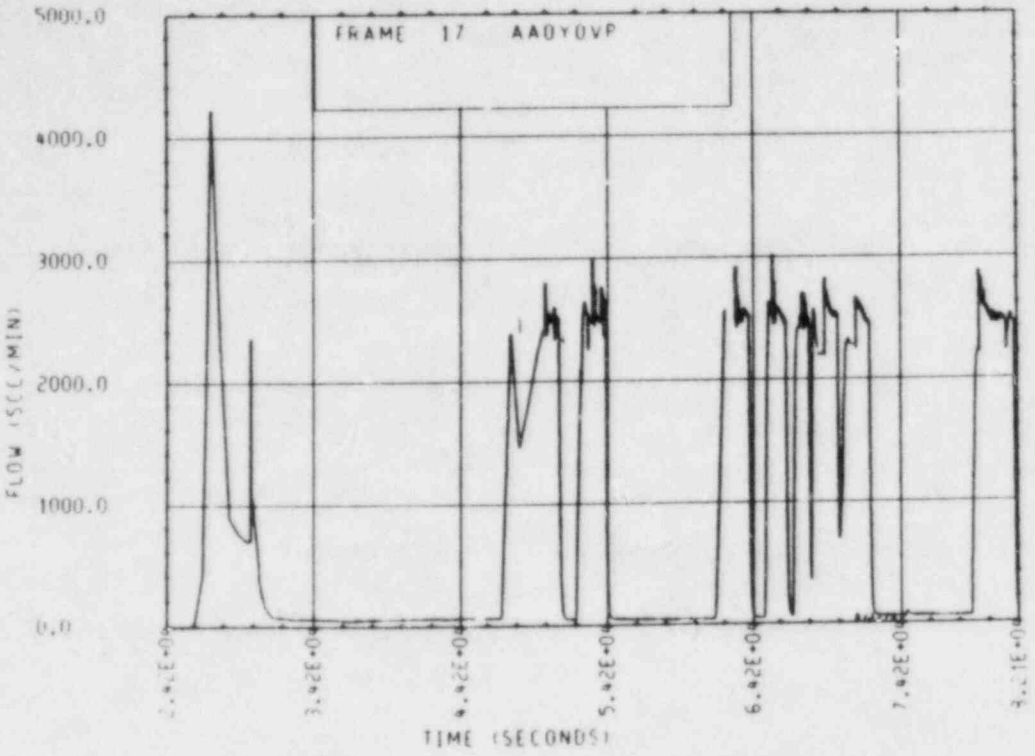

Figure A-171. Unbroken Loop Noncondensible Gas Injection Line Volumetric Flow Rate, Test 13

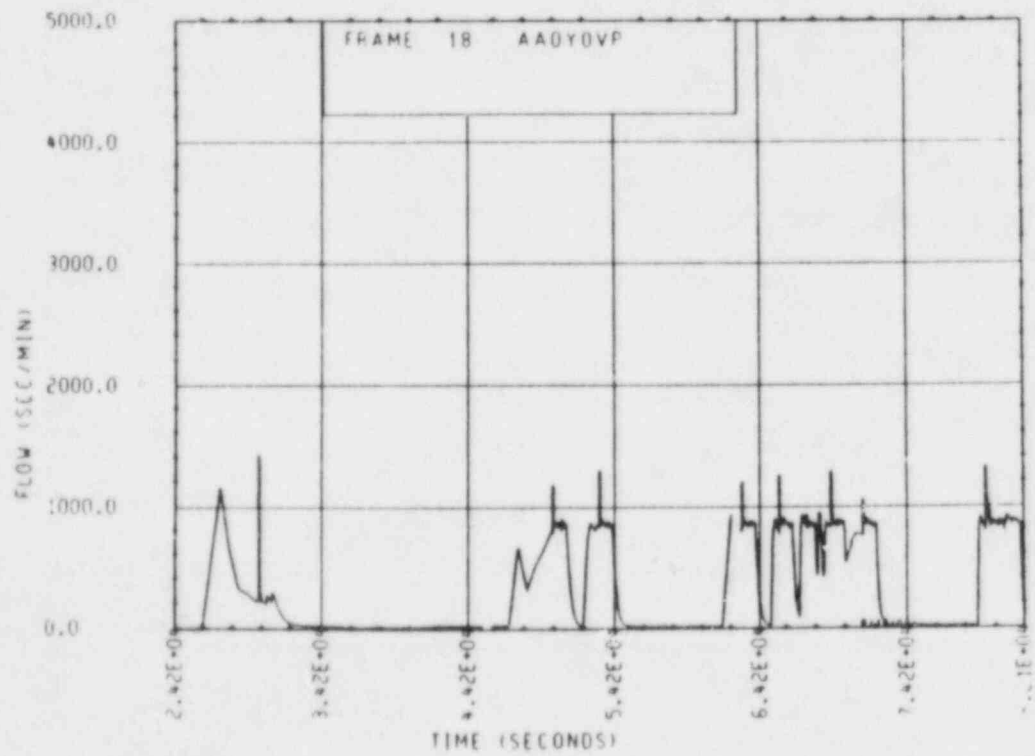

Figure A-172. Broken Loop Noncondensible Gas Injection Line Volumetric Flow Rate, Test 13

TEST 14: SINGLE-PHASE NATURAL CIRCULATION WITH MINIMUM SECONDARY SIDE HEAT SINK

Objective

To determine the minimum boiling level in the steam generator secondary sides which would maintain steady-state single-phase natural circulation

Test Procedure

The test was begun from a single-phase natural circulation mode with a nominal primary system pressure of 0.93 MPa (135 psia) and a nominal bundle power of 222 kw. The secondary side operated at a constant pressure of 0.21 MPa (30 psia) in a boiling mode with an initial collapsed liquid level of 7.62 m (25 ft) (71 percent full). The secondary side feedwater lines were valved out and the secondary side levels of both steam generators were allowed to decrease by means of boiloff. The pressurizer remained valved in to the primary system during the course of the boiloff; hence, a constant primary pressure was maintained. Boiloff was terminated when primary system natural circulation flow began to decrease. Feedwater flow was subsequently initiated to maintain secondary side collapsed liquid levels at this minimum heat sink level. After 15 minutes of steady-state operation at this minimum heat sink condition, the secondary side levels were recovered to their initial 7.62 m (25 ft) levels by injection of 140°C (220°F) water from accumulator 1. The test was terminated when the system returned to a steady-state condition.

Test Overview

Steam generator heat sink capability was sufficient to maintain steady-state single-phase natural circulation in the primary system for secondary side collapsed liquid levels as low as 4.11 m (13.5 ft) (39 percent full). As secondary side collapsed liquid levels were decreased below the 4.11 m (13.5 ft) level, the heat sink capability of the unbroken loop steam generator became sufficiently degraded to cause a decrease in mass flow through the

unbroken loop. Similar degradation of heat sink behavior was not observed in the broken loop, despite the fact that the broken loop secondary was allowed to boil off to the 7.62 m (6 ft) level (17.1 percent full). No explanation is offered at this time as to why the two steam generators acted so differently.

The unbroken loop mass flow decrease was of course echoed by a decrease in mass flow through the rod bundle. The decrease in mass flow through the rod bundle in turn caused bundle exit temperatures to increase. Higher exit temperatures coupled with a degraded unbroken loop heat sink caused the entire loop to heat up.

The steam leaving the secondary side became superheated as the primary system heated up. This indicates that heat transfer between the primary and secondary was not exclusively limited to those portions of the tube bundle below the secondary side collapsed liquid level.

TEST SCHEDULE
TEST 14

Time (sec)	Event
0	Computer on
40.2	Power to 90 kw; primary side operating in a forced circulation mode with pumps on
1164	Powr to 150 kw
1863	Power to 222 kw
6773	Pumps off; primary side transition into a natural circulation mode
10648	Secondary side feedwater shut off; began secondary side boiloff
15123	Secondary side levels had decreased enough to cause a decrease in primary side flow and a subsequent increase in temperature.
16383	Beginning of steady-state run at the minimum heat sink condition; secondary side operating with a collapsed liquid level of 1.83 m (6 ft)
17343	End of steady-state condition

Time (sec)	Event
17403	Beginning of secondary side recovery to a collapsed liquid level of 7.62 m (25 ft); injecting water into both steam generators from accumulator 2.
18063	Broken loop steam generator level reached 7.62 m (25 ft).
18123	Unbroken loop steam generator level reached 7.62 m (25 ft).
19503	End of test 14

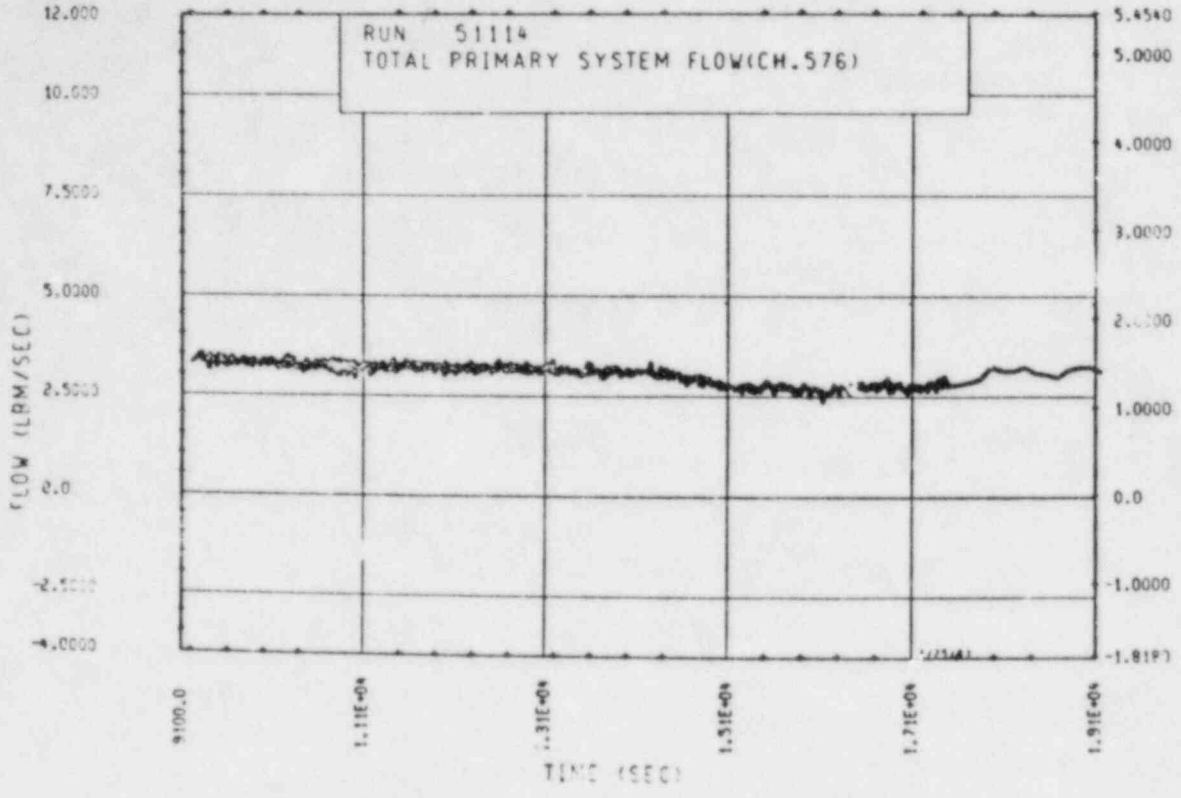

Figure A-173. Mass Flow Rate Through Rod Bundle, Test 14

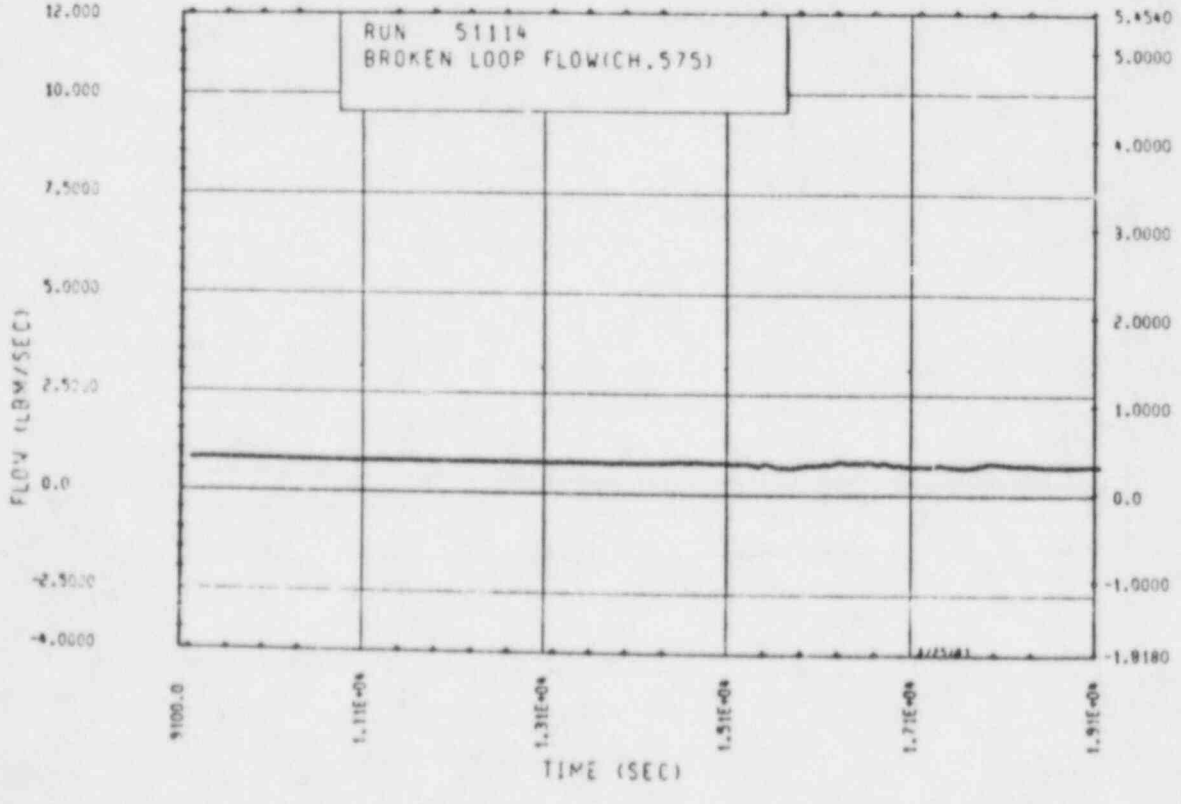

Figure A-174. Mass Flow Rate Through Broken Loop, Test 14

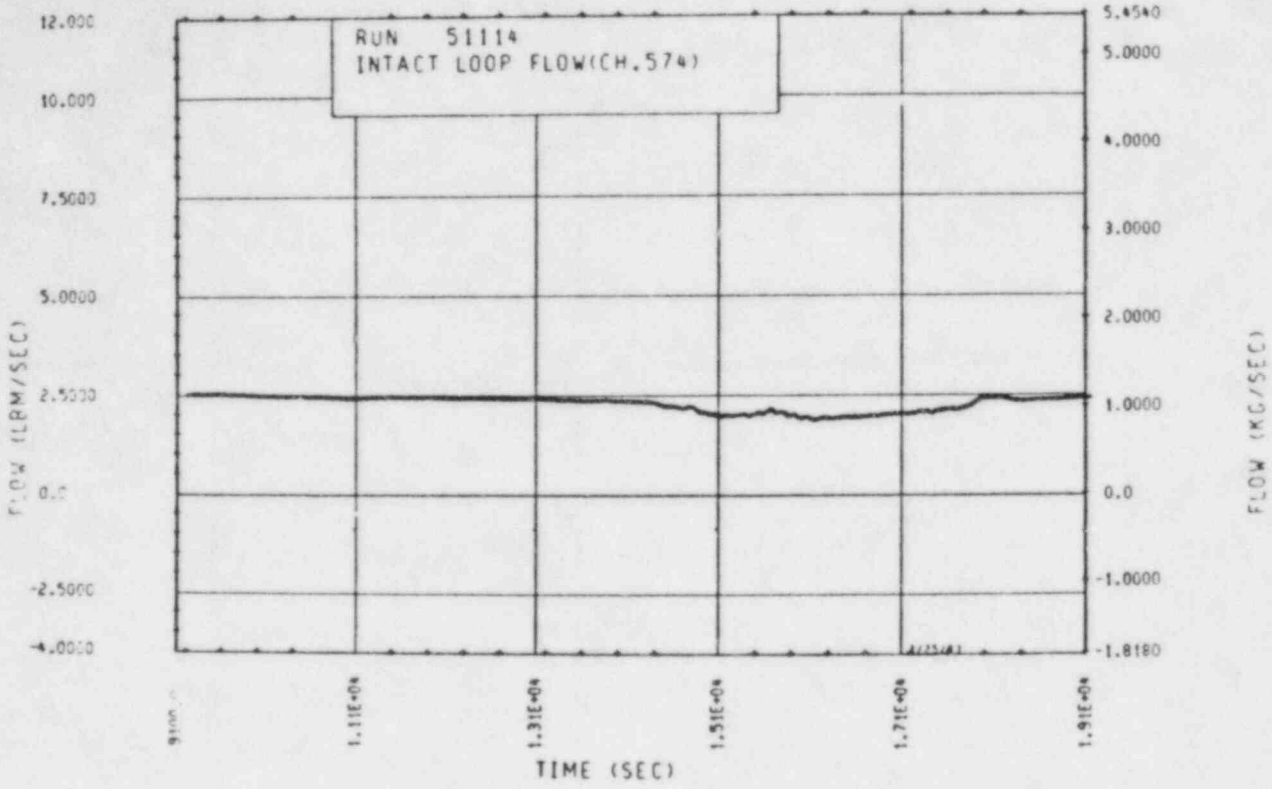

Figure A-175. Mass Flow Rate Through Unbroken Loop, Test 14

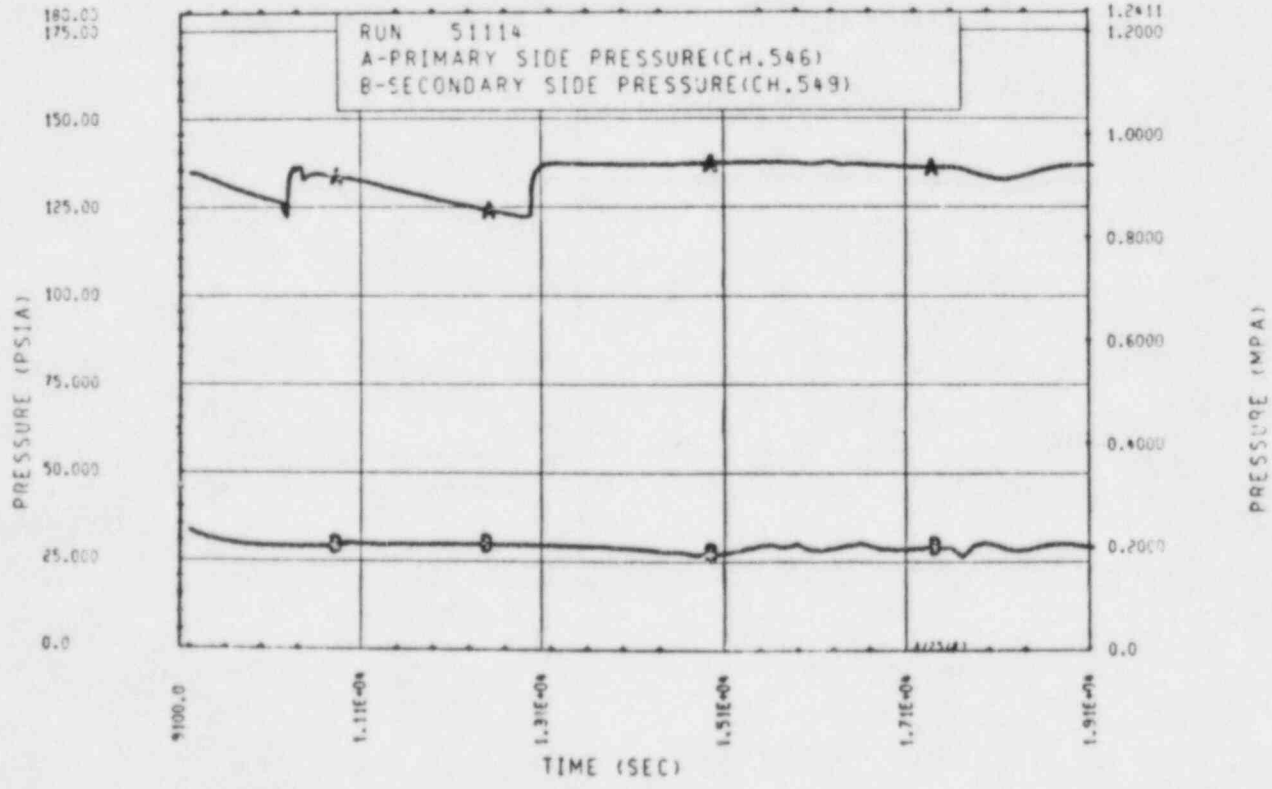

Figure A-176. Primary and Secondary System Pressure, Test 14

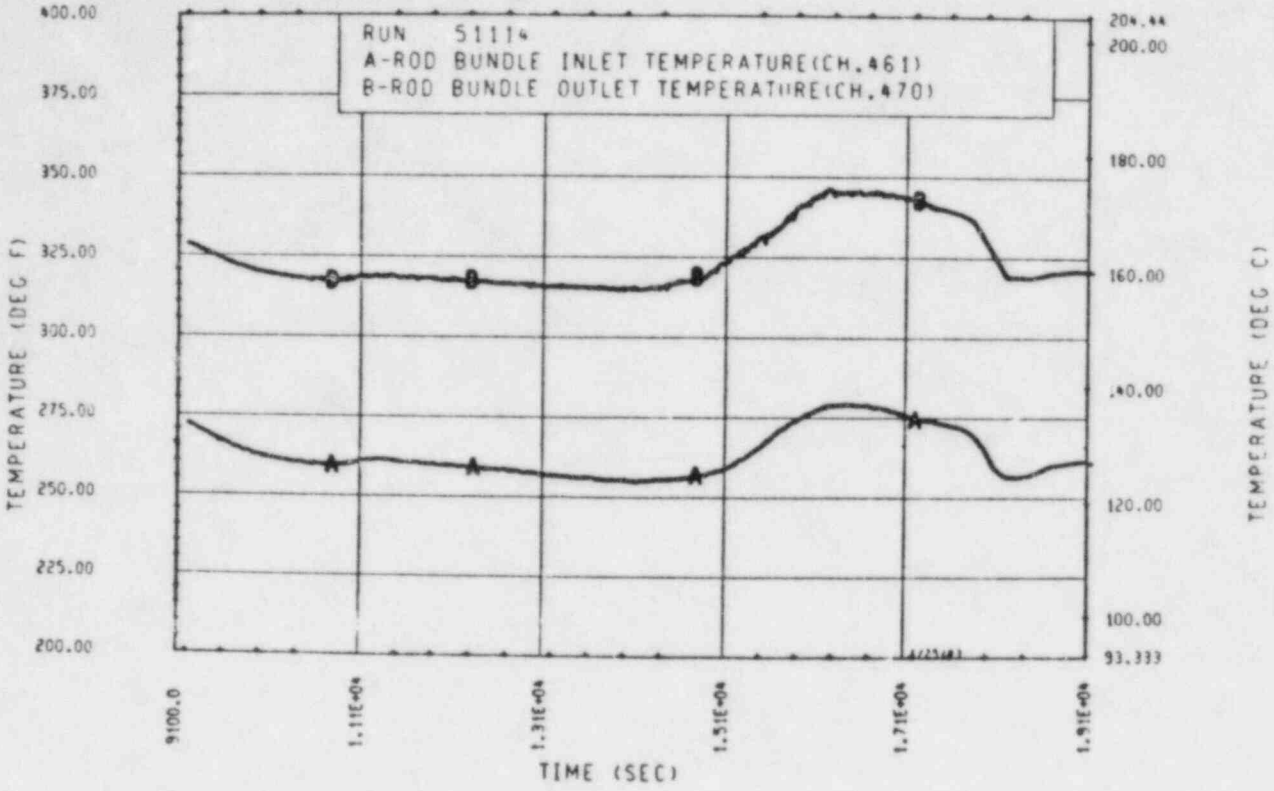

Figure A-177. Heater Rod Bundle Inlet and Outlet Temperature, Test 14

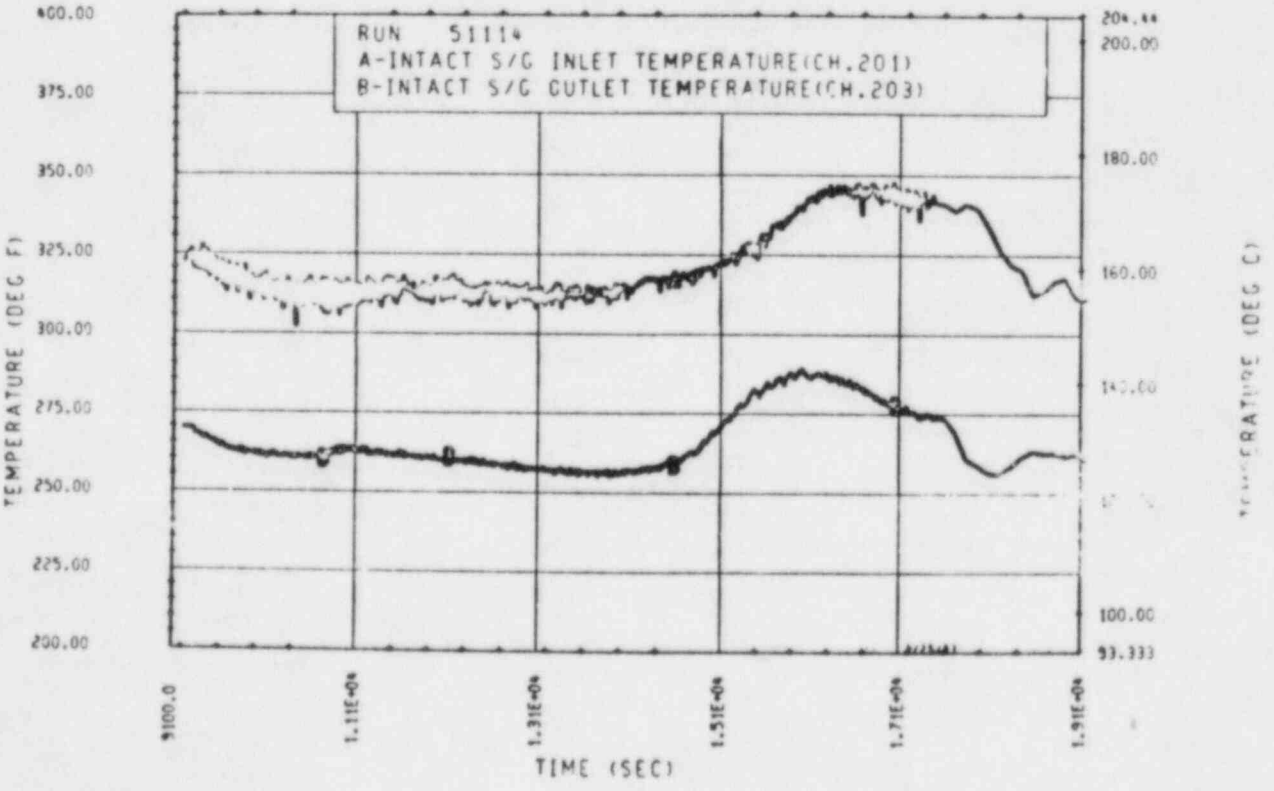

Figure A-178. Unbroken Loop Steam Generator Inlet and Outlet Temperature, Test 14

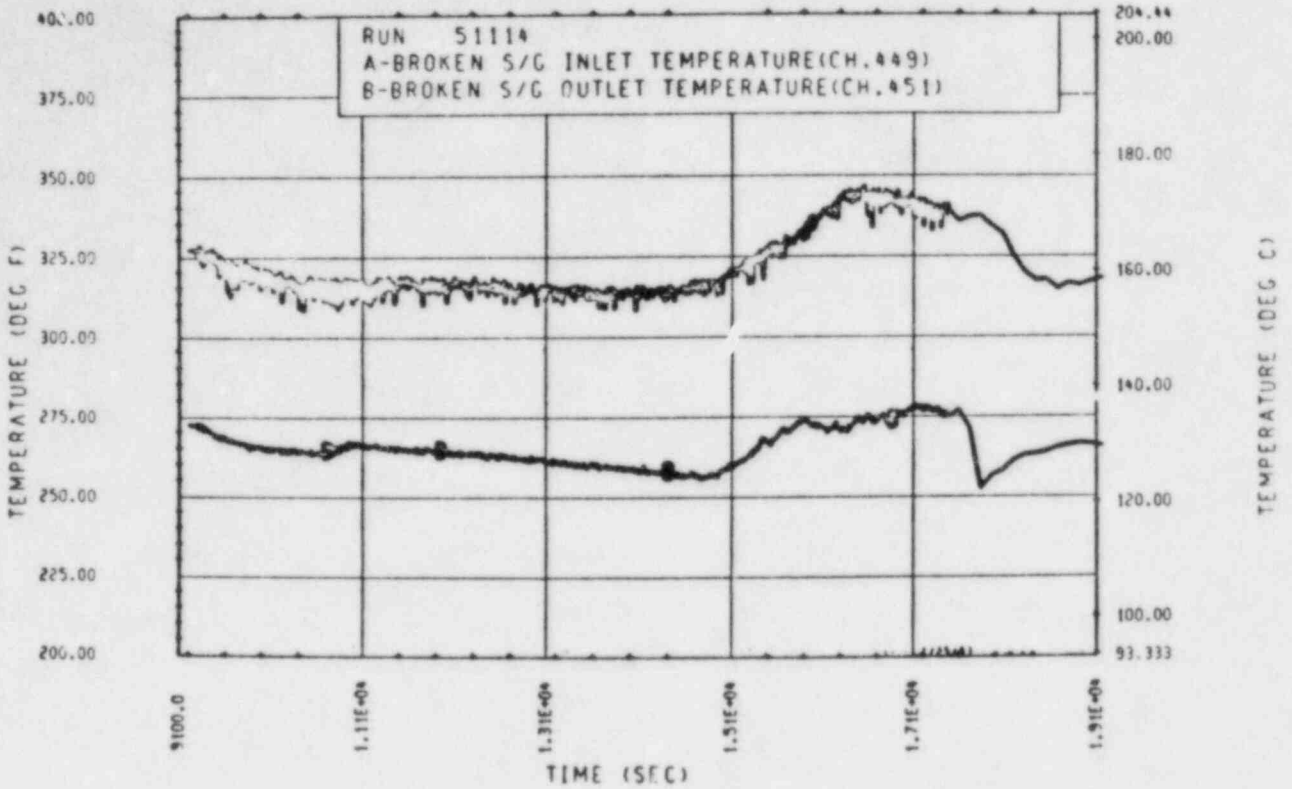

Figure A-179. Broken Loop Steam Generator Inlet and Outlet Temperature, Test 14

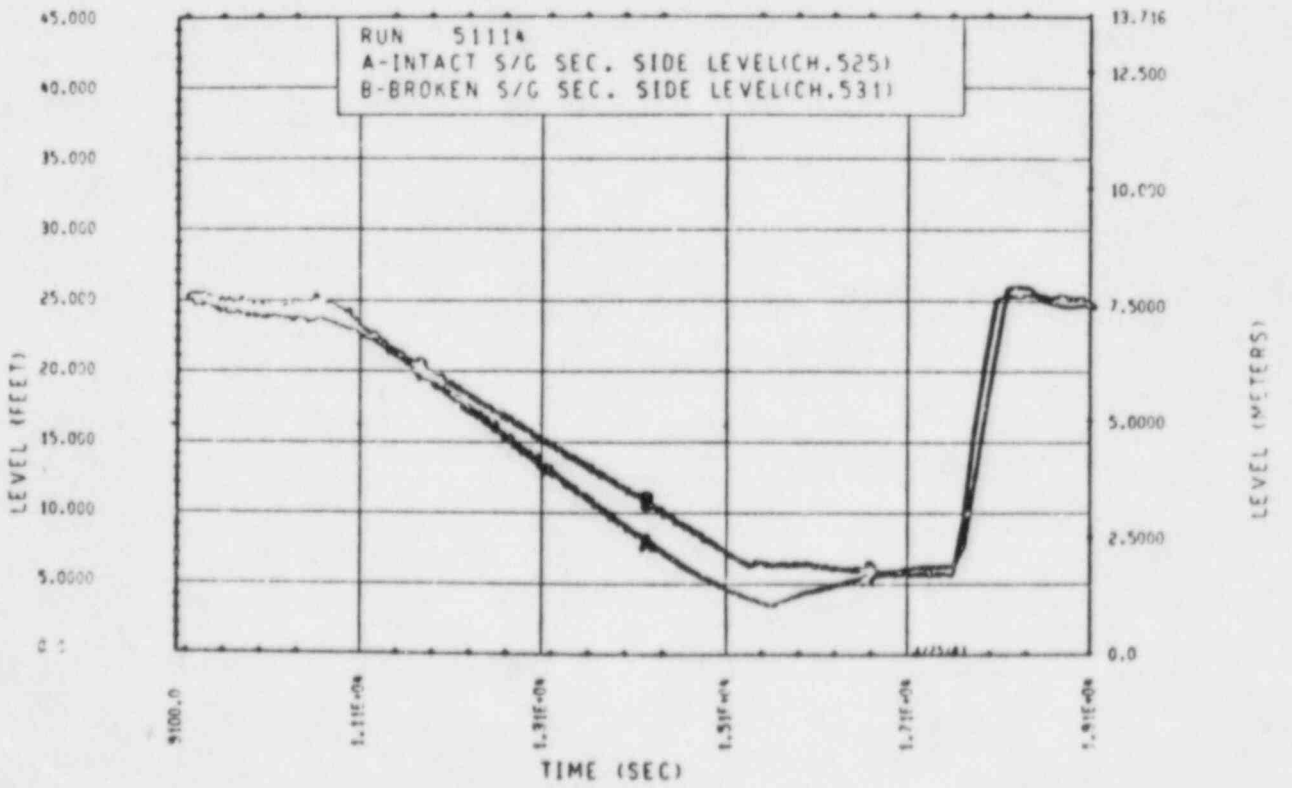

Figure A-180. Unbroken and Broken Loop Steam Generator Secondary Side Collapsed Liquid Levels, Test 14

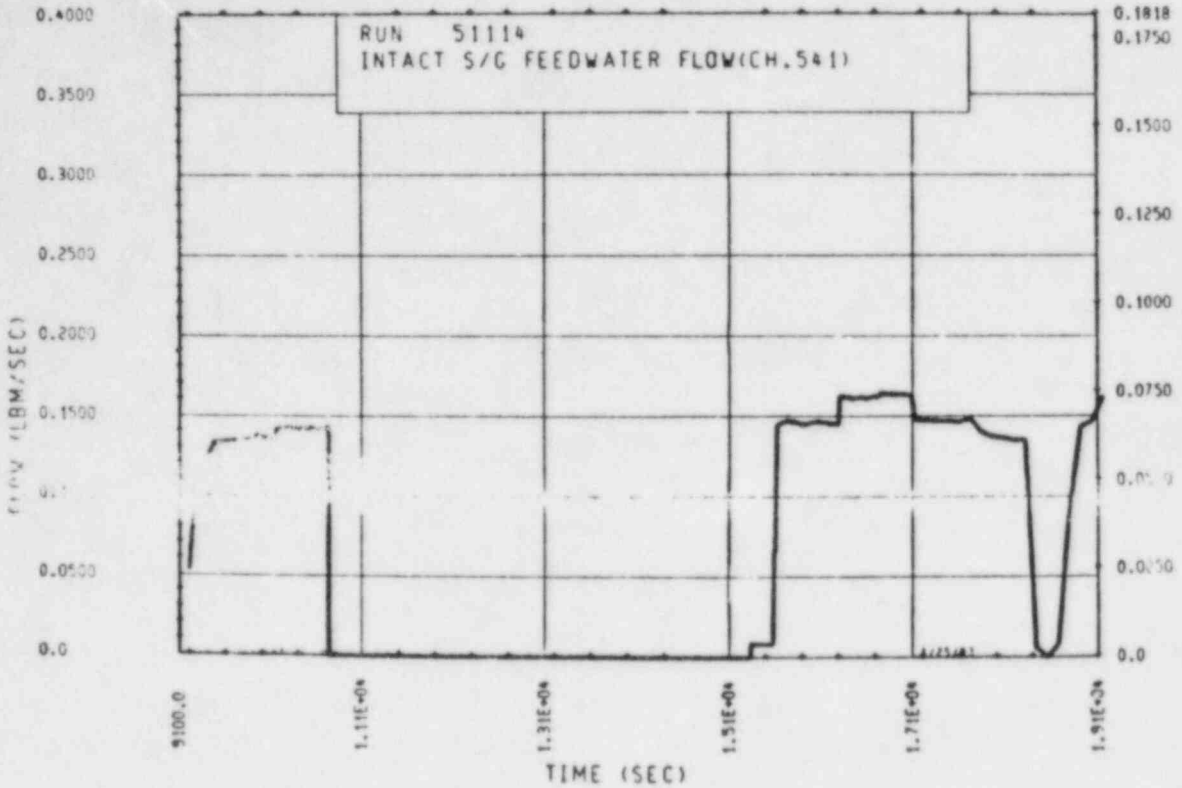

Figure A-181. Unbroken Loop Steam Generator Feedwater Mass Flow Rate, Test 14

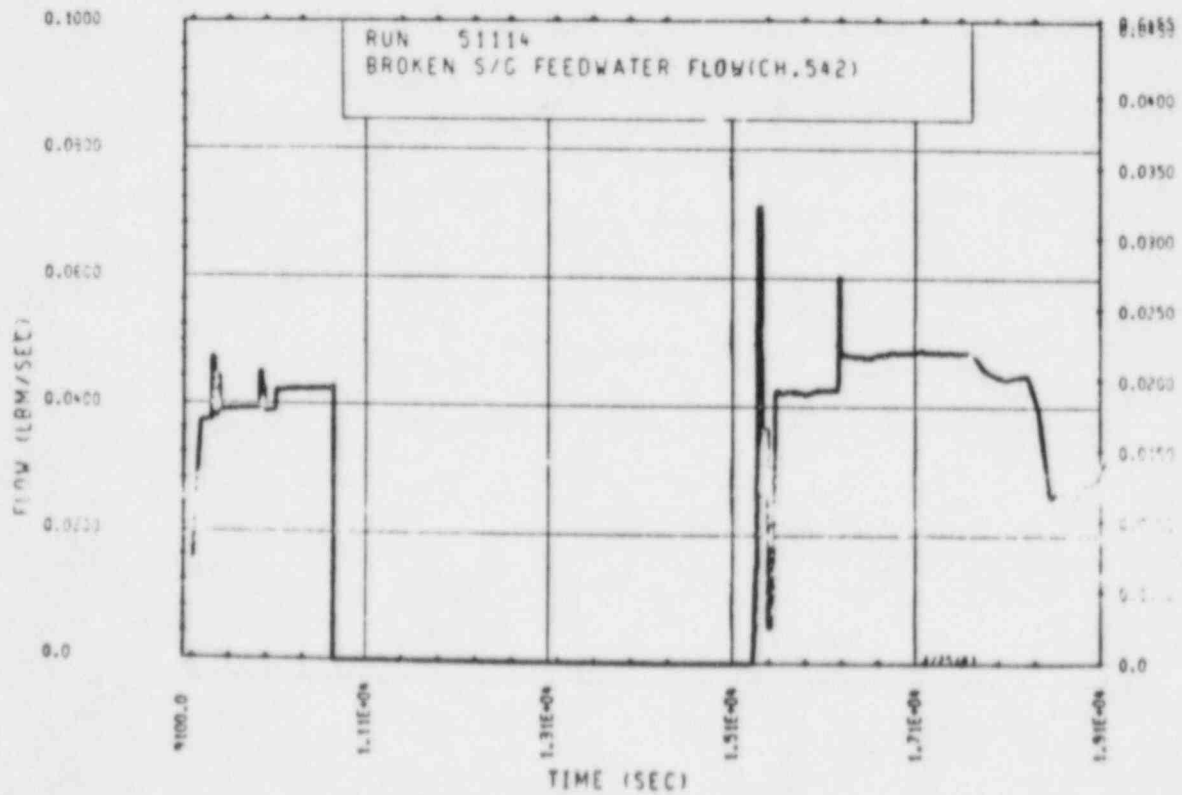

Figure A-182. Broken Loop Steam Generator Feedwater Mass Flow Rate, Test 14

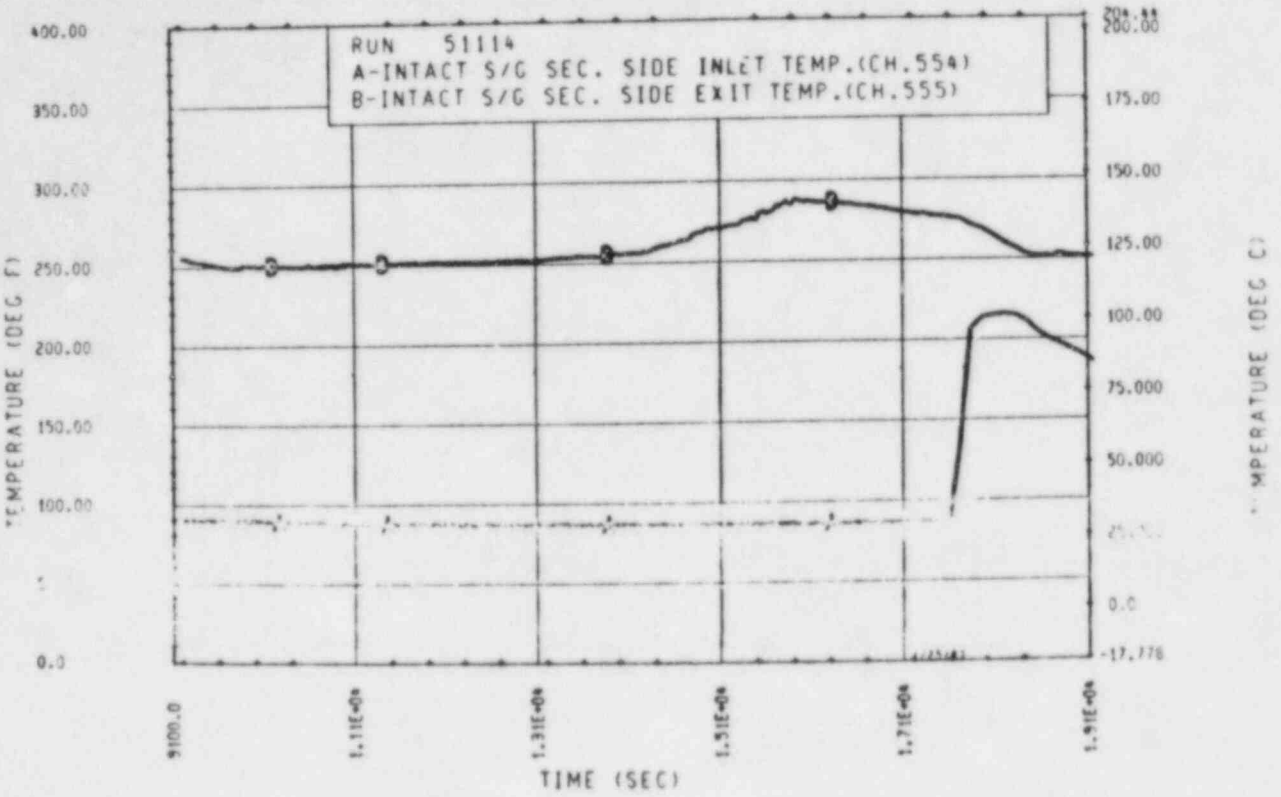

Figure A-183. Unbroken Loop Steam Generator Secondary Side Inlet and Outlet Temperature, Test 14

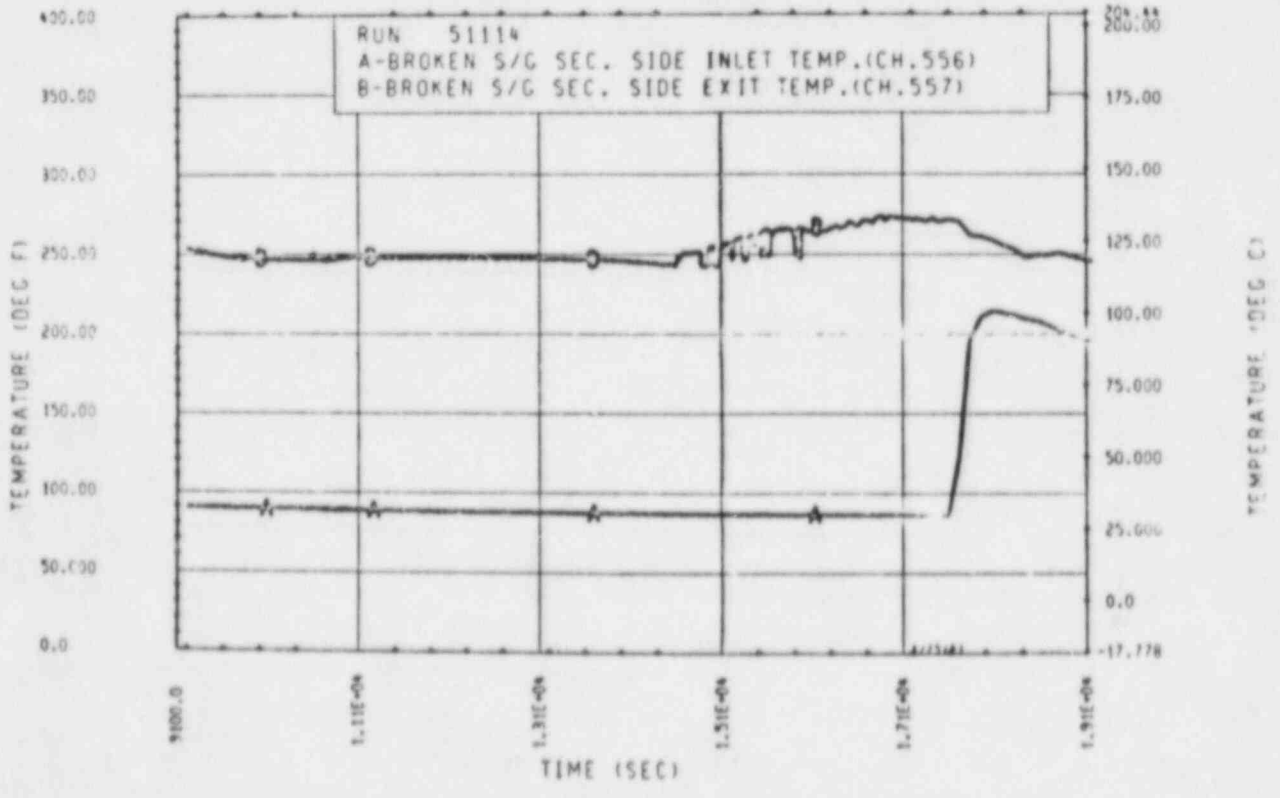

Figure A-184. Broken Loop Steam Generator Secondary Side Inlet and Outlet Temperature, Test 14

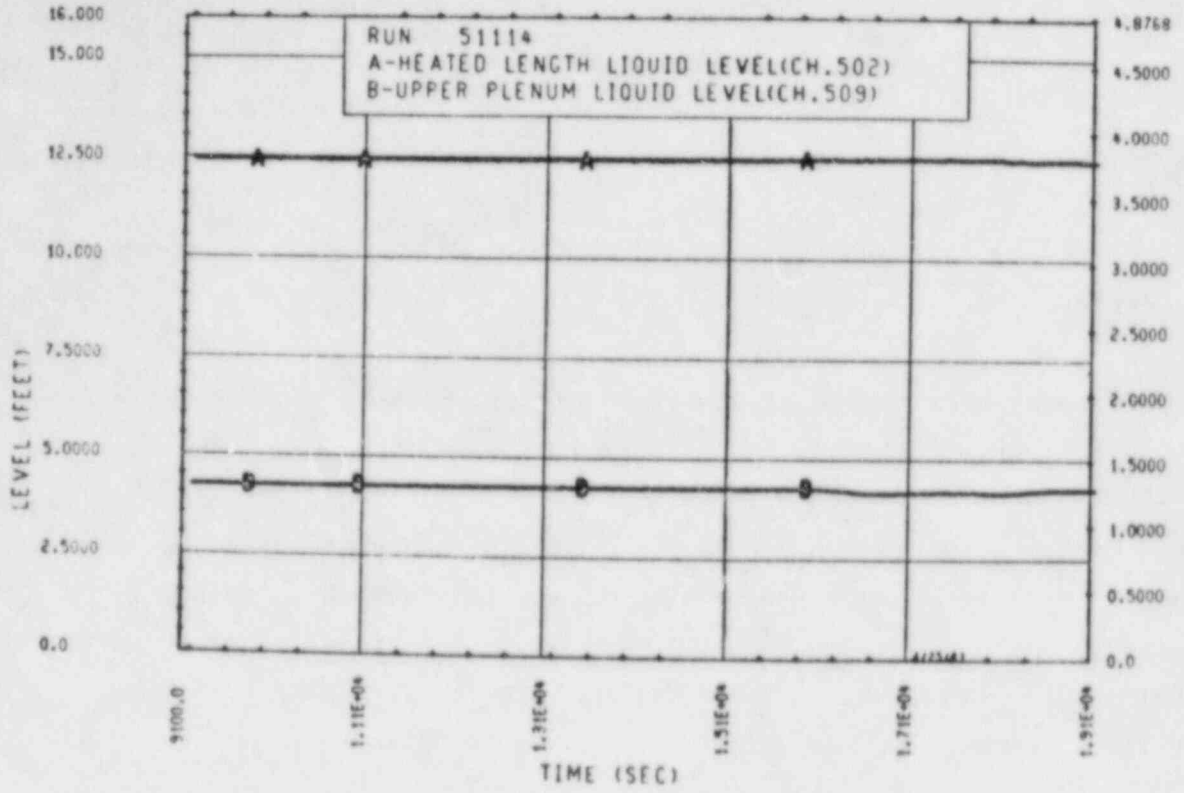

Figure A-185. Heated Length and Upper Plenum Liquid Levels, Test 14

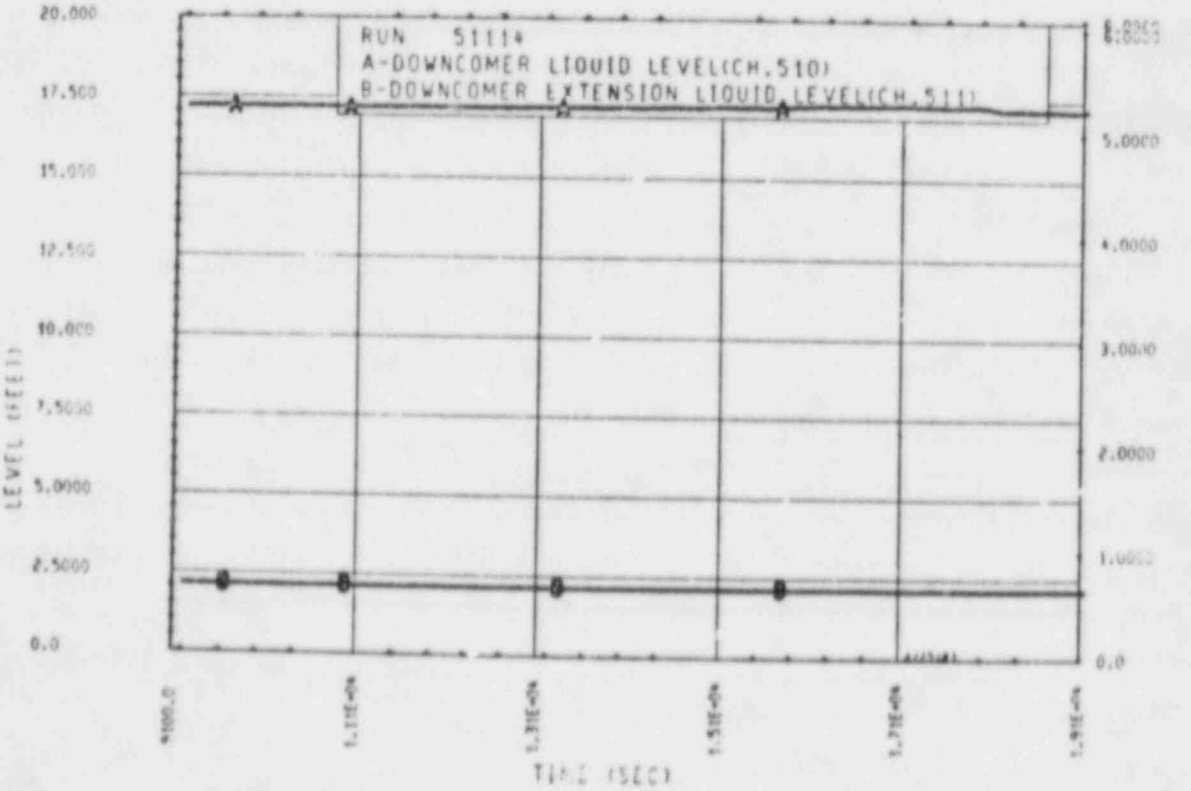

Figure A-186. Downcomer and Downcomer Extension Liquid Levels, Test 14

TEST 15: REFLUX CONDENSATION NONCONDENSIBLE GAS EFFECTS

Objective

To determine the effect of noncondensible gas on the reflux condensation cooling mode

Test Procedure:

The test was begun from a quasi-steady-state reflux condensation mode with a nominal bundle power of 222 kw. The primary system was operated with the pressurizer valved out and a reduced mass inventory consistent with previously established reflux condensation conditions. The secondary side was operated in a constant level feed-and-bleed boiling mode with a nominal pressure of 0.28 MPa (40 psia). The secondary side level was maintained at 7.62 m (25 ft) (71 percent full). Helium was proportionally injected into both the unbroken and the broken loop hot legs in a series of three injections.

Test Overview

Test 15 was designed to examine the effect of noncondensible gas on the reflux condensation mode of natural circulation. Prior to the initiation of noncondensible gas injections, the primary system was brought to a quasi-steady-state reflux condensation condition by reducing the primary system mass inventory to approximately 25.1 percent of its original single-phase liquid-solid condition. In this preinjection condition, the primary system exhibited periodic loop seal venting behavior consistent with that previously discussed in section 5. During the course of the test a total of 44.9 moles (9.89×10^{-2} lbm-mole) of helium were injected into the primary system by means of a series of three injections. As helium gas was introduced into the primary system, it was swept to the downhill side of the steam generators and loop seals, where it accumulated and reached thermal equilibrium with the secondary side. The pockets of helium gas on the downhill side of the steam generators blocked off previously available heat transfer area and forced more of the condensation process to occur on the uphill side of the steam generator

U-tubes. This same phenomenon was observed by Hein, et al.[1] As more helium was introduced into the primary system, these helium pockets blanketed the downhill side of the U-tubes and spread to the uphill side, removing more heat transfer area. Fluid thermocouple readings indicate that, by the end of the test, at least one pocket of helium in the unbroken loop steam generator had blanketed as much as 99 percent of a single U-tube. The condensation process now occurred exclusively on the uphill sides of the U-tubes. The primary system responded to this helium gas mass addition and subsequent degradation of heat sink by increasing its pressure from a preinjection condition of 0.31 to 0.52 MPa (45 to 75 psi) at test termination.

The presence of noncondensible helium gas affected more than just the primary-to-secondary heat transfer. It also affected the periodic loop seal venting phenomenon. Prior to the introduction of helium into the primary system, the unbroken loop seal vented steam into the cold leg every 18 to 28 minutes. This venting behavior was primarily driven by the condensation of steam trapped in the cold leg. This cold leg steam cavity was isolated from the remaining portion of the primary system by the liquid seals formed in the loop seals and downcomer-core regions. As the cold leg steam condensed, the differential pressure across these liquid seals increased. The liquid in these seals responded to this increase in differential pressure by redistributing liquid in a manner identical to that observed in a U-tube manometer. The loop seals moved water from the descending leg to the ascending leg. Similarly, in the seal formed by the core-downcomer region, liquid was moved from the core to the downcomer. Hence, as the ΔP increased, the liquid inventory in the core/upper plenum decreased and the potential for a degraded core cooling situation increased. The ΔP increase, and hence the decrease in core liquid inventory, was limited, however, by the maximum gravitational head that could be developed in the loop seals. This maximum gravitational

1. Hein, D., et al., "The Distribution of Gas in a U-Tube Heat Exchanger and Its Influence on the Condensation Process," The 7th International Heat Transfer Conference, Munich, Germany, September 6-10, 1982.

head occurred when the descending leg of the loop seal was liquid solid and the descending leg liquid level was coincident with the top of the loop seal horizontal pipe run. Any further ΔP increase pushed the descending leg liquid level below the top of the loop seal horizontal pipe run, allowing steam to vent through the loop seal and up into the cold leg. When this occurred, the cold leg was resupplied with fresh steam and the ΔP between the cold leg steam cavity and the upper plenum went to zero. The liquid seal formed by the downcomer and core responded to this ΔP decrease by moving water from the downcomer to the core. Similarly, the loop seals responded by moving liquid from the ascending legs to the descending legs. With the subsequent core liquid level recovery, any potential threat for a degraded core cooling condition vanished. Hence, core liquid level depression was limited to an elevation in the vicinity of the bottoms of the loop seals. The cycle, however, would begin again as the fresh steam in the cold leg steam cavity condensed as a result of ambient heat losses.

The injection of helium gas into the primary system interrupted this periodic loop seal venting behavior. Once helium gas was introduced into the primary system, any subsequent loop seal vents would vent helium gas into the cold leg cavity. The noncondensible nature of the helium gas mitigated the cold leg cavity condensation phenomenon, which previously acted as the driving force behind the periodic loop seal venting behavior. After a few vents during the first helium gas injection, the cold leg cavity was more than likely completely filled with noncondensible gas. Any subsequent pressure decrease in the cavity was the result of very slow cooling of the noncondensible gas by means of ambient heat loss. With the absence of any cold leg cavity condensation, the period associated with the loop seal venting phenomenon increased from minutes to hours.

In addition to changing the period of the loop seal venting phenomenon, the presence of helium gas caused periodic flooding on the uphill side of both the broken and unbroken loop steam generator U-tubes. This flooding behavior was the result of noncondensible gas blanketing the downhill sides of the U-tubes and forcing the condensation process to occur primarily on the uphill sides.

Consequently, the thickness of the condensate film increased on the uphill side and counter-current steam flow restricted the fallback of this film. Hence, the tubes flooded. As a result of the hydrostatic head associated with liquid holdup in the flooding U-tubes, the pressure drop across the affected steam generator increased. This additional pressure drop in the loop due to U-tube flooding significantly amplified the ΔP that already existed across the core-downcomer region. This ΔP was the result of the cooling of noncondensible vapor trapped in the cold leg, in conjunction with pressurization in the upper plenum due to degraded steam generator heat transfer. The core-downcomer liquid seal responded to this amplified ΔP by moving liquid inventory from the core to the downcomer. Consequently, the core's collapsed liquid level decreased beyond a level coincident with the bottom of the loop seals. It did so as a result of the restriction of the reflux condensation flow, as well as the redistribution of liquid inventory from the core to the downcomer.

In conclusion, when the flooding of U-tubes occurred in conjunction with an already-in-progress core liquid level depression, the extent of the core liquid level depression was no longer limited to a level coincident with the bottom of the loop seals. The core liquid level depression, however, recovered only if and when a loop seal vented.

During the course of the test, this flooding-enhanced core liquid level depression occurred four times. Each event was signaled by an increased steam generator plenum-to-plenum ΔP (indicative of uphill side liquid holdup) coincident with a core liquid level depression. The first two depressions occurred during the first helium injection and were minor in nature. The core liquid level depressions for both of these early events were terminated in a matter of seconds by a loop seal vent. These depressions reached elevations within the vicinity of the bottom of the loop seals. The third depression occurred during the second helium injection and was much more significant in its depth and duration. It penetrated to an elevation 0.30 to 0.61 m (1 to 2 ft) below the bottom of the loop seals and lasted for a period of approximately 15 minutes. The core liquid level depression was terminated and the level recovered with a loop seal vent. The fourth and final core liquid

level depression occurred during the third helium injection. This depression was severe enough to create a degraded core cooling situation, which consequently terminated the test as a result of a heater rod overtemperature signal [heater rod temperature in excess of 399°C (750°F)].

It is interesting to note that the first three core liquid level depressions discussed above were triggered by flooding in the unbroken loop steam generator. The broken loop steam generator did not exhibit any flooding behavior during the actual depressions. Upon loop seal venting and core recovery, the unbroken loop steam generator unflooded and the broken loop immediately began to flood. No explanation is offered for this flip-flop flooding behavior between the two steam generators. The fourth and final core liquid level depression, however, was triggered by flooding in the broken loop steam generator; the unbroken loop steam generator exhibited no such flooding behavior.

TEST SCHEDULE

TEST 15

Time (sec)	Event
0	Computer on
1959	Power to 222 kw while in forced circulation
7419	Pump off; began single-phase natural circulation
23199	Valved out accumulator 1 (pressurizer) and started continuously draining mass from the primary system (until reflux mode of natural circulation achieved)
27759	Valved in weir meters 569, 571, 572, 573
28359	499 kg (1100 lbm) drained from the primary; continuous draining stopped
28959	Began 18 kg (40 lbm) drain from primary
29079	Ended 18 kg (40 lbm) drain; 517 kg (1140 lbm) drained thus far from the primary
29259	Began 18 kg (40 lbm) drain from primary
29439	Ended 18 kg (40 lbm) drain; (535 kg (1180 lbm) drained thus far from primary
30999	Began 18 kg (40 lbm) drain from primary
31129	Ended 18 kg (40 lbm) drain; 553 kg (1220 lbm) drained thus far from primary

Time (sec)	Event
31839	Began 18 kg (40 lbm) drain from primary
31979	Ended 18 kg (40 lbm) drain; 572 kg (1260 lbm) drained thus far from primary
33099	Began 9 kg (20 lbm) drain from primary
33174	Ended 9 kg (20 lbm) drain; 581 kg (1280 lbm) drained thus far from primary
33879	Valved out weir meter 569, replaced by weir meter 570
35679	Began 5 kg (10 lbm) drain from primary
35724	Ended 5 kg (10 lbm) drain; 585 kg (1290 lbm) drained thus far from primary
36999	Began 18 kg (40 lbm) drain from primary
37179	Ended 18 kg (40 lbm) drain; 603 kg (1330 lbm) drained thus far from primary
38297	Began 18 kg (40 lbm) drain from primary
38415	Ended 18 kg (40 lbm) drain; 621 kg (1370 lbm) drained thus far from primary
39256	Began 14 kg (30 lbm) drain from primary
39369	Ended 14 kg (30 lbm drain); 635 kg (1400 lbm) drained thus far from primary

Time (sec)	Event
39459	Heater rod temperature rising [hot rod showed a temperature of 267°C (512°F)]; first indication that too much mass was drained from the primary resulting in a core uncovery
39579	Hot rod temperature of 324°C (615°F) observed; power reduced to 100 kw
39663	Hot rod temperature of 343°C (650°F) observed; critical rod temperature alarm sounded
39684	Test engineer scrammed bundle power.
42399	Accumulator 1 valved in to primary system, began injecting water from accumulator 1 at a nominal flow rate of 3×10^{-5} m^3/sec (2 gal/min).
42757	Ended accumulator 1 injection
42933	Began injecting water from accumulator 1 at a nominal flow rate of 3×10^{-5} m^3/sec (2 gal/min)
43228	Ended accumulator 1 injection; a liquid level observed at the upper plenum sight glass. An estimated 80.20 kg (176.8 lbm) were injected to the primary system through accumulator 1. Estimated amount of mass inventory removed from the primary system is 554.84 kg (1223.2 lbm).
43434	Ramped power up to 110 kw in attempt to recover to the reflux mode of natural circulation
44664	Ramped power to 222 kw

Time (sec)	Event
45924	Began 32 kg (70 lbm) drain from primary
46128	Ended 32 kg (70 lbm) drain; an estimated 586.60 kg (1293.2 lbm) have been drained from primary
47479	Began 18 kg (40 lbm) drain from primary
47600	Ended 18 kg (40 lbm) drain; an estimated 604.74 kg (1333.2 lbm) have been drained from primary
48129	Not satisfied with performance of weir meter 570. Wier meter 570 valved out; weir meter 569 valved in to replace 570
49076	Began 14 kg (30 lbm) drain from primary
49179	Ended 14 kg (30 lbm) drain; an estimated 618.35 kg (1363.2 lbm) have been drained from primary
50993	Satisfactory reflux mode of natural circulation achieved
57999	Began first helium injection
62379	Ended first helium injection, an estimated 15.8 moles (3.49×10^{-2} lbm-mole) of helium injected into primary system
63939	Began sampling steam generator U-tubes to determine helium concentration and distribution
69519	Ended helium sampling; primary system pressure decreased 0.019 MPa (10 psi) during sampling

Time (sec)	Event
72339	Began second helium injection
75399	Hot rod temperature of 266°C (510°F) observed
75636	Hot rod temperature of 300°C (572°F) observed
76359	Dramatic drop in small steam generator secondary side level
77679	Ended second helium injection; an estimated 19.3 moles (4.26×10^{-2} lbm-mole) of helium injected into primary system
79659	Began sampling steam generator U-tubes to determine helium concentration and distribution
83259	Ended helium sampling; primary system pressure decreased 0.041 MPa (5.9 psi) during sampling.
84219	Began third helium injection
86179	Hot rod temperature of 226.9°C (440.4°F) observed
86550	Hot rod temperature of 324°C (616°F) observed
86616	Hot rod temperature of 343°C (650°F) observed
86730	Hot rod temperature of 361.7°C (683.1°F) observed
86863.6	Rod bundle/computer scrammed because of hot rod temperature of 371°C (700°F). Ended third helium injection; an estimated 9.71 moles (2.14×10^{-2} lbm-mole) of helium injected into primary system

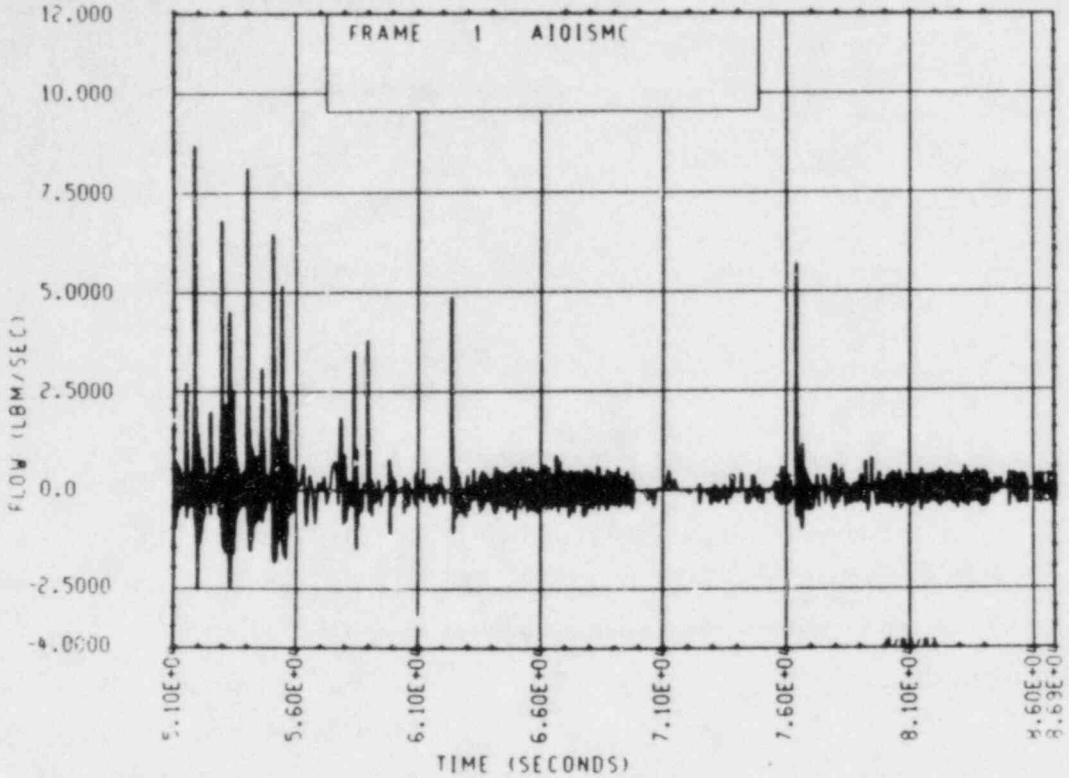

Figure A-187. Mass Flow Rate Through Rod Bundle, Test 15

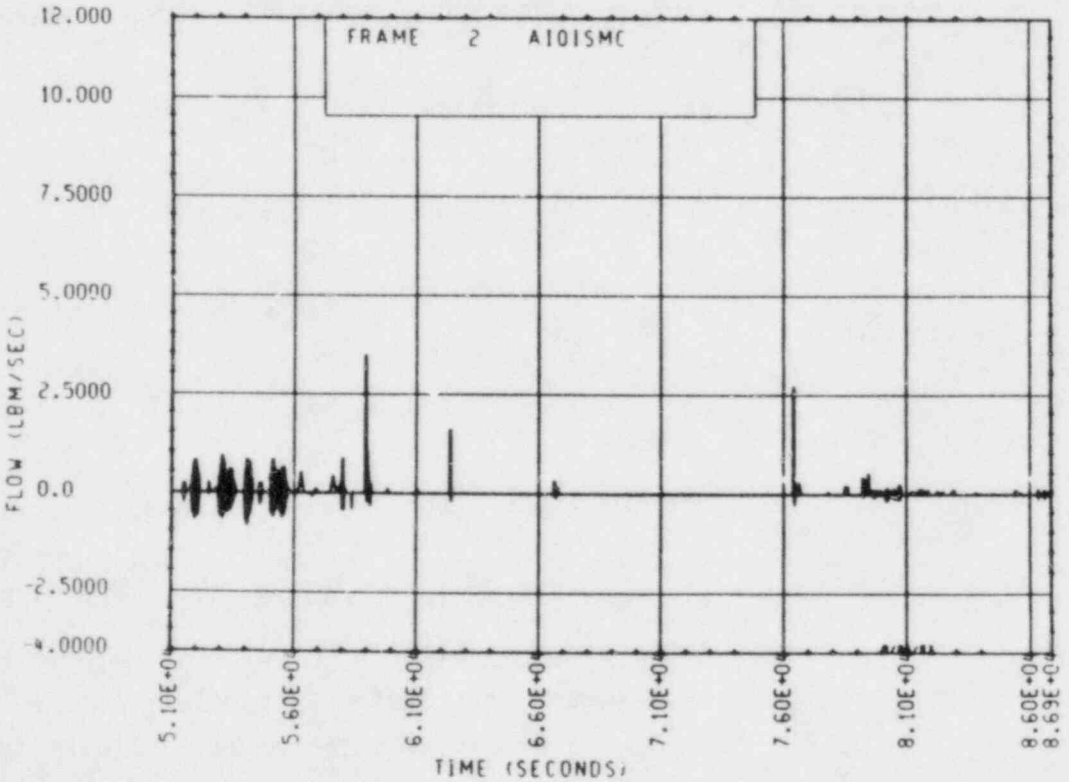

Figure A-188. Mass Flow Rate Through Broken Loop, Test 15

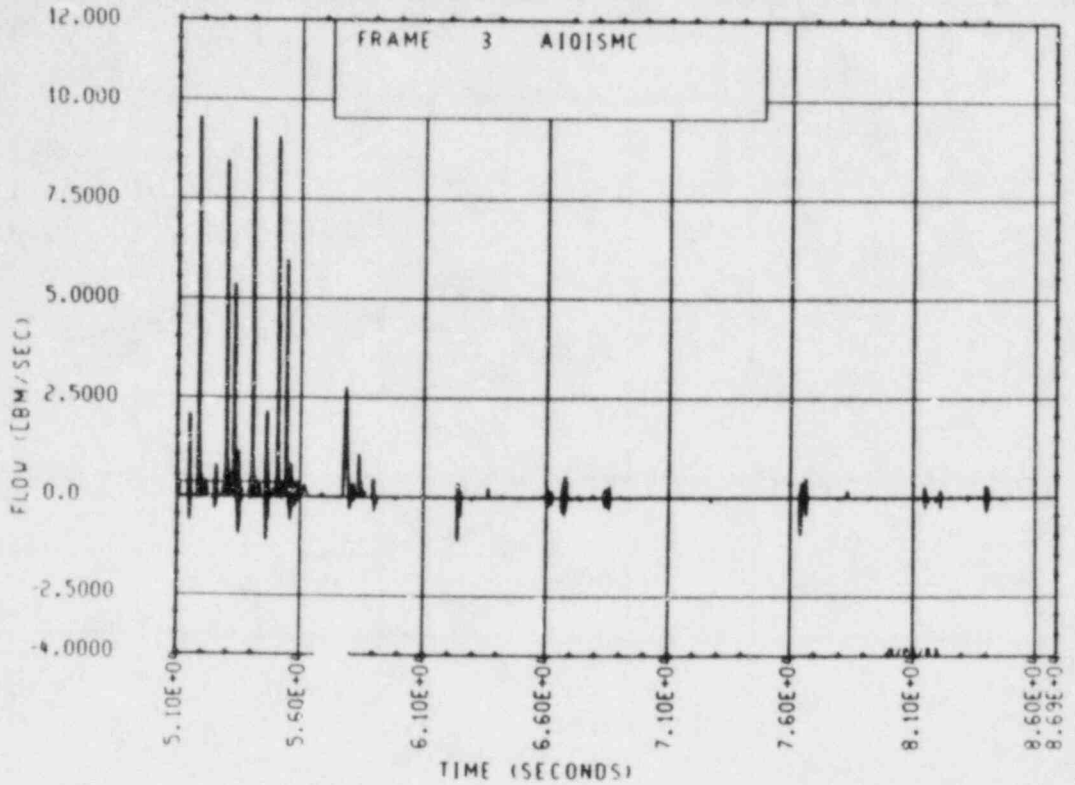

Figure A-189. Mass Flow Rate Through Unbroken Loop, Test 15

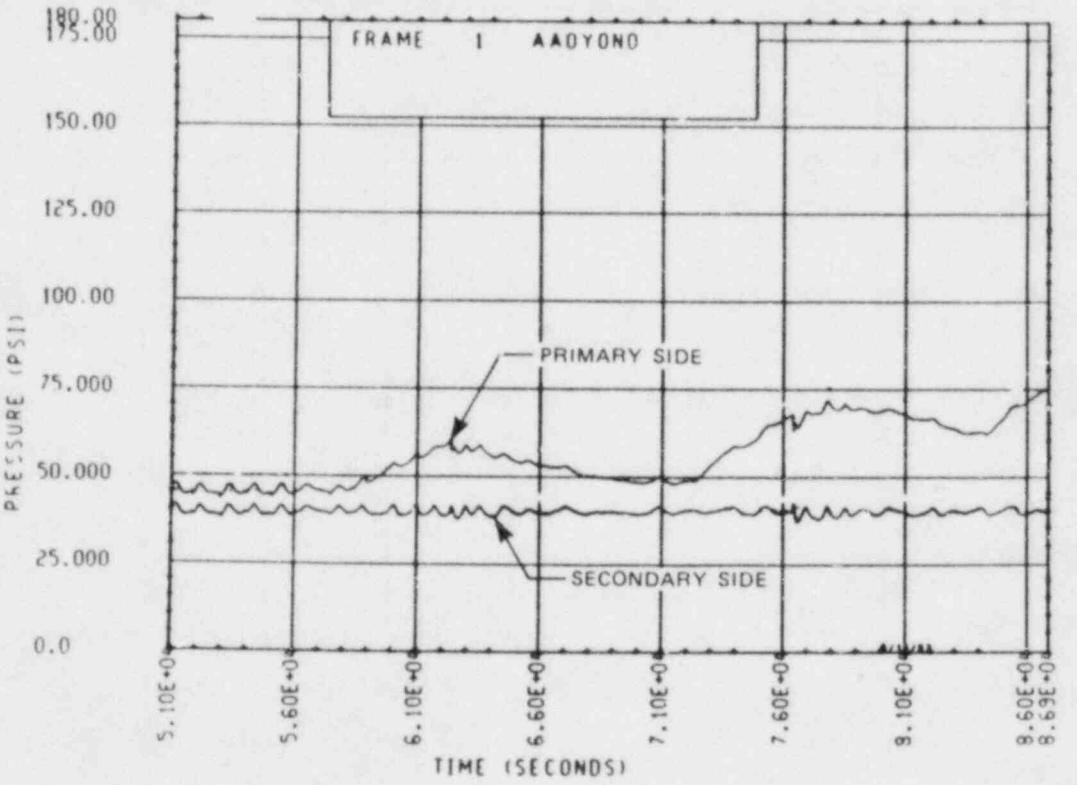

Figure A-190. Primary and Secondary System Pressure, Test 15

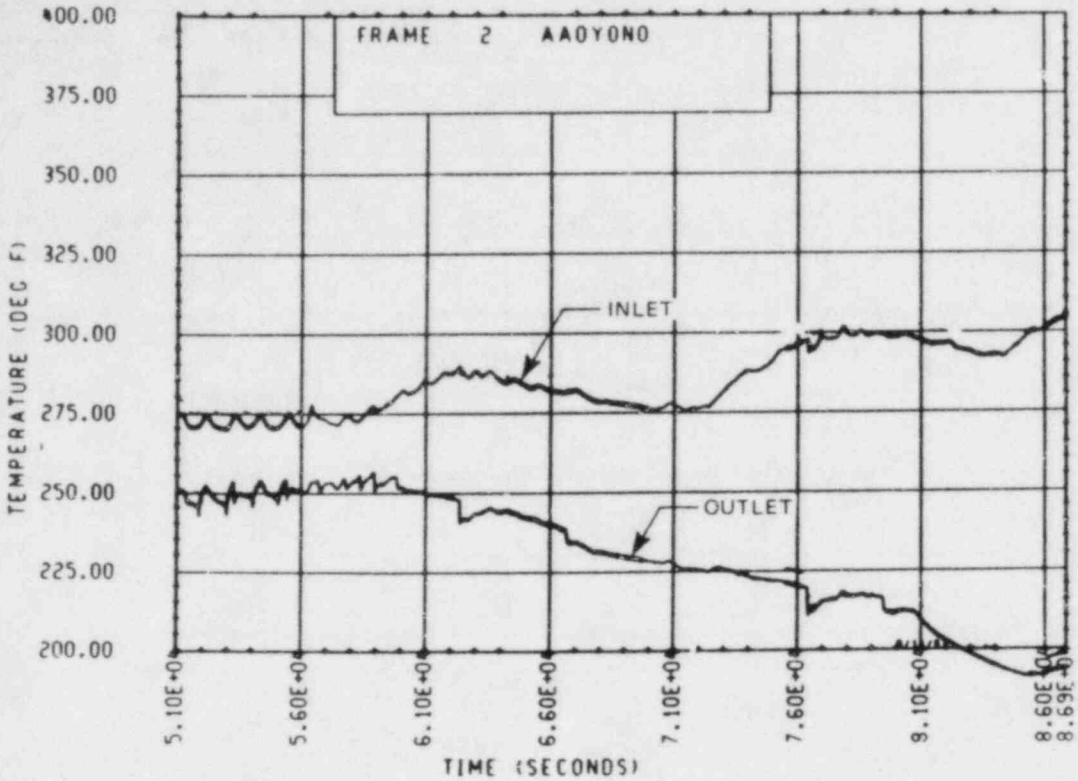

Figure A-191. Heater Rod Bundle Inlet and Outlet Temperature, Test 15

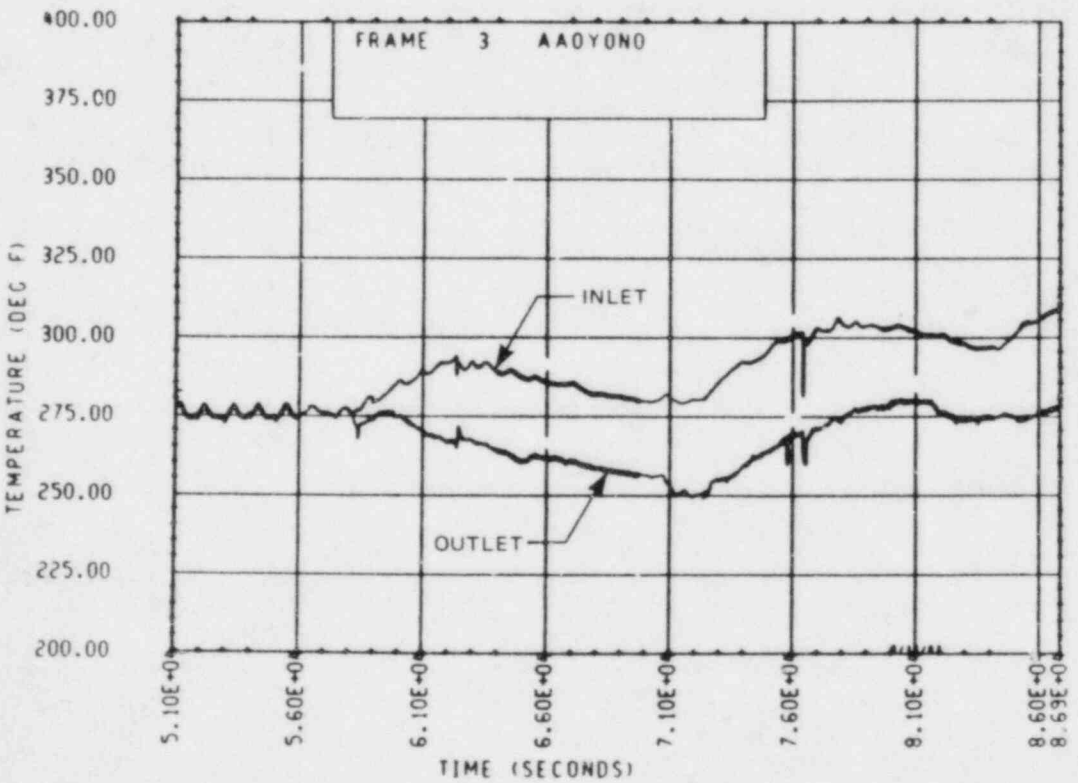

Figure A-192. Unbroken Loop Steam Generator Inlet and Outlet Temperature, Test 15

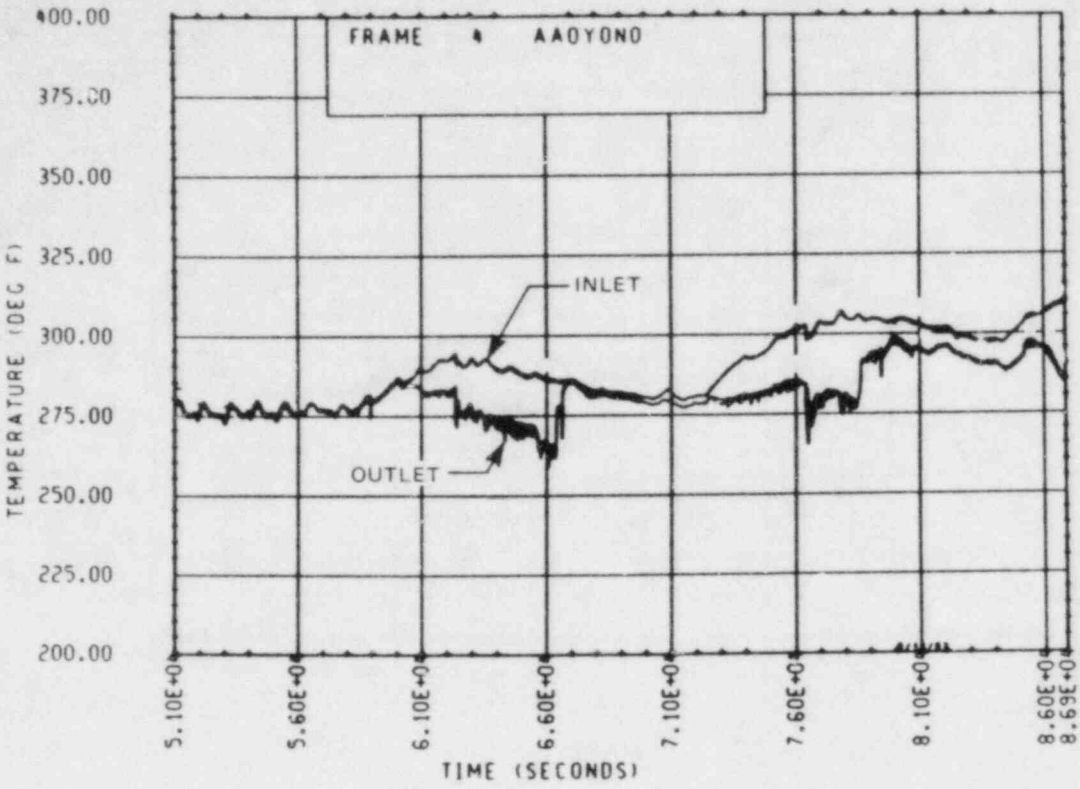

Figure A-193. Broken Loop Steam Generator Inlet and Outlet Temperature, Test 15

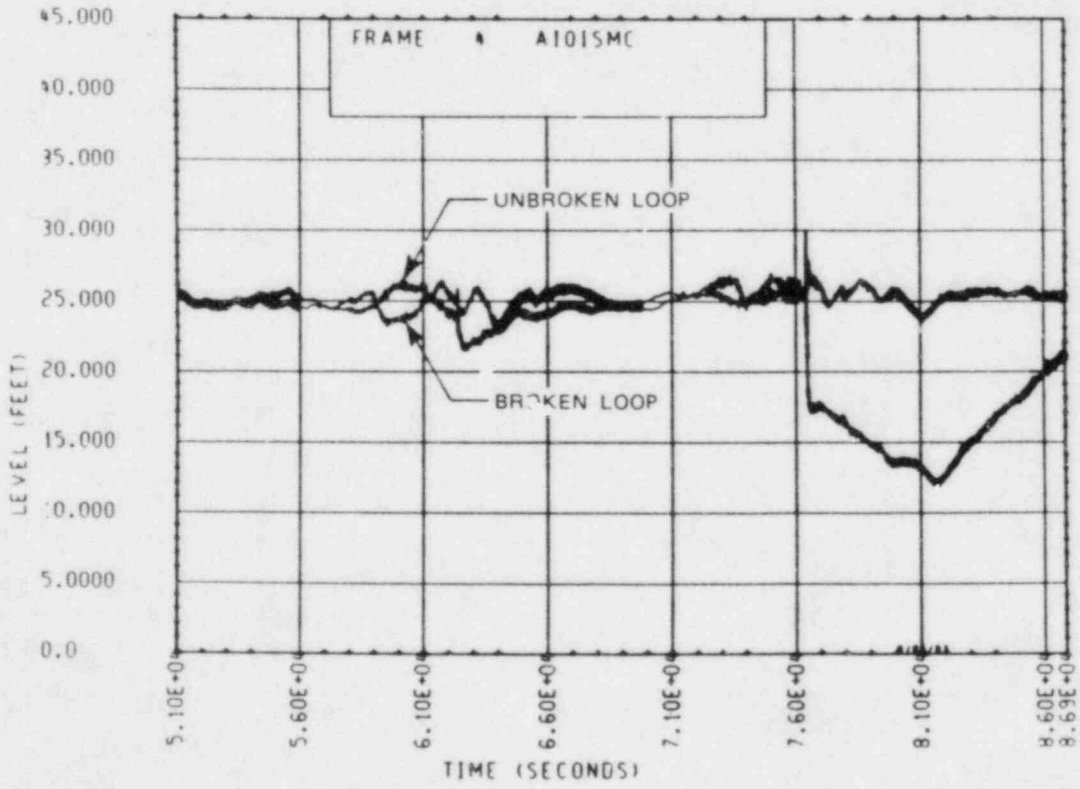

Figure A-194. Unbroken and Broken Loop Steam Generator Secondary Side Collapsed Liquid Levels, Test 15

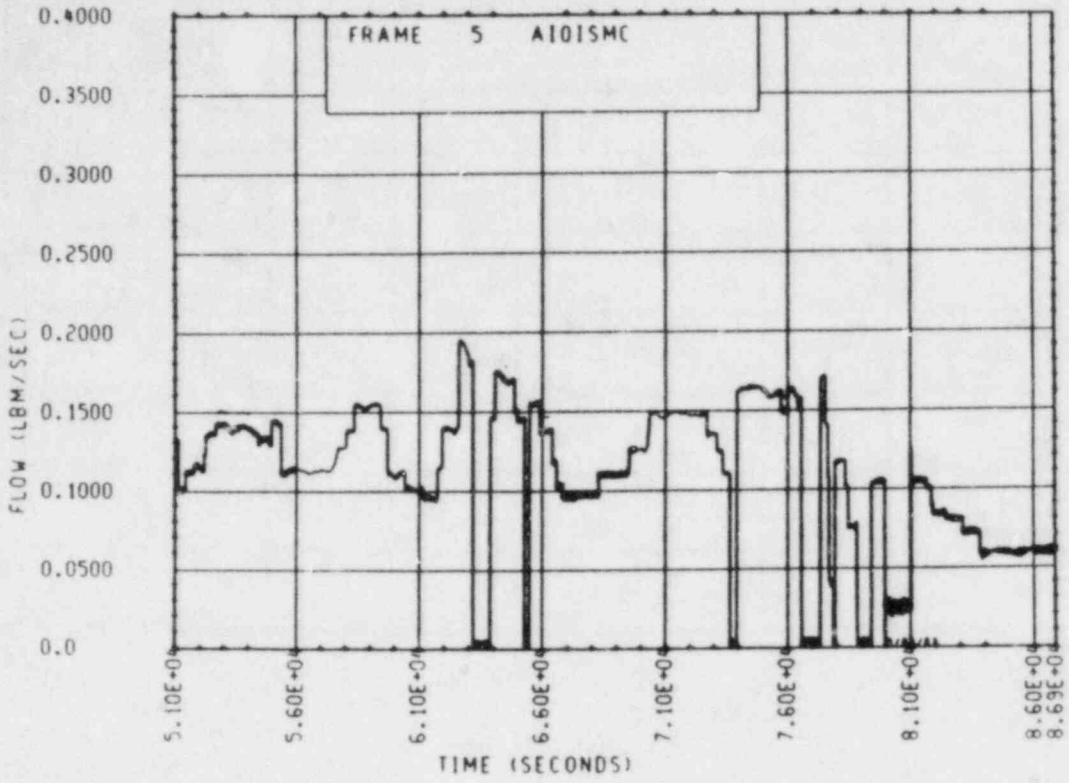

Figure A-195. Unbroken Loop Steam Generator Feedwater Mass Flow Rate, Test 15

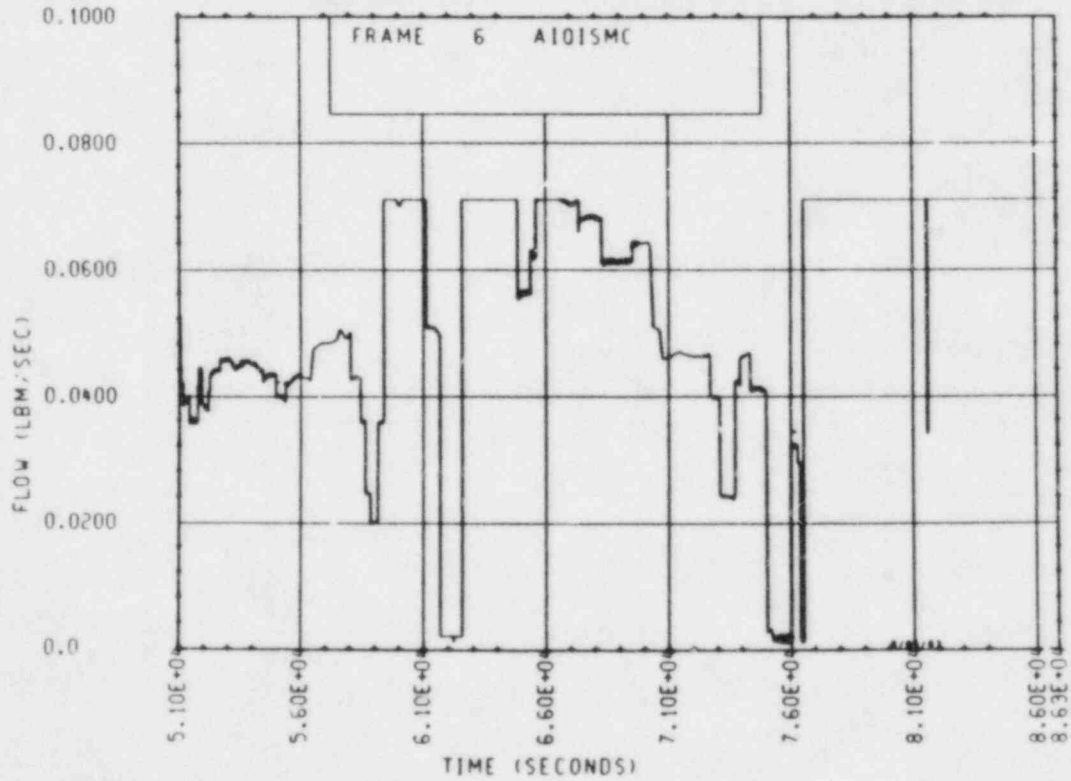

Figure A-196. Broken Loop Steam Generator Feedwater Mass Flow Rate, Test 15

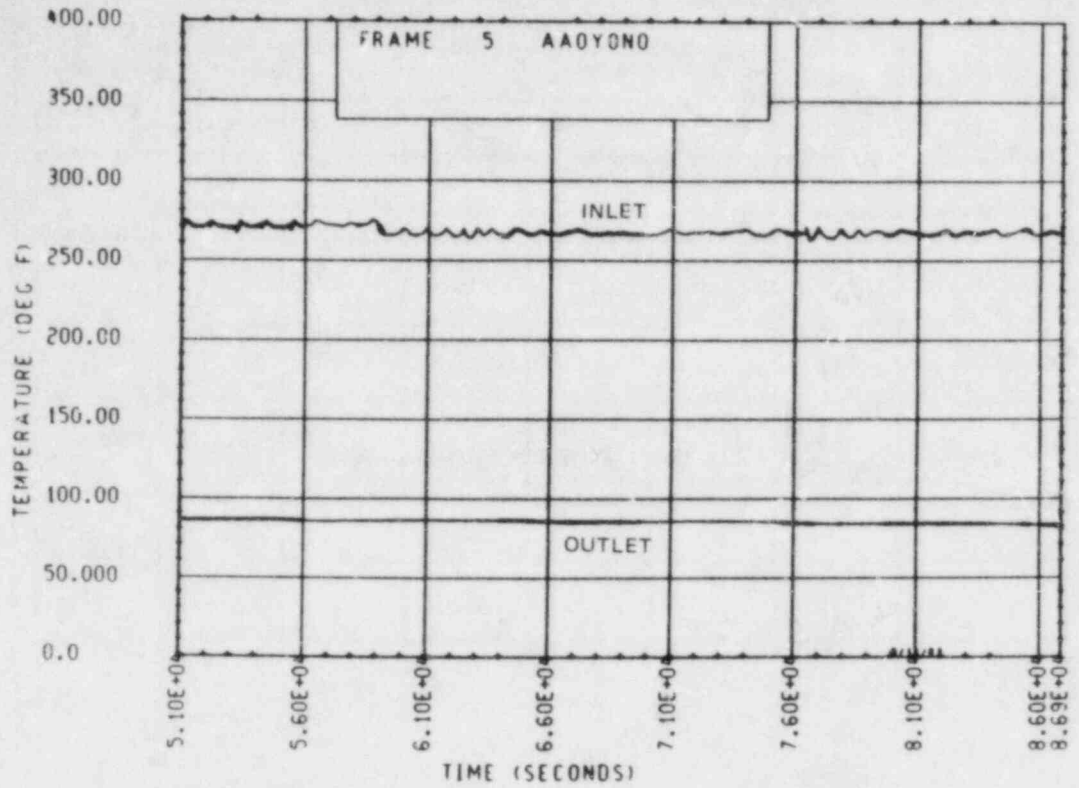

Figure A-197. Unbroken Loop Steam Generator Secondary Side Inlet and Outlet Temperature, Test 15

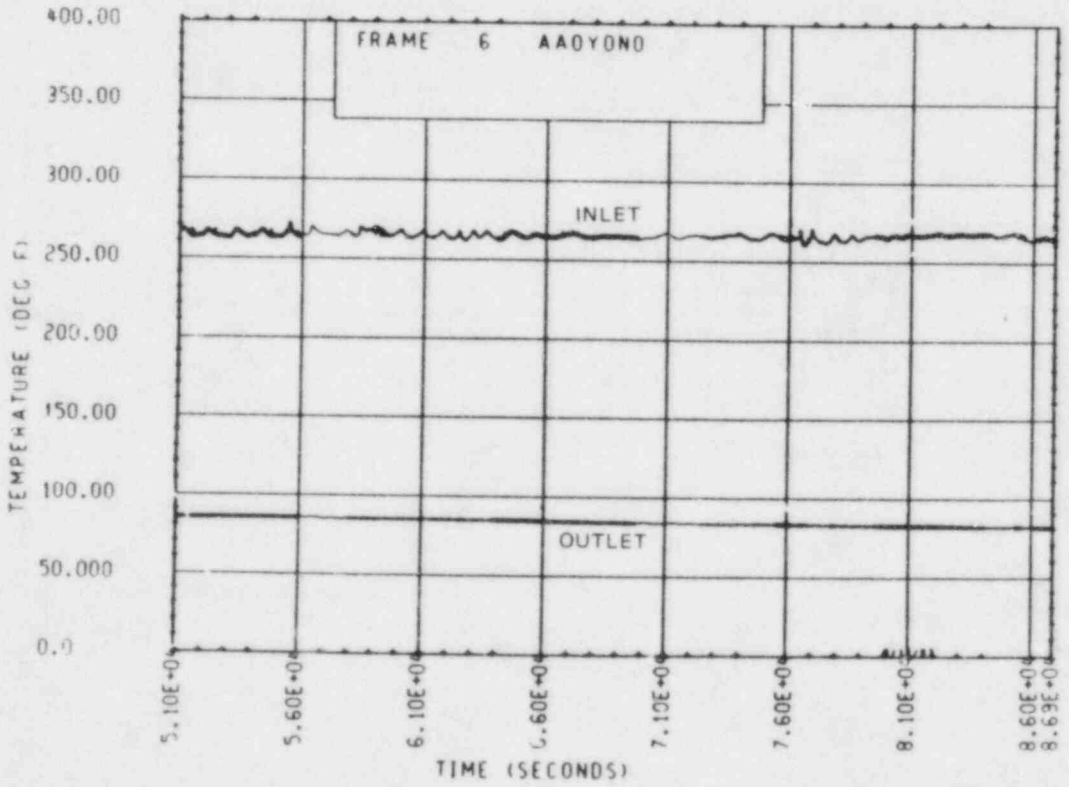

Figure A-198. Broken Loop Steam Generator Secondary Side Inlet and Outlet Temperature, Test 15

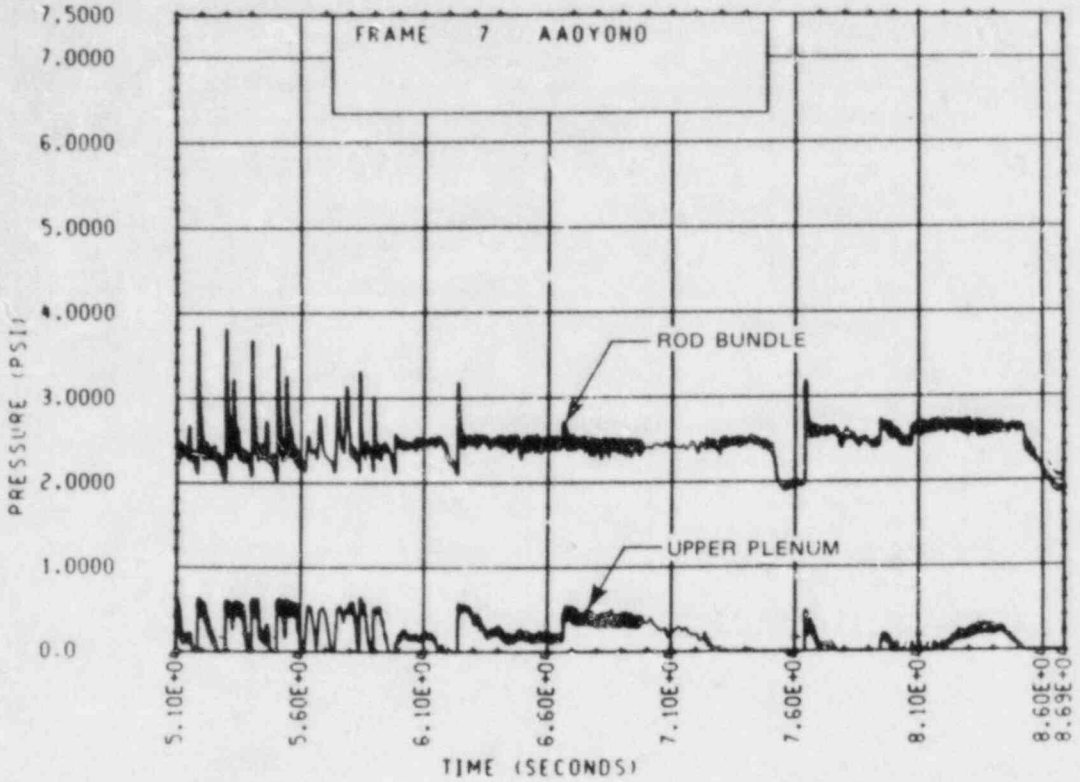

Figure A-199. Heater Rod Bundle and Upper Plenum Differential Pressure, Test 15

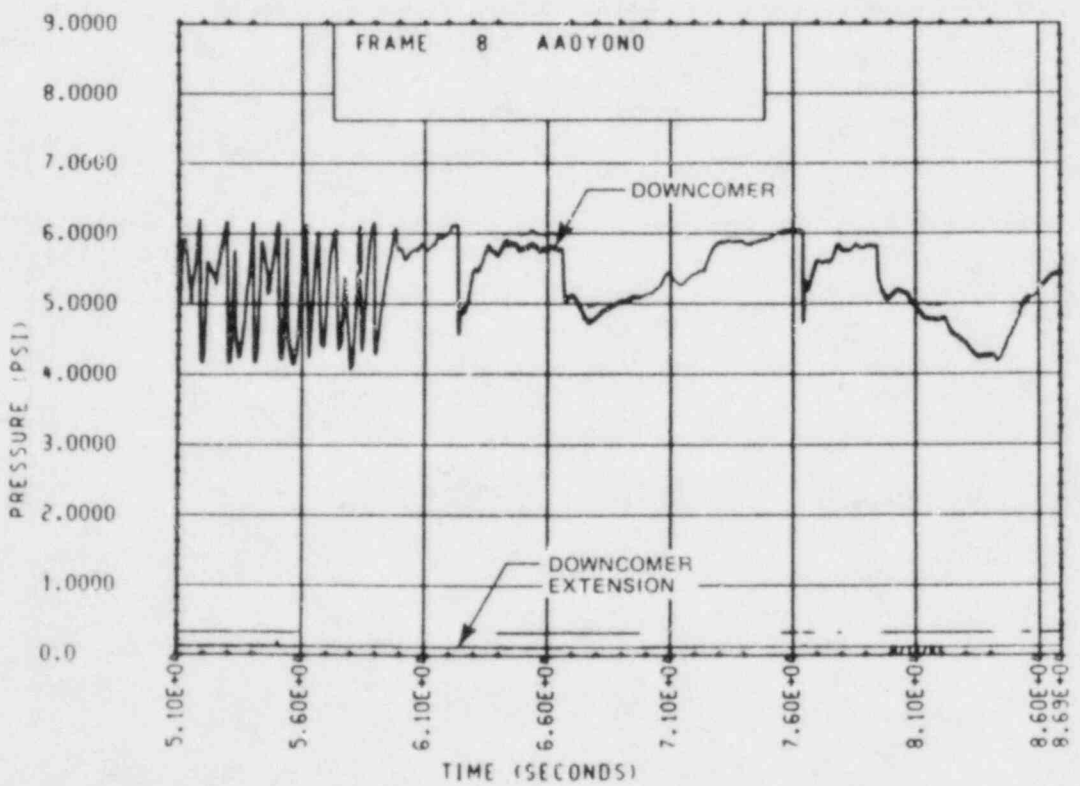

Figure A-200. Downcomer and Downcomer Extension Differential Pressure, Test 15

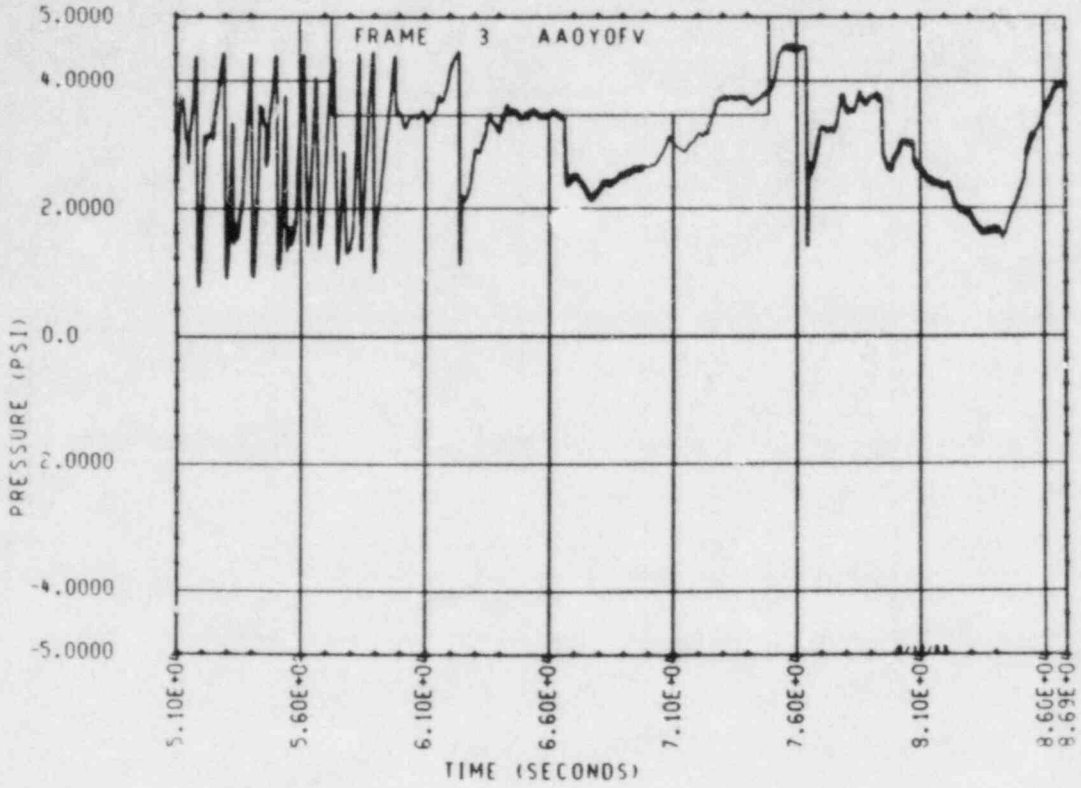

Figure A-201. Upper Plenum and Downcomer Extension Differential Pressure, Test 15

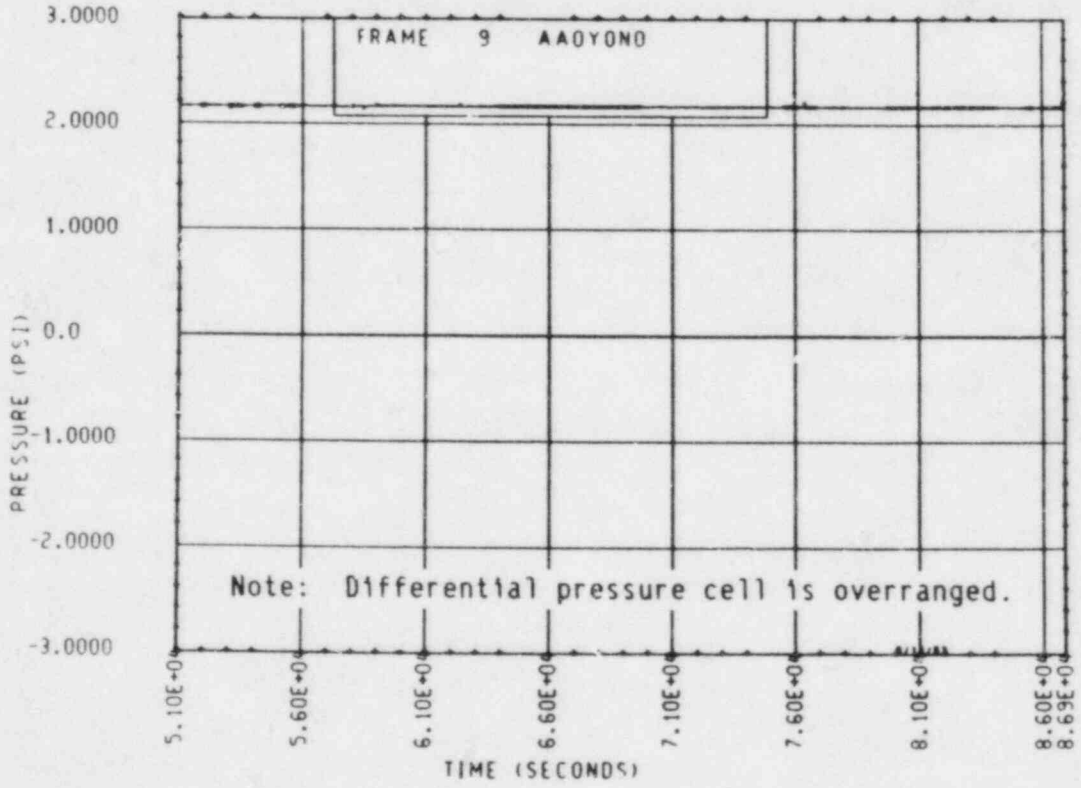

Figure A-202. Unbroken Loop Hot Leg Differential Pressure, Test 15

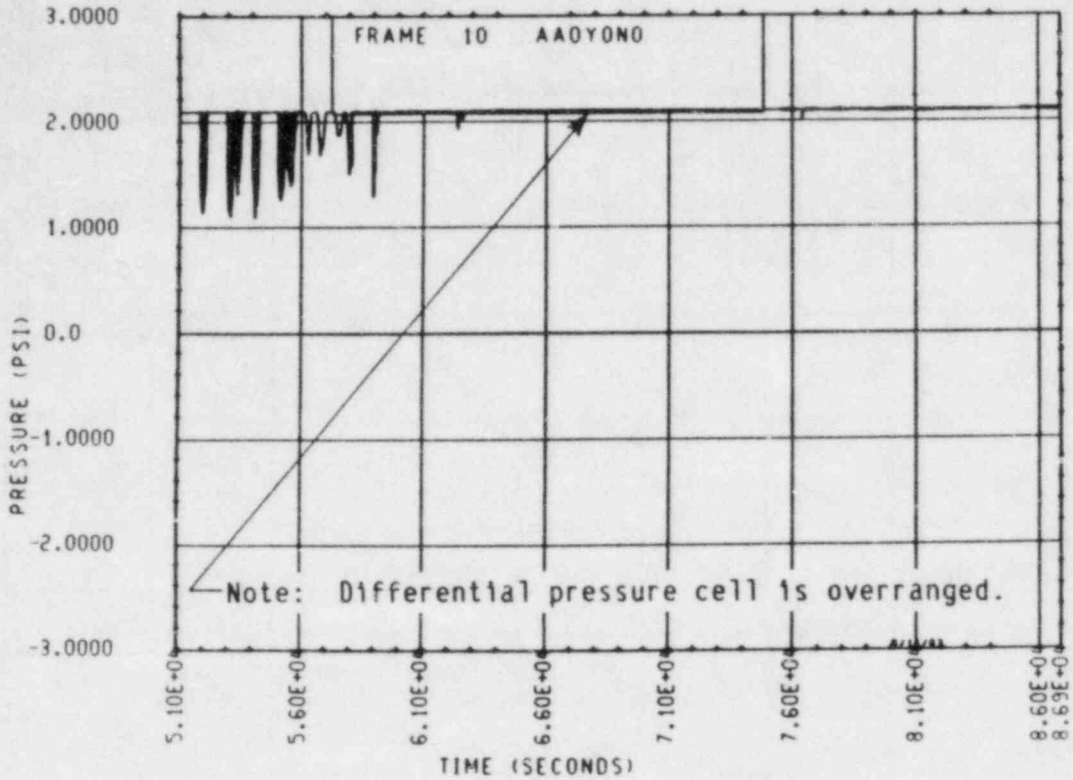

Figure A-203. Broken Loop Hot Leg Differential Pressure, Test 15

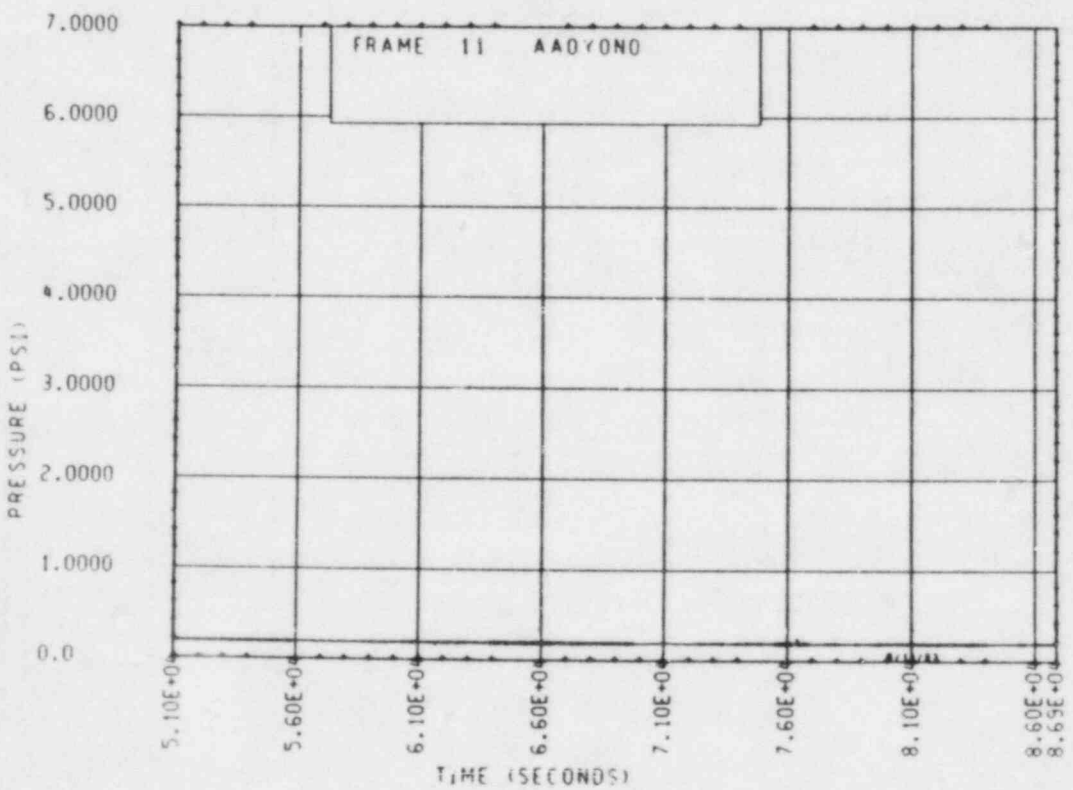

Figure A-204. Unbroken Loop Steam Generator Inlet Plenum Differential Pressure, Test 15

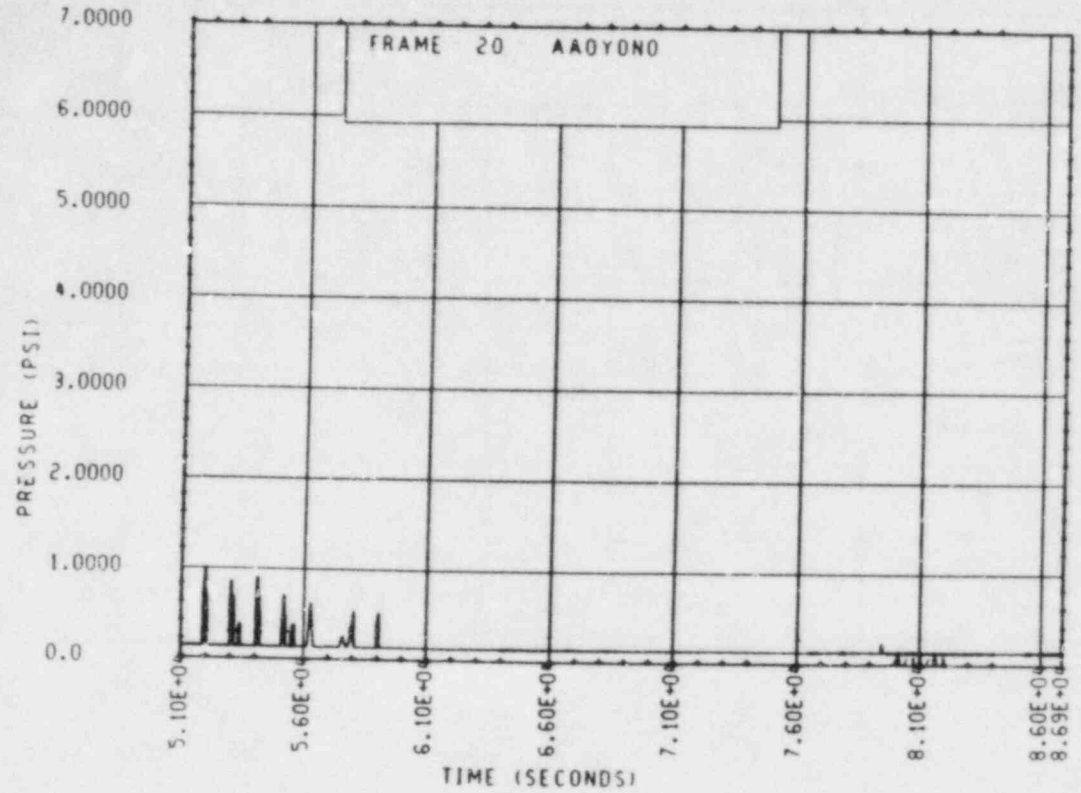

Figure A-205. Broken Loop Steam Generator Inlet Plenum Differential Pressure, Test 15

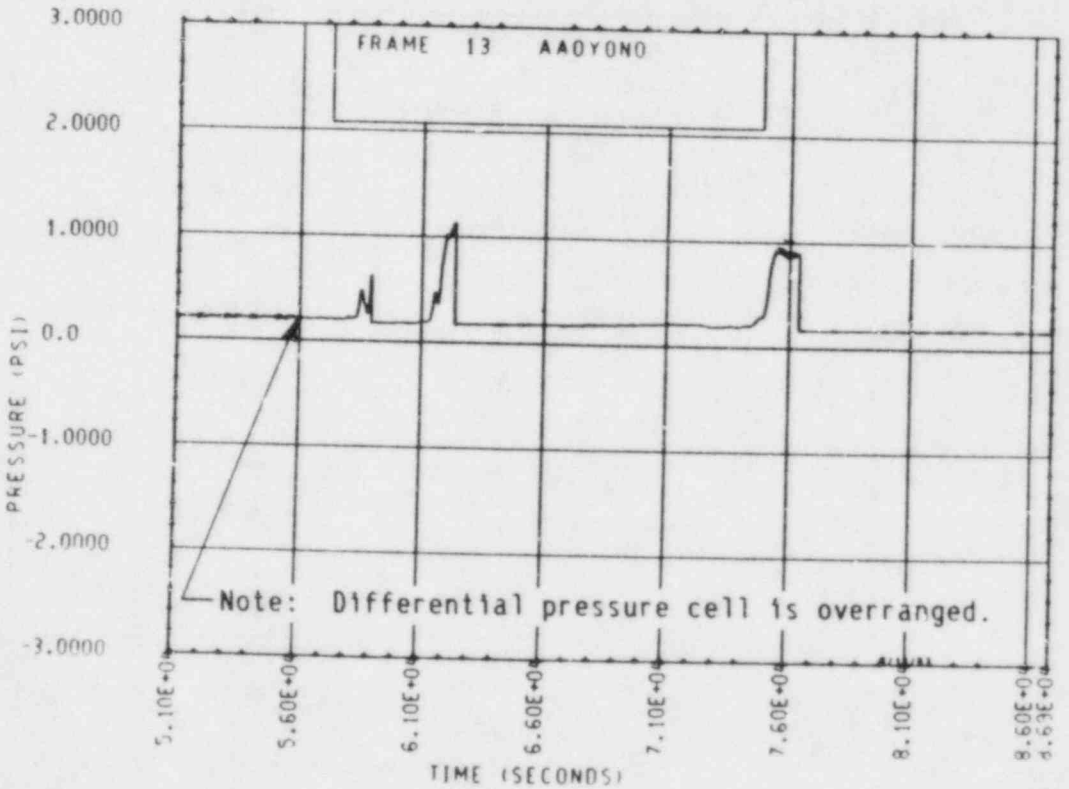

Figure A-206. Unbroken Loop Steam Generator Plenum-to-Plenum Differential Pressure, Test 15

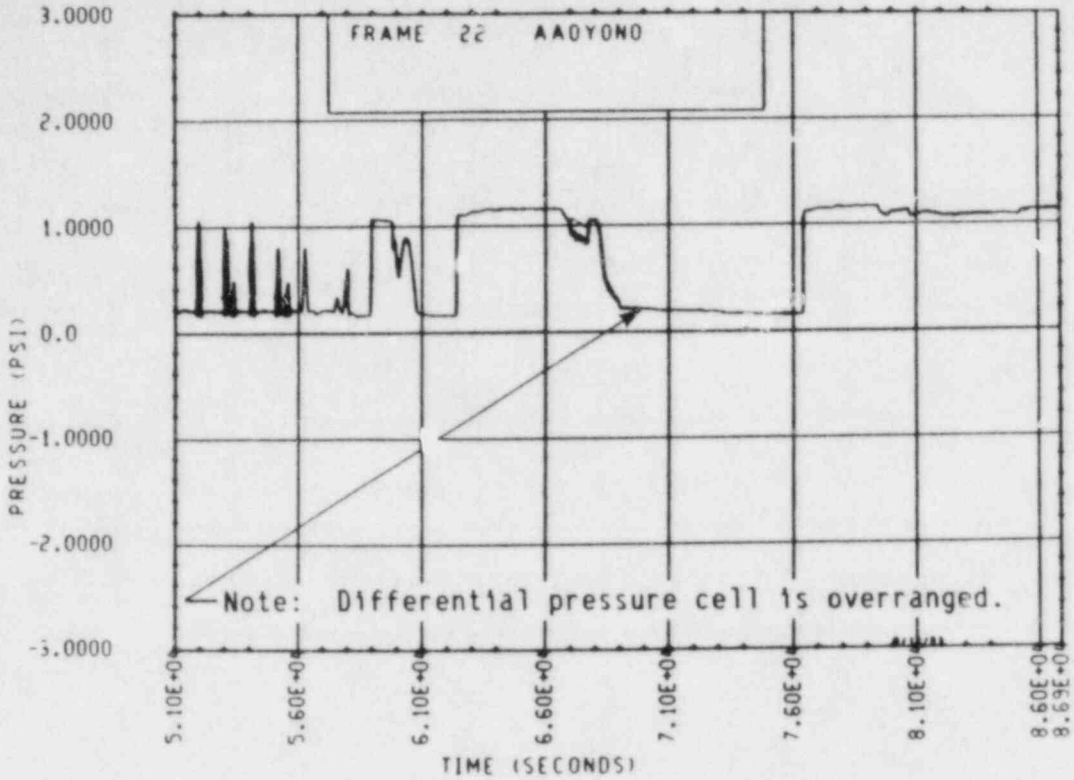

Figure A-207. Broken Loop Steam Generator Plenum-to-Plenum Differential Pressure, Test 15

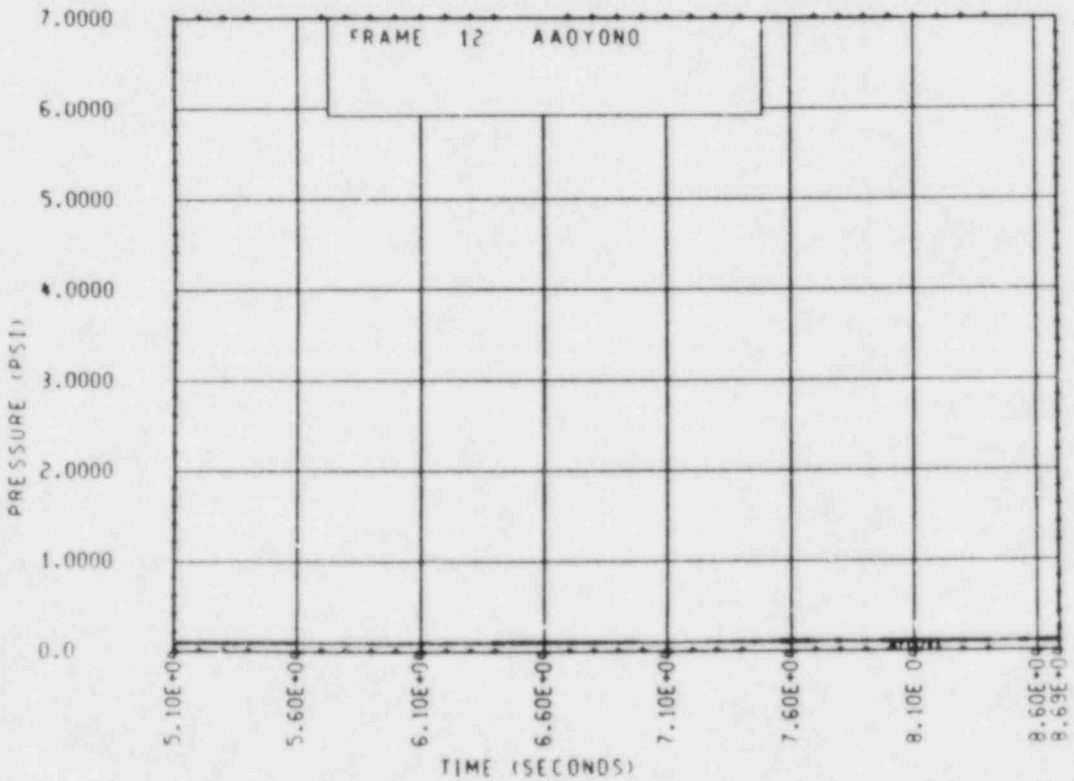

Figure A-208. Unbroken Loop Steam Generator Outlet Plenum Differential Pressure, Test 15

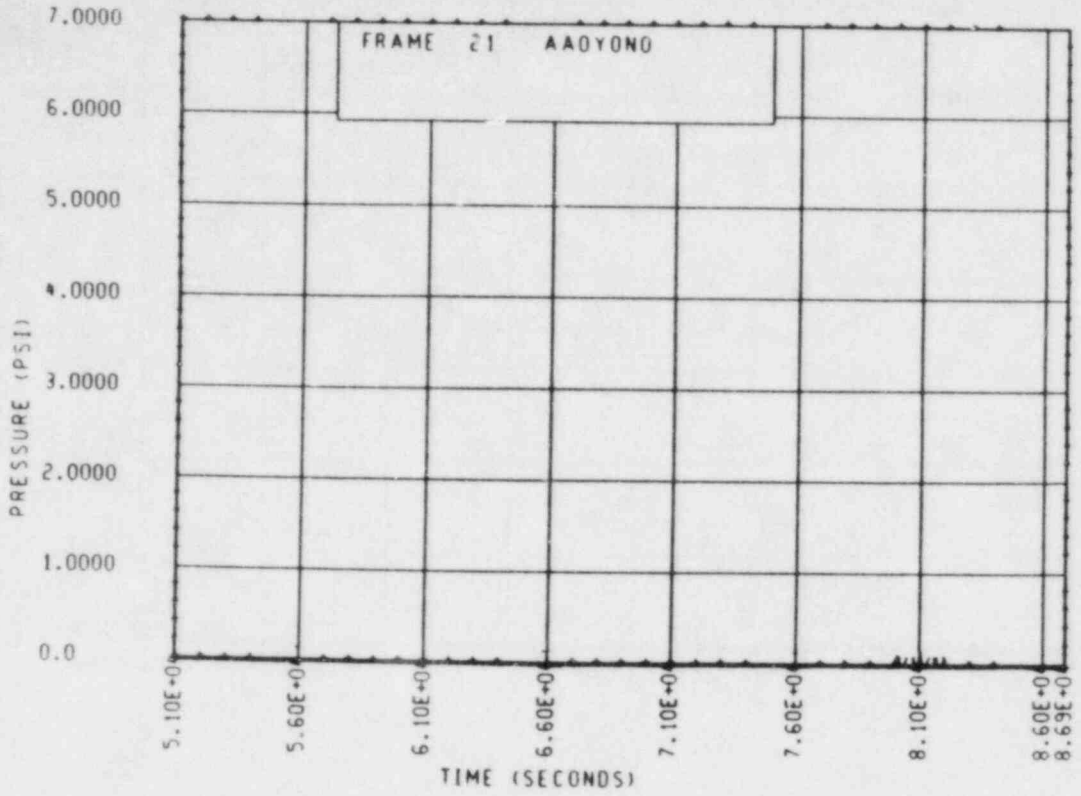

Figure A-209. Broken Loop Steam Generator Outlet Plenum Differential Pressure, Test 15

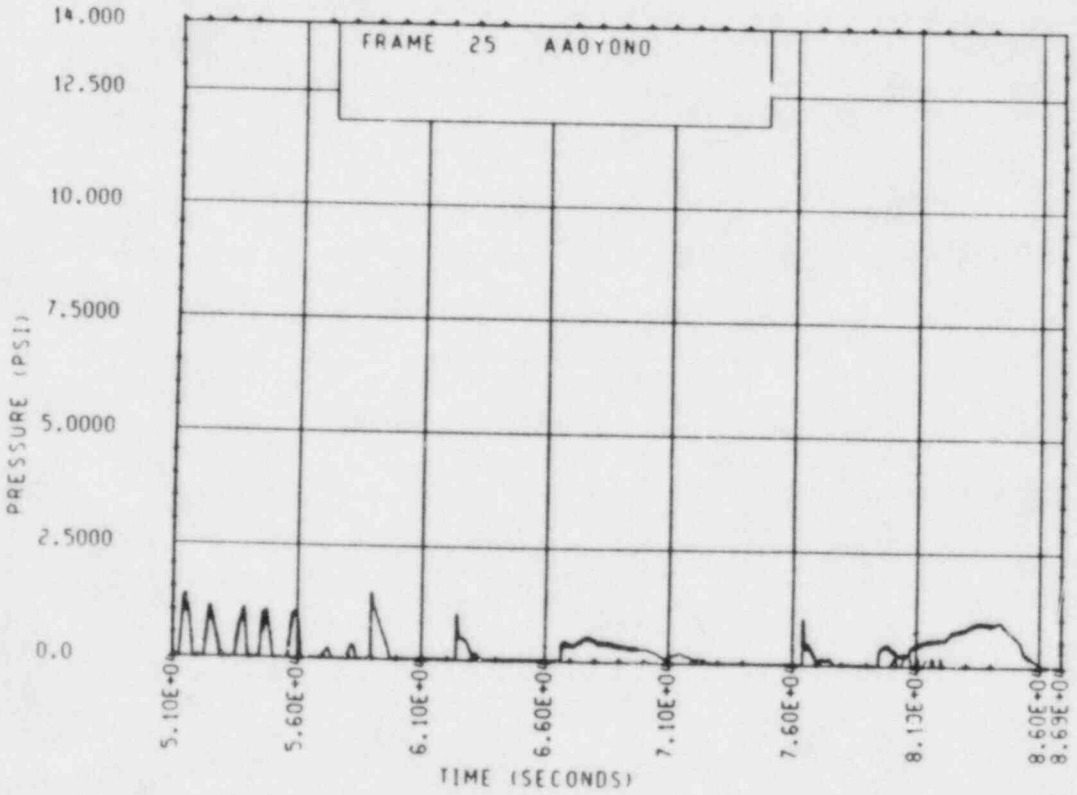

Figure A-210. Unbroken Loop Seal Descending Leg Differential Pressure, Test 15

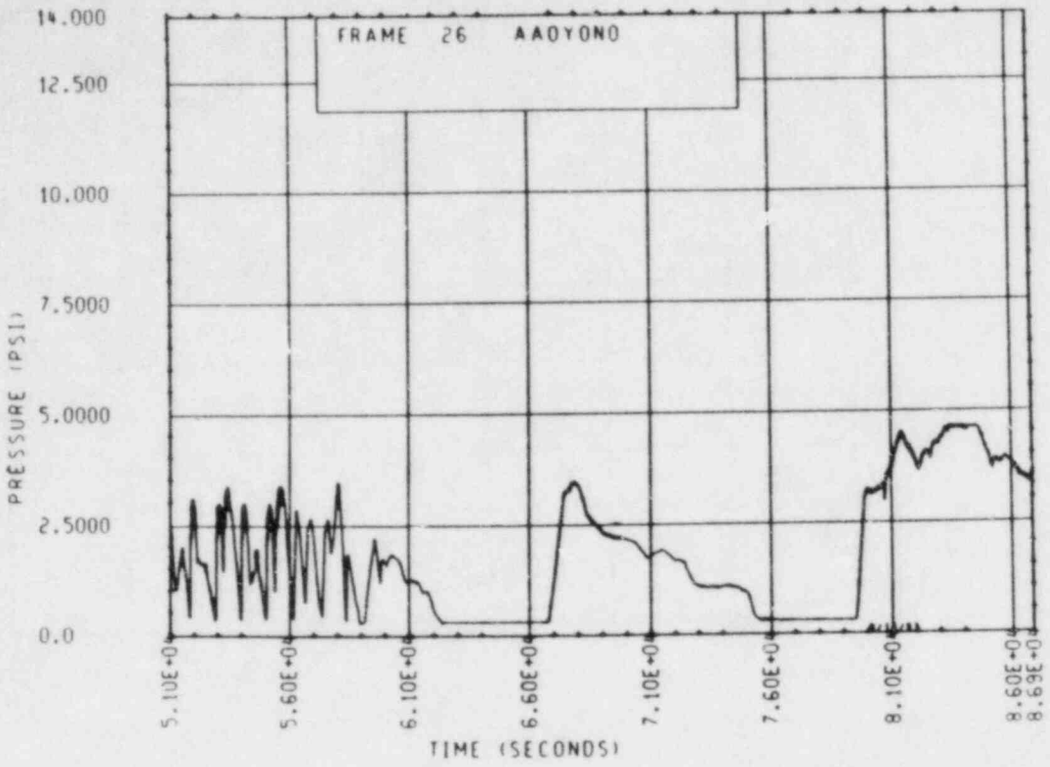

Figure A-211. Broken Loop Seal Descending Leg Differential Pressure, Test 15

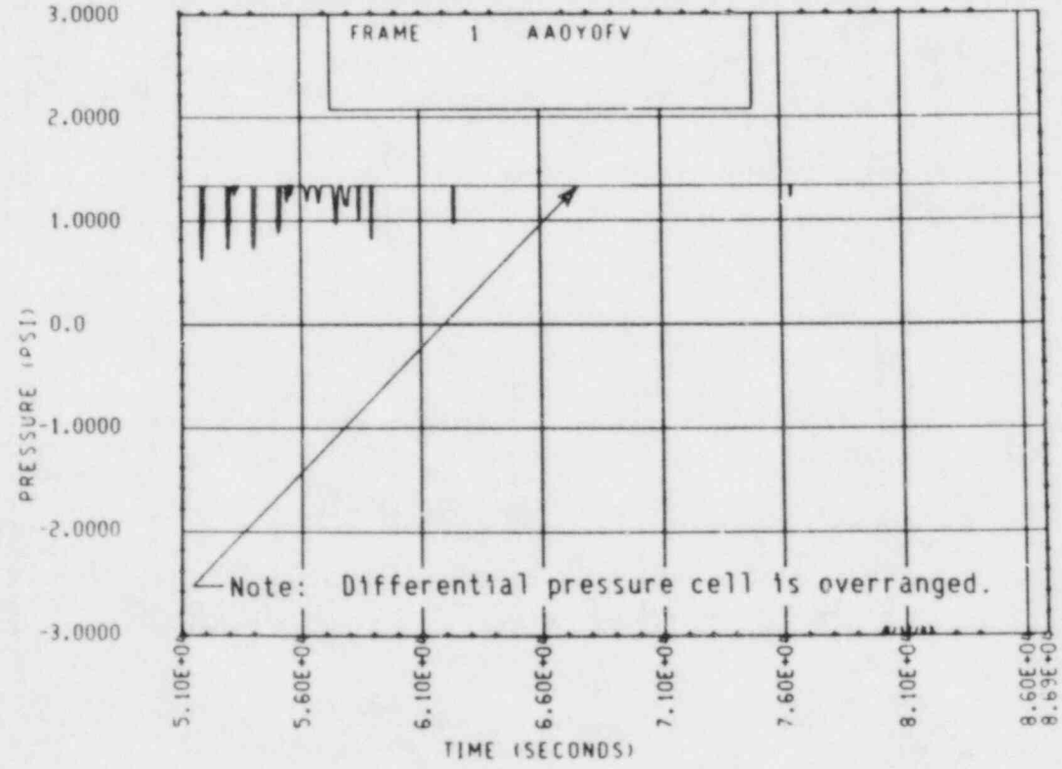

Figure A-212. Unbroken Loop Seal Cold Leg Differential Pressure, Test 15

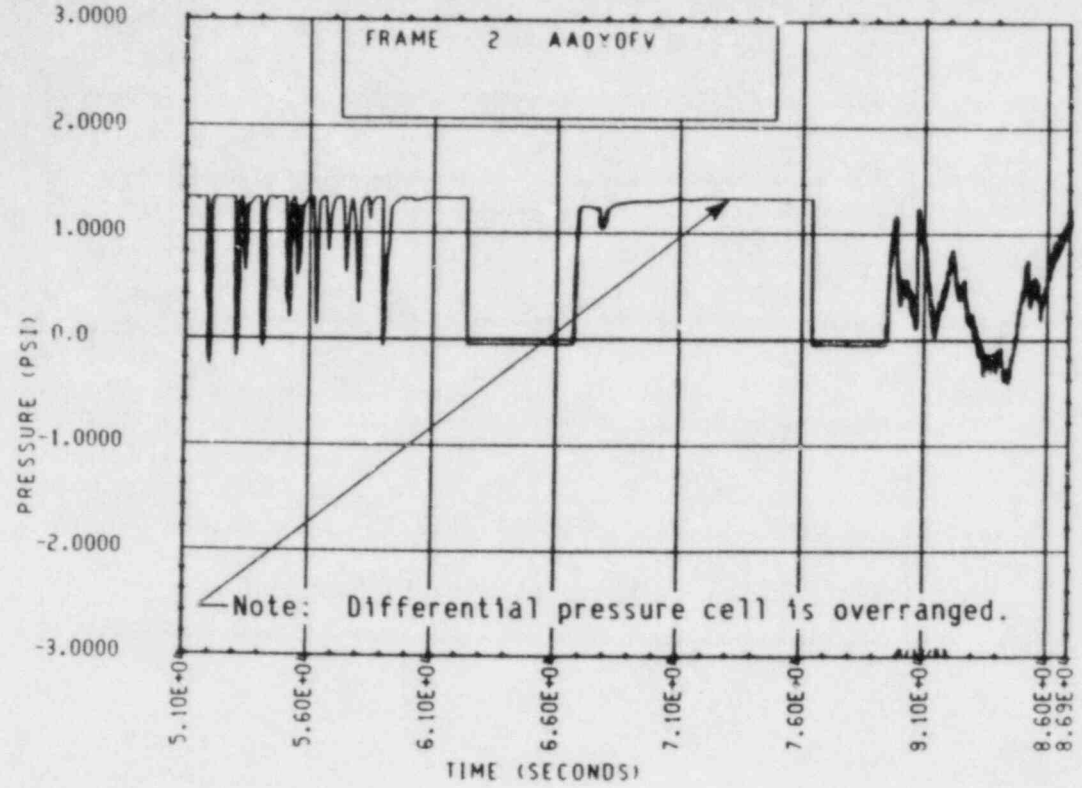

Figure A-213. Broken Loop Seal Cold Leg Differential Pressure, Test 15

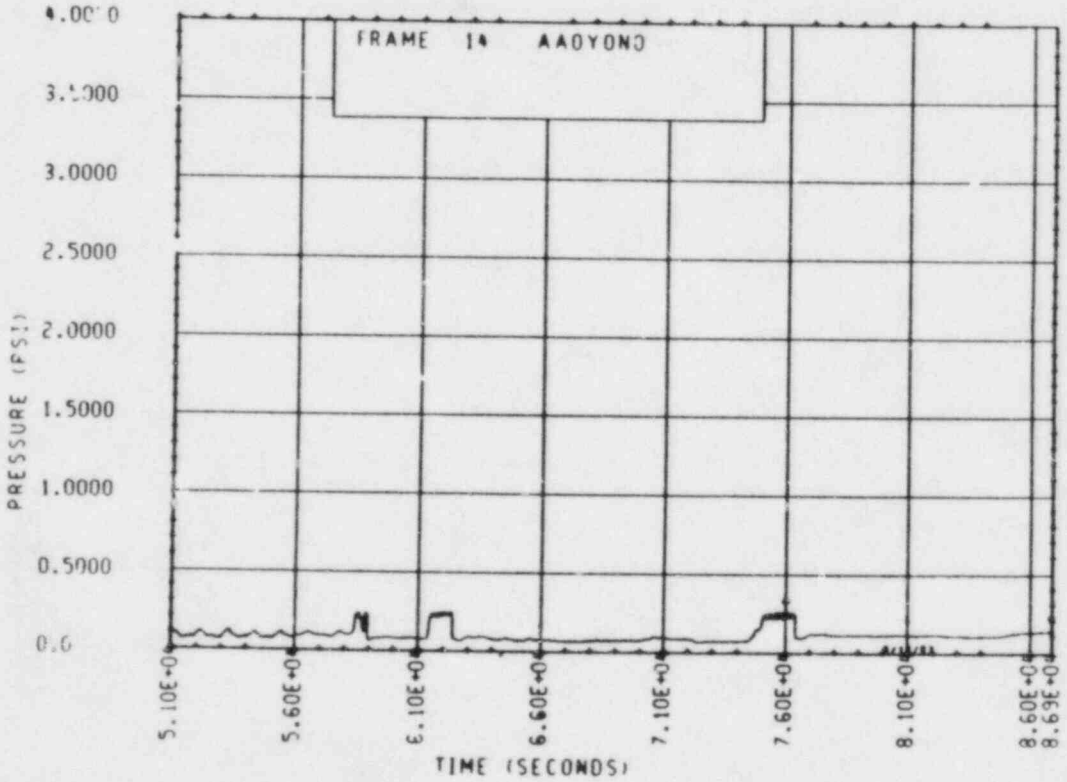

Figure A-214. Unbroken Loop Steam Generator Uphill Tube B-7 Differential Pressure, Test 15 [0-0.61 m (0-2 ft)]

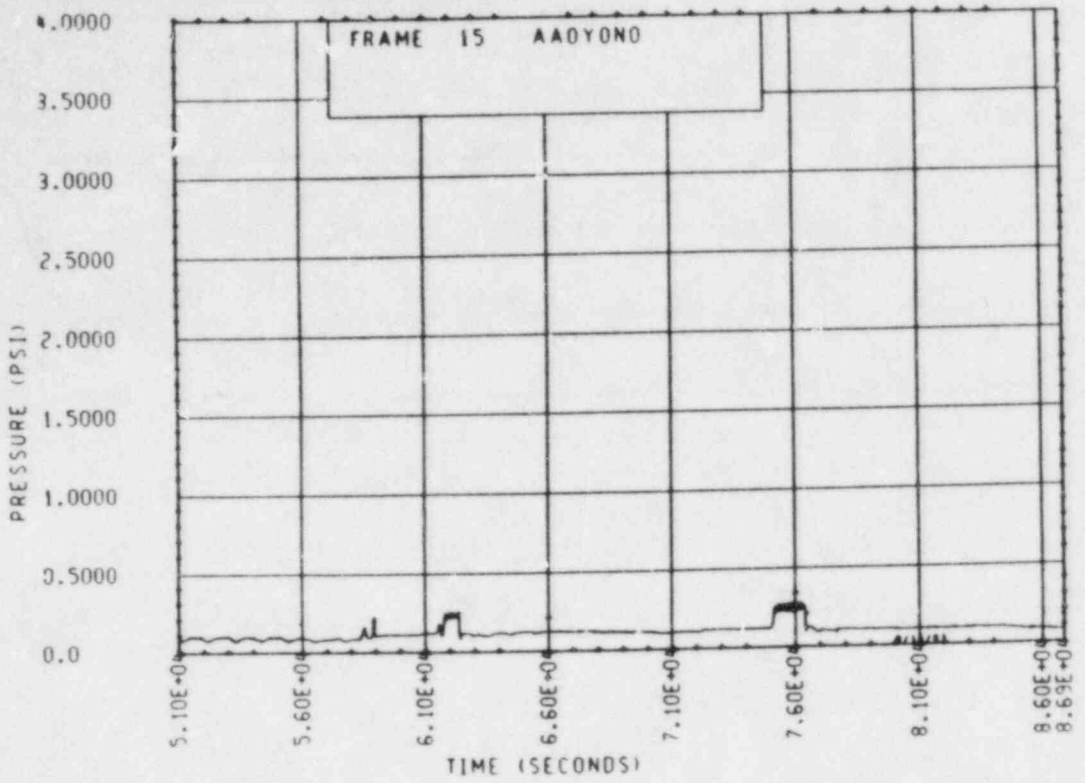

Figure A-215. Unbroken Loop Steam Generator Uphill Tube B-7 Differential Pressure, Test 15 [0.61-1.22 m (2-4 ft)]

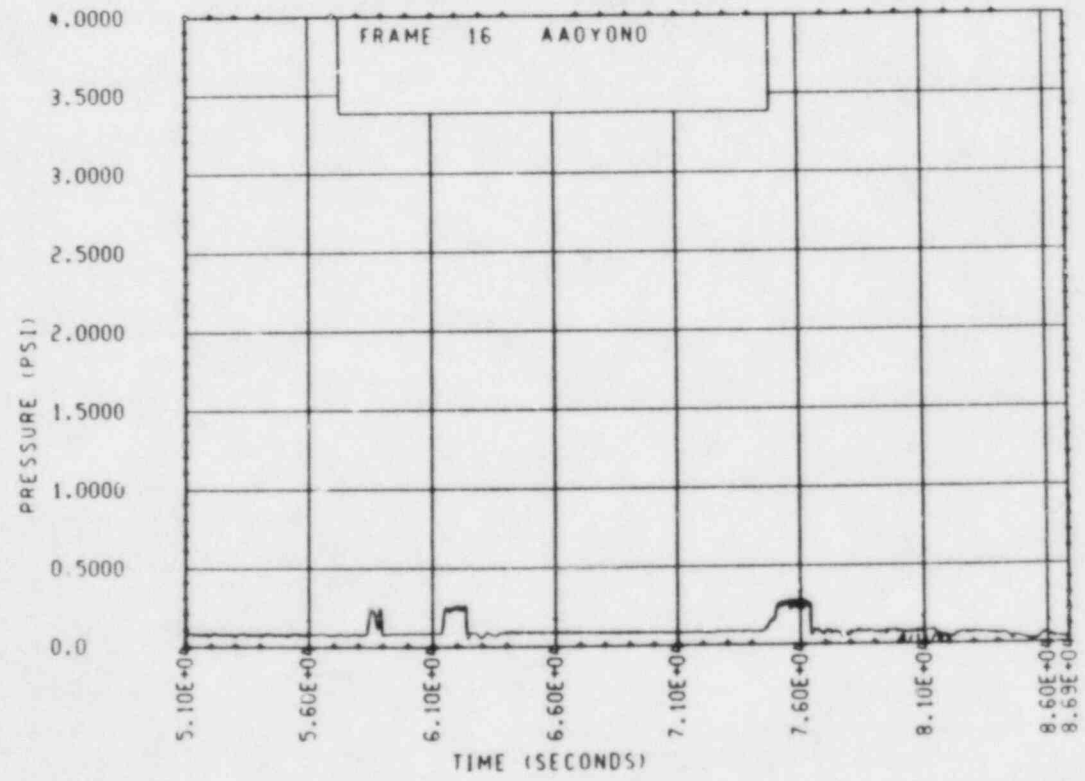

Figure A-216. Unbroken Loop Steam Generator Uphill Tube C-6 Differential Pressure, Test 15 [0-0.61 m (0-2 ft)]

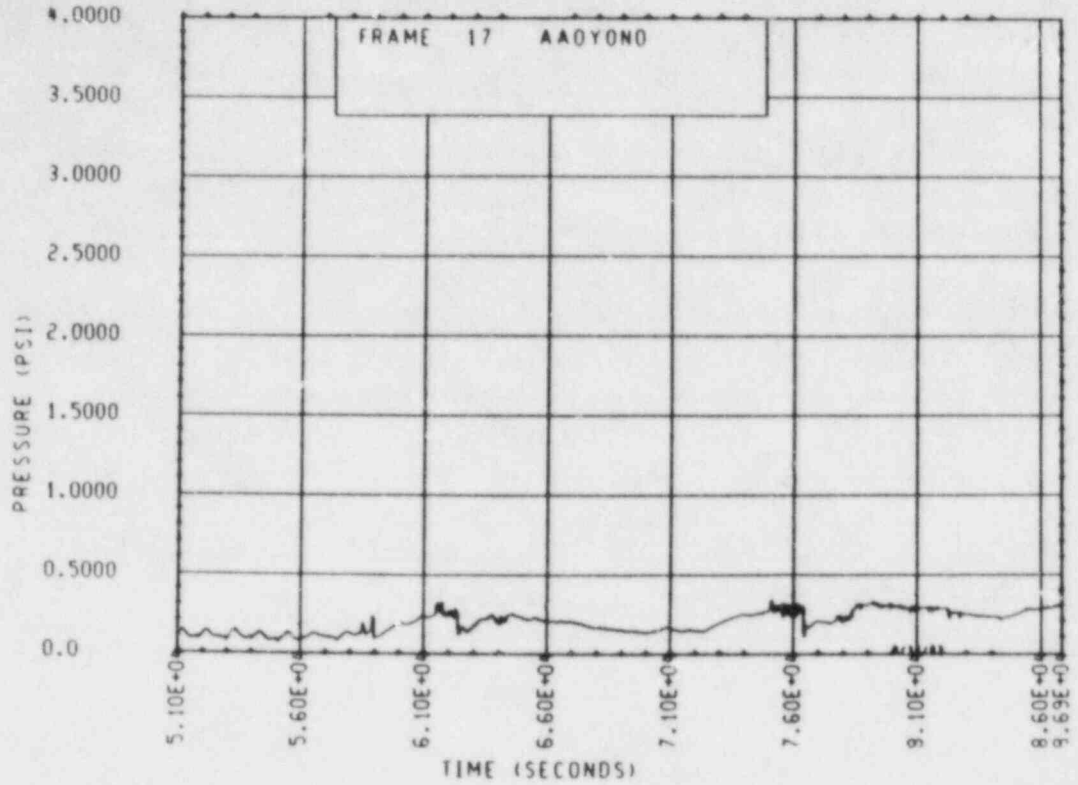

Figure A-217. Unbroken Loop Steam Generator Uph111 Tube C-6 Differential Pressure, Test 15 [0.61-1.22 m (2-4 ft)]

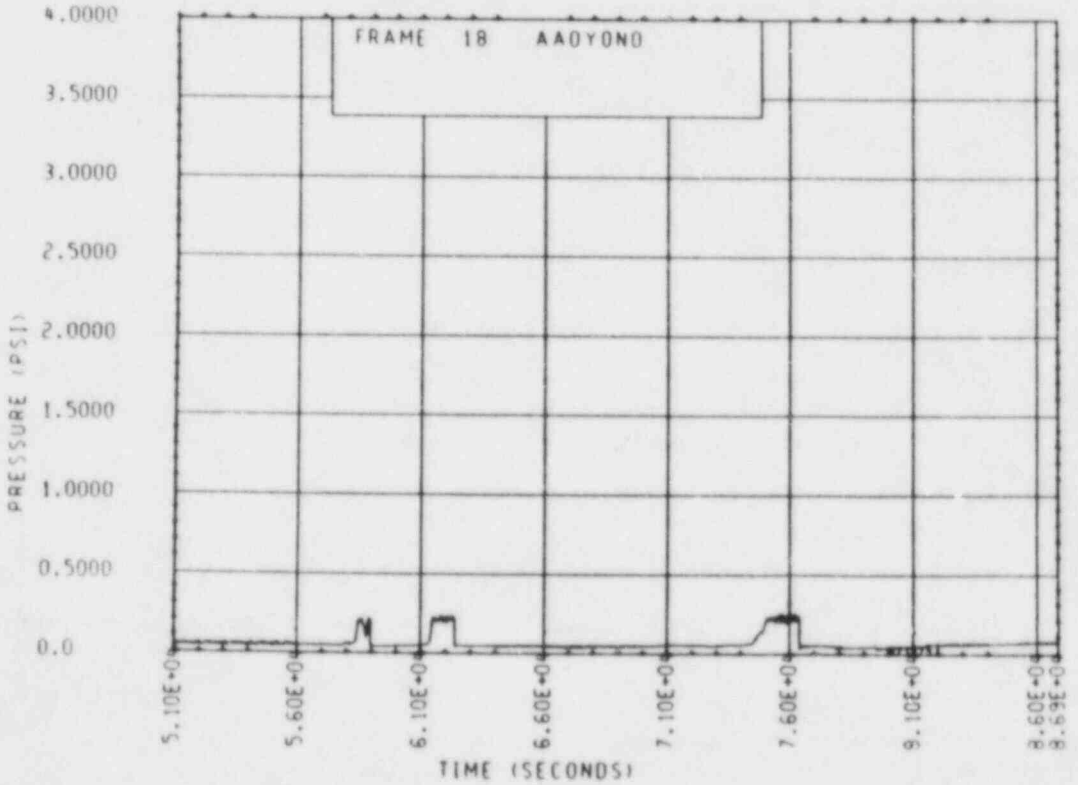

Figure A-218. Unbroken Loop Steam Generator Uph111 Tube E-5 Differential Pressure, Test 15 [0-0.61 m (0-2 ft)]

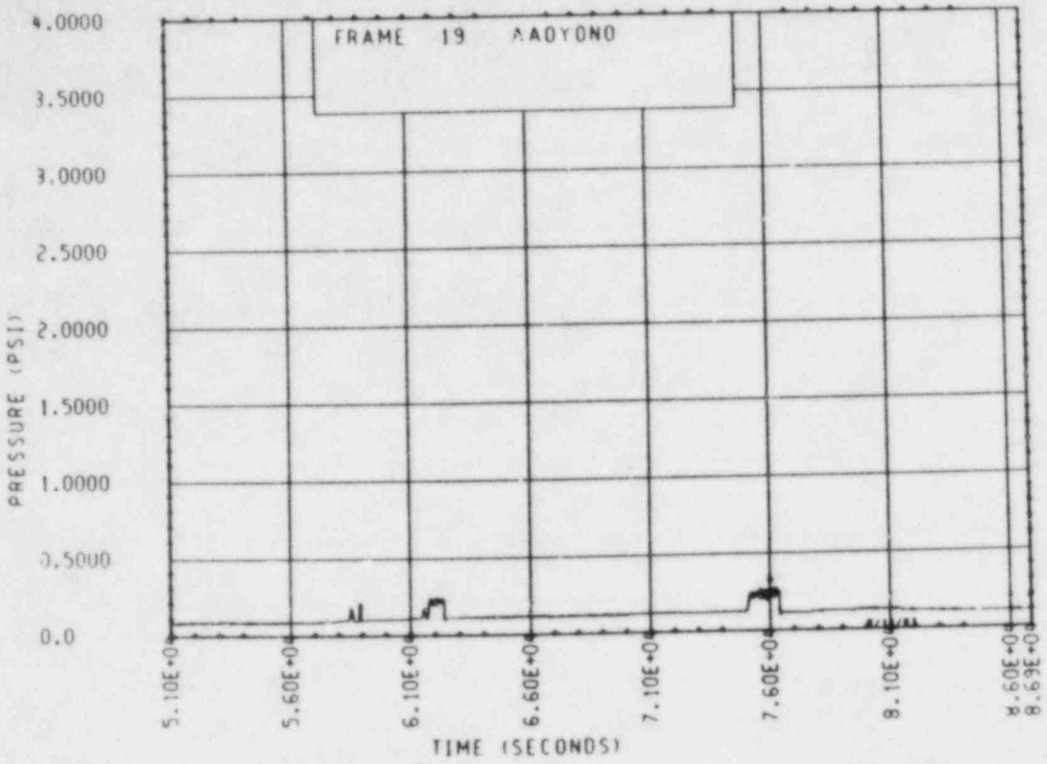

Figure A-219. Unbroken Loop Steam Generator Uphill Tube E-5 Differential Pressure, Test 15 [0.61-1.22 m (2-4 ft)]

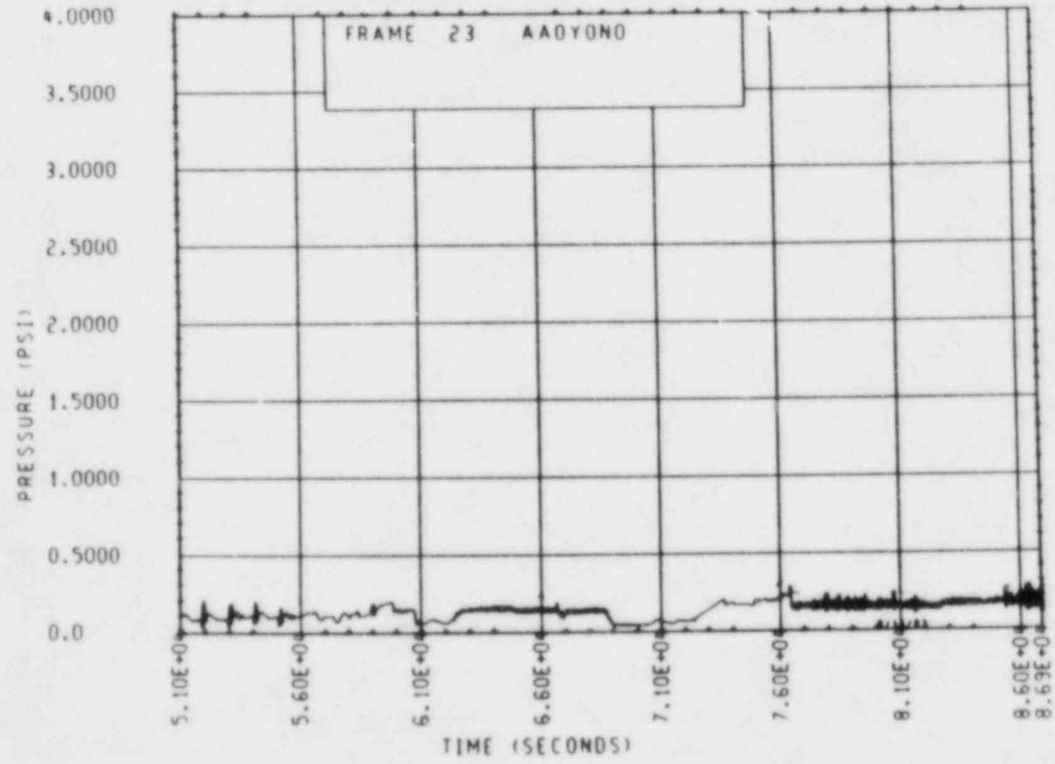

Figure A-220. Unbroken Loop Steam Generator Uphill Tube B-6 Differential Pressure, Test 15 [0-0.61 m (0-2 ft)]

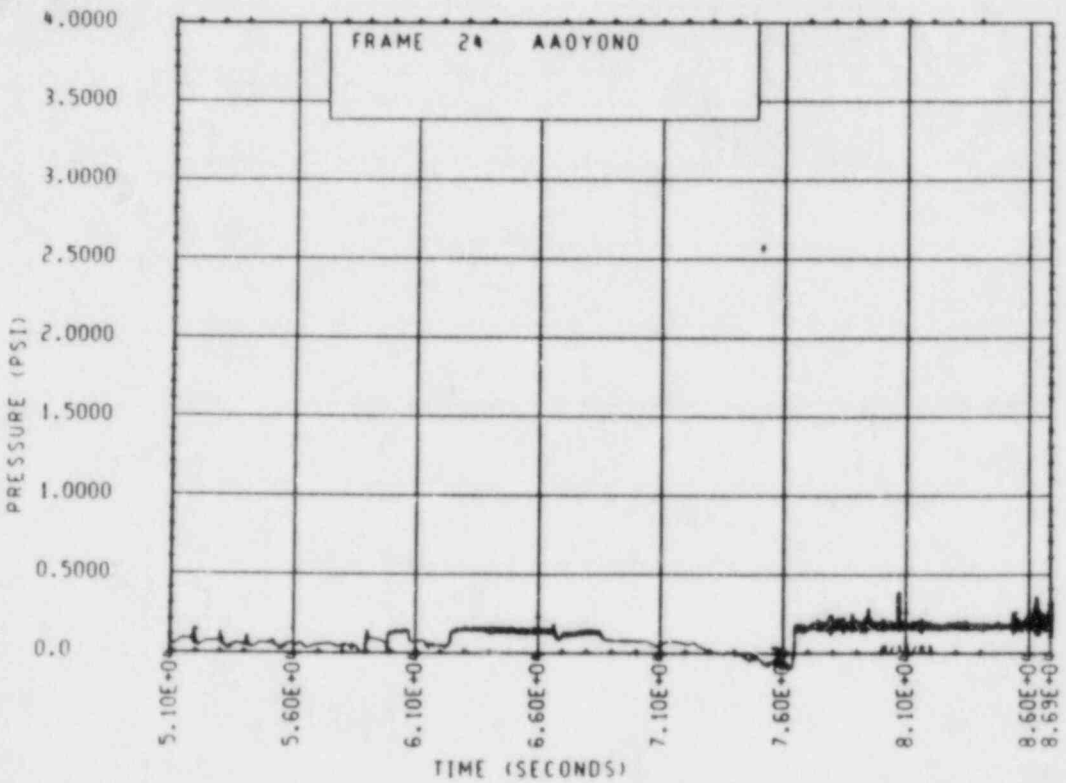

Figure A-221. Unbroken Loop Steam Generator Uphill Tube B-6 Differential Pressure, Test 15 [0.61-1.22 m (2-4 ft)]

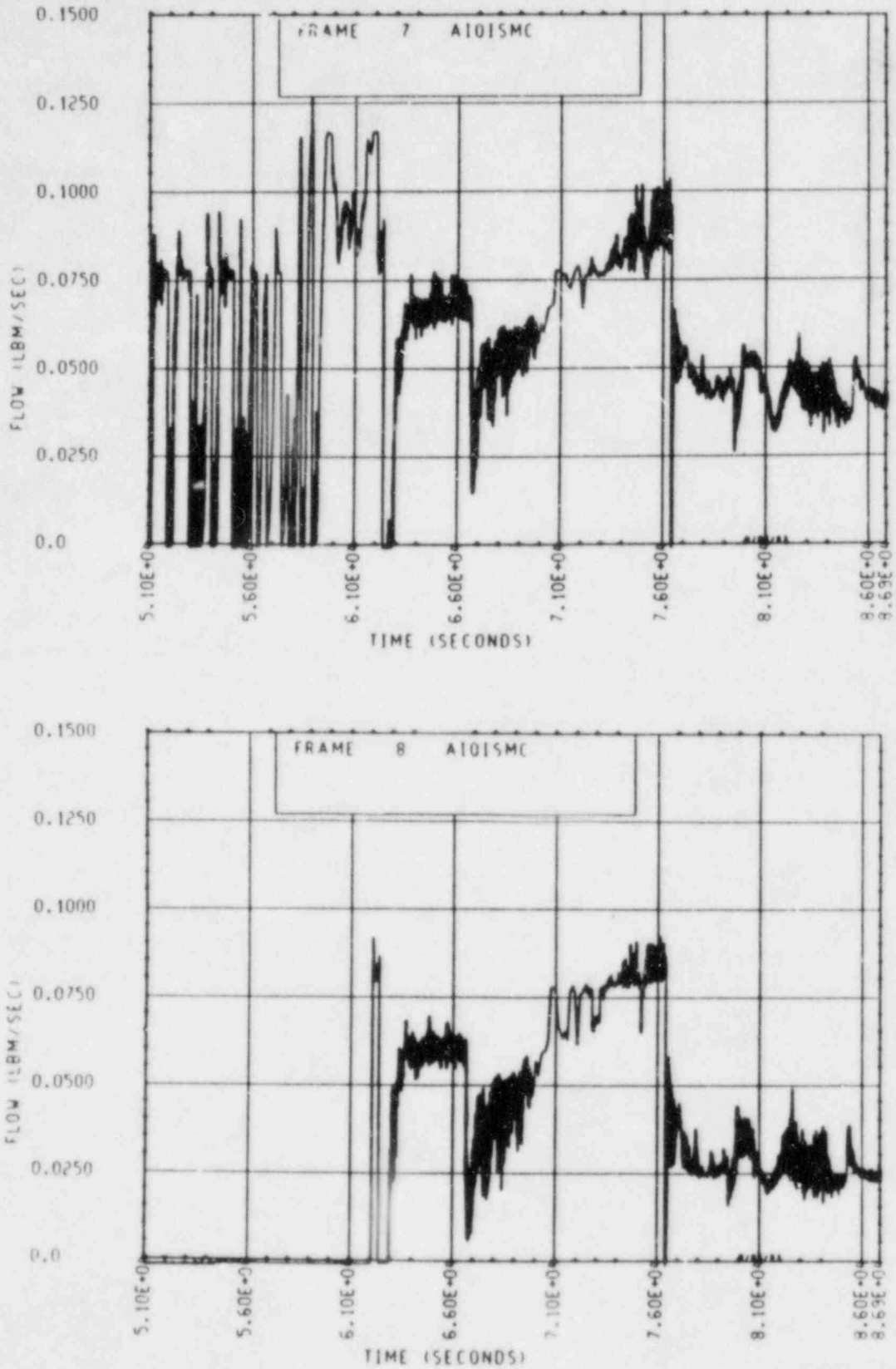

Figure A-222. Unbroken Loop Hot Leg Reflux Condensation Mass Flow Rate, Test 15

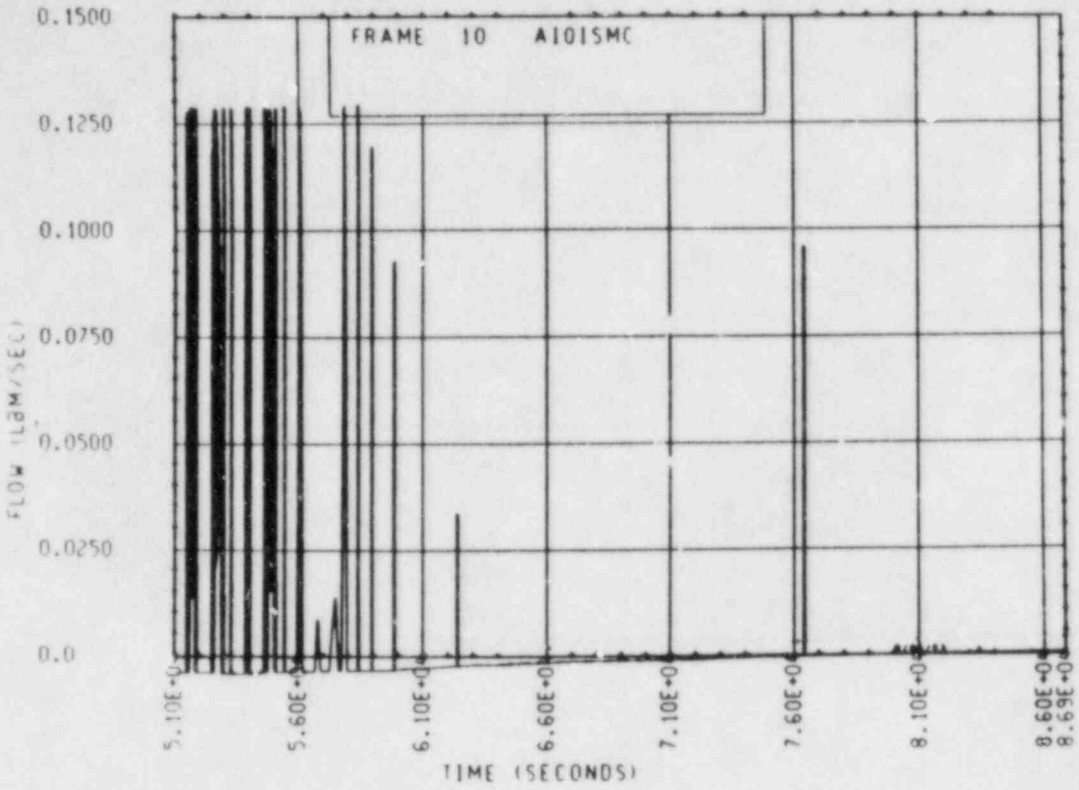

Figure A-223. Unbroken Loop Cold Leg Reflux Condensation Mass Flow Rate, Test 15

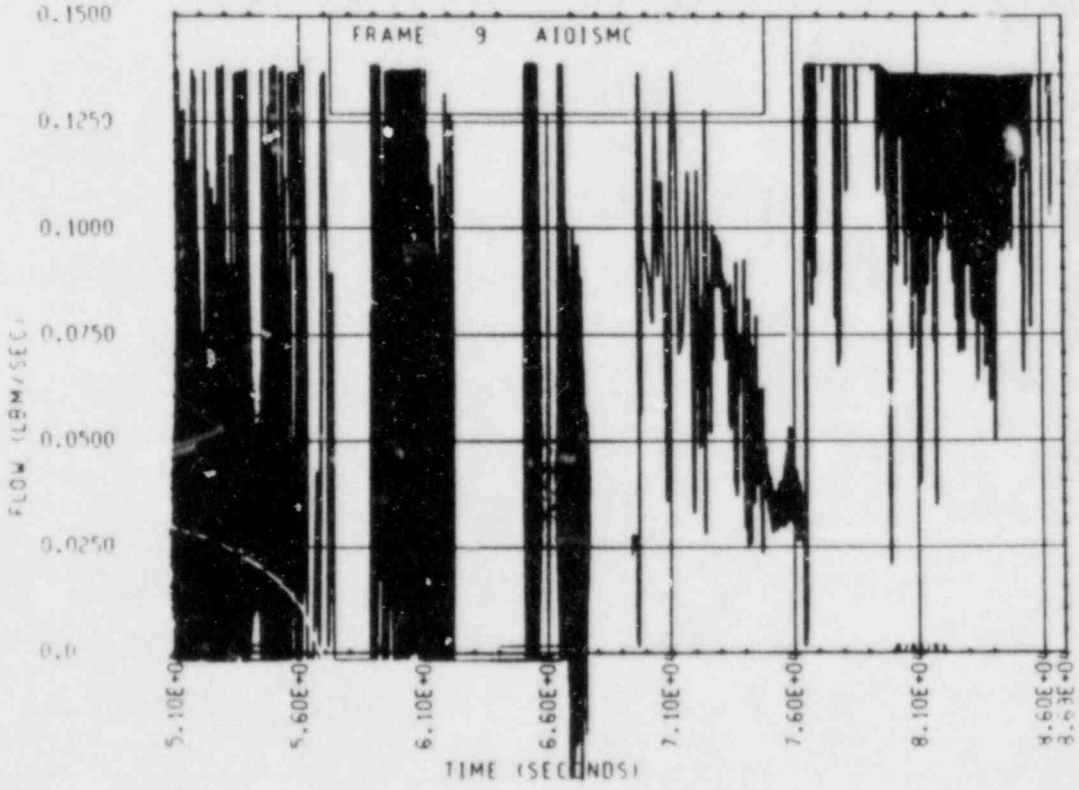

Figure A-224. Broken Loop Hot Leg Reflux Condensation Mass Flow Rate, Test 15

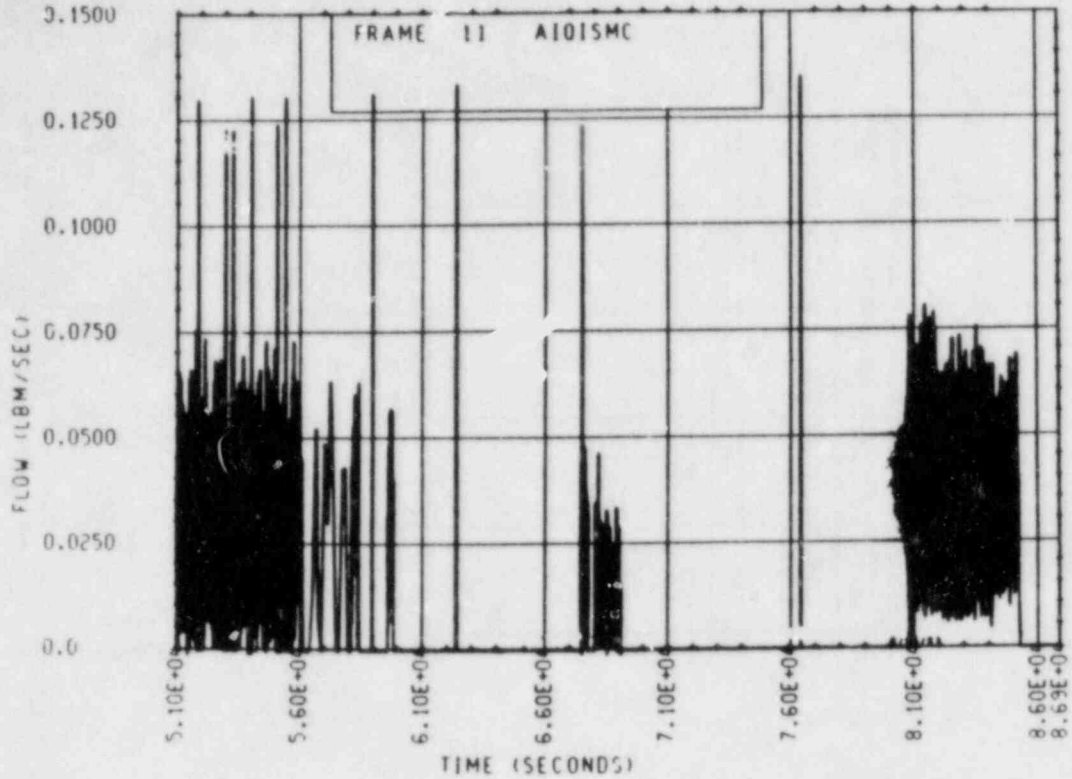

Figure A-225. Broken Loop Cold Leg Reflux Condensation Mass Flow Rate, Test 15

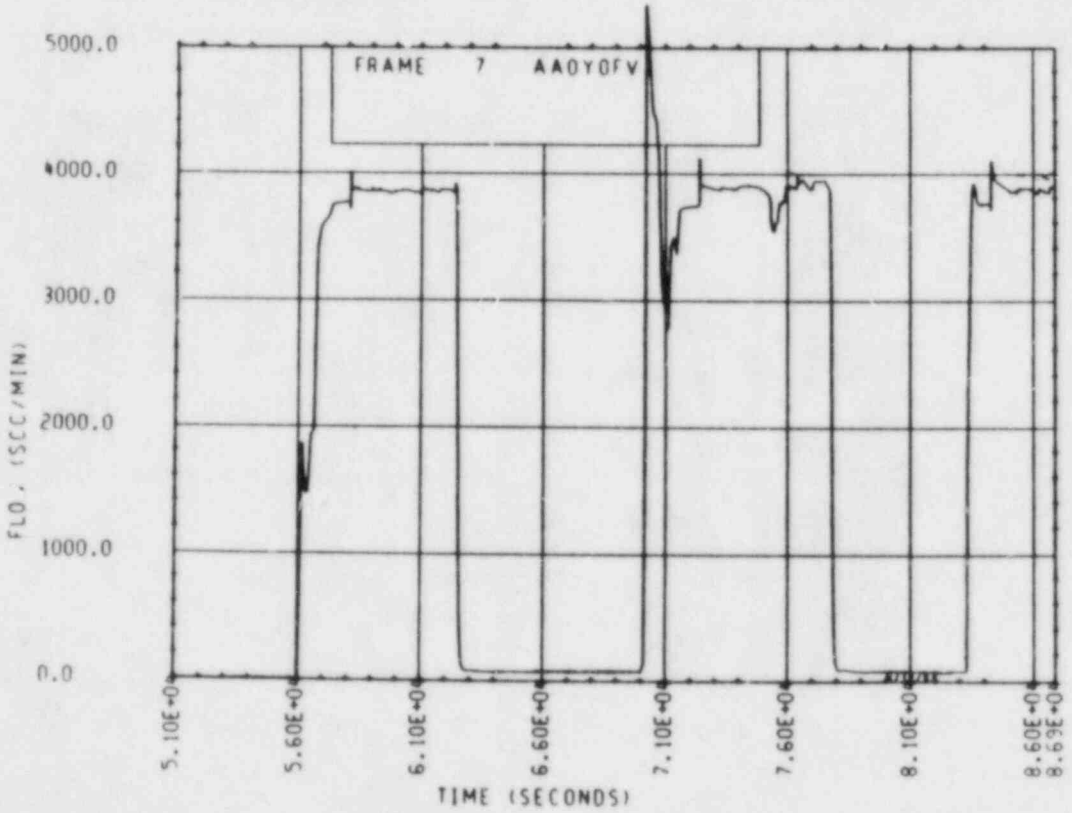

Figure A-226. Unbroken Loop Noncondensible Gas Injection Line Volumetric Flow Rate, Test 15

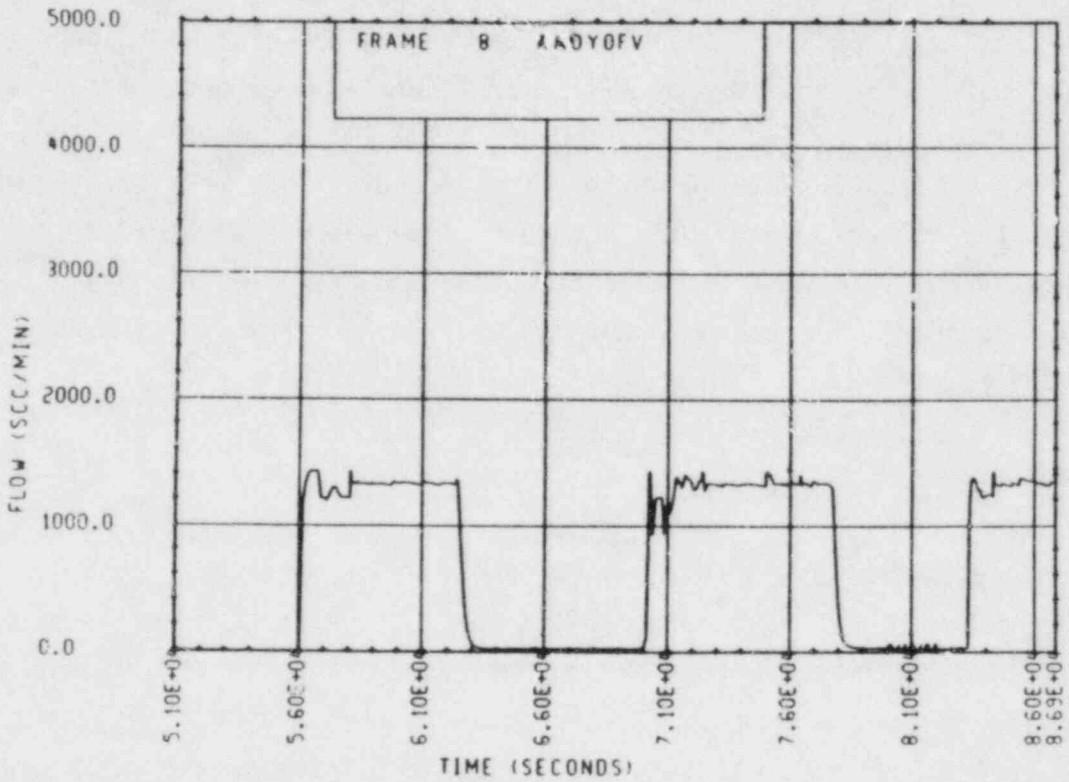

Figure A-227. Broken Loop Noncondensible Gas Injection Line Volumetric Flow Rate, Test 15

TEST 16: TWO-PHASE NATURAL CIRCULATION WITH SECONDARY SIDE DEPRESSURIZATION

Objective

To determine the effect of increased heat sink capacity on the primary side two-phase natural circulation

Test Procedure

The test was begun from a steady-state peak two-phase flow natural circulation mode with a nominal bundle power of 222 kw. The primary system was brought to the two-phase peak flow condition by draining 13.15 percent of the original single-phase mass inventory. The primary system was operated with the pressurizer valved out. The secondary sides were operated in a boiling mode with constant collapsed liquid levels of 7.62 m (25 ft) (71 percent full) and an initial pressure of 0.28 MPa (40 psia). The secondary side pressure regulator was incrementally lowered until the secondary side was operating at atmospheric pressure. Data were gathered at each secondary side pressure increment. The secondary side pressure was returned to 0.28 MPa (40 psia) and the test terminated when steady-state conditions were reestablished.

Test Overview

The primary system responded to the secondary side depressurization by correspondingly lowering its pressure and fluid temperatures around the loop. The primary to secondary pressure difference, however, did not remain a constant during the course of the depressurization, but decreased by approximately 25 percent. Before the start of the depressurization, the primary pressure was 0.14 MPa (21 psi) above the secondary side pressure. That difference was reduced to 0.10 MPa (15 psi) when the secondary side was completely depressurized to atmospheric conditions. It should be noted, however, that the primary and secondary were operating at low pressure conditions. Hence, the primary to secondary saturation temperature difference actually increased

while the pressure difference decreased. This would seem to indicate that the overall primary to secondary heat transfer coefficient was degraded during the depressurization.

The effect that the secondary side depressurization had on the peak two-phase flow throughout the loop was unclear. The mass flow rate slightly increased during the initial phases of the depressurization, only to slightly decrease in the later phases of the depressurization. This mass flow decrease was only temporary. The system returned to pretest conditions once the secondary side pressure was stabilized at 0.25 MPa (40 psi). The broken loop remained stalled during the course of the test.

TEST SCHEDULE
TEST 16

Time[a] (sec)	Event
27070	Secondary side pressure regulator adjusted to drop pressure from 0.28 to 0.24 MPa (40 to 35 psi)
28270	Secondary side pressure regulator adjusted to drop pressure to 0.21 MPa (30 psi)
29176	Secondary side pressure regulator adjusted to drop pressure to 0.17 MPa (25 psi)
29830	Secondary side pressure regulator opened all the way
32410	Secondary side pressure regulator adjusted to increase pressure to 0.14 MPa (20 psi); beginning of recovery to reference conditions
32590	Secondary side pressure regulator adjusted to increase pressure to 0.21 MPa (30 psi)
32770	Both steam generator feedwater flows shut off
33310	Secondary side pressure regulator adjusted to increase pressure to 0.28 MPa (40 psi)

a. Test 16 was run in series with test 8. Time zero therefore corresponds with time zero of test 8. All computer times are referenced to this time.

Time (sec)	Event
33790	Artificially drained both steam generators to recover to a 7.62 m (25 ft) collapsed liquid level; end of test 16

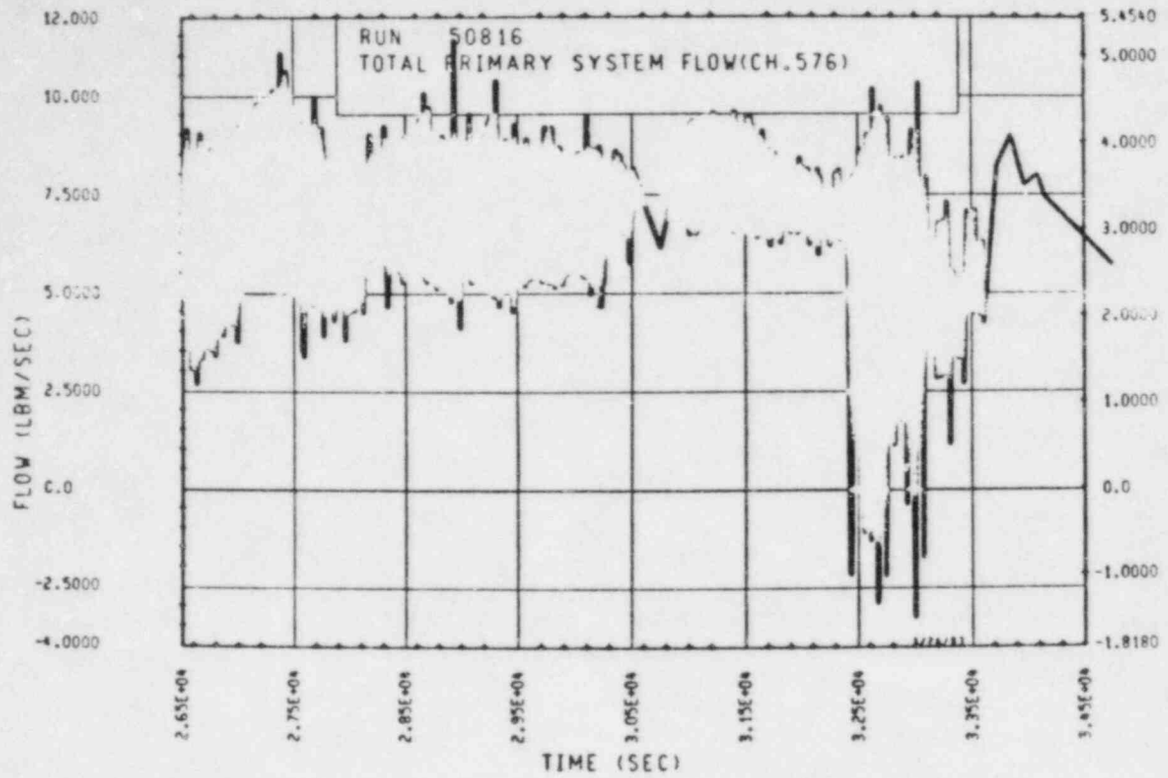

Figure A-228. Mass Flow Rate Through Rod Bundle, Test 16

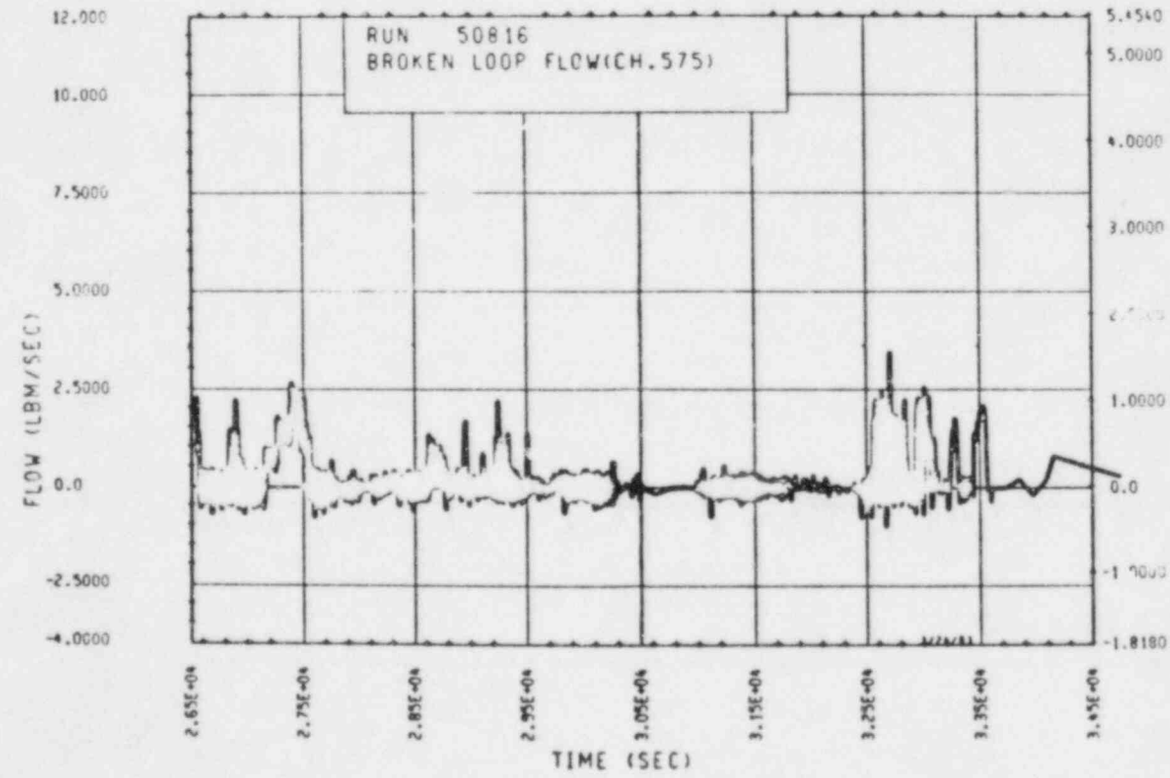

Figure A-229. Mass Flow Rate Through Broken Loop, Test 16

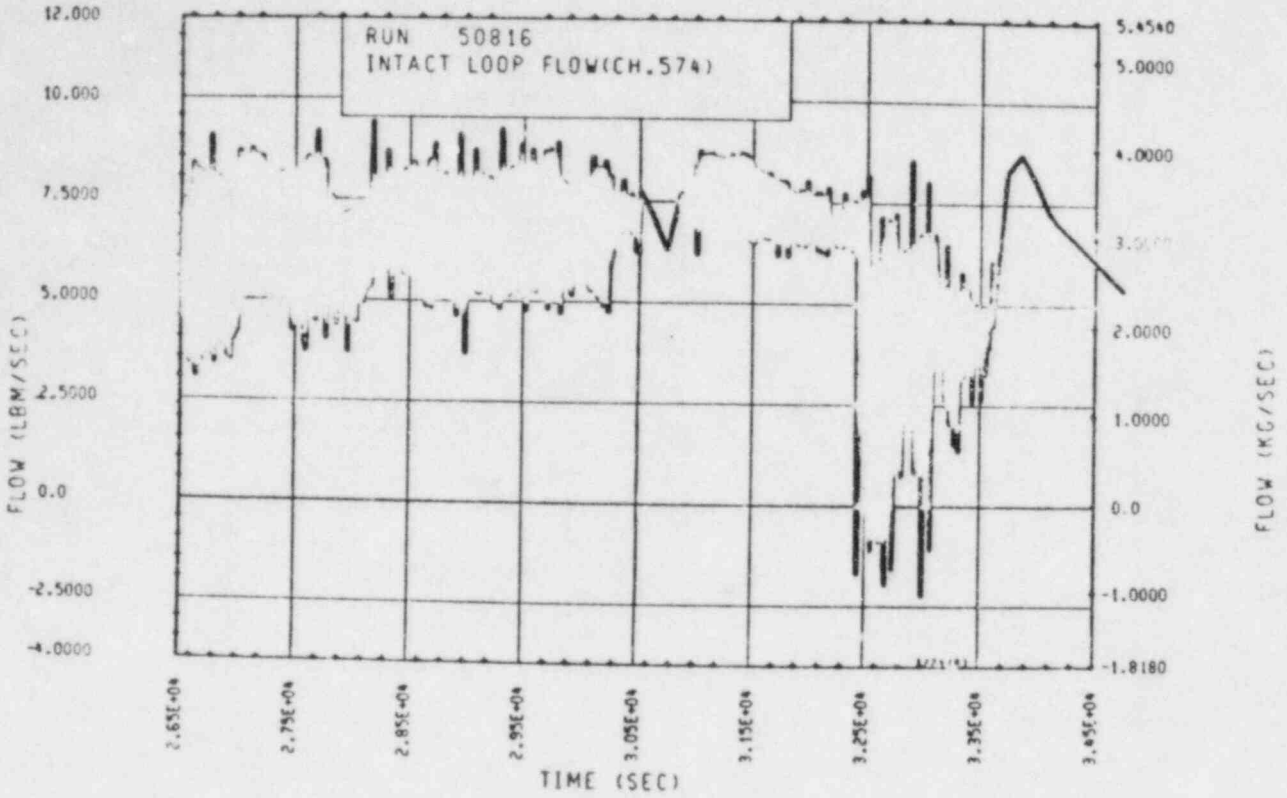

Figure A-230. Mass Flow Rate Through Unbroken Loop, Test 16

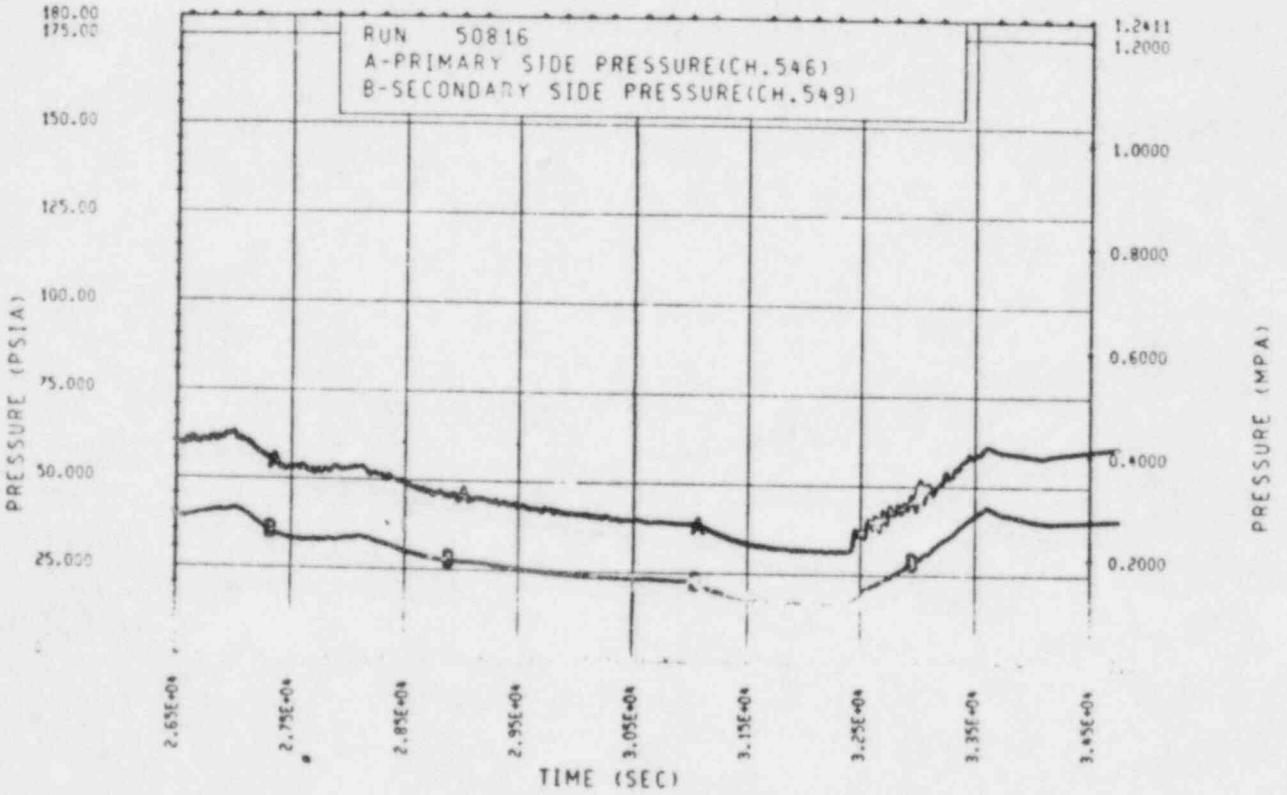

Figure A-231. Primary and Secondary System Pressure, Test 16

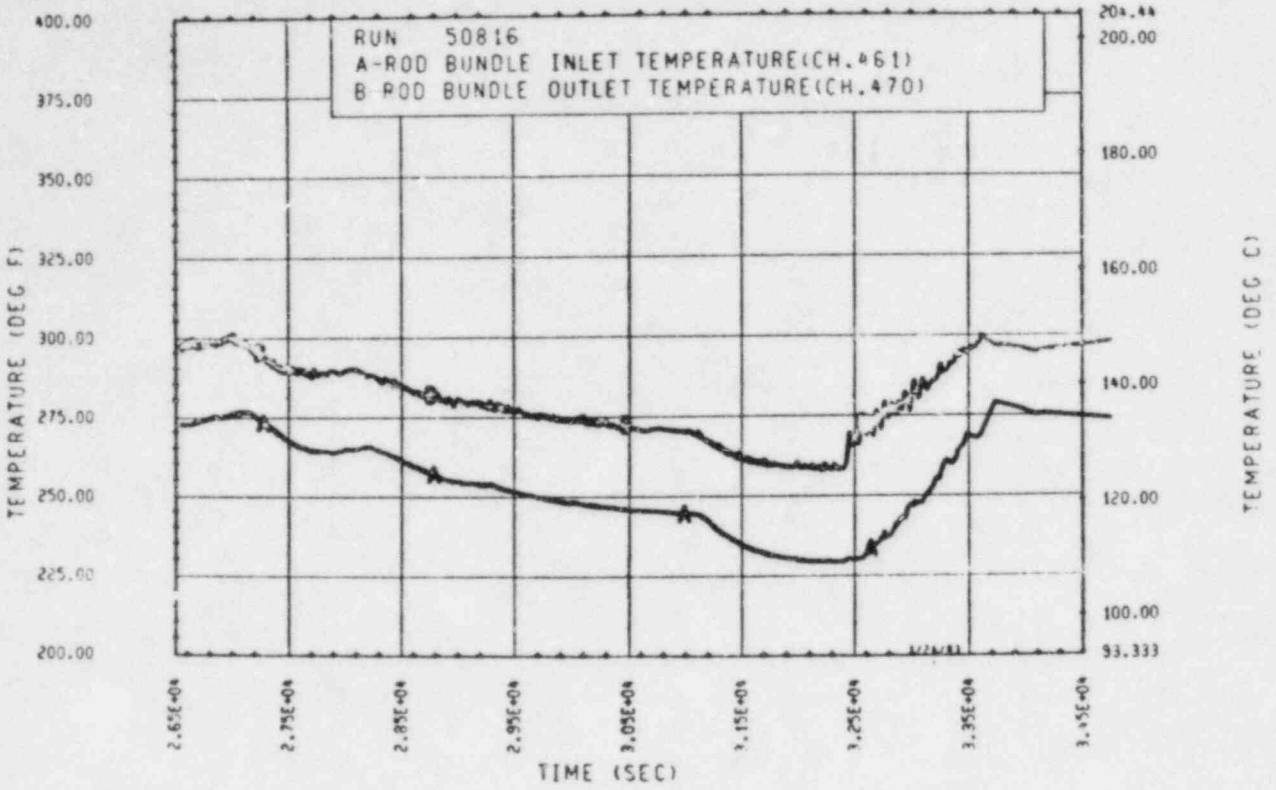

Figure A-232. Heater Rod Bundle Inlet and Outlet Temperature, Test 16

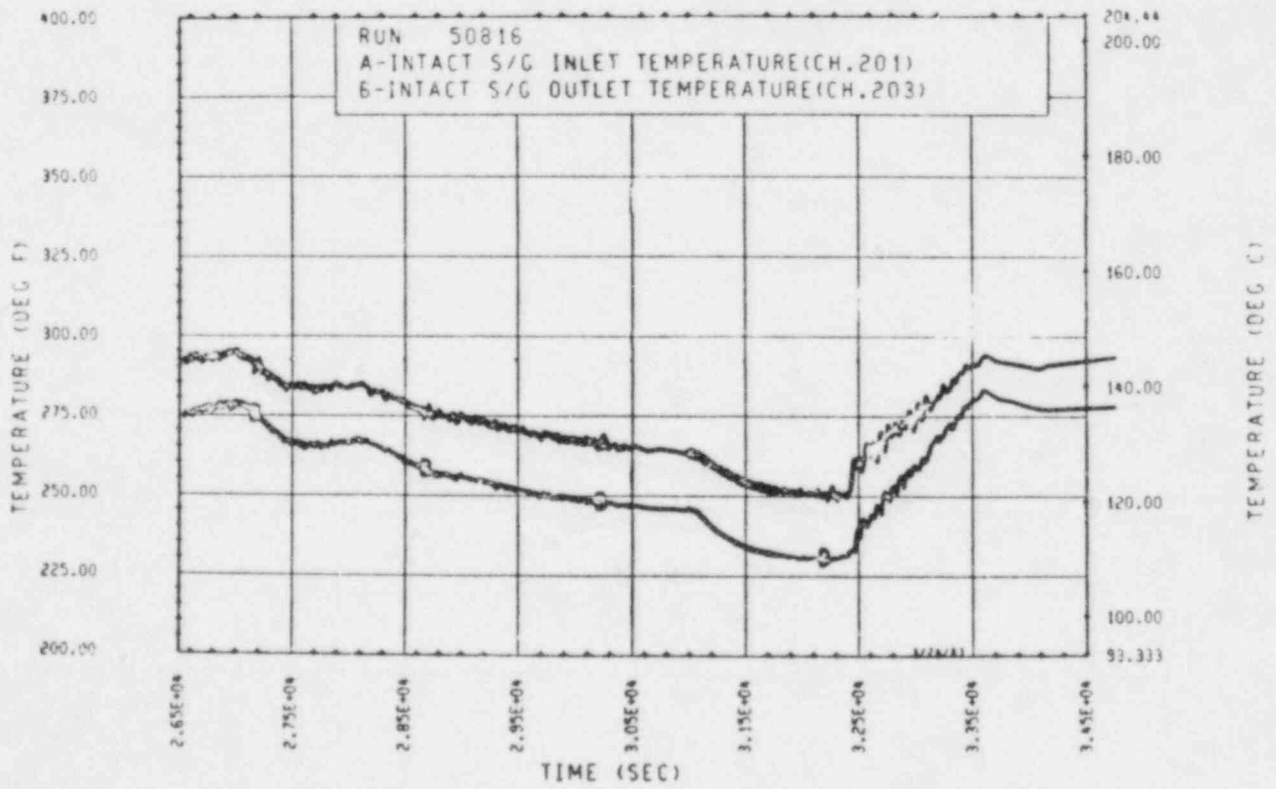

Figure A-233. Unbroken Loop Steam Generator Inlet and Outlet Temperature, Test 16

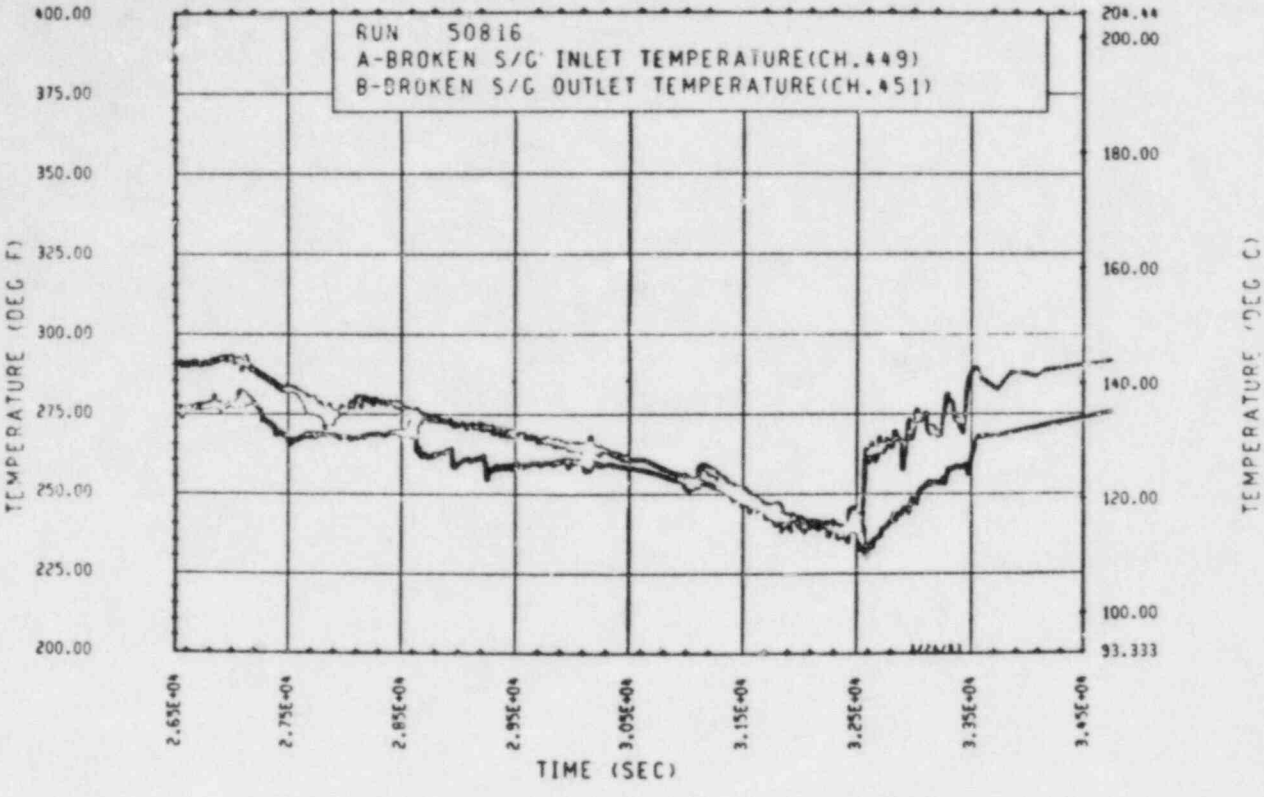

Figure A-234. Broken Loop Steam Generator Inlet and Outlet Temperature, Test 16

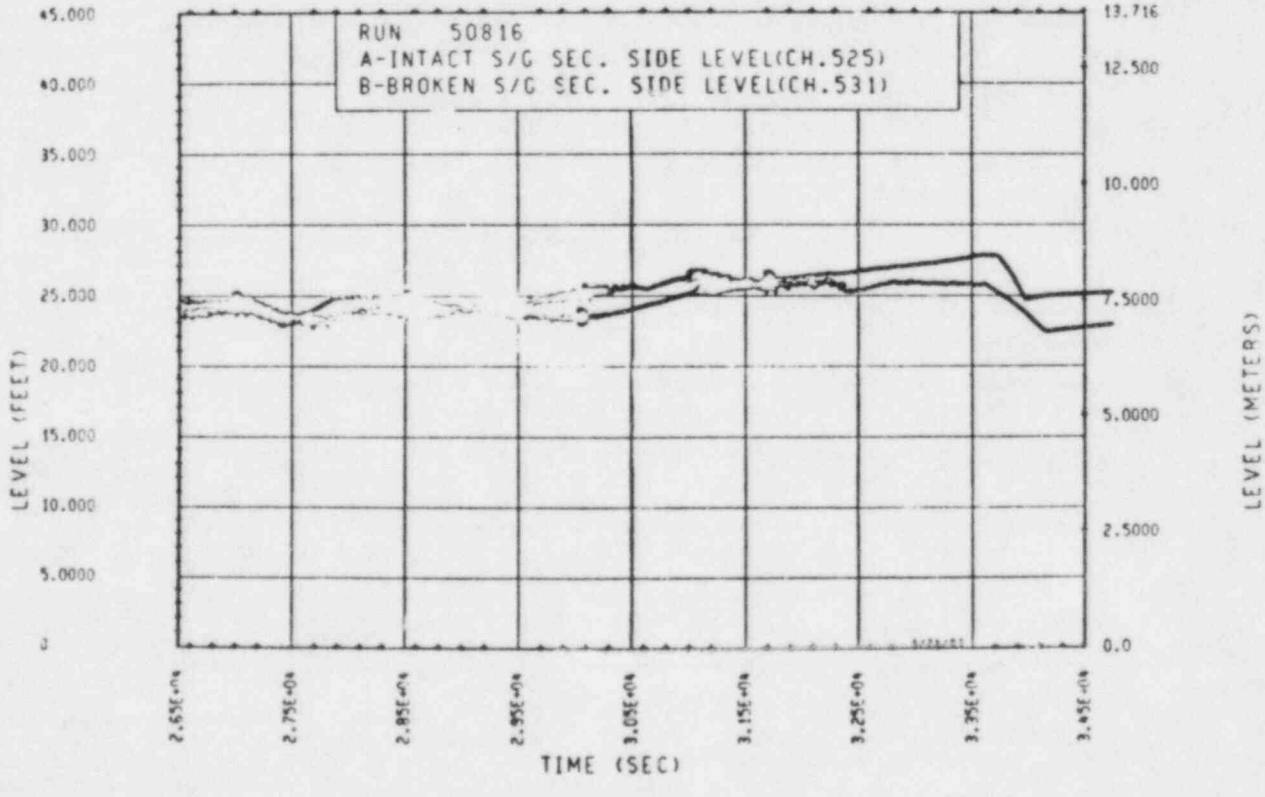

Figure A-235. Unbroken and Broken Loop Steam Generator Secondary Side Collapsed Liquid Levels, Test 16

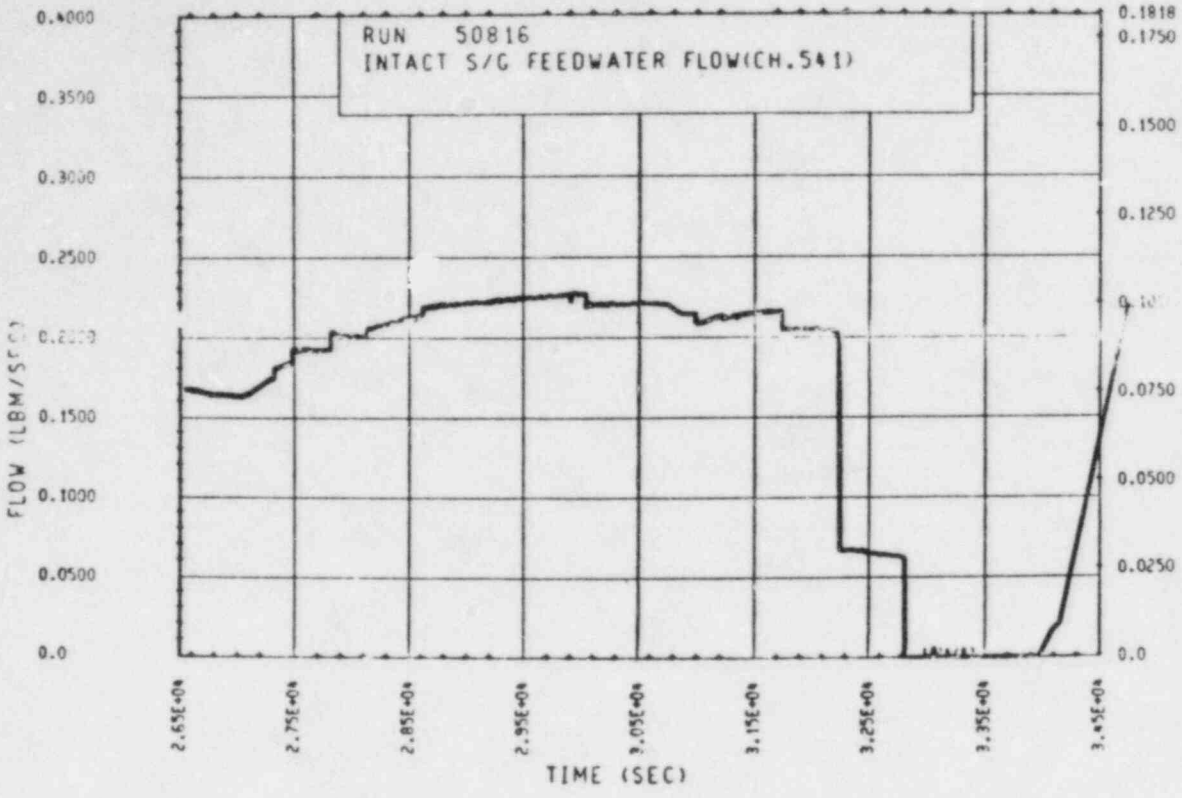

Figure A-236. Unbroken Loop Steam Generator Feedwater Mass Flow Rate, Test 16

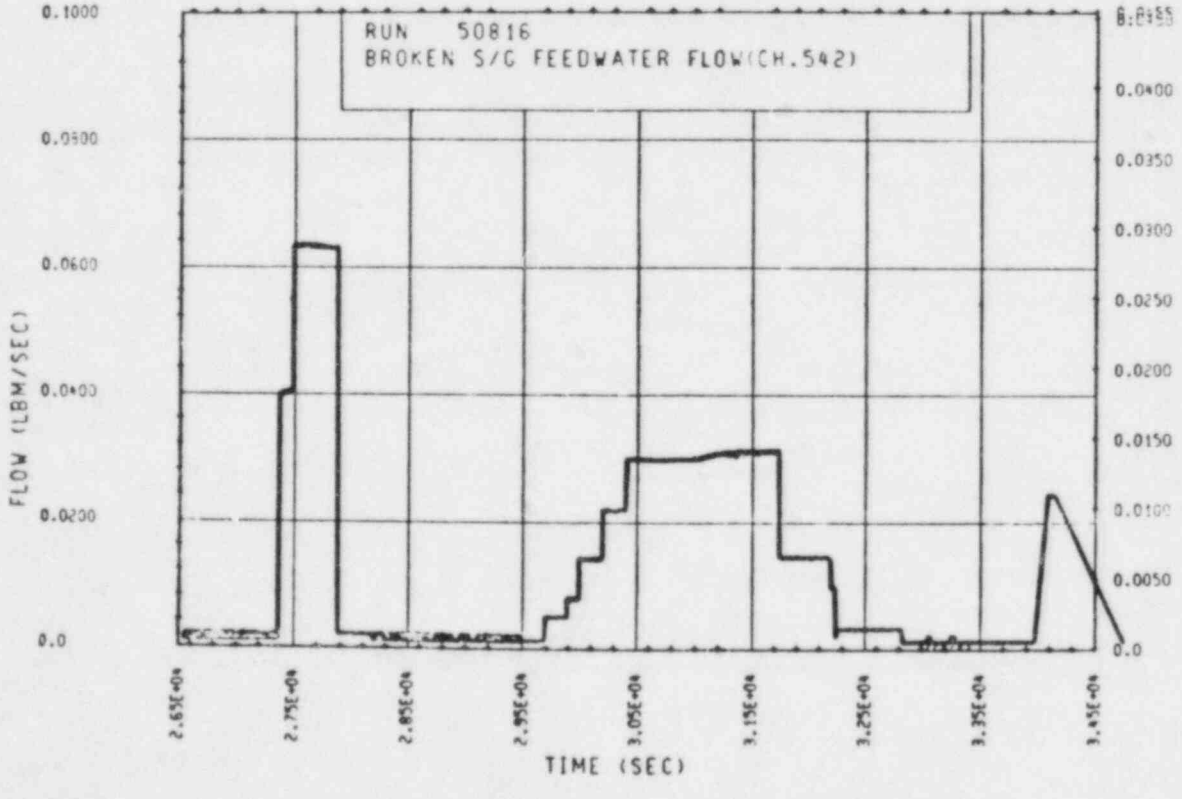

Figure A-237. Broken Loop Steam Generator Feedwater Mass Flow Rate, Test 16

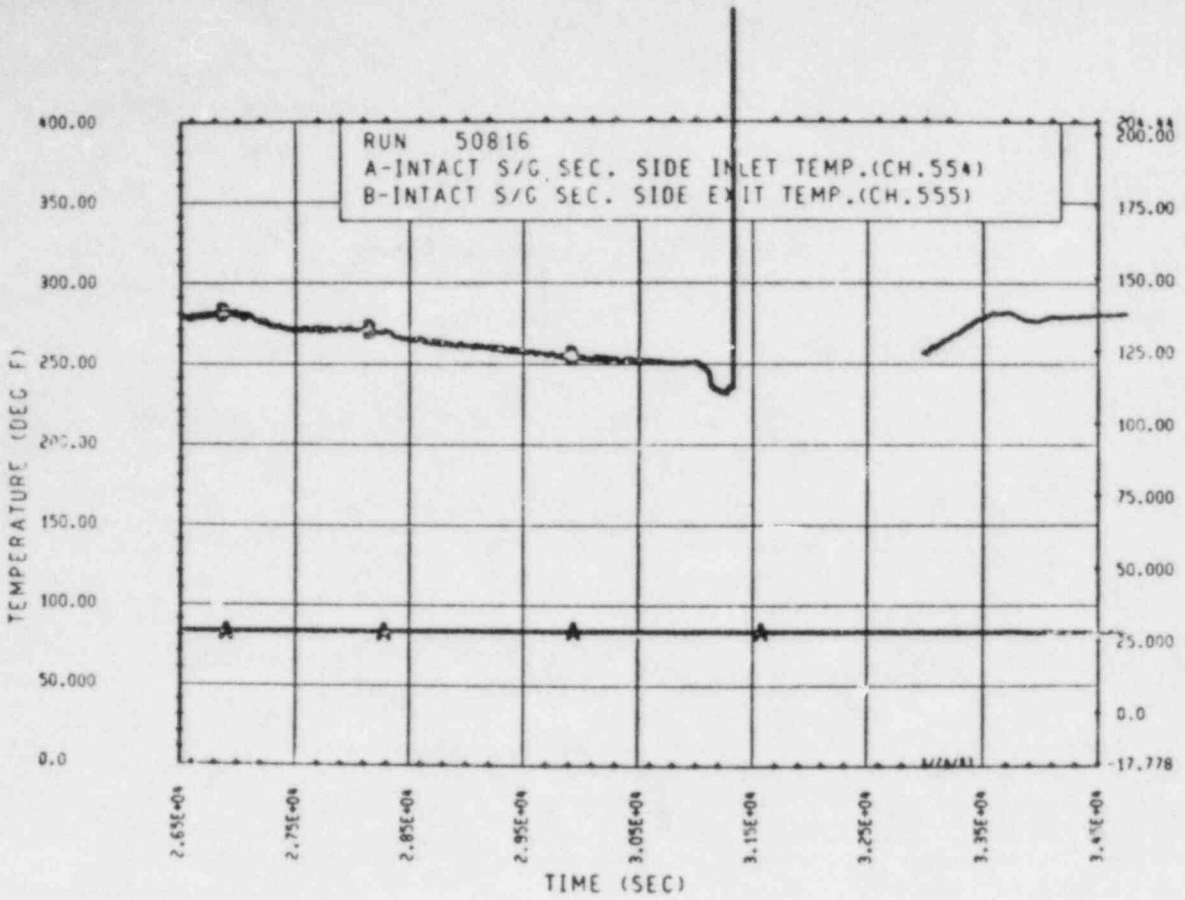

Figure A-238. Unbroken Loop Steam Generator Secondary Side Inlet and Outlet Temperature, Test 16

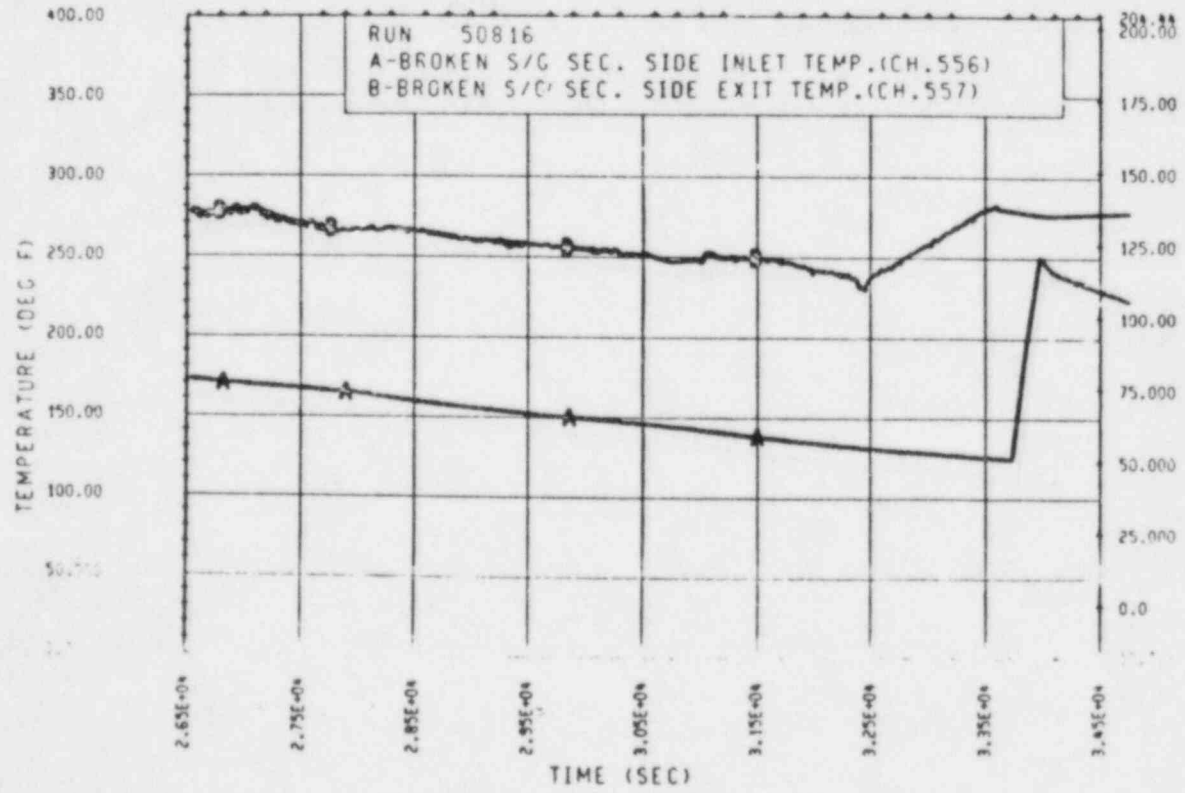

Figure A-239. Broken Loop Steam Generator Secondary Side Inlet and Outlet Temperature, Test 16

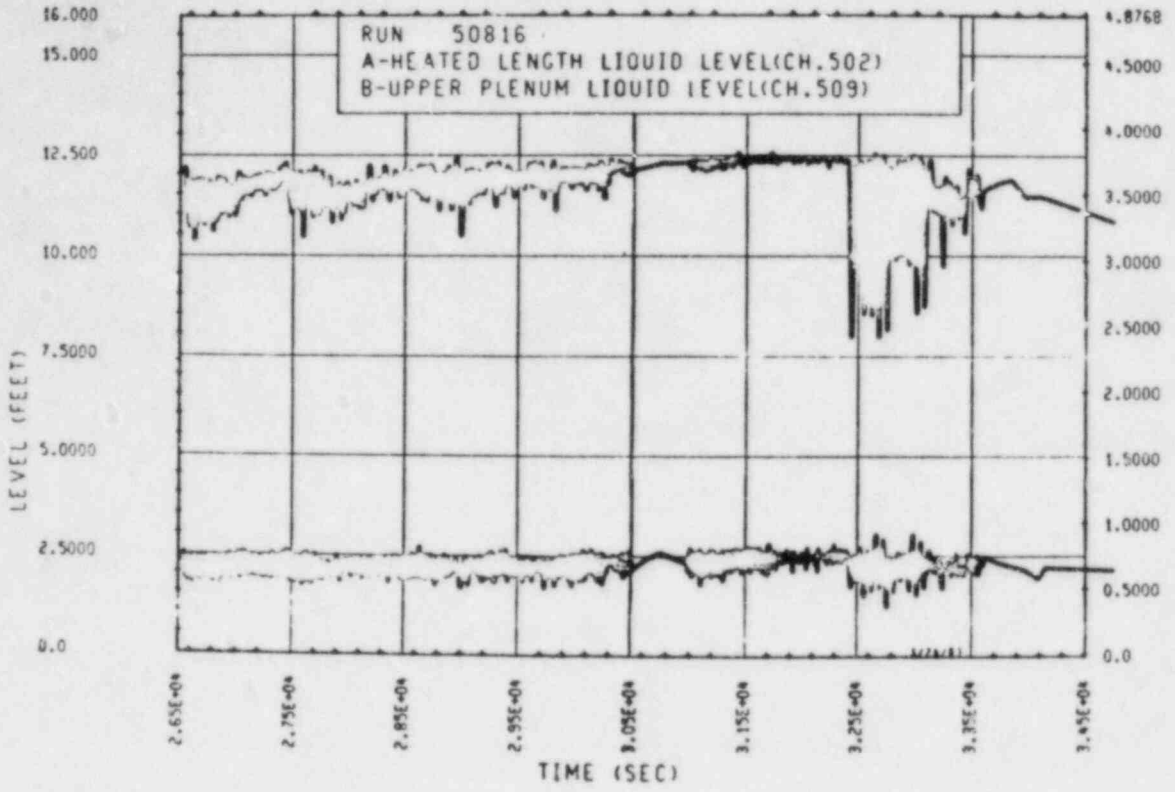

Figure A-240. Heated Length and Upper Plenum Liquid Levels, Test 16

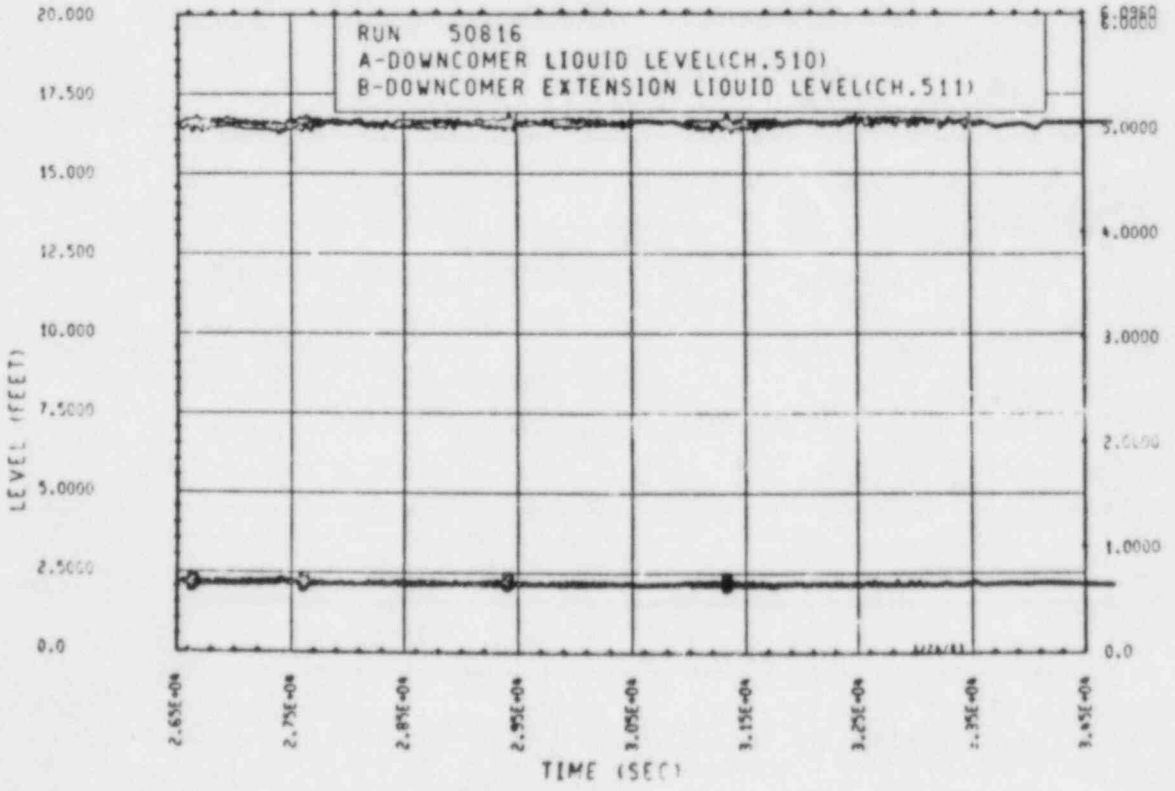

Figure A-241. Downcomer and Downcomer Extension Liquid Levels, Test 16

TEST 17: TWO-PHASE NATURAL CIRCULATION WITH BROKEN LOOP STEAM GENERATOR BOILOFF

Objective:

To determine the effect of a heat sink imbalance on peak two-phase natural circulation

Test Procedure

The test was begun from a steady-state peak two-phase flow natural circulation mode with a nominal bundle power of 222 kw. The primary system was brought to the two-phase peak flow condition by draining 18.60 percent of the original single-phase mass inventory. The primary system was operated with the pressurizer valved out. The secondary side was operated in a boiling mode with a nominal pressure of 0.25 MPa (35 psia) and an initial collapsed liquid level of 7.62 m (25 ft) (71 percent full). The broken loop steam generator feedwater line was valved out, allowing the secondary side collapsed liquid level to boil dry. The unbroken loop steam generator secondary side was maintained at a constant collapsed liquid level of 7.62 m (25 ft). After a steady-state condition had been achieved with the broken loop steam generator boiled dry, the steam generator secondary side was refilled with 93°C (200°F) water from accumulator 2.

Test Overview

Prior to the initiation of the broken loop secondary side boiloff, the primary system was operated in a two-phase peak flow natural circulation mode. The broken loop was stalled, however, as it characteristically would do whenever the system was operated in a two-phase mode. As a result, the system was essentially operated in a N-1 loop configuration, with the unbroken loop steam generator acting as the sole heat sink. Hence the heat sink imbalance imposed on the primary system by boiling off the broken loop secondary had no effect. The broken loop remained stalled and the unbroken loop continued to operate quite efficiently as the sole heat sink.

TEST SCHEDULE
TEST 17

Time[a] (sec)	Event
19509	Pressurizer valved out
20343	Began incremental drains of the primary inventory to achieve a maximum two-phase flow situation; began drain 1
20709	Ended drain 1; 18 kg (40 lbm) drained
21015	Began drain 2
21128	Ended drain 2; total of 36 kg (80 lbm) drained
21639	Began drain 3
21766	Ended drain 3; total of 54 kg (120 lbm) drained
22591	Began drain 4
22715	Ended drain 4, total of 73 kg (160 lbm) drained
23620	Began drain 5

a. Test 17 was run in series with test 14. Time zero therefore corresponds with time zero of test 14. All computer times are referenced to this time.

Time (sec)	Event
23733	Ended drain 5; total of 91 kg (200 lbm) drained
24613	Began drain 6
24720	Ended drain 6; total of 109 kg (240 lbm) drained. Small steam generator stalled.
25273	Began drain 7
25383	Ended drain 7; total of 127 kg (280 lbm) drained
26075	Began drain 8
26193	Ended drain 8; total of 145 kg (320 lbm) drained
26323	Secondary side pressure manually raised from 0.19 to 0.28 MPa (28 to 40 psi) to run the system at conditions similar to test 8
28471	Began drain 9
28535	Ended drain 9; total of 154 kg (340 lbm) drained
29368	Total primary flow indicated that the primary system had achieved two-phase peak flow. Start of a 15-minute reference run.
30295	End of steady-state reference run
30385	Small steam generator secondary side feedwater shut off; began small steam generator secondary side boiloff

Time (sec)	Event
31236	Small steam generator boiled intermittently.
35936	Small steam generator boiled dry.
36152	Began small steam generator secondary side recovery
36723	Ended small steam generator secondary side recovery; end of test 17

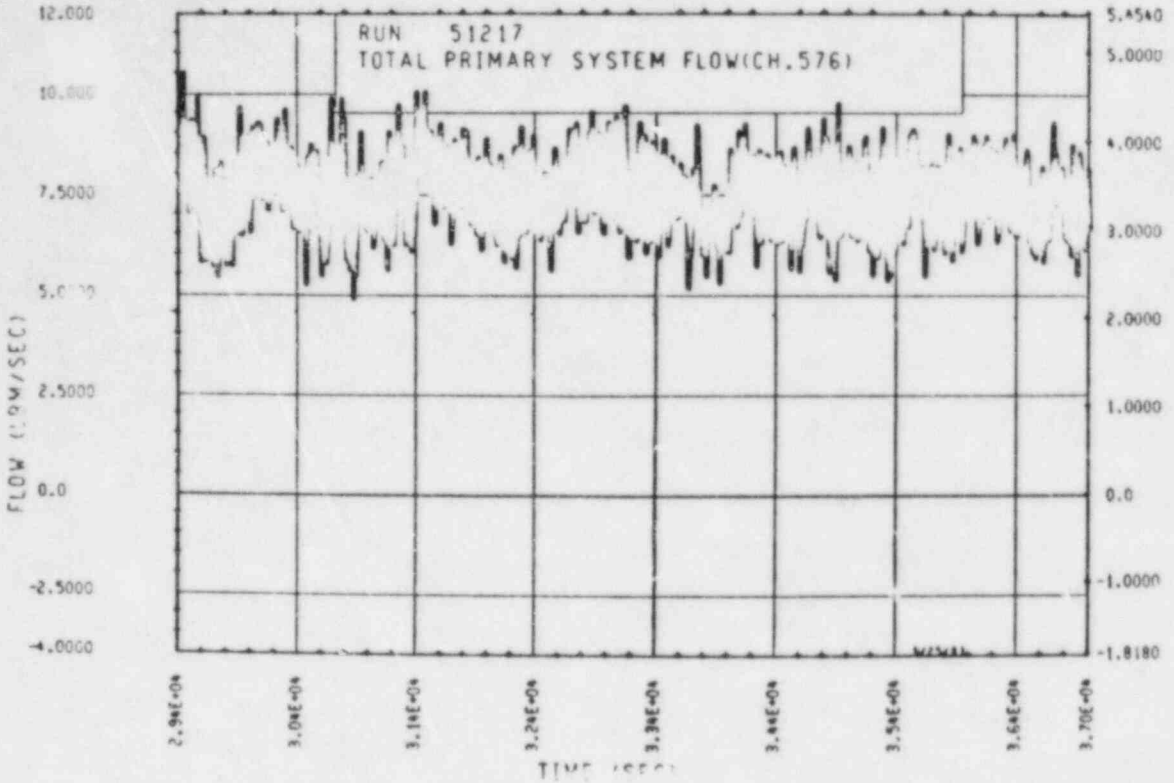

Figure A-242. Mass Flow Rate Through Rod Bundle, Test 17

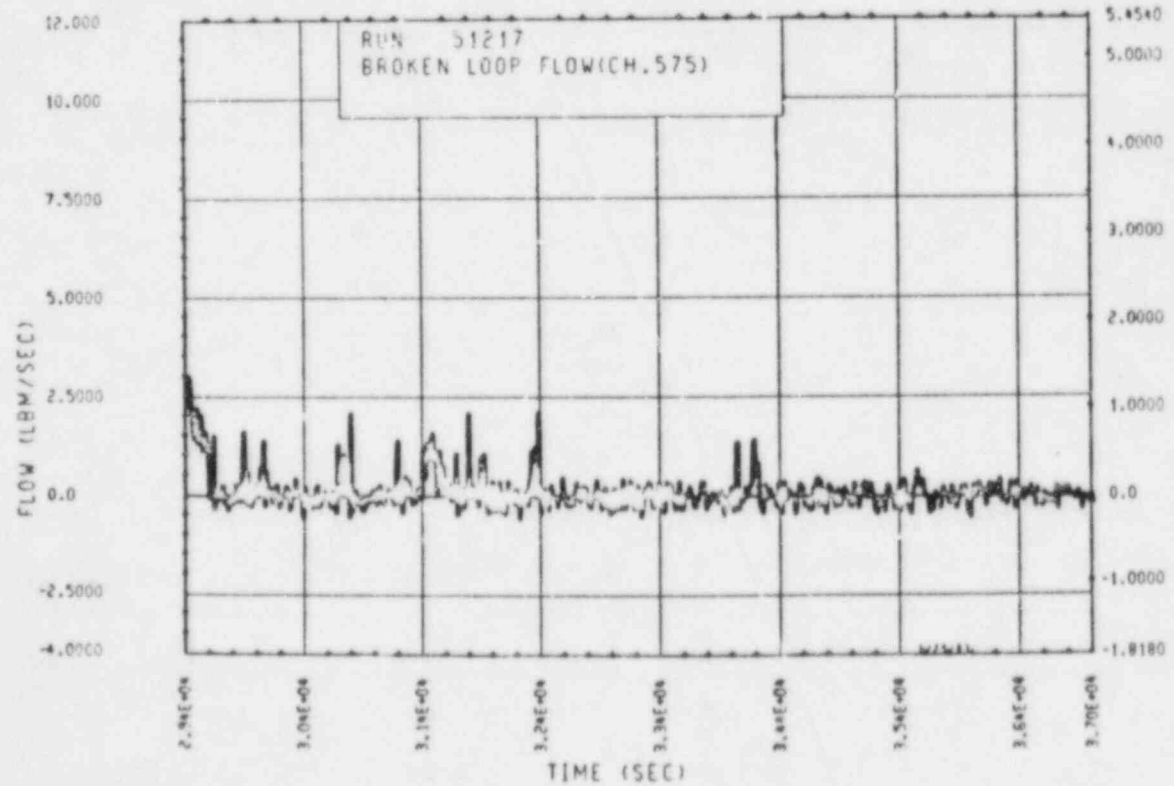

Figure A-243. Mass Flow Rate Through Broken Loop, Test 17

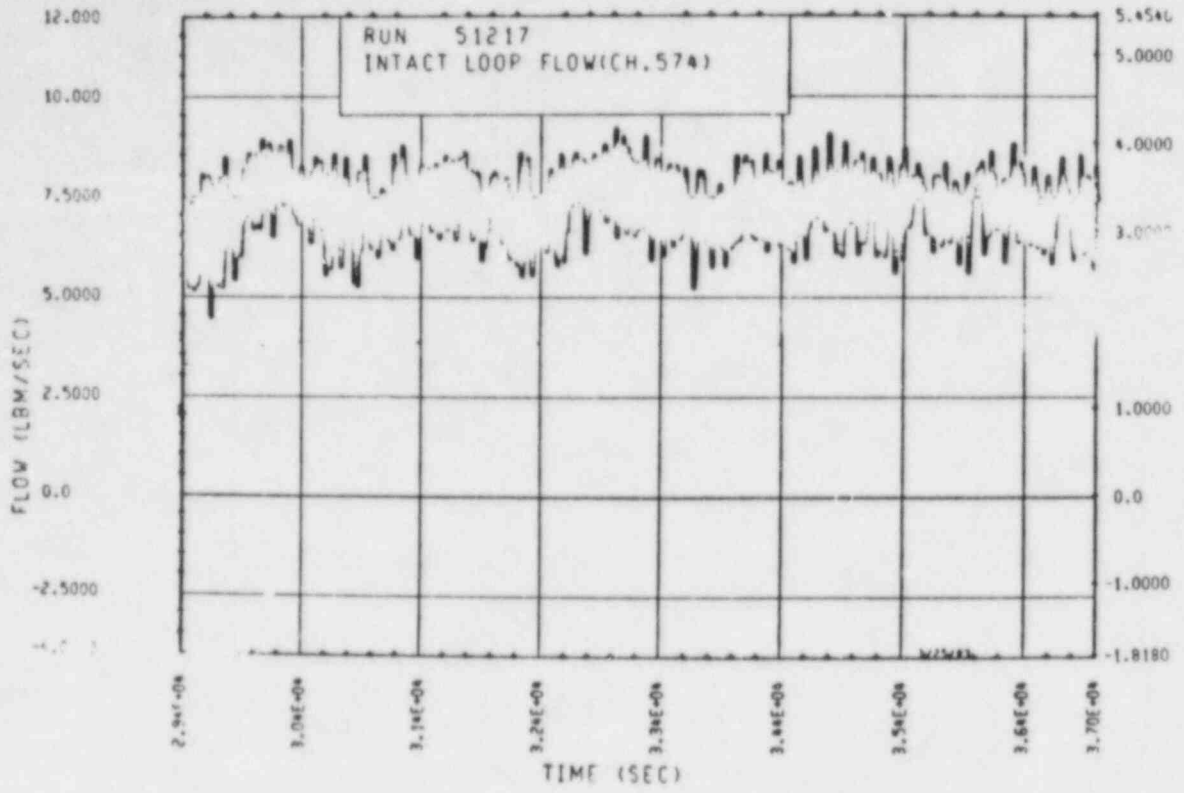

Figure A-244. Mass Flow Rate Through Unbroken Loop, Test 17

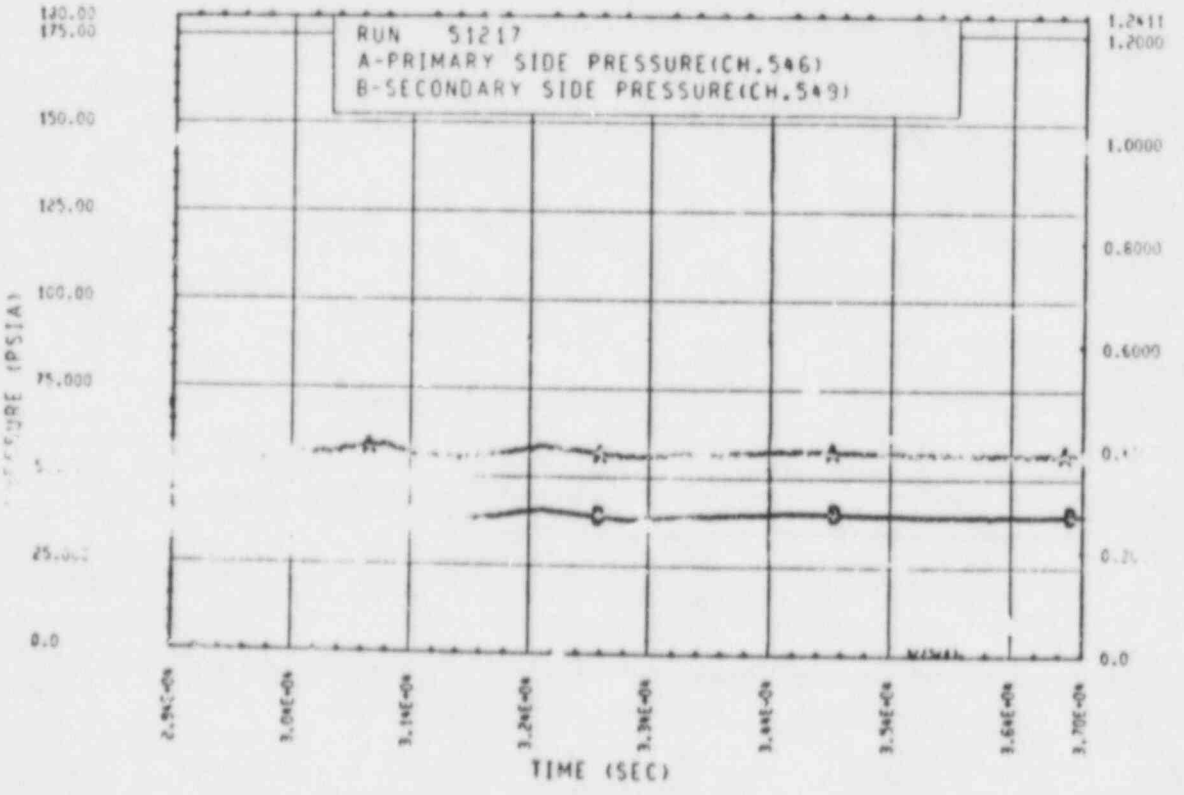

Figure A-245. Primary and Secondary System Pressure, Test 17

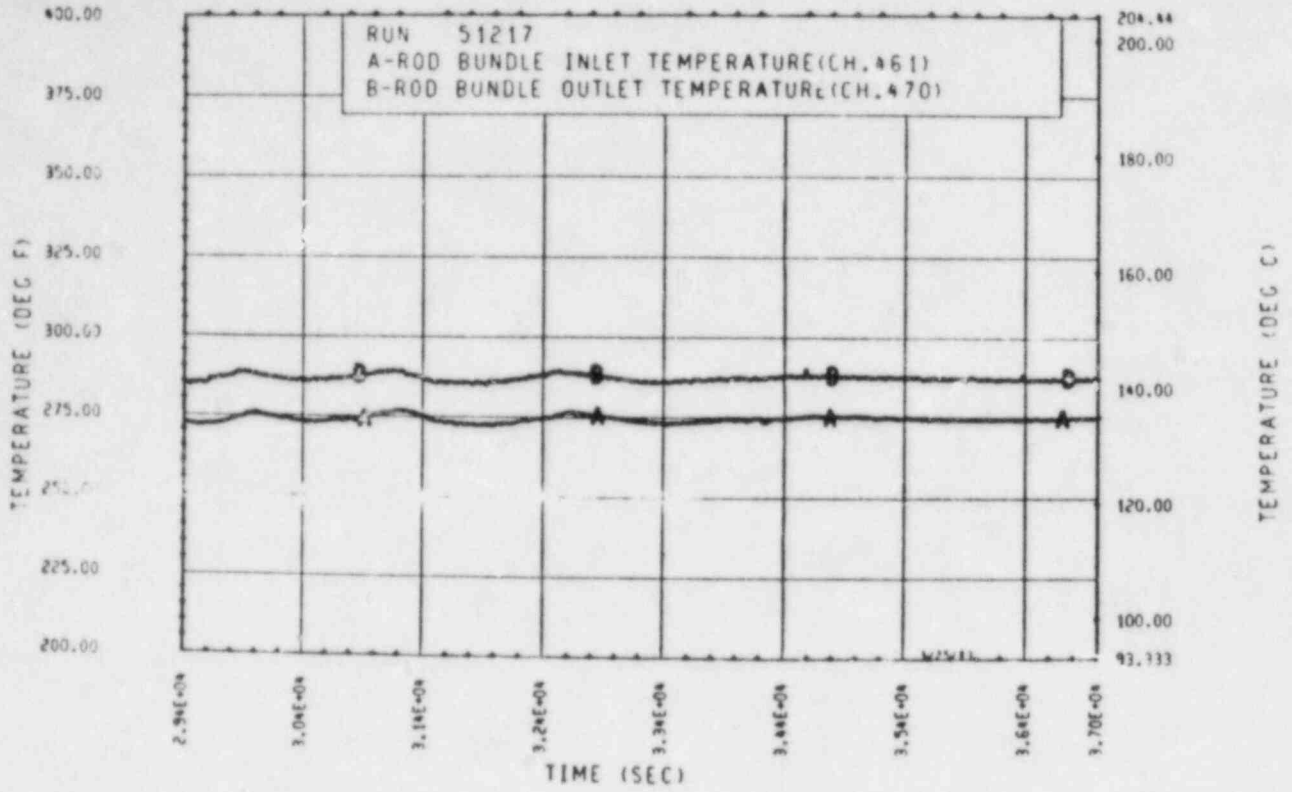

Figure A-246. Heater Rod Bundle Inlet and Outlet Temperature, Test 17

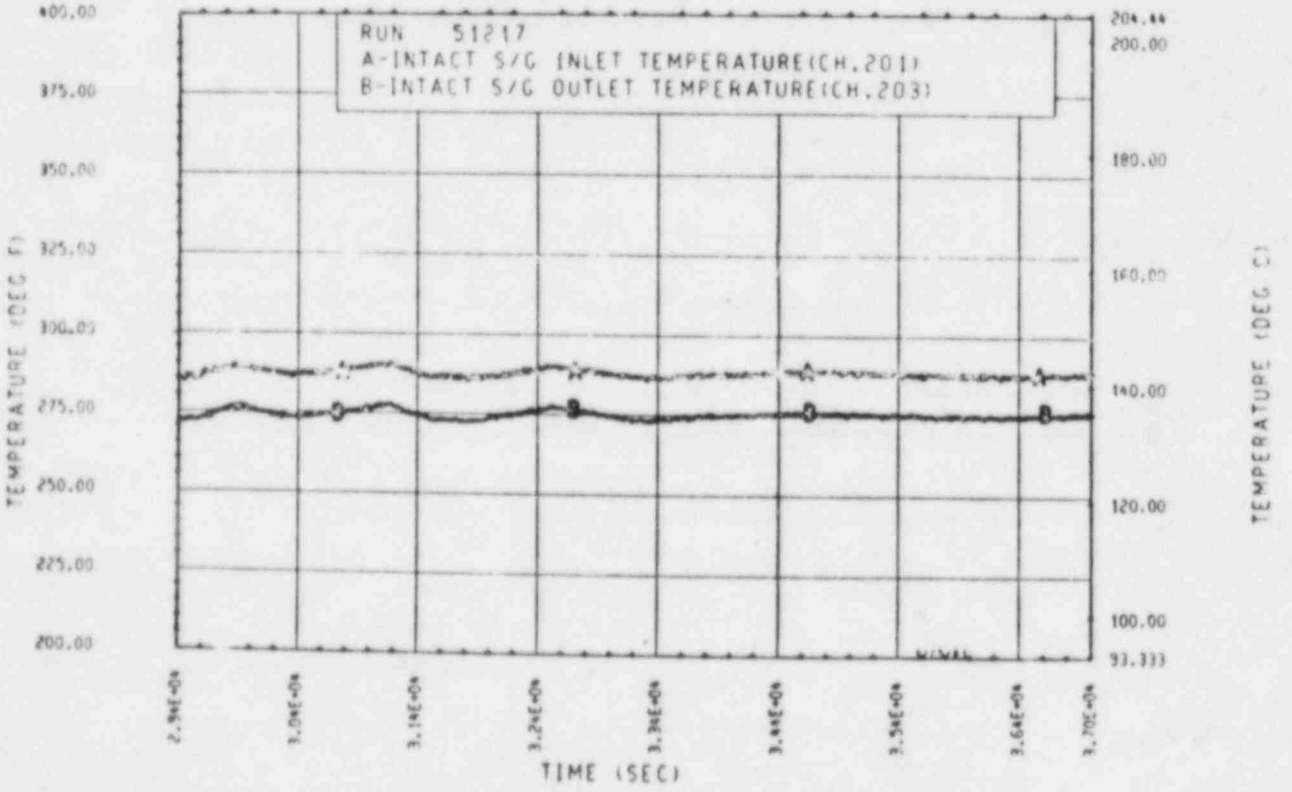

Figure A-247. Unbroken and Broken Loop Steam Generator Secondary Side Collapsed Liquid Levels, Test 17

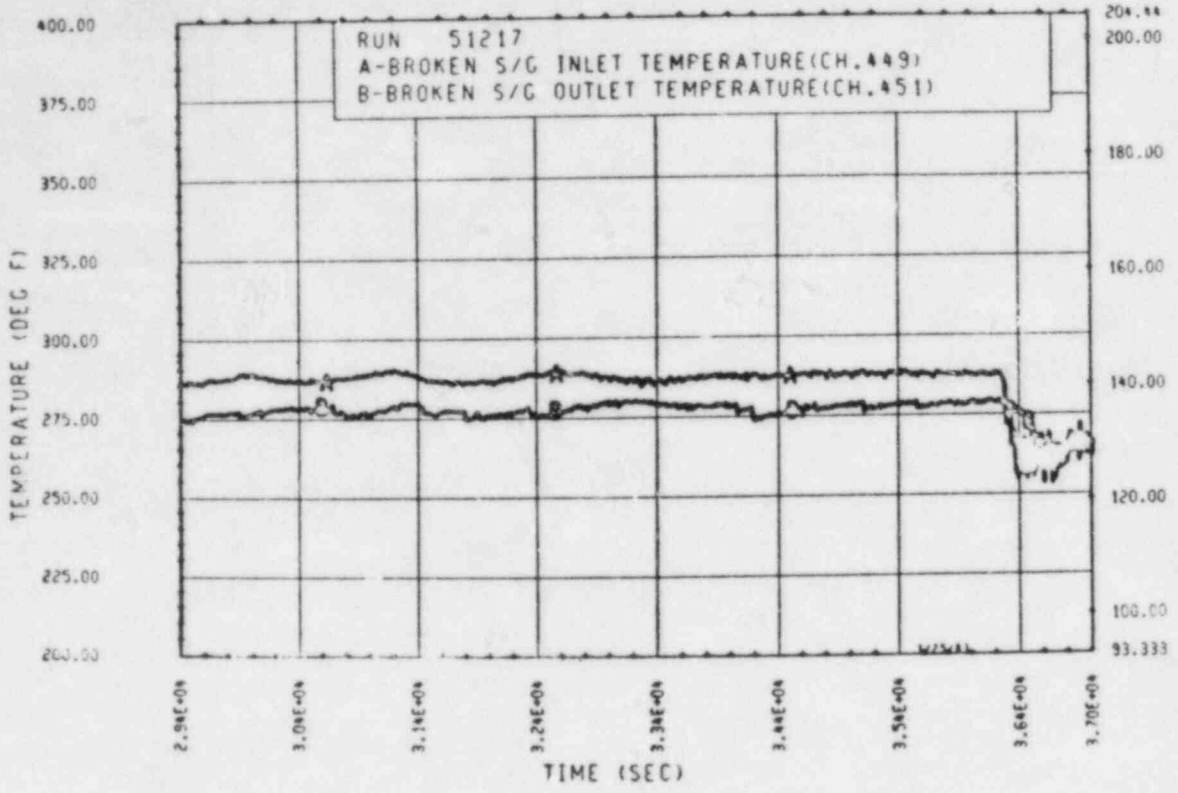

Figure A-248. Broken Loop Steam Generator Inlet and Outlet Temperature, Test 17

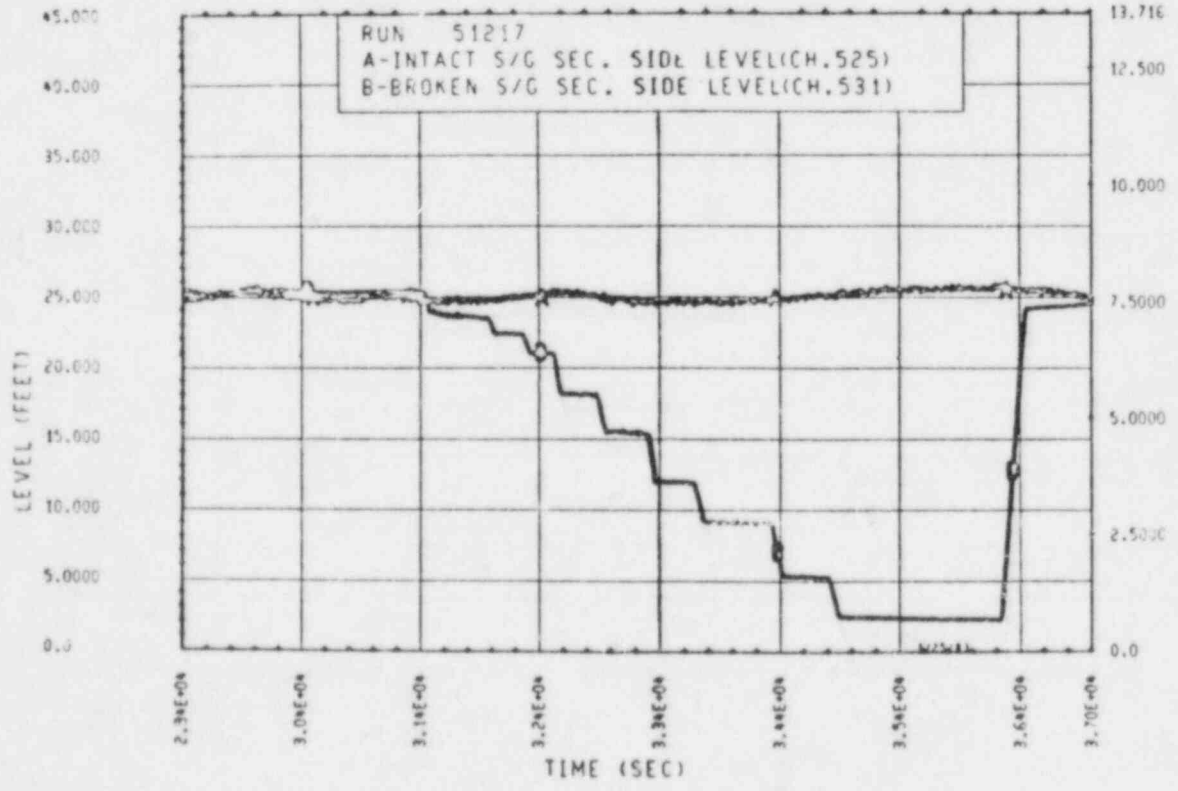

Figure A-249. Unbroken and Broken Loop Steam Generator Secondary Side Collapsed Liquid Levels, Test 17

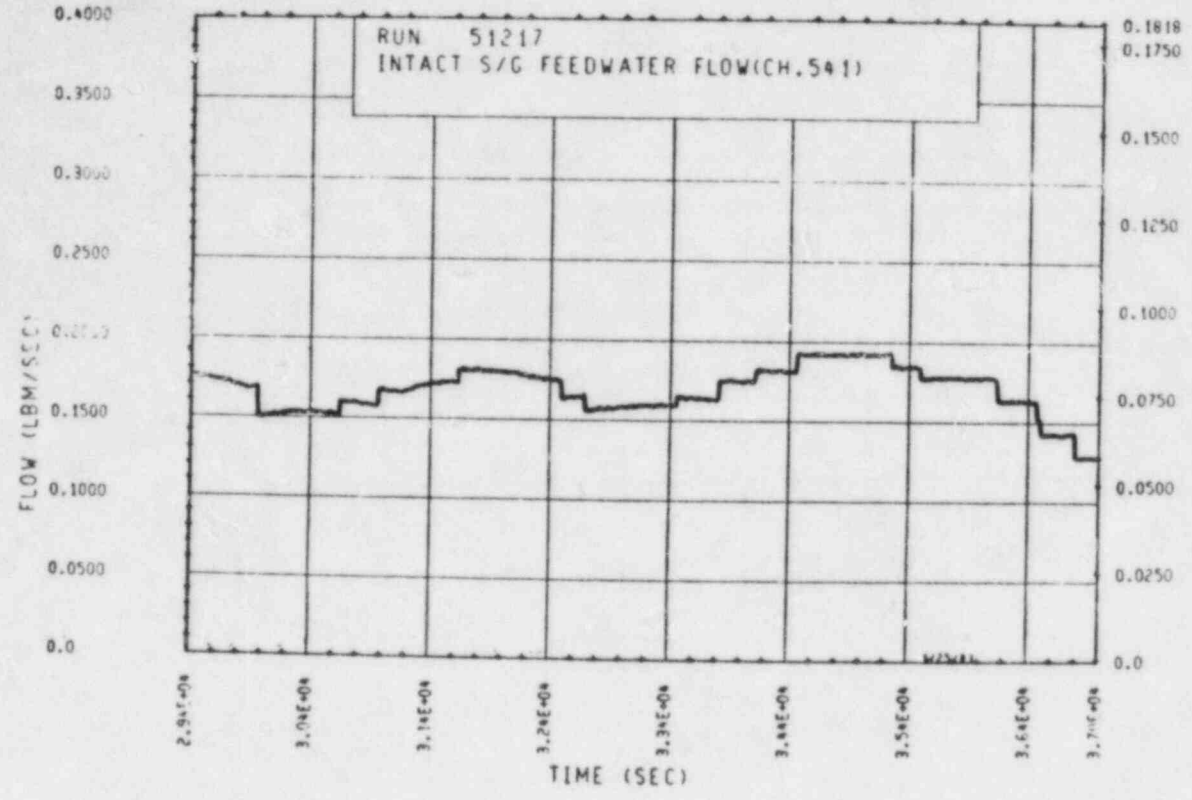

Figure A-250. Unbroken Loop Steam Generator Feedwater Mass Flow Rate, Test 17

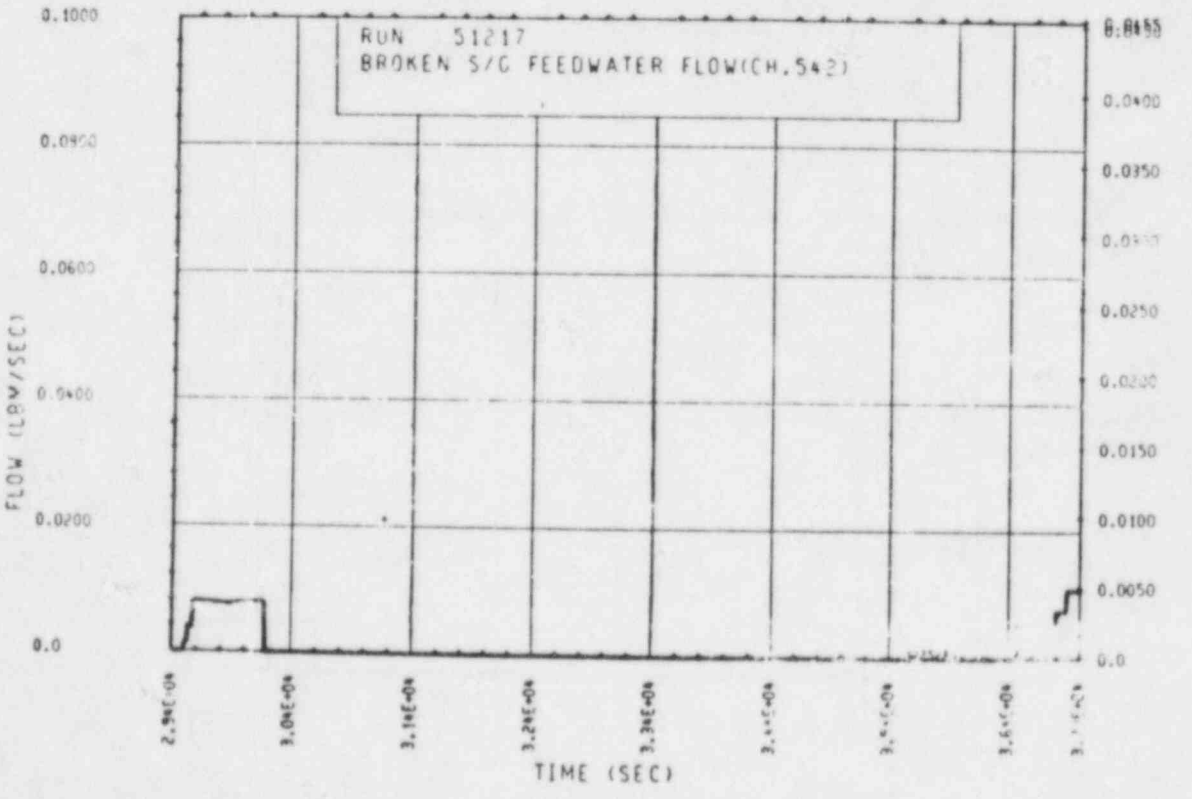

Figure A-251. Broken Loop Steam Generator Feedwater Mass Flow Rate, Test 17

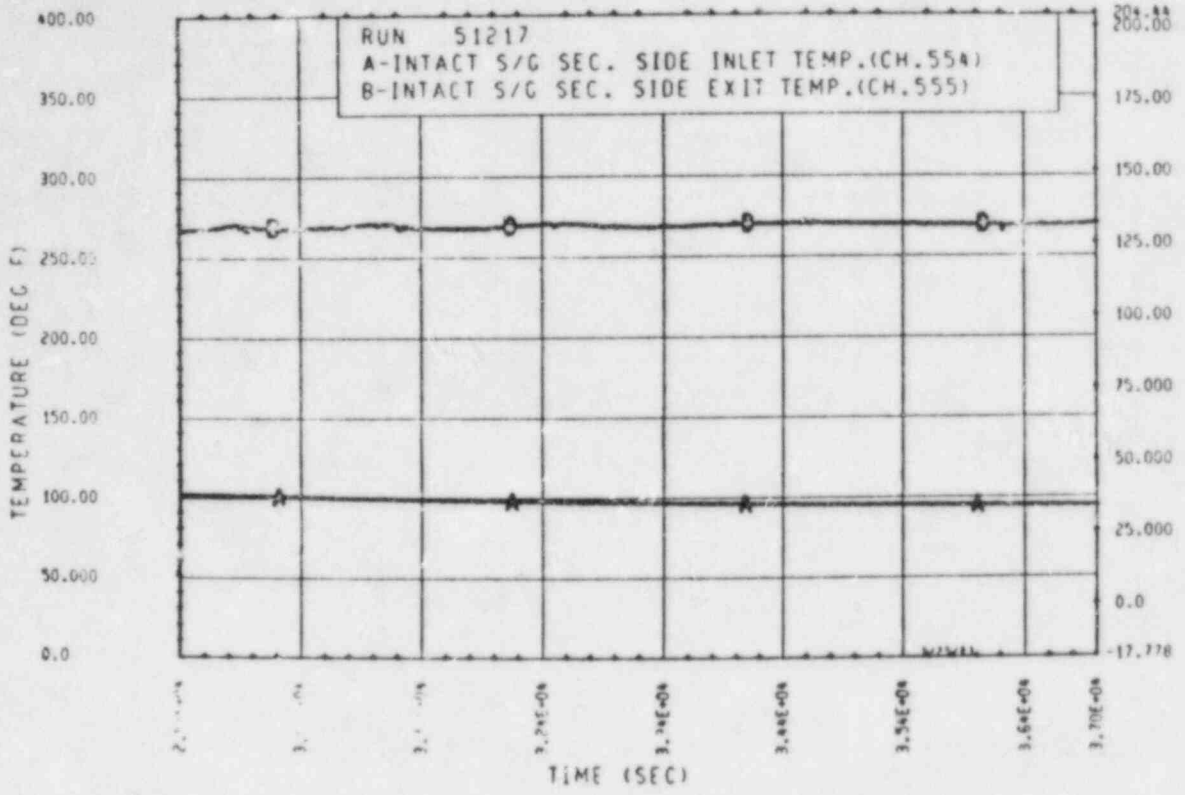

Figure A-252. Unbroken Loop Steam Generator Secondary Side Inlet and Outlet Temperature, Test 17

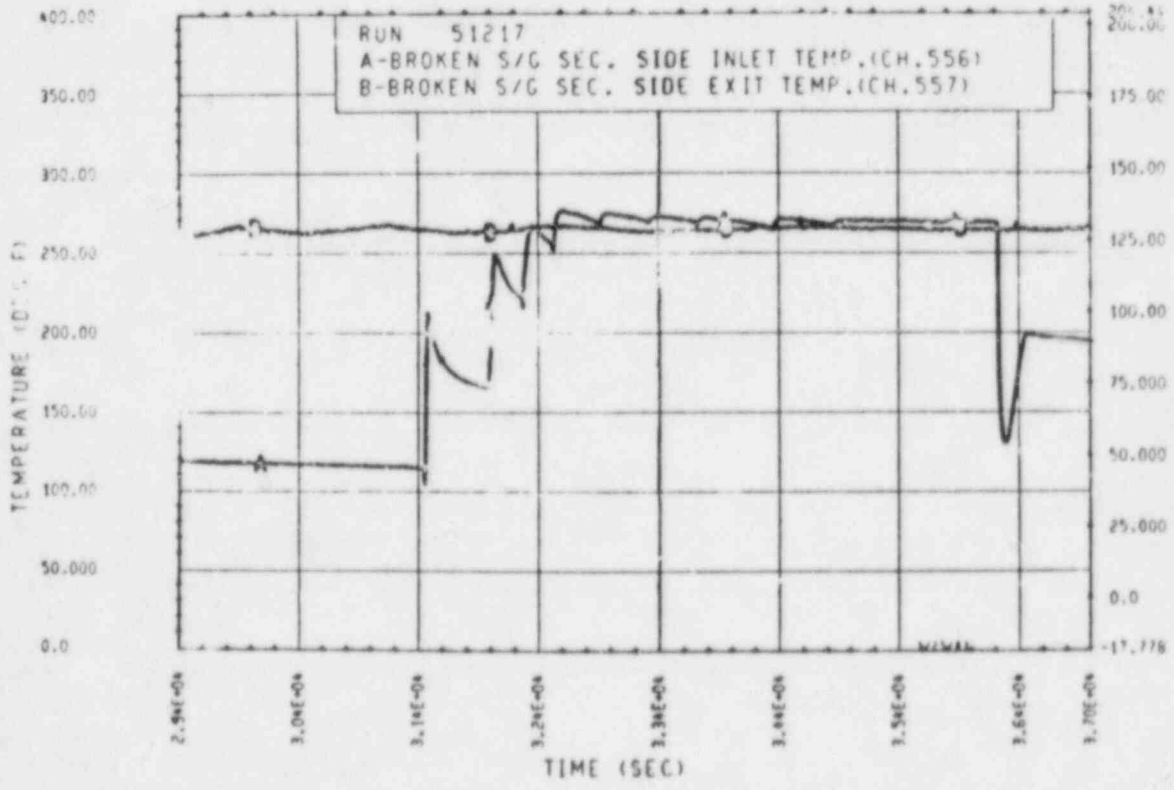

Figure A-253. Broken Loop Steam Generator Secondary Side Inlet and Outlet Temperature, Test 17

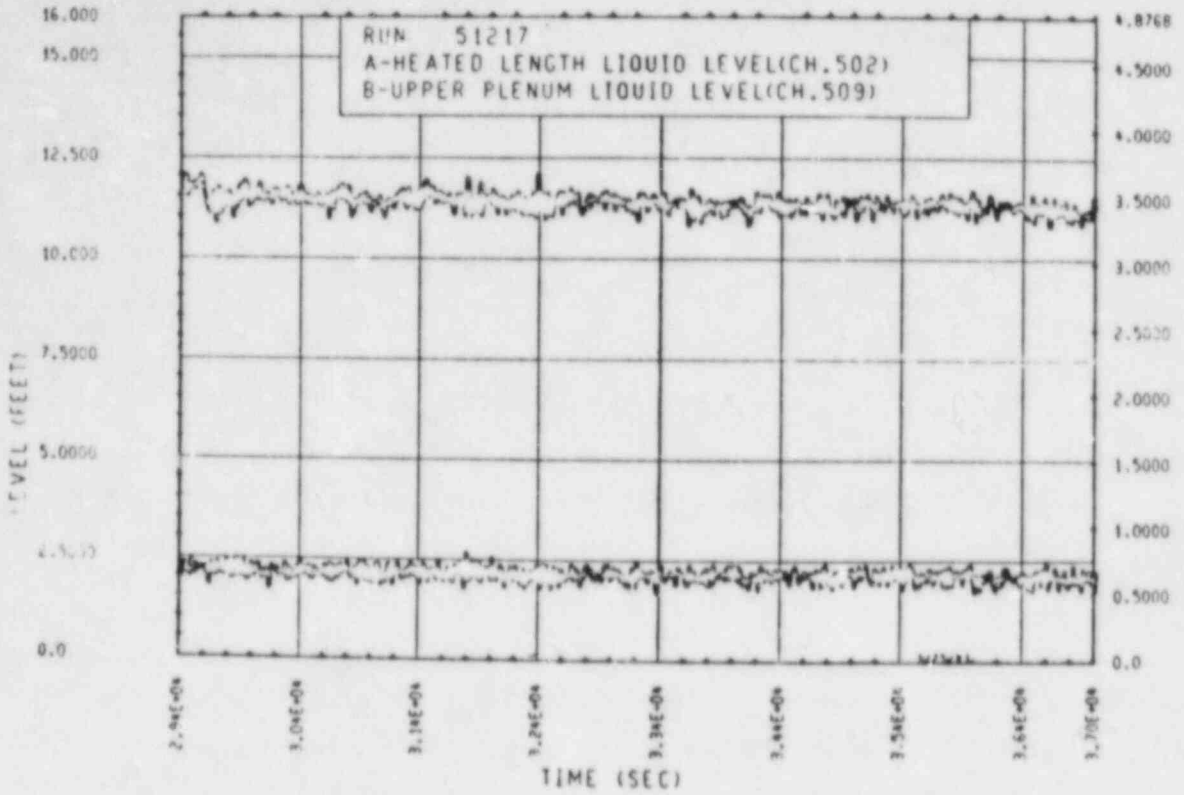

Figure A-254. Heated Length and Upper Plenum Liquid Levels, Test 17

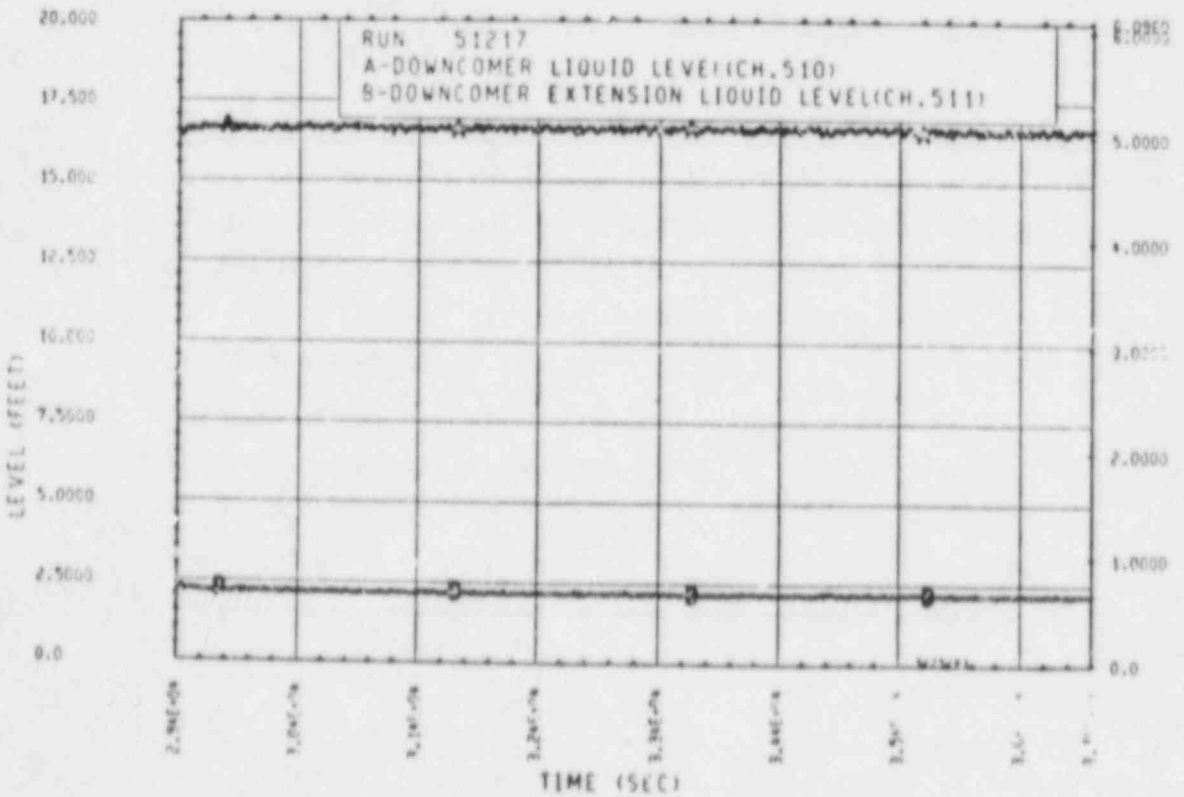

Figure A-255. Downcomer and Downcomer Extenston Liquid Levels, Test 17

TEST 18: REFLUX CONDENSATION WITH SECONDARY SIDE DEPRESSURIZATION

Objective

To determine the effect of increased heat sink capacity on the primary side reflux condensation mode of natural circulation

Test Procedure

The test was begun from a steady-state reflux condensation mode with a nominal bundle power of 222 kw. The primary system was operated with the pressurizer valved out and a reduced mass inventory consistent with previously established reflux condensation conditions. The secondary sides were operated in a boiling mode with collapsed liquid levels of 7.62 m (25 ft) (71 percent full) and an initial pressure of 0.28 MPa (40 psia). The secondary side pressure regulator was incrementally lowered until the secondary side was operated at atmospheric pressure. Data were gathered at each secondary side pressure increment. The secondary side pressure was returned to 0.28 MPa (40 psia) and the test terminated when steady-state conditions were reestablished.

Test Overview

As the secondary side pressure decreased, because of the slow depressurization, the feedwater flow into the generator was increased to maintain a constant secondary side level. This depressurization, combined with the increased feed flow, reduced both the secondary and primary temperatures. Since the primary presumed saturation temperature decreased, an additional amount of sensible energy in the primary system had to be removed in the steam generators. The additional energy that had to be removed is reflected in the increase in the hot leg and, to a lesser extent, cold leg reflux meter readings. Also, as the system pressure decreased, a larger fraction of the bundle was in the boiling mode, as observed by the decrease in the bundle collapsed liquid level and the near equality of the bundle inlet and exit temperatures.

At the very end of the test, the steam generator control valve was fully opened and the secondary side of the generator reached approximately 0.10 MPa (15 psia). At this point, the reflux meters indicated a reduced flow, which was the same value as that at the beginning of the transient. At this time the steam generator outlet fluid temperature became subcooled.

TEST SCHEDULE
TEST 18

Time[a] (sec)	Event
51221	Secondary side pressure regulator adjusted to drop pressure to a nominal 0.21 MPa (30 psi)
52279	Secondary side pressure regulator adjusted to drop pressure to a nominal 0.14 MPa (20 psi)
53611	Secondary side pressure regulator adjusted to a wide-open position
54358	End of test 18

a. Test 18 was run in series with test 8. Time zero therefore corresponds with time zero of test 8. All computer times are referenced to this time.

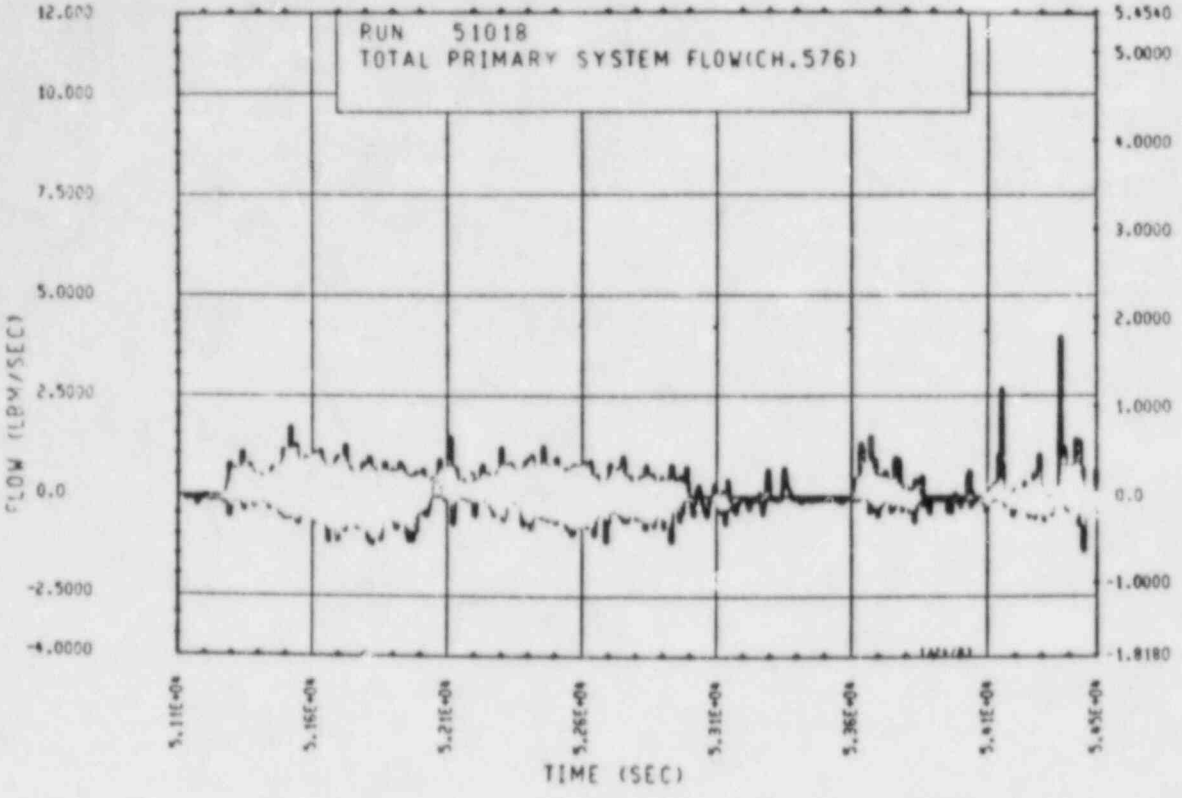

Figure A-256. Mass Flow Rate Through Rod Bundle, Test 18

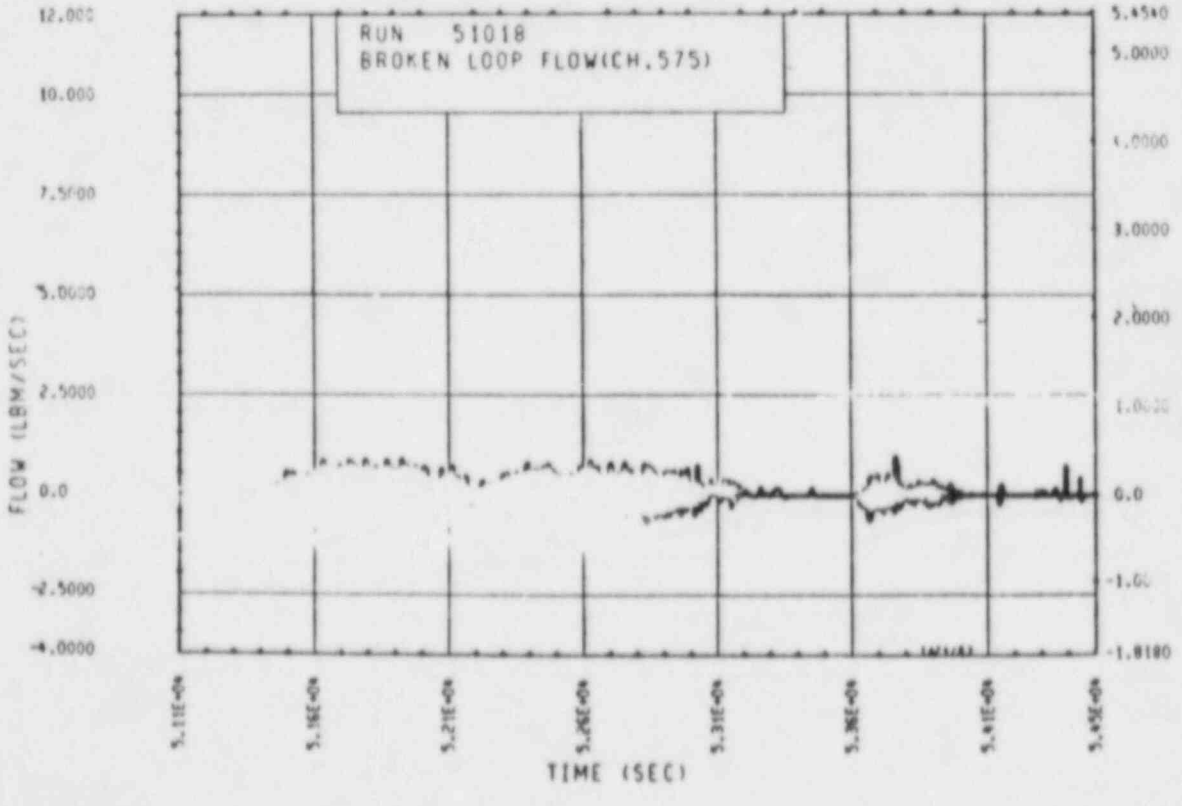

Figure A-257. Mass Flow Rate Through Broken Loop, Test 18

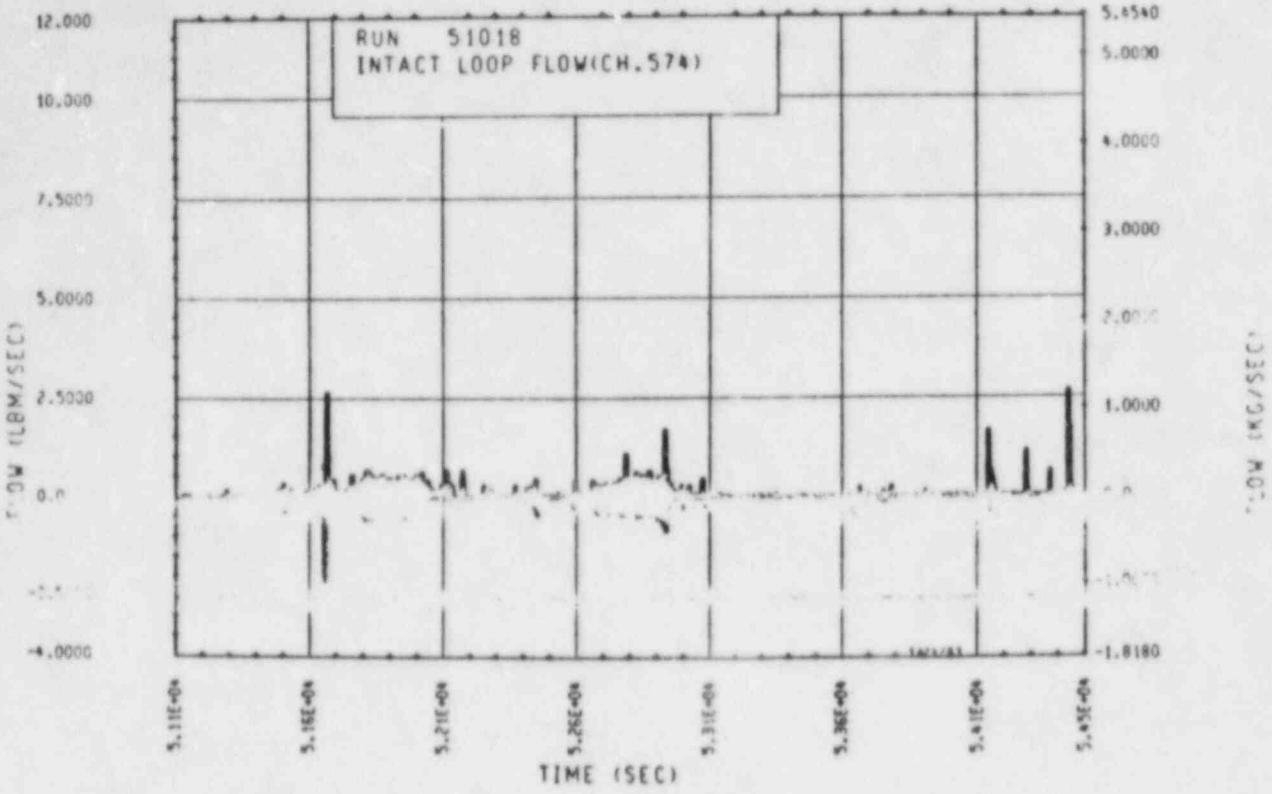

Figure A-258. Mass Flow Rate Through Unbroken Loop, Test 18

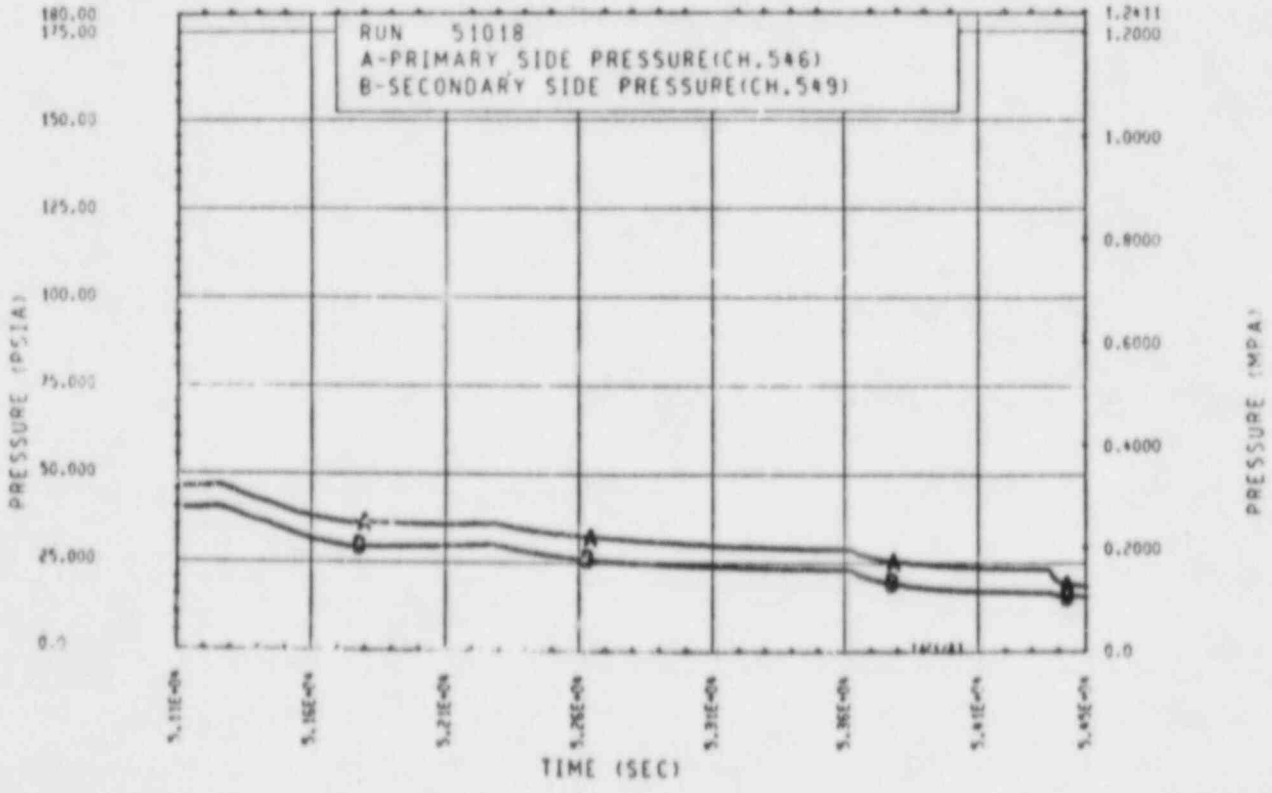

Figure A-259. Primary and Secondary System Pressure, Test 18

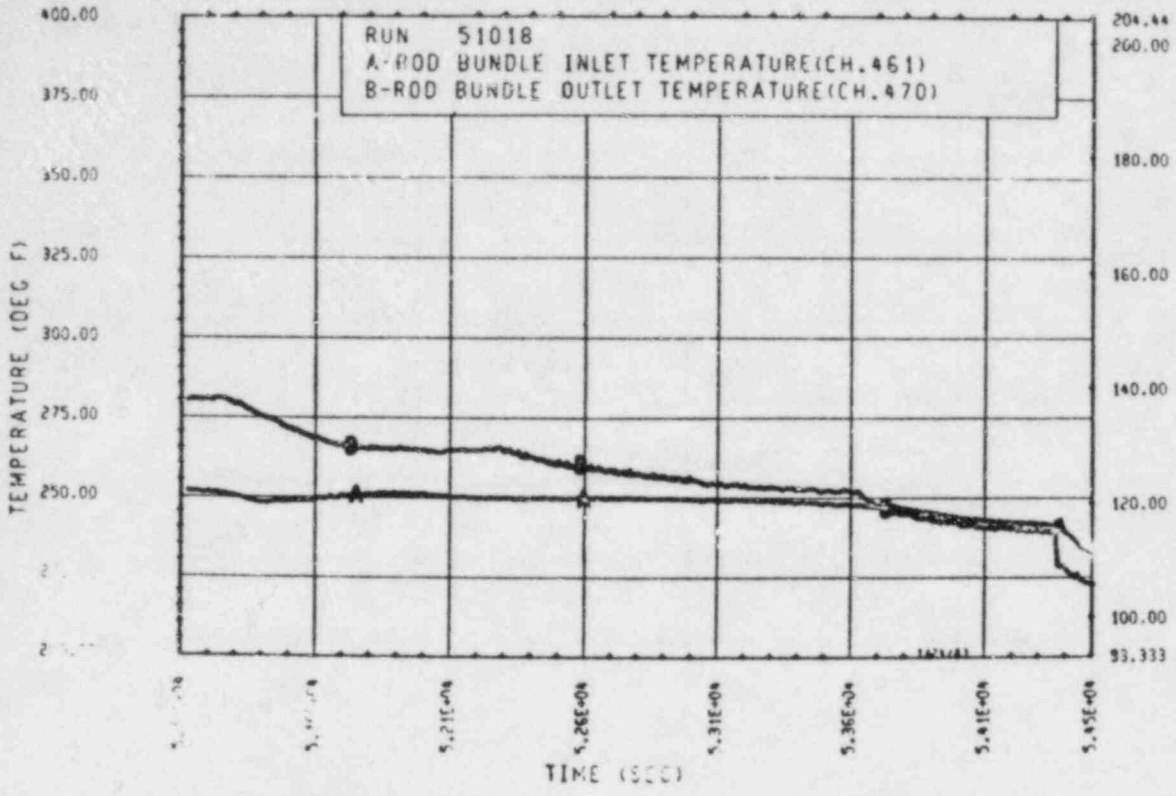

Figure A-260. Heater Rod Bundle Inlet and Outlet Temperature, Test 18

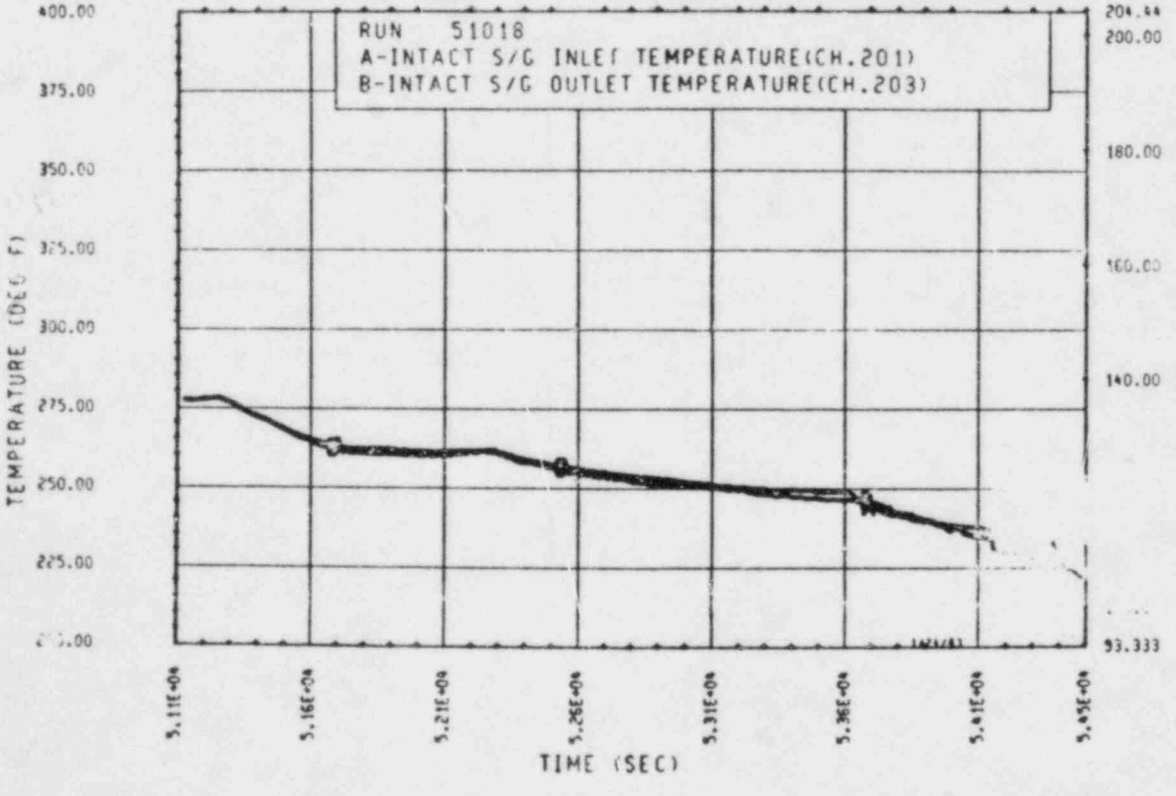

Figure A-261. Unbroken Loop Steam Generator Inlet and Outlet Temperature, Test 18

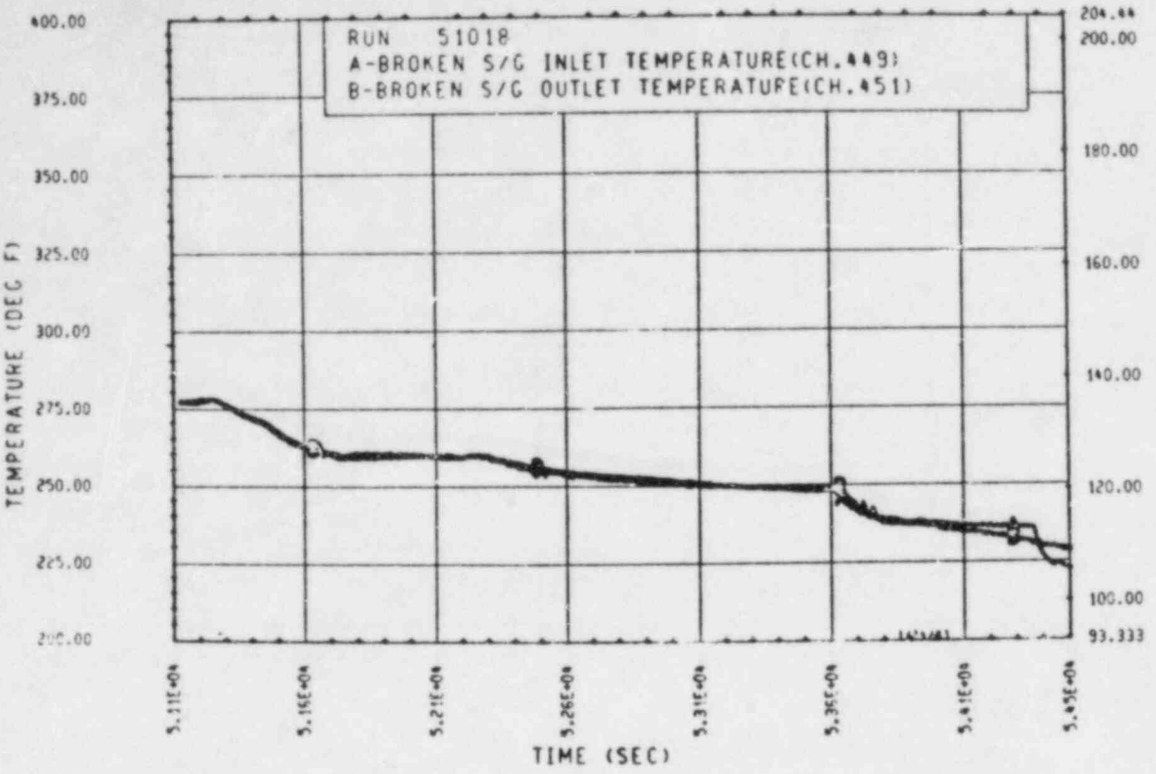

Figure A-262. Broken Loop Steam Generator Inlet and Outlet Temperature, Test 18

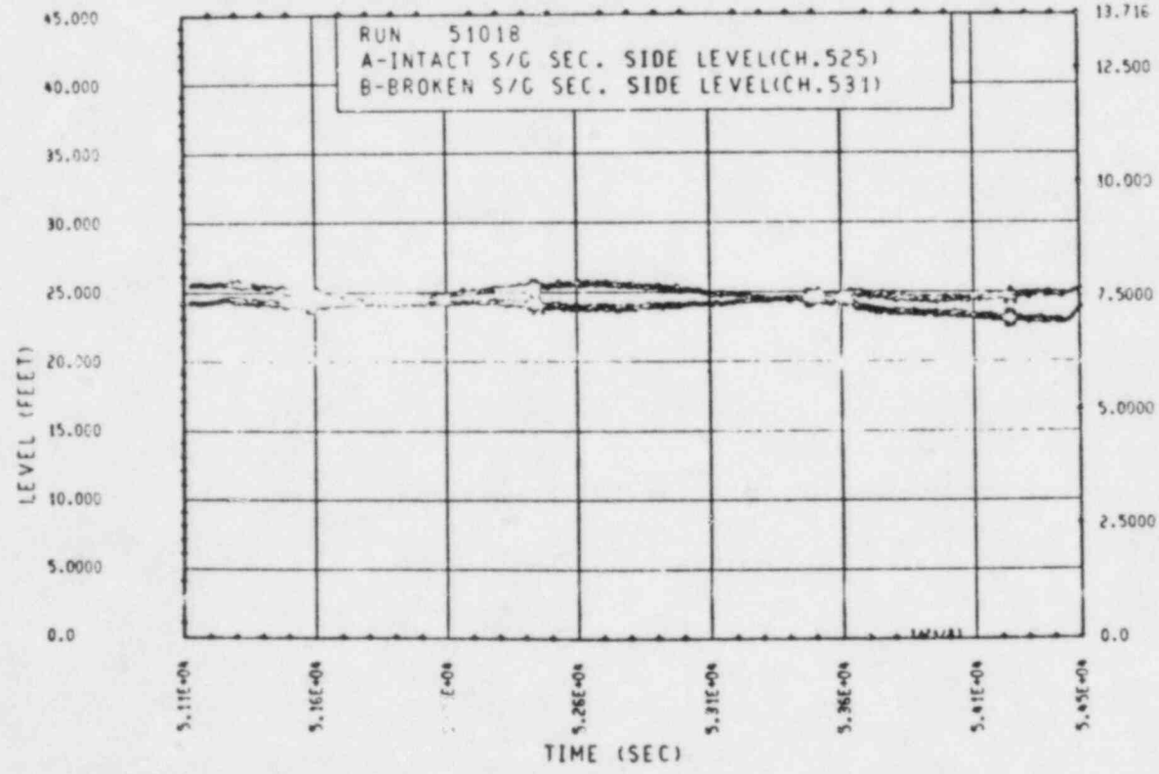

Figure A-263. Unbroken and Broken Loop Steam Generator Secondary Side Collapsed Liquid Levels, Test 18

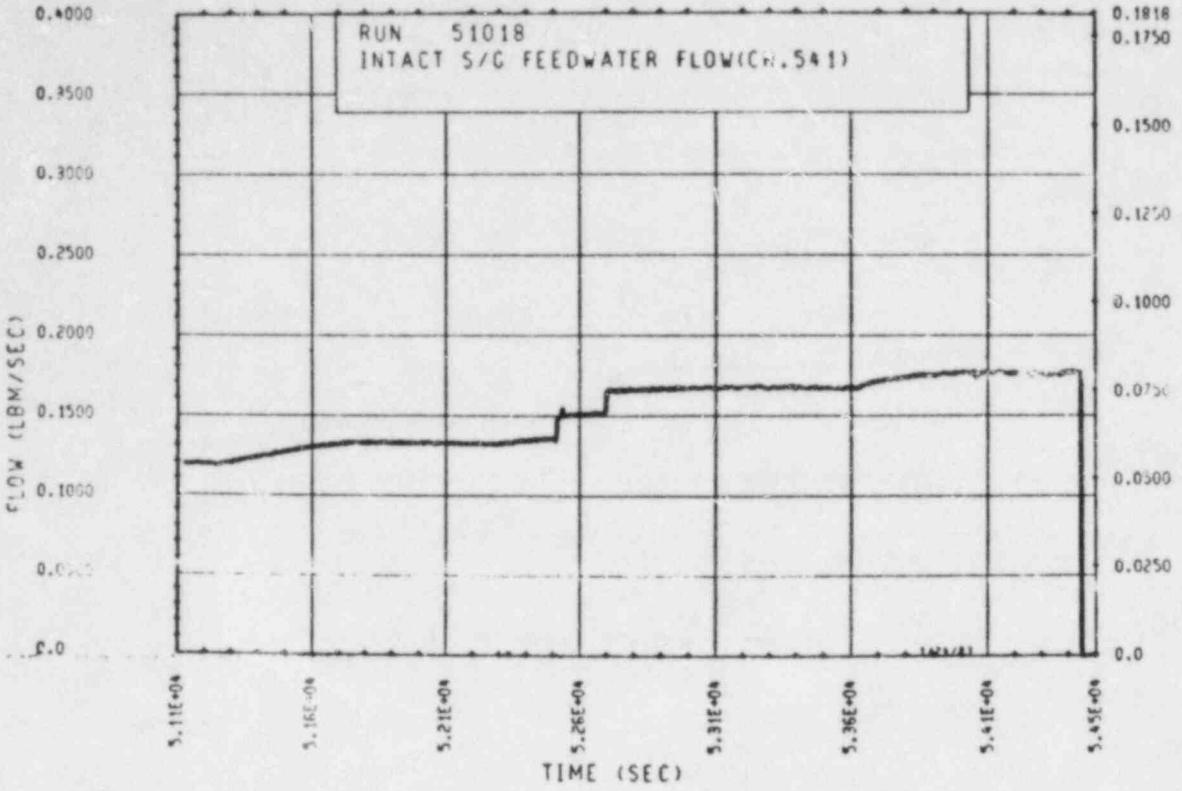

Figure A-264. Unbroken Loop Steam Generator Feedwater Mass Flow Rate, Test 18

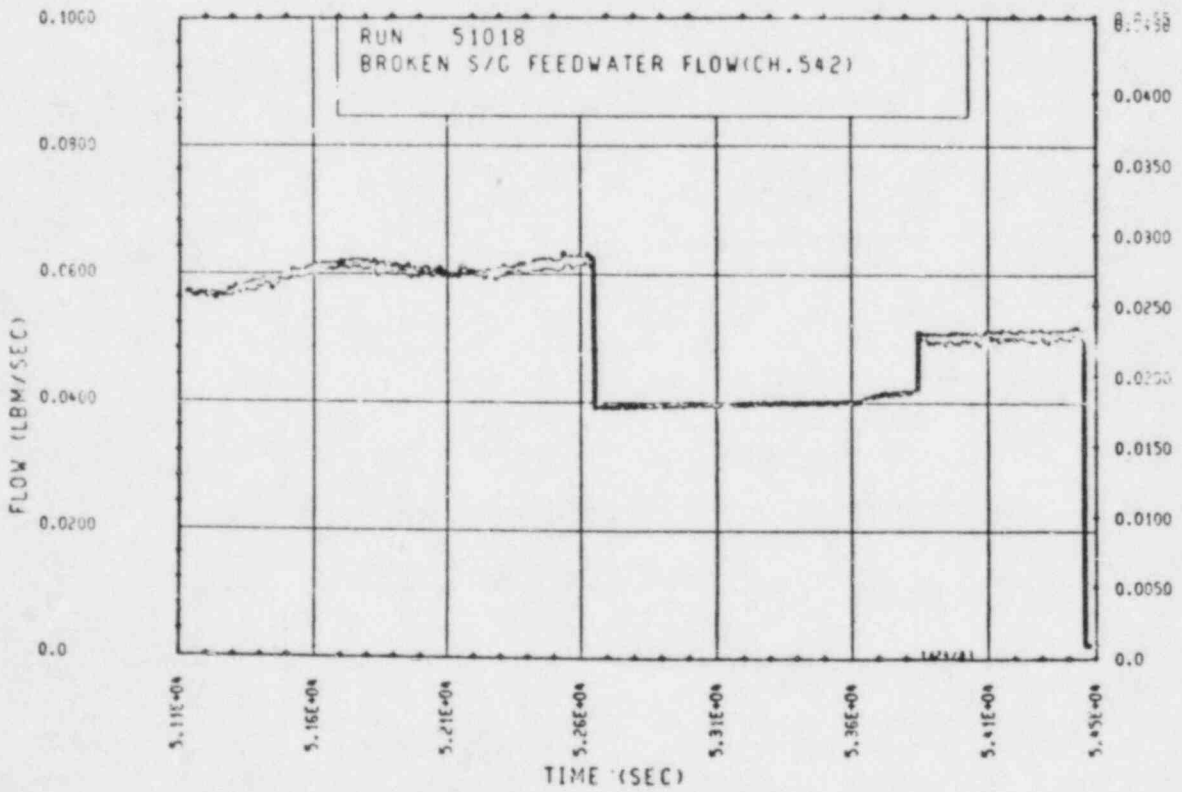

Figure A-265. Broken Loop Steam Generator Feedwater Mass Flow Rate, Test 18

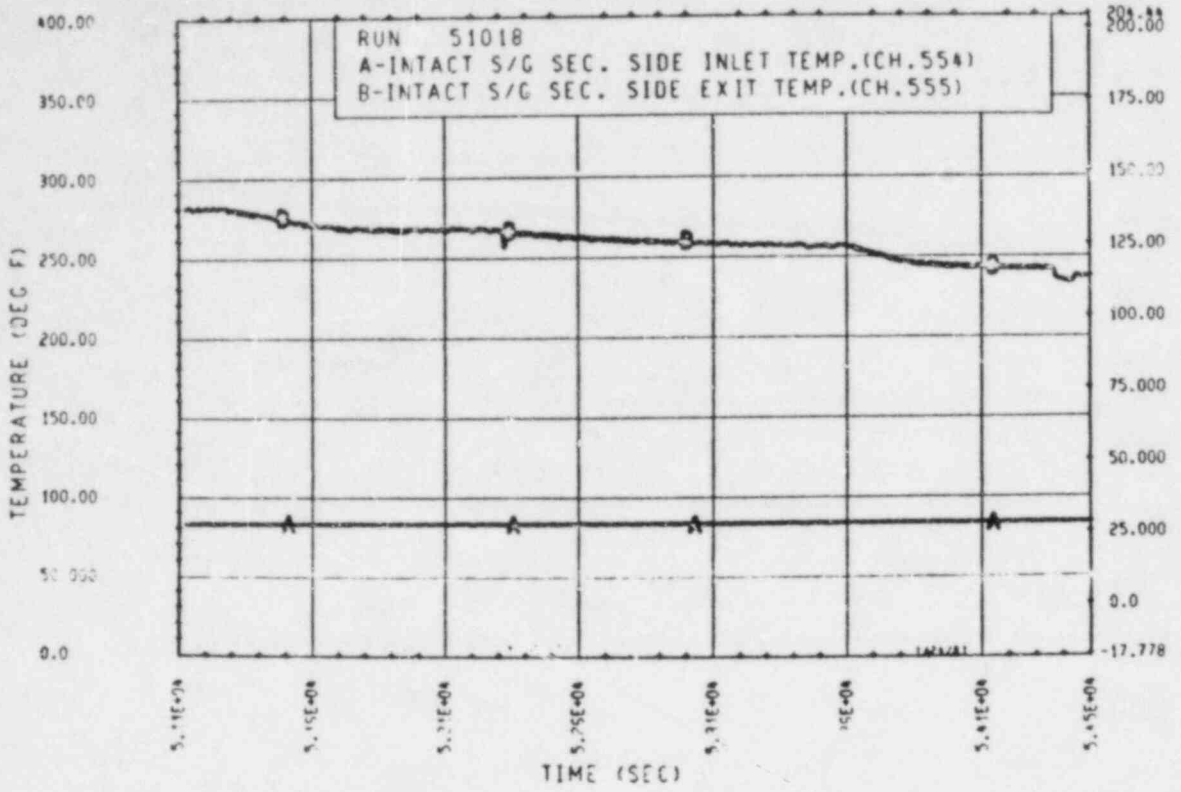

Figure A-266. Unbroken Loop Steam Generator Secondary Side Inlet and Outlet Temperature, Test 18

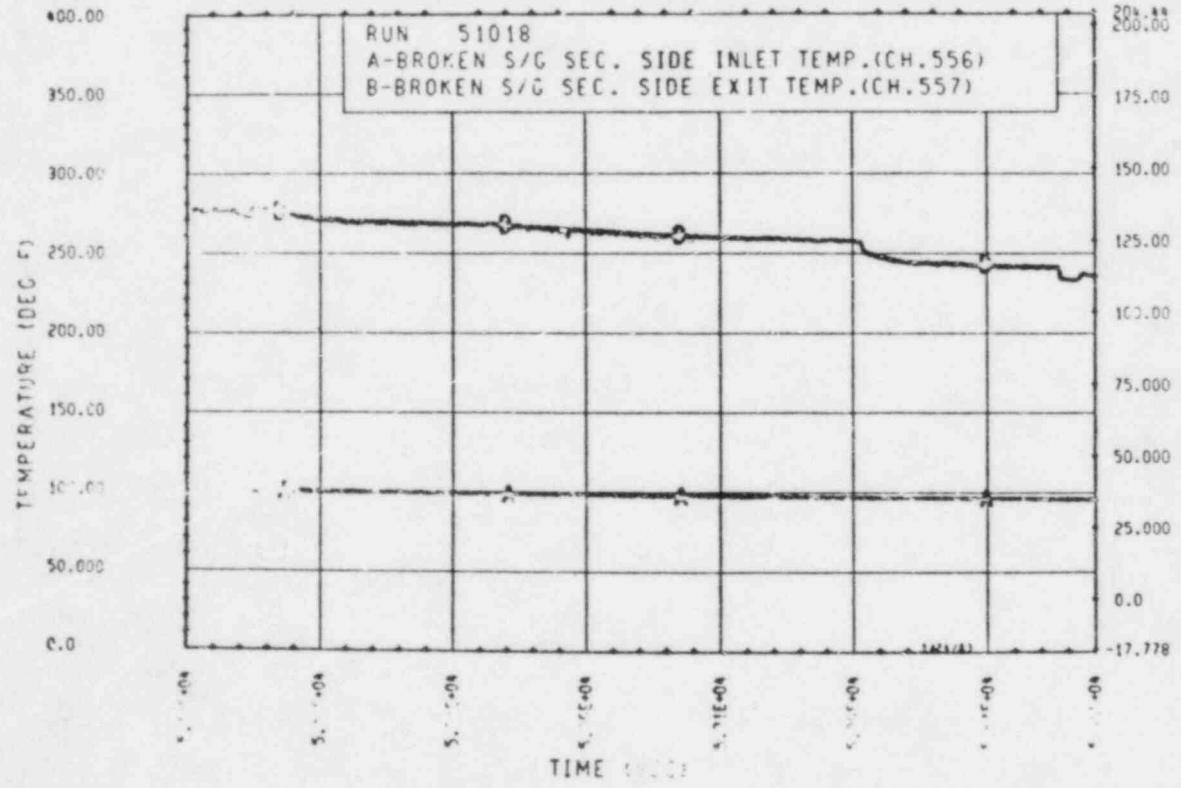

Figure A-267. Broken Loop Steam Generator Secondary Side Inlet and Outlet Temperature, Test 18

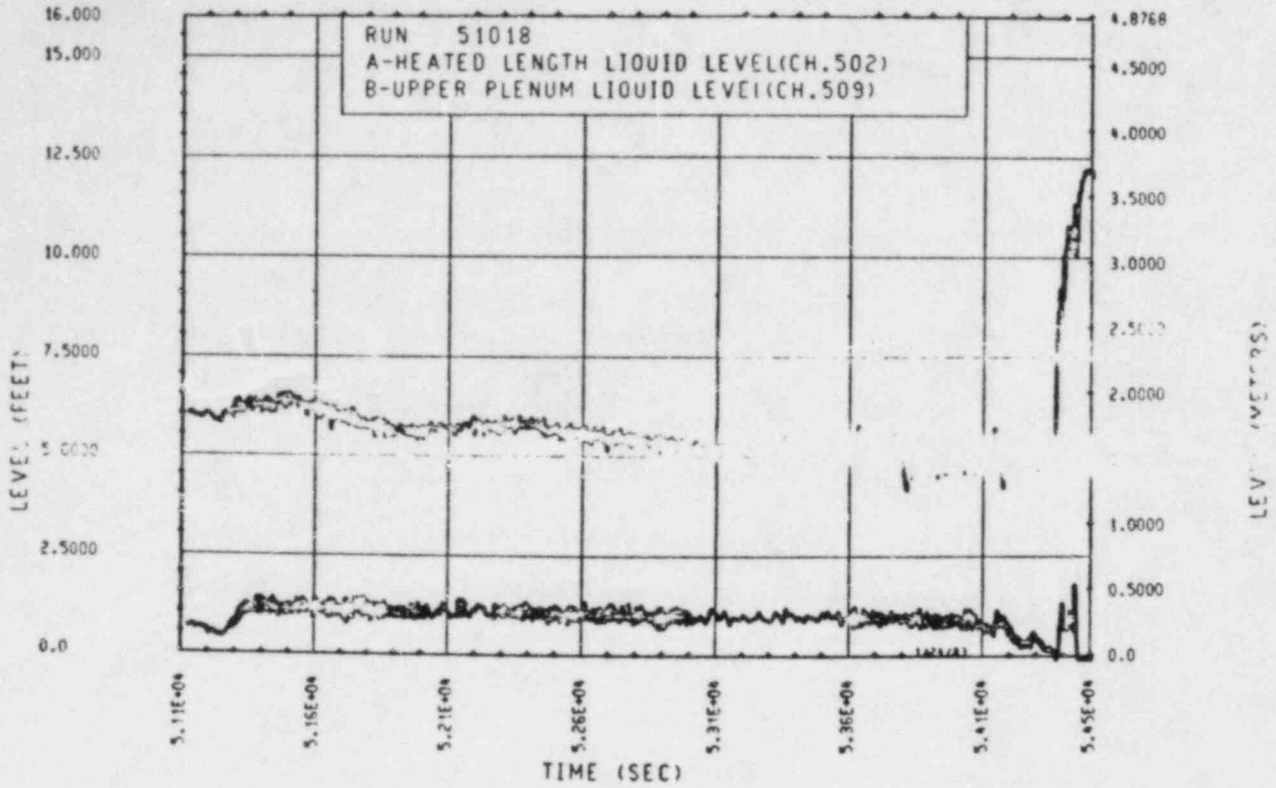

Figure A-268. Heated Length and Upper Plenum Liquid Levels, Test 18

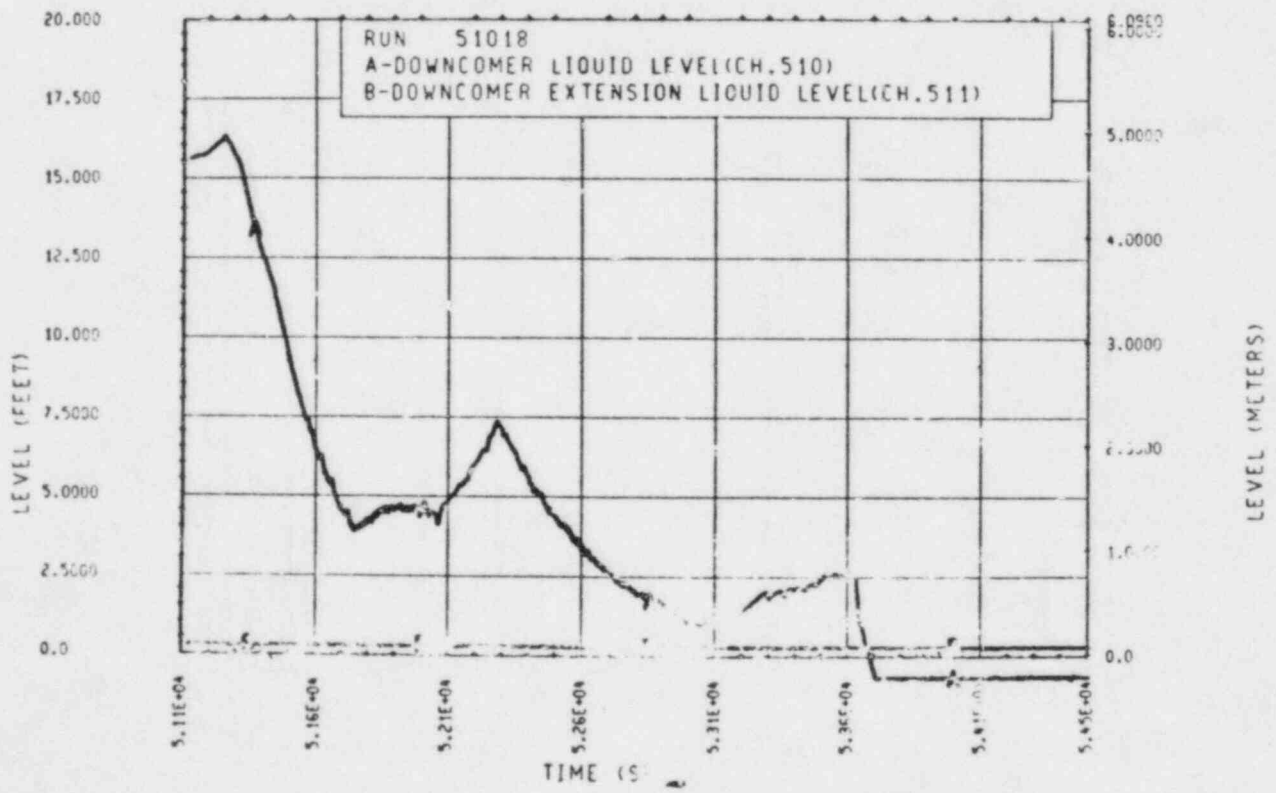

Figure A-269. Downcomer and Downcomer Extension Liquid Levels, Test 18

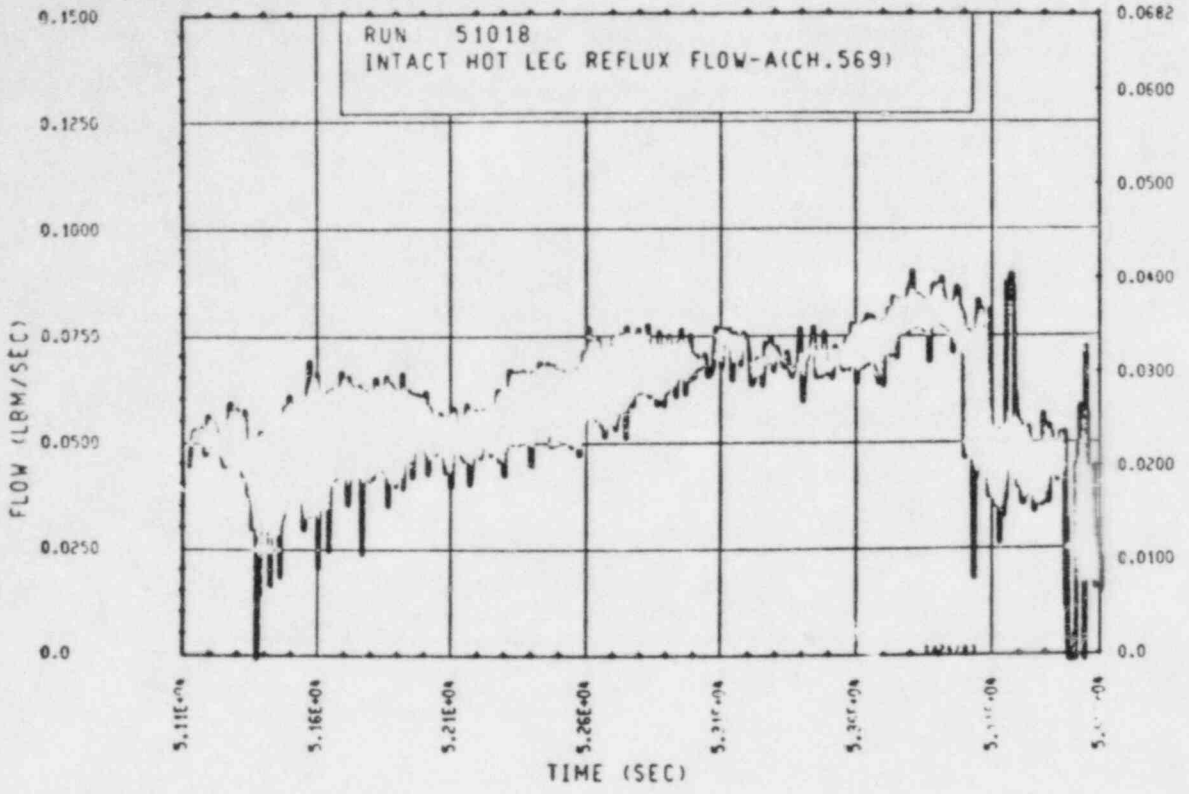

Figure A-270. Unbroken Loop Hot Leg Reflux Condensation Mass Flow Rate, Test 18

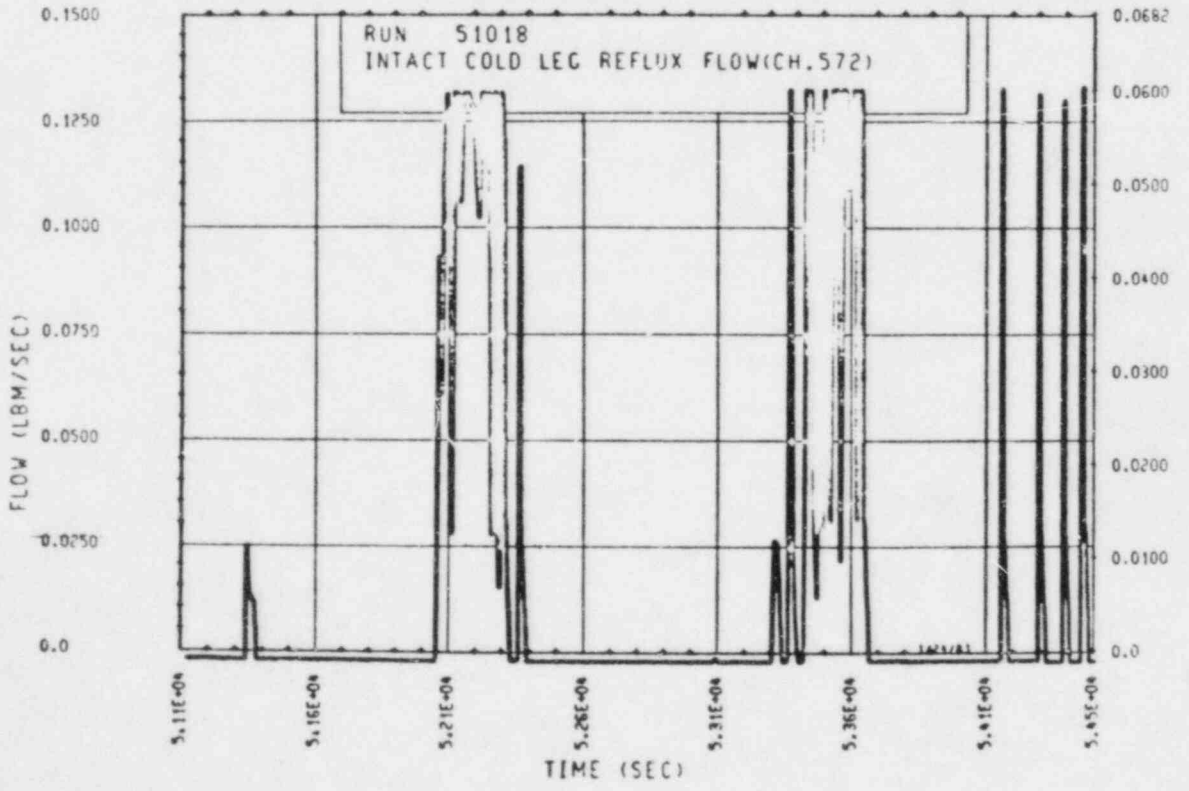

Figure A-271. Unbroken Loop Cold Leg Reflux Condensation Mass Flow Rate, Test 18

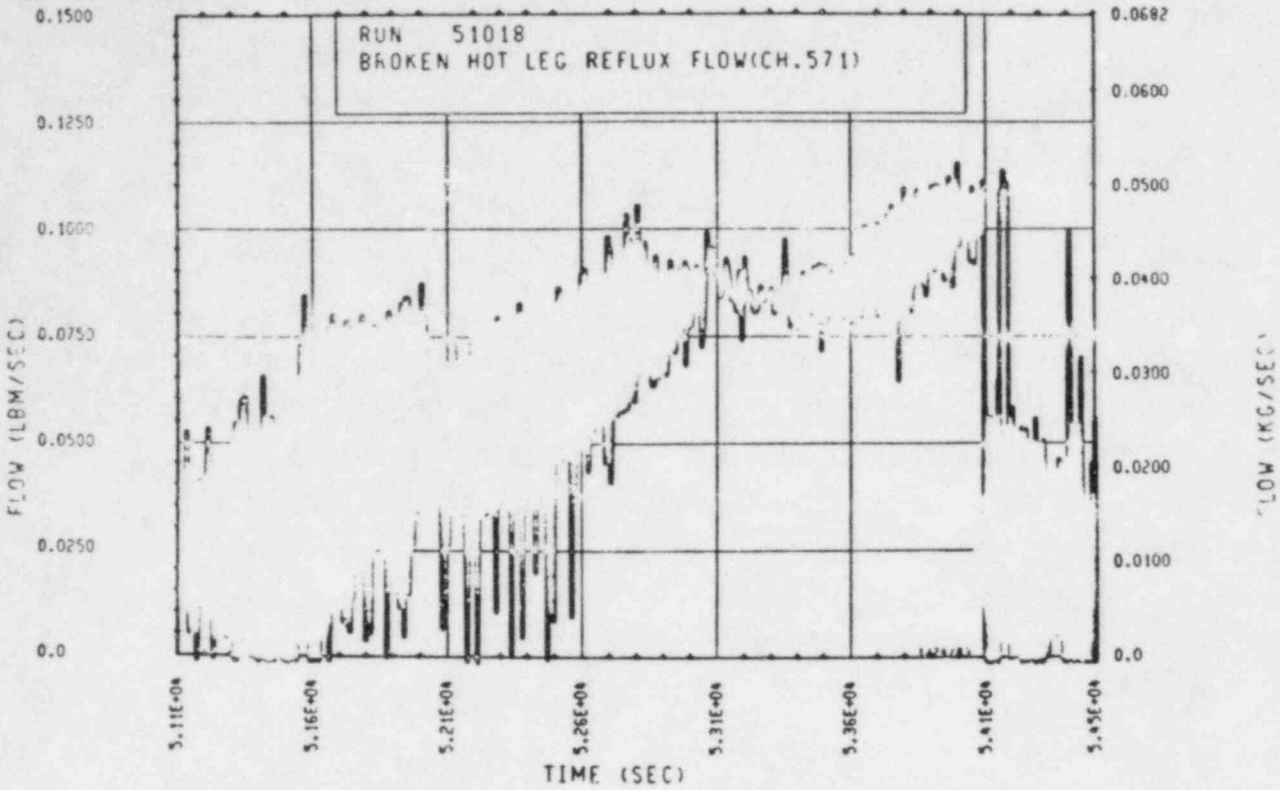

Figure A-272. Broken Loop Hot Leg Reflux Condensation Mass Flow Rate, Test 18

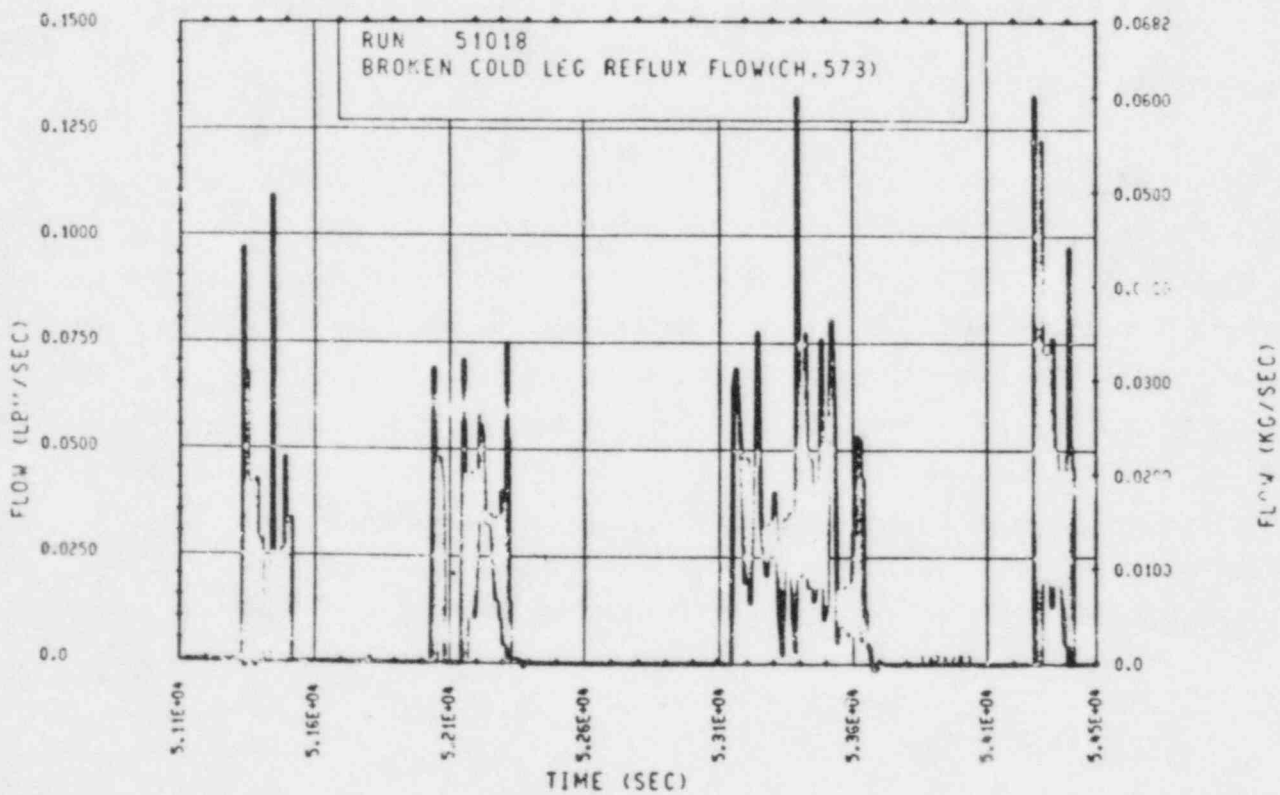

Figure A-273. Broken Loop Cold Leg Reflux Condensation Mass Flow Rate, Test 18

TEST 19: REFLUX CONDENSATION WITH BROKEN LOOP STEAM GENERATOR BOILOFF

Objective:

To determine the effect of a heat sink imbalance on reflux condensation

Test Procedure:

The test was begun from a steady-state reflux condensation mode with a nominal bundle power of 222 kw. The primary system was operated with the pressurizer valved out and a reduced mass inventory consistent with previously established reflux condensation conditions. The secondary side was operated in a boiling mode with a nominal pressure of 0.28 MPa (40 psia) and an initial collapsed liquid level of 7.62 m (25 ft) (71 percent full). The broken loop steam generator feedwater line was valved out allowing the secondary side collapsed liquid level to boil dry. The unbroken loop steam generator secondary side was maintained at a constant collapsed liquid level of 7.62 m (25 ft). After a steady-state condition had been achieved with the broken loop steam generator boiled dry, the broken loop steam generator secondary side was refilled with 93°C (200°F) water from accumulator 2.

Test Overview

The system was operating in the reflux condensation mode with both steam generators active. The feed flow to the unbroken loop was then isolated as the level in this generator decreased. The primary side pressure remained relatively constant, with oscillations caused by the unbroken loop blow-through, until the broken loop reached a level of 2.44 m (8 ft). At this point, the primary pressure began a very slow increase of 7 to 14 kPa (1 to 2 psia) while the secondary side pressure remained constant. Comparison of the difference in the primary and secondary saturation temperatures before the broken loop level decreased (t = 48,600 sec) and when the broken loop level was at 0.91 m (3.0 ft) (t = 57,300 sec) gives the following values:

- At t = 48,600 sec
  - -- $T_{primary_{sat}}$ = 136.5°C (277.8°F)
  - -- $T_{secondary_{sat}}$ = 131.4°C (268.6°F)
- At t = 57,300 sec
  - -- $T_{primary_{sat}}$ = 137.1°C (278.8°F)
  - -- $T_{secondary_{sat}}$ = 130.8°C (267.5°F)

The percentage increase in the driving temperature difference as the broken loop level decreased to approximately 0.91 m (3 ft) was 22 percent. The loss of heat transfer area relative to the original area (assuming that all tubes were initially covered) was 22.2 percent and the increase in the driving ΔT difference at this time was 22 percent. Therefore the loss of steam generator surface offset the increase in the total driving temperature difference. The exact balance as indicated above is more luck than science; however, examining other times does indicate that the primary system can easily accommodate the loss of the broken loop generator with modest loop pressurization.

TEST SCHEDULE
TEST 19

Time[a] (sec)	Event
37456	Began drain 10 (beginning of incremental drains of the primary mass inventory), to achieve a reflux natural circulation mode. 154 kg (340 lbm) had drained from the primary during test 17.
37731	Ended drain 10; total of 200 kg (440 lbm) drained
38643	Began drain 11
38917	Ended drain 11; total of 245 kg (540 lbm) drained
40347	Began drain 12
40657	Ended drain 12; total of 290 kg (640 lbm) drained
40683	Both steam generators observed to be active
41179	Began drain 13
41439	Ended drain 13; total of 336 kg (740 lbm) drained
42307	Began drain 14
42573	Ended drain 14; total of 391 kg (840 lbm) drained

a. Test 19 was run in series with tests 14 and 17. Time zero therefore corresponds with time zero of test 14. All computer times are referenced to this time.

Time (sec)	Event
43296	Began drain 15
43586	Ended drain 15; total of 426 kg (940 lbm) drained
44168	Began drain 16
44439	Ended drain 16; total of 472 kg (1040 lbm) drained
44823	Began drain 17
44973	Ended drain 17; total of 494 kg (1090 lbm) drained
45041	Valved in weir meters
45303	Began drain 18
45423	Ended drain 18; total of 517 kg (1140 lbm) drained
46054	Began drain 19
46115	Ended drain 19; total of 535 kg (1180 lbm) drained
46563	Began drain 20
46615	Ended drain 20; total of 544 kg (1200 lbm) drained
47349	Began drain 21
47382	Ended drain 21; total of 549 kg (1210 lbm) drained
48162	Began drain 22

Time (sec)	Event
48193	Ended drain 22; total of 553 kg (1220 lbm) drained
48570	Started reflux reference run
48980	Secondary side feedwater shut off; began secondary side boiloff. Small steam generator allowed to boil off without any artificial secondary side drains.
58503	Small steam generator appeared to be boiled dry.
58595	Artificially drained small steam generator to ensure that it was boiled dry; system acted up as a result.
59043	Small steam generator boiled dry.
59403	Began secondary side recovery with accumulator 2
59583	Secondary side recovered to 7.62 m (25 ft); end of test 19

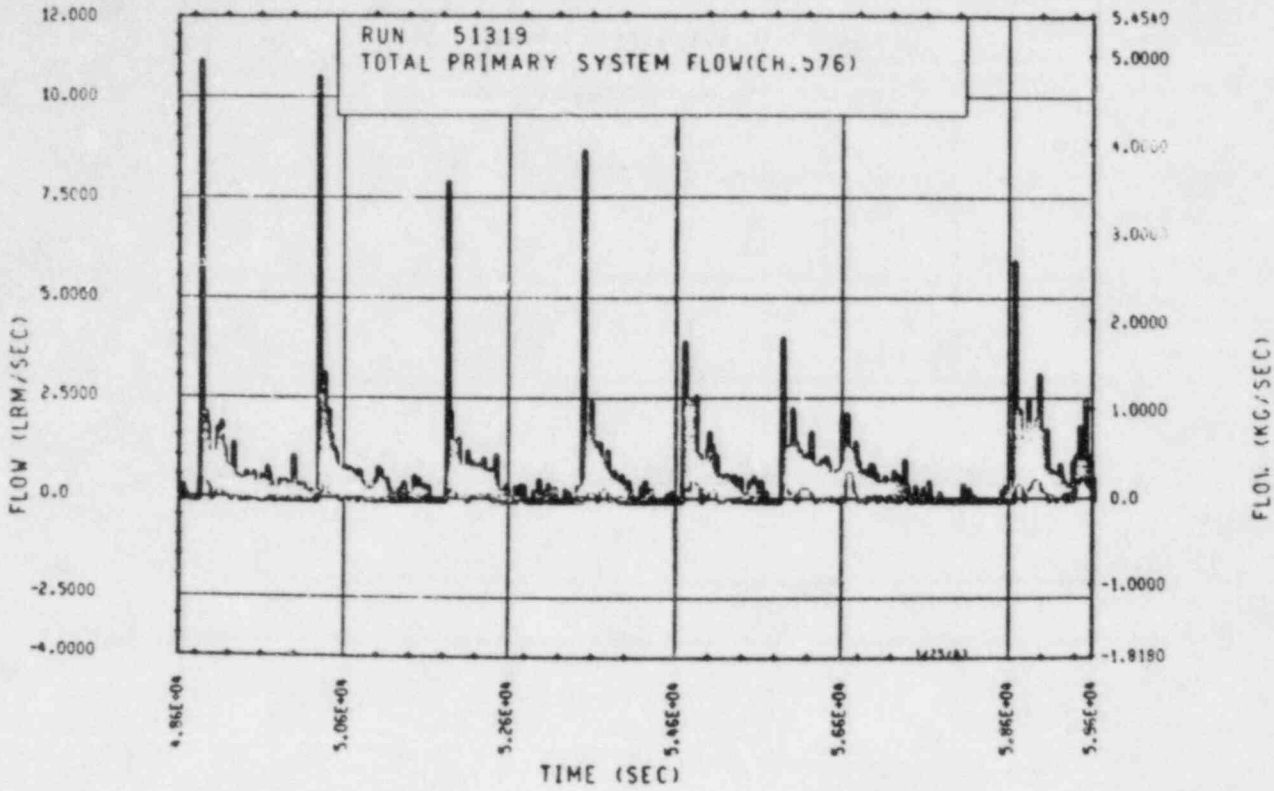

Figure A-274. Mass Flow Rate Through Rod Bundle, Test 19

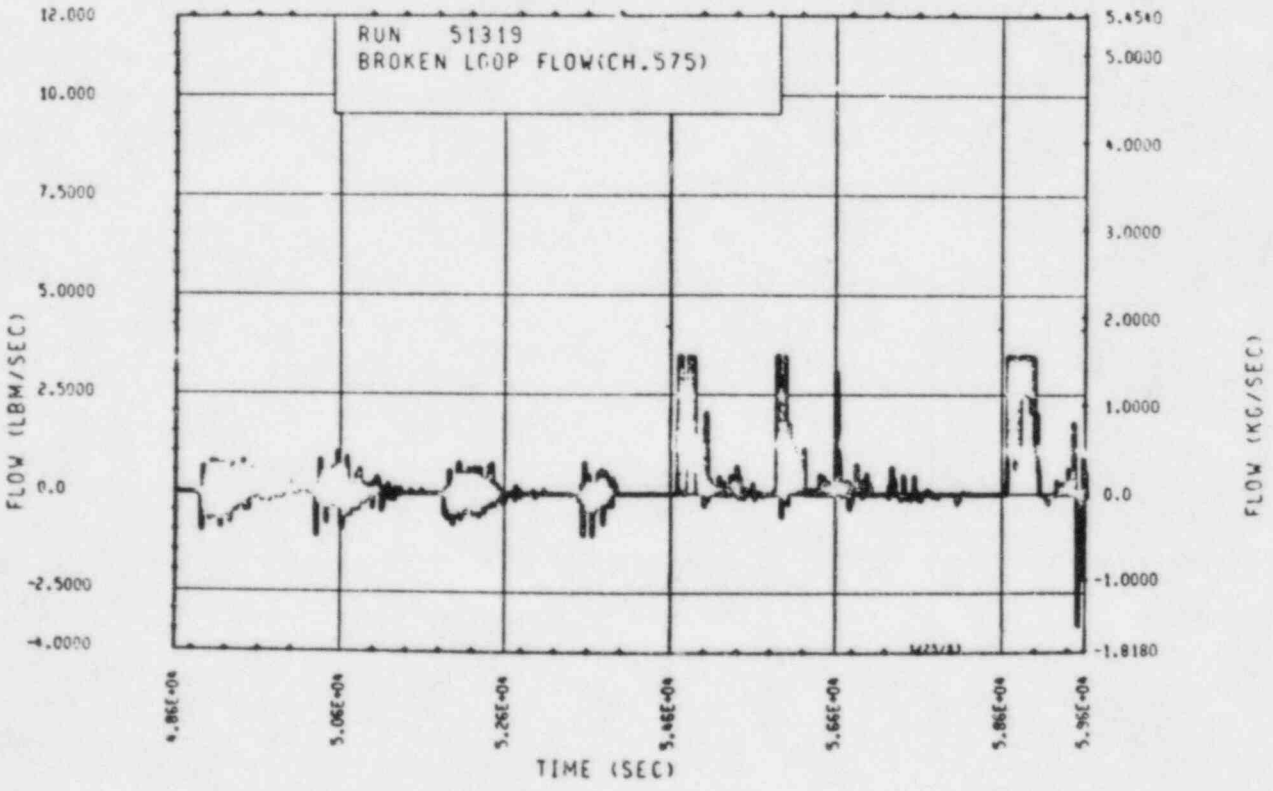

Figure A-275. Mass Flow Rate Through Broken Loop, Test 19

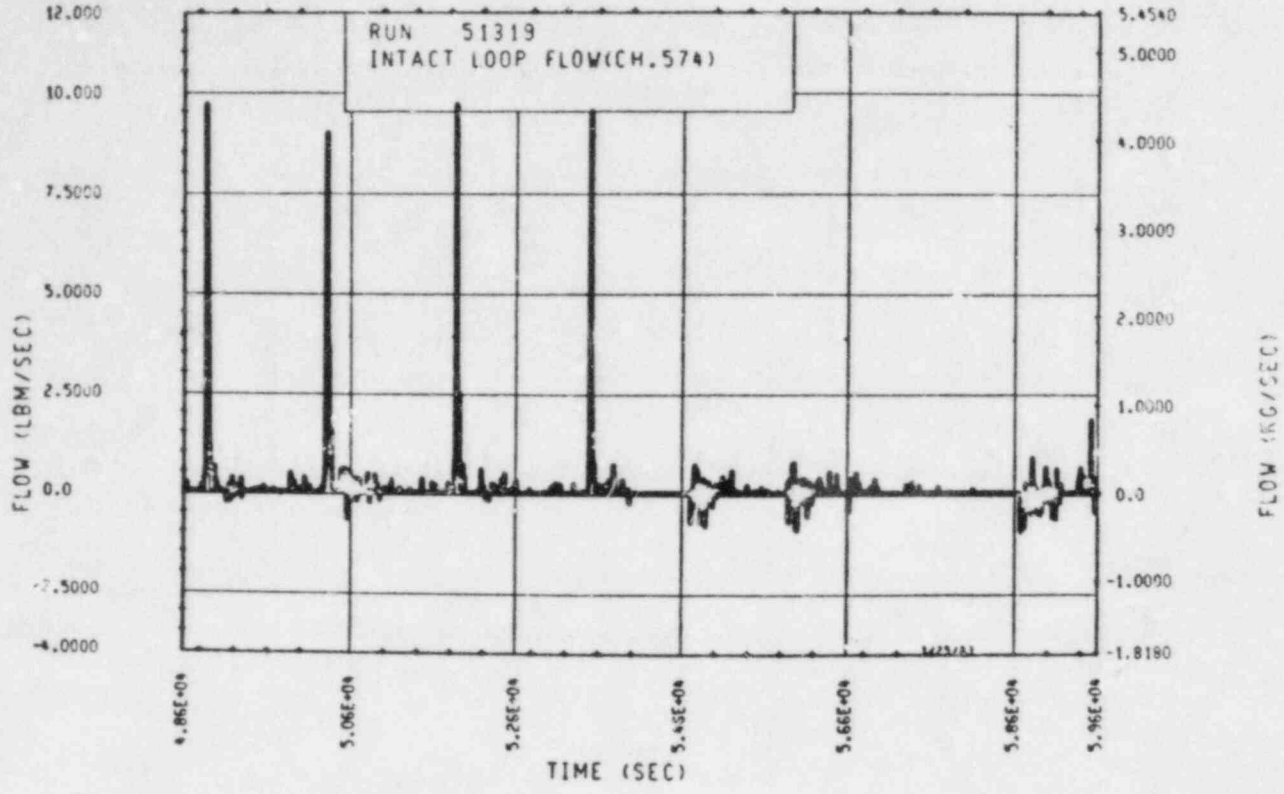

Figure A-276. Mass Flow Rate Through Unbroken Loop, Test 19

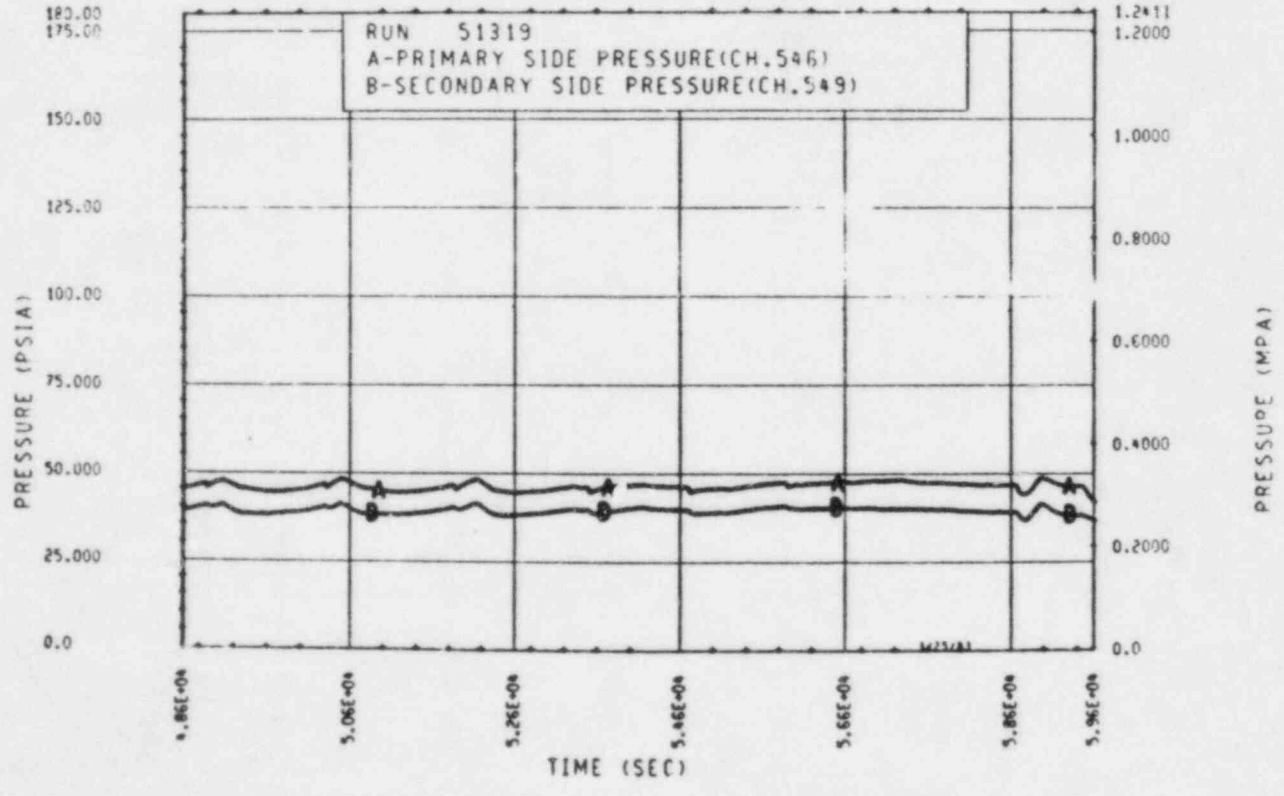

Figure A-277. Primary and Secondary System Pressure, Test 19

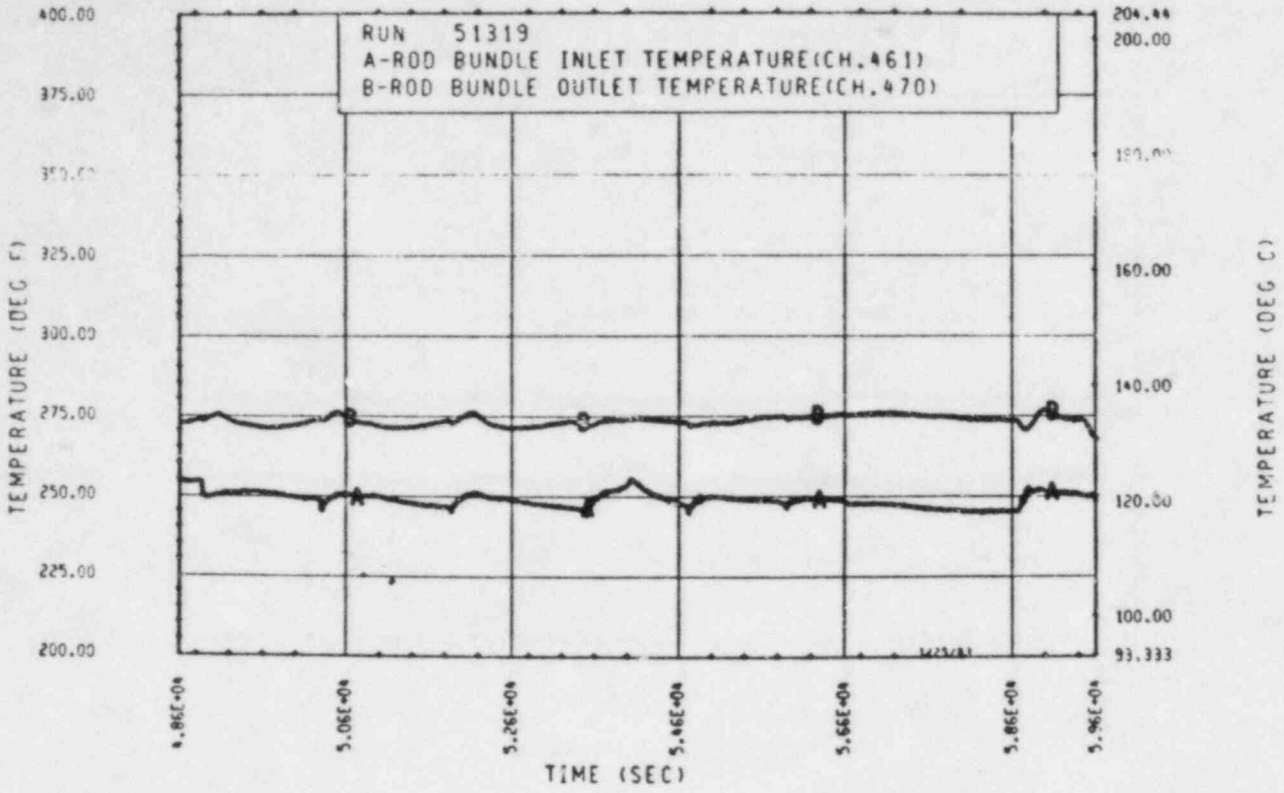

Figure A-278. Heater Rod Bundle Inlet and Outlet Temperature, Test 19

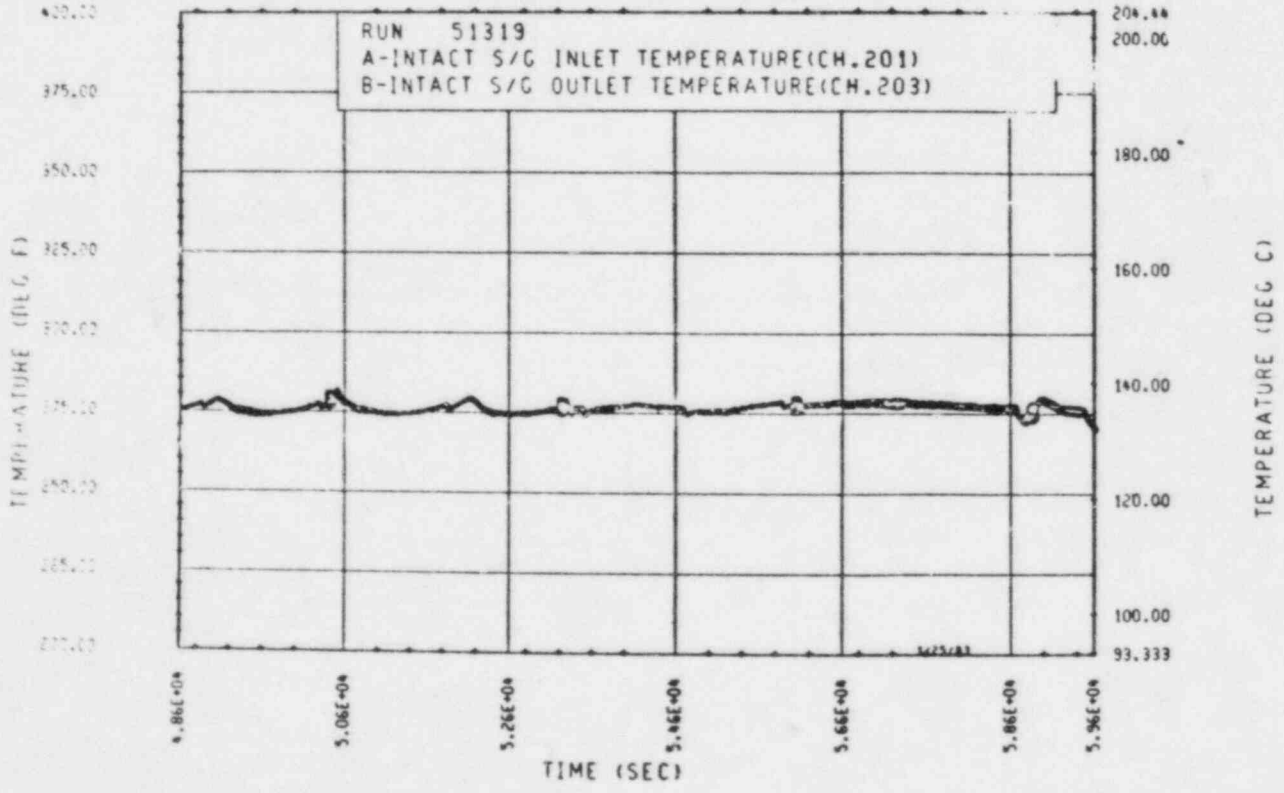

Figure A-279. Unbroken Loop Steam Generator Inlet and Outlet Temperature, Test 19

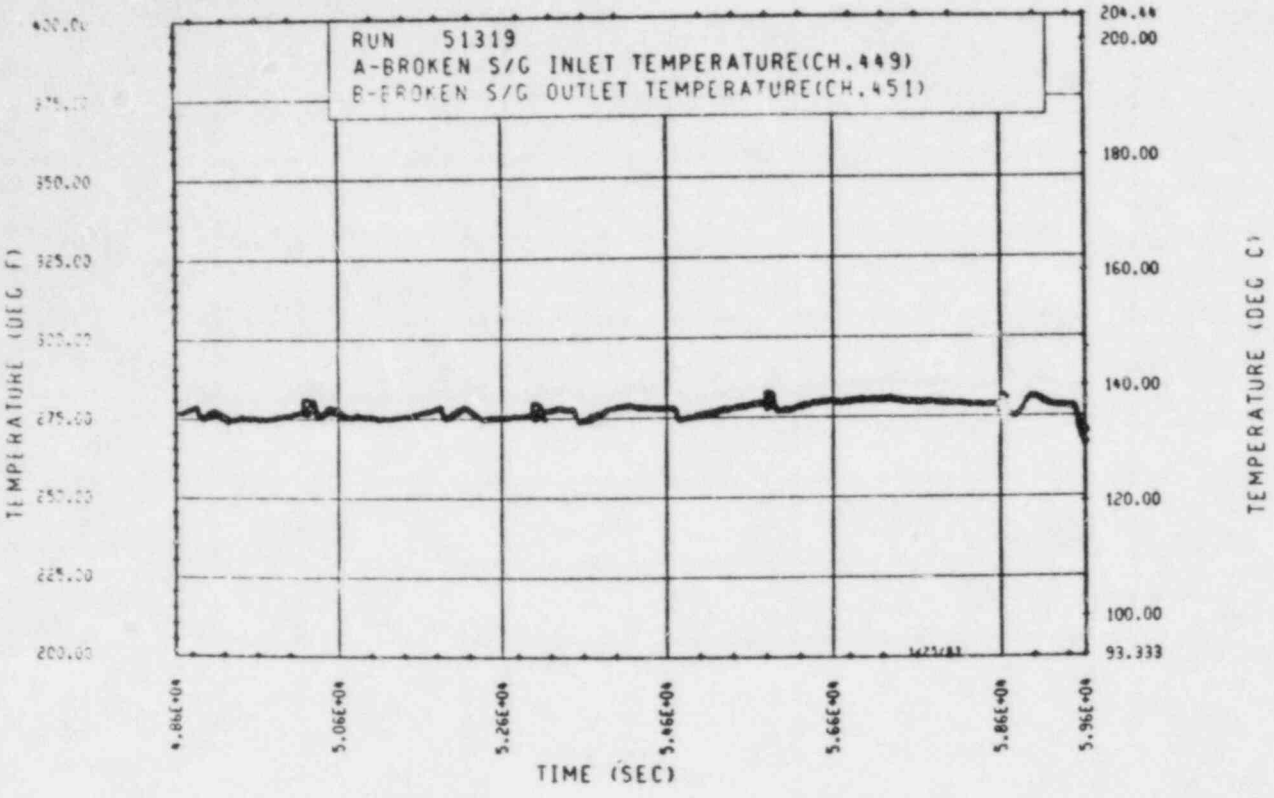

Figure A-280. Broken Loop Steam Generator Inlet and Outlet Temperature, Test 19

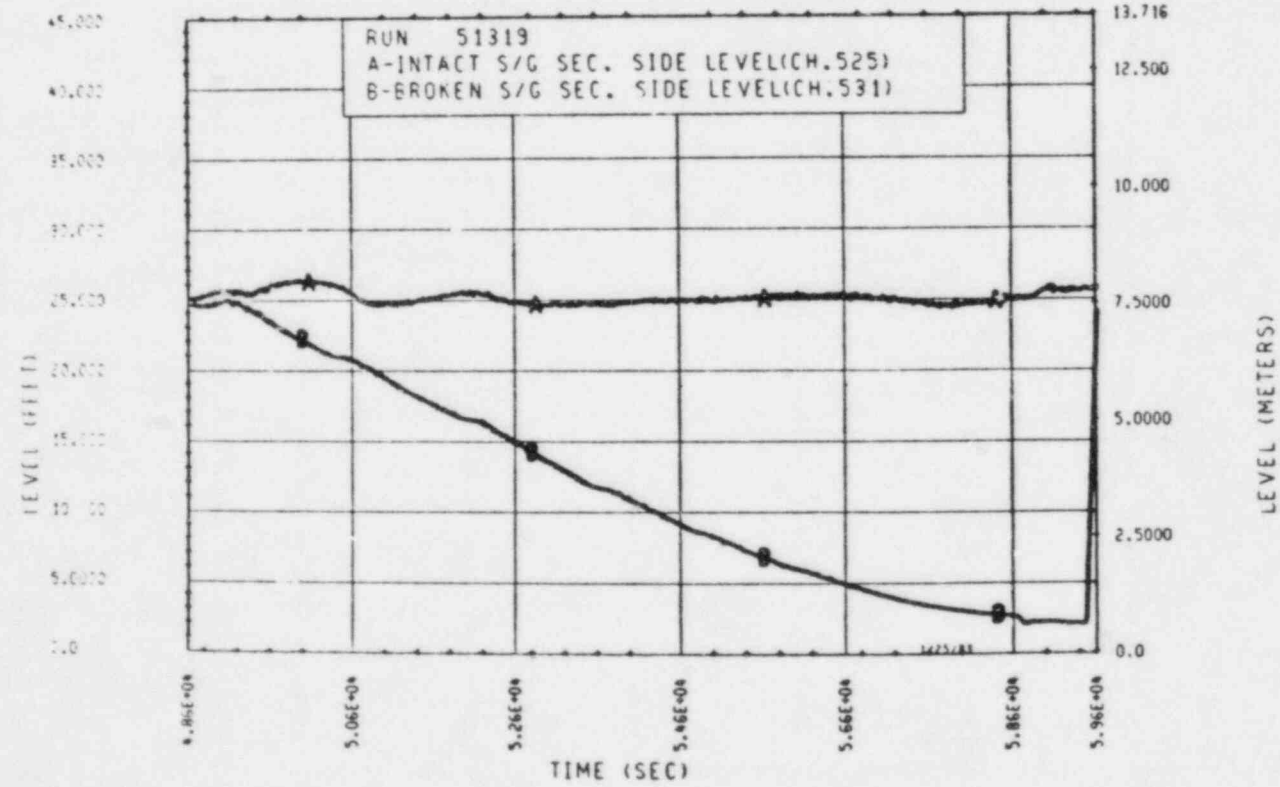

Figure A-281. Unbroken and Broken Loop Steam Generator Secondary Side Collapsed Liquid Levels, Test 19

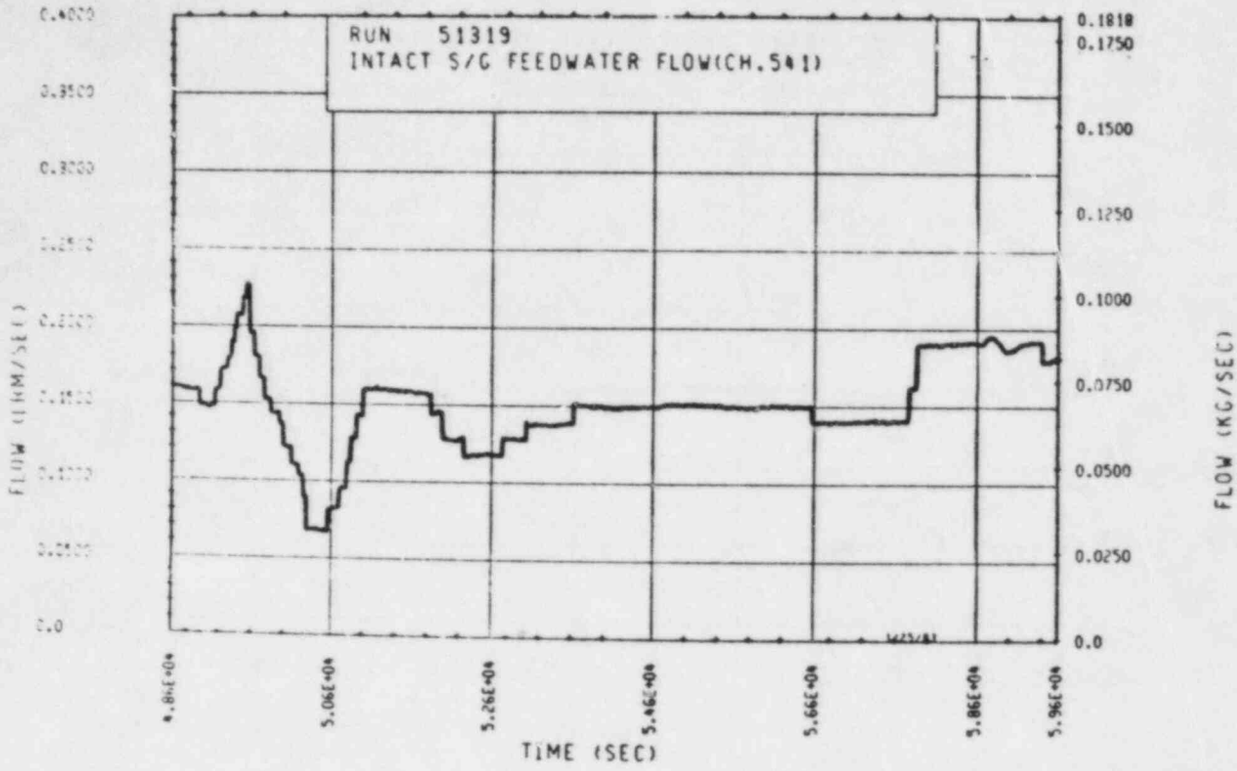

Figure A-282. Unbroken Loop Steam Generator Feedwater Mass Flow Rate, Test 19

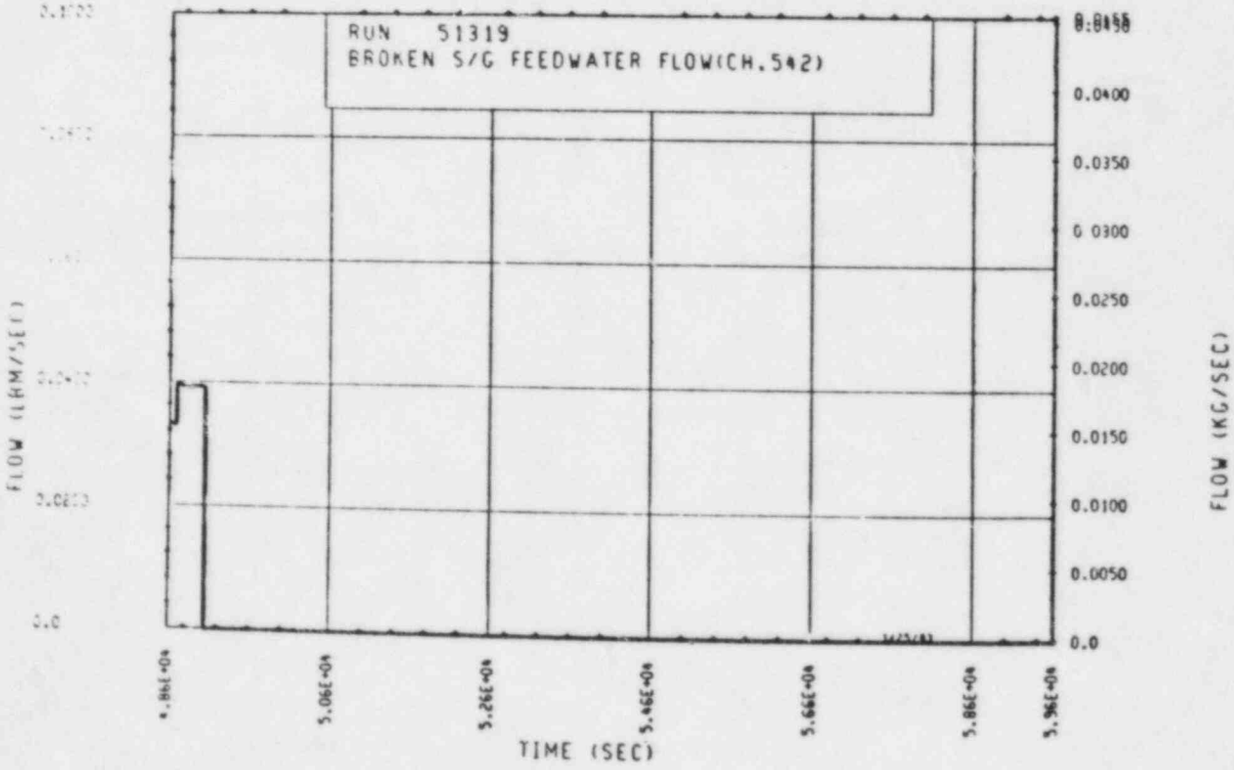

Figure A-283. Broken Loop Steam Generator Feedwater Mass Flow Rate, Test 19

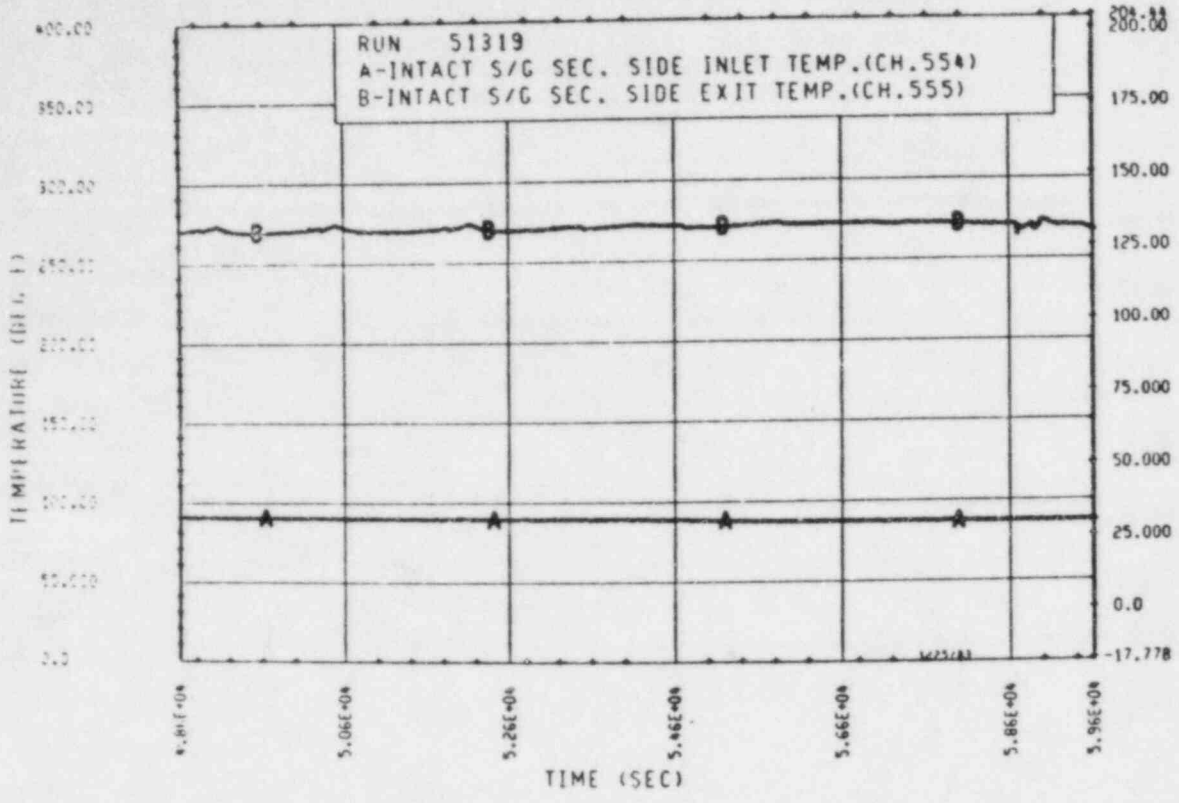

Figure A-284. Unbroken Loop Steam Generator Secondary Side Inlet and Outlet Temperature, Test 19

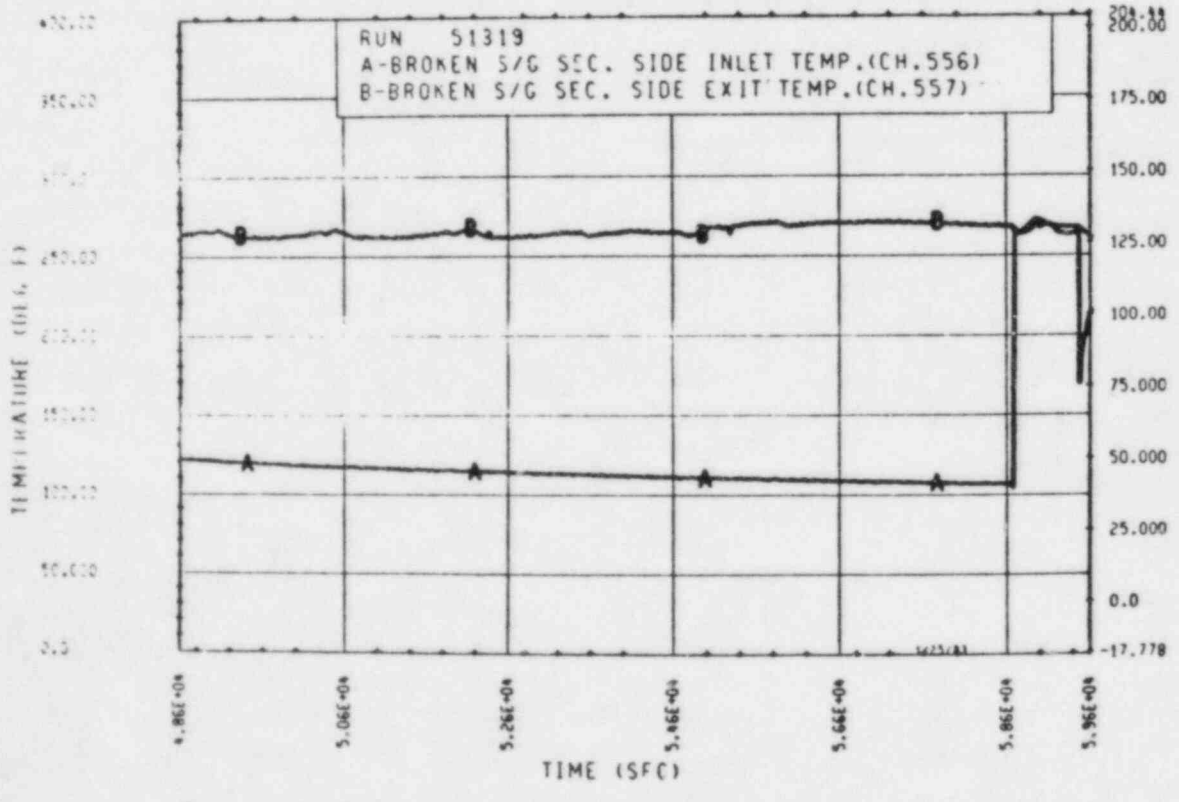

Figure A-285. Broken Loop Steam Generator Secondary Side Inlet and Outlet Temperature, Test 19

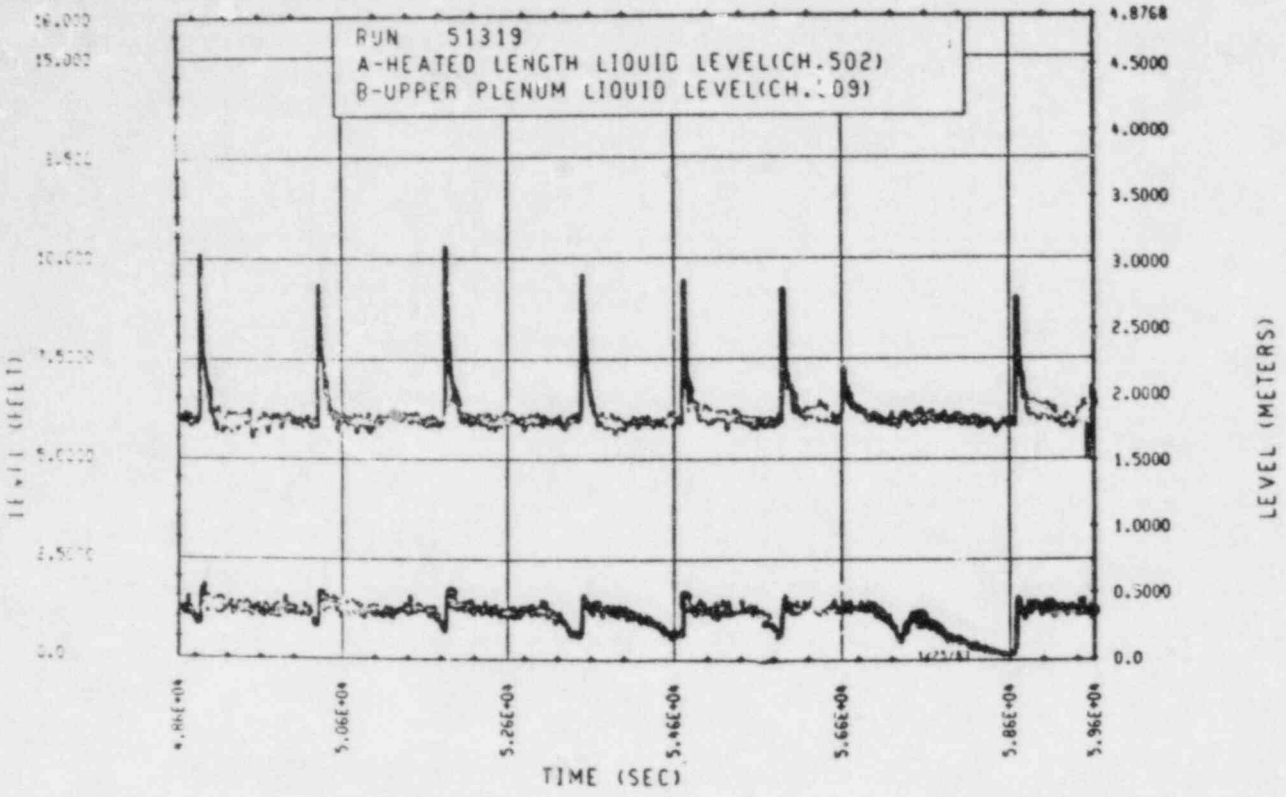

Figure A-286. Heated Length and Upper Plenum Liquid Levels, Test 19

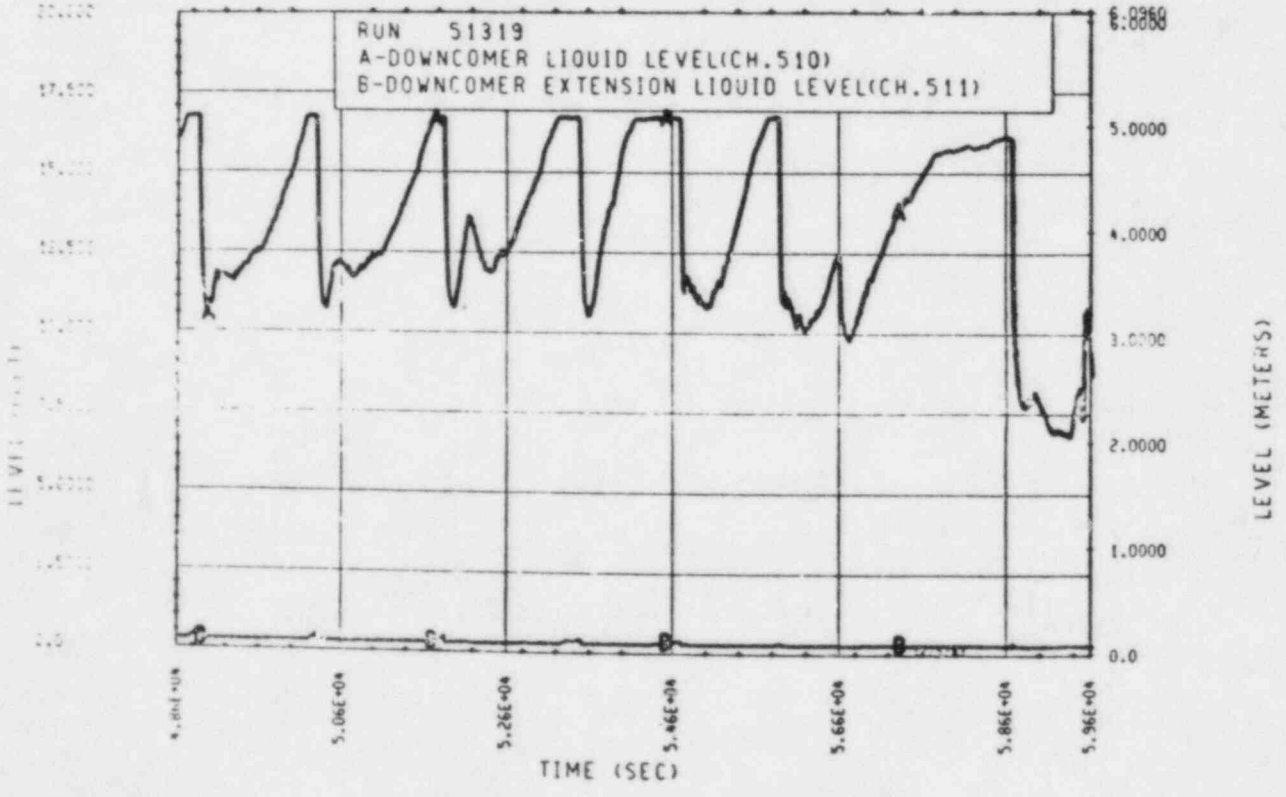

Figure A-287. Downcomer and Downcomer Extension Liquid Levels, Test 19

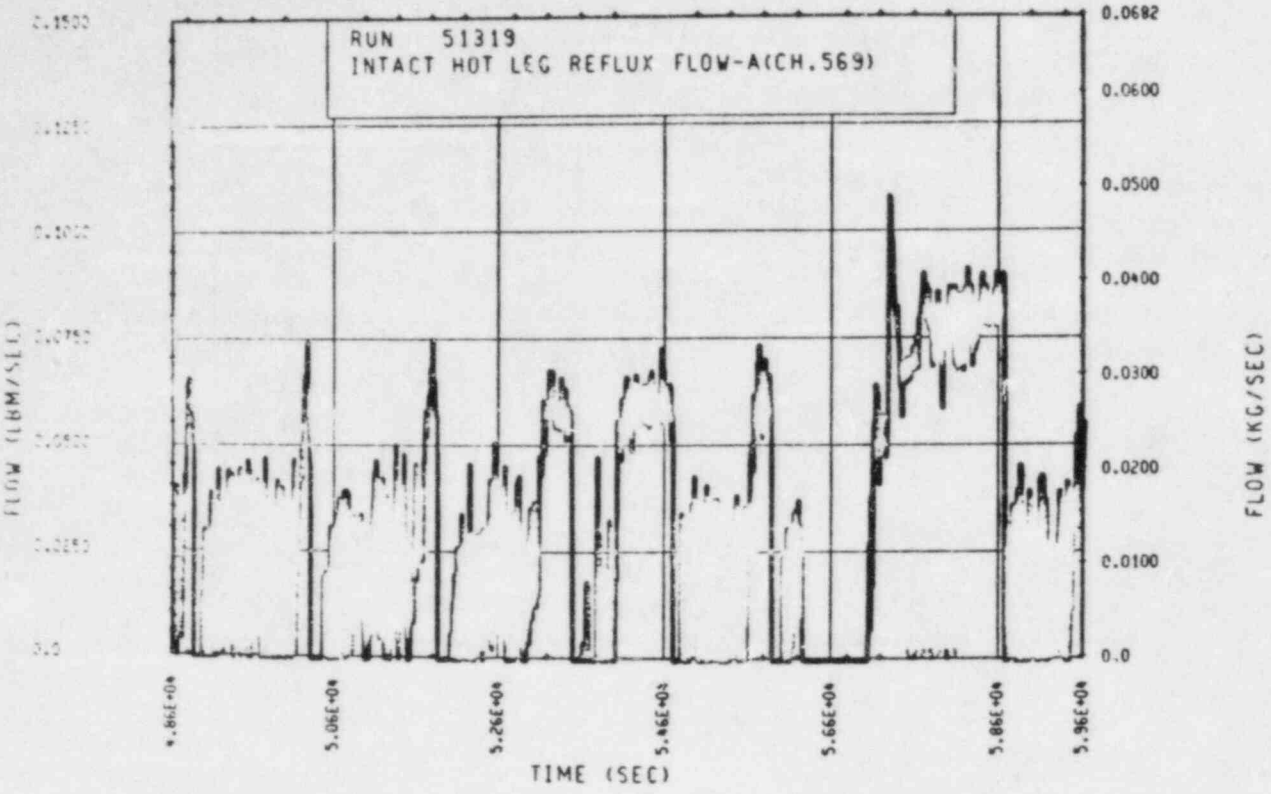

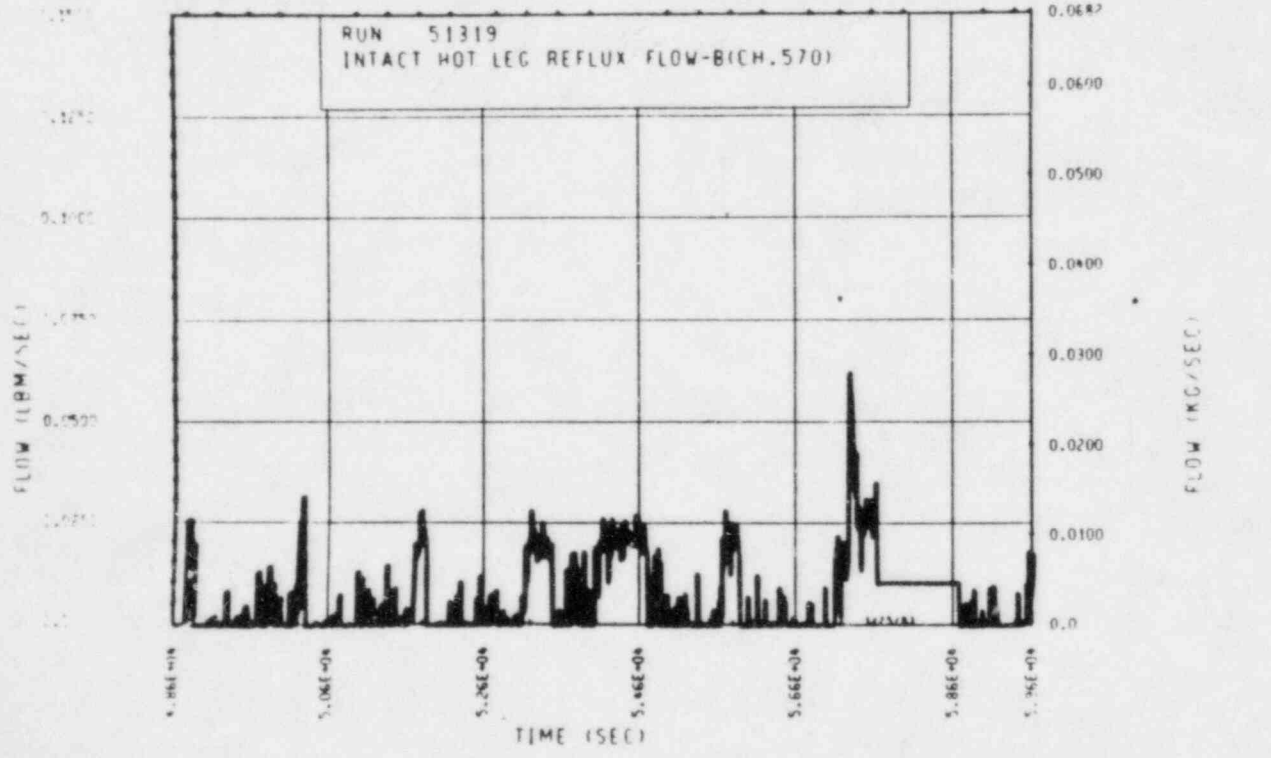

Figure A-288. Unbroken Loop Hot Leg Reflux Condensation Mass Flow Rate, Test 19

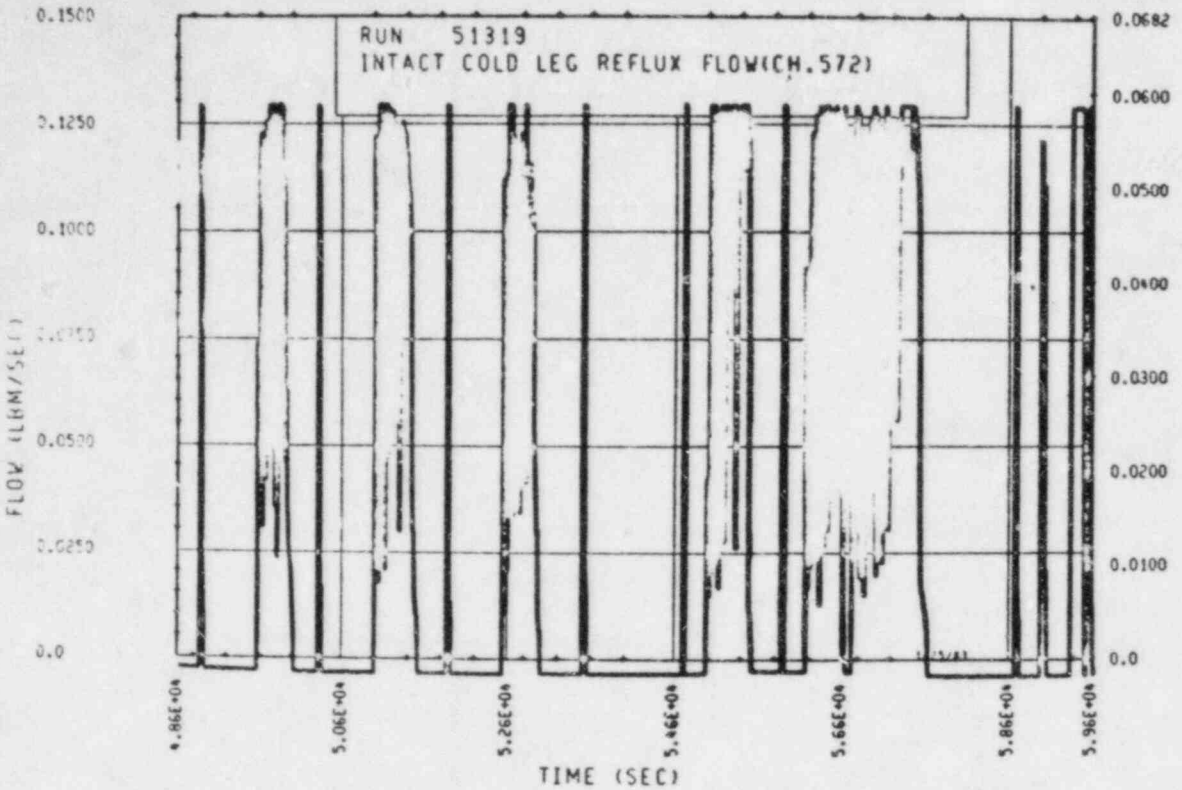

Figure A-289. Unbroken Loop Cold Leg Reflux Condensation Mass Flow Rate, Test 19

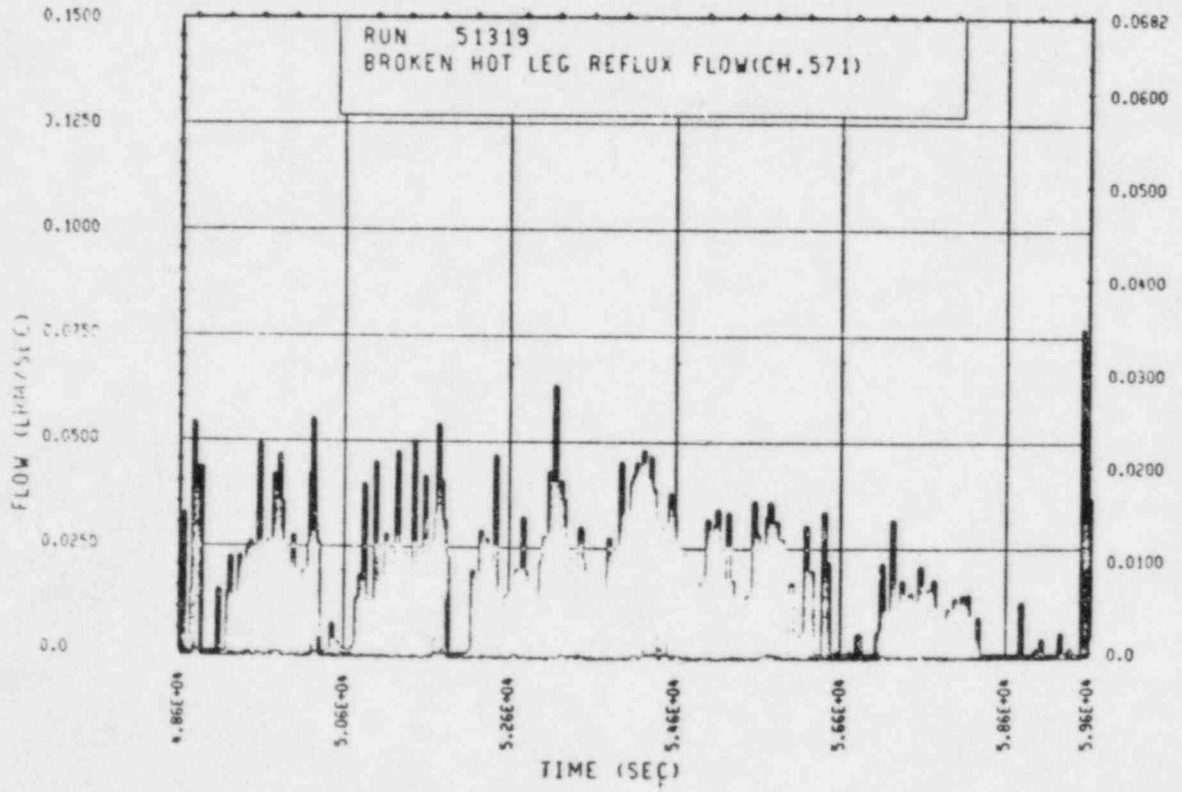

Figure A-290. Broken Loop Hot Leg Reflux Condensation Mass Flow Rate, Test 19

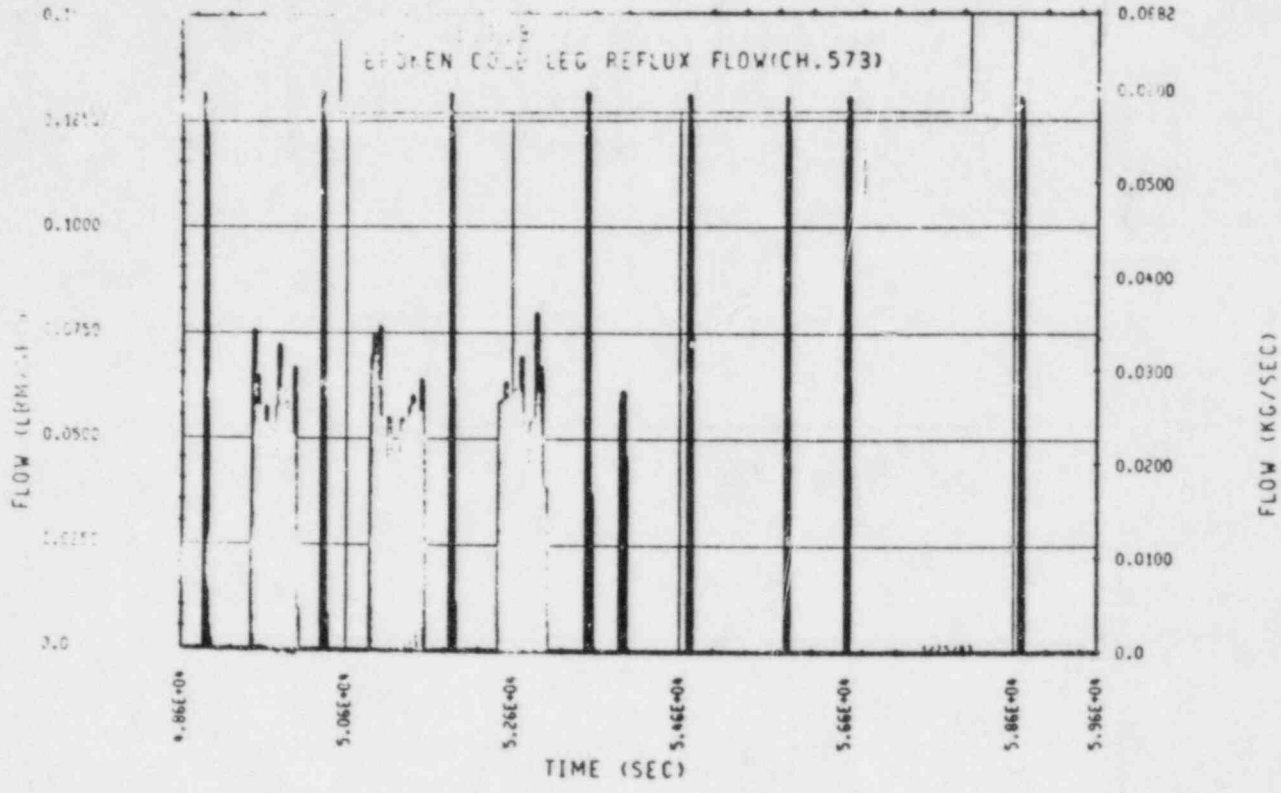

Figure A-291. Broken Loop Cold Leg Reflux Condensation Mass Flow Rate, Test 19

APPENDIX B

REPRESENTATIVE HEAT FLUX AND THERMOCOUPLE CORRECTION CURVES

Representative heat flux versus ΔT_{sat} curves for instrumented elevations are presented in figures B-1 through B-13. Representative wall thermocouple correction curves for the same locations are presented in figures B-14 through B-26.

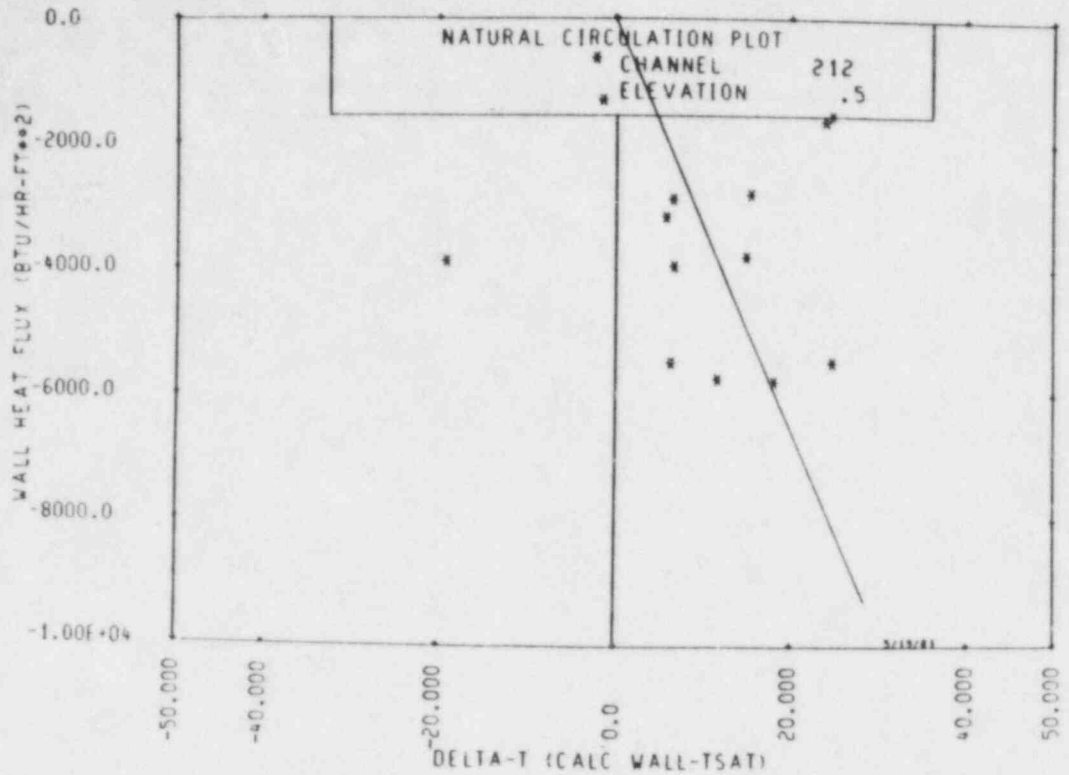

Figure B-1. Heat Flux Versus Calculated Wall Temperature Minus Saturation Temperature, 0.15 m (0.5 ft) Elevation

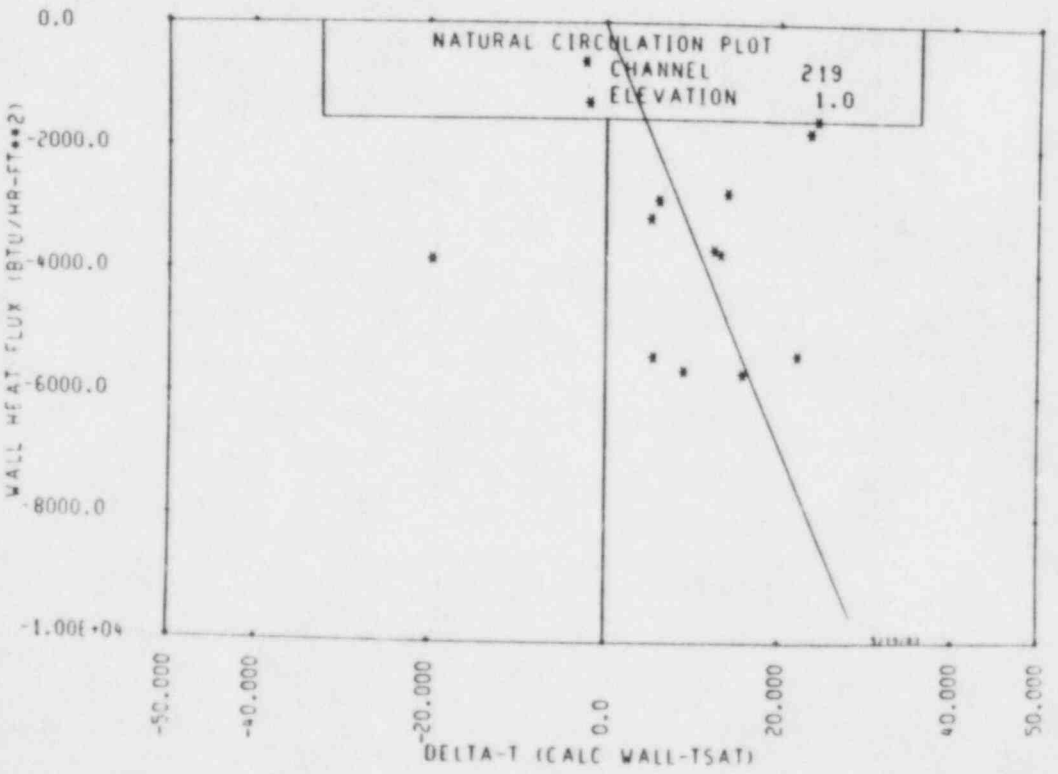

Figure B-2. Heat Flux Versus Calculated Wall Temperature Minus Saturation Temperature, 0.30 m (1 ft) Elevation

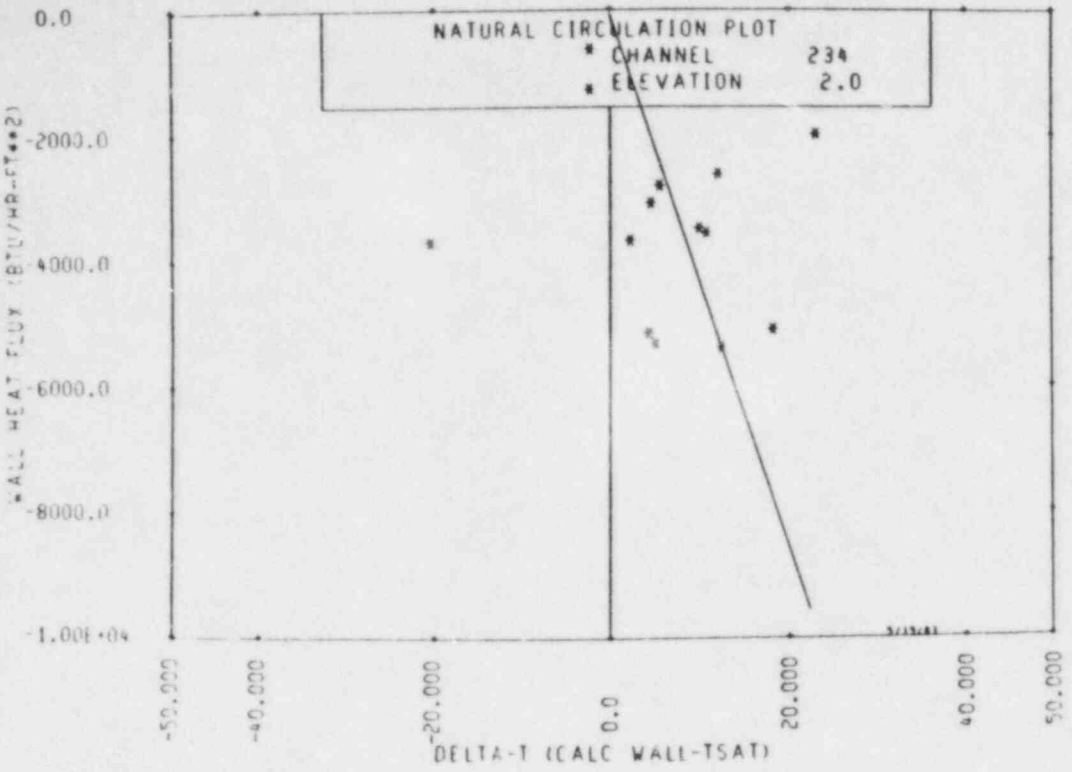

Figure B-3. Heat Flux Versus Calculated Wall Temperature Minus Saturation Temperature, 0.61 m (2 ft) Elevation

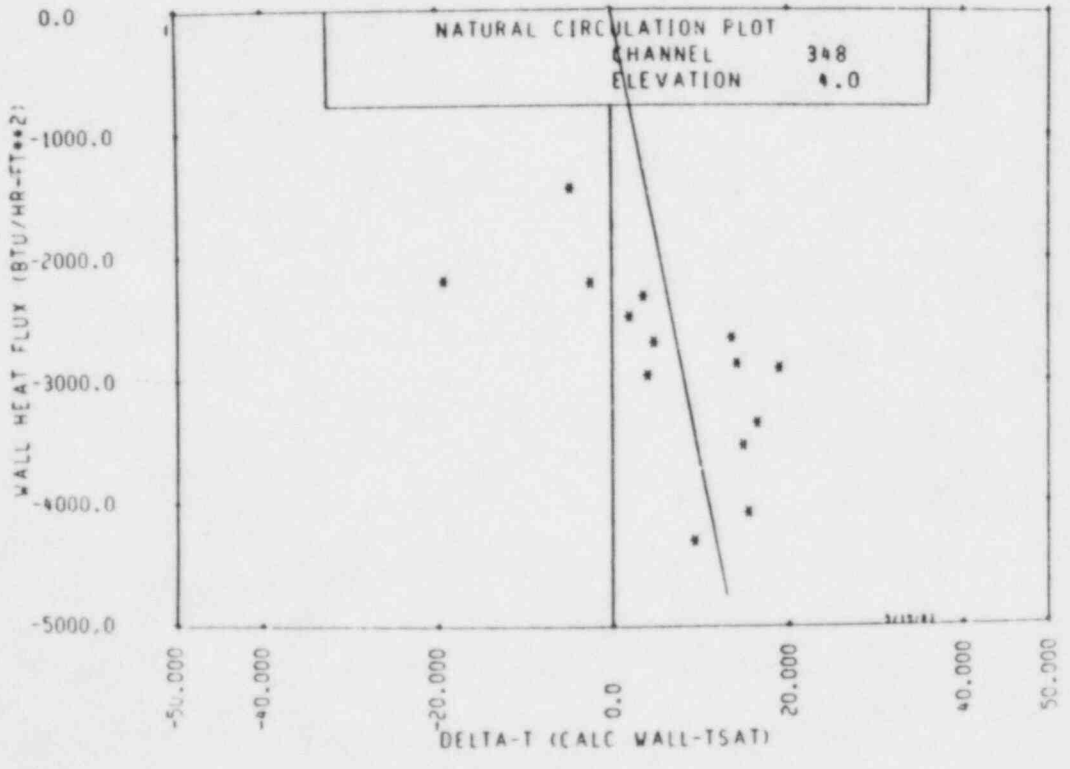

Figure B-4. Heat Flux Versus Calculated Wall Temperature Minus Saturation Temperature, 1.22 m (4 ft) Elevation

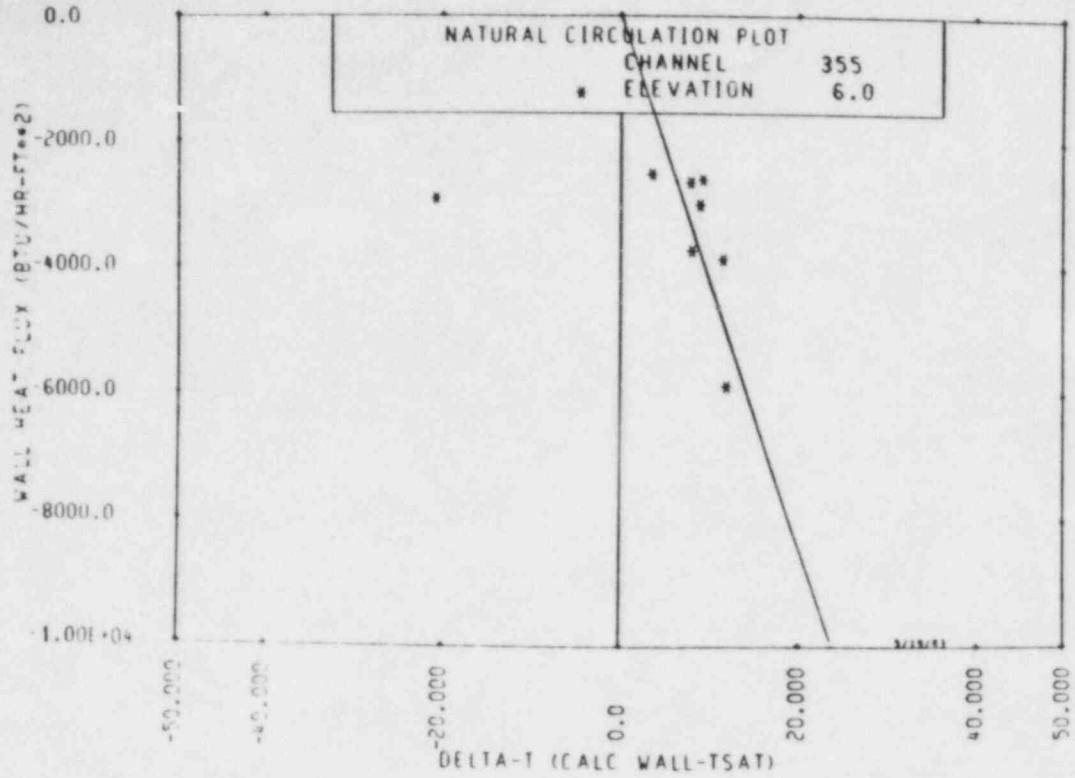

Figure B-5. Heat Flux Versus Calculated Wall Temperature Minus Saturation Temperature, 1.83 m (6 ft) Elevation

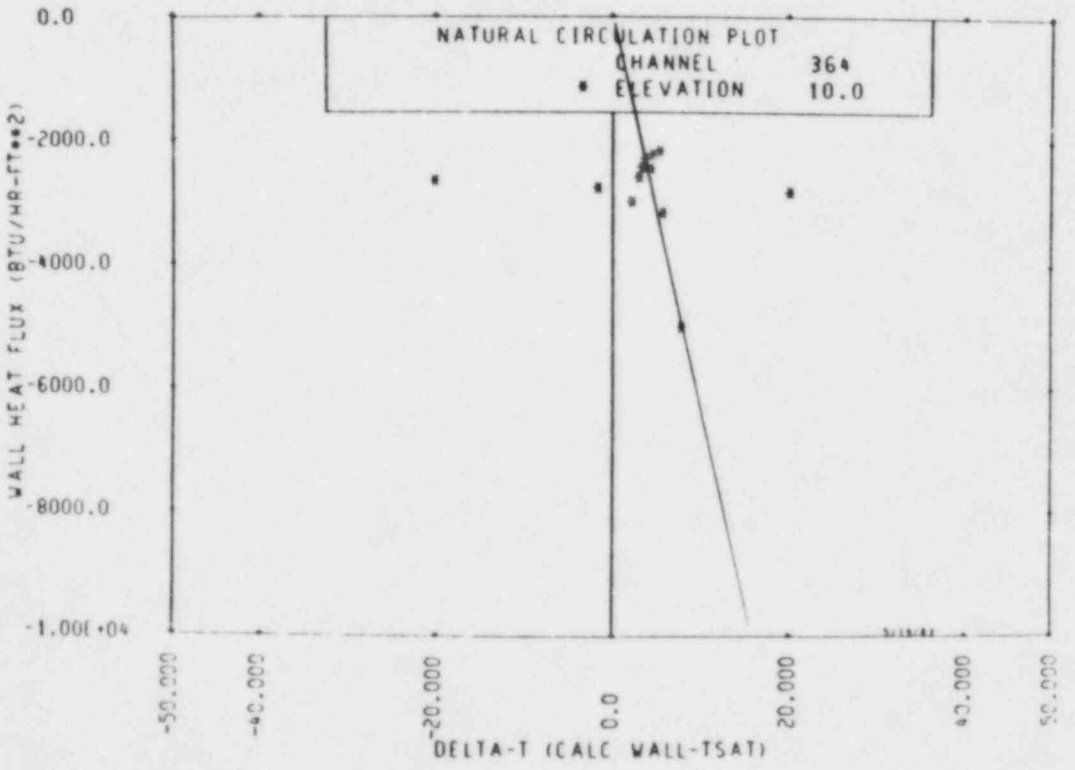

Figure B-6. Heat Flux Versus Calculated Wall Temperature Minus Saturation Temperature, 3.05 m (10 ft) Elevation

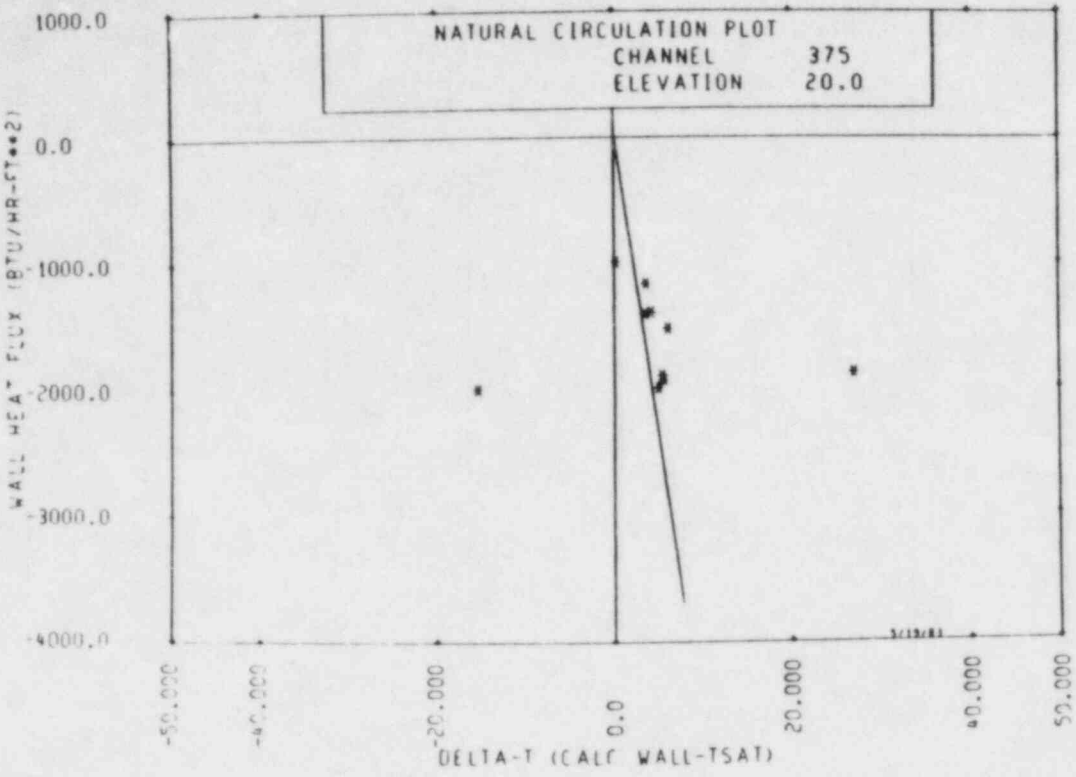

Figure B-7. Heat Flux Versus Calculated Wall Temperature Minus Saturation Temperature, 6.10 m (20 ft) Elevation

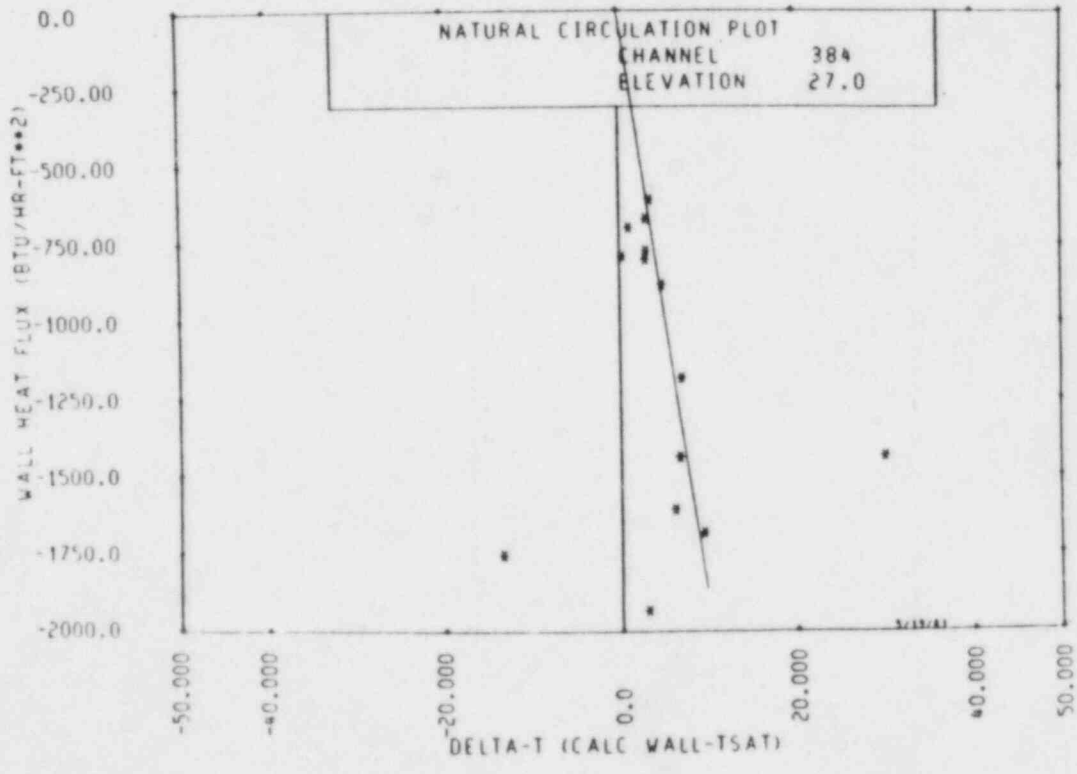

Figure B-8. Heat Flux Versus Calculated Wall Temperature Minus Saturation Temperature, 8.23 m (27 ft) Elevation

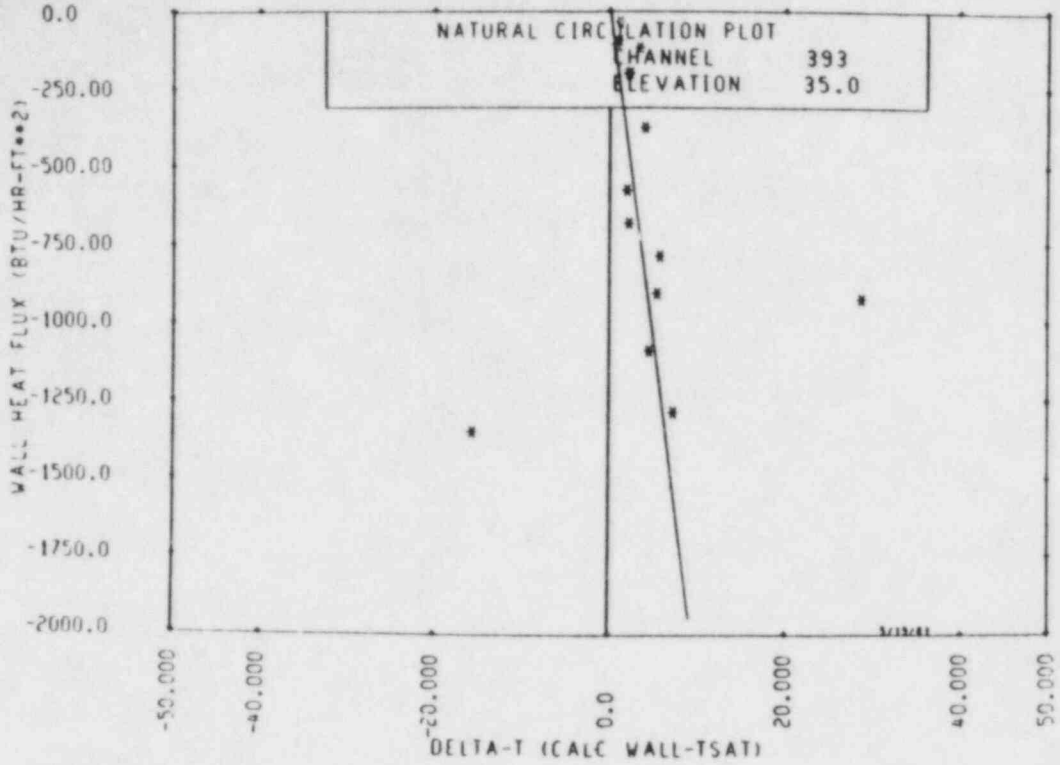

Figure B-9. Heat Flux Versus Calculated Wall Temperature Minus Saturation Temperature, 10.67 m (35 ft) Elevation

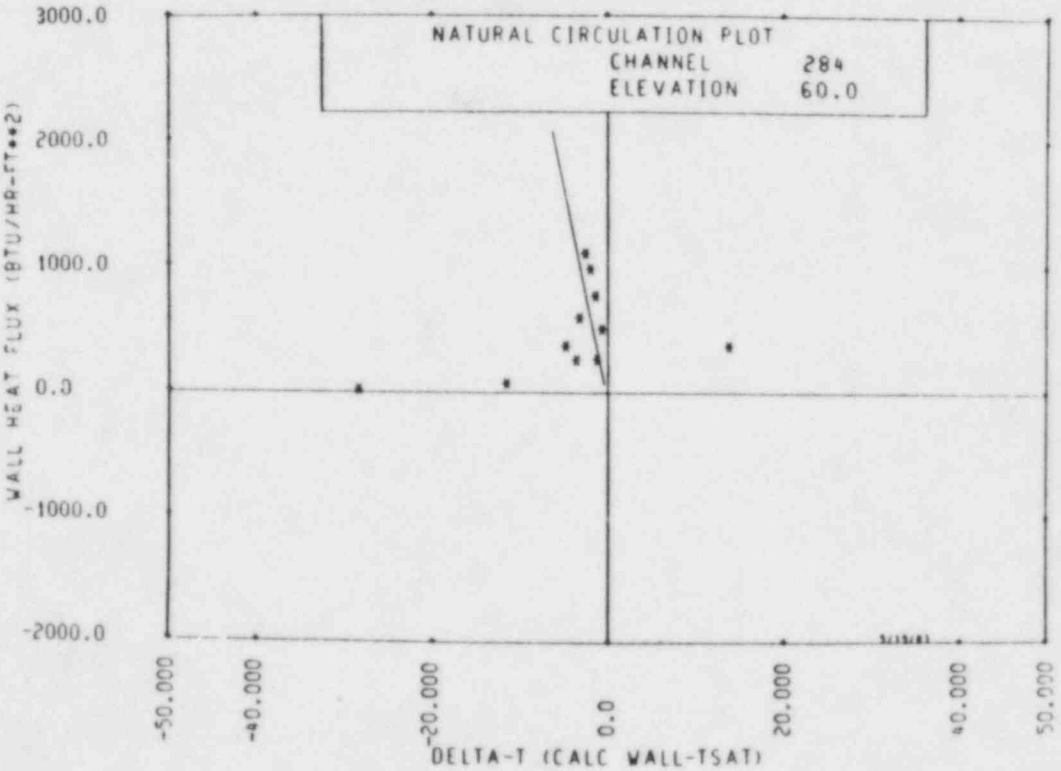

Figure B-10. Heat Flux Versus Calculated Wall Temperature Minus Saturation Temperature, 18.29 m (60 ft) Elevation

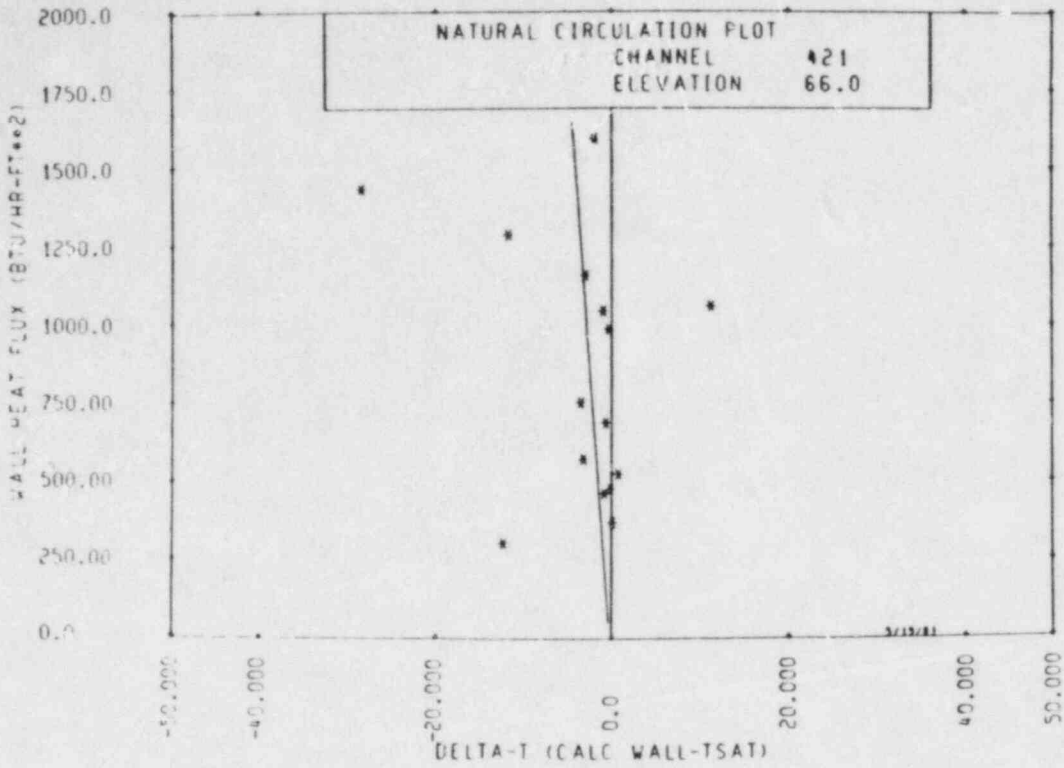

Figure B-11. Heat Flux Versus Calculated Wall Temperature Minus Saturation Temperature, 20.12 m (66 ft) Elevation

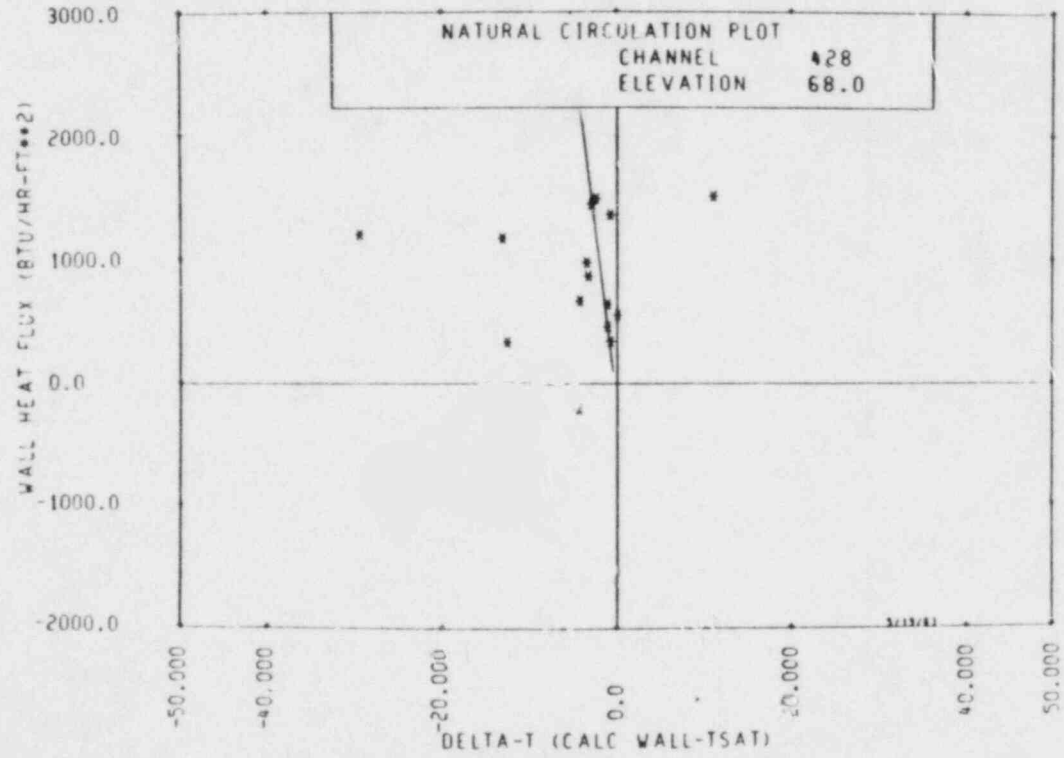

Figure B-12. Heat Flux Versus Calculated Wall Temperature Minus Saturation Temperature, 20.73 m (68 ft) Elevation

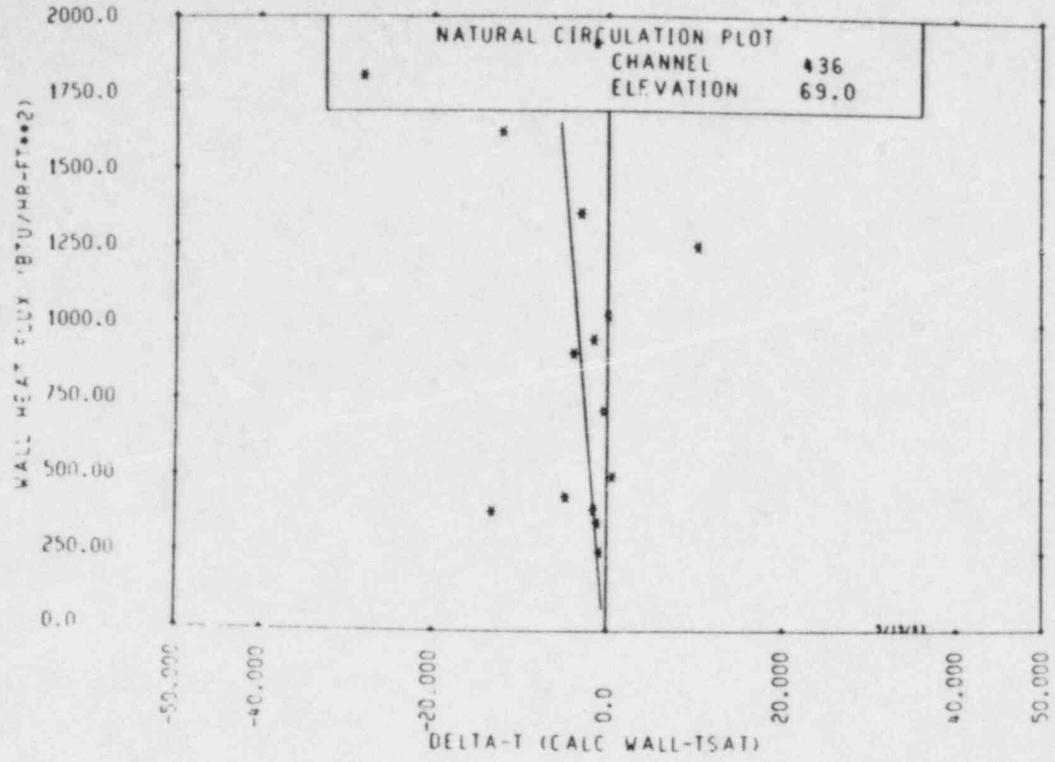

Figure B-13. Heat Flux Versus Calculated Wall Temperature Minus Saturation Temperature, 21.03 m (69 ft) Elevation

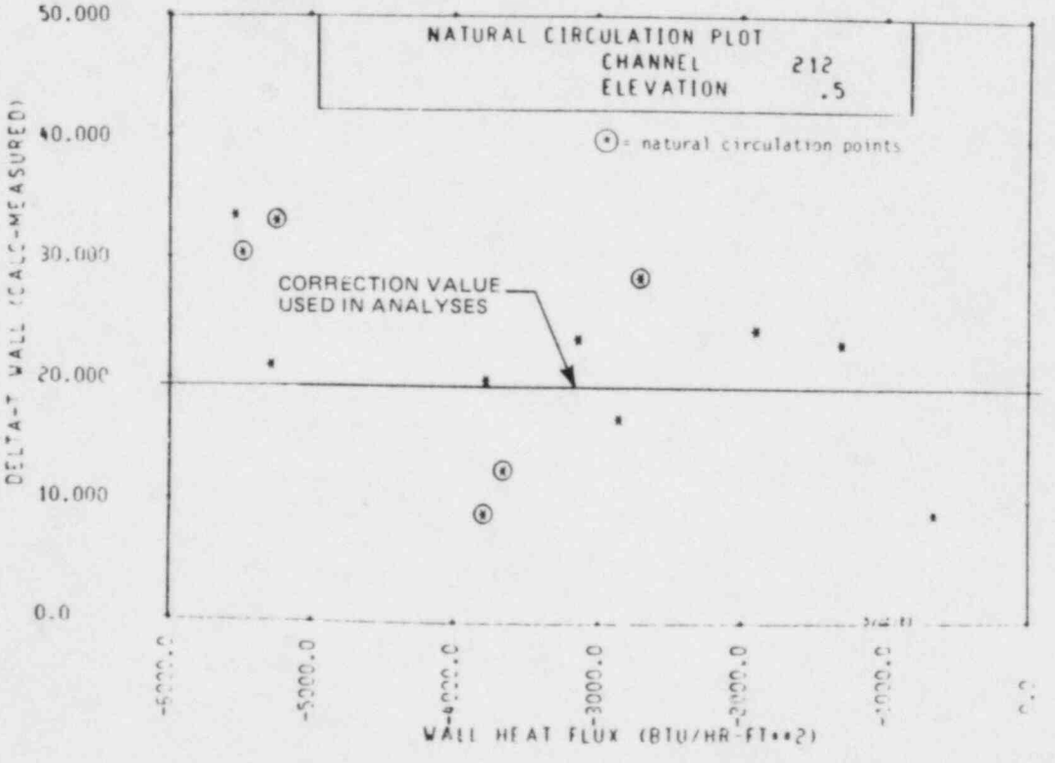

Figure B-14. Wall Thermocouple Correction Constant, 0.15 m (0.5 ft) Elevation

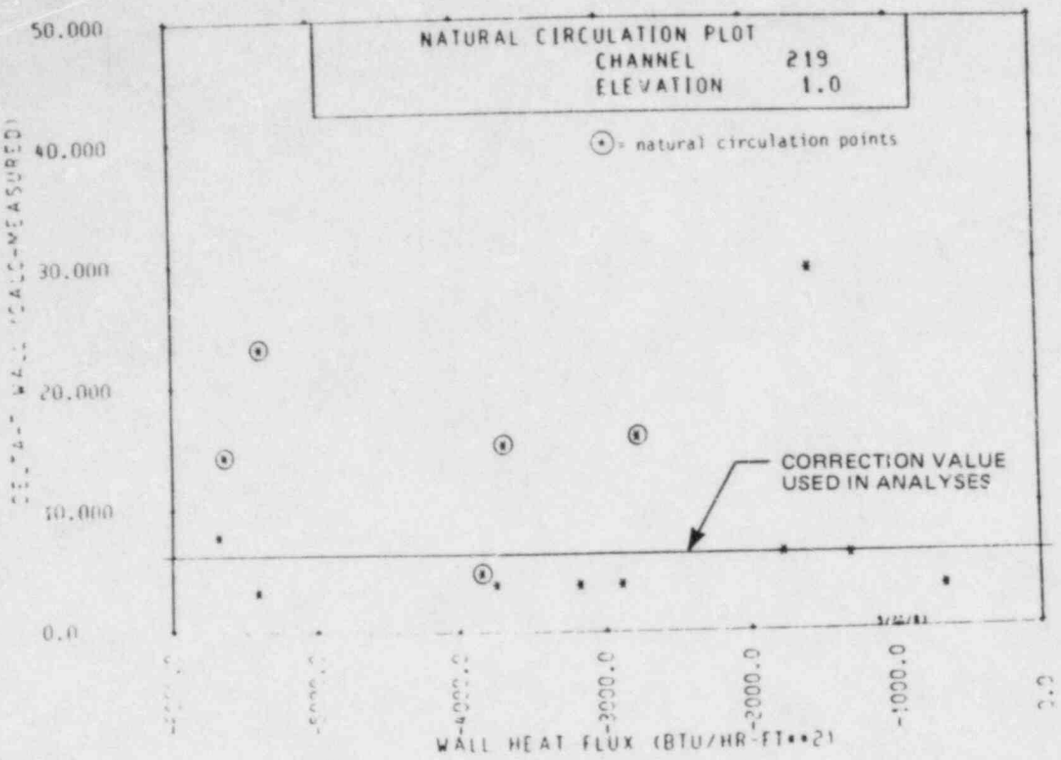

Figure B-15. Wall Thermocouple Correction Constant, 0.30 m (1 ft) Elevation

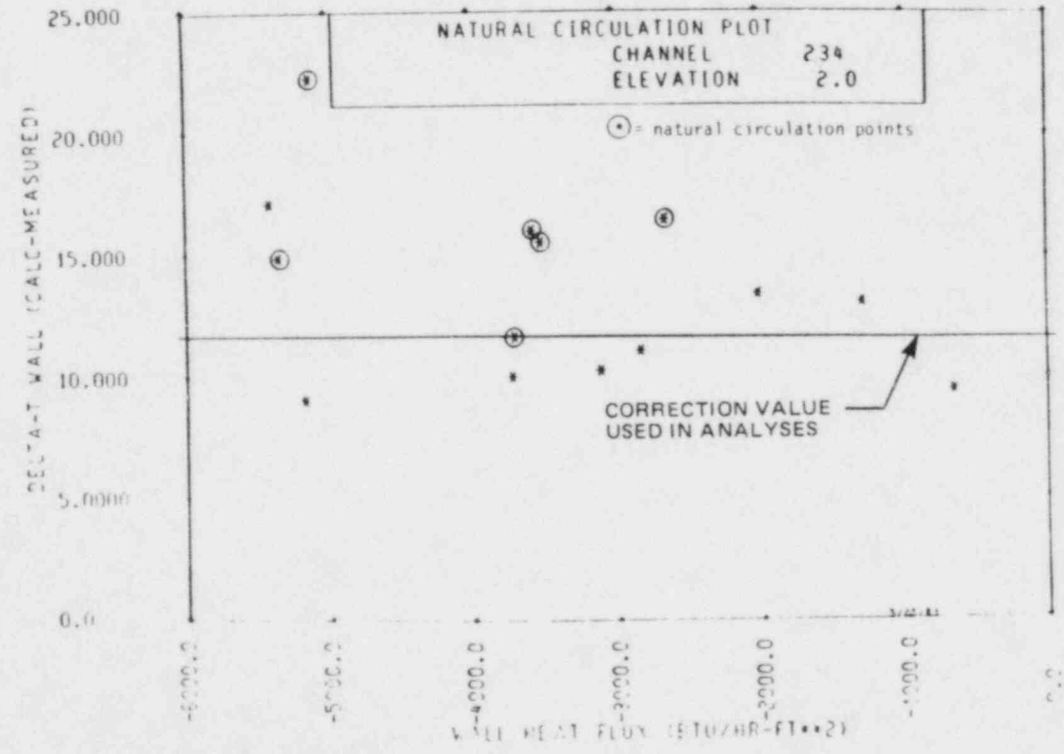

Figure B-16. Wall Thermocouple Correction Constant, 0.61 m (2 ft) Elevation

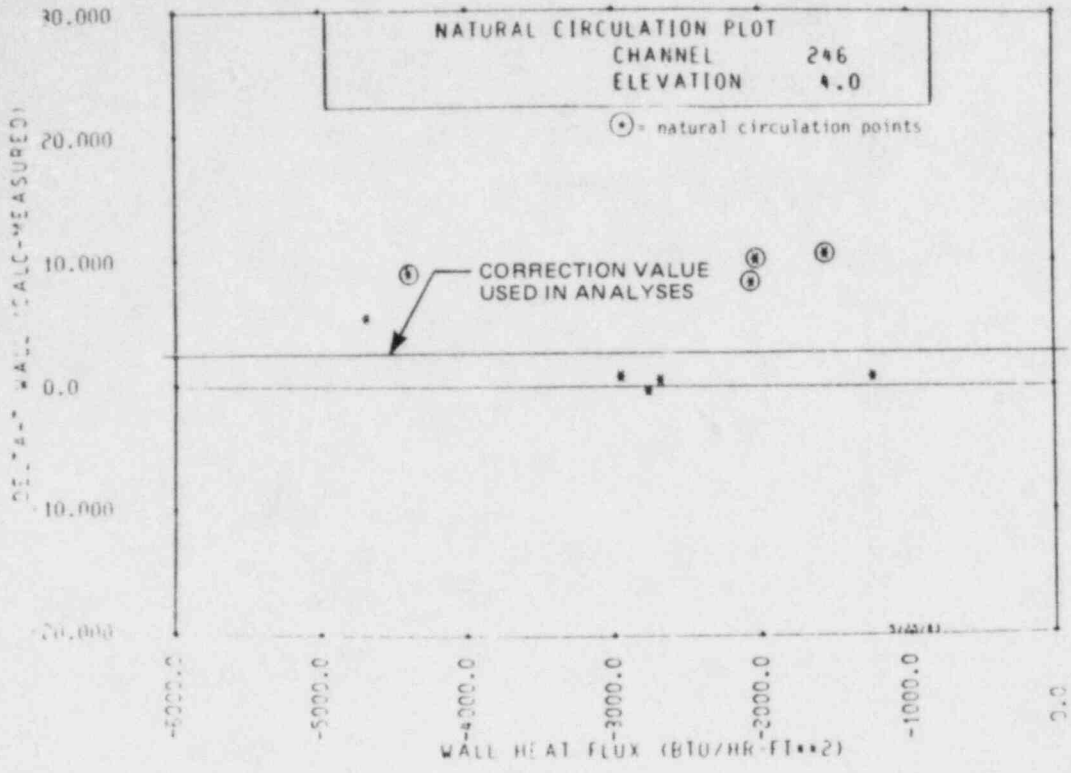

Figure B-17. Wall Thermocouple Correction Constant, 1.22 m (4 ft) Elevation

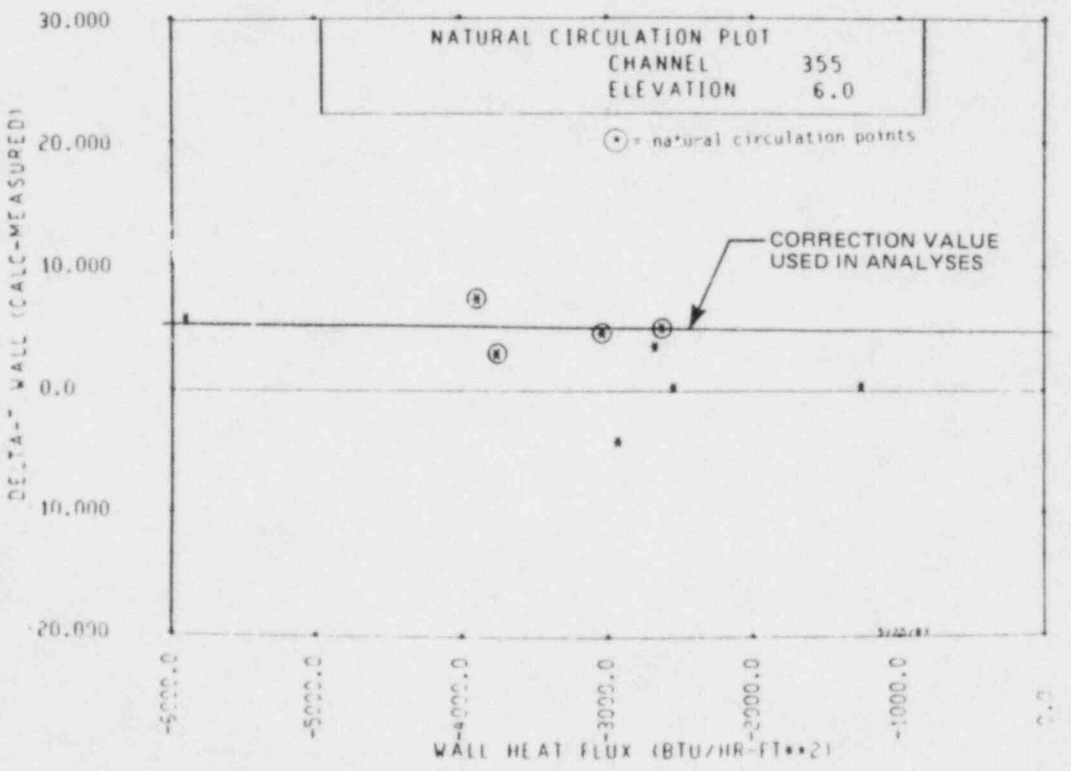

Figure B-18. Wall Thermocouple Correction Constant, 1.83 m (6 ft) Elevation

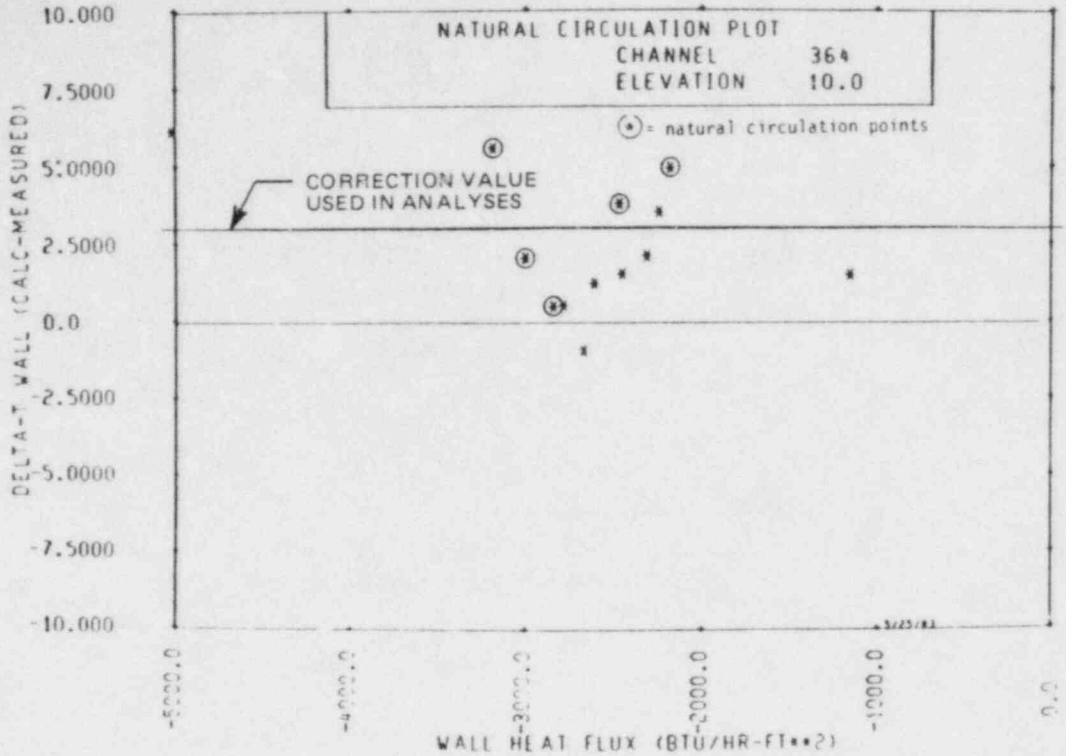

Figure B-19. Wall Thermocouple Correction Constant, 3.05 m (10 ft) Elevation

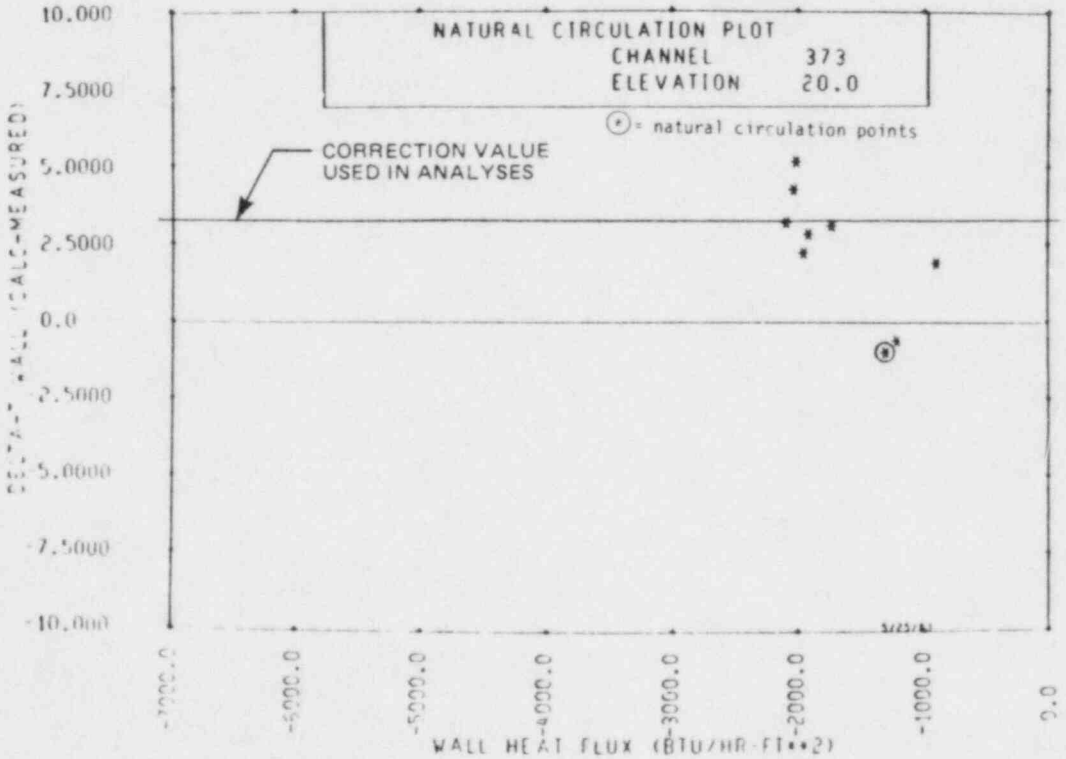

Figure B-20. Wall Thermocouple Correction Constant, 6.10 m (20 ft) Elevation

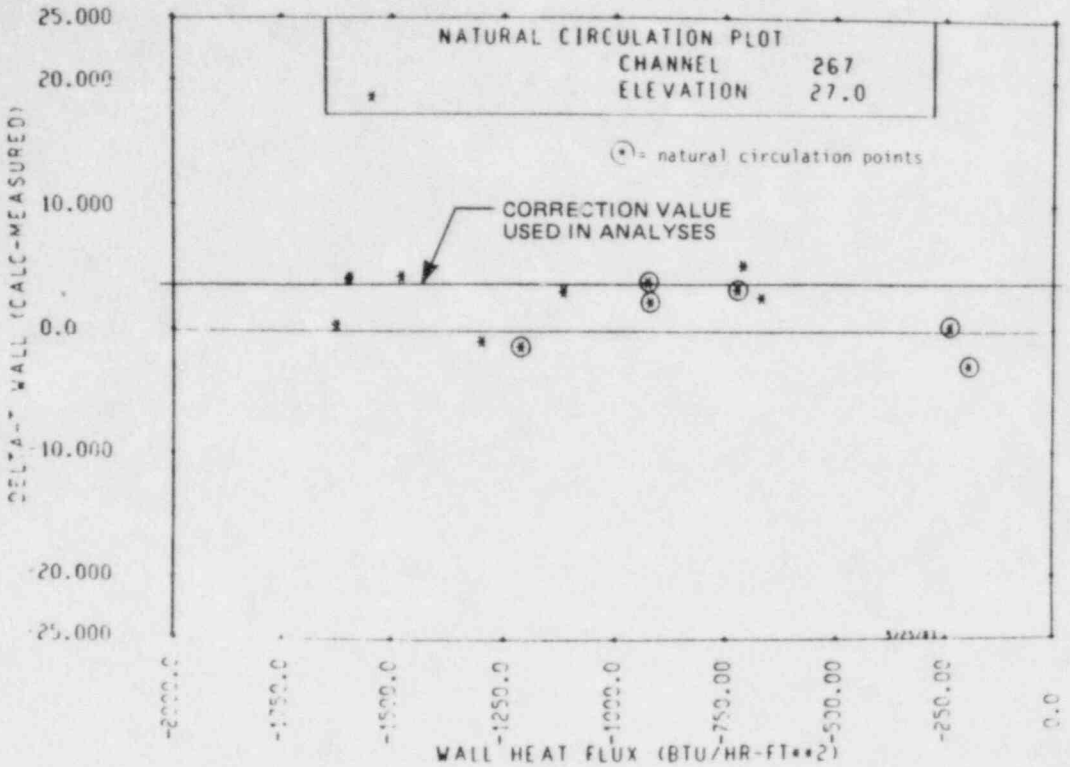

Figure B-21. Wall Thermocouple Correction Constant, 8.23 m (27 ft) Elevation

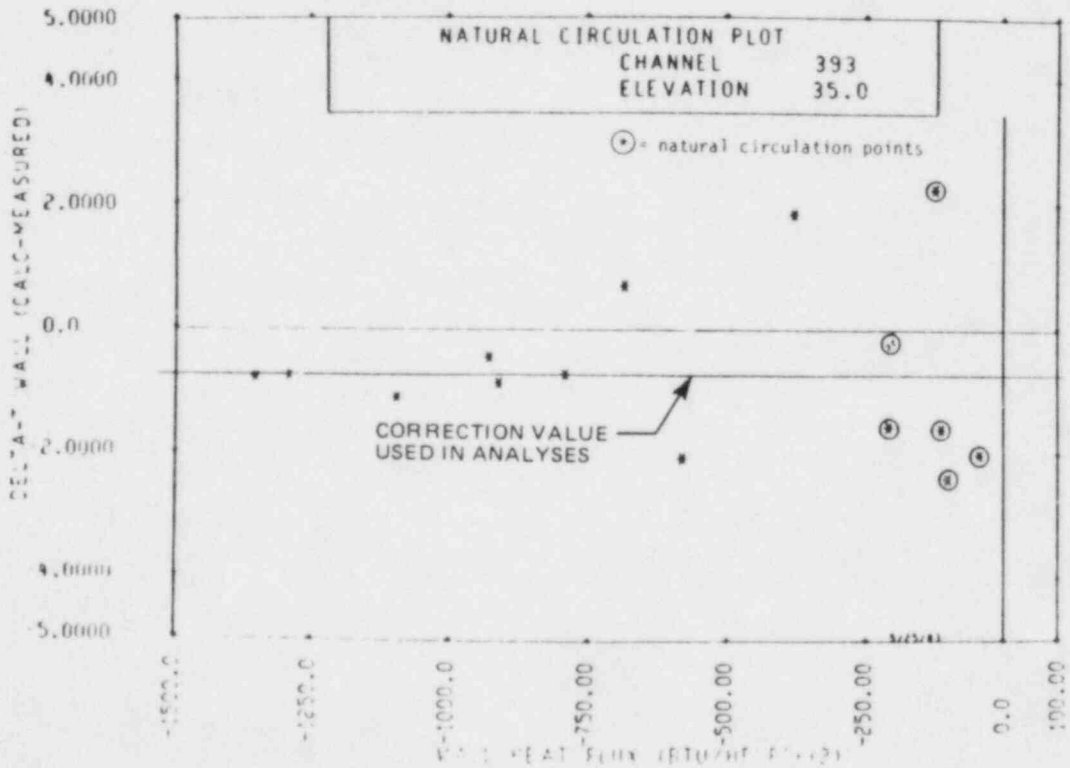

Figure B-22. Wall Thermocouple Correction Constant, 10.67 m (35 ft) Elevation

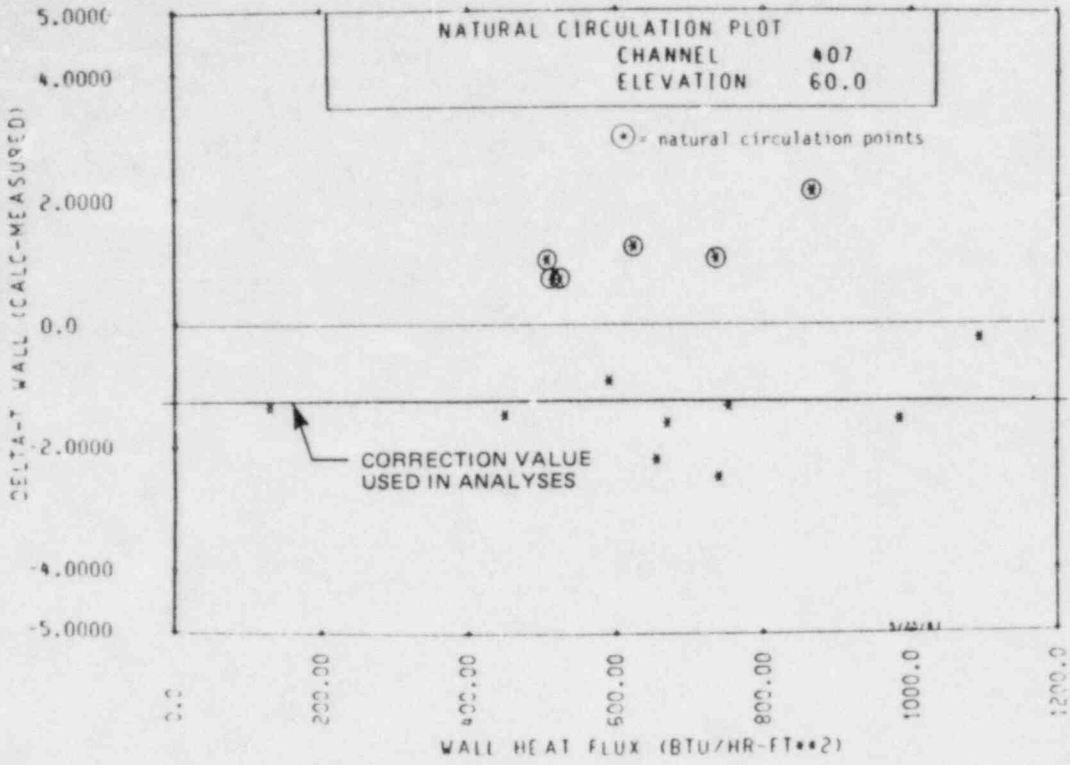

Figure B-23. Wall Thermocouple Correction Constant, 18.29 m (60 ft) Elevation

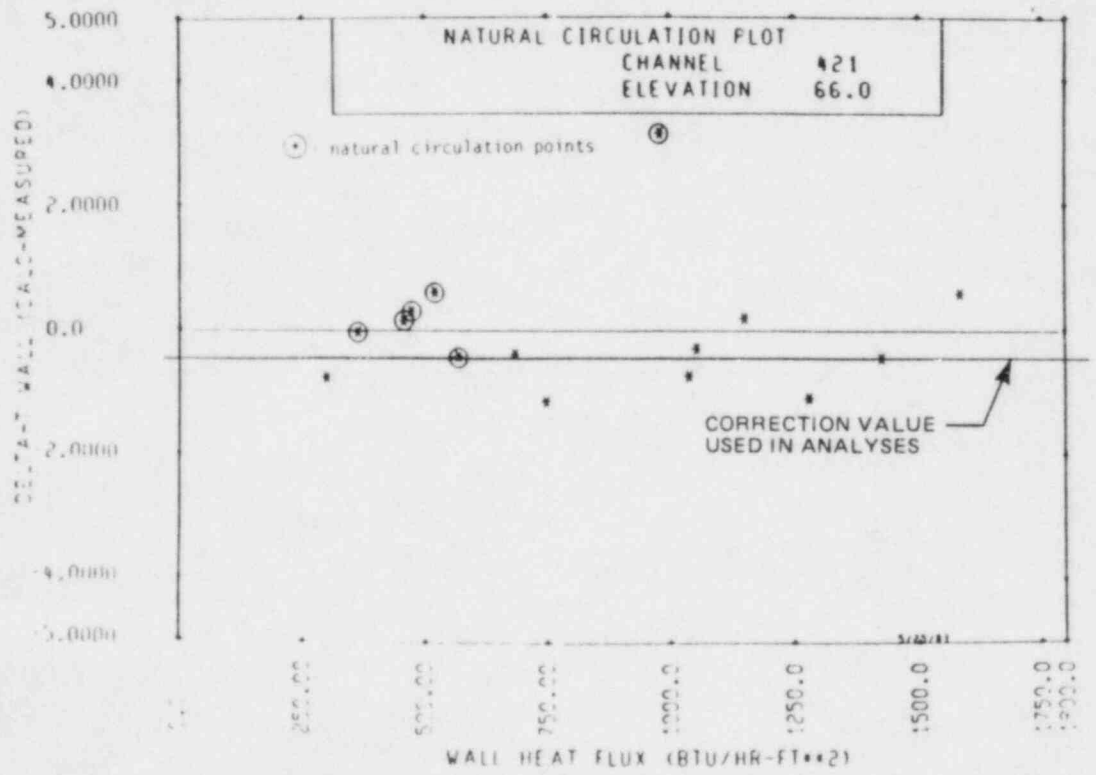

Figure B-24. Wall Thermocouple Correction Constant, 20.12 m (66 ft) Elevation

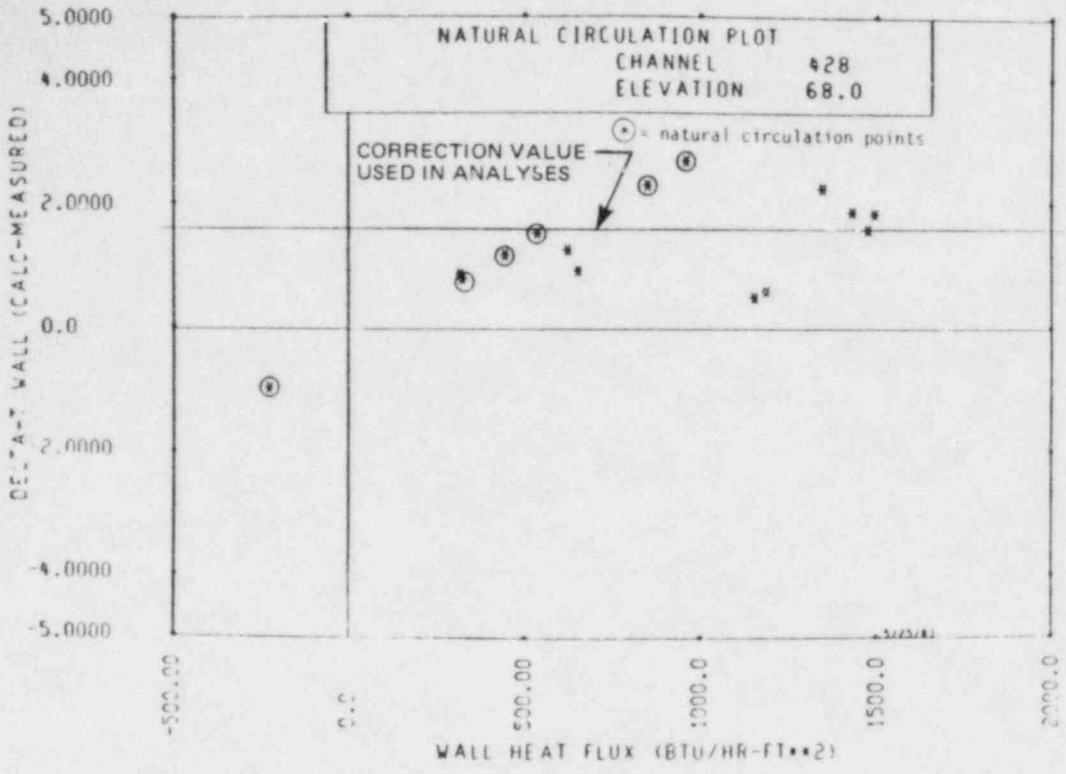

Figure B-25. Wall Thermocouple Correction Constant, 20.73 m (68 ft) Elevation

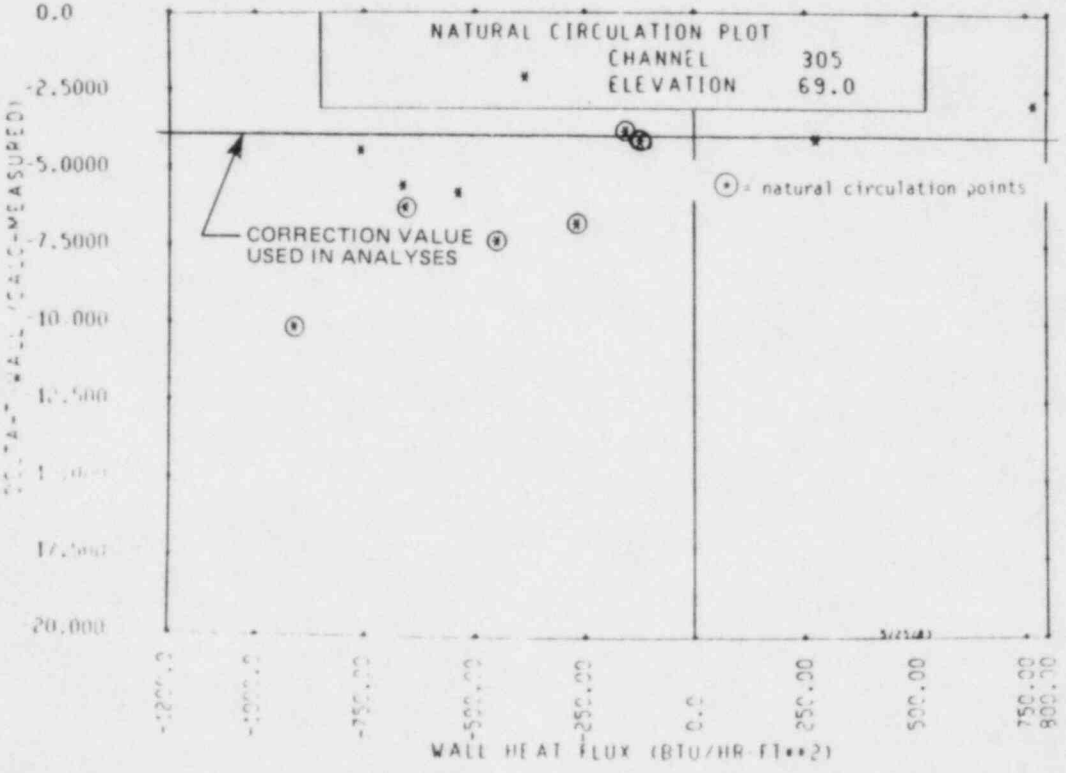

Figure B-26. Wall Thermocouple Correction Constant, 21.03 m (69 ft) Elevation

APPENDIX C
CORE AND STEAM GENERATOR ENERGY BALANCES

Calculations employed to obtain core and steam generator energy balances are presented on the following pages. The energy balance data are tabulated in table C-1, and the energy balance calculations are summarized in table C-2.

TABLE C-1

ENERGY BALANCE DATA

Parameter	Channel	Run Number					
		50708	51805	52809	51510	51114	51217
Time (sec)	--	12500	7995	6000	10200	9181	19161
Core flow [m^3/sec (gal/min)]	576	1.596 x 10^{-3} (25.29)	1.502 x 10^{-3} (23.81)	1.535 x 10^{-3} (24.330	1.509 x 10^{-3} (23.91)	1.595 x 10^{-3} (25.58)	1.608 x 10^{-3} (25.48)
Broken loop flow [m^3/sec (gal/min)]	575	3.98 x 10^{-4} (6.31)	3.81 x 10^{-4} (6.04)	3.74 x 10^{-4} (5.93)	3.76 x 10^{-4} (5.96)	4.02 x 10^{-4} (6.38)	3.63 x 10^{-4} (5.76)
Unbroken loop flow [m^3/sec (gal/min)]	574	1.181 x 10^{-3} (18.73)	1.161 x 10^{-3} (18.40)	1.111 x 10^{-3} (17.61)	1.154 x 10^{-3} (18.29)	1.237 x 10^{-3} (19.61)	1.187 x 10^{-3} (18.81)
Core T_{in} [°C (°F)]	461	136.74 (278.16)	111.33 (232.41)	132.69 (270.86)	110.61 (231.12)	133.64 (272.58)	127.44 (261.41)
Broken loop hot leg T_{in} [°C (°F)]	126	170.40 (338.75)	147.49 (297.50)	167.23 (333.04)	146.41 (295.57)	167.84 (334.14)	163.32 (326.01)
Broken loop hot leg T_{out} [°C (°F)]	151	170.28 (338.53)	147.60 (297.71)	164.91 (328.87)	146.53 (295.78)	167.84 (334.14)	162.59 (324.69)
Unbroken loop hot leg T_{in} [°C (°F)]	51	170.28 (338.53)	147.49 (297.50)	167.59 (333.70)	146.17 (295.14)	167.84 (334.14)	163.20 (325.79)
Unbroken loop hot leg T_{out} [°C (°F)]	78	170.03 (338.09)	147.25 (297.07)	167.11 (332.82)	145.81 (294.49)	168.45 (335.24)	164.18 (327.55)
Broken loop steam generator T_{out} [°C (°F)]	156	139.01 (282.25)	114.55 (238.21)	137.22 (279.02)	113.83 (236.92)	134.36 (273.87)	129.59 (265.28)

2128M:1E/121583

TABLE C-1 (cont)

ENERGY BALANCE DATA

Parameter	Channel	Run Number					
		50708	51805	52809	51510	51114	51217
Unbroken loop steam generator T_{out} [°C (°F)]	83	130.06 (280.53)	113.12 (235.63)	135.31 (275.59)	111.92 (233.48)	133.05 (271.51)	127.32 (261.19)
P_{sys} [MPa (psia)]	546	0.79382 (115.13)	0.5091 (73.88)	0.96171 (139.48)	0.5291 (76.73)	0.93117 (135.05)	0.94365 (136.86)
Core power (kw)	558	74.62	72.50	74.31	75.49	77.36	78.98
	560	73.9	73.96	73.80	71.16	72.07	71.83
	562	74.33	77.50	73.85	71.28	73.94	73.82

TABLE C-1 (cont)

ENERGY BALANCE DATA

Parameter	Channel	Run Number		
		51805	52309	52706
Time (sec)	--	5431	10230	10368
Core flow [m^3/sec (gal/min)]	576	4.688 x 10^{-3} (74.30)	4.300 x 10^{-3} (68.14)	4.623 x 10^{-3} (73.27)
Broken loop flow [m^3/sec (gal/min)]	575	1.165 x 10^{-3} (18.46)	1.117 x 10^{-3} (17.70)	1.126 x 10^{-3} (17.85)
Unbroken loop flow [m^3/sec (gal/min)]	574	3.464 x 10^{-3} (54.89)	3.180 x 10^{-3} (50.40)	3.280 x 10^{-3} (51.99)
Core T_{in} [°C (°F)]	461	107.15 (224.89)	106.79 (224.25)	120.39 (248.73)
Broken loop hot leg T_{in} [°C (°F)]	126	119.44 (247.02)	119.08 (246.37)	132.09 (269.79)
Broken loop hot leg T_{out} [°C (°F)]	151	119.68 (247.45)	119.32 (246.80)	131.85 (269.36)
Unbroken loop hot leg T_{in} [°C (°F)]	51	119.56 (247.23)	119.20 (246.59)	132.33 (270.22)
Unbroken loop hot leg T_{out} [°C (°F)]	78	119.44 (247.02)	119.32 (246.80)	133.05 (271.51)
Broken loop steam generator T_{out} [°C (°F)]	156	108.34 (227.04)	108.11 (226.61)	120.63 (249.16)
Unbroken loop steam generator T_{out} [°C (°F)]	83	108.11 (226.61)	107.74 (225.96)	120.39 (248.16)
P_{sys} [MPa (psia)]	546	0.5137 (74.50)	0.5171 (75.00)	0.6721 (97.47)
Core power (kw)	558	77.36	74.96	74.31
	560	74.39	75.09	73.80
	562	71.28	73.85	73.85

Run 50708

Natural circulation, 12500 sec

$T = 338.6°F$, $P = 115.13$ psia, $\rho \simeq 56.306$ lb/ft^3

Mass flow rates:

Broken loop: $\dot{m} = 6.31\ (471.64) = 2976.0$ lb/hr

Unbroken loop: $\dot{m} = 18.73\ (471.64) = 8833.8$ lb/hr

Core flow: $\dot{m} = 25.29\ (471.64) = 11{,}927.7$ lb/hr

Bundle power = 222.8 kw = 760,587 Btu/hr

Core balance using thermocouples:

$q = \dot{m}C_p\Delta T = 11{,}927.7\ (1.01)(338.6 - 278.16) = 728{,}119$ Btu/hr

$\Delta = (760{,}587 - 728{,}119)/760{,}587 = 4.26\%$

Broken loop steam generator heat loss:

$q = (2976)(1.01)(282.25 - 338.53) = -169{,}164$ Btu/hr

Unbroken loop steam generator heat loss:

$q = (8833.8)(1.01)(280.53 - 338.09) = -513{,}558$ Btu/hr

Broken loop hot leg heat loss:

$q = 2970.6\ (1.01)(338.53 - 338.75) = -660.06$ Btu/hr

Unbroken loop hot leg heat loss:

$q = (8833.8)(1.01)(338.0 - 338.53) = -3925.74$ Btu/hr

$\Sigma q = -687{,}307$ Btu/hr

$\Delta = (760{,}587 - 687{,}307)/760{,}587 = 9.6\%$

Run 51805

Natural Circulation, 7995 sec

$T = 297.50\ °F$, $P = 73.83$ psia, $\rho \simeq 57.306\ lb/ft^3$

Mass flow rates:

Broken loop: $\dot{m} = 6.04\ (459.64) = 2776.2$ lb/hr

Unbroken loop: $\dot{m} = 18.40\ (459.64) = 8457.3$ lb/hr

Core: $\dot{m} = 23.81\ (459.64) = 10,944.0$ lb/hr

Bundle power = 223.9 kw = 764,375 Btu/hr

Core balance using thermocouples:

$q = mC_p\Delta T = (10,944.0)(1.01)(297.5 - 232.41) = 719,468$ Btu/hr

$\Delta = 5.87\%$

Broken loop steam generator heat loss:

$q = 2776.2\ (1.01)(238.21 - 297.71) = -166,835$ Btu/hr

Unbroken loop steam generator heat loss:

$q = 8457.3\ (1.01)(235.63 - 297.07) = -524,812$ Btu/hr

Broken loop hot leg heat loss:

$q = 2776.2\ (1.01)(297.71 - 297.5) = 588.8$ Btu/hr

Unbroken loop hot leg heat loss:

$q = 8457.3\ (1.01)(297.07 - 297.5) = -3673.0$ Btu/hr

$\Sigma q = -694,731$ Btu/hr

$\Delta = 9.1\%$

Run 52809

Natural circulation, 600 sec

$T = 333.4\ °F$, $P = 139.48$ psia, $\rho \simeq 56.30\ lb/ft^3$

Mass flow rates:

Broken loop: $\dot{m} = 5.93\ (451.57) = 2677.8$ lb/hr

Unbroken loop: $\dot{m} = 17.61\ (45^{\prime} 57) = 7952.2$ lb/hr

Core: $\dot{m} = 24.33\ (451.57) = 10986.7$ lb/hr

Bundle power = 221.96 kw = 757,549 Btu/hr

Core balance using thermocouples:

$q = mC_p\Delta T = 10,986.7\ (1.01)(334.4 - 270.86) = 3,979$ Btu/hr

$\Delta = 8.39\%$

Broken loop steam generator heat loss:

$q = 2677.8\ (1.01)(279.02 - 328.87) = -134,823$ Btu/hr

Unbroken loop steam generator heat loss:

$q = 7952.2\ (1.01)(275.59 - 332.82) = -459,655$ Btu/hr

Broken loop hot leg heat loss:

$q = 2677.8\ (1.01)(328.87 - 333.04) = -11,278$ Btu/hr

Unbroken loop hot leg heat loss:

$q = 7952.2\ (1.01)(332.82 - 333.70) = -7067.9$ Btu/hr

$\Sigma q = -612,823$ Btu/hr

$\Delta = 19.1\%$

Run 51510

Natural circulation, 10,200 sec

$T = 295.3\ °F$, $P = 76.73$ psia, $\rho \simeq 57.47\ lb/ft^3$

Mass flow rates:

Broken loop: $\dot{m} = 5.96\ (460.96) = 2747.3$ lb/hr

Unbroken loop: $\dot{m} = 18.29\ (460.96) = 8431.1$ lb/hr

Core: $\dot{m} = 23.91\ (460.96) = 11021.7$ lb/hr

Bundle power = 217.93 kw = 743,795 Btu/hr

Core balance using thermocouples:

$q = mC_p\Delta T = (11021.7)(1.01)(295.57 - 231.12) = 717,452$ Btu/hr

$\Delta = 3.5\%$

Broken loop steam generator heat loss:

$q = 2747.3\ (1.01)(236.92 - 295.78) = -163,323$ Btu/hr

Unbroken loop steam generator heat loss:

$q = 8431.1\ (1.01)(233.48 - 294.49) = -519,525$ Btu/hr

Broken loop hot leg heat loss:

$q = 2747.3\ (1.01)(295.78 - 295.57) = 582.7$ Btu/hr

Unbroken loop hot leg heat loss:

$q = 8431.1\ (1.01)(294.49 - 295.14) = -5535$ Btu/hr

$\Sigma q = -687,800$ Btu/hr

$\Delta = 7.5\%$

Run 51114

Natural circulation, 9181 sec

$T = 334.14\ °F$, $P = 135.05$ psia, $\rho \simeq 56.14\ lb/ft^3$

Mass flow rates:

Broken loop: $\dot{m} = 6.38\ (450.35) = 2873$ lb/hr

Unbroken loop: $\dot{m} = 19.61\ (450.35) = 8831$ lb/hr

Core: $\dot{m} = 25.58\ (450.35) = 11{,}520$ lb/hr

Bundle power = 223.37 kw = 762,361 Btu/hr

Core balance using thermocouples:

$q = mC_p\Delta T = 11{,}520\ (1.01)(334.14 - 272.58) = 716{,}263$ Btu/hr

$\Delta = 6.04\%$

Broken loop steam generator heat loss:

$q = 2873\ (1.01)(273.87 - 334.14) = -174{,}887$ Btu/hr

Unbroken loop steam generator loss:

$q = 8831\ (1.01)(271.51 - 335.24) = -568{,}427$ Btu/hr

Broken loop hot leg heat loss:

$q = 2873.3\ (1.01)(334.14 - 334.14) = 0$ Btu/hr

Unbroken loop hot leg heat loss:

$q = 8831\ (1.01)(335.24 - 334.14) = 9811.2$ Btu/hr

$\Sigma q = -733{,}502$ Btu/hr

$\Delta = 3.78\%$

Run 51217

Natural circulation, 19,161 sec

$T = 325.9\ °F$, $P = 136.86$ psia, $\rho \simeq 56.49\ lb/ft^3$

Mass flow rates:

Broken loop: $\dot{m} = 5.76\ (453.15) = 2610$ lb/hr

Unbroken loop: $\dot{m} = 18.81\ (453.15) = 8523$ lb/hr

Core: $\dot{m} = 25.48\ (453.15) = 11,546$ lb/hr

Bundle power = 224.6 kw = 766,662 Btu/hr

Core balance using thermocouples:

$q = mC_p\Delta T = 11,546\ (1.01)(325.9 - 261.41) = 752,047$ Btu/hr

$\Delta = 1.9\%$

Broken loop steam generator heat loss:

$q = 2610\ (1.01)(265.28 - 324.69) = -156,610$ Btu/hr

Unbroken loop steam generator heat loss:

$q = 8523\ (1.01)(261.19 - 327.55) = -571,242$ Btu/hr

Broken loop hot leg heat loss:

$q = 2610\ (1.01)(324.69 - 326.01) = -3479.6$ Btu/hr

Unbroken loop hot leg heat loss:

$q = 8523\ (1.01)(327.55 - 325.79) = 15,150$ Btu/hr

$\Sigma q = -716,181$ Btu/hr

$\Delta = 6.58\%$

Run 51805

Forced circulation, 5431 sec

$T = 249.59\ ^{\circ}F$, $P = 74.5$ psia , $\rho \simeq 58.802\ lb/ft^3$

Mass flow rates:

Broken loop: $\dot{m} = 18.46\ (471.64) = 8706.5$ lb/hr

Unbroken loop: $\dot{m} = 54.89\ (471.64) = 25{,}888$ lb/hr

Core: $\dot{m} = 74.3\ (471.64) = 35{,}042$ lb/hr

Bundle power = 223.03 kw = 761,201 Btu/hr

Core balance using thermocouples:

$q = mC_p\Delta T = 35{,}042\ (1.01)(249.59 - 224.89) = 874{,}192$ Btu/hr

$\Delta = 14.8\%$

Broken loop steam generator heat loss:

$q = (8706.5)(1.01)(227.04 - 247.45) = -179{,}476$ Btu/hr

Unbroken loop steam generator heat loss:

$q = 25{,}888\ (1.01)(226.61 - 247.02) = -533{,}657$ Btu/hr

Broken loop hot leg heat loss:

$q = 8706.5\ (1.01)(247.45 - 247.02) = 3781.2$ Btu/hr

Unbroken loop hot leg heat loss:

$q = 25{,}888\ (1.01)(247.02 - 247.23) = -5490.8$ Btu/hr

$\Sigma q = -714{,}842$ Btu/hr

$\Delta = 6.0\%$

Run 52309

Forced circulation, 10,230.5 sec

$T = 250.0\ ^{\circ}F$, $P = 75$ psia , $\rho \simeq 58.823\ lb/ft^3$

Mass flow rates:

Broken loop: $\dot{m} = (17.7)(471.64) = 8348$ lb/hr

Unbroken loop: $\dot{m} = (50.4)(471.64) = 23,789$ lb/hr

Core: $\dot{m} = (68.14)(471.64) = 32,137$ lb/hr

Bundle power = 223.90 kw = 764,170 Btu/hr

Core balance using thermocouples:

$q = mC_p\Delta T = 32,137\ (1.01)(246.8 - 224.25) = 721,874$ Btu/hr

$\Delta = 5.5\%$

Broken loop steam generator heat loss:

$q = 8348\ (1.01)(226.61 - 246.8) = -170,231$ Btu/hr

Unbroken loop steam generator heat loss:

$q = 23,789\ (1.01)(225.96 - 246.8) = -500,720$ Btu/hr

Broken loop hot leg heat loss:

$q = 8348\ (1.01)(246.8 - 246.37) = 3652$ Btu/hr

Unbroken loop hot leg heat loss:

$q = 23,789\ (1.01)(246.8 - 246.59) = 5045.6$ Btu/hr

$\Sigma q = -662,253$ Btu/hr

$\Delta = 13.3\%$

Run 52706

Forced circulation, 10,368 sec

$T = 270\ °F$, $P = 97.47$ psia, $\rho \simeq 58.24\ lb/ft^3$

Mass flow rate:

Broken loop: $\dot{m} = 8422$ lb/hr

Unbroken loop: $\dot{m} = 24,524$ lb/hr

Core: $\dot{m} = 34,558$ lb/hr

Bundle power = 221.96 kw = 757,549 Btu/hr

Core balance using thermocouples:

$q = mC_p\Delta T = 34,558\ (1.01)(270.0 - 248.73) = 742,399$ Btu/hr

$\Delta = 1.9\%$

Broken loop steam generator heat loss:

$q = 8422\ (1.01)(249.16 - 269.36) = -171,825$ Btu/hr

Unbroken loop steam generator heat loss:

$q = 24,524\ (1.01)(248.73 - 271.51) = -564,243$ Btu/hr

Broken loop hot leg heat loss:

$q = 8422\ (1.01)(269.36 - 269.79) = -3657$ Btu/hr

Unbroken loop hot leg heat loss:

$q = 24,524\ (1.01)(271.51 - 270.22) = 31,952$ Btu/hr

$\Sigma q = -707,773$ Btu/hr

$\Delta = 6.5\%$

TABLE C-2

SUMMARY OF ENERGY BALANCE CALCULATIONS

Run Number	Time (sec)	Core Balance (%)	Steam Generator Balance (%)
50708	12,500	4.26	9.60
51805	7995	5.87	9.10
52809	6000	8.39	19.10
51510	10,200	3.50	7.50
51114	9181	6.04	3.78
51217	19,161	1.90	6.58
51805	5431	14.8	6.00
52309	10,230	5.50	13.30
52706	10,368	1.90	6.50

APPENDIX D
MEASUREMENT AND INSTRUMENTATION UNCERTAINTIES

D-1. STEAM GENERATOR TEMPERATURE MEASUREMENTS

Before actual testing on the natural circulation facility began, it was expected that the temperature differences within the steam generators would be very small, generally below 6°C (10°F). It therefore became imperative to attempt to reduce thermocouple uncertainty.

Calibrations were performed on 65 special-limit thermocouples before they were installed in the steam generators. The thermocouples were calibrated from 0°C (32°F) (ice point) to 277°C (530°F). The total number of data points taken was 973. A statistical regression analysis was performed on the calibration data and plotted (figure D-1). As a result, the temperature measurement uncertainty of the calibrated thermocouples was reduced from ±10°C (±2°F) to (±0.2°F). Since the calibrations were performed on both 0.51 and 1.02 mm (20- and 40-mil) thermocouples of varying locations from 3.05 to 10.67 m (10 to 35 ft), the confidence level of the regression analysis is enhanced. After all thermocouples had been installed in the steam generators, isothermal tests were performed to obtain additional data to verify past assumptions.

Two additional errors are also introduced into the total system error, conditioner error and readout error. Use of the actual reference junction calibrations produced an uncertainty of ±0.19°C (±0.35°F). By using the same method, it was also possible to obtain a readout error of ±0.23°C (±0.42°F). The three errors were then combined statistically by summing the square of each component error and then taking the square root to get the total system error. The result is a total system error of 0.32°C (±0.58°F).

Tests were performed in the Forest Hills calibration laboratory to determine whether absolute or differential temperature measurements are best for the measurement of the small temperature differentials seen in the steam generators.

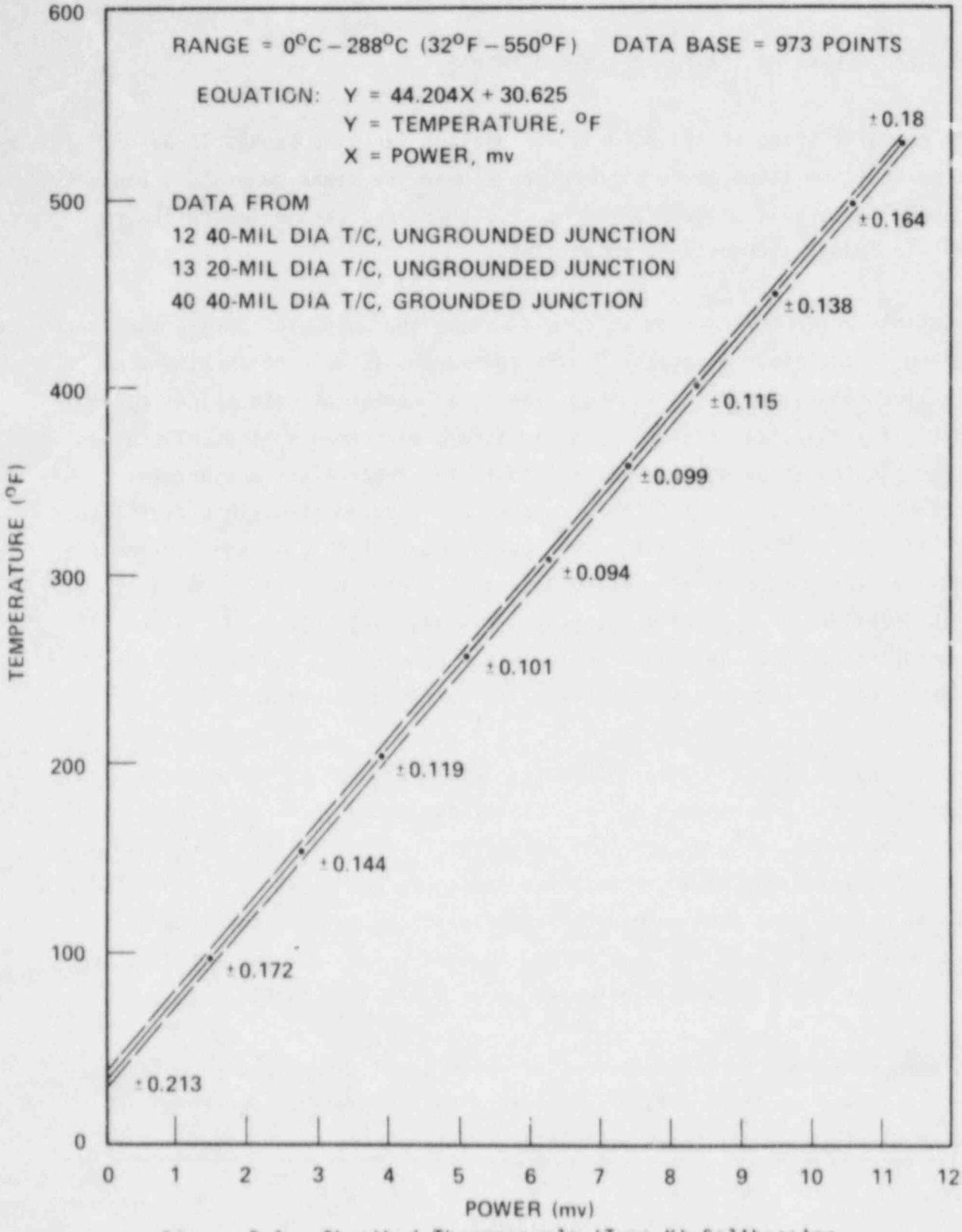

Figure D-1. Sheathed Thermocouple (Type K) Calibration Curve

To best simulate the actual conditions that exist on the facility, the thermocouple extention wire runs were kept at approximately 46 m (150 ft), existing loop thermocouples were calibrated for testing, and a reference junction and patch panel were used. The immersion mediums were as follows: an ice bath at 0°C ± 0.005°C (32°F ± 0.01°F), an oil bath with a constant temperature of 25°C ± 0.005°C (77°F ± 0.01°F), and an aluminum oxide bath at a constant temperature of 177°C ± 0.08°C (350°F ± 0.15°F). Thermocouple data were collected by the facility computer.

The tests were performed by, first, connecting the four calibrated thermocouples differentially, providing two EMF output sources. The thermocouples were placed in the immersion medium and allowed to stabilize. Readings were taken and recorded in each medium. Then the thermocouples were reconnected to provide an absolute reading. Again, readings were taken and recorded. To verify that extraneous electrical noise did not affect any of the test results, 75 kw of power was supplied to the bundle by phase-fired SCRs. Since the reference junction and patch panel were in close proximity to the SCRs, a check or the system noise rejection was performed. The final result was that the electrical noise had no influence on either the differential or absolute thermocouple readings. A summary of results of the 14 tests is given in table D-1. The difference in the maximum errors or uncertainties indicates that a differential connection would reduce the maximum error by 25 percent.

D-2. POWER CONTROL AND MEASUREMENT

The natural circulation test facility power control system consists of a main control cabinet and three water-cooled SCR control cabinets. Each SCR unit is rated at 2000 amperes at 480/277 volts. Extensive monitoring and control capabilities have been incorporated into each unit. Both primary and redundant metering circuits are inherent to each of the three units.

The power demand signal may be fed to the SCRs by one of three means: a manual potentiometer located on the control cabinet, a momentary switch which increments the demand signal by a predetermined value, and directly from the computer. The units may also be operated in several feedback modes. In the

TABLE D-1

COMPARISON OF ABSOLUTE AND

DIFFERENTIAL TEMPERATURE DATA

Test No.	Output	Immersion Medium	Computer Gain	SCR Power	Resulting Overall Error [°C (°F)]	Maximum Allowable Error [°C (°F)]
1	Absolute	Ice	1	No	≤ 0.5 (1)	± 1.79 (3.23)
2	Absolute	Ice	1	Yes	≤ 1.0 (1)	± 1.79 (3.23)
3	Absolute	Oil	1	No	≤ 1.0 (1.8)	± 1.79 (3.23)
4	Absolute	Oil	1	Yes	≤ 1.7 (1.8)	± 1.79 (3.23)
5	Absolute	Aluminum oxide	1	No	≤ 1.7 (3.1)	± 1.79 (3.23)
6	Absolute	Aluminum oxide	1	Yes	≤ 0.5 (3.1)	± 1.79 (3.23)
7	Differential	Aluminum oxide	0	No	≤ 0.5 (1)	± 1.32 (2.37)
8	Differential	Aluminum oxide	0	Yes	≤ 0.3 (1)	± 1.32 (2.37)
9	Differential	Oil	0	No	≤ 0.3 (0.5)	± 1.32 (2.37)
10	Differential	Oil	0	Yes	≤ 0.3 (0.5)	± 1.32 (2.37)
11	Differential	Ice	0	No	≤ 0.3 (0.5)	± 1.32 (2.37)
12	Differential	Ice	0	Yes	≤ 0.3 (0.5)	± 1.32 (2.37)
13	Differential	Oil/free air	0	No	≤ 0.3 (0.5)	± 1.32 (2.37)
14	Direct μvdc Input	N/A	0	(a) No (b) Yes	≤ ± 8.54 μvdc	± 8.54 μvdc

open loop mode, instantaneous response is obtained; however, the output may not remain constant. In the closed loop mode, the feedback signal is proportional to either power, voltage, or current. For natural circulation testing, closed loop voltage feedback was used.

Protection circuits built into the units provided an RMS overcurrent trip, instantaneous current trip, high-temperature SCR trip, and a water flow trip (for SCR protection). The RMS overcurrent trip and instantaneous trip could shut down the power controller within one-half cycle of line voltage.

Measurement of power is achieved by monitoring the voltage across the load and the current through the load. Each output is attenuated, converted to an RMS value, and scaled to its respective readout device. The actual power output is a result of a multiplier module (E x I). The output of this module is proportional to the instantaneous power consumed by the load. Additional stages also provide a scaled average power and scaled instantaneous power output.

D-3. INSTRUMENTATION UNCERTAINTY

A listing of the different sensors used in the FLECHT SEASET test facility with the manufacturer's quoted measurement uncertainty for each is given in table D-2. If the additional uncertainties due to signal conditioning and data acquisition computer uncertainties are statistically combined (square root of the sum of the squares), the total data path uncertainty can be estimated as in table D-3.

TABLE D-2

INSTRUMENTATION COMPONENT ERRORS

Device	Type	Manufacturer	Description	Error[a]
Sensor	1151DP	Rosemount	Differential pressure	± 0.2 percent of calibrated span
Sensor	1151AP	Rosemount	Absolute pressure	± 0.25 percent of calibrated span
Sensor	PM-385	Statham	Differential pressure	± 0.75 percent of full scale
Sensor	PM-8052	Statham	Differential pressure	± 0.50 percent of full scale
Sensor	PG-731TC	Statham	Gage pressure	± 0.50 percent of full scale
Sensor	PG-285	Statham	Gage pressure	± 0.50 percent of full scale
Sensor	K	--	Bundle thermocouple	± 1°C (2°F) [< 277°C (530°F)][b]
Sensor	K	--	Bundle thermocouple	± 0.375 percent [< 277°C (530°F)][b]
Sensor	K	--	Loop thermocouple	± 1°C (2°F) [< 277°C (530°F)][b]
Sensor	H-1K	Teledyne/ Hastings	Mass flowmeter (air)	± 1.0 percent of full scale
Sensor	H-5K	Teledyne/ Hastings	Mass flowmeter (air)	± 1.0 percent of full scale
Sensor	FT-12	Flow Technology	Flowmeter	± 0.05 percent of reading
Sensor	FT-20	Flow Technology	Bidirectional flowmeter	± 0.05 percent of reading
Sensor	5223M2600	Wallace/ Tiernan	Flowmeter (metal tube)	± 1.0 percent of full scale

a. Manufacturer's specified error except as otherwise noted
b. Thermocouple error based on National Bureau of Standards information

TABLE D-2 (cont)

INSTRUMENTATION COMPONENT ERRORS

Device	Type	Manufacturer	Description	Error[a]
Sensor	CI-320757	Flow Technology	Bidirectional flowmeter	± 0.05 percent of reading
Sensor	FTP-8C600	Flow Technology	Bidirectional flowmeter	± 0.05 percent of reading
Conditioning	K280-100	Joseph Kaye	150°F reference junction	± 0.3°C (0.5°F)
Conditioning	515	Uniloc	24 vdc dual supply	± 0.005 percent
Conditioning	UNI-76	Power Mate	5-10 vdc supply	± 0.05 percent
Readout	RTP-7470 series	Computer Products Corporation	Low-level analog input system	± 0.005 mv, 10 mv range[c]
Readout	RTP-7470 series	Computer Products Corporation	Low-level analog input system	± 0.015 mv, 20 mv range[c]
Readout	RTP-7470 series	Computer Products Corporation	Low-level analog input system	± 0.073 mv, 50 mv range[c]
Readout	RTP-7470 series	Computer Products Corporation	Low-level analog input system	± 0.488 mv, 1000 mv range[c]

a. Manufacturer's specified error except as otherwise noted
c. Error associated with the computer depends upon the selected millivolt calibration range.

Description	Range	Sensor		
		Type	Error	Ty
Bundle thermocouple	0°C-276°C (32°F-530°F)	Type K T/C	±1.1°C (2.0°F)	Refe junc
Bundle thermocouple	276°C-5[illegible]°C (530°F-[illegible]8°F)	Type K T/C	±2.10°C (3.78°F)	Refe junc
Loop thermocouple	0°C-276°C (32°F-530°F)	Type K T/C	±1.1°C[a] (2.0°F) ±0.1°C[b] (0.2°F)	Refe junc Refe junc
Differential pressure transducer	±3 kPa (0.5 psid)	Rosemount DP	0.01 kPa (0.002 psid)	Powe supp
Differential pressure transducer	±7 kPa (1.0 psid)	Rosemount DP	±0.03 kPa (0.004 psid)	Powe supp
Differential pressure transducer	±7 kPa (1.0 psid)	Statham DP	±0.07 kPa (0.01 psid)	Powe supp
Differential pressure transducer	±17 kPa (2.5 psid)	Statham DP Statham DP	±0.17 kPa (0.25 psid) ±0.26 kPa (0.038 psid)	Powe supp Powe supp
Differential pressure transducer	±34 kPa (5.0 psid)	Statham DP	±0.52 kPa (0.075 psid)	Powe supp
Differential pressure transducer	±69.0 kPa (10.0 psid)	Statham DP	±1.0 kPa (0.15 psid)	Powe supp
Differential pressure transducer	±138 kPa (20.0 psid)	Statham DP	±2.1 kPa (0.30 psid)	Powe supp
Pressure transducer	0-1.03 MPa (0-150 psi)	Rosemount AP	±2.59 kPa (0.375 psia)	Powe supp

a. Manufacturer's specified accuracy for type K special-limit the

b. Result of actual thermocouple calibrations and regression a. thermocouples installed in the steam generators

c. Error taken directly from actual reference junction calibratio

d. Error derived directly from actual system calibration data

TABLE D-3

OF ERROR ANALYSIS

Conditioner		Readout		Data Path	
e	Error	Type	Error	Expected Error	Maximum Error
ence ion	±0.3°C (0.5°F)	Computer	±0.28°C (0.52°F)	±1.18°C (2.13°F)	±1.68°C (3.02°F)
ence ion	±0.3°C (0.5°F)	Computer	±0.47°C (0.84°F)	±2.17°C (3.90°F)	±2.84°C (5.12°F)
ence ion	±0.3°C (0.5°F)	Computer	±0.28°C (0.52°F)	±1.18°C (2.13°F)	±1.68°C (3.02°F)
ence ion	±0.19°C(c) (0.35°F)	Computer	±0.23°C(d) (0.42°F)	±0.32°C (0.58°F)	±0.54°C (0.97°F)
y	≤ ±0.0083 kPa (0.0012 psid)	Computer	±0.005 kPa (0.0007 psid)	±0.01 kPa (0.002 psid)	±0.03 kPa (0.004 psid)
y	≤ ± 0.017 kPa (0.0024 psid)	Computer	±0.01 kPa (0.002 psid)	±0.03 kPa (0.005 psid)	±0.06 kPa (0.008 psid)
y	≤ ±0.007 kPa (0.001 psid)	Computer	±0.01 kPa (0.002 psid)	±0.07 kPa (0.01 psid)	±0.090 kPa (0.013 psid)
y	≤ ±0.017 kPa (0.0025 psid)	Computer	±0.03 kPa (0.004 psid)	±0.17 kPa (0.025 psid)	±0.22 kPa (0.032 psid)
y	≤ ±0.017 kPa (0.0025 psid)	Computer	±0.03 kPa (0.004 psid)	±0.26 kPa (0.038 psid)	±0.31 kPa (0.045 psid)
y	≤ ±0.03 kPa (0.005 psid)	Computer	±0.06 kPa (0.009 psid)	±0.52 kPa (0.076 psid)	±0.0.61 kPa (0.089 psid)
y	≤ ±0.07 kPa (0.01 psid)	Computer	±0.12 kPa ((0.018 psid)	±1.04 kPa (0.151 psid)	±1.23 kPa (0.178 psid)
y	≤ ±0.1 kPa (0.02 psid)	Computer	±0.24 kPa (0.035 psid)	+2.09 kPa (0.303 psid)	±2.45 kPa (0.355 psid)
y	≤ ±1.2 kPa (0.18 psi	Computer	±0.793 kPa (0.115 psia)	±2.98 kPa (0.432 psia)	±4.6 kPa 0.67 psia

rmocouples

ysis for

n data

TA

RESULTS

Description	Range	Sensor		
		Type	Error	T
Pressure transducer	0-1.38 MPa (0-200 psi)	Rosemount AP Teledyne GP	±3.4 kPa (0.50 psia) ±0.108 MPa (1.00 psig)	Pow sup Pow sup
Pressure transducer	0-2.07 MPa (0-300 psi)	Statham GP	±0.112 MPa (1.50 psig)	Pow sup
Gas flowmeter	0-1000 sccm	Teledyne/ Hastings	±10.0 sccm	Pow sup
Gas flowmeter	0-5000 sccm	Teledyne/ Hastings	±50.0 sccm	Pow sup
Flowmeter	0-6.3x10^{-5} m^3/sec (0-1.0 gal/min)	Wallace/ Tiernan	±6x10^{-7} m^3/sec (0.01 gal/min)	
Flowmeter	0-±1.6x10^{-3} m^3/sec (0-±25 gal/min)	Flow Technology	±1.5x10^{-7} m^3/sec (0.016 gal/min)	Pu ra co
Flowmeter	1.3x10^{-4}-1.3x10^{-3} m^3/sec (2-20 gal/min)	Flow Technology	±1.0x10^{-6} m^3/sec (0.016 gal/min)	Pu ra co
Flowmeter	1.3x10^{-4}-±4.7x10^{-3} m^3/sec (2-±75 gal/min)	Flow Technology	±4.7x10^{-6} m^3/sec (0.075 gal/min)	Pu ra co
Flowmeter	1.6-10^{-4}-±5x10^{-2} m^3/sec (2.5-±230 gal/min)	Flow Technology	±1.4x10^{-5} m^3/sec (0.23 gal/min)	Pu ra co
Flowmeter	4.9x10^{-5}-±1.7x10^{-3} m^3/sec (0.78-±27 gal/min)	Flow Technology	±1.7x10^{-6} m^3/sec (0.027 gal/min)	Pu ra co

BLE D-3 (cont)

OF ERROR ANALYSIS

Conditioner		Readout		Data Path	
ype	Error	Type	Error	Expected Error	Maximum Error
er ply	≤ ±1.7 kPa (0.24 psia)	Computer	±1.05 kPa (0.153 psia)	±3.96 kPa (0.575 psia)	±6.16 kPa (0.893 psia)
er ply	≤ ±0.10 MPa (0.10 psig)	Computer	±0.0977 MPa (0.175 psig)	±0.108 MPa (1.02 psig)	±0.1191 MPa (1.275 psig)
er ply	≤ ±0.10 MPa (0.15 psig)	Computer	±0.103 MPa (0.263 psig)	±0.112 MPa (1.53 psig)	±0.1145 MPa (1.913 psig)
er ply	≤ ±10.0 sccm	Computer	±0.875 sccm	±14.169 sccm	±20.875 sccm
er ply	≤ ± 50.0 sccm	Computer	±4.375 sccm	±70.846 sccm	±104.375 sccm
-	--	Computer	±5x10^{-8} m^3/sec (0.0008 gal/min)	±6x10^{-7} m^3/sec (0.01 gal/min)	±6.9x10^{-7} m^3/sec 0.011 gal/min)
se e version	±6x10^{-6} m^3/sec (0.1 gal/min)	Computer	±2.3x10^{-6} m^3/sec (0.038 gal/min)	±6.9x10^{-6} m^3/sec (0.11 gal/min)	±1.02x10^{-5} m^3/sec (0.163 gal/min)
se e version	±2.5x10^{-6} m^3/sec (0.04 gal/min)	Computer	9.4x10^{-7} m^3/sec (0.015 gal/min)	2.8x10^{-6} m^3/sec (0.044 gal/min)	4.1x10^{-6} m^3/sec (0.065 gal/min)
se e version	±2.3x10^{-5} m^3/sec (0.36 gal/min)	Computer	±9.4x10^{-7} m^3/sec (0.115 gal/min)	±2.42x10^{-5} m^3/sec (0.385 gal/min)	±3.5x10^{-5} m^3/sec (0.55 gal/min)
se e version	±5.8x10^{-5} m^3/sec (0.92 gal/min)	Computer	±2.22x10^{-5} m^3/sec (0.352 gal/min)	±6.38x10^{-5} m^3/sec (1.012 gal/min)	±9.47x10^{-5} m^3/sec (1.502 gal/min)
se e version	6.9x10^{-6} m^3/sec (0.11 gal/min)	Computer	±2.6x10^{-6} m^3/sec (0.041 gal/min)	±7.5x10^{-6} m^3/sec (0.120 gal/min)	±1.12x10^{-5} m^3/sec (0.178 gal/min)

APPENDIX E
STEAM GENERATOR TUBESHEET CONDUCTION

This calculation assesses the significance of heat conduction through the tubesheet on the steam generator energy balances. It is believed that the entering feedwater forms a cold layer [27°C - 38°C (80°F - 100°F)] on the shell side of the tubesheet, while the other side is exposed to the plenum fluid [166°C - 132°C (330°F - 270°F)]. The following calculation does not assume a film coefficient between the tubesheet and fluids and hence will yield a worst-case value for heat loss. The fluid temperatures are taken from run 50708 at 13,000 seconds.

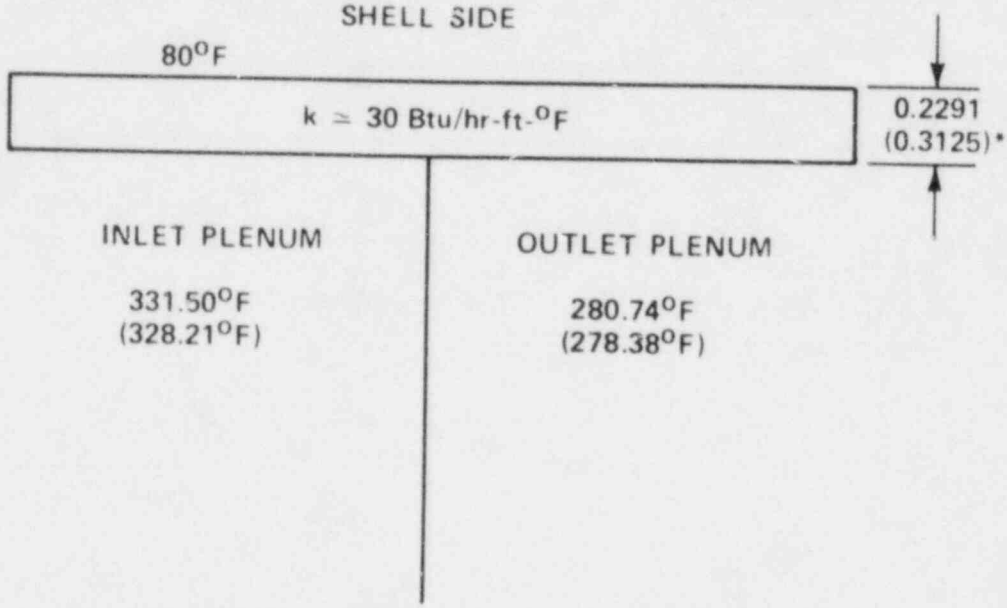

*QUANTITIES IN PARENTHESES REFER TO UNBROKEN LOOP

Unbroken loop steam generator tubesheet surface area = 0.2913 ft^2

Broken loop steam generator tubesheet surface area = 0.1173 ft^2

Broken loop steam generator:

Inlet plenum: $q_1 = (30)\ (0.1173)\ (331.5 - 80)/0.2291$

$= 3865$ Btu/hr

Outlet plenum: $q_2 = (30)\ (0.1173)\ (280.74 - 80)/0.2291$

$= 3085$ Btu/hr

Unbroken loop steam generator:

Inlet plenum: $q_3 = (30)\ (0.2913)\ (328.21 - 80)/0.3125$

$= 6941$ Btu/hr

Outlet plenum: $q_4 = (30)\ (0.2913)\ (278.38 - 80)/0.3125$

$= 5547$ Btu/hr

$\Sigma q = 19{,}438$ Btu/hr

% core power = 19,438/757,686 = 2.56%

APPENDIX F
NONUNIFORM TUBE FLOW ESTIMATE

This calculation performs a force balance on two steam generator tubes to determine whether a stalled condition may occur, or if significant tube-to-tube variations in flow are likely under natural circulation conditions.

The assumption is made that both tubes see the same plenum-to-plenum ΔP. These calculations were performed for run 52309, at 10230.5 seconds. The two tubes used for calculation are in tube model 1 and tube model 3, thus representing the maximum and minimum tube lengths [21.158 and 20.98 m (69.416 and 68.84 ft), respectively].

The test data are as follows:

Tube Model 1		Tube Model 2	
Elevation (ft)	Primary Temperature (°F)	Elevation (ft)	Primary Temperature (°F)
0	244.44	0	244.44
1	240.80	1	238.21
4	242.10	2	241.02
10	240.16	4	240.8
15	234.98	10	242.31
27	224.61	15	235.41
43	224.61	27	224.83
55	222.24	55	224.46
60	224.40	60	224.18
68	226.35	69	225.91
70	226.39	70	226.39

The averaged data are as follows:

Tube Model 1				Tube Model 3			
Δe	Elevation (ft)	Temperature (°F)	ρ (lb/ft^3)	Δe	Elevation (ft)	Temperature (°F)	ρ (lb/ft^3)
1	0-1	242.62	59.028	1	0-1	241.32	59.064
3	1-4	241.45	59.061	1	1-2	239.61	59.111
6	4-10	241.13	59.070	2	2-4	240.91	59.076
5	10-15	237.57	59.161	6	4-10	241.50	59.059
12	15-27	229.80	59.353	5	10-15	238.86	59.129
8	27-35	224.61	59.515	12	15-27	230.12	59.344
8	35-27	224.61	59.515	8	27-35	224.83	59.510
12	27-15	223.43	59.545	8	35-27	224.83	59.510
5	15-10	223.32	59.547	12	27-15	224.64	59.515
8	10-2	225.37	59.497	5	15-10	224.32	59.523
2	2-0	226.30	59.474	9	10-1	225.05	59.505
				1	1-0	226.15	59.477

Weighted densities are calculated as follows:

o Tube model 1

$$\bar{\rho}_{up} = [(59.028)(1) + (59.061)(3) + (59.07)(6) + (59.161)(5) + (59.353)(12) + (59.515)(7.42)]/34.42 = 59.277 \text{ lb/ft}^3$$

$$\bar{\rho}_{down} = [(59.515)(7.42) + (59.545)(12) + (59.547)(5) + (59.497)(8) + (59.474)(2)]/34.42 = 59.523 \text{ lb/ft}^3$$

o Tube model 3

$$\bar{\rho}_{up} = [(59.064)(1) + (59.111)(1) + (59.076)(2) + (59.059)(6) + (59.129)(5) + (59.344)(12) + (59.510)(7.708)]/34.708 = 59.270 \text{ lb/ft}^3$$

$$\bar{\rho}_{down} = [(59.510)(7.708) + (59.515)(12) + (59.523)(5) + (59.505)(9) + (59.477)]/34.708 = 59.511 \text{ lb/ft}^3$$

Taking the inlet-outlet plenum ΔP to be the same for each tube, a force balance yields

$$-f \frac{L_1}{D} \frac{V_1^2}{2g} \bar{\rho}_1 A + \bar{\Delta\rho}_1 \frac{g}{gc} (vol_1) = -f \frac{L_3}{D} \frac{V_3^2}{2g} \bar{\rho}_3 A + \bar{\Delta\rho}_3 \frac{g}{gc} (vol_3)$$

It should be noted that the friction loss components are negative because $\Delta\rho$ is defined as $\rho_{cold} - \rho_{hot}$ which is positive and thus the buoyancy term will be positive and hence drive the flow in a positive direction. The friction force direction is opposite to the flow direction.

Now let $V_3 = 0$ (stalled condition). If V_1 is positive, then a flow bias is predicted:

$$\Delta\rho_1 = 59.523 - 59.277 = 0.246$$
$$\Delta\rho_3 = 59.511 - 59.270 = 0.241$$

so

$$-f \frac{L_1}{D} \frac{V_1^2}{2g} \bar{\rho}_1 A = (\Delta\rho_3 \, vol_3 - \Delta\rho_1 \, vol_1) \frac{g}{gc}$$

$$vol_3 = \frac{\pi(0.775)^2}{4(144)} (34.708) = 0.1137 \text{ ft}^3$$

$$vol_1 = \frac{\pi(0.775)^2}{4(144)} (34.420) = 0.1127 \text{ ft}^3$$

Now taking averaged properties within tube model 1:

$$\bar{\rho} = 59.4 \text{ lb/ft}^3$$

$$\bar{T} = 230.92°F$$

$$\bar{\mu} = 54 \times 10^{-7} \text{ lb-sec/ft}^2$$

Therefore,

$$\frac{-f\ (68.84)\ V_1^2\ (12)\ (59.4)\ (\pi)\ (0.775)^2}{(0.775)\ (2)\ (32.17)\ (4)\ (144)} = -3.2236\ f\ V_1^2$$

$$-3.2236\ f\ V_1^2 = 0.241\ (0.1137) - 0.246\ (0.1127) = 0.000323$$

and

$$f\ v_1^2 = 0.000100 \qquad \text{(F-1)}$$

$$N_{RE} = \frac{VD\bar{\rho}}{\bar{\mu}} = \frac{V(0.775/12)\ (59.4)}{(54 \times 10^{-7})\ (32.17)} = 22{,}083\ V \qquad \text{(F-2)}$$

Iterating between equations (F-1) and (F-2) and pipe friction data[1] yields

$$f = 0.0900, \quad V_{tube} = 0.0333 \text{ ft/sec}$$

tube flow = (0.0333 ft/sec)(0.003276 ft^2/tube)(7.4805 gal/ft^3)(60 sec/min)

= 0.04896 gal/min-tube

This represents the amount of extra flow in tube model 1 due to buoyancy effects. If the flow were evenly split, each tube would carry approximately 0.5625 gal/min. Thus, a flow bias of approximately 0.04896/0.5625 or 8.7 percent can be expected under these conditions.

---

1. Vennard, J. K., Elementary Fluid Mechanics, John Wiley & Sons, New York, 1961, p. 283.

APPENDIX G
TUBE MODEL EQUATION FORMULATION

The equations used are the steady state two-phase continuity equations:

- Vapor phase

$$\cancel{\frac{\partial}{\partial t}(\alpha\rho_v)}^{\,0} + \frac{\partial}{\partial x}(\alpha\rho_v U_v) = \Gamma_c$$

- Liquid phase

$$\cancel{\frac{\partial}{\partial t}(1-\alpha)\rho_\ell}^{\,0} + \frac{\partial}{\partial x}((1-\alpha)\rho_\ell u_\ell) = -\Gamma_c$$

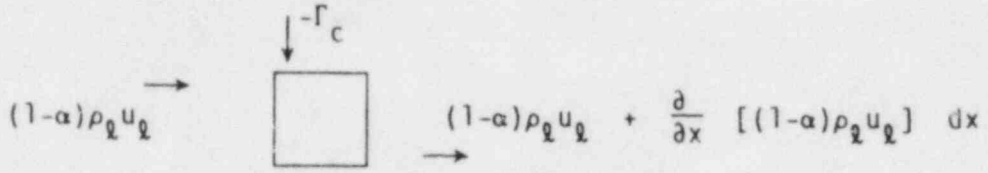

Heat transferred from primary to secondary is considered negative. Γ_c, the condensation rate, is thus a negative quantity since $\Gamma = Q/h_{fg}$.

In the above diagram, mass flow into the control volume is positive, and mass flow out is negative.

Hence, an additional negative sign accompanies Γ.

$$(1-\alpha)\rho_\ell u_\ell + \frac{\partial}{\partial x}((1-\alpha)\rho_\ell u_\ell)\,dx - (1-\alpha)\rho_\ell u_\ell - (-\Gamma_c) = 0$$

$$\frac{\partial}{\partial x}[(1-\alpha)\rho_\ell u_\ell] = -\Gamma_c \qquad \text{(G-1)}$$

Similarly,

$$\frac{\partial}{\partial x}(\alpha \rho_v u_v) = \Gamma_c \qquad \text{(G-2)}$$

Now, assume $\partial \rho_\ell / \partial x = \partial \rho_v / \partial x = 0$. Then, equations (G-1) and (G-2) become

$$\rho_\ell \frac{\partial}{\partial x}((1-\alpha) u_\ell) = -\Gamma_c \qquad \text{(G-3)}$$

$$\rho_v \frac{\partial}{\partial x}(\alpha\, u_v) = \Gamma_c \qquad \text{(G-4)}$$

Dividing equation (G-3) by ρ_ℓ and equation (G-4) by ρ_v and adding gives

$$\frac{\partial}{\partial x}[(1-\alpha) u_\ell + \alpha\, u_v] = \frac{-\Gamma_c}{\rho_\ell} + \frac{\Gamma_c}{\rho_v}$$

But

$$j = (1-\alpha)\, u_\ell + \alpha\, u_v$$

So,

$$\frac{\partial j}{\partial x} = \Gamma_c \left(\frac{1}{\rho_v} - \frac{1}{\rho_\ell} \right) \qquad \text{(G-5)}$$

Now, the two-phase mass flux is defined as:

$$G = \rho_\ell j_\ell + \rho_v j_v$$

and

$$j_\ell = (1-\alpha) j - \alpha(1-\alpha) u_r$$

$$j_v = \alpha j + \alpha(1-\alpha) u_r$$

Substituting,

$$G = \rho_\ell [(1-\alpha)j - \alpha(1-\alpha)u_r] + \rho_v [\alpha j + \alpha(1-\alpha)u_r] \tag{G-6}$$

Adding equations (G-3) and (G-4),

$$\frac{\partial}{\partial x} [\rho_\ell (1-\alpha)u_\ell + \rho_v \alpha u_v] = 0$$

or

$$\frac{\partial}{\partial x} [\rho_\ell j_\ell + \rho_v j_v] = 0 \tag{G-7}$$

Substituting equation (G-6) into equation (G-7) gives

$$\frac{\partial}{\partial x} \{\rho_\ell [(1-\alpha)j - \alpha (1-\alpha)u_r] + \rho_v [\alpha j + \alpha(1-\alpha)u_r]\} = 0 \tag{G-8}$$

Equations (G-5) and (G-8) are now to be solved using heat flux data from selected test runs. A first attempt uses only a constant relative velocity u_r.

Differencing equation (G-5) gives

$$(j_{i+1} - j_i) = \Gamma_c \left(\frac{1}{\rho_v} - \frac{1}{\rho_\ell}\right) (x_{i+1} - x_i) \tag{G-9}$$

This explicit scheme will solve for j_{i+1}, knowing j_i. The only problem is at i=1 where j_1 represents the inlet mixture volumetric flux. This quantity is estimated from data as follows:

Q ≡ unbroken loop seal volume flow rate

ρ_ℓ = unbroken loop seal liquid density

ρ_{ℓ_2} = saturated liquid density at inlet

ρ_{v_2} = saturated vapor density at inlet

A = cross-sectional area of tubes at inlet

$$Q \ \frac{gal}{min} \ \frac{60 \ min}{hr} \ \frac{1 \ ft^3}{7.4805 \ gal} = 8.0208 \ ft^3/hr$$

The average mixture density at the steam generator inlet is determined as

$$\bar{\rho}_{av} = \alpha \rho_{v_2} + (1-\alpha) \rho_{\ell_2}$$

$$\bar{v}_{av} = 1/\bar{\rho}_{av}$$

$$v_\ell' = 1/\rho_\ell'$$

So,

$$\dot{Q}_{inlet} \simeq \frac{\bar{v}_{av}}{v_\ell'} \ (Q_{loop \ seal})$$

$$\bar{j}_{mix\text{-}inlet} = Q_{inlet} / A$$

Now working with equation (G-8) and letting $\Delta\rho \equiv \rho_\ell - \rho_v$

$$\frac{d}{dx} \{[\rho_v \alpha + \rho_\ell (1-\alpha)]j - \Delta\rho\alpha (1-\alpha) u_r\} = 0$$

Let $\bar{\rho} = \rho_v \alpha + \rho_\ell (1-\alpha)$. Then,

$$\frac{d}{dx} [\bar{\rho} j - \Delta\rho\alpha(1-\alpha) u_r] = 0$$

Expanding,

$$\bar{\rho} \frac{dj}{dx} + j\frac{d\bar{\rho}}{dx} - \Delta\rho \frac{d}{dx} [\alpha(1-\alpha)] \frac{d\alpha}{dx} (u_r) - \Delta\rho\alpha (1-\alpha) \frac{du_r}{d\alpha} \frac{d\alpha}{dx} = 0$$

But

$$\frac{d\bar{\rho}}{dx} = \frac{d\bar{\rho}}{d\alpha}\frac{d\alpha}{dx} = (\rho_v - \rho_\ell)\frac{d\alpha}{dx} = -\Delta\rho\frac{d\alpha}{dx}$$

Thus,

$$\bar{\rho}\frac{dj}{dx} + j\{-\Delta\rho)\frac{d\alpha}{dx} - \Delta\rho(1-2\alpha)u_r\frac{d\alpha}{dx} - \Delta\rho\alpha(1-\alpha)\frac{du_r}{d\alpha}\frac{d\alpha}{dx} = 0$$

$$\bar{\rho}\frac{dj}{dx} + \Delta\rho\frac{d\alpha}{dx} - j - (1-2\alpha)u_r - \alpha(1-\alpha)\frac{du_r}{d\alpha} = 0$$

$$\bar{\rho}\frac{dj}{dx} + \Delta\rho\frac{d\alpha}{dx} j + (1-2\alpha)u_r + \alpha(1-\alpha)\frac{du_r}{d\alpha} \qquad \text{(G-10)}$$

Once the solution for j is found, this equation can be solved for α explicitly as follows.

Taking the simple case of u_r = constant,

$$\Delta\rho(\alpha_{i+1} - \alpha_i)\left[j_i + (1-2\alpha_{i+1})u_{r_{i+1}} + \alpha_{i+1}(1-\alpha_{i+1})\frac{d u_{r_{i+1}}}{d\alpha_{i+1}}\,0\right] = \bar{\rho}(j_{in} - j_i)$$

Expanding,

$$\Delta\rho\,\alpha_{i+1}[j_i + (1-2\alpha_{i+1})u_{r_{i+1}}] - \Delta\rho\alpha_i[j_i + (1-2\alpha_{i+1})u_{r_{i+1}}] = \bar{\rho}(j_{i+1} - j_i)$$

$$\Delta\rho\,\alpha_{i+1}j_i + \Delta\rho\alpha_{i+1}u_{r_{i+1}} = 2\Delta\rho\,u_{r_{i+1}}(\alpha_{i+1})^2 - \Delta\rho\,\alpha_i j_i$$

$$-\Delta\rho\alpha_i u_{r_{i+1}} + 2\Delta\rho\,\alpha_i\alpha_{i+1}u_{r_{i+1}} = \bar{\rho}(j_{i+1} - j_i) \qquad \text{(G-11)}$$

Collecting α_{i+1} terms, this equation can be written as

$$A\,(\alpha_{i+1})^2 + B\,(\alpha_{i+1}) + C = 0 \qquad \text{(G-12)}$$

with

$$A = -2\,\Delta\rho\,ur_{i+1} \qquad \text{(G-13)}$$

$$B = \Delta\rho j_i + \Delta\rho\,u_{r_{i+1}} + 2\Delta\rho\,\alpha_i\,u_{r_{i+1}} = \Delta\rho\,(j_i + u_{r_{i+1}} + 2\alpha_i\,u_{r_{i+1}}) \qquad \text{(G-14}$$

$$C = -\Delta\rho\alpha_i j_i - \Delta\rho\alpha_i\,u_{r_{i+1}} - \rho\,(j_{i+1} - j_i) \qquad \text{(G-15)}$$

Solving with the quadratic formula,

$$\alpha_{i+1} = \frac{-B \pm \sqrt{B^2 - 4AC}}{2A} \qquad \text{(G-16)}$$

The solution procedure is as follows

(1) Read in heat fluxes from 2-ϕ NCFLUX.

(2) Compute Γ values.

(3) Compute inlet j values (assume $\alpha_{in} = 0.95$).

(4) Solve for j_{i+1} ($i = 0, 1 \ldots, 69$) using equation (G-9).

(5) Solve equations (G-12) through (G-16) for α_{i+1} ($i = 0, 1 \ldots, 69$).

APPENDIX H

NUMERICAL PROCEDURES FOR NATURAL CIRCULATION PREDICTIVE CODE

In this appendix, the system geometry simulation is first described, the finite difference equations are developed, and finally the solution procedures are outlined. As in all other system codes, the code is constantly being updated, and it is impossible to give every detail that appears in the code. Only the key structures of the code and the numerical scheme are outlined; minor details not affecting the results of the code have been omitted.

H-1. SYSTEM GEOMETRY

A schematic diagram showing the FLECHT SEASET natural circulation test facility is shown in figure H-1. In simulation of the system, all detailed internal structures in the inlet and outlet plenums of the rod bundle and steam generator are neglected, and the system is simulated by only two types of geometric components:

- Flow channels with constant flow area are used to simulate the bundle flow area, the hot and cold legs, the steam generator U-tubes, the loop seals, the downcomer simulator, and the crossover leg. In the numerical calculations, each flow channel is further divided into numerical nodes of constant length to calculated detailed flow distributions along the flow channel. The maximum number of nodes allowed on each flow channel is 30.
- Fluid volumes connecting the constant area flow channels are used to simulate the inlet and outlet plenums of the rod bundle and steam generators. Each fluid volume is treated as a single numerical node and is not further subdivided into smaller nodal volumes; that is, flow property variations inside these fluid volumes are neglected.

To simulate the FLECHT SEASET natural circulation facility, a total of 18 flow channels and 10 fluid volumes are used, as shown schematically in figure H-2.

Note that multitube steam generators are modeled with four tube groups for each generator. The dimensions of the geometric components are given in table H-1.

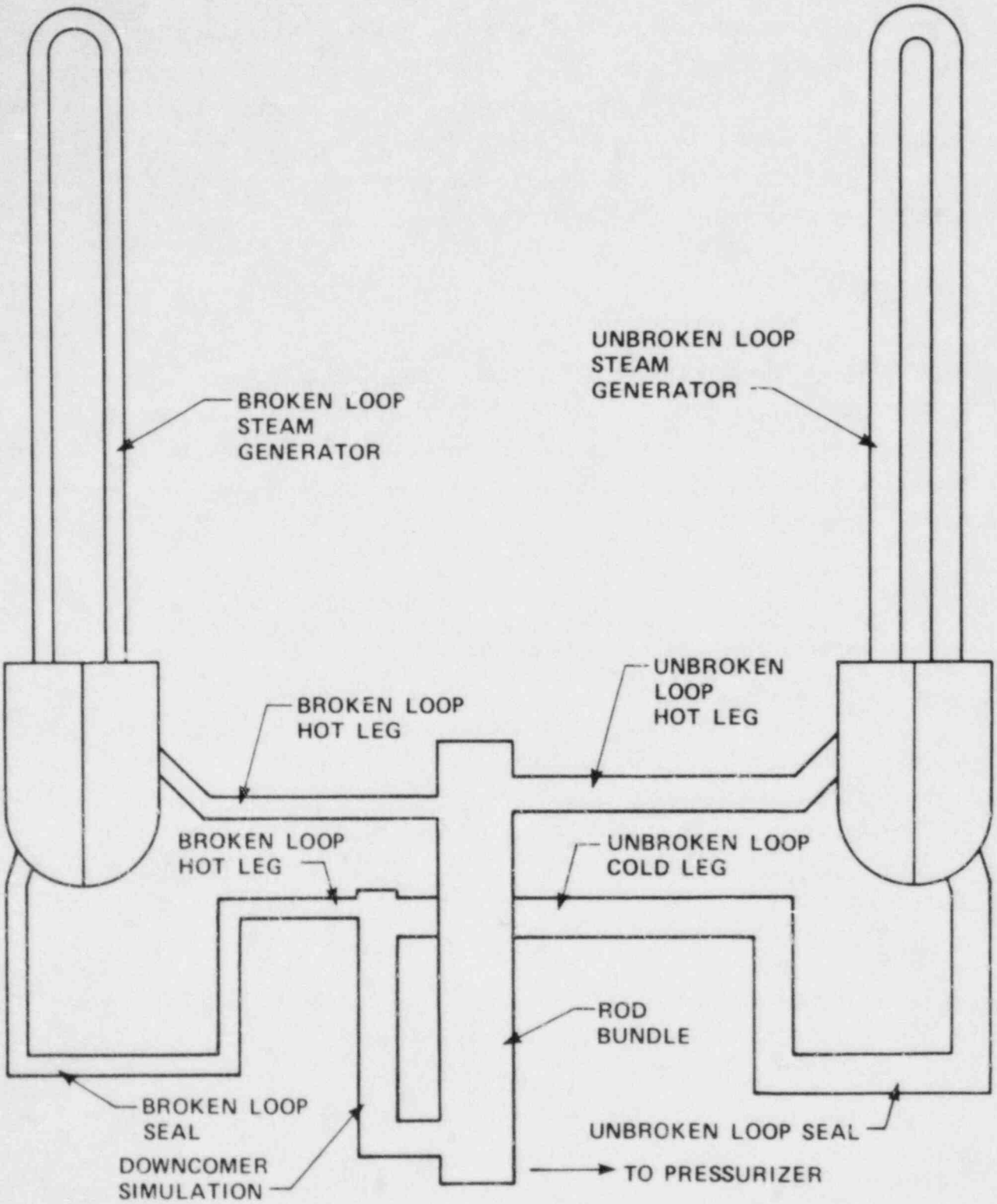

Figure H-1. Schematic Diagram of FLECHT SEASET Natural Circulation Test Loop

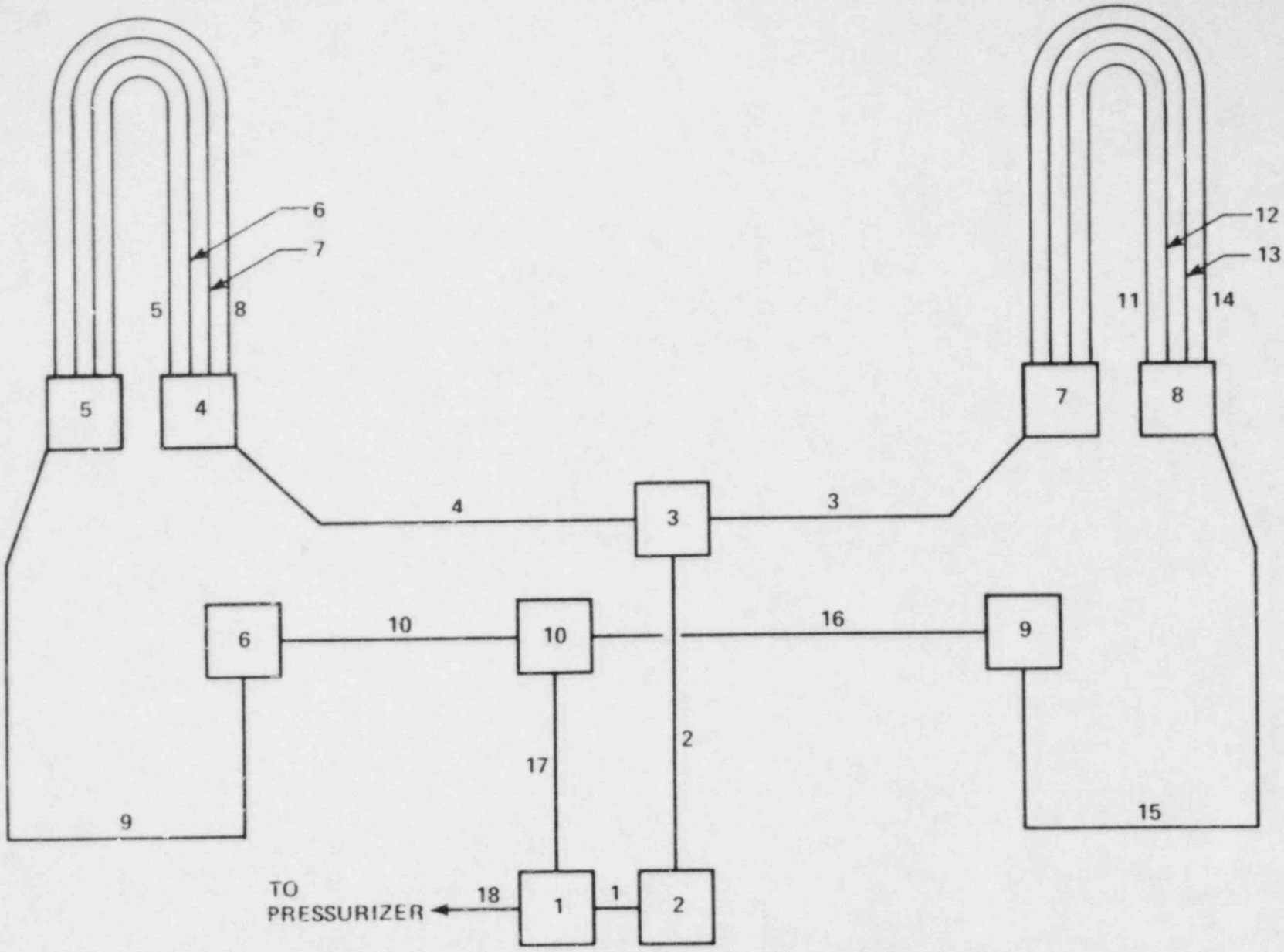

Figure H-2. Numerical Simulation of FLECHT SEASET Natural Circulation Loop

TABLE H-1

GEOMETRIC DIMENSIONS OF FLECHT SEASET NATURAL CIRCULATION LOOP

Fluid Volume Number	1	2	3	4	5	6	7	8	9	10
Volume [m^3 (ft^3)]	0.01946 (0.6875)	0.049203 (1.7380)	0.050160 (1.7718)	0.008963 (0.3166)	0.009031 (0.3190)	0.000481 (0.0170)	0.02626 (0.9276)	0.2626 (0.9276)	0.0000 (0.0004)	0.01165 (0.4114)

Component Number	Length [m (ft)]	Flow Area [m^2 (ft^2)]	Number of Nodes
1	0.97472 (3.1979)	0.01291 (0.1390)	2
2	3.66 (12.0)	0.01571 (0.1691)	6
3	6.71831 (22.0417)	0.01864 (0.2006)	10
4	5.95250 (19.5292)	0.00638 (0.00687)	10
5	20.9773 (68.8233)	0.0006086 (0.006552)	30
6	21.0792 (69.1576)	0.001522 (0.01638)	30
7	21.1582 (69.4167)	0.0006086 (0.006552)	30
8	21.03 (68.99)	0.0006086 (0.006552)	30
9	8.69064 (28.5126)	0.001587 (0.01708)	12
10	6.79652 (22.2983)	0.001316 (0.01417)	10
11	20.9264 (68.6563)	0.001522 (0.01638)	30
12	20.9772 (68.8229)	0.003347 (0.03603)	30
13	21.0534 (69.0729)	0.002739 (0.02948)	30
14	21.1535 (69.4011)	0.002130 (0.02293)	30
15	8.28574 (27.1842)	0.004768 (0.05132)	12
16	8.30376 (27.2433)	0.004264 (0.04590)	12
17	5.04953 (16.5667)	0.01637 (0.1762)	8
18	0.61 (2.0)	0.009 (0.1)	1

H-2. FINITE DIFFERENCE EQUATIONS

To develop the finite difference equations, a "staggered mesh" technique is used (figure H-3). Flow properties at the cell-center locations and at the cell-junction locations are distinguished. Usually, static fluid properties, such as fluid density, fluid enthalpy, and volumetric concentrations, are defined at the cell-center locations, while flowing fluid properties, such as velocities, mass flux, and steam quality, are defined at the cell-junction locations. There are occasions when static fluid properties must be defined at the cell-junctions and vice versa. For example, when one expresses the phase velocities in terms of volumetric concentrations by means of equations (7-14), (7-15), and (7-16), the proper volumetric concentrations must be used. For the present study, when a static fluid property must be defined at the cell-junction, the immediate upstream cell-center value is always used.

Figure H-3 illustrates the nomenclature used to denote cell locations. Integral index is used to represent cell-center locations and half-integral index is used to represent cell-junction locations. Other nomenclatures used in the finite difference equations are explained below:

- Subscript i is reserved to indicate cell locations, as illustrated in figure H-3.
- Subscripts v, ℓ, h are reserved to indicate the steam, liquid water, and noncondensible gas (helium) fields, respectively.
- Superscript n is used to denote time steps; n+1 usually denotes a new time step and n usually denotes a previous time step.
- If F is any variable, then

$$\Delta F_i^n \equiv F^n_{i+\frac{1}{2}} - F^n_{i-\frac{1}{2}} \qquad \text{(H-1)}$$

$$\delta F_i^n \equiv F_i^{n+1} - F_i^n \qquad \text{(H-2)}$$

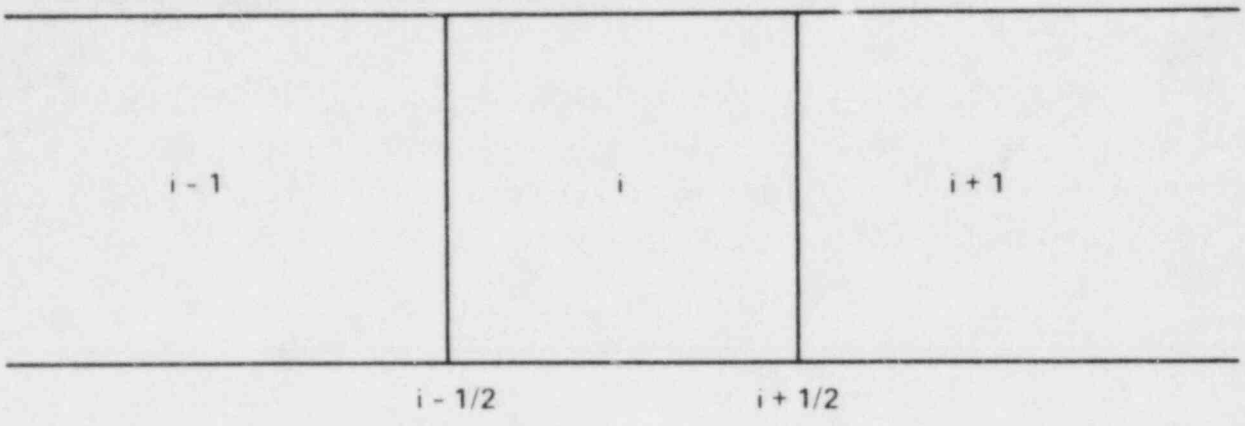

Figure H-3. Nomenclature for Numerical Cell Locations

With the above described definitions, equations (7-24), (7-23), (7-28), (7-1), and (7-2) are rewritten in the following finite difference forms, respectively:

$$h_{\ell_1}^{n+1} = \left(\frac{\alpha_{\ell_1}^n \rho_{\ell_1}^n}{\delta t^n} + \frac{G_{\ell_{1+\frac{1}{2}}}^n}{\Delta z_1} \right)^{-1} \left(\frac{\alpha_{\ell_1} \rho_{\ell_1} h_{\ell_1}^n}{\delta t^n} + \frac{G_{\ell_{1-\frac{1}{2}}}^n - G_{\ell_{1-\frac{1}{2}}}^{n+1}}{\delta z_1} \right.$$

$$\left. + \dot{q}_{\ell_1}''' + S_{\ell_1}^{n+1} + S_{\ell_1}^{n+1} h_{in_{\ell_1}}^{n+1} \right) \qquad \text{(H-3)}$$

$$j_{1+\frac{1}{2}}^{n+1} = \left(\sum_{\gamma=v,\ell,h} \frac{\rho_{\gamma_{1-1}} \alpha_{\gamma_{1-1}}}{\rho_{\gamma_1}^{n+1}} \right) j_{1-\frac{1}{2}}^{n+1} + \sum_{\gamma=v,\ell,h} \left(- \frac{\Delta (\rho_\gamma \alpha_\gamma u_{\gamma_1})_1^n}{\rho_{\gamma_1}^{n+1}} \right.$$

$$\left. - \frac{\alpha_{\gamma_1}^n \delta p_{\gamma_1}^n}{\rho_{\gamma_1}^{n+1} \delta t^n} \Delta z_1 + \frac{\Gamma_{\gamma_1}^{n+1}}{\rho_{\gamma_1}^{n+1}} \Delta z_1 + \frac{S_{\gamma_1}^{n+1}}{\rho_{\gamma_1}^{n+1}} \Delta z_1 \right) \qquad \text{(H-4)}$$

$$\Delta p_1^{n+1} = - \frac{\Delta G_1^*}{\delta t^n} - \Delta \left(\frac{G^2}{\rho_m} \right)_1^* - \frac{4 \tau_{w_1}^*}{D_h} \Delta z_1 + \Delta p_{S_1}^{n+1}$$

$$+ \Delta p_F^{n+1} + (\rho_v^{n+1} \alpha_v^n + \rho_\ell^n \alpha_\ell^n + \rho_h^{n+1} \alpha_h^n) g (\hat{z} \cdot \hat{g}) \Delta z_1 \qquad \text{(H-5)}$$

$$\frac{\delta (\rho_\ell \alpha_\ell)_1^n}{\delta t^n} + \frac{\Delta G_{\ell_1}^{n+1}}{\Delta z_1} - \Gamma_{\ell_1}^{n+1} - S_{\ell_1}^{n+1} = 0 \qquad \text{(H-6)}$$

$$\frac{\delta(\rho_v \alpha_v)_i^n}{\delta t^n} + \frac{\Delta G_{v_i}}{\Delta z_i} - \Gamma_{v_i}^{n+1} = 0 \qquad \text{(H-7)}$$

The superscript * in equation (H-5) has the following meaning: the G's contained in these expressions are calculated according to equations (7-13), (7-20), (7-21), and (7-22); the $(n+1)^{th}$ time step values of ρ's and j's are used while the previous n^{th} time step values of α's and $u_{\gamma j}$ are used in the calculations.

With the general rules described above, all other equations [equations (7-6) through (7-22)] can be easily written in finite difference form. Once the finite difference equations are written, an iterative procedure is used to solve these equations. The iterative procedures are described in more detail below.

H-3. NUMERICAL METHODS

The conservation equations are solved in the following order:

(1) The energy equation (H-3)

(2) The j equation and the momentum equation (H-4) and (H-5)

(3) The continuity equations (H-6) and (H-7)

The detailed solution method for each of the above equations is outlined below.

H-4. Solution Method of Energy Equation

It is apparent from equation (H-3) that one can easily calculate h_i^{n+1} if the enthalpy, h_{i-1}^{n+1}, at the immediate upstream cell is known. An iteration procedure is employed to solve equation (H-3) for the natural circulation loop. The procedure is best illustrated by considering a simple four-component loop, as shown in figure H-4. The following nomenclature is used:

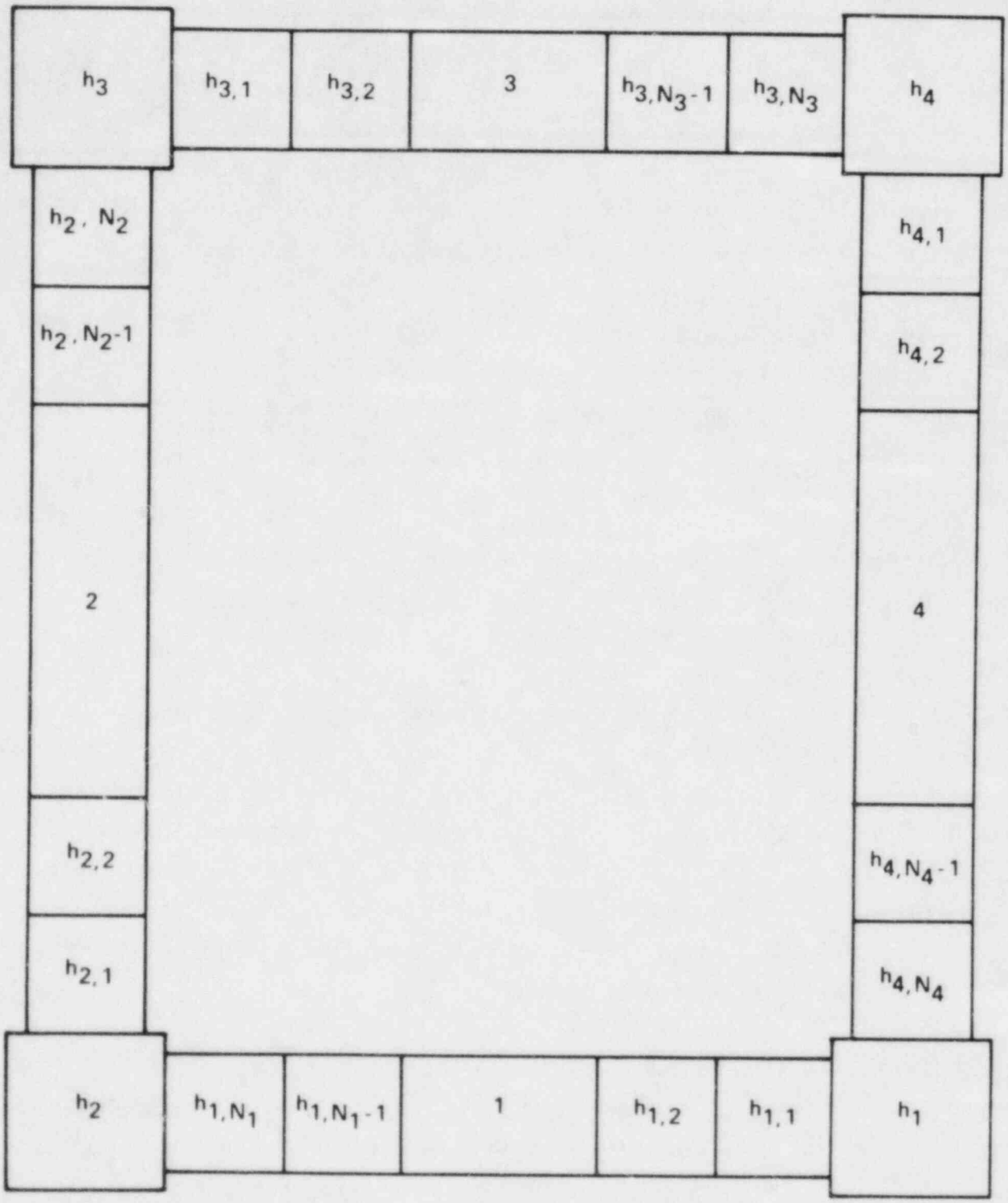

Figure H-4. Four-Component Loop Illustrating Numerical Solution Method for FLECHT SEASET Natural Circulation Loop

$h^{l}_{K,i}$ = the l^{th} iterative value for h^{n+1} at the i^{th} node of the K^{th} component (K=1, 2, 3, 4)

h^{l}_{M} = the l^{th} iterative value for h^{n+1} at the M^{th} fluid volume (M=1, 2, 3, 4)

N_K = number of nodes for the K^{th} component

Note also that equation (H-3) can easily be modified to apply to the fluid volumes 1, 2, 3, 4. Once this is done, it is apparent that the enthalpy in a given node is a function of the immediate upstream enthalpy:

$$h_{K,i} = h_{K,i}\,(h_{K,i-1}),\ i \neq 1 \qquad \text{(H-8)}$$

$$h_{K,1} = h_{K,1}\,(h_K) \qquad \text{(H-9)}$$

$$h_K = h_K\,(h_{K-1,N_{K-1}}),\ K \neq 1 \qquad \text{(H-10)}$$

$$h_1 = h_1\,(h_{4,N_4}) \qquad \text{(H-11)}$$

The iteration procedure is then performed as follows:

(1) Assume initial values (usually old time values) for h^{1}_{1}, h^{1}_{3}, $h^{1}_{K,i}$ (K=1, 2, 3, 4 and i=2, 4, 6,...N_K-2,N_K); that is, assume initial values for h at alternate numerical nodes.

(2) Calculate h^{1}_{2}, h^{1}_{4}, $h^{1}_{k,i}$ (K=1, 2, 3, 4 and i=1, 3, 5, N_K-3, N_K-1) as a function of the h values assumed in step (1).

(3) Calculate the 2nd iterative values of h^{2}_{1}, h^{2}_{3}, $h^{2}_{K,i}$ (K=1, 2, 3, 4 and i=2, 4, 6,...N_K-2, N_K) as a function of the h values calculated in step 2.

(4) Calculate the 2nd iterative values of h^{2}_{2}, h^{2}_{4}, h^{2}_{4}, h^{2}_{K1} (k=1, 2, 3, 4 and i=1, 3, 5,...N_K-3, N_K-1) as a function of the h values calculated in step (3).

(5) Repeat the procedure until all h_K, $h_{K,i}$ (k-1, 2, 3, 4 and i=1, 2, 3,...N_K) converges.

Once the fluid enthalpy has been calculated, physical properties are updated using the newly calculated enthalpy.

H-5. Solution Method of Mixture Velocity and Momentum Equations

The solution method of these two equations depends on whether one is calculating a constant pressure case or a constant inventory case. These two cases are considered separately below.

H-6. Constant Pressure Case -- In this case, the pressurizer is valved in to the system and the pressure at the junction of the loop seal and the downcomer (see figure H-1 and fluid volume 1 of figure H-2) is kept at a constant value. Fluid will run in and out of the loop (through component 18 in figure H-2), to maintain a constant system pressure. Equation (H-4) is then used to determine Δj_1^{n+1} for each node around the natural circulation loop, and these values are assumed to remain unchanged for the $(n+1)^{th}$ time step. While equation (H-4) gives the mixture velocity differences across each node around the natural circulation loop, the absolute magnitude of the $j_{i+1/2}^{n+1}$ values is determined by the momentum equation. The iteration procedures are carried out as follows:

(1) An initial guess for $j_{i+1/2}^{n+1}$ for component 1 (the loop seal in figure H-2) is first made. (Usually the value from the previous time step is used.)

(2) The j values around the loop are then calculated by the Δj values that have been already calculated.

(3) The j values are then used to update the G values [by means of equations (7-13), (7-20), (7-21) and (7-22), and using old time values of α and u_{Yj}] to be used in equation (H-7).

(4) Equation (H-5) is then used to calculate Δp^{n+1} around the loop and the calculated value is compared with zero.

(5) If Δp^{n+1} around the loop is not zero (to a specified margin), $j^{n+1}_{i+1/2}$ will be adjusted. (Normally, if $\Delta p^{n+1} > 0$, $j^{n+1}_{i+1/2}$ will be increased so that friction will increase, and if $\Delta p^{n+1} < 0$, j^{n+1}_{1} will be decreased so that friction will decrease.) The above procedures are repeated until convergence is achieved.

H-7. Constant Inventory Case -- In this case, the pressurizer is valved out of the system, and the system pressure responds to mass injection (helium gas injection) into the system, change in void fraction, thermal expansion of the gas and fluid, and so forth. Equation (H-4) is used to determine the system pressure as follows:

(1) Using an initial guess of the system pressure (usually previous time value), equation (H-4) is used to calculate the integrated Δj value around the loop. For a constant inventory situation, Δj around the loop must be zero or, equivalently, j at component 18 (figure H-2) must be zero.

(2) If the integrated Δj around the loop is not zero, the system pressure is adjusted (usually if $\int_{loop} \Delta j > 0$, the system pressure will be increased in order to increase the fluid density, and if $\int_{loop} \Delta j < 0$, the system pressure will be decreased so that fluid density will be reduced), and the fluid properties (especially fluid density) will be updated according to the new pressure. The above procedures will then be repeated until convergence is achieved.

Once the system pressure has been determined to satisfy the constant inventory criteria, calculations for the absolute magnitude of j's around the loop are carried out as in the constant pressure case.

H-8. Solution Method for Continuity Equation

The solution method for the continuity equations is identical to that of the energy equation, except for the following complications:

- Equations (H-6) and (H-7) are nonlinear in α_ℓ and α_v, since G_ℓ and G_v are quadratic functions of α's [see equations (7-14) through (7-22)]. So in order to solve for α in each cell, an iteration method is used. The bisection method[1] is used to calculate the local α's in the present study.

- Equations (H-6) and (H-7) must be solved simultaneously. However, since an interative procedure is employed, one can iterate equations (H-6) and (H-7) alternately and use the newest available α values in the calculations at all times.

---

1. The upper and lower bound values for α are first determined, and the solution of α is then determined by bisecting the difference between the upper and lower bound values.

NRC/EPRI/WESTINGHOUSE REPORT NO. 14
EXTERNAL DISTRIBUTION

Dr. L. S. Tong
9733 Lookout Place
Gaithersburg, MD

Dr. Richard Lee
Experimental Programs Research Branch
U. S. Nuclear Regulatory Commission
Washington, DC 20555

Mr. K. V. Morton, Chief
Research Contracts Branch
Division of Contracts
U. S. Nuclear Regulatory Commission
Washington, DC 20555

Dr. Wayne Hodges
DSS
U. S. Nuclear Regulatory Commission
Washington, DC 20555

Mr. L. Phillips
NRR
U. S. Nuclear Regulatory Commission
Washington, DC 20555

Mr. Harry Balukjan
NRR
U. S. Nuclear Regulatory Commission
Washington, DC 20555

Dr. D. Ross, Deputy Director
Office of Nuclear Regulatory Research
U. S. Nuclear Regulatory Commission
Washington, DC 20555

Dr. L. E. Hochreiter (10 copies)
MNC 426
Westinghouse Electric Corporation
P. O. Box 355
Pittsburgh, PA

Mr. F. D. Lang
Energy Incorporated
P. O. Box 763
Idaho Falls, ID 83415

Dr. J. Chen
Department of Mechanical Engineering
Lehigh University
Bethlehem, PA 18015

Mr. N. H. Shah
Babcock & Wilcox (NPGD)
P. O. Box 1260
Lynchburg, VA 24505

Mr. W. Kayser
Exxon Nuclear
2101 Horn Rapids Road
Richland, WA 99352

Dr. F. Aguilan
EG&G Idaho, Inc.
P. O. Box 1625
Idaho Falls, ID 83415

Dr. P. Griffith
Department of Mechanical Engineering
Massachusetts Institute of Technology
Cambridge, MA 02139

Dr. P. A. Lottes
Argonne National Laboratory
9700 South Cass Avenue
Argonne, IL 60439

Dr. L. Buxton
Sandia National Laboratory
P. O. Box 5800
Albuquerque, NM 87185

Mr. G. Otey
Sandia National Laboratory
P. S. Box 5800
Albuquerque, NM 87185

Mr. F. Mynatt
Engineering Technology Division
Oak Ridge National Laboratory
Box 7
Oak Ridge, TN 37830

Dr. W. Hancox
Whiteshell Nuclear Laboratory
Atomic Energy of Canada
Pinawa, Manitoba, Canada ROE 1LO

Professor T. Theofanous
Department of Nuclear Energy
Purdue University
West Lafayette, IN 47907

Dr. Avtar Singh (5 copies)
Nuclear Power Division
Electric Power Research Institute
P. O. Box 10412
Palo Alto, CA 94304

Dr. K. H. Sun
Nuclear Power Division
Electric Power Research Institute
P. O. Box 10412
Palo Alto, CA 94304

Dr. J. J. Cudlin
Power Generation Group
Babcock & Wilcox
P. O. Box 1260
Lynchburg, VA 24505

Mr. J. Longo, Jr. (2 copies)
Combustion Engineering
P. O. Box 500
Windsor, CT 06095

Dr. K. P. Galbraith
Nuclear Safety Engineering
Exxon Nuclear Company
2101 Horn Rapids Road
Richland, WA 99352

Dr. J. A. Block
Creare, Inc.
Hanover, NH 03755

Dr. S. Levy
S. Levy, Inc.
1901 S. Bascom Avenue, Suite 275
Campbell, CA 95008

Mr. Marv Thurgood
Numerical Applications, Inc.
GESA Building, 2nd floor
Richland, WA 99352

Mr. Don Ogden
EG&G Idaho, Inc.
P. O. Box 1625
Idaho Falls, ID 83415

Distribution Services Branch
(5 copies)
Nuclear Regulatory Commission
7920 Norfolk Avenue
Bethesda, MD 20555

Professor I. Catton
Department of Chemical, Nuclear, and
Thermal Engineering
University of California at Los Angeles
Los Angeles, CA 90024

Dr. Max W. Carbon
Department of Nuclear Engineering
University of Wisconsin
Madison, WI 53706

Dr. R. Lahey
Department of Nuclear Engineering
Rensselaer Polytechnic Institute
Troy, NY 12181

Dr. Owen Jones
Brookhaven National Laboratory
Building 820
Upton, NY 11973

Professor S. C. Yao
Department of Mechanical Engineering
Carnegie-Mellon University
Pittsburgh, PA 15213

Dr. S. J. Board
CEGB
Berkeley Nuclear Laboratory
Berkeley
Gloucestershire, England

Professor T. Wu
California Institute of Technology
Pasadena, CA 91109

Professor A. Tapucu
Ecole Polytechnique
Universite de Montreal
Institut d'Energie Nucleaire
Casier Postale 6079
Succursal "A,"
Montreal, Quebec, Canada H3C 3A7

Mr. Peter Davis
Inter-Mountain Technology
P. O. Box 1604
Idaho Falls, ID 83415

Mr. E. T. Laats
EG&G Idaho, Inc.
P. O. Box 1625
Idaho Falls, ID 83415

Dr. V. H. Dhir
University of California at
Los Angeles
5534 Boelter Hall
Los Angeles, CA 90024

Dr. Y. Y. Hsu
Department of Chemical and Nuclear
Engineering
University of Maryland
College Park, Maryland 20742

NRC FORM 335 (2-84) NRCM 1102, 3201, 3202

U.S. NUCLEAR REGULATORY COMMISSION

BIBLIOGRAPHIC DATA SHEET

SEE INSTRUCTIONS ON THE REVERSE

1 REPORT NUMBER (Assigned by TIDC add Vol. No., if any)
NUREG/CR-3654
EPRI NP-3497
WCAP-10415

2 TITLE AND SUBTITLE
PWR FLECHT SEASET Systems Effects Natural Circulation and Reflux Condensation Data Evaluation and Analysis Report
NRC/EPRI/Westinghouse Report No. 14

3 LEAVE BLANK

4 DATE REPORT COMPLETED
MONTH: August
YEAR: 1984

5 AUTHOR(S)
L.E. Hochreiter, S.D. Rupprecht, J.T. Dederer, S. Wong, E.R. Rosal, B.R. Sinwell, F.J. Kovdalski, R. Quaglia

6 DATE REPORT ISSUED
MONTH: September
YEAR: 1984

7 PERFORMING ORGANIZATION NAME AND MAILING ADDRESS (Include Zip Code)
Westinghouse Electric Corporation
Nuclear Energy Systems
P. O. Box 355
Pittsburgh, PA 15230

8 PROJECT/TASK/WORK UNIT NUMBER

9 FIN OR GRANT NUMBER
B6204

10 SPONSORING ORGANIZATION NAME AND MAILING ADDRESS (Include Zip Code)
Div. of Accident Evaluation
Off. of Nuclear Reg. Research
U.S. Nuclear Regulatory Comm.
Washington, D.C. 20555

Electric Power Res. Inst.
P. O. Box 10412
Palo Alto, CA 94303

11a TYPE OF REPORT
Technical

b PERIOD COVERED (Inclusive dates)

12 SUPPLEMENTARY NOTES

13 ABSTRACT (200 words or less)

A series of natural circulation tests were conducted at a FLECHT SEASET facility which is scaled 1/307 by volume to a full size PWR. The purpose of these tests was to identify hydraulic and heat transfer phenomena during natural circulation cooling modes. The resulting data, evaluation, and analysis are to be used for PWR codes and model assessments as well as to provide a comparison to similar experiments in other scaled systems. Steady-state single-phase, two-phase, and reflux condensation modes of natural circulation cooling were established in the FLECHT SEASET systems effects facility and the flow and heat transfer characteristics of the different cooling modes were identified. This report presents the test data; data reduction, analysis, and evaluations; and resulting model development and analysis. The models which have been developed include a reflux tube condensation model as well as a single- and two-phase model for the overall system.

14 DOCUMENT ANALYSIS - a KEYWORDS/DESCRIPTORS
FLECHT SEASET
Natural circulation
Single-phase, two-phase and reflux condensation

b IDENTIFIERS/OPEN-ENDED TERMS

15 AVAILABILITY STATEMENT
Unlimited

16 SECURITY CLASSIFICATION
(This page) Unclassified
(This report) Unclassified

17 NUMBER OF PAGES

18 PRICE

UNITED STATES
NUCLEAR REGULATORY COMMISSION
WASHINGTON, D.C. 20555